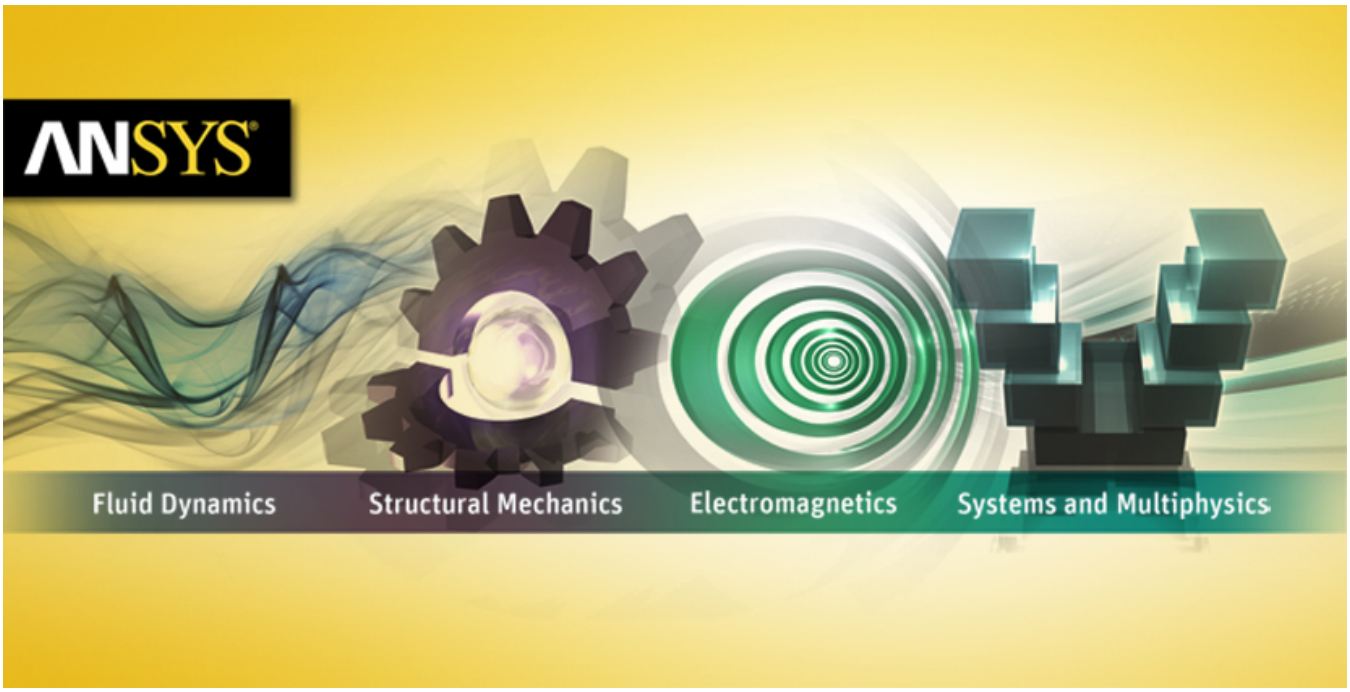


# ANSYS Fluent Theory Guide

ANSYS, Inc.
Southpointe
275 Technology Drive
Canonsburg, PA 15317
ansysinfo@ansys.com
http://www.ansys.com
(T) 724-746-3304
(F) 724-514-9494

Release 15.0
November 2013

ANSYS, Inc. is certified to ISO 9001:2008.

## Copyright and Trademark Information

© 2013 SAS IP, Inc. All rights reserved. Unauthorized use, distribution or duplication is prohibited.

ANSYS, ANSYS Workbench, Ansoft, AUTODYN, EKM, Engineering Knowledge Manager, CFX, FLUENT, HFSS and any and all ANSYS, Inc. brand, product, service and feature names, logos and slogans are registered trademarks or trademarks of ANSYS, Inc. or its subsidiaries in the United States or other countries. ICEM CFD is a trademark used by ANSYS, Inc. under license. CFX is a trademark of Sony Corporation in Japan. All other brand, product, service and feature names or trademarks are the property of their respective owners.

## Disclaimer Notice

THIS ANSYS SOFTWARE PRODUCT AND PROGRAM DOCUMENTATION INCLUDE TRADE SECRETS AND ARE CONFIDENTIAL AND PROPRIETARY PRODUCTS OF ANSYS, INC., ITS SUBSIDIARIES, OR LICENSORS. The software products and documentation are furnished by ANSYS, Inc., its subsidiaries, or affiliates under a software license agreement that contains provisions concerning non-disclosure, copying, length and nature of use, compliance with exporting laws, warranties, disclaimers, limitations of liability, and remedies, and other provisions. The software products and documentation may be used, disclosed, transferred, or copied only in accordance with the terms and conditions of that software license agreement.

ANSYS, Inc. is certified to ISO 9001:2008.

## U.S. Government Rights

For U.S. Government users, except as specifically granted by the ANSYS, Inc. software license agreement, the use, duplication, or disclosure by the United States Government is subject to restrictions stated in the ANSYS, Inc. software license agreement and FAR 12.212 (for non-DOD licenses).

## Third-Party Software

See the legal information in the product help files for the complete Legal Notice for ANSYS proprietary software and third-party software. If you are unable to access the Legal Notice, please contact ANSYS, Inc.

Published in the U.S.A.

# Table of Contents


Using This Manual ..... xxvii
1. The Contents of This Manual ..... xxvii
2. The Contents of the Fluent Manuals ..... xxviii
3. Typographical Conventions ..... xxix
4. Mathematical Conventions ..... xxx
5. Technical Support ..... xxxi
**1. Basic Fluid Flow** ..... 1
1.1. Overview of Physical Models in ANSYS Fluent ..... 1
1.2. Continuity and Momentum Equations ..... 2
1.2.1. The Mass Conservation Equation ..... 2
1.2.2. Momentum Conservation Equations ..... 3
1.3. User-Defined Scalar (UDS) Transport Equations ..... 4
1.3.1. Single Phase Flow ..... 4
1.3.2. Multiphase Flow ..... 5
1.4. Periodic Flows ..... 6
1.4.1. Overview ..... 6
1.4.2. Limitations ..... 7
1.4.3. Physics of Periodic Flows ..... 7
1.4.3.1. Definition of the Periodic Velocity ..... 7
1.4.3.2. Definition of the Streamwise-Periodic Pressure ..... 8
1.5. Swirling and Rotating Flows ..... 8
1.5.1. Overview of Swirling and Rotating Flows ..... 9
1.5.1.1. Axisymmetric Flows with Swirl or Rotation ..... 9
1.5.1.1.1. Momentum Conservation Equation for Swirl Velocity ..... 10
1.5.1.2. Three-Dimensional Swirling Flows ..... 10
1.5.1.3. Flows Requiring a Moving Reference Frame ..... 11
1.5.2. Physics of Swirling and Rotating Flows ..... 11
1.6. Compressible Flows ..... 12
1.6.1. When to Use the Compressible Flow Model ..... 13
1.6.2. Physics of Compressible Flows ..... 13
1.6.2.1. Basic Equations for Compressible Flows ..... 14
1.6.2.2. The Compressible Form of the Gas Law ..... 14
1.7. Inviscid Flows ..... 15
1.7.1. Euler Equations ..... 15
1.7.1.1. The Mass Conservation Equation ..... 15
1.7.1.2. Momentum Conservation Equations ..... 16
1.7.1.3. Energy Conservation Equation ..... 16
**2. Flows with Moving Reference Frames** ..... 17
2.1. Introduction ..... 17
2.2. Flow in a Moving Reference Frame ..... 18
2.2.1. Equations for a Moving Reference Frame ..... 19
2.2.1.1. Relative Velocity Formulation ..... 20
2.2.1.2. Absolute Velocity Formulation ..... 21
2.2.1.3. Relative Specification of the Reference Frame Motion ..... 21
2.3. Flow in Multiple Reference Frames ..... 22
2.3.1. The Multiple Reference Frame Model ..... 22
2.3.1.1. Overview ..... 22
2.3.1.2. Examples ..... 23
2.3.1.3. The MRF Interface Formulation ..... 24
2.3.1.3.1. Interface Treatment: Relative Velocity Formulation ..... 24


*Release 15.0 - © SAS IP, Inc. All rights reserved. - Contains proprietary and confidential information of ANSYS, Inc. and its subsidiaries and affiliates.*

2.3.1.3.2. Interface Treatment: Absolute Velocity Formulation ..... 25
2.3.2. The Mixing Plane Model ..... 25
2.3.2.1. Overview ..... 26
2.3.2.2. Rotor and Stator Domains ..... 26
2.3.2.3. The Mixing Plane Concept ..... 27
2.3.2.4. Choosing an Averaging Method ..... 28
2.3.2.4.1. Area Averaging ..... 28
2.3.2.4.2. Mass Averaging ..... 28
2.3.2.4.3. Mixed-Out Averaging ..... 29
2.3.2.5. Mixing Plane Algorithm of ANSYS Fluent ..... 29
2.3.2.6. Mass Conservation ..... 30
2.3.2.7. Swirl Conservation ..... 30
2.3.2.8. Total Enthalpy Conservation ..... 31
**3. Flows Using Sliding and Dynamic Meshes** ..... 33
3.1. Introduction ..... 33
3.2. Dynamic Mesh Theory ..... 34
3.2.1. Conservation Equations ..... 35
3.2.2. Six DOF (6DOF) Solver Theory ..... 36
3.3. Sliding Mesh Theory ..... 37
**4. Turbulence** ..... 39
4.1. Underlying Principles of Turbulence Modeling ..... 39
4.1.1. Reynolds (Ensemble) Averaging ..... 39
4.1.2. Filtered Navier-Stokes Equations ..... 40
4.1.3. Hybrid RANS-LES Formulations ..... 41
4.1.4. Boussinesq Approach vs. Reynolds Stress Transport Models ..... 42
4.2. Spalart-Allmaras Model ..... 42
4.2.1. Overview ..... 42
4.2.2. Transport Equation for the Spalart-Allmaras Model ..... 43
4.2.3. Modeling the Turbulent Viscosity ..... 43
4.2.4. Modeling the Turbulent Production ..... 44
4.2.5. Modeling the Turbulent Destruction ..... 45
4.2.6. Model Constants ..... 45
4.2.7. Wall Boundary Conditions ..... 45
4.2.8. Convective Heat and Mass Transfer Modeling ..... 46
4.3. Standard, RNG, and Realizable k-ε Models ..... 46
4.3.1. Standard k-ε Model ..... 47
4.3.1.1. Overview ..... 47
4.3.1.2. Transport Equations for the Standard k-ε Model ..... 47
4.3.1.3. Modeling the Turbulent Viscosity ..... 47
4.3.1.4. Model Constants ..... 48
4.3.2. RNG k-ε Model ..... 48
4.3.2.1. Overview ..... 48
4.3.2.2. Transport Equations for the RNG k-ε Model ..... 48
4.3.2.3. Modeling the Effective Viscosity ..... 49
4.3.2.4. RNG Swirl Modification ..... 50
4.3.2.5. Calculating the Inverse Effective Prandtl Numbers ..... 50
4.3.2.6. The R-ε Term in the ε Equation ..... 50
4.3.2.7. Model Constants ..... 51
4.3.3. Realizable k-ε Model ..... 51
4.3.3.1. Overview ..... 51
4.3.3.2. Transport Equations for the Realizable k-ε Model ..... 52
4.3.3.3. Modeling the Turbulent Viscosity ..... 53


*Release 15.0 - © SAS IP, Inc. All rights reserved. - Contains proprietary and confidential information of ANSYS, Inc. and its subsidiaries and affiliates.*

4.3.3.4. Model Constants ..... 54
4.3.4. Modeling Turbulent Production in the k-ε Models ..... 54
4.3.5. Effects of Buoyancy on Turbulence in the k-ε Models ..... 55
4.3.6. Effects of Compressibility on Turbulence in the k-ε Models ..... 56
4.3.7. Convective Heat and Mass Transfer Modeling in the k-ε Models ..... 56
4.4. Standard and SST k-ω Models ..... 57
4.4.1. Standard k-ω Model ..... 58
4.4.1.1. Overview ..... 58
4.4.1.2. Transport Equations for the Standard k-ω Model ..... 58
4.4.1.3. Modeling the Effective Diffusivity ..... 59
4.4.1.3.1. Low-Reynolds-Number Correction ..... 59
4.4.1.4. Modeling the Turbulence Production ..... 60
4.4.1.4.1. Production of k ..... 60
4.4.1.4.2. Production of ω ..... 60
4.4.1.5. Modeling the Turbulence Dissipation ..... 60
4.4.1.5.1. Dissipation of k ..... 60
4.4.1.5.2. Dissipation of ω ..... 61
4.4.1.5.3. Compressibility Correction ..... 61
4.4.1.6. Model Constants ..... 62
4.4.2. Shear-Stress Transport (SST) k-ω Model ..... 62
4.4.2.1. Overview ..... 62
4.4.2.2. Transport Equations for the SST k-ω Model ..... 63
4.4.2.3. Modeling the Effective Diffusivity ..... 63
4.4.2.4. Modeling the Turbulence Production ..... 64
4.4.2.4.1. Production of k ..... 64
4.4.2.4.2. Production of ω ..... 64
4.4.2.5. Modeling the Turbulence Dissipation ..... 65
4.4.2.5.1. Dissipation of k ..... 65
4.4.2.5.2. Dissipation of ω ..... 65
4.4.2.6. Cross-Diffusion Modification ..... 65
4.4.2.7. Model Constants ..... 65
4.4.3. Turbulence Damping ..... 66
4.4.4. Wall Boundary Conditions ..... 67
4.5. k-kl-ω Transition Model ..... 67
4.5.1. Overview ..... 67
4.5.2. Transport Equations for the k-kl-ω Model ..... 67
4.5.2.1. Model Constants ..... 71
4.6. Transition SST Model ..... 71
4.6.1. Overview ..... 71
4.6.2. Transport Equations for the Transition SST Model ..... 71
4.6.2.1. Separation-Induced Transition Correction ..... 74
4.6.2.2. Coupling the Transition Model and SST Transport Equations ..... 74
4.6.2.3. Transition SST and Rough Walls ..... 75
4.6.3. Mesh Requirements ..... 75
4.6.4. Specifying Inlet Turbulence Levels ..... 78
4.7. Intermittency Transition Model ..... 79
4.7.1. Overview ..... 79
4.7.2. Transport Equations for the Intermittency Transition Model ..... 80
4.7.3. Coupling with the Other Models ..... 82
4.7.4. Intermittency Transition Model and Rough Walls ..... 82
4.8. The V2F Model ..... 82
4.9. Reynolds Stress Model (RSM) ..... 83

*Release 15.0 - © SAS IP, Inc. All rights reserved. - Contains proprietary and confidential information of ANSYS, Inc. and its subsidiaries and affiliates.*

4.9.1. Overview ..... 83
4.9.2. Reynolds Stress Transport Equations ..... 83
4.9.3. Modeling Turbulent Diffusive Transport ..... 84
4.9.4. Modeling the Pressure-Strain Term ..... 85
4.9.4.1. Linear Pressure-Strain Model ..... 85
4.9.4.2. Low-Re Modifications to the Linear Pressure-Strain Model ..... 86
4.9.4.3. Quadratic Pressure-Strain Model ..... 86
4.9.4.4. Low-Re Stress-Omega Model ..... 87
4.9.5. Effects of Buoyancy on Turbulence ..... 89
4.9.6. Modeling the Turbulence Kinetic Energy ..... 89
4.9.7. Modeling the Dissipation Rate ..... 90
4.9.8. Modeling the Turbulent Viscosity ..... 90
4.9.9. Wall Boundary Conditions ..... 90
4.9.10. Convective Heat and Mass Transfer Modeling ..... 91
4.10. Scale-Adaptive Simulation (SAS) Model ..... 92
4.10.1. Overview ..... 92
4.10.2. Transport Equations for the SST-SAS Model ..... 93
4.10.3. SAS with Other ω-Based Turbulence Models ..... 94
4.11. Detached Eddy Simulation (DES) ..... 95
4.11.1. Overview ..... 95
4.11.2. DES with the Spalart-Allmaras Model ..... 95
4.11.3. DES with the Realizable k-ε Model ..... 96
4.11.4. DES with the SST k-ω Model ..... 97
4.11.5. DES with the Transition SST Model ..... 97
4.11.6. Improved Delayed Detached Eddy Simulation (IDDES) ..... 98
4.11.6.1. Overview of IDDES ..... 98
4.11.6.2. IDDES Model Formulation ..... 98
4.12. Large Eddy Simulation (LES) Model ..... 99
4.12.1. Overview ..... 99
4.12.2. Subgrid-Scale Models ..... 100
4.12.2.1. Smagorinsky-Lilly Model ..... 101
4.12.2.2. Dynamic Smagorinsky-Lilly Model ..... 101
4.12.2.3. Wall-Adapting Local Eddy-Viscosity (WALE) Model ..... 102
4.12.2.4. Algebraic Wall-Modeled LES Model (WMLES) ..... 103
4.12.2.4.1. Algebraic WMLES Model Formulation ..... 104
4.12.2.4.1.1. Reynolds Number Scaling ..... 104
4.12.2.4.2. Algebraic WMLES S-Omega Model Formulation ..... 105
4.12.2.5. Dynamic Kinetic Energy Subgrid-Scale Model ..... 106
4.12.3. Inlet Boundary Conditions for the LES Model ..... 106
4.12.3.1. Vortex Method ..... 106
4.12.3.2. Spectral Synthesizer ..... 108
4.13. Embedded Large Eddy Simulation (ELES) ..... 109
4.13.1. Overview ..... 109
4.13.2. Selecting a Model ..... 109
4.13.3. Interfaces Treatment ..... 109
4.13.3.1. RANS-LES Interface ..... 110
4.13.3.2. LES-RANS Interface ..... 110
4.13.3.3. Internal Interface Without LES Zone ..... 111
4.13.3.4. Grid Generation Guidelines ..... 111
4.14. Near-Wall Treatments for Wall-Bounded Turbulent Flows ..... 112
4.14.1. Overview ..... 112
4.14.1.1. Wall Functions vs. Near-Wall Model ..... 113


*Release 15.0 - © SAS IP, Inc. All rights reserved. - Contains proprietary and confidential information of ANSYS, Inc. and its subsidiaries and affiliates.*

4.14.1.2. Wall Functions ..... 115
4.14.2. Standard Wall Functions ..... 115
4.14.2.1. Momentum ..... 115
4.14.2.2. Energy ..... 116
4.14.2.3. Species ..... 118
4.14.2.4. Turbulence ..... 118
4.14.3. Scalable Wall Functions ..... 119
4.14.4. Non-Equilibrium Wall Functions ..... 120
4.14.4.1. Standard Wall Functions vs. Non-Equilibrium Wall Functions ..... 121
4.14.4.2. Limitations of the Wall Function Approach ..... 121
4.14.5. Enhanced Wall Treatment ε-Equation (EWT-ε) ..... 122
4.14.5.1. Two-Layer Model for Enhanced Wall Treatment ..... 122
4.14.5.2. Enhanced Wall Treatment for Momentum and Energy Equations ..... 124
4.14.6. Enhanced Wall Treatment ω-Equation (EWT-ω) ..... 127
4.14.7. User-Defined Wall Functions ..... 127
4.14.8. LES Near-Wall Treatment ..... 127
4.15. Curvature Correction for the Spalart-Allmaras and Two-Equation Models ..... 128
4.16. Production Limiters for Two-Equation Models ..... 130
**5. Heat Transfer** ..... 133
5.1. Introduction ..... 133
5.2. Modeling Conductive and Convective Heat Transfer ..... 133
5.2.1. Heat Transfer Theory ..... 133
5.2.1.1. The Energy Equation ..... 133
5.2.1.2. The Energy Equation in Moving Reference Frames ..... 134
5.2.1.3. The Energy Equation for the Non-Premixed Combustion Model ..... 134
5.2.1.4. Inclusion of Pressure Work and Kinetic Energy Terms ..... 135
5.2.1.5. Inclusion of the Viscous Dissipation Terms ..... 135
5.2.1.6. Inclusion of the Species Diffusion Term ..... 135
5.2.1.7. Energy Sources Due to Reaction ..... 136
5.2.1.8. Energy Sources Due To Radiation ..... 136
5.2.1.9. Interphase Energy Sources ..... 136
5.2.1.10. Energy Equation in Solid Regions ..... 136
5.2.1.11. Anisotropic Conductivity in Solids ..... 137
5.2.1.12. Diffusion at Inlets ..... 137
5.2.2. Natural Convection and Buoyancy-Driven Flows Theory ..... 137
5.3. Modeling Radiation ..... 138
5.3.1. Overview and Limitations ..... 138
5.3.1.1. Advantages and Limitations of the DTRM ..... 139
5.3.1.2. Advantages and Limitations of the P-1 Model ..... 139
5.3.1.3. Advantages and Limitations of the Rosseland Model ..... 140
5.3.1.4. Advantages and Limitations of the DO Model ..... 140
5.3.1.5. Advantages and Limitations of the S2S Model ..... 140
5.3.2. Radiative Transfer Equation ..... 141
5.3.3. P-1 Radiation Model Theory ..... 142
5.3.3.1. The P-1 Model Equations ..... 143
5.3.3.2. Anisotropic Scattering ..... 144
5.3.3.3. Particulate Effects in the P-1 Model ..... 144
5.3.3.4. Boundary Condition Treatment for the P-1 Model at Walls ..... 145
5.3.3.5. Boundary Condition Treatment for the P-1 Model at Flow Inlets and Exits ..... 146
5.3.4. Rosseland Radiation Model Theory ..... 146
5.3.4.1. The Rosseland Model Equations ..... 146
5.3.4.2. Anisotropic Scattering ..... 147

*Release 15.0 - © SAS IP, Inc. All rights reserved. - Contains proprietary and confidential information of ANSYS, Inc. and its subsidiaries and affiliates.*

5.3.4.3. Boundary Condition Treatment at Walls ..... 147
5.3.4.4. Boundary Condition Treatment at Flow Inlets and Exits ..... 147
5.3.5. Discrete Transfer Radiation Model (DTRM) Theory ..... 148
5.3.5.1. The DTRM Equations ..... 148
5.3.5.2. Ray Tracing ..... 148
5.3.5.3. Clustering ..... 149
5.3.5.4. Boundary Condition Treatment for the DTRM at Walls ..... 150
5.3.5.5. Boundary Condition Treatment for the DTRM at Flow Inlets and Exits ..... 150
5.3.6. Discrete Ordinates (DO) Radiation Model Theory ..... 150
5.3.6.1. The DO Model Equations ..... 151
5.3.6.2. Energy Coupling and the DO Model ..... 152
5.3.6.2.1. Limitations of DO/Energy Coupling ..... 153
5.3.6.3. Angular Discretization and Pixelation ..... 153
5.3.6.4. Anisotropic Scattering ..... 156
5.3.6.5. Particulate Effects in the DO Model ..... 157
5.3.6.6. Boundary and Cell Zone Condition Treatment at Opaque Walls ..... 157
5.3.6.6.1. Gray Diffuse Walls ..... 159
5.3.6.6.2. Non-Gray Diffuse Walls ..... 159
5.3.6.7. Cell Zone and Boundary Condition Treatment at Semi-Transparent Walls ..... 160
5.3.6.7.1. Semi-Transparent Interior Walls ..... 160
5.3.6.7.2. Specular Semi-Transparent Walls ..... 161
5.3.6.7.3. Diffuse Semi-Transparent Walls ..... 163
5.3.6.7.4. Partially Diffuse Semi-Transparent Walls ..... 164
5.3.6.7.5. Semi-Transparent Exterior Walls ..... 164
5.3.6.7.6. Limitations ..... 166
5.3.6.7.7. Solid Semi-Transparent Media ..... 167
5.3.6.8. Boundary Condition Treatment at Specular Walls and Symmetry Boundaries ..... 167
5.3.6.9. Boundary Condition Treatment at Periodic Boundaries ..... 167
5.3.6.10. Boundary Condition Treatment at Flow Inlets and Exits ..... 167
5.3.7. Surface-to-Surface (S2S) Radiation Model Theory ..... 167
5.3.7.1. Gray-Diffuse Radiation ..... 167
5.3.7.2. The S2S Model Equations ..... 168
5.3.7.3. Clustering ..... 169
5.3.7.3.1. Clustering and View Factors ..... 169
5.3.7.3.2. Clustering and Radiosity ..... 169
5.3.8. Radiation in Combusting Flows ..... 170
5.3.8.1. The Weighted-Sum-of-Gray-Gases Model ..... 170
5.3.8.1.1. When the Total (Static) Gas Pressure is Not Equal to 1 atm ..... 171
5.3.8.2. The Effect of Soot on the Absorption Coefficient ..... 172
5.3.8.3. The Effect of Particles on the Absorption Coefficient ..... 172
5.3.9. Choosing a Radiation Model ..... 172
5.3.9.1. External Radiation ..... 173
**6. Heat Exchangers** ..... 175
6.1. The Macro Heat Exchanger Models ..... 175
6.1.1. Overview of the Macro Heat Exchanger Models ..... 175
6.1.2. Restrictions of the Macro Heat Exchanger Models ..... 176
6.1.3. Macro Heat Exchanger Model Theory ..... 177
6.1.3.1. Streamwise Pressure Drop ..... 178
6.1.3.2. Heat Transfer Effectiveness ..... 179
6.1.3.3. Heat Rejection ..... 180
6.1.3.4. Macro Heat Exchanger Group Connectivity ..... 182
6.2. The Dual Cell Model ..... 183


*Release 15.0 - © SAS IP, Inc. All rights reserved. - Contains proprietary and confidential information of ANSYS, Inc. and its subsidiaries and affiliates.*

6.2.1. Overview of the Dual Cell Model ..... 183
6.2.2. Restrictions of the Dual Cell Model ..... 183
6.2.3. Dual Cell Model Theory ..... 183
6.2.3.1. NTU Relations ..... 184
6.2.3.2. Heat Rejection ..... 184
**7. Species Transport and Finite-Rate Chemistry** ..... 187
7.1. Volumetric Reactions ..... 187
7.1.1. Species Transport Equations ..... 187
7.1.1.1. Mass Diffusion in Laminar Flows ..... 188
7.1.1.2. Mass Diffusion in Turbulent Flows ..... 188
7.1.1.3. Treatment of Species Transport in the Energy Equation ..... 188
7.1.1.4. Diffusion at Inlets ..... 189
7.1.2. The Generalized Finite-Rate Formulation for Reaction Modeling ..... 189
7.1.2.1. The Laminar Finite-Rate Model ..... 189
7.1.2.2. Pressure-Dependent Reactions ..... 192
7.1.2.3. The Eddy-Dissipation Model ..... 193
7.1.2.4. The Eddy-Dissipation Model for LES ..... 194
7.1.2.5. The Eddy-Dissipation-Concept (EDC) Model ..... 195
7.1.2.6. The Thickened Flame Model ..... 196
7.1.2.7. The Relaxation to Chemical Equilibrium Model ..... 198
7.2. Wall Surface Reactions and Chemical Vapor Deposition ..... 199
7.2.1. Surface Coverage Reaction Rate Modification ..... 201
7.2.2. Reaction-Diffusion Balance for Surface Chemistry ..... 201
7.2.3. Slip Boundary Formulation for Low-Pressure Gas Systems ..... 202
7.3. Particle Surface Reactions ..... 204
7.3.1. General Description ..... 204
7.3.2. ANSYS Fluent Model Formulation ..... 205
7.3.3. Extension for Stoichiometries with Multiple Gas Phase Reactants ..... 206
7.3.4. Solid-Solid Reactions ..... 207
7.3.5. Solid Decomposition Reactions ..... 207
7.3.6. Solid Deposition Reactions ..... 207
7.3.7. Gaseous Solid Catalyzed Reactions on the Particle Surface ..... 208
7.4. Reacting Channel Model ..... 208
7.4.1. Overview and Limitations ..... 208
7.4.2. Reacting Channel Model Theory ..... 208
7.4.2.1. Flow Inside the Reacting Channel ..... 209
7.4.2.2. Surface Reactions in the Reacting Channel ..... 210
7.4.2.3. Porous Medium Inside Reacting Channel ..... 211
7.4.2.4. Outer Flow in the Shell ..... 211
7.5. Reactor Network Model ..... 212
7.5.1. Reactor Network Model Theory ..... 212
7.5.1.1. Reactor network temperature solution ..... 213
**8. Non-Premixed Combustion** ..... 215
8.1. Introduction ..... 215
8.2. Non-Premixed Combustion and Mixture Fraction Theory ..... 215
8.2.1. Mixture Fraction Theory ..... 216
8.2.1.1. Definition of the Mixture Fraction ..... 216
8.2.1.2. Transport Equations for the Mixture Fraction ..... 218
8.2.1.3. The Non-Premixed Model for LES ..... 219
8.2.1.4. Mixture Fraction vs. Equivalence Ratio ..... 219
8.2.1.5. Relationship of Mixture Fraction to Species Mass Fraction, Density, and Temperature ..... 220
8.2.2. Modeling of Turbulence-Chemistry Interaction ..... 221

*Release 15.0 - © SAS IP, Inc. All rights reserved. - Contains proprietary and confidential information of ANSYS, Inc. and its subsidiaries and affiliates.*

8.2.2.1. Description of the Probability Density Function ..... 221
8.2.2.2. Derivation of Mean Scalar Values from the Instantaneous Mixture Fraction ..... 222
8.2.2.3. The Assumed-Shape PDF ..... 222
8.2.2.3.1. The Double Delta Function PDF ..... 223
8.2.2.3.2. The β-Function PDF ..... 223
8.2.3. Non-Adiabatic Extensions of the Non-Premixed Model ..... 224
8.2.4. Chemistry Tabulation ..... 227
8.2.4.1. Look-Up Tables for Adiabatic Systems ..... 227
8.2.4.2. 3D Look-Up Tables for Non-Adiabatic Systems ..... 228
8.2.4.3. Generating Lookup Tables Through Automated Grid Refinement ..... 230
8.3. Restrictions and Special Cases for Using the Non-Premixed Model ..... 232
8.3.1. Restrictions on the Mixture Fraction Approach ..... 232
8.3.2. Using the Non-Premixed Model for Liquid Fuel or Coal Combustion ..... 235
8.3.3. Using the Non-Premixed Model with Flue Gas Recycle ..... 236
8.3.4. Using the Non-Premixed Model with the Inert Model ..... 237
8.3.4.1. Mixture Composition ..... 237
8.3.4.1.1. Property Evaluation ..... 238
8.4. The Diffusion Flamelet Models Theory ..... 238
8.4.1. Restrictions and Assumptions ..... 238
8.4.2. The Flamelet Concept ..... 239
8.4.2.1. Overview ..... 239
8.4.2.2. Strain Rate and Scalar Dissipation ..... 240
8.4.2.3. Embedding Diffusion Flamelets in Turbulent Flames ..... 241
8.4.3. Flamelet Generation ..... 242
8.4.4. Flamelet Import ..... 242
8.5. The Steady Diffusion Flamelet Model Theory ..... 244
8.5.1. Overview ..... 244
8.5.2. Multiple Steady Flamelet Libraries ..... 245
8.5.3. Steady Diffusion Flamelet Automated Grid Refinement ..... 245
8.5.4. Non-Adiabatic Steady Diffusion Flamelets ..... 246
8.6. The Unsteady Diffusion Flamelet Model Theory ..... 246
8.6.1. The Eulerian Unsteady Laminar Flamelet Model ..... 247
8.6.1.1. Liquid Reactions ..... 249
8.6.2. The Diesel Unsteady Laminar Flamelet Model ..... 249
8.6.3. Multiple Diesel Unsteady Flamelets ..... 250
8.6.4. Multiple Diesel Unsteady Flamelets with Flamelet Reset ..... 251
8.6.4.1. Resetting the Flamelets ..... 251
**9. Premixed Combustion** ..... 253
9.1. Overview and Limitations ..... 253
9.1.1. Overview ..... 253
9.1.2. Limitations ..... 254
9.2. C-Equation Model Theory ..... 254
9.2.1. Propagation of the Flame Front ..... 254
9.3. G-Equation Model Theory ..... 255
9.3.1. Numerical Solution of the G-equation ..... 257
9.4. Turbulent Flame Speed Models ..... 257
9.4.1. Zimont Turbulent Flame Speed Closure Model ..... 257
9.4.1.1. Zimont Turbulent Flame Speed Closure for LES ..... 259
9.4.1.2. Flame Stretch Effect ..... 259
9.4.1.3. Gradient Diffusion ..... 260
9.4.1.4. Wall Damping ..... 260
9.4.2. Peters Flame Speed Model ..... 260


*Release 15.0 - © SAS IP, Inc. All rights reserved. - Contains proprietary and confidential information of ANSYS, Inc. and its subsidiaries and affiliates.*

9.4.2.1. Peters Flame Speed Model for LES ..... 262
9.5. Extended Coherent Flamelet Model Theory ..... 262
9.5.1. Closure for ECFM Source Terms ..... 264
9.5.2. Turbulent Flame Speed in ECFM ..... 267
9.5.3. LES and ECFM ..... 267
9.6. Calculation of Properties ..... 269
9.6.1. Calculation of Temperature ..... 270
9.6.1.1. Adiabatic Temperature Calculation ..... 270
9.6.1.2. Non-Adiabatic Temperature Calculation ..... 270
9.6.2. Calculation of Density ..... 270
9.6.3. Laminar Flame Speed ..... 271
9.6.4. Unburnt Density and Thermal Diffusivity ..... 271
**10. Partially Premixed Combustion** ..... 273
10.1. Overview ..... 273
10.2. Limitations ..... 273
10.3. Partially Premixed Combustion Theory ..... 274
10.3.1. Chemical Equilibrium and Steady Diffusion Flamelet Models ..... 274
10.3.2. Flamelet Generated Manifold (FGM) model ..... 275
10.3.2.1. Premixed FGMs ..... 275
10.3.2.2. Diffusion FGMs ..... 277
10.3.3. FGM Turbulent Closure ..... 278
10.3.4. Calculation of Unburnt Properties ..... 279
10.3.5. Laminar Flame Speed ..... 279
**11. Composition PDF Transport** ..... 281
11.1. Overview and Limitations ..... 281
11.2. Composition PDF Transport Theory ..... 281
11.3. The Lagrangian Solution Method ..... 282
11.3.1. Particle Convection ..... 283
11.3.2. Particle Mixing ..... 284
11.3.2.1. The Modified Curl Model ..... 284
11.3.2.2. The IEM Model ..... 285
11.3.2.3. The EMST Model ..... 285
11.3.2.4. Liquid Reactions ..... 285
11.3.3. Particle Reaction ..... 285
11.4. The Eulerian Solution Method ..... 286
11.4.1. Reaction ..... 287
11.4.2. Mixing ..... 287
11.4.3. Correction ..... 288
11.4.4. Calculation of Composition Mean and Variance ..... 288
**12. Chemistry Acceleration** ..... 289
12.1. Overview and Limitations ..... 289
12.2. In-Situ Adaptive Tabulation (ISAT) ..... 289
12.3. Dynamic Mechanism Reduction ..... 291
12.3.1. Directed Relation Graph (DRG) Method for Mechanism Reduction ..... 292
12.4. Chemistry Agglomeration ..... 293
12.4.1. Binning Algorithm ..... 295
12.5. Chemical Mechanism Dimension Reduction ..... 296
12.5.1. Selecting the Represented Species ..... 297
**13. Engine Ignition** ..... 299
13.1. Spark Model ..... 299
13.1.1. Overview and Limitations ..... 299
13.1.2. Spark Model Theory ..... 299

*Release 15.0 - © SAS IP, Inc. All rights reserved. - Contains proprietary and confidential information of ANSYS, Inc. and its subsidiaries and affiliates.*

13.1.3. ECFM Spark Model Variants ..... 302
13.2. Autoignition Models ..... 303
13.2.1. Model Overview ..... 303
13.2.2. Model Limitations ..... 304
13.2.3. Ignition Model Theory ..... 304
13.2.3.1. Transport of Ignition Species ..... 304
13.2.3.2. Knock Modeling ..... 305
13.2.3.2.1. Modeling of the Source Term ..... 305
13.2.3.2.2. Correlations ..... 305
13.2.3.2.3. Energy Release ..... 306
13.2.3.3. Ignition Delay Modeling ..... 306
13.2.3.3.1. Modeling of the Source Term ..... 306
13.2.3.3.2. Correlations ..... 307
13.2.3.3.3. Energy Release ..... 308
13.3. Crevice Model ..... 308
13.3.1. Overview ..... 308
13.3.1.1. Model Parameters ..... 309
13.3.2. Limitations ..... 310
13.3.3. Crevice Model Theory ..... 310
**14. Pollutant Formation** ..... 313
14.1. NOx Formation ..... 313
14.1.1. Overview ..... 313
14.1.1.1. NOx Modeling in ANSYS Fluent ..... 313
14.1.1.2. NOx Formation and Reduction in Flames ..... 314
14.1.2. Governing Equations for NOx Transport ..... 314
14.1.3. Thermal NOx Formation ..... 315
14.1.3.1. Thermal NOx Reaction Rates ..... 315
14.1.3.2. The Quasi-Steady Assumption for [N] ..... 316
14.1.3.3. Thermal NOx Temperature Sensitivity ..... 316
14.1.3.4. Decoupled Thermal NOx Calculations ..... 316
14.1.3.5. Approaches for Determining O Radical Concentration ..... 316
14.1.3.5.1. Method 1: Equilibrium Approach ..... 317
14.1.3.5.2. Method 2: Partial Equilibrium Approach ..... 317
14.1.3.5.3. Method 3: Predicted O Approach ..... 317
14.1.3.6. Approaches for Determining OH Radical Concentration ..... 317
14.1.3.6.1. Method 1: Exclusion of OH Approach ..... 318
14.1.3.6.2. Method 2: Partial Equilibrium Approach ..... 318
14.1.3.6.3. Method 3: Predicted OH Approach ..... 318
14.1.3.7. Summary ..... 318
14.1.4. Prompt NOx Formation ..... 318
14.1.4.1. Prompt NOx Combustion Environments ..... 318
14.1.4.2. Prompt NOx Mechanism ..... 319
14.1.4.3. Prompt NOx Formation Factors ..... 319
14.1.4.4. Primary Reaction ..... 319
14.1.4.5. Modeling Strategy ..... 319
14.1.4.6. Rate for Most Hydrocarbon Fuels ..... 320
14.1.4.7. Oxygen Reaction Order ..... 321
14.1.5. Fuel NOx Formation ..... 321
14.1.5.1. Fuel-Bound Nitrogen ..... 321
14.1.5.2. Reaction Pathways ..... 321
14.1.5.3. Fuel NOx from Gaseous and Liquid Fuels ..... 322
14.1.5.3.1. Fuel NOx from Intermediate Hydrogen Cyanide (HCN) ..... 322


*Release 15.0 - © SAS IP, Inc. All rights reserved. - Contains proprietary and confidential information of ANSYS, Inc. and its subsidiaries and affiliates.*

14.1.5.3.1.1. HCN Production in a Gaseous Fuel ..... 323
14.1.5.3.1.2. HCN Production in a Liquid Fuel ..... 323
14.1.5.3.1.3. HCN Consumption ..... 323
14.1.5.3.1.4. HCN Sources in the Transport Equation ..... 324
14.1.5.3.1.5. NOx Sources in the Transport Equation ..... 324
14.1.5.3.2. Fuel NOx from Intermediate Ammonia (NH3) ..... 324
14.1.5.3.2.1. NH3 Production in a Gaseous Fuel ..... 325
14.1.5.3.2.2. NH3 Production in a Liquid Fuel ..... 325
14.1.5.3.2.3. NH3 Consumption ..... 326
14.1.5.3.2.4. NH3 Sources in the Transport Equation ..... 326
14.1.5.3.2.5. NOx Sources in the Transport Equation ..... 326
14.1.5.3.3. Fuel NOx from Coal ..... 327
14.1.5.3.3.1. Nitrogen in Char and in Volatiles ..... 327
14.1.5.3.3.2. Coal Fuel NOx Scheme A ..... 327
14.1.5.3.3.3. Coal Fuel NOx Scheme B ..... 328
14.1.5.3.3.4. HCN Scheme Selection ..... 328
14.1.5.3.3.5. NOx Reduction on Char Surface ..... 328
14.1.5.3.3.5.1. BET Surface Area ..... 329
14.1.5.3.3.5.2. HCN from Volatiles ..... 329
14.1.5.3.3.6. Coal Fuel NOx Scheme C ..... 330
14.1.5.3.3.7. Coal Fuel NOx Scheme D ..... 330
14.1.5.3.3.8. NH3 Scheme Selection ..... 331
14.1.5.3.3.8.1. NH3 from Volatiles ..... 331
14.1.5.3.4. Fuel Nitrogen Partitioning for HCN and NH3 Intermediates ..... 331
14.1.6. NOx Formation from Intermediate N2O ..... 332
14.1.6.1. N2O - Intermediate NOx Mechanism ..... 332
14.1.7. NOx Reduction by Reburning ..... 333
14.1.7.1. Instantaneous Approach ..... 333
14.1.7.2. Partial Equilibrium Approach ..... 334
14.1.7.2.1. NOx Reduction Mechanism ..... 335
14.1.8. NOx Reduction by SNCR ..... 336
14.1.8.1. Ammonia Injection ..... 337
14.1.8.2. Urea Injection ..... 338
14.1.8.3. Transport Equations for Urea, HNCO, and NCO ..... 339
14.1.8.4. Urea Production due to Reagent Injection ..... 340
14.1.8.5. NH3 Production due to Reagent Injection ..... 340
14.1.8.6. HNCO Production due to Reagent Injection ..... 340
14.1.9. NOx Formation in Turbulent Flows ..... 341
14.1.9.1. The Turbulence-Chemistry Interaction Model ..... 341
14.1.9.2. The PDF Approach ..... 342
14.1.9.3. The General Expression for the Mean Reaction Rate ..... 342
14.1.9.4. The Mean Reaction Rate Used in ANSYS Fluent ..... 342
14.1.9.5. Statistical Independence ..... 342
14.1.9.6. The Beta PDF Option ..... 343
14.1.9.7. The Gaussian PDF Option ..... 343
14.1.9.8. The Calculation Method for the Variance ..... 343
14.2. SOx Formation ..... 344
14.2.1. Overview ..... 344
14.2.1.1. The Formation of SOx ..... 345
14.2.2. Governing Equations for SOx Transport ..... 345
14.2.3. Reaction Mechanisms for Sulfur Oxidation ..... 346
14.2.4. SO2 and H2S Production in a Gaseous Fuel ..... 348

*Release 15.0 - © SAS IP, Inc. All rights reserved. - Contains proprietary and confidential information of ANSYS, Inc. and its subsidiaries and affiliates.*

14.2.5. SO2 and H2S Production in a Liquid Fuel ..... 348
14.2.6. SO2 and H2S Production from Coal ..... 348
14.2.6.1. SO2 and H2S from Char ..... 348
14.2.6.2. SO2 and H2S from Volatiles ..... 349
14.2.7. SOx Formation in Turbulent Flows ..... 349
14.2.7.1. The Turbulence-Chemistry Interaction Model ..... 349
14.2.7.2. The PDF Approach ..... 349
14.2.7.3. The Mean Reaction Rate ..... 350
14.2.7.4. The PDF Options ..... 350
14.3. Soot Formation ..... 350
14.3.1. Overview and Limitations ..... 350
14.3.1.1. Predicting Soot Formation ..... 350
14.3.1.2. Restrictions on Soot Modeling ..... 351
14.3.2. Soot Model Theory ..... 351
14.3.2.1. The One-Step Soot Formation Model ..... 351
14.3.2.2. The Two-Step Soot Formation Model ..... 352
14.3.2.2.1. Soot Generation Rate ..... 353
14.3.2.2.2. Nuclei Generation Rate ..... 353
14.3.2.3. The Moss-Brookes Model ..... 354
14.3.2.3.1. The Moss-Brookes-Hall Model ..... 356
14.3.2.3.2. Soot Formation in Turbulent Flows ..... 357
14.3.2.3.2.1. The Turbulence-Chemistry Interaction Model ..... 358
14.3.2.3.2.2. The PDF Approach ..... 358
14.3.2.3.2.3. The Mean Reaction Rate ..... 358
14.3.2.3.2.4. The PDF Options ..... 358
14.3.2.3.3. The Effect of Soot on the Radiation Absorption Coefficient ..... 358
14.4. Decoupled Detailed Chemistry Model ..... 358
14.4.1. Overview ..... 358
14.4.1.1. Limitations ..... 359
14.4.2. Decoupled Detailed Chemistry Model Theory ..... 359
**15. Aerodynamically Generated Noise** ..... 361
15.1. Overview ..... 361
15.1.1. Direct Method ..... 361
15.1.2. Integral Method Based on Acoustic Analogy ..... 362
15.1.3. Broadband Noise Source Models ..... 363
15.2. Acoustics Model Theory ..... 363
15.2.1. The Ffowcs-Williams and Hawkings Model ..... 363
15.2.2. Broadband Noise Source Models ..... 366
15.2.2.1. Proudman's Formula ..... 366
15.2.2.2. The Jet Noise Source Model ..... 367
15.2.2.3. The Boundary Layer Noise Source Model ..... 369
15.2.2.4. Source Terms in the Linearized Euler Equations ..... 369
15.2.2.5. Source Terms in Lilley's Equation ..... 370
**16. Discrete Phase** ..... 373
16.1. Introduction ..... 373
16.1.1. The Euler-Lagrange Approach ..... 373
16.2. Particle Motion Theory ..... 374
16.2.1. Equations of Motion for Particles ..... 374
16.2.1.1. Particle Force Balance ..... 374
16.2.1.2. Inclusion of the Gravity Term ..... 374
16.2.1.3. Other Forces ..... 374
16.2.1.4. Forces in Moving Reference Frames ..... 375


*Release 15.0 - © SAS IP, Inc. All rights reserved. - Contains proprietary and confidential information of ANSYS, Inc. and its subsidiaries and affiliates.*

16.2.1.5. Thermophoretic Force ..... 375
16.2.1.6. Brownian Force ..... 376
16.2.1.7. Saffman's Lift Force ..... 376
16.2.2. Turbulent Dispersion of Particles ..... 377
16.2.2.1. Stochastic Tracking ..... 377
16.2.2.1.1. The Integral Time ..... 377
16.2.2.1.2. The Discrete Random Walk Model ..... 378
16.2.2.1.3. Using the DRW Model ..... 379
16.2.2.2. Particle Cloud Tracking ..... 379
16.2.2.2.1. Using the Cloud Model ..... 382
16.2.3. Integration of Particle Equation of Motion ..... 382
16.3. Laws for Drag Coefficients ..... 385
16.3.1. Spherical Drag Law ..... 385
16.3.2. Non-spherical Drag Law ..... 385
16.3.3. Stokes-Cunningham Drag Law ..... 386
16.3.4. High-Mach-Number Drag Law ..... 386
16.3.5. Dynamic Drag Model Theory ..... 386
16.3.6. Dense Discrete Phase Model Drag Laws ..... 387
16.4. Laws for Heat and Mass Exchange ..... 387
16.4.1. Inert Heating or Cooling (Law 1/Law 6) ..... 388
16.4.2. Droplet Vaporization (Law 2) ..... 390
16.4.2.1. Mass Transfer During Law 2—Diffusion Controlled Model ..... 390
16.4.2.2. Mass Transfer During Law 2—Convection/Diffusion Controlled Model ..... 391
16.4.2.3. Defining the Saturation Vapor Pressure and Diffusion Coefficient (or Binary Diffusivity) ..... 392
16.4.2.4. Defining the Boiling Point and Latent Heat ..... 393
16.4.2.5. Heat Transfer to the Droplet ..... 393
16.4.3. Droplet Boiling (Law 3) ..... 394
16.4.4. Devolatilization (Law 4) ..... 396
16.4.4.1. Choosing the Devolatilization Model ..... 396
16.4.4.2. The Constant Rate Devolatilization Model ..... 396
16.4.4.3. The Single Kinetic Rate Model ..... 397
16.4.4.4. The Two Competing Rates (Kobayashi) Model ..... 398
16.4.4.5. The CPD Model ..... 398
16.4.4.5.1. General Description ..... 398
16.4.4.5.2. Reaction Rates ..... 399
16.4.4.5.3. Mass Conservation ..... 400
16.4.4.5.4. Fractional Change in the Coal Mass ..... 400
16.4.4.5.5. CPD Inputs ..... 401
16.4.4.5.6. Particle Swelling During Devolatilization ..... 403
16.4.4.5.7. Heat Transfer to the Particle During Devolatilization ..... 403
16.4.5. Surface Combustion (Law 5) ..... 404
16.4.5.1. The Diffusion-Limited Surface Reaction Rate Model ..... 404
16.4.5.2. The Kinetic/Diffusion Surface Reaction Rate Model ..... 405
16.4.5.3. The Intrinsic Model ..... 405
16.4.5.4. The Multiple Surface Reactions Model ..... 407
16.4.5.4.1. Limitations ..... 407
16.4.5.5. Heat and Mass Transfer During Char Combustion ..... 408
16.4.6. Multicomponent Particle Definition (Law 7) ..... 408
16.4.6.1. Raoult's Law ..... 410
16.4.6.2. Peng-Robinson Real Gas Model ..... 410
16.5. Vapor Liquid Equilibrium Theory ..... 410

*Release 15.0 - © SAS IP, Inc. All rights reserved. - Contains proprietary and confidential information of ANSYS, Inc. and its subsidiaries and affiliates.*

16.6. Wall-Jet Model Theory ..... 412
16.7. Wall-Film Model Theory ..... 413
16.7.1. Introduction ..... 414
16.7.2. Interaction During Impact with a Boundary ..... 415
16.7.3. Splashing ..... 416
16.7.4. Separation Criteria ..... 419
16.7.5. Conservation Equations for Wall-Film Particles ..... 419
16.7.5.1. Momentum ..... 419
16.7.5.2. Mass Transfer from the Film ..... 421
16.7.5.3. Energy Transfer from the Film ..... 422
16.8. Particle Erosion and Accretion Theory ..... 424
16.9. Atomizer Model Theory ..... 425
16.9.1. The Plain-Orifice Atomizer Model ..... 426
16.9.1.1. Internal Nozzle State ..... 428
16.9.1.2. Coefficient of Discharge ..... 429
16.9.1.3. Exit Velocity ..... 430
16.9.1.4. Spray Angle ..... 430
16.9.1.5. Droplet Diameter Distribution ..... 431
16.9.2. The Pressure-Swirl Atomizer Model ..... 432
16.9.2.1. Film Formation ..... 433
16.9.2.2. Sheet Breakup and Atomization ..... 434
16.9.3. The Air-Blast/Air-Assist Atomizer Model ..... 436
16.9.4. The Flat-Fan Atomizer Model ..... 437
16.9.5. The Effervescent Atomizer Model ..... 438
16.10. Secondary Breakup Model Theory ..... 439
16.10.1. Taylor Analogy Breakup (TAB) Model ..... 440
16.10.1.1. Introduction ..... 440
16.10.1.2. Use and Limitations ..... 440
16.10.1.3. Droplet Distortion ..... 440
16.10.1.4. Size of Child Droplets ..... 442
16.10.1.5. Velocity of Child Droplets ..... 442
16.10.1.6. Droplet Breakup ..... 442
16.10.2. Wave Breakup Model ..... 444
16.10.2.1. Introduction ..... 444
16.10.2.2. Use and Limitations ..... 444
16.10.2.3. Jet Stability Analysis ..... 444
16.10.2.4. Droplet Breakup ..... 446
16.10.3. KHRT Breakup Model ..... 447
16.10.3.1. Introduction ..... 447
16.10.3.2. Use and Limitations ..... 447
16.10.3.3. Liquid Core Length ..... 447
16.10.3.4. Rayleigh-Taylor Breakup ..... 448
16.10.3.5. Droplet Breakup Within the Liquid Core ..... 449
16.10.3.6. Droplet Breakup Outside the Liquid Core ..... 449
16.10.4. Stochastic Secondary Droplet (SSD) Model ..... 449
16.10.4.1. Theory ..... 449
16.11. Collision and Droplet Coalescence Model Theory ..... 450
16.11.1. Introduction ..... 450
16.11.2. Use and Limitations ..... 451
16.11.3. Theory ..... 451
16.11.3.1. Probability of Collision ..... 451
16.11.3.2. Collision Outcomes ..... 452


*Release 15.0 - © SAS IP, Inc. All rights reserved. - Contains proprietary and confidential information of ANSYS, Inc. and its subsidiaries and affiliates.*

16.12. Discrete Element Method Collision Model ..... 453
16.12.1. Theory ..... 453
16.12.1.1. The Spring Collision Law ..... 455
16.12.1.2. The Spring-Dashpot Collision Law ..... 455
16.12.1.3. The Friction Collision Law ..... 456
16.12.1.4. DEM Parcels ..... 457
16.12.1.5. Cartesian Collision Mesh ..... 457
16.13. One-Way and Two-Way Coupling ..... 458
16.13.1. Coupling Between the Discrete and Continuous Phases ..... 459
16.13.2. Momentum Exchange ..... 459
16.13.3. Heat Exchange ..... 460
16.13.4. Mass Exchange ..... 461
16.13.5. Under-Relaxation of the Interphase Exchange Terms ..... 461
16.13.6. Interphase Exchange During Stochastic Tracking ..... 462
16.13.7. Interphase Exchange During Cloud Tracking ..... 463
16.14. Node Based Averaging ..... 463
**17. Multiphase Flows** ..... 465
17.1. Introduction ..... 465
17.1.1. Multiphase Flow Regimes ..... 465
17.1.1.1. Gas-Liquid or Liquid-Liquid Flows ..... 465
17.1.1.2. Gas-Solid Flows ..... 466
17.1.1.3. Liquid-Solid Flows ..... 466
17.1.1.4. Three-Phase Flows ..... 466
17.1.2. Examples of Multiphase Systems ..... 467
17.2. Choosing a General Multiphase Model ..... 468
17.2.1. Approaches to Multiphase Modeling ..... 468
17.2.1.1. The Euler-Euler Approach ..... 468
17.2.1.1.1. The VOF Model ..... 468
17.2.1.1.2. The Mixture Model ..... 469
17.2.1.1.3. The Eulerian Model ..... 469
17.2.2. Model Comparisons ..... 469
17.2.2.1. Detailed Guidelines ..... 470
17.2.2.1.1. The Effect of Particulate Loading ..... 470
17.2.2.1.2. The Significance of the Stokes Number ..... 471
17.2.2.1.2.1. Examples ..... 472
17.2.2.1.3. Other Considerations ..... 472
17.2.3. Time Schemes in Multiphase Flow ..... 472
17.2.4. Stability and Convergence ..... 473
17.3. Volume of Fluid (VOF) Model Theory ..... 474
17.3.1. Overview of the VOF Model ..... 474
17.3.2. Limitations of the VOF Model ..... 474
17.3.3. Steady-State and Transient VOF Calculations ..... 475
17.3.4. Volume Fraction Equation ..... 475
17.3.4.1. The Implicit Scheme ..... 476
17.3.4.2. The Explicit Scheme ..... 476
17.3.4.3. Interpolation Near the Interface ..... 477
17.3.4.3.1. The Geometric Reconstruction Scheme ..... 478
17.3.4.3.2. The Donor-Acceptor Scheme ..... 478
17.3.4.3.3. The Compressive Interface Capturing Scheme for Arbitrary Meshes (CICSAM) ..... 479
17.3.4.3.4. The Compressive and Zonal Discretization Schemes ..... 479
17.3.4.3.5. Bounded Gradient Maximization (BGM) ..... 480
17.3.5. Material Properties ..... 480

*Release 15.0 - © SAS IP, Inc. All rights reserved. - Contains proprietary and confidential information of ANSYS, Inc. and its subsidiaries and affiliates.*

17.3.6. Momentum Equation ..... 480
17.3.7. Energy Equation ..... 481
17.3.8. Additional Scalar Equations ..... 481
17.3.9. Time Dependence ..... 481
17.3.10. Surface Tension and Adhesion ..... 481
17.3.10.1. Surface Tension ..... 482
17.3.10.1.1. The Continuum Surface Force Model ..... 482
17.3.10.1.2. The Continuum Surface Stress Model ..... 483
17.3.10.1.3. Comparing the CSS and CSF Methods ..... 484
17.3.10.1.4. When Surface Tension Effects Are Important ..... 484
17.3.10.2. Wall Adhesion ..... 484
17.3.10.3. Jump Adhesion ..... 485
17.3.11. Open Channel Flow ..... 485
17.3.11.1. Upstream Boundary Conditions ..... 486
17.3.11.1.1. Pressure Inlet ..... 486
17.3.11.1.2. Mass Flow Rate ..... 487
17.3.11.1.3. Volume Fraction Specification ..... 487
17.3.11.2. Downstream Boundary Conditions ..... 487
17.3.11.2.1. Pressure Outlet ..... 487
17.3.11.2.2. Outflow Boundary ..... 487
17.3.11.2.3. Backflow Volume Fraction Specification ..... 488
17.3.11.3. Numerical Beach Treatment ..... 488
17.3.12. Open Channel Wave Boundary Conditions ..... 489
17.3.12.1. Airy Wave Theory ..... 490
17.3.12.2. Stokes Wave Theories ..... 491
17.3.12.3. Cnoidal/Solitary Wave Theory ..... 492
17.3.12.4. Nomenclature for Open Channel Waves ..... 494
17.3.12.5. Choosing a Wave Theory ..... 495
17.3.12.6. Superposition of Waves ..... 497
17.3.13. Coupled Level-Set and VOF Model ..... 498
17.3.13.1. Theory ..... 498
17.3.13.1.1. Re-initialization of the Level-set Function via the Geometrical Method ..... 499
17.3.13.2. Limitations ..... 500
17.4. Mixture Model Theory ..... 500
17.4.1. Overview ..... 501
17.4.2. Limitations ..... 501
17.4.3. Continuity Equation ..... 502
17.4.4. Momentum Equation ..... 502
17.4.5. Energy Equation ..... 503
17.4.6. Relative (Slip) Velocity and the Drift Velocity ..... 503
17.4.7. Volume Fraction Equation for the Secondary Phases ..... 505
17.4.8. Granular Properties ..... 505
17.4.8.1. Collisional Viscosity ..... 505
17.4.8.2. Kinetic Viscosity ..... 505
17.4.9. Granular Temperature ..... 506
17.4.10. Solids Pressure ..... 507
17.4.11. Interfacial Area Concentration ..... 507
17.4.11.1. Hibiki-Ishii Model ..... 508
17.4.11.2. Ishii-Kim Model ..... 509
17.4.11.3. Yao-Morel Model ..... 510
17.5. Eulerian Model Theory ..... 511
17.5.1. Overview of the Eulerian Model ..... 512


*Release 15.0 - © SAS IP, Inc. All rights reserved. - Contains proprietary and confidential information of ANSYS, Inc. and its subsidiaries and affiliates.*

17.5.2. Limitations of the Eulerian Model ..... 512
17.5.3. Volume Fraction Equation ..... 513
17.5.4. Conservation Equations ..... 513
17.5.4.1. Equations in General Form ..... 514
17.5.4.1.1. Conservation of Mass ..... 514
17.5.4.1.2. Conservation of Momentum ..... 514
17.5.4.1.3. Conservation of Energy ..... 515
17.5.4.2. Equations Solved by ANSYS Fluent ..... 515
17.5.4.2.1. Continuity Equation ..... 515
17.5.4.2.2. Fluid-Fluid Momentum Equations ..... 516
17.5.4.2.3. Fluid-Solid Momentum Equations ..... 516
17.5.4.2.4. Conservation of Energy ..... 516
17.5.5. Interfacial Area Concentration ..... 517
17.5.6. Interphase Exchange Coefficients ..... 518
17.5.6.1. Fluid-Fluid Exchange Coefficient ..... 518
17.5.6.1.1. Schiller and Naumann Model ..... 518
17.5.6.1.2. Morsi and Alexander Model ..... 519
17.5.6.1.3. Symmetric Model ..... 520
17.5.6.1.4. Grace et al. Model ..... 520
17.5.6.1.5. Tomiyama et al. Model ..... 521
17.5.6.1.6. Ishii Model ..... 522
17.5.6.1.7. Universal Drag Laws for Bubble-Liquid and Droplet-Gas Flows ..... 522
17.5.6.1.7.1. Bubble-Liquid Flow ..... 523
17.5.6.1.7.2. Droplet-Gas Flow ..... 524
17.5.6.2. Fluid-Solid Exchange Coefficient ..... 524
17.5.6.3. Solid-Solid Exchange Coefficient ..... 527
17.5.6.4. Drag Modification ..... 528
17.5.6.4.1. Brucato Correlation ..... 528
17.5.7. Lift Force ..... 528
17.5.7.1. Lift Coefficient Models ..... 529
17.5.7.1.1. Moraga Lift Force Model ..... 530
17.5.7.1.2. Saffman-Mei Lift Force Model ..... 530
17.5.7.1.3. Legendre-Magnaudet Lift Force Model ..... 531
17.5.7.1.4. Tomiyama Lift Force Model ..... 531
17.5.8. Wall Lubrication Force ..... 532
17.5.8.1. Wall Lubrication Models ..... 532
17.5.8.1.1. Antal et al. Model ..... 533
17.5.8.1.2. Tomiyama Model ..... 533
17.5.8.1.3. Frank Model ..... 534
17.5.8.1.4. Hosokawa Model ..... 534
17.5.9. Turbulent Dispersion Force ..... 534
17.5.9.1. Models for Turbulent Dispersion Force ..... 535
17.5.9.1.1. Lopez de Bertodano Model ..... 535
17.5.9.1.2. Simonin Model ..... 535
17.5.9.1.3. Burns et al. Model ..... 536
17.5.9.1.4. Diffusion in VOF Model ..... 536
17.5.9.2. Limiting Functions for the Turbulent Dispersion Force ..... 537
17.5.10. Virtual Mass Force ..... 538
17.5.11. Solids Pressure ..... 538
17.5.11.1. Radial Distribution Function ..... 539
17.5.12. Maximum Packing Limit in Binary Mixtures ..... 541
17.5.13. Solids Shear Stresses ..... 541

*Release 15.0 - © SAS IP, Inc. All rights reserved. - Contains proprietary and confidential information of ANSYS, Inc. and its subsidiaries and affiliates.*

17.5.13.1. Collisional Viscosity ..... 542
17.5.13.2. Kinetic Viscosity ..... 542
17.5.13.3. Bulk Viscosity ..... 542
17.5.13.4. Frictional Viscosity ..... 542
17.5.14. Granular Temperature ..... 544
17.5.15. Description of Heat Transfer ..... 545
17.5.15.1. The Heat Exchange Coefficient ..... 546
17.5.15.1.1. Constant ..... 546
17.5.15.1.2. Nusselt Number ..... 546
17.5.15.1.3. Ranz-Marshall Model ..... 546
17.5.15.1.4. Tomiyama Model ..... 547
17.5.15.1.5. Hughmark Model ..... 547
17.5.15.1.6. Gunn Model ..... 547
17.5.15.1.7. Two-Resistance Model ..... 547
17.5.15.1.8. User Defined ..... 548
17.5.16. Turbulence Models ..... 548
17.5.16.1. k-$\varepsilon$ Turbulence Models ..... 549
17.5.16.1.1. k-$\varepsilon$ Mixture Turbulence Model ..... 549
17.5.16.1.2. k-$\varepsilon$ Dispersed Turbulence Model ..... 550
17.5.16.1.2.1. Assumptions ..... 550
17.5.16.1.2.2. Turbulence in the Continuous Phase ..... 551
17.5.16.1.2.3. Turbulence in the Dispersed Phase ..... 552
17.5.16.1.3. k-$\varepsilon$ Turbulence Model for Each Phase ..... 552
17.5.16.1.3.1. Transport Equations ..... 552
17.5.16.2. RSM Turbulence Models ..... 553
17.5.16.2.1. RSM Dispersed Turbulence Model ..... 554
17.5.16.2.2. RSM Mixture Turbulence Model ..... 555
17.5.16.3. Turbulence Interaction Models ..... 556
17.5.16.3.1. Simonin et al. ..... 556
17.5.16.3.1.1. Formulation in Dispersed Turbulence Models ..... 556
17.5.16.3.1.1.1. Continuous Phase ..... 556
17.5.16.3.1.1.2. Dispersed Phases ..... 557
17.5.16.3.1.2. Formulation in Per Phase Turbulence Models ..... 558
17.5.16.3.2. Troshko-Hassan ..... 559
17.5.16.3.2.1. Troshko-Hassan Formulation in Mixture Turbulence Models ..... 559
17.5.16.3.2.2. Troshko-Hassan Formulation in Dispersed Turbulence Models ..... 559
17.5.16.3.2.2.1. Continuous Phase ..... 559
17.5.16.3.2.2.2. Dispersed Phases ..... 560
17.5.16.3.2.3. Troshko-Hassan Formulation in Per-Phase Turbulence Models ..... 560
17.5.16.3.2.3.1. Continuous Phase ..... 560
17.5.16.3.2.3.2. Dispersed Phases ..... 560
17.5.16.3.3. Sato ..... 560
17.5.16.3.4. None ..... 561
17.5.17. Solution Method in ANSYS Fluent ..... 561
17.5.17.1. The Pressure-Correction Equation ..... 561
17.5.17.2. Volume Fractions ..... 561
17.5.18. Dense Discrete Phase Model ..... 561
17.5.18.1. Limitations ..... 562
17.5.18.2. Granular Temperature ..... 563
17.5.19. Multi-Fluid VOF Model ..... 563
17.5.20. Wall Boiling Models ..... 565
17.5.20.1. Overview ..... 565


*Release 15.0 - © SAS IP, Inc. All rights reserved. - Contains proprietary and confidential information of ANSYS, Inc. and its subsidiaries and affiliates.*

17.5.20.2. RPI Model ..... 565
17.5.20.3. Non-equilibrium Subcooled Boiling ..... 568
17.5.20.4. Critical Heat Flux ..... 568
17.5.20.4.1. Wall Heat Flux Partition ..... 569
17.5.20.4.2. Flow Regime Transition ..... 569
17.5.20.5. Interfacial Momentum Transfer ..... 570
17.5.20.5.1. Interfacial Area ..... 571
17.5.20.5.2. Bubble and Droplet Diameters ..... 571
17.5.20.5.2.1. Bubble Diameter ..... 571
17.5.20.5.2.2. Droplet Diameter ..... 571
17.5.20.5.3. Interfacial Drag Force ..... 572
17.5.20.5.4. Interfacial Lift Force ..... 572
17.5.20.5.5. Turbulent Dispersion Force ..... 572
17.5.20.5.6. Wall Lubrication Force ..... 572
17.5.20.5.7. Virtual Mass Force ..... 572
17.5.20.6. Interfacial Heat Transfer ..... 572
17.5.20.6.1. Interface to Liquid Heat Transfer ..... 572
17.5.20.6.2. Interface to Vapor Heat Transfer ..... 573
17.5.20.7. Mass Transfer ..... 573
17.5.20.7.1. Mass Transfer From the Wall to Vapor ..... 573
17.5.20.7.2. Interfacial Mass Transfer ..... 573
17.5.20.8. Turbulence Interactions ..... 573
17.6. Wet Steam Model Theory ..... 573
17.6.1. Overview of the Wet Steam Model ..... 574
17.6.2. Limitations of the Wet Steam Model ..... 574
17.6.3. Wet Steam Flow Equations ..... 574
17.6.4. Phase Change Model ..... 576
17.6.5. Built-in Thermodynamic Wet Steam Properties ..... 577
17.6.5.1. Equation of State ..... 577
17.6.5.2. Saturated Vapor Line ..... 578
17.6.5.3. Saturated Liquid Line ..... 578
17.6.5.4. Mixture Properties ..... 579
17.7. Modeling Mass Transfer in Multiphase Flows ..... 579
17.7.1. Source Terms due to Mass Transfer ..... 579
17.7.1.1. Mass Equation ..... 579
17.7.1.2. Momentum Equation ..... 579
17.7.1.3. Energy Equation ..... 580
17.7.1.4. Species Equation ..... 580
17.7.1.5. Other Scalar Equations ..... 580
17.7.2. Unidirectional Constant Rate Mass Transfer ..... 580
17.7.3. UDF-Prescribed Mass Transfer ..... 581
17.7.4. Cavitation Models ..... 581
17.7.4.1. Limitations of the Cavitation Models ..... 582
17.7.4.2. Vapor Transport Equation ..... 582
17.7.4.3. Bubble Dynamics Consideration ..... 583
17.7.4.4. Singhal et al. Model ..... 583
17.7.4.5. Zwart-Gerber-Belamri Model ..... 586
17.7.4.6. Schnerr and Sauer Model ..... 587
17.7.4.7. Additional Guidelines for the Cavitation Models ..... 588
17.7.4.8. Extended Cavitation Model Capabilities ..... 590
17.7.4.9. Multiphase Cavitation Models ..... 590
17.7.4.10. Multiphase Species Transport Cavitation Model ..... 590

*Release 15.0 - © SAS IP, Inc. All rights reserved. - Contains proprietary and confidential information of ANSYS, Inc. and its subsidiaries and affiliates.*

17.7.5. Evaporation-Condensation Model ..... 591
17.7.5.1. Lee Model ..... 591
17.7.5.2. Thermal Phase Change Model ..... 594
17.8. Modeling Species Transport in Multiphase Flows ..... 595
17.8.1. Limitations ..... 596
17.8.2. Mass and Momentum Transfer with Multiphase Species Transport ..... 596
17.8.2.1. Source Terms Due to Heterogeneous Reactions ..... 597
17.8.2.1.1. Mass Transfer ..... 597
17.8.2.1.2. Momentum Transfer ..... 597
17.8.2.1.3. Species Transfer ..... 598
17.8.2.1.4. Heat Transfer ..... 598
17.8.3. The Stiff Chemistry Solver ..... 599
17.8.4. Heterogeneous Phase Interaction ..... 599
**18. Solidification and Melting** ..... 601
18.1. Overview ..... 601
18.2. Limitations ..... 602
18.3. Introduction ..... 602
18.4. Energy Equation ..... 602
18.5. Momentum Equations ..... 603
18.6. Turbulence Equations ..... 604
18.7. Species Equations ..... 604
18.8. Back Diffusion ..... 606
18.9. Pull Velocity for Continuous Casting ..... 607
18.10. Contact Resistance at Walls ..... 608
18.11. Thermal and Solutal Buoyancy ..... 608
**19. Eulerian Wall Films** ..... 611
19.1. Introduction ..... 611
19.2. Mass, Momentum, and Energy Conservation Equations for Wall Film ..... 612
19.2.1. Film Sub-Models ..... 613
19.2.1.1. DPM Collection ..... 613
19.2.1.2. Splashing ..... 613
19.2.1.3. Film Separation ..... 613
19.2.1.3.1. Separation Criteria ..... 614
19.2.1.3.1.1. Foucart Separation ..... 614
19.2.1.3.1.2. O'Rourke Separation ..... 614
19.2.1.3.1.3. Friedrich Separation ..... 615
19.2.1.4. Film Stripping ..... 615
19.2.1.5. Secondary Phase Accretion ..... 616
19.2.1.6. Coupling of Wall Film with Mixture Species Transport ..... 617
19.2.2. Boundary Conditions ..... 618
19.2.3. Obtaining Film Velocity Without Solving the Momentum Equations ..... 618
19.2.3.1. Shear-Driven Film Velocity ..... 618
19.2.3.2. Gravity-Driven Film Velocity ..... 619
19.3. Numerical Schemes and Solution Algorithm ..... 620
19.3.1. Temporal Differencing Schemes ..... 620
19.3.1.1. First-Order Explicit Method ..... 620
19.3.1.2. First-Order Implicit Method ..... 621
19.3.1.3. Second-Order Implicit Method ..... 621
19.3.2. Spatial Differencing Schemes ..... 622
19.3.3. Solution Algorithm ..... 623
19.3.3.1. Steady Flow ..... 623
19.3.3.2. Transient Flow ..... 623


*Release 15.0 - © SAS IP, Inc. All rights reserved. - Contains proprietary and confidential information of ANSYS, Inc. and its subsidiaries and affiliates.*

**20. Solver Theory** ..... 625
20.1. Overview of Flow Solvers ..... 625
20.1.1. Pressure-Based Solver ..... 626
20.1.1.1. The Pressure-Based Segregated Algorithm ..... 626
20.1.1.2. The Pressure-Based Coupled Algorithm ..... 627
20.1.2. Density-Based Solver ..... 628
20.2. General Scalar Transport Equation: Discretization and Solution ..... 630
20.2.1. Solving the Linear System ..... 632
20.3. Discretization ..... 632
20.3.1. Spatial Discretization ..... 632
20.3.1.1. First-Order Upwind Scheme ..... 633
20.3.1.2. Power-Law Scheme ..... 633
20.3.1.3. Second-Order Upwind Scheme ..... 634
20.3.1.4. First-to-Higher Order Blending ..... 635
20.3.1.5. Central-Differencing Scheme ..... 635
20.3.1.6. Bounded Central Differencing Scheme ..... 636
20.3.1.7. QUICK Scheme ..... 636
20.3.1.8. Third-Order MUSCL Scheme ..... 637
20.3.1.9. Modified HRIC Scheme ..... 638
20.3.1.10. High Order Term Relaxation ..... 639
20.3.2. Temporal Discretization ..... 639
20.3.2.1. Implicit Time Integration ..... 640
20.3.2.2. Bounded Second Order Implicit Time Integration ..... 640
20.3.2.2.1. Limitations ..... 641
20.3.2.3. Explicit Time Integration ..... 641
20.3.3. Evaluation of Gradients and Derivatives ..... 641
20.3.3.1. Green-Gauss Theorem ..... 642
20.3.3.2. Green-Gauss Cell-Based Gradient Evaluation ..... 642
20.3.3.3. Green-Gauss Node-Based Gradient Evaluation ..... 642
20.3.3.4. Least Squares Cell-Based Gradient Evaluation ..... 643
20.3.4. Gradient Limiters ..... 644
20.3.4.1. Standard Limiter ..... 645
20.3.4.2. Multidimensional Limiter ..... 645
20.3.4.3. Differentiable Limiter ..... 645
20.4. Pressure-Based Solver ..... 645
20.4.1. Discretization of the Momentum Equation ..... 646
20.4.1.1. Pressure Interpolation Schemes ..... 646
20.4.2. Discretization of the Continuity Equation ..... 647
20.4.2.1. Density Interpolation Schemes ..... 648
20.4.3. Pressure-Velocity Coupling ..... 649
20.4.3.1. Segregated Algorithms ..... 649
20.4.3.1.1. SIMPLE ..... 649
20.4.3.1.2. SIMPLEC ..... 650
20.4.3.1.2.1. Skewness Correction ..... 650
20.4.3.1.3. PISO ..... 650
20.4.3.1.3.1. Neighbor Correction ..... 651
20.4.3.1.3.2. Skewness Correction ..... 651
20.4.3.1.3.3. Skewness - Neighbor Coupling ..... 651
20.4.3.2. Fractional-Step Method (FSM) ..... 651
20.4.3.3. Coupled Algorithm ..... 651
20.4.3.3.1. Limitations ..... 653
20.4.4. Steady-State Iterative Algorithm ..... 653

*Release 15.0 - © SAS IP, Inc. All rights reserved. - Contains proprietary and confidential information of ANSYS, Inc. and its subsidiaries and affiliates.*

20.4.4.1. Under-Relaxation of Variables ..... 653
20.4.4.2. Under-Relaxation of Equations ..... 653
20.4.5. Time-Advancement Algorithm ..... 654
20.4.5.1. Iterative Time-Advancement Scheme ..... 654
20.4.5.1.1. The Frozen Flux Formulation ..... 655
20.4.5.2. Non-Iterative Time-Advancement Scheme ..... 656
20.5. Density-Based Solver ..... 658
20.5.1. Governing Equations in Vector Form ..... 658
20.5.2. Preconditioning ..... 659
20.5.3. Convective Fluxes ..... 661
20.5.3.1. Roe Flux-Difference Splitting Scheme ..... 661
20.5.3.2. AUSM+ Scheme ..... 662
20.5.3.3. Low Diffusion Roe Flux Difference Splitting Scheme ..... 662
20.5.4. Steady-State Flow Solution Methods ..... 663
20.5.4.1. Explicit Formulation ..... 663
20.5.4.1.1. Implicit Residual Smoothing ..... 664
20.5.4.2. Implicit Formulation ..... 664
20.5.4.2.1. Convergence Acceleration for Stretched Meshes ..... 665
20.5.5. Unsteady Flows Solution Methods ..... 666
20.5.5.1. Explicit Time Stepping ..... 666
20.5.5.2. Implicit Time Stepping (Dual-Time Formulation) ..... 666
20.6. Pseudo Transient Under-Relaxation ..... 667
20.6.1. Automatic Pseudo Transient Time Step ..... 668
20.7. Multigrid Method ..... 670
20.7.1. Approach ..... 670
20.7.1.1. The Need for Multigrid ..... 670
20.7.1.2. The Basic Concept in Multigrid ..... 671
20.7.1.3. Restriction and Prolongation ..... 671
20.7.1.4. Unstructured Multigrid ..... 672
20.7.2. Multigrid Cycles ..... 672
20.7.2.1. The V and W Cycles ..... 672
20.7.3. Algebraic Multigrid (AMG) ..... 676
20.7.3.1. AMG Restriction and Prolongation Operators ..... 676
20.7.3.2. AMG Coarse Level Operator ..... 677
20.7.3.3. The F Cycle ..... 677
20.7.3.4. The Flexible Cycle ..... 678
20.7.3.4.1. The Residual Reduction Rate Criteria ..... 678
20.7.3.4.2. The Termination Criteria ..... 679
20.7.3.5. The Coupled and Scalar AMG Solvers ..... 679
20.7.3.5.1. Gauss-Seidel ..... 680
20.7.3.5.2. Incomplete Lower Upper (ILU) ..... 680
20.7.4. Full-Approximation Storage (FAS) Multigrid ..... 681
20.7.4.1. FAS Restriction and Prolongation Operators ..... 682
20.7.4.2. FAS Coarse Level Operator ..... 682
20.8. Hybrid Initialization ..... 683
20.9. Full Multigrid (FMG) Initialization ..... 685
20.9.1. Overview of FMG Initialization ..... 685
20.9.2. Limitations of FMG Initialization ..... 686
**21. Adapting the Mesh** ..... 687
21.1. Static Adaption Process ..... 687
21.1.1. Hanging Node Adaption ..... 687
21.1.1.1. Hanging Node Refinement ..... 688


*Release 15.0 - © SAS IP, Inc. All rights reserved. - Contains proprietary and confidential information of ANSYS, Inc. and its subsidiaries and affiliates.*

21.1.1.2. Hanging Node Coarsening ..... 689
21.2. Boundary Adaption ..... 689
21.3. Gradient Adaption ..... 691
21.3.1. Gradient Adaption Approach ..... 691
21.3.2. Example of Steady Gradient Adaption ..... 693
21.4. Dynamic Gradient Adaption ..... 695
21.5. Isovalue Adaption ..... 695
21.6. Region Adaption ..... 697
21.6.1. Defining a Region ..... 697
21.6.2. Region Adaption Example ..... 698
21.7. Volume Adaption ..... 699
21.7.1. Volume Adaption Approach ..... 699
21.7.2. Volume Adaption Example ..... 700
21.8. Yplus/Ystar Adaption ..... 701
21.8.1. Yplus/Ystar Adaption Approach ..... 701
21.9. Anisotropic Adaption ..... 703
21.10. Geometry-Based Adaption ..... 703
21.10.1. Geometry-Based Adaption Approach ..... 704
21.10.1.1. Node Projection ..... 704
21.10.1.2. Example of Geometry-Based Adaption ..... 706
21.11. Registers ..... 709
21.11.1. Adaption Registers ..... 709
21.11.2. Mask Registers ..... 710
**22. Reporting Alphanumeric Data** ..... 713
22.1. Fluxes Through Boundaries ..... 713
22.2. Forces on Boundaries ..... 714
22.2.1. Computing Forces, Moments, and the Center of Pressure ..... 714
22.3. Surface Integration ..... 716
22.3.1. Computing Surface Integrals ..... 717
22.3.1.1. Area ..... 717
22.3.1.2. Integral ..... 718
22.3.1.3. Area-Weighted Average ..... 718
22.3.1.4. Flow Rate ..... 718
22.3.1.5. Mass Flow Rate ..... 718
22.3.1.6. Mass-Weighted Average ..... 718
22.3.1.7. Sum of Field Variable ..... 718
22.3.1.8. Facet Average ..... 719
22.3.1.9. Facet Minimum ..... 719
22.3.1.10. Facet Maximum ..... 719
22.3.1.11. Vertex Average ..... 719
22.3.1.12. Vertex Minimum ..... 719
22.3.1.13. Vertex Maximum ..... 719
22.3.1.14. Standard-Deviation ..... 719
22.3.1.15. Uniformity Index ..... 720
22.3.1.16. Volume Flow Rate ..... 720
22.4. Volume Integration ..... 721
22.4.1. Computing Volume Integrals ..... 721
22.4.1.1. Volume ..... 721
22.4.1.2. Sum ..... 722
22.4.1.3. Sum*2Pi ..... 722
22.4.1.4. Volume Integral ..... 722
22.4.1.5. Volume-Weighted Average ..... 722

*Release 15.0 - © SAS IP, Inc. All rights reserved. - Contains proprietary and confidential information of ANSYS, Inc. and its subsidiaries and affiliates.*

22.4.1.6. Mass-Weighted Integral ..... 722
22.4.1.7. Mass ..... 723
22.4.1.8. Mass-Weighted Average ..... 723
A. Nomenclature ..... 725
Bibliography ..... 729
Index ..... 759


*Release 15.0 - © SAS IP, Inc. All rights reserved. - Contains proprietary and confidential information of ANSYS, Inc. and its subsidiaries and affiliates.*

# Using This Manual

This preface is divided into the following sections:

1. The Contents of This Manual
2. The Contents of the Fluent Manuals
3. Typographical Conventions
4. Mathematical Conventions
5. Technical Support

## 1. The Contents of This Manual

The ANSYS Fluent Theory Guide provides you with theoretical information about the models used in ANSYS Fluent.

**Important**

Under U.S. and international copyright law, ANSYS, Inc. is unable to distribute copies of the papers listed in the bibliography, other than those published internally by ANSYS, Inc. Use your library or a document delivery service to obtain copies of copyrighted papers.

A brief description of what is in each chapter follows:

- Basic Fluid Flow (p. 1), describes the governing equations and physical models used by ANSYS Fluent to compute fluid flow (including periodic flow, swirling and rotating flows, compressible flows, and inviscid flows).
- Flows with Moving Reference Frames (p. 17), describes single moving reference frames, multiple moving reference frames, and mixing planes.
- Flows Using Sliding and Dynamic Meshes (p. 33), describes sliding and deforming meshes.
- Turbulence (p. 39), describes various turbulent flow models.
- Heat Transfer (p. 133), describes the physical models used to compute heat transfer (including convective and conductive heat transfer, natural convection, radiative heat transfer, and periodic heat transfer).
- Heat Exchangers (p. 175), describes the physical models used to simulate the performance of heat exchangers.
- Species Transport and Finite-Rate Chemistry (p. 187), describes the finite-rate chemistry models. This chapter also provides information about modeling species transport in non-reacting flows.
- Non-Premixed Combustion (p. 215), describes the non-premixed combustion model.
- Premixed Combustion (p. 253), describes the premixed combustion model.
- Partially Premixed Combustion (p. 273), describes the partially premixed combustion model.
- Composition PDF Transport (p. 281), describes the composition PDF transport model.
- Chemistry Acceleration (p. 289), describes the methods used to accelerate computations for detailed chemical mechanisms involving laminar and turbulent flames.

*Release 15.0 - © SAS IP, Inc. All rights reserved. - Contains proprietary and confidential information of ANSYS, Inc. and its subsidiaries and affiliates.*

- Engine Ignition (p. 299), describes the engine ignition models.
- Pollutant Formation (p. 313), describes the models for the formation of NOx, SOx, and soot.
- Aerodynamically Generated Noise (p. 361), describes the acoustics model.
- Discrete Phase (p. 373), describes the discrete phase models.
- Multiphase Flows (p. 465), describes the general multiphase models (VOF, mixture, and Eulerian).
- Solidification and Melting (p. 601), describes the solidification and melting model.
- Eulerian Wall Films (p. 611), describes the Eulerian wall film model.
- Solver Theory (p. 625), describes the Fluent solvers.
- Adapting the Mesh (p. 687), describes the solution-adaptive mesh refinement feature.
- Reporting Alphanumeric Data (p. 713), describes how to obtain reports of fluxes, forces, surface integrals, and other solution data.

## 2. The Contents of the Fluent Manuals

The manuals listed below form the Fluent product documentation set. They include descriptions of the procedures, commands, and theoretical details needed to use Fluent products.

- Fluent Getting Started Guide contains general information about getting started with using Fluent and provides details about starting, running, and exiting the program.
- Fluent Migration Manual contains information about transitioning from the previous release of Fluent, including details about new features, solution changes, and text command list changes.
- Fluent User's Guide contains detailed information about running a simulation using the solution mode of Fluent, including information about the user interface, reading and writing files, defining boundary conditions, setting up physical models, calculating a solution, and analyzing your results.
- ANSYS Fluent Meshing User's Guide contains detailed information about creating 3D meshes using the meshing mode of Fluent.
- Fluent in Workbench User's Guide contains information about getting started with and using Fluent within the Workbench environment.
- Fluent Theory Guide contains reference information for how the physical models are implemented in Fluent.
- Fluent UDF Manual contains information about writing and using user-defined functions (UDFs).
- Fluent Tutorial Guide contains a number of examples of various flow problems with detailed instructions, commentary, and postprocessing of results.
- ANSYS Fluent Meshing Tutorials contains a number of examples of general mesh-generation techniques used in ANSYS Fluent Meshing.

  Tutorials for release 15.0 are available on the ANSYS Customer Portal. To access tutorials and their input files on the ANSYS Customer Portal, go to http://support.ansys.com/training.


Release 15.0 - © SAS IP, Inc. All rights reserved. - Contains proprietary and confidential information of ANSYS, Inc. and its subsidiaries and affiliates.

- Fluent Text Command List contains a brief description of each of the commands in Fluent's solution mode text interface.
- ANSYS Fluent Meshing Text Command List contains a brief description of each of the commands in Fluent's meshing mode text interface.
- Fluent Adjoint Solver Module Manual contains information about the background and usage of Fluent's Adjoint Solver Module that allows you to obtain detailed sensitivity data for the performance of a fluid system.
- Fluent Battery Module Manual contains information about the background and usage of Fluent's Battery Module that allows you to analyze the behavior of electric batteries.
- Fluent Continuous Fiber Module Manual contains information about the background and usage of Fluent's Continuous Fiber Module that allows you to analyze the behavior of fiber flow, fiber properties, and coupling between fibers and the surrounding fluid due to the strong interaction that exists between the fibers and the surrounding gas.
- Fluent Fuel Cell Modules Manual contains information about the background and the usage of two separate add-on fuel cell models for Fluent that allow you to model polymer electrolyte membrane fuel cells (PEMFC), solid oxide fuel cells (SOFC), and electrolysis with Fluent.
- Fluent Magnetohydrodynamics (MHD) Module Manual contains information about the background and usage of Fluent's Magnetohydrodynamics (MHD) Module that allows you to analyze the behavior of electrically conducting fluid flow under the influence of constant (DC) or oscillating (AC) electromagnetic fields.
- Fluent Population Balance Module Manual contains information about the background and usage of Fluent's Population Balance Module that allows you to analyze multiphase flows involving size distributions where particle population (as well as momentum, mass, and energy) require a balance equation.
- Fluent as a Server User's Guide contains information about the usage of Fluent as a Server which allows you to connect to a Fluent session and issue commands from a remote client application.
- Running Fluent Under LSF contains information about using Fluent with Platform Computing's LSF software, a distributed computing resource management tool.
- Running Fluent Under PBS Professional contains information about using Fluent with Altair PBS Professional, an open workload management tool for local and distributed environments.
- Running Fluent Under SGE contains information about using Fluent with Sun Grid Engine (SGE) software, a distributed computing resource management tool.

## 3. Typographical Conventions

Several typographical conventions are used in this manual's text to facilitate your learning process.

- Different type styles are used to indicate graphical user interface menu items and text interface menu items (for example, **Iso-Surface** dialog box, `surface/iso-surface` command).
- The text interface type style is also used when illustrating exactly what appears on the screen to distinguish it from the narrative text. In this context, user inputs are typically shown in boldface.

*Release 15.0 - © SAS IP, Inc. All rights reserved. - Contains proprietary and confidential information of ANSYS, Inc. and its subsidiaries and affiliates.*

- A mini flow chart is used to guide you through the navigation pane, which leads you to a specific task page or dialog box. For example,

  **Models** → **Multiphase** → **Edit...**

  indicates that **Models** is selected in the navigation pane, which then opens the corresponding task page. In the **Models** task page, **Multiphase** is selected from the list. Clicking the **Edit...** button opens the **Multiphase** dialog box.

  Also, a mini flow chart is used to indicate the menu selections that lead you to a specific command or dialog box. For example,

  **Define** → **Injections...**

  indicates that the **Injections...** menu item can be selected from the **Define** pull-down menu, and

  `display` → `mesh`

  indicates that the `mesh` command is available in the `display` text menu.

  In this manual, mini flow charts usually precede a description of a dialog box or command, or a screen illustration showing how to use the dialog box or command. They allow you to look up information about a command or dialog box and quickly determine how to access it without having to search the preceding material.

- The menu selections that will lead you to a particular dialog box or task page are also indicated (usually within a paragraph) using a "**/**". For example, **Define/Materials...** tells you to choose the **Materials...** menu item from the **Define** pull-down menu.

## 4. Mathematical Conventions

- Where possible, vector quantities are displayed with a raised arrow (e.g., $\vec{a}$, $\vec{A}$). Boldfaced characters are reserved for vectors and matrices as they apply to linear algebra (e.g., the identity matrix, $\mathbf{I}$).

- The operator $\nabla$, referred to as grad, nabla, or del, represents the partial derivative of a quantity with respect to all directions in the chosen coordinate system. In Cartesian coordinates, $\nabla$ is defined to be

$$\frac{\partial}{\partial x}\vec{\imath}+\frac{\partial}{\partial y}\vec{j}+\frac{\partial}{\partial z}\vec{k} \tag{1}$$

  $\nabla$ appears in several ways:

  – The gradient of a scalar quantity is the vector whose components are the partial derivatives; for example,

$$\nabla p=\frac{\partial p}{\partial x}\vec{\imath}+\frac{\partial p}{\partial y}\vec{j}+\frac{\partial p}{\partial z}\vec{k} \tag{2}$$

  – The gradient of a vector quantity is a second-order tensor; for example, in Cartesian coordinates,

$$\nabla(\vec{v})=\left(\frac{\partial}{\partial x}\vec{\imath}+\frac{\partial}{\partial y}\vec{j}+\frac{\partial}{\partial z}\vec{k}\right)\left(v_x\vec{\imath}+v_j\vec{j}+v_z\vec{k}\right) \tag{3}$$


Release 15.0 - © SAS IP, Inc. All rights reserved. - Contains proprietary and confidential information of ANSYS, Inc. and its subsidiaries and affiliates.

This tensor is usually written as

$$\begin{pmatrix} \frac{\partial v_x}{\partial x} & \frac{\partial v_x}{\partial y} & \frac{\partial v_x}{\partial z} \\ \frac{\partial v_y}{\partial x} & \frac{\partial v_y}{\partial y} & \frac{\partial v_y}{\partial z} \\ \frac{\partial v_z}{\partial x} & \frac{\partial v_z}{\partial y} & \frac{\partial v_z}{\partial z} \end{pmatrix} \tag{4}$$

– The divergence of a vector quantity, which is the inner product between $\nabla$ and a vector; for example,

$$\nabla \cdot \vec{v} = \frac{\partial v_x}{\partial x} + \frac{\partial v_y}{\partial y} + \frac{\partial v_z}{\partial z} \tag{5}$$

– The operator $\nabla \cdot \nabla$, which is usually written as $\nabla^2$ and is known as the Laplacian; for example,

$$\nabla^2 T = \frac{\partial^2 T}{\partial x^2} + \frac{\partial^2 T}{\partial y^2} + \frac{\partial^2 T}{\partial z^2} \tag{6}$$

$\nabla^2 T$ is different from the expression $(\nabla T)^2$, which is defined as

$$(\nabla T)^2 = \left(\frac{\partial T}{\partial x}\right)^2 + \left(\frac{\partial T}{\partial y}\right)^2 + \left(\frac{\partial T}{\partial z}\right)^2 \tag{7}$$

- An exception to the use of $\nabla$ is found in the discussion of Reynolds stresses in Turbulence in the *Fluent Theory Guide*, where convention dictates the use of Cartesian tensor notation. In this chapter, you will also find that some velocity vector components are written as $u$, $v$, and $w$ instead of the conventional $v$ with directional subscripts.

# 5. Technical Support

If you encounter difficulties while using ANSYS Fluent, please first refer to the section(s) of the manual containing information on the commands you are trying to use or the type of problem you are trying to solve. The product documentation is available from the online help, or from the ANSYS Customer Portal. To access documentation files on the ANSYS Customer Portal, go to http://support.ansys.com/documentation.

If you encounter an error, please write down the exact error message that appeared and note as much information as you can about what you were doing in ANSYS Fluent.

Technical Support for ANSYS, Inc. products is provided either by ANSYS, Inc. directly or by one of our certified ANSYS Support Providers. Please check with the ANSYS Support Coordinator (ASC) at your company to determine who provides support for your company, or go to www.ansys.com and select **Contact ANSYS > Contacts and Locations**.

*Release 15.0 - © SAS IP, Inc. All rights reserved. - Contains proprietary and confidential information of ANSYS, Inc. and its subsidiaries and affiliates.*

If your support is provided by ANSYS, Inc. directly, Technical Support can be accessed quickly and efficiently from the ANSYS Customer Portal, which is available from the ANSYS Website (www.ansys.com) under **Support > Customer Portal**. The direct URL is: support.ansys.com.

One of the many useful features of the Customer Portal is the Knowledge Resources Search, which can be found on the Home page of the Customer Portal.

Systems and installation Knowledge Resources are easily accessible via the Customer Portal by using the following keywords in the search box: `Systems/Installation`. These Knowledge Resources provide solutions and guidance on how to resolve installation and licensing issues quickly.

**NORTH AMERICA**

**All ANSYS, Inc. Products**

**Web:** Go to the ANSYS Customer Portal (http://support.ansys.com) and select the appropriate option.

**Toll-Free Telephone:** 1.800.711.7199

**Fax:** 1.724.514.5096

Support for University customers is provided only through the ANSYS Customer Portal.

**GERMANY**

**ANSYS Mechanical Products**

**Telephone:** +49 (0) 8092 7005-55 (CADFEM)

**Email:** support@cadfem.de

**All ANSYS Products**

**Web:** Go to the ANSYS Customer Portal (http://support.ansys.com) and select the appropriate option.

**National Toll-Free Telephone:**

German language: 0800 181 8499

English language: 0800 181 1565

Austria: 0800 297 835

Switzerland: 0800 546 318

**International Telephone:**

German language: +49 6151 152 9981

English language: +49 6151 152 9982

**Email:** support-germany@ansys.com

**UNITED KINGDOM**

**All ANSYS, Inc. Products**

**Web:** Go to the ANSYS Customer Portal (http://support.ansys.com) and select the appropriate option.

**Telephone:** Please have your Customer or Contact ID ready.

UK: 0800 048 0462

Republic of Ireland: 1800 065 6642

Outside UK: +44 1235 420130

**Email:** support-uk@ansys.com

Support for University customers is provided only through the ANSYS Customer Portal.


*Release 15.0 - © SAS IP, Inc. All rights reserved. - Contains proprietary and confidential information of ANSYS, Inc. and its subsidiaries and affiliates.*

**JAPAN**

**CFX , ICEM CFD and Mechanical Products**

**Telephone:** +81-3-5324-8333

**Fax:** +81-3-5324-7308

**Email:**

CFX: japan-cfx-support@ansys.com;

Mechanical: japan-ansys-support@ansys.com

**Fluent Products**

**Telephone:** +81-3-5324-7305

**Email:**

Fluent: japan-fluent-support@ansys.com;

Polyflow: japan-polyflow-support@ansys.com;

FfC: japan-ffc-support@ansys.com;

FloWizard: japan-flowizard-support@ansys.com

**Icepak**

**Telephone:** +81-3-5324-7444

**Email:** japan-icepak-support@ansys.com

***Licensing and Installation***

**Email:** japan-license-support@ansys.com

**INDIA**

**All ANSYS, Inc. Products**

**Web:** Go to the ANSYS Customer Portal (http://support.ansys.com) and select the appropriate option.

**Telephone:** +91 1 800 209 3475 (toll free) or +91 20 6654 3000 (toll)

**Fax:** +91 80 6772 2600

**Email:**

FEA products: feasup-india@ansys.com;

CFD products: cfdsup-india@ansys.com;

Ansoft products: ansoftsup-india@ansys.com;

Installation: installation-india@ansys.com

**FRANCE**

**All ANSYS, Inc. Products**

**Web:** Go to the ANSYS Customer Portal (http://support.ansys.com) and select the appropriate option.

**Toll-Free Telephone:** +33 (0) 800 919 225 **Toll Number:** +33 (0) 170 489 087

**Email:** support-france@ansys.com

**BELGIUM**

**All ANSYS Products**

*Release 15.0 - © SAS IP, Inc. All rights reserved. - Contains proprietary and confidential information of ANSYS, Inc. and its subsidiaries and affiliates.*

**Web:** Go to the ANSYS Customer Portal (http://support.ansys.com) and select the appropriate option.

**Telephone:** +32 (0) 10 45 28 61

**Email:** support-belgium@ansys.com

Support for University customers is provided only through the ANSYS Customer Portal.

**SWEDEN**

**All ANSYS Products**

**Web:** Go to the ANSYS Customer Portal (http://support.ansys.com) and select the appropriate option.

**Telephone:** +44 (0) 870 142 0300

**Email:** support-sweden@ansys.com

Support for University customers is provided only through the ANSYS Customer Portal.

**SPAIN and PORTUGAL**

**All ANSYS Products**

**Web:** Go to the ANSYS Customer Portal (http://support.ansys.com) and select the appropriate option.

**Telephone:** +34 900 933 407 (Spain), +351 800 880 513 (Portugal)

**Email:** support-spain@ansys.com, support-portugal@ansys.com

Support for University customers is provided only through the ANSYS Customer Portal.

**ITALY**

**All ANSYS Products**

**Web:** Go to the ANSYS Customer Portal (http://support.ansys.com) and select the appropriate option.

**Telephone:** +39 02 89013378

**Email:** support-italy@ansys.com

Support for University customers is provided only through the ANSYS Customer Portal.


*Release 15.0 - © SAS IP, Inc. All rights reserved. - Contains proprietary and confidential information of ANSYS, Inc. and its subsidiaries and affiliates.*

# Chapter 1: Basic Fluid Flow

This chapter describes the theoretical background for some of the basic physical models that ANSYS Fluent provides for fluid flow.

The information in this chapter is presented in the following sections:


1.1. Overview of Physical Models in ANSYS Fluent
1.2. Continuity and Momentum Equations
1.3. User-Defined Scalar (UDS) Transport Equations
1.4. Periodic Flows
1.5. Swirling and Rotating Flows
1.6. Compressible Flows
1.7. Inviscid Flows


| For more information about: | See |
|---|---|
| Models for flows in moving zones (including sliding and dynamic meshes) | Flows with Moving Reference Frames (p. 17) and Flows Using Sliding and Dynamic Meshes (p. 33) |
| Models for turbulence | Turbulence (p. 39) |
| Models for heat transfer (including radiation) | Heat Transfer (p. 133) |
| Models for species transport and reacting flows | Species Transport and Finite-Rate Chemistry (p. 187) – Composition PDF Transport (p. 281) |
| Models for pollutant formation | Pollutant Formation (p. 313) |
| Models for discrete phase | Discrete Phase (p. 373) |
| Models for general multiphase | Multiphase Flows (p. 465) |
| Models for melting and solidification | Solidification and Melting (p. 601) |
| Models for porous media, porous jumps, and lumped parameter fans and radiators | Cell Zone and Boundary Conditions in the User's Guide. |

## 1.1. Overview of Physical Models in ANSYS Fluent

ANSYS Fluent provides comprehensive modeling capabilities for a wide range of incompressible and compressible, laminar and turbulent fluid flow problems. Steady-state or transient analyses can be performed. In ANSYS Fluent, a broad range of mathematical models for transport phenomena (like heat transfer and chemical reactions) is combined with the ability to model complex geometries. Examples of ANSYS Fluent applications include laminar non-Newtonian flows in process equipment; conjugate heat transfer in turbomachinery and automotive engine components; pulverized coal combustion in utility boilers; external aerodynamics; flow through compressors, pumps, and fans; and multiphase flows in bubble columns and fluidized beds.

To permit modeling of fluid flow and related transport phenomena in industrial equipment and processes, various useful features are provided. These include porous media, lumped parameter (fan and heat exchanger), streamwise-periodic flow and heat transfer, swirl, and moving reference frame models. The moving reference frame family of models includes the ability to model single or multiple reference

Release 15.0 - © SAS IP, Inc. All rights reserved. - Contains proprietary and confidential information of ANSYS, Inc. and its subsidiaries and affiliates.

frames. A time-accurate sliding mesh method, useful for modeling multiple stages in turbomachinery applications, for example, is also provided, along with the mixing plane model for computing time-averaged flow fields.

Another very useful group of models in ANSYS Fluent is the set of free surface and multiphase flow models. These can be used for analysis of gas-liquid, gas-solid, liquid-solid, and gas-liquid-solid flows. For these types of problems, ANSYS Fluent provides the volume-of-fluid (VOF), mixture, and Eulerian models, as well as the discrete phase model (DPM). The DPM performs Lagrangian trajectory calculations for dispersed phases (particles, droplets, or bubbles), including coupling with the continuous phase. Examples of multiphase flows include channel flows, sprays, sedimentation, separation, and cavitation.

Robust and accurate turbulence models are a vital component of the ANSYS Fluent suite of models. The turbulence models provided have a broad range of applicability, and they include the effects of other physical phenomena, such as buoyancy and compressibility. Particular care has been devoted to addressing issues of near-wall accuracy via the use of extended wall functions and zonal models.

Various modes of heat transfer can be modeled, including natural, forced, and mixed convection with or without conjugate heat transfer, porous media, and so on. The set of radiation models and related submodels for modeling participating media are general and can take into account the complications of combustion. A particular strength of ANSYS Fluent is its ability to model combustion phenomena using a variety of models, including eddy dissipation and probability density function models. A host of other models that are very useful for reacting flow applications are also available, including coal and droplet combustion, surface reaction, and pollutant formation models.

## 1.2. Continuity and Momentum Equations

For all flows, ANSYS Fluent solves conservation equations for mass and momentum. For flows involving heat transfer or compressibility, an additional equation for energy conservation is solved. For flows involving species mixing or reactions, a species conservation equation is solved or, if the non-premixed combustion model is used, conservation equations for the mixture fraction and its variance are solved. Additional transport equations are also solved when the flow is turbulent.

In this section, the conservation equations for laminar flow in an inertial (non-accelerating) reference frame are presented. The equations that are applicable to moving reference frames are presented in Flows with Moving Reference Frames (p. 17). The conservation equations relevant to heat transfer, turbulence modeling, and species transport will be discussed in the chapters where those models are described.

The Euler equations solved for inviscid flow are presented in Inviscid Flows (p. 15).

For more information, see the following sections:

1.2.1. The Mass Conservation Equation
1.2.2. Momentum Conservation Equations

### 1.2.1. The Mass Conservation Equation

The equation for conservation of mass, or continuity equation, can be written as follows:

$$\frac{\partial \rho}{\partial t} + \nabla \cdot (\rho \vec{v}) = S_m \tag{1.1}$$

Equation 1.1 (p. 2) is the general form of the mass conservation equation and is valid for incompressible as well as compressible flows. The source $S_m$ is the mass added to the continuous phase from the dispersed second phase (for example, due to vaporization of liquid droplets) and any user-defined sources.


Release 15.0 - © SAS IP, Inc. All rights reserved. - Contains proprietary and confidential information of ANSYS, Inc. and its subsidiaries and affiliates.

For 2D axisymmetric geometries, the continuity equation is given by

$$\frac{\partial \rho}{\partial t}+\frac{\partial}{\partial x}(\rho v_x)+\frac{\partial}{\partial r}(\rho v_r)+\frac{\rho v_r}{r}=S_m \tag{1.2}$$

where $x$ is the axial coordinate, $r$ is the radial coordinate, $v_x$ is the axial velocity, and $v_r$ is the radial velocity.

## 1.2.2. Momentum Conservation Equations

Conservation of momentum in an inertial (non-accelerating) reference frame is described by [22] (p. 730)

$$\frac{\partial}{\partial t}(\rho \vec{v})+\nabla\cdot(\rho \vec{v}\,\vec{v})=-\nabla p+\nabla\cdot(\overline{\overline{\tau}})+\rho\vec{g}+\vec{F} \tag{1.3}$$

where $p$ is the static pressure, $\overline{\overline{\tau}}$ is the stress tensor (described below), and $\rho\vec{g}$ and $\vec{F}$ are the gravitational body force and external body forces (for example, that arise from interaction with the dispersed phase), respectively. $\vec{F}$ also contains other model-dependent source terms such as porous-media and user-defined sources.

The stress tensor $\overline{\overline{\tau}}$ is given by

$$\overline{\overline{\tau}}=\mu\left[\left(\nabla\vec{v}+\nabla\vec{v}^{\,T}\right)-\frac{2}{3}\nabla\cdot\vec{v}\,I\right] \tag{1.4}$$

where $\mu$ is the molecular viscosity, $I$ is the unit tensor, and the second term on the right hand side is the effect of volume dilation.

For 2D axisymmetric geometries, the axial and radial momentum conservation equations are given by

$$\begin{aligned}\frac{\partial}{\partial t}(\rho v_x)+\frac{1}{r}\frac{\partial}{\partial x}(r\rho v_x v_x)+\frac{1}{r}\frac{\partial}{\partial r}(r\rho v_r v_x)= & -\frac{\partial p}{\partial x}\\ & +\frac{1}{r}\frac{\partial}{\partial x}\left[r\mu\left(2\frac{\partial v_x}{\partial x}-\frac{2}{3}(\nabla\cdot\vec{v})\right)\right]\\ & +\frac{1}{r}\frac{\partial}{\partial r}\left[r\mu\left(\frac{\partial v_x}{\partial r}+\frac{\partial v_r}{\partial x}\right)\right]+F_x\end{aligned} \tag{1.5}$$

and

$$\begin{aligned}\frac{\partial}{\partial t}(\rho v_r)+\frac{1}{r}\frac{\partial}{\partial x}(r\rho v_x v_r)+\frac{1}{r}\frac{\partial}{\partial r}(r\rho v_r v_r)= & -\frac{\partial p}{\partial r}\\ & +\frac{1}{r}\frac{\partial}{\partial x}\left[r\mu\left(\frac{\partial v_r}{\partial x}+\frac{\partial v_x}{\partial r}\right)\right]\\ & +\frac{1}{r}\frac{\partial}{\partial r}\left[r\mu\left(2\frac{\partial v_r}{\partial r}-\frac{2}{3}(\nabla\cdot\vec{v})\right)\right]\\ & -2\mu\frac{v_r}{r^2}+\frac{2}{3}\frac{\mu}{r}(\nabla\cdot\vec{v})+\rho\frac{v_z^2}{r}+F_r\end{aligned} \tag{1.6}$$

where

Release 15.0 - © SAS IP, Inc. All rights reserved. - Contains proprietary and confidential information of ANSYS, Inc. and its subsidiaries and affiliates.

$$\nabla \cdot \vec{v} = \frac{\partial v_x}{\partial x} + \frac{\partial v_r}{\partial r} + \frac{v_r}{r} \tag{1.7}$$

and $v_z$ is the swirl velocity. (See Swirling and Rotating Flows (p. 8) for information about modeling axisymmetric swirl.)

## 1.3. User-Defined Scalar (UDS) Transport Equations

ANSYS Fluent can solve the transport equation for an arbitrary, user-defined scalar (UDS) in the same way that it solves the transport equation for a scalar such as species mass fraction. Extra scalar transport equations may be needed in certain types of combustion applications or for example in plasma-enhanced surface reaction modeling.

This section provides information on how you can specify user-defined scalar (UDS) transport equations to enhance the standard features of ANSYS Fluent. ANSYS Fluent allows you to define additional scalar transport equations in your model in the User-Defined Scalars Dialog Box. For more information about setting up user-defined scalar transport equations in ANSYS Fluent, see User-Defined Scalar (UDS) Transport Equations in the User's Guide.

Information in this section is organized in the following subsections:

1.3.1. Single Phase Flow
1.3.2. Multiphase Flow

### 1.3.1. Single Phase Flow

For an arbitrary scalar $\phi_k$, ANSYS Fluent solves the equation

$$\frac{\partial \rho \phi_k}{\partial t} + \frac{\partial}{\partial x_i}\left(\rho u_i \phi_k - \Gamma_k \frac{\partial \phi_k}{\partial x_i}\right) = S_{\phi_k} \quad k = 1, \ldots, N \tag{1.8}$$

where $\Gamma_k$ and $S_{\phi_k}$ are the diffusion coefficient and source term you supplied for each of the $N$ scalar equations. Note that $\Gamma_k$ is defined as a tensor in the case of anisotropic diffusivity. The diffusion term is therefore $\nabla \cdot \left(\Gamma_k \cdot \phi_k\right)$

For isotropic diffusivity, $\Gamma_k$ could be written as $\Gamma_k I$ where I is the identity matrix.

For the steady-state case, ANSYS Fluent will solve one of the three following equations, depending on the method used to compute the convective flux:

- If convective flux is *not* to be computed, ANSYS Fluent will solve the equation

  $$-\frac{\partial}{\partial x_i}\left(\Gamma_k \frac{\partial \phi_k}{\partial x_i}\right) = S_{\phi_k} \quad k = 1, \ldots, N \tag{1.9}$$

  where $\Gamma_k$ and $S_{\phi_k}$ are the diffusion coefficient and source term you supplied for each of the $N$ scalar equations.

- If convective flux is to be computed with mass flow rate, ANSYS Fluent will solve the equation


Release 15.0 - © SAS IP, Inc. All rights reserved. - Contains proprietary and confidential information of ANSYS, Inc. and its subsidiaries and affiliates.

$$\frac{\partial}{\partial x_i}\left(\rho u_i \phi_k - \Gamma_k \frac{\partial \phi_k}{\partial x_i}\right) = S_{\phi_k} \quad k = 1, \ldots, N \tag{1.10}$$

- It is also possible to specify a user-defined function to be used in the computation of convective flux. In this case, the user-defined mass flux is assumed to be of the form

$$F = \int_S \rho \vec{u} \cdot d\vec{S} \tag{1.11}$$

where $d\vec{S}$ is the face vector area.

## 1.3.2. Multiphase Flow

For multiphase flows, ANSYS Fluent solves transport equations for two types of scalars: *per phase* and *mixture*. For an arbitrary $k$ scalar in *phase-1*, denoted by $\phi_l^k$, ANSYS Fluent solves the transport equation inside the volume occupied by *phase-l*

$$\frac{\partial \alpha_l \rho_l \phi_l^k}{\partial t} + \nabla \cdot \left(\alpha_l \rho_l \vec{u}_l \phi_l^k - \alpha_l \Gamma_l^k \nabla \phi_l^k\right) = S_l^k \quad k = 1, \ldots, N \tag{1.12}$$

where $\alpha_l$, $\rho_l$, and $\vec{u}_l$ are the volume fraction, physical density, and velocity of *phase-l*, respectively. $\Gamma_l^k$ and $S_l^k$ are the diffusion coefficient and source term, respectively, which you will need to specify. In this case, scalar $\phi_l^k$ is associated only with one phase (*phase-l*) and is considered an individual field variable of *phase-l*.

The mass flux for *phase-l* is defined as

$$F_l = \int_S \alpha_l \rho_l \vec{u}_l \cdot d\vec{S} \tag{1.13}$$

If the transport variable described by scalar $\phi_l^k$ represents the physical field that is shared between phases, or is considered the same for each phase, then you should consider this scalar as being associated with a mixture of phases, $\phi^k$. In this case, the generic transport equation for the scalar is

$$\frac{\partial \rho_m \phi^k}{\partial t} + \nabla \cdot \left(\rho_m \vec{u}_m \phi^k - \Gamma_m^k \nabla \phi^k\right) = S^k{}_m \quad k = 1, \ldots, N \tag{1.14}$$

where mixture density $\rho_m$, mixture velocity $\vec{u}_m$, and mixture diffusivity for the scalar $k$ $\Gamma_m^k$ are calculated according to

$$\rho_m = \sum_l \alpha_l \rho_l \tag{1.15}$$

$$\rho_m \vec{u}_m = \sum_l \alpha_l \rho_l \vec{u}_l \tag{1.16}$$

$$F_m = \int_S \rho_m \vec{u}_m \cdot d\vec{S} \tag{1.17}$$

Release 15.0 - © SAS IP, Inc. All rights reserved. - Contains proprietary and confidential information of ANSYS, Inc. and its subsidiaries and affiliates.

$$\Gamma_m^k = \sum_l \alpha_l \Gamma_l^k \tag{1.18}$$

$$S_m^k = \sum_l S_l^k \tag{1.19}$$

To calculate mixture diffusivity, you will need to specify individual diffusivities for each material associated with individual phases.

Note that if the user-defined mass flux option is activated, then mass fluxes shown in Equation 1.13 (p. 5) and Equation 1.17 (p. 5) will need to be replaced in the corresponding scalar transport equations.

## 1.4. Periodic Flows

Periodic flow occurs when the physical geometry of interest and the expected pattern of the flow/thermal solution have a periodically repeating nature. Two types of periodic flow can be modeled in ANSYS Fluent. In the first type, no pressure drop occurs across the periodic planes. In the second type, a pressure drop occurs across translationally periodic boundaries, resulting in "fully-developed" or "streamwise-periodic" flow.

This section discusses streamwise-periodic flow. A description of no-pressure-drop periodic flow is provided in Periodic Boundary Conditions in the User's Guide, and a description of streamwise-periodic heat transfer is provided in Modeling Periodic Heat Transfer in the User's Guide. For more information about setting up periodic flows in ANSYS Fluent, see Periodic Flows in the User's Guide.

Information about streamwise-periodic flow is presented in the following sections:

1.4.1. Overview
1.4.2. Limitations
1.4.3. Physics of Periodic Flows

### 1.4.1. Overview

ANSYS Fluent provides the ability to calculate streamwise-periodic — or "fully-developed" — fluid flow. These flows are encountered in a variety of applications, including flows in compact heat exchanger channels and flows across tube banks. In such flow configurations, the geometry varies in a repeating manner along the direction of the flow, leading to a periodic fully-developed flow regime in which the flow pattern repeats in successive cycles. Other examples of streamwise-periodic flows include fully-developed flow in pipes and ducts. These periodic conditions are achieved after a sufficient entrance length, which depends on the flow Reynolds number and geometric configuration.

Streamwise-periodic flow conditions exist when the flow pattern repeats over some length $L$, with a constant pressure drop across each repeating module along the streamwise direction. Figure 1.1: Example of Periodic Flow in a 2D Heat Exchanger Geometry (p. 7) depicts one example of a periodically repeating flow of this type that has been modeled by including a single representative module.


Release 15.0 - © SAS IP, Inc. All rights reserved. - Contains proprietary and confidential information of ANSYS, Inc. and its subsidiaries and affiliates.

**Figure 1.1: Example of Periodic Flow in a 2D Heat Exchanger Geometry**

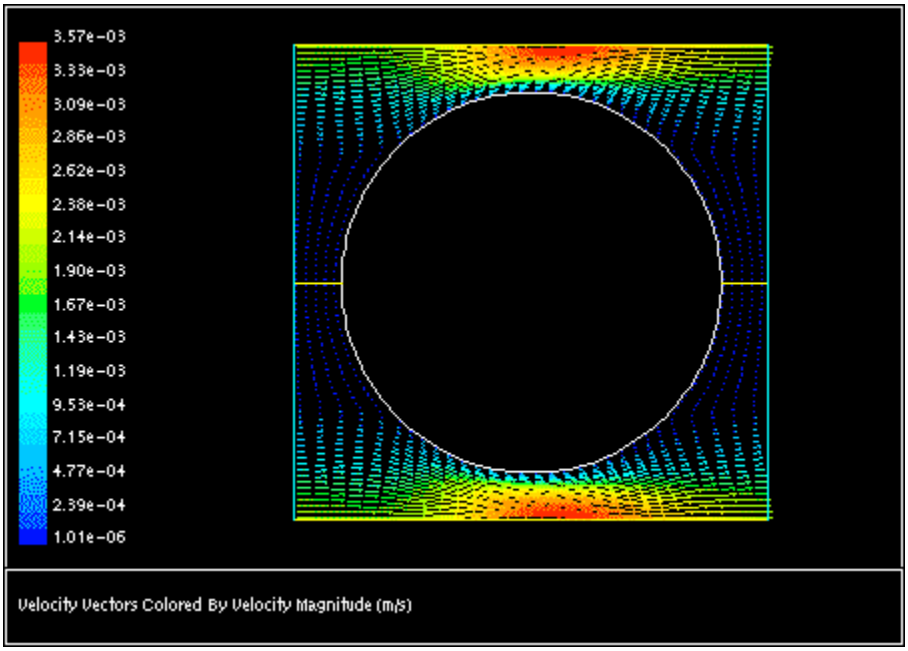


## 1.4.2. Limitations

The following limitations apply to modeling streamwise-periodic flow:

- The flow must be incompressible.
- When performing unsteady-state simulations with translational periodic boundary conditions, the specified pressure gradient is recommended.
- If one of the density-based solvers is used, you can specify only the pressure jump; for the pressure-based solver, you can specify either the pressure jump or the mass flow rate.
- No net mass addition through inlets/exits or extra source terms is allowed.
- Species can be modeled only if inlets/exits (without net mass addition) are included in the problem. Reacting flows are not permitted.
- Discrete phase and multiphase modeling are not allowed.
- When you specify a periodic mass-flow rate, Fluent will assume that the entire flow rate passes through one periodic continuous face zone only.

## 1.4.3. Physics of Periodic Flows

### *1.4.3.1. Definition of the Periodic Velocity*

The assumption of periodicity implies that the velocity components repeat themselves in space as follows:

$$\begin{aligned} u(\vec{r}) &= u(\vec{r}+\vec{L}) = u(\vec{r}+2\vec{L}) = \cdots \\ v(\vec{r}) &= v(\vec{r}+\vec{L}) = v(\vec{r}+2\vec{L}) = \cdots \\ w(\vec{r}) &= w(\vec{r}+\vec{L}) = w(\vec{r}+2\vec{L}) = \cdots \end{aligned} \tag{1.20}$$

Release 15.0 - © SAS IP, Inc. All rights reserved. - Contains proprietary and confidential information of ANSYS, Inc. and its subsidiaries and affiliates.

where $\vec{r}$ is the position vector and $\vec{L}$ is the periodic length vector of the domain considered (see Figure 1.2: Example of a Periodic Geometry (p. 8)).

**Figure 1.2: Example of a Periodic Geometry**

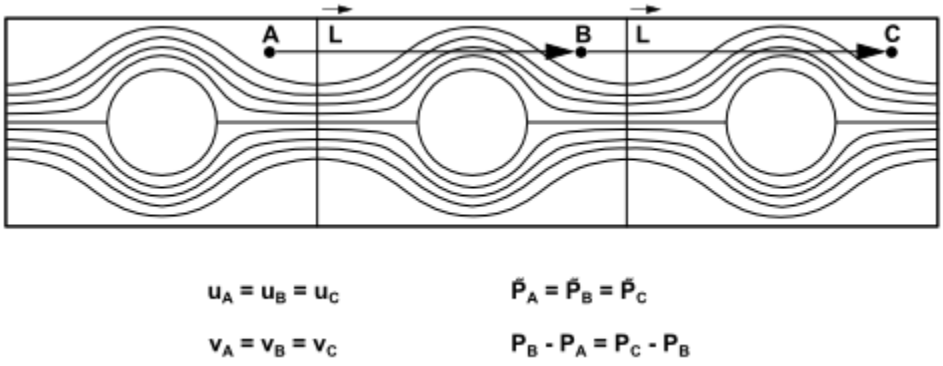


### 1.4.3.2. Definition of the Streamwise-Periodic Pressure

For viscous flows, the pressure is not periodic in the sense of Equation 1.20 (p. 7). Instead, the *pressure drop* between modules is periodic:

$$\Delta p = p(\vec{r}) - p(\vec{r}+\vec{L}) = p(\vec{r}+\vec{L}) - p(\vec{r}+2\vec{L}) = \cdots \tag{1.21}$$

If one of the density-based solvers is used, $\Delta p$ is specified as a constant value. For the pressure-based solver, the local pressure gradient can be decomposed into two parts: the gradient of a periodic component, $\nabla \tilde{p}(\vec{r})$, and the gradient of a linearly-varying component, $\beta \frac{\vec{L}}{|\vec{L}|}$:

$$\nabla p(\vec{r}) = \beta \frac{\vec{L}}{|\vec{L}|} + \nabla \tilde{p}(\vec{r}) \tag{1.22}$$

where $\tilde{p}(\vec{r})$ is the periodic pressure and $\beta |\vec{r}|$ is the linearly-varying component of the pressure. The periodic pressure is the pressure left over after subtracting out the linearly-varying pressure. The linearly-varying component of the pressure results in a force acting on the fluid in the momentum equations. Because the value of $\beta$ is not known a priori, it must be iterated on until the mass flow rate that you have defined is achieved in the computational model. This correction of $\beta$ occurs in the pressure correction step of the SIMPLE, SIMPLEC, or PISO algorithm where the value of $\beta$ is updated based on the difference between the desired mass flow rate and the actual one. You have some control over the number of sub-iterations used to update $\beta$. For more information about setting up parameters for $\beta$ in ANSYS Fluent, see Setting Parameters for the Calculation of $\beta$ in the User's Guide.

## 1.5. Swirling and Rotating Flows

Many important engineering flows involve swirl or rotation and ANSYS Fluent is well-equipped to model such flows. Swirling flows are common in combustion, with swirl introduced in burners and combustors in order to increase residence time and stabilize the flow pattern. Rotating flows are also encountered in turbomachinery, mixing tanks, and a variety of other applications.

When you begin the analysis of a rotating or swirling flow, it is essential that you classify your problem into one of the following five categories of flow:


Release 15.0 - © SAS IP, Inc. All rights reserved. - Contains proprietary and confidential information of ANSYS, Inc. and its subsidiaries and affiliates.

- axisymmetric flows with swirl or rotation
- fully three-dimensional swirling or rotating flows
- flows requiring a moving reference frame
- flows requiring multiple moving reference frames or mixing planes
- flows requiring sliding meshes

Modeling and solution procedures for the first two categories are presented in this section. The remaining three, which all involve "moving zones", are discussed in Flows with Moving Reference Frames (p. 17).

Information about rotating and swirling flows is provided in the following subsections:

1.5.1. Overview of Swirling and Rotating Flows
1.5.2. Physics of Swirling and Rotating Flows

For more information about setting up swirling and rotating flows in ANSYS Fluent, see Swirling and Rotating Flows in the User's Guide.

## 1.5.1. Overview of Swirling and Rotating Flows

### *1.5.1.1. Axisymmetric Flows with Swirl or Rotation*

You can solve a 2D axisymmetric problem that includes the prediction of the circumferential or swirl velocity. The assumption of axisymmetry implies that there are no circumferential gradients in the flow, but that there may be non-zero circumferential velocities. Examples of axisymmetric flows involving swirl or rotation are depicted in Figure 1.3: Rotating Flow in a Cavity (p. 9) and Figure 1.4: Swirling Flow in a Gas Burner (p. 10).

**Figure 1.3: Rotating Flow in a Cavity**

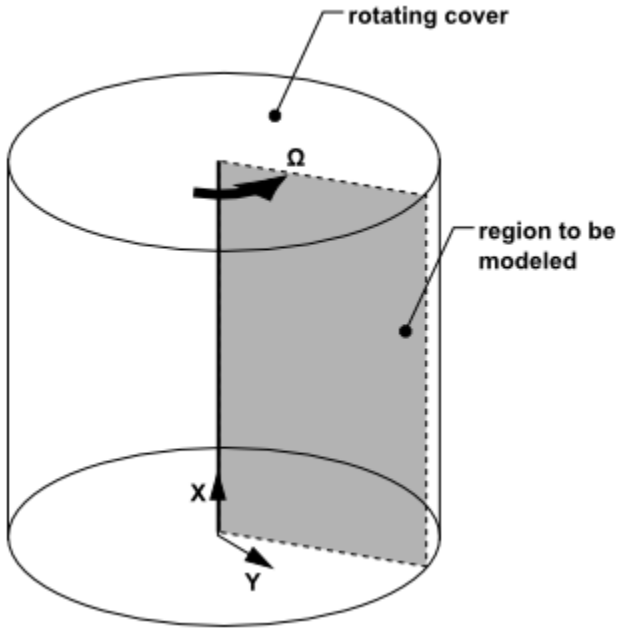

**Figure 1.4: Swirling Flow in a Gas Burner**

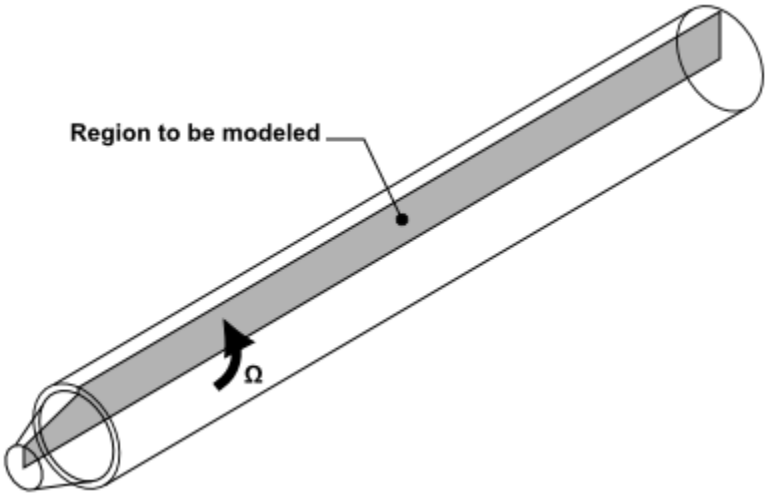


Your problem may be axisymmetric with respect to geometry and flow conditions but still include swirl or rotation. In this case, you can model the flow in 2D (that is, solve the axisymmetric problem) and include the prediction of the circumferential (or swirl) velocity. It is important to note that while the assumption of axisymmetry implies that there are no circumferential gradients in the flow, there may still be non-zero swirl velocities.

#### 1.5.1.1.1. Momentum Conservation Equation for Swirl Velocity

The tangential momentum equation for 2D swirling flows may be written as

$$\frac{\partial}{\partial t}(\rho w)+\frac{1}{r}\frac{\partial}{\partial x}(r\rho uw)+\frac{1}{r}\frac{\partial}{\partial r}(r\rho vw) = \frac{1}{r}\frac{\partial}{\partial x}\left[r\mu\frac{\partial w}{\partial x}\right] + \frac{1}{r^2}\frac{\partial}{\partial r}\left[r^3\mu\frac{\partial}{\partial r}\left(\frac{w}{r}\right)\right]-\rho\frac{vw}{r} \tag{1.23}$$

where $x$ is the axial coordinate, $r$ is the radial coordinate, $u$ is the axial velocity, $v$ is the radial velocity, and $w$ is the swirl velocity.

### *1.5.1.2. Three-Dimensional Swirling Flows*

When there are geometric changes and/or flow gradients in the circumferential direction, your swirling flow prediction requires a three-dimensional model. If you are planning a 3D ANSYS Fluent model that includes swirl or rotation, you should be aware of the setup constraints (Coordinate System Restrictions in the User's Guide). In addition, you may want to consider simplifications to the problem which might reduce it to an equivalent axisymmetric problem, especially for your initial modeling effort. Because of the complexity of swirling flows, an initial 2D study, in which you can quickly determine the effects of various modeling and design choices, can be very beneficial.

**Important**

For 3D problems involving swirl or rotation, there are no special inputs required during the problem setup and no special solution procedures. Note, however, that you may want to use the cylindrical coordinate system for defining velocity-inlet boundary condition inputs, as described in Defining the Velocity in the User's Guide. Also, you may find the gradual in-


Release 15.0 - © SAS IP, Inc. All rights reserved. - Contains proprietary and confidential information of ANSYS, Inc. and its subsidiaries and affiliates.

crease of the rotational speed (set as a wall or inlet boundary condition) helpful during the solution process. For more information, see Improving Solution Stability by Gradually Increasing the Rotational or Swirl Speed in the User's Guide.

### 1.5.1.3. Flows Requiring a Moving Reference Frame

If your flow involves a rotating boundary that moves through the fluid (for example, an impeller blade or a grooved or notched surface), you will need to use a moving reference frame to model the problem. Such applications are described in detail in Flow in a Moving Reference Frame (p. 18). If you have more than one rotating boundary (for example, several impellers in a row), you can use multiple reference frames (described in The Multiple Reference Frame Model (p. 22)) or mixing planes (described in The Mixing Plane Model (p. 25)).

## 1.5.2. Physics of Swirling and Rotating Flows

In swirling flows, conservation of angular momentum ($rw$ or $r^2\Omega$ = constant) tends to create a free vortex flow, in which the circumferential velocity, $w$, increases sharply as the radius, $r$, decreases (with $w$ finally decaying to zero near $r=0$ as viscous forces begin to dominate). A tornado is one example of a free vortex. Figure 1.5: Typical Radial Distribution of Circumferential Velocity in a Free Vortex (p. 11) depicts the radial distribution of $w$ in a typical free vortex.

**Figure 1.5: Typical Radial Distribution of Circumferential Velocity in a Free Vortex**




It can be shown that for an ideal free vortex flow, the centrifugal forces created by the circumferential motion are in equilibrium with the radial pressure gradient:

$$\frac{\partial p}{\partial r}=\frac{\rho w^2}{r} \tag{1.24}$$

As the distribution of angular momentum in a non-ideal vortex evolves, the form of this radial pressure gradient also changes, driving radial and axial flows in response to the highly non-uniform pressures that result. Thus, as you compute the distribution of swirl in your ANSYS Fluent model, you will also notice changes in the static pressure distribution and corresponding changes in the axial and radial flow velocities. It is this high degree of coupling between the swirl and the pressure field that makes the modeling of swirling flows complex.

In flows that are driven by wall rotation, the motion of the wall tends to impart a forced vortex motion to the fluid, wherein $w/r$ or $\Omega$ is constant. An important characteristic of such flows is the tendency of fluid with high angular momentum (for example, the flow near the wall) to be flung radially outward (see Figure 1.6: Stream Function Contours for Rotating Flow in a Cavity (p. 12) using the geometry of Figure 1.3: Rotating Flow in a Cavity (p. 9)). This is often referred to as "radial pumping", since the rotating wall is pumping the fluid radially outward.

Release 15.0 - © SAS IP, Inc. All rights reserved. - Contains proprietary and confidential information of ANSYS, Inc. and its subsidiaries and affiliates.

**Figure 1.6: Stream Function Contours for Rotating Flow in a Cavity**

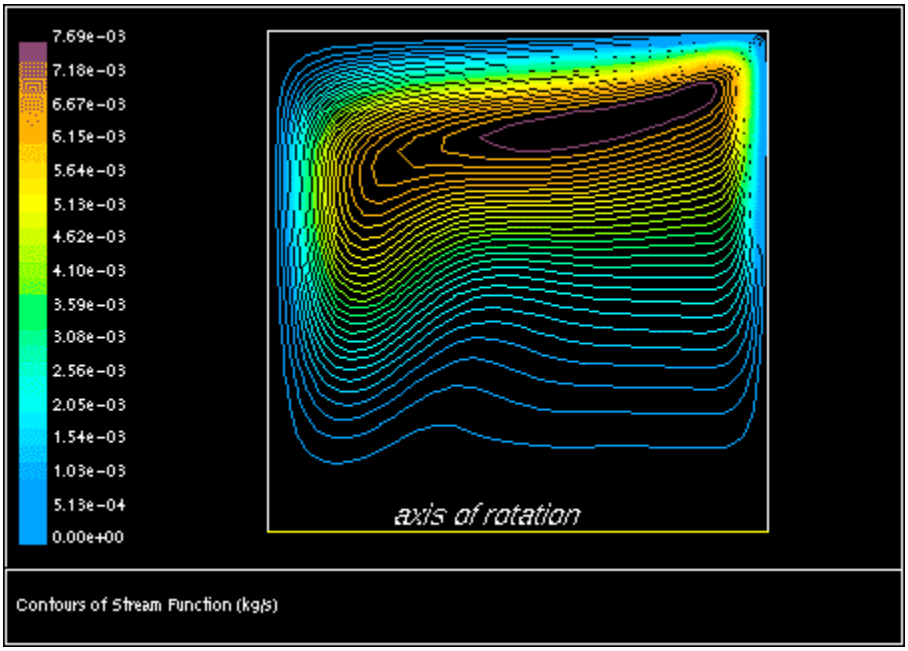


## 1.6. Compressible Flows

Compressibility effects are encountered in gas flows at high velocity and/or in which there are large pressure variations. When the flow velocity approaches or exceeds the speed of sound of the gas or when the pressure change in the system ($\Delta p/p$) is large, the variation of the gas density with pressure has a significant impact on the flow velocity, pressure, and temperature. Compressible flows create a unique set of flow physics for which you must be aware of the special input requirements and solution techniques described in this section. Figure 1.7: Transonic Flow in a Converging-Diverging Nozzle (p. 12) and Figure 1.8: Mach 0.675 Flow Over a Bump in a 2D Channel (p. 13) show examples of compressible flows computed using ANSYS Fluent.

**Figure 1.7: Transonic Flow in a Converging-Diverging Nozzle**

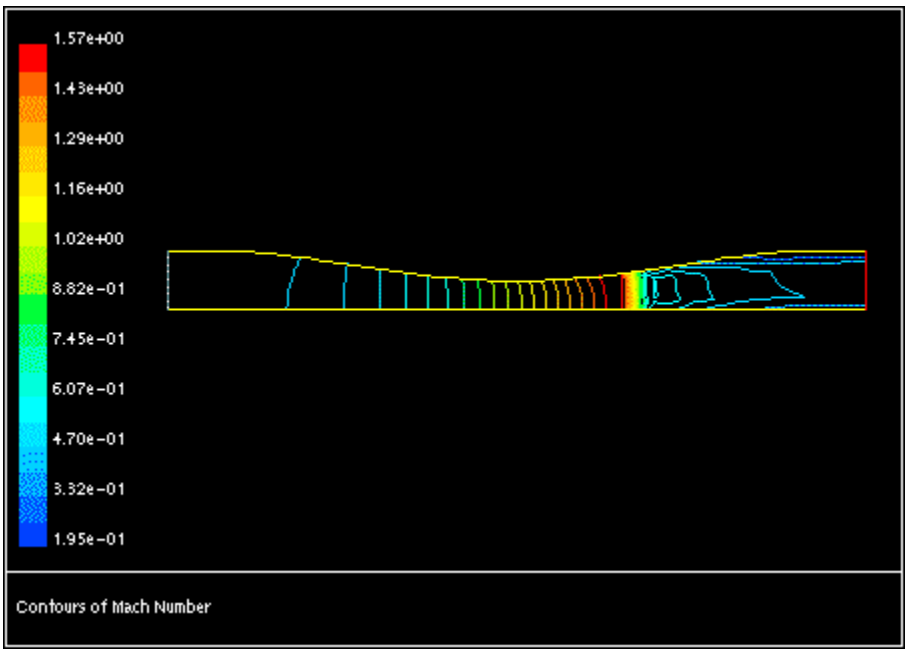



Release 15.0 - © SAS IP, Inc. All rights reserved. - Contains proprietary and confidential information of ANSYS, Inc. and its subsidiaries and affiliates.

**Figure 1.8: Mach 0.675 Flow Over a Bump in a 2D Channel**

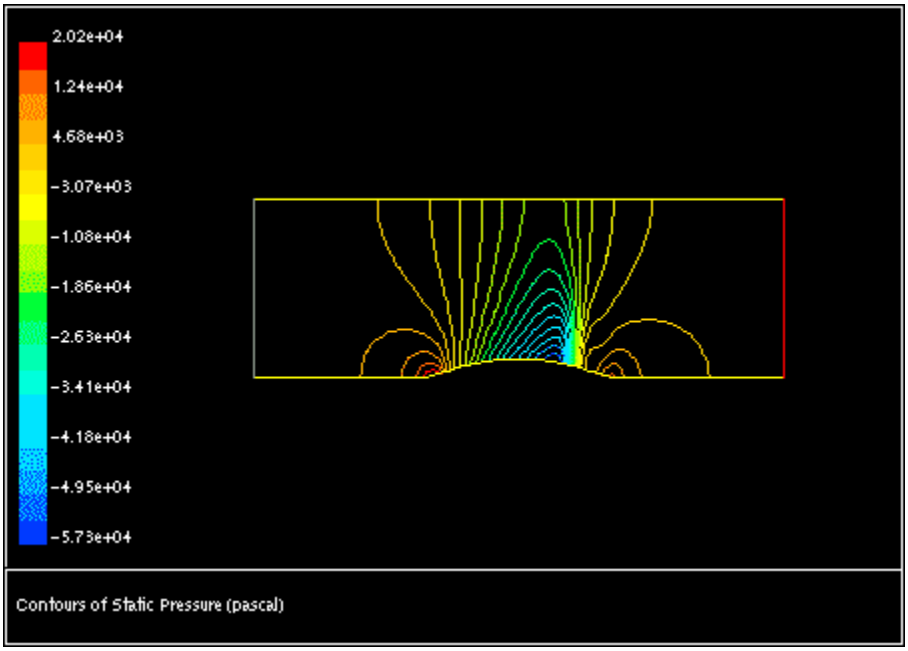


For more information about setting up compressible flows in ANSYS Fluent, see Compressible Flows in the User's Guide.

Information about compressible flows is provided in the following subsections:

1.6.1. When to Use the Compressible Flow Model
1.6.2. Physics of Compressible Flows

## 1.6.1. When to Use the Compressible Flow Model

Compressible flows can be characterized by the value of the Mach number:

$$M \equiv u/c \tag{1.25}$$

Here, $c$ is the speed of sound in the gas:

$$c = \sqrt{\gamma RT} \tag{1.26}$$

and $\gamma$ is the ratio of specific heats $\left(c_p/c_v\right)$.

When the Mach number is less than 1.0, the flow is termed subsonic. At Mach numbers much less than 1.0 ($M < 0.1$ or so), compressibility effects are negligible and the variation of the gas density with pressure can safely be ignored in your flow modeling. As the Mach number approaches 1.0 (which is referred to as the transonic flow regime), compressibility effects become important. When the Mach number exceeds 1.0, the flow is termed supersonic, and may contain shocks and expansion fans that can impact the flow pattern significantly. ANSYS Fluent provides a wide range of compressible flow modeling capabilities for subsonic, transonic, and supersonic flows.

## 1.6.2. Physics of Compressible Flows

Compressible flows are typically characterized by the total pressure $p_0$ and total temperature $T_0$ of the flow. For an ideal gas, these quantities can be related to the static pressure and temperature by the following:

Release 15.0 - © SAS IP, Inc. All rights reserved. - Contains proprietary and confidential information of ANSYS, Inc. and its subsidiaries and affiliates.

$$\frac{p_0}{p} = exp\left(\frac{\int_T^{T_0} \frac{C_p}{T} dT}{R}\right) \tag{1.27}$$

For constant $C_p$, Equation 1.27 (p. 14) reduces to

$$\frac{p_0}{p} = \left(1 + \frac{\gamma - 1}{2} M^2\right)^{\gamma/(\gamma-1)} \tag{1.28}$$

$$\frac{T_0}{T} = 1 + \frac{\gamma - 1}{2} M^2 \tag{1.29}$$

These relationships describe the variation of the static pressure and temperature in the flow as the velocity (Mach number) changes under isentropic conditions. For example, given a pressure ratio from inlet to exit (total to static), Equation 1.28 (p. 14) can be used to estimate the exit Mach number that would exist in a one-dimensional isentropic flow. For air, Equation 1.28 (p. 14) predicts a choked flow (Mach number of 1.0) at an isentropic pressure ratio, $p/p_0$, of 0.5283. This choked flow condition will be established at the point of minimum flow area (for example, in the throat of a nozzle). In the subsequent area expansion the flow may either accelerate to a supersonic flow in which the pressure will continue to drop, or return to subsonic flow conditions, decelerating with a pressure rise. If a supersonic flow is exposed to an imposed pressure increase, a shock will occur, with a sudden pressure rise and deceleration accomplished across the shock.

### 1.6.2.1. Basic Equations for Compressible Flows

Compressible flows are described by the standard continuity and momentum equations solved by ANSYS Fluent, and you do not need to activate any special physical models (other than the compressible treatment of density as detailed below). The energy equation solved by ANSYS Fluent correctly incorporates the coupling between the flow velocity and the static temperature, and should be activated whenever you are solving a compressible flow. In addition, if you are using the pressure-based solver, you should activate the viscous dissipation terms in Equation 5.1 (p. 134), which become important in high-Mach-number flows.

### 1.6.2.2. The Compressible Form of the Gas Law

For compressible flows, the ideal gas law is written in the following form:

$$\rho = \frac{p_{op} + p}{\frac{R}{M_w} T} \tag{1.30}$$

where $p_{op}$ is the operating pressure defined in the Operating Conditions Dialog Box, $p$ is the local static pressure relative to the operating pressure, $R$ is the universal gas constant, and $M_w$ is the molecular weight. The temperature, $T$, will be computed from the energy equation.

Some compressible flow problems involve fluids that do not behave as ideal gases. For example, flow under very high-pressure conditions cannot typically be modeled accurately using the ideal-gas assump-


Release 15.0 - © SAS IP, Inc. All rights reserved. - Contains proprietary and confidential information of ANSYS, Inc. and its subsidiaries and affiliates.

tion. Therefore, the real gas model described in Real Gas Models in the User's Guide should be used instead.

# 1.7. Inviscid Flows

Inviscid flow analyses neglect the effect of viscosity on the flow and are appropriate for high-Reynolds-number applications where inertial forces tend to dominate viscous forces. One example for which an inviscid flow calculation is appropriate is an aerodynamic analysis of some high-speed projectile. In a case like this, the pressure forces on the body will dominate the viscous forces. Hence, an inviscid analysis will give you a quick estimate of the primary forces acting on the body. After the body shape has been modified to maximize the lift forces and minimize the drag forces, you can perform a viscous analysis to include the effects of the fluid viscosity and turbulent viscosity on the lift and drag forces.

Another area where inviscid flow analyses are routinely used is to provide a good initial solution for problems involving complicated flow physics and/or complicated flow geometry. In a case like this, the viscous forces are important, but in the early stages of the calculation the viscous terms in the momentum equations will be ignored. Once the calculation has been started and the residuals are decreasing, you can turn on the viscous terms (by enabling laminar or turbulent flow) and continue the solution to convergence. For some very complicated flows, this may be the only way to get the calculation started.

For more information about setting up inviscid flows in ANSYS Fluent, see Inviscid Flows in the User's Guide.

Information about inviscid flows is provided in the following section.

1.7.1. Euler Equations

## 1.7.1. Euler Equations

For inviscid flows, ANSYS Fluent solves the Euler equations. The mass conservation equation is the same as for a laminar flow, but the momentum and energy conservation equations are reduced due to the absence of molecular diffusion.

In this section, the conservation equations for inviscid flow in an inertial (non-rotating) reference frame are presented. The equations that are applicable to non-inertial reference frames are described in Flows with Moving Reference Frames (p. 17). The conservation equations relevant for species transport and other models will be discussed in the chapters where those models are described.

### *1.7.1.1. The Mass Conservation Equation*

The equation for conservation of mass, or continuity equation, can be written as follows:

$$\frac{\partial \rho}{\partial t} + \nabla \cdot (\rho \vec{v}) = S_m \tag{1.31}$$

Equation 1.31 (p. 15) is the general form of the mass conservation equation and is valid for incompressible as well as compressible flows. The source $S_m$ is the mass added to the continuous phase from the dispersed second phase (for example, due to vaporization of liquid droplets) and any user-defined sources.

For 2D axisymmetric geometries, the continuity equation is given by

$$\frac{\partial \rho}{\partial t} + \frac{\partial}{\partial x}(\rho v_x) + \frac{\partial}{\partial r}(\rho v_r) + \frac{\rho v_r}{r} = S_m \tag{1.32}$$

Release 15.0 - © SAS IP, Inc. All rights reserved. - Contains proprietary and confidential information of ANSYS, Inc. and its subsidiaries and affiliates.

where $x$ is the axial coordinate, $r$ is the radial coordinate, $v_x$ is the axial velocity, and $v_r$ is the radial velocity.

### 1.7.1.2. Momentum Conservation Equations

Conservation of momentum is described by

$$\frac{\partial}{\partial t}(\rho \vec{v}) + \nabla \cdot (\rho \vec{v}\,\vec{v}) = -\nabla p + \rho \vec{g} + \vec{F} \tag{1.33}$$

where $p$ is the static pressure and $\rho \vec{g}$ and $\vec{F}$ are the gravitational body force and external body forces (for example, forces that arise from interaction with the dispersed phase), respectively. $\vec{F}$ also contains other model-dependent source terms such as porous-media and user-defined sources.

For 2D axisymmetric geometries, the axial and radial momentum conservation equations are given by

$$\frac{\partial}{\partial t}(\rho v_x) + \frac{1}{r}\frac{\partial}{\partial x}(r\rho v_x v_x) + \frac{1}{r}\frac{\partial}{\partial r}(r\rho v_r v_x) = -\frac{\partial p}{\partial x} + F_x \tag{1.34}$$

and

$$\frac{\partial}{\partial t}(\rho v_r) + \frac{1}{r}\frac{\partial}{\partial x}(r\rho v_x v_r) + \frac{1}{r}\frac{\partial}{\partial r}(r\rho v_r v_r) = -\frac{\partial p}{\partial r} + F_r \tag{1.35}$$

where

$$\nabla \cdot \vec{v} = \frac{\partial v_x}{\partial x} + \frac{\partial v_r}{\partial r} + \frac{v_r}{r} \tag{1.36}$$

### 1.7.1.3. Energy Conservation Equation

Conservation of energy is described by

$$\frac{\partial}{\partial t}(\rho E) + \nabla \cdot (\vec{v}\,(\rho E + p)) = -\nabla \cdot \left( \sum_j h_j J_j \right) + S_h \tag{1.37}$$


Release 15.0 - © SAS IP, Inc. All rights reserved. - Contains proprietary and confidential information of ANSYS, Inc. and its subsidiaries and affiliates.

# Chapter 2: Flows with Moving Reference Frames

This chapter describes the theoretical background for modeling flows in moving reference frames. Information about using the various models in this chapter can be found in Modeling Flows with Moving Reference Frames in the User's Guide. The information in this chapter is presented in the following sections:

2.1. Introduction
2.2. Flow in a Moving Reference Frame
2.3. Flow in Multiple Reference Frames

## 2.1. Introduction

ANSYS Fluent solves the equations of fluid flow and heat transfer by default in a stationary (or inertial) reference frame. However, there are many problems where it is advantageous to solve the equations in a moving (or non-inertial) reference frame. These problems typically involve moving parts, such as rotating blades, impellers, and moving walls, and it is the flow around the moving parts that is of interest. In most cases, the moving parts render the problem unsteady when viewed from a stationary frame. With a moving reference frame, however, the flow around the moving part can (with certain restrictions) be modeled as a steady-state problem with respect to the moving frame.

ANSYS Fluent's moving reference frame modeling capability allows you to model problems involving moving parts by allowing you to activate moving reference frames in selected cell zones. When a moving reference frame is activated, the equations of motion are modified to incorporate the additional acceleration terms that occur due to the transformation from the stationary to the moving reference frame.

For many problems, it may be possible to refer the entire computational domain to a single moving reference frame (see Figure 2.1: Single Component (Blower Wheel Blade Passage) (p. 18)). This is known as the single reference frame (or SRF) approach. The use of the SRF approach is possible; provided the geometry meets certain requirements (as discussed in Flow in a Moving Reference Frame (p. 18)). For more complex geometries, it may not be possible to use a single reference frame (see Figure 2.2: Multiple Component (Blower Wheel and Casing) (p. 18)). In such cases, you must break up the problem into multiple cell zones, with well-defined interfaces between the zones. The manner in which the interfaces are treated leads to two approximate, steady-state modeling methods for this class of problem: the multiple reference frame (or MRF) approach, and the mixing plane approach. These approaches will be discussed in The Multiple Reference Frame Model (p. 22) and The Mixing Plane Model (p. 25). If unsteady interaction between the stationary and moving parts is important, you can employ the sliding mesh approach to capture the transient behavior of the flow. The sliding meshing model will be discussed in Flows Using Sliding and Dynamic Meshes (p. 33).

Release 15.0 - © SAS IP, Inc. All rights reserved. - Contains proprietary and confidential information of ANSYS, Inc. and its subsidiaries and affiliates.

**Figure 2.1: Single Component (Blower Wheel Blade Passage)**

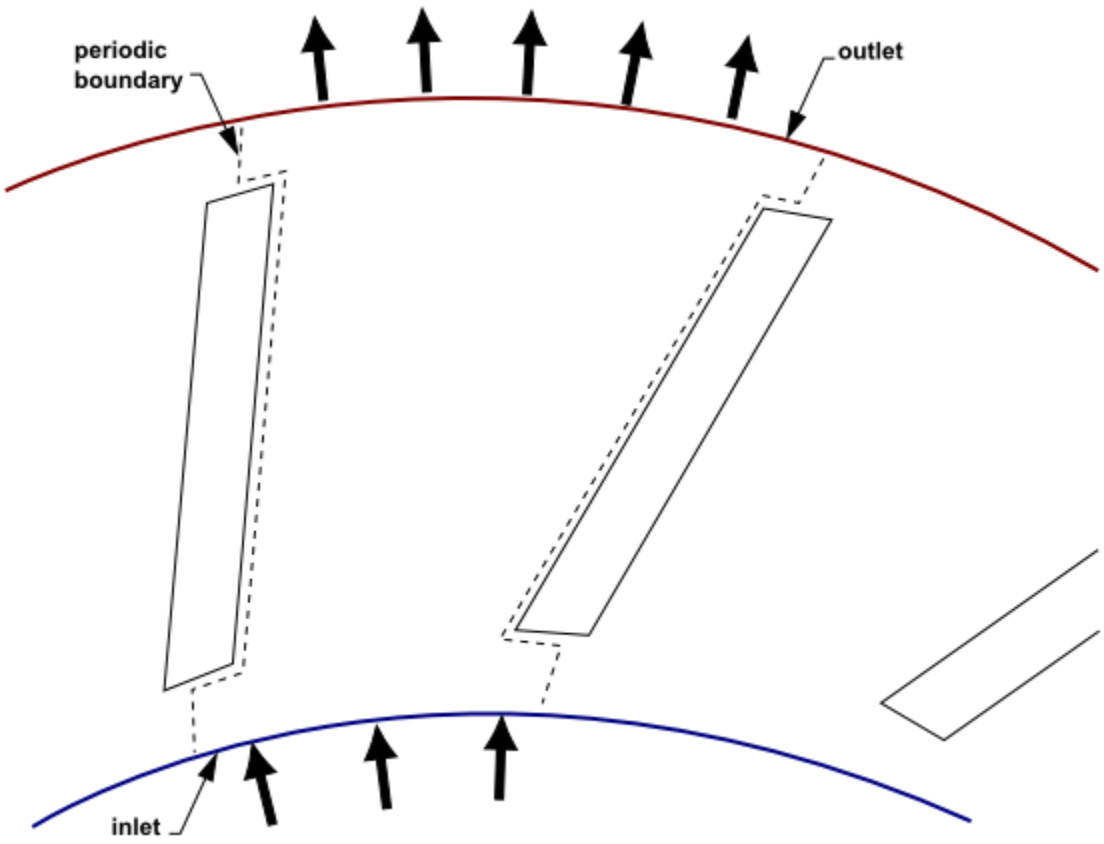


**Figure 2.2: Multiple Component (Blower Wheel and Casing)**

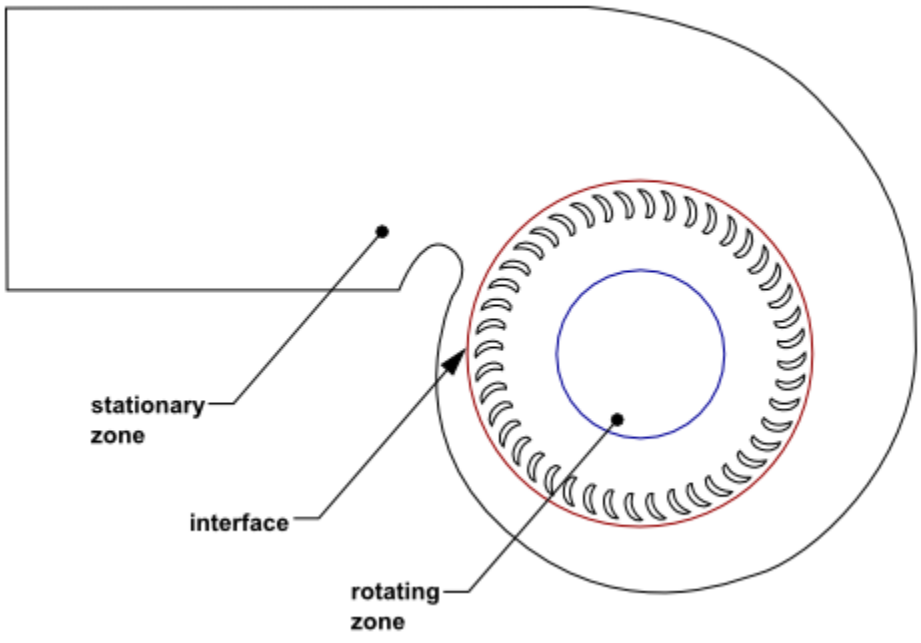


## 2.2. Flow in a Moving Reference Frame

The principal reason for employing a moving reference frame is to render a problem that is unsteady in the stationary (inertial) frame steady with respect to the moving frame. For a steadily moving frame


Release 15.0 - © SAS IP, Inc. All rights reserved. - Contains proprietary and confidential information
of ANSYS, Inc. and its subsidiaries and affiliates.

(for example, the rotational speed is constant), it is possible to transform the equations of fluid motion to the moving frame such that steady-state solutions are possible. It should also be noted that you can run an unsteady simulation in a moving reference frame with constant rotational speed. This would be necessary if you wanted to simulate, for example, vortex shedding from a rotating fan blade. The unsteadiness in this case is due to a natural fluid instability (vortex generation) rather than induced from interaction with a stationary component.

It is also possible in ANSYS Fluent to have frame motion with unsteady translational and rotational speeds. Again, the appropriate acceleration terms are added to the equations of fluid motion. Such problems are inherently unsteady with respect to the moving frame due to the unsteady frame motion

For more information, see the following section:
2.2.1. Equations for a Moving Reference Frame

## 2.2.1. Equations for a Moving Reference Frame

Consider a coordinate system that is translating with a linear velocity $\vec{v}_t$ and rotating with angular velocity $\vec{\omega}$ relative to a stationary (inertial) reference frame, as illustrated in Figure 2.3: Stationary and Moving Reference Frames (p. 19). The origin of the moving system is located by a position vector $\vec{r}_0$.

**Figure 2.3: Stationary and Moving Reference Frames**

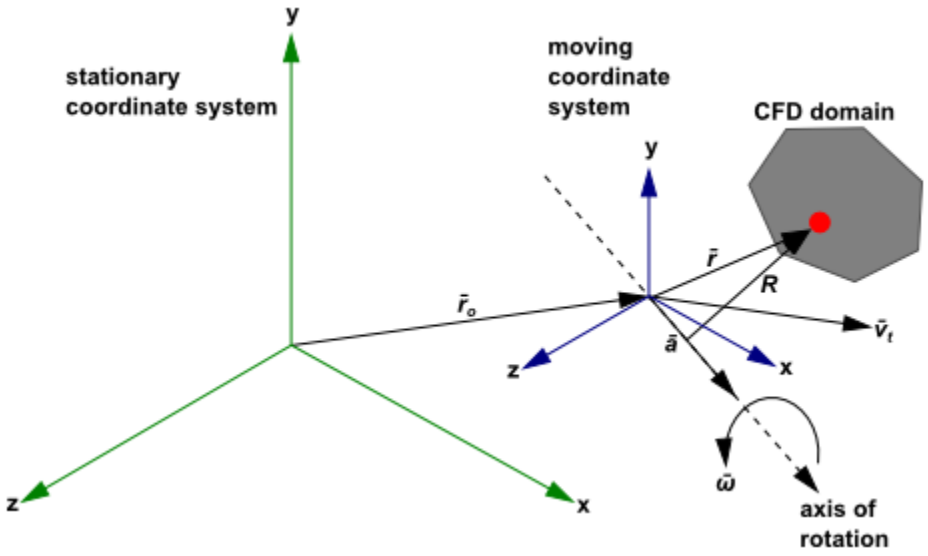


The axis of rotation is defined by a unit direction vector $\hat{a}$ such that

$$\vec{\omega} = \omega \hat{a} \tag{2.1}$$

The computational domain for the CFD problem is defined with respect to the moving frame such that an arbitrary point in the CFD domain is located by a position vector $\vec{r}$ from the origin of the moving frame.

The fluid velocities can be transformed from the stationary frame to the moving frame using the following relation:

$$\vec{v}_r = \vec{v} - \vec{u}_r \tag{2.2}$$

where

$$\vec{u}_r = \vec{v}_t + \vec{\omega} \times \vec{r} \tag{2.3}$$

Release 15.0 - © SAS IP, Inc. All rights reserved. - Contains proprietary and confidential information of ANSYS, Inc. and its subsidiaries and affiliates.

In the above equations, $\vec{v}_r$ is the relative velocity (the velocity viewed from the moving frame), $\vec{v}$ is the absolute velocity (the velocity viewed from the stationary frame), $\vec{u}_r$ is the velocity of the moving frame relative to the inertial reference frame, $\vec{v}_t$ is the translational frame velocity, and $\vec{\omega}$ is the angular velocity. It should be noted that both $\vec{\omega}$ and $\vec{v}_t$ can be functions of time.

When the equations of motion are solved in the moving reference frame, the acceleration of the fluid is augmented by additional terms that appear in the momentum equations [22] (p. 730). Moreover, the equations can be formulated in two different ways:

- Expressing the momentum equations using the relative velocities as dependent variables (known as the relative velocity formulation).
- Expressing the momentum equations using the absolute velocities as dependent variables in the momentum equations (known as the absolute velocity formulation).

The governing equations for these two formulations will be provided in the sections below. It can be noted here that ANSYS Fluent's pressure-based solvers provide the option to use either of these two formulations, whereas the density-based solvers always use the absolute velocity formulation. For more information about the advantages of each velocity formulation, see Choosing the Relative or Absolute Velocity Formulation in the User's Guide.

### 2.2.1.1. Relative Velocity Formulation

For the relative velocity formulation, the governing equations of fluid flow in a moving reference frame can be written as follows:

Conservation of mass:

$$\frac{\partial \rho}{\partial t} + \nabla \cdot \rho \vec{v}_r = 0 \tag{2.4}$$

Conservation of momentum:

$$\frac{\partial}{\partial t}(\rho \vec{v}_r) + \nabla \cdot (\rho \vec{v}_r \vec{v}_r) + \rho(2\vec{\omega} \times \vec{v}_r + \vec{\omega} \times \vec{\omega} \times \vec{r} + \vec{\alpha} \times \vec{r} + \vec{a}) = -\nabla p + \nabla \cdot \overline{\overline{\tau}}_r + \vec{F} \tag{2.5}$$

where $\vec{\alpha} = \frac{d\vec{\omega}}{dt}$ and $\vec{a} = \frac{d\vec{v}_t}{dt}$

Conservation of energy:

$$\frac{\partial}{\partial t}(\rho E_r) + \nabla \cdot (\rho \vec{v}_r H_r) = \nabla \cdot (k \nabla T + \overline{\overline{\tau}}_r \cdot \vec{v}_r) + S_h \tag{2.6}$$

The momentum equation contains four additional acceleration terms. The first two terms are the Coriolis acceleration ($2\vec{\omega} \times \vec{v}_r$) and the centripetal acceleration ($\vec{\omega} \times \vec{\omega} \times \vec{r}$), respectively. These terms appear for both steadily moving reference frames (that is, and are constant) and accelerating reference frames (that is, and/or are functions of time). The third and fourth terms are due to the unsteady change of the rotational speed and linear velocity, respectively. These terms vanish for constant translation and/or rotational speeds. In addition, the viscous stress ($\overline{\overline{\tau}}_r$) is identical to Equation 1.4 (p. 3) except that relative velocity derivatives are used. The energy equation is written in terms of the relative internal


Release 15.0 - © SAS IP, Inc. All rights reserved. - Contains proprietary and confidential information of ANSYS, Inc. and its subsidiaries and affiliates.

energy ($E_r$) and the relative total enthalpy ($H_r$), also known as the rothalpy. These variables are defined as:

$$E_r = h - \frac{p}{\rho} + \frac{1}{2}\left(v_r^2 - u_r^2\right) \tag{2.7}$$

$$H_r = E_r + \frac{p}{\rho} \tag{2.8}$$

### 2.2.1.2. Absolute Velocity Formulation

For the absolute velocity formulation, the governing equations of fluid flow for a steadily moving frame can be written as follows:

Conservation of mass:

$$\frac{\partial \rho}{\partial t} + \nabla \cdot \rho \vec{v}_r = 0 \tag{2.9}$$

Conservation of momentum:

$$\frac{\partial}{\partial t}\rho \vec{v} + \nabla \cdot (\rho \vec{v}_r \vec{v}) + \rho[\vec{\omega} \times (\vec{v} - \vec{v}_t)] = -\nabla p + \nabla \cdot \overline{\overline{\tau}} + \vec{F} \tag{2.10}$$

Conservation of energy:

$$\frac{\partial}{\partial t}\rho E + \nabla \cdot (\rho \vec{v}_r H + p \vec{u}_r) = \nabla \cdot (k \nabla T + \overline{\overline{\tau}} \cdot \vec{v}) + S_h \tag{2.11}$$

In this formulation, the Coriolis and centripetal accelerations can be simplified into a single term ($[\vec{\omega} \times (\vec{v} - \vec{v}_t)]$). Notice that the momentum equation for the absolute velocity formulation contains no explicit terms involving $\vec{\alpha}$ or $\vec{a}$.

### 2.2.1.3. Relative Specification of the Reference Frame Motion

ANSYS Fluent allows you to specify the frame of motion relative to an already moving (rotating and translating) reference frame. In this case, the resulting velocity vector is computed as

$$\vec{v}_r = \vec{v} - \vec{u}_r \tag{2.12}$$

where

$$\vec{u}_r = \vec{u_{r1}} + \vec{u_{r2}} \tag{2.13}$$

and

$$\vec{\omega} = \vec{\omega_1} + \vec{\omega_2} \tag{2.14}$$

Equation 2.13 (p. 21) is known as the Galilei transformation.

The rotation vectors are added together as in Equation 2.14 (p. 21), since the motion of the reference frame can be viewed as a solid body rotation, where the rotation rate is constant for every point on the body. In addition, it allows the formulation of the rotation to be an angular velocity axial (also known as pseudo) vector, describing infinitesimal instantaneous transformations. In this case, both rotation rates obey the commutative law. Note that such an approach is not sufficient when dealing with finite rotations. In this case, the formulation of rotation matrices based on Eulerian angles is necessary [368] (p. 749).

Release 15.0 - © SAS IP, Inc. All rights reserved. - Contains proprietary and confidential information of ANSYS, Inc. and its subsidiaries and affiliates.

To learn how to specify a moving reference frame within another moving reference frame, refer to Setting Up Multiple Reference Frames in the User's Guide.

## 2.3. Flow in Multiple Reference Frames

Problems that involve multiple moving parts cannot be modeled with the Single Reference Frame approach. For these problems, you must break up the model into multiple fluid/solid cell zones, with interface boundaries separating the zones. Zones that contain the moving components can then be solved using the moving reference frame equations (Equations for a Moving Reference Frame (p. 19)), whereas stationary zones can be solved with the stationary frame equations. The manner in which the equations are treated at the interface lead to two approaches that are supported in ANSYS Fluent:

- Multiple Moving Reference Frames
  - Multiple Reference Frame model (MRF) (see The Multiple Reference Frame Model (p. 22))
  - Mixing Plane Model (MPM) (see The Mixing Plane Model (p. 25))
- Sliding Mesh Model (SMM)

Both the MRF and mixing plane approaches are steady-state approximations, and differ primarily in the manner in which conditions at the interfaces are treated. These approaches will be discussed in the sections below. The sliding mesh model approach is, on the other hand, inherently unsteady due to the motion of the mesh with time. This approach is discussed in Flows Using Sliding and Dynamic Meshes (p. 33).

### 2.3.1. The Multiple Reference Frame Model

#### *2.3.1.1. Overview*

The MRF model [272] (p. 744) is, perhaps, the simplest of the two approaches for multiple zones. It is a steady-state approximation in which individual cell zones can be assigned different rotational and/or translational speeds. The flow in each moving cell zone is solved using the moving reference frame equations. (For details, see Flow in a Moving Reference Frame (p. 18)). If the zone is stationary ($\omega = 0$), the equations reduce to their stationary forms. At the interfaces between cell zones, a local reference frame transformation is performed to enable flow variables in one zone to be used to calculate fluxes at the boundary of the adjacent zone. The MRF interface formulation will be discussed in more detail in The MRF Interface Formulation (p. 24).

It should be noted that the MRF approach does not account for the relative motion of a moving zone with respect to adjacent zones (which may be moving or stationary); the mesh remains fixed for the computation. This is analogous to freezing the motion of the moving part in a specific position and observing the instantaneous flow field with the rotor in that position. Hence, the MRF is often referred to as the "frozen rotor approach."

While the MRF approach is clearly an approximation, it can provide a reasonable model of the flow for many applications. For example, the MRF model can be used for turbomachinery applications in which rotor-stator interaction is relatively weak, and the flow is relatively uncomplicated at the interface between the moving and stationary zones. In mixing tanks, since the impeller-baffle interactions are relatively weak, large-scale transient effects are not present and the MRF model can be used.

Another potential use of the MRF model is to compute a flow field that can be used as an initial condition for a transient sliding mesh calculation. This eliminates the need for a startup calculation. The multiple


Release 15.0 - © SAS IP, Inc. All rights reserved. - Contains proprietary and confidential information of ANSYS, Inc. and its subsidiaries and affiliates.

reference frame model should not be used, however, if it is necessary to actually simulate the transients that may occur in strong rotor-stator interactions, as the sliding mesh model alone should be used (see Modeling Flows Using Sliding and Dynamic Meshes in the User's Guide).

### 2.3.1.2. Examples

For a mixing tank with a single impeller, you can define a moving reference frame that encompasses the impeller and the flow surrounding it, and use a stationary frame for the flow outside the impeller region. An example of this configuration is illustrated in Figure 2.4: Geometry with One Rotating Impeller (p. 23). (The dashes denote the interface between the two reference frames.) Steady-state flow conditions are assumed at the interface between the two reference frames. That is, the velocity at the interface must be the same (in absolute terms) for each reference frame. *The mesh does not move.*

**Figure 2.4: Geometry with One Rotating Impeller**

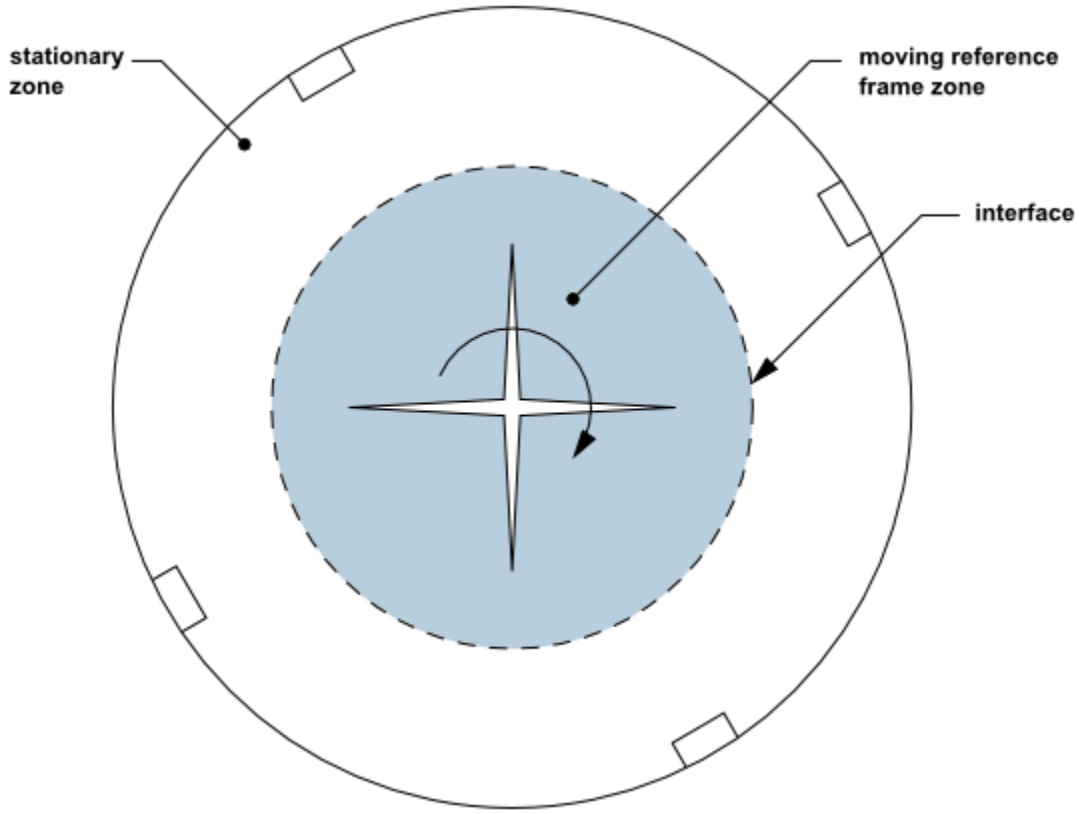


You can also model a problem that includes more than one moving reference frame. Figure 2.5: Geometry with Two Rotating Impellers (p. 24) shows a geometry that contains two rotating impellers side by side. This problem would be modeled using three reference frames: the stationary frame outside both impeller regions and two separate moving reference frames for the two impellers. (As noted above, the dashes denote the interfaces between reference frames.)

Release 15.0 - © SAS IP, Inc. All rights reserved. - Contains proprietary and confidential information
of ANSYS, Inc. and its subsidiaries and affiliates.

**Figure 2.5: Geometry with Two Rotating Impellers**

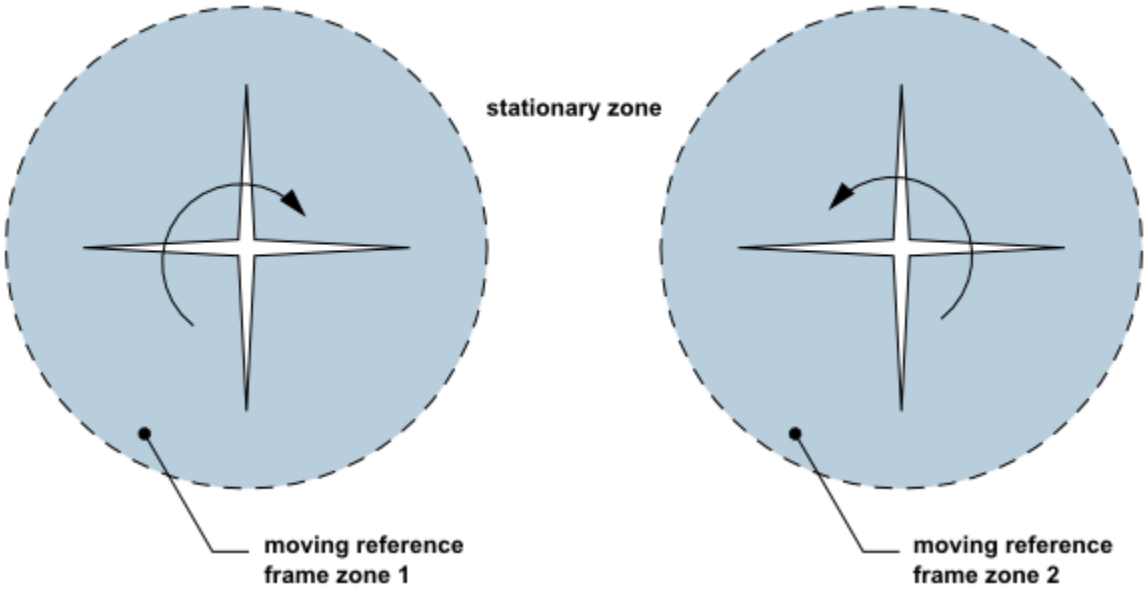


### *2.3.1.3. The MRF Interface Formulation*

The MRF formulation that is applied to the interfaces will depend on the velocity formulation being used. The specific approaches will be discussed below for each case. It should be noted that the interface treatment applies to the velocity and velocity gradients, since these vector quantities change with a change in reference frame. Scalar quantities, such as temperature, pressure, density, turbulent kinetic energy, and so on, do not require any special treatment, and therefore are passed locally without any change.

---

**Note**

The interface formulation used by ANSYS Fluent does not account for different normal (to the interface) cell zone velocities. You should specify the zone motion of both adjacent cell zones in a way that the interface-normal velocity difference is zero.

---

#### 2.3.1.3.1. Interface Treatment: Relative Velocity Formulation

In ANSYS Fluent's implementation of the MRF model, the calculation domain is divided into subdomains, each of which may be rotating and/or translating with respect to the laboratory (inertial) frame. The governing equations in each subdomain are written with respect to that subdomain's reference frame. Thus, the flow in stationary and translating subdomains is governed by the equations in Continuity and Momentum Equations (p. 2), while the flow in moving subdomains is governed by the equations presented in Equations for a Moving Reference Frame (p. 19).

At the boundary between two subdomains, the diffusion and other terms in the governing equations in one subdomain require values for the velocities in the adjacent subdomain (see Figure 2.6: Interface Treatment for the MRF Model (p. 25)). ANSYS Fluent enforces the continuity of the absolute velocity, $\vec{v}$, to provide the correct neighbor values of velocity for the subdomain under consideration. (This approach differs from the mixing plane approach described in The Mixing Plane Model (p. 25), where a circumferential averaging technique is used.)


Release 15.0 - © SAS IP, Inc. All rights reserved. - Contains proprietary and confidential information of ANSYS, Inc. and its subsidiaries and affiliates.

When the relative velocity formulation is used, velocities in each subdomain are computed relative to the motion of the subdomain. Velocities and velocity gradients are converted from a moving reference frame to the absolute inertial frame using Equation 2.15 (p. 25).

**Figure 2.6: Interface Treatment for the MRF Model**

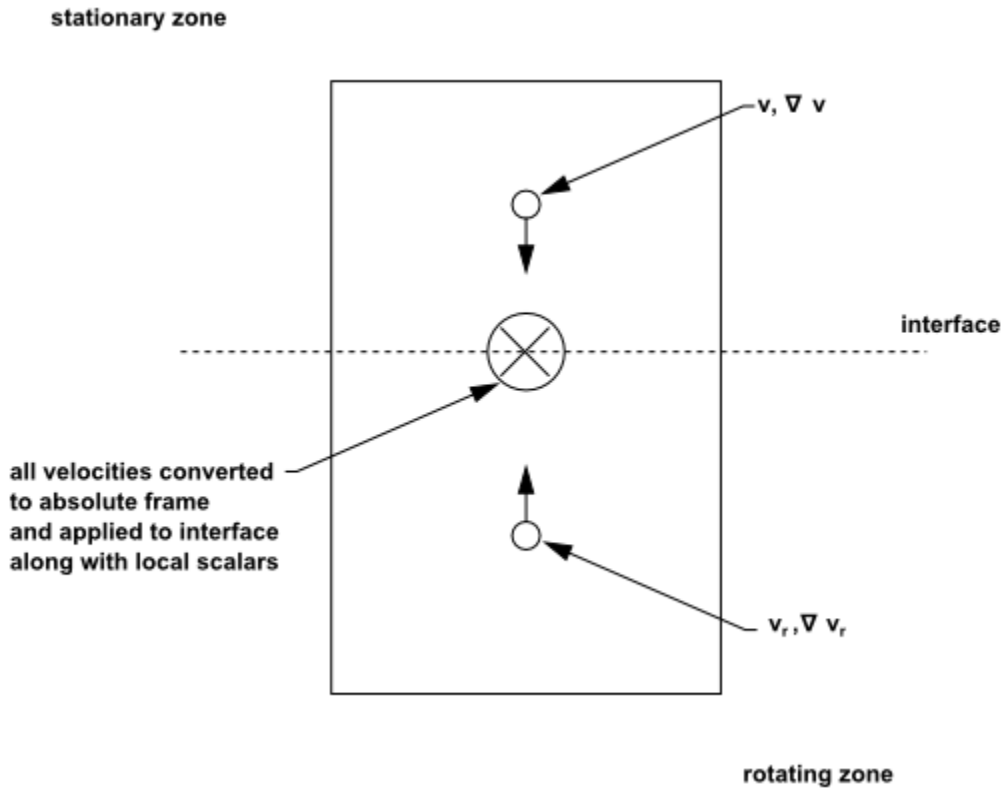


For a translational velocity $\vec{v}_t$, we have

$$\vec{v} = \vec{v}_r + (\vec{\omega} \times \vec{r}) + \vec{v}_t \tag{2.15}$$

From Equation 2.15 (p. 25), the gradient of the absolute velocity vector can be shown to be

$$\nabla \vec{v} = \nabla \vec{v}_r + \nabla (\vec{\omega} \times \vec{r}) \tag{2.16}$$

Note that scalar quantities such as density, static pressure, static temperature, species mass fractions, and so on, are simply obtained locally from adjacent cells.

#### 2.3.1.3.2. Interface Treatment: Absolute Velocity Formulation

When the absolute velocity formulation is used, the governing equations in each subdomain are written with respect to that subdomain's reference frame, but the velocities are stored in the absolute frame. Therefore, no special transformation is required at the interface between two subdomains. Again, scalar quantities are determined locally from adjacent cells.

### 2.3.2. The Mixing Plane Model

The mixing plane model in ANSYS Fluent provides an alternative to the multiple reference frame and sliding mesh models for simulating flow through domains with one or more regions in relative motion. This section provides a brief overview of the model and a list of its limitations.

Release 15.0 - © SAS IP, Inc. All rights reserved. - Contains proprietary and confidential information of ANSYS, Inc. and its subsidiaries and affiliates.

### 2.3.2.1. Overview

As discussed in The Multiple Reference Frame Model (p. 22), the MRF model is applicable when the flow at the interface between adjacent moving/stationary zones is nearly uniform ("mixed out"). If the flow at this interface is not uniform, the MRF model may not provide a physically meaningful solution. The sliding mesh model (see Modeling Flows Using Sliding and Dynamic Meshes in the User's Guide) may be appropriate for such cases, but in many situations it is not practical to employ a sliding mesh. For example, in a multistage turbomachine, if the number of blades is different for each blade row, a large number of blade passages is required in order to maintain circumferential periodicity. Moreover, sliding mesh calculations are necessarily unsteady, and therefore require significantly more computation to achieve a final, time-periodic solution. For situations where using the sliding mesh model is not feasible, the mixing plane model can be a cost-effective alternative.

In the mixing plane approach, each fluid zone is treated as a steady-state problem. Flow-field data from adjacent zones are passed as boundary conditions that are spatially averaged or "mixed" at the mixing plane interface. This mixing removes any unsteadiness that would arise due to circumferential variations in the passage-to-passage flow field (for example, wakes, shock waves, separated flow), therefore yielding a steady-state result. Despite the simplifications inherent in the mixing plane model, the resulting solutions can provide reasonable approximations of the time-averaged flow field.

### 2.3.2.2. Rotor and Stator Domains

Consider the turbomachine stages shown schematically in Figure 2.7: Axial Rotor-Stator Interaction (Schematic Illustrating the Mixing Plane Concept) (p. 26) and Figure 2.8: Radial Rotor-Stator Interaction (Schematic Illustrating the Mixing Plane Concept) (p. 27), each blade passage contains periodic boundaries. Figure 2.7: Axial Rotor-Stator Interaction (Schematic Illustrating the Mixing Plane Concept) (p. 26) shows a constant radial plane within a single stage of an axial machine, while Figure 2.8: Radial Rotor-Stator Interaction (Schematic Illustrating the Mixing Plane Concept) (p. 27) shows a constant $\theta$ plane within a mixed-flow device. In each case, the stage consists of two flow domains: the rotor domain, which is rotating at a prescribed angular velocity, followed by the stator domain, which is stationary. The order of the rotor and stator is arbitrary (that is, a situation where the rotor is downstream of the stator is equally valid).

**Figure 2.7: Axial Rotor-Stator Interaction (Schematic Illustrating the Mixing Plane Concept)**

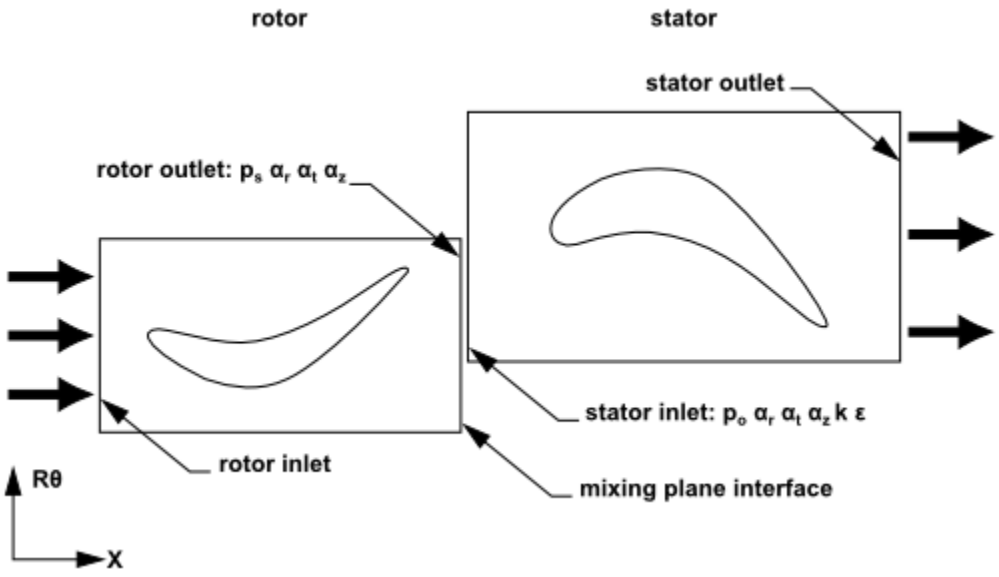



Release 15.0 - © SAS IP, Inc. All rights reserved. - Contains proprietary and confidential information of ANSYS, Inc. and its subsidiaries and affiliates.

**Figure 2.8: Radial Rotor-Stator Interaction (Schematic Illustrating the Mixing Plane Concept)**

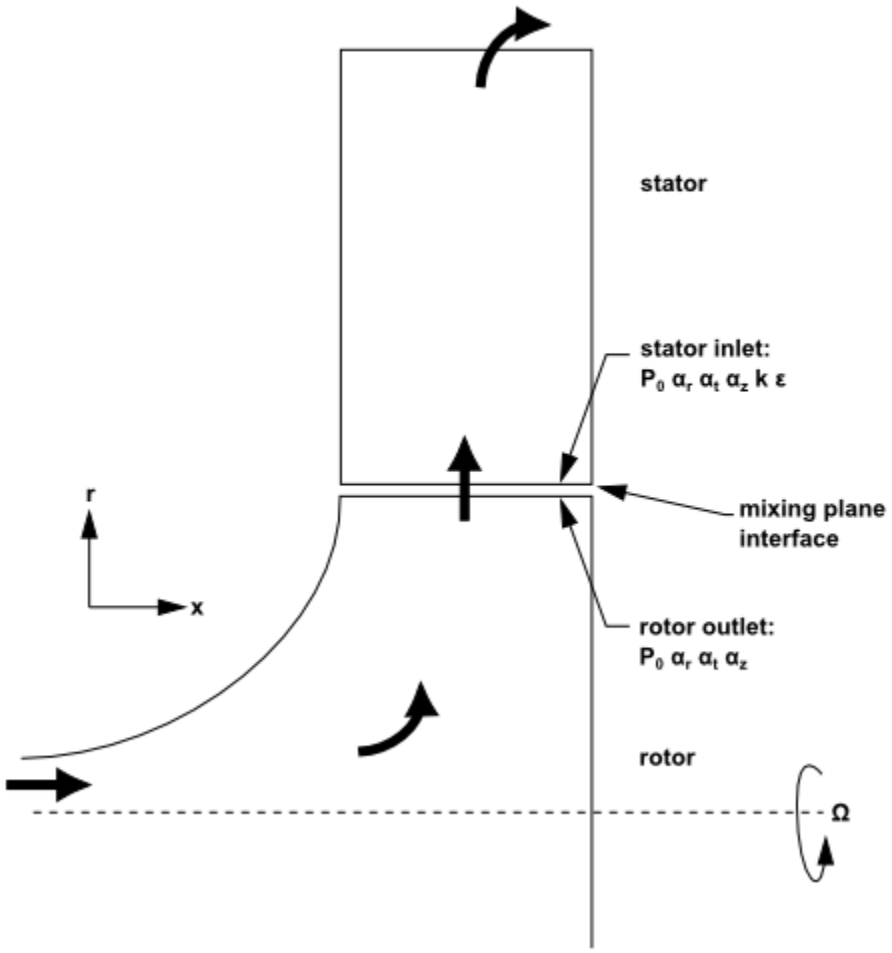


In a numerical simulation, each domain will be represented by a separate mesh. The flow information between these domains will be coupled at the mixing plane interface (as shown in Figure 2.7: Axial Rotor-Stator Interaction (Schematic Illustrating the Mixing Plane Concept) (p. 26) and Figure 2.8: Radial Rotor-Stator Interaction (Schematic Illustrating the Mixing Plane Concept) (p. 27)) using the mixing plane model. Note that you may couple any number of fluid zones in this manner; for example, four blade passages can be coupled using three mixing planes.

**Important**

Note that the stator and rotor passages are separate cell zones, each with their own inlet and outlet boundaries. You can think of this system as a set of SRF models for each blade passage coupled by boundary conditions supplied by the mixing plane model.

### 2.3.2.3. The Mixing Plane Concept

The essential idea behind the mixing plane concept is that each fluid zone is solved as a steady-state problem. At some prescribed iteration interval, the flow data at the mixing plane interface are averaged in the circumferential direction on both the stator outlet and the rotor inlet boundaries. The ANSYS Fluent implementation gives you the choice of three types of averaging methods: area-weighted aver-

Release 15.0 - © SAS IP, Inc. All rights reserved. - Contains proprietary and confidential information of ANSYS, Inc. and its subsidiaries and affiliates.

aging, mass averaging, and mixed-out averaging. By performing circumferential averages at specified radial or axial stations, "profiles" of boundary condition flow variables can be defined. These profiles—which will be functions of either the axial or the radial coordinate, depending on the orientation of the mixing plane—are then used to update boundary conditions along the two zones of the mixing plane interface. In the examples shown in Figure 2.7: Axial Rotor-Stator Interaction (Schematic Illustrating the Mixing Plane Concept) (p. 26) and Figure 2.8: Radial Rotor-Stator Interaction (Schematic Illustrating the Mixing Plane Concept) (p. 27), profiles of averaged total pressure ($p_0$), direction cosines of the local flow angles in the radial, tangential, and axial directions ($\alpha_r, \alpha_t, \alpha_z$), total temperature ($T_0$), turbulence kinetic energy ($k$), and turbulence dissipation rate ($\varepsilon$) are computed at the rotor exit and used to update boundary conditions at the stator inlet. Likewise, a profile of static pressure ($p_s$), direction cosines of the local flow angles in the radial, tangential, and axial directions ($\alpha_r, \alpha_t, \alpha_z$), are computed at the stator inlet and used as a boundary condition on the rotor exit.

Passing profiles in the manner described above assumes specific boundary condition types have been defined at the mixing plane interface. The coupling of an upstream outlet boundary zone with a downstream inlet boundary zone is called a "mixing plane pair". In order to create mixing plane pairs in ANSYS Fluent, the boundary zones must be of the following types:

| Upstream | Downstream |
|---|---|
| pressure outlet | pressure inlet |
| pressure outlet | velocity inlet |
| pressure outlet | mass flow inlet |

For specific instructions about setting up mixing planes, see Setting Up the Mixing Plane Model in the User's Guide.

### 2.3.2.4. Choosing an Averaging Method

Three profile averaging methods are available in the mixing plane model:

- area averaging
- mass averaging
- mixed-out averaging

#### 2.3.2.4.1. Area Averaging

Area averaging is the default averaging method and is given by

$$\overline{f} = \frac{1}{A}\int_A f dA \tag{2.17}$$

**Important**

The pressure and temperature obtained by the area average may not be representative of the momentum and energy of the flow.

#### 2.3.2.4.2. Mass Averaging

Mass averaging is given by


Release 15.0 - © SAS IP, Inc. All rights reserved. - Contains proprietary and confidential information of ANSYS, Inc. and its subsidiaries and affiliates.

$$\overline{f} = \frac{1}{\dot{m}} \int_A f \rho \vec{V} \cdot \hat{n} dA \tag{2.18}$$

where

$$\dot{m} = \int_A \rho \vec{V} \cdot \hat{n} dA \tag{2.19}$$

This method provides a better representation of the total quantities than the area-averaging method. Convergence problems could arise if severe reverse flow is present at the mixing plane. Therefore, for solution stability purposes, it is best if you initiate the solution with area averaging, then switch to mass averaging after reverse flow dies out.

**Important**

Mass averaging is not available with multiphase flows.

#### 2.3.2.4.3. Mixed-Out Averaging

The mixed-out averaging method is derived from the conservation of mass, momentum and energy:

$$\begin{aligned} F &= \int_A \rho (\vec{V} \cdot \hat{n}) dA \\ M_1 &= \int_A \rho (\vec{V} \cdot \hat{n}) u dA + \int_A P (\hat{e_x} \cdot \hat{n}) dA \\ M_2 &= \int_A \rho (\vec{V} \cdot \hat{n}) v dA + \int_A P \left(\hat{e_y} \cdot \hat{n}\right) dA \\ M_3 &= \int_A \rho (\vec{V} \cdot \hat{n}) w dA + \int_A P (\hat{e_z} \cdot \hat{n}) dA \\ E &= \frac{\gamma R}{(\gamma - 1)} \int_A \rho (\vec{V} \cdot \hat{n}) T dA + \frac{1}{2} \int_A \rho (\vec{V} \cdot \hat{n}) \left(u^2 + v^2 + w^2\right) dA \end{aligned} \tag{2.20}$$

Because it is based on the principles of conservation, the mixed-out average is considered a better representation of the flow since it reflects losses associated with non-uniformities in the flow profiles. However, like the mass-averaging method, convergence difficulties can arise when severe reverse flow is present across the mixing plane. Therefore, it is best if you initiate the solution with area averaging, then switch to mixed-out averaging after reverse flow dies out.

*Mixed-out averaging assumes that the fluid is a compressible ideal-gas with constant specific heat, $C_p$.*

**Important**

Mixed-out averaging is not available with multiphase flows.

### *2.3.2.5. Mixing Plane Algorithm of ANSYS Fluent*

ANSYS Fluent's basic mixing plane algorithm can be described as follows:

Release 15.0 - © SAS IP, Inc. All rights reserved. - Contains proprietary and confidential information of ANSYS, Inc. and its subsidiaries and affiliates.

1. Update the flow field solutions in the stator and rotor domains.
2. Average the flow properties at the stator exit and rotor inlet boundaries, obtaining profiles for use in updating boundary conditions.
3. Pass the profiles to the boundary condition inputs required for the stator exit and rotor inlet.
4. Repeat steps 1–3 until convergence.

**Important**

Note that it may be desirable to under-relax the changes in boundary condition values in order to prevent divergence of the solution (especially early in the computation). ANSYS Fluent allows you to control the under-relaxation of the mixing plane variables.

### 2.3.2.6. Mass Conservation

Note that the algorithm described above will not rigorously conserve mass flow across the mixing plane if it is represented by a pressure outlet and pressure inlet mixing plane pair. If you use a pressure outlet and mass flow inlet pair instead, ANSYS Fluent will force mass conservation across the mixing plane. The basic technique consists of computing the mass flow rate across the upstream zone (pressure outlet) and adjusting the mass flux profile applied at the mass flow inlet such that the downstream mass flow matches the upstream mass flow. This adjustment occurs at every iteration, therefore ensuring rigorous conservation of mass flow throughout the course of the calculation.

**Important**

Note that, since mass flow is being fixed in this case, there will be a jump in total pressure across the mixing plane. The magnitude of this jump is usually small compared with total pressure variations elsewhere in the flow field.

### 2.3.2.7. Swirl Conservation

By default, ANSYS Fluent does not conserve swirl across the mixing plane. For applications such as torque converters, where the sum of the torques acting on the components should be zero, enforcing swirl conservation across the mixing plane is essential, and is available in ANSYS Fluent as a modeling option. Ensuring conservation of swirl is important because, otherwise, sources or sinks of tangential momentum will be present at the mixing plane interface.

Consider a control volume containing a stationary or moving component (for example, a pump impeller or turbine vane). Using the moment of momentum equation from fluid mechanics, it can be shown that for steady flow,

$$T = \int_S \int r v_\theta \rho \vec{v} \cdot \hat{n} dS \tag{2.21}$$

where $T$ is the torque of the fluid acting on the component, $r$ is the radial distance from the axis of rotation, $v_\theta$ is the absolute tangential velocity, $\vec{v}$ is the total absolute velocity, and $S$ is the boundary surface. (The product $rv_\theta$ is referred to as swirl.)

For a circumferentially periodic domain, with well-defined inlet and outlet boundaries, Equation 2.21 (p. 30) becomes


Release 15.0 - © SAS IP, Inc. All rights reserved. - Contains proprietary and confidential information of ANSYS, Inc. and its subsidiaries and affiliates.

$$T = \int_{outlet} \int r v_\theta \rho \vec{v} \cdot \hat{n} dS + \int_{inlet} \int r v_\theta \rho \vec{v} \cdot \hat{n} dS \tag{2.22}$$

where inlet and outlet denote the inlet and outlet boundary surfaces.

Now consider the mixing plane interface to have a finite streamwise thickness. Applying Equation 2.22 (p. 31) to this zone and noting that, in the limit as the thickness shrinks to zero, the torque should vanish, the equation becomes

$$\int_{downstream} \int r v_\theta \rho \vec{v} \cdot \hat{n} dS = \int_{upstream} \int r v_\theta \rho \vec{v} \cdot \hat{n} dS \tag{2.23}$$

where upstream and downstream denote the upstream and downstream sides of the mixing plane interface. Note that Equation 2.23 (p. 31) applies to the full area (360 degrees) at the mixing plane interface.

Equation 2.23 (p. 31) provides a rational means of determining the tangential velocity component. That is, ANSYS Fluent computes a profile of tangential velocity and then uniformly adjusts the profile such that the swirl integral is satisfied. Note that interpolating the tangential (and radial) velocity component profiles at the mixing plane does not affect mass conservation because these velocity components are orthogonal to the face-normal velocity used in computing the mass flux.

### 2.3.2.8. Total Enthalpy Conservation

By default, ANSYS Fluent does not conserve total enthalpy across the mixing plane. For some applications, total enthalpy conservation across the mixing plane is very desirable, because global parameters such as efficiency are directly related to the change in total enthalpy across a blade row or stage. This is available in ANSYS Fluent as a modeling option.

The procedure for ensuring conservation of total enthalpy simply involves adjusting the downstream total temperature profile such that the integrated total enthalpy matches the upstream integrated total enthalpy. For multiphase flows, conservation of mass, swirl, and enthalpy are calculated for each phase. However, for the Eulerian multiphase model, since mass flow inlets are not permissible, conservation of the above quantities does not occur.

Release 15.0 - © SAS IP, Inc. All rights reserved. - Contains proprietary and confidential information of ANSYS, Inc. and its subsidiaries and affiliates.

Release 15.0 - © SAS IP, Inc. All rights reserved. - Contains proprietary and confidential information
of ANSYS, Inc. and its subsidiaries and affiliates.

# Chapter 3: Flows Using Sliding and Dynamic Meshes

This chapter describes the theoretical background of the sliding and dynamic mesh models in ANSYS Fluent. To learn more about using sliding meshes in ANSYS Fluent, see Using Sliding Meshes in the User's Guide. For more information about using dynamic meshes in ANSYS Fluent, see Using Dynamic Meshes in the User's Guide.

Theoretical information about sliding and dynamic mesh models is presented in the following sections:

3.1. Introduction
3.2. Dynamic Mesh Theory
3.3. Sliding Mesh Theory

## 3.1. Introduction

The dynamic mesh model allows you to move the boundaries of a cell zone relative to other boundaries of the zone, and to adjust the mesh accordingly. The motion of the boundaries can be *rigid*, such as pistons moving inside an engine cylinder (see Figure 3.1: A Mesh Associated With Moving Pistons (p. 33)) or a flap deflecting on an aircraft wing, or *deforming*, such as the elastic wall of a balloon during inflation or a flexible artery wall responding to the pressure pulse from the heart. In either case, the nodes that define the cells in the domain must be updated as a function of time, and hence the dynamic mesh solutions are inherently unsteady. The governing equations describing the fluid motion (which are different from those used for moving reference frames, as described in Flows with Moving Reference Frames (p. 17)) are described in Dynamic Mesh Theory (p. 34).

**Figure 3.1: A Mesh Associated With Moving Pistons**

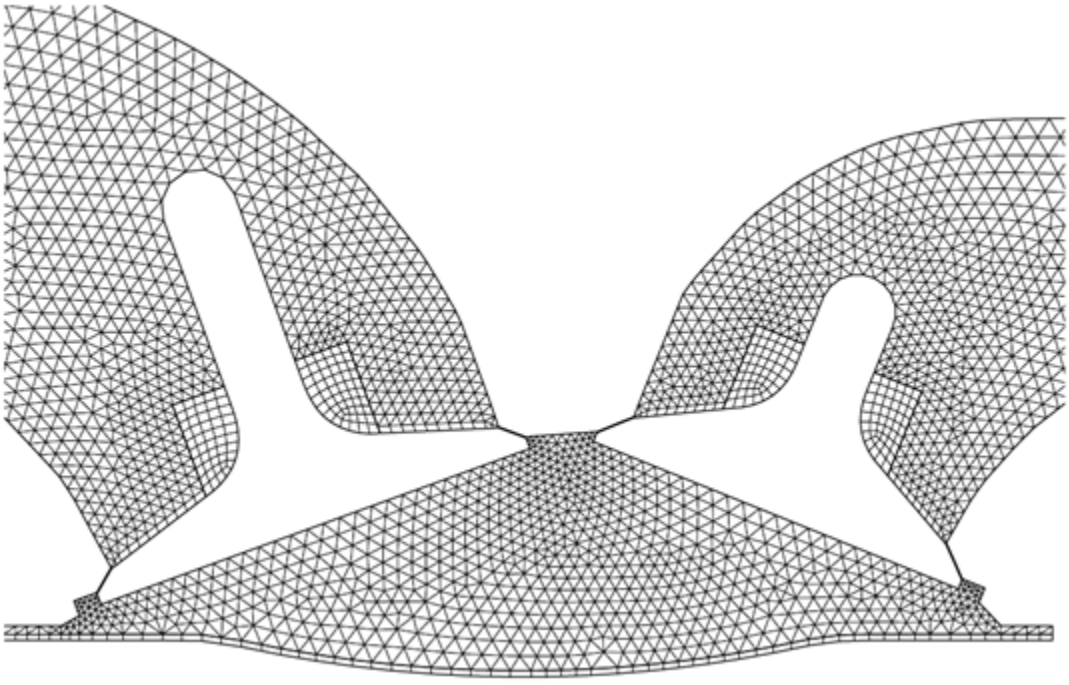

Release 15.0 - © SAS IP, Inc. All rights reserved. - Contains proprietary and confidential information of ANSYS, Inc. and its subsidiaries and affiliates.

An important special case of dynamic mesh motion is called the sliding mesh in which all of the boundaries and the cells of a given mesh zone move together in a rigid-body motion. In this situation, the nodes of the mesh move in space (relative to the fixed, global coordinates), but the cells defined by the nodes do not deform. Furthermore, mesh zones moving adjacent to one another can be linked across one or more non-conformal interfaces. As long as the interfaces stay in contact with one another (that is, "slide" along a common overlap boundary at the interface), the non-conformal interfaces can be dynamically updated as the meshes move, and fluid can pass from one zone to the other. Such a scenario is referred to as the sliding mesh model in ANSYS Fluent. Examples of sliding mesh model usage include modeling rotor-stator interaction between a moving blade and a stationary vane in a compressor or turbine, modeling a blower with rotating blades and a stationary casing (see Figure 3.2: Blower (p. 34)), and modeling a train moving in a tunnel by defining sliding interfaces between the train and the tunnel walls.

**Figure 3.2: Blower**

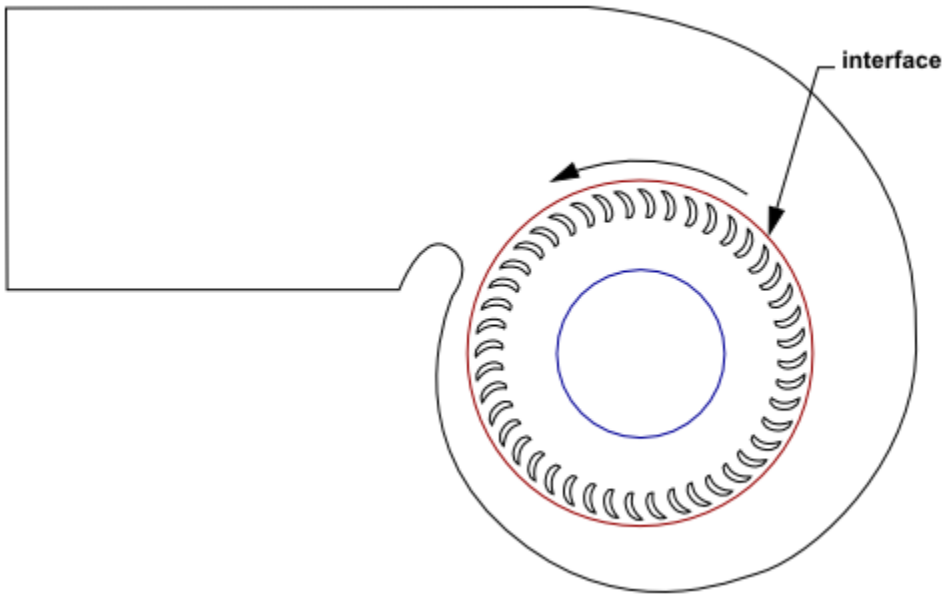


## 3.2. Dynamic Mesh Theory

The dynamic mesh model in ANSYS Fluent can be used to model flows where the shape of the domain is changing with time due to motion on the domain boundaries. The dynamic mesh model can be applied to single or multiphase flows (and multi-species flows). The generic transport equation (Equation 3.1 (p. 35)) applies to all applicable model equations, such as turbulence, energy, species, phases, etc. The dynamic mesh model can also be used for steady-state applications, when it is beneficial to move the mesh in the steady-state solver. The motion can be a prescribed motion (for example, you can specify the linear and angular velocities about the center of gravity of a solid body with time) or an unprescribed motion where the subsequent motion is determined based on the solution at the current time (for example, the linear and angular velocities are calculated from the force balance on a solid body, as is done by the six degree of freedom (6DOF) solver; see Using the Six DOF Solver in the User's Guide). The update of the volume mesh is handled automatically by ANSYS Fluent at each time step based on the new positions of the boundaries. To use the dynamic mesh model, you need to provide a starting volume mesh and the description of the motion of any moving zones in the model. ANSYS Fluent allows you to describe the motion using either boundary profiles, user-defined functions (UDFs), or the six degree of freedom solver.

ANSYS Fluent expects the description of the motion to be specified on either face or cell zones. If the model contains moving and non-moving regions, you need to identify these regions by grouping them


Release 15.0 - © SAS IP, Inc. All rights reserved. - Contains proprietary and confidential information of ANSYS, Inc. and its subsidiaries and affiliates.

into their respective face or cell zones in the starting volume mesh that you generate. Furthermore, regions that are deforming due to motion on their adjacent regions must also be grouped into separate zones in the starting volume mesh. The boundary between the various regions need not be conformal. You can use the non-conformal or sliding interface capability in ANSYS Fluent to connect the various zones in the final model.

Information about dynamic mesh theory is presented in the following sections:

3.2.1. Conservation Equations
3.2.2. Six DOF (6DOF) Solver Theory

## 3.2.1. Conservation Equations

With respect to dynamic meshes, the integral form of the conservation equation for a general scalar, $\phi$, on an arbitrary control volume, $V$, whose boundary is moving can be written as

$$\frac{d}{dt}\int_V \rho\phi dV + \int_{\partial V} \rho\phi\left(\vec{u}-\vec{u}_g\right)\cdot d\vec{A} = \int_{\partial V} \Gamma\nabla\phi\cdot d\vec{A} + \int_V S_\phi dV \tag{3.1}$$

where

$\rho$ is the fluid density

$\vec{u}$ is the flow velocity vector

$\vec{u}_g$ is the mesh velocity of the moving mesh

$\Gamma$ is the diffusion coefficient

$S_\phi$ is the source term of $\phi$

Here, $\partial V$ is used to represent the boundary of the control volume, $V$.

By using a first-order backward difference formula, the time derivative term in Equation 3.1 (p. 35) can be written as

$$\frac{d}{dt}\int_V \rho\phi dV = \frac{(\rho\phi V)^{n+1}-(\rho\phi V)^{n}}{\Delta t} \tag{3.2}$$

where $n$ and $n+1$ denote the respective quantity at the current and next time level, respectively. The $(n+1)$ th time level volume, $V^{n+1}$, is computed from

$$V^{n+1} = V^n + \frac{dV}{dt}\Delta t \tag{3.3}$$

where $dV/dt$ is the volume time derivative of the control volume. In order to satisfy the mesh conservation law, the volume time derivative of the control volume is computed from

$$\frac{dV}{dt} = \int_{\partial V} \vec{u}_g\cdot d\vec{A} = \sum_j^{n_f} \vec{u}_{g,j}\cdot\vec{A}_j \tag{3.4}$$

where $n_f$ is the number of faces on the control volume and $\vec{A}_j$ is the $j$ face area vector. The dot product $\vec{u}_{g,j}\cdot\vec{A}_j$ on each control volume face is calculated from

$$\vec{u}_{g,j} \cdot \vec{A}_j = \frac{\delta V_j}{\Delta t} \tag{3.5}$$

where $\delta V_j$ is the volume swept out by the control volume face $j$ over the time step $\Delta t$.

By using a second-order backward difference formula, the time derivative in Equation 3.1 (p. 35) can be written as

$$\frac{d}{dt}\int_V \rho\phi dV = \frac{3\,(\rho\phi V)^{n+1} - 4\,(\rho\phi V)^{n} + (\rho\phi V)^{n-1}}{2\,\Delta t} \tag{3.6}$$

where $n+1$, $n$, and $n-1$ denote the respective quantities from successive time levels with $n+1$ denoting the current time level.

In the case of a second-order difference scheme the volume time derivative of the control volume is computed in the same manner as in the first-order scheme as shown in Equation 3.4 (p. 35). For the second-order differencing scheme, the dot product $\vec{u}_{g,j} \cdot \vec{A}_j$ on each control volume face is calculated from

$$\left(\vec{u}_{g,j} \cdot \vec{A}_j\right)^{n+1} = \frac{3}{2}\left(\vec{u}_{g,j} \cdot \vec{A}_j\right)^{n} - \frac{1}{2}\left(\vec{u}_{g,j} \cdot \vec{A}_j\right)^{n-1} = \frac{3}{2}\left(\frac{\delta V_j}{\delta t}\right)^{n} - \frac{1}{2}\left(\frac{\delta V_j}{\delta t}\right)^{n-1} \tag{3.7}$$

where $\left(\delta V_j\right)^n$ and $\left(\delta V_j\right)^{n-1}$ are the volumes swept out by control volume faces at the current and previous time levels over a time step.

## 3.2.2. Six DOF (6DOF) Solver Theory

The 6DOF solver in ANSYS Fluent uses the object's forces and moments in order to compute the translational and angular motion of the center of gravity of an object. The governing equation for the translational motion of the center of gravity is solved for in the inertial coordinate system:

$$\dot{\vec{v}}_G = \frac{1}{m}\sum \vec{f}_G \tag{3.8}$$

where $\dot{\vec{v}}_G$ is the translational motion of the center of gravity, $m$ is the mass, and $\vec{f}_G$ is the force vector due to gravity.

The angular motion of the object, $\dot{\vec{\omega}}_B$, is more easily computed using body coordinates:

$$\dot{\vec{\omega}}_B = L^{-1}\left(\sum \vec{M}_B - \vec{\omega}_B \times L\vec{\omega}_B\right) \tag{3.9}$$

where $L$ is the inertia tensor, $\vec{M}_B$ is the moment vector of the body, and $\vec{\omega}_B$ is the rigid body angular velocity vector.

The moments are transformed from inertial to body coordinates using

$$\vec{M}_B = R\vec{M}_G \tag{3.10}$$

where, $R$ represents the following transformation matrix:


Release 15.0 - © SAS IP, Inc. All rights reserved. - Contains proprietary and confidential information of ANSYS, Inc. and its subsidiaries and affiliates.

$$\begin{matrix} C_\theta C_\psi & C_\theta S_\psi & -S_\theta \\ S_\phi S_\theta C_\psi - C_\phi S_\psi & S_\phi S_\theta S_\psi + C_\phi C_\psi & S_\phi C_\theta \\ C_\phi S_\theta C_\psi + S_\phi S_\psi & C_\phi S_\theta S_\psi - S_\phi C_\psi & C_\phi C_\theta \end{matrix}$$

where, in generic terms, $C_\chi = cos(\chi)$ and $S_\chi = sin(\chi)$. The angles $\phi, \theta$, and $\psi$ are Euler angles that represent the following sequence of rotations:

- rotation about the x-axis (for example, roll for airplanes)
- rotation about the y-axis (for example, pitch for airplanes)
- rotation about the z-axis (for example, yaw for airplanes)

After the angular and the translational accelerations are computed from Equation 3.8 (p. 36) and Equation 3.9 (p. 36), the rates are derived by numerical integration [421] (p. 752). The angular and translational velocities are used in the dynamic mesh calculations to update the rigid body position.

## 3.3. Sliding Mesh Theory

As mentioned previously, the sliding mesh model is a special case of general dynamic mesh motion wherein the nodes move rigidly in a given dynamic mesh zone. Additionally, multiple cells zones are connected with each other through non-conformal interfaces. As the mesh motion is updated in time, the non-conformal interfaces are likewise updated to reflect the new positions each zone. It is important to note that the mesh motion must be prescribed such that zones linked through non-conformal interfaces remain in contact with each other (that is, "slide" along the interface boundary) if you want fluid to be able to flow from one mesh to the other. Any portion of the interface where there is no contact is treated as a wall, as described in Non-Conformal Meshes in the User's Guide.

The general conservation equation formulation for dynamic meshes, as expressed in Equation 3.1 (p. 35), is also used for sliding meshes. Because the mesh motion in the sliding mesh formulation is rigid, all cells retain their original shape and volume. As a result, the time rate of change of the cell volume is zero, and Equation 3.3 (p. 35) simplifies to:

$$V^{n+1} = V^n \tag{3.11}$$

and Equation 3.2 (p. 35) becomes:

$$\frac{d}{dt}\int_V \rho\phi dV = \frac{\left[(\rho\phi)^{n+1} - (\rho\phi)^n\right]V}{\Delta t} \tag{3.12}$$

Additionally, Equation 3.4 (p. 35) simplifies to

$$\sum_j^{n_f} \vec{u}_{g,j} \cdot \vec{A}_j = 0 \tag{3.13}$$

Equation 3.1 (p. 35), in conjunction with the above simplifications, permits the flow in the moving mesh zones to be updated, provided that an appropriate specification of the rigid mesh motion is defined for each zone (usually this is simple linear or rotation motion, but more complex motions can be used). Note that due to the fact that the mesh is moving, the solutions to Equation 3.1 (p. 35) for sliding mesh applications will be inherently unsteady (as they are for all dynamic meshes).

Release 15.0 - © SAS IP, Inc. All rights reserved. - Contains proprietary and confidential information of ANSYS, Inc. and its subsidiaries and affiliates.

Release 15.0 - © SAS IP, Inc. All rights reserved. - Contains proprietary and confidential information
of ANSYS, Inc. and its subsidiaries and affiliates.

# Chapter 4: Turbulence

This chapter provides theoretical background about the turbulence models available in ANSYS Fluent. Information is presented in the following sections:


4.1. Underlying Principles of Turbulence Modeling
4.2. Spalart-Allmaras Model
4.3. Standard, RNG, and Realizable k-ε Models
4.4. Standard and SST k-ω Models
4.5. k-kl-ω Transition Model
4.6. Transition SST Model
4.7. Intermittency Transition Model
4.8. The V2F Model
4.9. Reynolds Stress Model (RSM)
4.10. Scale-Adaptive Simulation (SAS) Model
4.11. Detached Eddy Simulation (DES)
4.12. Large Eddy Simulation (LES) Model
4.13. Embedded Large Eddy Simulation (ELES)
4.14. Near-Wall Treatments for Wall-Bounded Turbulent Flows
4.15. Curvature Correction for the Spalart-Allmaras and Two-Equation Models
4.16. Production Limiters for Two-Equation Models


For more information about using these turbulence models in ANSYS Fluent, see Modeling Turbulence in the User's Guide.

## 4.1. Underlying Principles of Turbulence Modeling

The following sections provide an overview of the underlying principles for turbulence modeling.


4.1.1. Reynolds (Ensemble) Averaging
4.1.2. Filtered Navier-Stokes Equations
4.1.3. Hybrid RANS-LES Formulations
4.1.4. Boussinesq Approach vs. Reynolds Stress Transport Models


### 4.1.1. Reynolds (Ensemble) Averaging

In Reynolds averaging, the solution variables in the instantaneous (exact) Navier-Stokes equations are decomposed into the mean (ensemble-averaged or time-averaged) and fluctuating components. For the velocity components:

$$u_i = \bar{u}_i + u'_i \tag{4.1}$$

where $\bar{u}_i$ and $u'_i$ are the mean and fluctuating velocity components ($i = 1, 2, 3$).

Likewise, for pressure and other scalar quantities:

$$\phi = \overline{\phi} + \phi' \tag{4.2}$$

where $\phi$ denotes a scalar such as pressure, energy, or species concentration.


Release 15.0 - © SAS IP, Inc. All rights reserved. - Contains proprietary and confidential information of ANSYS, Inc. and its subsidiaries and affiliates.

Substituting expressions of this form for the flow variables into the instantaneous continuity and momentum equations and taking a time (or ensemble) average (and dropping the overbar on the mean velocity, $\bar{u}$) yields the ensemble-averaged momentum equations. They can be written in Cartesian tensor form as:

$$\frac{\partial \rho}{\partial t} + \frac{\partial}{\partial x_i}(\rho u_i) = 0 \tag{4.3}$$

$$\frac{\partial}{\partial t}(\rho u_i) + \frac{\partial}{\partial x_j}\left(\rho u_i u_j\right) = -\frac{\partial p}{\partial x_i} + \frac{\partial}{\partial x_j}\left[\mu\left(\frac{\partial u_i}{\partial x_j} + \frac{\partial u_j}{\partial x_i} - \frac{2}{3}\delta_{ij}\frac{\partial u_l}{\partial x_l}\right)\right] + \frac{\partial}{\partial x_j}\left(-\rho\overline{u_i' u_j'}\right) \tag{4.4}$$

Equation 4.3 (p. 40) and Equation 4.4 (p. 40) are called Reynolds-averaged Navier-Stokes (RANS) equations. They have the same general form as the instantaneous Navier-Stokes equations, with the velocities and other solution variables now representing ensemble-averaged (or time-averaged) values. Additional terms now appear that represent the effects of turbulence. These Reynolds stresses, $-\rho\overline{u_i' u_j'}$, must be modeled in order to close Equation 4.4 (p. 40).

For variable-density flows, Equation 4.3 (p. 40) and Equation 4.4 (p. 40) can be interpreted as Favre-averaged Navier-Stokes equations [164] (p. 738), with the velocities representing mass-averaged values. As such, Equation 4.3 (p. 40) and Equation 4.4 (p. 40) can be applied to variable-density flows.

### 4.1.2. Filtered Navier-Stokes Equations

The governing equations employed for LES are obtained by filtering the time-dependent Navier-Stokes equations in either Fourier (wave-number) space or configuration (physical) space. The filtering process effectively filters out the eddies whose scales are smaller than the filter width or grid spacing used in the computations. The resulting equations therefore govern the dynamics of large eddies.

A filtered variable (denoted by an overbar) is defined by flu_th_eq_turb_les_filter_variable

$$\overline{\phi}(x) = \int_D \phi(x')\, G(x, x')\, dx' \tag{4.5}$$

where $D$ is the fluid domain, and $G$ is the filter function that determines the scale of the resolved eddies.

In ANSYS Fluent, the finite-volume discretization itself implicitly provides the filtering operation:

$$\overline{\phi}(x) = \frac{1}{V}\int_v \phi(x')\, dx', x' \in v \tag{4.6}$$

where $V$ is the volume of a computational cell. The filter function, $G(x, x')$, implied here is then

$$G(x, x') = \begin{cases} 1/V, & x' \in v \\ 0, & x' otherwise \end{cases} \tag{4.7}$$

The LES capability in ANSYS Fluent is applicable to compressible and incompressible flows. For the sake of concise notation, however, the theory that follows begins with a discussion of incompressible flows.

Filtering the continuity and momentum equations, one obtains


Release 15.0 - © SAS IP, Inc. All rights reserved. - Contains proprietary and confidential information of ANSYS, Inc. and its subsidiaries and affiliates.

$$\frac{\partial \rho}{\partial t}+\frac{\partial}{\partial x_i}(\rho \overline{u}_i)=0 \tag{4.8}$$

and

$$\frac{\partial}{\partial t}(\rho \overline{u}_i)+\frac{\partial}{\partial x_j}\left(\rho \overline{u}_i \overline{u}_j\right)=\frac{\partial}{\partial x_j}\left(\sigma_{ij}\right)-\frac{\partial \overline{p}}{\partial x_i}-\frac{\partial \tau_{ij}}{\partial x_j} \tag{4.9}$$

where $\sigma_{ij}$ is the stress tensor due to molecular viscosity defined by

$$\sigma_{ij}\equiv\left[\mu\left(\frac{\partial \overline{u}_i}{\partial x_j}+\frac{\partial \overline{u}_j}{\partial x_i}\right)\right]-\frac{2}{3}\mu\frac{\partial \overline{u}_l}{\partial x_l}\delta_{ij} \tag{4.10}$$

and $\tau_{ij}$ is the subgrid-scale stress defined by and $\tau_{ij}$ is the subgrid-scale stress defined by

$$\tau_{ij}\equiv\rho\overline{u_i u_j}-\rho\overline{u}_i\overline{u}_j \tag{4.11}$$

Filtering the energy equation, one obtains:

$$\frac{\partial \rho \overline{h_s}}{\partial t}+\frac{\partial \rho \overline{u_i}\,\overline{h_s}}{\partial x_i}-\frac{\partial \overline{p}}{\partial t}-\overline{u_j}\frac{\partial \overline{p}}{\partial x_i}-\frac{\partial}{\partial x_i}\left(\lambda\frac{\partial \overline{T}}{\partial x_i}\right)=-\frac{\partial}{\partial x_j}\left[\underbrace{\rho(\overline{u_i h_s}-\overline{u_i}\,\overline{h_s})}_{\text{subgrid enthalpy flux}}\right] \tag{4.12}$$

where $h_s$ and $\lambda$ are the sensible enthalpy and thermal conductivity, respectively.

The subgrid enthalpy flux term in the Equation 4.12 (p. 41) is approximated using the gradient hypothesis:

$$\rho(\overline{u_i h_s}-\overline{u_i}\,\overline{h_s})=-\frac{\mu_{\text{SGS}}C_p}{\text{Pr}_{\text{SGS}}}\frac{\partial \overline{T}}{\partial x_j} \tag{4.13}$$

where $\mu_{\text{SGS}}$ is a subgrid viscosity, and $\text{Pr}_{\text{SGS}}$ is a subgrid Prandtl number equal to 0.85.

### 4.1.3. Hybrid RANS-LES Formulations

At first, the concepts of Reynolds Averaging and Spatial Filtering seem incompatible, as they result in different additional terms in the momentum equations (Reynolds Stresses and sub-grid stresses). This would preclude hybrid models like Scale-Adaptive Simulation (SAS) or Detached Eddy Simulation (DES), which are based on one set of momentum equations throughout the RANS and LES portions of the domain. However, it is important to note that once a turbulence model is introduced into the momentum equations, they no longer carry any information concerning their derivation (averaging). Case in point is that the most popular models, both in RANS and LES, are eddy viscosity models that are used to substitute either the Reynolds- or the sub-grid stress tensor. After the introduction of an eddy viscosity (turbulent viscosity), both the RANS and LES momentum equations are formally identical. The difference lies exclusively in the size of the eddy-viscosity provided by the underlying turbulence model. This allows the formulation of turbulence models that can switch from RANS to LES mode, by lowering the eddy viscosity in the LES zone appropriately, without any formal change to the momentum equations.

Release 15.0 - © SAS IP, Inc. All rights reserved. - Contains proprietary and confidential information of ANSYS, Inc. and its subsidiaries and affiliates.

### 4.1.4. Boussinesq Approach vs. Reynolds Stress Transport Models

The Reynolds-averaged approach to turbulence modeling requires that the Reynolds stresses in Equation 4.4 (p. 40) are appropriately modeled. A common method employs the Boussinesq hypothesis [164] (p. 738) to relate the Reynolds stresses to the mean velocity gradients:

$$-\rho\overline{u_i'u_j'} = \mu_t\left(\frac{\partial u_i}{\partial x_j}+\frac{\partial u_j}{\partial x_i}\right)-\frac{2}{3}\left(\rho k+\mu_t\frac{\partial u_k}{\partial x_k}\right)\delta_{ij} \tag{4.14}$$

The Boussinesq hypothesis is used in the Spalart-Allmaras model, the $k$-$\varepsilon$ models, and the $k$-$\omega$ models. The advantage of this approach is the relatively low computational cost associated with the computation of the turbulent viscosity, $\mu_t$. In the case of the Spalart-Allmaras model, only one additional transport equation (representing turbulent viscosity) is solved. In the case of the $k$-$\varepsilon$ and $k$-$\omega$ models, two additional transport equations (for the turbulence kinetic energy, $k$, and either the turbulence dissipation rate, $\varepsilon$, or the specific dissipation rate, $\omega$) are solved, and $\mu_t$ is computed as a function of $k$ and $\varepsilon$ or $k$ and $\omega$. The disadvantage of the Boussinesq hypothesis as presented is that it assumes $\mu_t$ is an isotropic scalar quantity, which is not strictly true. However the assumption of an isotropic turbulent viscosity typically works well for shear flows dominated by only one of the turbulent shear stresses. This covers many technical flows, such as wall boundary layers, mixing layers, jets, etc.

The alternative approach, embodied in the RSM, is to solve transport equations for each of the terms in the Reynolds stress tensor. An additional scale-determining equation (normally for $\varepsilon$ or $\omega$) is also required. This means that five additional transport equations are required in 2D flows and seven additional transport equations must be solved in 3D.

In many cases, models based on the Boussinesq hypothesis perform very well, and the additional computational expense of the Reynolds stress model is not justified. However, the RSM is clearly superior in situations where the anisotropy of turbulence has a dominant effect on the mean flow. Such cases include highly swirling flows and stress-driven secondary flows.

## 4.2. Spalart-Allmaras Model

This section describes the theory behind the Spalart-Allmaras model. Information is presented in the following sections:

4.2.1. Overview
4.2.2. Transport Equation for the Spalart-Allmaras Model
4.2.3. Modeling the Turbulent Viscosity
4.2.4. Modeling the Turbulent Production
4.2.5. Modeling the Turbulent Destruction
4.2.6. Model Constants
4.2.7. Wall Boundary Conditions
4.2.8. Convective Heat and Mass Transfer Modeling

For details about using the model in ANSYS Fluent, see Modeling Turbulence and Setting Up the Spalart-Allmaras Model in the User's Guide.

### 4.2.1. Overview

The Spalart-Allmaras model [426] (p. 752) is a one-equation model that solves a modeled transport equation for the kinematic eddy (turbulent) viscosity. The Spalart-Allmaras model was designed specifically for aerospace applications involving wall-bounded flows and has been shown to give good results for


Release 15.0 - © SAS IP, Inc. All rights reserved. - Contains proprietary and confidential information of ANSYS, Inc. and its subsidiaries and affiliates.

boundary layers subjected to adverse pressure gradients. It is also gaining popularity in turbomachinery applications.

In its original form, the Spalart-Allmaras model is effectively a low-Reynolds number model, requiring the viscosity-affected region of the boundary layer to be properly resolved ($y^+ \sim 1$ meshes). In ANSYS Fluent, the Spalart-Allmaras model has been extended with a $y^+$-insensitive wall treatment (Enhanced Wall Treatment), which allows the application of the model independent of the near wall $y^+$ resolution. The formulation blends automatically from a viscous sublayer formulation to a logarithmic formulation based on $y^+$. On intermediate grids, $(1 < y^+ < 30)$, the formulation maintains its integrity and provides consistent wall shear stress and heat transfer coefficients. While the $y^+$ sensitivity is removed, it still should be ensured that the boundary layer is resolved with a minimum resolution of 10-15 cells.

The Spalart-Allmaras model was developed for aerodynamic flows. It is not calibrated for general industrial flows, and does produce relatively larger errors for some free shear flows, especially plane and round jet flows. In addition, it cannot be relied on to predict the decay of homogeneous, isotropic turbulence.

## 4.2.2. Transport Equation for the Spalart-Allmaras Model

The transported variable in the Spalart-Allmaras model, $\tilde{\nu}$, is identical to the turbulent kinematic viscosity except in the near-wall (viscosity-affected) region. The transport equation for $\tilde{\nu}$ is

$$\frac{\partial}{\partial t}(\rho\tilde{\nu}) + \frac{\partial}{\partial x_i}(\rho\tilde{\nu}u_i) = G_\nu + \frac{1}{\sigma_{\tilde{\nu}}}\left[\frac{\partial}{\partial x_j}\left\{(\mu+\rho\tilde{\nu})\frac{\partial\tilde{\nu}}{\partial x_j}\right\} + C_{b2}\rho\left(\frac{\partial\tilde{\nu}}{\partial x_j}\right)^2\right] - Y_\nu + S_{\tilde{\nu}} \tag{4.15}$$

where $G_\nu$ is the production of turbulent viscosity, and $Y_\nu$ is the destruction of turbulent viscosity that occurs in the near-wall region due to wall blocking and viscous damping. $\sigma_{\tilde{\nu}}$ and $C_{b2}$ are the constants and $\nu$ is the molecular kinematic viscosity. $S_{\tilde{\nu}}$ is a user-defined source term. Note that since the turbulence kinetic energy, $k$, is not calculated in the Spalart-Allmaras model, the last term in Equation 4.14 (p. 42) is ignored when estimating the Reynolds stresses.

## 4.2.3. Modeling the Turbulent Viscosity

The turbulent viscosity, $\mu_t$, is computed from

$$\mu_t = \rho\tilde{\nu}f_{\nu 1} \tag{4.16}$$

where the viscous damping function, $f_{\nu 1}$, is given by

$$f_{\nu 1} = \frac{\chi^3}{\chi^3 + C_{\nu 1}^3} \tag{4.17}$$

and

$$\chi \equiv \frac{\tilde{\nu}}{\nu} \tag{4.18}$$

Release 15.0 - © SAS IP, Inc. All rights reserved. - Contains proprietary and confidential information of ANSYS, Inc. and its subsidiaries and affiliates.

## 4.2.4. Modeling the Turbulent Production

The production term, $G_v$, is modeled as

$$G_v = C_{b1}\rho\tilde{S}\tilde{\nu} \tag{4.19}$$

where

$$\tilde{S} \equiv S + \frac{\tilde{\nu}}{\kappa^2 d^2} f_{v2} \tag{4.20}$$

and

$$f_{v2} = 1 - \frac{\chi}{1 + \chi f_{v1}} \tag{4.21}$$

$C_{b1}$ and $\kappa$ are constants, $d$ is the distance from the wall, and $S$ is a scalar measure of the deformation tensor. By default in ANSYS Fluent, as in the original model proposed by Spalart and Allmaras, $S$ is based on the magnitude of the vorticity:

$$S \equiv \sqrt{2\Omega_{ij}\Omega_{ij}} \tag{4.22}$$

where $\Omega_{ij}$ is the mean rate-of-rotation tensor and is defined by

$$\Omega_{ij} = \frac{1}{2}\left(\frac{\partial u_i}{\partial x_j} - \frac{\partial u_j}{\partial x_i}\right) \tag{4.23}$$

The justification for the default expression for $S$ is that, for shear flows, vorticity and strain rate are identical. Vorticity has the advantage of being zero in inviscid flow regions like stagnation lines, where turbulence production due to strain rate can be unphysical. However, an alternative formulation has been proposed [83] (p. 733) and incorporated into ANSYS Fluent.

This modification combines the measures of both vorticity and the strain tensors in the definition of $S$:

$$S \equiv |\Omega_{ij}| + C_{prod} \min\left(0, |S_{ij}| - |\Omega_{ij}|\right) \tag{4.24}$$

where

$$C_{prod} = 2.0, \quad |\Omega_{ij}| \equiv \sqrt{2\Omega_{ij}\Omega_{ij}}, \quad |S_{ij}| \equiv \sqrt{2S_{ij}S_{ij}}$$

with the mean strain rate, $S_{ij}$, defined as

$$S_{ij} = \frac{1}{2}\left(\frac{\partial u_j}{\partial x_i} + \frac{\partial u_i}{\partial x_j}\right) \tag{4.25}$$

Including both the rotation and strain tensors reduces the production of eddy viscosity and consequently reduces the eddy viscosity itself in regions where the measure of vorticity exceeds that of strain rate. One such example can be found in vortical flows, that is, flow near the core of a vortex subjected to a pure rotation where turbulence is known to be suppressed. Including both the rotation and strain tensors more accurately accounts for the effects of rotation on turbulence. The default option (including the rotation tensor only) tends to overpredict the production of eddy viscosity and hence over-predicts the eddy viscosity itself inside vortices.


Release 15.0 - © SAS IP, Inc. All rights reserved. - Contains proprietary and confidential information of ANSYS, Inc. and its subsidiaries and affiliates.

You can select the modified form for calculating production in the Viscous Model Dialog Box.

## 4.2.5. Modeling the Turbulent Destruction

The destruction term is modeled as

$$Y_v = C_{w1}\rho f_w \left(\frac{\tilde{\nu}}{d}\right)^2 \tag{4.26}$$

where

$$f_w = g\left[\frac{1+C_{w3}^6}{g^6+C_{w3}^6}\right]^{1/6} \tag{4.27}$$

$$g = r + C_{w2}\left(r^6 - r\right) \tag{4.28}$$

$$r \equiv \frac{\tilde{\nu}}{\tilde{S}\kappa^2 d^2} \tag{4.29}$$

$C_{w1}$, $C_{w2}$, and $C_{w3}$ are constants, and $\tilde{S}$ is given by Equation 4.20 (p. 44). Note that the modification described above to include the effects of mean strain on $S$ will also affect the value of $\tilde{S}$ used to compute $r$.

## 4.2.6. Model Constants

The model constants $C_{b1}$, $C_{b2}$, $\sigma_{\tilde{\nu}}$, $C_{v1}$, $C_{w1}$, $C_{w2}$, $C_{w3}$, and $\kappa$ have the following default values [426] (p. 752):

$$C_{b1} = 0.1355,\ C_{b2} = 0.622,\ \sigma_{\tilde{\nu}} = \frac{2}{3},\ C_{v1} = 7.1$$

$$C_{w1} = \frac{C_{b1}}{\kappa^2} + \frac{(1+C_{b2})}{\sigma_{\tilde{\nu}}},\ C_{w2} = 0.3,\ C_{w3} = 2.0,\ \kappa = 0.4187$$

## 4.2.7. Wall Boundary Conditions

The Spalart-Allmaras model has been extended within ANSYS Fluent with a $y^+$-insensitive wall treatment (Enhanced Wall Treatment (EWT)). The EWT automatically blends all solution variables from their viscous sublayer formulation

$$\frac{u}{u_\tau} = \frac{\rho u_\tau y}{\mu} \tag{4.30}$$

to the corresponding logarithmic layer values depending on $y^+$.

$$\frac{u}{u_\tau} = \frac{1}{\kappa}\ln E\left(\frac{\rho u_\tau y}{\mu}\right) \tag{4.31}$$

where $u$ is the velocity parallel to the wall, $u_\tau$ is the shear velocity, $y$ is the distance from the wall, $\kappa$ is the von Kármán constant (0.4187), and $E = 9.793$.

Release 15.0 - © SAS IP, Inc. All rights reserved. - Contains proprietary and confidential information of ANSYS, Inc. and its subsidiaries and affiliates.

The blending is calibrated to also cover intermediate $y^+$ values in the buffer layer $(1<y^+<30)$.

### 4.2.8. Convective Heat and Mass Transfer Modeling

In ANSYS Fluent, turbulent heat transport is modeled using the concept of the Reynolds analogy to turbulent momentum transfer. The "modeled" energy equation is as follows:

$$\frac{\partial}{\partial t}(\rho E)+\frac{\partial}{\partial x_i}[u_i(\rho E+p)]=\frac{\partial}{\partial x_j}\left[\left(k+\frac{c_p\mu_t}{Pr_t}\right)\frac{\partial T}{\partial x_j}+u_i\left(\tau_{ij}\right)_{eff}\right]+S_h \tag{4.32}$$

where $k$, in this case, is the thermal conductivity, $E$ is the total energy, and $\left(\tau_{ij}\right)_{eff}$ is the deviatoric stress tensor, defined as

$$\left(\tau_{ij}\right)_{eff}=\mu_{eff}\left(\frac{\partial u_j}{\partial x_i}+\frac{\partial u_i}{\partial x_j}\right)-\frac{2}{3}\mu_{eff}\frac{\partial u_k}{\partial x_k}\delta_{ij}$$

## 4.3. Standard, RNG, and Realizable k-ε Models

This section describes the theory behind the Standard, RNG, and Realizable $k$-$\varepsilon$ models. Information is presented in the following sections:


4.3.1. Standard k-ε Model
4.3.2. RNG k-ε Model
4.3.3. Realizable k-ε Model
4.3.4. Modeling Turbulent Production in the k-ε Models
4.3.5. Effects of Buoyancy on Turbulence in the k-ε Models
4.3.6. Effects of Compressibility on Turbulence in the k-ε Models
4.3.7. Convective Heat and Mass Transfer Modeling in the k-ε Models


For details about using the models in ANSYS Fluent, see Modeling Turbulence and Setting Up the k-ε Model in the User's Guide.

This section presents the standard, RNG, and realizable $k$-$\varepsilon$ models. All three models have similar forms, with transport equations for $k$ and $\varepsilon$. The major differences in the models are as follows:

- the method of calculating turbulent viscosity
- the turbulent Prandtl numbers governing the turbulent diffusion of $k$ and $\varepsilon$
- the generation and destruction terms in the $\varepsilon$ equation

The transport equations, the methods of calculating turbulent viscosity, and model constants are presented separately for each model. The features that are essentially common to all models follow, including turbulent generation due to shear buoyancy, accounting for the effects of compressibility, and modeling heat and mass transfer.


Release 15.0 - © SAS IP, Inc. All rights reserved. - Contains proprietary and confidential information of ANSYS, Inc. and its subsidiaries and affiliates.

## 4.3.1. Standard k-ε Model

### 4.3.1.1. Overview

Two-equation turbulence models allow the determination of both, a turbulent length and time scale by solving two separate transport equations. The standard $k$-$\varepsilon$ model in ANSYS Fluent falls within this class of models and has become the workhorse of practical engineering flow calculations in the time since it was proposed by Launder and Spalding [231] (p. 741). Robustness, economy, and reasonable accuracy for a wide range of turbulent flows explain its popularity in industrial flow and heat transfer simulations. It is a semi-empirical model, and the derivation of the model equations relies on phenomenological considerations and empiricism.

The standard $k$-$\varepsilon$ model [231] (p. 741) is a model based on model transport equations for the turbulence kinetic energy ($k$) and its dissipation rate ($\varepsilon$). The model transport equation for $k$ is derived from the exact equation, while the model transport equation for $\varepsilon$ was obtained using physical reasoning and bears little resemblance to its mathematically exact counterpart.

In the derivation of the $k$-$\varepsilon$ model, the assumption is that the flow is fully turbulent, and the effects of molecular viscosity are negligible. The standard $k$-$\varepsilon$ model is therefore valid only for fully turbulent flows.

As the strengths and weaknesses of the standard $k$-$\varepsilon$ model have become known, modifications have been introduced to improve its performance. Two of these variants are available in ANSYS Fluent: the RNG $k$-$\varepsilon$ model [499] (p. 756) and the realizable $k$-$\varepsilon$ model [402] (p. 751).

### 4.3.1.2. Transport Equations for the Standard k-ε Model

The turbulence kinetic energy, $k$, and its rate of dissipation, $\varepsilon$, are obtained from the following transport equations:

$$\frac{\partial}{\partial t}(\rho k)+\frac{\partial}{\partial x_i}(\rho k u_i)=\frac{\partial}{\partial x_j}\left[\left(\mu+\frac{\mu_t}{\sigma_k}\right)\frac{\partial k}{\partial x_j}\right]+G_k+G_b-\rho\varepsilon-Y_M+S_k \tag{4.33}$$

and

$$\frac{\partial}{\partial t}(\rho \varepsilon)+\frac{\partial}{\partial x_i}(\rho \varepsilon u_i)=\frac{\partial}{\partial x_j}\left[\left(\mu+\frac{\mu_t}{\sigma_\varepsilon}\right)\frac{\partial \varepsilon}{\partial x_j}\right]+C_{1\varepsilon}\frac{\varepsilon}{k}(G_k+C_{3\varepsilon}G_b)-C_{2\varepsilon}\rho\frac{\varepsilon^2}{k}+S_\varepsilon \tag{4.34}$$

In these equations, $G_k$ represents the generation of turbulence kinetic energy due to the mean velocity gradients, calculated as described in Modeling Turbulent Production in the k-ε Models (p. 54). $G_b$ is the generation of turbulence kinetic energy due to buoyancy, calculated as described in Effects of Buoyancy on Turbulence in the k-ε Models (p. 55). $Y_M$ represents the contribution of the fluctuating dilatation in compressible turbulence to the overall dissipation rate, calculated as described in Effects of Compressibility on Turbulence in the k-ε Models (p. 56). $C_{1\varepsilon}$, $C_{2\varepsilon}$, and $C_{3\varepsilon}$ are constants. $\sigma_k$ and $\sigma_\varepsilon$ are the turbulent Prandtl numbers for $k$ and $\varepsilon$, respectively. $S_k$ and $S_\varepsilon$ are user-defined source terms.

### 4.3.1.3. Modeling the Turbulent Viscosity

The turbulent (or eddy) viscosity, $\mu_t$, is computed by combining $k$ and $\varepsilon$ as follows:

Release 15.0 - © SAS IP, Inc. All rights reserved. - Contains proprietary and confidential information of ANSYS, Inc. and its subsidiaries and affiliates.

$$\mu_t = \rho C_\mu \frac{k^2}{\varepsilon} \tag{4.35}$$

where $C_\mu$ is a constant.

#### 4.3.1.4. Model Constants

The model constants $C_{1\varepsilon}$, $C_{2\varepsilon}$, $C_\mu$, $\sigma_k$, and $\sigma_\varepsilon$ have the following default values [231] (p. 741):

$$C_{1\varepsilon} = 1.44,\ C_{2\varepsilon} = 1.92,\ C_\mu = 0.09,\ \sigma_k = 1.0,\ \sigma_\varepsilon = 1.3$$

These default values have been determined from experiments for fundamental turbulent flows including frequently encountered shear flows like boundary layers, mixing layers and jets as well as for decaying isotropic grid turbulence. They have been found to work fairly well for a wide range of wall-bounded and free shear flows.

Although the default values of the model constants are the standard ones most widely accepted, you can change them (if needed) in the Viscous Model Dialog Box.

### 4.3.2. RNG k-ε Model

#### 4.3.2.1. Overview

The RNG $k$-$\varepsilon$ model was derived using a statistical technique called renormalization group theory. It is similar in form to the standard $k$-$\varepsilon$ model, but includes the following refinements:

- The RNG model has an additional term in its $\varepsilon$ equation that improves the accuracy for rapidly strained flows.
- The effect of swirl on turbulence is included in the RNG model, enhancing accuracy for swirling flows.
- The RNG theory provides an analytical formula for turbulent Prandtl numbers, while the standard $k$-$\varepsilon$ model uses user-specified, constant values.
- While the standard $k$-$\varepsilon$ model is a high-Reynolds number model, the RNG theory provides an analytically-derived differential formula for effective viscosity that accounts for low-Reynolds number effects. Effective use of this feature does, however, depend on an appropriate treatment of the near-wall region.

These features make the RNG $k$-$\varepsilon$ model more accurate and reliable for a wider class of flows than the standard $k$-$\varepsilon$ model.

The RNG-based $k$-$\varepsilon$ turbulence model is derived from the instantaneous Navier-Stokes equations, using a mathematical technique called "renormalization group" (RNG) methods. The analytical derivation results in a model with constants different from those in the standard $k$-$\varepsilon$ model, and additional terms and functions in the transport equations for $k$ and $\varepsilon$. A more comprehensive description of RNG theory and its application to turbulence can be found in [334] (p. 747).

#### 4.3.2.2. Transport Equations for the RNG k-ε Model

The RNG $k$-$\varepsilon$ model has a similar form to the standard $k$-$\varepsilon$ model:


Release 15.0 - © SAS IP, Inc. All rights reserved. - Contains proprietary and confidential information of ANSYS, Inc. and its subsidiaries and affiliates.

$$\frac{\partial}{\partial t}(\rho k)+\frac{\partial}{\partial x_i}(\rho k u_i)=\frac{\partial}{\partial x_j}\left(\alpha_k \mu_{eff}\frac{\partial k}{\partial x_j}\right)+G_k+G_b-\rho\varepsilon-Y_M+S_k \tag{4.36}$$

and

$$\frac{\partial}{\partial t}(\rho \varepsilon)+\frac{\partial}{\partial x_i}(\rho \varepsilon u_i)=\frac{\partial}{\partial x_j}\left(\alpha_\varepsilon \mu_{eff}\frac{\partial \varepsilon}{\partial x_j}\right)+C_{1\varepsilon}\frac{\varepsilon}{k}(G_k+C_{3\varepsilon}G_b)-C_{2\varepsilon}\rho\frac{\varepsilon^2}{k}-R_\varepsilon+S_\varepsilon \tag{4.37}$$

In these equations, $G_k$ represents the generation of turbulence kinetic energy due to the mean velocity gradients, calculated as described in Modeling Turbulent Production in the k-ε Models (p. 54). $G_b$ is the generation of turbulence kinetic energy due to buoyancy, calculated as described in Effects of Buoyancy on Turbulence in the k-ε Models (p. 55). $Y_M$ represents the contribution of the fluctuating dilatation in compressible turbulence to the overall dissipation rate, calculated as described in Effects of Compressibility on Turbulence in the k-ε Models (p. 56). The quantities $\alpha_k$ and $\alpha_\varepsilon$ are the inverse effective Prandtl numbers for $k$ and $\varepsilon$, respectively. $S_k$ and $S_\varepsilon$ are user-defined source terms.

### 4.3.2.3. Modeling the Effective Viscosity

The scale elimination procedure in RNG theory results in a differential equation for turbulent viscosity:

$$d\left(\frac{\rho^2 k}{\sqrt{\varepsilon\mu}}\right)=1.72\frac{\hat{\nu}}{\sqrt{\hat{\nu}^3-1+C_\nu}}d\hat{\nu} \tag{4.38}$$

where

$$\hat{\nu}=\frac{\mu_{eff}}{\mu}$$

$$C_\nu \approx 100$$

Equation 4.38 (p. 49) is integrated to obtain an accurate description of how the effective turbulent transport varies with the effective Reynolds number (or eddy scale), allowing the model to better handle low-Reynolds number and near-wall flows.

In the high-Reynolds number limit, Equation 4.38 (p. 49) gives

$$\mu_t=\rho C_\mu\frac{k^2}{\varepsilon} \tag{4.39}$$

with $C_\mu=0.0845$, derived using RNG theory. It is interesting to note that this value of $C_\mu$ is very close to the empirically-determined value of 0.09 used in the standard $k$-$\varepsilon$ model.

In ANSYS Fluent, by default, the effective viscosity is computed using the high-Reynolds number form in Equation 4.39 (p. 49). However, there is an option available that allows you to use the differential relation given in Equation 4.38 (p. 49) when you need to include low-Reynolds number effects.

Release 15.0 - © SAS IP, Inc. All rights reserved. - Contains proprietary and confidential information of ANSYS, Inc. and its subsidiaries and affiliates.

### 4.3.2.4. RNG Swirl Modification

Turbulence, in general, is affected by rotation or swirl in the mean flow. The RNG model in ANSYS Fluent provides an option to account for the effects of swirl or rotation by modifying the turbulent viscosity appropriately. The modification takes the following functional form:

$$\mu_t = \mu_{t0} f\left(\alpha_s, \Omega, \frac{k}{\varepsilon}\right) \tag{4.40}$$

where $\mu_{t0}$ is the value of turbulent viscosity calculated without the swirl modification using either Equation 4.38 (p. 49) or Equation 4.39 (p. 49). $\Omega$ is a characteristic swirl number evaluated within ANSYS Fluent, and $\alpha_s$ is a swirl constant that assumes different values depending on whether the flow is swirl-dominated or only mildly swirling. This swirl modification always takes effect for axisymmetric, swirling flows and three-dimensional flows when the RNG model is selected. For mildly swirling flows (the default in ANSYS Fluent), $\alpha_s$ is set to 0.07. For strongly swirling flows, however, a higher value of $\alpha_s$ can be used.

### 4.3.2.5. Calculating the Inverse Effective Prandtl Numbers

The inverse effective Prandtl numbers, $\alpha_k$ and $\alpha_\varepsilon$, are computed using the following formula derived analytically by the RNG theory:

$$\left|\frac{\alpha - 1.3929}{\alpha_0 - 1.3929}\right|^{0.6321} \left|\frac{\alpha + 2.3929}{\alpha_0 + 2.3929}\right|^{0.3679} = \frac{\mu_{mol}}{\mu_{eff}} \tag{4.41}$$

where $\alpha_0 = 1.0$. In the high-Reynolds number limit ($\frac{\mu_{mol}}{\mu_{eff}} \ll 1$), $\alpha_k = \alpha_\varepsilon \approx 1.393$.

### 4.3.2.6. The R-$\varepsilon$ Term in the $\varepsilon$ Equation

The main difference between the RNG and standard $k$-$\varepsilon$ models lies in the additional term in the $\varepsilon$ equation given by

$$R_\varepsilon = \frac{C_\mu \rho \eta^3 \left(1 - \eta/\eta_0\right)}{1 + \beta \eta^3} \frac{\varepsilon^2}{k} \tag{4.42}$$

where $\eta \equiv Sk/\varepsilon$, $\eta_0 = 4.38$, $\beta = 0.012$.

The effects of this term in the RNG $\varepsilon$ equation can be seen more clearly by rearranging Equation 4.37 (p. 49). Using Equation 4.42 (p. 50), the third and fourth terms on the right-hand side of Equation 4.37 (p. 49) can be merged, and the resulting $\varepsilon$ equation can be rewritten as

$$\frac{\partial}{\partial t}(\rho\varepsilon) + \frac{\partial}{\partial x_i}(\rho\varepsilon u_i) = \frac{\partial}{\partial x_j}\left(\alpha_\varepsilon \mu_{eff} \frac{\partial \varepsilon}{\partial x_j}\right) + C_{1\varepsilon}\frac{\varepsilon}{k}(G_k + C_{3\varepsilon}G_b) - C_{2\varepsilon}^* \rho \frac{\varepsilon^2}{k} \tag{4.43}$$

where $C_{2\varepsilon}^*$ is given by

$$C_{2\varepsilon}^* \equiv C_{2\varepsilon} + \frac{C_\mu \eta^3 \left(1 - \eta/\eta_0\right)}{1 + \beta \eta^3} \tag{4.44}$$


Release 15.0 - © SAS IP, Inc. All rights reserved. - Contains proprietary and confidential information of ANSYS, Inc. and its subsidiaries and affiliates.

In regions where $\eta < \eta_0$, the $R$ term makes a positive contribution, and $C_{2\varepsilon}^*$ becomes larger than $C_{2\varepsilon}$.

In the logarithmic layer, for instance, it can be shown that $\eta \approx 3.0$, giving $C_{2\varepsilon}^* \approx 2.0$, which is close in magnitude to the value of $C_{2\varepsilon}$ in the standard $k$-$\varepsilon$ model (1.92). As a result, for weakly to moderately strained flows, the RNG model tends to give results largely comparable to the standard $k$-$\varepsilon$ model.

In regions of large strain rate ($\eta > \eta_0$), however, the $R$ term makes a negative contribution, making the value of $C_{2\varepsilon}^*$ less than $C_{2\varepsilon}$. In comparison with the standard $k$-$\varepsilon$ model, the smaller destruction of $\varepsilon$ augments $\varepsilon$, reducing $k$ and, eventually, the effective viscosity. As a result, in rapidly strained flows, the RNG model yields a lower turbulent viscosity than the standard $k$-$\varepsilon$ model.

Thus, the RNG model is more responsive to the effects of rapid strain and streamline curvature than the standard $k$-$\varepsilon$ model, which explains the superior performance of the RNG model for certain classes of flows.

#### 4.3.2.7. Model Constants

The model constants $C_{1\varepsilon}$ and $C_{2\varepsilon}$ in Equation 4.37 (p. 49) have values derived analytically by the RNG theory. These values, used by default in ANSYS Fluent, are

$$C_{1\varepsilon} = 1.42,\ C_{2\varepsilon} = 1.68$$

### 4.3.3. Realizable k-ε Model

#### 4.3.3.1. Overview

The realizable $k$-$\varepsilon$ model [402] (p. 751) differs from the standard $k$-$\varepsilon$ model in two important ways:

- The realizable $k$-$\varepsilon$ model contains an alternative formulation for the turbulent viscosity.
- A modified transport equation for the dissipation rate, $\varepsilon$, has been derived from an exact equation for the transport of the mean-square vorticity fluctuation.

The term "realizable" means that the model satisfies certain mathematical constraints on the Reynolds stresses, consistent with the physics of turbulent flows. Neither the standard $k$-$\varepsilon$ model nor the RNG $k$-$\varepsilon$ model is realizable.

To understand the mathematics behind the realizable $k$-$\varepsilon$ model, consider combining the Boussinesq relationship (Equation 4.14 (p. 42)) and the eddy viscosity definition (Equation 4.35 (p. 48)) to obtain the following expression for the normal Reynolds stress in an incompressible strained mean flow:

$$\overline{u^2} = \frac{2}{3}k - 2\nu_t \frac{\partial U}{\partial x} \tag{4.45}$$

Using Equation 4.35 (p. 48) for $\nu_t \equiv \mu_t / \rho$, one obtains the result that the normal stress, $\overline{u^2}$, which by definition is a positive quantity, becomes negative, that is, "non-realizable", when the strain is large enough to satisfy

$$\frac{k}{\varepsilon}\frac{\partial U}{\partial x} > \frac{1}{3C_\mu} \approx 3.7 \tag{4.46}$$

Release 15.0 - © SAS IP, Inc. All rights reserved. - Contains proprietary and confidential information of ANSYS, Inc. and its subsidiaries and affiliates.

Similarly, it can also be shown that the Schwarz inequality for shear stresses ($\overline{u_\alpha}\,\overline{u_\beta}^2 \le \overline{u_\alpha^2 u_\beta^2}$; no summation over $\alpha$ and $\beta$) can be violated when the mean strain rate is large. The most straightforward way to ensure the realizability (positivity of normal stresses and Schwarz inequality for shear stresses) is to make $C_\mu$ variable by sensitizing it to the mean flow (mean deformation) and the turbulence ($k$, $\varepsilon$). The notion of variable $C_\mu$ is suggested by many modelers including Reynolds [375] (p. 749), and is well substantiated by experimental evidence. For example, $C_\mu$ is found to be around 0.09 in the logarithmic layer of equilibrium boundary layers, and 0.05 in a strong homogeneous shear flow.

Both the realizable and RNG $k$-$\varepsilon$ models have shown substantial improvements over the standard $k$-$\varepsilon$ model where the flow features include strong streamline curvature, vortices, and rotation. Since the model is still relatively new, it is not clear in exactly which instances the realizable $k$-$\varepsilon$ model consistently outperforms the RNG model. However, initial studies have shown that the realizable model provides the best performance of all the $k$-$\varepsilon$ model versions for several validations of separated flows and flows with complex secondary flow features.

One of the weaknesses of the standard $k$-$\varepsilon$ model or other traditional $k$-$\varepsilon$ models lies with the modeled equation for the dissipation rate ($\varepsilon$). The well-known round-jet anomaly (named based on the finding that the spreading rate in planar jets is predicted reasonably well, but prediction of the spreading rate for axisymmetric jets is unexpectedly poor) is considered to be mainly due to the modeled dissipation equation.

The realizable $k$-$\varepsilon$ model proposed by Shih et al. [402] (p. 751) was intended to address these deficiencies of traditional $k$-$\varepsilon$ models by adopting the following:

- A new eddy-viscosity formula involving a variable $C_\mu$ originally proposed by Reynolds [375] (p. 749).
- A new model equation for dissipation ($\varepsilon$) based on the dynamic equation of the mean-square vorticity fluctuation.

One limitation of the realizable $k$-$\varepsilon$ model is that it produces non-physical turbulent viscosities in situations when the computational domain contains both rotating and stationary fluid zones (for example, multiple reference frames, rotating sliding meshes). This is due to the fact that the realizable $k$-$\varepsilon$ model includes the effects of mean rotation in the definition of the turbulent viscosity (see Equation 4.49 (p. 53) – Equation 4.51 (p. 54)). This extra rotation effect has been tested on single moving reference frame systems and showed superior behavior over the standard $k$-$\varepsilon$ model. However, due to the nature of this modification, its application to multiple reference frame systems should be taken with some caution. See Modeling the Turbulent Viscosity (p. 53) for information about how to include or exclude this term from the model.

### 4.3.3.2. Transport Equations for the Realizable k-ε Model

The modeled transport equations for $k$ and $\varepsilon$ in the realizable $k$-$\varepsilon$ model are

$$\frac{\partial}{\partial t}(\rho k) + \frac{\partial}{\partial x_j}\left(\rho k u_j\right) = \frac{\partial}{\partial x_j}\left[\left(\mu + \frac{\mu_t}{\sigma_k}\right)\frac{\partial k}{\partial x_j}\right] + G_k + G_b - \rho\varepsilon - Y_M + S_k \tag{4.47}$$

and


Release 15.0 - © SAS IP, Inc. All rights reserved. - Contains proprietary and confidential information of ANSYS, Inc. and its subsidiaries and affiliates.

$$\frac{\partial}{\partial t}(\rho\varepsilon)+\frac{\partial}{\partial x_j}\left(\rho\varepsilon u_j\right) = \frac{\partial}{\partial x_j}\left[\left(\mu+\frac{\mu_t}{\sigma_\varepsilon}\right)\frac{\partial\varepsilon}{\partial x_j}\right] + \rho C_1 S\varepsilon - \rho C_2\frac{\varepsilon^2}{k+\sqrt{\nu\varepsilon}} + C_{1\varepsilon}\frac{\varepsilon}{k}C_{3\varepsilon}G_b + S_\varepsilon \tag{4.48}$$

where

$$C_1 = \max\left[0.43, \frac{\eta}{\eta+5}\right],\ \eta = S\frac{k}{\varepsilon},\ S = \sqrt{2S_{ij}S_{ij}}$$

In these equations, $G_k$ represents the generation of turbulence kinetic energy due to the mean velocity gradients, calculated as described in Modeling Turbulent Production in the k-ε Models (p. 54). $G_b$ is the generation of turbulence kinetic energy due to buoyancy, calculated as described in Effects of Buoyancy on Turbulence in the k-ε Models (p. 55). $Y_M$ represents the contribution of the fluctuating dilatation in compressible turbulence to the overall dissipation rate, calculated as described in Effects of Compressibility on Turbulence in the k-ε Models (p. 56). $C_2$ and $C_{1\varepsilon}$ are constants. $\sigma_k$ and $\sigma_\varepsilon$ are the turbulent Prandtl numbers for $k$ and $\varepsilon$, respectively. $S_k$ and $S_\varepsilon$ are user-defined source terms.

Note that the $k$ equation (Equation 4.47 (p. 52)) is the same as that in the standard $k$-$\varepsilon$ model (Equation 4.33 (p. 47)) and the RNG $k$-$\varepsilon$ model (Equation 4.36 (p. 49)), except for the model constants. However, the form of the $\varepsilon$ equation is quite different from those in the standard and RNG-based $k$-$\varepsilon$ models (Equation 4.34 (p. 47) and Equation 4.37 (p. 49)). One of the noteworthy features is that the production term in the $\varepsilon$ equation (the second term on the right-hand side of Equation 4.48 (p. 53)) does not involve the production of $k$; that is, it does not contain the same $G_k$ term as the other $k$-$\varepsilon$ models. It is believed that the present form better represents the spectral energy transfer. Another desirable feature is that the destruction term (the third term on the right-hand side of Equation 4.48 (p. 53)) does not have any singularity; that is, its denominator never vanishes, even if $k$ vanishes or becomes smaller than zero. This feature is contrasted with traditional $k$-$\varepsilon$ models, which have a singularity due to $k$ in the denominator.

This model has been extensively validated for a wide range of flows [210] (p. 740), [402] (p. 751), including rotating homogeneous shear flows, free flows including jets and mixing layers, channel and boundary layer flows, and separated flows. For all these cases, the performance of the model has been found to be substantially better than that of the standard $k$-$\varepsilon$ model. Especially noteworthy is the fact that the realizable $k$-$\varepsilon$ model resolves the round-jet anomaly; that is, it predicts the spreading rate for axisymmetric jets as well as that for planar jets.

### 4.3.3.3. Modeling the Turbulent Viscosity

As in other $k$-$\varepsilon$ models, the eddy viscosity is computed from

$$\mu_t = \rho C_\mu \frac{k^2}{\varepsilon} \tag{4.49}$$

The difference between the realizable $k$-$\varepsilon$ model and the standard and RNG $k$-$\varepsilon$ models is that $C_\mu$ is no longer constant. It is computed from

Release 15.0 - © SAS IP, Inc. All rights reserved. - Contains proprietary and confidential information of ANSYS, Inc. and its subsidiaries and affiliates.

$$C_\mu = \frac{1}{A_0 + A_s \frac{kU^*}{\varepsilon}} \tag{4.50}$$

where

$$U^* \equiv \sqrt{S_{ij}S_{ij} + \tilde{\Omega}_{ij}\tilde{\Omega}_{ij}} \tag{4.51}$$

and

$$\begin{aligned} \tilde{\Omega}_{ij} &= \Omega_{ij} - 2\varepsilon_{ijk}\omega_k \\ \Omega_{ij} &= \overline{\Omega_{ij}} - \varepsilon_{ijk}\omega_k \end{aligned}$$

where $\overline{\Omega_{ij}}$ is the mean rate-of-rotation tensor viewed in a moving reference frame with the angular velocity $\omega_k$. The model constants $A_0$ and $A_s$ are given by

$$A_0 = 4.04, \quad A_s = \sqrt{6}\cos\phi \tag{4.52}$$

where

$$\phi = \frac{1}{3}\cos^{-1}(\sqrt{6}W), \quad W = \frac{S_{ij}S_{jk}S_{ki}}{\tilde{S}^3}, \quad \tilde{S} = \sqrt{S_{ij}S_{ij}}, \quad S_{ij} = \frac{1}{2}\left(\frac{\partial u_j}{\partial x_i} + \frac{\partial u_i}{\partial x_j}\right) \tag{4.53}$$

It can be seen that $C_\mu$ is a function of the mean strain and rotation rates, the angular velocity of the system rotation, and the turbulence fields ($k$ and $\varepsilon$). $C_\mu$ in Equation 4.49 (p. 53) can be shown to recover the standard value of 0.09 for an inertial sublayer in an equilibrium boundary layer.

**Important**

In ANSYS Fluent, the term $-2\varepsilon_{ijk}\omega_k$ is, by default, not included in the calculation of $\tilde{\Omega}_{ij}$. This is an extra rotation term that is not compatible with cases involving sliding meshes or multiple reference frames. If you want to include this term in the model, you can enable it by using the `define/models/viscous/turbulence-expert/rke-cmu-rotation-term?` text command and entering `yes` at the prompt.

#### 4.3.3.4. Model Constants

The model constants $C_2$, $\sigma_k$, and $\sigma_\varepsilon$ have been established to ensure that the model performs well for certain canonical flows. The model constants are

$$C_{1\varepsilon} = 1.44, \quad C_2 = 1.9, \quad \sigma_k = 1.0, \quad \sigma_\varepsilon = 1.2$$

### 4.3.4. Modeling Turbulent Production in the k-ε Models

The term $G_k$, representing the production of turbulence kinetic energy, is modeled identically for the standard, RNG, and realizable $k$-$\varepsilon$ models. From the exact equation for the transport of $k$, this term may be defined as


Release 15.0 - © SAS IP, Inc. All rights reserved. - Contains proprietary and confidential information of ANSYS, Inc. and its subsidiaries and affiliates.

$$G_k = -\rho \overline{u'_i u'_j} \frac{\partial u_j}{\partial x_i} \tag{4.54}$$

To evaluate $G_k$ in a manner consistent with the Boussinesq hypothesis,

$$G_k = \mu_t S^2 \tag{4.55}$$

where $S$ is the modulus of the mean rate-of-strain tensor, defined as

$$S \equiv \sqrt{2 S_{ij} S_{ij}} \tag{4.56}$$

**Important**

When using the high-Reynolds number $k$-$\varepsilon$ versions, $\mu_{eff}$ is used in lieu of $\mu_t$ in Equation 4.55 (p. 55).

## 4.3.5. Effects of Buoyancy on Turbulence in the k-ε Models

When a non-zero gravity field and temperature gradient are present simultaneously, the $k$-$\varepsilon$ models in ANSYS Fluent account for the generation of $k$ due to buoyancy ($G_b$ in Equation 4.33 (p. 47), Equation 4.36 (p. 49), and Equation 4.47 (p. 52)), and the corresponding contribution to the production of $\varepsilon$ in Equation 4.34 (p. 47), Equation 4.37 (p. 49), and Equation 4.48 (p. 53).

The generation of turbulence due to buoyancy is given by

$$G_b = \beta g_i \frac{\mu_t}{Pr_t} \frac{\partial T}{\partial x_i} \tag{4.57}$$

where $Pr_t$ is the turbulent Prandtl number for energy and $g_i$ is the component of the gravitational vector in the $i$th direction. For the standard and realizable $k$-$\varepsilon$ models, the default value of $Pr_t$ is 0.85. In the case of the RNG $k$-$\varepsilon$ model, $Pr_t = 1/\alpha$, where $\alpha$ is given by Equation 4.41 (p. 50), but with $\alpha_0 = 1/Pr = k/\mu c_p$. The coefficient of thermal expansion, $\beta$, is defined as

$$\beta = -\frac{1}{\rho}\left(\frac{\partial \rho}{\partial T}\right)_p \tag{4.58}$$

For ideal gases, Equation 4.57 (p. 55) reduces to

$$G_b = -g_i \frac{\mu_t}{\rho Pr_t} \frac{\partial \rho}{\partial x_i} \tag{4.59}$$

It can be seen from the transport equations for $k$ (Equation 4.33 (p. 47), Equation 4.36 (p. 49), and Equation 4.47 (p. 52)) that turbulence kinetic energy tends to be augmented ($G_b > 0$) in unstable stratification. For stable stratification, buoyancy tends to suppress the turbulence ($G_b < 0$). In ANSYS Fluent, the effects of buoyancy on the generation of $k$ are always included when you have both a non-zero gravity field and a non-zero temperature (or density) gradient.

While the buoyancy effects on the generation of $k$ are relatively well understood, the effect on $\varepsilon$ is less clear. In ANSYS Fluent, by default, the buoyancy effects on $\varepsilon$ are neglected simply by setting $G_b$ to zero in the transport equation for $\varepsilon$ (Equation 4.34 (p. 47), Equation 4.37 (p. 49), or Equation 4.48 (p. 53)).

Release 15.0 - © SAS IP, Inc. All rights reserved. - Contains proprietary and confidential information of ANSYS, Inc. and its subsidiaries and affiliates.

However, you can include the buoyancy effects on $\varepsilon$ in the Viscous Model Dialog Box. In this case, the value of $G_b$ given by Equation 4.59 (p. 55) is used in the transport equation for $\varepsilon$ (Equation 4.34 (p. 47), Equation 4.37 (p. 49), or Equation 4.48 (p. 53)).

The degree to which $\varepsilon$ is affected by the buoyancy is determined by the constant $C_{3\varepsilon}$. In ANSYS Fluent, $C_{3\varepsilon}$ is not specified, but is instead calculated according to the following relation [159] (p. 737):

$$C_{3\varepsilon}=tanh\left|\frac{v}{u}\right| \tag{4.60}$$

where $v$ is the component of the flow velocity parallel to the gravitational vector and $u$ is the component of the flow velocity perpendicular to the gravitational vector. In this way, $C_{3\varepsilon}$ will become 1 for buoyant shear layers for which the main flow direction is aligned with the direction of gravity. For buoyant shear layers that are perpendicular to the gravitational vector, $C_{3\varepsilon}$ will become zero.

## 4.3.6. Effects of Compressibility on Turbulence in the k-ε Models

For high-Mach-number flows, compressibility affects turbulence through so-called "dilatation dissipation", which is normally neglected in the modeling of incompressible flows [490] (p. 756). Neglecting the dilatation dissipation fails to predict the observed decrease in spreading rate with increasing Mach number for compressible mixing and other free shear layers. To account for these effects in the $k$-$\varepsilon$ models in ANSYS Fluent, the dilatation dissipation term, $Y_M$, can be included in the $k$ equation. This term is modeled according to a proposal by Sarkar [386] (p. 750):

$$Y_M=2\rho\varepsilon M_t^2 \tag{4.61}$$

where $M_t$ is the turbulent Mach number, defined as

$$M_t=\sqrt{\frac{k}{a^2}} \tag{4.62}$$

where $a$ ($\equiv\sqrt{\gamma RT}$) is the speed of sound.

**Note**

The Sarkar model has been tested for a very limited number of free shear test cases, and should be used with caution (and only when truly necessary), as it can negatively affect the wall boundary layer even at transonic and supersonic Mach numbers. It is disabled by default. For details, see Model Enhancements in the *Fluent User's Guide*.

## 4.3.7. Convective Heat and Mass Transfer Modeling in the k-ε Models

In ANSYS Fluent, turbulent heat transport is modeled using the concept of Reynolds' analogy to turbulent momentum transfer. The "modeled" energy equation is therefore given by

$$\frac{\partial}{\partial t}(\rho E)+\frac{\partial}{\partial x_i}\left[u_i(\rho E+p)\right]=\frac{\partial}{\partial x_j}\left(k_{eff}\frac{\partial T}{\partial x_j}+u_i\left(\tau_{ij}\right)_{eff}\right)+S_h \tag{4.63}$$

where $E$ is the total energy, $k_{eff}$ is the effective thermal conductivity, and


Release 15.0 - © SAS IP, Inc. All rights reserved. - Contains proprietary and confidential information of ANSYS, Inc. and its subsidiaries and affiliates.

$\left(\tau_{ij}\right)_{eff}$ is the deviatoric stress tensor, defined as

$$\left(\tau_{ij}\right)_{eff}=\mu_{eff}\left(\frac{\partial u_j}{\partial x_i}+\frac{\partial u_i}{\partial x_j}\right)-\frac{2}{3}\mu_{eff}\frac{\partial u_k}{\partial x_k}\delta_{ij}$$

The term involving $\left(\tau_{ij}\right)_{eff}$ represents the viscous heating, and is always computed in the density-based solvers. It is not computed by default in the pressure-based solver, but it can be enabled in the Viscous Model Dialog Box.

Additional terms may appear in the energy equation, depending on the physical models you are using. See Heat Transfer Theory (p. 133) for more details.

For the standard and realizable $k$-$\varepsilon$ models, the effective thermal conductivity is given by

$$k_{eff}=k+\frac{c_p\mu_t}{Pr_t}$$

where $k$, in this case, is the thermal conductivity. The default value of the turbulent Prandtl number is 0.85. You can change the value of the turbulent Prandtl number in the Viscous Model Dialog Box.

For the RNG $k$-$\varepsilon$ model, the effective thermal conductivity is

$$k_{eff}=\alpha c_p\mu_{eff}$$

where $\alpha$ is calculated from Equation 4.41 (p. 50), but with $\alpha_0=1/Pr=k/\mu c_p$.

The fact that $\alpha$ varies with $\mu_{mol}/\mu_{eff}$, as in Equation 4.41 (p. 50), is an advantage of the RNG $k$-$\varepsilon$ model. It is consistent with experimental evidence indicating that the turbulent Prandtl number varies with the molecular Prandtl number and turbulence [201] (p. 740). Equation 4.41 (p. 50) works well across a very broad range of molecular Prandtl numbers, from liquid metals ($Pr\approx 10^{-2}$) to paraffin oils ($Pr\approx 10^{3}$), which allows heat transfer to be calculated in low-Reynolds number regions. Equation 4.41 (p. 50) smoothly predicts the variation of effective Prandtl number from the molecular value ($\alpha=1/Pr$) in the viscosity-dominated region to the fully turbulent value ($\alpha=1.393$) in the fully turbulent regions of the flow.

Turbulent mass transfer is treated similarly. For the standard and realizable $k$-$\varepsilon$ models, the default turbulent Schmidt number is 0.7. This default value can be changed in the Viscous Model Dialog Box. For the RNG model, the effective turbulent diffusivity for mass transfer is calculated in a manner that is analogous to the method used for the heat transport. The value of $\alpha_0$ in Equation 4.41 (p. 50) is $\alpha_0=1/Sc$, where Sc is the molecular Schmidt number.

## 4.4. Standard and SST k-ω Models

This section describes the theory behind the Standard and SST $k$-$\omega$ models. Information is presented in the following sections:

4.4.1. Standard k-ω Model

Release 15.0 - © SAS IP, Inc. All rights reserved. - Contains proprietary and confidential information of ANSYS, Inc. and its subsidiaries and affiliates.

4.4.2. Shear-Stress Transport (SST) k-ω Model
4.4.3. Turbulence Damping
4.4.4. Wall Boundary Conditions

For details about using the models in ANSYS Fluent, see Modeling Turbulence and Setting Up the k-ω Model in the User's Guide.

This section presents the standard [490] (p. 756) and shear-stress transport (SST) [290] (p. 745) $k$-$\omega$ models. Both models have similar forms, with transport equations for $k$ and $\omega$. The major ways in which the SST model [293] (p. 745) differs from the standard model are as follows:

- gradual change from the standard $k$-$\omega$ model in the inner region of the boundary layer to a high-Reynolds number version of the $k$-$\varepsilon$ model in the outer part of the boundary layer
- modified turbulent viscosity formulation to account for the transport effects of the principal turbulent shear stress

The transport equations, methods of calculating turbulent viscosity, and methods of calculating model constants and other terms are presented separately for each model.

Low Reynolds number modifications have been proposed by Wilcox for the k-$\omega$ model and are available in ANSYS Fluent. It is important to note that all k-$\omega$ models can be integrated through the viscous sublayer without these terms. The terms were mainly added to reproduce the peak in the turbulence kinetic energy observed in DNS data very close to the wall. In addition, these terms affect the laminar-turbulent transition process. The low-Reynolds number terms can produce a delayed onset of the turbulent wall boundary layer and constitute therefore a very simple model for laminar-turbulent transition. In general, the use of the low-Reynolds number terms in the k-$\omega$ models is not recommended, and it is advised to use the more sophisticated, and more widely calibrated, models for laminar-turbulent transition instead.

## 4.4.1. Standard k-ω Model

### *4.4.1.1. Overview*

The standard $k$-$\omega$ model in ANSYS Fluent is based on the Wilcox $k$-$\omega$ model [490] (p. 756), which incorporates modifications for low-Reynolds number effects, compressibility, and shear flow spreading. One of the weak points of the Wilcox model is the sensitivity of the solutions to values for k and $\omega$ outside the shear layer (freestream sensitivity). While the new formulation implemented in ANSYS Fluent has reduced this dependency, it can still have a significant effect on the solution, especially for free shear flows [291] (p. 745).

The standard $k$-$\omega$ model is an empirical model based on model transport equations for the turbulence kinetic energy ($k$) and the specific dissipation rate ($\omega$), which can also be thought of as the ratio of $\varepsilon$ to $k$ [490] (p. 756).

As the $k$-$\omega$ model has been modified over the years, production terms have been added to both the $k$ and $\omega$ equations, which have improved the accuracy of the model for predicting free shear flows.

### *4.4.1.2. Transport Equations for the Standard k-ω Model*

The turbulence kinetic energy, $k$, and the specific dissipation rate, $\omega$, are obtained from the following transport equations:


Release 15.0 - © SAS IP, Inc. All rights reserved. - Contains proprietary and confidential information of ANSYS, Inc. and its subsidiaries and affiliates.

$$\frac{\partial}{\partial t}(\rho k)+\frac{\partial}{\partial x_i}(\rho k u_i)=\frac{\partial}{\partial x_j}\left(\Gamma_k\frac{\partial k}{\partial x_j}\right)+G_k-Y_k+S_k \tag{4.64}$$

and

$$\frac{\partial}{\partial t}(\rho \omega)+\frac{\partial}{\partial x_i}(\rho \omega u_i)=\frac{\partial}{\partial x_j}\left(\Gamma_\omega\frac{\partial \omega}{\partial x_j}\right)+G_\omega-Y_\omega+S_\omega \tag{4.65}$$

In these equations, $G_k$ represents the generation of turbulence kinetic energy due to mean velocity gradients. $G_\omega$ represents the generation of $\omega$. $\Gamma_k$ and $\Gamma_\omega$ represent the effective diffusivity of $k$ and $\omega$, respectively. $Y_k$ and $Y_\omega$ represent the dissipation of $k$ and $\omega$ due to turbulence. All of the above terms are calculated as described below. $S_k$ and $S_\omega$ are user-defined source terms.

### 4.4.1.3. Modeling the Effective Diffusivity

The effective diffusivities for the $k$-$\omega$ model are given by

$$\Gamma_k=\mu+\frac{\mu_t}{\sigma_k}$$
$$\Gamma_\omega=\mu+\frac{\mu_t}{\sigma_\omega} \tag{4.66}$$

where $\sigma_k$ and $\sigma_\omega$ are the turbulent Prandtl numbers for $k$ and $\omega$, respectively. The turbulent viscosity, $\mu_t$, is computed by combining $k$ and $\omega$ as follows:

$$\mu_t=\alpha^*\frac{\rho k}{\omega} \tag{4.67}$$

#### 4.4.1.3.1. Low-Reynolds-Number Correction

The coefficient $\alpha^*$ damps the turbulent viscosity causing a low-Reynolds number correction. It is given by

$$\alpha^*=\alpha_\infty^*\left(\frac{\alpha_0^*+Re_t/R_k}{1+Re_t/R_k}\right) \tag{4.68}$$

where

$$Re_t=\frac{\rho k}{\mu\omega} \tag{4.69}$$
$$R_k=6 \tag{4.70}$$
$$\alpha_0^*=\frac{\beta_i}{3} \tag{4.71}$$
$$\beta_i=0.072 \tag{4.72}$$

Note that in the high-Reynolds number form of the $k$-$\omega$ model, $\alpha^*=\alpha_\infty^*=1$.

Release 15.0 - © SAS IP, Inc. All rights reserved. - Contains proprietary and confidential information of ANSYS, Inc. and its subsidiaries and affiliates.

## 4.4.1.4. Modeling the Turbulence Production

### 4.4.1.4.1. Production of k

The term $G_k$ represents the production of turbulence kinetic energy. From the exact equation for the transport of $k$, this term may be defined as

$$G_k = -\rho \overline{u'_i u'_j} \frac{\partial u_j}{\partial x_i} \tag{4.73}$$

To evaluate $G_k$ in a manner consistent with the Boussinesq hypothesis,

$$G_k = \mu_t S^2 \tag{4.74}$$

where $S$ is the modulus of the mean rate-of-strain tensor, defined in the same way as for the $k$-$\varepsilon$ model (see Equation 4.56 (p. 55)).

### 4.4.1.4.2. Production of ω

The production of $\omega$ is given by

$$G_\omega = \alpha \frac{\omega}{k} G_k \tag{4.75}$$

where $G_k$ is given by Equation 4.73 (p. 60).

The coefficient $\alpha$ is given by

$$\alpha = \frac{\alpha_\infty}{\alpha^*} \left( \frac{\alpha_0 + Re_t/R_\omega}{1 + Re_t/R_\omega} \right) \tag{4.76}$$

where $R_\omega$ = 2.95. $\alpha^*$ and $Re_t$ are given by Equation 4.68 (p. 59) and Equation 4.69 (p. 59), respectively.

Note that in the high-Reynolds number form of the $k$-$\omega$ model, $\alpha = \alpha_\infty = 1$.

## 4.4.1.5. Modeling the Turbulence Dissipation

### 4.4.1.5.1. Dissipation of k

The dissipation of $k$ is given by

$$Y_k = \rho \beta^* f_{\beta^*} k \omega \tag{4.77}$$

where

$$f_{\beta^*} = \begin{cases} 1 & \chi_k \le 0 \\ \dfrac{1 + 680\chi_k^2}{1 + 400\chi_k^2} & \chi_k > 0 \end{cases} \tag{4.78}$$

where


Release 15.0 - © SAS IP, Inc. All rights reserved. - Contains proprietary and confidential information of ANSYS, Inc. and its subsidiaries and affiliates.

$$\chi_k \equiv \frac{1}{\omega^3}\frac{\partial k}{\partial x_j}\frac{\partial \omega}{\partial x_j} \tag{4.79}$$

and

$$\beta^* = \beta_i^* \left[1 + \zeta^* F(M_t)\right] \tag{4.80}$$

$$\beta_i^* = \beta_\infty^* \left( \frac{4/15 + \left(Re_t/R_\beta\right)^4}{1 + \left(Re_t/R_\beta\right)^4} \right) \tag{4.81}$$

$$\zeta^* = 1.5 \tag{4.82}$$

$$R_\beta = 8 \tag{4.83}$$

$$\beta_\infty^* = 0.09 \tag{4.84}$$

where $Re_t$ is given by Equation 4.69 (p. 59).

#### 4.4.1.5.2. Dissipation of ω

The dissipation of $\omega$ is given by

$$Y_\omega = \rho\beta f_\beta \omega^2 \tag{4.85}$$

where

$$f_\beta = \frac{1 + 70\chi_\omega}{1 + 80\chi_\omega} \tag{4.86}$$

$$\chi_\omega = \left| \frac{\Omega_{ij}\Omega_{jk}S_{ki}}{\left(\beta_\infty^*\omega\right)^3} \right| \tag{4.87}$$

$$\Omega_{ij} = \frac{1}{2}\left( \frac{\partial u_i}{\partial x_j} - \frac{\partial u_j}{\partial x_i} \right) \tag{4.88}$$

The strain rate tensor, $S_{ij}$ is defined in Equation 4.25 (p. 44). Also,

$$\beta = \beta_i \left[ 1 - \frac{\beta_i^*}{\beta_i}\zeta^* F(M_t) \right] \tag{4.89}$$

$\beta_i^*$ and $F(M_t)$ are defined by Equation 4.81 (p. 61) and Equation 4.90 (p. 62), respectively.

#### 4.4.1.5.3. Compressibility Correction

The compressibility function, $F(M_t)$, is given by

Release 15.0 - © SAS IP, Inc. All rights reserved. - Contains proprietary and confidential information of ANSYS, Inc. and its subsidiaries and affiliates.

$$F(M_t) = \begin{cases} 0 & M_t \le M_{t0} \\ M_t^2 - M_{t0}^2 & M_t > \mathrm{M}_{t0} \end{cases} \tag{4.90}$$

where

$$M_t^2 \equiv \frac{2k}{a^2} \tag{4.91}$$

$$M_{t0} = 0.25 \tag{4.92}$$

$$a = \sqrt{\gamma RT} \tag{4.93}$$

Note that, in the high-Reynolds number form of the $k$-$\omega$ model, $\beta_i^* = \beta_\infty^*$. In the incompressible form, $\beta^* = \beta_i^*$.

**Note**

The compressibility correction has been calibrated for a very limited number of free shear flow experiments, and it is not recommended for general use. It is disabled by default. For details, see Model Enhancements in the *Fluent User's Guide*.

#### 4.4.1.6. Model Constants

$$\alpha_\infty^* = 1,\ \alpha_\infty = 0.52,\ \alpha_0 = \frac{1}{9},\ \beta_\infty^* = 0.09,\ \beta_i = 0.072,\ R_\beta = 8$$

$$R_k = 6,\ R_\omega = 2.95,\ \zeta^* = 1.5,\ M_{t0} = 0.25,\ \sigma_k = 2.0,\ \sigma_\omega = 2.0$$

### 4.4.2. Shear-Stress Transport (SST) k-ω Model

#### 4.4.2.1. Overview

The shear-stress transport (SST) $k$-$\omega$ model was developed by Menter [290] (p. 745) to effectively blend the robust and accurate formulation of the $k$-$\omega$ model in the near-wall region with the freestream independence of the $k$-$\varepsilon$ model in the far field. To achieve this, the $k$-$\varepsilon$ model is converted into a $k$-$\omega$ formulation. The SST $k$-$\omega$ model is similar to the standard $k$-$\omega$ model, but includes the following refinements:

- The standard $k$-$\omega$ model and the transformed $k$-$\varepsilon$ model are both multiplied by a blending function and both models are added together. The blending function is designed to be one in the near-wall region, which activates the standard $k$-$\omega$ model, and zero away from the surface, which activates the transformed $k$-$\varepsilon$ model.
- The SST model incorporates a damped cross-diffusion derivative term in the $\omega$ equation.
- The definition of the turbulent viscosity is modified to account for the transport of the turbulent shear stress.
- The modeling constants are different.


Release 15.0 - © SAS IP, Inc. All rights reserved. - Contains proprietary and confidential information of ANSYS, Inc. and its subsidiaries and affiliates.

These features make the SST $k$-$\omega$ model more accurate and reliable for a wider class of flows (for example, adverse pressure gradient flows, airfoils, transonic shock waves) than the standard $k$-$\omega$ model.

### 4.4.2.2. Transport Equations for the SST k-ω Model

The SST $k$-$\omega$ model has a similar form to the standard $k$-$\omega$ model:

$$\frac{\partial}{\partial t}(\rho k)+\frac{\partial}{\partial x_i}(\rho k u_i)=\frac{\partial}{\partial x_j}\left(\Gamma_k\frac{\partial k}{\partial x_j}\right)+G_k-Y_k+S_k \tag{4.94}$$

and

$$\frac{\partial}{\partial t}(\rho\omega)+\frac{\partial}{\partial x_j}\left(\rho\omega u_j\right)=\frac{\partial}{\partial x_j}\left(\Gamma_\omega\frac{\partial \omega}{\partial x_j}\right)+G_\omega-Y_\omega+D_\omega+S_\omega \tag{4.95}$$

In these equations, the term $G_k$ represents the production of turbulence kinetic energy, and is defined in the same manner as in the standard k-$\omega$ model. $G_\omega$ represents the generation of $\omega$, calculated as described for the standard $k$-$\omega$ model in Modeling the Turbulence Production (p. 60). $\Gamma_k$ and $\Gamma_\omega$ represent the effective diffusivity of $k$ and $\omega$, respectively, which are calculated as described below. $Y_k$ and $Y_\omega$ represent the dissipation of $k$ and $\omega$ due to turbulence, calculated as described in Modeling the Turbulence Dissipation (p. 60). $D_\omega$ represents the cross-diffusion term, calculated as described below. $S_k$ and $S_\omega$ are user-defined source terms.

### 4.4.2.3. Modeling the Effective Diffusivity

The effective diffusivities for the SST $k$-$\omega$ model are given by

$$\Gamma_k=\mu+\frac{\mu_t}{\sigma_k} \tag{4.96}$$

$$\Gamma_\omega=\mu+\frac{\mu_t}{\sigma_\omega} \tag{4.97}$$

where $\sigma_k$ and $\sigma_\omega$ are the turbulent Prandtl numbers for $k$ and $\omega$, respectively. The turbulent viscosity, $\mu_t$, is computed as follows:

$$\mu_t=\frac{\rho k}{\omega}\frac{1}{\max\left[\frac{1}{\alpha^*},\frac{SF_2}{a_1\omega}\right]} \tag{4.98}$$

where $S$ is the strain rate magnitude and

$$\sigma_k=\frac{1}{F_1/\sigma_{k,1}+(1-F_1)/\sigma_{k,2}} \tag{4.99}$$

$$\sigma_\omega=\frac{1}{F_1/\sigma_{\omega,1}+(1-F_1)/\sigma_{\omega,2}} \tag{4.100}$$

$\alpha^*$ is defined in Equation 4.68 (p. 59). The blending functions, $F_1$ and $F_2$, are given by

Release 15.0 - © SAS IP, Inc. All rights reserved. - Contains proprietary and confidential information of ANSYS, Inc. and its subsidiaries and affiliates.

$$F_1 = \tanh\left(\Phi_1^4\right) \tag{4.101}$$

$$\Phi_1 = \min\left[\max\left(\frac{\sqrt{k}}{0.09\omega y}, \frac{500\mu}{\rho y^2 \omega}\right), \frac{4\rho k}{\sigma_{\omega,2} D_\omega^+ y^2}\right] \tag{4.102}$$

$$D_\omega^+ = \max\left[2\rho \frac{1}{\sigma_{\omega,2}} \frac{1}{\omega} \frac{\partial k}{\partial x_j} \frac{\partial \omega}{\partial x_j}, 10^{-10}\right] \tag{4.103}$$

$$F_2 = \tanh\left(\Phi_2^2\right) \tag{4.104}$$

$$\Phi_2 = \max\left[2\frac{\sqrt{k}}{0.09\omega y}, \frac{500\mu}{\rho y^2 \omega}\right] \tag{4.105}$$

where $y$ is the distance to the next surface and $D_\omega^+$ is the positive portion of the cross-diffusion term (see Equation 4.113 (p. 65)).

## 4.4.2.4. Modeling the Turbulence Production

### 4.4.2.4.1. Production of k

The term $G_k$ represents the production of turbulence kinetic energy, and is defined in the same manner as in the standard $k$-$\omega$ model. See Modeling the Turbulence Production (p. 60) for details.

### 4.4.2.4.2. Production of ω

The term $G_\omega$ represents the production of $\omega$ and is given by

$$G_\omega = \frac{\alpha}{v_t} G_k \tag{4.106}$$

Note that this formulation differs from the standard $k$-$\omega$ model. The difference between the two models also exists in the way the term $\alpha_\infty$ is evaluated. In the standard $k$-$\omega$ model, $\alpha_\infty$ is defined as a constant (0.52). For the SST $k$-$\omega$ model, $\alpha_\infty$ is given by

$$\alpha_\infty = F_1 \alpha_{\infty,1} + (1 - F_1)\alpha_{\infty,2} \tag{4.107}$$

where

$$\alpha_{\infty,1} = \frac{\beta_{i,1}}{\beta_\infty^*} - \frac{\kappa^2}{\sigma_{w,1}\sqrt{\beta_\infty^*}} \tag{4.108}$$

$$\alpha_{\infty,2} = \frac{\beta_{i,2}}{\beta_\infty^*} - \frac{\kappa^2}{\sigma_{w,2}\sqrt{\beta_\infty^*}} \tag{4.109}$$

where $\kappa$ is 0.41.


Release 15.0 - © SAS IP, Inc. All rights reserved. - Contains proprietary and confidential information of ANSYS, Inc. and its subsidiaries and affiliates.

### 4.4.2.5. Modeling the Turbulence Dissipation

#### 4.4.2.5.1. Dissipation of k

The term $Y_k$ represents the dissipation of turbulence kinetic energy, and is defined in a similar manner as in the standard $k$-$\omega$ model (see Modeling the Turbulence Dissipation (p. 60)). The difference is in the way the term $f_{\beta^*}$ is evaluated. In the standard $k$-$\omega$ model, $f_{\beta^*}$ is defined as a piecewise function. For the SST $k$-$\omega$ model, $f_{\beta^*}$ is a constant equal to 1. Thus,

$$Y_k = \rho\beta^* k\omega \tag{4.110}$$

#### 4.4.2.5.2. Dissipation of ω

The term $Y_\omega$ represents the dissipation of $\omega$, and is defined in a similar manner as in the standard $k$-$\omega$ model (see Modeling the Turbulence Dissipation (p. 60)). The difference is in the way the terms $\beta_i$ and $f_\beta$ are evaluated. In the standard $k$-$\omega$ model, $\beta_i$ is defined as a constant (0.072) and $f_\beta$ is defined in Equation 4.85 (p. 61). For the SST $k$-$\omega$ model, $f_\beta$ is a constant equal to 1. Thus,

$$Y_k = \rho\beta\omega^2 \tag{4.111}$$

Instead of having a constant value, $\beta_i$ is given by

$$\beta_i = F_1\beta_{i,1} + (1 - F_1)\beta_{i,2} \tag{4.112}$$

and $F_1$ is obtained from Equation 4.101 (p. 64).

### 4.4.2.6. Cross-Diffusion Modification

The SST $k$-$\omega$ model is based on both the standard $k$-$\omega$ model and the standard $k$-$\varepsilon$ model. To blend these two models together, the standard $k$-$\varepsilon$ model has been transformed into equations based on $k$ and $\omega$, which leads to the introduction of a cross-diffusion term ($D_\omega$ in Equation 4.95 (p. 63)). $D_\omega$ is defined as

$$D_\omega = 2(1 - F_1)\rho\frac{1}{\omega\sigma_{\omega,2}}\frac{\partial k}{\partial x_j}\frac{\partial \omega}{\partial x_j} \tag{4.113}$$

### 4.4.2.7. Model Constants

$$\sigma_{k,1} = 1.176,\ \sigma_{\omega,1} = 2.0,\ \sigma_{k,2} = 1.0,\ \sigma_{\omega,2} = 1.168$$

$$a_1 = 0.31,\ \beta_{i,1} = 0.075,\ \beta_{i,2} = 0.0828$$

All additional model constants ($\alpha^*_\infty$, $\alpha_\infty$, $\alpha_0$, $\beta^*_\infty$, $R_\beta$, $R_k$, $R_\omega$, $\zeta^*$, and $M_{t0}$) have the same values as for the standard $k$-$\omega$ model (see Model Constants (p. 62)).

Release 15.0 - © SAS IP, Inc. All rights reserved. - Contains proprietary and confidential information of ANSYS, Inc. and its subsidiaries and affiliates.

## 4.4.3. Turbulence Damping

In free surface flows, a high velocity gradient at the interface between two fluids results in high turbulence generation, in both phases. Hence, turbulence damping is required in the interfacial area to model such flows correctly.

**Important**

Turbulence damping is available only with the $k$-$\omega$ models.

The following term is added as a source to the $\omega$-equation [107] (p. 734)

$$S_i = A_i \Delta n \beta \rho_i \left( \frac{B 6 \mu_i}{\beta \rho_i \Delta n^2} \right)^2 \tag{4.114}$$

where

$A_i$ = Interfacial area density for phase $i$

$\Delta n$ = Cell height normal to interface

$\beta$ = $k$-$\omega$ model closure coefficient of destruction term, which is equal to 0.075

$B$ = Damping factor

$\mu_i$ = Viscosity of phase $i$

$\rho_i$ = Density of phase $i$

The interfacial area density for phase $i$ is calculated as

$$A_i = 2.0\ \alpha_i\ |\nabla \alpha_i| \tag{4.115}$$

where

$\alpha_i$ = Volume fraction of phase $i$

$|\nabla \alpha_i|$ = Magnitude of gradient of volume fraction

The grid size $\Delta n$ is calculated internally using grid information. You can specify the damping factor $B$ in the **Viscous Model** dialog box. The default value for the damping factor is 10.

Turbulence damping is available with the VOF and Mixture models. Note that it is also available with the Eulerian multiphase model when using the immiscible fluid model. To use this option, refer to Turbulence Damping.

If the Eulerian multiphase model is enabled, you can specify a turbulence multiphase model. If the **Per Phase** turbulence model is used, then the source term is added to the $\omega$-equation of each phase. If the VOF or mixture model is enabled, or the Eulerian multiphase model is used with the **Mixture** turbulence model, the term is summed over all the phases and added as a source term to the mixture level $\omega$-equation. For information about turbulence multiphase modeling, see Modeling Turbulence.


Release 15.0 - © SAS IP, Inc. All rights reserved. - Contains proprietary and confidential information of ANSYS, Inc. and its subsidiaries and affiliates.

### 4.4.4. Wall Boundary Conditions

The wall boundary conditions for the $k$ equation in the $k$-$\omega$ models are treated in the same way as the $k$ equation is treated when enhanced wall treatments are used with the $k$-$\varepsilon$ models. This means that all boundary conditions for wall-function meshes will correspond to the wall function approach, while for the fine meshes, the appropriate low-Reynolds number boundary conditions will be applied.

In ANSYS Fluent the value of $\omega$ at the wall is specified as

$$\omega_w = \frac{\rho (u^*)^2}{\mu} \omega^+ \tag{4.116}$$

Analytical solutions can be given for both the laminar sublayer

$$\omega^+ = \frac{6}{\beta_i (y^+)^2} \tag{4.117}$$

and the logarithmic region:

$$\omega^+ = \frac{1}{\sqrt{\beta_\infty^*}} \frac{d u_{turb}^+}{d y^+} \tag{4.118}$$

Therefore, a wall treatment can be defined for the $\omega$-equation, which switches automatically from the viscous sublayer formulation to the wall function, depending on the grid. This blending has been optimized using Couette flow in order to achieve a grid independent solution of the skin friction value and wall heat transfer. This improved blending is the default behavior for near wall treatment.

## 4.5. k-kl-ω Transition Model

This section describes the theory behind the $k$-$kl$-$\omega$ Transition model. For details about using the model in ANSYS Fluent, see Modeling Turbulence and Setting Up the Transition k-kl-ω Model in the User's Guide.

For more information, see the following sections:

4.5.1. Overview
4.5.2. Transport Equations for the k-kl-ω Model

### 4.5.1. Overview

The $k$-$kl$-$\omega$ transition model [474] (p. 755) is used to predict boundary layer development and calculate transition onset. This model can be used to effectively address the transition of the boundary layer from a laminar to a turbulent regime.

### 4.5.2. Transport Equations for the k-kl-ω Model

The $k$-$kl$-$\omega$ model is considered to be a three-equation eddy-viscosity type, which includes transport equations for turbulent kinetic energy ($k_T$), laminar kinetic energy ($k_L$), and the inverse turbulent time scale ($\omega$)

$$\frac{Dk_T}{Dt} = P_{K_T} + R + R_{NAT} - \omega k_T - D_T + \frac{\partial}{\partial x_j}\left[\left(\nu + \frac{\alpha_T}{\alpha_k}\right)\frac{\partial k_T}{\partial x_j}\right] \tag{4.119}$$

$$\frac{Dk_L}{Dt}=P_{K_L}-R-R_{NAT}-D_L+\frac{\partial}{\partial x_j}\left[v\frac{\partial k_L}{\partial x_j}\right] \tag{4.120}$$

$$\begin{aligned}\frac{D_\omega}{D_t}= \quad & C_{\omega 1}\frac{\omega}{k_T}P_{k_T}+\left(\frac{C_{\omega R}}{f_W}-1\right)\frac{\omega}{k_T}(R+R_{NAT})-C_{\omega 2}\omega^2 \\ & +C_{\omega 3}f_\omega\alpha_T f_W^2\frac{\sqrt{k_T}}{d^3}+\frac{\partial}{\partial x_j}\left[\left(v+\frac{\alpha_T}{\alpha_\omega}\right)\frac{\partial\omega}{\partial x_j}\right]\end{aligned} \tag{4.121}$$

The inclusion of the turbulent and laminar fluctuations on the mean flow and energy equations via the eddy viscosity and total thermal diffusivity is as follows:

$$\overline{-u_i u_j}=v_{TOT}\left(\frac{\partial U_i}{\partial x_j}+\frac{\partial U_j}{\partial x_i}\right)-\frac{2}{3}k_{TOT}\delta_{ij} \tag{4.122}$$

$$\overline{-u_i\theta}=\alpha_{\theta,TOT}\frac{\partial\theta}{\partial x_i} \tag{4.123}$$

The effective length is defined as

$$\lambda_{eff}=MIN\,(C_\lambda d,\lambda_T) \tag{4.124}$$

where $\lambda_T$ is the turbulent length scale and is defined by

$$\lambda_T=\frac{\sqrt{k}}{\omega} \tag{4.125}$$

and the small scale energy is defined by

$$k_{T,s}=f_{ss}f_W k_T \tag{4.126}$$

$$f_W=\frac{\lambda_{eff}}{\lambda_T} \tag{4.127}$$

$$f_{ss}=exp\left[-\left(\frac{C_{ss}v\Omega}{k_T}\right)^2\right] \tag{4.128}$$

The large scale energy is given by

$$k_{T,l}=k_T-k_{T,s} \tag{4.129}$$

Note that the sum of Equation 4.126 (p. 68) and Equation 4.129 (p. 68) yields the turbulent kinetic energy $k_T$.

The turbulence production term generated by turbulent fluctuations is given by

$$P_{k_T}=v_{T,s}S^2 \tag{4.130}$$

where the small-scale turbulent viscosity is $v_{T,s}$

$$v_{T,s}=f_v f_{INT}C_\mu\sqrt{k_{T,s}}\lambda_{eff} \tag{4.131}$$


Release 15.0 - © SAS IP, Inc. All rights reserved. - Contains proprietary and confidential information of ANSYS, Inc. and its subsidiaries and affiliates.

and

$$C_{\mu}=\frac{1}{A_0+A_s(S/\omega)} \tag{4.132}$$

$$f_v=1-exp\left(-\frac{\sqrt{Re_{T,s}}}{A_v}\right) \tag{4.133}$$

A damping function defining the turbulent production due to intermittency is given by

$$f_{INT}=MIN\left(\frac{k_L}{C_{INT}k_{TOT}},1\right) \tag{4.134}$$

$$Re_{T,s}=\frac{f_W^2 k_T}{v\omega} \tag{4.135}$$

In Equation 4.120 (p. 68), $P_{k_L}$ is the production of laminar kinetic energy by large scale turbulent fluctuations, such that

$$P_{k_L}=v_{T,l}S^2 \tag{4.136}$$

The large-scale turbulent viscosity $v_{T,1}$ is modeled as

$$v_{T,1}=MIN\left\{v_{T,1}^*,\frac{0.5\left(k_L+k_{T,1}\right)}{S}\right\} \tag{4.137}$$

where

$$v_{T,1}^*=f_{\tau,1}C_{11}\left(\frac{\Omega\lambda_{eff}^2}{v}\right)\sqrt{k_{T,1}}\lambda_{eff}+\beta_{TS}C_{12}\phi_{NAT}d^2\Omega \tag{4.138}$$

The limit in Equation 4.137 (p. 69) binds the realizability such that it is not violated in the two-dimensional developing boundary layer. The time-scale-based damping function $f_{\tau,1}$ is

$$f_{\tau,1}=1-exp\left[-C_{\tau,1}\frac{k_{T,1}}{\lambda_{eff}^2\Omega^2}\right] \tag{4.139}$$

where $\beta_{TS}$ from Equation 4.138 (p. 69) is

$$\beta_{TS}=1-exp\left(-\frac{MAX\left(\phi_{NAT}-C_{TS,crit},0\right)^2}{A_{TS}}\right) \tag{4.140}$$

$$\phi_{NAT}=\frac{d^2\Omega}{v} \tag{4.141}$$

Near-wall dissipation is given by

$$D_T=2v\frac{\partial\sqrt{k_T}}{\partial x_j}\frac{\partial\sqrt{k_T}}{\partial x_j} \tag{4.142}$$

Release 15.0 - © SAS IP, Inc. All rights reserved. - Contains proprietary and confidential information of ANSYS, Inc. and its subsidiaries and affiliates.

$$D_L = 2\nu \frac{\partial \sqrt{k_L}}{\partial x_j} \frac{\partial \sqrt{k_L}}{\partial x_j} \tag{4.143}$$

In Equation 4.119 (p. 67) – Equation 4.121 (p. 68), $R$ represents the averaged effect of the breakdown of streamwise fluctuations into turbulence during bypass transition:

$$R = C_R \beta_{BP} k_L \omega / f_W \tag{4.144}$$

$\beta_{BP}$, which is the threshold function controls the bypass transition process:

$$\beta_{BP} = 1 - exp\left(-\frac{\phi_{BP}}{A_{BP}}\right) \tag{4.145}$$

$$\phi_{BP} = MAX\left[\left(\frac{k_T}{\nu \Omega} - C_{BP,crit}\right), 0\right] \tag{4.146}$$

The breakdown to turbulence due to instabilities is considered to be a natural transition production term, given by

$$R_{NAT} = C_{R,NAT} \beta_{NAT} k_L \Omega \tag{4.147}$$

$$\beta_{NAT} = 1 - exp\left[-\frac{MAX\left(\phi_{NAT} - C_{NAT,crit}/f_{NAT,crit}, 0\right)}{A_{NAT}}\right] \tag{4.148}$$

$$f_{NAT,crit} = 1 - exp\left(C_{NC} \frac{\sqrt{k_L}\, d}{\nu}\right) \tag{4.149}$$

The use of $\omega$ as the scale-determining variable can lead to a reduced intermittency effect in the outer region of a turbulent boundary layer, and consequently an elimination of the wake region in the velocity profile. From Equation 4.121 (p. 68), the following damping is defined as

$$f_\omega = 1 - exp\left[-0.41\left(\frac{\lambda_{eff}}{\lambda_T}\right)^4\right] \tag{4.150}$$

The total eddy viscosity and eddy diffusivity included in Equation 4.122 (p. 68) and Equation 4.123 (p. 68) are given by

$$\nu_{TOT} = \nu_{T,s} + \nu_{T,l} \tag{4.151}$$

$$\alpha_{\theta,TOT} = f_W\left(\frac{k_T}{k_{TOT}}\right)\frac{\nu_{T,s}}{Pr_\theta} + \left(1 - f_W\right) C_{\alpha,\theta} \sqrt{k_T} \lambda_{eff} \tag{4.152}$$

The turbulent scalar diffusivity in Equation 4.119 (p. 67) – Equation 4.121 (p. 68) is defined as

$$\alpha_T = f_\nu C_{\mu,std} \sqrt{k_{T,s}} \lambda_{eff} \tag{4.153}$$

$$k_{TOT} = k_T + k_L \tag{4.154}$$

A compressibility correction, similar to the one in the $k$-$\varepsilon$ model (Effects of Compressibility on Turbulence in the k-ε Models) is available for the $k$-$kl$-$\omega$ model. By default, this compressibility correction option is turned off. For details see, Model Enhancements in the *Fluent User's Guide*.


Release 15.0 - © SAS IP, Inc. All rights reserved. - Contains proprietary and confidential information of ANSYS, Inc. and its subsidiaries and affiliates.

#### 4.5.2.1. Model Constants

The model constants for the $k$-$kl$-$\omega$ transition model are listed below [474] (p. 755)

$A_0=4.04$, $A_s=2.12$, $A_v=6.75$, $A_{BP}=0.6$

$A_{NAT}=200$, $A_{TS}=200$, $C_{BP,crit}=1.2$, $C_{NC}=0.1$

$C_{NAT,crit}=1250$, $C_{INT}=0.75$, $C_{TS,crit}=1000$, $C_{R,NAT}=0.02$

$C_{11}=3.4\times10^{-6}$, $C_{12}=1.0\times10^{-10}$, $C_R=0.12$, $C_{\alpha,\theta}=0.035$

$C_{SS}=1.5$, $C_{\tau,1}=4360$, $C_{\omega1}=0.44$, $C_{\omega2}=0.92$

$C_{\omega3}=0.3$, $C_{\omega R}=1.5$, $C_{\lambda}=2.495$, $C_{\mu,std}=0.09$

$Pr_{\theta}=0.85$, $\sigma_k=1$, $\sigma_{\omega}=1.17$

## 4.6. Transition SST Model

This section describes the theory behind the Transition SST model. Information is presented in the following sections:

4.6.1. Overview
4.6.2. Transport Equations for the Transition SST Model
4.6.3. Mesh Requirements
4.6.4. Specifying Inlet Turbulence Levels

For details about using the model in ANSYS Fluent, see Modeling Turbulence and Setting Up the Transition SST Model in the User's Guide.

### 4.6.1. Overview

The transition SST model is based on the coupling of the SST $k-\omega$ transport equations with two other transport equations, one for the intermittency and one for the transition onset criteria, in terms of momentum-thickness Reynolds number. An ANSYS empirical correlation (Langtry and Menter) has been developed to cover standard bypass transition as well as flows in low freestream turbulence environments.

In addition, a very powerful option has been included to allow you to enter your own user-defined empirical correlation, which can then be used to control the transition onset momentum thickness Reynolds number equation. To learn how to set up the transition SST model, see Setting Up the Transition SST Model (in the User's Guide).

### 4.6.2. Transport Equations for the Transition SST Model

The transport equation for the intermittency $\gamma$ is defined as:

$$\frac{\partial(\rho\gamma)}{\partial t}+\frac{\partial\left(\rho U_j\gamma\right)}{\partial x_j}=P_{\gamma1}-E_{\gamma1}+P_{\gamma2}-E_{\gamma2}+\frac{\partial}{\partial x_j}\left[\left(\mu+\frac{\mu_t}{\sigma_{\gamma}}\right)\frac{\partial\gamma}{\partial x_j}\right] \tag{4.155}$$

The transition sources are defined as follows:

Release 15.0 - © SAS IP, Inc. All rights reserved. - Contains proprietary and confidential information of ANSYS, Inc. and its subsidiaries and affiliates.

$$\begin{aligned} P_{\gamma 1} &= C_{a1} F_{length} \rho S [\gamma F_{onset}]^{c_{\gamma 3}} \\ E_{\gamma 1} &= C_{e1} P_{\gamma 1} \gamma \end{aligned} \tag{4.156}$$

where $S$ is the strain rate magnitude, $F_{length}$ is an empirical correlation that controls the length of the transition region, and $C_{a1}$ and $C_{e1}$ hold the values of 2 and 1, respectively. The destruction/relaminarization sources are defined as follows:

$$\begin{aligned} P_{\gamma 2} &= C_{a2} \rho \Omega \gamma F_{turb} \\ E_{\gamma 2} &= C_{e2} P_{\gamma 2} \gamma \end{aligned} \tag{4.157}$$

where $\Omega$ is the vorticity magnitude. The transition onset is controlled by the following functions:

$$\begin{aligned} Re_V &= \frac{\rho y^2 S}{\mu} \\ R_T &= \frac{\rho k}{\mu \omega} \end{aligned} \tag{4.158}$$

$$\begin{aligned} F_{onset1} &= \frac{Re_V}{2.193 Re_{\theta c}} \\ F_{onset2} &= min\left( max\left( F_{onset1}, F_{onset1}^4 \right), 2.0 \right) \end{aligned} \tag{4.159}$$

$$\begin{aligned} F_{onset3} &= max\left( 1 - \left( \frac{R_T}{2.5} \right)^3, 0 \right) \\ F_{onset} &= max\left( F_{onset2} - F_{onset3}, 0 \right) \\ F_{turb} &= e^{-\left( \frac{R_T}{4} \right)^4} \end{aligned} \tag{4.160}$$

where $y$ is the wall distance and $Re_{\theta c}$ is the critical Reynolds number where the intermittency first starts to increase in the boundary layer. This occurs upstream of the transition Reynolds number $\tilde{Re}_{\theta t}$ and the difference between the two must be obtained from an empirical correlation. Both the $F_{length}$ and $Re_{\theta c}$ correlations are functions of $\tilde{Re}_{\theta t}$.

The constants for the intermittency equation are:

$$C_{a1} = 2;\ C_{e1} = 1;\ C_{a2} = 0.06;\ C_{e2} = 50;\ c_{\gamma 3} = 0.5;\ \sigma_\gamma = 1.0 \tag{4.161}$$

The transport equation for the transition momentum thickness Reynolds number $\tilde{Re}_{\theta t}$ is

$$\frac{\partial (\rho \tilde{Re}_{\theta t})}{\partial t} + \frac{\partial \left( \rho U_j \tilde{Re}_{\theta t} \right)}{\partial x_j} = P_{\theta t} + \frac{\partial}{\partial x_j} \left[ \sigma_{\theta t} \left( \mu + \mu_t \right) \frac{\partial \tilde{Re}_{\theta t}}{\partial x_j} \right] \tag{4.162}$$

The source term is defined as follows:


Release 15.0 - © SAS IP, Inc. All rights reserved. - Contains proprietary and confidential information of ANSYS, Inc. and its subsidiaries and affiliates.

$$\begin{aligned} P_{\theta t} &= c_{\theta t}\frac{\rho}{t}(Re_{\theta t}-\tilde{Re}_{\theta t})\,(1.0-F_{\theta t}) \\ t &= \frac{500\mu}{\rho U^2} \end{aligned} \tag{4.163}$$

$$F_{\theta t}=min\left(max\left(F_{wake}e^{\left(-\frac{y}{\delta}\right)^4},1.0-\left(\frac{\gamma-1/50}{1.0-1/50}\right)^2\right),1.0\right) \tag{4.164}$$

$$\begin{aligned} \theta_{BL} &= \frac{\tilde{Re}_{\theta t}\mu}{\rho U} \\ \delta_{BL} &= \frac{15}{2}\theta_{BL} \\ \delta &= \frac{50\Omega y}{U}\delta_{BL} \end{aligned} \tag{4.165}$$

$$\begin{aligned} Re_{\omega} &= \frac{\rho\omega y^2}{\mu} \\ F_{wake} &= e^{-\left(\frac{Re_{\omega}}{1E+5}\right)^2} \end{aligned} \tag{4.166}$$

The model constants for the $\tilde{Re}_{\theta t}$ equation are:

$$c_{\theta t}=0.03\,;\quad \sigma_{\theta t}=2.0 \tag{4.167}$$

The boundary condition for $\tilde{Re}_{\theta t}$ at a wall is zero flux. The boundary condition for $\tilde{Re}_{\theta t}$ at an inlet should be calculated from the empirical correlation based on the inlet turbulence intensity.

The model contains three empirical correlations. $Re_{\Theta t}$ is the transition onset as observed in experiments. This has been modified from Menter et al. [294] (p. 745) in order to improve the predictions for natural transition. It is used in Equation 4.162 (p. 72). $F_{length}$ is the length of the transition zone and is substituted in Equation 4.155 (p. 71). $Re_{\Theta c}$ is the point where the model is activated in order to match both $Re_{\Theta t}$ and $F_{length}$, and is used in Equation 4.159 (p. 72). These empirical correlations are provided by Langtry and Menter [225] (p. 741).

$$\begin{aligned} Re_{\Theta t} &= f\,(Tu\,,\lambda\,) \\ F_{length} &= f\,(\tilde{Re}_{\Theta t}) \\ Re_{\Theta c} &= f\,(\tilde{Re}_{\Theta t}) \end{aligned} \tag{4.168}$$

The first empirical correlation is a function of the local turbulence intensity, $Tu$:

$$Tu=\frac{100}{U}\sqrt{\frac{2}{3}k} \tag{4.169}$$

where $k$ is the turbulent energy.

The Thwaites' pressure gradient coefficient $\lambda_\theta$ is defined as

Release 15.0 - © SAS IP, Inc. All rights reserved. - Contains proprietary and confidential information of ANSYS, Inc. and its subsidiaries and affiliates.

$$\lambda_\theta = \left(\theta^2/\nu\right) dU/ds \tag{4.170}$$

where $dU/ds$ is the acceleration in the streamwise direction.

### 4.6.2.1. Separation-Induced Transition Correction

The modification for separation-induced transition is:

$$\begin{aligned} \gamma_{sep} &= min\left(C_{s1} max\left[\left(\frac{Re_v}{3.235 Re_{\theta c}}\right) - 1, 0\right] F_{reattch}, 2\right) F_{\theta t} \\ F_{reattch} &= e^{-\left(\frac{R_T}{20}\right)^4} \\ \gamma_{eff} &= max\left(\gamma, \gamma_{sep}\right) \end{aligned} \tag{4.171}$$

Here, $C_{s1}$ is a constant with a value of 2.

The model constants in Equation 4.171 (p. 74) have been adjusted from those of Menter et al. [294] (p. 745) in order to improve the predictions of separated flow transition. The main difference is that the constant that controls the relation between $Re_v$ and $Re_{\theta c}$ was changed from 2.193, its value for a Blasius boundary layer, to 3.235, the value at a separation point where the shape factor is 3.5 [294] (p. 745). The boundary condition for $\gamma$ at a wall is zero normal flux, while for an inlet, $\gamma$ is equal to 1.0.

### 4.6.2.2. Coupling the Transition Model and SST Transport Equations

The transition model interacts with the SST turbulence model by modification of the $k$-equation (Equation 4.94 (p. 63)), as follows:

$$\frac{\partial}{\partial t}(\rho k) + \frac{\partial}{\partial x_i}(\rho k u_i) = \frac{\partial}{\partial x_j}\left(\Gamma_k \frac{\partial k}{\partial x_j}\right) + G_k^* - Y_k^* + S_k \tag{4.172}$$

$$G_k^* = \gamma_{eff} \tilde{G}_k \tag{4.173}$$

$$Y_k^* = min\left(max\left(\gamma_{eff}, 0.1\right), 1.0\right) Y_k \tag{4.174}$$

where $\tilde{G}_k$ and $Y_k$ are the original production and destruction terms for the SST model. Note that the production term in the $\omega$-equation is not modified. The rationale behind the above model formulation is given in detail in Menter et al. [294] (p. 745).

In order to capture the laminar and transitional boundary layers correctly, the mesh must have a $y^+$ of approximately one. If the $y^+$ is too large (that is, > 5), then the transition onset location moves upstream with increasing $y^+$. It is recommended that you use the bounded second order upwind based discretization for the mean flow, turbulence and transition equations.


Release 15.0 - © SAS IP, Inc. All rights reserved. - Contains proprietary and confidential information of ANSYS, Inc. and its subsidiaries and affiliates.

### 4.6.2.3. Transition SST and Rough Walls

When the Transition SST Model is used together with rough walls, the roughness correlation must be enabled in the Viscous Model Dialog Box. This correlation requires the geometric roughness height $K$ as an input parameter, since, for the transition process from laminar to turbulent flow, the geometric roughness height is more important than the equivalent sand-grain roughness height $K_s$. Guidance to determine the appropriate equivalent sand-grain roughness height (based on the geometric roughness height, shape and distribution of the roughness elements) can be obtained, for example, from Schlichting and Gersten [394] (p. 750) and Coleman et al. [75] (p. 733).

The roughness correlation is a modification of the built-in correlation for $\tilde{\mathrm{Re}}_{\theta t}$ and is defined as:

$$\mathrm{Re}_{\theta t,rough} = \tilde{\mathrm{Re}}_{\theta t} \cdot f(K) \tag{4.175}$$

The new defined $\mathrm{Re}_{\theta t,rough}$ is then used in the correlations for $F_{length}$ and $\mathrm{Re}_{\theta c}$. $\tilde{\mathrm{Re}}_{\theta t}$ represents the transition momentum thickness Reynolds number. The value specified for the geometric roughness will apply to all walls. In case a different value is required for different walls, a user defined function can be specified. It is important to note that the function for K is used in the volume (not at the wall). The function therefore must cover the region of the boundary layer and beyond where it should be applied. As an example, assume a roughness strip on a flat plate (x-streamwise direction, y wall normal z-spanwise) at the location $1 < x < 1.2$ (m) and a boundary layer thickness in that region of perhaps $\delta = 0.01\mathrm{m}$ (spanwise extent $-0.1 < z < 0.1$ (m)). The following pseudo-code will switch between roughness K0 everywhere (could be zero) and K1 at the transition strip. The height in the y-direction does not have to be exactly the boundary layer thickness – it can be much larger – as long as it does not impact other walls in the vicinity.

$$\begin{aligned} &fstep = 0 \\ &if\ ((1 < x < 1.2)\ and\ (0 < y < 0.02)\ and\ (-0.1 < z < 0.1))\ fstep = 1 \\ &K = K0 \cdot (1 - fstep) + K1 \cdot fstep \end{aligned} \tag{4.176}$$

## 4.6.3. Mesh Requirements

The effect of increasing and decreasing $y^+$ for a flat plate test case (T3A) is shown in Figure 4.1: Effect of Increasing y+ for the Flat Plate T3A Test Case (p. 76) and Figure 4.2: Effect of Decreasing y+ for the Flat Plate T3A Test Case (p. 76). For $y^+$ values between 0.001 and 1, there is almost no effect on the solution. Once the maximum $y^+$ increases above 8, the transition onset location begins to move upstream. At a maximum $y^+$ of 25, the boundary layer is almost completely turbulent. For $y^+$ values below 0.001, the transition location appears to move downstream. This is presumably caused by the large surface value of the specific turbulence frequency $\omega$, which scales with the first mesh node height. For these reasons, very small $y^+$ values (below 0.001) should be avoided.

Release 15.0 - © SAS IP, Inc. All rights reserved. - Contains proprietary and confidential information of ANSYS, Inc. and its subsidiaries and affiliates.

**Figure 4.1: Effect of Increasing y+ for the Flat Plate T3A Test Case**

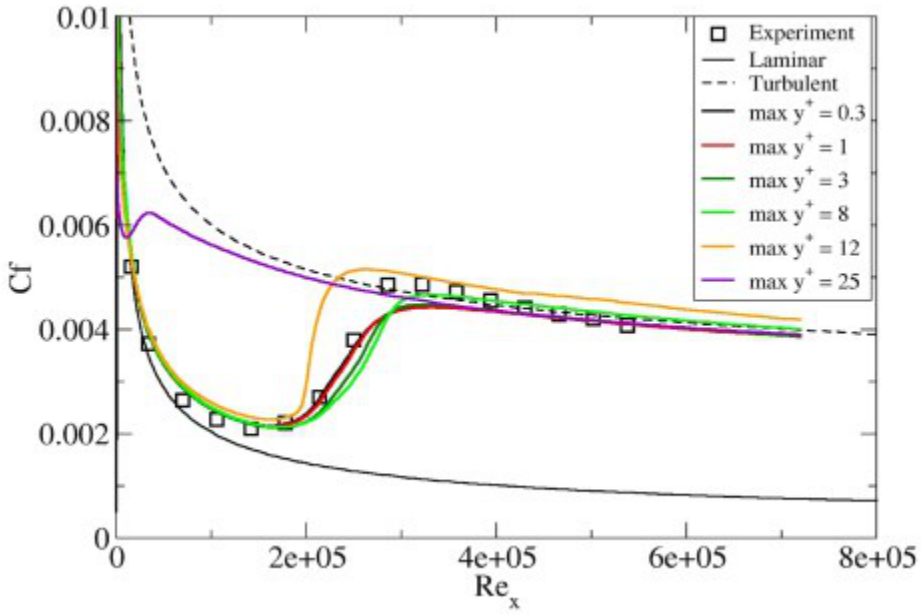


**Figure 4.2: Effect of Decreasing y+ for the Flat Plate T3A Test Case**

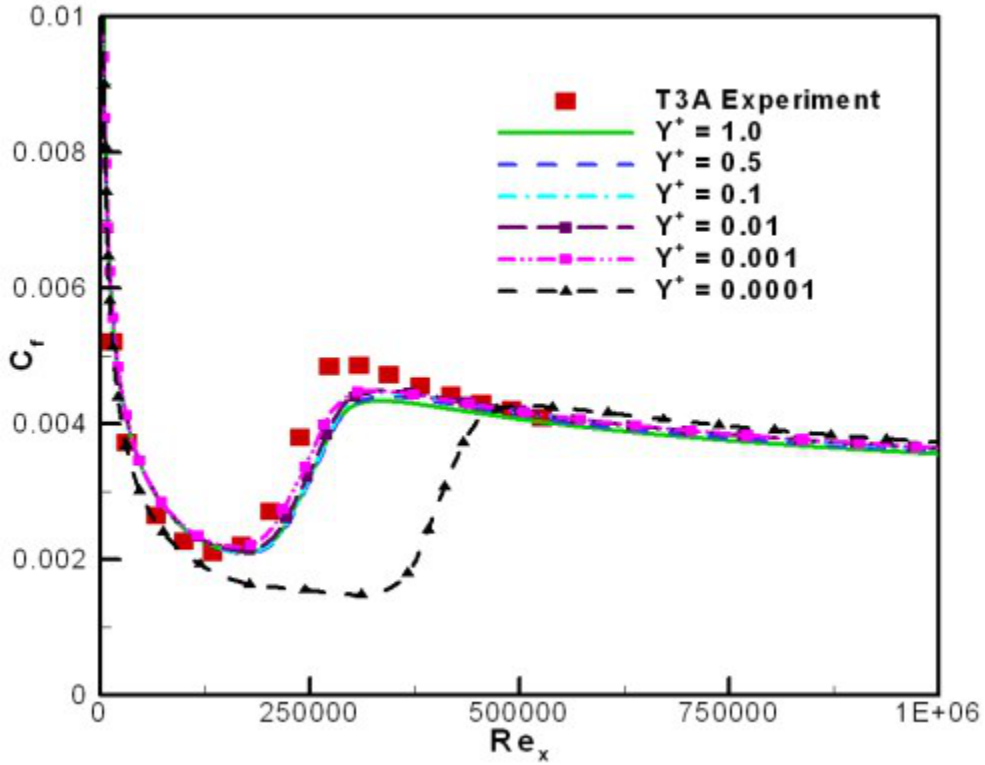


The effect of the wall normal expansion ratio from a $y^+$ value of 1 is shown in Figure 4.3: Effect of Wall Normal Expansion Ratio for the Flat Plate T3A Test Case (p. 77). For expansion factors of 1.05 and 1.1, there is no effect on the solution. For larger expansion factors of 1.2 and 1.4, there is a small but noticeable upstream shift in the transition location. Because the sensitivity of the solution to wall-normal mesh resolution can increase for flows with pressure gradients, it is recommended that you apply meshes with $y^+ < 1$ and expansion factors smaller than 1.1.


Release 15.0 - © SAS IP, Inc. All rights reserved. - Contains proprietary and confidential information of ANSYS, Inc. and its subsidiaries and affiliates.

**Figure 4.3: Effect of Wall Normal Expansion Ratio for the Flat Plate T3A Test Case**

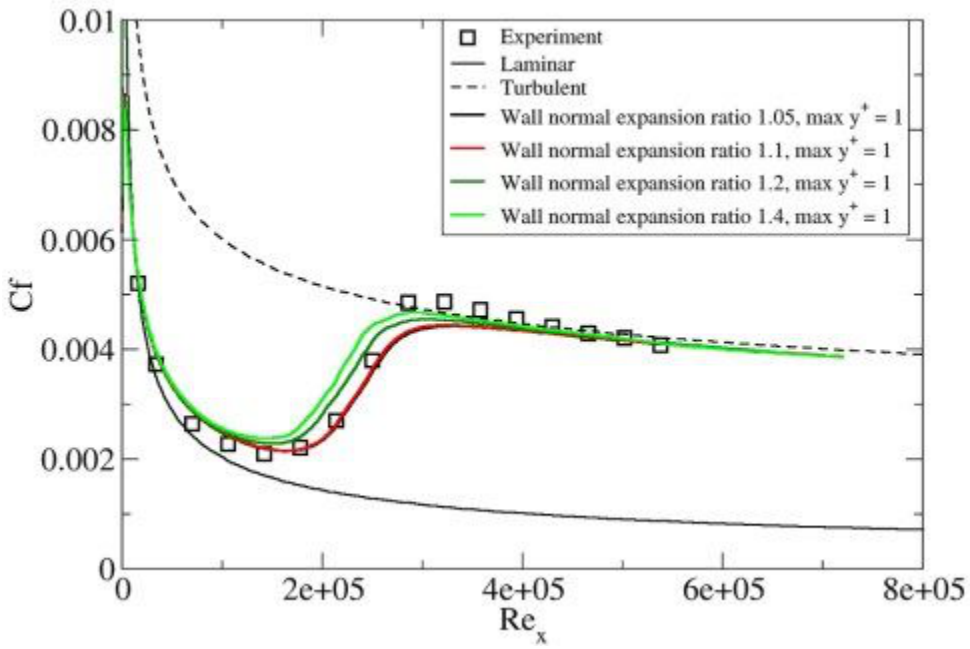


The effect of streamwise mesh refinement is shown in Figure 4.4: Effect of Streamwise Mesh Density for the Flat Plate T3A Test Case (p. 77). Surprisingly, the model was not very sensitive to the number of streamwise nodes. The solution differed significantly from the mesh-independent one only for the case of 25 streamwise nodes where there was only one cell in the transitional region. Nevertheless, the mesh-independent solution appears to occur when there is approximately 75–100 streamwise mesh nodes on the flat plate. Also, separation-induced transition occurs over a very short length; for cases where this is important, a fine mesh is necessary.

**Figure 4.4: Effect of Streamwise Mesh Density for the Flat Plate T3A Test Case**

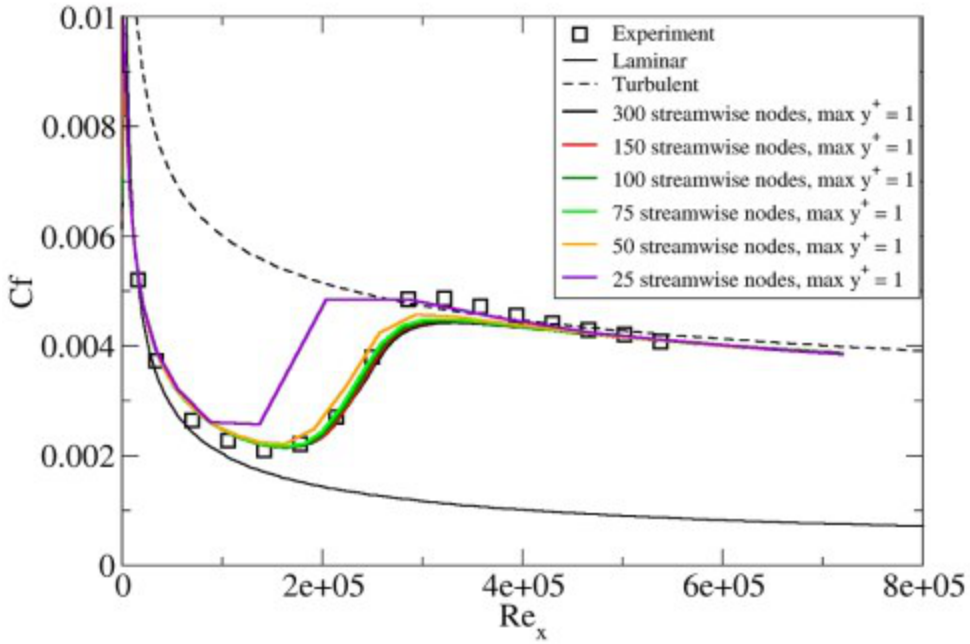


Release 15.0 - © SAS IP, Inc. All rights reserved. - Contains proprietary and confidential information of ANSYS, Inc. and its subsidiaries and affiliates.

One point to note is that for sharp leading edges, often transition can occur due to a small leading edge separation bubble. If the mesh is too coarse, the rapid transition caused by the separation bubble is not captured.

Based on the mesh sensitivity study, the recommended best practice mesh guidelines are a max $y^+$ of 1, a wall normal expansion ratio that is less than 1.1, and about 75–100 mesh nodes in the streamwise direction. Note that if separation-induced transition is present, additional mesh nodes in the streamwise direction are most likely needed. For a turbine blade, that would translate into 100–150 cells in the streamwise direction on each side of the blade.

## 4.6.4. Specifying Inlet Turbulence Levels

It has been observed that the turbulence intensity specified at an inlet can decay quite rapidly depending on the inlet viscosity ratio ($\mu_t/\mu$) (and hence turbulence eddy frequency). As a result, the local turbulence intensity downstream of the inlet can be much smaller than the inlet value (see Figure 4.5: Exemplary Decay of Turbulence Intensity (Tu) as a Function of Streamwise Distance (x) (p. 79)). Typically, the larger the inlet viscosity ratio, the smaller the turbulent decay rate. However, if too large a viscosity ratio is specified (that is, > 100), the skin friction can deviate significantly from the laminar value. There is experimental evidence that suggests that this effect occurs physically; however, at this point it is not clear how accurately the transition model reproduces this behavior. For this reason, if possible, it is desirable to have a relatively low (that is, ≈1 – 10) inlet viscosity ratio and to estimate the inlet value of turbulence intensity such that at the leading edge of the blade/airfoil, the turbulence intensity has decayed to the desired value. The decay of turbulent kinetic energy can be calculated with the following analytical solution:

$$k = k_{inlet}\left(1+\omega_{inlet}\beta t\right)^{\frac{-\beta^*}{\beta}} \tag{4.177}$$

For the SST turbulence model in the freestream the constants are:

$$\beta = 0.09,\ \beta^* = 0.0828 \tag{4.178}$$

The time scale can be determined as follows:

$$t = \frac{x}{V} \tag{4.179}$$

where $x$ is the streamwise distance downstream of the inlet and $V$ is the mean convective velocity. The eddy viscosity is defined as:

$$\mu_t = \frac{\rho k}{\omega} \tag{4.180}$$

The decay of turbulent kinetic energy equation can be rewritten in terms of inlet turbulence intensity ($Tu_{inlet}$) and inlet eddy viscosity ratio ($\mu_t/\mu$) as follows:

$$Tu = \left( Tu_{inlet}^2 \left[ 1 + \frac{3\rho V x \beta \left( Tu_{inlet}^2 \right)}{2\mu \left( \mu_t/\mu \right)_{inlet}} \right]^{\frac{-\beta^*}{\beta}} \right)^{0.5} \tag{4.181}$$


Release 15.0 - © SAS IP, Inc. All rights reserved. - Contains proprietary and confidential information of ANSYS, Inc. and its subsidiaries and affiliates.

**Figure 4.5: Exemplary Decay of Turbulence Intensity (Tu) as a Function of Streamwise Distance (x)**

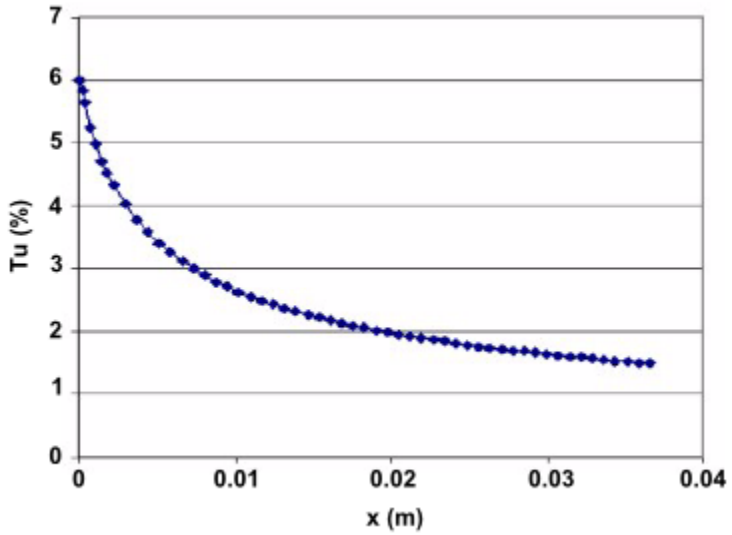


You should ensure that the $Tu$ values around the body of interest roughly satisfy $Tu$>0.1%. For smaller values of $Tu$, the reaction of the SST model production terms to the transition onset becomes too slow, and transition can be delayed past the physically correct location.

## 4.7. Intermittency Transition Model

This section describes the theory behind the Intermittency Transition model. Information is presented in the following sections:

4.7.1. Overview
4.7.2. Transport Equations for the Intermittency Transition Model
4.7.3. Coupling with the Other Models
4.7.4. Intermittency Transition Model and Rough Walls

For details about using the model in ANSYS Fluent, see Modeling Turbulence and Setting Up the Intermittency Transition Model in the User's Guide.

### 4.7.1. Overview

The $\gamma$ (intermittency) transition model is a further development based on the $\gamma$-$\mathrm{Re}_\theta$ transition model (referred to as the Transition SST model in ANSYS Fluent, as described in Transition SST Model (p. 71)). The $\gamma$ transition model solves only one transport equation for the turbulence intermittency $\gamma$, and avoids the need for the second $\mathrm{Re}_\theta$ equation of the $\gamma$-$\mathrm{Re}_\theta$ transition model. The $\gamma$ transition model has the following advantages over the $\gamma$-$\mathrm{Re}_\theta$ transition model:

- It reduces the computational effort (by solving one transport equation instead of two).
- It avoids the dependency of the $\mathrm{Re}_\theta$ equation on the velocity $U$. This makes the $\gamma$ transition model Galilean invariant. It can therefore be applied to surfaces that move relative to the coordinate system for which the velocity field is computed.

Release 15.0 - © SAS IP, Inc. All rights reserved. - Contains proprietary and confidential information of ANSYS, Inc. and its subsidiaries and affiliates.

- The model has provisions for crossflow instability that are not available for the $k$-$kl$ or the $\gamma$-$\mathrm{Re}_\theta$ transition model.
- The model formulation is simple and can be fine-tuned based on a small number of user parameters.

Like the $\gamma$-$\mathrm{Re}_\theta$ transition model, the $\gamma$ transition model is based strictly on local variables. The $\gamma$ transition model is also only available in combination with the following turbulence models:

- SST $k$-$\omega$ model
- Scale-Adaptive Simulation with SST
- Detached Eddy Simulation with SST

## 4.7.2. Transport Equations for the Intermittency Transition Model

The transport equation for intermittency is the following:

$$\frac{\partial\ (\rho\gamma)}{\partial\, t} + \frac{\partial\ \left(\rho U_j \gamma\right)}{\partial\, x_j} = P_\gamma - E_\gamma + \frac{\partial}{\partial\, x_j}\left[\left(\mu + \frac{\mu_t}{\sigma_\gamma}\right)\frac{\partial\,\gamma}{\partial\, x_j}\right] \tag{4.182}$$

The formulation of the source terms is similar in nature to the corresponding terms in the $\gamma$-$\mathrm{Re}_\theta$ transition model, but the precise details are proprietary.

As in the $\gamma$-$\mathrm{Re}_\theta$ transition model, the source terms includes a correlation to trigger the transition model.

$$\mathrm{Re}_{\theta c}\left(Tu\,,\ \lambda_\theta\right) = C_{TU1} + C_{TU2}\exp\left[-C_{TU3}\,Tu\ F_{PG}\left(\lambda_\theta\right)\right] \tag{4.183}$$

In this correlation, $\mathrm{Re}_{\theta c}$ is the critical momentum thickness Reynolds number, and $Tu$ and $\lambda_\theta$ are locally defined variables that approximate the freestream turbulence intensity and the pressure gradient parameter, respectively (see Transport Equations for the Transition SST Model (p. 71)). The function $F_{PG}$ accounts for the influence of the pressure gradient on transition, and is defined as:

$$F_{PG}\left(\lambda_\theta\right) = \begin{cases} \min\left(1 + C_{PG1}\,\lambda_\theta\ ,\ C_{PG1}^{\lim}\right) & \text{for } \lambda_\theta \geq 0 \\ \min\left(1 + C_{PG2}\,\lambda_\theta\ + C_{PG3}\min\left[\lambda_\theta + 1\,,\ 0\right]\,,\ C_{PG2}^{\lim}\right) & \text{for } \lambda_\theta < 0 \end{cases} \tag{4.184}$$

The $\gamma$ transition model has been calibrated against a wide range of generic as well as turbomachinery and external aeronautical test cases. While you should not have to adjust the model coefficients in most situations, the model provides access to the coefficients so that you can fine-tune the model. This should only be done based on detailed experimental data. You can adjust the following constants in the correlations: $C_{TU1}$, $C_{TU2}$, $C_{TU3}$, $C_{PG1}$, $C_{PG2}$, $C_{PG3}$, $C_{PG1}^{\lim}$, $C_{PG2}^{\lim}$, $C_{SEP}$, and $C_{RSF}$

The $C_{TU1}$ constant defines the minimal value of the critical $\mathrm{Re}_{\theta c}$ number, whereas the sum of $C_{TU1}$ and $C_{TU2}$ defines the maximal value of $\mathrm{Re}_{\theta c}$. The $C_{TU3}$ constant controls how fast $\mathrm{Re}_{\theta c}$ decreases as the freestream turbulence intensity ($Tu$) increases.


Release 15.0 - © SAS IP, Inc. All rights reserved. - Contains proprietary and confidential information of ANSYS, Inc. and its subsidiaries and affiliates.

The $C_{PG1}$ and $C_{PG2}$ constants adjust the value of the critical $\mathrm{Re}_{\theta c}$ number in areas with favorable and adverse pressure gradients, respectively. The $C_{PG3}$ constant becomes active in regions with separation, correcting the $\mathrm{Re}_{\theta c}$ value if necessary. Additionally, the size of the separation bubble can be tuned by another constant, $C_{SEP}$, which enters the model through the source terms directly rather than the correlations. It should be noted, however, that the $C_{SEP}$ constant has an effect only for the bubbles developing under low $Tu$ conditions (<0.5%). It might also slightly affect the length of transition in attached boundary layers under very low freestream turbulence intensity. The $C_{PG1}^{\lim}$ and $C_{PG2}^{\lim}$ constants define the limits of the $F_{PG}$ function; while they typically do not need to be adjusted, it is possible to do so (for details, contact your support engineer).

For crossflow transition, a widely used experimental correlation is the C1 correlation proposed by Arnal [13] (p. 729). According to this correlation, transition occurs when the following condition is met:

$$\frac{\mathrm{Re}_{\delta 2t}^{*}}{f\,(H_S)} \geq 1 \tag{4.185}$$

where

$$f\,(H_S) = \begin{cases} \dfrac{300}{\pi}\arctan\left(\dfrac{0.106}{(H_S-2.3)^{2.05}}\right) & \text{for } 2.3<H_S<2.7 \\ 150 & \text{for } H_S<2.3 \end{cases} \tag{4.186}$$

$$\mathrm{Re}_{\delta_{\delta 2}^{*}} = \frac{U_{S,\delta}\delta_{\delta 2}^{*}}{\nu} \tag{4.187}$$

$$\delta_{\delta 2}^{*} = \int_0^{\infty} \frac{W_S}{U_{S,\delta}} dy \tag{4.188}$$

$$H_S = \frac{\delta_{XS}^{*}}{\theta_{XS}} \tag{4.189}$$

$$\delta_{XS}^{*} = \int_0^{\infty} \left(1 - \left(\frac{U_S}{U_{S,\delta}}\right)\right) dy \tag{4.190}$$

$$\theta_{XS} = \int_0^{\infty} \left(1 - \frac{U_S}{U_{S,\delta}}\right)\frac{U_S}{U_{S,\delta}} dy \tag{4.191}$$

In the previous equations, $\mathrm{Re}_{\delta_{\delta 2}^{*}}$ is the crossflow Reynolds number, and $S$ refers to a coordinate system that is aligned with the freestream velocity $U_{S,\delta}$ (where $\delta$ refers to the boundary layer edge). $W_S$ is the crossflow velocity normal to the direction of the freestream velocity.

The $\gamma$ transition model accounts for the crossflow transition through a separate correlation, which approximates the C1 correlation through a local formulation that is proprietary. The correlation can be adjusted by the constant $C_{RSF}$. The transition location due to the crossflow instability will move upstream as $C_{RSF}$ increases.

The default values for the model constants are the following:

Release 15.0 - © SAS IP, Inc. All rights reserved. - Contains proprietary and confidential information of ANSYS, Inc. and its subsidiaries and affiliates.

$C_{TU1}$ = 100.0

$C_{TU2}$ = 1000.0

$C_{TU3}$ = 1.0

$C_{PG1}$ = 1.0

$C_{PG2}$ = -0.5

$C_{PG3}$ = 0.0

$C_{PG1}^{\lim}$ = 1.5

$C_{PG2}^{\lim}$ = 3.0

$C_{SEP}$ = 1.0

$C_{RSF}$ = 1.0

### 4.7.3. Coupling with the Other Models

The coupling between the $\gamma$ transition model and the SST $k$-$\omega$, SAS with SST, and DES with SST models is similar as for the $\gamma$-$\mathrm{Re}_\theta$ transition model (see Coupling the Transition Model and SST Transport Equations (p. 74)).

### 4.7.4. Intermittency Transition Model and Rough Walls

Note that the correlation does not include the effects of rough walls. If you plan to include rough walls, it is recommended that you switch to the $\gamma$-$\mathrm{Re}_\theta$ transition model (that is, the Transition SST model).

## 4.8. The V2F Model

The $v^2-f$ model (V2F) is similar to the standard $k$-$\varepsilon$ model, but incorporates near-wall turbulence anisotropy and non-local pressure-strain effects. A limitation of the $v^2-f$ model is that it cannot be used to solve Eulerian multiphase problems, whereas the $k$-$\varepsilon$ model is typically used in such applications. The $v^2-f$ model is a general low-Reynolds number turbulence model that is valid all the way up to solid walls, and therefore does not need to make use of wall functions. Although the model was originally developed for attached or mildly separated boundary layers [102] (p. 734), it also accurately simulates flows dominated by separation [30] (p. 730).

The distinguishing feature of the $v^2-f$ model is its use of the velocity scale, $\overline{v^2}$, instead of the turbulent kinetic energy, $k$, for evaluating the eddy viscosity. $\overline{v^2}$ can be thought of as the velocity fluctuation normal to the streamlines.

For more information about the theoretical background and usage of the $v^2-f$ model, visit the ANSYS Customer Portal (`http://www.ansys.com`).


Release 15.0 - © SAS IP, Inc. All rights reserved. - Contains proprietary and confidential information of ANSYS, Inc. and its subsidiaries and affiliates.

# 4.9. Reynolds Stress Model (RSM)

This section describes the theory behind the Reynolds Stress model (RSM). Information is presented in the following sections:

4.9.1. Overview
4.9.2. Reynolds Stress Transport Equations
4.9.3. Modeling Turbulent Diffusive Transport
4.9.4. Modeling the Pressure-Strain Term
4.9.5. Effects of Buoyancy on Turbulence
4.9.6. Modeling the Turbulence Kinetic Energy
4.9.7. Modeling the Dissipation Rate
4.9.8. Modeling the Turbulent Viscosity
4.9.9. Wall Boundary Conditions
4.9.10. Convective Heat and Mass Transfer Modeling

For details about using the model in ANSYS Fluent, see Modeling Turbulence and Setting Up the Reynolds Stress Model in the User's Guide.

## 4.9.1. Overview

The Reynolds stress model (RSM) [137] (p. 736), [228] (p. 741), [229] (p. 741) is the most elaborate type of RANS turbulence model that ANSYS Fluent provides. Abandoning the isotropic eddy-viscosity hypothesis, the RSM closes the Reynolds-averaged Navier-Stokes equations by solving transport equations for the Reynolds stresses, together with an equation for the dissipation rate. This means that five additional transport equations are required in 2D flows, in comparison to seven additional transport equations solved in 3D.

Since the RSM accounts for the effects of streamline curvature, swirl, rotation, and rapid changes in strain rate in a more rigorous manner than one-equation and two-equation models, it has greater potential to give accurate predictions for complex flows. However, the fidelity of RSM predictions is still limited by the closure assumptions employed to model various terms in the exact transport equations for the Reynolds stresses. The modeling of the pressure-strain and dissipation-rate terms is particularly challenging, and often considered to be responsible for compromising the accuracy of RSM predictions. In addition, even RSM rely on scale equations ($\varepsilon$- or $\omega$-) and inherit deficiencies resulting from the underlying assumptions in these equations.

The RSM might not always yield results that are clearly superior to the simpler models in all classes of flows to warrant the additional computational expense. However, use of the RSM is a must when the flow features of interest are the result of anisotropy in the Reynolds stresses. Among the examples are cyclone flows, highly swirling flows in combustors, rotating flow passages, and the stress-induced secondary flows in ducts.

The exact form of the Reynolds stress transport equations may be derived by taking moments of the exact momentum equation. This is a process wherein the exact momentum equations for the fluctuations are multiplied by the fluctuating velocities and averaged, the product then being Reynolds-averaged. Unfortunately, several of the terms in the exact equation are unknown and modeling assumptions are required in order to close the equations.

## 4.9.2. Reynolds Stress Transport Equations

The exact transport equations for the transport of the Reynolds stresses, $\rho \overline{u'_i u'_j}$, may be written as follows:

Release 15.0 - © SAS IP, Inc. All rights reserved. - Contains proprietary and confidential information of ANSYS, Inc. and its subsidiaries and affiliates.

$$\underbrace{\frac{\partial}{\partial t}\left(\rho\overline{u_i'u_j'}\right)}_{\text{Local Time Derivative}} + \underbrace{\frac{\partial}{\partial x_k}\left(\rho u_k\overline{u_i'u_j'}\right)}_{C_{ij}\equiv\text{ Convection}} = \underbrace{-\frac{\partial}{\partial x_k}\left[\rho\overline{u_i'u_j'u_k'} + \overline{p'\left(\delta_{kj}u_i'+\delta_{ik}u_j'\right)}\right]}_{D_{T,ij}\equiv\text{ Turbulent Diffusion}}$$
$$+ \underbrace{\frac{\partial}{\partial x_k}\left[\mu\frac{\partial}{\partial x_k}\left(\overline{u_i'u_j'}\right)\right]}_{D_{L,ij}\equiv\text{ Molecular Diffusion}}$$
$$\underbrace{-\rho\left(\overline{u_i'u_k'}\frac{\partial u_j}{\partial x_k}+\overline{u_j'u_k'}\frac{\partial u_i}{\partial x_k}\right)}_{P_{ij}\equiv\text{ Stress Production}}$$
$$\underbrace{-\rho\beta\left(g_i\overline{u_j'\theta}+g_j\overline{u_i'\theta}\right)}_{G_{ij}\equiv\text{ Buoyancy Production}}$$
$$+ \underbrace{\overline{p'\left(\frac{\partial u_i'}{\partial x_j}+\frac{\partial u_j'}{\partial x_i}\right)}}_{\phi_{ij}\equiv\text{ Pressure Strain}}$$
$$\underbrace{-2\mu\overline{\frac{\partial u_i'}{\partial x_k}\frac{\partial u_j'}{\partial x_k}}}_{\varepsilon_{ij}\equiv\text{ Dissipation}}$$
$$\underbrace{-2\rho\Omega_k\left(\overline{u_j'u_m'}\varepsilon_{ikm}+\overline{u_i'u_m'}\varepsilon_{jkm}\right)}_{F_{ij}\equiv\text{ Production by System Rotation}}$$
$$+ \underbrace{S_{user}}_{\text{User-Defined Source Term}} \tag{4.192}$$

Of the various terms in these exact equations, $C_{ij}$, $D_{L,ij}$, $P_{ij}$, and $F_{ij}$ do not require any modeling. However, $D_{T,ij}$, $G_{ij}$, $\phi_{ij}$, and $\varepsilon_{ij}$ need to be modeled to close the equations. The following sections describe the modeling assumptions required to close the equation set.

## 4.9.3. Modeling Turbulent Diffusive Transport

$D_{T,ij}$ can be modeled by the generalized gradient-diffusion model of Daly and Harlow [86] (p. 733):

$$D_{T,ij} = C_s\frac{\partial}{\partial x_k}\left(\rho\frac{k\overline{u_k'u_\ell'}}{\varepsilon}\frac{\partial\overline{u_i'u_j'}}{\partial x_\ell}\right) \tag{4.193}$$

However, this equation can result in numerical instabilities, so it has been simplified in ANSYS Fluent to use a scalar turbulent diffusivity as follows [250] (p. 742):

$$D_{T,ij} = \frac{\partial}{\partial x_k}\left(\frac{\mu_t}{\sigma_k}\frac{\partial\overline{u_i'u_j'}}{\partial x_k}\right) \tag{4.194}$$


Release 15.0 - © SAS IP, Inc. All rights reserved. - Contains proprietary and confidential information of ANSYS, Inc. and its subsidiaries and affiliates.

The turbulent viscosity, $\mu_t$, is computed using Equation 4.224 (p. 90).

Lien and Leschziner [250] (p. 742) derived a value of $\sigma_k = 0.82$ by applying the generalized gradient-diffusion model, Equation 4.193 (p. 84), to the case of a planar homogeneous shear flow. Note that this value of $\sigma_k$ is different from that in the standard and realizable $k$-$\varepsilon$ models, in which $\sigma_k = 1.0$.

## 4.9.4. Modeling the Pressure-Strain Term

### 4.9.4.1. Linear Pressure-Strain Model

By default in ANSYS Fluent, the pressure-strain term, $\phi_{ij}$, in Equation 4.192 (p. 84) is modeled according to the proposals by Gibson and Launder [137] (p. 736), Fu et al. [131] (p. 736), and Launder [227] (p. 741), [228] (p. 741).

The classical approach to modeling $\phi_{ij}$ uses the following decomposition:

$$\phi_{ij} = \phi_{ij,1} + \phi_{ij,2} + \phi_{ij,w} \tag{4.195}$$

where $\phi_{ij,1}$ is the slow pressure-strain term, also known as the return-to-isotropy term, $\phi_{ij,2}$ is called the rapid pressure-strain term, and $\phi_{ij,w}$ is the wall-reflection term.

The slow pressure-strain term, $\phi_{ij,1}$, is modeled as

$$\phi_{ij,1} \equiv -C_1 \rho \frac{\varepsilon}{k}\left[\overline{u'_i u'_j} - \frac{2}{3}\delta_{ij}k\right] \tag{4.196}$$

with $C_1$ = 1.8.

The rapid pressure-strain term, $\phi_{ij,2}$, is modeled as

$$\phi_{ij,2} \equiv -C_2\left[\left(P_{ij} + F_{ij} + 5/6 G_{ij} - C_{ij}\right) - \frac{2}{3}\delta_{ij}\left(P + 5/6 G - C\right)\right] \tag{4.197}$$

where $C_2$ = 0.60, $P_{ij}$, $F_{ij}$, $G_{ij}$, and $C_{ij}$ are defined as in Equation 4.192 (p. 84), $P = \frac{1}{2}P_{kk}$, $G = \frac{1}{2}G_{kk}$, and $C = \frac{1}{2}C_{kk}$.

The wall-reflection term, $\phi_{ij,w}$, is responsible for the redistribution of normal stresses near the wall. It tends to damp the normal stress perpendicular to the wall, while enhancing the stresses parallel to the wall. This term is modeled as

$$\begin{aligned} \phi_{ij,w} \equiv\ & C'_1 \frac{\varepsilon}{k}\left(\overline{u'_k u'_m} n_k n_m \delta_{ij} - \frac{3}{2}\overline{u'_i u'_k} n_j n_k - \frac{3}{2}\overline{u'_j u'_k} n_i n_k\right)\frac{C_\ell k^{3/2}}{\varepsilon d} \\ & + C'_2\left(\phi_{km,2} n_k n_m \delta_{ij} - \frac{3}{2}\phi_{ik,2} n_j n_k - \frac{3}{2}\phi_{jk,2} n_i n_k\right)\frac{C_\ell k^{3/2}}{\varepsilon d} \end{aligned} \tag{4.198}$$

where $C_1'=0.5$, $C_2'=0.3$, $n_k$ is the $x_k$ component of the unit normal to the wall, $d$ is the normal distance to the wall, and $C_\ell=C_\mu^{3/4}/\kappa$, where $C_\mu=0.09$ and $\kappa$ is the von Kármán constant (= 0.4187).

$\phi_{ij,w}$ is included by default in the Reynolds stress model.

### 4.9.4.2. Low-Re Modifications to the Linear Pressure-Strain Model

When the RSM is applied to near-wall flows using the enhanced wall treatment described in Two-Layer Model for Enhanced Wall Treatment (p. 122), the pressure-strain model must be modified. The modification used in ANSYS Fluent specifies the values of $C_1$, $C_2$, $C_1'$, and $C_2'$ as functions of the Reynolds stress invariants and the turbulent Reynolds number, according to the suggestion of Launder and Shima [230] (p. 741):

$$C_1 = 1+2.58AA_2^{0.25}\left\{1-\exp\left[-(0.0067Re_t)^2\right]\right\} \tag{4.199}$$

$$C_2 = 0.75\sqrt{A} \tag{4.200}$$

$$C_1' = -\frac{2}{3}C_1+1.67 \tag{4.201}$$

$$C_2' = \max\left[\frac{\frac{2}{3}C_2-\frac{1}{6}}{C_2},0\right] \tag{4.202}$$

with the turbulent Reynolds number defined as $Re_t=\left(\rho k^2/\mu\varepsilon\right)$. The flatness parameter $A$ and tensor invariants, $A_2$ and $A_3$, are defined as

$$A \equiv \left[1-\frac{9}{8}(A_2-A_3)\right] \tag{4.203}$$

$$A_2 \equiv a_{ik}a_{ki} \tag{4.204}$$

$$A_3 \equiv a_{ik}a_{kj}a_{ji} \tag{4.205}$$

$a_{ij}$ is the Reynolds-stress anisotropy tensor, defined as

$$a_{ij}=-\left(\frac{-\rho\overline{u_i'u_j'}+\frac{2}{3}\rho k\delta_{ij}}{\rho k}\right) \tag{4.206}$$

The modifications detailed above are employed only when the enhanced wall treatment is selected in the Viscous Model Dialog Box.

### 4.9.4.3. Quadratic Pressure-Strain Model

An optional pressure-strain model proposed by Speziale, Sarkar, and Gatski [430] (p. 752) is provided in ANSYS Fluent. This model has been demonstrated to give superior performance in a range of basic shear flows, including plane strain, rotating plane shear, and axisymmetric expansion/contraction. This improved accuracy should be beneficial for a wider class of complex engineering flows, particularly


Release 15.0 - © SAS IP, Inc. All rights reserved. - Contains proprietary and confidential information of ANSYS, Inc. and its subsidiaries and affiliates.

those with streamline curvature. The quadratic pressure-strain model can be selected as an option in the Viscous Model Dialog Box.

This model is written as follows:

$$\begin{aligned}\phi_{ij} = & -(C_1\rho\varepsilon + C_1^* P)\, b_{ij} + C_2\rho\varepsilon\left(b_{ik}b_{kj} - \frac{1}{3}b_{mn}b_{mn}\delta_{ij}\right) + \left(C_3 - C_3^*\sqrt{b_{ij}b_{ij}}\right)\rho k S_{ij} \\ & + C_4\rho k\left(b_{ik}S_{jk} + b_{jk}S_{ik} - \frac{2}{3}b_{mn}S_{mn}\delta_{ij}\right) + C_5\rho k\left(b_{ik}\Omega_{jk} + b_{jk}\Omega_{ik}\right)\end{aligned} \tag{4.207}$$

where $b_{ij}$ is the Reynolds-stress anisotropy tensor defined as

$$b_{ij} = -\left(\frac{-\rho\overline{u'_i u'_j} + \frac{2}{3}\rho k\delta_{ij}}{2\rho k}\right) \tag{4.208}$$

The mean strain rate, $S_{ij}$, is defined as

$$S_{ij} = \frac{1}{2}\left(\frac{\partial u_j}{\partial x_i} + \frac{\partial u_i}{\partial x_j}\right) \tag{4.209}$$

The mean rate-of-rotation tensor, $\Omega_{ij}$, is defined by

$$\Omega_{ij} = \frac{1}{2}\left(\frac{\partial u_i}{\partial x_j} - \frac{\partial u_j}{\partial x_i}\right) \tag{4.210}$$

The constants are

$$C_1 = 3.4, C_1^* = 1.8, C_2 = 4.2, C_3 = 0.8, C_3^* = 1.3, C_4 = 1.25, C_5 = 0.4$$

The quadratic pressure-strain model does not require a correction to account for the wall-reflection effect in order to obtain a satisfactory solution in the logarithmic region of a turbulent boundary layer. It should be noted, however, that the quadratic pressure-strain model is not available when the enhanced wall treatment is selected in the Viscous Model Dialog Box.

### 4.9.4.4. Low-Re Stress-Omega Model

The low-Re stress-omega model is a stress-transport model that is based on the omega equations and LRR model [490] (p. 756). This model is ideal for modeling flows over curved surfaces and swirling flows. The low-Re stress-omega model can be selected in the Viscous Model Dialog Box and requires no treatments of wall reflections. The closure coefficients are identical to the $k$-$\omega$ model (Model Constants (p. 62)), however, there are additional closure coefficients, $C_1$ and $C_2$, noted below.

The low-Re stress-omega model resembles the $k$-$\omega$ model due to its excellent predictions for a wide range of turbulent flows. Furthermore, low Reynolds number modifications and surface boundary conditions for rough surfaces are similar to the $k$-$\omega$ model.

Equation 4.195 (p. 85) can be re-written for the low-Re stress-omega model such that wall reflections are excluded:

Release 15.0 - © SAS IP, Inc. All rights reserved. - Contains proprietary and confidential information of ANSYS, Inc. and its subsidiaries and affiliates.

$$\phi_{ij}=\phi_{ij,1}+\phi_{ij,2} \tag{4.211}$$

Therefore,

$$\begin{aligned}\phi_{ij} = \quad & -C_1\rho\beta^*_{RSM}\omega\left[\overline{u'_i u'_j}-{}^2\!/\!_3\delta_{ij}k\right]-\hat{\alpha}_0\left[P_{ij}-{}^1\!/\!_3P_{kk}\delta_{ij}\right] \\ & -\hat{\beta}_0\left[D_{ij}-{}^1\!/\!_3P_{kk}\delta_{ij}\right]-k\hat{\gamma}_0\left[S_{ij}-{}^1\!/\!_3S_{kk}\delta_{ij}\right]\end{aligned} \tag{4.212}$$

where $D_{ij}$ is defined as

$$D_{ij}=-\rho\left[\overline{u_i'u_m'}\frac{\partial u_m}{\partial x_j}+\overline{u_j'u_m'}\frac{\partial u_m}{\partial x_i}\right] \tag{4.213}$$

The mean strain rate $S_{ij}$ is defined in Equation 4.209 (p. 87) and $\beta^*_{RSM}$ is defined by

$$\beta^*_{RSM}=\beta^* f^*_\beta \tag{4.214}$$

where $\beta^*$ and $f^*_\beta$ are defined in the same way as for the standard $k-\omega$, using Equation 4.78 (p. 60) and Equation 4.84 (p. 61), respectively. The only difference here is that the equation for $f^*_\beta$ uses a value of 640 instead of 680, as in Equation 4.78 (p. 60).

The constants are

$$\hat{\alpha}_0=\frac{8+C_2}{11},\hat{\beta}_0=\frac{8C_2-2}{11},\hat{\gamma}_0=\frac{60C_2-4}{55}$$

$$C_1=1.8,C_2=0.52$$

The above formulation does not require viscous damping functions to resolve the near-wall sublayer. However, inclusion of the viscous damping function [490] (p. 756) could improve model predictions for certain flows. This results in the following changes:

$$\hat{\alpha}=\frac{1+\hat{\alpha}_0 Re_T/R_k}{1+Re_T/R_k}$$

$$\hat{\beta}=\hat{\beta}_0\frac{Re_T/R_k}{1+Re_T/R_k}$$

$$\hat{\gamma}=\hat{\gamma}_0\frac{0.007+Re_T/R_k}{1+Re_T/R_k}$$

$$C_1=1.8\left[\frac{5/3+Re_T/R_k}{1+Re_T/R_k}\right]$$

where $\hat{\alpha}$, $\hat{\beta}$, and $\hat{\gamma}$ would replace $\hat{\alpha}_0$, $\hat{\beta}_0$, and $\hat{\gamma}_0$ in Equation 4.212 (p. 88). The constants are


Release 15.0 - © SAS IP, Inc. All rights reserved. - Contains proprietary and confidential information of ANSYS, Inc. and its subsidiaries and affiliates.

$R_\beta = 12, R_k = 12, R_\omega = 6.20$

Inclusion of the low-Re viscous damping is controlled by enabling **Low-Re Corrections** under **k-omega Options** in the Viscous Model Dialog Box.

## 4.9.5. Effects of Buoyancy on Turbulence

The production terms due to buoyancy are modeled as

$$G_{ij} = -\rho\beta\left(g_i\overline{u'_j\theta} + g_j\overline{u'_i\theta}\right) \tag{4.215}$$

$$\overline{U_i\theta} = \frac{\mu_t}{Pr_t}\left(\frac{\partial T}{\partial x_i}\right) \tag{4.216}$$

where $\mathrm{Pr}_t$ is the turbulent Prandtl number for energy, with a default value of 0.85.

Using the definition of the coefficient of thermal expansion, $\beta$, given by Equation 4.58 (p. 55), the following expression is obtained for $G_{ij}$ for ideal gases:

$$G_{ij} = -\frac{\mu_t}{\rho Pr_t}\left(g_i\frac{\partial \rho}{\partial x_j} + g_j\frac{\partial \rho}{\partial x_i}\right) \tag{4.217}$$

**Important**

Note that the buoyancy effects are not included if low-Re omega based RSM model is used.

## 4.9.6. Modeling the Turbulence Kinetic Energy

In general, when the turbulence kinetic energy is needed for modeling a specific term, it is obtained by taking the trace of the Reynolds stress tensor:

$$k = \frac{1}{2}\overline{u'_i u'_i} \tag{4.218}$$

As described in Wall Boundary Conditions (p. 90), an option is available in ANSYS Fluent to solve a transport equation for the turbulence kinetic energy in order to obtain boundary conditions for the Reynolds stresses. In this case, the following model equation is used:

$$\begin{aligned}\frac{\partial}{\partial t}(\rho k) + \frac{\partial}{\partial x_i}(\rho k u_i) &= \frac{\partial}{\partial x_j}\left[\left(\mu + \frac{\mu_t}{\sigma_k}\right)\frac{\partial k}{\partial x_j}\right] + \frac{1}{2}(P_{ii} + G_{ii}) \\ &\quad -\rho\varepsilon\left(1 + 2M_t^2\right) + S_k\end{aligned} \tag{4.219}$$

where $\sigma_k = 0.82$ and $S_k$ is a user-defined source term. Equation 4.219 (p. 89) is obtainable by contracting the modeled equation for the Reynolds stresses (Equation 4.192 (p. 84)). As one might expect, it is essentially identical to Equation 4.33 (p. 47) used in the standard $k$-$\varepsilon$ model.

Although Equation 4.219 (p. 89) is solved, the values of $k$ obtained are used only for boundary conditions. In every other case, $k$ is obtained from Equation 4.218 (p. 89). This is a minor point, however, since the values of $k$ obtained with either method should be very similar.

Release 15.0 - © SAS IP, Inc. All rights reserved. - Contains proprietary and confidential information of ANSYS, Inc. and its subsidiaries and affiliates.

## 4.9.7. Modeling the Dissipation Rate

The dissipation tensor, $\varepsilon_{ij}$, is modeled as

$$\varepsilon_{ij} = \frac{2}{3}\delta_{ij}(\rho\varepsilon + Y_M) \tag{4.220}$$

where $Y_M = 2\rho\varepsilon M_t^2$ is an additional "dilatation dissipation" term according to the model by Sarkar [386] (p. 750). The turbulent Mach number in this term is defined as

$$M_t = \sqrt{\frac{k}{a^2}} \tag{4.221}$$

where $a$ ($\equiv\sqrt{\gamma RT}$) is the speed of sound. This compressibility modification is available when the compressible form of the ideal gas law is used.

The scalar dissipation rate, $\varepsilon$, is computed with a model transport equation similar to that used in the standard $k$-$\varepsilon$ model:

$$\frac{\partial}{\partial t}(\rho\varepsilon) + \frac{\partial}{\partial x_i}(\rho\varepsilon u_i) = \frac{\partial}{\partial x_j}\left[\left(\mu + \frac{\mu_t}{\sigma_\varepsilon}\right)\frac{\partial\varepsilon}{\partial x_j}\right] + C_{\varepsilon 1}\frac{1}{2}[P_{ii} + C_{\varepsilon 3}G_{ii}]\frac{\varepsilon}{k} - C_{\varepsilon 2}\rho\frac{\varepsilon^2}{k} + S_\varepsilon \tag{4.222}$$

where $\sigma_\varepsilon = 1.0$, $C_{\varepsilon 1} = 1.44$, $C_{\varepsilon 2} = 1.92$, $C_{\varepsilon 3}$ is evaluated as a function of the local flow direction relative to the gravitational vector, as described in Effects of Buoyancy on Turbulence in the k-ε Models (p. 55), and $S_\varepsilon$ is a user-defined source term.

In the case when the Reynolds Stress model is coupled with the omega equation, the dissipation tensor $\varepsilon_{ij}$ is modeled as

$$\varepsilon_{ij} = 2/3\,\delta_{ij}\rho\beta^*_{RSM}k\omega \tag{4.223}$$

Where $\beta^*_{RSM}$ is defined in Modeling the Pressure-Strain Term (p. 85) and the specific dissipation rate $\omega$ is computed in the same way as for the standard $k-\omega$ model, using Equation 4.65 (p. 59).

## 4.9.8. Modeling the Turbulent Viscosity

The turbulent viscosity, $\mu_t$, is computed similarly to the $k$-$\varepsilon$ models:

$$\mu_t = \rho C_\mu \frac{k^2}{\varepsilon} \tag{4.224}$$

where $C_\mu = 0.09$.

## 4.9.9. Wall Boundary Conditions

The RSM model in ANSYS Fluent requires boundary conditions for individual Reynolds stresses, $\overline{u'_i u'_j}$, and for the turbulence dissipation rate, $\varepsilon$ (or $\omega$ if the low-Re stress-omega model is used). These quantities can be input directly or derived from the turbulence intensity and characteristic length (Reynolds Stress Model in the User's Guide).


Release 15.0 - © SAS IP, Inc. All rights reserved. - Contains proprietary and confidential information of ANSYS, Inc. and its subsidiaries and affiliates.

At walls, ANSYS Fluent computes the near-wall values of the Reynolds stresses and $\varepsilon$ from wall functions (see Standard Wall Functions (p. 115), Non-Equilibrium Wall Functions (p. 120), and Enhanced Wall Treatment for Momentum and Energy Equations (p. 124)). ANSYS Fluent applies explicit wall boundary conditions for the Reynolds stresses by using the log-law and the assumption of equilibrium, disregarding convection and diffusion in the transport equations for the stresses (Equation 4.192 (p. 84)). Using a local coordinate system, where $\tau$ is the tangential coordinate, $\eta$ is the normal coordinate, and $\lambda$ is the binormal coordinate, the Reynolds stresses at the wall-adjacent cells (assuming standard wall functions or non-equilibrium wall functions) are computed from

$$\frac{\overline{u_\tau'^2}}{k}=1.098,\frac{\overline{u_\eta'^2}}{k}=0.247,\frac{\overline{u_\lambda'^2}}{k}=0.655,-\frac{\overline{u_\tau' u_\eta'}}{k}=0.255 \tag{4.225}$$

To obtain $k$, ANSYS Fluent solves the transport equation of Equation 4.219 (p. 89). For reasons of computational convenience, the equation is solved globally, even though the values of $k$ therefore computed are needed only near the wall; in the far field $k$ is obtained directly from the normal Reynolds stresses using Equation 4.218 (p. 89). By default, the values of the Reynolds stresses near the wall are fixed using the values computed from Equation 4.225 (p. 91), and the transport equations in Equation 4.192 (p. 84) are solved only in the bulk flow region.

Alternatively, the Reynolds stresses can be explicitly specified in terms of wall-shear stress, instead of $k$:

$$\frac{\overline{u_\tau'^2}}{u_\tau^2}=5.1,\frac{\overline{u_\eta'^2}}{u_\tau^2}=1.0,\frac{\overline{u_\lambda'^2}}{u_\tau^2}=2.3,-\frac{\overline{u_\tau' u_\eta'}}{u_\tau^2}=1.0 \tag{4.226}$$

where $u_\tau$ is the friction velocity defined by $u_\tau \equiv \sqrt{\frac{\tau_w}{\rho}}$, where $\tau_w$ is the wall-shear stress. When this option is chosen, the $k$ transport equation is not solved.

When using enhanced wall treatments as the near-wall treatment, ANSYS Fluent applies zero flux wall boundary conditions to the Reynolds stress equations.

## 4.9.10. Convective Heat and Mass Transfer Modeling

With the Reynolds stress model in ANSYS Fluent, turbulent heat transport is modeled using the concept of Reynolds' analogy to turbulent momentum transfer. The "modeled" energy equation is therefore given by the following:

$$\frac{\partial}{\partial t}(\rho E)+\frac{\partial}{\partial x_i}[u_i(\rho E+p)]=\frac{\partial}{\partial x_j}\left[\left(k+\frac{c_p\mu_t}{Pr_t}\right)\frac{\partial T}{\partial x_j}+u_i\left(\tau_{ij}\right)_{eff}\right]+S_h \tag{4.227}$$

where $E$ is the total energy and $\left(\tau_{ij}\right)_{eff}$ is the deviatoric stress tensor, defined as

$$\left(\tau_{ij}\right)_{eff}=\mu_{eff}\left(\frac{\partial u_j}{\partial x_i}+\frac{\partial u_i}{\partial x_j}\right)-\frac{2}{3}\mu_{eff}\frac{\partial u_k}{\partial x_k}\delta_{ij}$$

The term involving $\left(\tau_{ij}\right)_{eff}$ represents the viscous heating, and is always computed in the density-based solvers. It is not computed by default in the pressure-based solver, but it can be enabled in the

Release 15.0 - © SAS IP, Inc. All rights reserved. - Contains proprietary and confidential information of ANSYS, Inc. and its subsidiaries and affiliates.

Viscous Model Dialog Box. The default value of the turbulent Prandtl number is 0.85. You can change the value of $\mathrm{Pr}_t$ in the Viscous Model Dialog Box.

Turbulent mass transfer is treated similarly, with a default turbulent Schmidt number of 0.7. This default value can be changed in the Viscous Model Dialog Box.

# 4.10. Scale-Adaptive Simulation (SAS) Model

This section describes the theory behind the Scale-Adaptive Simulation (SAS) model. For details about using the model in ANSYS Fluent, see Setting Up Scale-Adaptive Simulation (SAS) Modeling in the User's Guide.

For more information, see the following sections:

4.10.1. Overview
4.10.2. Transport Equations for the SST-SAS Model
4.10.3. SAS with Other ω-Based Turbulence Models

## 4.10.1. Overview

The Scale-Adaptive Simulation (SAS) is an improved URANS formulation, which allows the resolution of the turbulent spectrum in unstable flow conditions. Figure 4.6: Resolved Structures for Cylinder in Cross Flow (top: URANS; bottom: SST-SAS) (p. 92) shows isosurfaces where $S-\Omega=10^5 1/s^2$ for a cylinder in cross flow ($Re=3.6*10^6$), calculated using the SST model (URANS) and the SST-SAS model. The URANS simulation produces only the large-scale unsteadiness, whereas the SST-SAS model adjusts to the already resolved scales in a dynamic way and allows the development of a turbulent spectrum in the detached regions.

**Figure 4.6: Resolved Structures for Cylinder in Cross Flow (top: URANS; bottom: SST-SAS)**

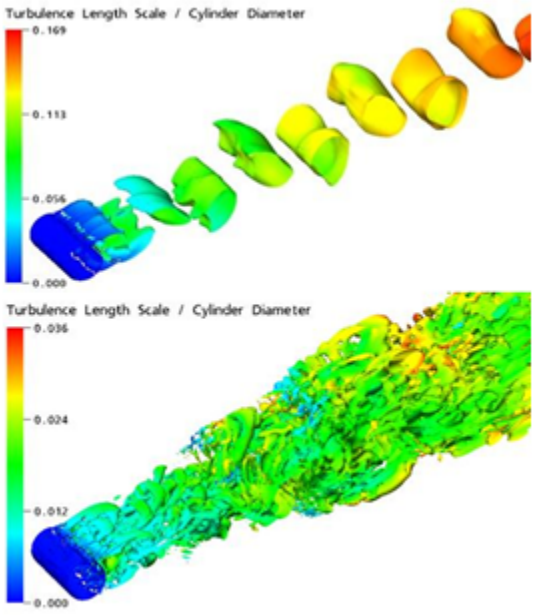


The SAS concept is based on the introduction of the von Karman length-scale into the turbulence scale equation. The information provided by the von Karman length-scale allows SAS models to dynamically adjust to resolved structures in a URANS simulation, which results in an LES-like behavior in unsteady


Release 15.0 - © SAS IP, Inc. All rights reserved. - Contains proprietary and confidential information of ANSYS, Inc. and its subsidiaries and affiliates.

regions of the flow field. At the same time, the model provides standard RANS capabilities in stable flow regions.

For information about the synthetic turbulence generation on inlets, refer to Inlet Boundary Conditions for the LES Model (p. 106).

## 4.10.2. Transport Equations for the SST-SAS Model

From a fundamental standpoint, all the currently used two-equation models suffer from lack of an underlying exact transport equation, which can serve as a guide for the model development on a term by term basis. The reason for this deficiency lies in the fact that the exact equation for $\varepsilon$ does not describe the large scales, but the dissipative scales. The goal of a two-equation model is however the modeling of the influence of the large scale motions on the mean flow. Due to the lack of an exact equation, the $\varepsilon$- and the $\omega$-equations are modeled in analogy with the equation for the turbulent kinetic energy, $k$, using purely heuristic arguments. A more consistent approach for formulating a scale-equation has been developed by Rotta (1968, 1972). Instead of using purely heuristic and dimensional arguments, Rotta formulated an exact transport equation for turbulent kinetic energy times length scale, $kL$. Rotta's equation represents the large scales of turbulence and can therefore serve as a basis for term-by-term modeling. The transport equations for the SST-SAS model as implemented in ANSYS Fluent are based on transforming Rotta's approach to $k$-$\omega$ (SST) and defined as:

$$\frac{\partial \rho k}{\partial t}+\frac{\partial}{\partial x_i}(\rho u_i k)=G_k-\rho c_\mu k\omega+\frac{\partial}{\partial x_j}\left[\left(\mu+\frac{\mu_t}{\sigma_k}\right)\frac{\partial k}{\partial x_j}\right] \tag{4.228}$$

$$\begin{aligned}\frac{\partial \rho\omega}{\partial t}+\frac{\partial}{\partial x_i}(\rho u_i\omega)= &\ \alpha\frac{\omega}{k}G_k-\rho\beta\omega^2+Q_{SAS}+\frac{\partial}{\partial x_i}\left[\left(\mu+\frac{\mu_t}{\sigma_\omega}\right)\frac{\partial \omega}{\partial x_j}\right] \\ &+(1-F_1)\frac{2\rho}{\sigma_{\omega,2}}\frac{1}{\omega}\frac{\partial k}{\partial x_j}\frac{\partial \omega}{\partial x_j}\end{aligned} \tag{4.229}$$

For the detailed derivation see Egorov and Menter [148] (p. 737). The transport equations of the SST-SAS model Equation 4.228 (p. 93) and Equation 4.229 (p. 93) differ from those of the SST RANS model [290] (p. 745) by the additional SAS source term $Q_{SAS}$ in the transport equation for the turbulence eddy frequency $\omega$, Equation 4.229 (p. 93). In Equation 4.229 (p. 93) $\sigma_{\omega,2}$ is the $\sigma_\omega$ value for the $k$-$\varepsilon$ regime of the SST model.

The additional source term $Q_{SAS}$ reads (see Egorov and Menter [148] (p. 737) for details):

$$Q_{SAS}=max\left[\rho\eta_2\kappa S^2\left(\frac{L}{L_{\nu\kappa}}\right)^2-C\cdot\frac{2\rho k}{\sigma_\Phi}max\left(\frac{1}{\omega^2}\frac{\partial\omega}{\partial x_j}\frac{\partial\omega}{\partial x_j},\frac{1}{k^2}\frac{\partial k}{\partial x_j}\frac{\partial k}{\partial x_j}\right),0\right] \tag{4.230}$$

This SAS source term originates from a second order derivative term in Rotta's transport equations [292] (p. 745). The model parameters in the SAS source term Equation 4.230 (p. 93) are

$$\eta_2=3.51$$
$$\sigma_\Phi=2/3$$
$$C=2$$

Release 15.0 - © SAS IP, Inc. All rights reserved. - Contains proprietary and confidential information of ANSYS, Inc. and its subsidiaries and affiliates.

Here $L$ is the length scale of the modeled turbulence

$$L = \sqrt{k} / \left( c_{\mu}^{1/4} \cdot \omega \right) \tag{4.231}$$

and the von Karman length scale $L_{vK}$ is a three-dimensional generalization of the classic boundary layer definition $L_{BL}^{vK} = \kappa \frac{\partial U}{\partial y} / \frac{\partial^2 U}{\partial y^2}$

$$L_{vK} = \kappa \left| \frac{U'}{U''} \right| \tag{4.232}$$

The first velocity derivative $\frac{\partial U}{\partial y}$ is represented in $L_{vK}$ by $U'$, which is equal to $S$, a scalar invariant of the strain rate tensor $S_{ij}$:

$$U' = S = \sqrt{2 \cdot S_{ij} S_{ij}}; \qquad S_{ij} = \frac{1}{2} \left( \frac{\partial U_i}{\partial x_j} + \frac{\partial U_j}{\partial x_i} \right) \tag{4.233}$$

Note, that the same $S$ also directly participates in $Q_{SAS}$ (Equation 4.230 (p. 93)) and in the turbulence production term $P_k = \mu_t S^2$. The second velocity derivative $U''$ is generalized to 3D using the magnitude of the velocity Laplacian:

$$U'' = \sqrt{\frac{\partial^2 U_i}{\partial x_k^2} \frac{\partial^2 U_i}{\partial x_j^2}} \tag{4.234}$$

So defined $L$ and $L_{vK}$ are both equal to $(\kappa y)$ in the logarithmic part of the boundary layer, where $\kappa = 0.41$ is the von Karman constant.

The model also provides a direct control of the high wave number damping. This is realized by a lower constraint on the $L_{vK}$ value in the following way:

$$L_{vK} = max \left( \kappa \left| \frac{U'}{U''} \right|, C_S \sqrt{\frac{\kappa \eta_2}{\left( \beta / c_{\mu} \right) - \alpha}} \cdot \Delta \right), \Delta = \Omega_{CV}^{1/3} \tag{4.235}$$

This limiter is proportional to the mesh cell size $\Delta$, which is calculated as the cubic root of the control volume size $\Omega_{CV}$. The purpose of this limiter is to control damping of the finest resolved turbulent fluctuations. The structure of the limiter is derived from analyzing the equilibrium eddy viscosity of the SST-SAS model [148] (p. 737).

## 4.10.3. SAS with Other ω-Based Turbulence Models

The SAS approach can be combined not only with the SST model, but also with several other $\omega$-based turbulence models:

- Standard ($k$-$\omega$) and Transition SST
- $\omega$-based Reynolds Stress Model (RSM)


Release 15.0 - © SAS IP, Inc. All rights reserved. - Contains proprietary and confidential information of ANSYS, Inc. and its subsidiaries and affiliates.

Adding the SAS capability to one of these models will enable the additional source term $Q_{SAS}$ (as defined in Equation 4.230 (p. 93)) in the $\omega$-based equation.

# 4.11. Detached Eddy Simulation (DES)

This section describes the theory behind the Detached Eddy Simulation (DES) model. Information is presented in the following sections:

4.11.1. Overview
4.11.2. DES with the Spalart-Allmaras Model
4.11.3. DES with the Realizable k-ε Model
4.11.4. DES with the SST k-ω Model
4.11.5. DES with the Transition SST Model
4.11.6. Improved Delayed Detached Eddy Simulation (IDDES)

For details about using the model in ANSYS Fluent, see Modeling Turbulence and Setting Up the Detached Eddy Simulation Model in the User's Guide.

## 4.11.1. Overview

ANSYS Fluent offers four different models for the detached eddy simulation: the Spalart-Allmaras model, the realizable $k$-$\varepsilon$ model, the SST $k$-$\omega$ model, and the Transition SST model.

In the DES approach, the unsteady RANS models are employed in the boundary layer, while the LES treatment is applied to the separated regions. The LES region is normally associated with the core turbulent region where large unsteady turbulence scales play a dominant role. In this region, the DES models recover LES-like subgrid models. In the near-wall region, the respective RANS models are recovered.

DES models have been specifically designed to address high Reynolds number wall bounded flows, where the cost of a near-wall resolving Large Eddy Simulation would be prohibitive. The difference with the LES model is that it relies only on the required RANS resolution in the boundary layers. The application of DES, however, may still require significant CPU resources and therefore, as a general guideline, it is recommended that the conventional turbulence models employing the Reynolds-averaged approach be used for most practical calculations.

The DES models, often referred to as the hybrid LES/RANS models, combine RANS modeling with LES for applications such as high-Re external aerodynamics simulations. In ANSYS Fluent, the DES model is based on the one-equation Spalart-Allmaras model, the realizable $k$-$\varepsilon$ model, the SST $k$-$\omega$ model, and the Transition SST model. The computational costs, when using the DES models, is less than LES computational costs, but greater than RANS.

For information about the synthetic turbulence generation on inlets, refer to Inlet Boundary Conditions for the LES Model (p. 106).

## 4.11.2. DES with the Spalart-Allmaras Model

The standard Spalart-Allmaras model uses the distance to the closest wall as the definition for the length scale $d$, which plays a major role in determining the level of production and destruction of turbulent viscosity (Equation 4.20 (p. 44), Equation 4.26 (p. 45), and Equation 4.29 (p. 45)). The DES model, as proposed by Shur et al. [404] (p. 751) replaces $d$ everywhere with a new length scale $\tilde{d}$, defined as

$$\tilde{d} = \min\left(d, C_{des}\Delta_{\max}\right) \tag{4.236}$$

Release 15.0 - © SAS IP, Inc. All rights reserved. - Contains proprietary and confidential information of ANSYS, Inc. and its subsidiaries and affiliates.

where the grid spacing, $\Delta_{\max}$, is based on the largest grid space in the $x$, $y$, or $z$ directions forming the computational cell. The empirical constant $C_{des}$ has a value of 0.65.

For a typical RANS grid with a high aspect ratio in the boundary layer, and where the wall-parallel grid spacing usually exceeds $\delta$, where $\delta$ is the size of the boundary layer, Equation 4.236 (p. 95) will ensure that the DES model is in the RANS mode for the entire boundary layer. However, in case of an ambiguous grid definition, where $\Delta_{\max} < \delta$, the DES limiter can activate the LES mode inside the boundary layer, where the grid is not fine enough to sustain resolved turbulence. Therefore, a new formulation [427] (p. 752) of DES is available in ANSYS Fluent to preserve the RANS mode throughout the boundary layer. This is known as the delayed option or DDES for delayed DES.

The DES length scale $\tilde{d}$ is re-defined according to:

$$\tilde{d} = d - f_d \max\left(0, d - C_{des}\Delta_{\max}\right) \tag{4.237}$$

where $f_d$ is given by:

$$f_d = 1 - \tanh\left((8r_d)^3\right) \tag{4.238}$$

and

$$r_d = \frac{\tilde{\nu}}{\sqrt{U_{i,j}U_{i,j}}\kappa^2 d^2}; \qquad \kappa = 0.41 \tag{4.239}$$

This formulation is the default settings.

## 4.11.3. DES with the Realizable k-ε Model

This DES model is similar to the Realizable $k$-$\varepsilon$ model discussed in Realizable k-ε Model (p. 51), with the exception of the dissipation term in the $k$ equation. In the DES model, the Realizable $k$-$\varepsilon$ RANS dissipation term is modified such that:

$$Y_k = \frac{\rho k^{\frac{3}{2}}}{l_{des}} \tag{4.240}$$

where

$$l_{des} = min\left(l_{rke}, l_{les}\right) \tag{4.241}$$

$$l_{rke} = \frac{k^{\frac{3}{2}}}{\varepsilon} \tag{4.242}$$

$$l_{les} = C_{des}\Delta_{\max} \tag{4.243}$$

where $C_{des}$ is a calibration constant used in the DES model and has a value of 0.61 and $\Delta_{\max}$ is the maximum local grid spacing ($\Delta x$, $\Delta y$, $\Delta z$).

For the case where $l_{des} = l_{rke}$, you will obtain an expression for the dissipation of the $k$ formulation for the Realizable $k$-$\varepsilon$ model (Realizable k-ε Model (p. 51)): $Y_k = \rho\varepsilon$. Similarly to the Spalart-Allmaras model, the delayed concept can be applied as well to the Realizable DES model to preserve the RANS mode throughout the boundary layer. The DES length $l_{des}$ in Equation 4.240 (p. 96) is redefined such that


Release 15.0 - © SAS IP, Inc. All rights reserved. - Contains proprietary and confidential information of ANSYS, Inc. and its subsidiaries and affiliates.

$$l_{des} = l_{rke} - f_d \max\left(0, l_{rke} - C_{des}\Delta_{\max}\right) \tag{4.244}$$

**Note**

In Equation 4.244 (p. 97) $f_d$ is used as defined for the Spalart-Allmaras model in Equation 4.238 (p. 96) with the exception that the value of the constant is changed from 8 to 20 and $\tilde{\nu}$ is replaced with $(\nu_t + \nu)$ in the calculation of $r_d$ in Equation 4.239 (p. 96).

## 4.11.4. DES with the SST k-ω Model

The dissipation term of the turbulent kinetic energy (see Modeling the Turbulence Dissipation (p. 60)) is modified for the DES turbulence model as described in Menter's work [293] (p. 745) such that

$$Y_k = \rho\beta^* k\omega F_{DES} \tag{4.245}$$

where $F_{DES}$ is expressed as

$$F_{DES} = max\left(\frac{L_t}{C_{des}\Delta_{\max}}, 1\right) \tag{4.246}$$

where $C_{des}$ is a calibration constant used in the DES model and has a value of 0.61, $\Delta_{\max}$ is the maximum local grid spacing ($\Delta x$, $\Delta y$, $\Delta z$).

The turbulent length scale is the parameter that defines this RANS model:

$$L_t = \frac{\sqrt{k}}{\beta^* \omega} \tag{4.247}$$

The DES-SST model also offers the option to "protect" the boundary layer from the limiter (delayed option). This is achieved with the help of the zonal formulation of the SST model. $F_{DES}$ is modified according to

$$F_{DES} = max\left(\frac{L_t}{C_{des}\Delta_{\max}}(1 - F_{SST}), 1\right) \tag{4.248}$$

with $F_{SST} = 0, F_1, F_2$, where $F_1$ and $F_2$ are the blending functions of the SST model. Alternatively, the DDES shielding function or the IDDES function can be selected [403] (p. 751), [427] (p. 752). The default setting is to use DDES.

**Note**

In the DDES and IDDES implementations, $f_d$ is used as defined for the Spalart-Allmaras model in Equation 4.238 (p. 96) with the exception that the value of the constant is changed from 8 to 20.

## 4.11.5. DES with the Transition SST Model

The Transition SST model can be combined with the DES approach. The dissipation term of the transport equation for the turbulence kinetic energy will be modified in the same way as for the SST $k$-$\omega$ turbulence

model (see Equation 4.245 (p. 97)). All shielding functions outlined in DES with the SST k-ω Model (p. 97) are also available for DES with the Transition SST model.

## 4.11.6. Improved Delayed Detached Eddy Simulation (IDDES)

### 4.11.6.1. Overview of IDDES

The Improved Delayed Detached Eddy Simulation (IDDES) model ([403] (p. 751)) is a hybrid RANS-LES model (consisting of a combination of various new and existing techniques) that provides a more flexible and convenient scale-resolving simulation (SRS) model for high Reynolds number flows. Since the model formulation is relatively complex and the application of the model is non-trivial, it is recommended that you consult the original publications of Shur et al. [403] (p. 751).

The IDDES model has the following goals in addition to the formulation of the standard DES model:

- Provide shielding against Grid Induced Separation (GIS), similar to the DDES model ([427] (p. 752)).
- Allow the model to run in Wall-Modeled LES (WMLES) mode in case unsteady inlet conditions are provided to simulate wall boundary layers in unsteady mode. The IDDES model is designed to allow the LES simulation of wall boundary layers at much higher Reynolds numbers than standard LES models. As an alternative to unsteady inlet conditions, unsteadiness could also be triggered by an obstacle (such as a backward facing step, or a rib inside or upstream of the boundary layer).

The IDDES model implemented in ANSYS Fluent is based on the SST model ([290] (p. 745)) with the application of IDDES modifications as given in [403] (p. 751). Similar to DES, the k-equation of the SST model is modified to include information on the local grid spacing. In case the grid resolution is sufficiently fine, the model will switch to LES mode. However, the goal is to cover stable boundary layers (meaning no unsteady inlet conditions and no upstream obstacles generating unsteadiness) in RANS mode. In order to avoid affecting the SST model under such conditions, the IDDES function provides shielding similar to the DDES model, meaning it attempts to keep the boundary layer in steady RANS mode even under grid refinement.

If you want to resolve the wall boundary layer in WMLES mode, unsteady inlet conditions need to be provided (see Vortex Method (p. 106) or Spectral Synthesizer (p. 108)). The model can also be run with the Embedded LES (ELES) option (see Embedded Large Eddy Simulation (ELES) (p. 109)) and the IDDES option (see Detached Eddy Simulation (DES) in the User's Guide) in ANSYS Fluent.

### 4.11.6.2. IDDES Model Formulation

The SST-IDDES model is based on modifying the sink term in the k-equation of the SST model. (The $\omega$-equation remains unmodified.)

$$\frac{\partial \rho k}{\partial t}+\nabla \cdot (\overline{\rho}\widetilde{U k}) = \nabla \cdot [(\mu+\frac{\mu_T}{\sigma_{k3}})\nabla k]+P_k-\rho\beta^* k\omega F_{IDDES}$$
$$\frac{\partial \rho \omega}{\partial t}+\nabla \cdot (\overline{\rho}\widetilde{U \omega}) = \nabla \cdot [(\mu+\frac{\mu_T}{\sigma_{\omega 3}})\nabla \omega]+(1-F_1)2\rho\frac{\nabla k \cdot \nabla \omega}{\sigma_{\omega 2}\omega}+\alpha_3\frac{\omega}{k}P_k-\beta_3\rho\omega^2 \quad (4.249)$$

$$F_{IDDES} = \frac{l_{RANS}}{l_{IDDES}} \quad (4.250)$$

Where, $l_{RANS}=\sqrt{k}/(\beta^*\omega)$.


Release 15.0 - © SAS IP, Inc. All rights reserved. - Contains proprietary and confidential information of ANSYS, Inc. and its subsidiaries and affiliates.

In Equation 4.250 (p. 98), $F_{IDDES}$ is based on the RANS turbulent length scale and the LES grid length scales. Note that the sub-grid length scale $\Delta$ differs from the DES formulation, where it is equal to the maximum local edge length $h_{\max}$ for the considered cell. In the IDDES formulation, instead of $h_{\max}$, a more general formulation for $\Delta$ is used that combines local grid scales and the wall distance $d_w$. The values $h_{\max}$ and $h_{\min}$ are the maximum and the minimum edge length of each cell, respectively.

The complete formulation is relatively complex and has been implemented as published by [403] (p. 751).

## 4.12. Large Eddy Simulation (LES) Model

This section describes the theory behind the Large Eddy Simulation (LES) model. Information is presented in the following sections:

4.12.1. Overview
4.12.2. Subgrid-Scale Models
4.12.3. Inlet Boundary Conditions for the LES Model

For details about using the model in ANSYS Fluent, see Modeling Turbulence and Setting Up the Large Eddy Simulation Model in the User's Guide.

### 4.12.1. Overview

Turbulent flows are characterized by eddies with a wide range of length and time scales. The largest eddies are typically comparable in size to the characteristic length of the mean flow (for example, shear layer thickness). The smallest scales are responsible for the dissipation of turbulence kinetic energy.

It is possible, in theory, to directly resolve the whole spectrum of turbulent scales using an approach known as direct numerical simulation (DNS). No modeling is required in DNS. However, DNS is not feasible for practical engineering problems involving high Reynolds number flows. The cost required for DNS to resolve the entire range of scales is proportional to $Re_t^3$, where $Re_t$ is the turbulent Reynolds number. Clearly, for high Reynolds numbers, the cost becomes prohibitive.

In LES, large eddies are resolved directly, while small eddies are modeled. Large eddy simulation (LES) therefore falls between DNS and RANS in terms of the fraction of the resolved scales. The rationale behind LES can be summarized as follows:

- Momentum, mass, energy, and other passive scalars are transported mostly by large eddies.
- Large eddies are more problem-dependent. They are dictated by the geometries and boundary conditions of the flow involved.
- Small eddies are less dependent on the geometry, tend to be more isotropic, and are consequently more universal.
- The chance of finding a universal turbulence model is much higher for small eddies.

Resolving only the large eddies allows one to use much coarser mesh and larger time-step sizes in LES than in DNS. However, LES still requires substantially finer meshes than those typically used for RANS calculations. In addition, LES has to be run for a sufficiently long flow-time to obtain stable statistics of the flow being modeled. As a result, the computational cost involved with LES is normally orders of magnitudes higher than that for steady RANS calculations in terms of memory (RAM) and CPU time. Therefore, high-performance computing (for example, parallel computing) is a necessity for LES, especially for industrial applications. The main shortcoming of LES lies in the high resolution requirements for

Release 15.0 - © SAS IP, Inc. All rights reserved. - Contains proprietary and confidential information of ANSYS, Inc. and its subsidiaries and affiliates.

wall boundary layers. Near the wall, even the 'large' eddies become relatively small and require a Reynolds number dependent resolution. This limits LES for wall bounded flows to very low Reynolds numbers ($\mathrm{Re} \sim 10^4 - 10^5$) and limited computational domains.

The following sections give details of the governing equations for LES, the subgrid-scale turbulence models, and the boundary conditions.

## 4.12.2. Subgrid-Scale Models

The subgrid-scale stresses resulting from the filtering operation are unknown, and require modeling. The subgrid-scale turbulence models in ANSYS Fluent employ the Boussinesq hypothesis [164] (p. 738) as in the RANS models, computing subgrid-scale turbulent stresses from

$$\tau_{ij} - \frac{1}{3}\tau_{kk}\delta_{ij} = -2\mu_t \overline{S}_{ij} \tag{4.251}$$

where $\mu_t$ is the subgrid-scale turbulent viscosity. The isotropic part of the subgrid-scale stresses $\tau_{kk}$ is not modeled, but added to the filtered static pressure term. $\overline{S}_{ij}$ is the rate-of-strain tensor for the resolved scale defined by

$$\overline{S}_{ij} \equiv \frac{1}{2}\left(\frac{\partial \overline{u}_i}{\partial x_j} + \frac{\partial \overline{u}_j}{\partial x_i}\right) \tag{4.252}$$

For compressible flows, it is convenient to introduce the density-weighted (or Favre) filtering operator:

$$\tilde{\phi} = \frac{\overline{\rho\phi}}{\overline{\rho}} \tag{4.253}$$

The Favre Filtered Navier-Stokes equation takes the same form as Equation 4.9 (p. 41). The compressible form of the subgrid stress tensor is defined as:

$$\tau_{ij} = \overline{\rho} u \tilde{u}_j - \overline{\rho}\tilde{u}_i\tilde{u}_j \tag{4.254}$$

This term is split into its isotropic and deviatoric parts

$$\tau_{ij} = \underbrace{\tau_{ij} - \frac{1}{3}\tau_{kk}\delta_{ij}}_{\text{deviatoric}} + \underbrace{\frac{1}{3}\tau_{kk}\delta_{ij}}_{\text{isotropic}} \tag{4.255}$$

The deviatoric part of the subgrid-scale stress tensor is modeled using the compressible form of the Smagorinsky model:

$$\tau_{ij} - \frac{1}{3}\tau_{kk}\delta_{ij} = -2\mu_t\left(S_{ij} - \frac{1}{3}S_{kk}\delta_{ij}\right) \tag{4.256}$$

As for incompressible flows, the term involving $\tau_{kk}$ can be added to the filtered pressure or simply neglected [110] (p. 735). Indeed, this term can be re-written as $\tau_{kk} = \gamma M^2_{sgs}\overline{p}$ where $M_{sgs}$ is the subgrid Mach number. This subgrid Mach number can be expected to be small when the turbulent Mach number of the flow is small.

ANSYS Fluent offers four models for $\mu_t$: the Smagorinsky-Lilly model, the dynamic Smagorinsky-Lilly model, the WALE model, and the dynamic kinetic energy subgrid-scale model.


Release 15.0 - © SAS IP, Inc. All rights reserved. - Contains proprietary and confidential information of ANSYS, Inc. and its subsidiaries and affiliates.

The subgrid-scale turbulent flux of a scalar, $\phi$, is modeled using a subgrid-scale turbulent Prandtl number by

$$q_j = -\frac{\mu_t}{\sigma_t}\frac{\partial \phi}{\partial x_j} \tag{4.257}$$

where $q_j$ is the subgrid-scale flux.

The compressible subgrid enthalpy flux term is modeled in the same manner:

$$\overline{\rho}\left(\widetilde{u_i h_s} - \tilde{u}_i \tilde{h}_s\right) = -\frac{\mu_{\text{SGS}} C_p}{\text{Pr}_{\text{SGS}}}\frac{\partial \tilde{T}}{\partial x_j} \tag{4.258}$$

where $h_s$ is the sensible enthalpy, $\mu_{\text{SGS}}$ is a subgrid viscosity, and $\text{Pr}_{\text{SGS}}$ is a subgrid Prandtl number equal to 0.85.

In the dynamic models, the subgrid-scale turbulent Prandtl number or Schmidt number is obtained by applying the dynamic procedure originally proposed by Germano [134] (p. 736) to the subgrid-scale flux.

### 4.12.2.1. Smagorinsky-Lilly Model

This simple model was first proposed by Smagorinsky [412] (p. 751). In the Smagorinsky-Lilly model, the eddy-viscosity is modeled by

$$\mu_t = \rho L_s^2 \left|\overline{S}\right| \tag{4.259}$$

where $L_s$ is the mixing length for subgrid scales and $\left|\overline{S}\right| \equiv \sqrt{2\overline{S}_{ij}\overline{S}_{ij}}$. In ANSYS Fluent, $L_s$ is computed using

$$L_s = min\left(\kappa d, C_s \Delta\right) \tag{4.260}$$

where $\kappa$ is the von Kármán constant, $d$ is the distance to the closest wall, $C_s$ is the Smagorinsky constant, and $\Delta$ is the local grid scale. In ANSYS Fluent, $\Delta$ is computed according to the volume of the computational cell using

$$\Delta = V^{1/3} \tag{4.261}$$

Lilly derived a value of 0.23 for $C_s$ for homogeneous isotropic turbulence in the inertial subrange. However, this value was found to cause excessive damping of large-scale fluctuations in the presence of mean shear and in transitional flows as near solid boundary, and has to be reduced in such regions. In short, $C_s$ is not a universal constant, which is the most serious shortcoming of this simple model. Nonetheless, a $C_s$ value of around 0.1 has been found to yield the best results for a wide range of flows, and is the default value in ANSYS Fluent.

### 4.12.2.2. Dynamic Smagorinsky-Lilly Model

Germano et al. [134] (p. 736) and subsequently Lilly [253] (p. 743) conceived a procedure in which the Smagorinsky model constant, $C_s$, is dynamically computed based on the information provided by the resolved scales of motion. The dynamic procedure therefore obviates the need for users to specify the model constant $C_s$ in advance.

Release 15.0 - © SAS IP, Inc. All rights reserved. - Contains proprietary and confidential information of ANSYS, Inc. and its subsidiaries and affiliates.

The concept of the dynamic procedure is to apply a second filter (called the test filter) to the equations of motion. The new filter width $\hat{\Delta}$ is equal to twice the grid filter width $\Delta$. Both filters produce a resolved flow field. The difference between the two resolved fields is the contribution of the small scales whose size is in between the grid filter and the test filter. The information related to these scales is used to compute the model constant. In ANSYS Fluent, the variable density formulation of the model is considered as explained below.

At the test filtered field level, the SGS stress tensor can be expressed as:

$$T_{ij} = \overline{\rho u}_i \hat{u}_j - \left( \overline{\rho \hat{u}}_i \overline{\rho \hat{u}}_j / \hat{\overline{\rho}} \right) \tag{4.262}$$

Both $T_{ij}$ and $\tau_{ij}$ are modeled in the same way with the Smagorinsky-Lilly model, assuming scale similarity:

$$\tau_{ij} = -2C\overline{\rho}\Delta^2 \tilde{S} \mid \left( \tilde{S}_{ij} - \frac{1}{3}\tilde{S}_{kk}\delta_{ij} \right) \tag{4.263}$$

$$T_{ij} = -2C\hat{\overline{\rho}}\hat{\Delta}^2 \mid \hat{\tilde{S}} \mid \left( \hat{\tilde{S}}_{ij} - \frac{1}{3}\hat{\tilde{S}}_{kk}\delta_{ij} \right) \tag{4.264}$$

In Equation 4.263 (p. 102) and Equation 4.264 (p. 102), the coefficient C is assumed to be the same and independent of the filtering process (note that per Equation 4.260 (p. 101), $C = C_s^2$). The grid filtered SGS and the test-filtered SGS are related by the Germano identity [134] (p. 736) such that:

$$Ł_{ij} = T_{ij} - \hat{\tau}_{ij} = \overline{\rho}\hat{\tilde{u}}_i\tilde{u}_j - \frac{1}{\hat{\overline{\rho}}}\left( \overline{\rho}\hat{\tilde{u}}_i \overline{\rho}\hat{\tilde{u}}_j \right) \tag{4.265}$$

Where $L_{ij}$ is computable from the resolved large eddy field. Substituting the grid-filter Smagorinsky-Lilly model and Equation 4.264 (p. 102) into Equation 4.265 (p. 102), the following expressions can be derived to solve for C with the contraction obtained from the least square analysis of Lilly (1992).

$$C = \frac{\left( L_{ij} - L_{kk}\delta_{ij}/3 \right)}{M_{ij}M_{ij}} \tag{4.266}$$

With

$$M_{ij} = -2\left( \hat{\Delta}^2 \hat{\overline{\rho}} \mid \hat{\tilde{S}} \mid \hat{\tilde{S}}_{ij} - \Delta^2 \overline{\rho} \mid \hat{\tilde{S}} \mid \tilde{S}_{ij} \right) \tag{4.267}$$

More details of the model implementation in ANSYS Fluent and its validation can be found in [208] (p. 740).

The $C_s = \sqrt{C}$ obtained using the dynamic Smagorinsky-Lilly model varies in time and space over a fairly wide range. To avoid numerical instability, both the numerator and the denominator in Equation 4.266 (p. 102) are locally averaged (or filtered) using the test-filter. In ANSYS Fluent, $C_s$ is also clipped at zero and 0.23 by default.

### 4.12.2.3. Wall-Adapting Local Eddy-Viscosity (WALE) Model

In the WALE model [320] (p. 746), the eddy viscosity is modeled by

$$\mu_t = \rho L_s^2 \frac{\left( S_{ij}^d S_{ij}^d \right)^{3/2}}{\left( \overline{S}_{ij}\overline{S}_{ij} \right)^{5/2} + \left( S_{ij}^d S_{ij}^d \right)^{5/4}} \tag{4.268}$$


Release 15.0 - © SAS IP, Inc. All rights reserved. - Contains proprietary and confidential information of ANSYS, Inc. and its subsidiaries and affiliates.

where $L_s$ and $S_{ij}^d$ in the WALE model are defined, respectively, as

$$L_s = min\left(\kappa d, C_w V^{1/3}\right) \tag{4.269}$$

$$S_{ij}^d = \frac{1}{2}\left(\overline{g}_{ij}^2 + \overline{g}_{ji}^2\right) - \frac{1}{3}\delta_{ij}\overline{g}_{kk}^2, \quad \overline{g}_{ij} = \frac{\partial \overline{u}_i}{\partial x_j} \tag{4.270}$$

In ANSYS Fluent, the default value of the WALE constant, $C_w$, is 0.325 and has been found to yield satisfactory results for a wide range of flow. The rest of the notation is the same as for the Smagorinsky-Lilly model. With this spatial operator, the WALE model is designed to return the correct wall asymptotic ($y^3$) behavior for wall bounded flows.

Another advantage of the WALE model is that it returns a zero turbulent viscosity for laminar shear flows. This allows the correct treatment of laminar zones in the domain. In contrast, the Smagorinsky-Lilly model produces non-zero turbulent viscosity. The WALE model is therefore preferable compared to the Smagorinsky-Lilly model.

### 4.12.2.4. Algebraic Wall-Modeled LES Model (WMLES)

While widely used in the academic community, LES has had very limited impact on industrial simulations. The reason lies in the excessively high resolution requirements for wall boundary layers. Near the wall, the largest scales in the turbulent spectrum are nevertheless geometrically very small and require a very fine grid and a small time step. In addition, unlike RANS, the grid cannot only be refined in the wall normal direction, but also must resolve turbulence in the wall parallel plane. This can only be achieved for flows at very low Reynolds number and on very small geometric scales (the extent of the LES domain cannot be much larger than 10-100 times the boundary layer thickness parallel to the wall). For this reason, using LES is only recommended for flows where wall boundary layers are not relevant and need not be resolved, or for flows where the boundary layers are laminar due to the low Reynolds number.

However, there are only very few such flows and other approaches need to be employed. A promising approach to overcome the Reynolds number scaling limitations of LES is the algebraic Wall-Modeled LES (WMLES) approach [403] (p. 751). In WMLES, the RANS portion of the model is only activated in the inner part of the logarithmic layer and the outer part of the boundary layer is covered by a modified LES formulation. Since the inner portion of the boundary layer is responsible for the Reynolds number dependency of the LES model, the WMLES approach can be applied at the same grid resolution to an ever increasing Reynolds number for channel flow simulations.

Note that for wall boundary layers, the Reynolds number scaling is not entirely avoided, as the thickness of the boundary layer declines relative to body dimensions with increasing Reynolds number. Assuming a certain number of grid nodes per 'boundary layer volume', the overall grid spacing will decrease and the overall number of cells will increase with the Reynolds number.

Another interesting option, and possibly the best use of the WMLES option, is when it is combined with the Embedded LES (ELES) implementation in ANSYS Fluent. ELES limits the LES zone to small regions of the domain and covers the less critical areas with RANS. WMLES extends this functionality to high Reynolds numbers in the LES domain. To apply this option, refer to Setting Up the Large Eddy Simulation Model and Setting Up the Embedded Large Eddy Simulation (ELES) Model in the User's Guide.

Release 15.0 - © SAS IP, Inc. All rights reserved. - Contains proprietary and confidential information of ANSYS, Inc. and its subsidiaries and affiliates.

### 4.12.2.4.1. Algebraic WMLES Model Formulation

The original Algebraic WMLES formulation was proposed in the works of Shur et.al. [403] (p. 751). It combines a mixing length model with a modified Smagorinsky model [412] (p. 751) and with the wall-damping function of Piomelli [351] (p. 748).

In the Shur et al. model [403] (p. 751), the eddy viscosity is calculated with the use of a hybrid length scale:

$$v_t = \min\left[ (\kappa d_w)^2, (C_{Smag}\Delta)^2 \right] \cdot S \cdot \left\{ 1 - \exp\left[ -\left( y^+ / 25 \right)^3 \right] \right\} \tag{4.271}$$

where $d_w$ is the wall distance, $S$ is the strain rate, $\kappa = 0.41$ and $C_{S_{mag}} = 0.2$ are constants, and $y^+$ is the normal to the wall inner scaling. The LES model is based on a modified grid scale to account for the grid anisotropies in wall-modeled flows:

$$\Delta = \min(\max(C_w \cdot d_w;\ C_w \cdot h_{max}, h_{wn});\ h_{max}) \tag{4.272}$$

Here $h_{max}$ is the maximum edge length of the cell, $h_{wn}$ is the wall-normal grid spacing, and $C_w = 0.15$ is a constant.

The above model has been optimized for use in ANSYS Fluent but remains within the spirit of the original model.

#### *4.12.2.4.1.1. Reynolds Number Scaling*

The main advantage of the WMLES formulation is the improved Reynolds number scaling. The classical resolution requirements for wall resolved LES is

$$\Delta_x^+ = 40, \quad Ny = 30, \quad \Delta_z^+ = 20 \tag{4.273}$$

where

$$\Delta_x^+ = \frac{u_\tau \Delta x}{v}, \quad \Delta_z^+ = \frac{u_\tau \Delta z}{v} \tag{4.274}$$

and $Ny$ is the number of cells across the boundary layer, *h*, (or half channel height *h*) and $\nu$ is the kinematic viscosity. The wall friction velocity is defined as

$$u_\tau = \sqrt{\frac{\tau_w}{\rho}} \tag{4.275}$$

where $\tau_w$ is the wall shear stress and $\rho$ is the density.

The resolution requirement for WMLES is

$$\Delta_x = \frac{h}{10}, \quad Ny = 30 - 40, \quad \Delta_z = \frac{h}{20} \tag{4.276}$$

Again with $h = \frac{H}{2}$ for a channel (where *H* is the channel height), or $h = \delta$ (where $\delta$ is the boundary layer thickness).

Considering a periodic channel (in the span and streamwise direction) with the geometry dimensions:


Release 15.0 - © SAS IP, Inc. All rights reserved. - Contains proprietary and confidential information of ANSYS, Inc. and its subsidiaries and affiliates.

$$Lx = 8h, \quad Ly = 2h, \quad Lz = 3h \tag{4.277}$$

you obtain the following cell numbers ($N_T$ total number of cells in channel) for the wall-resolved LES and WMLES:

**Wall-Resolved LES:**

**Table 4.1: Wall-Resolved Grid Size as a Function of Reynolds Number**

| $Re_\tau$ | 500 | $10^3$ | $10^4$ | $10^5$ |
|---|---|---|---|---|
| $N_T$ | 5.0e5 | 1.8e6 | 1.8e8 | 1.8e10 |

**WMLES:**

**Table 4.2: WMLES Grid Size as a Function of Reynolds Number**

| $Re_\tau$ | 500 | $10^3$ | $10^4$ | $10^5$ |
|---|---|---|---|---|
| $N_T$ | 5.0e5 | 5.0e5 | 5.0e5 | 5.0e5 |
| Ratio LES/WMLES | 1 | 4 | $4x10^2$ | $4x10^4$ |
| Ratio CPU LES/WMLES (CFL=0.3) | 1 | $10^1$ | $10^4$ | $10^7$ |

The Reynolds number is based on the friction velocity:

$$Re_\tau = \sqrt{\frac{u_\tau h}{\nu}} \tag{4.278}$$

From the above tables, it can be seen that the quadratic Reynolds number dependence of the Wall-Resolved LES has been avoided by WMLES and that the CPU effort is substantially reduced.

However, it is still important to keep in mind that WMLES is much more computationally expensive than RANS. Considering a wall boundary layer flow, with WMLES one must cover every boundary layer volume $(\delta \times \delta \times \delta)$ with 10 x (30-40) x 20 = 6000-8000 cells in the stream-wise, normal, and span-wise direction. RANS can be estimated to 1 x (30-40) x 1 =30-40 cells. In addition, RANS can be computed steady state whereas WMLES requires an unsteady simulation with CFL~0.3.

## 4.12.2.4.2. Algebraic WMLES S-Omega Model Formulation

One of the deficiencies of the WMLES approach is that the model does not provide zero eddy-viscosity for flows with constant shear when you use a modified Smagorinsky model in the LES zone. For this reason, the WMLES model does not allow the computation of transitional effects, and can produce overly large eddy-viscosities in separating shear layers (like from a backstep).

A way to enhance the WMLES formulation given in Equation 4.271 (p. 104) is to compute the LES portion of the model using the difference $\mathrm{abs}\,(S - \Omega)$ instead of $S$, where $S$ is the strain rate and $\Omega$ is the vorticity magnitude. This enhancement is referred to as the WMLES $S$-$\Omega$ formulation.

Release 15.0 - © SAS IP, Inc. All rights reserved. - Contains proprietary and confidential information of ANSYS, Inc. and its subsidiaries and affiliates.

#### 4.12.2.5. Dynamic Kinetic Energy Subgrid-Scale Model

The original and dynamic Smagorinsky-Lilly models, discussed previously, are essentially algebraic models in which subgrid-scale stresses are parameterized using the resolved velocity scales. The underlying assumption is the local equilibrium between the transferred energy through the grid-filter scale and the dissipation of kinetic energy at small subgrid scales. The subgrid-scale turbulence can be better modeled by accounting for the transport of the subgrid-scale turbulence kinetic energy.

The dynamic subgrid-scale kinetic energy model in ANSYS Fluent replicates the model proposed by Kim and Menon [211] (p. 740).

The subgrid-scale kinetic energy is defined as

$$k_{sgs}=\frac{1}{2}\left(\overline{u_k^2}-\overline{u}_k^2\right) \tag{4.279}$$

which is obtained by contracting the subgrid-scale stress in Equation 4.11 (p. 41).

The subgrid-scale eddy viscosity, $\mu_t$, is computed using $k_{sgs}$ as

$$\mu_t=C_k\rho k_{sgs}^{1/2}\Delta_f \tag{4.280}$$

where $\Delta_f$ is the filter-size computed from $\Delta_f \equiv V^{1/3}$.

The subgrid-scale stress can then be written as

$$\tau_{ij}-\frac{2}{3}\rho k_{sgs}\delta_{ij}=-2C_k\rho k_{sgs}^{1/2}\Delta_f\overline{S}_{ij} \tag{4.281}$$

$k_{sgs}$ is obtained by solving its transport equation

$$\rho\frac{\partial \overline{k}_{sgs}}{\partial t}+\rho\frac{\partial \overline{u}_j\overline{k}_{sgs}}{\partial x_j}=-\tau_{ij}\frac{\partial \overline{u}_i}{\partial x_j}-C_\varepsilon\rho\frac{k_{sgs}^{3/2}}{\Delta_f}+\frac{\partial}{\partial x_j}\left(\frac{\mu_t}{\sigma_k}\frac{\partial k_{sgs}}{\partial x_j}\right) \tag{4.282}$$

In the above equations, the model constants, $C_k$ and $C_\varepsilon$, are determined dynamically [211] (p. 740). $\sigma_k$ is hardwired to 1.0. The details of the implementation of this model in ANSYS Fluent and its validation is given by Kim [208] (p. 740).

## 4.12.3. Inlet Boundary Conditions for the LES Model

This section describes the algorithms available in ANSYS Fluent to model the fluctuating velocity at velocity inlet boundaries or pressure inlet boundaries.

The stochastic components of the flow at the velocity-specified inlet boundaries are neglected if the **No Perturbations** option is used. In such cases, individual instantaneous velocity components are simply set equal to their mean velocity counterparts. This option is suitable only when the level of turbulence at the inflow boundaries is negligible or does not play a major role in the accuracy of the overall solution.

#### 4.12.3.1. Vortex Method

To generate a time-dependent inlet condition, a random 2D vortex method is considered. With this approach, a perturbation is added on a specified mean velocity profile via a fluctuating vorticity field


Release 15.0 - © SAS IP, Inc. All rights reserved. - Contains proprietary and confidential information of ANSYS, Inc. and its subsidiaries and affiliates.

(that is, two-dimensional in the plane normal to the streamwise direction). The vortex method is based on the Lagrangian form of the 2D evolution equation of the vorticity and the Biot-Savart law. A particle discretization is used to solve this equation. These particles, or "vortex points" are convected randomly and carry information about the vorticity field. If $N$ is the number of vortex points and $A$ is the area of the inlet section, the amount of vorticity carried by a given particle $i$ is represented by the circulation $\Gamma_i$ and an assumed spatial distribution $\eta$:

$$\Gamma_i(x,y) = 4\sqrt{\frac{\pi A k(x,y)}{3N[2\ln(3)-3\ln(2)]}} \tag{4.283}$$

$$\eta(\vec{x}) = \frac{1}{2\pi\sigma^2}\left(2e^{-|x|^2/2\sigma^2}-1\right)2e^{-|x|^2/2\sigma^2} \tag{4.284}$$

where $k$ is the turbulence kinetic energy. The parameter $\sigma$ provides control over the size of a vortex particle. The resulting discretization for the velocity field is given by

$$\vec{u}(\vec{x}) = \frac{1}{2\pi}\sum_{i=1}^{N}\Gamma_i\frac{((\vec{x}_i-\vec{x})\times\vec{z})\left(1-e^{|\vec{x}-\vec{x}'|^2/2\sigma^2}\right)}{|\vec{x}-\vec{x}'_i|^2} \tag{4.285}$$

Where $\vec{z}$ is the unit vector in the streamwise direction. Originally [400] (p. 751), the size of the vortex was fixed by an ad hoc value of $\sigma$. To make the vortex method generally applicable, a local vortex size is specified through a turbulent mixing length hypothesis. $\sigma$ is calculated from a known profile of mean turbulence kinetic energy and mean dissipation rate at the inlet according to the following:

$$\sigma = \frac{ck^{3/2}}{2\varepsilon} \tag{4.286}$$

where $c = 0.16$. To ensure that the vortex will always belong to resolved scales, the minimum value of $\sigma$ in Equation 4.286 (p. 107) is bounded by the local grid size. The sign of the circulation of each vortex is changed randomly each characteristic time scale $\tau$. In the general implementation of the vortex method, this time scale represents the time necessary for a 2D vortex convected by the bulk velocity in the boundary normal direction to travel along $n$ times its mean characteristic 2D size ($\sigma_m$), where $n$ is fixed equal to 100 from numerical testing. The vortex method considers only velocity fluctuations in the plane normal to the streamwise direction.

In ANSYS Fluent however, a simplified linear kinematic model (LKM) for the streamwise velocity fluctuations is used [283] (p. 744). It is derived from a linear model that mimics the influence of the two-dimensional vortex in the streamwise mean velocity field. If the mean streamwise velocity $U$ is considered as a passive scalar, the fluctuation $u'$ resulting from the transport of $U$ by the planar fluctuating velocity field $v'$ is modeled by

$$u' = -\vec{v}' \cdot \vec{g} \tag{4.287}$$

where $\vec{g}$ is the unit vector aligned with the mean velocity gradient $\overrightarrow{\nabla U}$. When this mean velocity gradient is equal to zero, a random perturbation can be considered instead.

Since the fluctuations are equally distributed among the velocity components, only the prescribed kinetic energy profile can be fulfilled at the inlet of the domain. Farther downstream, the correct fluctuation distribution is recovered [283] (p. 744). However, if the distribution of the normal fluctuations is known or can be prescribed at the inlet, a rescaling technique can be applied to the synthetic flow field in order to fulfill the normal statistic fluctuations $<uu>$, $<vv>$, and $<ww>$ as given at the inlet.

Release 15.0 - © SAS IP, Inc. All rights reserved. - Contains proprietary and confidential information of ANSYS, Inc. and its subsidiaries and affiliates.

With the rescaling procedure, the velocity fluctuations are expressed according to:

$$u_i'^{*} = u_i' \frac{\sqrt{<u_i u_i>}}{\sqrt{2/3k}} \tag{4.288}$$

This also results in an improved representation of the turbulent flow field downstream of the inlet. This rescaling procedure is used only if the **Reynolds-Stress Components** is specified as the **Reynolds-Stress Specification Method**, instead of the default option **K or Turbulence Intensity**.

**Important**

Since the vortex method theory is based on the modification of the velocity field normal to the streamwise direction, it is imperative that you create an inlet plane normal (or as close as possible) to the streamwise velocity direction. Problems can arise if the inlet convective velocity is of the same order or lower than $k^{0.5}$, as this can cause local outflow. For this reason it should be applied with caution for Tu~1 or smaller).

The vortex method covers the entire boundary for which it is selected with vortices, even in regions, where the incoming turbulence level is low (freestream). For efficiency reasons, it is therefore recommended that you restrict the domain of the VM to the region where you which to generate unsteady turbulence. As an example, assume a thin mixing layer enters through a much larger inlet region. It is then advised to split the inlet boundary into three parts. One below the mixing layer with constant inlet velocity, one where the mixing layer enters the domain using the VM and a third above the mixing layer, again with a constant velocity. Thereby the vortices are concentrated at the domain of interest. Otherwise, a very large number of vortices would have to be generated to ensure a sufficient number of them in the thin mixing layer region.

### 4.12.3.2. Spectral Synthesizer

The spectral synthesizer provides an alternative method of generating fluctuating velocity components. It is based on the random flow generation technique originally proposed by Kraichnan [218] (p. 741) and modified by Smirnov et al. [414] (p. 751). In this method, fluctuating velocity components are computed by synthesizing a divergence-free velocity-vector field from the summation of Fourier harmonics. In ANSYS Fluent, the number of Fourier harmonics is fixed to 100.

**Important**

Both the vortex method and the spectral synthesizer are available for velocity inlet and pressure inlet boundary conditions. For the velocity inlet, the fluctuations are added on the mean specified velocity. For the pressure inlet, virtual body forces are employed in the momentum equations to add the reconstructed turbulent fluctuations to the velocity field. These virtual body forces are considered only in the first LES cells close to the inlet.

Both methods are also available for the SAS and DES models. If unsteadiness inside the domain can be sustained depends on the flow and the grid spacing, especially when using the SAS or the DDES models for wall bounded flows.

Finally it should be noted that both methods require realistic inlet conditions (U,k, $\varepsilon$ profiles) that can be obtained from separate RANS simulations. Unrealistic ("flat") turbulent profiles at inlets will generate unrealistic turbulent eddies at inlets.


Release 15.0 - © SAS IP, Inc. All rights reserved. - Contains proprietary and confidential information of ANSYS, Inc. and its subsidiaries and affiliates.

# 4.13. Embedded Large Eddy Simulation (ELES)

This section describes the theory behind the Embedded Large Eddy Simulation (ELES) model. Information is presented in the following sections:

4.13.1. Overview
4.13.2. Selecting a Model
4.13.3. Interfaces Treatment

## 4.13.1. Overview

Large Eddy Simulation (LES) has had very limited impact on industrial CFD simulations, mainly due to its high computational costs. There are only very few technical applications, where LES can be applied within the entire computational domain. Such flows are typically of very low Reynolds number, or flows where wall boundary layers are not important (free shear flows). Especially the high resolution requirements for wall bounded flows even at moderate Reynolds numbers have severely limited the usage of LES.

In order to allow the resolution of large turbulent structures in industrial flow simulations, hybrid models like Scale-Adaptive Simulation (SAS) (see Scale-Adaptive Simulation (SAS) Model (p. 92)) or Detached Eddy Simulation (DES) (see Detached Eddy Simulation (DES) (p. 95)) have been developed. For these models, the wall boundary layers are typically covered by the RANS part of the model and turbulence is only resolved in large separated (detached) zones. The unsteadiness in the simulations is generated from a global flow instability as observed behind bluff bodies. However, such an approach is not always suitable, as not all flows exhibit a sufficiently strong instability to generate turbulent structures by themselves. In such situations, zonal models are desirable, where a clear distinction between RANS and LES regions can be made and where turbulence is converted from RANS to LES by suitable methods at the interface. One such approach is ELES, where you generate RANS and LES zones during the grid generation phase, select appropriate models for each zone, and define the appropriate treatment at the interface. ELES is therefore not a new turbulence model, but the combination of RANS and LES models joined by appropriate interface conditions.

## 4.13.2. Selecting a Model

In principle, there are a large number of models that can be combined. Generally, all RANS models in ANSYS Fluent can be selected in the RANS region. The RANS model not compatible with ELES is the Spalart-Allmaras model, as a one-equation model cannot provide the required turbulent length scale to the interface method.

With respect to LES models, all algebraic LES models are available (this excludes the Dynamic Kinetic Energy Subgrid-Scale Model — see Dynamic Kinetic Energy Subgrid-Scale Model (p. 106)). While for the RANS portion, a general recommendation is difficult due to the different strength of RANS models for different applications, for the LES region, the WALE model is generally considered a suitable choice.

## 4.13.3. Interfaces Treatment

Figure 4.7: Backward Facing Step Flow Using ELES (p. 110) shows a typical example of an ELES scenario. The geometry of the simulation is divided into RANS and LES zones with interfaces between them. The upstream and the downstream zone are covered by RANS and the middle section with the reversed flow is covered by LES.

Release 15.0 - © SAS IP, Inc. All rights reserved. - Contains proprietary and confidential information of ANSYS, Inc. and its subsidiaries and affiliates.

**Figure 4.7: Backward Facing Step Flow Using ELES**

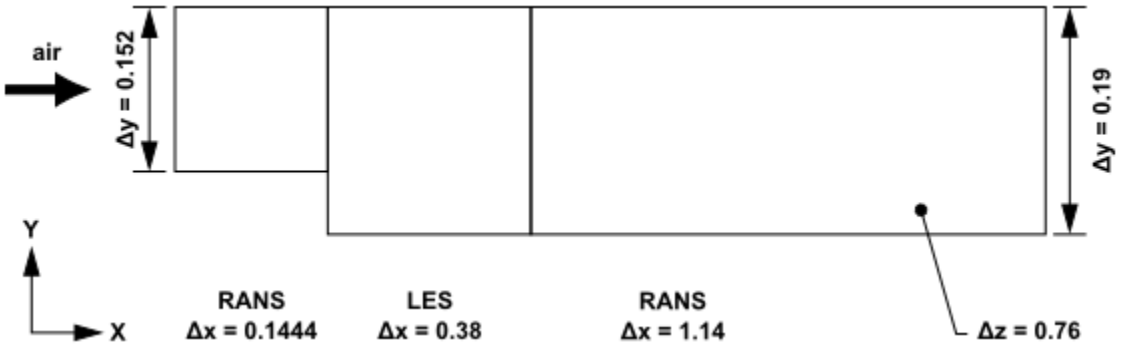


As the flow passes between the RANS domain and the LES domain, and from the LES domain into the downstream RANS domain, the treatment of the interfaces must be considered, as described in the following sections.

4.13.3.1. RANS-LES Interface
4.13.3.2. LES-RANS Interface
4.13.3.3. Internal Interface Without LES Zone
4.13.3.4. Grid Generation Guidelines

## 4.13.3.1. RANS-LES Interface

The most critical interface is the interface where the flow leaves the RANS domain and enters the LES region (RANS-LES interface). At this interface, it is necessary to convert modeled turbulence kinetic energy into resolved energy and you must select an appropriate method for this transfer. This can be achieved by selecting one of the two existing methods for generating resolved turbulence at inlets – namely the Vortex Method (VM, see Vortex Method (p. 106)) or the Spectral Synthesizer (SS, see Spectral Synthesizer (p. 108)). Both methods have been augmented so that they can be used at interior interfaces between the RANS and LES zone. The RANS information is obtained from the RANS model used upstream of the interface. For details and recommendations on these methods, see Zonal Modeling and Embedded LES (ELES) and Setting Up the Embedded Large Eddy Simulation (ELES) Model in the User's Guide.

If a DDES or SAS model is run in the entire domain, the interface treatment ensures that the turbulent kinetic energy that is converted from RANS to LES is subtracted from the RANS model. Thereby avoiding double-accounting of turbulence.

## 4.13.3.2. LES-RANS Interface

There is also an ambiguity concerning how to revert back from the LES to the RANS zone (LES-RANS interface). The first option is to freeze the background RANS model during the ELES simulation in the LES zone. This assumes that the ELES is started from a reasonably converged RANS simulation (this is recommended in any case). The momentum equations in the LES zone are not affected by the freeze as they are provided by the eddy-viscosity from the LES model. At the 'downstream' LES-RANS interface, the RANS model is then simply reactivated, using the frozen RANS solution inside the LES zone as an 'inlet' condition for the downstream RANS zone. This works well, as long as there is no significant change in mean flow topology between the full RANS and the ELES run, or if the flow downstream of the LES-RANS interface is not relevant to the goals of the simulation. It should be stressed, however, that for this option, any non-converged RANS starting solution will affect the flow for all times downstream of the LES-RANS interface. The option of freezing the turbulence variables of the underlying RANS model inside the LES domain is employed with all standard RANS models.


Release 15.0 - © SAS IP, Inc. All rights reserved. - Contains proprietary and confidential information of ANSYS, Inc. and its subsidiaries and affiliates.

A second option would be to run the RANS model in passive mode within the LES zone, meaning the model is solved on the unsteady velocity field, but the resulting eddy-viscosity is overwritten by the LES model eddy-viscosity for the momentum equations. The RANS model is then reactivated at the LES-RANS interface. It turns out that this approach fails for standard RANS models, as they severely over-predict the turbulent kinetic energy in the LES zone. The reason lies in the high strain rates computed from the unsteady velocity field. These strain rates enter into the production term Pk and generate very high turbulence levels in the LES zone. However, this option is sensible in combination with the SST-SAS model. This model recognizes the resolved scale and adjusts turbulence levels accordingly. When reactivated at the downstream interface, the model gradually converts back to RANS as the grid coarsens, or stays in LES-mode if time step and grid resolution permits.

### 4.13.3.3. Internal Interface Without LES Zone

There is a final option, where only a single hybrid model is run in the entire domain, that is, there is no change in the model between the RANS and LES zone. The choice is between the (rke- or SST-) DDES and the (SST-) SAS model, both of which can be run in RANS and LES mode. At the interface, again, the Vortex Method or the Spectral Synthesizer can be selected to generate resolved turbulence. When using the (rke- or SST-) DDES model, one has to consider that the model will not be in RANS mode for free shear flows (flows away from walls where the DDES shielding function is not active) if the grid is sufficiently fine to activate the DES limiter in the RANS zone. The combination of the (I)DDES model with the interface option is therefore mostly limited to wall-bounded internal flows. For more information about DDES, see Detached Eddy Simulation (DES) (p. 95), and for more information about IDDES, see Improved Delayed Detached Eddy Simulation (IDDES) (p. 98)

The current option of using an internal interface works more naturally in combination with the SST-SAS model, where little attention is required to carry the model in RANS mode to the interface. The current interface treatment can therefore be used in situations, where the internal flow instability is not strong enough to convert the SAS model into scale-resolving ('LES') mode at a desired location. Downstream of the interface, the SAS model will then remain in LES mode if the grid and time step size permit, or will gradually turn back to RANS otherwise.

If a DDES or SAS model is run in the entire domain, the interface treatment ensures that the turbulent kinetic energy that is converted from RANS to LES is subtracted from the RANS model. Thereby avoiding double-accounting of turbulence.

### 4.13.3.4. Grid Generation Guidelines

The grids used in the RANS and LES zones have to be conforming to the resolution requirements of the underlying turbulence model. Figure 4.8: Typical Grid for ELES for Backward Facing Step (p. 112) shows an example of an ELES grid. Frequently, the LES zone will be connected to the RANS zones by Non-Conformal Interfaces (NCI) to allow a more refined grid in the LES zone.

Release 15.0 - © SAS IP, Inc. All rights reserved. - Contains proprietary and confidential information of ANSYS, Inc. and its subsidiaries and affiliates.

**Figure 4.8: Typical Grid for ELES for Backward Facing Step**

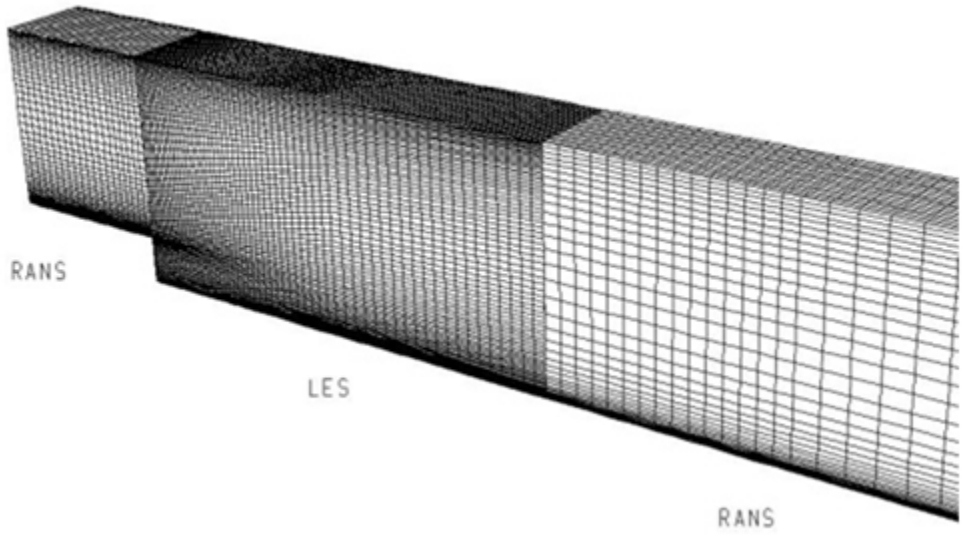


## 4.14. Near-Wall Treatments for Wall-Bounded Turbulent Flows

Information about near-wall treatments for wall-bounded turbulent flows is presented in the following sections:

4.14.1. Overview
4.14.2. Standard Wall Functions
4.14.3. Scalable Wall Functions
4.14.4. Non-Equilibrium Wall Functions
4.14.5. Enhanced Wall Treatment ε-Equation (EWT-ε)
4.14.6. Enhanced Wall Treatment ω-Equation (EWT-ω)
4.14.7. User-Defined Wall Functions
4.14.8. LES Near-Wall Treatment

### 4.14.1. Overview

Turbulent flows are significantly affected by the presence of walls. Obviously, the mean velocity field is affected through the no-slip condition that has to be satisfied at the wall. However, the turbulence is also changed by the presence of the wall in non-trivial ways. Very close to the wall, viscous damping reduces the tangential velocity fluctuations, while kinematic blocking reduces the normal fluctuations. Toward the outer part of the near-wall region, however, the turbulence is rapidly augmented by the production of turbulence kinetic energy due to the large gradients in mean velocity.

The near-wall modeling significantly impacts the fidelity of numerical solutions, inasmuch as walls are the main source of mean vorticity and turbulence. After all, it is in the near-wall region that the solution variables have large gradients, and the momentum and other scalar transports occur most vigorously. Therefore, accurate representation of the flow in the near-wall region determines successful predictions of wall-bounded turbulent flows.

Numerous experiments have shown that the near-wall region can be largely subdivided into three layers. In the innermost layer, called the "viscous sublayer", the flow is almost laminar, and the (molecular) viscosity plays a dominant role in momentum and heat or mass transfer. In the outer layer, called the fully-turbulent layer, turbulence plays a major role. Finally, there is an interim region between the viscous


Release 15.0 - © SAS IP, Inc. All rights reserved. - Contains proprietary and confidential information of ANSYS, Inc. and its subsidiaries and affiliates.

sublayer and the fully turbulent layer where the effects of molecular viscosity and turbulence are equally important. Figure 4.9: Subdivisions of the Near-Wall Region (p. 113) illustrates these subdivisions of the near-wall region, plotted in semi-log coordinates.

**Figure 4.9: Subdivisions of the Near-Wall Region**

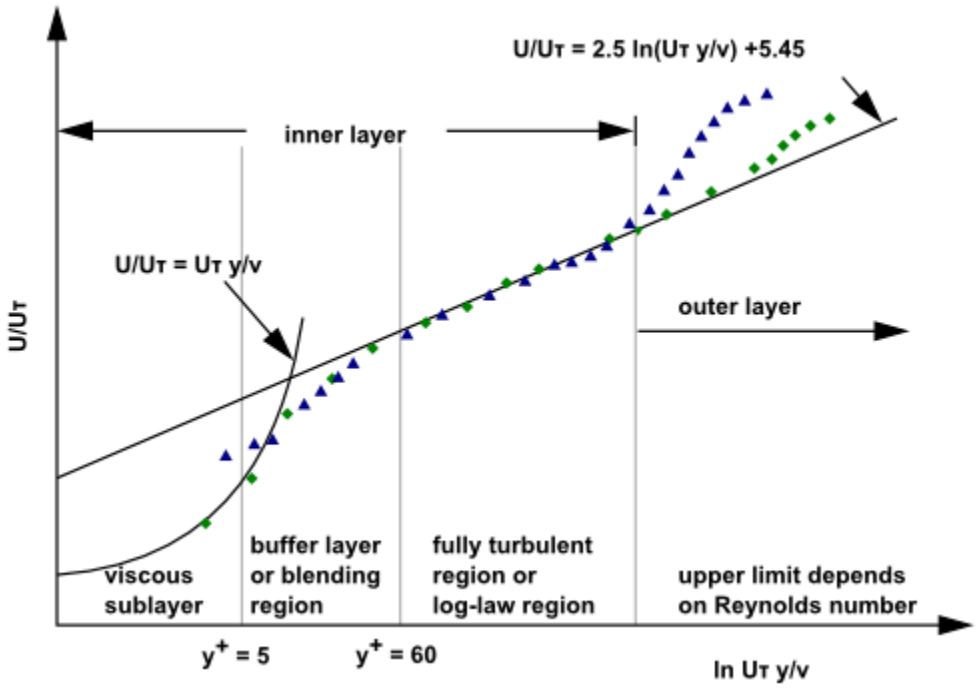


In Figure 4.9: Subdivisions of the Near-Wall Region (p. 113), $y^+ \equiv \rho u_\tau y/\mu$, where $u_\tau$ is the friction velocity, defined as $\sqrt{\frac{\tau_w}{\rho}}$.

### 4.14.1.1. Wall Functions vs. Near-Wall Model

Traditionally, there are two approaches to modeling the near-wall region. In one approach, the viscosity-affected inner region (viscous sublayer and buffer layer) is not resolved. Instead, semi-empirical formulas called "wall functions" are used to bridge the viscosity-affected region between the wall and the fully-turbulent region. The use of wall functions obviates the need to modify the turbulence models to account for the presence of the wall.

In another approach, the turbulence models are modified to enable the viscosity-affected region to be resolved with a mesh all the way to the wall, including the viscous sublayer. For the purposes of discussion, this will be termed the "near-wall modeling" approach. These two approaches are depicted schematically in Figure 4.10: Near-Wall Treatments in ANSYS Fluent (p. 114).

Release 15.0 - © SAS IP, Inc. All rights reserved. - Contains proprietary and confidential information of ANSYS, Inc. and its subsidiaries and affiliates.

**Figure 4.10: Near-Wall Treatments in ANSYS Fluent**

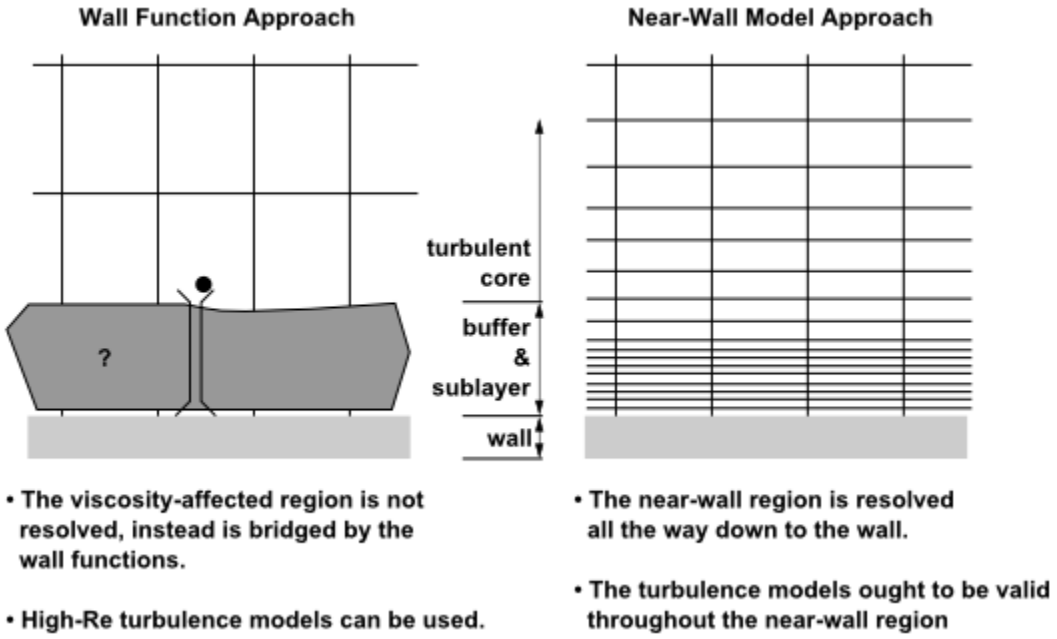


The main shortcoming of all wall functions (except the scalable wall function) is that the numerical results deteriorate under refinement of the grid in wall normal direction. $Y^+$ values of below 15 will gradually result in unbounded errors in wall shear stress and wall heat transfer. While this was the industrial standard some years ago, ANSYS Fluent has taken steps to offer more advanced wall formulations which allow a consistent mesh refinement without a deterioration of the results. Such $y^+$-independent formulations are the default for all $\omega$-equation based turbulence models. For the $\varepsilon$-equation based models, the Enhance Wall Treatment (EWT) serves the same purpose. This option is also the default for the Spalart-Allmaras model and allows you to run this model independent of the near wall $y^+$-resolution.

High quality numerical results for the wall boundary layer will only be obtained if the overall resolution of the boundary layer is sufficient. This requirement is actually more important than achieving certain $y^+$ values. The minimum number of cells to cover a boundary layer accurately is around 10, but values of 20 are desirable. It should also be noted that an improvement of boundary layer resolution can often be achieved with moderate increase in numerical effort, as it requires only a mesh refinement in the wall-normal direction. The associated increase in accuracy is typically well worth the additional computing costs. For unstructured meshes, it is recommended that you generate prism layers near the wall with 10–20 or more layers for an accurate prediction of the wall boundary layers. The thickness of the prism layer should be designed to ensure that around 15 or more nodes are actually covering the boundary layer. This can be checked after a solution is obtained, by looking at the turbulent viscosity, which has a maximum in the middle of the boundary layer – this maximum gives an indication of the thickness of the boundary layer (twice the location of the maximum gives the boundary layer edge). It is essential that the prism layer is thicker than the boundary layer as otherwise there is a danger that the prism layer confines the growth of the boundary layer.

**Recommendations:**

- For the $\varepsilon$-equation, use Enhanced Wall Treatment – EWT-$\varepsilon$
- If wall functions are favored with the $\varepsilon$-equation, use scalable wall functions
- For the $\omega$-equation based models, use the default – EWT-$\omega$


Release 15.0 - © SAS IP, Inc. All rights reserved. - Contains proprietary and confidential information of ANSYS, Inc. and its subsidiaries and affiliates.

- For the Spalart-Allmaras model, use the default Enhanced Wall Treatment.

#### 4.14.1.2. Wall Functions

Wall functions are a set of semi-empirical formulas and functions that in effect "bridge" or "link" the solution variables at the near-wall cells and the corresponding quantities on the wall. The wall functions comprise

- law-of-the-wall for the mean velocity and temperature (or other scalars)
- formulae for the near-wall turbulent quantities

Depending on the choice of turbulent model, ANSYS Fluent offers four to five choices of wall-function approaches:

- **Standard Wall Functions**
- **Scalable Wall Functions**
- **Non-Equilibrium Wall Functions**
- **Enhanced Wall Functions (as a part of EWT)**
- **User-Defined Wall Functions**

### 4.14.2. Standard Wall Functions

The standard wall functions in ANSYS Fluent are based on the work of Launder and Spalding [232] (p. 741), and have been most widely used in industrial flows. They are provided as a default option in ANSYS Fluent.

#### 4.14.2.1. Momentum

The law-of-the-wall for mean velocity yields

$$U^* = \frac{1}{\kappa} \ln (E y^*) \tag{4.289}$$

where

$$U^* \equiv \frac{U_P C_\mu^{1/4} k_P^{1/2}}{\tau_w / \rho} \tag{4.290}$$

is the dimensionless velocity.

$$y^* \equiv \frac{\rho C_\mu^{1/4} k_P^{1/2} y_P}{\mu} \tag{4.291}$$

is the dimensionless distance from the wall.

and

$\kappa$ = von Kármán constant (= 0.4187)

$E$ = empirical constant (= 9.793)

Release 15.0 - © SAS IP, Inc. All rights reserved. - Contains proprietary and confidential information of ANSYS, Inc. and its subsidiaries and affiliates.

$U_P$ = mean velocity of the fluid at the wall-adjacent cell centroid, $P$

$k_P$ = turbulence kinetic energy at the wall-adjacent cell centroid, $P$

$y_P$ = distance from the centroid of the wall-adjacent cell to the wall, $P$

$\mu$ = dynamic viscosity of the fluid

The range of $y^*$ values for which wall functions are suitable depend on the overall Reynolds number of the flow. The lower limit always lies in the order of $y^*$~15. Below this limit, wall functions will typically deteriorate and the accuracy of the solutions cannot be maintained (for exceptions, see Scalable Wall Functions (p. 119)). The upper limit depends strongly on the Reynolds number. For very high Reynolds numbers (for example, ships, airplanes), the logarithmic layer can extend to values as high as several thousand, whereas for low Reynolds number flows (for example, turbine blades, etc.) the upper limit can be as small as 100. For these low Reynolds number flows, the entire boundary layer is frequently only of the order of a few hundred $y^*$ units. The application of wall functions for such flows should therefore be avoided as they limit the overall number of nodes one can sensibly place in the boundary layer. In general, it is more important to ensure that the boundary layer is covered with a sufficient number of (structured) cells than to ensure a certain $y^*$ value.

In ANSYS Fluent, the log-law is employed when $y^* > 11.225$. When the mesh is such that $y^* < 11.225$ at the wall-adjacent cells, ANSYS Fluent applies the laminar stress-strain relationship that can be written as

$$U^* = y^* \tag{4.292}$$

It should be noted that, in ANSYS Fluent, the law-of-the-wall for mean velocity and temperature are based on the wall unit, $y^*$, rather than $y^+$ ($\equiv \rho u_\tau y/\mu$). These quantities are approximately equal in equilibrium turbulent boundary layers.

### 4.14.2.2. Energy

Reynolds' analogy between momentum and energy transport gives a similar logarithmic law for mean temperature. As in the law-of-the-wall for mean velocity, the law-of-the-wall for temperature employed in ANSYS Fluent comprises the following two different laws:

- linear law for the thermal conduction sublayer, or thermal viscous sublayer, where conduction is important
- logarithmic law for the turbulent region where effects of turbulence dominate conduction

The thickness of the thermal conduction layer is, in general, different from the thickness of the (momentum) viscous sublayer, and changes from fluid to fluid. For example, the thickness of the thermal sublayer for a high-Prandtl-number fluid (for example, oil) is much less than its momentum sublayer thickness. For fluids of low Prandtl numbers (for example, liquid metal), on the contrary, it is much larger than the momentum sublayer thickness.

$$\frac{\delta}{\delta_T} \approx \sqrt{Pr} \tag{4.293}$$

In highly compressible flows, the temperature distribution in the near-wall region can be significantly different from that of low subsonic flows, due to the heating by viscous dissipation. In ANSYS Fluent, the temperature wall functions include the contribution from the viscous heating [467] (p. 754).


Release 15.0 - © SAS IP, Inc. All rights reserved. - Contains proprietary and confidential information of ANSYS, Inc. and its subsidiaries and affiliates.

The law-of-the-wall implemented in ANSYS Fluent has the following composite form:

$$T^* \equiv \frac{(T_w - T_P)\rho c_p C_\mu^{1/4} k_P^{1/2}}{\dot{q}} = \begin{cases} \mathrm{Pr} y^* + \frac{1}{2}\rho \mathrm{Pr} \frac{C_\mu^{1/4} k_P^{1/2}}{\dot{q}} U_P^2 & (y^* < y_T^*) \\ \mathrm{Pr}_t \left[ \frac{1}{\kappa} \ln(E y^*) + P \right] + & \\ \frac{1}{2}\rho \frac{C_\mu^{1/4} k_P^{1/2}}{\dot{q}} \left\{ \mathrm{Pr}_t U_P^2 + (\mathrm{Pr} - \mathrm{Pr}_t) U_c^2 \right\} & (y^* > y_T^*) \end{cases} \tag{4.294}$$

where $P$ is computed by using the formula given by Jayatilleke [189] (p. 739):

$$P = 9.24 \left[ \left( \frac{Pr}{Pr_t} \right)^{3/4} - 1 \right] \left[ 1 + 0.28 e^{-0.007 Pr/Pr_t} \right] \tag{4.295}$$

and

$k_P$ = turbulent kinetic energy at the wall-adjacent cell centroid, $P$

$\rho$ = density of fluid

$c_p$ = specific heat of fluid

$\dot{q}$ = wall heat flux

$T_P$ = temperature at the wall-adjacent cell centroid, $P$

$T_w$ = temperature at the wall

$Pr$ = molecular Prandtl number ($\mu c_p / k_f$)

$Pr_t$ = turbulent Prandtl number (0.85 at the wall)

$A$ = Van Driest constant (= 26)

$U_c$ = mean velocity magnitude at $y^* = y_T^*$

Note that, for the pressure-based solver, the terms

$$\frac{1}{2}\rho Pr \frac{C_\mu^{1/4} k_P^{1/2}}{\dot{q}} U_P^2$$

and

$$\frac{1}{2}\rho \frac{C_\mu^{1/4} k_P^{1/2}}{\dot{q}} \left\{ Pr_t U_P^2 + (Pr - Pr_t) U_c^2 \right\}$$

will be included in Equation 4.294 (p. 117) only for compressible flow calculations.

The non-dimensional thermal sublayer thickness, $y_T^*$, in Equation 4.294 (p. 117) is computed as the $y^*$ value at which the linear law and the logarithmic law intersect, given the molecular Prandtl number of the fluid being modeled.

Release 15.0 - © SAS IP, Inc. All rights reserved. - Contains proprietary and confidential information of ANSYS, Inc. and its subsidiaries and affiliates.

The procedure of applying the law-of-the-wall for temperature is as follows. Once the physical properties of the fluid being modeled are specified, its molecular Prandtl number is computed. Then, given the molecular Prandtl number, the thermal sublayer thickness, $y_T^*$, is computed from the intersection of the linear and logarithmic profiles, and stored.

During the iteration, depending on the $y^*$ value at the near-wall cell, either the linear or the logarithmic profile in Equation 4.294 (p. 117) is applied to compute the wall temperature $T_w$ or heat flux $\dot{q}$ (depending on the type of the thermal boundary conditions).

The function for $P$ given by Equation 4.295 (p. 117) is relevant for the smooth walls. For the rough walls, however, this function is modified as follows:

$$P_{rough} = 3.15 Pr^{0.695} \left( \frac{1}{E'} - \frac{1}{E} \right)^{0.359} + \left( \frac{E'}{E} \right)^{0.6} P \tag{4.296}$$

where $E'$ is the wall function constant modified for the rough walls, defined by $E' = E/f_r$. To find a description of the roughness function $f_r$, you may refer to Equation 6.89 in Wall Roughness Effects in Turbulent Wall-Bounded Flows in the User's Guide.

### 4.14.2.3. Species

When using wall functions for species transport, ANSYS Fluent assumes that species transport behaves analogously to heat transfer. Similarly to Equation 4.294 (p. 117), the law-of-the-wall for species can be expressed for constant property flow with no viscous dissipation as

$$Y^* \equiv \frac{\left(Y_{i,w} - Y_i\right) \rho C_\mu^{1/4} k_P^{1/2}}{J_{i,w}} = \begin{cases} Sc y^* & \left(y^* < y_c^*\right) \\ Sc_t \left[ \frac{1}{\kappa} \ln\left(E y^*\right) + P_c \right] & \left(y^* > y_c^*\right) \end{cases} \tag{4.297}$$

where $Y_i$ is the local species mass fraction, $Sc$ and $Sc_t$ are molecular and turbulent Schmidt numbers, and $J_{i,w}$ is the diffusion flux of species $i$ at the wall. Note that $P_c$ and $y_c^*$ are calculated in a similar way as $P$ and $y_T^*$, with the difference being that the Prandtl numbers are always replaced by the corresponding Schmidt numbers.

### 4.14.2.4. Turbulence

In the $k$-$\varepsilon$ models and in the RSM (if the option to obtain wall boundary conditions from the $k$ equation is enabled), the $k$ equation is solved in the whole domain including the wall-adjacent cells. The boundary condition for $k$ imposed at the wall is

$$\frac{\partial k}{\partial n} = 0 \tag{4.298}$$

where $n$ is the local coordinate normal to the wall.

The production of kinetic energy, $G_k$, and its dissipation rate, $\varepsilon$, at the wall-adjacent cells, which are the source terms in the $k$ equation, are computed on the basis of the local equilibrium hypothesis.


Release 15.0 - © SAS IP, Inc. All rights reserved. - Contains proprietary and confidential information of ANSYS, Inc. and its subsidiaries and affiliates.

Under this assumption, the production of $k$ and its dissipation rate are assumed to be equal in the wall-adjacent control volume.

Thus, the production of $k$ is based on the logarithmic law and is computed from

$$G_k \approx \tau_w \frac{\partial U}{\partial y} = \tau_w \frac{\tau_w}{\kappa \rho C_\mu^{1/4} k_P^{1/2} y_P} \tag{4.299}$$

and $\varepsilon$ is computed from

$$\varepsilon_P = \frac{C_\mu^{3/4} k_P^{3/2}}{\kappa y_P} \tag{4.300}$$

The $\varepsilon$ equation is not solved at the wall-adjacent cells, but instead is computed using Equation 4.300 (p. 119). $\omega$ and Reynolds stress equations are solved as detailed in Wall Boundary Conditions (p. 67) and Wall Boundary Conditions (p. 90), respectively.

Note that, as shown here, the wall boundary conditions for the solution variables, including mean velocity, temperature, species concentration, $k$, and $\varepsilon$, are all taken care of by the wall functions. Therefore, you do not need to be concerned about the boundary conditions at the walls.

The standard wall functions described so far are provided as a default option in ANSYS Fluent. The standard wall functions work reasonably well for a broad range of wall-bounded flows. However, they tend to become less reliable when the flow situations depart from the ideal conditions that are assumed in their derivation. Among others, the constant-shear and local equilibrium assumptions are the ones that most restrict the universality of the standard wall functions. Accordingly, when the near-wall flows are subjected to severe pressure gradients, and when the flows are in strong non-equilibrium, the quality of the predictions is likely to be compromised.

The non-equilibrium wall functions are offered as an additional option, which can potentially improve the results in such situations.

---

**Important**

Standard wall functions are available with the following viscous models:

- $k$-$\varepsilon$ models
- Reynolds Stress models

---

## 4.14.3. Scalable Wall Functions

Scalable wall functions avoid the deterioration of standard wall functions under grid refinement below $y^* < 11$. These wall functions produce consistent results for grids of arbitrary refinement. For grids that are coarser than $y^* > 11$, the standard wall functions are identical.

The purpose of scalable wall functions is to force the usage of the log law in conjunction with the standard wall functions approach. This is achieved by introducing a limiter in the y* calculations such that

$$\tilde{y^*} = MAX(y^*, y^*_{limit}) \tag{4.301}$$

Release 15.0 - © SAS IP, Inc. All rights reserved. - Contains proprietary and confidential information of ANSYS, Inc. and its subsidiaries and affiliates.

where $y^*_{limit} = 11.225$. The use of Equation 4.301 (p. 119) in the context of the scalable wall functions concept is straightforward, that is, the y* formulation used for any standard wall function formula is replaced by $\tilde{y}^*$.

Scalable wall functions can be enabled in the **Viscous Model** dialog box under **Near-Wall Treatment**.

## 4.14.4. Non-Equilibrium Wall Functions

In addition to the standard wall function described above (which is the default near-wall treatment) a two-layer-based, non-equilibrium wall function [209] (p. 740) is also available. The key elements in the non-equilibrium wall functions are as follows:

- Launder and Spalding's log-law for mean velocity is sensitized to pressure-gradient effects.
- The two-layer-based concept is adopted to compute the budget of turbulence kinetic energy ($\overline{G_k}$, $\overline{\varepsilon}$) in the wall-neighboring cells.

The law-of-the-wall for mean temperature or species mass fraction remains the same as in the standard wall functions described above.

The log-law for mean velocity sensitized to the pressure gradients is

$$\frac{\tilde{U}C_\mu^{1/4}k^{1/2}}{\tau_w/\rho} = \frac{1}{\kappa}\ln\left(E\frac{\rho C_\mu^{1/4}k^{1/2}y}{\mu}\right) \tag{4.302}$$

where

$$\tilde{U} = U - \frac{1}{2}\frac{dp}{dx}\left[\frac{y_v}{\rho\kappa\sqrt{k}}\ln\left(\frac{y}{y_v}\right) + \frac{y-y_v}{\rho\kappa\sqrt{k}} + \frac{y_v^2}{\mu}\right] \tag{4.303}$$

and $y_v$ is the physical viscous sublayer thickness, and is computed from

$$y_v \equiv \frac{\mu y_v^*}{\rho C_\mu^{1/4}k_P^{1/2}} \tag{4.304}$$

where $y_v^* = 11.225$.

The non-equilibrium wall function employs the two-layer concept in computing the budget of turbulence kinetic energy at the wall-adjacent cells, which is needed to solve the $k$ equation at the wall-neighboring cells. The wall-neighboring cells are assumed to consist of a viscous sublayer and a fully turbulent layer. The following profile assumptions for turbulence quantities are made:

$$\tau_t = \begin{cases} 0, & y<y_v \\ \tau_w, & y>y_v \end{cases} \quad k = \begin{cases} \left(\frac{y}{y_v}\right)^2 k_P, & y<y_v \\ k_P, & y>y_v \end{cases} \quad \varepsilon = \begin{cases} \frac{2\nu k}{y^2}, & y<y_v \\ \frac{k^{3/2}}{C_\ell^* y}, & y>y_v \end{cases} \tag{4.305}$$


Release 15.0 - © SAS IP, Inc. All rights reserved. - Contains proprietary and confidential information of ANSYS, Inc. and its subsidiaries and affiliates.

where $C_\ell{}^* = \kappa C_\mu^{-3/4}$, and $y_\nu$ is the dimensional thickness of the viscous sublayer, defined in Equation 4.304 (p. 120).

Using these profiles, the cell-averaged production of $k$, $\overline{G_k}$, and the cell-averaged dissipation rate, $\overline{\varepsilon}$, can be computed from the volume average of $G_k$ and $\varepsilon$ of the wall-adjacent cells. For quadrilateral and hexahedral cells for which the volume average can be approximated with a depth-average,

$$\overline{G_k} \equiv \frac{1}{y_n}\int_0^{y_n} \tau_t \frac{\partial U}{\partial y} dy = \frac{1}{\kappa y_n}\frac{\tau_w^2}{\rho C_\mu^{1/4} k_P^{1/2}} \ln\left(\frac{y_n}{y_\nu}\right) \tag{4.306}$$

and

$$\overline{\varepsilon} \equiv \frac{1}{y_n}\int_0^{y_n} \varepsilon dy = \frac{1}{y_n}\left[\frac{2\nu}{y_\nu} + \frac{k_P^{1/2}}{C_\ell{}^*}\ln\left(\frac{y_n}{y_\nu}\right)\right] k_P \tag{4.307}$$

where $y_n$ is the height of the cell ($y_n = 2y_P$). For cells with other shapes (for example, triangular and tetrahedral grids), the appropriate volume averages are used.

In Equation 4.306 (p. 121) and Equation 4.307 (p. 121), the turbulence kinetic energy budget for the wall-neighboring cells is effectively depends on the proportions of the viscous sublayer and the fully turbulent layer, which varies widely from cell to cell in highly non-equilibrium flows. The nonequilibrium wall functions account for the effect of pressure gradients on the distortion of the velocity profiles. In such cases the assumption of local equilibrium, when the production of the turbulent kinetic energy is equal to the rate of its destruction, is no longer valid. Therefore, the non-equilibrium wall functions, in effect, partly account for the non-equilibrium effects that are neglected in the standard wall functions.

### 4.14.4.1. Standard Wall Functions vs. Non-Equilibrium Wall Functions

Because of the capability to partly account for the effects of pressure gradients, the non-equilibrium wall functions are recommended for use in complex flows involving separation, reattachment, and impingement where the mean flow and turbulence are subjected to pressure gradients and rapid changes. In such flows, improvements can be obtained, particularly in the prediction of wall shear (skin-friction coefficient) and heat transfer (Nusselt or Stanton number).

**Important**

Non-equilibrium wall functions are available with the following turbulence closures:

- $k$-$\varepsilon$ models
- Reynolds Stress Transport models

### 4.14.4.2. Limitations of the Wall Function Approach

The standard wall functions give reasonable predictions for the majority of high-Reynolds number wall-bounded flows. The non-equilibrium wall functions further extend the applicability of the wall function approach by including the effects of pressure gradient; however, the above wall functions become less

Release 15.0 - © SAS IP, Inc. All rights reserved. - Contains proprietary and confidential information of ANSYS, Inc. and its subsidiaries and affiliates.

reliable when the flow conditions depart too much from the ideal conditions underlying the wall functions. Examples are as follows:

- Pervasive low-Reynold-number or near-wall effects (for example, flow through a small gap or highly viscous, low-velocity fluid flow).
- Massive transpiration through the wall (blowing/suction).
- Severe pressure gradients leading to boundary layer separations.
- Strong body forces (for example, flow near rotating disks, buoyancy-driven flows).
- High three-dimensionality in the near-wall region (for example, Ekman spiral flow, strongly skewed 3D boundary layers).

If any of the above listed features prevail in the flow you are modeling, and if it is considered critically important for the success of your simulation, you must employ the near-wall modeling approach combined with the adequate mesh resolution in the near-wall region. ANSYS Fluent provides the enhanced wall treatment for such situations. This approach can be used with the $k$-$\varepsilon$ and the RSM models.

## 4.14.5. Enhanced Wall Treatment ε-Equation (EWT-ε)

Enhanced Wall Treatment for the $\varepsilon$-equation is a near-wall modeling method that combines a two-layer model with so-called enhanced wall functions. If the near-wall mesh is fine enough to be able to resolve the viscous sublayer (typically with the first near-wall node placed at $y^+ \approx 1$), then the enhanced wall treatment will be identical to the traditional two-layer zonal model (see below for details). However, the restriction that the near-wall mesh must be sufficiently fine everywhere might impose too large a computational requirement. Ideally, one would like to have a near-wall formulation that can be used with coarse meshes (usually referred to as wall-function meshes) as well as fine meshes (low-Reynolds number meshes). In addition, excessive error should not be incurred for the intermediate meshes where the first near-wall node is placed neither in the fully turbulent region, where the wall functions are suitable, nor in the direct vicinity of the wall at $y^+ \approx 1$, where the low-Reynold-number approach is adequate.

To achieve the goal of having a near-wall modeling approach that will possess the accuracy of the standard two-layer approach for fine near-wall meshes and that, at the same time, will not significantly reduce accuracy for wall-function meshes, ANSYS Fluent can combine the two-layer model with enhanced wall functions, as described in the following sections.

### 4.14.5.1. Two-Layer Model for Enhanced Wall Treatment

In ANSYS Fluent's near-wall model, the viscosity-affected near-wall region is completely resolved all the way to the viscous sublayer. The two-layer approach is an integral part of the enhanced wall treatment and is used to specify both $\varepsilon$ and the turbulent viscosity in the near-wall cells. In this approach, the whole domain is subdivided into a viscosity-affected region and a fully-turbulent region. The demarcation of the two regions is determined by a wall-distance-based, turbulent Reynolds number, $\mathrm{Re}_y$, defined as

$$Re_y \equiv \frac{\rho y \sqrt{k}}{\mu} \tag{4.308}$$


Release 15.0 - © SAS IP, Inc. All rights reserved. - Contains proprietary and confidential information of ANSYS, Inc. and its subsidiaries and affiliates.

where $y$ is the wall-normal distance calculated at the cell centers. In ANSYS Fluent, $y$ is interpreted as the distance to the nearest wall:

$$y \equiv \min_{\vec{r}_w \in \Gamma_w} \left\| \vec{r} - \vec{r}_w \right\| \tag{4.309}$$

where $\vec{r}$ is the position vector at the field point, and $\vec{r}_w$ is the position vector of the wall boundary. $\Gamma_w$ is the union of all the wall boundaries involved. This interpretation allows $y$ to be uniquely defined in flow domains of complex shape involving multiple walls. Furthermore, $y$ defined in this way is independent of the mesh topology.

In the fully turbulent region ($Re_y > Re_y^*$; $Re_y^* = 200$), the $k$-$\varepsilon$ models or the RSM (described in Standard, RNG, and Realizable k-ε Models (p. 46) and Reynolds Stress Model (RSM) (p. 83)) are employed.

In the viscosity-affected near-wall region ($Re_y < Re_y^*$), the one-equation model of Wolfstein [497] (p. 756) is employed. In the one-equation model, the momentum equations and the $k$ equation are retained as described in Standard, RNG, and Realizable k-ε Models (p. 46) and Reynolds Stress Model (RSM) (p. 83). However, the turbulent viscosity, $\mu_t$, is computed from

$$\mu_{t,2layer} = \rho C_\mu \ell_\mu \sqrt{k} \tag{4.310}$$

where the length scale that appears in Equation 4.310 (p. 123) is computed from [63] (p. 732)

$$\ell_\mu = y C_\ell^* \left(1 - e^{-Re_y/A_\mu}\right) \tag{4.311}$$

The two-layer formulation for turbulent viscosity described above is used as a part of the enhanced wall treatment, in which the two-layer definition is smoothly blended with the high-Reynolds number $\mu_t$ definition from the outer region, as proposed by Jongen [192] (p. 739):

$$\mu_{t,enh} = \lambda_\varepsilon \mu_t + (1 - \lambda_\varepsilon)\mu_{t,2layer} \tag{4.312}$$

where $\mu_t$ is the high-Reynolds number definition as described in Standard, RNG, and Realizable k-ε Models (p. 46) or Reynolds Stress Model (RSM) (p. 83) for the $k$-$\varepsilon$ models or the RSM. A blending function, $\lambda_\varepsilon$, is defined in such a way that it is equal to unity away from walls and is zero in the vicinity of the walls. The blending function has the following form:

$$\lambda_\varepsilon = \frac{1}{2}\left[1 + \tanh\left(\frac{Re_y - Re_y^*}{A}\right)\right] \tag{4.313}$$

The constant $A$ determines the width of the blending function. By defining a width such that the value of $\lambda_\varepsilon$ will be within 1% of its far-field value given a variation of $\Delta Re_y$, the result is

$$A = \frac{|\Delta Re_y|}{artanh(0.98)} \tag{4.314}$$

Typically, $\Delta Re_y$ would be assigned a value that is between 5% and 20% of $Re_y^*$. The main purpose of the blending function $\lambda_\varepsilon$ is to prevent solution convergence from being impeded when the value of $\mu_t$ obtained in the outer layer does not match with the value of $\mu_t$ returned by the Wolfstein model at the edge of the viscosity-affected region.

Release 15.0 - © SAS IP, Inc. All rights reserved. - Contains proprietary and confidential information of ANSYS, Inc. and its subsidiaries and affiliates.

The $\varepsilon$ field in the viscosity-affected region is computed from

$$\varepsilon = \frac{k^{3/2}}{\ell_\varepsilon} \tag{4.315}$$

The length scales that appear in Equation 4.315 (p. 124) are computed from Chen and Patel [63] (p. 732):

$$\ell_\varepsilon = y C_\ell{}^* \left(1 - e^{-Re_y/A_\varepsilon}\right) \tag{4.316}$$

If the whole flow domain is inside the viscosity-affected region ($Re_y < 200$), $\varepsilon$ is not obtained by solving the transport equation; it is instead obtained algebraically from Equation 4.315 (p. 124). ANSYS Fluent uses a procedure for the blending of $\varepsilon$ that is similar to the $\mu_t$-blending in order to ensure a smooth transition between the algebraically-specified $\varepsilon$ in the inner region and the $\varepsilon$ obtained from solution of the transport equation in the outer region.

The constants in Equation 4.311 (p. 123) and Equation 4.316 (p. 124), are taken from [63] (p. 732) and are as follows:

$$C_\ell{}^* = \kappa C_\mu^{-3/4}, A_\mu = 70, A_\varepsilon = 2C_\ell{}^* \tag{4.317}$$

### 4.14.5.2. Enhanced Wall Treatment for Momentum and Energy Equations

To have a method that can extend its applicability throughout the near-wall region (that is, viscous sublayer, buffer region, and fully-turbulent outer region) it is necessary to formulate the law-of-the wall as a single wall law for the entire wall region. ANSYS Fluent achieves this by blending the linear (laminar) and logarithmic (turbulent) law-of-the-wall using a function suggested by Kader [194] (p. 739):

$$u^+ = e^{\Gamma} u^+_{lam} + e^{1/\Gamma} u^+_{turb} \tag{4.318}$$

where the blending function is given by:

$$\Gamma = -\frac{a(y^+)^4}{1 + by^+} \tag{4.319}$$

where $a = 0.01$ and $b = 5$.

Similarly, the general equation for the derivative $\frac{du^+}{dy^+}$ is

$$\frac{du^+}{dy^+} = e^{\Gamma} \frac{du^+_{lam}}{dy^+} + e^{1/\Gamma} \frac{du^+_{turb}}{dy^+} \tag{4.320}$$

This approach allows the fully turbulent law to be easily modified and extended to take into account other effects such as pressure gradients or variable properties. This formula also guarantees the correct asymptotic behavior for large and small values of $y^+$ and reasonable representation of velocity profiles in the cases where $y^+$ falls inside the wall buffer region ($3 < y^+ < 10$).

The enhanced wall functions were developed by smoothly blending the logarithmic layer formulation with the laminar formulation. The enhanced turbulent law-of-the-wall for compressible flow with heat transfer and pressure gradients has been derived by combining the approaches of White and Cristoph [489] (p. 756) and Huang et al. [169] (p. 738):


Release 15.0 - © SAS IP, Inc. All rights reserved. - Contains proprietary and confidential information of ANSYS, Inc. and its subsidiaries and affiliates.

$$\frac{du^+_{turb}}{dy^+} = \frac{1}{\kappa y^+}\left[S'\left(1-\beta u^+ - \gamma (u^+)^2\right)\right]^{1/2} \tag{4.321}$$

where

$$S' = \begin{cases} 1+\alpha y^+ & \text{for } y^+ < y_s^+ \\ 1+\alpha y_s^+ & \text{for } y^+ \geq y_s^+ \end{cases} \tag{4.322}$$

and

$$\alpha \equiv \frac{v_w}{\tau_w u^*}\frac{dp}{dx} = \frac{\mu}{\rho^2 (u^*)^3}\frac{dp}{dx} \tag{4.323}$$

$$\beta \equiv \frac{\sigma_t q_w u^*}{c_p \tau_w T_w} = \frac{\sigma_t q_w}{\rho c_p u^* T_w} \tag{4.324}$$

$$\gamma \equiv \frac{\sigma_t (u^*)^2}{2 c_p T_w} \tag{4.325}$$

where $y_s^+$ is the location at which the log-law slope is fixed. By default, $y_s^+ = 60$. The coefficient $\alpha$ in Equation 4.321 (p. 125) represents the influences of pressure gradients while the coefficients $\beta$ and $\gamma$ represent the thermal effects. Equation 4.321 (p. 125) is an ordinary differential equation and ANSYS Fluent will provide an appropriate analytical solution. If $\alpha$, $\beta$, and $\gamma$ all equal 0, an analytical solution would lead to the classical turbulent logarithmic law-of-the-wall.

The laminar law-of-the-wall is determined from the following expression:

$$\frac{du^+_{lam}}{dy^+} = 1+\alpha y^+ \tag{4.326}$$

Note that the above expression only includes effects of pressure gradients through $\alpha$, while the effects of variable properties due to heat transfer and compressibility on the laminar wall law are neglected. These effects are neglected because they are thought to be of minor importance when they occur close to the wall. Integration of Equation 4.326 (p. 125) results in

$$u^+_{lam} = y^+\left(1+\frac{\alpha}{2}y^+\right) \tag{4.327}$$

Enhanced thermal wall functions follow the same approach developed for the profile of $u^+$. The unified wall thermal formulation blends the laminar and logarithmic profiles according to the method of Kader [194] (p. 739):

$$T^+ \equiv \frac{(T_w - T_P)\rho c_p u_T}{\dot{q}} = e^{\Gamma} T^+_{lam} + e^{1/\Gamma} T^+_{turb} \tag{4.328}$$

where the notation for $T_P$ and $\dot{q}$ is the same as for standard thermal wall functions (see Equation 4.294 (p. 117)). Furthermore, the blending factor $\Gamma$ is defined as

$$\Gamma = -\frac{a(Pry^+)^4}{1+bPr^3y^+} \tag{4.329}$$

where $Pr$ is the molecular Prandtl number, and the coefficients $a$ and $b$ are defined as in Equation 4.319 (p. 124).

Apart from the formulation for $T^+$ in Equation 4.328 (p. 125), the enhanced thermal wall functions follow the same logic as for standard thermal wall functions (see Energy (p. 116)), resulting in the following definition for turbulent and laminar thermal wall functions:

$$T^+_{lam} = Pr\left(u^+_{lam} + \frac{\rho u_*}{2\dot{q}}u^2\right) \tag{4.330}$$

$$T^+_{turb} = Pr_t\left\{u^+_{turb} + P + \frac{\rho u_*}{2\dot{q}}\left[u^2 - \left(\frac{Pr}{Pr_t}-1\right)(u_c^+)^2(u_*)^2\right]\right\} \tag{4.331}$$

where the quantity $u_c^+$ is the value of $u^+$ at the fictitious "crossover" between the laminar and turbulent region. The function $P$ is defined in the same way as for the standard wall functions.

A similar procedure is also used for species wall functions when the enhanced wall treatment is used. In this case, the Prandtl numbers in Equation 4.330 (p. 126) and Equation 4.331 (p. 126) are replaced by adequate Schmidt numbers. See Species (p. 118) for details about the species wall functions.

The boundary conditions for the turbulence kinetic energy are similar to the ones used with the standard wall functions (Equation 4.298 (p. 118)). However, the production of turbulence kinetic energy, $G_k$, is computed using the velocity gradients that are consistent with the enhanced law-of-the-wall (Equation 4.318 (p. 124) and Equation 4.320 (p. 124)), ensuring a formulation that is valid throughout the near-wall region.

**Important**

The enhanced wall treatment is available with the following turbulence closures:

- All $\varepsilon$ — equation models (except the Quadratic RSM)
- All $\omega$ — equation models (default)
- For the Spalart-Allmaras model, this option is not available. However, the model works consistently for wall function grids ($y^* > 15$) and for viscous sublayer grids ($y^* < 2$). Intermediate grids should be avoided as they will reduce the accuracy of the model.

Note that an alternative blending compared to the Kader-blending for $u^+$ and $\frac{du^+_{turb}}{dy^+}$ is used for the improved near wall treatment for turbulence models based on the $\omega$-equation, which is the new default near wall treatment.


Release 15.0 - © SAS IP, Inc. All rights reserved. - Contains proprietary and confidential information of ANSYS, Inc. and its subsidiaries and affiliates.

## 4.14.6. Enhanced Wall Treatment ω-Equation (EWT-ω)

Unlike the standard $\varepsilon$-equation, the $\omega$-equation can be integrated through the viscous sublayer without the need for a two-layer approach. This feature can be utilized for a $y^*$-insensitive wall treatment by blending the viscous sublayer formulation and the logarithmic layer formulation based on $y^*$. This formulation is the default for all $\omega$-equation based models.

## 4.14.7. User-Defined Wall Functions

This option is only available when one of the $k$-$\varepsilon$ model is enabled. Selecting the **User-Defined Wall Functions** under **Near-wall Treatment** allows you to hook a **Law-of-the-Wall** UDF. For more information about user-defined wall functions, see `DEFINE_WALL_FUNCTIONS` in the UDF Manual.

**Important**

User-defined wall functions are available with the $k$-$\varepsilon$ turbulence closure model:

## 4.14.8. LES Near-Wall Treatment

When the mesh is fine enough to resolve the laminar sublayer, the wall shear stress is obtained from the laminar stress-strain relationship:

$$\frac{\overline{u}}{u_\tau} = \frac{\rho u_\tau y}{\mu} \tag{4.332}$$

If the mesh is too coarse to resolve the laminar sublayer, it is assumed that the centroid of the wall-adjacent cell falls within the logarithmic region of the boundary layer, and the law-of-the-wall is employed:

$$\frac{\overline{u}}{u_\tau} = \frac{1}{\kappa}\ln E\left(\frac{\rho u_\tau y}{\mu}\right) \tag{4.333}$$

where $\kappa$ is the von Kármán constant and $E = 9.793$. If the mesh is such that the first near-wall point is within the buffer region, then two above laws are blended in accordance with Equation 4.318 (p. 124).

For the LES simulations in ANSYS Fluent, there is an alternative near-wall approach based on the work of Werner and Wengle [486] (p. 755), who proposed an analytical integration of the power-law near-wall velocity distribution resulting in the following expressions for the wall shear stress:

$$|\tau_w| = \begin{cases} \dfrac{2\mu|u_p|}{\Delta z} & \text{for } |u_p| \le \dfrac{\mu}{2\rho\Delta z} A^{\frac{2}{1-B}} \\ \rho\left[\dfrac{1-B}{2} A^{\frac{1+B}{1-B}}\left(\dfrac{\mu}{\rho\Delta z}\right)^{1+B} + \dfrac{1+B}{A}\left(\dfrac{\mu}{\rho\Delta z}\right)^{B}|u_p|\right]^{\frac{2}{1+B}} & \text{for } |u_p| > \dfrac{\mu}{2\rho\Delta z} A^{\frac{2}{1-B}} \end{cases} \tag{4.334}$$

where $u_p$ is the wall-parallel velocity, $A = 8.3$, $B = 1/7$ are the constants, and $\Delta z$ is the near-wall control volume length scale.

The Werner-Wengle wall functions can be enabled using the `define/models/viscous/near-wall-treatment/werner-wengle-wall-fn?` text command.

## 4.15. Curvature Correction for the Spalart-Allmaras and Two-Equation Models

One drawback of the eddy-viscosity models is that these models are insensitive to streamline curvature and system rotation, which play a significant role in many turbulent flows of practical interest. A modification to the turbulence production term is available to sensitize the following standard eddy-viscosity models to the effects of streamline curvature and system rotation:

- Spalart-Allmaras one-equation model
- Standard, RNG, and Realizable ($k$-$\varepsilon$)-models
- Standard ($k$-$\omega$), SST and Transition SST
- Scale-Adaptive Simulation (SAS) and Detached Eddy Simulation with SST (DES-SST).

Note that both the RNG and Realizable ($k$-$\varepsilon$) turbulence models already have their own terms to include rotational or swirl effects (see RNG Swirl Modification (p. 50) and Modeling the Turbulent Viscosity (p. 53), respectively, for more information). The curvature correction option should therefore be used with caution for these two models and is offered mainly for completeness for RNG and Realizable ($k$-$\varepsilon$).

Spalart and Shur [428] (p. 752) and Shur et al. [405] (p. 751) have derived a modification of the production term for the Spalart-Allmaras one-equation turbulence model to take streamline curvature and system rotation effects into account. Based on this work, a modification of the production term has been derived that allows you to sensitize the standard two-equation turbulence models to these effects (Smirnov and Menter [413] (p. 751)). The empirical function suggested by Spalart and Shur [428] (p. 752) to account for streamline curvature and system rotation effects is defined by

$$f_{rotation} = (1+c_{r1})\frac{2r^*}{1+r^*}\left[1-c_{r3}\tan^{-1}(c_{r2}\tilde{r})\right]-c_{r1} \tag{4.335}$$

It is used as a multiplier of the production term and has been limited in ANSYS Fluent in the following way:

$$P_k \rightarrow P_k \cdot f_r \tag{4.336}$$

with

$$f_r = \max\left\{0, 1+C_{scale}(\tilde{f}_r-1)\right\} \tag{4.337}$$

$$\tilde{f}_r = \max\left\{\min(f_{rotation}, 1.25), 0\right\} \tag{4.338}$$

The original function is limited in the range from 0 corresponding to, for example, a strong convex curvature (stabilized flow, no turbulence production) up to 1.25 (strong concave curvature, enhanced turbulence production). The lower limit is introduced for numerical stability reasons, whereas the upper limit is needed to avoid over-generation of the eddy viscosity in flows with a destabilizing curvature/rotation. The specific limiter 1.25 provides a good compromise for different test cases that have been considered with the SST model (such as U-turn flow, flow in hydro cyclone, NACA 0012 wing tip vortex [413] (p. 751)).


Release 15.0 - © SAS IP, Inc. All rights reserved. - Contains proprietary and confidential information of ANSYS, Inc. and its subsidiaries and affiliates.

$C_{scale}$ in Equation 4.337 (p. 128) has been introduced to allow you to influence the strength of the curvature correction if needed for a specific flow. The default value is 1 and can be changed using the `/define/models/viscous/turbulence-expert/curvature-correction-coefficient` text command, when the curvature correction option has been enabled.

Assuming that all the variables and their derivatives are defined with respect to the reference frame of the calculation, which is rotating with a rate $\Omega^{rot}$, the arguments $r^*$ and $\tilde{r}$ of the function $f_{rotation}$ are defined in the following way:

$$r^* = \frac{S}{\Omega} \tag{4.339}$$

$$\tilde{r} = 2\Omega_{ik}S_{jk}\left[\frac{DS_{ij}}{Dt} + \left(\varepsilon_{imn}S_{jn} + \varepsilon_{jmn}S_{in}\right)\Omega_m^{Rot}\right]\frac{1}{\tilde{D}} \tag{4.340}$$

Where the first term in brackets is equivalent to the second velocity gradient (in this case the Lagrangian derivative of the strain rate tensor) and the second term in the brackets is a measure of the system rotation. The strain rate and vorticity tensor are defined as

$$S_{ij} = \frac{1}{2}\left(\frac{\partial u_i}{\partial x_j} + \frac{\partial u_j}{\partial x_i}\right) \tag{4.341}$$

$$\Omega_{ij} = \frac{1}{2}\left(\frac{\partial u_i}{\partial x_j} - \frac{\partial u_j}{\partial x_i}\right) + 2\varepsilon_{mji}\Omega_m^{rot} \tag{4.342}$$

with

$$S^2 = 2S_{ij}S_{ij} \tag{4.343}$$

$$\Omega^2 = 2\Omega_{ij}\Omega_{ij} \tag{4.344}$$

The denominator in Equation 4.340 (p. 129) takes the following form for the Spalart-Allmaras turbulence model (Shur et al. [405] (p. 751)):

$$\tilde{D} = D^4 \tag{4.345}$$

$$D^2 = 0.5\left(S^2 - \Omega^2\right) \tag{4.346}$$

and for all other turbulence models (Smirnov and Menter [413] (p. 751)) :

$$\tilde{D} = \Omega D^3 \tag{4.347}$$

$$D^2 = \max\left(S^2, 0.09\omega^2\right) \tag{4.348}$$

$\frac{DS_{ij}}{Dt}$ are the components of the Lagrangian derivative of the strain rate tensor. The Einstein summation convention is used.

The empirical constants $c_{r1}$, $c_{r2}$ and $c_{r3}$ involved in Equation 4.335 (p. 128) are set equal to

- 1.0, 12.0, and 1.0, respectively, for the Spalart-Allmaras model [405] (p. 751)
- 1.0, 2.0, and 1.0, respectively, for all other turbulence models based on the performed tests in [413] (p. 751)

Release 15.0 - © SAS IP, Inc. All rights reserved. - Contains proprietary and confidential information of ANSYS, Inc. and its subsidiaries and affiliates.

To enable curvature correction, see Including the Curvature Correction for the Spalart-Allmaras and Two-Equation Turbulence Models in the User's Guide.

## 4.16. Production Limiters for Two-Equation Models

A disadvantage of standard two-equation turbulence models is the excessive generation of the turbulence energy, $G_k$, in the vicinity of stagnation points. In order to avoid the buildup of turbulent kinetic energy in the stagnation regions, the production term in the turbulence equations can be limited by one of the two formulations presented below.

The first formulation takes the following form (Menter [290] (p. 745)):

$$G_k = \min ( G_k , C_{\lim} \rho \varepsilon ) \tag{4.349}$$

where the coefficient $C_{\lim}$ has a default value of 10. This limiter does not affect the shear layer performance of the model, but avoids the stagnation point buildup in aerodynamic simulations. The first formulation is available for the following turbulence models:

- Standard, RNG, and Realizable ($k$-$\varepsilon$)-models
- Standard ($k$-$\omega$), SST and Transition SST
- Scale-Adaptive Simulation (SAS)
- Detached Eddy Simulation with SST (DES-SST) and with Realizable ($k$-$\varepsilon$)-models (DES-rke)

By default, this limiter is enabled for all turbulence models based on the $\omega$ equation.

Using the standard Boussinesq approximation for the Reynolds stress tensor, the production term $G_k$ for an incompressible flow can be expressed as:

$$G_k = \mu_t S^2 \tag{4.350}$$

where $S$ is the magnitude of the strain rate:

$$S = \sqrt{2 S_{ij} S_{ij}} \tag{4.351}$$

The strain rate tensor $S_{ij}$ is calculated as:

$$S_{ij} = \frac{1}{2} \left( \frac{\partial U_i}{\partial x_j} + \frac{\partial U_j}{\partial x_i} \right) \tag{4.352}$$

The second formulation is based on the work of Kato and Launder ([198] (p. 739)) who noticed that the excessive level of turbulence kinetic energy production is caused by the very high level of shear strain rate $S$ in the stagnation regions. As the flow field near a stagnation point is nearly irrotational, with a very small vorticity rate $\Omega$, the alternative form of the production term proposed by Kato-Launder is written as:

$$G_k = \mu_t S \Omega \tag{4.353}$$

where $\Omega$ is the magnitude of the vorticity rate:

$$\Omega = \sqrt{2 \Omega_{ij} \Omega_{ij}} \tag{4.354}$$


Release 15.0 - © SAS IP, Inc. All rights reserved. - Contains proprietary and confidential information of ANSYS, Inc. and its subsidiaries and affiliates.

where the vorticity tensor $\Omega_{ij}$ is calculated as:

$$\Omega_{ij} = \frac{1}{2}\left(\frac{\partial U_i}{\partial x_j} - \frac{\partial U_j}{\partial x_i}\right) \tag{4.355}$$

In a simple shear flow, $S$ and $\Omega$ are equal and thus Equation 4.350 (p. 130) is recovered. The Kato-Launder formulation for the production term is available for the following turbulence models:

- Standard, and RNG ($k$-$\varepsilon$)-models
- Standard ($k$-$\omega$), SST and Transition SST
- Scale-Adaptive Simulation (SAS)
- Detached Eddy Simulation with SST (DES-SST)

The Kato-Launder formulation is enabled by default only for the Transition SST model.

Both modifications for the production term can be accessed in the Viscous Model panel. For more details, see Including Production Limiters for Two-Equation Models in the *Fluent User's Guide*. The Kato-Launder formulation and production limiter can be applied simultaneously, as is done for the Transition SST model by default.

*Release 15.0 - © SAS IP, Inc. All rights reserved. - Contains proprietary and confidential information of ANSYS, Inc. and its subsidiaries and affiliates.*

Release 15.0 - © SAS IP, Inc. All rights reserved. - Contains proprietary and confidential information
of ANSYS, Inc. and its subsidiaries and affiliates.

# Chapter 5: Heat Transfer

This chapter describes the theory behind heat transfer in ANSYS Fluent. Information is provided in the following sections:

5.1. Introduction
5.2. Modeling Conductive and Convective Heat Transfer
5.3. Modeling Radiation

For more information about using heat transfer in ANSYS Fluent, see Modeling Heat Transfer in the User's Guide.

## 5.1. Introduction

The flow of thermal energy from matter occupying one region in space to matter occupying a different region in space is known as heat transfer. Heat transfer can occur by three main methods: conduction, convection, and radiation. Physical models involving conduction and/or convection only are the simplest (Modeling Conductive and Convective Heat Transfer (p. 133)), while buoyancy-driven flow or natural convection (Natural Convection and Buoyancy-Driven Flows Theory (p. 137)), and radiation models (Modeling Radiation (p. 138)) are more complex. Depending on your problem, ANSYS Fluent will solve a variation of the energy equation that takes into account the heat transfer methods you have specified. ANSYS Fluent is also able to predict heat transfer in periodically repeating geometries (Modeling Periodic Heat Transfer in the User's Guide), therefore greatly reducing the required computational effort in certain cases.

For more information about using heat transfer models in ANSYS Fluent, see Modeling Conductive and Convective Heat Transfer, Modeling Radiation, and Modeling Periodic Heat Transfer in the User's Guide.

## 5.2. Modeling Conductive and Convective Heat Transfer

ANSYS Fluent allows you to include heat transfer within the fluid and/or solid regions in your model. Problems ranging from thermal mixing within a fluid to conduction in composite solids can therefore be handled by ANSYS Fluent. When your ANSYS Fluent model includes heat transfer you will need to activate the relevant physical models, supply thermal boundary conditions, and input material properties that govern heat transfer and/or vary with temperature as part of the setup. For information about setting up and using heat transfer models in your ANSYS Fluent model, see Modeling Heat Transfer in the User's Guide.

Information about heat transfer theory is presented in the following subsections.

5.2.1. Heat Transfer Theory
5.2.2. Natural Convection and Buoyancy-Driven Flows Theory

### 5.2.1. Heat Transfer Theory

#### *5.2.1.1. The Energy Equation*

ANSYS Fluent solves the energy equation in the following form:

*Release 15.0 - © SAS IP, Inc. All rights reserved. - Contains proprietary and confidential information of ANSYS, Inc. and its subsidiaries and affiliates.*

$$\frac{\partial}{\partial t}(\rho E)+\nabla\cdot(\vec{v}(\rho E+p))=\nabla\cdot\left(k_{eff}\nabla T-\sum_j h_j\vec{J}_j+\left(\overline{\overline{\tau}}_{eff}\cdot\vec{v}\right)\right)+S_h \tag{5.1}$$

where $k_{eff}$ is the effective conductivity ($k+k_t$, where $k_t$ is the turbulent thermal conductivity, defined according to the turbulence model being used), and $\vec{J}_j$ is the diffusion flux of species $j$. The first three terms on the right-hand side of Equation 5.1 (p. 134) represent energy transfer due to conduction, species diffusion, and viscous dissipation, respectively. $S_h$ includes the heat of chemical reaction, and any other volumetric heat sources you have defined.

In Equation 5.1 (p. 134),

$$E=h-\frac{p}{\rho}+\frac{v^2}{2} \tag{5.2}$$

where sensible enthalpy $h$ is defined for ideal gases as

$$h=\sum_j Y_j h_j \tag{5.3}$$

and for incompressible flows as

$$h=\sum_j Y_j h_j+\frac{p}{\rho} \tag{5.4}$$

In Equation 5.3 (p. 134) and Equation 5.4 (p. 134), $Y_j$ is the mass fraction of species $j$ and

$$h_j=\int_{T_{ref}}^{T} c_{p,j}dT \tag{5.5}$$

The value used for $T_{ref}$ in the sensible enthalpy calculation depends on the solver and models in use. For the pressure-based solver $T_{ref}$ is 298.15 K except for PDF models in which case $T_{ref}$ is a user input for the species. For the density-based solver $T_{ref}$ is 0 K except when modeling species transport with reactions in which case $T_{ref}$ is a user input for the species.

### 5.2.1.2. The Energy Equation in Moving Reference Frames

The energy equation is solved in moving (relative) frames of reference. In moving frames of reference, the energy transport equation uses rothalpy as a conservative quantity. See Equation 2.6 (p. 20) for the energy equation in moving frames of reference.

### 5.2.1.3. The Energy Equation for the Non-Premixed Combustion Model

When the non-adiabatic non-premixed combustion model is enabled, ANSYS Fluent solves the total enthalpy form of the energy equation:

$$\frac{\partial}{\partial t}(\rho H)+\nabla\cdot(\rho\vec{v}H)=\nabla\cdot\left(\frac{k_t}{c_p}\nabla H\right)+S_h \tag{5.6}$$

Under the assumption that the Lewis number (Le) = 1, the conduction and species diffusion terms combine to give the first term on the right-hand side of the above equation while the contribution


Release 15.0 - © SAS IP, Inc. All rights reserved. - Contains proprietary and confidential information of ANSYS, Inc. and its subsidiaries and affiliates.

from viscous dissipation appears in the non-conservative form as the second term. The total enthalpy $H$ is defined as

$$H = \sum_j Y_j H_j \tag{5.7}$$

where $Y_j$ is the mass fraction of species $j$ and

$$H_j = \int_{T_{ref,j}}^{T} c_{p,j} dT + h_j^0\left(T_{ref,j}\right) \tag{5.8}$$

$h_j^0\left(T_{ref,j}\right)$ is the formation enthalpy of species $j$ at the reference temperature $T_{ref,j}$.

### 5.2.1.4. Inclusion of Pressure Work and Kinetic Energy Terms

Equation 5.1 (p. 134) includes pressure work and kinetic energy terms, which are often negligible in incompressible flows. For this reason, the pressure-based solver by default does not include the pressure work or kinetic energy when you are solving incompressible flow. If you want to include these terms, use the `define/models/energy?` text command. When asked to `include pressure work in energy equation?` and `include kinetic energy in energy equation?`, respond by entering `yes` in the console window.

Pressure work and kinetic energy are *always* accounted for when you are modeling compressible flow or using the density-based solver.

### 5.2.1.5. Inclusion of the Viscous Dissipation Terms

Equation 5.1 (p. 134) and Equation 5.6 (p. 134) describe the thermal energy created by viscous shear in the flow.

When the pressure-based solver is used, ANSYS Fluent's default form of the energy equation does not include them (because viscous heating is often negligible). Viscous heating will be important when the Brinkman number, $Br$, approaches or exceeds unity, where

$$Br = \frac{\mu U_e^2}{k \Delta T} \tag{5.9}$$

and $\Delta T$ represents the temperature difference in the system.

When your problem requires inclusion of the viscous dissipation terms and you are using the pressure-based solver, you should activate the terms using the **Viscous Heating** option in the Viscous Model Dialog Box. Compressible flows typically have $Br \geq 1$. Note, however, that when the pressure-based solver is used, ANSYS Fluent does not automatically activate the viscous dissipation if you have defined a compressible flow model.

When the density-based solver is used, the viscous dissipation terms are *always* included when the energy equation is solved.

### 5.2.1.6. Inclusion of the Species Diffusion Term

Equation 5.1 (p. 134) and Equation 5.6 (p. 134) both include the effect of enthalpy transport due to species diffusion.

Release 15.0 - © SAS IP, Inc. All rights reserved. - Contains proprietary and confidential information of ANSYS, Inc. and its subsidiaries and affiliates.

When the pressure-based solver is used, the term

$$\nabla \cdot \left( \sum_j h_j \vec{J}_j \right)$$

is included in Equation 5.1 (p. 134) by default. If you do not want to include it, you can disable the **Diffusion Energy Source** option in the Species Model Dialog Box.

When the non-adiabatic non-premixed combustion model is being used, this term does not explicitly appear in the energy equation, because it is included in the first term on the right-hand side of Equation 5.6 (p. 134).

When the density-based solver is used, this term is *always* included in the energy equation.

### 5.2.1.7. Energy Sources Due to Reaction

Sources of energy, $S_h$, in Equation 5.1 (p. 134) include the source of energy due to chemical reaction:

$$S_{h,rxn} = -\sum_j \frac{h_j^0}{M_j} \mathcal{R}_j \tag{5.10}$$

where $h_j^0$ is the enthalpy of formation of species $j$ and $\mathcal{R}_j$ is the volumetric rate of creation of species $j$.

In the energy equation used for non-adiabatic non-premixed combustion (Equation 5.6 (p. 134)), the heat of formation is included in the definition of enthalpy (see Equation 5.7 (p. 135)), so reaction sources of energy are not included in $S_h$.

### 5.2.1.8. Energy Sources Due To Radiation

When one of the radiation models is being used, $S_h$ in Equation 5.1 (p. 134) or Equation 5.6 (p. 134) also includes radiation source terms. For details, see Modeling Radiation (p. 138).

### 5.2.1.9. Interphase Energy Sources

It should be noted that the energy sources, $S_h$, also include heat transfer between the continuous and the discrete phase. This is further discussed in Coupling Between the Discrete and Continuous Phases (p. 459).

### 5.2.1.10. Energy Equation in Solid Regions

In solid regions, the energy transport equation used by ANSYS Fluent has the following form:

$$\frac{\partial}{\partial t}(\rho h) + \nabla \cdot (\vec{v} \rho h) = \nabla \cdot (k \nabla T) + S_h \tag{5.11}$$

where

$\rho$ = density


Release 15.0 - © SAS IP, Inc. All rights reserved. - Contains proprietary and confidential information of ANSYS, Inc. and its subsidiaries and affiliates.

$h$ = sensible enthalpy, $\int_{T_{ref}}^{T} c_p dT$

$k$ = conductivity

$T$ = temperature

$S_h$ = volumetric heat source

The second term on the left-hand side of Equation 5.11 (p. 136) represents convective energy transfer due to rotational or translational motion of the solids. The velocity field $\vec{v}$ is computed from the motion specified for the solid zone. (For details, see Solid Conditions in the User's Guide). The terms on the right-hand side of Equation 5.11 (p. 136) are the heat flux due to conduction and volumetric heat sources within the solid, respectively.

### 5.2.1.11. Anisotropic Conductivity in Solids

When you use the pressure-based solver, ANSYS Fluent allows you to specify anisotropic conductivity for solid materials. The conduction term for an anisotropic solid has the form

$$\nabla \cdot \left( k_{ij} \nabla T \right) \tag{5.12}$$

where $k_{ij}$ is the conductivity matrix. See Anisotropic Thermal Conductivity for Solids in the User's Guide for details on specifying anisotropic conductivity for solid materials.

### 5.2.1.12. Diffusion at Inlets

The net transport of energy at inlets consists of both the convection and diffusion components. The convection component is fixed by the inlet temperature specified by you. The diffusion component, however, depends on the gradient of the computed temperature field. Thus the diffusion component (and therefore the net inlet transport) is not specified a priori.

In some cases, you may want to specify the net inlet transport of energy rather than the inlet temperature. If you are using the pressure-based solver, you can do this by disabling inlet energy diffusion. By default, ANSYS Fluent includes the diffusion flux of energy at inlets. To turn off inlet diffusion, use the `define/models/energy?` text command and respond `no` when asked to `Include diffusion at inlets?`

Inlet diffusion cannot be turned off if you are using the density-based solver.

## 5.2.2. Natural Convection and Buoyancy-Driven Flows Theory

When heat is added to a fluid and the fluid density varies with temperature, a flow can be induced due to the force of gravity acting on the density variations. Such buoyancy-driven flows are termed natural-convection (or mixed-convection) flows and can be modeled by ANSYS Fluent.

The importance of buoyancy forces in a mixed convection flow can be measured by the ratio of the Grashof and Reynolds numbers:

$$\frac{Gr}{Re^2} = \frac{g\beta \Delta TL}{v^2} \tag{5.13}$$

When this number approaches or exceeds unity, you should expect strong buoyancy contributions to the flow. Conversely, if it is very small, buoyancy forces may be ignored in your simulation. In pure natural convection, the strength of the buoyancy-induced flow is measured by the Rayleigh number:

$$Ra = \frac{g\beta \Delta T L^3 \rho}{\mu \alpha} \tag{5.14}$$

where $\beta$ is the thermal expansion coefficient:

$$\beta = -\frac{1}{\rho}\left(\frac{\partial \rho}{\partial T}\right)_p \tag{5.15}$$

and $\alpha$ is the thermal diffusivity:

$$\alpha = \frac{k}{\rho c_p} \tag{5.16}$$

Rayleigh numbers less than $10^8$ indicate a buoyancy-induced laminar flow, with transition to turbulence occurring over the range of $10^8 < Ra < 10^{10}$.

## 5.3. Modeling Radiation

Information about radiation modeling theory is presented in the following sections:

5.3.1. Overview and Limitations
5.3.2. Radiative Transfer Equation
5.3.3. P-1 Radiation Model Theory
5.3.4. Rosseland Radiation Model Theory
5.3.5. Discrete Transfer Radiation Model (DTRM) Theory
5.3.6. Discrete Ordinates (DO) Radiation Model Theory
5.3.7. Surface-to-Surface (S2S) Radiation Model Theory
5.3.8. Radiation in Combusting Flows
5.3.9. Choosing a Radiation Model

For information about setting up and using radiation models in ANSYS Fluent, see Modeling Radiation in the User's Guide.

### 5.3.1. Overview and Limitations

ANSYS Fluent provides five radiation models that allow you to include radiation, with or without a participating medium, in your heat transfer simulations.

Heating or cooling of surfaces due to radiation and/or heat sources or sinks due to radiation within the fluid phase can be included in your model using one of the following radiation models.

- Discrete Transfer Radiation Model (DTRM) [57] (p. 732), [401] (p. 751)
- P-1 Radiation Model [64] (p. 732), [406] (p. 751)
- Rosseland Radiation Model [406] (p. 751)
- Surface-to-Surface (S2S) Radiation Model [406] (p. 751)
- Discrete Ordinates (DO) Radiation Model [68] (p. 732), [364] (p. 749)


Release 15.0 - © SAS IP, Inc. All rights reserved. - Contains proprietary and confidential information of ANSYS, Inc. and its subsidiaries and affiliates.

In addition to these radiation models, ANSYS Fluent also provides a solar load model that allows you to include the effects of solar radiation in your simulation.

Typical applications well suited for simulation using radiative heat transfer include the following:

- radiative heat transfer from flames
- surface-to-surface radiant heating or cooling
- coupled radiation, convection, and/or conduction heat transfer
- radiation through windows in HVAC applications, and cabin heat transfer analysis in automotive applications
- radiation in glass processing, glass fiber drawing, and ceramic processing

You should include radiative heat transfer in your simulation when the radiant heat flux, $Q_{rad}=\sigma\left(T_{max}^4-T_{min}^4\right)$, is large compared to the heat transfer rate due to convection or conduction. Typically this will occur at high temperatures where the fourth-order dependence of the radiative heat flux on temperature implies that radiation will dominate.

### 5.3.1.1. Advantages and Limitations of the DTRM

The primary advantages of the DTRM are threefold: it is a relatively simple model, you can increase the accuracy by increasing the number of rays, and it applies to a wide range of optical thicknesses.

You should be aware of the following limitations when using the DTRM in ANSYS Fluent:

- DTRM assumes that all surfaces are diffuse. This means that the reflection of incident radiation at the surface is isotropic with respect to the solid angle.
- The effect of scattering is not included.
- The implementation assumes gray radiation.
- Solving a problem with a large number of rays is CPU-intensive.
- DTRM is not compatible with non-conformal interfaces or sliding meshes.
- DTRM is not compatible with parallel processing.

### 5.3.1.2. Advantages and Limitations of the P-1 Model

The P-1 model has several advantages over the DTRM. For the P-1 model, the RTE (Equation 5.17 (p. 141)) is a diffusion equation, which is easy to solve with little CPU demand. The model includes the effect of scattering. For combustion applications where the optical thickness is large, the P-1 model works reasonably well. In addition, the P-1 model can easily be applied to complicated geometries with curvilinear coordinates.

You should be aware of the following limitations when using the P-1 radiation model:

- The P-1 model assumes that all surfaces are diffuse. This means that the reflection of incident radiation at the surface is isotropic with respect to the solid angle.

Release 15.0 - © SAS IP, Inc. All rights reserved. - Contains proprietary and confidential information of ANSYS, Inc. and its subsidiaries and affiliates.

- The implementation is restricted to either gray radiation or non-gray radiation using a gray-band model. The non-gray implementation assumes a constant absorption coefficient within each wavelength band. The weighted-sum-of-gray-gases model (WSGGM) cannot be used to specify the absorption coefficient in each band. The non-gray implementation also assumes the spectral emissivity at walls to be constant within each band. Further information about the gray-band model is provided in Advantages and Limitations of the DO Model (p. 140).

- There may be a loss of accuracy, depending on the complexity of the geometry, if the optical thickness is small.

- The P-1 model tends to over-predict radiative fluxes from localized heat sources or sinks.

### 5.3.1.3. Advantages and Limitations of the Rosseland Model

The Rosseland model has two advantages over the P-1 model. Since it does not solve an extra transport equation for the incident radiation (as the P-1 model does), the Rosseland model is faster than the P-1 model and requires less memory.

The Rosseland model can be used only for optically thick media. It is recommended for use when the optical thickness exceeds 3. Note also that the Rosseland model is not available when the density-based solver is being used; it is available with the pressure-based solver, only.

### 5.3.1.4. Advantages and Limitations of the DO Model

The DO model spans the entire range of optical thicknesses, and allows you to solve problems ranging from surface-to-surface radiation to participating radiation in combustion problems. It also allows the solution of radiation at semi-transparent walls. Computational cost is moderate for typical angular discretizations, and memory requirements are modest.

The current implementation is restricted to either gray radiation or non-gray radiation using a gray-band model. Solving a problem with a fine angular discretization may be CPU-intensive.

The non-gray implementation in ANSYS Fluent is intended for use with participating media with a spectral absorption coefficient $a_\lambda$ that varies in a stepwise fashion across spectral bands, but varies smoothly within the band. Glass, for example, displays banded behavior of this type. The current implementation does not model the behavior of gases such as carbon dioxide or water vapor, which absorb and emit energy at distinct wave numbers [304] (p. 745). The modeling of non-gray gas radiation is still an evolving field. However, some researchers [121] (p. 735) have used gray-band models to model gas behavior by approximating the absorption coefficients within each band as a constant. The implementation in ANSYS Fluent can be used in this fashion if desired.

The non-gray implementation in ANSYS Fluent is compatible with all the models with which the gray implementation of the DO model can be used. Thus, it is possible to include scattering, anisotropy, semi-transparent media, and particulate effects. However, the non-gray implementation assumes a constant absorption coefficient within each wavelength band. The weighted-sum-of-gray-gases model (WSGGM) cannot be used to specify the absorption coefficient in each band. The implementation allows the specification of spectral emissivity at walls. The emissivity is assumed to be constant within each band.

### 5.3.1.5. Advantages and Limitations of the S2S Model

The surface-to-surface (S2S) radiation model is good for modeling the enclosure radiative transfer without participating media (for example, spacecraft heat rejection systems, solar collector systems,


Release 15.0 - © SAS IP, Inc. All rights reserved. - Contains proprietary and confidential information of ANSYS, Inc. and its subsidiaries and affiliates.

radiative space heaters, and automotive underhood cooling systems). In such cases, the methods for participating radiation may not always be efficient. As compared to the DTRM and the DO radiation models, the S2S model has a much faster time per iteration, although the view factor calculation itself is CPU-intensive. This increased time for view factor calculation will be especially pronounced when the emitting/absorbing surfaces are the polygonal faces of polyhedral cells.

You should be aware of the following limitations when using the S2S radiation model:

- The S2S model assumes that all surfaces are diffuse.
- The implementation assumes gray radiation.
- The storage and memory requirements increase very rapidly as the number of surface faces increases. This can be minimized by using a cluster of surface faces, although the CPU time will be independent of the number of clusters that are used if the face to face basis is used to calculate the view factors.
- The S2S model cannot be used to model participating radiation problems.
- The S2S model with the hemicube view factor method cannot be used if your model contains symmetry or periodic boundary conditions.
- The S2S model does not support hanging nodes or mesh adaption on radiating boundary zones.

## 5.3.2. Radiative Transfer Equation

The radiative transfer equation (RTE) for an absorbing, emitting, and scattering medium at position $\vec{r}$ in the direction $\vec{s}$ is

$$\frac{dI(\vec{r},\vec{s})}{ds}+(a+\sigma_s)I(\vec{r},\vec{s})=an^2\frac{\sigma T^4}{\pi}+\frac{\sigma_s}{4\pi}\int_0^{4\pi} I(\vec{r},\vec{s}')\Phi(\vec{s}\cdot\vec{s}')d\Omega' \tag{5.17}$$

where

$\vec{r}$ = position vector

$\vec{s}$ = direction vector

$\vec{s}'$ = scattering direction vector

$s$ = path length

$a$ = absorption coefficient

$n$ = refractive index

$\sigma_s$ = scattering coefficient

$\sigma$ = Stefan-Boltzmann constant ($5.669 \times 10^{-8} W/m^2-K^4$)

$I$ = radiation intensity, which depends on position ($\vec{r}$) and direction ($\vec{s}$)

$T$ = local temperature

$\Phi$ = phase function

$\Omega'$ = solid angle

Release 15.0 - © SAS IP, Inc. All rights reserved. - Contains proprietary and confidential information of ANSYS, Inc. and its subsidiaries and affiliates.

$(a+\sigma_s)s$ is the optical thickness or opacity of the medium. The refractive index $n$ is important when considering radiation in semi-transparent media. Figure 5.1: Radiative Heat Transfer (p. 142) illustrates the process of radiative heat transfer.

**Figure 5.1: Radiative Heat Transfer**

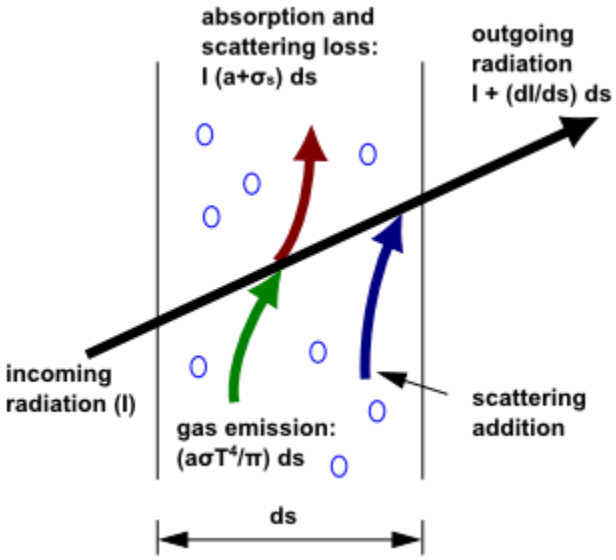


The DTRM and the P-1, Rosseland, and DO radiation models require the absorption coefficient $a$ as input. $a$ and the scattering coefficient $\sigma_s$ can be constants, and $a$ can also be a function of local concentrations of $H_2O$ and $CO_2$, path length, and total pressure. ANSYS Fluent provides the weighted-sum-of-gray-gases model (WSGGM) for computation of a variable absorption coefficient. For details, see Radiation in Combusting Flows (p. 170). The discrete ordinates implementation can model radiation in semi-transparent media. The refractive index $n$ of the medium must be provided as a part of the calculation for this type of problem. The Rosseland model also requires you to enter a refractive index, or use the default value of 1.

The P1 and DO radiation model is solved for the mixture material. In other words, the radiative properties, such as the absorption coefficient, refractive index, and scattering coefficients of the mixture, is computed based on the volume fraction based averaging of the radiative properties of the individual phases.

In simulations that use the porous media model with a radiation model, the contributions of the radiative heat flux and radiative heat source in the energy calculation are scaled by the local porosity. Note that the modeling treatment for the interaction of porous media and radiation in ANSYS Fluent is strictly valid only for values of local fluid porosity that are very close or equal to 1.0.

## 5.3.3. P-1 Radiation Model Theory

The P-1 radiation model is the simplest case of the more general P-N model, which is based on the expansion of the radiation intensity $I$ into an orthogonal series of spherical harmonics [64] (p. 732), [406] (p. 751). This section provides details about the equations used in the P-1 model. For information about setting up the model, see Using the Radiation Models in the User's Guide.


Release 15.0 - © SAS IP, Inc. All rights reserved. - Contains proprietary and confidential information of ANSYS, Inc. and its subsidiaries and affiliates.

### 5.3.3.1. The P-1 Model Equations

As mentioned above, the P-1 radiation model is the simplest case of the P-N model. When modeling gray radiation, the following equation is obtained for the radiation flux $q_r$ if only four terms in the series are used:

$$q_r = -\frac{1}{3(a+\sigma_s) - C\sigma_s} \nabla G \tag{5.18}$$

where $a$ is the absorption coefficient, $\sigma_s$ is the scattering coefficient, $G$ is the incident radiation, and $C$ is the linear-anisotropic phase function coefficient, described below. After introducing the parameter

$$\Gamma = \frac{1}{(3(a+\sigma_s) - C\sigma_s)} \tag{5.19}$$

Equation 5.18 (p. 143) simplifies to

$$q_r = -\Gamma \nabla G \tag{5.20}$$

The transport equation for $G$ is

$$\nabla \cdot (\Gamma \nabla G) - aG + 4an^2\sigma T^4 = S_G \tag{5.21}$$

where $n$ is the refractive index of the medium, $\sigma$ is the Stefan-Boltzmann constant and $S_G$ is a user-defined radiation source. ANSYS Fluent solves this equation to determine the local incident radiation when the P-1 model is active.

Combining Equation 5.20 (p. 143) and Equation 5.21 (p. 143) yields the following equation:

$$-\nabla \cdot q_r = aG - 4an^2\sigma T^4 \tag{5.22}$$

The expression for $-\nabla \cdot q_r$ can be directly substituted into the energy equation to account for heat sources (or sinks) due to radiation.

ANSYS Fluent also allows for the modeling of non-gray radiation using a gray-band model. For non-gray radiation, Equation 5.21 (p. 143) is rewritten as:

$$\nabla \cdot (\Gamma_\lambda \nabla G_\lambda) - a_\lambda G_\lambda + 4a_\lambda n^2\sigma T^4 = S_{G\lambda} \tag{5.23}$$

where $G_\lambda$ is the spectral incident radiation, $a_\lambda$ is a spectral absorption coefficient, $n$ is the refractive index of the medium, $S_{G\lambda}$ is a user-defined source term, and $\sigma$ is the Stefan-Boltzmann constant. $\Gamma_\lambda$ is defined as:

$$\Gamma_\lambda = \frac{1}{(3(a_\lambda+\sigma_{s\lambda}) - C\sigma_{s\lambda})} \tag{5.24}$$

where $\sigma_{s\lambda}$ is a spectral scattering coefficient and $C$ is the linear anisotropic phase function coefficient.

The spectral black body emission ($G_{b\lambda}$) between wavelength $\lambda_1$ and $\lambda_2$ is given as

$$G_{b\lambda} = 4\left[F(0 \rightarrow n\lambda_2 T) - F(0 \rightarrow n\lambda_1 T)\right]\sigma T^4 \tag{5.25}$$

where $F(0 \rightarrow n\lambda T)$ is the fraction of radiant energy emitted by a black body in the wavelength interval from 0 to $\lambda$ at temperature $T$ in a medium of refractive index $n$. $\lambda_2$ and $\lambda_1$ are the wavelength boundaries of the band.

Release 15.0 - © SAS IP, Inc. All rights reserved. - Contains proprietary and confidential information of ANSYS, Inc. and its subsidiaries and affiliates.

The spectral radiative flux is calculated as

$$q_\lambda = -\Gamma_\lambda \nabla G_\lambda \tag{5.26}$$

The radiation source term in the energy equation is given as

$$-\nabla q_r = \sum_{\text{All Bands}} -\nabla q_{r,\lambda} = \sum_{\text{All Bands}} a_\lambda (G_\lambda - n^2 G_{b\lambda}) \tag{5.27}$$

### 5.3.3.2. Anisotropic Scattering

Included in the P-1 radiation model is the capability for modeling anisotropic scattering. ANSYS Fluent models anisotropic scattering by means of a linear-anisotropic scattering phase function:

$$\Phi(\vec{s}' \cdot \vec{s}) = 1 + C\,\vec{s}' \cdot \vec{s} \tag{5.28}$$

where

$\vec{s}$ = unit vector in the direction of scattering

$\vec{s}'$ = unit vector in the direction of the incident radiation

$C$ = linear-anisotropic phase function coefficient, which is a property of the fluid

Value of $C$ ranges from –1 to 1. A positive value indicates that more radiant energy is scattered forward than backward, and a negative value means that more radiant energy is scattered backward than forward. A zero value defines isotropic scattering (that is, scattering that is equally likely in all directions), which is the default in ANSYS Fluent. You should modify the default value only if you are certain of the anisotropic scattering behavior of the material in your problem.

### 5.3.3.3. Particulate Effects in the P-1 Model

When your ANSYS Fluent model includes a dispersed second phase of particles, you can include the effect of particles in the P-1 radiation model. Note that when particles are present, ANSYS Fluent ignores scattering in the gas phase. That is, Equation 5.29 (p. 144) assumes that all scattering is due to particles.

For a gray, absorbing, emitting, and scattering medium containing absorbing, emitting, and scattering particles, the transport equation for the incident radiation can be written as

$$\nabla \cdot (\Gamma \nabla G) + 4\pi \left( an^2 \frac{\sigma T^4}{\pi} + E_p \right) - \left( a + a_p \right) G = 0 \tag{5.29}$$

where $E_p$ is the equivalent emission of the particles, $a_p$ is the equivalent absorption coefficient, and $n$ is the refractive index of the medium. These are defined as follows:

$$E_p = \lim_{V \to 0} \sum_{n=1}^{N} \varepsilon_{pn} A_{pn} \frac{\sigma T_{pn}^4}{\pi V} \tag{5.30}$$

and

$$a_p = \lim_{V \to 0} \sum_{n=1}^{N} \varepsilon_{pn} \frac{A_{pn}}{V} \tag{5.31}$$

In Equation 5.30 (p. 144) and Equation 5.31 (p. 144), $\varepsilon_{pn}$, $A_{pn}$, and $T_{pn}$ are the emissivity, projected area, and temperature of particle $n$. The summation is over $N$ particles in volume $V$. These quantities are computed during particle tracking in ANSYS Fluent.


Release 15.0 - © SAS IP, Inc. All rights reserved. - Contains proprietary and confidential information of ANSYS, Inc. and its subsidiaries and affiliates.

The projected area $A_{pn}$ of particle $n$ is defined as

$$A_{pn}=\frac{\pi d_{pn}^2}{4} \tag{5.32}$$

where $d_{pn}$ is the diameter of the $n$th particle.

The quantity $\Gamma$ in Equation 5.29 (p. 144) is defined as

$$\Gamma=\frac{1}{3\left(a+a_p+\sigma_p\right)} \tag{5.33}$$

where the equivalent particle scattering factor is computed during particle tracking and is defined as

$$\sigma_p=\lim_{V\to 0}\sum_{n=1}^{N}\left(1-f_{pn}\right)\left(1-\varepsilon_{pn}\right)\frac{A_{pn}}{V} \tag{5.34}$$

Here, $f_{pn}$ is the scattering factor associated with the $n$th particle.

Heat sources (sinks) due to particle radiation are included in the energy equation as follows:

$$-\nabla\cdot q_r=-4\pi\left(an^2\frac{\sigma T^4}{\pi}+E_p\right)+\left(a+a_p\right)G \tag{5.35}$$

### 5.3.3.4. Boundary Condition Treatment for the P-1 Model at Walls

To get the boundary condition for the incident radiation equation when modeling gray radiation, the dot product of the outward normal vector $\vec{n}$ and Equation 5.20 (p. 143) is computed:

$$q_r\cdot\vec{n} \quad = \quad -\Gamma\nabla G\cdot\vec{n} \tag{5.36}$$

$$q_{r,w} \quad = \quad -\Gamma\frac{\partial G}{\partial n} \tag{5.37}$$

Thus the flux of the incident radiation, $G$, at a wall is $-q_{r,w}$. The wall radiative heat flux is computed using the following boundary condition:

$$I_w(\vec{r},\vec{s})=f_w(\vec{r},\vec{s}) \tag{5.38}$$

$$f_w(\vec{r},\vec{s})=\epsilon_w\frac{n^2\sigma T_w^4}{\pi}+\rho_w I(\vec{r},-\vec{s}) \tag{5.39}$$

where $\rho_w$ is the wall reflectivity. The Marshak boundary condition is then used to eliminate the angular dependence [338] (p. 747):

$$\int_0^{2\pi} I_w(\vec{r},\vec{s})\,\vec{n}\cdot\vec{s}\,d\Omega=\int_0^{2\pi} f_w(\vec{r},\vec{s})\,\vec{n}\cdot\vec{s}\,d\Omega \tag{5.40}$$

Substituting Equation 5.38 (p. 145) and Equation 5.39 (p. 145) into Equation 5.40 (p. 145) and performing the integrations yields

Release 15.0 - © SAS IP, Inc. All rights reserved. - Contains proprietary and confidential information of ANSYS, Inc. and its subsidiaries and affiliates.

$$q_{r,w} = -\frac{4\pi\varepsilon_w \frac{n^2\sigma T_w^4}{\pi} - \left(1-\rho_w\right)G_w}{2\left(1+\rho_w\right)} \tag{5.41}$$

If it is assumed that the walls are diffuse gray surfaces, then $\rho_w = 1-\varepsilon_w$, and Equation 5.41 (p. 146) becomes

$$q_{r,w} = -\frac{\varepsilon_w}{2\,(2-\varepsilon_w)}\left(4n^2\sigma T_w^4 - G_w\right) \tag{5.42}$$

Equation 5.42 (p. 146) is used to compute $q_{r,w}$ for the energy equation and for the incident radiation equation boundary conditions.

When using the gray-band model, the flux at the wall can be written as the following (assuming that the wall is a diffuse surface):

$$q_{\lambda,w} = -\frac{\varepsilon_{\lambda,w}}{2\,(2-\varepsilon_{\lambda,w})}\left(4n^2\left[F\left(0\rightarrow n\lambda_2 T\right) - F\left(0\rightarrow n\lambda_1 T\right)\right]\sigma T^4 - G_{\lambda,w}\right) \tag{5.43}$$

where $\varepsilon_{\lambda,w}$ is the wall emissivity, $q_{\lambda,w}$ is the spectral radiative flux at the wall, and $G_{\lambda,w}$ is the spectral incident radiation at the wall.

### 5.3.3.5. Boundary Condition Treatment for the P-1 Model at Flow Inlets and Exits

The net radiative heat flux at flow inlets and outlets is computed in the same manner as at walls, as described above. ANSYS Fluent assumes that the emissivity of all flow inlets and outlets is 1.0 (black body absorption) unless you choose to redefine this boundary treatment.

ANSYS Fluent includes an option that allows you to use different temperatures for radiation and convection at inlets and outlets. This can be useful when the temperature outside the inlet or outlet differs considerably from the temperature in the enclosure. For details, see Defining Boundary Conditions for Radiation in the User's Guide.

## 5.3.4. Rosseland Radiation Model Theory

The Rosseland or diffusion approximation for radiation is valid when the medium is optically thick ($(a+\sigma_s)L \gg 1$), and is recommended for use in problems where the optical thickness is greater than 3. It can be derived from the P-1 model equations, with some approximations. This section provides details about the equations used in the Rosseland model. For information about setting up the model, see Using the Radiation Models in the User's Guide.

### 5.3.4.1. The Rosseland Model Equations

As with the P-1 model, the radiative heat flux vector in a gray medium can be approximated by Equation 5.20 (p. 143):

$$q_r = -\Gamma \nabla G \tag{5.44}$$

where $\Gamma$ is given by Equation 5.19 (p. 143).

The Rosseland radiation model differs from the P-1 model in that the Rosseland model assumes that the intensity is the black-body intensity at the gas temperature. (The P-1 model actually calculates a


Release 15.0 - © SAS IP, Inc. All rights reserved. - Contains proprietary and confidential information of ANSYS, Inc. and its subsidiaries and affiliates.

transport equation for $G$.) Thus $G=4\sigma n^2 T^4$, where $n$ is the refractive index. Substituting this value for $G$ into Equation 5.44 (p. 146) yields

$$q_r = -16\sigma\Gamma n^2 T^3 \nabla T \tag{5.45}$$

Since the radiative heat flux has the same form as the Fourier conduction law, it is possible to write

$$q = q_c + q_r \tag{5.46}$$

$$q = -(k + k_r)\nabla T \tag{5.47}$$

$$k_r = 16\sigma\Gamma n^2 T^3 \tag{5.48}$$

where $k$ is the thermal conductivity and $k_r$ is the radiative conductivity. Equation 5.46 (p. 147) is used in the energy equation to compute the temperature field.

### 5.3.4.2. Anisotropic Scattering

The Rosseland model allows for anisotropic scattering, using the same phase function (Equation 5.28 (p. 144)) described for the P-1 model in Anisotropic Scattering (p. 144).

### 5.3.4.3. Boundary Condition Treatment at Walls

Since the diffusion approximation is not valid near walls, it is necessary to use a temperature slip boundary condition. The radiative heat flux at the wall boundary, $q_{r,w}$, is defined using the slip coefficient $\psi$:

$$q_{r,w} = -\frac{\sigma\left(T_w^4 - T_g^4\right)}{\psi} \tag{5.49}$$

where $T_w$ is the wall temperature, $T_g$ is the temperature of the gas at the wall, and the slip coefficient $\psi$ is approximated by a curve fit to the plot given in [406] (p. 751):

$$\psi = \begin{cases} 1/2 & N_w < 0.01 \\ \dfrac{2x^3 + 3x^2 - 12x + 7}{54} & 0.01 \le N_w \le 10 \\ 0 & N_w > 10 \end{cases} \tag{5.50}$$

where $N_w$ is the conduction to radiation parameter at the wall:

$$N_w = \frac{k(a + \sigma_s)}{4\sigma T_w^3} \tag{5.51}$$

and $x = \log_{10} N_w$.

### 5.3.4.4. Boundary Condition Treatment at Flow Inlets and Exits

No special treatment is required at flow inlets and outlets for the Rosseland model. The radiative heat flux at these boundaries can be determined using Equation 5.46 (p. 147).

Release 15.0 - © SAS IP, Inc. All rights reserved. - Contains proprietary and confidential information of ANSYS, Inc. and its subsidiaries and affiliates.

## 5.3.5. Discrete Transfer Radiation Model (DTRM) Theory

The main assumption of the DTRM is that the radiation leaving the surface element in a certain range of solid angles can be approximated by a single ray. This section provides details about the equations used in the DTRM. For information about setting up the model, see Setting Up the DTRM in the User's Guide.

### 5.3.5.1. The DTRM Equations

The equation for the change of radiant intensity, $dI$, along a path, $ds$, can be written as

$$\frac{dI}{ds}+aI=\frac{a\sigma T^4}{\pi} \tag{5.52}$$

where

$a$ = gas absorption coefficient

$I$ = intensity

$T$ = gas local temperature

$\sigma$ = Stefan-Boltzmann constant ($5.669\times10^{-8}W/m^2-K^4$)

Here, the refractive index is assumed to be unity. The DTRM integrates Equation 5.52 (p. 148) along a series of rays emanating from boundary faces. If $a$ is constant along the ray, then $I(s)$ can be estimated as

$$I(s)=\frac{\sigma T^4}{\pi}(1-e^{-as})+I_0e^{-as} \tag{5.53}$$

where $I_0$ is the radiant intensity at the start of the incremental path, which is determined by the appropriate boundary condition (see the description of boundary conditions, below). The energy source in the fluid due to radiation is then computed by summing the change in intensity along the path of each ray that is traced through the fluid control volume.

The "ray tracing" technique used in the DTRM can provide a prediction of radiative heat transfer between surfaces without explicit view factor calculations. The accuracy of the model is limited mainly by the number of rays traced and the computational mesh.

### 5.3.5.2. Ray Tracing

The ray paths are calculated and stored prior to the fluid flow calculation. At each radiating face, rays are fired at discrete values of the polar and azimuthal angles (see Figure 5.2: Angles θ and ϕ Defining the Hemispherical Solid Angle About a Point P (p. 149)). To cover the radiating hemisphere, $\theta$ is varied from $0$ to $\frac{\pi}{2}$ and $\phi$ from $0$ to $2\pi$. Each ray is then traced to determine the control volumes it intercepts as well as its length within each control volume. This information is then stored in the radiation file, which must be read in before the fluid flow calculations begin.


Release 15.0 - © SAS IP, Inc. All rights reserved. - Contains proprietary and confidential information of ANSYS, Inc. and its subsidiaries and affiliates.

**Figure 5.2: Angles θ and ϕ Defining the Hemispherical Solid Angle About a Point P**

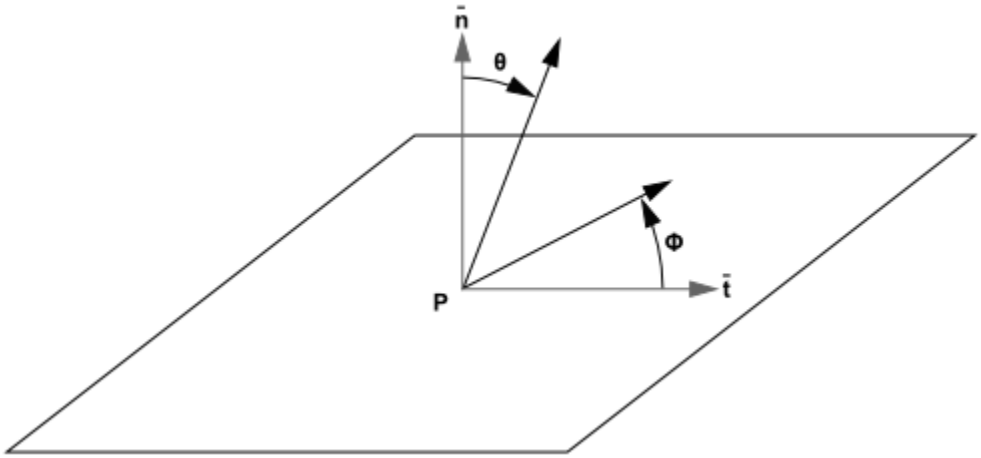


### 5.3.5.3. Clustering

DTRM is computationally very expensive when there are too many surfaces to trace rays from and too many volumes crossed by the rays. To reduce the computational time, the number of radiating surfaces and absorbing cells is reduced by clustering surfaces and cells into surface and volume "clusters". The volume clusters are formed by starting from a cell and simply adding its neighbors and their neighbors until a specified number of cells per volume cluster is collected. Similarly, surface clusters are made by starting from a face and adding its neighbors and their neighbors until a specified number of faces per surface cluster is collected.

The incident radiation flux, $q_{in}$, and the volume sources are calculated for the surface and volume clusters respectively. These values are then distributed to the faces and cells in the clusters to calculate the wall and cell temperatures. Since the radiation source terms are highly non-linear (proportional to the fourth power of temperature), care must be taken to calculate the average temperatures of surface and volume clusters and distribute the flux and source terms appropriately among the faces and cells forming the clusters.

The surface and volume cluster temperatures are obtained by area and volume averaging as shown in the following equations:

$$T_{sc} = \left( \frac{\sum_f A_f T_f^4}{\sum A_f} \right)^{1/4} \tag{5.54}$$

$$T_{vc} = \left( \frac{\sum_c V_c T_c^4}{\sum V_c} \right)^{1/4} \tag{5.55}$$

where $T_{sc}$ and $T_{vc}$ are the temperatures of the surface and volume clusters respectively, $A_f$ and $T_f$ are the area and temperature of face $f$, and $V_c$ and $T_c$ are the volume and temperature of cell $c$. The summations are carried over all faces of a surface cluster and all cells of a volume cluster.

Release 15.0 - © SAS IP, Inc. All rights reserved. - Contains proprietary and confidential information of ANSYS, Inc. and its subsidiaries and affiliates.

### 5.3.5.4. Boundary Condition Treatment for the DTRM at Walls

The radiation intensity approaching a point on a wall surface is integrated to yield the incident radiative heat flux, $q_{in}$, as

$$q_{in} = \int_{\vec{s}\cdot\vec{n}>0} I_{in}\,\vec{s}\cdot\vec{n}\,d\Omega \tag{5.56}$$

where $\Omega$ is the hemispherical solid angle, $I_{in}$ is the intensity of the incoming ray, $\vec{s}$ is the ray direction vector, and $\vec{n}$ is the normal pointing out of the domain. The net radiative heat flux from the surface, $q_{out}$, is then computed as a sum of the reflected portion of $q_{in}$ and the emissive power of the surface:

$$q_{out} = (1-\varepsilon_w)\,q_{in} + \varepsilon_w \sigma T_w^4 \tag{5.57}$$

where $T_w$ is the surface temperature of the point $P$ on the surface and $\varepsilon_w$ is the wall emissivity which you input as a boundary condition. ANSYS Fluent incorporates the radiative heat flux (Equation 5.57 (p. 150)) in the prediction of the wall surface temperature. Equation 5.57 (p. 150) also provides the surface boundary condition for the radiation intensity $I_0$ of a ray emanating from the point $P$, as

$$I_0 = \frac{q_{out}}{\pi} \tag{5.58}$$

### 5.3.5.5. Boundary Condition Treatment for the DTRM at Flow Inlets and Exits

The net radiative heat flux at flow inlets and outlets is computed in the same manner as at walls, as described above. ANSYS Fluent assumes that the emissivity of all flow inlets and outlets is 1.0 (black body absorption) unless you choose to redefine this boundary treatment.

ANSYS Fluent includes an option that allows you to use different temperatures for radiation and convection at inlets and outlets. This can be useful when the temperature outside the inlet or outlet differs considerably from the temperature in the enclosure. For details, see Defining Boundary Conditions for Radiation in the User's Guide.

## 5.3.6. Discrete Ordinates (DO) Radiation Model Theory

The discrete ordinates (DO) radiation model solves the radiative transfer equation (RTE) for a finite number of discrete solid angles, each associated with a vector direction $\vec{s}$ fixed in the global Cartesian system $(x, y, z)$. You control the fineness of the angular discretization, analogous to choosing the number of rays for the DTRM. Unlike the DTRM, however, the DO model does not perform ray tracing. Instead, the DO model transforms Equation 5.17 (p. 141) into a transport equation for radiation intensity in the spatial coordinates $(x, y, z)$. The DO model solves for as many transport equations as there are directions $\vec{s}$. The solution method is identical to that used for the fluid flow and energy equations.

Two implementations of the DO model are available in ANSYS Fluent: uncoupled and (energy) coupled. The uncoupled implementation is sequential in nature and uses a conservative variant of the DO model called the finite-volume scheme [68] (p. 732), [364] (p. 749), and its extension to unstructured meshes [313] (p. 746). In the uncoupled case, the equations for the energy and radiation intensities are solved one by one, assuming prevailing values for other variables.

Alternatively, in the coupled ordinates method (or COMET) [284] (p. 744), the discrete energy and intensity equations at each cell are solved simultaneously, assuming that spatial neighbors are known. The advantages of using the coupled approach is that it speeds up applications involving high optical thick-


Release 15.0 - © SAS IP, Inc. All rights reserved. - Contains proprietary and confidential information of ANSYS, Inc. and its subsidiaries and affiliates.

nesses and/or high scattering coefficients. Such applications slow down convergence drastically when the sequential approach is used. For information about setting up the model, see Setting Up the DO Model in the User's Guide.

### 5.3.6.1. The DO Model Equations

The DO model considers the radiative transfer equation (RTE) in the direction $\vec{s}$ as a field equation. Thus, Equation 5.17 (p. 141) is written as

$$\nabla \cdot (I(\vec{r},\vec{s})\vec{s}) + (a+\sigma_s) I(\vec{r},\vec{s}) = an^2\frac{\sigma T^4}{\pi} + \frac{\sigma_s}{4\pi}\int_0^{4\pi} I(\vec{r},\vec{s}\,')\Phi(\vec{s}\cdot\vec{s}\,')\,d\Omega' \tag{5.59}$$

ANSYS Fluent also allows the modeling of non-gray radiation using a gray-band model. The RTE for the spectral intensity $I_\lambda(\vec{r},\vec{s})$ can be written as

$$\nabla \cdot (I_\lambda(\vec{r},\vec{s})\vec{s}) + (a_\lambda+\sigma_s) I_\lambda(\vec{r},\vec{s}) = a_\lambda n^2 I_{b\lambda} + \frac{\sigma_s}{4\pi}\int_0^{4\pi} I_\lambda(\vec{r},\vec{s}\,')\Phi(\vec{s}\cdot\vec{s}\,')\,d\Omega' \tag{5.60}$$

Here $\lambda$ is the wavelength, $a_\lambda$ is the spectral absorption coefficient, and $I_{b\lambda}$ is the black body intensity given by the Planck function. The scattering coefficient, the scattering phase function, and the refractive index $n$ are assumed independent of wavelength.

The non-gray DO implementation divides the radiation spectrum into $N$ wavelength bands, which need not be contiguous or equal in extent. The wavelength intervals are supplied by you, and correspond to values in vacuum ($n = 1$). The RTE is integrated over each wavelength interval, resulting in transport equations for the quantity $I_\lambda \Delta\lambda$, the radiant energy contained in the wavelength band $\Delta\lambda$. The behavior in each band is assumed gray. The black body emission in the wavelength band per unit solid angle is written as

$$[F(0 \to n\lambda_2 T) - F(0 \to n\lambda_1 T)]n^2\frac{\sigma T^4}{\pi} \tag{5.61}$$

where $F(0 \to n\lambda T)$ is the fraction of radiant energy emitted by a black body [304] (p. 745) in the wavelength interval from 0 to $\lambda$ at temperature $T$ in a medium of refractive index $n$. $\lambda_2$ and $\lambda_1$ are the wavelength boundaries of the band.

The total intensity $I(\vec{r},\vec{s})$ in each direction $\vec{s}$ at position $\vec{r}$ is computed using

$$I(\vec{r},\vec{s}) = \sum_k I_{\lambda_k}(\vec{r},\vec{s})\,\Delta\lambda_k \tag{5.62}$$

where the summation is over the wavelength bands.

Boundary conditions for the non-gray DO model are applied on a band basis. The treatment within a band is the same as that for the gray DO model.

Release 15.0 - © SAS IP, Inc. All rights reserved. - Contains proprietary and confidential information of ANSYS, Inc. and its subsidiaries and affiliates.

### 5.3.6.2. Energy Coupling and the DO Model

The coupling between energy and radiation intensities at a cell (which is also known as COMET) [284] (p. 744) accelerates the convergence of the finite volume scheme for radiative heat transfer. This method results in significant improvement in the convergence for applications involving optical thicknesses greater than 10. This is typically encountered in glass-melting applications. This feature is advantageous when scattering is significant, resulting in strong coupling between directional radiation intensities. This DO model implementation is utilized in ANSYS Fluent by enabling the **DO/Energy Coupling** option for the DO model in the **Radiation Model** dialog box. The discrete energy equations for the coupled method are presented below.

The energy equation when integrated over a control volume $i$, yields the discrete energy equation:

$$\sum_{j=1}^{N} \mu_{ij}^{T} T_j - \beta_i^{T} T_i = \alpha_i^{T} \sum_{k=1}^{L} I_i^k \omega_k - S_i^{T} + S_i^{h} \tag{5.63}$$

where

$$\alpha_i^{T} = \kappa \Delta V_i$$

$$\beta_i^{T} = 16 \kappa \sigma T_i^{*3} \Delta V_i$$

$$S_i^{T} = 12 \kappa \sigma T_i^{*4} \Delta V_i$$

$\kappa$ = absorption coefficient

$\Delta V$ control volume

The coefficient $\mu_{ij}^{T}$ and the source term $S_i^{h}$ are due to the discretization of the convection and diffusion terms as well as the non-radiative source terms.

Combining the discretized form of Equation 5.59 (p. 151) and the discretized energy equation, Equation 5.63 (p. 152), yields [284] (p. 744):

$$\vec{P}_i \vec{q}_i + \vec{r}_i = 0 \tag{5.64}$$

where

$$\vec{q}_i = \begin{bmatrix} I_i^1 \\ I_i^2 \\ \vdots \\ \vdots \\ I_i^L \\ T_i \end{bmatrix} \tag{5.65}$$


Release 15.0 - © SAS IP, Inc. All rights reserved. - Contains proprietary and confidential information of ANSYS, Inc. and its subsidiaries and affiliates.

$$\vec{P}_i = \begin{bmatrix} M_{ii}^1 + \eta_i^{11} + \gamma_i^1 \omega_1 & \eta_i^{12} + \gamma_i^1 \omega_2 & \ldots \beta_i^1 \\ \eta_i^{21} + \gamma_i^2 \omega_1 & M_{ii}^2 + \eta_i^{22} + \gamma_i^2 \omega_2 & \ldots \beta_i^2 \\ \vdots & & \\ -\alpha_i^T \omega_1 & -\alpha_i^T \omega_2 & \ldots M_{ii}^T \end{bmatrix} \tag{5.66}$$

$$\vec{r}_i = \begin{bmatrix} \sum_{j=1, i \neq j}^{N} \mu_{ij}^l I_j^l - S_i^1 - S_i^B \\ \vdots \\ \sum_{j=1, i \neq j}^{N} \mu_{ij}^T T_j + S_i^T + S_i^h \end{bmatrix} \tag{5.67}$$

#### 5.3.6.2.1. Limitations of DO/Energy Coupling

There are some instances when using DO/Energy coupling is not recommended or is incompatible with certain models:

- DO/Energy coupling is not recommended for cases with weak coupling between energy and directional radiation intensities. This may result in slower convergence of the coupled approach compared to the sequential approach.
- DO/Energy coupling is not available when solving enthalpy equations instead of temperature equations. Specifically, DO/Energy coupling is not compatible with the non-premixed or partially premixed combustion models.

To find out how to apply DO/Energy coupling, refer to Setting Up the DO Model in the User's Guide.

### 5.3.6.3. Angular Discretization and Pixelation

Each octant of the angular space $4\pi$ at any spatial location is discretized into $N_\theta \times N_\phi$ solid angles of extent $\omega_i$, called control angles. The angles $\theta$ and $\phi$ are the polar and azimuthal angles respectively, and are measured with respect to the global Cartesian system $(x, y, z)$ as shown in Figure 5.3: Angular Coordinate System (p. 154). The $\theta$ and $\phi$ extents of the control angle, $\Delta\theta$ and $\Delta\phi$, are constant. In two-dimensional calculations, only four octants are solved due to symmetry, making a total of $4N_\theta N_\phi$ directions in all. In three-dimensional calculations, a total of $8N_\theta N_\phi$ directions are solved. In the case of the non-gray model, $4N_\theta N_\phi$ or $8N_\theta N_\phi$ equations are solved for each band.

Release 15.0 - © SAS IP, Inc. All rights reserved. - Contains proprietary and confidential information of ANSYS, Inc. and its subsidiaries and affiliates.

**Figure 5.3: Angular Coordinate System**

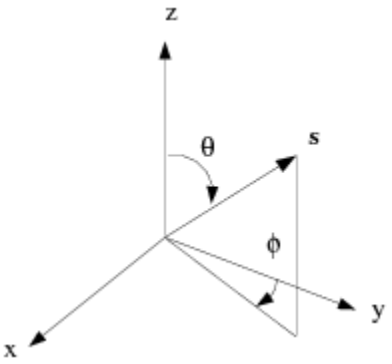


When Cartesian meshes are used, it is possible to align the global angular discretization with the control volume face, as shown in Figure 5.4: Face with No Control Angle Overhang (p. 154). For generalized unstructured meshes, however, control volume faces do not in general align with the global angular discretization, as shown in Figure 5.5: Face with Control Angle Overhang (p. 155), leading to the problem of control angle overhang [313] (p. 746).

**Figure 5.4: Face with No Control Angle Overhang**

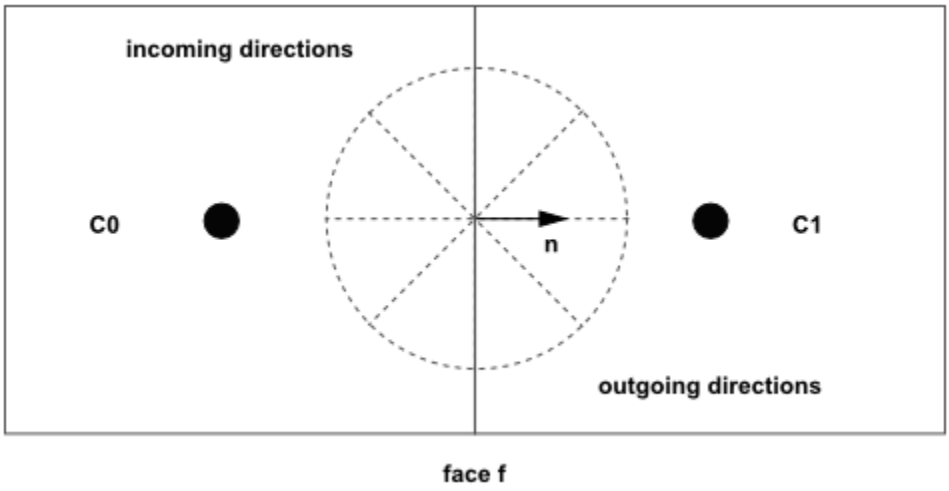



Release 15.0 - © SAS IP, Inc. All rights reserved. - Contains proprietary and confidential information of ANSYS, Inc. and its subsidiaries and affiliates.

**Figure 5.5: Face with Control Angle Overhang**

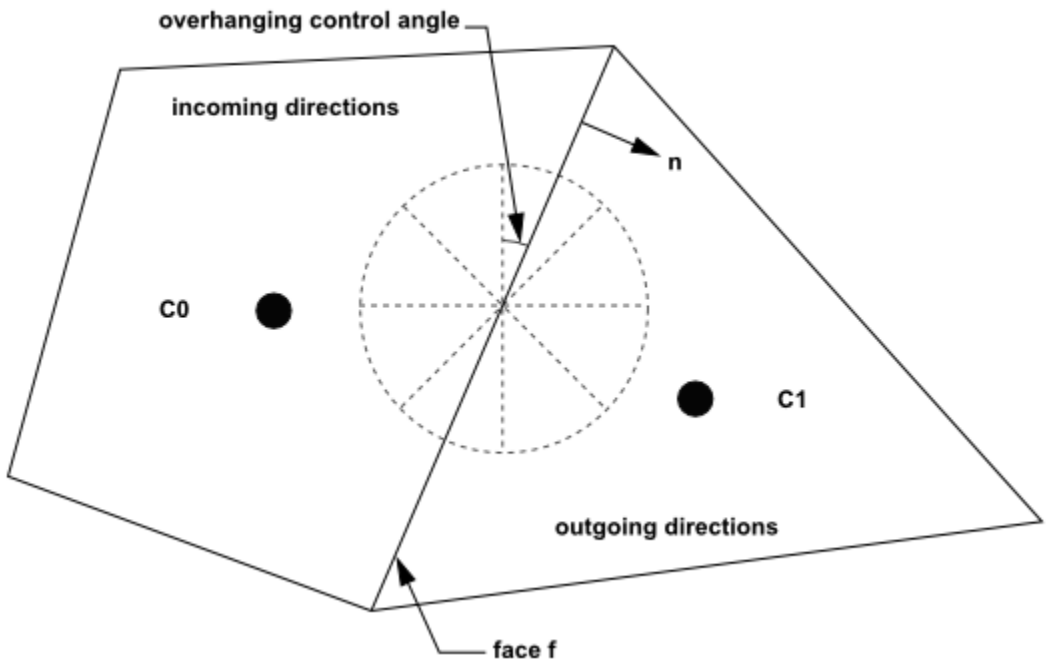


Essentially, control angles can straddle the control volume faces, so that they are partially incoming and partially outgoing to the face. Figure 5.6: Face with Control Angle Overhang (3D) (p. 155) shows a 3D example of a face with control angle overhang.

**Figure 5.6: Face with Control Angle Overhang (3D)**

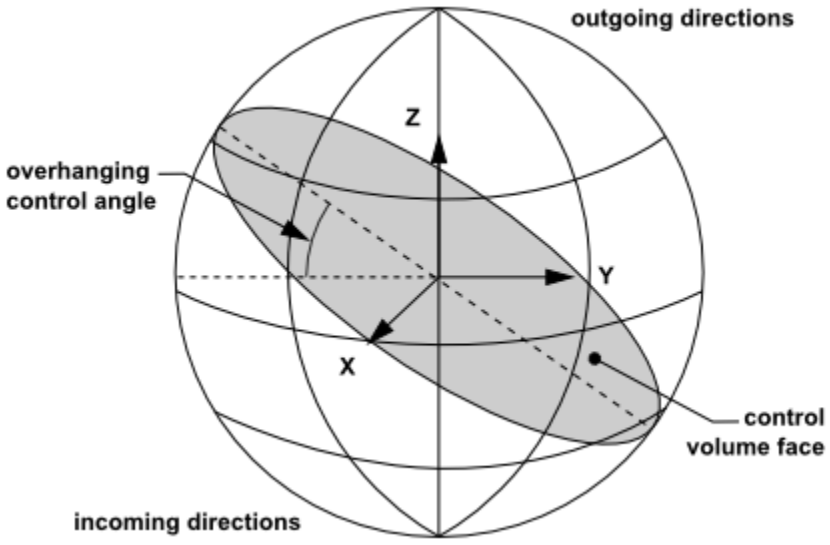


The control volume face cuts the sphere representing the angular space at an arbitrary angle. The line of intersection is a great circle. Control angle overhang may also occur as a result of reflection and refraction. It is important in these cases to correctly account for the overhanging fraction. This is done through the use of pixelation [313] (p. 746).

Each overhanging control angle is divided into $N_{\theta_p} \times N_{\phi_p}$ pixels, as shown in Figure 5.7: Pixelation of Control Angle (p. 156).

Release 15.0 - © SAS IP, Inc. All rights reserved. - Contains proprietary and confidential information of ANSYS, Inc. and its subsidiaries and affiliates.

**Figure 5.7: Pixelation of Control Angle**

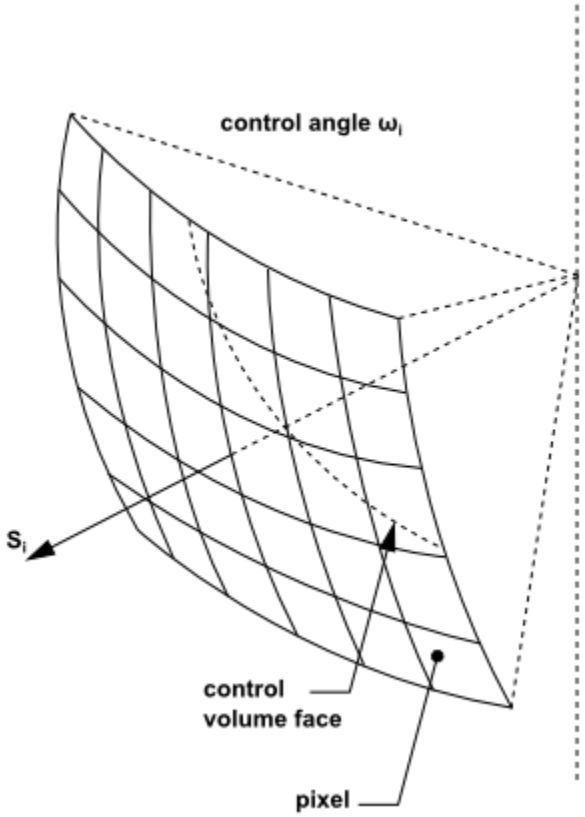


The energy contained in each pixel is then treated as incoming or outgoing to the face. The influence of overhang can therefore be accounted for within the pixel resolution. ANSYS Fluent allows you to choose the pixel resolution. For problems involving gray-diffuse radiation, the default pixelation of $1 \times 1$ is usually sufficient. For problems involving symmetry, periodic, specular, or semi-transparent boundaries, a pixelation of $3 \times 3$ is recommended. You should be aware, however, that increasing the pixelation adds to the cost of computation.

## 5.3.6.4. Anisotropic Scattering

The DO implementation in ANSYS Fluent admits a variety of scattering phase functions. You can choose an isotropic phase function, a linear anisotropic phase function, a Delta-Eddington phase function, or a user-defined phase function. The linear anisotropic phase function is described in Equation 5.28 (p. 144). The Delta-Eddington function takes the following form:

$$\Phi(\vec{s} \cdot \vec{s}') = 2f\delta(1 - \vec{s} \cdot \vec{s}') + (1 - f)(1 + C\vec{s} \cdot \vec{s}') \tag{5.68}$$

Here, $f$ is the forward-scattering factor and $\delta(\vec{s} \cdot \vec{s}')$ is the Dirac delta function. The $f$ term essentially cancels a fraction $f$ of the out-scattering; therefore, for $f = 1$, the Delta-Eddington phase function will cause the intensity to behave as if there is no scattering at all. $C$ is the asymmetry factor. When the Delta-Eddington phase function is used, you will specify values for $f$ and $C$.

When a user-defined function is used to specify the scattering phase function, ANSYS Fluent assumes the phase function to be of the form

$$\Phi(\vec{s} \cdot \vec{s}') = 2f\delta(1 - \vec{s} \cdot \vec{s}') + (1 - f)\Phi^*(\vec{s} \cdot \vec{s}') \tag{5.69}$$


Release 15.0 - © SAS IP, Inc. All rights reserved. - Contains proprietary and confidential information of ANSYS, Inc. and its subsidiaries and affiliates.

The user-defined function will specify $\Phi^*$ and the forward-scattering factor $f$.

The scattering phase functions available for gray radiation can also be used for non-gray radiation. However, the scattered energy is restricted to stay within the band.

### 5.3.6.5. Particulate Effects in the DO Model

The DO model allows you to include the effect of a discrete second phase of particulates on radiation. In this case, ANSYS Fluent will neglect all other sources of scattering in the gas phase.

The contribution of the particulate phase appears in the RTE as:

$$\nabla \cdot (I\vec{s}) + \left(a + a_p + \sigma_p\right) I(\vec{r}, \vec{s}) = an^2 \frac{\sigma T^4}{\pi} + E_p + \frac{\sigma_p}{4\pi} \int_0^{4\pi} I(\vec{r}, \vec{s}\,') \Phi(\vec{s} \cdot \vec{s}\,') \, d\Omega' \tag{5.70}$$

where $a_p$ is the equivalent absorption coefficient due to the presence of particulates, and is given by Equation 5.31 (p. 144). The equivalent emission $E_p$ is given by Equation 5.30 (p. 144). The equivalent particle scattering factor $\sigma_p$, defined in Equation 5.34 (p. 145), is used in the scattering terms.

For non-gray radiation, absorption, emission, and scattering due to the particulate phase are included in each wavelength band for the radiation calculation. Particulate emission and absorption terms are also included in the energy equation.

### 5.3.6.6. Boundary and Cell Zone Condition Treatment at Opaque Walls

The discrete ordinates radiation model allows the specification of opaque walls that are interior to a domain (with adjacent fluid or solid zones on both sides of the wall), or external to the domain (with an adjacent fluid or solid zone on one side, only). Opaque walls are treated as gray if gray radiation is being computed, or non-gray if the non-gray DO model is being used.

Figure 5.8: DO Radiation on Opaque Wall (p. 158) shows a schematic of radiation on an opaque wall in ANSYS Fluent.

Release 15.0 - © SAS IP, Inc. All rights reserved. - Contains proprietary and confidential information of ANSYS, Inc. and its subsidiaries and affiliates.

**Figure 5.8: DO Radiation on Opaque Wall**

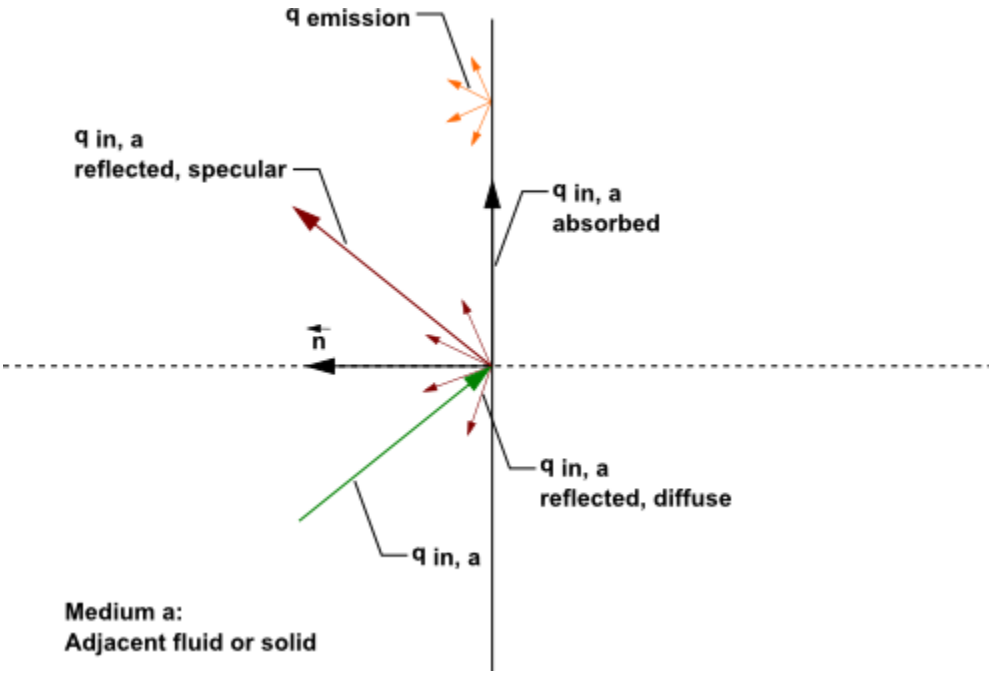


The diagram in Figure 5.8: DO Radiation on Opaque Wall (p. 158) shows incident radiation $q_{in,a}$ on side a of an opaque wall. Some of the radiant energy is reflected diffusely and specularly, depending on the diffuse fraction $f_d$ for side a of the wall that you specify as a boundary condition.

Some of the incident radiation is absorbed at the surface of the wall and some radiation is emitted from the wall surface as shown in Figure 5.8: DO Radiation on Opaque Wall (p. 158). The amount of incident radiation absorbed at the wall surface and the amount emitted back depends on the emissivity of that surface and the diffuse fraction. For non-gray DO models, you must specify internal emissivity for each wavelength band. Radiation is not transmitted through an opaque wall.

Radiant incident energy that impacts an opaque wall can be reflected back to the surrounding medium and absorbed by the wall. The radiation that is reflected can be diffusely reflected and/or specularly reflected, depending on the diffuse fraction $f_d$. If $q_{in}$ is the amount of radiative energy incident on the opaque wall, then the following general quantities are computed by ANSYS Fluent for opaque walls:

- emission from the wall surface $= n^2 \varepsilon_w \sigma T_w^4$
- diffusely reflected energy $= f_d (1 - \varepsilon_w) q_{in}$
- specularly reflected energy $= \left(1 - f_d\right)(1 - \varepsilon_w) q_{in}$
- absorption at the wall surface $= \varepsilon_w q_{in}$

where $f_d$ is the diffuse fraction, $n$ is the refractive index of the adjacent medium, $\varepsilon_w$ is the wall emissivity, $\sigma$ is the Stefan-Boltzmann Constant, and $T_w$ is the wall temperature.

Note that although ANSYS Fluent uses emissivity in its computation of radiation quantities, it is not available for postprocessing. Absorption at the wall surface assumes that the absorptivity is equal to


Release 15.0 - © SAS IP, Inc. All rights reserved. - Contains proprietary and confidential information of ANSYS, Inc. and its subsidiaries and affiliates.

the emissivity. For a purely diffused wall, $f_d$ is equal to $1$ and there is no specularly reflected energy. Similarly, for a purely specular wall, $f_d$ is equal to $0$ and there is no diffusely reflected energy. A diffuse fraction between $0$ and $1$ will result in partially diffuse and partially reflected energy.

#### 5.3.6.6.1. Gray Diffuse Walls

For gray diffuse radiation, the incident radiative heat flux, $q_{in}$, at the wall is

$$q_{in} = \int_{\vec{s}\cdot\vec{n}>0} I_{in}\,\vec{s}\cdot\vec{n}\,d\Omega \tag{5.71}$$

The net radiative flux leaving the surface is given by

$$q_{out} = (1-\varepsilon_w)\,q_{in} + n^2\varepsilon_w\sigma T_w^4 \tag{5.72}$$

where

$n$ = the refractive index of the medium next to the wall

$\varepsilon_w$ = wall emissivity

$\sigma$ = Stefan-Boltzmann Constant

$T_w$

This equation is also valid for specular radiation with emissivity = $0$.

The boundary intensity for all outgoing directions $\vec{s}$ at the wall is given by

$$I_0 = \frac{q_{out}}{\pi} \tag{5.73}$$

#### 5.3.6.6.2. Non-Gray Diffuse Walls

There is a special set of equations that apply uniquely to non-gray diffuse opaque walls. These equations assume that the absorptivity is equal to the emissivity for the wall surface. For non-gray diffuse radiation, the incident radiative heat flux $q_{in,\lambda}$ in the band $\Delta\lambda$ at the wall is

$$q_{in,\lambda} = \Delta\lambda \int_{\vec{s}\cdot\vec{n}>0} I_{in,\lambda}\,\vec{s}\cdot\vec{n}\,d\Omega \tag{5.74}$$

The net radiative flux leaving the surface in the band $\Delta\lambda$ is given by

$$q_{out,\lambda} = (1-\varepsilon_{w\lambda})\,q_{in,\lambda} + \varepsilon_{w\lambda}[F(0\rightarrow n\lambda_2 T_w) - F(0\rightarrow n\lambda_1 T_w)]\,n^2\sigma T_w^4 \tag{5.75}$$

where $\varepsilon_{w\lambda}$ is the wall emissivity in the band. $F(n,\lambda,T)$ provides the Planck distribution function. This defines the emittance for each radiation band as a function of the temperature of the source surface. The boundary intensity for all outgoing directions $\vec{s}$ in the band $\Delta\lambda$ at the wall is given by

$$I_{0\lambda} = \frac{q_{out,\lambda}}{\pi\,\Delta\lambda} \tag{5.76}$$

Release 15.0 - © SAS IP, Inc. All rights reserved. - Contains proprietary and confidential information of ANSYS, Inc. and its subsidiaries and affiliates.

## 5.3.6.7. Cell Zone and Boundary Condition Treatment at Semi-Transparent Walls

ANSYS Fluent allows the specification of interior and exterior semi-transparent walls for the DO model. In the case of interior semi-transparent walls, incident radiation can pass through the wall and be transmitted to the adjacent medium (and possibly refracted), it can be reflected back into the surrounding medium, and absorbed through the wall thickness. Transmission and reflection can be diffuse and/or specular. You specify the diffuse fraction for all transmitted and reflected radiation; the rest is treated specularly. For exterior semi-transparent walls, there are two possible sources of radiation on the boundary wall: an irradiation beam from outside the computational domain and incident radiation from cells in adjacent fluid or solid zones.

For non-gray radiation, semi-transparent wall boundary conditions are applied on a per-band basis. The radiant energy within a band is transmitted, reflected, and refracted as in the gray case; there is no transmission, reflection, or refraction of radiant energy from one band to another.

By default the DO equations are solved in all fluid zones, but not in any solid zones. Therefore, if you have an adjacent solid zone for your thin wall, you will need to specify the solid zone as participating in radiation in the **Solid** dialog box as part of the boundary condition setup.

---

**Important**

If you are interested in the detailed temperature distribution inside your semi-transparent media, then you will need to model a semi-transparent wall as a solid zone with adjacent fluid zone(s), and treat the solid as a semi-transparent medium. This is discussed in a subsequent section.

---

### 5.3.6.7.1. Semi-Transparent Interior Walls

Figure 5.9: DO Radiation on Interior Semi-Transparent Wall (p. 161) shows a schematic of an interior (two-sided) wall that is treated as semi-transparent in ANSYS Fluent and has zero thickness. Incident radiant energy depicted by $q_{in,a}$ can pass through the semi-transparent wall if and only if the contiguous fluid or solid cell zones participate in radiation, thereby allowing the radiation to be coupled. Radiation coupling is set when a wall is specified as semi-transparent. Note that by default, radiation is *not* coupled and you will need to explicitly specify radiation coupling on the interior wall by changing the boundary condition type to semi-transparent in the **Wall** dialog box (under the **Radiation** tab).


Release 15.0 - © SAS IP, Inc. All rights reserved. - Contains proprietary and confidential information of ANSYS, Inc. and its subsidiaries and affiliates.

**Figure 5.9: DO Radiation on Interior Semi-Transparent Wall**

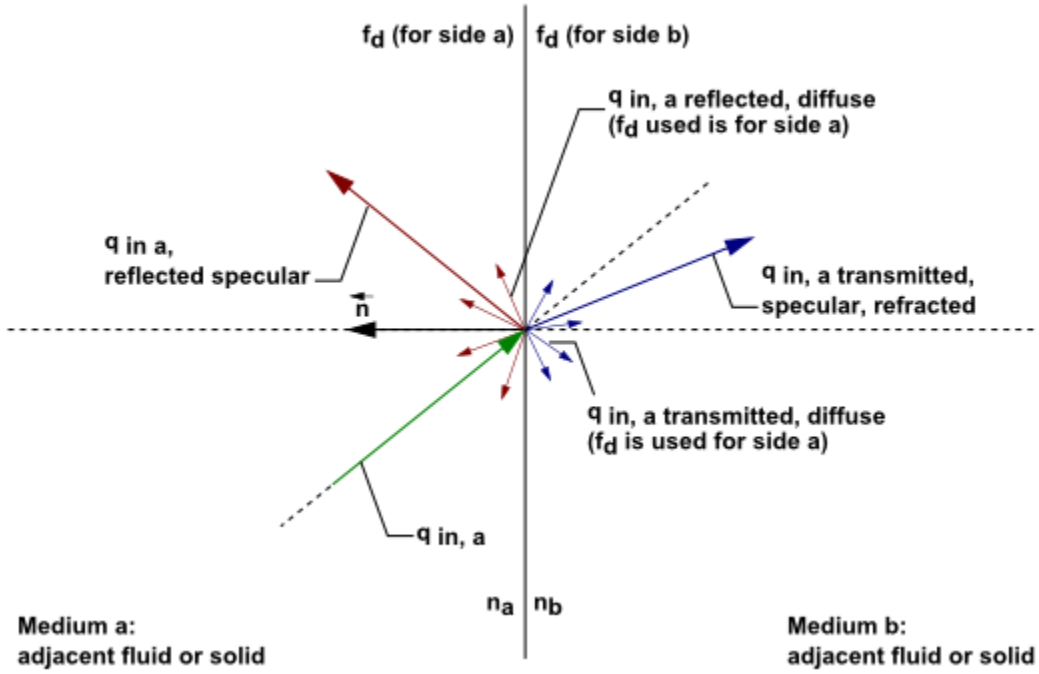


Incident radiant energy that is transmitted through a semi-transparent wall can be transmitted specularly and diffusely. Radiation can also be reflected at the interior wall back to the surrounding medium if the refractive index $n_a$ for the fluid zone that represents medium $a$ is different than the refractive index $n_b$ for medium $b$. Reflected radiation can be reflected specularly and diffusely. The fraction of diffuse versus specular radiation that is transmitted and reflected depends on the diffuse fraction for the wall. The special cases of purely diffuse and purely specular transmission and reflection on semi-transparent walls is presented in the following sections.

If the semi-transparent wall has thickness, then the thickness and the absorption coefficient determine the absorptivity of the 'thin' wall. If either the wall thickness or absorption coefficient is set to $0$, then the wall has no absorptivity. Although incident radiation can be absorbed in a semi-transparent wall that has thickness, the default is that the absorbed radiation flux does not affect the energy equation, which can result in an energy imbalance and possibly an unexpected temperature field. The exception is when shell conduction is used (available in 3D only). With shell conduction there is full correspondence between energy and radiation. If the wall is expected to have significant absorption/emission, then it may be better to model the thickness explicitly with solid cells, where practical. ANSYS Fluent does not include emission from the surface of semi-transparent walls (due to defined internal emissivity), except when a temperature boundary condition is defined.

### 5.3.6.7.2. Specular Semi-Transparent Walls

Consider the special case for a semi-transparent wall, when the diffuse fraction $f_d$ is equal to $0$ and all of the transmitted and reflected radiant energy at the semi-transparent wall is purely specular.

Figure 5.10: Reflection and Refraction of Radiation at the Interface Between Two Semi-Transparent Media (p. 162) shows a ray traveling from a semi-transparent medium $a$ with refractive index $n_a$ to a semi-transparent medium $b$ with a refractive index $n_b$ in the direction $\vec{s}$. Surface $a$ of the interface is the side that faces medium $a$; similarly, surface $b$ faces medium $b$. The interface normal $\vec{n}$ is assumed to

point into side $a$. We distinguish between the intensity $I_a(\vec{s})$, the intensity in the direction $\vec{s}$ on side $a$ of the interface, and the corresponding quantity on the side $b$, $I_b(\vec{s})$.

**Figure 5.10: Reflection and Refraction of Radiation at the Interface Between Two Semi-Transparent Media**

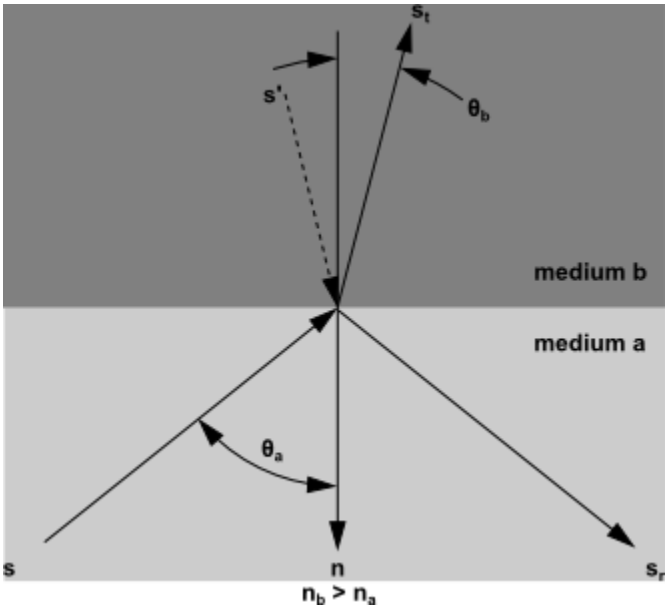


A part of the energy incident on the interface is reflected, and the rest is transmitted. The reflection is specular, so that the direction of reflected radiation is given by

$$\vec{s}_r = \vec{s} - 2(\vec{s}\cdot\vec{n})\,\vec{n} \tag{5.77}$$

The radiation transmitted from medium $a$ to medium $b$ undergoes refraction. The direction of the transmitted energy, $\vec{s}_t$, is given by Snell's law:

$$\sin\theta_b = \frac{n_a}{n_b}\sin\theta_a \tag{5.78}$$

where $\theta_a$ is the angle of incidence and $\theta_b$ is the angle of transmission, as shown in Figure 5.10: Reflection and Refraction of Radiation at the Interface Between Two Semi-Transparent Media (p. 162). We also define the direction

$$\vec{s}' = \vec{s}_t - 2(\vec{s}_t\cdot\vec{n})\,\vec{n} \tag{5.79}$$

shown in Figure 5.10: Reflection and Refraction of Radiation at the Interface Between Two Semi-Transparent Media (p. 162).

The interface reflectivity on side $a$ [304] (p. 745)

$$r_a(\vec{s}) = \frac{1}{2}\left(\frac{n_a\cos\theta_b - n_b\cos\theta_a}{n_a\cos\theta_b + n_b\cos\theta_a}\right)^2 + \frac{1}{2}\left(\frac{n_a\cos\theta_a - n_b\cos\theta_b}{n_a\cos\theta_a + n_b\cos\theta_b}\right)^2 \tag{5.80}$$

represents the fraction of incident energy transferred from $\vec{s}$ to $\vec{s}_r$.

The boundary intensity $I_{w,a}(\vec{s}_r)$ in the outgoing direction $\vec{s}_r$ on side $a$ of the interface is determined from the reflected component of the incoming radiation and the transmission from side $b$. Thus


Release 15.0 - © SAS IP, Inc. All rights reserved. - Contains proprietary and confidential information of ANSYS, Inc. and its subsidiaries and affiliates.

$$I_{w,a}(\vec{s}_r) = r_a(\vec{s})\, I_{w,a}(\vec{s}) + \tau_b(\vec{s}')\, I_{w,b}(\vec{s}') \tag{5.81}$$

where $\tau_b(\vec{s}')$ is the transmissivity of side $b$ in direction $\vec{s}'$. Similarly, the outgoing intensity in the direction $\vec{s}_t$ on side $b$ of the interface, $I_{w,b}(\vec{s}_t)$, is given by

$$I_{w,b}(\vec{s}_t) = r_b(\vec{s}')\, I_{w,b}(\vec{s}') + \tau_a(\vec{s})\, I_{w,a}(\vec{s}) \tag{5.82}$$

For the case $n_a < n_b$, the energy transmitted from medium $a$ to medium $b$ in the incoming solid angle $2\pi$ must be refracted into a cone of apex angle $\theta_c$ (see Figure 5.11: Critical Angle θc (p. 163)) where

$$\theta_c = \sin^{-1}\frac{n_a}{n_b} \tag{5.83}$$

**Figure 5.11: Critical Angle θc**

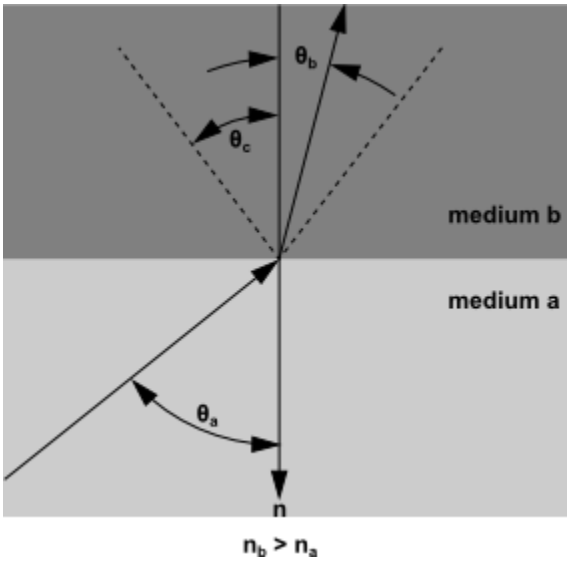


Similarly, the transmitted component of the radiant energy going from medium $b$ to medium $a$ in the cone of apex angle $\theta_c$ is refracted into the outgoing solid angle $2\pi$. For incident angles greater than $\theta_c$, total internal reflection occurs and all the incoming energy is reflected specularly back into medium $b$. The equations presented above can be applied to the general case of interior semi-transparent walls that is shown in Figure 5.9: DO Radiation on Interior Semi-Transparent Wall (p. 161).

When medium $b$ is external to the domain as in the case of an external semi-transparent wall (Figure 5.12: DO Irradiation on External Semi-Transparent Wall (p. 165)), $I_{w,b}(\vec{s}')$ is given in Equation 5.81 (p. 163) as a part of the boundary condition inputs. You supply this incoming irradiation flux in terms of its magnitude, beam direction, and the solid angle over which the radiative flux is to be applied. Note that the refractive index of the external medium is assumed to be 1.

### 5.3.6.7.3. Diffuse Semi-Transparent Walls

Consider the special case for a semi-transparent wall, when the diffuse fraction $f_d$ is equal to 1 and all of the transmitted and reflected radiant energy at the semi-transparent wall is purely diffuse.

Release 15.0 - © SAS IP, Inc. All rights reserved. - Contains proprietary and confidential information of ANSYS, Inc. and its subsidiaries and affiliates.

In many engineering problems, the semi-transparent interface may be a diffuse reflector. For such a case, the interfacial reflectivity $r(\vec{s})$ is assumed independent of $\vec{s}$, and equal to the hemispherically averaged value $r_d$. For $n = n_a/n_b > 1$, $r_{d,a}$ and $r_{d,b}$ are given by [407] (p. 751)

$$r_{d,a} = 1 - \frac{\left(1 - r_{d,b}\right)}{n^2} \tag{5.84}$$

$$r_{d,b} = \frac{1}{2} + \frac{(3n+1)(n-1)}{6(n+1)^2} + \frac{n^2\left(n^2-1\right)^2}{\left(n^2+1\right)^3}\ln\left(\frac{n-1}{n+1}\right) - \frac{2n^3\left(n^2+2n-1\right)}{\left(n^2+1\right)\left(n^4-1\right)} + \frac{8n^4\left(n^4+1\right)}{\left(n^2+1\right)\left(n^4-1\right)^2}\ln(n) \tag{5.85}$$

The boundary intensity for all outgoing directions on side $a$ of the interface is given by

$$I_{w,a} = \frac{r_{d,a}q_{in,a} + \tau_{d,b}q_{in,b}}{\pi} \tag{5.86}$$

Similarly for side $b$,

$$I_{w,b} = \frac{r_{d,b}q_{in,b} + \tau_{d,a}q_{in,a}}{\pi} \tag{5.87}$$

where

$$q_{in,a} = -\int_{4\pi} I_{w,a}\,\vec{s}\cdot\vec{n}\,d\Omega,\ \vec{s}\cdot\vec{n} < 0 \tag{5.88}$$

$$q_{in,b} = \int_{4\pi} I_{w,b}\,\vec{s}\cdot\vec{n}\,d\Omega,\ \vec{s}\cdot\vec{n} \geq 0 \tag{5.89}$$

When medium $b$ is external to the domain as in the case of an external semi-transparent wall (Figure 5.12: DO Irradiation on External Semi-Transparent Wall (p. 165)), $q_{in,b}$ is given as a part of the boundary condition inputs. You supply this incoming irradiation flux in terms of its magnitude, beam direction, and the solid angle over which the radiative flux is to be applied. Note that the refractive index of the external medium is assumed to be 1.

### 5.3.6.7.4. Partially Diffuse Semi-Transparent Walls

When the diffuse fraction $f_d$ that you enter for a semi-transparent wall is between 0 and 1, the wall is partially diffuse and partially specular. In this case, ANSYS Fluent includes the reflective and transmitted radiative flux contributions from both diffuse and specular components to the defining equations.

### 5.3.6.7.5. Semi-Transparent Exterior Walls

Figure 5.12: DO Irradiation on External Semi-Transparent Wall (p. 165) shows the general case of an irradiation beam $q_{irrad}$ applied to an exterior semi-transparent wall with zero thickness and a non-zero


Release 15.0 - © SAS IP, Inc. All rights reserved. - Contains proprietary and confidential information of ANSYS, Inc. and its subsidiaries and affiliates.

absorption coefficient for the material property. Refer to the previous section for the radiation effects of wall thickness on semi-transparent walls.

**Figure 5.12: DO Irradiation on External Semi-Transparent Wall**

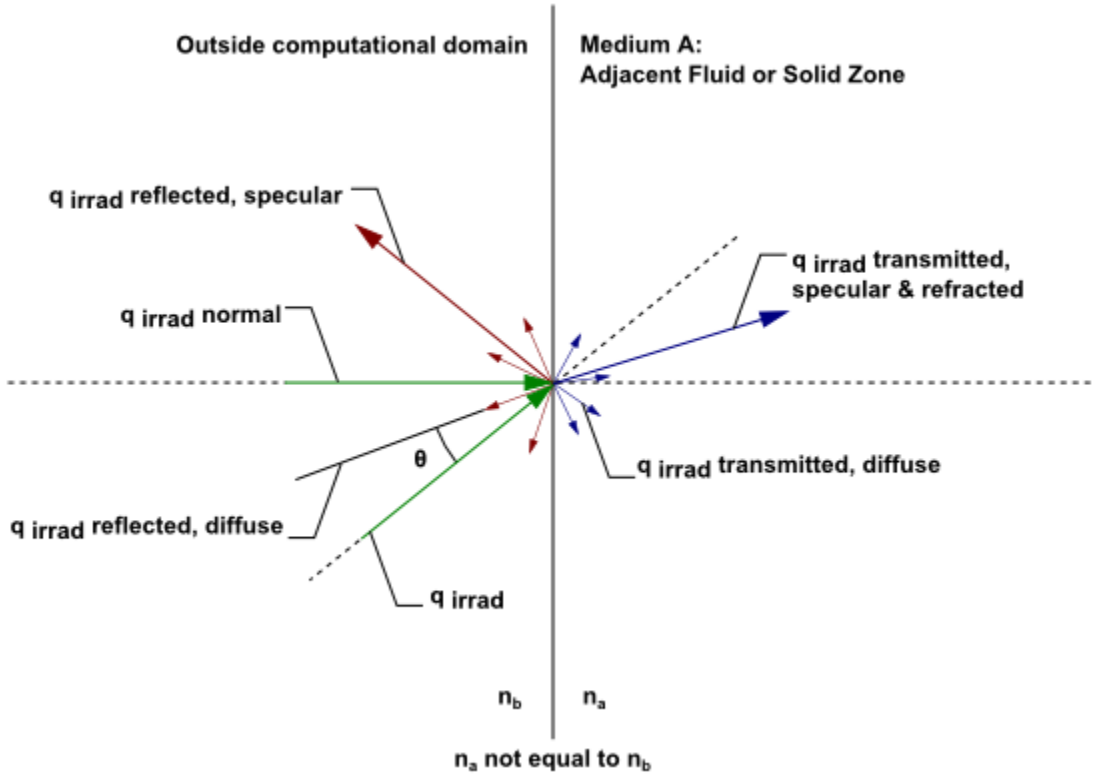


An irradiation flux passes through the semi-transparent wall from outside the computational domain (Figure 5.12: DO Irradiation on External Semi-Transparent Wall (p. 165)) into the adjacent fluid or solid medium a. The transmitted radiation can be refracted (bent) and dispersed specularly and diffusely, depending on the refractive index and the diffuse fraction that you provide as a boundary condition input. Note that there is a reflected component of $q_{irrad}$ when the refractive index of the wall ($n_b$) is not equal to 1, as shown.

There is an additional flux beyond $q_{irrad}$ that is applied when the **Mixed** or **Radiation** wall boundary conditions are selected in the **Thermal** tab. This external flux at the semi-transparent wall is computed by ANSYS Fluent as

$$Q_{ext} = \varepsilon_{external} \sigma T_{rad}^4 \tag{5.90}$$

The fraction of the above energy that will enter into the domain depends on the transmissivity of the semi-transparent wall under consideration. Note that this energy is distributed across the solid angles (that is, similar treatment as diffuse component.)

Incident radiation can also occur on external semi-transparent walls. Refer to the previous discussion on interior walls for details, since the radiation effects are the same.

The irradiation beam is defined by the magnitude, beam direction, and beam width that you supply.

The irradiation magnitude is specified in terms of an incident radiant heat flux ($W/m^2$). Beam width is specified as the solid angle over which the irradiation is distributed (that is, the beam $\theta$ and $\phi$ extents). The default beam width in ANSYS Fluent is $1e-6$ degrees which is suitable for collimated beam radiation.

Release 15.0 - © SAS IP, Inc. All rights reserved. - Contains proprietary and confidential information of ANSYS, Inc. and its subsidiaries and affiliates.

Beam direction is defined by the vector of the centroid of the solid angle. If you select the feature **Apply Direct Irradiation Parallel to the Beam** in the **Wall** boundary condition dialog box, then you supply $q_{irrad}$ for irradiation (Figure 5.12: DO Irradiation on External Semi-Transparent Wall (p. 165)) and ANSYS Fluent computes and uses the surface normal flux $q_{irrad,normal}$ in its radiation calculation. If this feature is not checked, then you must supply the surface normal flux $q_{irrad,normal}$ for irradiation.

Figure 5.13: Beam Width and Direction for External Irradiation Beam (p. 166) shows a schematic of the beam direction and beam width for the irradiation beam. You provide these inputs (in addition to irradiation magnitude) as part of the boundary conditions for a semi-transparent wall.

**Figure 5.13: Beam Width and Direction for External Irradiation Beam**

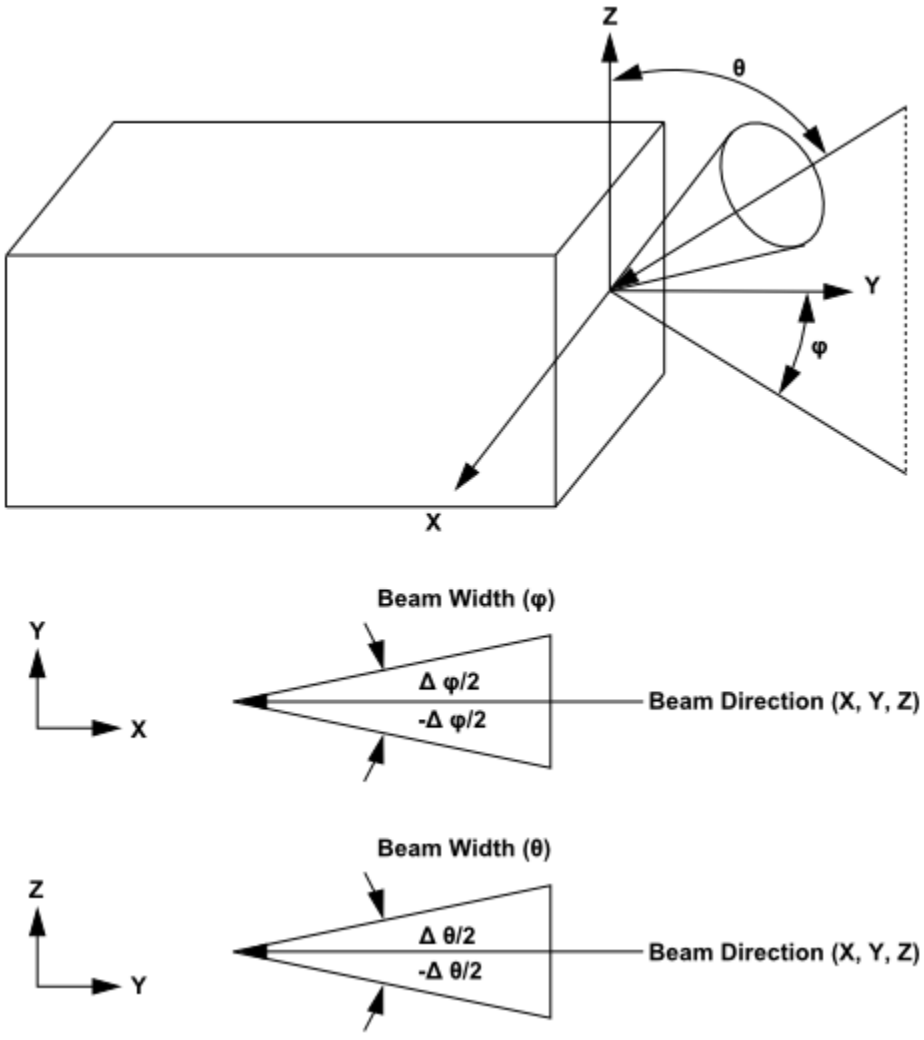


The irradiation beam can be refracted in medium a depending on the refractive index that is specified for the particular fluid or solid zone material.

## 5.3.6.7.6. Limitations

Where shell conduction is not active, there is only limited support for absorbing and emitting semi-transparent thin walls. In cases with significant emission or absorption of radiation in a participating solid material, such as the absorption of long wavelength radiation in a glass window, the use of semi-transparent thin walls can result in the prediction of unphysical temperatures in the numerical solution.


Release 15.0 - © SAS IP, Inc. All rights reserved. - Contains proprietary and confidential information of ANSYS, Inc. and its subsidiaries and affiliates.

In a 3-dimensional model this can be overcome by activating the shell conduction option for the respective thin wall. Otherwise, where possible, it is advisable to represent the solid wall thickness explicitly with one or more layers of cells across the wall thickness.

#### 5.3.6.7.7. Solid Semi-Transparent Media

The discrete ordinates radiation model allows you to model a solid zone that has adjacent fluid or solid zones on either side as a "semi-transparent" medium. This is done by designating the solid zone to participate in radiation as part of the boundary condition setup. Modeling a solid zone as a semi-transparent medium allows you to obtain a detailed temperature distribution inside the semi-transparent zone since ANSYS Fluent solves the energy equation on a per-cell basis for the solid and provides you with the thermal results. By default, however, the DO equations are solved in fluid zones, but not in any solid zones. Therefore, you will need to specify the solid zone as participating in radiation in the **Solid** dialog box as part of the boundary condition setup.

### 5.3.6.8. Boundary Condition Treatment at Specular Walls and Symmetry Boundaries

At specular walls and symmetry boundaries, the direction of the reflected ray $\vec{s}_r$ corresponding to the incoming direction $\vec{s}$ is given by Equation 5.77 (p. 162). Furthermore,

$$I_w(\vec{s}_r) = I_w(\vec{s}) \tag{5.91}$$

### 5.3.6.9. Boundary Condition Treatment at Periodic Boundaries

When rotationally periodic boundaries are used, it is important to use pixelation in order to ensure that radiant energy is correctly transferred between the periodic and shadow faces. A pixelation between $3 \times 3$ and $10 \times 10$ is recommended.

### 5.3.6.10. Boundary Condition Treatment at Flow Inlets and Exits

The treatment at flow inlets and exits is described in Boundary Condition Treatment for the DTRM at Flow Inlets and Exits (p. 150).

## 5.3.7. Surface-to-Surface (S2S) Radiation Model Theory

The surface-to-surface radiation model can be used to account for the radiation exchange in an enclosure of gray-diffuse surfaces. The energy exchange between two surfaces depends in part on their size, separation distance, and orientation. These parameters are accounted for by a geometric function called a "view factor".

The main assumption of the S2S model is that any absorption, emission, or scattering of radiation can be ignored; therefore, only "surface-to-surface" radiation need be considered for analysis.

For information about setting up the model, see Setting Up the S2S Model in the User's Guide.

### 5.3.7.1. Gray-Diffuse Radiation

ANSYS Fluent's S2S radiation model assumes the surfaces to be gray and diffuse. Emissivity and absorptivity of a gray surface are independent of the wavelength. Also, by Kirchoff's law [304] (p. 745), the emissivity equals the absorptivity ($\varepsilon = \alpha$). For a diffuse surface, the reflectivity is independent of the outgoing (or incoming) directions.

The gray-diffuse model is what is used in ANSYS Fluent. Also, as stated earlier, for applications of interest, the exchange of radiative energy between surfaces is virtually unaffected by the medium that separates

Release 15.0 - © SAS IP, Inc. All rights reserved. - Contains proprietary and confidential information of ANSYS, Inc. and its subsidiaries and affiliates.

them. Thus, according to the gray-body model, if a certain amount of radiant energy ($E$) is incident on a surface, a fraction ($\rho E$) is reflected, a fraction ($\alpha E$) is absorbed, and a fraction ($\tau E$) is transmitted. Since for most applications the surfaces in question are opaque to thermal radiation (in the infrared spectrum), the surfaces can be considered opaque. The transmissivity, therefore, can be neglected. It follows, from the conservation of energy, that $\alpha+\rho=1$, since $\alpha=\varepsilon$ (emissivity), and $\rho=1-\varepsilon$.

### 5.3.7.2. The S2S Model Equations

The energy flux leaving a given surface is composed of directly emitted and reflected energy. The reflected energy flux is dependent on the incident energy flux from the surroundings, which then can be expressed in terms of the energy flux leaving all other surfaces. The energy leaving from surface $k$ is

$$q_{out,k}=\varepsilon_k\sigma T_k^4+\rho_k q_{in,k} \tag{5.92}$$

where $q_{out,k}$ is the energy flux leaving the surface, $\varepsilon_k$ is the emissivity, $\sigma$ is the Stefan-Boltzmann constant, and $q_{in,k}$ is the energy flux incident on the surface from the surroundings.

The amount of incident energy upon a surface from another surface is a direct function of the surface-to-surface "view factor," $F_{jk}$. The view factor $F_{jk}$ is the fraction of energy leaving surface $j$ that is incident on surface $k$. The surfaces used in the calculation of a view factor can be mesh faces or (for 3D cases only) clusters of faces; see Clustering and View Factors (p. 169) for details about clusters. The incident energy flux $q_{in,k}$ can be expressed in terms of the energy flux leaving all other surfaces as

$$A_k q_{in,k}=\sum_{j=1}^{N} A_j q_{out,j} F_{jk} \tag{5.93}$$

where $A_k$ is the area of surface $k$ and $F_{jk}$ is the view factor between surface $k$ and surface $j$. For $N$ surfaces, using the view factor reciprocity relationship gives

$$A_j F_{jk}=A_k F_{kj} \text{ for } j=1,2,3,\ldots N \tag{5.94}$$

so that

$$q_{in,k}=\sum_{j=1}^{N} F_{kj} q_{out,j} \tag{5.95}$$

Therefore,

$$q_{out,k}=\varepsilon_k\sigma T_k^4+\rho_k\sum_{j=1}^{N} F_{kj} q_{out,j} \tag{5.96}$$

which can be written as

$$J_k=E_k+\rho_k\sum_{j=1}^{N} F_{kj} J_j \tag{5.97}$$

where $J_k$ represents the energy that is given off (or radiosity) of surface $k$, and $E_k$ represents the emissive power of surface $k$. This represents $N$ equations, which can be recast into matrix form as

$$KJ=E \tag{5.98}$$

where $K$ is an $N\times N$ matrix, $J$ is the radiosity vector, and $E$ is the emissive power vector.


Release 15.0 - © SAS IP, Inc. All rights reserved. - Contains proprietary and confidential information of ANSYS, Inc. and its subsidiaries and affiliates.

Equation 5.98 (p. 168) is referred to as the radiosity matrix equation. The view factor between two finite surfaces $i$ and $j$ is given by

$$F_{ij} = \frac{1}{A_i} \int_{A_i} \int_{A_j} \frac{\cos\theta_i \cos\theta_j}{\pi r^2} \delta_{ij} dA_i dA_j \tag{5.99}$$

where $\delta_{ij}$ is determined by the visibility of $dA_j$ to $dA_i$. $\delta_{ij}$ = 1 if $dA_j$ is visible to $dA_i$ and 0 otherwise.

## 5.3.7.3. Clustering

The S2S radiation model is computationally very expensive when you calculate the radiation and view factors for a large number of surfaces. To reduce the computational time as well as the storage requirement, the number of surfaces is reduced by creating surface "clusters". The surface clusters are made by starting from a face and adding its neighbors and their neighbors until a specified number of faces per surface cluster is collected.

### 5.3.7.3.1. Clustering and View Factors

By default, view factors are calculated using a face to face basis, in which clustering is used in a limited way only. The boundary faces act as the surfaces for the view factor calculation, and then a cluster view factor is obtained by taking the area-weighted average of the view factors of the faces within the cluster.

For 3D cases, you have the option of using the cluster to cluster basis instead of the face to face basis, which can reduce the computational expense and storage requirements. In this approach, ANSYS Fluent internally creates polygon faces by combining all of the faces from non-polyhedral cells in each cluster, and these are then used as the surfaces for the view factor calculation. The `.s2s` file will contain the connectivity information of the cluster itself instead of the individual faces in the cluster, and the coarser, polyhedral mesh that is written requires less disk space. Note that accuracy can be impacted by the use of the cluster to cluster basis, because of the following reasons:

- Clusters are assumed to be planar for view factor computation, even though they may not be exactly planar. This discrepancy reduces the accuracy, especially as the surface becomes more convex / concave, and as the number of faces per surface clusters for the boundary zones increases.
- The option of dividing faces into subfaces as part of the hemicube algorithm (which increases accuracy) is not available with the cluster to cluster basis.

### 5.3.7.3.2. Clustering and Radiosity

The radiosity, $J$, is calculated for the surface clusters. These values are then distributed to the faces in the clusters to calculate the wall temperatures. Since the radiation source terms are highly non-linear (proportional to the fourth power of temperature), care must be taken to calculate the average temperature of the surface clusters and distribute the flux and source terms appropriately among the faces forming the clusters.

The surface cluster temperature is obtained by area averaging as shown in the following equation:

$$T_{sc} = \left( \frac{\sum_f A_f T_f^4}{\sum A_f} \right)^{1/4} \tag{5.100}$$

where $T_{sc}$ is the temperature of the surface cluster, and $A_f$ and $T_f$ are the area and temperature of face $f$. The summation is carried over all faces of a surface cluster.

## 5.3.8. Radiation in Combusting Flows

### 5.3.8.1. The Weighted-Sum-of-Gray-Gases Model

The weighted-sum-of-gray-gases model (WSGGM) is a reasonable compromise between the oversimplified gray gas model and a complete model which takes into account particular absorption bands. The basic assumption of the WSGGM is that the total emissivity over the distance $s$ can be presented as

$$\varepsilon = \sum_{i=0}^{I} a_{\varepsilon,i}(T)\left(1 - e^{-\kappa_i ps}\right) \tag{5.101}$$

where $a_{\varepsilon,i}$ is the emissivity weighting factor for the $i$th fictitious gray gas, the bracketed quantity is the $i$th fictitious gray gas emissivity, $\kappa_i$ is the absorption coefficient of the $i$th gray gas, $p$ is the sum of the partial pressures of all absorbing gases, and $s$ is the path length. For $a_{\varepsilon,i}$ and $\kappa_i$ ANSYS Fluent uses values obtained from [77] (p. 733) and [419] (p. 752). These values depend on gas composition, and $a_{\varepsilon,i}$ also depend on temperature. When the total pressure is not equal to 1 atm, scaling rules for $\kappa_i$ are used (see Equation 5.108 (p. 171)).

The absorption coefficient for $i=0$ is assigned a value of zero to account for windows in the spectrum between spectral regions of high absorption ($\sum_{i=1}^{I} a_{\varepsilon,i} < 1$) and the weighting factor for $i=0$ is evaluated from [419] (p. 752):

$$a_{\varepsilon,0} = 1 - \sum_{i=1}^{I} a_{\varepsilon,i} \tag{5.102}$$

The temperature dependence of $a_{\varepsilon,i}$ can be approximated by any function, but the most common approximation is

$$a_{\varepsilon,i} = \sum_{j=1}^{J} b_{\varepsilon,i,j} T^{j-1} \tag{5.103}$$

where $b_{\varepsilon,i,j}$ are the emissivity gas temperature polynomial coefficients. The coefficients $b_{\varepsilon,i,j}$ and $\kappa_i$ are estimated by fitting Equation 5.101 (p. 170) to the table of total emissivities, obtained experimentally [77] (p. 733), [89] (p. 733), [419] (p. 752).

The absorptivity $\alpha$ of the radiation from the wall can be approximated in a similar way [419] (p. 752), but, to simplify the problem, it is assumed that $\varepsilon = \alpha$ [303] (p. 745). This assumption is justified unless the medium is optically thin and the wall temperature differs considerably from the gas temperature.

Since the coefficients $b_{\varepsilon,i,j}$ and $\kappa_i$ are slowly varying functions of $ps$ and $T$, they can be assumed constant for a wide range of these parameters. In [419] (p. 752) these constant coefficients are presented for different relative pressures of the $CO_2$ and $H_2O$ vapor, assuming that the total pressure $p_T$ is 1 atm. The values of the coefficients shown in [419] (p. 752) are valid for $0.001 \le ps \le 10.0$ atm-m and $600 \le T \le 2400$ K. For $T > 2400$ K, coefficient values suggested by [77] (p. 733) are used. If $\kappa_i ps \ll 1$ for all $i$, Equation 5.101 (p. 170) simplifies to


Release 15.0 - © SAS IP, Inc. All rights reserved. - Contains proprietary and confidential information of ANSYS, Inc. and its subsidiaries and affiliates.

$$\varepsilon = \sum_{i=0}^{I} a_{\varepsilon,i} \kappa_i p s \tag{5.104}$$

Comparing Equation 5.104 (p. 171) with the gray gas model with absorption coefficient $a$, it can be seen that the change of the radiation intensity over the distance $s$ in the WSGGM is exactly the same as in the gray gas model with the absorption coefficient

$$a = \sum_{i=0}^{I} a_{\varepsilon,i} \kappa_i p \tag{5.105}$$

which does not depend on $s$. In the general case, $a$ is estimated as

$$a = -\frac{\ln(1-\varepsilon)}{s} \tag{5.106}$$

where the emissivity $\varepsilon$ for the WSGGM is computed using Equation 5.101 (p. 170). $a$ as defined by Equation 5.106 (p. 171) depends on $s$, reflecting the non-gray nature of the absorption of thermal radiation in molecular gases. In ANSYS Fluent, Equation 5.105 (p. 171) is used when $s \leq 10^{-4}$ m and Equation 5.106 (p. 171) is used for $s > 10^{-4}$ m. Note that for $s \approx 10^{-4}$ m, the values of $a$ predicted by Equation 5.105 (p. 171) and Equation 5.106 (p. 171) are practically identical (since Equation 5.106 (p. 171) reduces to Equation 5.105 (p. 171) in the limit of small $s$).

ANSYS Fluent allows you to set $s$ equal to the mean beam length. You can specify the mean beam length or have ANSYS Fluent compute it according to the following equation from Siegel [406] (p. 751).

$$s = 3.6\frac{V}{A} \tag{5.107}$$

Where $V$ is the volume and $A$ is the total surface area of the boundaries (walls, inlets, outlets; not symmetry).

See Inputs for a Composition-Dependent Absorption Coefficient in the User's Guide for details about setting properties for the WSGGM.

**Important**

The WSGGM cannot be used to specify the absorption coefficient in each band when using the non-gray DO model or the non-gray P-1 model. If the WSGGM is used with a non-gray model, the absorption coefficient will be the same in all bands.

#### 5.3.8.1.1. When the Total (Static) Gas Pressure is Not Equal to 1 atm

The WSGGM, as described above, assumes that $p_{tot}$—the total (static) gas pressure—is equal to 1 atm. In cases where $p_{tot}$ is not unity (for example, combustion at high temperatures), scaling rules suggested in [104] (p. 734) are used to introduce corrections. When $p_{tot} < 0.9$ atm or $p_{tot} > 1.1$ atm, the values for $\kappa_i$ in Equation 5.101 (p. 170) and Equation 5.105 (p. 171) are rescaled:

$$\kappa_i \rightarrow \kappa_i p_{tot}^{m} \tag{5.108}$$

where $m$ is a non-dimensional value obtained from [104] (p. 734), which depends on the partial pressures and temperature $T$ of the absorbing gases, as well as on $p_{tot}$.

Release 15.0 - © SAS IP, Inc. All rights reserved. - Contains proprietary and confidential information of ANSYS, Inc. and its subsidiaries and affiliates.

### 5.3.8.2. The Effect of Soot on the Absorption Coefficient

When soot formation is computed, ANSYS Fluent can include the effect of the soot concentration on the radiation absorption coefficient. The generalized soot model estimates the effect of the soot on radiative heat transfer by determining an effective absorption coefficient for soot. The absorption coefficient of a mixture of soot and an absorbing (radiating) gas is then calculated as the sum of the absorption coefficients of pure gas and pure soot:

$$a_{s+g}=a_g+a_s \tag{5.109}$$

where $a_g$ is the absorption coefficient of gas without soot (obtained from the WSGGM) and

$$a_s=b_1\rho_{soot}Y_{soot}[1+b_T(T-2000)] \tag{5.110}$$

with

$$b_1=1232.4\mathrm{m}^2/\mathrm{kg}$$

and

$$b_T\approx 4.8\times 10^{-4}\mathrm{K}^{-1}$$

$\rho_{\mathrm{soot}}$ is the soot density in $kg/m^3$ and $Y_{\mathrm{soot}}$ is the soot mass fraction.

The coefficients $b_1$ and $b_T$ were obtained [389] (p. 750) by fitting Equation 5.110 (p. 172) to data based on the Taylor-Foster approximation [447] (p. 753) and data based on the Smith et al. approximation [419] (p. 752).

See Radiation Properties and Using the Soot Models in the User's Guide for information about including the soot-radiation interaction effects.

### 5.3.8.3. The Effect of Particles on the Absorption Coefficient

ANSYS Fluent can also include the effect of discrete phase particles on the radiation absorption coefficient, provided that you are using either the P-1 or the DO model. When the P-1 or DO model is active, radiation absorption by particles can be enabled. The particle emissivity, reflectivity, and scattering effects are then included in the calculation of the radiative heat transfer. See Setting Material Properties for the Discrete Phase in the User's Guide for more details on the input of radiation properties for the discrete phase.

## 5.3.9. Choosing a Radiation Model

For certain problems one radiation model may be more appropriate than the others. When deciding which radiation model to use, consider the following:

- Optical thickness: The optical thickness $aL$ is a good indicator of which model to use in your problem. Here, $L$ is an appropriate length scale for your domain. For flow in a combustor, for example, $L$ is the diameter of the combustion chamber. If $aL \gg 1$, your best alternatives are the P-1 and Rosseland models. The P-1 model should typically be used for optical thicknesses $>1$. For optical thickness $>3$, the Rosseland model is cheaper and more efficient. For high optical thickness cases, a second-order discretization scheme for the DO model is recommended. The DTRM and the DO model work across the full range of optical thicknesses, but are substantially more expensive to use. Consequently, you should use the "thick-limit"


Release 15.0 - © SAS IP, Inc. All rights reserved. - Contains proprietary and confidential information of ANSYS, Inc. and its subsidiaries and affiliates.

models, P-1 and Rosseland, if the problem allows it. For optically thin problems ($aL < 1$), the DTRM and the DO model, only, are appropriate.

- Scattering and emissivity: The P-1, Rosseland, and DO models account for scattering, while the DTRM neglects it. Since the Rosseland model uses a temperature slip condition at walls, it is insensitive to wall emissivity.
- Particulate effects: Only the P-1 and DO models account for exchange of radiation between gas and particulates (see Equation 5.29 (p. 144)).
- Semi-transparent walls:(interior and exterior) Only the DO model allows you to model semi-transparent walls of various types (for example, glass).
- Specular walls: Only the DO model allows specular reflection (for example, for dust-free mirror).
- Partially specular walls: Only the DO model allows specular reflection (for example, dusty mirror).
- Non-gray radiation: Only the P-1 and DO models allow you to compute non-gray radiation using a gray-band model.
- Localized heat sources: In problems with localized sources of heat, the P-1 model may over-predict the radiative fluxes. The DO model is probably the best suited for computing radiation for this case, although the DTRM, with a sufficiently large number of rays, is also acceptable.
- Enclosure radiative transfer with non-participating media: The surface-to-surface (S2S) model is suitable for this type of problem. The radiation models used with participating media may, in principle, be used to compute the surface-to-surface radiation, but they are not always efficient.

#### 5.3.9.1. External Radiation

If you need to include radiative heat transfer from the exterior of your physical model, you can include an external radiation boundary condition in your model (for details, see Thermal Boundary Conditions at Walls in the User's Guide). If you are not concerned with radiation within the domain, this boundary condition can be used without activating one of the radiation models.

Release 15.0 - © SAS IP, Inc. All rights reserved. - Contains proprietary and confidential information of ANSYS, Inc. and its subsidiaries and affiliates.

Release 15.0 - © SAS IP, Inc. All rights reserved. - Contains proprietary and confidential information
of ANSYS, Inc. and its subsidiaries and affiliates.

# Chapter 6: Heat Exchangers

Many engineering systems, including power plants, climate control, and engine cooling systems typically contain tubular heat exchangers. However, for most engineering problems, it is impractical to model individual fins and tubes of a heat exchanger core. In principle, heat exchanger cores introduce a pressure drop to the primary fluid stream and transfer heat to a second fluid, a coolant, referred to here as the auxiliary fluid.

In ANSYS Fluent, lumped-parameter models are used to account for the pressure loss and auxiliary fluid heat rejection. ANSYS Fluent provides two heat exchanger models: the macro (ungrouped and grouped) models and the dual cell model. The macro model allows you to choose between two heat transfer models, namely the **simple-effectiveness-model** and the number-of-transfer-units (NTU) model. The models can be used to compute auxiliary fluid inlet temperature for a fixed heat rejection or total heat rejection for a fixed auxiliary fluid inlet temperature. For the **simple-effectiveness-model**, the auxiliary fluid may be single-phase or two-phase. The dual cell model uses the NTU method for heat transfer calculations. This model allows the solution of auxiliary flow on a separate mesh (other than the primary fluid mesh), unlike the macro model, where the auxiliary flow is modeled as 1D flow. The dual cell model also offers more flexibility as far as the shape of the heat exchanger is concerned, and overcomes some of the major limitations present in the macro model.

For more information about using the heat exchanger models, see Modeling Heat Exchangers in the User's Guide.

The following sections contain information about the theory behind the heat exchanger models:

6.1. The Macro Heat Exchanger Models
6.2. The Dual Cell Model

## 6.1. The Macro Heat Exchanger Models

The following sections contain information about the theory behind the macro heat exchanger models:

6.1.1. Overview of the Macro Heat Exchanger Models
6.1.2. Restrictions of the Macro Heat Exchanger Models
6.1.3. Macro Heat Exchanger Model Theory

### 6.1.1. Overview of the Macro Heat Exchanger Models

In a typical heat exchanger core, the auxiliary fluid temperature is stratified in the direction of the auxiliary fluid flow. As a result, heat rejection is not constant over the entire core. In ANSYS Fluent, the fluid zone representing the heat exchanger core is subdivided into macroscopic cells or *macros* along the auxiliary fluid path, as in Figure 6.1: Core Discretized Into 3x4x2 Macros (p. 176). In this figure, the core is discretized into 3x4x2 macros. This configuration consists of 2 passes, each pass having four rows and three columns of macros. The auxiliary fluid inlet temperature to each macro is computed and then subsequently used to compute the heat rejection from each macro. This approach provides a realistic heat rejection distribution over the heat exchanger core.

To use the heat exchanger models, you must define one or more fluid zone(s) to represent the heat exchanger core. Typically, the fluid zone is sized to the dimension of the core itself. As part of the setup

Release 15.0 - © SAS IP, Inc. All rights reserved. - Contains proprietary and confidential information of ANSYS, Inc. and its subsidiaries and affiliates.

procedure, you will define the auxiliary fluid path, the number of macros, and the physical properties and operating conditions of the core (pressure drop parameters, heat exchanger effectiveness, auxiliary fluid flow rate, and so on).

You can also combine several fluid zones as a single heat exchanger group. In this situation each fluid zone acts as a separate heat exchanger core, and the auxiliary fluid mass flow rate of the heat exchanger group is divided among the zones in the ratio of the respective volumes. For the purpose of auxiliary fluid flow, heat exchanger groups can also be connected in series. In addition, a heat exchanger group can have an auxiliary fluid pressure drop (for example, for pressure dependent properties) and a supplementary auxiliary fluid stream entering or leaving it. For more information on heat exchanger groups, see Using the Grouped Macro Heat Exchanger Model.

The heat exchanger models were designed for "compact" heat exchangers, implying that the primary fluid side flow is unidirectional. The auxiliary fluid is assumed to flow through a large number of parallel tubes, which can optionally double back in a serpentine pattern to create a number of "passes". You can independently choose the principal auxiliary fluid flow direction, the pass-to-pass direction and the external primary fluid flow direction.

**Important**

It is highly recommended that the free-form **Tet** mesh is not used in the macro heat exchanger model. Instead, evenly distributed **Hex/Wedge** cells should be used for improved accuracy and a more robust solution process.

**Figure 6.1: Core Discretized Into 3x4x2 Macros**

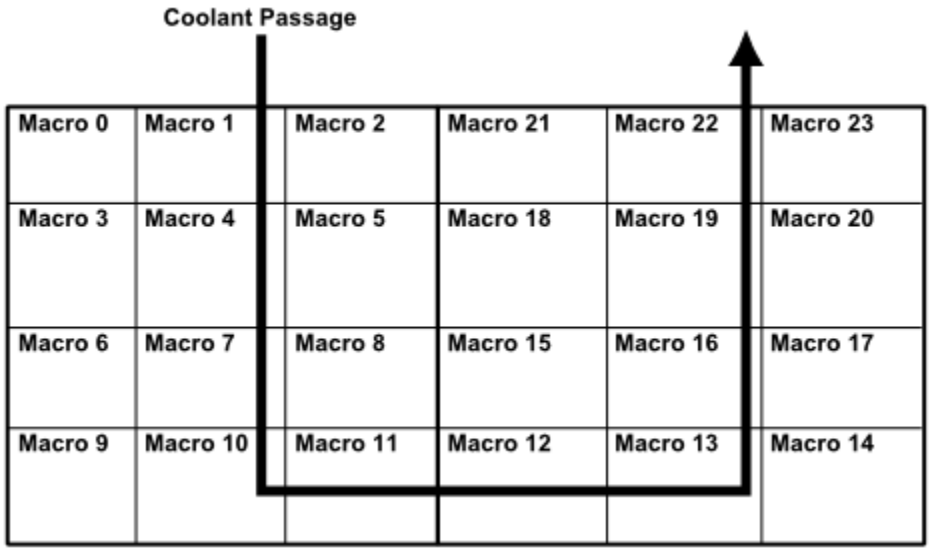


## 6.1.2. Restrictions of the Macro Heat Exchanger Models

The following restrictions exist for the macro heat exchanger models:

- The core must be a 3D mesh with a cross section that is approximately rectangular in shape.
- The primary fluid streamwise direction (see Equation 6.1 (p. 178)) must be aligned with one of the three orthogonal axes defined by the rectangular core.
- The pass-to-pass plane must be perpendicular to the primary fluid streamwise direction.


Release 15.0 - © SAS IP, Inc. All rights reserved. - Contains proprietary and confidential information of ANSYS, Inc. and its subsidiaries and affiliates.

- Flow acceleration effects are neglected in calculating the pressure loss coefficient.
- For the **simple-effectiveness-model**, the primary fluid capacity rate must be less than the auxiliary fluid capacity rate.
- Auxiliary fluid phase change cannot be modeled using the **ntu-model**.
- The macro-based method requires that an equal number of cells reside in each macro of equal size and shape.
- Auxiliary fluid flow is assumed to be 1D.
- The pass width has to be uniform.
- Accuracy is not guaranteed when the mesh is not structured or layered.
- Accuracy is not guaranteed when there is upstream diffusion of temperature at the inlet/outlet of the core.
- Non-conformal meshes cannot be attached to the inlet/outlet of the core. An extra layer has to be created to avoid it.

### 6.1.3. Macro Heat Exchanger Model Theory

In ANSYS Fluent, the heat exchanger core is treated as a fluid zone with momentum and heat transfer. Pressure loss is modeled as a momentum sink in the momentum equation, and heat transfer is modeled as a heat source in the energy equation.

ANSYS Fluent provides two heat transfer models: the default **ntu-model** and the **simple-effectiveness-model**. The **simple-effectiveness-model** interpolates the effectiveness from the velocity vs effectiveness curve that you provide. For the **ntu-model**, ANSYS Fluent calculates the effectiveness, $\varepsilon$, from the NTU value that is calculated by ANSYS Fluent from the heat transfer data provided by you in tabular format. ANSYS Fluent will automatically convert this heat transfer data to a primary fluid mass flow rate vs NTU curve (this curve will be piecewise linear). This curve will be used by ANSYS Fluent to calculate the NTU for macros based on their size and primary fluid flow rate.

The **ntu-model** provides the following features:

- The model can be used to check the heat capacity for both the primary and the auxiliary fluid, and takes the lesser of the two for the calculation of heat transfer.
- The model can be used to model heat transfer to the primary fluid from the auxiliary fluid and vice versa.
- The model can be used to model primary fluid-side reverse flow.
- The model can be used with variable density of the primary fluid.
- The model can be used in either the serial or parallel ANSYS Fluent solvers.
- Transient profiles can be used for the auxiliary fluid inlet temperature and for total heat rejection.
- Transient profiles can be used for auxiliary mass flow rates.

The **simple-effectiveness-model** provides the following features:

- The model can be used to model heat transfer from the auxiliary fluid to the primary fluid.

*Release 15.0 - © SAS IP, Inc. All rights reserved. - Contains proprietary and confidential information of ANSYS, Inc. and its subsidiaries and affiliates.*

- The auxiliary fluid properties can be a function of pressure and temperature, therefore allowing phase change of the auxiliary fluid.
- The model can be used by serial as well as parallel solvers.
- The model can be used to make a network of heat exchangers using a heat exchanger group (Using the Grouped Macro Heat Exchanger Model).
- Transient profiles can be used for the auxiliary fluid inlet temperature and for total heat rejection.
- Transient profiles can be used for auxiliary mass flow rates.

### 6.1.3.1. Streamwise Pressure Drop

In both heat transfer models, pressure loss is modeled using the porous media model in ANSYS Fluent. For the dual cell model (The Dual Cell Model (p. 183)), pressure loss is used for both streams, while for the macro model, it is used only for the primary side.

The loss coefficients of the porous media model are computed using curve fitting of the pressure-versus-flow rate data outside of ANSYS Fluent, which you will specify for the cell zone conditions. However, in some cases, the data for curve-fitting is not available. The macro model provides an additional means of getting the coefficients if the data is not available. The coefficients can also be automatically computed (and updated) using a known pressure loss coefficient as a function of some geometric parameters, the theory of which is defined below:

$$\Delta p = \frac{1}{2} f \rho_m U^2_{A_{min}} \tag{6.1}$$

where

$\Delta p$ = streamwise pressure drop

$f$ = streamwise pressure loss coefficient

$\rho_m$ = mean primary fluid density

$U_{A_{min}}$ = primary fluid velocity at the minimum flow area

The pressure loss coefficient is computed from

$$f = \left(K_c + 1 - \sigma^2\right) - \left(1 - \sigma^2 - K_e\right)\frac{v_e}{v_i} + 2\left(\frac{v_e}{v_i} - 1\right) + f_c \frac{A}{A_c}\frac{v_m}{v_i} \tag{6.2}$$

where

$\sigma$ = minimum flow to face area ratio

$K_c$ = entrance loss coefficient

$K_e$ = exit loss coefficient

$A$ = primary fluid-side surface area

$A_c$ = minimum cross-sectional flow area

$f_c$ = core friction factor

$v_e$ = specific volume at the exit

$v_i$ = specific volume at the inlet


Release 15.0 - © SAS IP, Inc. All rights reserved. - Contains proprietary and confidential information of ANSYS, Inc. and its subsidiaries and affiliates.

$v_m$ = mean specific volume $\equiv \frac{1}{2}(v_e + v_i)$

$K_c$ and $K_e$ are empirical quantities obtained from experimental data. You will need to specify these parameters based on graphs that are closest to the heat exchanger configuration that you are setting up [202] (p. 740), [200] (p. 740). These parameters are used to set up large resistances in the two non-streamwise directions, effectively forcing the primary fluid flow through the core to be unidirectional.

In Equation 6.2 (p. 178), the core friction factor is defined as

$$f_c = a Re_{min}^{b} \tag{6.3}$$

where

$a$ = core friction coefficient

$b$ = core friction exponent

$Re_{min}$ = Reynolds number for velocity at the minimum flow area

$a$ and $b$ are empirical quantities obtained from experimental data. You will need to specify the core friction coefficient and exponent based on graphs that are closest to the heat exchanger models that you set up [202] (p. 740), [200] (p. 740).

The Reynolds number in Equation 6.3 (p. 179) is defined as

$$Re_{min} = \frac{\rho_m U_{A_{min}} D_h}{\mu_m} \tag{6.4}$$

where

$\rho_m$ = mean primary fluid density

$\mu_m$ = mean primary fluid viscosity

$D_h$ = hydraulic diameter

$U_{A_{min}}$ = primary fluid velocity at the minimum flow area

For a heat exchanger core, the hydraulic diameter can be defined as

$$D_h = 4L\left(\frac{A_c}{A}\right) \tag{6.5}$$

where $L$ is the flow length of the heat exchanger. If the tubes are normal to the primary fluid flow, then $L$ is the length in the primary fluid flow direction. Note that $U_{A_{min}}$ can be calculated from

$$U_{A_{min}} = \frac{U}{\sigma} \tag{6.6}$$

where $U$ is the primary fluid velocity and $\sigma$ is the minimum flow to face area ratio.

### 6.1.3.2. Heat Transfer Effectiveness

For the **simple-effectiveness-model**, the heat-exchanger effectiveness, $\varepsilon$, is defined as the ratio of actual rate of heat transfer from the hot to cold fluid to the maximum possible rate of heat transfer. The maximum possible heat transfer is given by

Release 15.0 - © SAS IP, Inc. All rights reserved. - Contains proprietary and confidential information of ANSYS, Inc. and its subsidiaries and affiliates.

$$q_{max} = C_{min}\left(T_{in,hot} - T_{in,cold}\right) \tag{6.7}$$

where $T_{in,hot}$ and $T_{in,cold}$ are the inlet temperatures of the hot and cold fluids and

$$C_{min} = \min\left[\left(\dot{m}c_p\right)_{hot}, \left(\dot{m}c_p\right)_{cold}\right] \tag{6.8}$$

Thus, the actual rate of heat transfer, $q$, is defined as

$$q = \varepsilon C_{min}\left(T_{in,hot} - T_{in,cold}\right) \tag{6.9}$$

The value of $\varepsilon$ depends on the heat exchanger geometry and flow pattern (parallel flow, counter flow, cross flow, and so on). Even though the effectiveness of the primary fluid is computed using uniform conditions on the entire heat exchanger core, it is being applied to a small portion of the core represented by a computational cell. This can make it less accurate for some heat exchanger cores, where there is a strong variation in the primary flow. For a core with a strong primary flow variation, the NTU model must be used.

For the **ntu-model**, given the heat exchanger performance data (total heat rejection versus primary flow rate) based on uniform test conditions, ANSYS Fluent calculates the effectiveness of the entire heat exchanger from the ratio of heat capacity and the number of transfer units using the relation

$$\varepsilon = 1 - \exp\left[-\frac{1}{C_r}N_{tu}^{0.22}\left(1 - e^{-C_r N_{tu}^{0.78}}\right)\right] \tag{6.10}$$

where $C_r$ is the ratio of $C_{min}$ to $C_{max}$.

The heat exchanger performance data should be specified for a number of auxiliary flow rates so that ANSYS Fluent can compute the number of transfer units versus the primary fluid flow rate for a number of auxiliary fluid flow rates. This NTU, which is based on the full heat exchanger and uniform conditions, is scaled for each macro using the ratio of their volumes and minimum heat capacities.

For each macro, the primary fluid inlet temperature is calculated using the mass average of the incoming primary fluid temperatures at the boundaries. This automatically takes into account any reverse flow of the primary fluid at the boundaries.

### 6.1.3.3. Heat Rejection

Heat rejection is computed for each cell within a macro and added as a source term to the energy equation for the primary fluid flow. Note that heat rejection from the auxiliary fluid to primary fluid can be either positive or negative.

For the **simple-effectiveness-model**, the heat transfer for a given cell is computed from

$$q_{cell} = \varepsilon\left(\dot{m}c_p\right)_g\left(T_{in,auxiliary} - T_{cell}\right) \tag{6.11}$$

where

$\varepsilon$ = heat exchanger effectiveness

$\left(\dot{m}c_p\right)_g$ = primary fluid capacity rate (flow rate $\times$ specific heat)

$T_{in,auxiliary}$ = auxiliary fluid inlet temperature of macro containing the cell


Release 15.0 - © SAS IP, Inc. All rights reserved. - Contains proprietary and confidential information of ANSYS, Inc. and its subsidiaries and affiliates.

$T_{cell}$ = cell temperature

For the **simple-effectiveness-model**, the heat rejection from a macro is calculated by summing the heat transfer of all the cells contained within the macro

$$q_{macro} = \sum_{all\ cells\ in\ macro} q_{cell} \tag{6.12}$$

For the **ntu-model**, the heat transfer for a macro is calculated from

$$q_{macro} = \varepsilon C_{min}\left(T_{in,auxiliary} - T_{in,primary}\right) \tag{6.13}$$

where

$\varepsilon$ = macro effectiveness

$T_{in,auxiliary}$ = macro auxiliary fluid inlet temperature

$T_{in,primary}$ = macro primary fluid inlet temperature

For the **ntu-model**, the heat transfer for a given cell is computed from

$$q_{cell} = q_{macro}\frac{V_{cell}}{V_{macro}} \tag{6.14}$$

For both heat exchanger models, the total heat rejection from the heat exchanger core is computed as the sum of the heat rejection from all the macros:

$$q_{total} = \sum_{all\ macros} q_{macro} \tag{6.15}$$

The auxiliary fluid inlet temperature to each macro ($T_{in,auxiliary}$ in Equation 6.11 (p. 180) and Equation 6.13 (p. 181)) is computed based on the energy balance of the auxiliary fluid at a previous macro computation. For a given macro,

$$q_{macro} = (\dot{m})_{auxiliary}(h_{out} - h_{in}) \tag{6.16}$$

where $h_{in}$ and $h_{out}$ are the inlet and outlet enthalpies of the auxiliary fluid in the macro. The auxiliary fluid outlet temperature from the macro is calculated as

$$T_{out} = \begin{cases} \dfrac{h_{out}}{c_{p,auxiliary}} & constant\ specific\ heat\ method \\ f(h_{out}, p) & UDF\ method \end{cases} \tag{6.17}$$

where

$f$ = user-defined function

$p$ = auxiliary fluid pressure

The values of $h_{out}$ and $T_{out}$ then become the inlet conditions to the next macro.

The first row of macros (Macros 0, 1, and 2 in Figure 6.1: Core Discretized Into 3x4x2 Macros (p. 176)) are assumed to be where the auxiliary fluid enters the heat exchanger core. When the fixed total heat rejection from the heat exchanger core is specified, the inlet temperature to the first row of macros is iteratively computed, so that all of the equations are satisfied simultaneously. When a fixed auxiliary

Release 15.0 - © SAS IP, Inc. All rights reserved. - Contains proprietary and confidential information of ANSYS, Inc. and its subsidiaries and affiliates.

fluid inlet temperature is specified, the heat transfer for the first row of macros are used to calculate their exit enthalpy, which becomes the inlet condition for the next row macros. At the end of each pass, the outlet enthalpy of each macro (in the last row) is mass averaged to obtain the inlet condition for the next pass macros.

### 6.1.3.4. Macro Heat Exchanger Group Connectivity

If the optional macro heat exchanger group is used, a single heat exchanger may be consist of multiple fluid zones. In this case, the auxiliary fluid is assumed to flow through these zones in parallel. Thus, after taking into account any auxiliary stream effects, the auxiliary fluid inlet mass flow rate is automatically apportioned to each zone in the group as follows:

$$\dot{m}_i = \left( \frac{\sum_k V_{i,k}}{\sum_i \sum_k V_{i,k}} \right) \dot{m} \tag{6.18}$$

where $\dot{m}_i$ is the total auxiliary mass flow rate for the heat exchanger group. $V_{i,k}$ refers to the volume of the $k$th finite volume cell within the $i$th fluid zone. Within each zone, the auxiliary fluid flows through each macro in series as usual.

At the outlet end of the group, the parallel auxiliary fluid streams through the individual zones are re-combined, and the outlet auxiliary fluid enthalpy is calculated on a mass-averaged basis:

$$\overline{h} = \left( \frac{\sum_i \dot{m}_i h_i}{\sum_i \dot{m}_i} \right) \tag{6.19}$$

With user-defined functions, the **simple-effectiveness-model** allows you to simulate two-phase auxiliary fluid flows and other complex auxiliary fluid enthalpy relationships of the form

$$h = h(T, p, x) \tag{6.20}$$

where $p$ is the absolute pressure and $x$ is the quality (mass fraction of vapor) of a two-phase vapor-liquid mixture. When pressure-dependent auxiliary fluid properties are used, the mean pressure within each macro is calculated and passed to the user-defined function as

$$\overline{p}_j = p_{in} + \left( j + \frac{1}{2} \right) \frac{\Delta p}{N} \tag{6.21}$$

where

$j$ = macro row index

$p_{in}$ = inlet auxiliary fluid pressure

$\Delta p$ = overall pressure drop across a heat exchanger group

$N$ = number of rows per pass $\times$ number of passes.

To learn how to use the macro heat exchanger models, refer to Using the Ungrouped Macro Heat Exchanger Model and Using the Grouped Macro Heat Exchanger Model in the User's Guide.


Release 15.0 - © SAS IP, Inc. All rights reserved. - Contains proprietary and confidential information of ANSYS, Inc. and its subsidiaries and affiliates.

## 6.2. The Dual Cell Model

The following sections contain information about the theory behind the dual cell heat exchanger model:

6.2.1. Overview of the Dual Cell Model
6.2.2. Restrictions of the Dual Cell Model
6.2.3. Dual Cell Model Theory

### 6.2.1. Overview of the Dual Cell Model

The Macro Model is quite suitable for thin rectangular heat exchanger cores, where the pass-to-pass is perpendicular to the primary flow direction and the auxiliary flow is uniform. Moreover, the mesh should be uniform and structured. However, many practical heat exchangers have a non-rectangular core and the auxiliary fluid, before reaching the core, may pass through arbitrary shaped inlet tanks, which make them highly non-uniform. It is quite possible that due to the complex shape of the core and or ease of meshing, the structured mesh may not be the obvious choice. These shortcomings of the macro model can be easily overcome by using the dual cell heat exchanger model. This model allows the solution of both the primary and auxiliary flow on separate co-located meshes and couples the two flows only through heat transfer at the heat exchanger core.

### 6.2.2. Restrictions of the Dual Cell Model

The following restrictions exist for the dual cell heat exchanger models:

- Heat transfer calculations are based on the NTU method only.
- Multipass heat exchangers cannot be modeled. This will require hooking a UDF.
- In the case of a heat exchanger core with non-matching meshes, the total cell count for the primary and auxiliary core should approximately be the same.

### 6.2.3. Dual Cell Model Theory

The dual cell heat exchanger consists of two porous fluid zones, namely a primary zone and an auxiliary zone. The two zones are solved simultaneously and are coupled only through heat transfer. The common region in each zone, where heat transfer takes place, represents the heat exchanger core. The cores for both primary and auxiliary zones occupy the same physical space, as shown in Figure 6.2: Core with Matching Quad Meshes for Primary and Auxiliary Zones in a Cross-Flow Pattern (p. 184). The cells in the two cores should overlap completely in the physical space to ensure conservative heat transfer. Heat transfer occurs between cells in close proximity based on the cell centroid. In other words, a primary zone cell exchanges heat with one, and only one, auxiliary zone cell and vice versa. Therefore, if one of the core (say primary) mesh is too coarse or fine relative to the other core (say auxiliary) conservation of heat transfer is not ensured. Heat transfer calculations in the dual cell model are based on the NTU method.

*Release 15.0 - © SAS IP, Inc. All rights reserved. - Contains proprietary and confidential information of ANSYS, Inc. and its subsidiaries and affiliates.*

**Figure 6.2: Core with Matching Quad Meshes for Primary and Auxiliary Zones in a Cross-Flow Pattern**

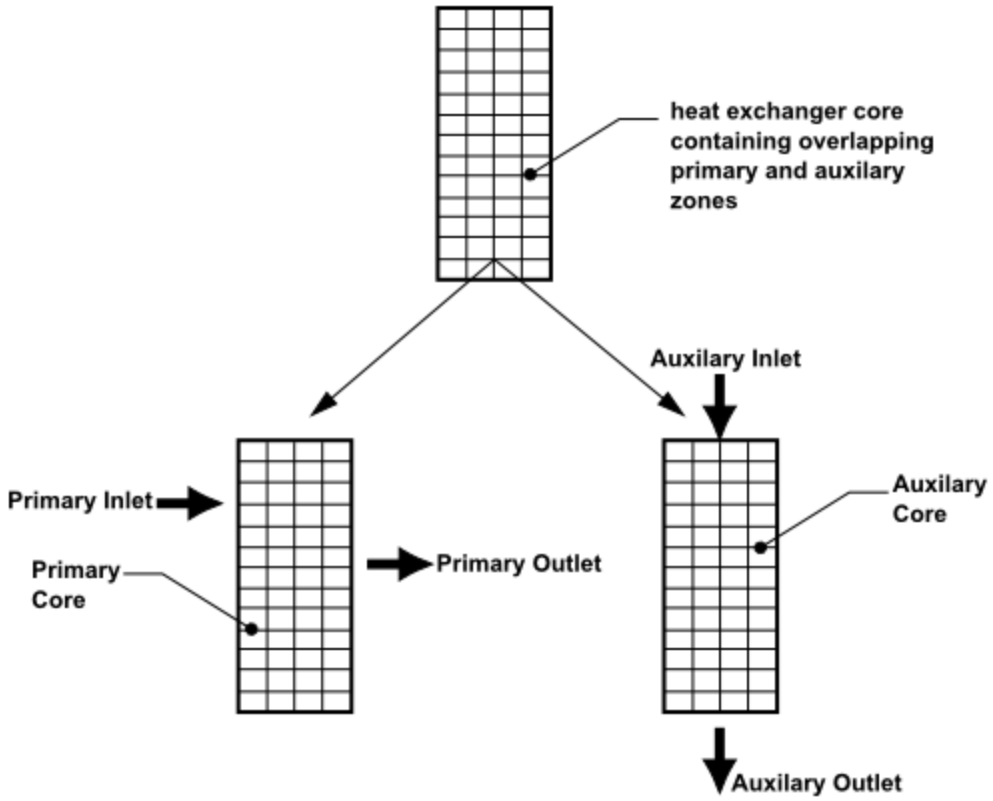


### 6.2.3.1. NTU Relations

In a cross-flow pattern, the NTU values are calculated as in Equation 6.10 (p. 180). The equation is solved iteratively using the Newton-Raphson. For parallel flow, the NTU value is calculated as follows:

$$NTU = \frac{-ln(1-\varepsilon-\varepsilon C_r)}{(C_r+1)} \tag{6.22}$$

and for counter flow, the following equation is used:

$$NTU_{C_r=1} = \frac{\varepsilon}{1-\varepsilon} \tag{6.23}$$

Otherwise,

$$NTU = \frac{1}{(C_r-1)} ln\left[\frac{(1-\varepsilon)}{(1-\varepsilon C_r)}\right] \tag{6.24}$$

where $C_r$ is the heat capacity ratio and $\varepsilon$ is the effectiveness.

### 6.2.3.2. Heat Rejection

Heat rejection is computed for each cell in the two cores (primary and auxiliary) and added as a source term to the energy equation for the respective flows. This is illustrated in Figure 6.3: Core with Primary and Auxiliary Zones with Possible Overlap of Cells (p. 185).


Release 15.0 - © SAS IP, Inc. All rights reserved. - Contains proprietary and confidential information of ANSYS, Inc. and its subsidiaries and affiliates.

**Figure 6.3: Core with Primary and Auxiliary Zones with Possible Overlap of Cells**

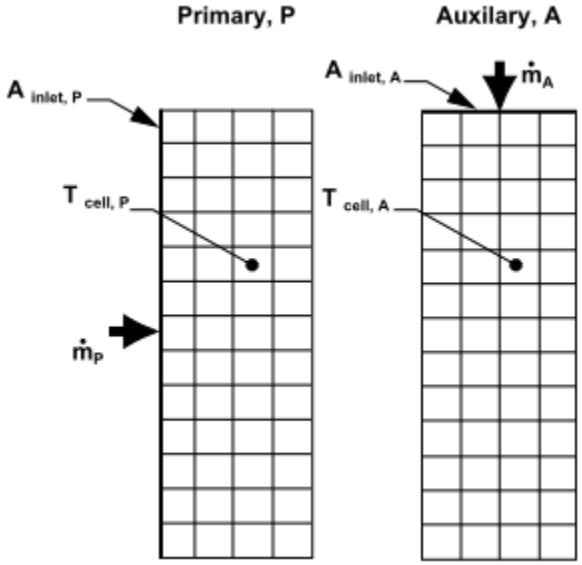


$$\dot{m}_{scaled,A} = \rho_{cell,A} \vec{V}_{cell,A} A_{inlet,A} \tag{6.25}$$

$$\dot{m}_{scaled,P} = \rho_{cell,P} \vec{V}_{cell,P} A_{inlet,P} \tag{6.26}$$

$$C_{min,scaled} = min\left[ \left( C_{p,cell} \dot{m}_{scale} \right) |_P \ , \left( C_{p,cell} \dot{m}_{scale} \right) |_A \right] \tag{6.27}$$

$$NTU_{scaled} = \left[ NTU_{full}\left( \dot{m}_{scaled,P}, \dot{m}_{scaled,A} \right) \right]_{bilinear\ interpolation} \tag{6.28}$$

$$(UA)_{scaled} = NTU_{scaled} C_{min,scaled} \tag{6.29}$$

$$q_{cell} = \frac{(UA)_{scaled}\left( T_{cell,A} - T_{cell,P} \right) V_{cell}}{V_{core}} \tag{6.30}$$

where

$T_{cell,A}$ = auxiliary cell temperature

$T_{cell,P}$ = primary cell temperature

$U$ = overall heat transfer coefficient

$A$ = total heat transfer area

$C_{min,scaled}$ = scaled minimum heat capacity rate

$V_{cell}$ = volume of cell

$V_{core}$

You can supply the NTU values, or it can be calculated using the supplied raw data and the effectiveness-NTU relation that you specify.

To learn how to use the dual cell heat exchanges model, refer to Using the Dual Cell Heat Exchanger Model in the User's Guide.

Release 15.0 - © SAS IP, Inc. All rights reserved. - Contains proprietary and confidential information of ANSYS, Inc. and its subsidiaries and affiliates.

Release 15.0 - © SAS IP, Inc. All rights reserved. - Contains proprietary and confidential information
of ANSYS, Inc. and its subsidiaries and affiliates.

# Chapter 7: Species Transport and Finite-Rate Chemistry

ANSYS Fluent can model the mixing and transport of chemical species by solving conservation equations describing convection, diffusion, and reaction sources for each component species. Multiple simultaneous chemical reactions can be modeled, with reactions occurring in the bulk phase (volumetric reactions) and/or on wall or particle surfaces, and in the porous region. Species transport modeling capabilities, both with and without reactions, are described in this chapter.

Note that you may also want to consider modeling your turbulent reacting flame using the mixture fraction approach (for non-premixed systems, described in Non-Premixed Combustion (p. 215)), the reaction progress variable approach (for premixed systems, described in Premixed Combustion (p. 253)), the partially premixed approach (described in Partially Premixed Combustion (p. 273)), or the composition PDF Transport approach (described in Composition PDF Transport (p. 281)). Modeling multiphase species transport and finite-rate chemistry can be found in Multiphase Flows (p. 465).

Information is divided into the following sections:


7.1. Volumetric Reactions
7.2. Wall Surface Reactions and Chemical Vapor Deposition
7.3. Particle Surface Reactions
7.4. Reacting Channel Model
7.5. Reactor Network Model


For more information about using these models in ANSYS Fluent, see Modeling Species Transport and Finite-Rate Chemistry in the User's Guide.

## 7.1. Volumetric Reactions

Theoretical information about species transport and finite-rate chemistry as related to volumetric reactions is presented in this section. Additional information can be found in the following sections:


7.1.1. Species Transport Equations
7.1.2. The Generalized Finite-Rate Formulation for Reaction Modeling


For more information about using species transport and finite-rate chemistry as related to volumetric reactions, see Volumetric Reactions in the User's Guide.

### 7.1.1. Species Transport Equations

When you choose to solve conservation equations for chemical species, ANSYS Fluent predicts the local mass fraction of each species, $Y_i$, through the solution of a convection-diffusion equation for the $i^{\text{th}}$ species. This conservation equation takes the following general form:

$$\frac{\partial}{\partial t}(\rho Y_i) + \nabla \cdot (\rho \vec{v} Y_i) = -\nabla \cdot \vec{J}_i + R_i + S_i \tag{7.1}$$

where $R_i$ is the net rate of production of species $i$ by chemical reaction (described later in this section) and $S_i$ is the rate of creation by addition from the dispersed phase plus any user-defined sources. An equation of this form will be solved for $N-1$ species where $N$ is the total number of fluid phase

Release 15.0 - © SAS IP, Inc. All rights reserved. - Contains proprietary and confidential information of ANSYS, Inc. and its subsidiaries and affiliates.

chemical species present in the system. Since the mass fraction of the species must sum to unity, the $N$th mass fraction is determined as one minus the sum of the $N-1$ solved mass fractions. To minimize numerical error, the $N^{\text{th}}$ species should be selected as that species with the overall largest mass fraction, such as $N_2$ when the oxidizer is air.

### 7.1.1.1. Mass Diffusion in Laminar Flows

In Equation 7.1 (p. 187), $\vec{J}_i$ is the diffusion flux of species $i$, which arises due to gradients of concentration and temperature. By default, ANSYS Fluent uses the dilute approximation (also called Fick's law) to model mass diffusion due to concentration gradients, under which the diffusion flux can be written as

$$\vec{J}_i = -\rho D_{i,m} \nabla Y_i - D_{T,i} \frac{\nabla T}{T} \tag{7.2}$$

Here $D_{i,m}$ is the mass diffusion coefficient for species $i$ in the mixture, and $D_{T,i}$ is the thermal (Soret) diffusion coefficient.

For certain laminar flows, the dilute approximation may not be acceptable, and full multicomponent diffusion is required. In such cases, the Maxwell-Stefan equations can be solved; see Full Multicomponent Diffusion in the User's Guide for details.

### 7.1.1.2. Mass Diffusion in Turbulent Flows

In turbulent flows, ANSYS Fluent computes the mass diffusion in the following form:

$$\vec{J}_i = -\left(\rho D_{i,m} + \frac{\mu_t}{Sc_t}\right) \nabla Y_i - D_{T,i} \frac{\nabla T}{T} \tag{7.3}$$

where $Sc_t$ is the turbulent Schmidt number ($\frac{\mu_t}{\rho D_t}$ where $\mu_t$ is the turbulent viscosity and $D_t$ is the turbulent diffusivity). The default $Sc_t$ is 0.7. Note that turbulent diffusion generally overwhelms laminar diffusion, and the specification of detailed laminar diffusion properties in turbulent flows is generally not necessary.

### 7.1.1.3. Treatment of Species Transport in the Energy Equation

For many multicomponent mixing flows, the transport of enthalpy due to species diffusion

$$\nabla \cdot \left[ \sum_{i=1}^{n} h_i \vec{J}_i \right]$$

can have a significant effect on the enthalpy field and should not be neglected. In particular, when the Lewis number

$$Le_i = \frac{k}{\rho c_p D_{i,m}} \tag{7.4}$$

for any species is far from unity, neglecting this term can lead to significant errors. ANSYS Fluent will include this term by default. In Equation 7.4 (p. 188), $k$ is the thermal conductivity.


Release 15.0 - © SAS IP, Inc. All rights reserved. - Contains proprietary and confidential information of ANSYS, Inc. and its subsidiaries and affiliates.

#### 7.1.1.4. Diffusion at Inlets

For the pressure-based solver in ANSYS Fluent, the net transport of species at inlets consists of both convection and diffusion components. For the density-based solvers, only the convection component is included. The convection component is fixed by the inlet species mass fraction specified by you. The diffusion component, however, depends on the gradient of the computed species field at the inlet. Thus the diffusion component (and therefore the net inlet transport) is not specified a priori. For information about specifying the net inlet transport of species, see Defining Cell Zone and Boundary Conditions for Species in the User's Guide.

### 7.1.2. The Generalized Finite-Rate Formulation for Reaction Modeling

The reaction rates that appear as source terms in Equation 7.1 (p. 187) are computed in ANSYS Fluent, for turbulent flows, by one of three models:

- Laminar finite-rate model: The effect of turbulent fluctuations are ignored, and reaction rates are determined by Arrhenius kinetic expressions.
- Eddy-dissipation model: Reaction rates are assumed to be controlled by the turbulence, so expensive Arrhenius chemical kinetic calculations can be avoided. The model is computationally cheap, but, for realistic results, only one or two step heat-release mechanisms should be used.
- Eddy-dissipation-concept (EDC) model: Detailed Arrhenius chemical kinetics can be incorporated in turbulent flames. Note that detailed chemical kinetic calculations are computationally expensive.

The generalized finite-rate formulation is suitable for a wide range of applications including laminar or turbulent reaction systems, and combustion systems with premixed, non-premixed, or partially-premixed flames.

#### 7.1.2.1. The Laminar Finite-Rate Model

The laminar finite-rate model computes the chemical source terms using Arrhenius expressions, and ignores the effects of turbulent fluctuations. The model is exact for laminar flames, but is generally inaccurate for turbulent flames due to highly non-linear Arrhenius chemical kinetics. The laminar model may, however, be acceptable for combustion with relatively slow chemistry and small turbulence-chemistry interaction, such as supersonic flames.

The net source of chemical species $i$ due to reaction is computed as the sum of the Arrhenius reaction sources over the $N_R$ reactions that the species participate in:

$$R_i = M_{w,i} \sum_{r=1}^{N_R} \hat{R}_{i,r} \tag{7.5}$$

where $M_{w,i}$ is the molecular weight of species $i$ and $\hat{R}_{i,r}$ is the Arrhenius molar rate of creation/destruction of species $i$ in reaction $r$. Reaction may occur in the continuous phase at wall surfaces.

Consider the $r$th reaction written in general form as follows:

$$\sum_{i=1}^{N} \nu'_{i,r} \mathcal{M}_i \underset{k_{b,r}}{\overset{k_{f,r}}{\rightleftharpoons}} \sum_{i=1}^{N} \nu''_{i,r} \mathcal{M}_i \tag{7.6}$$

where,

$N$ = number of chemical species in the system

$v'_{i,r}$ = stoichiometric coefficient for reactant $i$ in reaction $r$

$v''_{i,r}$ = stoichiometric coefficient for product $i$ in reaction $r$

$\mathcal{M}_i$ = symbol denoting species $i$

$k_{f,r}$ = forward rate constant for reaction $r$

$k_{b,r}$ = backward rate constant for reaction $r$

Equation 7.6 (p. 189) is valid for both reversible and non-reversible reactions. (Reactions in ANSYS Fluent are non-reversible by default.) For non-reversible reactions, the backward rate constant, $k_{b,r}$, is simply omitted.

The summations in Equation 7.6 (p. 189) are for all chemical species in the system, but only species that appear as reactants or products will have non-zero stoichiometric coefficients. Hence, species that are not involved will drop out of the equation.

For a non-reversible reaction (that is, the **Include Backward Reaction** button is disabled), the molar rate of creation/destruction of species $i$ in reaction $r$ ($\hat{R}_{i,r}$ in Equation 7.5 (p. 189)) is given by

$$\hat{R}_{i,r} = \Gamma \left(v''_{i,r} - v'_{i,r}\right) \left( k_{f,r} \prod_{j=1}^{N} \left[C_{j,r}\right]^{\left(\eta'_{j,r} + \eta''_{j,r}\right)} \right) \tag{7.7}$$

where,

$C_{j,r}$ = molar concentration of species $j$ in reaction $r$ ($\mathrm{kmol/m^3}$)

$\eta'_{j,r}$ = rate exponent for reactant species $j$ in reaction $r$

$\eta''_{j,r}$ = rate exponent for product species $j$ in reaction $r$

For a reversible reaction, the molar rate of creation/destruction of species $i$ in reaction $r$ is given by

$$\hat{R}_{i,r} = \Gamma \left(v''_{i,r} - v'_{i,r}\right) \left( k_{f,r} \prod_{j=1}^{N} \left[C_{j,r}\right]^{\eta'_{j,r}} - k_{b,r} \prod_{j=1}^{N} \left[C_{j,r}\right]^{v''_{j,r}} \right) \tag{7.8}$$

Note that the rate exponent for the reverse reaction part in Equation 7.8 (p. 190) is always the product species stoichiometric coefficient ($v''_{j,r}$).

For information about inputting the stoichiometric coefficients and rate exponents for both global forward (non-reversible) reactions and elementary (reversible) reactions, see Inputs for Reaction Definition in the User's Guide.

$\Gamma$ represents the net effect of third bodies on the reaction rate. This term is given by

$$\Gamma = \sum_{j}^{N} \gamma_{j,r} C_j \tag{7.9}$$


Release 15.0 - © SAS IP, Inc. All rights reserved. - Contains proprietary and confidential information of ANSYS, Inc. and its subsidiaries and affiliates.

where $\gamma_{j,r}$ is the third-body efficiency of the $j^{\text{th}}$ species in the $r$th reaction. By default, ANSYS Fluent does not include third-body effects in the reaction rate calculation. You can, however, opt to include the effect of third-body efficiencies if you have data for them.

The forward rate constant for reaction $r$, $k_{f,r}$, is computed using the Arrhenius expression

$$k_{f,r} = A_r T^{\beta_r} e^{-E_r/RT} \tag{7.10}$$

where,

$A_r$ = pre-exponential factor (consistent units)

$\beta_r$ = temperature exponent (dimensionless)

$E_r$ = activation energy for the reaction (J/kmol)

$R$ = universal gas constant (J/kmol-K)

You (or the database) will provide values for $v'_{i,r}$, $v''_{i,r}$, $\eta'_{j,r}$, $\eta''_{j,r}$, $\beta_r$, $A_r$, $E_r$, and, optionally, $\gamma_{j,r}$ during the problem definition in ANSYS Fluent.

If the reaction is reversible, the backward rate constant for reaction $r$, $k_{b,r}$, is computed, by default, from the forward rate constant using the following relation:

$$k_{b,r} = \frac{k_{f,r}}{K_r} \tag{7.11}$$

where $K_r$ is the equilibrium constant for the $r$th reaction, computed from

$$K_r = \exp\left(\frac{\Delta S_r}{R} - \frac{\Delta H_r}{RT}\right)\left(\frac{p_{\text{atm}}}{RT}\right)^{\sum_{i=1}^{N}(v''_{i,r} - v'_{i,r})} \tag{7.12}$$

where $p_{atm}$ denotes atmospheric pressure (101325 Pa). The term within the exponential function represents the change in Gibbs free energy, and its components are computed as follows:

$$\frac{\Delta S_r}{R} = \sum_{i=1}^{N}\left(v''_{i,r} - v'_{i,r}\right)\frac{S_i}{R} \tag{7.13}$$

$$\frac{\Delta H_r}{RT} = \sum_{i=1}^{N}\left(v''_{i,r} - v'_{i,r}\right)\frac{h_i}{RT} \tag{7.14}$$

where $S_i$ and $h_i$ are the entropy and enthalpy of the $i^{\text{th}}$ species evaluated at temperature $T$ and atmospheric pressure. These values are specified in ANSYS Fluent as properties of the mixture material.

ANSYS Fluent also provides the option to explicitly specify the reversible reaction rate parameters (pre-exponential factor, temperature exponent , and activation energy for the reaction) if desired. In this case, the backward rate constant of the reversible reaction $r$ is computed using the relationship similar to Equation 7.10 (p. 191):

$$k_{b,r} = A_{b,r} T^{\beta_{b,r}} e^{-E_{b,r}/RT} \tag{7.15}$$

where,

$A_{b,r}$ = backward reaction pre-exponential factor (consistent units)

$\beta_{b,r}$ = backward reaction temperature exponent (dimensionless)

$E_{b,r}$ = backward reaction activation energy for the reaction (J/kmol)

For more information about specifying the backward reaction rate parameters, see Inputs for Reaction Definition in the *Fluent User's Guide*.

### 7.1.2.2. Pressure-Dependent Reactions

ANSYS Fluent can use one of three methods to represent the rate expression in pressure-dependent (or pressure fall-off) reactions. A "fall-off" reaction is one in which the temperature and pressure are such that the reaction occurs between Arrhenius high-pressure and low-pressure limits, and therefore is no longer solely dependent on temperature.

There are three methods of representing the rate expressions in this fall-off region. The simplest one is the Lindemann [255] (p. 743) form. There are also two other related methods, the Troe method [140] (p. 736) and the SRI method [436] (p. 753), that provide a more accurate description of the fall-off region.

Arrhenius rate parameters are required for both the high- and low-pressure limits. The rate coefficients for these two limits are then blended to produce a smooth pressure-dependent rate expression. In Arrhenius form, the parameters for the high-pressure limit ($k$) and the low-pressure limit ($k_{low}$) are as follows:

$$k = AT^{\beta}e^{-E/RT} \tag{7.16}$$

$$k_{low} = A_{low}T^{\beta_{low}}e^{-E_{low}/RT} \tag{7.17}$$

The net rate constant at any pressure is then taken to be

$$k_{net}=k\left(\frac{p_r}{1+p_r}\right)F \tag{7.18}$$

where $p_r$ is defined as

$$p_r=\frac{k_{low}[M]}{k} \tag{7.19}$$

and $[M]$ is the concentration of the bath gas, which can include third-body efficiencies. If the function $F$ in Equation 7.18 (p. 192) is unity, then this is the Lindemann form. ANSYS Fluent provides two other forms to describe $F$, namely the Troe method and the SRI method.

In the Troe method, $F$ is given by

$$\log F=\left\{1+\left[\frac{\log p_r+c}{n-d\left(\log p_r+c\right)}\right]^2\right\}^{-1}\log F_{cent} \tag{7.20}$$

where


Release 15.0 - © SAS IP, Inc. All rights reserved. - Contains proprietary and confidential information of ANSYS, Inc. and its subsidiaries and affiliates.

$$\begin{aligned} c &= -0.4 - 0.67 \log F_{cent} \\ n &= 0.75 - 1.27 \log F_{cent} \\ d &= 0.14 \end{aligned} \tag{7.21}$$

and

$$F_{cent} = (1-\alpha)\, e^{-T/T_1} + \alpha e^{-T/T_2} + e^{-T_3/T} \tag{7.22}$$

The parameters $\alpha$, $T_3$, $T_2$, and $T_1$ are specified as inputs.

In the SRI method, the blending function $F$ is approximated as

$$F = d\left[ a \exp\left(\frac{-b}{T}\right) + \exp\left(\frac{-T}{c}\right)\right]^{X} T^{e} \tag{7.23}$$

where

$$X = \frac{1}{1 + \log^2 p_r} \tag{7.24}$$

In addition to the three Arrhenius parameters for the low-pressure limit ($k_{low}$) expression, you must also supply the parameters $a$, $b$, $c$, $d$, and $e$ in the $F$ expression.

For Chemically Activated Bimolecular pressure dependent reactions, the net rate constant at any pressure is

$$k_{net} = k_{low}\left(\frac{1}{1+p_r}\right) F \tag{7.25}$$

**Important**

Chemical kinetic mechanisms usually contain a wide range of time scales and form a set of highly non-linear, stiff coupled equations. For solution procedure guidelines, see Solution Procedures for Chemical Mixing and Finite-Rate Chemistry in the User's Guide. Also, if you have a chemical mechanism in CHEMKIN [203] (p. 740) format, you can import this mechanism into ANSYS Fluent. See Importing a Volumetric Kinetic Mechanism in CHEMKIN Format in the User's Guide.

### 7.1.2.3. The Eddy-Dissipation Model

Most fuels are fast burning, and the overall rate of reaction is controlled by turbulent mixing. In non-premixed flames, turbulence slowly convects/mixes fuel and oxidizer into the reaction zones where they burn quickly. In premixed flames, the turbulence slowly convects/mixes cold reactants and hot products into the reaction zones, where reaction occurs rapidly. In such cases, the combustion is said to be mixing-limited, and the complex, and often unknown, chemical kinetic rates can be safely neglected.

ANSYS Fluent provides a turbulence-chemistry interaction model, based on the work of Magnussen and Hjertager [280] (p. 744), called the eddy-dissipation model. The net rate of production of species $i$ due to reaction $r$, $R_{i,r}$, is given by the smaller (that is, limiting value) of the two expressions below:

Release 15.0 - © SAS IP, Inc. All rights reserved. - Contains proprietary and confidential information of ANSYS, Inc. and its subsidiaries and affiliates.

$$R_{i,r} = v'_{i,r} M_{w,i} A \rho \frac{\varepsilon}{k} \min_{\mathcal{R}} \left( \frac{Y_{\mathcal{R}}}{v'_{\mathcal{R},r} M_{w,\mathcal{R}}} \right) \tag{7.26}$$

$$R_{i,r} = v'_{i,r} M_{w,i} A B \rho \frac{\varepsilon}{k} \frac{\sum_P Y_P}{\sum_j^N v''_{j,r} M_{w,j}} \tag{7.27}$$

where,

$Y_P$ = the mass fraction of any product species, $P$

$Y_{\mathcal{R}}$ = the mass fraction of a particular reactant, $\mathcal{R}$

$A$ = an empirical constant equal to 4.0

$B$ = an empirical constant equal to 0.5

In Equation 7.26 (p. 194) and Equation 7.27 (p. 194), the chemical reaction rate is governed by the large-eddy mixing time scale, $k/\varepsilon$, as in the eddy-breakup model of Spalding [429] (p. 752). Combustion proceeds whenever turbulence is present ($k/\varepsilon > 0$), and an ignition source is not required to initiate combustion. This is usually acceptable for non-premixed flames, but in premixed flames, the reactants will burn as soon as they enter the computational domain, upstream of the flame stabilizer. To remedy this, ANSYS Fluent provides the finite-rate/eddy-dissipation model, where both the Arrhenius (Equation 7.8 (p. 190)), and eddy-dissipation (Equation 7.26 (p. 194) and Equation 7.27 (p. 194)) reaction rates are calculated. The net reaction rate is taken as the minimum of these two rates. In practice, the Arrhenius rate acts as a kinetic "switch", preventing reaction before the flame holder. Once the flame is ignited, the eddy-dissipation rate is generally smaller than the Arrhenius rate, and reactions are mixing-limited.

**Important**

- Although ANSYS Fluent allows multi-step reaction mechanisms (number of reactions $>2$) with the eddy-dissipation and finite-rate/eddy-dissipation models, these will likely produce incorrect solutions. The reason is that multi-step chemical mechanisms are based on Arrhenius rates, which differ for each reaction. In the eddy-dissipation model, every reaction has the same, turbulent rate, and therefore the model should be used only for one-step (reactant → product), or two-step (reactant → intermediate, intermediate → product) global reactions. The model cannot predict kinetically controlled species such as radicals. To incorporate multi-step chemical kinetic mechanisms in turbulent flows, use the EDC model (described in The Eddy-Dissipation Model for LES (p. 194)).
- The eddy-dissipation model requires products to initiate reaction (see Equation 7.27 (p. 194)). When you initialize the solution for steady flows, ANSYS Fluent sets all species mass fractions to a maximum in the user-specified initial value and 0.01. This is usually sufficient to start the reaction. However, if you converge a mixing solution first, where all product mass fractions are zero, you may then have to patch products into the reaction zone to ignite the flame. For details, see Ignition in Combustion Simulations in the User's Guide.

### 7.1.2.4. The Eddy-Dissipation Model for LES

When the LES turbulence model is used, the turbulent mixing rate, $\varepsilon/k$ in Equation 7.26 (p. 194) and Equation 7.27 (p. 194), is replaced by the subgrid-scale mixing rate. This is calculated as


Release 15.0 - © SAS IP, Inc. All rights reserved. - Contains proprietary and confidential information of ANSYS, Inc. and its subsidiaries and affiliates.

$$\tau_{sgs}^{-1} = \sqrt{2S_{ij}S_{ij}} \tag{7.28}$$

where,

$\tau_{sgs}^{-1}$ = subgrid-scale mixing rate ($s^{-1}$)

$S_{ij} = \frac{1}{2}\left(\frac{\partial u_i}{\partial x_j} + \frac{\partial u_j}{\partial x_i}\right)$ = strain rate tensor ($s^{-1}$)

### 7.1.2.5. The Eddy-Dissipation-Concept (EDC) Model

The eddy-dissipation-concept (EDC) model is an extension of the eddy-dissipation model to include detailed chemical mechanisms in turbulent flows [279] (p. 744). It assumes that reaction occurs in small turbulent structures, called the fine scales. The length fraction of the fine scales is modeled as [145] (p. 736)

$$\xi^* = C_\xi \left(\frac{\nu\varepsilon}{k^2}\right)^{1/4} \tag{7.29}$$

where $^*$ denotes fine-scale quantities and

$C_\xi$ = volume fraction constant = 2.1377

$\nu$ = kinematic viscosity

The volume fraction of the fine scales is calculated as $\xi^{*3}$. Species are assumed to react in the fine structures over a time scale

$$\tau^* = C_\tau \left(\frac{\nu}{\varepsilon}\right)^{1/2} \tag{7.30}$$

where $C_\tau$ is a time scale constant equal to 0.4082.

When the LES turbulence model is used, $k$ and $\varepsilon$ represent the sub-grid scale turbulent kinetic energy and its dissipation, respectively.

In ANSYS Fluent, combustion at the fine scales is assumed to occur as a constant pressure reactor, with initial conditions taken as the current species and temperature in the cell. Reactions proceed over the time scale $\tau^*$, governed by the Arrhenius rates of Equation 7.8 (p. 190), and are integrated numerically using the ISAT algorithm [358] (p. 748). ISAT can accelerate the chemistry calculations by two to three orders of magnitude, offering substantial reductions in run-times. Details about the ISAT algorithm may be found in Particle Reaction (p. 285) and In-Situ Adaptive Tabulation (ISAT) (p. 289). ISAT is very powerful, but requires some care. See Using ISAT Efficiently the User's Guide for details on using ISAT efficiently.

The source term in the conservation equation for the mean species $i$, Equation 7.1 (p. 187), is modeled as

$$R_i = \frac{\rho(\xi^*)^2}{\tau^*\left[1-(\xi^*)^3\right]}(Y_i^* - Y_i) \tag{7.31}$$

Release 15.0 - © SAS IP, Inc. All rights reserved. - Contains proprietary and confidential information of ANSYS, Inc. and its subsidiaries and affiliates.

where $Y_i^*$ is the fine-scale species mass fraction after reacting over the time $\tau^*$.

The EDC model can incorporate detailed chemical mechanisms into turbulent reacting flows. However, typical mechanisms are invariably stiff and their numerical integration is computationally costly. Hence, the model should be used only when the assumption of fast chemistry is invalid, such as modeling the slow CO burnout in rapidly quenched flames, or the NO conversion in selective non-catalytic reduction (SNCR).

For guidelines on obtaining a solution using the EDC model, see Solution of Stiff Laminar Chemistry Systems in the User's Guide.

### 7.1.2.6. The Thickened Flame Model

Premixed flames have typical laminar flame thicknesses of the order of a millimeter. Since the laminar flame propagation speed is determined by species diffusion, heat conduction and chemical reaction within the flame, sufficient grid resolution inside the flame is necessary to predict the correct laminar flame velocity. In contrast, the combustor dimensions are usually much larger than the laminar flame thickness and the flame cannot be affordably resolved, even with unstructured and solution-adaptive grids.

The premixed laminar flame speed, denoted $U_l$, is proportional to $\sqrt{DR}$ where $D$ is a diffusivity and $R$ is a reaction rate. The laminar flame thickness is proportional to $D/U_l$. Hence, the laminar flame can be artificially thickened, without altering the laminar flame speed, by increasing the diffusivity and decreasing the reaction rate proportionally. The thickened flame can then be feasibly resolved on a coarse mesh while still capturing the correct laminar flame speed.

The thickening factor $F$ is calculated in ANSYS Fluent as

$$F = \frac{N\Delta}{\delta} \tag{7.32}$$

where $\Delta$ is the grid size, $\delta$ is the laminar flame thickness, and $N$ is the user-specified number of points in the flame (default of 8). The grid-size, $\Delta$, is determined as $V^{1/d}$ where $V$ is the cell volume and $d$ is the spatial dimension (2 or 3). The laminar flame thickness, $\delta$, is a user-input, and may be specified as a constant, a User-Defined Function, or calculated as $D/U_l$, where $D$ is the thermal diffusivity evaluated as $k/\rho c_p$ ($k$ is the thermal conductivity, $\rho$ is the density and $c_p$ is the specific heat).

All species diffusion coefficients, as well as the thermal conductivity, are multiplied by the thickening factor, $F$, and all reaction rates are divided by $F$. However, away from the flame, these enhanced diffusivities can cause erroneous mixing and heat-transfer, so the flame is dynamically thickened only in a narrow band around the reaction front. This band is calculated by multiplying $F$ with, a factor $\Omega$ calculated as

$$\Omega = \tanh\left(\beta \frac{\overline{|R|}}{\max\left(\overline{|R|}\right)}\right) \tag{7.33}$$

In Equation 7.33 (p. 196), $\overline{|R|}$ is the spatially filtered absolute value of the reaction rate, and $\beta$ is a constant with a default value of 10. The absolute reaction rate is filtered several times, and $\max\left(\overline{|R|}\right)$ is the


Release 15.0 - © SAS IP, Inc. All rights reserved. - Contains proprietary and confidential information of ANSYS, Inc. and its subsidiaries and affiliates.

maximum value of $\beta$ in the domain. $\Omega$ ranges from unity in the band around the flame to zero outside this band.

The Thickened Flame Model (TFM) [333] (p. 747) is most often used with a single step chemical mechanism where the global reaction has been tuned to provide the correct laminar flame speed. Since the flame is thickened to be resolved on the mesh, the non-stiff species solver is usually stable. The TFM can, in principal, be used with multi-step reaction mechanisms, however all composition profiles should be adequately resolved within the flame. The stiff-chemistry solver may be necessary for numerical stability when all species time and length scales are not resolved. The TFM is available in both the pressure-based as well as density-based solvers.

While the TFM can be used to model laminar flames, its most common application is as an LES combustion model for turbulent premixed and partially-premixed flames. The turbulent flame speed of a premixed flame is determined principally by the flame wrinkling, which increases the flame surface area. In a turbulent flow-field, a thick flame wrinkles less than a thin flame, so the diffusivities and reaction rates in the TFM are both multiplied by an efficiency factor, denoted $E$, to increase the flame speed. This efficiency factor is calculated using the turbulent flame speed closure model of Zimont (see Equation 9.9 (p. 257)), which can be written as

$$\frac{U_t}{U_l} = 1 + A\left(\frac{u'}{U_l}\right)^{3/4}\left(\frac{l_t}{\delta}\right)^{1/4} \tag{7.34}$$

where $U_t$ is the turbulent flame speed, $A$ is a constant, and $u'$ and $l_t$ are turbulent velocity and length scales. Note that $U_t$ is the turbulent flame speed due to the wrinkling effect of turbulence with eddy length scales less than $l_t$. In a RANS simulation, $u'$ is the RMS velocity and $l_t$ is the turbulence integral scale, as Equation 9.9. In an LES, $u'$ and $l_t$ are the sub-grid velocity fluctuation and length scales, as in Equation 9.13 (p. 259) and Equation 9.14 (p. 259). The TFM efficiency factor, $E$, is then calculated as the ratio of the sub-grid turbulent flame speeds at length scales of $\mathrm{F}\Delta$ and $\Delta$:

$$E = \frac{1 + A\left(\frac{u'}{U_l}\right)^{3/4}\left(\frac{\Delta}{\delta}\right)^{1/4}}{1 + A\left(\frac{u'}{U_l}\right)^{3/4}\left(\frac{\Delta}{F\delta}\right)^{1/4}} \tag{7.35}$$

All species reaction rates are multiplied by $E/F$. The effective species diffusivities (and thermal conductivity) in each cell are dynamically determined as

$$D_{eff} = D_{lam}E\left(1 + (F-1)\Omega\right) + D_{turb}\left(1-\Omega\right) \tag{7.36}$$

where $D_{lam}$ is the molecular (laminar) diffusivity and $D_{turb}$ is the turbulent diffusivity. $D_{lam}$ may be computed with any of the available methods in ANSYS Fluent, including kinetic theory and User Defined Functions (UDFs). Since the kinetic coefficients of 1-step reactions are invariably adjusted to capture the actual laminar flame speed, the same transport properties that are used in this tuning simulation should be used in the TFM simulation. In the narrow band around the flame where $\Omega$ is one, the turbulent diffusivities are switched off and the molecular diffusivities are enhanced by a factor $\mathrm{EF}$. Away from the flame where $\Omega$ is zero, the effective diffusivity is the non-thickened value of $D_{lam}+D_{turb}$.

Release 15.0 - © SAS IP, Inc. All rights reserved. - Contains proprietary and confidential information of ANSYS, Inc. and its subsidiaries and affiliates.

### 7.1.2.7. The Relaxation to Chemical Equilibrium Model

When using the laminar-finite-rate (LFR), eddy-dissipation (ED), finite-rate/eddy-dissipation (FR/ED) or EDC model, as described above, chemical species evolve according to the prescribed kinetic mechanism. In the Relaxation to Chemical Equilibrium model, the reaction source term in the $i$th mean species conservation equation (Equation 7.1 (p. 187)), is modeled as

$$R_i = \rho \frac{Y_i^{eq} - Y_i}{\tau_{char}} \tag{7.37}$$

where,

$\rho$ = the density

$Y_i$ = the mean mass fraction of species $i$

superscript $eq$ denotes chemical equilibrium

$\tau_{char}$ = a characteristic time-scale

Equation 7.37 (p. 198) implies that species react toward their chemical equilibrium state over the characteristic time, $\tau_{char}$, as in the Characteristic Time model [217] (p. 741). Since chemical equilibrium does not depend on any kinetic mechanism, for a given $\tau_{char}$, the reaction source term in Equation 7.37 (p. 198) is independent of the reaction mechanism.

The Relaxation to Chemical Equilibrium model is an option available for LFR, ED and FR/ED turbulence-chemistry interaction models. For the LFR model, the characteristic time is calculated as

$$\tau_{char} = \tau_{flow} + \tau_{chem} \tag{7.38}$$

where $\tau_{flow}$ is a convection/diffusion time-scale in a cell. $\tau_{chem}$ is a cell chemical time-scale modeled as

$$\tau_{chem} = c_{chem} \min_f \left( \frac{Y_f}{dY_f/dt} \right) \tag{7.39}$$

In Equation 7.39 (p. 198), $c_{chem}$ is a model constant (default of 1), index $f$ denotes the user-specified fuel species, $Y_f$ is the fuel species mass fraction, and $dY_f/dt$ is the rate of change of the fuel species mass fraction, while $\min$ denotes the minimum over all specified fuel species. Hence, $\tau_{chem}$ represents a chemical ignition time-scale for the fuel species, and is used to prevent a premixed flame from auto-igniting, similar to the FR/ED model. Note that a kinetic mechanism is required to evaluate $\tau_{chem}$.

For the ED model, the characteristic time-scale is evaluated as $\tau_{char} = \tau_{turb}$. where the turbulent time-scale is $\tau_{turb} = k / (\epsilon A)$, and the default turbulent rate constant is $A = 4$. For the FR/ED model, the characteristic time-scale is calculated as $\tau_{char} = \tau_{turb} + \tau_{chem}$. Typically, the ED and FR/ED models employ a 1-step reaction, or a 2-step reaction where hydrocarbons pyrolize to $CO$, which then oxidizes to $CO_2$. The Relaxation to Chemical Equilibrium model can be considered as an extension of the ED type models where species react towards chemical equilibrium instead of complete reaction. The model should provide more accurate predictions of intermediate species such as $CO$ and radicals required for NOx modeling such as $O$ and $OH$.

Since chemical equilibrium calculations are typically less computationally expensive than detailed chemistry simulations, the Relaxation to Chemical equilibrium can be used as a good initial condition


Release 15.0 - © SAS IP, Inc. All rights reserved. - Contains proprietary and confidential information of ANSYS, Inc. and its subsidiaries and affiliates.

for full kinetic simulations. The model can also be used in lieu of the Eddy-Dissipation model where the solution tends to chemical equilibrium instead of complete reaction.

The assumption of chemical equilibrium can lead to large errors in rich zones for hydrocarbon fuels. ANSYS Fluent offers the option of reducing the reaction rate in Equation 7.37 (p. 198) by increasing the characteristic time-scale $\tau_{char}$ in rich zones. With this option, the local equivalence ratio in a cell is calculated as

$$\phi = \frac{2X_C + X_H/2}{X_O} \tag{7.40}$$

where $Y_O$, $Y_H$, and $Y_C$ denote the atomic mass fraction of oxygen, hydrogen and carbon. The time-scale, $\tau_{char}$, is then multiplied by a factor $e^{\beta(\phi-\phi_{rich})}$ when the local equivalence ratio $\phi$ exceeds the specified rich equivalence ratio $\phi_{rich}$. The default rich equivalence ratio is 1, and the default exponential factor, $\beta$, is 2. The option to enable the slow reaction rate in rich mixtures is available in the text interface.

Since chemical equilibrium calculations are computationally costly, ISAT tabulation is always used. Initial ANSYS Fluent iterations are relatively slow as the ISAT table is built, but speed up significantly as the table is filled and queries to the table are interpolated. Since chemical equilibrium compositions are uniquely determined by the species elements and initial temperature and pressure of the mixture, the ISAT table dimensions are $\mathrm{N}_{elements}+1$ for isobaric systems. In most combustion cases, the number of elements are much smaller than the number of chemical species, and the ISAT table is filled relatively quickly.

## 7.2. Wall Surface Reactions and Chemical Vapor Deposition

For gas-phase reactions, the reaction rate is defined on a volumetric basis and the rate of creation and destruction of chemical species becomes a source term in the species conservation equations. For surface reactions, the rate of adsorption and desorption is governed by both chemical kinetics and diffusion to and from the surface. Wall surface reactions therefore create sources and sinks of chemical species in the gas phase, as well as on the reacting surface.

Theoretical information about wall surface reactions and chemical vapor deposition is presented in this section. Information can be found in the following sections:

7.2.1. Surface Coverage Reaction Rate Modification
7.2.2. Reaction-Diffusion Balance for Surface Chemistry
7.2.3. Slip Boundary Formulation for Low-Pressure Gas Systems

For more information about using wall surface reactions and chemical vapor deposition, see Wall Surface Reactions and Chemical Vapor Deposition in the User's Guide.

Consider the $r$th wall surface reaction written in general form as follows:

$$\sum_{i=1}^{N_g} g'_{i,r} G_i + \sum_{i=1}^{N_b} b'_{i,r} B_i + \sum_{i=1}^{N_s} s'_{i,r} S_i \quad \Leftrightarrow \frac{k_{f,r}}{k_{b,r}} \Leftrightarrow \quad \sum_{i=1}^{N_g} g''_{i,r} G_i + \sum_{i=1}^{N_b} b''_{i,r} B_i + \sum_{i=1}^{N_s} s''_{i,r} S_i \tag{7.41}$$

where $G_i$, $B_i$, and $S_i$ represent the gas phase species, the bulk (or solid) species, and the surface-adsorbed (or site) species, respectively. $N_g$, $N_b$, and $N_s$ are the total numbers of these species. $g'_{i,r}$, $b'_{i,r}$, and $s'_{i,r}$ are the stoichiometric coefficients for each reactant species $i$, and $g''_{i,r}$, $b''_{i,r}$, and $s''_{i,r}$ are the stoichiometric

coefficients for each product species $i$. $k_{f,r}$ and $k_{b,r}$ are the forward and backward rate of reactions, respectively.

The summations in Equation 7.41 (p. 199) are for all chemical species in the system, but only species involved as reactants or products will have non-zero stoichiometric coefficients. Hence, species that are not involved will drop out of the equation.

The rate of the $r$th reaction is

$$\mathcal{R}_r = k_{f,r}\left(\prod_{i=1}^{N_g}[C_i]_{wall}^{\eta'_{i,g,r}}\right)\left(\prod_{j=1}^{N_s}[S_j]_{wall}^{\eta'_{j,s,r}}\right) - k_{b,r}\left(\prod_{i=1}^{N_g}[C_i]_{wall}^{\eta''_{i,g,r}}\right)\left(\prod_{j=1}^{N_s}[S_j]_{wall}^{\eta''_{j,s,r}}\right) \tag{7.42}$$

where $[]_{wall}$ represents molar concentrations of surface-adsorbed species on the wall. $\eta'_{i,g,r}$ and $\eta''_{i,g,r}$ are the rate exponents for the $i^{th}$ gaseous species as reactant and product, respectively, in the reaction. The variables $\eta'_{j,s,r}$ and $\eta''_{j,s,r}$ are the rate exponents for the $j^{th}$ site species as reactant and product in the reaction. It is assumed that the reaction rate does not depend on concentrations of the bulk (solid) species. From this, the net molar rate of production or consumption of each species $i$ is given by

$$\hat{R}_{i,gas} = \sum_{r=1}^{N_{rxn}}\left(g''_{i,r} - g'_{i,r}\right)\mathcal{R}_r \quad i = 1,2,3,\ldots,N_g \tag{7.43}$$

$$\hat{R}_{i,bulk} = \sum_{r=1}^{N_{rxn}}\left(b''_{i,r} - b'_{i,r}\right)\mathcal{R}_r \quad i = 1,2,3,\ldots,N_b \tag{7.44}$$

$$\hat{R}_{i,site} = \sum_{r=1}^{N_{rxn}}\left(s''_{i,r} - s'_{i,r}\right)\mathcal{R}_r \quad i = 1,2,3,\ldots,N_s \tag{7.45}$$

The forward rate constant for reaction $r$ ($k_{f,r}$) is computed using the Arrhenius expression,

$$k_{f,r} = A_r T^{\beta_r} e^{-E_r/RT} \tag{7.46}$$

where,

$A_r$ = pre-exponential factor (consistent units)

$\beta_r$ = temperature exponent (dimensionless)

$E_r$ = activation energy for the reaction (J/kmol)

$R$ = universal gas constant (J/kmol-K)

You (or the database) will provide values for $g'_{i,r}$, $g''_{i,r}$, $b'_{i,r}$, $b''_{i,r}$, $s'_{i,r}$, $s''_{i,r}$, $\beta_r$, $A_r$, and $E_r$.

To include the mass transfer effects and model heat release, refer to Including Mass Transfer To Surfaces in Continuity, Wall Surface Mass Transfer Effects in the Energy Equation, and Modeling the Heat Release Due to Wall Surface Reactions in the User's Guide.


Release 15.0 - © SAS IP, Inc. All rights reserved. - Contains proprietary and confidential information of ANSYS, Inc. and its subsidiaries and affiliates.

If the reaction is reversible, the backward rate constant for reaction $r$, $k_{b,r}$ is computed from the forward rate constant using the following relation:

$$k_{b,r}=\frac{k_{f,r}}{K_r} \tag{7.47}$$

where $K_r$ is the equilibrium constant for $r$th reaction computed from

$$K_r=\exp\left(\frac{\Delta S_r}{R}-\frac{\Delta H_r}{RT}\right)\left(\frac{p_{atm}}{RT}\right)^{\sum_{i=1}^{N_g}\left(\upsilon''_{i,r}-\upsilon'_{i,r}\right)}\prod_{k=1}^{N_{types}}\left(\rho_s\right)_k^{\sum_{j=1}^{N_{s,k}}\left(\upsilon''_{j,k,r}-\upsilon'_{j,k,r}\right)} \tag{7.48}$$

where $p_{atm}$ denotes the atmospheric pressure (101325 Pa). The term within the exponential function represents the change in the Gibbs free energy, and its components are computed per Equation 7.13 (p. 191) and Equation 7.14 (p. 191).

$N_{types}$ is the number of different types of sites, $\left(\rho_s\right)_k$ is the site density of site type $k$. $\upsilon'_{j,k,r}$ and $\upsilon''_{j,k,r}$ are the stoichiometric coefficients of the $j$th site species of type $k$ in reaction $r$.

## 7.2.1. Surface Coverage Reaction Rate Modification

ANSYS Fluent has the option to modify the surface reaction rate as a function of species site coverages. In such cases, the forward rate constant for the $r$th reaction is evaluated as,

$$k_{f,r}=A_r T^{\beta_r} e^{-E_r/RT}\prod_{k_{site}}\left(10^{Z_k\eta_{k,r}}\right)\left(Z_k{}^{\mu_{k,r}}\right)\left(e^{-\varepsilon_{k,r}Z_k/RT}\right) \tag{7.49}$$

In Equation 7.49 (p. 201), the three surface coverage rate modification parameters for species $k$ in reaction $r$ are $\eta_{k,r}$, $\mu_{k,r}$ and $\varepsilon_{k,r}$. These parameters default to zero for reaction species that are not surface rate modifying. The surface (coverage) site fraction, $Z_k$ is the fraction of surface sites covered by species $k$, and is defined as,

$$Z_k=[S_k]/\rho_{site} \tag{7.50}$$

where $[S_k]$ is the surface site concentration and $\rho_{site}$ is the surface site density (see Equation 7.55 (p. 202)).

## 7.2.2. Reaction-Diffusion Balance for Surface Chemistry

Reactions at surfaces change gas-phase, surface-adsorbed (site) and bulk (solid) species. On reacting surfaces, the mass flux of each gas species due to diffusion and convection to/from the surface is balanced with its rate of consumption/production on the surface,

$$\rho_{wall}D_i\frac{\partial Y_{i,wall}}{\partial n}-\dot{m}_{dep}Y_{i,wall} = M_{w,i}\hat{R}_{i,gas} \quad i=1,2,3,\ldots,N_g \tag{7.51}$$

$$\frac{\partial [S_i]_{wall}}{\partial t} = \hat{R}_{i,site} \quad i=1,2,3,\ldots,N_s \tag{7.52}$$

The wall mass fraction $Y_{i,wall}$ is related to concentration by

$$[G_i]_{wall}=\frac{\rho_{wall}Y_{i,wall}}{M_{w,i}} \tag{7.53}$$

$\dot{m}_{dep}$ is the net rate of mass deposition or etching as a result of surface reaction; that is,

$$\dot{m}_{dep} = \sum_{i=1}^{N_b} M_{w,i} \hat{R}_{i,bulk} \tag{7.54}$$

$[S_i]_{wall}$ is the site species concentration at the wall, and is defined as

$$[S_i]_{wall} = \rho_{site} Z_i \tag{7.55}$$

where $\rho_{site}$ is the site density and $Z_i$ is the site coverage of species $i$.

Equation 7.51 (p. 201) and Equation 7.52 (p. 201) are solved for the dependent variables $Y_{i,wall}$ and $Z_i$ using a point-by-point coupled Newton solver. When the Newton solver fails, Equation 7.51 (p. 201) and Equation 7.52 (p. 201) are solved by time marching in an ODE solver until convergence. If the ODE solver fails, reaction-diffusion balance is disabled, $Y_{i,wall}$ is assumed equal to the cell-center value $Y_{i,cell}$, and only the site coverages $Z_i$ are advanced in the ODE solver to convergence. You can manually disable reaction-diffusion balance with the text interface command `define/models/species/disable-diffusion-reaction-balance`.

The effective gas-phase reaction source terms are then available for solution of the gas-phase species transport Equation 7.1 (p. 187).

The diffusion term in Equation 7.51 (p. 201) is calculated as the difference in the species mass fraction at the cell center and the wall-face center, divided by the normal distance between these center points. ANSYS Fluent can model unresolved surface washcoats, which greatly increase the catalytic surface area, with the **Surface Area Washcoat Factor**. The surface washcoat increases the area available for surface reaction. ANSYS Fluent can also model surface chemistry on unresolved walls using a porous media model. This model is appropriate for catalytic tube-banks or porous foam matrices where it is not feasible to resolve the individual walls. When surface reaction is enabled in porous cell zones, the **Surface-to-Volume Ratio** must be specified. The wall normal distance required for the diffusion term in Equation 7.51 (p. 201) is calculated as the inverse of the surface-to-volume ratio.

## 7.2.3. Slip Boundary Formulation for Low-Pressure Gas Systems

Most semiconductor fabrication devices operate far below atmospheric pressure, typically only a few millitorrs. At such low pressures, the fluid flow is in the slip regime and the normally used no-slip boundary conditions for velocity and temperature are no longer valid.

The Knudsen number, denoted $Kn$, and defined as the ratio of mean free path to a characteristic length scale of the system, is used to quantify continuum flow regimes. Since the mean free path increases as the pressure is lowered, the high end of $Kn$ values represents *free molecular flow* and the low end the continuum regime. The range in between these two extremes is called the slip regime ($0.01<Kn<0.1$) [34] (p. 730) In the slip regime, the gas-phase velocity at a solid surface differs from the velocity at which the wall moves, and the gas temperature at the surface differs from the wall temperature. Maxwell's models are adopted for these physical phenomena in ANSYS Fluent for their simplicity and effectiveness.

- velocity slip

$$U_w - U_g = \left( \frac{2-\alpha_v}{\alpha_v} \right) Kn L_c \frac{\partial U}{\partial n} \approx \left( \frac{2-\alpha_v}{\alpha_v} \right) \frac{\lambda}{\delta} (U_g - U_c) \tag{7.56}$$

$$V_g \equiv (\vec{V} \cdot \vec{n})_g = V_w \tag{7.57}$$


Release 15.0 - © SAS IP, Inc. All rights reserved. - Contains proprietary and confidential information of ANSYS, Inc. and its subsidiaries and affiliates.

Here, $U$ and $V$ represent the velocity components that are parallel and normal to the wall, respectively. The subscripts $g$, $w$ and $c$ indicate gas, wall and cell-center velocities. $\delta$ is the distance from cell center to the wall. $L_c$ is the characteristic length. $\alpha_v$ is the momentum accommodation coefficient of the gas mixture and its value is calculated as mass-fraction weighted average of each gas species in the system.

$$\alpha_v = \sum_{i=1}^{N_g} Y_i \alpha_i \tag{7.58}$$

The mean free path, $\lambda$, is computed as follows:

$$\lambda = \frac{k_B T}{\sqrt{2}\pi\sigma^2 p} \tag{7.59}$$

$$\sigma = \sum_{i=1}^{N_g} Y_i \sigma_i \tag{7.60}$$

$\sigma_i$ is the Lennard-Jones characteristic length of species $i$. $k_B$ is the Boltzmann constant, $1.38066 \times 10^{-23} J/K$.

Equation 7.56 (p. 202) and Equation 7.57 (p. 202) indicate that while the gas velocity component normal to the wall is the same as the wall normal velocity, the tangential components slip. The values lie somewhere between the cell-center and the wall values. These two equations can be combined to give a generalized formulation:

$$\vec{V}_g = \frac{\vec{V}_w + \frac{k}{\delta}\left[ (\vec{V}_w \cdot \vec{n})\,\vec{n} + \vec{V}_c - (\vec{V}_c \cdot \vec{n})\,\vec{n} \right]}{1 + \frac{k}{\delta}} \tag{7.61}$$

where

$$k \equiv \lambda \left( \frac{2 - \alpha_v}{\alpha_v} \right) \tag{7.62}$$

- temperature jump

$$T_w - T_g = 2\left( \frac{2 - \alpha_T}{\alpha_T} \right) Kn L_c \frac{\partial T}{\partial n} \approx 2\left( \frac{2 - \alpha_T}{\alpha_T} \right) \frac{\lambda}{\delta} (T_g - T_c) \tag{7.63}$$

or equivalently

$$T_g = \frac{T_w + \beta T_c}{1 + \beta} \tag{7.64}$$

where

$$\beta = \frac{2(2 - \alpha_T)\lambda}{\alpha_T \delta} \tag{7.65}$$

Release 15.0 - © SAS IP, Inc. All rights reserved. - Contains proprietary and confidential information of ANSYS, Inc. and its subsidiaries and affiliates.

$\alpha_T$ is the thermal accommodation coefficient of the gas mixture and is calculated as $\alpha_T = \sum Y_i \alpha_{T,i}$.

**Important**

The low-pressure slip boundary formulation is available only with the pressure-based solver.

## 7.3. Particle Surface Reactions

As described in The Multiple Surface Reactions Model (p. 407), it is possible to define multiple particle surface reactions to model the surface combustion of a combusting discrete-phase particle. This section provides theoretical background about particle surface reactions. Information can be found in the following sections:

7.3.1. General Description
7.3.2. ANSYS Fluent Model Formulation
7.3.3. Extension for Stoichiometries with Multiple Gas Phase Reactants
7.3.4. Solid-Solid Reactions
7.3.5. Solid Decomposition Reactions
7.3.6. Solid Deposition Reactions
7.3.7. Gaseous Solid Catalyzed Reactions on the Particle Surface

For more information about using particle surface reactions, see Particle Surface Reactions in the User's Guide.

### 7.3.1. General Description

The relationships for calculating char particle burning rates are presented and discussed in detail by Smith [417] (p. 752). The particle reaction rate, $\mathcal{R}$ ($\mathrm{kg/m^2}$-s), can be expressed as

$$\mathcal{R} = D_0 \left( C_g - C_s \right) = R_c \left( C_s \right)^N \tag{7.66}$$

where,

$D_0$ = bulk diffusion coefficient (m/s)

$C_g$ = mean reacting gas species concentration in the bulk ($\mathrm{kg/m^3}$)

$C_s$ = mean reacting gas species concentration at the particle surface ($\mathrm{kg/m^3}$)

$R_c$ = chemical reaction rate coefficient (units vary)

$N$ = apparent reaction order (dimensionless)

In Equation 7.66 (p. 204), the concentration at the particle surface, $C_s$, is not known, so it should be eliminated, and the expression is recast as follows:

$$\mathcal{R} = R_c \left[ C_g - \frac{\mathcal{R}}{D_0} \right]^N \tag{7.67}$$

This equation has to be solved by an iterative procedure, with the exception of the cases when $N = 1$ or $N = 0$. When $N = 1$, Equation 7.67 (p. 204) can be written as


Release 15.0 - © SAS IP, Inc. All rights reserved. - Contains proprietary and confidential information of ANSYS, Inc. and its subsidiaries and affiliates.

$$\mathcal{R}=\frac{C_g R_c D_0}{D_0+R_c} \tag{7.68}$$

In the case of $N=0$, if there is a finite concentration of reactant at the particle surface, the solid depletion rate is equal to the chemical reaction rate. If there is no reactant at the surface, the solid depletion rate changes abruptly to the diffusion-controlled rate. In this case, however, ANSYS Fluent will always use the chemical reaction rate for stability reasons.

## 7.3.2. ANSYS Fluent Model Formulation

A particle undergoing an exothermic reaction in the gas phase is shown schematically in Figure 7.1: A Reacting Particle in the Multiple Surface Reactions Model (p. 205). $T_p$ and $T_\infty$ are the temperatures in Equation 16.157 (p. 408).

**Figure 7.1: A Reacting Particle in the Multiple Surface Reactions Model**

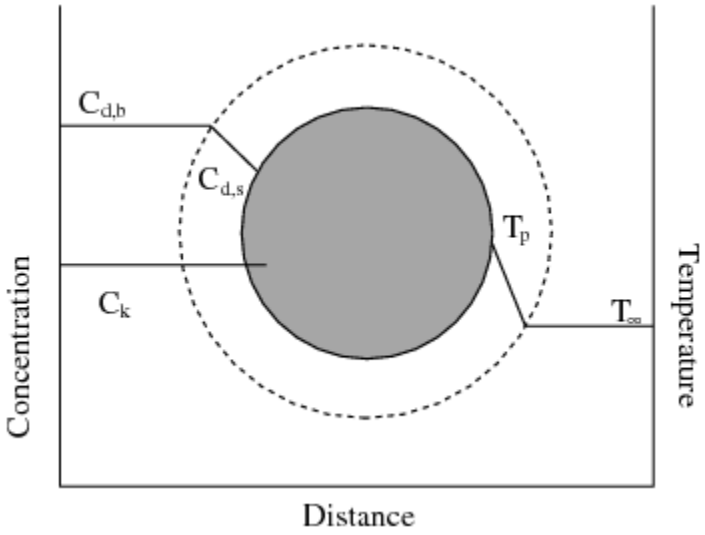


Based on the analysis above, ANSYS Fluent uses the following equation to describe the rate of reaction $r$ of a particle surface species $j$ with the gas phase species $n$. The reaction stoichiometry of reaction $r$ in this case is described by

$$\text{particle species}j\text{(s)}+\text{gas phase species}n\rightarrow\text{products} \tag{7.69}$$

and the rate of reaction is given as

$$\overline{\mathcal{R}}_{j,r}=A_p\eta_r Y_j \mathcal{R}_{j,r} \tag{7.70}$$

$$\mathcal{R}_{j,r}=\mathcal{R}_{kin,r}\left(p_n-\frac{\mathcal{R}_{j,r}}{D_{0,r}}\right)^N \tag{7.71}$$

where,

$\overline{\mathcal{R}}_{j,r}$ = rate of particle surface species depletion (kg/s)

$A_p$ = particle surface area ($\text{m}^2$)

$Y_j$ = mass fraction of surface species $j$ in the particle

Release 15.0 - © SAS IP, Inc. All rights reserved. - Contains proprietary and confidential information of ANSYS, Inc. and its subsidiaries and affiliates.

$\eta_r$ = effectiveness factor (dimensionless)

$\mathcal{R}_{j,r}$ = rate of particle surface species reaction per unit area ($\mathrm{kg/m^2-s}$)

$p_n$ = bulk partial pressure of the gas phase species (Pa)

$D_{0,r}$ = diffusion rate coefficient for reaction $r$

$\mathcal{R}_{kin,r}$ = kinetic rate of reaction $r$ (units vary)

$N_r$ = apparent order of reaction $r$

The effectiveness factor, $\eta_r$, is related to the surface area, and can be used in each reaction in the case of multiple reactions. $D_{0,r}$ is given by

$$D_{0,r}=C_{1,r}\frac{\left[\left(T_p+T_\infty\right)/2\right]^{0.75}}{d_p} \tag{7.72}$$

The kinetic rate of reaction $r$ is defined as

$$\mathcal{R}_{kin,r}=A_r T_p^{\beta_r} e^{-\left(E_r/RT_p\right)} \tag{7.73}$$

The rate of the particle surface species depletion for reaction order $N_r=1$ is given by

$$\overline{\mathcal{R}}_{j,r}=A_p\eta_r Y_j p_n\frac{\mathcal{R}_{kin,r}D_{0,r}}{D_{0,r}+\mathcal{R}_{kin,r}} \tag{7.74}$$

For reaction order $N_r=0$,

$$\overline{\mathcal{R}}_{j,r}=A_p\eta_r Y_j\mathcal{R}_{kin,r} \tag{7.75}$$

## 7.3.3. Extension for Stoichiometries with Multiple Gas Phase Reactants

When more than one gas phase reactant takes part in the reaction, the reaction stoichiometry must be extended to account for this case:

$$\begin{aligned}\text{particle species}\,j(\mathrm{s}) \quad &+\text{gas phase species}\,1+\text{gas phase species}\,2+\ldots\\ &+\text{gas phase species}\,n_{max}\rightarrow\text{products}\end{aligned} \tag{7.76}$$

To describe the rate of reaction $r$ of a particle surface species $j$ in the presence of $n_{max}$ gas phase species $n$, it is necessary to define the diffusion-limited species for each solid particle reaction, that is, the species for which the concentration gradient between the bulk and the particle surface is the largest. For the rest of the species, the surface and the bulk concentrations are assumed to be equal. The concentration of the diffusion-limited species is shown as $C_{d,b}$ and $C_{d,s}$ in Figure 7.1: A Reacting Particle in the Multiple Surface Reactions Model (p. 205), and the concentrations of all other species are denoted as $C_k$. For stoichiometries with multiple gas phase reactants, the bulk partial pressure $p_n$ in Equation 7.70 (p. 205) and Equation 7.74 (p. 206) is the bulk partial pressure of the diffusion-limited species, $p_{r,d}$ for reaction $r$.

The kinetic rate of reaction $r$ is then defined as


Release 15.0 - © SAS IP, Inc. All rights reserved. - Contains proprietary and confidential information of ANSYS, Inc. and its subsidiaries and affiliates.

$$\mathcal{R}_{kin,r} = \frac{A_r T^{\beta_r} e^{-(E_r/RT)} \prod_{n=1}^{n_{max}} p_n^{N_{r,n}}}{\left(p_{r,d}\right)^{N_{r,d}}} \tag{7.77}$$

where,

$p_n$ = bulk partial pressure of gas species $n$

$N_{r,n}$ = reaction order in species $n$

When this model is enabled, the constant $C_{1,r}$ (Equation 7.72 (p. 206)) and the effectiveness factor $\eta_r$ (Equation 7.70 (p. 205)) are entered in the **Reactions** dialog box (see User Inputs for Particle Surface Reactions in the User's Guide).

## 7.3.4. Solid-Solid Reactions

Reactions involving only particle surface reactants can be modeled, provided that the particle surface reactants and products exist on the same particle.

$$\text{particle species1(s)} + \text{particle species2(s)} + \ldots \rightarrow \text{products}$$

The reaction rate for this case is given by Equation 7.75 (p. 206).

## 7.3.5. Solid Decomposition Reactions

The decomposition reactions of particle surface species can be modeled.

$$\begin{aligned} &\text{particle species1(s)} + \text{particle species2(s)} + \ldots \quad + \text{particle species}n_{max}\text{(s)} \\ &\qquad\qquad\qquad\qquad\qquad\qquad \rightarrow \text{gas species}j + \text{products} \end{aligned} \tag{7.78}$$

The reaction rate for this case is given by Equation 7.70 (p. 205) – Equation 7.77 (p. 207), where the diffusion-limited species is now the gaseous product of the reaction. If there are more than one gaseous product species in the reaction, it is necessary to define the diffusion-limited species for the particle reaction as the species for which the concentration gradient between the bulk and the particle surface is the largest.

## 7.3.6. Solid Deposition Reactions

The deposition reaction of a solid species on a particle can be modeled with the following assumptions:

$$\text{gas species1} + \text{gas species2} + \ldots + \text{gas species}n_{max} \rightarrow \text{solid species}j\text{(s)} + \text{products} \tag{7.79}$$

The theoretical analysis and Equation 7.70 (p. 205) – Equation 7.77 (p. 207) are applied for the surface reaction rate calculation, with the mass fraction of the surface species set to unity in Equation 7.70 (p. 205), Equation 7.74 (p. 206), and Equation 7.75 (p. 206).

In ANSYS Fluent, for the particle surface species to be deposited on a particle, a finite mass of the species must already exist in the particle. This allows for activation of the deposition reaction selectively to particular injection particles. It follows that, to initiate the solid species deposition reaction on a particle, the particle must be defined in the Set Injection Properties Dialog Box (or Set Multiple Injection Properties Dialog Box) to contain a small mass fraction of the solid species to be deposited. For details on defining the particle surface species mass fractions, see Using the Multiple Surface Reactions Model for Discrete-Phase Particle Combustion in the User's Guide.

Release 15.0 - © SAS IP, Inc. All rights reserved. - Contains proprietary and confidential information of ANSYS, Inc. and its subsidiaries and affiliates.

### 7.3.7. Gaseous Solid Catalyzed Reactions on the Particle Surface

Reactions of gaseous species catalyzed on the particle surface can also be modeled following Equation 7.70 (p. 205) – Equation 7.77 (p. 207) for the surface reaction rate calculation, with the mass fraction of the surface species set to unity in Equation 7.70 (p. 205), Equation 7.74 (p. 206), and Equation 7.75 (p. 206). To apply this type of reaction, see Modeling Gaseous Solid Catalyzed Reactions in the User's Guide. For details on defining the particle surface species mass fractions, see Using the Multiple Surface Reactions Model for Discrete-Phase Particle Combustion in the User's Guide.

## 7.4. Reacting Channel Model

This section provides theoretical background about the reacting channel model. Information can be found in the following sections:

7.4.1. Overview and Limitations
7.4.2. Reacting Channel Model Theory

For more information about using the reacting channel model, see Reacting Channel Model in the User's Guide.

### 7.4.1. Overview and Limitations

Some flow geometries contain long, thin channels (also called pipes or ducts) with reacting fluid inside the channels exchanging heat with the fluid outside the channels. Examples of such shell-and-tube configurations include fuel reformers and cracking furnaces. The flow inside the channels rapidly establishes a stationary, fully-developed radial profile. The evolution of chemical species and temperature in these channels can be accurately modeled with lower dimensional models, often assuming parabolic flow. This is much more efficient than resolving the mesh in the channels and using an elliptic code to solve both the flow and chemistry inside and outside the channels simultaneously. The reacting channel model inside ANSYS Fluent allows affordable simulations of reactors with simple flow but complex chemistry occurring in long, thin channels, thermally coupled to geometrically complex outer flows with simple, or no, chemistry.

---

**Note**

The **Reacting Channel Model** is only available for steady-state, 3D cases using the pressure-based solver.

---

### 7.4.2. Reacting Channel Model Theory

In the reacting channel model, all channel walls must be geometrically resolved in three-dimensions. However, only the geometry in the outer shell should be meshed; no cells should be included inside the channel walls. Figure 7.2: Cross-section of a Channel and Outer Shell Around It. (p. 209) shows a typical configuration with two circular channels and an outer shell around it. The flow inside the channels is reacting, while the outer flow in the shell can be reacting or non-reacting. The channel walls are non-permeable and only heat transfer can take place through them.


Release 15.0 - © SAS IP, Inc. All rights reserved. - Contains proprietary and confidential information of ANSYS, Inc. and its subsidiaries and affiliates.

**Figure 7.2: Cross-section of a Channel and Outer Shell Around It.**

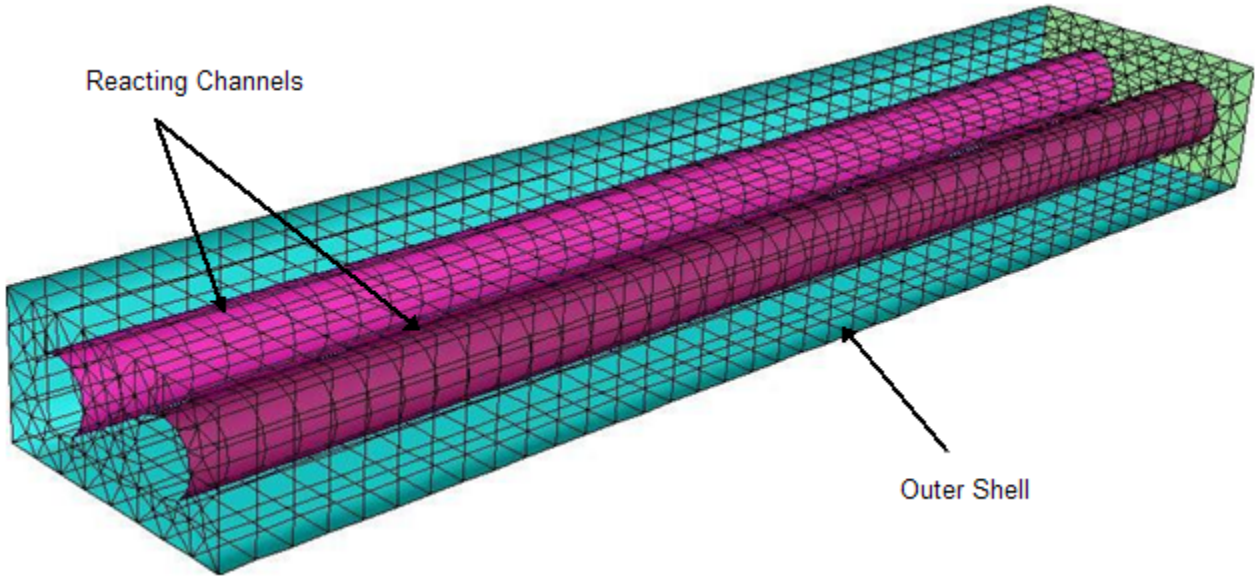


During an ANSYS Fluent iteration, the flow inside the reacting channel is solved using fixed wall temperatures from the 3D outer flow, and then the 3D outer flow is solved using fixed heat fluxes from the channel solver.

### 7.4.2.1. Flow Inside the Reacting Channel

The flow inside the channels is assumed to be a plug flow, which means that the flow variables at any axial location are radially uniform. Axial diffusion of heat and species are also ignored and therefore change only by reaction. The plug flow evolution equations for the channel species and temperatures are

$$\frac{dY_k}{dt} = \frac{W_k \dot{\omega}_k}{\rho}$$
$$\frac{dT}{dt} = \frac{\sum_k W_k \dot{\omega}_k h_k + \dot{Q}_C}{\rho\, c_p} \tag{7.80}$$

where,

$Y_k = k^{th}$ species mass fraction

$W_k = k^{th}$ molecular weight

$\dot{\omega}_k = k^{th}$ net molar reaction rate

$h_k = k^{th}$ total enthalpy

$\rho$ = mixture density

$T$ = bulk temperature

$c_p$ = specific heat

$\dot{Q}_C$ = convective heat transfer source

Release 15.0 - © SAS IP, Inc. All rights reserved. - Contains proprietary and confidential information of ANSYS, Inc. and its subsidiaries and affiliates.

The reaction channel convective heat transfer source $\dot{Q}_C$ is determined as

$$\dot{Q}_C = h_f \frac{A_C}{V_C} (T_W - T) \tag{7.81}$$

where,

$h_f$ = convective heat transfer coefficient on the channel side

$A_c$ = wall area of the channel element

$V_c$ = volume of the channel element

The channel wall temperature $T_w$ (not to be mistaken with the channel bulk temperature $T$) is averaged from the 3D outer flow temperature field on the resolved channel wall, as described below.

The heat transfer coefficient $h_f$ in Equation 7.81 (p. 210) is calculated as

$$h_f = \frac{Nu K_C}{D_C} \tag{7.82}$$

where $K_c$ and $D_c$ are the gas-phase thermal conductivity and the channel diameter, respectively. The Nusselt number, $Nu$, in the above equation is calculated from empirical correlations for fully developed pipe flow as follows:

- For Laminar flow (Re < 3000)
  $$Nu = 3.66 \tag{7.83}$$
- For Turbulent flow (Re > 3000), Gnielinski's correlation for turbulent flow is used:
  $$Nu = \frac{f(\mathrm{Re} - 1000)\mathrm{Pr}}{1 + 2.7\sqrt{f}(\mathrm{Pr}^{2/3} - 1)} \left( \frac{T_c}{T_w} \right)^{0.36} \tag{7.84}$$
  where $f$ is the friction factor. For smooth tubes of circular cross-section, $f$ is given by
  $$f = = \frac{0.125}{(0.79 \log(\mathrm{Re}) - 1.64)^2} \tag{7.85}$$

The plug flow equations are solved with a stiff ODE solver using time-steps based on the grid size (size of channel element) and the local channel velocity.

### 7.4.2.2. Surface Reactions in the Reacting Channel

When the surface reaction option is enabled, additional source terms due to surface reactions are added to Equation 7.80 (p. 209). Details of the heat and mass sources due to surface reactions are described in Wall Surface Reactions and Chemical Vapor Deposition (p. 199). The reacting surface area of a reacting channel element is calculated as

$$A_{surf} = V_C \, (A/V)_{Ratio} \tag{7.86}$$


Release 15.0 - © SAS IP, Inc. All rights reserved. - Contains proprietary and confidential information of ANSYS, Inc. and its subsidiaries and affiliates.

where $V_C$ is the volume of the channel element and $(A/V)_{Ratio}$ is the area to volume ratio of the catalytic surface.

**Note**

In the reacting channel model, the heat source due to surface reaction and the heat and mass source due to mass deposition are always included.

### 7.4.2.3. Porous Medium Inside Reacting Channel

The porous medium option in the reacting channel model uses the superficial velocity porous formulation. ANSYS Fluent calculates the superficial mixture velocities based on the volumetric flow rate in a porous region.

When the **Porous Medium** option is enabled, the heat transfer coefficient calculated from Equation 7.82 (p. 210) is modified to account for the solid material of the porous medium in the following manner.

$$h_f = \alpha \frac{Nu K_C}{D_C} + (1-\alpha)\frac{K_{S,C}}{D_C} \tag{7.87}$$

where $\alpha$ is the porosity and $K_{S,C}$ is the conductivity of the solid material. Also, the reaction rates $\dot{\omega}_k$ are modified by multiplying $\dot{\omega}_k$ by medium porosity $\alpha$ to account for the displacement of the gas by the solid.

The **Porous Medium** option provides the capability to model pressure drop inside the reacting channel. The pressure drop in the channel is calculated only in the axial direction and has contributions from viscous and inertial resistances:

$$\Delta p = \Delta p_{Viscous} + \Delta p_{Inertial} \tag{7.88}$$

The pressure drop due to viscous resistance is calculated using Darcy's law

$$\Delta p_{Viscous} = C_{Viscous}\, \mu\, u\, \Delta x \tag{7.89}$$

where $C_{Viscous}$ is the viscous resistance along axial direction and $\Delta x$ is the length of the channel element.

The pressure drop due to inertial losses is modeled as

$$\Delta p_{Inertial} = \frac{\rho}{2} C_{Inertial}\, u^2\, \Delta x \tag{7.90}$$

where $C_{Inertial}$ is the inertial resistance along axial direction and $\Delta x$ is the length of the channel element.

### 7.4.2.4. Outer Flow in the Shell

The outer shell can be any arbitrarily shaped 3D geometry, but must resolve the channel walls. Note that while this outer shell is meshed in ANSYS Fluent with finite-volume cells, the inside of the channels should not be meshed. This outer flow can be a reacting or non-reacting mixture, which is typically a different mixture material than the complex mechanism material used for the reacting channel plug flow.

Release 15.0 - © SAS IP, Inc. All rights reserved. - Contains proprietary and confidential information of ANSYS, Inc. and its subsidiaries and affiliates.

The ANSYS Fluent energy solution of the outer shell flow uses a prescribed heat flux boundary condition at the channel walls from the solution of the reacting channel. The value of this heat flux is calculated as an under-relaxation of the heat gained from the channel:

$$\dot{Q}_{3D} = -\alpha \dot{Q}_C - (1-\alpha)\dot{Q}_C^o \tag{7.91}$$

where $\dot{Q}_C$ is the channel heat gain/loss, $\alpha$ is a user-specified under relaxation parameter, and $\dot{Q}_C^o$ is the heat flux from the previous iteration. At convergence, the heat loss/gain from the channel is equal to the heat gain/loss in the shell outer flow.

## 7.5. Reactor Network Model

The reactor network model is used to simulate species and temperature fields in a combustor using a detailed chemical kinetic mechanism. The reactor network is constructed from a converged ANSYS Fluent simulation modeled with a fast chemistry combustion model, such as the Non-Premixed, Partially-Premixed, or Eddy-Dissipation model. A full chemical mechanism in CHEMKIN format can be imported into Fluent and solved on the reactor network. The combustor volume is automatically subdivided into a small number of connected perfectly stirred reactors. The mass fluxes through the network are determined from the CFD solution, and the species and temperatures in the reactor network are solved together. Hence, the reactor network model is used to simulate finite-rate chemistry effects with detailed kinetic mechanisms, in particular pollutant emissions such as NOx, CO, and unburnt hydro-carbons. Since the specified number of stirred reactors is much smaller than the number of CFD cells, the reactor network model allows much faster simulations of the species and temperature fields than solving for detailed chemistry in every cell, as in the Laminar, EDC, and PDF Transport models.

Typically, the reactor network model is executed on a converged steady-state RANS solution or a time-averaged unsteady solution. The model can also be run on an unsteady flow representing a “snap-shot” in time. Since there is no backward coupling of the reactor-network solution to the flow, the model is useful for predictions where the detailed chemistry has little impact on the flow, such as pollutant formation. The model is inappropriate for highly unsteady flows such as flame ignition or global extinction and also for flows that are strongly influenced by the chemistry, such as soot with significant soot-radiation interaction.

For more information about using reactor network, see Reactor Network Model in the *Fluent User's Guide*.

### 7.5.1. Reactor Network Model Theory

The first step in a reactor network simulation involves agglomerating the CFD cells into the specified number of reactors, $N_{reactor}$.

Since each reactor is a perfectly mixed representation of a region of the combustor, ideally cells that are closest in composition space should be grouped together. In other words, for optimal performance, the CFD cells grouped together in each reactor should have temperatures and species mass fractions that are as similar as possible.

By default, for Non-Premixed and Partially-Premixed cases, Fluent groups cells that have similar temperatures and mixture fractions, and for Species Transport cases, Fluent groups cells that have similar temperatures and mass fractions of $N_2$ and $H_2O$. These defaults should provide good cell clustering in most cases. However, Fluent allows user-controlled clustering through custom-field functions when these defaults are not sufficient.


Release 15.0 - © SAS IP, Inc. All rights reserved. - Contains proprietary and confidential information of ANSYS, Inc. and its subsidiaries and affiliates.

After similar cells have been clustered, Fluent splits non-contiguous groups, then agglomerates clusters with the smallest number of cells to their closest neighbors until the specified number of reactors, $N_{reactor}$, is obtained.

The second step in a reactor network simulation involves the solution of the reactor network, which proceeds as follows.

The mass flux matrix, $\dot{m}$, is calculated from the cell fluxes in the CFD solution, where each matrix component $\dot{m}_{ij}$ is the mass flux from reactor $i$ to reactor $j$. The $k^{\text{th}}$ species mass fraction in reactor $i$, $Y_k^i$, is governed by the algebraic equation:

$$\sum_{j=1, j\neq i}^{N_{reactor}} \dot{m}_{ij} Y_k^j - \dot{m}_i Y_k^i = V_i \dot{\omega}_k^i + S_k^i \tag{7.92}$$

where $V_i$ is the volume of reactor $i$, $\dot{\omega}_k^i$ is the $k^{\text{th}}$ species reaction rate in the $i$th reactor, and $S_k^i$ is a mass source term. $\dot{m}_i$ is the net mass flux into reactor $i$ and is calculated as:

$$\dot{m}_i = \sum_{j=1, j\neq i}^{N_{reactor}} \dot{m}_{ij} \tag{7.93}$$

The mass source term, $S_k^i$, accounts for contributions from the CFD inlet species mass fluxes through the CFD boundaries and from volume sources, such as the Discrete Phase Model (DPM).

The system of equations for $Y_k^i$, Equation 7.92 (p. 213), has the dimension of $N_{reactor} \times N_{species}$, where $N_{reactor}$ is the user-specified number of reactors, and $N_{species}$ is the number of species in the chemical mechanism. ANSYS Fluent solves this system with a segregated algorithm by default, although the option to use a fully coupled algorithm is available.

### 7.5.1.1. Reactor network temperature solution

An energy equation is not solved in the reactor network. Instead, by default, the temperature in each reactor is calculated from the equation of state. The reactor pressure is fixed and determined as the mass-averaged pressure of the CFD cells in the reactor. Note that the density of each reactor is fixed since both the reactor volume and the reactor mass are constant. This approach ensures that heat loss (or gain) in the CFD simulation is appropriately accounted for in the reactor network. Fluent also provides an option to not solve for temperature, in which case the temperature is fixed as the mass-average temperature of the CFD cells in the reactor.

Release 15.0 - © SAS IP, Inc. All rights reserved. - Contains proprietary and confidential information of ANSYS, Inc. and its subsidiaries and affiliates.

Release 15.0 - © SAS IP, Inc. All rights reserved. - Contains proprietary and confidential information
of ANSYS, Inc. and its subsidiaries and affiliates.

# Chapter 8: Non-Premixed Combustion

In non-premixed combustion, fuel and oxidizer enter the reaction zone in distinct streams. This is in contrast to premixed systems, in which reactants are mixed at the molecular level before burning. Examples of non-premixed combustion include pulverized coal furnaces, diesel internal-combustion engines and pool fires.

Under certain assumptions, the thermochemistry can be reduced to a single parameter: the mixture fraction. The mixture fraction, denoted by $f$, is the mass fraction that originated from the fuel stream. In other words, it is the local mass fraction of burnt and unburnt fuel stream elements ($C$, $H$, and so on) in all the species ($CO_2$, $H_2O$, $O_2$, and so on). The approach is elegant because atomic elements are conserved in chemical reactions. In turn, the mixture fraction is a conserved scalar quantity, and therefore its governing transport equation does not have a source term. Combustion is simplified to a mixing problem, and the difficulties associated with closing non-linear mean reaction rates are avoided. Once mixed, the chemistry can be modeled as being in chemical equilibrium with the Equilibrium model, being near chemical equilibrium with the Steady Diffusion Flamelet model, or significantly departing from chemical equilibrium with the Unsteady Diffusion Flamelet model.

For more information about using the non-premixed combustion model, see Modeling Non-Premixed Combustion in the User's Guide. Theoretical information about the non-premixed combustion model is presented in the following sections:


8.1. Introduction
8.2. Non-Premixed Combustion and Mixture Fraction Theory
8.3. Restrictions and Special Cases for Using the Non-Premixed Model
8.4. The Diffusion Flamelet Models Theory
8.5. The Steady Diffusion Flamelet Model Theory
8.6. The Unsteady Diffusion Flamelet Model Theory


## 8.1. Introduction

Non-premixed modeling involves the solution of transport equations for one or two conserved scalars (the mixture fractions). Equations for individual species are not solved. Instead, species concentrations are derived from the predicted mixture fraction fields. The thermochemistry calculations are preprocessed and then tabulated for look-up in ANSYS Fluent. Interaction of turbulence and chemistry is accounted for with an assumed-shape Probability Density Function (PDF).

## 8.2. Non-Premixed Combustion and Mixture Fraction Theory

Information about non-premixed combustion and mixture fraction theory are presented in the following sections:


8.2.1. Mixture Fraction Theory
8.2.2. Modeling of Turbulence-Chemistry Interaction
8.2.3. Non-Adiabatic Extensions of the Non-Premixed Model
8.2.4. Chemistry Tabulation


Release 15.0 - © SAS IP, Inc. All rights reserved. - Contains proprietary and confidential information of ANSYS, Inc. and its subsidiaries and affiliates.

## 8.2.1. Mixture Fraction Theory

### 8.2.1.1. Definition of the Mixture Fraction

The basis of the non-premixed modeling approach is that under a certain set of simplifying assumptions, the instantaneous thermochemical state of the fluid is related to a conserved scalar quantity known as the mixture fraction, $f$. The mixture fraction can be written in terms of the atomic mass fraction as [411] (p. 751)

$$f = \frac{Z_i - Z_{i,ox}}{Z_{i,fuel} - Z_{i,ox}} \tag{8.1}$$

where $Z_i$ is the elemental mass fraction for element, $i$. The subscript *ox* denotes the value at the oxidizer stream inlet and the subscript fuel denotes the value at the fuel stream inlet. If the diffusion coefficients for all species are equal, then Equation 8.1 (p. 216) is identical for all elements, and the mixture fraction definition is unique. The mixture fraction is therefore the elemental mass fraction that originated from the fuel stream.

If a secondary stream (another fuel or oxidant, or a non-reacting stream) is included, the fuel and secondary mixture fractions are simply the elemental mass fractions of the fuel and secondary streams, respectively. The sum of all three mixture fractions in the system (fuel, secondary stream, and oxidizer) is always equal to 1:

$$f_{fuel} + f_{sec} + f_{ox} = 1 \tag{8.2}$$

This indicates that only points on the plane ABC (shown in Figure 8.1: Relationship of Mixture Fractions (Fuel, Secondary Stream, and Oxidizer) (p. 217)) in the mixture fraction space are valid. Consequently, the two mixture fractions, $f_{fuel}$ and $f_{sec'}$ cannot vary independently; their values are valid only if they are both within the triangle OBC shown in Figure 8.1: Relationship of Mixture Fractions (Fuel, Secondary Stream, and Oxidizer) (p. 217).


Release 15.0 - © SAS IP, Inc. All rights reserved. - Contains proprietary and confidential information of ANSYS, Inc. and its subsidiaries and affiliates.

**Figure 8.1: Relationship of Mixture Fractions (Fuel, Secondary Stream, and Oxidizer)**

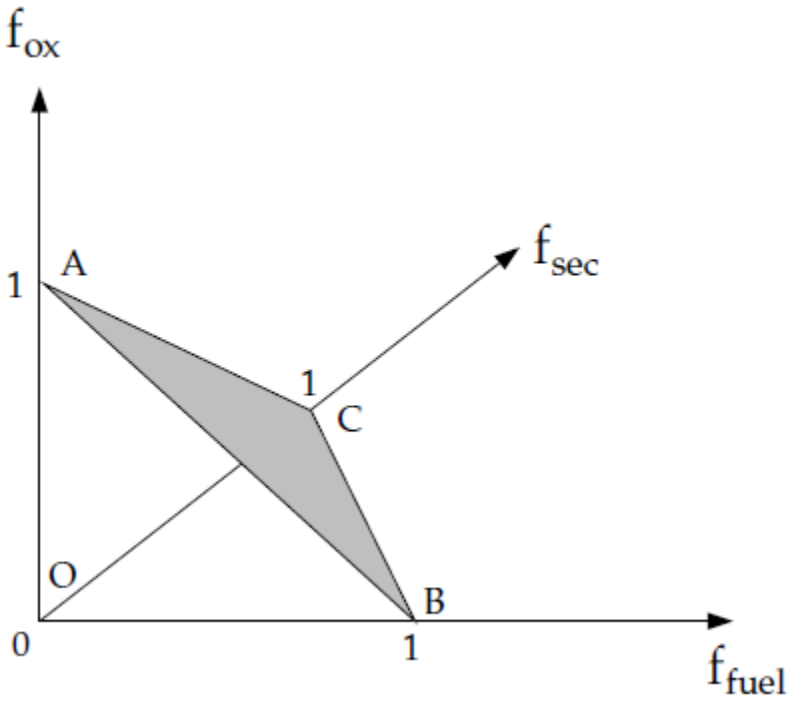


**Figure 8.2: Relationship of Mixture Fractions (Fuel, Secondary Stream, and Normalized Secondary Mixture Fraction)**

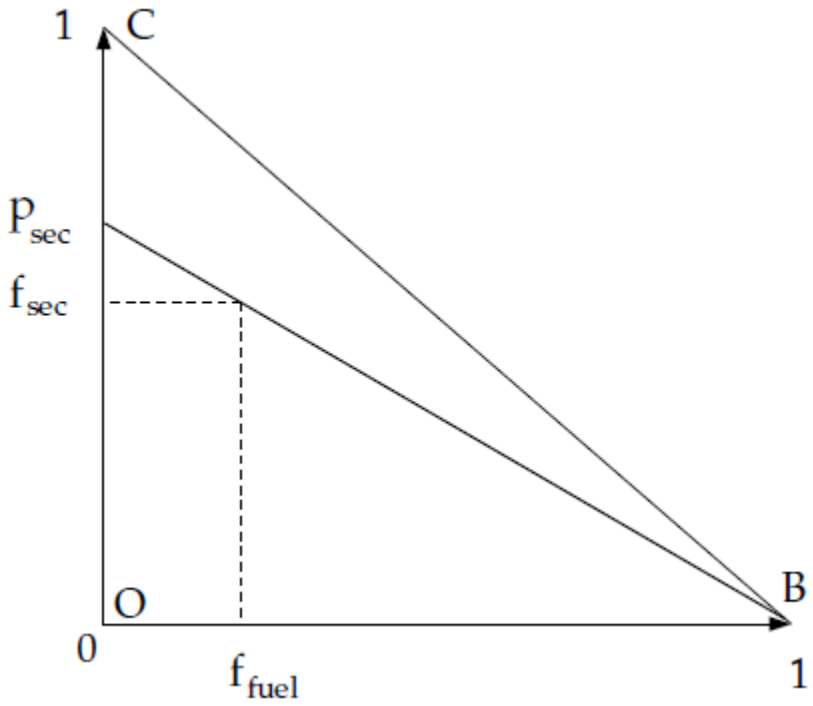


ANSYS Fluent discretizes the triangle OBC as shown in Figure 8.2: Relationship of Mixture Fractions (Fuel, Secondary Stream, and Normalized Secondary Mixture Fraction) (p. 217). Essentially, the primary mixture

Release 15.0 - © SAS IP, Inc. All rights reserved. - Contains proprietary and confidential information of ANSYS, Inc. and its subsidiaries and affiliates.

fraction, $f_{fuel}$, is allowed to vary between zero and one, as for the single mixture fraction case, while the secondary mixture fraction lies on lines with the following equation:

$$f_{sec} = p_{sec} \times \left(1 - f_{fuel}\right) \tag{8.3}$$

where $p_{sec}$ is the normalized secondary mixture fraction and is the value at the intersection of a line with the secondary mixture fraction axis. Note that unlike $f_{sec}$, $p_{sec}$ is bounded between zero and one, regardless of the $f_{fuel}$ value.

An important characteristic of the normalized secondary mixture fraction, $p_{sec}$, is its assumed statistical independence from the fuel mixture fraction, $f_{fuel}$. Note that unlike $f_{sec}$, $p_{sec}$ is not a conserved scalar. This normalized mixture fraction definition, $p_{sec}$, is used everywhere in ANSYS Fluent when prompted for Secondary Mixture Fraction except when defining the rich limit for a secondary fuel stream, which is defined in terms of $f_{sec}$.

### 8.2.1.2. Transport Equations for the Mixture Fraction

Under the assumption of equal diffusivities, the species equations can be reduced to a single equation for the mixture fraction, $f$. The reaction source terms in the species equations cancel (since elements are conserved in chemical reactions), and therefore $f$ is a conserved quantity. While the assumption of equal diffusivities is problematic for laminar flows, it is generally acceptable for turbulent flows where turbulent convection overwhelms molecular diffusion. The Favre mean (density-averaged) mixture fraction equation is

$$\frac{\partial}{\partial t}(\rho \overline{f}) + \nabla \cdot (\rho \vec{v} \overline{f}) = \nabla \cdot \left( \frac{\mu_l + \mu_t}{\sigma_t} \nabla \overline{f} \right) + S_m + S_{user} \tag{8.4}$$

where $\mu_l$ is the laminar viscosity and $\mu_t$ is the turbulent viscosity.

The source term $S_m$ is due solely to transfer of mass into the gas phase from liquid fuel droplets or reacting particles (for example, coal). $S_{user}$ is any user-defined source term.

In addition to solving for the Favre mean mixture fraction, ANSYS Fluent solves a conservation equation for the mixture fraction variance, $\overline{f'^2}$ [191] (p. 739):

$$\frac{\partial}{\partial t}\left(\rho \overline{f'^2}\right) + \nabla \cdot \left(\rho \vec{v} \overline{f'^2}\right) = \nabla \cdot \left( \frac{\mu_l + \mu_t}{\sigma_t} \nabla \overline{f'^2} \right) + C_g \mu_t \cdot (\nabla \overline{f})^2 - C_d \rho \frac{\varepsilon}{k} \overline{f'^2} + S_{user} \tag{8.5}$$

where $f' = f - \overline{f}$. The default values for the constants $\sigma_t$, $C_g$, and $C_d$ are 0.85, 2.86, and 2.0, respectively, and $S_{user}$ is any user-defined source term.

The mixture fraction variance is used in the closure model describing turbulence-chemistry interactions (see Modeling of Turbulence-Chemistry Interaction (p. 221)).


Release 15.0 - © SAS IP, Inc. All rights reserved. - Contains proprietary and confidential information of ANSYS, Inc. and its subsidiaries and affiliates.

For a two-mixture-fraction problem, $\overline{f_{fuel}}$ and $\overline{f'^2_{fuel}}$ are obtained from Equation 8.4 (p. 218) and Equation 8.5 (p. 218) by substituting $\overline{f_{fuel}}$ for $\overline{f}$ and $\overline{f'^2_{fuel}}$ for $\overline{f'^2}$. $\overline{f_{sec}}$ is obtained from Equation 8.4 (p. 218) by substituting $\overline{f_{sec}}$ for $\overline{f}$. $\overline{p_{sec}}$ is then calculated using Equation 8.3 (p. 218), and $\overline{p'^2_{sec}}$ is obtained by solving Equation 8.5 (p. 218) with $\overline{p_{sec}}$ substituted for $\overline{f}$. To a first-order approximation, the variances in $\overline{p_{sec}}$ and $\overline{f_{sec}}$ are relatively insensitive to $\overline{f_{fuel}}$, and therefore the equation for $\overline{p'^2_{sec}}$ is essentially the same as $\overline{f'^2_{sec}}$.

**Important**

The equation for $\overline{p'^2_{sec}}$ instead of $\overline{f'^2_{sec}}$ is valid when the mass flow rate of the secondary stream is relatively small compared with the total mass flow rate.

### 8.2.1.3. The Non-Premixed Model for LES

For Large Eddy Simulations, the transport equation is not solved for the mixture fraction variance. Instead, it is modeled as

$$\overline{f'^2} = C_{var} L_s^2 |\nabla \overline{f}|^2 \tag{8.6}$$

where

$C_{var}$ = constant

$L_s$ = subgrid length scale (see Equation 4.260 (p. 101))

The constant $C_{var}$ is computed dynamically when the **Dynamic Stress** option is enabled in the **Viscous** dialog box, else a constant value (with a default of 0.5) is used.

If the **Dynamic Scalar Flux** option is enabled, the turbulent Sc ($\sigma_t$ in Equation 8.4 (p. 218)) is computed dynamically.

### 8.2.1.4. Mixture Fraction vs. Equivalence Ratio

The mixture fraction definition can be understood in relation to common measures of reacting systems. Consider a simple combustion system involving a fuel stream (F), an oxidant stream (O), and a product stream (P) symbolically represented at stoichiometric conditions as

$$F + rO \rightarrow (1 + r) P \tag{8.7}$$

where $r$ is the air-to-fuel ratio on a mass basis. Denoting the equivalence ratio as $\phi$, where

$$\phi = \frac{(fuel/air)_{actual}}{(fuel/air)_{stoichiometric}} \tag{8.8}$$

the reaction in Equation 8.7 (p. 219), under more general mixture conditions, can then be written as

$$\phi F + rO \rightarrow (\phi + r) P \tag{8.9}$$

Looking at the left side of this equation, the mixture fraction for the system as a whole can then be deduced to be

$$f = \frac{\phi}{\phi + r} \tag{8.10}$$

Equation 8.10 (p. 220) allows the computation of the mixture fraction at stoichiometric conditions ($\phi$ = 1) or at fuel-rich conditions (for example, $\phi$ > 1), or fuel-lean conditions (for example, $\phi$ < 1).

### 8.2.1.5. Relationship of Mixture Fraction to Species Mass Fraction, Density, and Temperature

The power of the mixture fraction modeling approach is that the chemistry is reduced to one or two conserved mixture fractions. Under the assumption of chemical equilibrium, all thermochemical scalars (species fractions, density, and temperature) are uniquely related to the mixture fraction(s).

For a single mixture fraction in an adiabatic system, the instantaneous values of mass fractions, density, and temperature depend solely on the instantaneous mixture fraction, $f$:

$$\phi_i = \phi_i(f) \tag{8.11}$$

If a secondary stream is included, the instantaneous values will depend on the instantaneous fuel mixture fraction, $f_{fuel}$, and the secondary partial fraction, $p_{sec}$:

$$\phi_i = \phi_i\left(f_{fuel}, p_{sec}\right) \tag{8.12}$$

In Equation 8.11 (p. 220) and Equation 8.12 (p. 220), $\phi_i$ represents the instantaneous species mass fraction, density, or temperature. In the case of non-adiabatic systems, the effect of heat loss/gain is parameterized as

$$\phi_i = \phi_i(f, H) \tag{8.13}$$

for a single mixture fraction system, where $H$ is the instantaneous enthalpy (see Equation 5.7 (p. 135)).

If a secondary stream is included,

$$\phi_i = \phi_i\left(f_{fuel}, p_{sec}, H\right) \tag{8.14}$$

Examples of non-adiabatic flows include systems with radiation, heat transfer through walls, heat transfer to/from discrete phase particles or droplets, and multiple inlets at different temperatures. Additional detail about the mixture fraction approach in such non-adiabatic systems is provided in Non-Adiabatic Extensions of the Non-Premixed Model (p. 224).

In many reacting systems, the combustion is not in chemical equilibrium. ANSYS Fluent offers several approaches to model chemical non-equilibrium, including the finite-rate (see The Generalized Finite-Rate Formulation for Reaction Modeling (p. 189)), EDC (see The Eddy-Dissipation-Concept (EDC) Model (p. 195)), and PDF transport (see Composition PDF Transport (p. 281)) models, where detailed kinetic mechanisms can be incorporated.

There are three approaches in the non-premixed combustion model to simulate chemical non-equilibrium. The first is to use the Rich Flammability Limit (RFL) option in the Equilibrium model, where rich regions are modeled as a mixed-but-unburnt mixture of pure fuel and a leaner equilibrium burnt mixture (see Enabling the Rich Flammability Limit (RFL) Option in the User's Guide). The second approach is the


Release 15.0 - © SAS IP, Inc. All rights reserved. - Contains proprietary and confidential information of ANSYS, Inc. and its subsidiaries and affiliates.

Steady Diffusion Flamelet model, where chemical non-equilibrium due to diffusion flame stretching by turbulence can be modeled. The third approach is the Unsteady Diffusion Flamelet model where slow-forming product species that are far from chemical equilibrium can be modeled. See The Diffusion Flamelet Models Theory (p. 238) and The Unsteady Diffusion Flamelet Model Theory (p. 246) for details about the Steady and Unsteady Diffusion Flamelet models in ANSYS Fluent.

## 8.2.2. Modeling of Turbulence-Chemistry Interaction

Equation 8.11 (p. 220) through Equation 8.14 (p. 220) describe the instantaneous relationships between mixture fraction and species fractions, density, and temperature under the assumption of chemical equilibrium. The ANSYS Fluent prediction of the turbulent reacting flow, however, is concerned with prediction of the averaged values of these fluctuating scalars. How these averaged values are related to the instantaneous values depends on the turbulence-chemistry interaction model. ANSYS Fluent applies the assumed-shape probability density function (PDF) approach as its closure model when the non-premixed model is used. The assumed shape PDF closure model is described in this section.

### 8.2.2.1. Description of the Probability Density Function

The Probability Density Function, written as $p(f)$, can be thought of as the fraction of time that the fluid spends in the vicinity of the state $f$. Figure 8.3: Graphical Description of the Probability Density Function (p. 221) plots the time trace of mixture fraction at a point in the flow (right-hand side) and the probability density function of $f$ (left-hand side). The fluctuating value of $f$, plotted on the right side of the figure, spends some fraction of time in the range denoted as $\Delta f$. $p(f)$, plotted on the left side of the figure, takes on values such that the area under its curve in the band denoted, $\Delta f$, is equal to the fraction of time that $f$ spends in this range. Written mathematically,

$$p(f)\,\Delta f = \lim_{T\to\infty} \frac{1}{T} \sum_i \tau_i \tag{8.15}$$

where $T$ is the time scale and $\tau_i$ is the amount of time that $f$ spends in the $\Delta f$ band. The shape of the function $p(f)$ depends on the nature of the turbulent fluctuations in $f$. In practice, $p(f)$ is unknown and is modeled as a mathematical function that approximates the actual PDF shapes that have been observed experimentally.

**Figure 8.3: Graphical Description of the Probability Density Function**

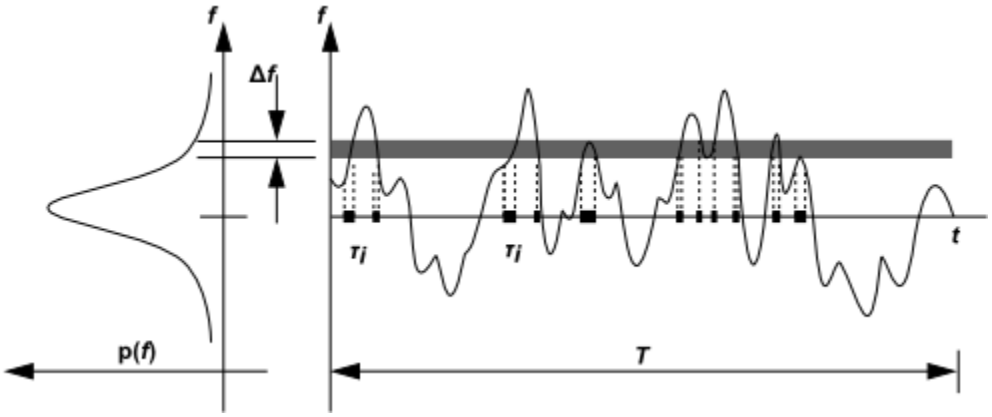

### 8.2.2.2. Derivation of Mean Scalar Values from the Instantaneous Mixture Fraction

The probability density function $p(f)$, describing the temporal fluctuations of $f$ in the turbulent flow, can be used to compute averaged values of variables that depend on $f$. Density-weighted mean species mass fractions and temperature can be computed (in adiabatic systems) as

$$\overline{\phi}_i = \int_0^1 p(f)\,\phi_i(f)\,df \tag{8.16}$$

for a single-mixture-fraction system. When a secondary stream exists, mean values are calculated as

$$\overline{\phi}_i = \int_0^1 \int_0^1 p_1\left(f_{fuel}\right) p_2\left(p_{sec}\right) \phi_i\left(f_{fuel}, p_{sec}\right) df_{fuel}\, dp_{sec} \tag{8.17}$$

where $p_1$ is the PDF of $f_{fuel}$ and $p_2$ is the PDF of $p_{sec}$. Here, statistical independence of $f_{fuel}$ and $p_{sec}$ is assumed, so that $p\left(f_{fuel}, p_{sec}\right) = p_1\left(f_{fuel}\right) p_2\left(p_{sec}\right)$.

Similarly, the mean time-averaged fluid density, $\overline{\rho}$, can be computed as

$$\frac{1}{\overline{\rho}} = \int_0^1 \frac{p(f)}{\rho(f)} df \tag{8.18}$$

for a single-mixture-fraction system, and

$$\frac{1}{\overline{\rho}} = \int_0^1 \int_0^1 \frac{p_1\left(f_{fuel}\right) p_2\left(p_{sec}\right)}{\rho\left(f_{fuel}, p_{sec}\right)} df_{fuel}\, dp_{sec} \tag{8.19}$$

when a secondary stream exists. $\rho(f)$ or $\rho\left(f_{fuel}, p_{sec}\right)$ is the instantaneous density obtained using the instantaneous species mass fractions and temperature in the ideal gas law equation.

Using Equation 8.16 (p. 222) and Equation 8.18 (p. 222) (or Equation 8.17 (p. 222) and Equation 8.19 (p. 222)), it remains only to specify the shape of the function $p(f)$ (or $p_1\left(f_{fuel}\right)$ and $p_2\left(p_{sec}\right)$) in order to determine the local mean fluid state at all points in the flow field.

### 8.2.2.3. The Assumed-Shape PDF

The shape of the assumed PDF, $p(f)$, is described in ANSYS Fluent by one of two mathematical functions:

- the double-delta function (two-mixture-fraction cases only)
- the $\beta$-function (single- and two-mixture-fraction cases)

The double-delta function is the most easily computed, while the $\beta$-function most closely represents experimentally observed PDFs. The shape produced by this function depends solely on the mean mixture fraction, $\overline{f}$, and its variance, $\overline{f'^2}$. A detailed description of each function follows.


Release 15.0 - © SAS IP, Inc. All rights reserved. - Contains proprietary and confidential information of ANSYS, Inc. and its subsidiaries and affiliates.

#### 8.2.2.3.1. The Double Delta Function PDF

The double delta function is given by

$$p(f) = \begin{cases} 0.5, & f = \overline{f} - \sqrt{\overline{f'^2}} \\ 0.5, & f = \overline{f} + \sqrt{\overline{f'^2}} \\ 0, & \text{elsewhere} \end{cases} \tag{8.20}$$

with suitable bounding near $f$ = 1 and $f$ = 0. One example of the double delta function is illustrated in Figure 8.4: Example of the Double Delta Function PDF Shape (p. 223). As noted above, the double delta function PDF is very easy to compute but is invariably less accurate than the alternate $\beta$-function PDF because it assumes that only two states occur in the turbulent flow. For this reason, it is available only for two-mixture-fraction simulations where the savings in computational cost is significant.

**Figure 8.4: Example of the Double Delta Function PDF Shape**

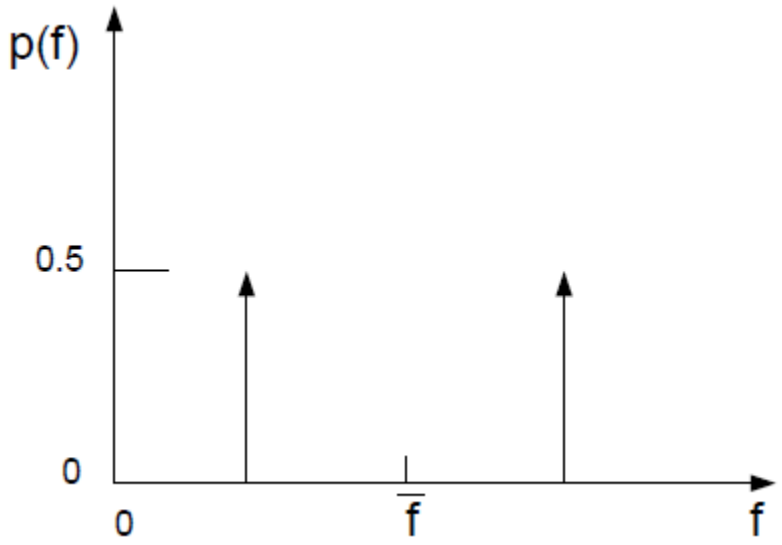


#### 8.2.2.3.2. The β-Function PDF

The $\beta$-function PDF shape is given by the following function of $\overline{f}$ and $\overline{f'^2}$:

$$p(f) = \frac{f^{\alpha-1}(1-f)^{\beta-1}}{\int f^{\alpha-1}(1-f)^{\beta-1} df} \tag{8.21}$$

where

$$\alpha = \overline{f}\left[\frac{\overline{f}(1-\overline{f})}{\overline{f'^2}} - 1\right] \tag{8.22}$$

and

$$\beta = (1-\overline{f})\left[\frac{\overline{f}(1-\overline{f})}{\overline{f'^2}}-1\right] \tag{8.23}$$

Importantly, the PDF shape $p(f)$ is a function of only its first two moments, namely the mean mixture fraction, $\overline{f}$, and the mixture fraction variance, $\overline{f'^2}$. Thus, given ANSYS Fluent's prediction of $\overline{f}$ and $\overline{f'^2}$ at each point in the flow field (Equation 8.4 (p. 218) and Equation 8.5 (p. 218)), the assumed PDF shape can be computed and used as the weighting function to determine the mean values of species mass fractions, density, and temperature using, Equation 8.16 (p. 222) and Equation 8.18 (p. 222) (or, for a system with a secondary stream, Equation 8.17 (p. 222) and Equation 8.19 (p. 222)).

This logical dependence is depicted visually in Figure 8.5: Logical Dependence of Averaged Scalars on Mean Mixture Fraction, the Mixture Fraction Variance, and the Chemistry Model (Adiabatic, Single-Mixture-Fraction Systems) (p. 224) for a single mixture fraction.

**Figure 8.5: Logical Dependence of Averaged Scalars on Mean Mixture Fraction, the Mixture Fraction Variance, and the Chemistry Model (Adiabatic, Single-Mixture-Fraction Systems)**

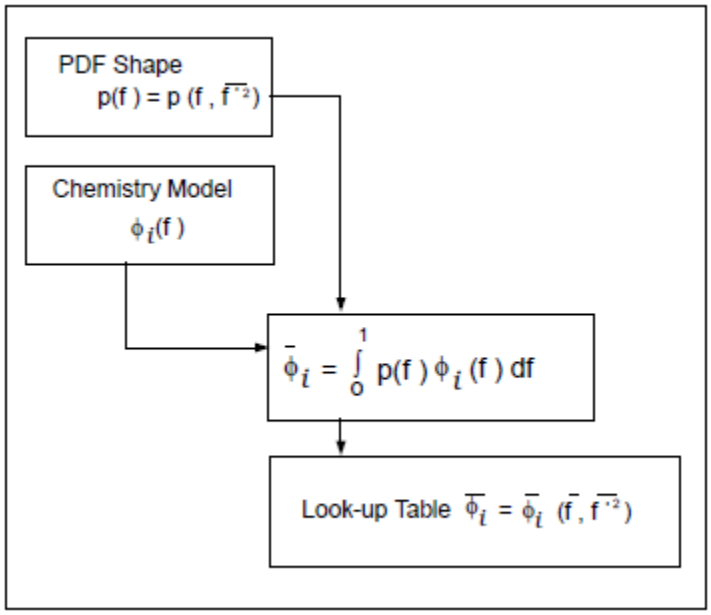


## 8.2.3. Non-Adiabatic Extensions of the Non-Premixed Model

Many reacting systems involve heat transfer through wall boundaries, droplets, and/or particles. In such flows the local thermochemical state is no longer related only to $f$, but also to the enthalpy, $H$. The system enthalpy impacts the chemical equilibrium calculation and the temperature and species of the reacting flow. Consequently, changes in enthalpy due to heat loss must be considered when computing scalars from the mixture fraction, as in Equation 8.13 (p. 220).

In such non-adiabatic systems, turbulent fluctuations should be accounted for by means of a joint PDF, $p(f, H)$. The computation of $p(f, H)$, however, is not practical for most engineering applications. The problem can be simplified significantly by assuming that the enthalpy fluctuations are independent


Release 15.0 - © SAS IP, Inc. All rights reserved. - Contains proprietary and confidential information of ANSYS, Inc. and its subsidiaries and affiliates.

of the enthalpy level (that is, heat losses do not significantly impact the turbulent enthalpy fluctuations). With this assumption, $p(f,H) = p(f)\,\delta(H-\overline{H})$ and mean scalars are calculated as

$$\overline{\phi_i} = \int_0^1 \phi_i(f,\overline{H})\,p(f)\,df \tag{8.24}$$

Determination of $\overline{\phi_i}$ in the non-adiabatic system therefore requires solution of the modeled transport equation for mean enthalpy:

$$\frac{\partial}{\partial t}(\rho\overline{H}) + \nabla\cdot(\rho\overline{v}\,\overline{H}) = \nabla\cdot\left(\frac{k_t}{c_p}\nabla\overline{H}\right) + S_h \tag{8.25}$$

where $S_h$ accounts for source terms due to radiation, heat transfer to wall boundaries, and heat exchange with the dispersed phase.

Figure 8.6: Logical Dependence of Averaged Scalars on Mean Mixture Fraction, the Mixture Fraction Variance, Mean Enthalpy, and the Chemistry Model (Non-Adiabatic, Single-Mixture-Fraction Systems) (p. 225) depicts the logical dependence of mean scalar values (species mass fraction, density, and temperature) on ANSYS Fluent's prediction of $\overline{f}$, $\overline{f'^2}$, and $\overline{H}$ in non-adiabatic single-mixture-fraction systems.

**Figure 8.6: Logical Dependence of Averaged Scalars on Mean Mixture Fraction, the Mixture Fraction Variance, Mean Enthalpy, and the Chemistry Model (Non-Adiabatic, Single-Mixture-Fraction Systems)**

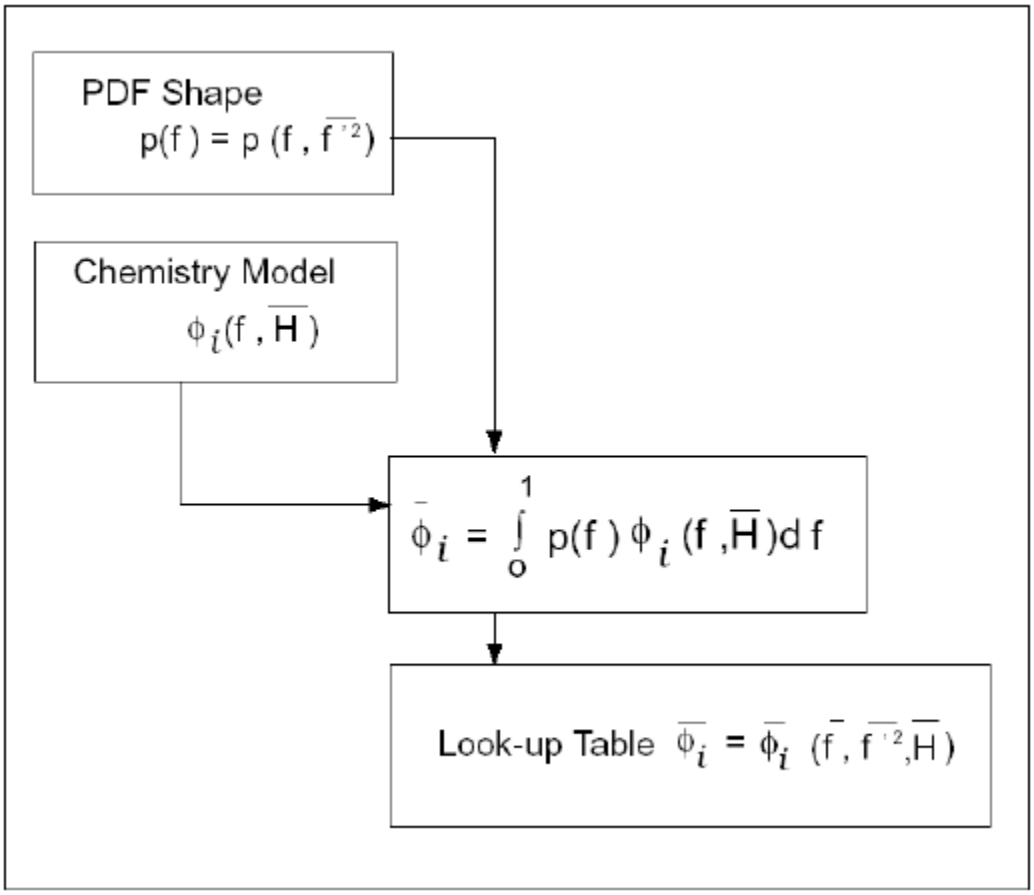

When a secondary stream is included, the mean values are calculated from

$$\overline{\phi}_i = \int_0^1 \int_0^1 \phi_i\left(f_{fuel}, p_{sec}, \overline{H}\right) p_1\left(f_{fuel}\right) p_2\left(p_{sec}\right) d f_{fuel} d p_{sec} \tag{8.26}$$

As noted above, the non-adiabatic extensions to the PDF model are required in systems involving heat transfer to walls and in systems with radiation included. In addition, the non-adiabatic model is required in systems that include multiple fuel or oxidizer inlets with different inlet temperatures. Finally, the non-adiabatic model is required in particle-laden flows (for example, liquid fuel systems or coal combustion systems) when such flows include heat transfer to the dispersed phase. Figure 8.7: Reacting Systems Requiring Non-Adiabatic Non-Premixed Model Approach (p. 226) illustrates several systems that must include the non-adiabatic form of the PDF model.

**Figure 8.7: Reacting Systems Requiring Non-Adiabatic Non-Premixed Model Approach**

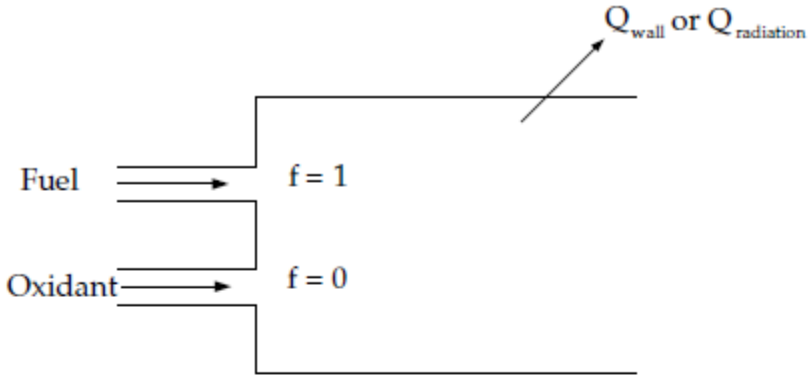


(a) Heat Transfer to Domain Boundaries and/or Radiation Heat Transfer

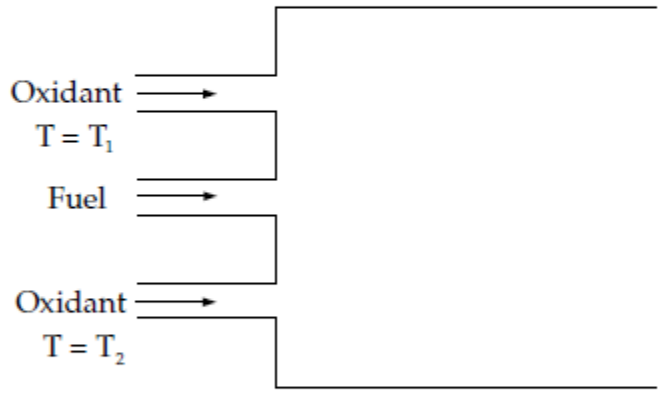


(b) Multiple Fuel or Oxidant Inlets at Different Temperatures

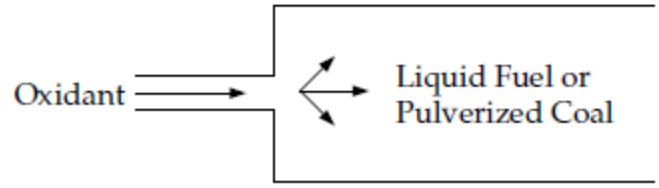


(c) Dispersed Phase Heat or Mass Transfer (e.g., Liquid Fuel or Coal Combustion)


Release 15.0 - © SAS IP, Inc. All rights reserved. - Contains proprietary and confidential information of ANSYS, Inc. and its subsidiaries and affiliates.

## 8.2.4. Chemistry Tabulation

### *8.2.4.1. Look-Up Tables for Adiabatic Systems*

For an equilibrium, adiabatic, single-mixture-fraction case, the mean temperature, density, and species fraction are functions of the $\overline{f}$ and $\overline{f'^2}$ only (see Equation 8.16 (p. 222) and Equation 8.21 (p. 223)). Significant computational time can be saved by computing these integrals once, storing them in a look-up table, and retrieving them during the ANSYS Fluent simulation.

Figure 8.8: Visual Representation of a Look-Up Table for the Scalar (Mean Value of Mass Fractions, Density, or Temperature) as a Function of Mean Mixture Fraction and Mixture Fraction Variance in Adiabatic Single-Mixture-Fraction Systems (p. 227) illustrates the concept of the look-up tables generated for a single-mixture-fraction system. Given ANSYS Fluent's predicted value for $\overline{f}$ and $\overline{f'^2}$ at a point in the flow domain, the mean value of mass fractions, density, or temperature ($\overline{\phi}_i$) at that point can be obtained by table interpolation.

The table, Figure 8.8: Visual Representation of a Look-Up Table for the Scalar (Mean Value of Mass Fractions, Density, or Temperature) as a Function of Mean Mixture Fraction and Mixture Fraction Variance in Adiabatic Single-Mixture-Fraction Systems (p. 227), is the mathematical result of the integration of Equation 8.16 (p. 222). There is one look-up table of this type for each scalar of interest (species mass fractions, density, and temperature). In adiabatic systems, where the instantaneous enthalpy is a function of only the instantaneous mixture fraction, a two-dimensional look-up table, like that in Figure 8.8: Visual Representation of a Look-Up Table for the Scalar (Mean Value of Mass Fractions, Density, or Temperature) as a Function of Mean Mixture Fraction and Mixture Fraction Variance in Adiabatic Single-Mixture-Fraction Systems (p. 227), is all that is required.

**Figure 8.8: Visual Representation of a Look-Up Table for the Scalar (Mean Value of Mass Fractions, Density, or Temperature) as a Function of Mean Mixture Fraction and Mixture Fraction Variance in Adiabatic Single-Mixture-Fraction Systems**

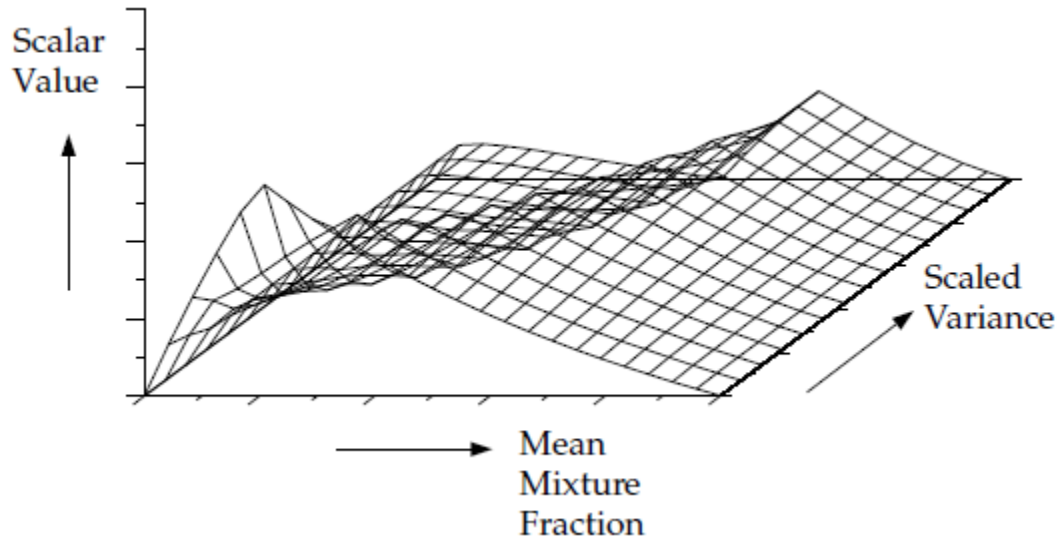


For systems with two mixture fractions, the creation and interpolation costs of four-dimensional look-up tables are computationally expensive. By default, the instantaneous properties $\phi_i$ are tabulated as a function of the fuel mixture fraction $f_{fuel}$ and the secondary partial fraction $p_{sec}$ (see Equa-

tion 8.12 (p. 220)), and the PDF integrations (see Equation 8.14 (p. 220)) are performed at run-time. This two-dimensional table is illustrated in Figure 8.9: Visual Representation of a Look-Up Table for the Scalar $\phi$_I as a Function of Fuel Mixture Fraction and Secondary Partial Fraction in Adiabatic Two-Mixture-Fraction Systems (p. 228). Alternatively, 4D look-up tables can be created before the simulation and interpolated at run time (see Full Tabulation of the Two-Mixture-Fraction Model in the User's Guide).

**Figure 8.9: Visual Representation of a Look-Up Table for the Scalar $\phi$_I as a Function of Fuel Mixture Fraction and Secondary Partial Fraction in Adiabatic Two-Mixture-Fraction Systems**

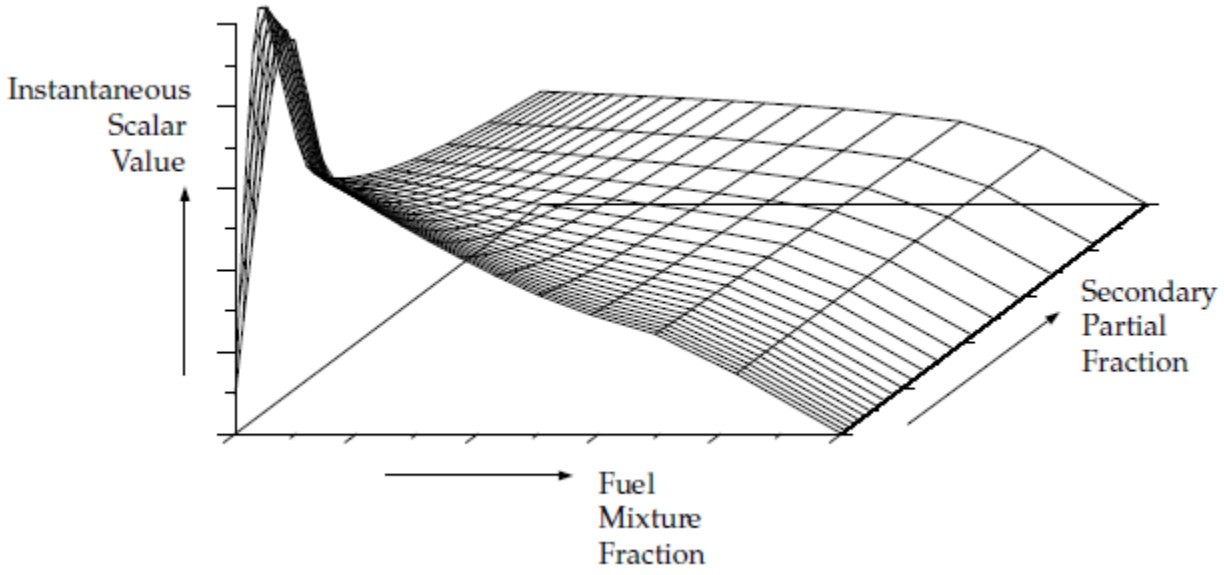


## 8.2.4.2. 3D Look-Up Tables for Non-Adiabatic Systems

In non-adiabatic systems, where the enthalpy is not linearly related to the mixture fraction, but depends also on wall heat transfer and/or radiation, a look-up table is required for each possible enthalpy value in the system. The result, for single mixture fraction systems, is a three-dimensional look-up table, as illustrated in Figure 8.10: Visual Representation of a Look-Up Table for the Scalar as a Function of Mean Mixture Fraction and Mixture Fraction Variance and Normalized Heat Loss/Gain in Non-Adiabatic Single-Mixture-Fraction Systems (p. 229), which consists of layers of two-dimensional tables, each one corresponding to a normalized heat loss or gain. The first slice corresponds to the maximum heat loss from the system, the last slice corresponds to the maximum heat gain to the system, and the zero heat loss/gain slice corresponds to the adiabatic table. Slices interpolated between the adiabatic and maximum slices correspond to heat gain, and those interpolated between the adiabatic and minimum slices correspond to heat loss.

The three-dimensional look-up table allows ANSYS Fluent to determine the value of each mass fraction, density, and temperature from calculated values of $\overline{f}$, $\overline{f'^2}$, and $\overline{H}$. This three-dimensional table in Figure 8.10: Visual Representation of a Look-Up Table for the Scalar as a Function of Mean Mixture Fraction and Mixture Fraction Variance and Normalized Heat Loss/Gain in Non-Adiabatic Single-Mixture-Fraction Systems (p. 229) is the visual representation of the integral in Equation 8.24 (p. 225).


Release 15.0 - © SAS IP, Inc. All rights reserved. - Contains proprietary and confidential information of ANSYS, Inc. and its subsidiaries and affiliates.

**Figure 8.10: Visual Representation of a Look-Up Table for the Scalar as a Function of Mean Mixture Fraction and Mixture Fraction Variance and Normalized Heat Loss/Gain in Non-Adiabatic Single-Mixture-Fraction Systems**

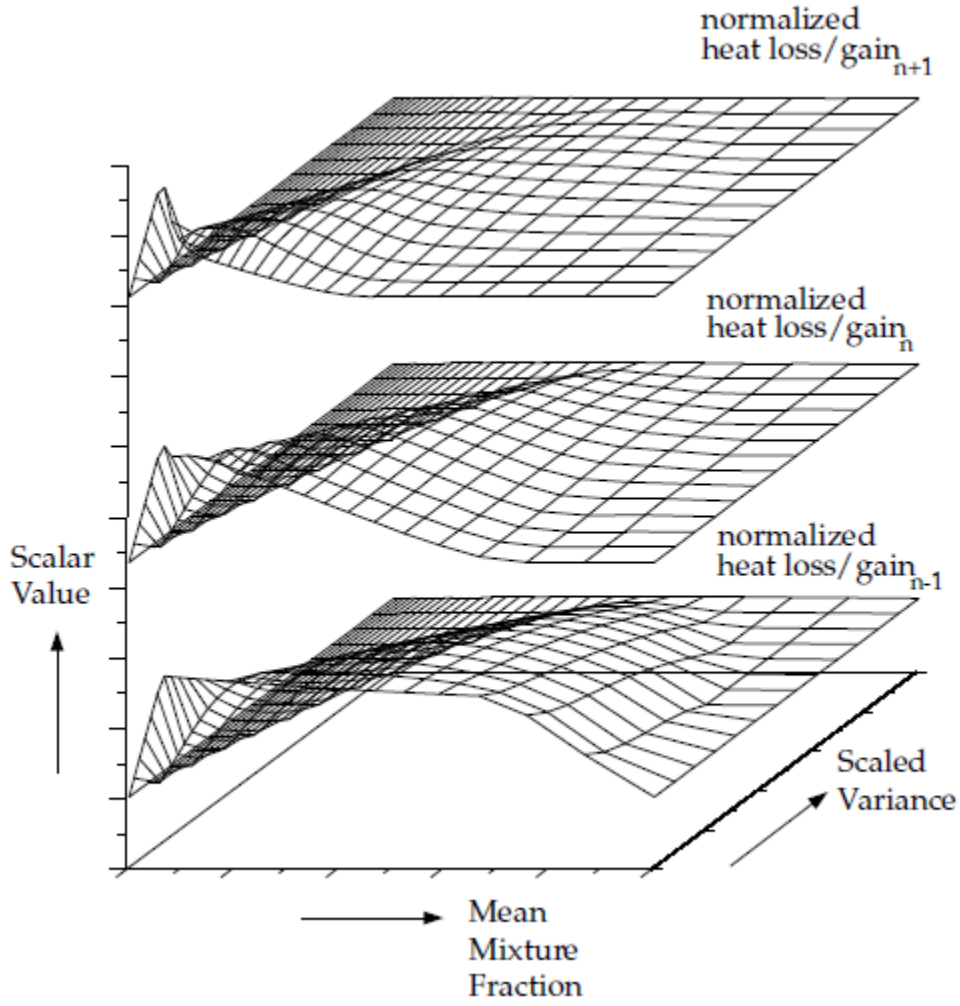


For non-adiabatic, two-mixture-fraction problems, it is very expensive to tabulate and retrieve Equation 8.26 (p. 226) since five-dimensional tables are required. By default, 3D lookup tables of the instantaneous state relationship given by Equation 8.14 (p. 220) are created. The 3D table in Figure 8.11: Visual Representation of a Look-Up Table for the Scalar $\phi$_I as a Function of Fuel Mixture Fraction and Secondary Partial Fraction, and Normalized Heat Loss/Gain in Non-Adiabatic Two-Mixture-Fraction Systems (p. 230) is the visual representation of Equation 8.14 (p. 220). The mean density during the ANSYS Fluent solution is calculated by integrating the instantaneous density over the fuel and secondary mixture fraction space (see Equation 8.26 (p. 226)). Alternatively, 5D look-up tables can be created before the simulation and interpolated at run time (see Full Tabulation of the Two-Mixture-Fraction Model in the User's Guide). The one-time pre-generation of the 5D look-up table is very expensive, but, once built, interpolating the table during an ANSYS Fluent solution is usually significantly faster than performing the integrations at run-time. This is especially true for cases with a large number of cells that require many iteration or time-steps to converge.

**Important**

Note that the computation time in ANSYS Fluent for a two-mixture-fraction case will be much greater than for a single-mixture-fraction problem. This expense should be carefully considered

Release 15.0 - © SAS IP, Inc. All rights reserved. - Contains proprietary and confidential information of ANSYS, Inc. and its subsidiaries and affiliates.

before choosing the two-mixture-fraction model. Also, it is usually expedient to start a two-mixture-fraction simulation from a converged single-mixture-fraction solution.

**Figure 8.11: Visual Representation of a Look-Up Table for the Scalar $\phi$_I as a Function of Fuel Mixture Fraction and Secondary Partial Fraction, and Normalized Heat Loss/Gain in Non-Adiabatic Two-Mixture-Fraction Systems**

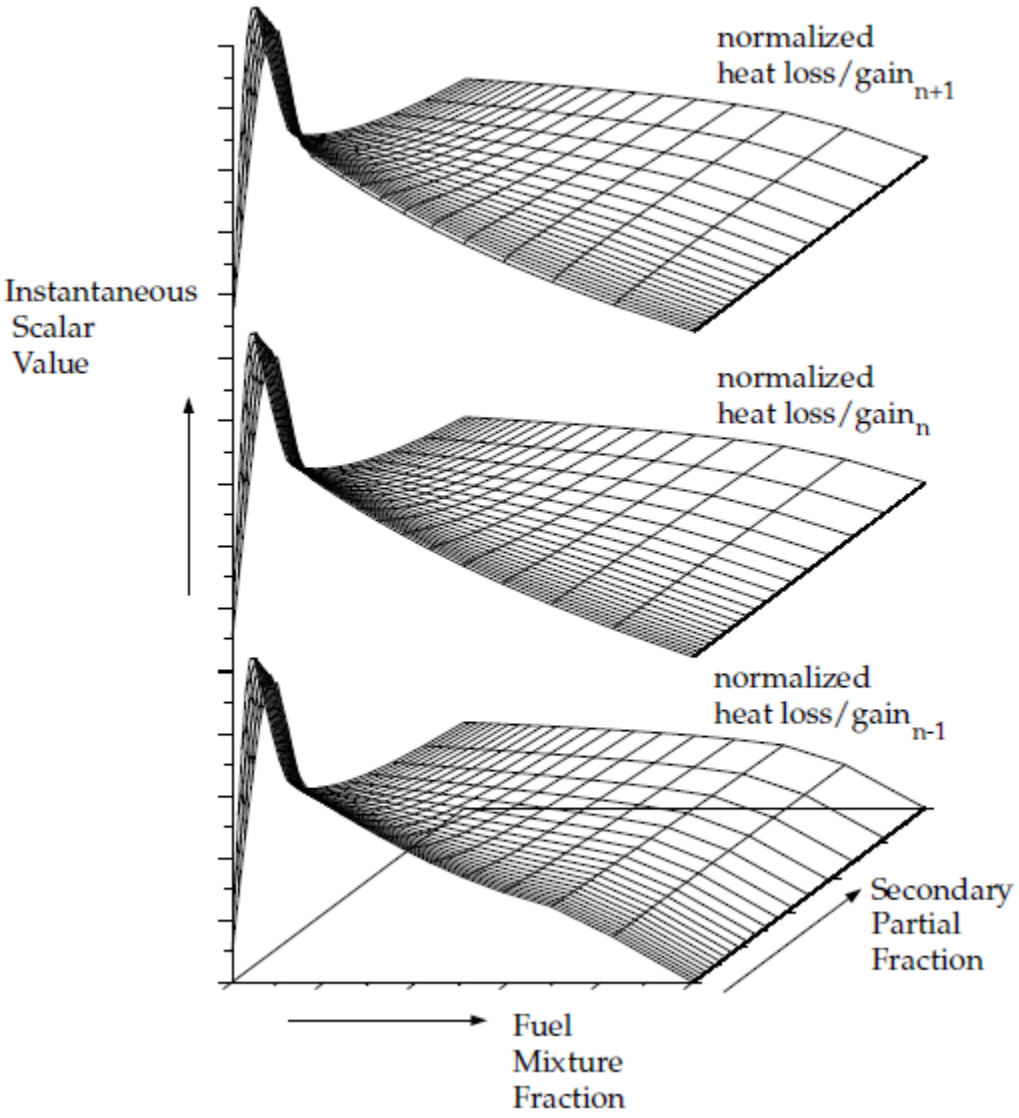


## 8.2.4.3. Generating Lookup Tables Through Automated Grid Refinement

ANSYS Fluent has the capability of generating lookup tables using **Automated Grid Refinement**. This is where an adaptive algorithm inserts grid points in all table dimensions so that changes in the values of tabulated variables (such as mean temperature, density and species mass fractions) between successive grid points, as well as changes in their slopes, are less than a user specified tolerance. The advantage of automated grid refinement is that tabulated quantities are resolved only in regions of rapid change, therefore, more accurate and/or smaller PDF tables are generated, compared to the alternative of an a priori fixed grid.


Release 15.0 - © SAS IP, Inc. All rights reserved. - Contains proprietary and confidential information of ANSYS, Inc. and its subsidiaries and affiliates.

When using automated grid refinement, table points are calculated on a coarse grid with a user specified **Initial Number of Grid Points** (default of $15$). A new grid point is inserted midway between a point $i$ and its neighbor $i+1$ if,

$$| v_i - v_{i+1} | > \varepsilon_v ( v_{max} - v_{min} ) \tag{8.27}$$

where $v_i$ is the value of a table variable at grid point $i$, $\varepsilon_v$ is a user specified **Maximum Change in Value Ratio** (default of $0.25$), and $v_{max}$ ($v_{min}$) are the maximum (minimum) table values over all grid points.

In addition to ensuring gradual change in value between successive table points, a grid point is added if

$$| s_i - s_{i+1} | > \varepsilon_s ( s_{max} - s_{min} ) \tag{8.28}$$

where the slope at any point $s_i$ is defined as,

$$s_i = \frac{v_{i+1} - v_i}{\varphi_{i+1} - \varphi_i} \tag{8.29}$$

In Equation 8.28 (p. 231) and Equation 8.29 (p. 231), $\varepsilon_s$ is a user specified **Maximum Change in Slope Ratio** (default of $0.25$), $s_{max}$ ($s_{min}$) are the maximum (minimum) slopes over all grid points, and $\varphi_i$ is the value of the independent grid variable being refined (that is, mean mixture fraction, mixture fraction variance or mean enthalpy).

The automated grid refinement algorithm is summarized as follows: an initial grid in the mean mixture fraction dimension is created with the specified **Initial Number of Grid Points**. Grid points are then inserted when the change in table mean temperature, and mean H2, CO and OH mole fractions, between two grid points, or the change in their slope between three grid points, is less than what you specified in **Maximum Change in Value/Slope Ratio**. This process is repeated until all points satisfy the specified value and slope change requirements, or the **Maximum Number of Grid Points** is exceeded. This procedure is then repeated for the mixture fraction variance dimension, which is calculated at the mean stoichiometric mixture fraction. Finally, if the non-adiabatic option is enabled, the procedure is repeated for the mean enthalpy grid, evaluated at the mean stoichiometric mixture fraction and zero mixture fraction variance.

When steady diffusion flamelets are used, the **Automated Grid Refinement** can generate different mean mixture fraction grid points than specified in the diffusion flamelets. For such cases, a 4th order polynomial interpolation is used to obtain the flamelet solution at the inserted points.

**Note**

The second order interpolation option is faster than fourth order interpolation, especially for tables with high dimensions, such as non-adiabatic flamelets. However, under-resolved tables that are interpolated with second order can lead to convergence difficulties. Therefore, the Automated Grid Refinement (AGR) option places grid points optimally when generating PDF tables. Hence, AGR should be used in general, and especially for second order interpolation.

**Note**

Automated grid refinement is not available with two mixture fractions.

Release 15.0 - © SAS IP, Inc. All rights reserved. - Contains proprietary and confidential information of ANSYS, Inc. and its subsidiaries and affiliates.

For more information about the input parameters used to generate lookup tables, refer to Calculating the Look-Up Tables in the User's Guide.

## 8.3. Restrictions and Special Cases for Using the Non-Premixed Model

For information about restrictions and special cases for using the non-premixed model, see the following sections:

8.3.1. Restrictions on the Mixture Fraction Approach
8.3.2. Using the Non-Premixed Model for Liquid Fuel or Coal Combustion
8.3.3. Using the Non-Premixed Model with Flue Gas Recycle
8.3.4. Using the Non-Premixed Model with the Inert Model

### 8.3.1. Restrictions on the Mixture Fraction Approach

The unique dependence of $\phi_i$ (species mass fractions, density, or temperature) on $f$ (Equation 8.11 (p. 220) or Equation 8.13 (p. 220)) requires that the reacting system meet the following conditions:

- The chemical system must be of the diffusion type with discrete fuel and oxidizer inlets (spray combustion and pulverized fuel flames may also fall into this category).
- The Lewis number must be unity. (This implies that the diffusion coefficients for all species and enthalpy are equal, a good approximation in turbulent flow).
- When a single mixture fraction is used, the following conditions must be met:
  - Only one type of fuel is involved. The fuel may be made up of a burnt mixture of reacting species (for example, 90% $CH_4$ and 10% $CO$) and you may include multiple fuel inlets. The multiple fuel inlets must have the same composition; two or more fuel inlets with different fuel composition are not allowed (for example, one inlet of $CH_4$ and one inlet of $CO$). Similarly, in spray combustion systems or in systems involving reacting particles, only one off-gas is permitted.
  - Only one type of oxidizer is involved. The oxidizer may consist of a mixture of species (for example, 21% $O_2$ and 79% $N_2$) and you may have multiple oxidizer inlets. The multiple oxidizer inlets must, however, have the same composition. Two or more oxidizer inlets with different compositions are not allowed (for example, one inlet of air and a second inlet of pure oxygen).
- When two mixture fractions are used, three streams can be involved in the system. Valid systems are as follows:
  - Two fuel streams with different compositions and one oxidizer stream. Each fuel stream may be made up of a mixture of reacting species (for example, 90% $CH_4$ and 10% $CO$). You may include multiple inlets of each fuel stream, but each fuel inlet must have one of the two defined compositions (for example, one inlet of $CH_4$ and one inlet of $CO$).
  - Mixed fuel systems including gas-liquid, gas-coal, or liquid-coal fuel mixtures with a single oxidizer. In systems with a gas-coal or liquid-coal fuel mixture, the coal volatiles and char can be treated as a single composite fuel stream and the secondary stream can represent another fuel. Alternatively, for coal combustion, the volatile and char off-gases are tracked separately as distinct fuel streams.
  - Two oxidizer streams with different compositions and one fuel stream. Each oxidizer stream may consist of a mixture of species (for example 21% $O_2$ and 79% $N_2$). You may have multiple inlets of each oxidizer


Release 15.0 - © SAS IP, Inc. All rights reserved. - Contains proprietary and confidential information of ANSYS, Inc. and its subsidiaries and affiliates.

stream, but each oxidizer inlet must have one of the two defined compositions (for example, one inlet of air and a second inlet of pure oxygen).

  – A fuel stream, an oxidizer stream, and a non-reacting secondary stream.

- The flow must be turbulent.

It is important to emphasize that these restrictions eliminate the use of the non-premixed approach for directly modeling premixed combustion. This is because the unburned premixed stream is far from chemical equilibrium. Note, however, that an extended mixture fraction formulation, the partially premixed model (see Partially Premixed Combustion (p. 273)), can be applied to non-premixed (with mixed-but-unburnt regions), as well as partially premixed flames.

Figure 8.12: Chemical Systems That Can Be Modeled Using a Single Mixture Fraction (p. 234) and Figure 8.13: Chemical System Configurations That Can Be Modeled Using Two Mixture Fractions (p. 235) illustrate typical reacting system configurations that can be handled by the non-premixed model in ANSYS Fluent. Figure 8.14: Premixed Systems That Cannot Be Modeled Using the Non-Premixed Model (p. 235) shows a premixed configuration that cannot be modeled using the non-premixed model.

Release 15.0 - © SAS IP, Inc. All rights reserved. - Contains proprietary and confidential information of ANSYS, Inc. and its subsidiaries and affiliates.

**Figure 8.12: Chemical Systems That Can Be Modeled Using a Single Mixture Fraction**

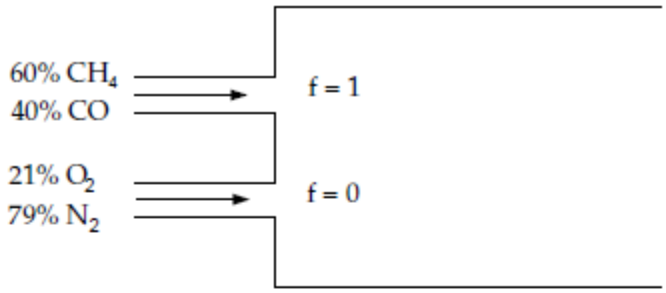


(a) Simple Fuel/Oxidant Diffusion Flame

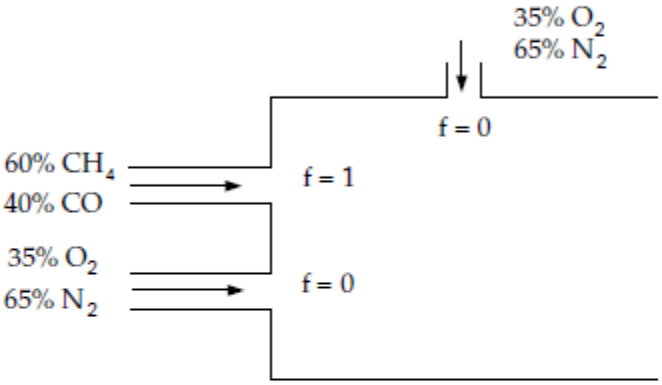


(b) Diffusion System Using Multiple Oxidant Inlets

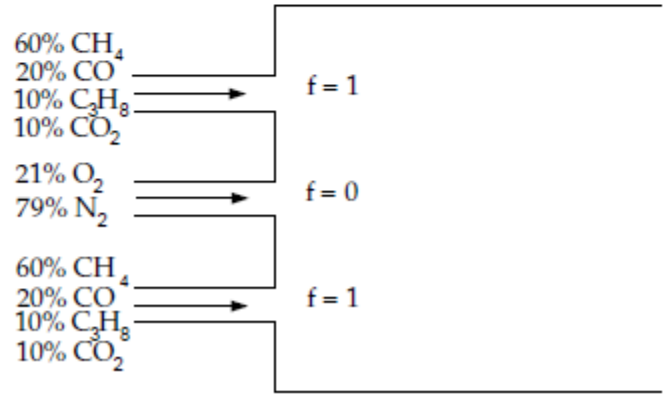


(c) System Using Multiple Fuel Inlets


Release 15.0 - © SAS IP, Inc. All rights reserved. - Contains proprietary and confidential information of ANSYS, Inc. and its subsidiaries and affiliates.

**Figure 8.13: Chemical System Configurations That Can Be Modeled Using Two Mixture Fractions**

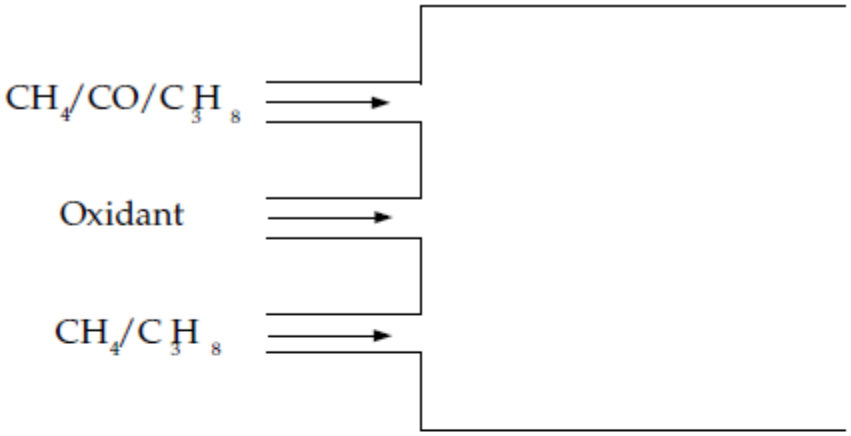


(a) System Containing Two Dissimilar Fuel Inlets

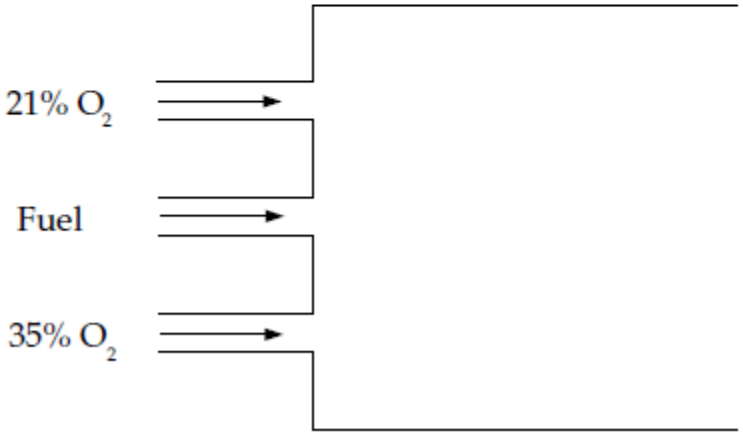


(b) System Containing Two Dissimilar Oxidant Inlets

**Figure 8.14: Premixed Systems That Cannot Be Modeled Using the Non-Premixed Model**

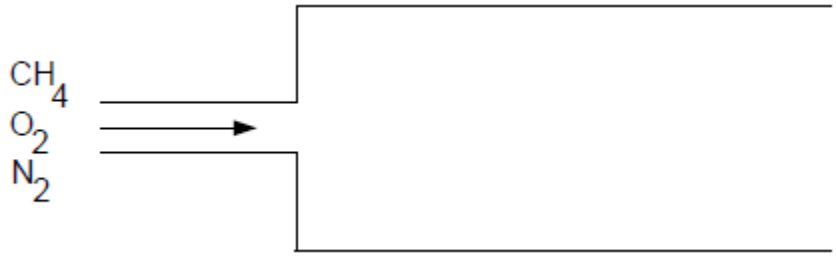


## 8.3.2. Using the Non-Premixed Model for Liquid Fuel or Coal Combustion

You can use the non-premixed model if your ANSYS Fluent simulation includes liquid droplets and/or coal particles. In this case, fuel enters the gas phase within the computational domain at a rate determined by the evaporation, devolatilization, and char combustion laws governing the dispersed phase. In the case of coal, the volatiles and the products of char can be defined as two different types of fuel

Release 15.0 - © SAS IP, Inc. All rights reserved. - Contains proprietary and confidential information of ANSYS, Inc. and its subsidiaries and affiliates.

(using two mixture fractions) or as a single composite off-gas (using one mixture fraction), as described in Modeling Coal Combustion Using the Non-Premixed Model in the User's Guide.

## 8.3.3. Using the Non-Premixed Model with Flue Gas Recycle

While most problems you solve using the non-premixed model will involve inlets that contain either pure oxidant or pure fuel ($f = 0$ or 1), you can include an inlet that has an intermediate value of mixture fraction ($0 < f < 1$) provided that this inlet represents a completely reacted mixture. Such cases arise when there is flue gas recirculation, as depicted schematically in Figure 8.15: Using the Non-Premixed Model with Flue Gas Recycle (p. 236). Since $f$ is a conserved quantity, the mixture fraction at the flue gas recycle inlet can be computed as

$$\dot{m}_{fuel} + \dot{m}_{recyc} f_{exit} = \left(\dot{m}_{fuel} + \dot{m}_{ox} + \dot{m}_{recyc}\right) f_{exit} \tag{8.30}$$

or

$$f_{exit} = \frac{\dot{m}_{fuel}}{\dot{m}_{fuel} + \dot{m}_{ox}} \tag{8.31}$$

where $f_{exit}$ is the exit mixture fraction (and the mixture fraction at the flue gas recycle inlet), $\dot{m}_{ox}$ is the mass flow rate of the oxidizer inlet, $\dot{m}_{fuel}$ is the mass flow rate of the fuel inlet, $\dot{m}_{recyc}$ is the mass flow rate of the recycle inlet.

If a secondary stream is included,

$$f_{fuel,exit} = \frac{\dot{m}_{fuel}}{\dot{m}_{fuel} + \dot{m}_{sec} + \dot{m}_{ox}} \tag{8.32}$$

and

$$p_{sec,exit} = \frac{\dot{m}_{sec}}{\dot{m}_{sec} + \dot{m}_{ox}} \tag{8.33}$$

**Figure 8.15: Using the Non-Premixed Model with Flue Gas Recycle**

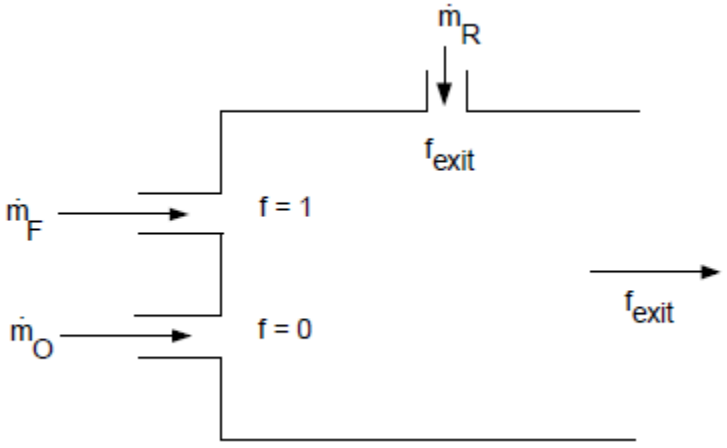



Release 15.0 - © SAS IP, Inc. All rights reserved. - Contains proprietary and confidential information of ANSYS, Inc. and its subsidiaries and affiliates.

## 8.3.4. Using the Non-Premixed Model with the Inert Model

To model the effect of dilution on combustion without the expense of using two mixture fractions, ANSYS Fluent allows the introduction of an inert stream into the domain. Unlike a secondary mixture fraction, the inert does not chemically equilibrate with the primary fuel and oxidizer - instead, its composition remains constant after mixing. However the inert stream does affect the solution due to its influence on enthalpy, specific heat, and density of the mixture. The equation for conservation of inert is written as:

$$\frac{\partial \rho Y_I}{\partial t} + \nabla \cdot ( \vec{v} \rho Y_I) = \nabla \cdot \left( \frac{\mu_l + \mu_t}{Sc_t} \nabla ( Y_I) \right) \tag{8.34}$$

where

$Y_I$ = inert stream tracer

$Sc_t$ = turbulent Schmidt number

$\mu_t$ = turbulent viscosity

$\rho$ = density

Equation 8.34 (p. 237) has no sources or sinks, because the problem is reduced to tracking a conserved scalar when it is assumed that the inert components have the same turbulent diffusivities.

### 8.3.4.1. Mixture Composition

The mixture properties are computed from the mean ($\overline{f}$) and variance ($\overline{f'}$) of the mixture fraction in the cell, the reaction progress variable ($c$, when the partially premixed model is enabled), the cell enthalpy ($H$, for non-adiabatic flows), and the inert tracer ($Y_I$). The mixture is modeled as a blend of inert and active species, but the PDF tables need to be accessed with *conditioned* variables. Conditioning is necessary to take into account the volume taken up by the inert fraction, yet still be able to utilize previously built tables by straightforward lookup. The mean mixture fraction and mixture fraction variance used to access the PDF table is given by:

$$\overline{f_I} = \frac{\overline{f}}{1 - Y_I} \tag{8.35}$$

$$f'^2_I = \frac{\overline{f'^2}}{(1 - Y_I)^2} \tag{8.36}$$

The reaction progress variable $c$ is not conditioned, however the cell enthalpy must be conditioned to account for the inert enthalpy. The inert enthalpy and active enthalpy are obtained from the following relationships:

$$H ( T ) = ( 1 - Y_I ) H^{pdf} ( T ) + Y_I H^I ( T ) \tag{8.37}$$

where $H$ is the enthalpy of the cell at temperature $T$, $H^{pdf}$ is the enthalpy of the active mixture-fraction stream and $H^I$ is the enthalpy of the inert stream. Here it is assumed that the inert and the active streams have the same temperature, but different enthalpies. To calculate the temperature in the cell,

Equation 8.37 (p. 237) is solved for the temperature and for $H^{pdf}$, which gives the partitioning of the energy between the inert and active streams.

The inert enthalpy is defined as

$$H^I(T) = \sum_{i=0}^{N_I} Y_i \int_{T_0}^{T} C_{p_i} dT \tag{8.38}$$

where $Y_i$ refers to the mass fraction of species $i$ defined in the inert stream, $T_0$ is the reference temperature, $C_{p_i}$ the specific heat of species $i$, and $N_I$ is the number of inert species.

The inert and PDF enthalpies are defined further in Equation 33.13 in the User's Guide.

#### 8.3.4.1.1. Property Evaluation

The specific heat of the mixture is evaluated by mixing the inert and active streams in the following way:

$$C_p(T) = (1 - Y_I)\, C_p^{pdf}(T) + Y_I C_p^I(T) \tag{8.39}$$

The density of the mixture is calculated by using a harmonic average of the densities of the active and inert streams, weighted by the inert tracer:

$$\rho(T) = \left[ \frac{(1 - Y_I)}{\rho^{pdf}(T)} + \frac{Y_I}{\rho^I(T)} \right]^{-1} \tag{8.40}$$

Here, the inert density ($\rho^I$) is calculated from the ideal gas law.

For information on how to set up the inert model, see Setting Up the Inert Model in the User's Guide.

## 8.4. The Diffusion Flamelet Models Theory

Information about the flamelet models are presented in the following sections:

8.4.1. Restrictions and Assumptions
8.4.2. The Flamelet Concept
8.4.3. Flamelet Generation
8.4.4. Flamelet Import

## 8.4.1. Restrictions and Assumptions

The following restrictions apply to all diffusion flamelet models in ANSYS Fluent:

- Only a single mixture fraction can be modeled; two-mixture-fraction flamelet models are not allowed.
- The mixture fraction is assumed to follow the $\beta$-function PDF, and scalar dissipation fluctuations are ignored.
- Empirically-based streams cannot be used with the flamelet model.


Release 15.0 - © SAS IP, Inc. All rights reserved. - Contains proprietary and confidential information of ANSYS, Inc. and its subsidiaries and affiliates.

## 8.4.2. The Flamelet Concept

### 8.4.2.1. Overview

The flamelet concept views the turbulent flame as an ensemble of thin, laminar, locally one-dimensional flamelet structures embedded within the turbulent flow field [44] (p. 731), [345] (p. 748), [346] (p. 748) (see Figure 8.16: Laminar Opposed-Flow Diffusion Flamelet (p. 239)).

**Figure 8.16: Laminar Opposed-Flow Diffusion Flamelet**

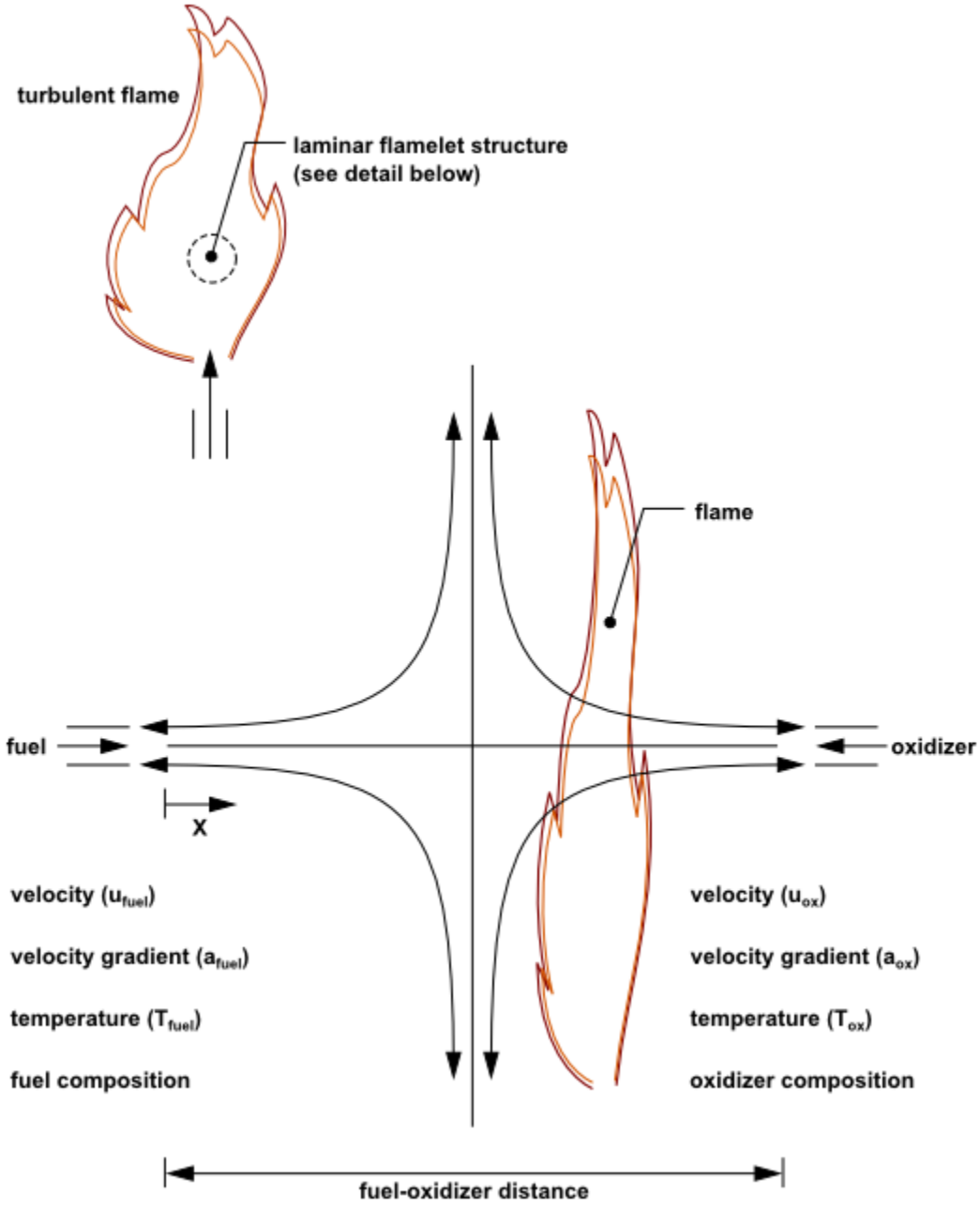


A common laminar flame type used to represent a flamelet in a turbulent flow is the counterflow diffusion flame. This geometry consists of opposed, axisymmetric fuel and oxidizer jets. As the distance between the jets is decreased and/or the velocity of the jets increased, the flame is strained and increasingly departs from chemical equilibrium until it is eventually extinguished. The species mass fraction and temperature fields can be measured in laminar counterflow diffusion flame experiments, or, most

Release 15.0 - © SAS IP, Inc. All rights reserved. - Contains proprietary and confidential information of ANSYS, Inc. and its subsidiaries and affiliates.

commonly, calculated. For the latter, a self-similar solution exists, and the governing equations can be simplified to one dimension along the axis of the fuel and oxidizer jets, where complex chemistry calculations can be affordably performed.

In the laminar counterflow flame, the mixture fraction, $f$, (see Definition of the Mixture Fraction (p. 216)) decreases monotonically from unity at the fuel jet to zero at the oxidizer jet. If the species mass fraction and temperature along the axis are mapped from physical space to mixture fraction space, they can be uniquely described by two parameters: the mixture fraction and the strain rate (or, equivalently, the scalar dissipation, $\chi$, defined in Equation 8.42 (p. 240)). Hence, the chemistry is reduced and completely described by the two quantities, $f$ and $\chi$.

This reduction of the complex chemistry to two variables allows the flamelet calculations to be preprocessed, and stored in look-up tables. By preprocessing the chemistry, computational costs are reduced considerably.

The balance equations, solution methods, and sample calculations of the counterflow laminar diffusion flame can be found in several references. Comprehensive reviews and analyses are presented in the works of Bray and Peters, and Dixon-Lewis [44] (p. 731), [92] (p. 734).

### 8.4.2.2. Strain Rate and Scalar Dissipation

A characteristic strain rate for a counterflow diffusion flamelet can be defined as $a_s = v/2d$, where $v$ is the relative speed of the fuel and oxidizer jets, and $d$ is the distance between the jet nozzles.

Instead of using the strain rate to quantify the departure from equilibrium, it is expedient to use the scalar dissipation, denoted by $\chi$. The scalar dissipation is defined as

$$\chi = 2D|\nabla f|^2 \tag{8.41}$$

where $D$ is a representative diffusion coefficient.

Note that the scalar dissipation, $\chi$, varies along the axis of the flamelet. For the counterflow geometry, the flamelet strain rate $a_s$ can be related to the scalar dissipation at the position where $f$ is stoichiometric by [345] (p. 748):

$$\chi_{st} = \frac{a_s \exp\left(-2\left[erfc^{-1}\left(2f_{st}\right)\right]^2\right)}{\pi} \tag{8.42}$$

where

$\chi_{st}$ = scalar dissipation at $f = f_{st}$

$a_s$ = characteristic strain rate

$f_{st}$ = stoichiometric mixture fraction

$erfc^{-1}$ = inverse complementary error function

Physically, as the flame is strained, the width of the reaction zone diminishes, and the gradient of $f$ at the stoichiometric position $f = f_{st}$ increases. The instantaneous stoichiometric scalar dissipation, $\chi_{st}$, is used as the essential non-equilibrium parameter. It has the dimensions $\mathrm{s}^{-1}$ and may be interpreted as


Release 15.0 - © SAS IP, Inc. All rights reserved. - Contains proprietary and confidential information of ANSYS, Inc. and its subsidiaries and affiliates.

the inverse of a characteristic diffusion time. In the limit $\chi_{st} \rightarrow 0$ the chemistry tends to equilibrium, and as $\chi_{st}$ increases due to aerodynamic straining, the non-equilibrium increases. Local quenching of the flamelet occurs when $\chi_{st}$ exceeds a critical value.

### 8.4.2.3. Embedding Diffusion Flamelets in Turbulent Flames

A turbulent flame brush is modeled as an ensemble of discrete diffusion flamelets. Since, for adiabatic systems, the species mass fraction and temperature in the diffusion flamelets are completely parameterized by $f$ and $\chi_{st}$, density-weighted mean species mass fractions and temperature in the turbulent flame can be determined from the PDF of $f$ and $\chi_{st}$ as

$$\overline{\phi} = \int \int \phi\left(f, \chi_{st}\right) p\left(f, \chi_{st}\right) df \, d\chi_{st} \tag{8.43}$$

where $\phi$ represents species mass fractions and temperature.

In ANSYS Fluent, $f$ and $\chi_{st}$ are assumed to be statistically independent, so the joint PDF $p\left(f, \chi_{st}\right)$ can be simplified as $p_f(f) p_\chi\left(\chi_{st}\right)$. A $\beta$ PDF shape is assumed for $p_f$, and transport equations for $\overline{f}$ and $\overline{f'^2}$ are solved in ANSYS Fluent to specify $p_f$. Fluctuations in $\chi_{st}$ are ignored so that the PDF of $\chi$ is a delta function: $p_\chi = \delta(\chi - \overline{\chi})$. The first moment, namely the mean scalar dissipation, $\overline{\chi_{st}}$, is modeled in ANSYS Fluent as

$$\overline{\chi_{st}} = \frac{C_\chi \varepsilon \overline{f'^2}}{k} \tag{8.44}$$

where $C_\chi$ is a constant with a default value of 2.

For LES, the mean scalar dissipation is modeled as

$$\overline{\chi_{st}} = C_\chi \frac{\left(\mu_t + \mu\right)}{\rho \sigma_t} |\nabla \overline{f}|^2 \tag{8.45}$$

To avoid the PDF convolutions at ANSYS Fluent run-time, the integrations in Equation 8.43 (p. 241) are preprocessed and stored in look-up tables. For adiabatic flows, flamelet tables have three dimensions: $\overline{f}$, $\overline{f'^2}$ and $\overline{\chi_{st}}$.

For non-adiabatic steady diffusion flamelets, the additional parameter of enthalpy is required. However, the computational cost of modeling steady diffusion flamelets over a range of enthalpies is prohibitive, so some approximations are made. Heat gain/loss to the system is assumed to have a negligible effect on the species mass fractions, and adiabatic mass fractions are used [33] (p. 730), [311] (p. 746). The temperature is then calculated from Equation 5.7 (p. 135) for a range of mean enthalpy gain/loss, $\overline{H}$. Accordingly, mean temperature and density PDF tables have an extra dimension of mean enthalpy. The approximation of constant adiabatic species mass fractions is, however, not applied for the case corresponding to a scalar dissipation of zero. Such a case is represented by the non-adiabatic equilibrium solution. For $\overline{\chi_{st}} = 0$, the species mass fractions are computed as functions of $\overline{f}$, $\overline{f'^2}$, and $\overline{H}$.

Release 15.0 - © SAS IP, Inc. All rights reserved. - Contains proprietary and confidential information of ANSYS, Inc. and its subsidiaries and affiliates.

In ANSYS Fluent, you can either generate your own diffusion flamelets, or import them as flamelet files calculated with other stand-alone packages. Such stand-alone codes include OPPDIF [273] (p. 744) , CFX-RIF [20] (p. 730), [21] (p. 730), [353] (p. 748) and RUN-1DL [349] (p. 748). ANSYS Fluent can import flamelet files in OPPDIF format or standard flamelet file format.

Instructions for generating and importing diffusion flamelets are provided in Flamelet Generation (p. 242) and Flamelet Import (p. 242).

## 8.4.3. Flamelet Generation

The laminar counterflow diffusion flame equations can be transformed from physical space (with $x$ as the independent variable) to mixture fraction space (with $f$ as the independent variable) [354] (p. 748). In ANSYS Fluent, a simplified set of the mixture fraction space equations are solved [353] (p. 748). Here, $N$ equations are solved for the species mass fractions, $Y_i$,

$$\rho\frac{\partial Y_i}{\partial t}=\frac{1}{2}\rho\chi\frac{\partial^2 Y_i}{\partial f^2}+S_i \tag{8.46}$$

and one equation for temperature:

$$\rho\frac{\partial T}{\partial t}=\frac{1}{2}\rho\chi\frac{\partial^2 T}{\partial f^2}-\frac{1}{c_p}\sum_i H_i S_i+\frac{1}{2c_p}\rho\chi\left[\frac{\partial c_p}{\partial f}+\sum_i c_{p,i}\frac{\partial Y_i}{\partial f}\right]\frac{\partial T}{\partial f} \tag{8.47}$$

The notation in Equation 8.46 (p. 242) and Equation 8.47 (p. 242) is as follows: $Y_i$, $T$, $\rho$, and $f$ are the $i^{\text{th}}$ species mass fraction, temperature, density, and mixture fraction, respectively. $c_{p,i}$ and $c_p$ are the $i^{\text{th}}$ species specific heat and mixture-averaged specific heat, respectively. $S_i$ is the $i^{\text{th}}$ species reaction rate, and $H_i$ is the specific enthalpy of the $i^{\text{th}}$ species.

The scalar dissipation, $\chi$, must be modeled across the flamelet. An extension of Equation 8.42 (p. 240) to variable density is used [205] (p. 740):

$$\chi(f)=\frac{a_s}{4\pi}\frac{3\left(\sqrt{\rho_\infty/\rho}+1\right)^2}{2\sqrt{\rho_\infty/\rho}+1}\exp\left(-2\left[erfc^{-1}(2f)\right]^2\right) \tag{8.48}$$

where $\rho_\infty$ is the density of the oxidizer stream.

## 8.4.4. Flamelet Import

ANSYS Fluent can import one or more flamelet files, convolute these diffusion flamelets with the assumed-shape PDFs (see Equation 8.43 (p. 241)), and construct look-up tables. The flamelet files can be generated in ANSYS Fluent, or with separate stand-alone computer codes.

Three types of flamelet files can be imported into ANSYS Fluent: binary files generated by the OPPDIF code [273] (p. 744), ASCII files generated by the CFX-RIF code [20] (p. 730), [21] (p. 730), [353] (p. 748), and standard format files described in Standard Flamelet Files in the User's Guide and in Peters and Rogg [349] (p. 748).

When diffusion flamelets are generated in physical space (such as with OPPDIF), the species and temperature vary in one spatial dimension. The species and temperature must then be mapped from physical space to mixture fraction space. If the diffusion coefficients of all species are equal, a unique


Release 15.0 - © SAS IP, Inc. All rights reserved. - Contains proprietary and confidential information of ANSYS, Inc. and its subsidiaries and affiliates.

definition of the mixture fraction exists. However, with differential diffusion, the mixture fraction can be defined in a number of ways.

ANSYS Fluent provides four methods of computing the mixture fraction profile along the diffusion flamelet:

- Average of C and H: Following the work of Drake and Blint [97] (p. 734), the mixture fraction is calculated as the mean value of $f_C$ and $f_H$, where $f_C$ and $f_H$ are the mixture fraction values based on the carbon and hydrogen elements.

- Hydrocarbon formula: Following the work of Bilger et al. [32] (p. 730), the mixture fraction is calculated as

  $$f = \frac{b - b_{ox}}{b_{fuel} - b_{ox}} \tag{8.49}$$

  where

  $$b = 2\frac{Y_C}{M_{w,C}} + 0.5\frac{Y_H}{M_{w,H}} - \frac{Y_O}{M_{w,O}} \tag{8.50}$$

  $Y_C$, $Y_H$, and $Y_O$ are the mass fractions of carbon, hydrogen, and oxygen atoms, and $M_{w,C}$, $M_{w,H}$, and $M_{w,O}$ are the molecular weights. $b_{ox}$ and $b_{fuel}$ are the values of $b$ at the oxidizer and fuel inlets.

- Nitrogen method: The mixture fraction is computed in terms of the mass fraction of the nitrogen species:

  $$f = \frac{Y_N - Y_{N,ox}}{Y_{N,fuel} - Y_{N,ox}} \tag{8.51}$$

  where $Y_N$ is the elemental mass fraction of nitrogen along the flamelet, $Y_{N,ox}$ is the mass fraction of nitrogen at the oxidizer inlet, and $Y_{N,fuel}$ is the mass fraction of nitrogen at the fuel inlet.

- Read from a file (standard format files only):

  This option is for diffusion flamelets solved in mixture fraction space. If you choose this method, ANSYS Fluent will search for the mixture fraction keyword Z, as specified in Peter and Roggs's work [349] (p. 748), and retrieve the data. If ANSYS Fluent does not find mixture fraction data in the flamelet file, it will instead use the hydrocarbon formula method described above.

The flamelet profiles in the multiple-flamelet data set should vary only in the strain rate imposed; the species and the boundary conditions should be the same. In addition, it is recommended that an extinguished flamelet is excluded from the multiple-flamelet data set. The formats for multiple diffusion flamelets are as follows:

- OPPDIF format: The multiple-flamelet OPPDIF files should be produced using the CNTN keyword in the OPPDIF script. Alternatively, you can use ANSYS Fluent to merge a number of single-flamelet OPPDIF files into a multiple-flamelet file.

- Standard format: If you have a set of standard format flamelet files, you can import them all at the same time, and ANSYS Fluent will merge them internally into a multiple-flamelet file. When you import the set of flamelet files, ANSYS Fluent will search for and count the occurrences of the HEADER keyword to determine the number of diffusion flamelets in the file.

Release 15.0 - © SAS IP, Inc. All rights reserved. - Contains proprietary and confidential information of ANSYS, Inc. and its subsidiaries and affiliates.

- CFX-RIF format: A CFX-RIF flamelet file contains multiple diffusion flamelets at various strains and the file should not be modified manually. Only one CFX-RIF flamelet file should be imported.

For either type of file, ANSYS Fluent will determine the number of flamelet profiles and sort them in ascending strain-rate order. For diffusion flamelets generated in physical space, you can select one of the four methods available for the calculation of mixture fraction. The scalar dissipation will be calculated from the strain rate using Equation 8.42 (p. 240).

## 8.5. The Steady Diffusion Flamelet Model Theory

The steady flamelet approach models a turbulent flame brush as an ensemble of discrete, steady laminar flames, called diffusion flamelets. The individual diffusion flamelets are assumed to have the same structure as laminar flames in simple configurations, and are obtained by experiments or calculations. Using detailed chemical mechanisms, ANSYS Fluent can calculate laminar opposed-flow diffusion flamelets for non-premixed combustion. The diffusion flamelets are then embedded in a turbulent flame using statistical PDF methods.

The advantage of the diffusion flamelet approach is that realistic chemical kinetic effects can be incorporated into turbulent flames. The chemistry can then be preprocessed and tabulated, offering tremendous computational savings. However, the steady diffusion flamelet model is limited to modeling combustion with relatively fast chemistry. The flame is assumed to respond instantaneously to the aerodynamic strain, and therefore the model cannot capture deep non-equilibrium effects such as ignition, extinction, and slow chemistry (like NOx).

Information pertaining strictly to the steady diffusion flamelet model is presented in the following sections:

8.5.1. Overview
8.5.2. Multiple Steady Flamelet Libraries
8.5.3. Steady Diffusion Flamelet Automated Grid Refinement
8.5.4. Non-Adiabatic Steady Diffusion Flamelets

For general information about the mixture fraction model, see Introduction (p. 215).

### 8.5.1. Overview

In a diffusion flame, at the molecular level, fuel and oxidizer diffuse into the reaction zone. Here, they encounter high temperatures and radical species and ignite. More heat and radicals are generated in the reaction zone and some diffuse out. In near-equilibrium flames, the reaction rate is much faster than the diffusion rate. However, as the flame is stretched and strained by the turbulence, species and temperature gradients increase, and radicals and heat diffuse more quickly out of the flame. The species have less time to reach chemical equilibrium, and the degree of local non-equilibrium increases.

The steady diffusion flamelet model is suited to predict chemical non-equilibrium due to aerodynamic straining of the flame by the turbulence. The chemistry, however, is assumed to respond rapidly to this strain, so as the strain relaxes to zero, the chemistry tends to equilibrium.

When the chemical time-scale is comparable to the fluid mixing time-scale, the species can be considered to be in global chemical non-equilibrium. Such cases include NOx formation and low-temperature CO oxidation. The steady diffusion flamelet model is not suitable for such slow-chemistry flames. Instead, you can model slow chemistry using one of the following:

- the Unsteady Diffusion Flamelet model (see The Unsteady Diffusion Flamelet Model Theory (p. 246))
- the trace species assumption in the NOx model (see Pollutant Formation (p. 313))


Release 15.0 - © SAS IP, Inc. All rights reserved. - Contains proprietary and confidential information of ANSYS, Inc. and its subsidiaries and affiliates.

- the Laminar Finite-Rate model (see The Generalized Finite-Rate Formulation for Reaction Modeling (p. 189)), where the turbulence-chemistry interaction is ignored.
- the EDC model (see The Eddy-Dissipation-Concept (EDC) Model (p. 195))
- the PDF transport model (see Composition PDF Transport (p. 281)).

## 8.5.2. Multiple Steady Flamelet Libraries

ANSYS Fluent can generate multiple steady diffusion flamelets over a range of strain rates to account for the varying strain field in your multi-dimensional simulation. If you specify the number of diffusion flamelets to be greater than one, diffusion flamelets are generated at scalar dissipation values as determined by Equation 8.52 (p. 245).

$$\chi_i = \begin{cases} 10\chi_{i-1} & for\ \chi_{i-1} < 1s^{-1} \\ \chi_{i-1} + \Delta\chi & for\ \chi_{i-1} \geq 1s^{-1} \end{cases} \tag{8.52}$$

where $i$ ranges from 1 up to the specified maximum number of diffusion flamelets, $\chi_0$ is the initial scalar dissipation, and $\Delta\chi$ is the scalar dissipation step. Diffusion flamelets are generated until either the maximum number of flamelets is reached, or the flamelet extinguishes. Extinguished flamelets are excluded from the flamelet library.

## 8.5.3. Steady Diffusion Flamelet Automated Grid Refinement

By default, 1D flamelet grids are discretized by clustering a fixed number of points about the stoichiometric mixture fraction, which is approximated as the location of peak temperature. ANSYS Fluent also has the option for **Automated Grid Refinement** of steady diffusion flamelets, where an adaptive algorithm inserts grid points so that the change of values, as well as the change of slopes, between successive grid points is less than user specified tolerances.

When using automated grid refinement, a steady solution is calculated on a coarse grid with a user specified **Initial Number of Grid Points in Flamelet** (default of $8$). At convergence, a new grid point is inserted midway between a point $i$ and its neighbor $i+1$ if,

$$| v_i - v_{i+1} | > \varepsilon_v ( v_{max} - v_{min} ) \tag{8.53}$$

where $v_i$ is the value for each temperature and species mass fraction at grid point $i$, $\varepsilon_v$ is a user specified **Maximum Change in Value Ratio** (default of $0.5$), and $v_{max}$ ($v_{min}$) are the maximum (minimum) values over all grid points.

In addition a grid point is added if,

$$| s_i - s_{i+1} | > \varepsilon_s ( s_{max} - s_{min} ) \tag{8.54}$$

where the slope $s_i$ is defined as,

$$s_i = \frac{v_{i+1} - v_i}{f_{i+1} - f_i} \tag{8.55}$$

In Equation 8.54 (p. 245) and Equation 8.55 (p. 245), $\varepsilon_s$ is a user specified **Maximum Change in Slope Ratio** (default of $0.5$), $s_{max}$ ($s_{min}$) are the maximum (minimum) slopes over all grid points, and $f_i$ is the mixture fraction value of grid point $i$.

Release 15.0 - © SAS IP, Inc. All rights reserved. - Contains proprietary and confidential information of ANSYS, Inc. and its subsidiaries and affiliates.

The refined flamelet is reconverged, and the refinement process is repeated until no further grid points are added by Equation 8.53 (p. 245) and Equation 8.54 (p. 245), or the user-specified **Maximum Number of Grid Points in Flamelet** (default of 64) is exceeded.

### 8.5.4. Non-Adiabatic Steady Diffusion Flamelets

For non-adiabatic steady diffusion flamelets, ANSYS Fluent follows the approach of [33] (p. 730), [311] (p. 746) and assumes that flamelet species profiles are unaffected by heat loss/gain from the flamelet. No special non-adiabatic flamelet profiles need to be generated, avoiding a very cumbersome preprocessing step. In addition, the compatibility of ANSYS Fluent with external steady diffusion flamelet generation packages (for example, OPPDIF, CFX-RIF, RUN-1DL) is retained. The disadvantage to this model is that the effect of the heat losses on the species mass fractions is not taken into account. Also, the effect of the heat loss on the extinction limits is not taken into account.

After diffusion flamelet generation, the flamelet profiles are convoluted with the assumed-shape PDFs as in Equation 8.43 (p. 241), and then tabulated for look-up in ANSYS Fluent. The non-adiabatic PDF tables have the following dimensions:

$\overline{T}\left(\overline{f}, \overline{f'^2}, \overline{H}, \overline{\chi}\right)$

$\overline{Y_i}\left(\overline{f}, \overline{f'^2}, \overline{H}\right)$ for $\chi = 0$ (that is, equilibrium solution)

$\overline{Y_i}\left(\overline{f}, \overline{f'^2}, \overline{\chi}\right)$ for $\chi \neq 0$

$\overline{\rho}\left(\overline{f}, \overline{f'^2}, \overline{H}, \overline{\chi}\right)$

During the ANSYS Fluent solution, the equations for the mean mixture fraction, mixture fraction variance, and mean enthalpy are solved. The scalar dissipation field is calculated from the turbulence field and the mixture fraction variance (Equation 8.44 (p. 241)). The mean values of cell temperature, density, and species mass fraction are obtained from the PDF look-up table.

## 8.6. The Unsteady Diffusion Flamelet Model Theory

The *steady* diffusion flamelet model, described in The Diffusion Flamelet Models Theory (p. 238) and The Steady Diffusion Flamelet Model Theory (p. 244), models local chemical non-equilibrium due to the straining effect of turbulence. In many combustors the strain is small at the outlet and the steady diffusion flamelet model predicts all species, including slow-forming species like NOx, to be near equilibrium, which is often inaccurate. The cause of this inaccuracy is the disparity between the flamelet time-scale, which is the inverse of the scalar dissipation, and the slow-forming species time-scale, which is the residence time since the species started accumulating after mixing in the combustor.

The *unsteady* diffusion flamelet model in ANSYS Fluent can predict slow-forming species, such as gaseous pollutants or product yields in liquid reactors, more accurately than the steady diffusion flamelet model. Computationally expensive chemical kinetics are reduced to one dimension and the model is significantly faster than the laminar-finite-rate, EDC or PDF Transport models where kinetics are calculated in two or three dimensions. There are two variants of the unsteady flamelet model, namely an Eulerian unsteady flamelet model (described in The Eulerian Unsteady Laminar Flamelet Model (p. 247)) and a diesel unsteady flamelet model for predicting combustion in compression-ignition engines (described in The Diesel Unsteady Laminar Flamelet Model (p. 249)).


Release 15.0 - © SAS IP, Inc. All rights reserved. - Contains proprietary and confidential information of ANSYS, Inc. and its subsidiaries and affiliates.

Information pertaining strictly to the unsteady flamelet model is presented in the following sections:

8.6.1. The Eulerian Unsteady Laminar Flamelet Model
8.6.2. The Diesel Unsteady Laminar Flamelet Model
8.6.3. Multiple Diesel Unsteady Flamelets
8.6.4. Multiple Diesel Unsteady Flamelets with Flamelet Reset

## 8.6.1. The Eulerian Unsteady Laminar Flamelet Model

The Eulerian unsteady laminar flamelet model can be used to predict slow-forming intermediate and product species that are not in chemical equilibrium. Typical examples of slow-forming species are gas-phase pollutants like NOx, and product compounds in liquid reactors. By reducing the chemistry computations to one dimension, detailed kinetics with multiple species and stiff reactions can be economically simulated in complex 3D geometries.

The model, following the work of Barths et al. [21] (p. 730) and Coelho and Peters [70] (p. 732), postprocesses unsteady marker probability equations on a steady-state converged flow field. The marker field represents the probability of finding a flamelet at any point in time and space. A probability marker transport equation is solved for each flamelet.

In ANSYS Fluent, the steady flow solution must be computed with the steady diffusion flamelet model (see The Steady Diffusion Flamelet Model Theory (p. 244)) before starting the unsteady flamelets simulation. Since the unsteady flamelet equations are postprocessed on a steady-state flamelet solution, the effect of the unsteady flamelet species on the flow-field is neglected.

When multiple flamelets are enabled, ANSYS Fluent solves Eulerian transport equations representing the probability of fuel from $n$th flamelet, $I_n$, as follows

$$\frac{\partial (\rho I_n)}{\partial t} + \nabla \cdot (\rho \vec{v} I_n) = \nabla \cdot \left( \frac{\mu_l + \mu_t}{\sigma_t} \cdot \nabla I_n \right) \tag{8.56}$$

Each marker probability is initialized as,

$$I_n = \begin{cases} 1 & for\ \chi_{\min,n} < \chi \leq \chi_{\max,n}\ and\ \overline{f} \geq f_{init} \\ 0 & for\ \chi < \chi_{\min,n}\ or\ \chi > \chi_{\max,n}\ or\ \overline{f} < f_{init} \end{cases} \tag{8.57}$$

where $\chi$ is the scalar dissipation, $\chi_{\min,n}$ $and$ $\chi_{\max,n}$ are the minimum and maximum scalar dissipation values for $n$th flamelet marker probability, $\overline{f}$ is the mean mixture fraction, and $f_{init}$ is a user-specified constant that should be set greater than the stoichiometric mixture fraction. Hence the marker probabilities are initialized to unity in regions of the domain where the mean mixture fraction is greater than a user specified value (typically greater than stoichiometric), and multiple flamelets subdivide this initial region by the scalar dissipation.

As previously mentioned, the Eulerian Unsteady Laminar Flamelet Model is only available for steady-state simulations. However, marker probability transport equations (Equation 8.56 (p. 247)) are always solved time-accurately as the initial marker probabilities convect and diffuse through the steady flow field. At the inlet boundaries, $I_n$ is set to zero, and hence the $I_n$ field decreases to zero with time as it is convected and diffused out of the domain (for cases with outlet boundaries).

The unsteady flamelet species Equation 8.46 (p. 242)) is integrated simultaneously with the marker probability Equation 8.56 (p. 247) for each marker probability $I_n$. For liquid-phase chemistry, the initial flamelet field is the mixed-but-unburnt flamelet, as liquid reactions are assumed to proceed immediately

Release 15.0 - © SAS IP, Inc. All rights reserved. - Contains proprietary and confidential information of ANSYS, Inc. and its subsidiaries and affiliates.

upon mixing. Gas-phase chemistry involves ignition, so the initial flamelet field is calculated from a steady diffusion flamelet solution. All of the slow-forming species, such as NOx, must be identified before solving the unsteady flamelet equations. The mass fractions of all slow-forming species are set to zero in this initial flamelet profile, since, at ignition, little residence time has elapsed for any significant formation.

The scalar dissipation at stoichiometric mixture fraction ($\chi_{st,n}$) is required by each flamelet species equation. This is calculated from the steady-state ANSYS Fluent field at each time step as a probability-weighted volume integral:

$$\chi_{st,n}(t) = \frac{\int_V I_n \left( \overline{\chi}_{st}(\vec{x}) \right)^{\frac{3}{2}} \rho(\vec{x})\, dV}{\int_V I_n \left( \overline{\chi}_{st}(\vec{x}) \right)^{\frac{1}{2}} \rho(\vec{x})\, dV} \tag{8.58}$$

where $\overline{\chi_{st}}$ is defined in Equation 8.44 (p. 241), and $V$ denotes the fluid volume. ANSYS Fluent provides the option of limiting $\overline{\chi_{st}}$ to a user-specified maximum value, which should be approximately equal to the flamelet extinction scalar dissipation (the steady diffusion flamelet solver can be used to calculate this extinction scalar dissipation in a separate simulation).

The unsteady flamelet energy equation is not solved in order to avoid flamelet extinction for high scalar dissipation, and to account for non-adiabatic heat loss or gain. For adiabatic cases, the flamelet temperature, $T^{ad}(f,t)$, is calculated at each time step from the steady diffusion flamelet library at the probability-weighted scalar dissipation $\chi_{st}$ from Equation 8.58 (p. 248). For non-adiabatic cases, the flamelet temperature at time $t$ is calculated from

$$T(f,t) = T^{ad}(f,t)\,\xi(f,t) \tag{8.59}$$

where

$$\xi(f,t) = \frac{\int_V I \rho \overline{T}(\vec{x} \,|\, f) / T^{ad}(f,t)\, dV}{\int_V I \rho\, dV} \tag{8.60}$$

Here, the subscript $n$ referring to $n$th flamelet has been omitted for simplicity, and $\overline{T}(\vec{x} \,|\, f)$ represents the ANSYS Fluent steady-state mean cell temperature conditioned on the local cell mixture fraction.

Unsteady flamelet mean species mass fractions in each cell are accumulated over time and can be expressed as:

$$\tilde{Y}_k = \frac{\sum_n \int_t I_n(t) \left\langle Y_{k,n} \right\rangle dt}{\sum_n \int_t I_n(t)\, dt} \tag{8.61}$$

where $\tilde{Y}_k$ denotes the $k^{\text{th}}$ species unsteady flamelet mass fraction, and $Y_{k,n}$ is the $k$th unsteady flamelet mass fraction of $n$th flamelet and is calculated using a Beta pdf as,


Release 15.0 - © SAS IP, Inc. All rights reserved. - Contains proprietary and confidential information of ANSYS, Inc. and its subsidiaries and affiliates.

$$\left\langle Y_{k,n} \right\rangle = \int_0^1 Y_{k,n}(f)\, P(f)\, df \tag{8.62}$$

The probability marker equation (Equation 8.56 (p. 247)) and the flamelet species equation (Equation 8.46 (p. 242)) are advanced together in time until the probability marker has substantially convected and diffused out of the domain. The unsteady flamelet mean species, calculated from Equation 8.60 (p. 248), reach steady-state as the probability marker $I_n$ vanishes.

#### 8.6.1.1. Liquid Reactions

Liquid reactors are typically characterized by:

- Near constant density and temperature.
- Relatively slow reactions and species far from chemical equilibrium.
- High Schmidt number ($Sc$) and hence reduced molecular diffusion.

The Eulerian unsteady laminar flamelet model can be used to model liquid reactions. When the **Liquid Micro-Mixing** model is enabled, ANSYS Fluent uses the **volume-weighted-mixing-law** formula to calculate the density.

The effect of high $Sc$ is to decrease mixing at the smallest (micro) scales and increase the mixture fraction variance, which is modeled with the Turbulent Mixer Model [16] (p. 729). Three transport equations are solved for the inertial-convective ($\overline{f_{ic}'^2}$), viscous-convective ($\overline{f_{vc}'^2}$), and viscous-diffusive ($\overline{f_{vd}'^2}$) subranges of the turbulent scalar spectrum,

$$\frac{\partial}{\partial t}\left(\rho \overline{f_{ic}'^2}\right) + \nabla\cdot\left(\rho \vec{v}\, \overline{f_{ic}'^2}\right) = \nabla\cdot\left(\frac{\mu_l+\mu_t}{\sigma_t}\nabla \overline{f_{ic}'^2}\right) + C_1\mu_t\cdot(\nabla \overline{f})^2 - C_2\rho\frac{\varepsilon}{k}\overline{f_{ic}'^2} \tag{8.63}$$

$$\frac{\partial}{\partial t}\left(\rho \overline{f_{vc}'^2}\right) + \nabla\cdot\left(\rho \vec{v}\, \overline{f_{vc}'^2}\right) = \nabla\cdot\left(\frac{\mu_l+\mu_t}{\sigma_t}\nabla \overline{f_{vc}'^2}\right) + C_2\rho\frac{\varepsilon}{k}\overline{f_{ic}'^2} - C_3\rho\sqrt{\frac{\varepsilon}{\nu}}\cdot\overline{f_{vc}'^2} \tag{8.64}$$

$$\frac{\partial}{\partial t}\left(\rho \overline{f_{vd}'^2}\right) + \nabla\cdot\left(\rho \vec{v}\, \overline{f_{vd}'^2}\right) = \nabla\cdot\left(\frac{\mu_l+\mu_t}{\sigma_t}\nabla \overline{f_{vd}'^2}\right) + C_3\rho\sqrt{\frac{\varepsilon}{\nu}}\cdot\left(\overline{f_{vc}'^2} - \left(C_4+\frac{C_5}{Sc}\right)\overline{f_{vd}'^2}\right) \tag{8.65}$$

where the constants $C_1$ through $C_5$ have values of 2, 1.86, 0.058, 0.303, and 17050, respectively. The total mixture fraction variance is the sum of $\overline{f_{ic}'^2}$, $\overline{f_{vc}'^2}$ and $\overline{f_{vd}'^2}$.

In Equation 8.65 (p. 249), the cell Schmidt number, $Sc$, is calculated as $Sc = \mu/\rho D$ where $\mu$ is the viscosity, $\rho$ the density, and $D$ the mass diffusivity as defined for the *pdf-mixture* material.

### 8.6.2. The Diesel Unsteady Laminar Flamelet Model

In diesel engines, fuel sprayed into the cylinder evaporates, mixes with the surrounding gases, and then auto-ignites as compression raises the temperature and pressure. The diesel unsteady laminar flamelet model, based on the work of Pitsch et al. and Barths et al. [353] (p. 748), [20] (p. 730), models the chemistry by a finite number of one-dimensional laminar flamelets. By reducing the costly chemical

kinetic calculation to 1D, substantial savings in run-time can be achieved over the laminar-finite-rate, EDC or PDF Transport models.

The flamelet species and energy equations (Equation 8.46 (p. 242) and Equation 8.47 (p. 242)) are solved simultaneously with the flow. The flamelet equations are advanced for a fractional step using properties from the flow, and then the flow is advanced for the same fractional time-step using properties from the flamelet.

The initial condition of each flamelet at the time of its introduction into computational domain is a mixed-but-unburnt distribution. For the flamelet fractional time-step, the volume-averaged scalar dissipation and pressure, as well as the fuel and oxidizer temperatures, are passed from the flow solver to the flamelet solver. To account for temperature rise during compression, the flamelet energy equation (Equation 8.47 (p. 242)) has an additional term on the right-hand side as

$$\dot{q}=\frac{1}{c_p}\frac{\partial p}{\partial t} \tag{8.66}$$

where $c_p$ is the specific heat and $p$ is the volume-averaged pressure in the cylinder. This rise in flamelet temperature due to compression eventually leads to ignition of the flamelet.

After the flamelet equations have been advanced for the fractional time-step, the PDF Table is created as a Non-Adiabatic Steady Flamelet table (see Non-Adiabatic Steady Diffusion Flamelets (p. 246)). Using the properties from this table, the CFD flow field is then advanced for the same fractional time-step.

## 8.6.3. Multiple Diesel Unsteady Flamelets

In certain applications where the ignition in different regions of the combustion domain occurs at different times, the chemistry cannot be accurately represented by a single flamelet. Among the examples are split-injections and sprays with high residence times. In these cases, evaporated spray injected at early stage ignites before spray injected at later stage due to the longer residence time. A single flamelet cannot model the local ignition delay for the late spray as the single flamelet represents a burnt state. This deficiency is overcome with the use of multiple flamelets, which are generated in the reacting domain at user-specified times during the simulation. The new flamelet inherits the preceding flamelet boundary temperature calculated at the time of the new flamelet introduction, and the flamelet species field is initialized as mixed-but-unburnt.

The marker probability equations (Equation 8.56 (p. 247)) are solved for $N-1$ flamelets, where $N$ is the total number of unsteady flamelets. The marker probability of the last flamelet is obtained as follows:

$$I_N=\overline{f}-\sum_{n=1}^{N-1} I_n \tag{8.67}$$

where $\overline{f}$ is the mean mixture fraction, and $I_n$ is the marker probability of the $n$th unsteady flamelet. The scalar dissipation of the $n$th flamelet is calculated using Equation 8.58 (p. 248).

The properties from the PDF tables $\varphi(t)$ (such as mass fraction, specific heat, and so on) are calculated using the weighted contribution from each flamelet:

$$\langle \varphi(t) \rangle=\frac{\sum_{n=1}^{N-1} I_n(t) \left\langle \varphi_n(t) \right\rangle}{\sum_{n=1}^{N-1} I_n(t)} \tag{8.68}$$


Release 15.0 - © SAS IP, Inc. All rights reserved. - Contains proprietary and confidential information of ANSYS, Inc. and its subsidiaries and affiliates.

where $\varphi_n$ is the property for $n$th flamelet.

The diesel unsteady flamelet approach can model ignition as well as formation of product, intermediate, and pollutant species. The setting of the **Diesel Unsteady Flamelet** model is described in Using the Diesel Unsteady Laminar Flamelet Model in the *Fluent User's Guide*.

## 8.6.4. Multiple Diesel Unsteady Flamelets with Flamelet Reset

As the multiple diesel unsteady flamelets ignite, their species and temperature fields tend toward the same chemical equilibrium state as the scalar dissipation (mixing) decreases. To model multiple engine cycles, ANSYS Fluent allows flamelet reset events, which resets multiple flamelets to a single flamelet. Additionally, at the end of a cycle, some burnt gases typically remain trapped and mix later with the fresh charge introduced in the next cycle. The presence of the exhaust gas in the engine chamber can be modeled using either a **Diesel Unsteady Flamelet Reset** or the inert model (via **Inert EGR Reset**).

For information on how to use and set up the **Diesel Unsteady Flamelet Reset** and **Inert EGR Reset** options, see Resetting Diesel Unsteady Flamelets in the *Fluent User's Guide*.

### 8.6.4.1. Resetting the Flamelets

At the end of combustion stroke and just before the inlet valves open, all existing flamelets, except the first one, are deleted, and the probability of the first flamelet is set as:

$$I_1 = \sum_{n=1}^{n=N} I_n$$

where, $I_n$ is the probability of the $n^{\text{th}}$ flamelet, and $N$ is the total number of flamelets. The mixture composition (and similarly the temperature) of the reset flamelet is set as:

$$\langle Y_k \rangle_1 = \sum_{n=1}^{N} I_n(t) \langle Y_k \rangle_n$$

where $\langle Y_k \rangle_n$ is the species mass fraction of the $k^{\text{th}}$ species from the $n^{\text{th}}$ flamelet.

After resetting the flamelets, the computations are performed with this single, typically burnt, flamelet. The flamelet start time of subsequent flamelets should be set to just before the fuel injection. Hence, the injected fuel is modeled in the second and higher flamelets. The process is controlled through dynamic mesh events described in Diesel Unsteady Flamelet Reset in the *Fluent User's Guide*.

Release 15.0 - © SAS IP, Inc. All rights reserved. - Contains proprietary and confidential information of ANSYS, Inc. and its subsidiaries and affiliates.

Release 15.0 - © SAS IP, Inc. All rights reserved. - Contains proprietary and confidential information
of ANSYS, Inc. and its subsidiaries and affiliates.

# Chapter 9: Premixed Combustion

ANSYS Fluent has several models to simulate premixed turbulent combustion. For more information about using the premixed turbulent combustion models, see Modeling Premixed Combustion in the User's Guide. Theoretical information about these models is provided in the following sections:


9.1. Overview and Limitations
9.2. C-Equation Model Theory
9.3. G-Equation Model Theory
9.4. Turbulent Flame Speed Models
9.5. Extended Coherent Flamelet Model Theory
9.6. Calculation of Properties


## 9.1. Overview and Limitations

For more information, see the following sections:


9.1.1. Overview
9.1.2. Limitations


### 9.1.1. Overview

In premixed combustion, fuel and oxidizer are mixed at the molecular level prior to ignition. Combustion occurs as a flame front propagating into the unburnt reactants. Examples of premixed combustion include aspirated internal combustion engines, lean-premixed gas turbine combustors, and gas-leak explosions.

Premixed combustion is much more difficult to model than non-premixed combustion. The reason for this is that premixed combustion usually occurs as a thin, propagating flame that is stretched and contorted by turbulence. For subsonic flows, the overall rate of propagation of the flame is determined by both the laminar flame speed and the turbulent eddies. The laminar flame speed is determined by the rate that species and heat diffuse upstream into the reactants and burn. To capture the laminar flame speed, the internal flame structure would need to be resolved, as well as the detailed chemical kinetics and molecular diffusion processes. Since practical laminar flame thicknesses are of the order of millimeters or smaller, resolution requirements are usually unaffordable.

The effect of turbulence is to wrinkle and stretch the propagating laminar flame sheet, increasing the sheet area and, in turn, the effective flame speed. The large turbulent eddies tend to wrinkle and corrugate the flame sheet, while the small turbulent eddies, if they are smaller than the laminar flame thickness, may penetrate the flame sheet and modify the laminar flame structure.

Non-premixed combustion, in comparison, can be greatly simplified to a mixing problem (see the mixture fraction approach in Introduction (p. 215)). The essence of premixed combustion modeling lies in capturing the turbulent flame speed, which is influenced by both the laminar flame speed and the turbulence.

In premixed flames, the fuel and oxidizer are intimately mixed before they enter the combustion device. Reaction then takes place in a combustion zone that separates unburnt reactants and burnt combustion products. Partially premixed flames exhibit the properties of both premixed and diffusion flames. They occur when an additional oxidizer or fuel stream enters a premixed system, or when a diffusion flame becomes lifted off the burner so that some premixing takes place prior to combustion.


Release 15.0 - © SAS IP, Inc. All rights reserved. - Contains proprietary and confidential information of ANSYS, Inc. and its subsidiaries and affiliates.

Premixed and partially premixed flames can be modeled using ANSYS Fluent's finite-rate/eddy-dissipation formulation (see Species Transport and Finite-Rate Chemistry (p. 187)). If finite-rate chemical kinetic effects are important, the Laminar Finite-Rate model (see The Laminar Finite-Rate Model (p. 189)), the EDC model (see The Eddy-Dissipation-Concept (EDC) Model (p. 195)) or the composition PDF transport model (see Composition PDF Transport (p. 281)) can be used. For information about ANSYS Fluent's partially premixed combustion model, see Partially Premixed Combustion (p. 273). If the flame is perfectly premixed (all streams entering the combustor have the same equivalence ratio), it is possible to use the premixed combustion model, as described in this chapter.

### 9.1.2. Limitations

The following limitations apply to the premixed combustion model:

- You must use the pressure-based solver. The premixed combustion model is not available with either of the density-based solvers.
- The premixed combustion model is valid only for turbulent, subsonic flows. These types of flames are called deflagrations. Explosions, also called detonations, where the combustible mixture is ignited by the heat behind a shock wave, can be modeled with the finite-rate model using the density-based solver. See Species Transport and Finite-Rate Chemistry (p. 187) for information about the finite-rate model.
- The premixed combustion model cannot be used in conjunction with the pollutant (that is, soot and NOx) models. However, a perfectly premixed system can be modeled with the partially premixed model (see Partially Premixed Combustion (p. 273)), which can be used with the pollutant models.
- You cannot use the premixed combustion model to simulate reacting discrete-phase particles, since these would result in a partially premixed system. Only inert particles can be used with the premixed combustion model.

## 9.2. C-Equation Model Theory

A scalar variable representing the progress of reaction from unburnt to burnt is denoted by c. The transport equation for c describes the spatial and temporal evolution of the reaction progress in a turbulent flow field. Ahead of the flame, c is defined as zero in the unburnt reactants, and behind the flame c is unity in the burnt products. Within the flame brush c varies between zero and one. The flame brush propagates upstream at a modeled turbulent flame speed. Fluent offers two models for the turbulent flame speed, namely the Zimont model [506] (p. 757), [507] (p. 757), [509] (p. 757) and the Peters model [347] (p. 748), as detailed in Peters Flame Speed Model (p. 260).

For more information, see the following section:
9.2.1. Propagation of the Flame Front

### 9.2.1. Propagation of the Flame Front

In many industrial premixed systems, combustion takes place in a thin flame sheet. As the flame front moves, combustion of unburnt reactants occurs, converting unburnt premixed reactants to burnt products. The premixed combustion model therefore considers the reacting flow field to be divided into regions of burnt and unburnt species, separated by the flame sheet. Note that the C-equation model assumes that the laminar flame is thin in comparison to the turbulent flame brush, so a value of reaction progress between 0 and 1 implies that the fluctuating flame spends some time at the unburnt state and the remainder at the burnt state; it does not represent an intermediate reaction state between unburnt and burnt.


Release 15.0 - © SAS IP, Inc. All rights reserved. - Contains proprietary and confidential information of ANSYS, Inc. and its subsidiaries and affiliates.

The flame front propagation is modeled by solving a transport equation for the density-weighted mean reaction progress variable, denoted by $\overline{c}$:

$$\frac{\partial}{\partial t}(\rho \overline{c}) + \nabla \cdot (\rho \overline{v} \overline{c}) = \nabla \cdot \left( \frac{\mu_t}{\mathrm{Sc}_t} \nabla \overline{c} \right) + \rho S_c \tag{9.1}$$

where

$\overline{c}$ = mean reaction progress variable

$Sc_t$ = turbulent Schmidt number

$S_c$ = reaction progress source term ($s^{-1}$)

The progress variable is defined as a normalized sum of the product species mass fractions,

$$c = \frac{\sum_k \alpha_k (Y_k - Y_k^u)}{\sum_k \alpha_k Y_k^{eq}} = \frac{Y_c}{Y_c^{eq}} \tag{9.2}$$

where

superscript $u$ denotes the unburnt reactant

$Y_k$ denotes the $k^{th}$ species mass fraction

superscript $eq$ denotes chemical equilibrium

$\alpha_k$ are constants that are typically zero for reactants and unity for a few product species

Based on this definition, $c = 0$ where the mixture is unburnt and $c = 1$ where the mixture is burnt:

- $c = 0$: unburnt mixture
- $c = 1$: burnt mixture

The value of $\overline{c}$ is defined as a boundary condition at all flow inlets. It is usually specified as either 0 (unburnt) or 1 (burnt).

The mean reaction rate in Equation 9.1 (p. 255) is modeled as [507] (p. 757)

$$\rho S_c = \rho_u U_t \, | \nabla c | \tag{9.3}$$

where

$\rho_u$ = density of unburnt mixture

$U_t$ = turbulent flame speed

ANSYS Fluent provides two models for the turbulent flame speed. Many other models for $U_t$ exist [44] (p. 731) and can be specified using user-defined functions. More information about user-defined functions can be found in the UDF Manual.

## 9.3. G-Equation Model Theory

The G-equation is a premixed flame-front tracking model. The transport equation governing the unsteady evolution of a propagating flame interface is (derivation can be found in [347] (p. 748)),

$$\rho\frac{\partial G}{\partial t}+\rho v \bullet \nabla G=\rho U_l|\nabla G|-\rho D\kappa|\nabla G| \tag{9.4}$$

where $\rho$ is the fluid density, $v$ is the fluid velocity vector, $U_l$ is the laminar flame speed (interface normal propagation), $D$ is the diffusivity and $\kappa$ is the flame curvature. For turbulent flames, Equation 9.4 (p. 256) can be Favre Reynolds-averaged or spatially-filtered to provide transport equations for the flame mean position,

$$\tilde{\rho}\frac{\partial \overline{G}}{\partial t}+\tilde{\rho}\tilde{v}\bullet\nabla\overline{G}=\rho_u U_t\mid\nabla\overline{G}\mid-\rho_u D_t'\tilde{\kappa}\mid\nabla\overline{G}\mid \tag{9.5}$$

and the variance of the flame position,

$$\tilde{\rho}\frac{\partial \overline{G}''^2}{\partial t}+\tilde{\rho}\tilde{v}\bullet\nabla\overline{G}''^2=\nabla_{||}\bullet(\rho_u D_t\nabla_{||}\nabla\overline{G}''^2)+2\rho_u D_t(\nabla\overline{G})^2-c_s\rho_u\frac{u'}{l_t}\overline{G}''^2 \tag{9.6}$$

where

$U_t$ is the turbulent flame speed

$D_t'$ is a diffusivity term defined as $D_t'=\sqrt{\frac{c_\mu c_s}{2Sc_t}}l_t u''$

$u'$ is the turbulent velocity scale

$c_\mu$ is a modeling constant taken from the $k-\varepsilon$ turbulence model (default=0.09)

$c_s$ is a modeling constant = 2.0

$Sc_t$ is the turbulent Schmidt number

$l_t$ is the turbulent length scale

$\kappa$ is the flame curvature, defined as $\kappa=\nabla\bullet n$, where $n=-\frac{\nabla\overline{G}}{|\nabla\overline{G}|}$

In Equation 9.6 (p. 256), $\nabla_{||}$ indicates that the diffusion term is only applied parallel to the flame front [347] (p. 748), the normal component being accounted for in the turbulent burning velocity. In practice this makes only a minor difference to results and can lead to convergence problems, and is therefore disabled by default.

ANSYS Fluent also offers the option of using an algebraic expression to calculate the flame position variance, $\overline{G}''^2$, instead of Equation 9.6 (p. 256):

$$\overline{G}''^2=\frac{l_t}{u'}\frac{\mu_{eff}}{\tilde{\rho}Sc_t} \tag{9.7}$$

where $\mu_{eff}$ is the effective turbulent viscosity.

For more information, see the following section:
9.3.1. Numerical Solution of the G-equation


Release 15.0 - © SAS IP, Inc. All rights reserved. - Contains proprietary and confidential information of ANSYS, Inc. and its subsidiaries and affiliates.

### 9.3.1. Numerical Solution of the G-equation

Equation 9.4 (p. 256) and Equation 9.5 (p. 256) do not contain a diffusion term and sharp interfaces remain sharp at all times. Special numerical techniques such as the Volume-of-Fluid (VOF) and Marker-and-Cell (MAC) have been devised to solve such equations. In ANSYS Fluent, the mean G-equation Equation 9.5 (p. 256) is solved using a Level-set method. Here, $\overline{G}$ represents the signed mean distance to the flame front, and hence the flame front is the $\overline{G}=0$ iso-surface. Since $\overline{G}$ is the distance to the flame front, $|\nabla \overline{G}|$ is constrained to be unity everywhere in the flow field. The standard ANSYS Fluent transport equation machinery is used to solve for $\overline{G}$ (Equation 9.5 (p. 256)) over a time-step. However, at the end of the time-step, the $\overline{G}$ field is typically is not exactly equal to the mean flame distance (and $|\nabla \overline{G}|$ is not identically equal to 1), and this condition is enforced by a process called re-initialization. In ANSYS Fluent this is done by constructing a faceted representation of the flame front from the $\overline{G}$ field. Then, in every cell, $\overline{G}$ is set to the geometric distance to the nearest flame front facet. $\overline{G}$ is positive in the burnt region downstream of the flame front and negative in the unburnt region upstream of the flame front.

Given the mean flame front position, the mean progress variable is calculated according to a Gaussian distribution depending on proximity to the flame front and the G-equation variance:

$$\overline{c}=\int_{G=0}^{\infty}\frac{1}{\sqrt{2\pi\,\overline{G}''^{2}}}\exp\left(-\frac{(G-\overline{G})^{2}}{2\,\overline{G}''^{2}}\right)dG \tag{9.8}$$

Mean properties, such as the mean density, temperature and species mass fractions, are calculated from the mean reaction progress variable, as in the C-equation model.

## 9.4. Turbulent Flame Speed Models

The key to the premixed combustion model is the prediction of $U_t$, the turbulent flame speed normal to the mean surface of the flame. The turbulent flame speed is influenced by the following:

- laminar flame speed, which is, in turn, determined by the fuel concentration, temperature, and molecular diffusion properties, as well as the detailed chemical kinetics
- flame front wrinkling and stretching by large eddies, and flame thickening by small eddies

ANSYS Fluent has two turbulent flame speed models, namely the Zimont turbulent flame speed closure model and the Peters flame speed model.

For more information, see the following sections:
9.4.1. Zimont Turbulent Flame Speed Closure Model
9.4.2. Peters Flame Speed Model

### 9.4.1. Zimont Turbulent Flame Speed Closure Model

In ANSYS Fluent, the Zimont turbulent flame speed closure is computed using a model for wrinkled and thickened flame fronts [507] (p. 757):

$$U_t = A\,(u')^{3/4}U_l^{1/2}\alpha^{-1/4}\ell_t^{1/4} \tag{9.9}$$

Release 15.0 - © SAS IP, Inc. All rights reserved. - Contains proprietary and confidential information of ANSYS, Inc. and its subsidiaries and affiliates.

$$U_t = Au' \left( \frac{\tau_t}{\tau_c} \right)^{1/4} \tag{9.10}$$

where

$A$ = model constant

$u'$ = RMS (root-mean-square) velocity (m/s)

$U_l$ = laminar flame speed (m/s)

$\alpha = k/\rho c_p$ = unburnt thermal diffusivity ($m^2/s$)

$\ell_t$ = turbulence length scale (m)

$\tau_t = \ell_t / u'$ = turbulence time scale (s)

$\tau_c = \alpha / U_l^2$ = chemical time scale (s)

The turbulence length scale, $\ell_t$, is computed from

$$\ell_t = C_D \frac{(u')^3}{\varepsilon} \tag{9.11}$$

where $\varepsilon$ is the turbulence dissipation rate.

The model is based on the assumption of equilibrium small-scale turbulence inside the laminar flame, resulting in a turbulent flame speed expression that is purely in terms of the large-scale turbulent parameters. The default value of 0.52 for $A$ is recommended [507] (p. 757), and is suitable for most premixed flames. The default value of 0.37 for $C_D$ should also be suitable for most premixed flames.

The model is strictly applicable when the smallest turbulent eddies in the flow (the Kolmogorov scales) are smaller than the flame thickness, and penetrate into the flame zone. This is called the thin reaction zone combustion region, and can be quantified by Karlovitz numbers, $Ka$, greater than unity. $Ka$ is defined as

$$Ka = \frac{t_l}{t_\eta} = \frac{v_\eta^2}{U_l^2} \tag{9.12}$$

where

$t_l$ = characteristic flame time scale

$t_\eta$ = smallest (Kolmogorov) turbulence time scale

$v_\eta = (v\varepsilon)^{1/4}$ = Kolmogorov velocity

$v$ = kinematic viscosity

Lastly, the model is valid for premixed systems where the flame brush width increases in time, as occurs in most industrial combustors. Flames that propagate for a long period of time equilibrate to a constant flame width, which cannot be captured in this model.


Release 15.0 - © SAS IP, Inc. All rights reserved. - Contains proprietary and confidential information of ANSYS, Inc. and its subsidiaries and affiliates.

#### 9.4.1.1. Zimont Turbulent Flame Speed Closure for LES

For simulations that use the LES turbulence model, the Reynolds-averaged quantities in the turbulent flame speed expression (Equation 9.9 (p. 257)) are replaced by their equivalent subgrid quantities. In particular, the large eddy length scale $\ell_t$ is modeled as

$$\ell_t = C_s \Delta \tag{9.13}$$

where $C_s$ is the Smagorinsky constant and $\Delta$ is the cell characteristic length.

The RMS velocity in Equation 9.9 (p. 257) is replaced by the subgrid velocity fluctuation, calculated as

$$u' = \ell_t \tau_{sgs}^{-1} \tag{9.14}$$

where $\tau_{sgs}^{-1}$ is the subgrid scale mixing rate (inverse of the subgrid scale time scale), given in Equation 7.28 (p. 195).

#### 9.4.1.2. Flame Stretch Effect

Since industrial low-emission combustors often operate near lean blow-off, flame stretching will have a significant effect on the mean turbulent heat release intensity. To take this flame stretching into account, the source term for the progress variable ($\rho S_c$ in Equation 9.1 (p. 255)) is multiplied by a stretch factor, $G$ [509] (p. 757). This stretch factor represents the probability that the stretching will not quench the flame; if there is no stretching ($G = 1$), the probability that the flame will be unquenched is 100%.

The stretch factor, $G$, is obtained by integrating the log-normal distribution of the turbulence dissipation rate, $\varepsilon$:

$$G = \frac{1}{2} erfc\left\{ -\sqrt{\frac{1}{2\sigma}} \left[ \ln\left(\frac{\varepsilon_{cr}}{\varepsilon}\right) + \frac{\sigma}{2} \right] \right\} \tag{9.15}$$

where erfc is the complementary error function, and $\sigma$ and $\varepsilon_{cr}$ are defined below.

$\sigma$ is the standard deviation of the distribution of $\varepsilon$:

$$\sigma = \mu_{str} \ln\left(\frac{L}{\eta}\right) \tag{9.16}$$

where $\mu_{str}$ is the stretch factor coefficient for dissipation pulsation, $L$ is the turbulent integral length scale, and $\eta$ is the Kolmogorov micro-scale. The default value of 0.26 for $\mu_{str}$ (measured in turbulent non-reacting flows) is recommended by [507] (p. 757), and is suitable for most premixed flames.

$\varepsilon_{cr}$ is the turbulence dissipation rate at the critical rate of strain [507] (p. 757):

$$\varepsilon_{cr} = 15 \nu g_{cr}^2 \tag{9.17}$$

By default, $g_{cr}$ is set to a very high value ($1 \times 10^8$) so no flame stretching occurs. To include flame stretching effects, the critical rate of strain $g_{cr}$ should be adjusted based on experimental data for the burner. Numerical models can suggest a range of physically plausible values [507] (p. 757), or an appropriate value can be determined from experimental data. A reasonable model for the critical rate of strain $g_{cr}$ is

Release 15.0 - © SAS IP, Inc. All rights reserved. - Contains proprietary and confidential information of ANSYS, Inc. and its subsidiaries and affiliates.

$$g_{cr} = \frac{BU_l^2}{\alpha} \tag{9.18}$$

where $B$ is a constant (typically 0.5) and $\alpha$ is the unburnt thermal diffusivity. Equation 9.18 (p. 260) can be implemented in ANSYS Fluent using a property user-defined function. More information about user-defined functions can be found in the UDF Manual.

#### 9.4.1.3. Gradient Diffusion

Volume expansion at the flame front can cause counter-gradient diffusion. This effect becomes more pronounced when the ratio of the reactant density to the product density is large, and the turbulence intensity is small. It can be quantified by the ratio $\left(\rho_u/\rho_b\right)\left(U_l/I\right)$, where $\rho_u$, $\rho_b$, $U_l$, and $I$ are the unburnt and burnt densities, laminar flame speed, and turbulence intensity, respectively. Values of this ratio greater than one indicate a tendency for counter-gradient diffusion, and the premixed combustion model may be inappropriate. Recent arguments for the validity of the turbulent-flame-speed model in such regimes can be found in Zimont et al. [508] (p. 757).

#### 9.4.1.4. Wall Damping

High turbulent kinetic energy levels at the walls in some problems can cause an unphysical acceleration of the flame along the wall. In reality, radical quenching close to walls decreases reaction rates and therefore the flame speed, but is not included in the model. To approximate this effect, ANSYS Fluent includes a constant multiplier for the turbulent flame speed, $\alpha_w$, which modifies the flame speed in the vicinity of wall boundaries:

$$U_t = \alpha_w A \left(\frac{\tau_t}{\tau_c}\right)^{1/4} \tag{9.19}$$

The default for this constant is 1 which does not change the flame speed. Values of $\alpha_w$ larger than 1 increase the flame speed, while values less than 1 decrease the flame speed in the cells next to the wall boundary.

ANSYS Fluent will solve the transport equation for the reaction progress variable $c$ (Equation 9.1 (p. 255)), computing the source term, $\rho S_c$, based on the theory outlined above:

$$\begin{aligned} \rho S_c &= AG\rho_u I^{3/4}\left[U_l\left(\lambda_{lp}\right)\right]^{1/2}\left[\alpha\left(\lambda_{lp}\right)\right]^{-1/4}\ell_t^{1/4}\,|\,\nabla c\,| \\ &= AG\rho_u I\left[\frac{\tau_t}{\tau_c\left(\lambda_{lp}\right)}\right]^{1/4}\,|\,\nabla c\,| \end{aligned} \tag{9.20}$$

### 9.4.2. Peters Flame Speed Model

The Peters model [347] (p. 748) for turbulent flame speed is used in the form proposed by Ewald [111] (p. 735):

$$U_t = U_l\left(1+\sigma_t\right) \tag{9.21}$$

where


Release 15.0 - © SAS IP, Inc. All rights reserved. - Contains proprietary and confidential information of ANSYS, Inc. and its subsidiaries and affiliates.

$$\sigma_t = -\frac{a_4 b_3^2}{4b_1}\frac{l_f}{\delta} l_*^q + \left[ \left( \frac{a_4 b_3^2}{4b_1}\frac{l_f}{\delta} l_*^q \right)^2 + \frac{c_s b_3^2}{2}\frac{u' l_f^2}{U_l \delta l_t} \right]^{1/2} \tag{9.22}$$

The term $l_*^q$ is Ewald's corrector and may be disabled by you, in which case $l_*^q = 1$ and the formulation reduces to that of Peters flame speed model.

In Equation 9.22 (p. 261):

$U_l$ is the laminar flame speed

$\delta = \left( \frac{\lambda / c_p}{\rho U_l} \right)_{unburned}$ is the laminar flame thickness

$u'$ is the turbulent velocity scale

$l_f$ is the flame brush thickness, given below

$l_*^q = \frac{l_f}{l_{alg}}$

$l_{alg} = \sqrt{\frac{2C_\mu}{C_s Sc_t}}\, l_t$ is an algebraic flame brush thickness

$a_4 = \sqrt{\frac{3C_\mu C_s}{Sc_t}}$

$b_3$ is a constant with a default value of 1.0

$b_1$ is a constant with a default value of 2.0

$q$ is a constant with a default value of 0.66

$c_\mu$ is a modeling constant taken from the $k-\varepsilon$ turbulence model with a default value of 0.09

$C_s$ is a constant with a default value of 2.0

$Sc_t$ is the turbulent Schmidt number with a default value of 0.7

If the Blint modifier is being used

$$\delta = \left( \frac{\lambda / C_p}{\rho U_l} \right)_{unburned} B_1 \left( \frac{\rho_u}{\rho_b} \right)^{B_2}$$

where

$B_1$ = 2.0

Release 15.0 - © SAS IP, Inc. All rights reserved. - Contains proprietary and confidential information of ANSYS, Inc. and its subsidiaries and affiliates.

$B_2 = 0.7$

$\rho_u$ is the unburned density

$\rho_b$ is the burned density

The flame brush thickness is calculated differently for the C-equation and G-equation models.

For the G equation model [347] (p. 748):

$$l_f = \frac{\sqrt{\tilde{G}''^2}}{|\nabla \tilde{G}|} \tag{9.23}$$

For the C-equation model an algebraic form of this is used giving:

$$l_f = \sqrt{\frac{l_t}{u'}\frac{\mu_{eff}}{\tilde{\rho} Sc_t}} \tag{9.24}$$

Note that for the C-equation model the Ewald corrector has no affect.

To reduce the flame speed along walls, ANSYS Fluent includes a constant multiplier for the turbulent flame speed, $\alpha_w$, which modifies the flame speed in the vicinity of wall boundaries by multiplying the $U_t$ expression in Equation 9.21 (p. 260) by a constant between 0 and 1.

### 9.4.2.1. Peters Flame Speed Model for LES

For LES the Peters model [347] (p. 748) for turbulent flame speed must be modified to use the subgrid quantities. Here we use the form derived by Pitsch [352] (p. 748).

$$S_t = S_l . MAX(1.0, \sigma_t) \tag{9.25}$$

$$\sigma_t = -\frac{b_3^2}{2b_1 Sc_t}\frac{1}{\delta}\frac{v_t}{u'} + \left[\left(\frac{b_3^2}{2b_1 Sc_t}\frac{1}{\delta}\frac{v_t}{u'}\right)^2 + \frac{b_3^2}{Sc_t}\frac{v_t}{D}\right]^{1/2} \tag{9.26}$$

where $D = \left(\frac{\lambda/c_p}{\rho}\right)_{unburned}$ is the thermal diffusivity.

The turbulent velocity scale $u'$ is the subgrid quantity as given in Equation 9.14 (p. 259).

## 9.5. Extended Coherent Flamelet Model Theory

The Extended Coherent Flamelet Model (ECFM) [355] (p. 748) is a more refined premixed combustion model than the C-equation or G-equation models. It has theoretically greater accuracy, but is less robust and requires greater computational effort to converge.

Information in this section is provided in the following sections:

9.5.1. Closure for ECFM Source Terms
9.5.2. Turbulent Flame Speed in ECFM
9.5.3. LES and ECFM


Release 15.0 - © SAS IP, Inc. All rights reserved. - Contains proprietary and confidential information of ANSYS, Inc. and its subsidiaries and affiliates.

The ECFM model solves an additional equation for the flame area density, denoted $\Sigma$, which is ultimately used to model the mean reaction rate in Equation 9.1 (p. 255). The model assumes that the smallest turbulence length scales (Kolmogorov eddies) are larger than the laminar flame thickness, so the effect of turbulence is to wrinkle the laminar flame sheet, however the internal laminar flame profile is not distorted. The increased surface area of the flame results in increased net fuel consumption and an increased flame speed. The range of applicability of the ECFM model is illustrated on the Borghi diagram in Figure 9.1: Borghi Diagram for Turbulent Combustion (p. 263), where the wrinkled flamelets regime is indicated below the $Da = 1$ line. Typical Internal Combustion (IC) engines typically operate in this wrinkled flamelet range.

**Figure 9.1: Borghi Diagram for Turbulent Combustion**

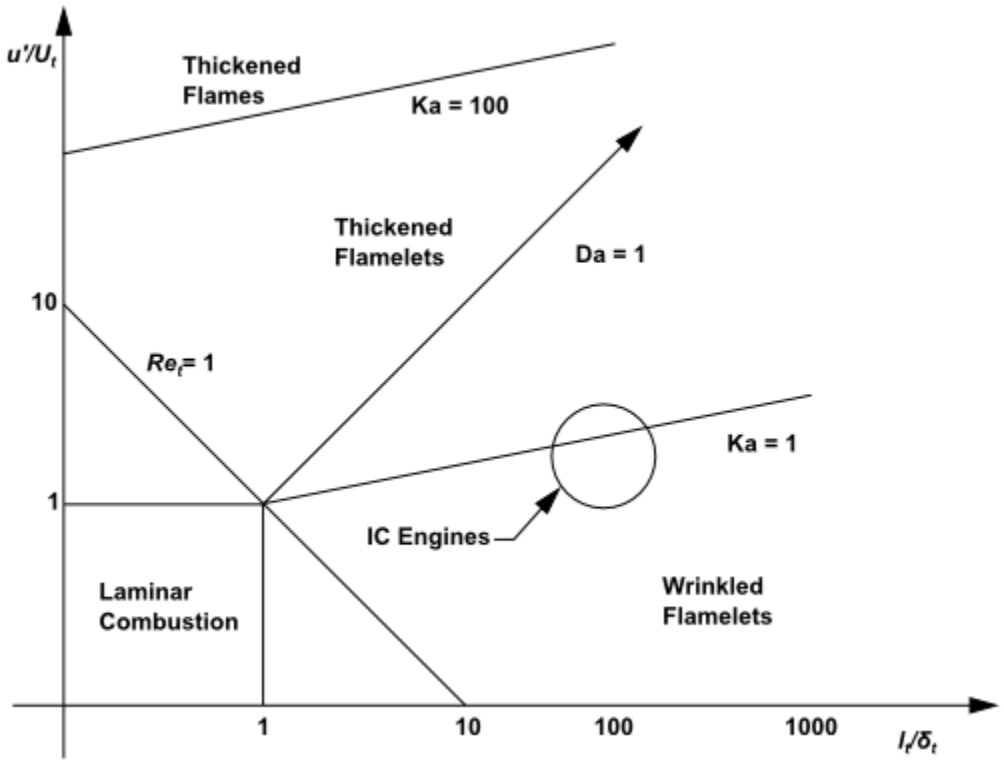


An expression for the transport of the net flame area per unit volume, or flame area density, $\Sigma$, can be derived based on these assumptions [54] (p. 731):

$$\frac{\partial \Sigma}{\partial t} + \nabla \cdot (\vec{u}\,\Sigma) = \nabla \cdot \left( \frac{\mu_t}{Sc_t} \nabla \left( \frac{\Sigma}{\rho} \right) \right) + (P_1 + P_2 + P_3)\Sigma + P_4 - D \tag{9.27}$$

where

$\Sigma$ = mean flame area density

$Sc_t$ = turbulent Schmidt number

$\mu_t$ = turbulent viscosity

$\rho$ = density

$P_1$ = Source due to turbulence interaction

Release 15.0 - © SAS IP, Inc. All rights reserved. - Contains proprietary and confidential information of ANSYS, Inc. and its subsidiaries and affiliates.

$P_2$ = Source due to dilatation in the flame [466] (p. 754)

$P_3$ = Source due to expansion of burned gas [466] (p. 754)

$P_4$ = Source due to normal propagation [466] (p. 754)

$D$ = Dissipation of flame area

Equation 9.27 (p. 263) requires closure terms for the production and destruction terms for flame area density. Several families of closure terms have been put forth in the literature [355] (p. 748). ANSYS Fluent uses the closure described in the following section.

## 9.5.1. Closure for ECFM Source Terms

There are four ECFM model variants available. The default Veynante scheme is the recommended scheme, because it provides the best accuracy in most situations. You can access the other models by using the `define/models/species/ecfm-controls` text command, and revise the model constants as necessary.

The source terms for each model are shown in Table 9.1: Source Terms for ECFM Models (p. 264):

**Table 9.1: Source Terms for ECFM Models**

| Model Name | $P_1$ | $P_2$ | $P_3$ | $P_4$ | $D$ |
|---|---|---|---|---|---|
| Veynante [466] (p. 754) (default) | $\alpha_1 K_t$ | $\frac{2}{3}\cdot\frac{\alpha_2}{\rho}\nabla(\rho\vec{u})$ | $\alpha_3\beta_1 U_l\frac{\Sigma}{\overline{c}(1-\overline{c})}$ | $\alpha_4 U_l\nabla^2\overline{c}$ | $\beta_1 U_l\frac{\Sigma^2}{1-\overline{c}}$ |
| Meneveau [76] (p. 733) | $\alpha_1 K_t$ | $\frac{2}{3}\cdot\frac{\alpha_2}{\rho}\nabla(\rho\vec{u})$ | $\alpha_3 U_l\frac{1-\tilde{c}}{\tilde{c}}\Sigma$ | N/A | $\beta_1 U_l\frac{\Sigma^2}{1-\tilde{c}}$ |
| Poinsot [76] (p. 733) | $\alpha_1 K_t$ | $\frac{2}{3}\cdot\frac{\alpha_2}{\rho}\nabla(\rho\vec{u})$ | $\alpha_3\frac{\rho_u}{\rho_b}U_l\frac{1-\tilde{c}}{\tilde{c}}\Sigma$ | N/A | $\beta_1 U_l\frac{\Sigma^2}{1-\overline{c}}$ |
| Teraji [449] (p. 753) | $\alpha_1\sqrt{Re_t}K_t$ | N/A | $\alpha_2 e^{(-\alpha_3 \mathrm{Ka})}\frac{T_b}{T_u}U_l\Sigma$ | N/A | $\beta_1\left(U_l+\beta_2 u'\right)\frac{\Sigma^2}{1-\tilde{c}}$ |

The values of the constants shown in Table 9.1: Source Terms for ECFM Models (p. 264) are detailed in Table 9.2: Values of Constants for ECFM Model Source Terms (p. 264):

**Table 9.2: Values of Constants for ECFM Model Source Terms**

| Model Name | $\alpha_1$ | $\alpha_2$ | $\alpha_3$ | $\alpha_4$ | $\beta_1$ | $\beta_2$ |
|---|---|---|---|---|---|---|
| Veynante (default) | 1.6 | 1.0 | 0.5 | 1.0 | 0.4 | N/A |
| Meneveau | 1.6 | 1.0 | 1.0 | N/A | 1.0 | N/A |
| Poinsot | 1.6 | 1.0 | 1.0 | N/A | 1.0 | N/A |
| Teraji | 0.012 | 8.5 | 1.4 | N/A | 1.0 | 0.1 |

In Table 9.1: Source Terms for ECFM Models (p. 264), $\mathrm{Ka}$ is the Karlovitz number, and $\overline{c}$ is calculated from $\tilde{c}$ in the following manner:


Release 15.0 - © SAS IP, Inc. All rights reserved. - Contains proprietary and confidential information of ANSYS, Inc. and its subsidiaries and affiliates.

$$\overline{c} = \frac{\tilde{c}\frac{\rho_u}{\rho_b}}{1-\tilde{c}\left(1-\frac{\rho_u}{\rho_b}\right)} \tag{9.28}$$

where $\tilde{c}$ is the Favre-averaged progress variable, which is provided by ANSYS Fluent.

$P_1$ represents the flame area density that results from turbulent flame stretching, which is calculated using the turbulent time scale $K_t$:

$$K_t = \frac{\varepsilon}{k}\left[\left(1-\alpha_0\right)+\alpha_0\Gamma_K\right] \tag{9.29}$$

where $\varepsilon$ is the turbulent dissipation rate and $k$ is the turbulent kinetic energy. The constant $\alpha_0$ is a user-defined coefficient that determines the weight of the intermediate turbulent net flame stretch (ITNFS) term, $\Gamma_K$, relative to a straightforward turbulent time scale. The value of $\alpha_0$ is 1 for low turbulence levels (the default), and 0 for high turbulence levels.

The ITNFS term, $\Gamma_K$, can be specified either as a constant or calculated as a function of the two parameters $\frac{u'}{U_l}$ and $\frac{l_t}{\delta_l^0}$, where $u'$ is the turbulent velocity fluctuation, $U_l$ is the laminar flame speed, $l_t$ is the integral turbulent length scale, and $\delta_l^0$ is the laminar flame thickness.

The expression for $\Gamma_K$ is given by:

$$\begin{aligned}\log_{10}(\Gamma_K) = \quad & -\frac{1}{(s+0.4)}\exp(-(s+0.4)) \\ & +\left(1-\exp(-(s+0.4))\right)\left(\sigma_1\left(\frac{u'}{U_l}\right)s-0.11\right)\end{aligned} \tag{9.30}$$

where $s$ is defined as

$$s = \log_{10}\left(\frac{l_t}{\delta_l^0}\right) \tag{9.31}$$

and $\sigma_1$ is

$$\sigma_1\left(\frac{u'}{U_l}\right) = \frac{2}{3}\left(1-\frac{1}{2}\exp\left(-\left(\frac{u'}{U_l}\right)^{\frac{1}{3}}\right)\right) \tag{9.32}$$

ANSYS Fluent allows you to set the ITNFS term ($\Gamma_K$) directly, in a manner that is referred to as the constant ITNFS treatment. Otherwise, you can influence $\Gamma_K$ by defining the laminar flame thickness $\delta_l^0$ as one of the following:

- a constant, user-defined value

  This is referred to as the constant delta ITNFS treatment.

Release 15.0 - © SAS IP, Inc. All rights reserved. - Contains proprietary and confidential information of ANSYS, Inc. and its subsidiaries and affiliates.

- the Meneveau flame thickness [289] (p. 745)

  In this case, the laminar flame thickness is calculated as:

$$\delta_l^0 = \frac{2\alpha}{U_l} \tag{9.33}$$

  where $\alpha$ is the local unburned thermal diffusivity.

- the Poinsot flame thickness [355] (p. 748)

  In this case, the flame thickness is evaluated as in Equation 9.33 (p. 266), but $\Gamma_K$ in Equation 9.29 (p. 265) is replaced by $\Gamma_K + \Gamma_P$. $\Gamma_P$ is calculated as:

$$\Gamma_P = -\frac{3}{2}\frac{l_t U_l}{\delta_l^0 u'} \log\left(\frac{1}{1-p_q}\right) \tag{9.34}$$

  where

$$p_q = \frac{1}{2}\left(1 + \tanh\left(\frac{b^3}{|b|}\right)\right) \tag{9.35}$$

$$b = \frac{\left[\log_{10}\left(u'/U_l\right) - g_l\right]}{0.04s} \tag{9.36}$$

$$g_l = \left(0.7 + \frac{1}{s}\right)e^{-s} + \left(1 + e^{-s}\right)\left(1 + 0.36s\right) \tag{9.37}$$

  and $s$ is defined in Equation 9.31 (p. 265).

- the Blint Correction flame thickness [36] (p. 731)

  In this case, a correction is added in order to account for the rapid expansion of the gases:

$$\delta_l^0 = 2\left(\frac{T_b}{T_u}\right)^{0.7}\frac{\alpha}{U_l} \tag{9.38}$$

  where $T_u$ is the unburned temperature and $T_b$ denotes the burned temperature.

As formulated, a singularity can result when $\bar{c} = 0$, $\bar{c} = 1$, $\tilde{c} = 0$, or $\tilde{c} = 1$, and so ANSYS Fluent limits $\bar{c}$ and $\tilde{c}$ in order to avoid such values. Furthermore, the production terms $P_1$ and $P_2$ can be nonzero values in regions where the mixture is outside of the flammability limits, which is not physically possible. Accordingly, ANSYS Fluent sets the production terms to zero when the laminar flame speed is less than a very small value. The stability of the solution is enhanced by ensuring that the laminar flame speed in the destruction term is always greater than a small finite value. Inspection of the function for $\Gamma_K$ shows that a singularity exists in Equation 9.30 (p. 265) when $s = -0.4$, which can occur when the turbulent length scale is small compared to the laminar flame thickness. To prevent such a singularity, the quantity $(s + 0.4)$ is limited to a small positive number. As a result, the net turbulent flame stretch is small in laminar zones. These numerical limiting constants can be adjusted via the text user interface.


Release 15.0 - © SAS IP, Inc. All rights reserved. - Contains proprietary and confidential information of ANSYS, Inc. and its subsidiaries and affiliates.

### 9.5.2. Turbulent Flame Speed in ECFM

The mean reaction rate term in the reaction progress variable Equation 9.1 (p. 255) is closed as

$$\rho S_c = \rho_u U_l \Sigma \tag{9.39}$$

which is the product of the unburnt density, $\rho_u$, laminar flame speed, $U_l$, and flame surface area density, $\Sigma$.

### 9.5.3. LES and ECFM

When LES turbulence modeling is used in conjunction with the ECFM model, it is necessary to recast Equation 9.27 (p. 263) using terms that are resolved by the mesh and those that are unresolved (that is, subgrid terms):

$$\underbrace{\frac{\partial \Sigma}{\partial t} + \nabla \cdot (\vec{u}\Sigma) = \left(P_{2,\text{res}} + P_{3,\text{res}}\right)\Sigma + P_{4,\text{res}} - D_{\text{res}}}_{\text{resolved terms}}$$
$$\underbrace{\nabla \cdot \left(\sigma_c \frac{\hat{\mu}_t}{Sc_t} \nabla \left(\frac{\Sigma}{\rho}\right)\right) + \left(P_{1,\text{sgs}} + P_{3,\text{sgs}}\right)\Sigma - D_{\text{sgs}}}_{\text{subgrid terms}} \tag{9.40}$$

The resolved terms remain the same as given previously in Table 9.1: Source Terms for ECFM Models (p. 264). The subgrid terms are derived from those defined by Veynante et al. [378] (p. 749) [465] (p. 754). The $P_{1,\text{sgs}}$ term takes the same form as the $P_1$ term given in Table 9.1: Source Terms for ECFM Models (p. 264), but $K_t$ is now defined as:

$$K_t = \frac{\hat{u}'}{\sigma_c \hat{\Delta}} [(1-\alpha_0) + \alpha_0 \Gamma_K] \tag{9.41}$$

where $\hat{\Delta}$ is the combustion filter size and $\hat{u}'$ is the turbulent velocity fluctuation at scale $\hat{\Delta}$. The ECFM equation is filtered at a larger scale than the momentum equations, because it has been shown that eddies smaller than this size do not wrinkle the flame front. Consequently, $\hat{\Delta}$ is defined as:

$$\hat{\Delta} = n_{\text{res}} \Delta_x \tag{9.42}$$

where $n_{\text{res}}$ is a user-defined coefficient with a default value of 5, and $\Delta_x$ is the grid size. $\hat{u}'$ is then defined as:

$$\hat{u}' = u' n_{\text{res}}^{\frac{1}{3}} \tag{9.43}$$

where $u'$ is the usual LES subgrid scale turbulent velocity fluctuation.

With LES turbulence modeling, the definition of $\Gamma_K$ in Equation 9.41 (p. 267) also changes to become a sub-filter scale function, as given by Meneveau et al. [61] (p. 732):

Release 15.0 - © SAS IP, Inc. All rights reserved. - Contains proprietary and confidential information of ANSYS, Inc. and its subsidiaries and affiliates.

$$\Gamma_K = \frac{1}{\left( \left( \frac{1}{f_u^a} + \frac{1}{f_\Delta^a} \right)^{b/a} + \frac{1}{f_{Re}^b} \right)^{1/b}} \tag{9.44}$$

The denominator on the right side of Equation 9.44 (p. 268) is defined by the following:

$$f_u = 4 \left( \frac{27 C_k}{110} \right)^{1/2} \left( \frac{18 C_k}{55} \right) \left( \frac{\hat{u}'}{U_l} \right)^2 \tag{9.45}$$

$$f_\Delta = \left( \frac{27 C_k \pi^{4/3}}{110} \left( \left( \frac{\hat{\Delta}}{\delta_l^0} \right) - 1 \right) \right)^{1/2} \tag{9.46}$$

$$f_{Re} = \left( \frac{9 Re_\Delta}{55} \exp\left( -\frac{3}{2} \frac{C_k \pi^{4/3}}{Re_\Delta} \right) \right)^{1/2} \tag{9.47}$$

$$a = 0.6 + 0.2 \exp\left( -0.1 \frac{\hat{u}'}{U_l} \right) - 0.2 \exp\left( -0.01 \frac{\hat{\Delta}}{\delta_l^0} \right) \tag{9.48}$$

$$b = 1.4 \tag{9.49}$$

where:

$$C_k = 1.5 \tag{9.50}$$

$$Re_\Delta = \frac{\rho \hat{u}' \hat{\Delta}}{\mu_l} \tag{9.51}$$

The coefficient $\sigma_c$ in Equation 9.40 (p. 267) and Equation 9.41 (p. 267) is designed to ensure that a correct flame brush thickness is maintained. This coefficient is applied not only to the diffusion term of the ECFM equation, but also to the diffusion terms of the progress variable and mixture fraction equations:

$$\sigma_c = \frac{\hat{\Delta}}{\delta_{cn}} \tag{9.52}$$

where $\delta_{cn}$ is the flame brush thickness of a 1D steady flame:

$$\delta_{cn} = \frac{4 U_l \left( \Xi_{\text{eq}} - 1 \right) \beta_{2,\text{les}} \frac{\rho_b}{\rho_u} \left( \frac{\rho_u}{\rho_b} \left( \frac{1}{2} + \frac{\tau}{3} \right) - \alpha_{3,\text{les}} \left( \frac{\rho_u}{\rho_b} + \frac{\tau^2}{3} \right) \right)}{a_t} \tag{9.53}$$

In the previous equation, $\rho_u$ represents the unburnt density, $\rho_b$ represents the burnt density, and $\tau$ is calculated as follows:

$$\tau = \frac{\rho_u}{\rho_b} - 1 \tag{9.54}$$


Release 15.0 - © SAS IP, Inc. All rights reserved. - Contains proprietary and confidential information of ANSYS, Inc. and its subsidiaries and affiliates.

$\Xi_{eq}$ is the equilibrium wrinkling factor given by the following:

$$\Xi_{eq} = 1 + \frac{2}{U_l}\left(\frac{\hat{v}_t a_t}{1-\beta_{2,les}\alpha_{3,les}\frac{\rho_b}{\rho_u}}\right)^{1/2} \tag{9.55}$$

where

$$a_t = \Gamma_K \frac{\hat{u}'}{\hat{\Delta}} \tag{9.56}$$

$$\hat{v}_t = v_t n_{res}^{\frac{4}{3}} \tag{9.57}$$

$v_t$ represents the turbulent viscosity.

Similarly, in Equation 9.40 (p. 267):

$$\hat{\mu}_t = \mu_t n_{res}^{\frac{4}{3}} \tag{9.58}$$

The remaining subgrid terms are:

$$P_{3,sgs} = \beta_{2,les} U_l \frac{1}{1-\bar{c}}\left(\alpha_{3,les}\frac{\Sigma}{\bar{c}} + \Sigma_{lam}\right) \tag{9.59}$$

$$D_{sgs} = \beta_{2,les} U_l \frac{1}{1-\bar{c}}\left(\alpha_{3,les}\frac{\Sigma_{lam}}{\bar{c}} + \Sigma\right)\Sigma \tag{9.60}$$

where

$$\Sigma_{lam} = |\nabla \tilde{c}| + \beta_{1,les}\frac{(\bar{c}-\tilde{c})}{1-\bar{c}}\left(\frac{\alpha_{3,les}}{\bar{c}} - 1\right)\Sigma \tag{9.61}$$

The defaults for the user-defined constants used in the subgrid terms are:

$$\alpha_{3,les} = 0.5 \tag{9.62}$$

$$\beta_{1,les} = 0.4 \tag{9.63}$$

$$\beta_{2,les} = \frac{4}{3} \tag{9.64}$$

## 9.6. Calculation of Properties

The C-equation, G-equation and ECFM turbulent premixed combustion models require properties for temperature, density, unburnt density, unburnt thermal diffusivity and laminar flame speed, which are modeled as described in the sections that follow.

For more information, see the following sections:

9.6.1. Calculation of Temperature
9.6.2. Calculation of Density
9.6.3. Laminar Flame Speed
9.6.4. Unburnt Density and Thermal Diffusivity

Release 15.0 - © SAS IP, Inc. All rights reserved. - Contains proprietary and confidential information of ANSYS, Inc. and its subsidiaries and affiliates.

## 9.6.1. Calculation of Temperature

The calculation method for temperature will depend on whether the model is adiabatic or non-adiabatic.

### 9.6.1.1. Adiabatic Temperature Calculation

For the adiabatic premixed combustion model, the temperature is assumed to be a linear function of reaction progress between the lowest temperature of the unburnt mixture, $T_u$, and the highest adiabatic burnt temperature $T_{ad}$:

$$T = (1-c)\,T_u + cT_{ad} \tag{9.65}$$

### 9.6.1.2. Non-Adiabatic Temperature Calculation

For the non-adiabatic premixed combustion model, ANSYS Fluent solves an energy transport equation in order to account for any heat losses or gains within the system. The energy equation in terms of sensible enthalpy, $h$, for the fully premixed fuel (see Equation 5.3 (p. 134)) is as follows:

$$\frac{\partial}{\partial t}(\rho h) + \nabla \cdot (\rho \vec{v} h) = \nabla \cdot \left( \frac{k+k_t}{c_p} \nabla h \right) + S_{h,chem} + S_{h,rad} \tag{9.66}$$

$S_{h,rad}$ represents the heat losses due to radiation and $S_{h,chem}$ represents the heat gains due to chemical reaction:

$$S_{h,chem} = \rho S_c H_{comb} Y_{fuel} \tag{9.67}$$

where

$S_c$ = normalized average rate of product formation ($s^{-1}$)

$H_{comb}$ = heat of combustion for burning 1 kg of fuel (J/kg)

$Y_{fuel}$ = fuel mass fraction of unburnt mixture

## 9.6.2. Calculation of Density

ANSYS Fluent calculates the premixed density using the ideal gas law. For the adiabatic model, pressure variations are neglected and the mean molecular weight is assumed to be constant. The burnt gas density is then calculated from the following relation:

$$\rho_b T_b = \rho_u T_u \tag{9.68}$$

where the subscript $u$ refers to the unburnt cold mixture, and the subscript $b$ refers to the burnt hot mixture. The required inputs are the unburnt density ($\rho_u$), the unburnt temperature ($T_u$), and the burnt adiabatic flame temperature ($T_b$).

For the non-adiabatic model, you can choose to either include or exclude pressure variations in the ideal gas equation of state. If you choose to ignore pressure fluctuations, ANSYS Fluent calculates the density from

$$\rho T = \rho_u T_u \tag{9.69}$$

where $T$ is computed from the energy transport equation, Equation 9.66 (p. 270). The required inputs are the unburnt density ($\rho_u$) and the unburnt temperature ($T_u$). Note that, from the incompressible ideal


Release 15.0 - © SAS IP, Inc. All rights reserved. - Contains proprietary and confidential information of ANSYS, Inc. and its subsidiaries and affiliates.

gas equation, the expression $\rho_u RT_u/p_{op}$ may be considered to be the effective molecular weight of the gas, where $R$ is the gas constant and $p_{op}$ is the operating pressure.

If you want to include pressure fluctuations for a compressible gas, you will need to input the effective molecular weight of the gas, and the density will be calculated from the ideal gas equation of state.

## 9.6.3. Laminar Flame Speed

The laminar flame speed ($U_l$ in Equation 9.3 (p. 255)) can be specified as constant, or as a user-defined function. A third option appears for non-adiabatic premixed and partially-premixed flames and is based on the correlation proposed by Metghalchi and Keck [296] (p. 745),

$$U_l = U_{l,ref}\left(\frac{T_u}{T_{u,ref}}\right)^{\gamma}\left(\frac{p_u}{p_{u,ref}}\right)^{\beta} \tag{9.70}$$

In Equation 9.70 (p. 271), $T_u$ and $p_u$ are the unburnt reactant temperature and pressure ahead of the flame, $T_{u,ref}=298K$ and $p_{u,ref}=1\,atm$.

The reference laminar flame speed, $U_{l,ref}$, is calculated from

$$U_{l,ref}=C_1+C_2(\phi-C_3)^2 \tag{9.71}$$

where $\phi$ is the equivalence ratio ahead of the flame front, and $C_1$, $C_2$ and $C_3$ are fuel-specific constants. The exponents $\gamma$ and $\beta$ are calculated from,

$$\begin{aligned}\gamma &= 2.18-0.8(\phi-1)\\ \beta &= -0.16+0.22(\phi-1)\end{aligned} \tag{9.72}$$

The Metghalchi-Keck laminar flame speeds are available for fuel-air mixtures of methane, methanol, propane, iso-octane and indolene fuels.

## 9.6.4. Unburnt Density and Thermal Diffusivity

The unburnt density ($\rho_u$ in Equation 9.3 (p. 255)) and unburnt thermal diffusivity ($\alpha$ in Equation 9.9 (p. 257) and Equation 9.10 (p. 258)) are specified constants that are set in the **Materials** dialog box. However, for compressible cases, such as in-cylinder combustion, these can change significantly in time and/or space. When the ideal gas model is selected for density, the unburnt density and thermal diffusivity are calculated by evaluating the local cell at the unburnt state c=0.

Release 15.0 - © SAS IP, Inc. All rights reserved. - Contains proprietary and confidential information of ANSYS, Inc. and its subsidiaries and affiliates.

Release 15.0 - © SAS IP, Inc. All rights reserved. - Contains proprietary and confidential information
of ANSYS, Inc. and its subsidiaries and affiliates.

# Chapter 10: Partially Premixed Combustion

ANSYS Fluent provides a partially premixed combustion model that is based on the non-premixed combustion model described in Non-Premixed Combustion (p. 215) and the premixed combustion model described in Premixed Combustion (p. 253). For information about using the partially premixed combustion model, see Modeling Partially Premixed Combustion in the User's Guide. Information about the theory behind the partially premixed combustion model is presented in the following sections:

10.1. Overview
10.2. Limitations
10.3. Partially Premixed Combustion Theory

## 10.1. Overview

Partially premixed combustion systems are premixed flames with non-uniform fuel-oxidizer mixtures (equivalence ratios). Such flames include premixed jets discharging into a quiescent atmosphere, lean premixed combustors with diffusion pilot flames and/or cooling air jets, and imperfectly premixed inlets. ANSYS Fluent has three types of partially premixed models, namely Chemical Equilibrium, Steady Diffusion Flamelet, and Flamelet Generated Manifold.

The Chemical Equilibrium and Steady Diffusion Flamelet partially-premixed models assume that the premixed flame front is infinitely thin, with unburnt reactants ahead and burnt products behind the flame front. The composition of the burnt products can be modeled assuming chemical equilibrium or with steady laminar diffusion flamelets. The flame-brush is indicated by a value of mean reaction progress $\overline{c}$ between 0 and 1. Note that at a point within the turbulent premixed flame brush, $0 < \overline{c} < 1$, the fluctuating thin flame spends some time at the unburnt state ($c = 0$) and the remaining time at the burnt state ($c = 1$), with a mean reaction progress between zero and one. It should not be interpreted that the instantaneous premixed flame reaction progress is intermediate between the unburnt and burnt state.

The Flamelet Generated Manifold (FGM) model [460] (p. 754) assumes that the thermochemical states in a turbulent flame are similar to the states in a laminar flame, and parameterize these by mixture fraction and reaction progress. Within the laminar flame, reaction progress increases from $c = 0$ in the unburnt reactants to $c = 1$ in the burnt products, over a non-zero flame thickness. A point within the turbulent flame brush with $0 < \overline{c} < 1$ has contributions from both fluctuating flame fronts, as well as intermediate reaction progress. ANSYS Fluent has the option to model the FGM with either premixed or diffusion laminar flames.

## 10.2. Limitations

The underlying theory, assumptions, and limitations of the non-premixed and premixed models apply directly to the partially premixed model. In particular, the single-mixture-fraction approach is limited to two inlet streams, which may be pure fuel, pure oxidizer, or a mixture of fuel and oxidizer. The two-mixture-fraction model extends the number of inlet streams to three, but incurs a major computational overhead. See Limitations (p. 254) for additional limitations.

Release 15.0 - © SAS IP, Inc. All rights reserved. - Contains proprietary and confidential information of ANSYS, Inc. and its subsidiaries and affiliates.

## 10.3. Partially Premixed Combustion Theory

The partially premixed model solves a transport equation for the mean reaction progress variable, $\overline{c}$, or the mean flame position, $\overline{G}$ (to determine the position of the flame front), as well as the mean mixture fraction, $\overline{f}$ and the mixture fraction variance, $\overline{f'^2}$. The Flamelet Generated Manifold model has an option to solve a transport equation for the reaction progress variable variance, $\overline{c'^2}$, or to use an algebraic expression. Ahead of the flame ($c=0$), the fuel and oxidizer are mixed but unburnt and behind the flame ($c=1$), the mixture is burnt.

For more information, see the following sections:

10.3.1. Chemical Equilibrium and Steady Diffusion Flamelet Models
10.3.2. Flamelet Generated Manifold (FGM) model
10.3.3. FGM Turbulent Closure
10.3.4. Calculation of Unburnt Properties
10.3.5. Laminar Flame Speed

### 10.3.1. Chemical Equilibrium and Steady Diffusion Flamelet Models

Density weighted mean scalars (such as species fractions and temperature), denoted by $\overline{\phi}$, are calculated from the probability density function (PDF) of $f$ and $c$ as

$$\overline{\phi}=\int_0^1\int_0^1 \phi(f,c)\,p(f,c)\,df\,dc \tag{10.1}$$

Under the assumption of thin flames, so that only unburnt reactants and burnt products exist, the mean scalars are determined from

$$\overline{\phi}=\overline{c}\int_0^1 \phi_b(f)\,p(f)\,df+(1-\overline{c})\int_0^1 \phi_u(f)\,p(f)\,df \tag{10.2}$$

where the subscripts $b$ and $u$ denote burnt and unburnt, respectively.

The burnt scalars, $\phi_b$, are functions of the mixture fraction and are calculated by mixing a mass $f$ of fuel with a mass $(1-f)$ of oxidizer and allowing the mixture to equilibrate. When non-adiabatic mixtures and/or diffusion laminar flamelets are considered, $\phi_b$ is also a function of enthalpy and/or strain, but this does not alter the basic formulation. The unburnt scalars, $\phi_u$, are calculated similarly by mixing a mass $f$ of fuel with a mass $(1-f)$ of oxidizer, but the mixture is not reacted.

Just as in the non-premixed model, the chemistry calculations and PDF integrations for the burnt mixture are performed in ANSYS Fluent, and look-up tables are constructed.

It is important to understand that in the limit of perfectly premixed combustion, the equivalence ratio and hence mixture fraction is constant. Hence, the mixture fraction variance and its scalar dissipation are zero. If you are using laminar diffusion flamelets, the flamelet at the lowest strain will always be interpolated, and if you have **Include Equilibrium Flamelet** enabled, the ANSYS Fluent solution will be identical to a calculation with a chemical equilibrium PDF table.


Release 15.0 - © SAS IP, Inc. All rights reserved. - Contains proprietary and confidential information of ANSYS, Inc. and its subsidiaries and affiliates.

## 10.3.2. Flamelet Generated Manifold (FGM) model

The Laminar Flamelet model (see The Diffusion Flamelet Models Theory (p. 238)) postulates that a turbulent flame is an ensemble of laminar flames that have an internal structure not significantly altered by the turbulence. These laminar flamelets are embedded in the turbulent flame brush using statistical averaging. The Flamelet Generated Manifold (FGM) [460] (p. 754) model assumes that the scalar evolution (that is the realized trajectories on the thermochemical manifold) in a turbulent flame can be approximated by the scalar evolution in a laminar flame. Both Laminar Flamelet and FGM parameterize all species and temperature by a few variables, such as mixture-fraction, scalar-dissipation and/or reaction-progress, and solve transport equations for these parameters in a 3D CFD simulation.

Note that the FGM model is fundamentally different from the Laminar Flamelet model. For instance, since Laminar Flamelets are parameterized by strain, the thermochemistry always tends to chemical equilibrium as the strain rate decays towards the outlet of the combustor. In contrast, the FGM model is parameterized by reaction progress and the flame can be fully quenched, for example, by adding dilution air. No assumption of thin and intact flamelets is made by FGM, and the model can theoretically be applied to the stirred reactor limit, as well as to ignition and extinction modeling.

Any type of laminar flame can be used to parameterize an FGM. ANSYS Fluent can either import an FGM calculated in a third-party flamelet code and written in Standard file format (see Standard Flamelet Files in the User's Guide), or calculate an FGM from 1D steady premixed flamelets or 1D diffusion flamelets.

In general, premixed FGMs should be used for turbulent partially-premixed flames that are predominantly premixed. Similarly, diffusion FGMs should be used for turbulent partially-premixed flames that are predominantly non-premixed.

### 10.3.2.1. Premixed FGMs

While the only possible configuration for a diffusion flamelet in 1D is opposed flow, 1D steady premixed flamelets can have several configurations. These include unstrained adiabatic freely-propagating, unstrained non-adiabatic burner-stabilized, as well as a strained opposed flow premixed flames.

1D premixed flamelets can be solved in physical space (for example, [370] (p. 749), [59] (p. 732)), then transformed to reaction-progress space in the ANSYS Fluent premixed flamelet file format, and imported into ANSYS Fluent. Alternatively 1D premixed flamelets can be generated in ANSYS Fluent, which solves the flamelets in reaction-progress space. The reaction progress variable is defined by Equation 9.2 (p. 255)

where the sum is over all species in the chemical mechanism, $Y_k$ denotes the $k^{th}$ species mass fraction, superscript $u$ denotes the unburnt reactant at the flame inlet, and superscript $eq$ denotes chemical equilibrium at the flame outlet. The coefficients $\alpha_k$ should be prescribed so that the reaction progress, $c$, increases monotonically through the flame. By default, $\alpha_k = 0$ for all species other than $\alpha_{CO_2} = \alpha_{CO} = 1$, which are selected for hydrocarbon combustion. In the case where the element $C$ is missing from the chemical mechanism, such as $H_2$ combustion, ANSYS Fluent uses $\alpha_k = 0$ except $\alpha_{H_2O} = 1$, by default. The coefficients $\alpha_k$ can be set in the text user interface when generating FGM using the text user interface.

The 1D adiabatic premixed flame equations can be transformed from physical-space to reaction-progress space [319] (p. 746), [265] (p. 743). Neglecting differential-diffusion, these equations are

$$\rho \frac{\partial Y_k}{\partial t} + \frac{\partial Y_k}{\partial c} \dot{\omega}_c = \rho \chi_c \frac{\partial^2 Y_k}{\partial c^2} + \dot{\omega}_k \tag{10.3}$$

$$\rho\frac{\partial T}{\partial t}+\frac{\partial T}{\partial c}\dot{\omega}_c=\rho\chi_c\frac{\partial^2 T}{\partial c^2}-\frac{1}{c_p}\sum_k h_k\dot{\omega}_k+\frac{\rho\chi_c}{c_p}\left(\frac{\partial c_p}{\partial c}+\sum_k c_{p,k}\frac{\partial Y_k}{\partial c}\right)\frac{\partial T}{\partial c} \tag{10.4}$$

where $Y_k$ is the $k^{th}$ species mass fraction, $T$ is the temperature, $\rho$ is the fluid density, $t$ is time, $\dot{\omega}_k$ is the $k^{th}$ species mass reaction rate, $h_k$ is the total enthalpy, and $c_{p,k}$ is the $k^{th}$ species specific heat at constant pressure.

The scalar-dissipation rate, $\chi_c$ in Equation 10.3 (p. 275) and Equation 10.4 (p. 276) is defined as

$$\chi_c=\frac{\lambda}{\rho c_p}|\nabla c|^2 \tag{10.5}$$

where $\lambda$ is the thermal conductivity. Note that $\chi_c$ varies with $c$ and is an input to the equation set. If $\chi_c(c)$ is taken from a 1D physical-space, adiabatic, equi-diffusivity flamelet calculation, either freely-propagating (unstrained) or opposed-flow (strained), the $c$-space species and temperature distributions would be identical to the physical-space solution. However, $\chi_c(c)$ is generally not known and is modeled in ANSYS Fluent as

$$\chi_c(c)=\chi_{\max}\exp\left(-2\left(erfc^{-1}(2c)\right)^2\right) \tag{10.6}$$

where $\chi_{\max}$ is a user-specified maximum scalar dissipation within the premixed flamelet, and $erfc^{-1}$ is the inverse complementary error function.

A 1D premixed flamelet is calculated at a single equivalence ratio, which can be directly related to a corresponding mixture fraction. For partially-premixed combustion, premixed laminar flamelets must be generated over a range of mixture fractions. Premixed flamelets at different mixture fractions have different maximum scalar dissipations, $\chi_{\max}$. In ANSYS Fluent, the scalar dissipation $\chi_c(f,c)$ at any mixture fraction $f$ is modeled as

$$\chi_c(f,c)=\chi_{\max}^{sto}\exp\left(-2\left(erfc^{-1}\left(\frac{f}{f_{sto}}\right)\right)^2\right)\exp\left(-2\left(erfc^{-1}(2c)\right)^2\right) \tag{10.7}$$

where $sto$ indicates stoichiometric mixture fraction.

Hence, the only model input to the premixed flamelet generator in ANSYS Fluent is the scalar dissipation at stoichiometric mixture fraction, $\chi_{\max}^{sto}$. The default value is $\chi_{\max}^{sto}=1000/s$, which reasonably matches solutions of unstrained (freely propagating) physical-space flamelets for rich, lean, and stoichiometric hydrocarbon and hydrogen flames at standard temperature and pressure.

The following are important points to consider about premixed flamelet generation in ANSYS Fluent in general and when specifying $\chi_{\max}^{sto}$ in particular:

- It is common in the FGM approach to use unstrained, freely-propagating premixed flamelets. However, for highly turbulent flames where the instantaneous premixed flame front is stretched and distorted by the turbulence, a strained premixed flamelet may be a better representation of the manifold. The ANSYS Fluent FGM model allows a premixed flamelet generated manifold at a single, representative strain rate, $\chi_{\max}^{sto}$.


Release 15.0 - © SAS IP, Inc. All rights reserved. - Contains proprietary and confidential information of ANSYS, Inc. and its subsidiaries and affiliates.

- Calculating flamelets in physical-space can be compute-intensive and difficult to converge over the entire mixture fraction range, especially with large kinetic mechanisms at the flammability limits. The ANSYS Fluent solution in reaction-progress space is substantially faster and more robust than a corresponding physical-space solution. However, if physical-space solutions (for example, from [370] (p. 749), [59] (p. 732)) are preferred, they can be generated with an external code, transformed to reaction-progress space, and imported in ANSYS Fluent's Standard Flamelet file format.

- A more appropriate value of $\chi_{\max}^{sto}$ than the default (1000/s) for the specific fuel and operating conditions of your combustor can be determined from a physical-space premixed flamelet solution at stoichiometric mixture fraction. This premixed flamelet solution can be unstrained or strained. $\chi_c(c)$ through the flamelet is then calculated from Equation 10.5 (p. 276) and $\chi_{\max}^{sto}$ is the maximum value of $\chi_c(c)$.

- As $\chi_{\max}^{sto}$ is increased, the solution of temperature and species fractions as a function of $c$ tends to the thin-flamelet chemical equilibrium solution, which is linear between unburnt at $c=0$ and chemical equilibrium at $c=1$. The minimum specified $\chi_{\max}^{sto}$ should be that in a freely-propagating flame.

  For smaller values of $\chi_{\max}^{sto}$, the ANSYS Fluent premixed flamelet generator will have difficulties converging. When ANSYS Fluent fails to converge steady premixed flamelets at rich mixture fractions, equilibrium thin-flamelet solutions are used.

- The ANSYS Fluent partially-premixed model can be used to model partially-premixed flames ranging from the non-premixed to the perfectly-premixed limit. In the non-premixed limit, reaction progress is unity everywhere in the domain and all premixed streams are fully burnt. In the premixed limit, the mixture fraction is constant in the domain. When creating a partially-premixed PDF table, the interface requires specification of the fuel and oxidizer compositions and temperatures. For partially-premixed flames, the fuel composition can be modeled as pure fuel, in which case any premixed inlet would be set to the corresponding mixture fraction, which is less than one. Alternatively, the fuel composition can be specified in the interface as a premixed inlet composition, containing both fuel and oxidizer components. In this latter case, the mixture fraction at premixed inlets would be set to one.

#### 10.3.2.2. Diffusion FGMs

For turbulent partially-premixed flames that are predominantly non-premixed, diffusion FGMs are a better representation of the thermochemistry than premixed FGMs. An example of this is modeling $CO$ emissions from a gas-turbine combustor where the primary combustion zone is quenched by rapid mixing with dilution air. If the outlet equivalence ratio is less than the flammability limit of a corresponding premixed flamelet, the premixed FGM will predict sub-equilibrium $CO$, even if the combustor is quenched ($\overline{c}<1$). A diffusion FGM, however, will better predict super-equilibrium $CO$ for $\overline{c}<1$.

Diffusion FGMs are calculated in ANSYS Fluent using the diffusion laminar flamelet generator as detailed in Flamelet Generation (p. 242). Steady diffusion flamelets are generated over a range of scalar dissipation rates by starting from a very small strain (0.01/s by default) and increasing this in increments (5/s by default) until the flamelet extinguishes. The diffusion FGM is calculated from the steady diffusion laminar flamelets by converting the flamelet species fields to reaction progress, $c$ (see Equation 10.2 (p. 274)). As the strain rate increases, the flamelet chemistry departs further from chemical equilibrium and $c$ decreases from unity towards the extinction reaction, $c_{extinction}$.

Release 15.0 - © SAS IP, Inc. All rights reserved. - Contains proprietary and confidential information of ANSYS, Inc. and its subsidiaries and affiliates.

The FGM between $c_{extinction}$ and the unburnt state $c=0$, is determined from the thermochemical states of the final, extinguishing diffusion flamelet.

## 10.3.3. FGM Turbulent Closure

The reaction progress variable is defined as a normalized fraction of product species (see Equation 9.2 (p. 255)), namely $c=\frac{Y_c}{Y_c^{eq}}$. Note that the denominator, $Y_c^{eq}$, is only a function of the local mixture fraction. When the **Flamelet Generated Manifold** model is enabled, ANSYS Fluent solves a transport equation for the un-normalized progress variable, $Y_c$, and not the normalized progress variable, $c$. This has two advantages. Firstly, since there are usually no products in the oxidizer stream, $Y_c^{eq}$ is zero and $c$ is undefined here (in other words, burnt air is the same as unburnt air). This can lead to difficulties in specifying oxidizer boundary conditions where oxidizer is mixed into unburnt reactants before the flame, as well as into burnt products behind the flame. Solving for $Y_c$ avoids these issues and the solution is independent of the specified boundary value of $c$ for pure oxidizer inlets. The second advantage of solving for $Y_c$ is that flame quenching can be modeled naturally. Consider a burnt stream in chemical equilibrium ($c=1$) that is rapidly quenched with an air jet. Since the $c$ equation in ANSYS Fluent does not have a source term dependent on changes in mixture fraction, $c$ remains at unity and hence the diluted mixture remains at chemical equilibrium. Solving for $Y_c$ can capture quenching since $Y_c^{eq}$ changes with mixture fraction, and the normalized reaction progress $c$ is correctly less than unity after mixing. To model these two effects with the normalized $c$ equation, additional terms involving derivatives and cross-derivatives of mixture fraction are required [43] (p. 731). These terms do not appear in the transport equation for $Y_c$:

$$\overline{\rho}\frac{\partial \tilde{Y}_c}{\partial t}+\frac{\partial}{\partial x_i}(\overline{\rho}\tilde{u}_i\tilde{Y}_c)=\frac{\partial}{\partial x_i}\left(\overline{\rho}D_{eff}\frac{\partial \tilde{Y}_c}{\partial x_i}\right)+\overline{S}_c \tag{10.8}$$

Typically, in the FGM model, the mean source term $\overline{S}_c$ is modeled from the finite-rate kinetic rate obtained from the FGM, namely,

$$\overline{S}_c=\overline{\rho}\iint S_{FR}(c,f)\,P(c,f)\,dc\,df=\overline{S}_{FR} \tag{10.9}$$

where $S_{FR}$ is the Finite-Rate flamelet source term from the flamelet library, and $P$ is the joint PDF of reaction-progress ($c$) and mixture fraction ($f$).

The source term $\overline{S}_c$ determines the turbulent flame position. Errors in both the approximation of the $c$ variance, as well as the assumed shape Beta PDF, can cause inaccurate flame positions. ANSYS Fluent has the option of two other turbulence-chemistry interaction models for the source term $\overline{S}_c$. One option is to use a turbulent flame speed,

$$\overline{S}_c=\rho_u S_t|\nabla\tilde{c}|=\overline{S}_{TFS} \tag{10.10}$$

which is essentially the same source term when using the chemical equilibrium and diffusion flamelet partially-premixed models. An advantage of using a turbulent flame speed is that model constants can be calibrated to predict the correct flame position. In contrast, there are no direct parameters to control the FGM finite-rate source (Equation 10.9 (p. 278)), and hence the flame position.

The third option is to use the minimum of the Finite-Rate and Turbulent-Flame-Speed expressions:

$$\overline{S}_c=Min(\overline{S}_{FR},\overline{S}_{TFS}) \tag{10.11}$$

The idea behind Equation 10.11 (p. 278) is to use the turbulent flame speed model to predict the flame location and the finite-rate model to predict post-flame quenching, for example, by dilution with cold air.


Release 15.0 - © SAS IP, Inc. All rights reserved. - Contains proprietary and confidential information of ANSYS, Inc. and its subsidiaries and affiliates.

The joint PDF, $P(c,f)$ in Equation 10.9 (p. 278), is specified as the product of two beta PDFs. The beta PDFs require second moments (that is, variances). The variance of the un-normalized reaction progress variable is modeled either with a transport equation

$$\overline{\rho}\frac{\partial \tilde{Y}_c^{"2}}{\partial t}+\frac{\partial}{\partial x_i}\left(\overline{\rho}\tilde{u}_i\tilde{Y}_c^{"2}\right)=\frac{\partial}{\partial x_i}\left(\overline{\rho}D_{eff}\frac{\partial \tilde{Y}_c^{"2}}{\partial x_i}\right)+c_\varphi D_{eff}|\nabla \tilde{Y}_c|^2-\frac{\overline{\rho}c_\varphi}{\tau_{turb}}\tilde{Y}_c^{"2} \tag{10.12}$$

or with an algebraic expression

$$\widetilde{Y''_c}^2=c_{\text{var}}\frac{l_{turb}^2}{Sc_t}\left(\nabla \widetilde{Y}_c\right)^2 \tag{10.13}$$

where $l_{turb}$ is the turbulence length scale and $c_{\text{var}}$ is a constant with a default value of 0.1.

The mean thermochemical properties are determined from the modeled PDF as

$$\overline{\varphi}=\iint \varphi(c,f)\,P(c,f)\,dc\,df \tag{10.14}$$

where $\varphi$ denotes temperature or species fractions from the premixed flamelet library.

For non-adiabatic flows, ANSYS Fluent neglects the effect of heat loss or heat gain on the species compositions within the flame brush ($0<\overline{c}<1$). However, in burnt product zones ($c=1$), where by definition the thermochemistry is in chemical equilibrium, non-adiabatic effects are accounted for in the species fields.

## 10.3.4. Calculation of Unburnt Properties

Turbulent fluctuations are neglected for the unburnt mixture, so the mean unburnt scalars, $\overline{\phi}_u$, are functions of $\overline{f}$ only. The unburnt density, temperature, specific heat, and thermal diffusivity are fitted in ANSYS Fluent to third-order polynomials of $\overline{f}$ using linear least squares:

$$\overline{\phi}_u=\sum_{n=0}^{3}c_n\overline{f}^{\,n} \tag{10.15}$$

Since the unburnt scalars are smooth and slowly-varying functions of $\overline{f}$, these polynomial fits are generally accurate. Access to polynomials is provided in case you want to modify them.

When the secondary mixture fraction model is enabled, the unburnt density, temperature, specific heat, thermal diffusivity, and laminar flame speed are calculated as follows: polynomial functions are calculated for a mixture of pure primary fuel and oxidizer, as described above, and are a function of the mean primary mixture fraction, $\overline{f}$. Similar polynomial functions are calculated for a mixture of pure secondary fuel and oxidizer, and are a function of the normalized secondary mixture fraction, $\overline{p}$. The unburnt properties in a cell are then calculated as a weighted function of the mean primary mixture fraction and mean secondary normalized mixture fraction as,

$$\phi_u=\frac{\overline{f}}{\overline{f}+\overline{p}}\phi_u^{primary}+\frac{\overline{p}}{\overline{f}+\overline{p}}\phi_u^{secondary} \tag{10.16}$$

## 10.3.5. Laminar Flame Speed

The premixed models require the laminar flame speed (see Equation 9.9 (p. 257)), which depends strongly on the composition, temperature, and pressure of the unburnt mixture. For adiabatic perfectly premixed

Release 15.0 - © SAS IP, Inc. All rights reserved. - Contains proprietary and confidential information of ANSYS, Inc. and its subsidiaries and affiliates.

systems as in Premixed Combustion (p. 253), the reactant stream has one composition, and the laminar flame speed is constant throughout the domain. However, in partially premixed systems, the laminar flame speed will change as the reactant composition (equivalence ratio) changes, and this must be taken into account.

Accurate laminar flame speeds are difficult to determine analytically, and are usually measured from experiments or computed from 1D simulations. For the partially-premixed model, in addition to the laminar flame speed model options described in Laminar Flame Speed (p. 271), namely constant, UDF, and Metghalchi-Keck,, ANSYS Fluent has fitted curves obtained from numerical simulations of the laminar flame speed [144] (p. 736). These curves were determined for hydrogen ($H_2$), methane ($CH_4$), acetylene ($C_2H_2$), ethylene ($C_2H_4$), ethane ($C_2H_6$), and propane ($C_3H_8$) fuels. They are valid for inlet compositions ranging from the lean limit through unity equivalence ratio (stoichiometric), for unburnt temperatures from 298 K to 800 K, and for pressures from 1 bar to 40 bars.

ANSYS Fluent fits these curves to a piecewise-linear polynomial. Mixtures leaner than the lean limit or richer than the rich limit will not burn, and have zero flame speed. The required inputs are values for the laminar flame speed at ten mixture fraction ($\overline{f}$) points. The first (minimum) and last (maximum) $\overline{f}$ inputs are the flammability limits of the mixture and the laminar flame speed is zero outside these values.

For non-adiabatic simulations, such as heat transfer at walls or compressive heating, the unburnt mixture temperature may deviate from its adiabatic value. The piecewise-linear function of mixture fraction is unable to account for this effect on the laminar flame speed. You can include non-adiabatic effects on the laminar flame speed by enabling **Non-Adiabatic Laminar Flame Speed**, which tabulates the laminar speeds in the PDF table by evaluating the curve fits from [144] (p. 736) at the enthalpy levels in the PDF table. Note that the tabulated mean laminar flame speed accounts for fluctuations in the mixture fraction.

**Important**

These flame speed fits are accurate for air mixtures with pure fuels of $H_2$, $CH_4$, $C_2H_2$, $C_2H_4$, $C_2H_6$, and $C_3H_8$. If an oxidizer other than air or a different fuel is used, or if the unburnt temperature or pressure is outside the range of validity, then the curve fits will be incorrect. Although ANSYS Fluent defaults to a methane-air mixture, the laminar flame speed polynomial and the rich and lean limits are most likely incorrect for your specified fuel/oxidizer and unburnt temperature/pressure conditions. The laminar flame speed polynomial should be determined from other sources, such as measurements from the relevant literature or detailed 1D simulations, and then input into ANSYS Fluent. Alternatively, you can use a user-defined function for the laminar flame speed.


Release 15.0 - © SAS IP, Inc. All rights reserved. - Contains proprietary and confidential information of ANSYS, Inc. and its subsidiaries and affiliates.

# Chapter 11: Composition PDF Transport

ANSYS Fluent provides a composition PDF transport model for modeling finite-rate chemistry effects in turbulent flames. For information about using the composition PDF transport model, see Modeling a Composition PDF Transport Problem in the User's Guide. Information about the theory behind this model is presented in the following sections:


11.1. Overview and Limitations
11.2. Composition PDF Transport Theory
11.3. The Lagrangian Solution Method
11.4. The Eulerian Solution Method


## 11.1. Overview and Limitations

The composition PDF transport model, like the Laminar Finite-Rate (see The Laminar Finite-Rate Model (p. 189)) and EDC model (see The Eddy-Dissipation-Concept (EDC) Model (p. 195)), should be used when you are interested in simulating finite-rate chemical kinetic effects in turbulent reacting flows. With an appropriate chemical mechanism, kinetically-controlled species such as CO and NOx, as well as flame extinction and ignition, can be predicted. PDF transport simulations are computationally expensive, and it is recommended that you start your modeling with small meshes, and preferably in 2D.

A limitation that applies to the composition PDF transport model is that you must use the pressure-based solver as the model is not available with the density-based solver.

ANSYS Fluent has two different discretizations of the composition PDF transport equation, namely Lagrangian and Eulerian. The Lagrangian method is strictly more accurate than the Eulerian method, but requires significantly longer run time to converge.

## 11.2. Composition PDF Transport Theory

Turbulent combustion is governed by the reacting Navier-Stokes equations. While this equation set is accurate, its direct solution (where all turbulent scales are resolved) is far too expensive for practical turbulent flows. In Species Transport and Finite-Rate Chemistry (p. 187), the species equations are Reynolds-averaged, which leads to unknown terms for the turbulent scalar flux and the mean reaction rate. The turbulent scalar flux is modeled in ANSYS Fluent by gradient diffusion, treating turbulent convection as enhanced diffusion. The mean reaction rate can be modeled with the Laminar, Eddy-Dissipation or EDC Finite-Rate chemistry models. Since the reaction rate is invariably highly non-linear, modeling the mean reaction rate in a turbulent flow is difficult and prone to error.

An alternative to Reynolds-averaging the species and energy equations is to derive a transport equation for their single-point, joint probability density function (PDF). This PDF, denoted by $P$, can be considered to represent the fraction of the time that the fluid spends at each species, temperature and pressure state. $P$ has $N+2$ dimensions for the $N$ species, temperature and pressure spaces. From the PDF, any single-point thermo-chemical moment (for example, mean or RMS temperature, mean reaction rate) can be calculated. The composition PDF transport equation is derived from the Navier-Stokes equations as [357] (p. 748):


Release 15.0 - © SAS IP, Inc. All rights reserved. - Contains proprietary and confidential information of ANSYS, Inc. and its subsidiaries and affiliates.

$$\frac{\partial}{\partial t}(\rho P)+\frac{\partial}{\partial x_i}(\rho u_i P)+\frac{\partial}{\partial \psi_k}(\rho S_k P)= -\frac{\partial}{\partial x_i}[\rho\langle u_i'' \mid \psi\rangle P] + \frac{\partial}{\partial \psi_k}\left[\rho\left\langle \frac{1}{\rho}\frac{\partial J_{i,k}}{\partial x_i} \;\middle|\; \psi\right\rangle P\right] \tag{11.1}$$

where

$P$ = Favre joint PDF of composition

$\rho$ = mean fluid density

$u_i$ = Favre mean fluid velocity vector

$S_k$ = reaction rate for species $k$

$\psi$ = composition space vector

$u_i''$ = fluid velocity fluctuation vector

$J_{i,k}$ = molecular diffusion flux vector

The notation of $\langle \ldots \rangle$ denotes expectations, and $\langle A \mid B \rangle$ is the conditional probability of event $A$, given that event $B$ occurs.

In Equation 11.1 (p. 282), the terms on the left-hand side are closed, while those on the right-hand side are not and require modeling. The first term on the left-hand side is the unsteady rate of change of the PDF, the second term is the change of the PDF due to convection by the mean velocity field, and the third term is the change due to chemical reactions. The principal strength of the PDF transport approach is that the highly-non-linear reaction term is completely closed and requires no modeling. The two terms on the right-hand side represent the PDF change due to scalar convection by turbulence (turbulent scalar flux), and molecular mixing/diffusion, respectively.

The turbulent scalar flux term is unclosed, and is modeled in ANSYS Fluent by the gradient-diffusion assumption

$$-\frac{\partial}{\partial x_i}[\rho\langle u_i'' \mid \psi\rangle P]=\frac{\partial}{\partial x_i}\left(\frac{\rho\mu_t}{Sc_t}\frac{\partial P}{\partial x_i}\right) \tag{11.2}$$

where $\mu_t$ is the turbulent viscosity and $Sc_t$ is the turbulent Schmidt number. A turbulence model, as described in Turbulence (p. 39), is required for composition PDF transport simulations, and this determines $\mu_t$.

Since single-point PDFs are described, information about neighboring points is missing and all gradient terms, such as molecular mixing, are unclosed and must be modeled. The mixing model is critical because combustion occurs at the smallest molecular scales when reactants and heat diffuse together. Modeling mixing in PDF methods is not straightforward, and is the weakest link in the PDF transport approach. See Particle Mixing (p. 284) for a description of the mixing models.

## 11.3. The Lagrangian Solution Method

A Lagrangian Monte Carlo method is used to solve for the $N+1$ dimensional PDF Transport equation. Monte Carlo methods are appropriate for high-dimensional equations since the computational cost in-


Release 15.0 - © SAS IP, Inc. All rights reserved. - Contains proprietary and confidential information of ANSYS, Inc. and its subsidiaries and affiliates.

creases linearly with the number of dimensions. The disadvantage is that statistical errors are introduced, and these must be carefully controlled.

To solve the modeled PDF transport equation, an analogy is made with a stochastic differential equation (SDE) that has identical solutions. The Monte Carlo algorithm involves notional particles that move randomly through physical space due to particle convection, and also through composition space due to molecular mixing and reaction. The particles have mass and, on average, the sum of the particle masses in a cell equals the cell mass (cell density times cell volume). Since practical meshes have large changes in cell volumes, the particle masses are adjusted so that the number of particles in a cell is controlled to be approximately constant and uniform.

The processes of convection, diffusion, and reaction are treated in fractional steps as described in the sections that follow. For information on the fractional step method, refer to [55] (p. 732).

Information about this method is described in the following sections:

11.3.1. Particle Convection
11.3.2. Particle Mixing
11.3.3. Particle Reaction

## 11.3.1. Particle Convection

A spatially second-order-accurate Lagrangian method is used in ANSYS Fluent, consisting of two steps. At the first convection step, particles are advanced to a new position

$$x_i^{1/2} = x_i^0 + \frac{1}{2} u_i^0 \Delta t \tag{11.3}$$

where

$x_i$ = particle position vector

$u_i$ = Favre mean fluid-velocity vector at the particle position

$\Delta t$ = particle time step

For unsteady flows, the particle time step is the physical time step. For steady-state flows, local time steps are calculated for each cell as

$$\Delta t = \min\left(\Delta t_{conv}, \Delta t_{diff}, \Delta t_{mix}\right) \tag{11.4}$$

where

$\Delta t_{conv}$ = *convection number* $\times \Delta x$ / (*cell fluid velocity*)

$\Delta t_{diff}$ = *diffusion number* $\times (\Delta x)^2$ / (*cell turbulent diffusivity*)

$\Delta t_{mix}$ = *mixing number* $\times$ *turbulent time scale*

$\Delta x$ = characteristic cell length = $volume^{1/D}$ where $D$ is the problem dimension

After the first convection step, all other sub-processes, including diffusion and reaction are treated. Finally, the second convection step is calculated as

$$x_i^1 = x_i^{1/2} + \Delta t\left(u_i^{1/2} - \frac{1}{2} u_i^0 + \frac{1}{\rho Sc_t}\frac{\partial \mu_{eff}}{\partial x_i} + \xi_i\sqrt{\frac{2\mu_{eff}}{\rho \Delta t Sc_t}}\right) \tag{11.5}$$

where

$\rho$ = mean cell fluid density

$u_i$ = mean fluid-velocity vector at the particle position

$\mu_{eff}$ = effective viscosity

$Sc_t$ = turbulent Schmidt number

$\xi_i$ = standardized normal random vector

## 11.3.2. Particle Mixing

Molecular mixing of species and heat must be modeled and is usually the source of the largest modeling error in the PDF transport approach. ANSYS Fluent provides three models for molecular diffusion: the Modified Curl model [186] (p. 739), [322] (p. 746), the IEM model (which is sometimes called the LSME model) [95] (p. 734) and the EMST model [437] (p. 753).

### 11.3.2.1. The Modified Curl Model

For the Modified Curl model, a few particle pairs are selected at random from all the particles in a cell, and their individual compositions are moved toward their mean composition. For the special case of equal particle mass, the number of particle pairs selected is calculated as

$$N_{pair}=\frac{1.5C_{\phi}N\Delta t}{\tau_t} \tag{11.6}$$

where

$N$ = total number of particles in the cell

$C_{\phi}$ = mixing constant (default = 2)

$\tau_t$ = turbulent time scale (for the $k$-$\varepsilon$ model this is $k/\varepsilon$)

The algorithm in [322] (p. 746) is used for the general case of variable particle mass.

For each particle pair, a uniform random number $\xi$ is selected and each particle's composition $\phi$ is moved toward the pair's mean composition by a factor proportional to $\xi$:

$$\begin{aligned}\phi_i^1&=(1-\xi)\phi_i^0+\xi\frac{\left(\phi_i^0 m_i+\phi_j^0 m_j\right)}{\left(m_i+m_j\right)}\\ \phi_j^1&=(1-\xi)\phi_j^0+\xi\frac{\left(\phi_i^0 m_i+\phi_j^0 m_j\right)}{\left(m_i+m_j\right)}\end{aligned} \tag{11.7}$$

where $\phi_i$ and $\phi_j$ are the composition vectors of particles $i$ and $j$, and $m_i$ and $m_j$ are the masses of particles $i$ and $j$.


Release 15.0 - © SAS IP, Inc. All rights reserved. - Contains proprietary and confidential information of ANSYS, Inc. and its subsidiaries and affiliates.

#### 11.3.2.2. The IEM Model

For the Interaction by Exchange with the Mean (IEM) model, the composition of all particles in a cell are moved a small distance toward the mean composition:

$$\phi^1 = \phi^0 - \left(1 - e^{-0.5 C_\phi / \tau_t}\right)\left(\phi^0 - \tilde{\phi}\right) \tag{11.8}$$

where $\phi^0$ is the composition before mixing, $\phi^1$ is the composition after mixing, and $\tilde{\phi}$ is the Favre mean-composition vector at the particle's location.

#### 11.3.2.3. The EMST Model

Physically, mixing occurs between fluid particles that are adjacent to each other. The Modified Curl and IEM mixing models take no account of this localness, which can be a source of error. The Euclidean Minimum Spanning Tree (EMST) model mixes particle pairs that are close to each other in composition space. Since scalar fields are locally smooth, particles that are close in composition space are likely to be close in physical space. The particle pairing is determined by a Euclidean Minimum Spanning Tree, which is the minimum length of the set of edges connecting one particle to at least one other particle. The EMST mixing model is more accurate than the Modified Curl and IEM mixing models, but incurs a slightly greater computational expense. Details on the EMST model can be found in reference [437] (p. 753).

#### 11.3.2.4. Liquid Reactions

Reactions in liquids often occur at low turbulence levels (small Re), among reactants with low diffusivities (large Sc). For such flows, the mixing constant default of $C_\phi = 2$ overestimates the mixing rate. The **Liquid Micro-Mixing** option interpolates $C_\phi$ from model turbulence [359] (p. 748) and scalar [126] (p. 735) spectra.

### 11.3.3. Particle Reaction

The particle composition vector is represented as

$$\phi = (Y_1, Y_2, \ldots, Y_N, T, p) \tag{11.9}$$

where $Y_k$ is the $k$th species mass fraction, $T$ is the temperature and $p$ the pressure.

For the reaction fractional step, the reaction source term is integrated as

$$\phi^1 = \phi^0 + \int_0^{\Delta t} S\,dt \tag{11.10}$$

where $S$ is the chemical source term. Most realistic chemical mechanisms consist of tens of species and hundreds of reactions. Typically, a reaction does not occur until an ignition temperature is reached, but then proceeds very quickly until reactants are consumed. Hence, some reactions have very fast time scales, in the order of $10^{-10}$ s, while others have much slower time scales, on the order of 1 s. This time-scale disparity results in numerical stiffness, which means that extensive computational work is required to integrate the chemical source term in Equation 11.10 (p. 285). In ANSYS Fluent, the reaction step (that is, the calculation of $\phi^1$) can be performed either by Direct Integration or by In-Situ Adaptive Tabulation (ISAT), as described in the following paragraphs.

Release 15.0 - © SAS IP, Inc. All rights reserved. - Contains proprietary and confidential information of ANSYS, Inc. and its subsidiaries and affiliates.

A typical steady-state PDF transport simulation in ANSYS Fluent may have 50000 cells, with 20 particles per cell, and requires 1000 iterations to converge. Hence, at least $10^9$ stiff ODE integrations are required. Since each integration typically takes tens or hundreds of milliseconds, on average, the direct integration of the chemistry is extremely CPU-demanding.

For a given reaction mechanism, Equation 11.10 (p. 285) may be considered as a mapping. With an initial composition vector $\phi^0$, the final state $\phi^1$ depends only on $\phi^0$ and the mapping time $\Delta t$. In theory, if a table could be built before the simulation, covering all realizable $\phi^0$ states and time steps, the integrations could be avoided by table look-ups. In practice, this *a priori* tabulation is not feasible since a full table in $N+3$ dimensions ($N$ species, temperature, pressure and time-step) is required. To illustrate this, consider a structured table with $M$ points in each dimension. The required table size is $M^{N+3}$, and for a conservative estimate of $M=10$ discretization points and $N=7$ species, the table would contain $10^{10}$ entries.

On closer examination, the full storage of the entire realizable space is very wasteful because most regions are never accessed. For example, it would be unrealistic to find a composition of $Y_{OH}=1$ and $T=300K$ in a real combustor. In fact, for steady-state, 3D laminar simulations, the chemistry can be parameterized by the spatial position vector. Thus, mappings must lie on a three dimensional manifold within the $N+3$ dimensional composition space. It is, hence, sufficient to tabulate only this accessed region of the composition space.

The accessed region, however, depends on the particular chemical mechanism, molecular transport properties, flow geometry, and boundary conditions. For this reason, the accessed region is not known before the simulation and the table cannot be preprocessed. Instead, the table must be built during the simulation, and this is referred to as *in-situ* tabulation. ANSYS Fluent employs ISAT [358] (p. 748) to dynamically tabulate the chemistry mappings and accelerate the time to solution. ISAT is a method to tabulate the accessed composition space region "on the fly" (in-situ) with error control (adaptive tabulation). When ISAT is used correctly, accelerations of two to three orders of magnitude are typical. However, it is important to understand how ISAT works in order to use it optimally.

## 11.4. The Eulerian Solution Method

The Lagrangian solution method solves the composition PDF transport equation by stochastically tracking Lagrangian particles through the domain. It is computationally expensive since a large number of particles are required to represent the PDF, and a large number of iterations are necessary to reduce statistical errors and explicitly convect the particles through the domain. The Eulerian PDF transport model overcomes these limitations by assuming a shape for the PDF, which allows Eulerian transport equations to be derived. Stochastic errors are eliminated and the transport equations are solved implicitly, which is computationally economical. The multi-dimensional PDF shape is assumed as a product of delta functions. As with the Lagrangian PDF model, the highly non-linear chemical source term is closed. However, the turbulent scalar flux and molecular mixing terms must be modeled, and are closed with the gradient diffusion and the IEM models, respectively.

The composition PDF of $N_s+1$ dimension ($N_s$ species and enthalpy) is represented as a collection of $N_e$ delta functions (or modes). This presumed PDF has the following form:

$$P(\psi;\ \vec{x},t)=\sum_{n=1}^{N_e}p_n(\vec{x},t)\prod_{k=1}^{N_s}\delta\left[\psi_k-<\phi_k>_n(\vec{x},t)\right] \tag{11.11}$$


Release 15.0 - © SAS IP, Inc. All rights reserved. - Contains proprietary and confidential information of ANSYS, Inc. and its subsidiaries and affiliates.

where $p_n$ is the probability in each mode, $<\phi_k>_n$ is the conditional mean composition of species $k$ in the $n$th mode, $\psi_k$ is the composition space variable of species $k$, and $\delta(\ \dots\ )$ is the delta function.

The Eulerian PDF transport equations are derived by substituting Equation 11.11 (p. 286) into the closed composition PDF transport equation (Equation 11.1 (p. 282) with Equation 11.2 (p. 282) and Equation 11.8 (p. 285)). The unknown terms, $p_n$ and $<\phi_k>_n$, are determined by forcing lower moments of this transported PDF to match the RANS lower moment transport equations, using the Direct Quadrature Method of Moments (DQMOM) approach [126] (p. 735), [282] (p. 744). The resulting transport equations are:

- Probability (magnitude of the $n$th delta function):

$$\frac{\partial \rho p_n}{\partial t}+\frac{\partial}{\partial x_i}\left(\rho u_i p_n\right)=\nabla\left(\rho\Gamma\nabla p_n\right) \tag{11.12}$$

- Probability weighted conditional mean of composition $k$:

$$\frac{\partial \rho s_{k,n}}{\partial t}+\frac{\partial}{\partial x_i}\left(\rho u_i s_{k,n}\right)=\nabla\left(\rho\Gamma\nabla s_{k,n}\right)+\rho\left(M_{k,n}+S_{k,n}+C_{k,n}\right) \tag{11.13}$$

where $p_n$ is the probability of the $n$th mode, and $s_{k,n}=p_n<\phi_k>_n$ is the $k$th species probability weighted conditional mean composition of the $n$th mode. $\Gamma=\mu_l+\mu_t/Sc_t$ is the effective turbulent diffusivity. The terms $M_{k,n}$, $S_{k,n}$ and $C_{k,n}$ represent mixing, reaction and correction terms respectively. Note that only $N_e-1$ probability equations are solved and the $N$th probability is calculated as one minus the sum of the $N_e-1$ solved probabilities.

For more information, see the following sections:

11.4.1. Reaction
11.4.2. Mixing
11.4.3. Correction
11.4.4. Calculation of Composition Mean and Variance

## 11.4.1. Reaction

The reaction source term $S_{k,n}$ in Equation 11.13 (p. 287) for the $k$th composition and the $n$th mode is calculated as,

$$S_{k,n}=p_n S\left(<\phi_k>_n\right)_k \tag{11.14}$$

where $S(\ )_k$ is the net reaction rate for the $k$th component.

## 11.4.2. Mixing

The micro-mixing term $M_{k,n}$ is modeled with the IEM mixing model:

$$M_{k,n}=\frac{C_\phi}{\tau}\left(<\phi_k>_n-\psi_k\right) \tag{11.15}$$

where $\tau$ is the turbulence time-scale and $C_\phi$ is the mixing constant.

Release 15.0 - © SAS IP, Inc. All rights reserved. - Contains proprietary and confidential information of ANSYS, Inc. and its subsidiaries and affiliates.

Hence, for the two-mode DQMOM-IEM model, the mixing terms for component $k$ are,

$$\begin{aligned} M_{k,1} &= \frac{C_\phi}{\tau}\left(p_1 s_{k,2} - p_2 s_{k,1}\right) \\ M_{k,2} &= \frac{C_\phi}{\tau}\left(p_2 s_{k,1} - p_1 s_{k,2}\right) \end{aligned} \tag{11.16}$$

The default value of $C_\phi$ is 2, which is appropriate for gas-phase combustion. For reactions in liquids, where the diffusivities are much smaller than gases, the **Liquid Micro-Mixing** option interpolates $C_\phi$ from model turbulence [359] (p. 748) and scalar [126] (p. 735) spectra.

## 11.4.3. Correction

Using assumptions to ensure realizability and boundedness, the correction terms $C_{k,n}$ in Equation 11.13 (p. 287) for the $k$th composition are determined from the linear system,

$$\sum_{n=1}^{N_e} <\phi_k>_n^{m_k-1} C_{k,n} = \sum_{n=1}^{N_e} (m_k - 1) <\phi_k>_n^{m_k-2} p_n c_{k,n} \tag{11.17}$$

where $m_k$ are the non-negative integer lower moments (1.. $N_e$) for each component $k$. Note that the condition of the matrix decreases with increasing $m_k$, which reduces the stability of higher mode simulations.

The dissipation term $c_{k,n}$ in Equation 11.17 (p. 288) is calculated as,

$$c_{k,n} = \Gamma \nabla\left(<\phi_k>_n\right) \cdot \nabla\left(<\phi_k>_n\right) \tag{11.18}$$

For the two-mode DQMOM-IEM model, the correction terms for the $k$th component are,

$$\begin{aligned} C_{k,1} &= \frac{\Gamma}{<\phi_k>_1 - <\phi_k>_2}\left(p_1\left(\nabla <\phi_k>_1\right)^2 + p_2\left(\nabla <\phi_k>_2\right)^2\right) \\ C_{k,2} &= -C_{k,1} \end{aligned} \tag{11.19}$$

## 11.4.4. Calculation of Composition Mean and Variance

The mean composition (species $k$ or energy) is calculated as,

$$\overline{\phi_k} = \sum_{n=1}^{N_e} s_{k,n} \tag{11.20}$$

and its variance is calculated as

$$\overline{\phi_k'^2} = \left(\sum_{n=1}^{N_e} s_{k,n} <\phi_k>_n\right) - \overline{\phi_k}^2 \tag{11.21}$$


Release 15.0 - © SAS IP, Inc. All rights reserved. - Contains proprietary and confidential information of ANSYS, Inc. and its subsidiaries and affiliates.

# Chapter 12: Chemistry Acceleration

ANSYS Fluent provides several methods to reduce the computational expense of solving detailed chemistry in multi-dimensional CFD. For information about using these chemistry acceleration methods, see Using Chemistry Acceleration in the User's Guide. Information about the theory behind these approaches is presented in the following sections:


12.1. Overview and Limitations
12.2. In-Situ Adaptive Tabulation (ISAT)
12.3. Dynamic Mechanism Reduction
12.4. Chemistry Agglomeration
12.5. Chemical Mechanism Dimension Reduction


## 12.1. Overview and Limitations

ANSYS Fluent has four turbulence-chemistry interaction models for simulating combustors with detailed chemical kinetics:

- Laminar Finite-Rate (for laminar as well as turbulent flames)
- Eddy-Dissipation Concept (for turbulent flames)
- Lagrangian Composition PDF Transport (for turbulent flames)
- Eulerian Composition PDF Transport (for turbulent flames)

Using detailed chemistry is appropriate when modeling kinetically controlled phenomena, such as slowly forming product and pollutant species, as well as flame ignition and extinction. Comprehensive chemical mechanisms contain a multitude of intermediate species in addition to the major fuel, oxidizer, and product species. These intermediate species evolve at widely different reaction rates resulting in disparate species formation and destruction time-scales. The numerical time integration to accurately calculate the species evolution requires very small time substeps, called stiffness, and causes large computational run-times. The chemistry acceleration tools in ANSYS Fluent can mitigate this cost, but with some loss of accuracy. Care must be taken to set controlling parameters so that these inaccuracies are within acceptable limits.

## 12.2. In-Situ Adaptive Tabulation (ISAT)

ISAT is ANSYS Fluent's most powerful tool to accelerate detailed stiff chemistry. A speedup of two to three orders of magnitude is common, which is significant in that a simulation that would take months without ISAT can be run in days instead.

For kinetic mechanisms that are deterministic, the final reacted state is a unique function of the initial unreacted state and the time-step. This reaction mapping can, in theory, be performed once and tabulated. The table can then be interpolated with run-time speedup as long as interpolation is more efficient than chemistry integration. In practice, pre-tabulation is prohibitive since the table dimensions are too large: the number of species (N), plus the temperature, pressure, and time-step. However, in a reacting flow, only a very small sub-space of the full composition space is accessed. For example, it is unlikely

Release 15.0 - © SAS IP, Inc. All rights reserved. - Contains proprietary and confidential information of ANSYS, Inc. and its subsidiaries and affiliates.

that a state consisting of pure radical OH (mass fraction of one) at a temperature of 300 K will exist, and it is unnecessary to pre-tabulate this state. The chemistry is said to lie on a low-dimensional manifold. In fact, for steady-state, 3D, laminar simulations, the chemistry can be parameterized by the spatial position vector. Thus, mappings must lie on a three dimensional manifold within the N+3 dimensional composition space. It is, hence, sufficient to tabulate only this accessed region of the composition space. The accessed region, however, depends on the particular chemical mechanism, the thermodynamic and transport properties, the flow geometry, and the boundary conditions. For this reason, the accessed region is not known before the simulation and the table cannot be preprocessed. Instead, the table must be built during the simulation, and this is referred to as in-situ tabulation. ANSYS Fluent employs ISAT [358] (p. 748) to dynamically tabulate the chemistry mappings and accelerate the time to solution. ISAT is a method to tabulate the accessed composition space region "on the fly" (in-situ) with error control (adaptive tabulation). It is important to understand how ISAT works in order to use it optimally.

Reaction over a time-step $\Delta t$ from an initial composition $\phi^0$ to a final composition $\phi^1$ is calculated as:

$$\phi^1 = \phi^0 + \int_0^{\Delta t} S dt \tag{12.1}$$

where $S$ is the chemical source term.

At the start of an ANSYS Fluent simulation using ISAT, the ISAT table is empty. For the first reaction step, Equation 12.1 (p. 290) is integrated with a stiff ODE solver. This is called Direct Integration (DI). The first table entry is created and consists of:

- the initial composition $\phi^0$ (where the superscript 0 denotes the composition vector *before* the reaction)
- the mapping $\phi^1$ (where the superscript 1 denotes the composition vector *after* the reaction)
- the mapping gradient matrix $A = \partial \phi^1 / \partial \phi^0$
- a hyper-ellipsoid of accuracy

The next reaction mapping is calculated as follows: The initial composition vector for this particle is denoted by $\phi_q^0$, where the subscript $q$ denotes a *query*. The existing table (consisting of one entry at this stage) is queried by interpolating the new mapping as

$$\phi_q^1 = \phi^1 + A\left(\phi_q^0 - \phi^0\right) \tag{12.2}$$

The mapping gradient is hence used to linearly interpolate the table when queried. The ellipsoid of accuracy (EOA) is the elliptical space around the table point $\phi^0$ where the linear approximation to the mapping is accurate to the specified tolerance, $\varepsilon_{tol}$.

If the query point $\phi_q^0$ is within the EOA, then the linear interpolation by Equation 12.2 (p. 290) is sufficiently accurate, and the mapping is *retrieved*. Otherwise, a direct integration (DI) is performed and the mapping error $\varepsilon = | B\left(\phi_{DI}^1 - \phi_q^1\right) |$ is calculated (here, $B$ is a scaling matrix). If this error is smaller than the specified error tolerance ($\varepsilon_{tol}$), then the original interpolation $\phi_q^1$ is accurate and the EOA is *grown* so as to include


Release 15.0 - © SAS IP, Inc. All rights reserved. - Contains proprietary and confidential information of ANSYS, Inc. and its subsidiaries and affiliates.

$\phi_q^0$. If not, and if the table size is smaller than the user-specified maximum RAM (**Max. Storage**), a new table entry is added.

Table entries are stored as leaves in a binary tree. When a new table entry is *added*, the original leaf becomes a node with two leaves—the original leaf and the new entry. A cutting hyper-plane is created at the new node, so that the two leaves are on either side of this cutting plane. A composition vector $\phi_q^0$ will hence lie on either side of this hyper-plane.

The ISAT algorithm is summarized as follows:

1. The ISAT table is *queried* for every composition vector during the reaction step.
2. For each query $\phi_q^0$ the table is traversed to identify a leaf whose composition $\phi^0$ is close to $\phi_q^0$.
3. If the query composition $\phi_q^0$ lies within the EOA of the leaf, then the mapping $\phi_q^1$ is *retrieved* using interpolation by Equation 12.2 (p. 290). Otherwise, Direct Integration (DI) is performed and the error $\varepsilon$ between the DI and the linear interpolation is measured.
4. If the error $\varepsilon$ is less than the tolerance, then the ellipsoid of accuracy is *grown* and the DI result is returned. Otherwise, a new table entry is *added*.

At the start of the simulation, most operations are *adds* and *grows*. Later, as more of the composition space is tabulated, *retrieves* become frequent. Since *adds* and *grows* are very slow whereas *retrieves* are relatively quick, initial ANSYS Fluent iterations are slow but accelerate as the table is built.

There are two inputs to ISAT, namely the ISAT error tolerance ($\varepsilon_{tol}$) and the maximum ISAT table size (in Mbytes). Large values of $\varepsilon_{tol}$ provide faster run-times, but larger error. For steady-state simulations, it is advised to start the simulation with a large $\varepsilon_{tol}$ and reduce $\varepsilon_{tol}$ as the solution stabilizes and nears convergence. For this reason, the default ISAT error tolerance of 0.001 is relatively large and should be decreased for unsteady simulations or when a steady-state simulation converges. It is recommended that you monitor the species of interest and re-converge with reduced $\varepsilon_{tol}$ until these species change in acceptably small increments. The maximum ISAT table size should be set to just below the available RAM memory on the computer.

## 12.3. Dynamic Mechanism Reduction

The solution time for a chemically reacting flow problem increases with the size of the reaction mechanism used. Typically, this relationship is

$$t_{CPU} \propto c_1 N_{species}^3 + c_2 N_{species}^2 + c_3 N_{species} + c_4 N_{reactions}$$

where $c_1$, $c_2$, $c_3$, and $c_4$ are constants.

Dynamic Mechanism Reduction can accelerate the simulation by decreasing the number of species ($N_{species}$) and number of reactions ($N_{reactions}$) in the chemical mechanism. In general, more reduction results in faster, but less accurate simulations. Mechanism reduction seeks to decrease the mechanism size while limiting accuracy loss to some predefined tolerances.

Release 15.0 - © SAS IP, Inc. All rights reserved. - Contains proprietary and confidential information of ANSYS, Inc. and its subsidiaries and affiliates.

Unlike skeletal reduction where mechanism reduction is completed at the pre-solution stage to create a single reduced mechanism that is used throughout the simulation, Dynamic Mechanism Reduction is performed "on the fly" in every cell (or particle), at every flow iteration (for steady simulations) or time-step (for transient simulations). Since the mechanism is only required to be accurate at the local cell conditions, Dynamic Mechanism Reduction can be used with a higher level of reduction yet less accuracy loss than skeletal mechanism [[270] (p. 743), [328] (p. 747)].

Mechanism reduction in ANSYS Fluent is performed using the Directed Relation Graph (DRG) approach [[268] (p. 743), [269] (p. 743)], described next.

## 12.3.1. Directed Relation Graph (DRG) Method for Mechanism Reduction

Given a list of species that need to be modeled accurately (called "targets"), DRG eliminates all species and reactions in the mechanism that do not contribute significantly (directly or indirectly) to predicting the evolution of the targets.

To generate the reduced mechanism, DRG implements the following steps.

1. DRG considers normalized contribution of each non-target species $B$ to overall production of each target species $A$ within a single cell:

$$r_{AB} \equiv \frac{\max_i \left(|\nu_{A,i}\omega_i\delta_{Bi}|\right)}{\max_i \left(|\nu_{A,i}\omega_i|\right)} \tag{12.3}$$

where

$$\delta_{Bi} = \begin{cases} 1, & \text{If reaction } i \text{ involves species } B \\ 0, & \text{otherwise} \end{cases}$$

$\omega_i(T, P, Y)$ is a chemical rate of elementary reaction $i$ at a local cell condition defined by the temperature $T$, the pressure $P$, and the species mass fraction $Y$

$\nu_{A,i}$ is a stoichiometric coefficient of species $A$ in reaction $i$

Species $B$ is retained in the mechanism if and only if the largest reaction rate involving both species, $A$ and $B$, is larger than a fraction $\varepsilon$ of the largest reaction rate involving species $A$ within the cell:

$$r_{AB} > \varepsilon \tag{12.4}$$

where $\varepsilon$ is a specified error tolerance.

Normalized contribution value $r_{Ak}$ is computed for every non-target species $k$ in the mechanism, to identify all non-target species that directly contribute significantly to modeling target species $A$. These species constitute the *dependent set* of $A$. This process is repeated for all target species, and a comprehensive dependent set is created as the union of individual dependent sets for all targets.

2. In the next step, DRG algorithm, in a similar manner, identifies indirect contributors, which are species that directly impact the dependent set, rather than the targets. In other words, if species $B$ is included in the comprehensive dependent set created in step 1, then all the remaining species $k$ with $r_{Bk} > \varepsilon$ must also be included. The procedure outlined in step 1 is applied to each species $B$ in the dependent set to generate the list of species that contribute to its production or consumption.


Release 15.0 - © SAS IP, Inc. All rights reserved. - Contains proprietary and confidential information of ANSYS, Inc. and its subsidiaries and affiliates.

This process is continued for each species added to the mechanism, until no new species qualifies to be added to the comprehensive dependent set.

The resulting set of species (including the targets) constitutes the species retained in the mechanism. All the other species, that is all the species $B$ for which $r_{Bi}<\varepsilon$ for all species $i$ included in the resulting set of species, are considered unimportant and are eliminated from the mechanism.

3. Finally, all reactions that do not involve any of the retained species are also eliminated from the mechanism. The resulting mechanism is the final reduced mechanism.

   A lower-dimensional ODE system is solved, involving only the retained species and reactions. The eliminated species mass fractions are stored for computing mixture quantities such as density and heat capacity.

It is important to note that computational expense of the DRG method has been shown to be linear in the number of reactions $N_{reactions}$ in the full detailed mechanism. This small additional overhead is typically significantly outweighed by the acceleration due to Dynamic Mechanism Reduction using DRG.

Mechanism reduction is controlled by the following two parameters in ANSYS Fluent:

- Error Tolerance $\varepsilon$

  The default value for error tolerance $\varepsilon$ is `0.01`.

- Target Species List (adjustable only in expert mode, accessible in the TUI)

  The default list of target species consists of 3 constituents. Hydrogen radical is explicitly defined as the first target species. Hydrogen radical is used as a default target species because it is strongly linked to heat release in combustion; accurate prediction of this species should ensure accurate prediction of heat release. Two other species with the largest mass fractions are added to the target species list by DRG algorithm at each time step or flow iteration.

There is also an option to remove a species from the target list whenever its mass fraction is below a given threshold. This option is disabled by default in ANSYS Fluent (that is, the default value for minimum mass fraction is 0).

In general, a smaller value of error tolerance $\varepsilon$ and a larger value of number of targets $N_{target}$ yield larger, more accurate mechanisms, but slower simulations. The default settings should balance accuracy and efficiency well for most simulations. However, these parameters may require more careful selection for some problems, such as auto-ignition of highly complex fuels. For further instructions on how to use Dynamic Mechanism Reduction, see Using Dynamic Mechanism Reduction in the *Fluent User's Guide*.

## 12.4. Chemistry Agglomeration

Reacting flow computations with detailed mechanisms can be computationally demanding, even with the speedup provided by ISAT. Chemistry agglomeration (CA) provides additional run-time improvement, with a corresponding additional decrease in accuracy. The idea behind chemistry agglomeration is to collect cells (or particles for the Lagrangian PDF Transport model) that are close in composition space, average these to a single composition, call the reaction step integrator, then map this reaction step back to the cells. In summary:

1. Just before the reaction step, bin CFD cells that are close in composition space.

2. Average their compositions.

Release 15.0 - © SAS IP, Inc. All rights reserved. - Contains proprietary and confidential information of ANSYS, Inc. and its subsidiaries and affiliates.

3. Call ISAT to perform the chemistry integration with the single, averaged composition.

4. Map this reaction step back to the cells in the group.

The number of calls to the relatively costly chemistry integration routine (ISAT) is less than the number of cells in the domain. Chemistry agglomeration is hence similar to Reactor Network, or Multi-Zone models, which calculate reaction on a smaller number of zones than the number of cells in the CFD simulation.

A reaction mapping is represented as,

$$\phi \rightarrow \phi^* \tag{12.5}$$

where $\phi$ and $\phi^*$ are the thermo-chemical compositions (temperature, pressure, and species fractions) before and after reaction, respectively. By default, ANSYS Fluent loops over all cells (or particles for the Lagrangian PDF Transport model) and calculates the reaction mapping.

Chemistry agglomeration loops through all CFD cells before reaction and bins those that are 'close' in composition space to within a specified tolerance. The composition in each bin is averaged as,

$$\overline{\phi} = \frac{\sum_i \phi_i \rho_i V_i}{\sum_i \rho_i V_i} \tag{12.6}$$

where $\overline{\phi}$ represents the agglomerated composition, subscript $i$ is an index over the cells in the bin, and $\rho_i$ and $V_i$ denote the density and volume of the $i$th cell, respectively.

After agglomeration, the ISAT reaction mapping routine is called,

$$\overline{\phi} \rightarrow \overline{\phi}^* \tag{12.7}$$

Finally, the reacted cluster composition is mapped back to all the CFD cells in the corresponding bin,

$$\phi_i^* = \phi_i + \left( \overline{\phi}^* - \overline{\phi} \right) \tag{12.8}$$

for every cell $i$ within the bin.

To ensure an iso-enthalpic reaction, the enthalpy of each cell after reaction, $h_i^*$, is set according to:

$$h_i^* = h_i + \sum_k h_k^o \left( \overline{Y_k}^* - Y_{i,k} \right) \tag{12.9}$$

where $h_i$ denotes the enthalpy of cell $i$ before the reaction step, $h_k^o$ is the formation enthalpy of species $k$, $\overline{Y_k}^*$ is the mass fraction after reaction for the cell cluster, and $Y_{i,k}$ is the cell mass fraction before reaction.

To learn how to enable Chemistry Agglomeration, see Using Chemistry Agglomeration in the User's Guide.

For more information, see the following section:
12.4.1. Binning Algorithm


Release 15.0 - © SAS IP, Inc. All rights reserved. - Contains proprietary and confidential information of ANSYS, Inc. and its subsidiaries and affiliates.

### 12.4.1. Binning Algorithm

A uniform Cartesian mesh is used to bin cells at every reaction step. The composition space has $N = N_{spe} + 2$ dimensions, where $N_{spe}$ are the number of species and the additional two dimensions are temperature and pressure. To reduce the cost of tabulating in $N$-dimensions, a subset of size $M$ representative composition coordinates are selected.

For tabulation purposes, each coordinate $k$ of the $M$-dimensional reduced composition space is normalized as,

$$\hat{\phi}_k = \frac{\phi_k - \phi_k^{min}}{\phi_k^{max} - \phi_k^{min}} \tag{12.10}$$

where $\phi_k^{min}$ and $\phi_k^{max}$ are the minimum and maximum of composition space variable $k$ in the CFD computational domain. Hence, the reduced composition space binning mesh extends from zero to one in each of the $M$ coordinate of the hyper-cube is discretized into $L = 1/\varepsilon_{tol}$ constant spaced intervals, where $\varepsilon_{tol}$ is a user specified CA tolerance. All CFD cell compositions that fall within a reduced composition space bin are agglomerated.

Since most of the bins in the $M$-dimensional hyper-cube are likely to be empty, a dynamic hash table [4] (p. 729) is employed to efficiently store the bins. The hash table maps a unique bin index in the $M$-dimensional hyper-cube to a 1D line. Since the reduced space hyper-cube is discretized into equispaced bins, a unique index for every bin can be defined as,

$$j = \sum_{l=0}^{M-1} i_l L^l \tag{12.11}$$

where $i_l = \hat{\phi}_l L$ is the bin index in the $l$'th dimension.

The hash table maps $j$ to a 1D table of size $H$, which is much smaller than the number of entries in the reduced space hyper-cube, $L^M$. A simple hash mapping function is the modulo function:

$$h = j \bmod H \tag{12.12}$$

Different $M$-space indices $j$ may have the same hash mapping index $h$, which results in collisions. In the dynamic hash table, the number of collisions, as well as the number of empty hash table entries are monitored, and the hash table size, $H$, is adjusted at each iteration to set these to be within acceptable limits.

The $M$ compositions representing the reduced space coordinates are selected from the $N_{spe} + 2$ dimensional composition space as follows. By default, temperature is included and pressure is excluded. The current algorithm orders the species with largest total mass in the computational domain. For example, $N_2$ is typically first in this list for combustors using air as the oxidizer. The first $M - 1$ species of this list are selected as the reduced composition space variables.

By selecting species with the largest mass, minor species are invariably neglected. Since $CO$ and $NO$ are of interest in many practical applications, $CO$ and $NO$ are inserted at the front of the list if they exist in the computational domain. It was found that inclusion of these species in the table coordinates consistently provided increased accuracy for all thermo-chemical variables.

Release 15.0 - © SAS IP, Inc. All rights reserved. - Contains proprietary and confidential information of ANSYS, Inc. and its subsidiaries and affiliates.

In summary, the default coordinate algorithm selects $T$ as a reduced space coordinate, then $NO$ (if $NO$ is present in the CFD domain), then $CO$ (if $CO$ is present in the CFD domain), followed by the species with largest mass in the domain until $M$ variables are reached (with $M$=4 as default). The default reduced table size ($M=4$) and species list should be suitable for most reacting flow applications, but can be changed. Contact your technical support engineer to learn how to make the changes.

As with the ISAT error tolerance, the Chemistry Agglomeration error tolerance should be reduced so that changes in the monitored species of interest are acceptably small.

## 12.5. Chemical Mechanism Dimension Reduction

Dimension Reduction is a chemistry acceleration method in addition to ISAT storage-retrieval, Dynamic Mechanism Reduction, and Cell Agglomeration, providing faster chemistry calculations with a corresponding loss of accuracy. To learn how to use chemical mechanism Dimension Reduction, see Dimension Reduction in the User's Guide.

Dimension Reduction solves a smaller number ($N_r$) of species transport equations (see Equation 7.1 (p. 187)) than the number of species in the full chemical mechanism ($N_f$). These are termed the represented species. The remaining $N_f - N_r$ species are termed the unrepresented species. In ANSYS Fluent, the unrepresented species are reconstructed assuming that they are in chemical equilibrium [360] (p. 749). The Dimension Reduction algorithm is implemented as follows:

- ANSYS Fluent solves transport equations for the mixture enthalpy and the $N_r$ represented species mass fractions. Transport equations are also solved for the unrepresented element mass fractions, which are the cumulative mass fraction of each atomic element in all the unrepresented species.
- For the reaction step, the initial unrepresented species in a cell are reconstructed by assuming that they are in chemical equilibrium at the cell pressure and enthalpy, subject to the constraints of the represented species mass fractions and the unrepresented element mass fractions. That is, the unrepresented species are determined as those that give maximum mixture entropy with the represented species held fixed, while also satisfying the unrepresented element mass fractions and mixture enthalpy. At the end of this reconstruction step, all $N_f$ species mass fractions of the full mechanism are available in the cell.
- Next, the full detailed reaction mechanism with all $N_f$ species is integrated for the reaction time-step. Reaction mappings for the $N_r$ represented species are available after the reaction step, and the mappings for the unrepresented species are discarded.

As Dimension Reduction integrates the full chemical mechanism, which is computationally expensive, its advantage lies in coupling with ISAT. An ISAT table with $N_r$ dimensions will cover more of the reaction manifold than ISAT tabulation of the full $N_f$ dimensions in the same time. Consequently, a simulation with Dimension Reduction is initially not much faster than a simulation with the full mechanism, but iterations can be substantially faster at later times when the ISAT table is retrieved. Additionally, the retrieval time with Dimension Reduction enabled (proportional to $N_r^2$), is much smaller than that with the Full Mechanism (proportional to $N_f^2$). For this reason, Dimension Reduction is only available with ISAT.

Note that Dimension Reduction allows CFD simulations with full chemical mechanisms consisting of more than the ANSYS Fluent transported species limit of 500, as long as the number of represented species is less than 500.


Release 15.0 - © SAS IP, Inc. All rights reserved. - Contains proprietary and confidential information of ANSYS, Inc. and its subsidiaries and affiliates.

For more information, see the following section:
12.5.1. Selecting the Represented Species

## 12.5.1. Selecting the Represented Species

Judicious selection of the represented species is important for simulation accuracy. Boundary and initial species must be included in the represented species list. Species of interest, especially species that are far from chemical equilibrium, such as pollutants, should also be included. Intermediate species that occur in large mass fractions relative to the fuel and oxidizer species should be included, as well as species important in the chemical pathway. For example, for methane combustion in air, $CH_3$ should be included as a represented species since $CH_4$ pyrolizes to $CH_3$ first.

In ANSYS Fluent, you will input the number of represented species, as well as selected represented species, such as the boundary **Fuel** and **Oxidizer** species. When the selected represented species are less than the input number of represented species, the remaining represented species are taken from the full mechanism in the order they appear in the **Mixture Species** list.

After you obtain a preliminary solution with **Dimension Reduction**, it is a good idea to check the magnitude of all unrepresented species, which are available in the **Full Mechanism Species...** option in the **Contours** dialog box. If the mass fraction of an unrepresented species is larger than other represented species, you should repeat the simulation with this species included in the represented species list. In turn, the mass fraction of unrepresented elements should decrease.

Release 15.0 - © SAS IP, Inc. All rights reserved. - Contains proprietary and confidential information of ANSYS, Inc. and its subsidiaries and affiliates.

Release 15.0 - © SAS IP, Inc. All rights reserved. - Contains proprietary and confidential information
of ANSYS, Inc. and its subsidiaries and affiliates.

# Chapter 13: Engine Ignition

This chapter discusses the theory behind the engine ignition models available in ANSYS Fluent. Information can be found in the following sections.

13.1. Spark Model
13.2. Autoignition Models
13.3. Crevice Model

For information about using these ignition models, see Modeling Engine Ignition in the User's Guide.

## 13.1. Spark Model

The spark model in ANSYS Fluent will be described in the context of the premixed turbulent combustion model. For information about using this model, see Spark Model in the User's Guide. Information regarding the theory behind this model is detailed in the following sections:

13.1.1. Overview and Limitations
13.1.2. Spark Model Theory
13.1.3. ECFM Spark Model Variants

### 13.1.1. Overview and Limitations

Initiation of combustion at a desired time and location in a combustion chamber can be accomplished by sending a high voltage across two narrowly separated wires, creating a spark. The spark event in typical engines happens very quickly relative to the main combustion in the engine. The physical description of this simple event is very involved and complex, making it difficult to accurately model the spark in the context of a multidimensional engine simulation. Additionally, the energy from the spark event is several orders of magnitude less than the chemical energy release from the fuel. Despite the amount of research devoted to spark ignition physics and ignition devices, the ignition of a mixture at a point in the domain is more dependent on the local composition than on the spark energy (see Heywood [161] (p. 737)). Thus, for situations in which ANSYS Fluent is utilized for combustion engine modeling, including internal combustion engines, the spark event does not need to be modeled in great detail, but simply as the initiation of combustion over a duration, which you will set.

Since spark ignition is inherently transient, the spark model is only available in the transient solver. Additionally, the spark model requires chemical reactions to be solved. The spark model is available for all of the combustion models.

### 13.1.2. Spark Model Theory

Typically, the initial spark size is small relative to the cell size, and the spark is under-resolved on the CFD mesh. Modeling the spark by burning a few cells around the spark location shows strong sensitivity to the grid and time-step size, and flame speed and flame brush diffusion can be erroneous due to the insufficient space and time resolution. In addition, for cases where the initial spark is smaller than the cell size, ignition proceeds too quickly.

Release 15.0 - © SAS IP, Inc. All rights reserved. - Contains proprietary and confidential information of ANSYS, Inc. and its subsidiaries and affiliates.

To mitigate this sensitivity, ANSYS Fluent solves a sub-grid equation for the spark evolution. The spark shape is assumed to be perfectly spherical, with an infinitely thin flame front. The spark radius, $r$, grows in time, $t$, according to the ODE,

$$\frac{dr}{dt} = \frac{\rho_u}{\rho_b} S_t \tag{13.1}$$

where $\rho_u$ is the density of the unburned fluid ahead of the flame front, $\rho_b$ is the density of the burnt fluid behind of the flame, and $S_t$ is the turbulent flame speed.

The sub-grid spark model is transferred to the CFD grid through a representative volume of CFD cells. This volume is spherical and has a fixed diameter computed as the local turbulent length scale at the spark location. However, in order to ensure that this representative volume is not too large (relative to the size of the combustor) or too small (relative to the cell size), the radius of the representative sphere, $r_t$, is calculated as,

$$r_t = \max\left( r_o + 3\Delta,\ 3r_o,\ \min\left( \frac{1}{2} l_t, r_o + 10\Delta \right) \right) \tag{13.2}$$

where $r_o$ is the user-specified initial spark radius, $\Delta$ is the cell length scale, and $l_t$ is the turbulent length scale.

Alternatively $r_t$ may be specified as a fixed value via the spark-model text interface.

$l_t$ is taken to define the representative volume because, once the spark diameter reaches this size, the flame speed is affected by all the turbulent scales present. The spark radius will continue to increase until the length scale is reached, even if the simulation time exceeds the user-specified duration. Note, that the specified duration is only used to calculate the rate of spark energy input and the time when this input ceases. At this condition ANSYS Fluent automatically switches the spark flame speed model off, so that the flame speed is modeled using the flame speed model that you have selected in the **Species** dialog box, throughout the domain.

For the Extended Coherent Flamelet model (ECFM) and C-Equation model, ANSYS Fluent fixes the reaction progress in the representative volume, $c$, as,

$$c = \left( \frac{r}{r_t} \right)^3 \tag{13.3}$$

For the G-Equation model, reaction progress in the spark is calculated in the usual way for this model as given by Equation 9.8 (p. 257).

The temperature and species composition (denoted by $\varphi$) within the representative spherical volume at every time-step are calculated as,

$$\varphi = c\varphi^b + (1 - c)\,\varphi^u \tag{13.4}$$

where $\varphi^b$ denotes the equilibrium burnt composition, and $\varphi^u$ is the unburned composition. These compositions are fixed in time and uniform in space.

Since the thermo-chemical state behind the spark flame front is instantaneously equilibrated as the spark propagates, spark energy is not required to ignite the mixture. By default, the spark energy is set to zero for all combustion models, and the burnt temperature is the equilibrium temperature. However,


Release 15.0 - © SAS IP, Inc. All rights reserved. - Contains proprietary and confidential information of ANSYS, Inc. and its subsidiaries and affiliates.

spark energy can be set to a positive value in the user interface, in which case the temperature behind the spark will be higher than the equilibrium temperature.

ANSYS Fluent offers the following models for the turbulent flame speed, $S_t$ in Equation 13.1 (p. 300):

## Turbulent Curvature

In the Turbulent Curvature model, the turbulent flame speed is calculated as,

$$S_t = \max\left( S_l - \frac{2D}{r}, S_t(r) - \frac{2D_t}{r} \right) \tag{13.5}$$

where $S_l$ is the laminar flame speed, $r$ is the current spark radius, $D$ is the laminar diffusivity, and $D_t$ is the turbulent diffusivity. $D$ and $D_t$ are evaluated at the spark location, and $S_t(r)$ is the turbulent flame speed evaluated at the turbulent length scale of the spark radius. Since turbulent scales larger than the spark radius convect the spark but do not increase its area and flame speed, only turbulent length scales up to the spark radius $r$ can affect the turbulent flame speed of the spark. For the premixed and partially-premixed models, the spark flame speed model is the same flame speed model as selected for the main combustion. For Species Transport cases, by default the Zimont flame speed model is used. $S_l$ and $D$ are added as additional material inputs in the interface for the species transport models.

Note that the effect of the flame curvature is to decrease both the laminar and turbulent flames speeds. Since the initial spark radius $r_o$ is a user-input, decreasing $r_o$ slows the spark propagation and increases the burning time.

## Turbulent Length

In the Turbulent Length model, the turbulent flame speed is calculated as,

$$S_t = \max\left( S_l, S_t(r) \right) \tag{13.6}$$

That is, the Turbulent Length model ignores the effects of flame curvature on the flame speed.

## Herweg-Maly

The turbulent flame speed is calculated using the model proposed by Herweg and Maly [162] (p. 737):

$$_t = \max\left( S_l, S_l\left( I_0 + I_0^{\frac{1}{2}}\left( \frac{u'}{u' + S_l} \right)^{\frac{1}{2}}\left[ 1 - exp\left( -\frac{r}{l_t} \right) \right]^{\frac{1}{2}}\left[ 1 - exp\left( -\frac{t - t_0}{\tau_s} \right) \right]^{\frac{1}{2}}\left( \frac{u'}{S_l} \right)^{\frac{5}{6}} \right) \right) \tag{13.7}$$

where $I_0$ is a function for effect of strain on the laminar burning velocity calculated as,

$$I_0 = \max\left( 0, \quad 1 - \left( \frac{\delta}{15 l_t} \right)^{\frac{1}{2}}\left( \frac{u'}{S_l} \right)^{\frac{3}{2}} - 2\frac{\delta}{r}\frac{\rho_u}{\rho_b} \right)$$

and

$t$ = current time

Release 15.0 - © SAS IP, Inc. All rights reserved. - Contains proprietary and confidential information of ANSYS, Inc. and its subsidiaries and affiliates.

$t_0$ = start time

$u'$ = turbulent velocity scale

$\tau_s = \frac{l_t}{u' + S_l}$

$\delta$ = laminar flame thickness = $\frac{D}{S_l}$

If the Blint modifier is being used

$$\delta = \text{laminar flame thickness} = \frac{D}{S_l} B_1 \left( \frac{\rho_u}{\rho_b} \right)^{B_2}$$

where

$B_1$ = 2.0

$B_2$ = 0.7

$\rho_u$ is the unburned density

$\rho_b$ is the burned density

### Laminar

In the Laminar model, the turbulent flame speed $S_t$ in Equation 13.1 (p. 300) is modeled as the laminar flame speed, $S_l$. Since the Laminar flame speed can be modeled with a user-defined function (UDF), the Laminar option can be used to define your own function for the turbulent flame speed.

## 13.1.3. ECFM Spark Model Variants

When the ECFM combustion model is used the value of the flame surface density must be set within the spark region. The following ECFM spark model variants provide different methods of doing this:

### Turbulent Model

The flame surface density is calculated as:

$$\Sigma = \frac{S_t}{S_l} \frac{3}{r}$$

with $S_t$ being calculated using the spark flame speed model that you choose. In this equation $\frac{S_t}{S_l}$ represents a flame wrinkling factor and $\frac{3}{r}$ is the ratio of the spherical flame area to its volume.

### Zimont Model

The flame surface density is calculated as:


Release 15.0 - © SAS IP, Inc. All rights reserved. - Contains proprietary and confidential information of ANSYS, Inc. and its subsidiaries and affiliates.

$$\Sigma = \frac{1}{Max(r,\ 0.0001\mathrm{m})}$$

### Constant Value Model

In this case you supply the value of flame surface density.

### User-Defined Sigma Source

In this instance you supply a source for the flame surface density via a UDF. This is detailed in the UDF manual.

## 13.2. Autoignition Models

Autoignition phenomena in engines are due to the effects of chemical kinetics of the reacting flow inside the cylinder. There are two types of autoignition models considered in ANSYS Fluent:

- knock model in spark-ignited (SI) engines
- ignition delay model in diesel engines

For information regarding using autoignition models, see Autoignition Models in the User's Guide. The theory behind the autoignition models is described in the following sections:

13.2.1. Model Overview
13.2.2. Model Limitations
13.2.3. Ignition Model Theory

### 13.2.1. Model Overview

The concept of knock has been studied extensively in the context of premixed engines, as it defines a limit in terms of efficiency and power production of that type of engine. As the compression ratio increases, the efficiency of the engine as a function of the work extracted from the fuel increases.

However, as the compression ratio increases, the temperature and pressure of the air/fuel mixture in the cylinder also increase during the cycle compressions. The temperature and pressure increase can be large enough for the mixture to spontaneously ignite and release its heat before the spark plug fires. The premature release of all of the energy in the air/fuel charge is almost never desirable, as this results in the spark event no longer controlling the combustion. As a result of the premature release of the energy, catastrophic damage to the engine components can occur. The sudden, sharp rise in pressure inside the engine can be heard clearly through the engine block as a knocking sound, hence the term "knock". For commonly available gasoline pumps, knock usually limits the highest practical compression ratio to less than 11:1 for premium fuels and around 9:1 for less expensive fuels.

By comparison, ignition delay in diesel engines has not been as extensively studied as SI engines, mainly because it does not have such a sharply defining impact on engine efficiency. Ignition delay in diesel engines refers to the time between when the fuel is injected into the combustion chamber and when the pressure starts to increase as the fuel releases its energy. The fuel is injected into a gas that is usually air, however, it can have a considerable amount of exhaust gas mixed in (or EGR) to reduce nitrogen oxide emissions (NOx). Ignition delay depends on the composition of the gas in the cylinder, the temperature of the gas, the turbulence level, and other factors. Since ignition delay changes the combustion phasing, which in turn impacts efficiency and emissions, it is important to account for it in a diesel engine simulation.

Release 15.0 - © SAS IP, Inc. All rights reserved. - Contains proprietary and confidential information of ANSYS, Inc. and its subsidiaries and affiliates.

## 13.2.2. Model Limitations

The main difference between the knock model and the ignition delay model is the manner in which the model is coupled with the chemistry. The knock model always releases energy from the fuel while the ignition delay model prevents energy from being released prematurely.

The knock model in ANSYS Fluent is compatible with the premixed and partially premixed combustion models. The autoignition model is compatible with any volumetric combustion model, with the exception of the purely premixed models. The autoignition models are inherently transient and so are not available with steady simulations.

The autoignition models in general require adjustment of parameters to reproduce engine data and are likely to require tuning to improve accuracy. Once the model is calibrated to a particular engine configuration, then different engine speeds and loads can be reasonably well represented. Detailed chemical kinetics may be more applicable over a wider range of conditions, though are more expensive to solve. The single equation autoignition models are appropriate for the situation where geometric fidelity or resolution of particular flow details is more important than chemical effects on the simulation.

## 13.2.3. Ignition Model Theory

Both the knock and the ignition delay models are treated similarly in ANSYS Fluent, in that they share the same infrastructure. These models belong to the family of *single equation* autoignition models and use correlations to account for complex chemical kinetics. They differ from the eight step reaction models, such as Halstead's "Shell" model [153] (p. 737), in that only a single transport equation is solved. The source term in the transport equation is typically not stiff, therefore making the equation relatively inexpensive to solve.

This approach is appropriate for large simulations where geometric accuracy is more important than fully resolved chemical kinetics. The model can be used on less resolved meshes to explore a range of designs quickly, and to obtain trends before utilizing more expensive and presumably more accurate chemical mechanisms in multidimensional simulations.

### 13.2.3.1. Transport of Ignition Species

Autoignition is modeled using the transport equation for an *Ignition Species*, $Y_{ig}$, which is given by

$$\frac{\partial \rho Y_{ig}}{\partial t} + \nabla \cdot \left( \rho \vec{v} Y_{ig} \right) = \nabla \cdot \left( \frac{\mu_t}{Sc_t} \nabla Y_{ig} \right) + \rho S_{ig} \tag{13.8}$$

where $Y_{ig}$ is a "mass fraction" of a passive species representing radicals that form when the fuel in the domain breaks down. $Sc_t$ is the turbulent Schmidt number. The term $S_{ig}$ is the source term for the ignition species, which has a form,

$$S_{ig} = \int_{t=t_0}^{t} \frac{dt}{\tau_{ig}}$$

where $t_0$ corresponds to the time at which fuel is introduced into the domain. The $\tau_{ig}$ term is a correlation of ignition delay with the units of time. Ignition has occurred when the ignition species reaches a value of 1 in the domain. It is assumed that all the radical species represented by $Y_{ig}$ diffuse at the same rate as the mean flow.


Release 15.0 - © SAS IP, Inc. All rights reserved. - Contains proprietary and confidential information of ANSYS, Inc. and its subsidiaries and affiliates.

Note that the source term for these radical species is treated differently for knock and ignition delay. Furthermore, the form of the correlation of ignition delay differs between the two models. Details of how the source term is treated are covered in the following sections.

### 13.2.3.2. Knock Modeling

When modeling knock or ignition delay, chemical energy in the fuel is released when the ignition species reaches a value of 1 in the domain. For the knock model, two correlations are built into ANSYS Fluent. One is given by Douaud [96] (p. 734), while the other is a generalized model that reproduces several correlations, given by Heywood [161] (p. 737).

#### 13.2.3.2.1. Modeling of the Source Term

In order to model knock in a physically realistic manner, the source term is accumulated under appropriate conditions in a cell. Consider the one dimensional flame in Figure 13.1: Flame Front Showing Accumulation of Source Terms for the Knock Model (p. 305). Here, the flame is propagating from left to right, and the temperature is relatively low in front of the flame and high behind the flame. In this figure, $T_b$ and $T_u$ represent the temperatures at the burned and unburned states, respectively. The ignition species accumulates only when there is fuel. In the premixed model, the fuel is defined as $fuel = 1 - c$, where $c$ is the progress variable. If the progress variable has a value of zero, the mixture is considered unburned. If the progress variable is 1, then the mixture is considered burned.

**Figure 13.1: Flame Front Showing Accumulation of Source Terms for the Knock Model**

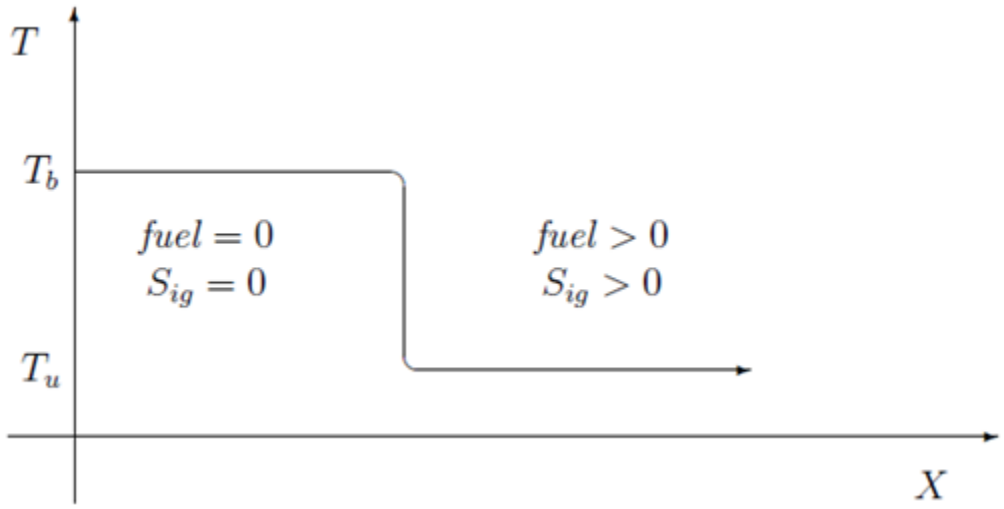


When the ignition species reaches a value of 1 in the domain, knock has occurred at that point. The value of the ignition species can exceed unity. In fact, values well above that can be obtained in a short time. The ignition species will continue to accumulate until there is no more fuel present.

#### 13.2.3.2.2. Correlations

An extensively tested correlation for knock in SI engines is given by Douaud and Eyzat [96] (p. 734):

$$\tau = 0.01768 \left( \frac{ON}{100} \right)^{3.402} p^{-1.7} \exp\left( \frac{3800}{T} \right) \tag{13.9}$$

Release 15.0 - © SAS IP, Inc. All rights reserved. - Contains proprietary and confidential information of ANSYS, Inc. and its subsidiaries and affiliates.

where $ON$ is the octane number of the fuel, $p$ is the absolute pressure in atmospheres and $T$ is the temperature in Kelvin.

A generalized expression for $\tau$ is also available that can reproduce many existing Arrhenius correlations. The form of the correlation is

$$\tau = A\left(\frac{ON}{100}\right)^{a} p^{b} T^{c} \mathrm{RPM}^{d} \Phi^{d} \exp\left(\frac{-E_a}{RT}\right) \tag{13.10}$$

where $A$ is the pre-exponential (with units in seconds), RPM is the engine speed in cycles per minute and $\Phi$ is the fuel/air equivalence ratio.

#### 13.2.3.2.3. Energy Release

Once ignition has occurred in the domain, the knock event is modeled by releasing the remaining fuel energy with a single-step Arrhenius reaction. An additional source term, which burns the remaining fuel in that cell, is added to the rate term in the premixed model. The reaction rate is given by

$$\dot{\omega} = A_0 \exp\frac{-E_a}{RT} \tag{13.11}$$

where $A_0 = 8.6 \times 10^{9}$, and $E_a = -15078$. These values are chosen to reflect single-step reaction rates appropriate for propane as described in Amsden [5] (p. 729). The rate at which the fuel is consumed is limited such that a completely unburned cell will burn during three of the current time steps. Limiting the reaction rate is done purely for numerical stability.

### 13.2.3.3. Ignition Delay Modeling

When modeling ignition delay in diesel engines, chemical reactions are allowed to occur when the ignition species reaches a value of 1 in the domain. For the ignition delay model, two correlations are built into ANSYS Fluent, one given by Hardenburg and Hase [157] (p. 737) and the other, a generalized model that reproduces several Arrhenius correlations from the literature.

If the ignition species is less than 1 when using the ignition delay model, the chemical source term is suppressed by not activating the combustion model at that particular time step; therefore, the energy release is delayed. This approach is reasonable if you have a good high-temperature chemical model, but do not want to solve for typically expensive low temperature chemistry.

#### 13.2.3.3.1. Modeling of the Source Term

In order to model ignition in a physically realistic manner, the source term is accumulated under appropriate conditions in a cell. Consider the one dimensional spray in Figure 13.2: Propagating Fuel Cloud Showing Accumulation of Source Terms for the Ignition Delay Model (p. 307).


Release 15.0 - © SAS IP, Inc. All rights reserved. - Contains proprietary and confidential information of ANSYS, Inc. and its subsidiaries and affiliates.

**Figure 13.2: Propagating Fuel Cloud Showing Accumulation of Source Terms for the Ignition Delay Model**

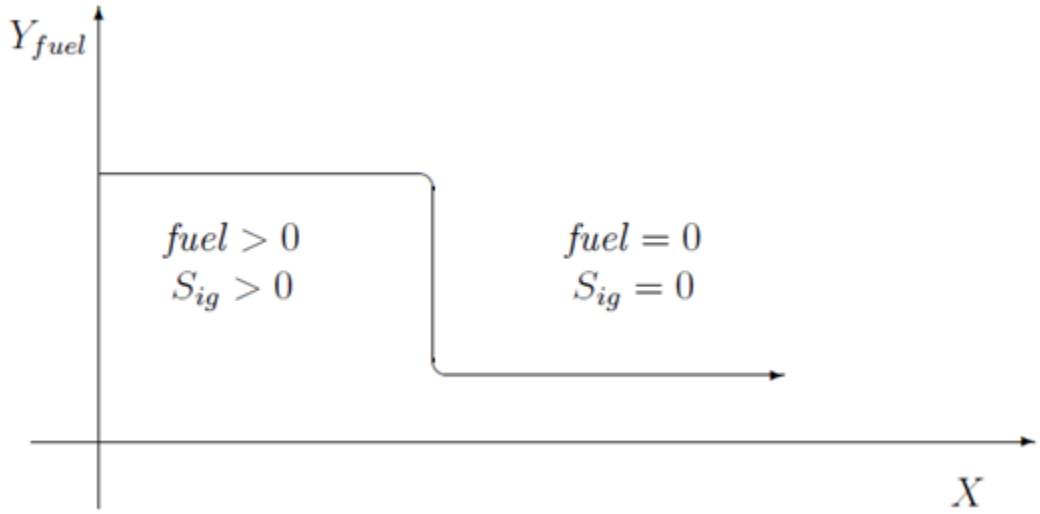


Here, the spray is propagating from left to right and the fuel mass fraction is relatively low in front of the spray and high behind the spray. If there is no fuel in the cell, the model will set the local source term to zero, nevertheless, the value of $Y_{ig}$ can be nonzero due to convection and diffusion.

### 13.2.3.3.2. Correlations

If fuel is present in the cell, there are two built-in options in ANSYS Fluent to calculate the local source term. The first correlation was done by Hardenburg and Hase and was developed at Daimler Chrysler for heavy duty diesel engines. The correlation works over a reasonably wide range of conditions and is given by

$$\tau_{id} = \left( \frac{C_1 + 0.22 \overline{S}_p}{6N} \right) \exp \left[ E_a \left( \frac{1}{RT} - \frac{1}{17,190} \right) + \left( \frac{21.2}{p - 12.4} \right)^{e_p} \right] \tag{13.12}$$

where $\tau_{id}$ is in seconds, $C_1$ is 0.36, $N$ is engine speed in revolutions per minute, $E_a$ is the effective activation energy and $e_p$ is the pressure exponent. The expression for the effective activation energy is given by

$$E_a = \frac{E_{hh}}{CN + 25} \tag{13.13}$$

**Table 13.1: Default Values of the Variables in the Hardenburg Correlation**

| *Variable* | $E_{hh}$ | $CN$ | $C_1$ | $e_p$ |
|---|---|---|---|---|
| *Default* | 618,840 | 25 | 0.36 | 0.63 |

The second correlation, which is the generalized correlation, is given by Equation 13.10 (p. 306) and is available for ignition delay calculations.

*Release 15.0 - © SAS IP, Inc. All rights reserved. - Contains proprietary and confidential information of ANSYS, Inc. and its subsidiaries and affiliates.*

#### 13.2.3.3.3. Energy Release

If the ignition species is greater than or equal to 1 anywhere in the domain, ignition has occurred and combustion is no longer delayed. The ignition species acts as a switch to turn on the volumetric reactions in the domain. Note that the ignition species "mass fraction" can exceed 1 in the domain, therefore, it is not truly a mass fraction, but rather a passive scalar that represents the integrated correlation as a function of time.

## 13.3. Crevice Model

This section describes the theory behind the crevice model. Information can be found in the following sections:

13.3.1. Overview
13.3.2. Limitations
13.3.3. Crevice Model Theory

For information regarding using the crevice model, see Crevice Model in the User's Guide.

## 13.3.1. Overview

The crevice model implemented in ANSYS Fluent is a zero-dimensional ring-flow model based on the model outlined in Namazian and Heywood [316] (p. 746) and Roberts and Matthews [380] (p. 750). The model is geared toward in-cylinder specific flows, and more specifically, direct-injection (DI) diesel engines, and therefore is available only for time-dependent simulations.

The model takes mass, momentum, and energy from cells adjoining two boundaries and accounts for the storage of mass in the volumes of the crevices in the piston. Detailed geometric information regarding the ring and piston—typically a ring pack around the bore of an engine—is necessary to use the crevice model. An example representation is shown in Figure 13.3: Crevice Model Geometry (Piston) (p. 308) — Figure 13.5: Crevice Model "Network" Representation (p. 309).

**Figure 13.3: Crevice Model Geometry (Piston)**

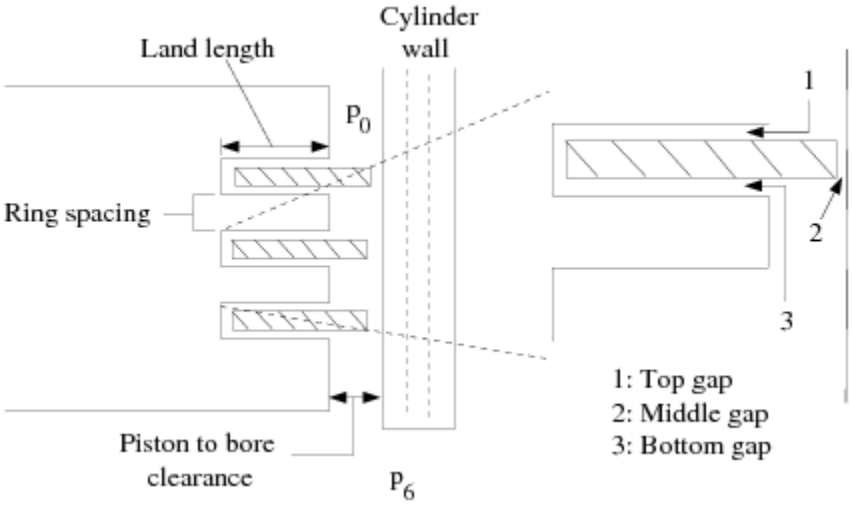



Release 15.0 - © SAS IP, Inc. All rights reserved. - Contains proprietary and confidential information of ANSYS, Inc. and its subsidiaries and affiliates.

**Figure 13.4: Crevice Model Geometry (Ring)**

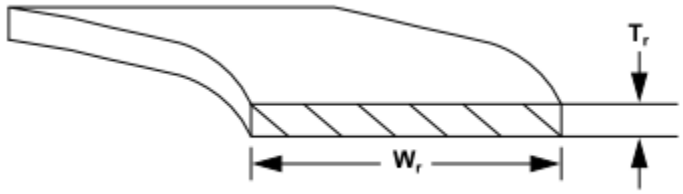


**Figure 13.5: Crevice Model "Network" Representation**

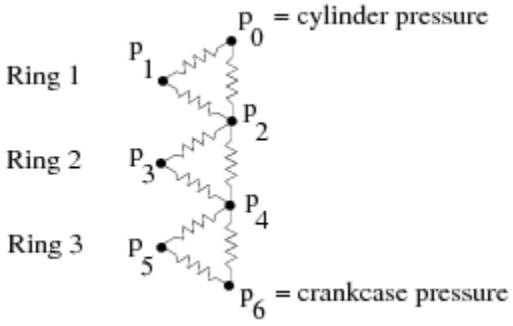


## 13.3.1.1. Model Parameters

- The *piston to bore clearance* is the distance between the piston and the bore. Typical values are 2 to 5 mil (80 to 120 µm) in a spark engine (SI) and 4 to 7 mil (100 to 240 µm) in some diesel engines (DI).
- The *ring thickness* is the variable $T_r$ in Figure 13.4: Crevice Model Geometry (Ring) (p. 309). Typical values range from 1 to 3 mm for SI engines and 2 to 4 mm for DI engines.
- The *ring width* is the variable $W_r$ in Figure 13.4: Crevice Model Geometry (Ring) (p. 309). Typical values range from 3 to 3.5 mm for SI engines and 4 to 6 mm for DI diesel engines.
- The *ring spacing* is the distance between the bottom of one ring land and the top of the next ring land. Typical values of the ring spacing are 3 to 5 mm for SI engines and 4 to 8 mm for DI diesel engines.
- The *land length* is the depth of the ring land (that is, the cutout into the piston); always deeper than the width of the ring by about 1 mm. Typical values are 4 to 4.5 mm for SI engines and 5 to 7 mm for DI diesel engines.
- The *top gap* is the clearance between the ring land and the top of the ring (40 to 80 µm).
- The *middle gap* is the distance between the ring and the bore (10 to 40 µm).
- The *bottom gap* is the clearance between the ring land and the bottom of the ring (40 to 80 µm).
- The *shared boundary and leaking wall* is the piston (for example, `wall-8`) and the cylinder wall (for example, `wall.1`) in most in-cylinder simulations. Cells that share a boundary with the top of the piston and the cylinder wall are defined as the *crevice* cells.

The ring pack is the set of rings that seal the piston in the cylinder bore. As the piston moves upward in the cylinder when the valves are closed (for example, during the compression stroke in a four-stroke cycle engine), the pressure in the cylinder rises and flow begins to move past the rings. The pressure distribution in the ring pack is modeled by assuming either fully-developed compressible flow through

Release 15.0 - © SAS IP, Inc. All rights reserved. - Contains proprietary and confidential information of ANSYS, Inc. and its subsidiaries and affiliates.

the spaces between the rings and the piston, or choked compressible flow between the rings and the cylinder wall.

Since the temperature in the ring pack is fixed and the geometry is known, once a pressure distribution is calculated, the mass in each volume can be found using the ideal gas equation of state. The overall mass flow out of the ring pack (that is, the flow past the last ring specified) is also calculated at each discrete step in the ANSYS Fluent solution.

## 13.3.2. Limitations

The limitations of the crevice model are that it is zero dimensional, transient, and currently limited to two threads that share a boundary.

A zero-dimensional approach is used because it is difficult to accurately predict lateral diffusion of species in the crevice. If the lateral diffusion of species is important in the simulation, as in when a spray plume in a DI engine is in close proximity to the boundary and the net mass flow is into the crevice, it is recommended that the full multidimensional crevice geometry be simulated in ANSYS Fluent using a nonconformal mesh. Additionally, this approach does not specifically track individual species, as any individual species would be instantly distributed over the entire ring pack. The mass flux into the domain from the crevice is assumed to have the same composition as the cell into which mass is flowing.

The formulation of the crevice flow equations is inherently transient and is solved using ANSYS Fluent's stiff-equation solver. A steady problem with leakage flow can be solved by running the transient problem to steady state. Additional limitations of the crevice model in its current form are that only a single crevice is allowed and only one thread can have leakage. Ring dynamics are not explicitly accounted for, although ring positions can be set during the simulation.

In this context, the crevice model solution is a stiff initial boundary-value problem. The stiffness increases as the pressure difference between the ring crevices increases and also as the overall pressure difference across the ring pack increases. Thus, if the initial conditions are very far from the solution during a time step, the ODE solver may not be able to integrate the equations successfully. One solution to this problem is to decrease the flow time step for several iterations. Another solution is to start with initial conditions that are closer to the solution at the end of the time step.

## 13.3.3. Crevice Model Theory

ANSYS Fluent solves the equations for mass conservation in the crevice geometry by assuming laminar compressible flow in the region between the piston and the top and bottom faces of the ring, and by assuming an orifice flow between the ring and the cylinder wall. The equation for the mass flow through the ring end gaps is of the form

$$\dot{m}_{ij} = C_d A_{ij} \rho c \eta_{ij} \tag{13.14}$$

where $C_d$ is the discharge coefficient, $A_{ij}$ is the gap area, $\rho$ is the gas density, $c$ is the local speed of sound, and $\eta_{ij}$ is a compressibility factor given by


Release 15.0 - © SAS IP, Inc. All rights reserved. - Contains proprietary and confidential information of ANSYS, Inc. and its subsidiaries and affiliates.

$$\eta_{ij}=\begin{cases}\dfrac{2}{\gamma-1}\left[\left(\dfrac{p_i}{p_j}\right)^{\frac{2}{\gamma}}-\left(\dfrac{p_i}{p_j}\right)^{\frac{2}{\gamma}}\right]^{0.5} & \dfrac{p_i}{p_j}>0.52 \\ \left(\dfrac{2}{\gamma-1}\right)^{\frac{\gamma+1}{2(\gamma-1)}} & \dfrac{p_i}{p_j}\le 0.52\end{cases} \tag{13.15}$$

where $\gamma$ is the ratio of specific heats, $p_i$ the upstream pressure and $p_j$ the downstream pressure. The equation for the mass flow through the top and bottom faces of the ring (that is, into and out of the volume behind the piston ring) is given by

$$\dot{m}_{ij}=\frac{h_{ij}^2\left(p_i^2-p_j^2\right)A_{ij}}{24W_r\mu_{gas}RT} \tag{13.16}$$

where $h_{ij}$ is the cross-sectional area of the gap, $W_r$ is the width of the ring along which the gas is flowing, $\mu_{gas}$ is the local gas viscosity, $T$ is the temperature of the gas and $R$ is the universal gas constant. The system of equations for a set of three rings is of the following form:

$$\frac{dp_1}{dt}=\frac{p_1}{m_1}(\dot{m}_{01}-\dot{m}_{12}) \tag{13.17}$$

$$\frac{dp_2}{dt}=\frac{p_2}{m_2}(\dot{m}_{02}+\dot{m}_{12}-\dot{m}_{23}-\dot{m}_{24}) \tag{13.18}$$

$$\frac{dp_3}{dt}=\frac{p_3}{m_3}(\dot{m}_{23}-\dot{m}_{34}) \tag{13.19}$$

$$\frac{dp_4}{dt}=\frac{p_4}{m_4}(\dot{m}_{24}+\dot{m}_{34}-\dot{m}_{45}-\dot{m}_{46}) \tag{13.20}$$

$$\frac{dp_5}{dt}=\frac{p_5}{m_5}(\dot{m}_{45}-\dot{m}_{56}) \tag{13.21}$$

where $p_0$ is the average pressure in the crevice cells and $p_6$ is the crankcase pressure input from the text interface. The expressions for the mass flows for numerically adjacent zones (for example, 0-1, 1-2, 2-3, and so on) are given by Equation 13.16 (p. 311) and expressions for the mass flows for zones separated by two integers (for example, 0-2, 2-4, 4-6) are given by Equation 13.14 (p. 310) and Equation 13.15 (p. 311). Thus, there are $2n_r-1$ equations needed for the solution to the ring-pack equations, where $n_r$ is the number of rings in the simulation.

Release 15.0 - © SAS IP, Inc. All rights reserved. - Contains proprietary and confidential information of ANSYS, Inc. and its subsidiaries and affiliates.

Release 15.0 - © SAS IP, Inc. All rights reserved. - Contains proprietary and confidential information
of ANSYS, Inc. and its subsidiaries and affiliates.

# Chapter 14: Pollutant Formation

This chapter discusses the theory behind the models available in ANSYS Fluent for modeling pollutant formation.

Information is presented in the following sections:

14.1. NOx Formation
14.2. SOx Formation
14.3. Soot Formation
14.4. Decoupled Detailed Chemistry Model

For information about using the models in ANSYS Fluent, see Modeling Pollutant Formation in the User's Guide.

## 14.1. NOx Formation

The following sections present the theoretical background of $NO_x$ prediction. For information about using the $NO_x$ models in ANSYS Fluent, see Using the NOx Model in the User's Guide.

14.1.1. Overview
14.1.2. Governing Equations for NOx Transport
14.1.3. Thermal NOx Formation
14.1.4. Prompt NOx Formation
14.1.5. Fuel NOx Formation
14.1.6. NOx Formation from Intermediate N2O
14.1.7. NOx Reduction by Reburning
14.1.8. NOx Reduction by SNCR
14.1.9. NOx Formation in Turbulent Flows

### 14.1.1. Overview

$NO_x$ emission consists of mostly nitric oxide ($NO$), and to a lesser degree nitrogen dioxide ($NO_2$) and nitrous oxide ($N_2O$). $NO_x$ is a precursor for photochemical smog, contributes to acid rain, and causes ozone depletion. Thus, $NO_x$ is a pollutant. The ANSYS Fluent $NO_x$ model provides a tool to understand the sources of $NO_x$ production and to aid in the design of $NO_x$ control measures.

#### *14.1.1.1. NOx Modeling in ANSYS Fluent*

The ANSYS Fluent $NO_x$ model provides the capability to model thermal, prompt, and fuel $NO_x$ formation, as well as $NO_x$ consumption due to reburning in combustion systems. It uses rate models developed at the Department of Fuel and Energy at The University of Leeds in England, as well as from the open literature. $NO_x$ reduction using reagent injection, such as selective non-catalytic reduction (SNCR), can be modeled in ANSYS Fluent, along with an $N_2O$ intermediate model that has also been incorporated.

To predict $NO_x$ emissions, ANSYS Fluent solves a transport equation for nitric oxide ($NO$) concentration. When fuel $NO_x$ sources are present, ANSYS Fluent solves additional transport equations for intermediate

Release 15.0 - © SAS IP, Inc. All rights reserved. - Contains proprietary and confidential information of ANSYS, Inc. and its subsidiaries and affiliates.

species ($HCN$ and/or $NH_3$). When the $N_2O$ intermediate model is activated, an additional transport equation for $N_2O$ will be solved. The $NO_x$ transport equations are solved based on a given flow field and combustion solution. In other words, $NO_x$ is postprocessed from a combustion simulation. It is therefore evident that an accurate combustion solution becomes a prerequisite of $NO_x$ prediction. For example, thermal $NO_x$ production doubles for every 90 K temperature increase when the flame temperature is about 2200 K. Great care must be exercised to provide accurate thermophysical data and boundary condition inputs for the combustion model. Appropriate turbulence, chemistry, radiation, and other submodels must be employed.

To be realistic, you can only expect results to be as accurate as the input data and the selected physical models. Under most circumstances, $NO_x$ variation trends can be accurately predicted, but the $NO_x$ quantity itself cannot be pinpointed. Accurate prediction of $NO_x$ parametric trends can cut down on the number of laboratory tests, allow more design variations to be studied, shorten the design cycle, and reduce product development cost. That is truly the power of the ANSYS Fluent $NO_x$ model and, in fact, the power of CFD in general.

### 14.1.1.2. NOx Formation and Reduction in Flames

In laminar flames and at the molecular level within turbulent flames, the formation of $NO_X$ can be attributed to four distinct chemical kinetic processes: thermal $NO_x$ formation, prompt $NO_x$ formation, fuel $NO_x$ formation, and intermediate $N_2O$. Thermal $NO_x$ is formed by the oxidation of atmospheric nitrogen present in the combustion air. Prompt $NO_x$ is produced by high-speed reactions at the flame front. Fuel $NO_x$ is produced by oxidation of nitrogen contained in the fuel. At elevated pressures and oxygen-rich conditions, $NO_x$ may also be formed from molecular nitrogen ($N_2$) via $N_2O$. The reburning and SNCR mechanisms reduce the total $NO_x$ formation by accounting for the reaction of $NO$ with hydrocarbons and ammonia, respectively.

**Important**

The $NO_x$ models cannot be used in conjunction with the premixed combustion model.

## 14.1.2. Governing Equations for NOx Transport

ANSYS Fluent solves the mass transport equation for the $NO$ species, taking into account convection, diffusion, production, and consumption of $NO$ and related species. This approach is completely general, being derived from the fundamental principle of mass conservation. The effect of residence time in $NO_x$ mechanisms (a Lagrangian reference frame concept) is included through the convection terms in the governing equations written in the Eulerian reference frame. For thermal and prompt $NO_x$ mechanisms, only the $NO$ species transport equation is needed:

$$\frac{\partial}{\partial t}(\rho Y_{NO}) + \nabla \cdot (\rho \vec{v} Y_{NO}) = \nabla \cdot (\rho \mathcal{D} \nabla Y_{NO}) + S_{NO} \tag{14.1}$$

As discussed in Fuel NOx Formation (p. 321), the fuel $NO_x$ mechanisms are more involved. The tracking of nitrogen-containing intermediate species is important. ANSYS Fluent solves a transport equation for the $HCN$, $NH_3$, or $N_2O$ species, in addition to the $NO$ species:

$$\frac{\partial}{\partial t}(\rho Y_{HCN}) + \nabla \cdot (\rho \vec{v} Y_{HCN}) = \nabla \cdot (\rho \mathcal{D} Y_{HCN}) + S_{HCN} \tag{14.2}$$


Release 15.0 - © SAS IP, Inc. All rights reserved. - Contains proprietary and confidential information of ANSYS, Inc. and its subsidiaries and affiliates.

$$\frac{\partial}{\partial t}\left(\rho Y_{NH_3}\right)+\nabla\cdot\left(\rho\vec{v}\,Y_{NH_3}\right)=\nabla\cdot\left(\rho\mathcal{D}Y_{NH_3}\right)+S_{NH_3} \tag{14.3}$$

$$\frac{\partial}{\partial t}\left(\rho Y_{N_2O}\right)+\nabla\cdot\left(\rho\vec{v}\,Y_{N_2O}\right)=\nabla\cdot\left(\rho\mathcal{D}Y_{N_2O}\right)+S_{N_2O} \tag{14.4}$$

where $Y_{HCN}$, $Y_{NH_3}$, $Y_{N_2O}$, and $Y_{NO}$ are mass fractions of $\mathrm{HCN}$, $\mathrm{NH_3}$, $\mathrm{N_2O}$, and $\mathrm{NO}$ in the gas phase, and $\mathcal{D}$ is the effective diffusion coefficient. The source terms $S_{HCN}$, $S_{NH_3}$, $S_{N_2O}$, and $S_{NO}$ are to be determined next for different $\mathrm{NO}_x$ mechanisms.

## 14.1.3. Thermal NOx Formation

The formation of thermal $\mathrm{NO}_x$ is determined by a set of highly temperature-dependent chemical reactions known as the extended Zeldovich mechanism. The principal reactions governing the formation of thermal $\mathrm{NO}_x$ from molecular nitrogen are as follows:

$$\mathrm{O}+\mathrm{N_2}\rightleftharpoons\mathrm{N}+\mathrm{NO} \tag{14.5}$$

$$\mathrm{N}+\mathrm{O_2}\rightleftharpoons\mathrm{O}+\mathrm{NO} \tag{14.6}$$

A third reaction has been shown to contribute to the formation of thermal $\mathrm{NO}_x$, particularly at near-stoichiometric conditions and in fuel-rich mixtures:

$$\mathrm{N}+\mathrm{OH}\rightleftharpoons\mathrm{H}+\mathrm{NO} \tag{14.7}$$

### 14.1.3.1. Thermal NOx Reaction Rates

The rate constants for these reactions have been measured in numerous experimental studies [35] (p. 730), [125] (p. 735), [306] (p. 745), and the data obtained from these studies have been critically evaluated by Baulch et al. [23] (p. 730) and Hanson and Salimian [156] (p. 737). The expressions for the rate coefficients for Equation 14.5 (p. 315) – Equation 14.7 (p. 315) used in the $\mathrm{NO}_x$ model are given below. These were selected based on the evaluation of Hanson and Salimian [156] (p. 737).

$$k_{f,1}=1.8\times10^{8}e^{-38370/T} \qquad k_{r,1}=3.8\times10^{7}e^{-425/T}$$

$$k_{f,2}=1.8\times10^{4}Te^{-4680/T} \qquad k_{r,2}=3.81\times10^{3}Te^{-20820/T}$$

$$k_{f,3}=7.1\times10^{7}e^{-450/T} \qquad k_{r,3}=1.7\times10^{8}e^{-24560/T}$$

In the above expressions, $k_{f,1}$, $k_{f,2}$, and $k_{f,3}$ are the rate constants for the forward reactions Equation 14.5 (p. 315) – Equation 14.7 (p. 315), respectively, and $k_{r,1}$, $k_{r,2}$, and $k_{r,3}$ are the corresponding reverse rate constants. All of these rate constants have units of $\mathrm{m^3/mol\text{-}s}$.

The net rate of formation of $\mathrm{NO}$ via the reactions in Equation 14.5 (p. 315) – Equation 14.7 (p. 315) is given by

$$\begin{aligned}\frac{d[\mathrm{NO}]}{dt} &= k_{f,1}[\mathrm{O}][\mathrm{N_2}]+k_{f,2}[\mathrm{N}][\mathrm{O_2}]+k_{f,3}[\mathrm{N}][\mathrm{OH}]\\ &\quad -k_{r,1}[\mathrm{NO}][\mathrm{N}]-k_{r,2}[\mathrm{NO}][\mathrm{O}]-k_{r,3}[\mathrm{NO}][\mathrm{H}]\end{aligned} \tag{14.8}$$

Release 15.0 - © SAS IP, Inc. All rights reserved. - Contains proprietary and confidential information of ANSYS, Inc. and its subsidiaries and affiliates.

where all concentrations have units of $mol/m^3$.

To calculate the formation rates of $NO$ and $N$, the concentrations of $O$, $H$, and $OH$ are required.

### 14.1.3.2. The Quasi-Steady Assumption for [N]

The rate of formation of $NO_x$ is significant only at high temperatures (greater than 1800 K) because fixation of nitrogen requires the breaking of the strong $N_2$ triple bond (dissociation energy of 941 kJ/mol). This effect is represented by the high activation energy of reaction Equation 14.5 (p. 315), which makes it the rate-limiting step of the extended Zeldovich mechanism. However, the activation energy for oxidation of $N$ atoms is small. When there is sufficient oxygen, as in a fuel-lean flame, the rate of consumption of free nitrogen atoms becomes equal to the rate of its formation, and therefore a quasi-steady state can be established. This assumption is valid for most combustion cases, except in extremely fuel-rich combustion conditions. Hence the $NO$ formation rate becomes

$$\frac{d[\mathrm{NO}]}{dt} = 2k_{f,1}[\mathrm{O}][\mathrm{N_2}] \frac{\left(1 - \frac{k_{r,1}k_{r,2}[NO]^2}{k_{f,1}[N_2]k_{f,2}[O_2]}\right)}{\left(1 + \frac{k_{r,1}[NO]}{k_{f,2}[O_2] + k_{f,3}[OH]}\right)} \quad \left(\mathrm{mol/m^3\text{-}s}\right) \tag{14.9}$$

### 14.1.3.3. Thermal NOx Temperature Sensitivity

From Equation 14.9 (p. 316) it is clear that the rate of formation of $NO$ will increase with increasing oxygen concentration. It also appears that thermal $NO$ formation should be highly dependent on temperature but independent of fuel type. In fact, based on the limiting rate described by $k_{f,1}$, the thermal $NO_x$ production rate doubles for every 90 K temperature increase beyond 2200 K.

### 14.1.3.4. Decoupled Thermal NOx Calculations

To solve Equation 14.9 (p. 316), the concentration of $O$ atoms and the free radical $OH$ will be required, in addition to the concentration of stable species (that is, $O_2$, $N_2$). Following the suggestion by Zeldovich, the thermal $NO_x$ formation mechanism can be decoupled from the main combustion process by assuming equilibrium values of temperature, stable species, $O$ atoms, and $OH$ radicals. However, radical concentrations ($O$ atoms in particular) are observed to be more abundant than their equilibrium levels. The effect of partial equilibrium $O$ atoms on $NO_x$ formation rate has been investigated [302] (p. 745) during laminar methane-air combustion. The results of these investigations indicate that the level of $NO_x$ emission can be under-predicted by as much as 28% in the flame zone, when assuming equilibrium $O$-atom concentrations.

### 14.1.3.5. Approaches for Determining O Radical Concentration

There has been little detailed study of radical concentration in industrial turbulent flames, but work [99] (p. 734) has demonstrated the existence of this phenomenon in turbulent diffusion flames. Presently, there is no definitive conclusion as to the effect of partial equilibrium on $NO_x$ formation rates in turbulent flames. Peters and Donnerhack [348] (p. 748) suggest that partial equilibrium radicals can account for no more than a 25% increase in thermal $NO_x$ and that fluid dynamics has the dominant effect on the $NO_x$ formation rate. Bilger et al. [31] (p. 730) suggest that in turbulent diffusion flames, the effect of $O$ atom overshoot on the $NO_x$ formation rate is very important.


Release 15.0 - © SAS IP, Inc. All rights reserved. - Contains proprietary and confidential information of ANSYS, Inc. and its subsidiaries and affiliates.

To overcome this possible inaccuracy, one approach would be to couple the extended Zeldovich mechanism with a detailed hydrocarbon combustion mechanism involving many reactions, species, and steps. This approach has been used previously for research purposes [298] (p. 745). However, long computer processing time has made the method economically unattractive and its extension to turbulent flows difficult.

To determine the $\mathrm{O}$ radical concentration, ANSYS Fluent uses one of three approaches—the equilibrium approach, the partial equilibrium approach, and the predicted concentration approach—in recognition of the ongoing controversy discussed above.

#### 14.1.3.5.1. Method 1: Equilibrium Approach

The kinetics of the thermal $\mathrm{NO}_x$ formation rate is much slower than the main hydrocarbon oxidation rate, and so most of the thermal $\mathrm{NO}_x$ is formed after completion of combustion. Therefore, the thermal $\mathrm{NO}_x$ formation process can often be decoupled from the main combustion reaction mechanism and the $\mathrm{NO}_x$ formation rate can be calculated by assuming equilibration of the combustion reactions. Using this approach, the calculation of the thermal $\mathrm{NO}_x$ formation rate is considerably simplified. The assumption of equilibrium can be justified by a reduction in the importance of radical overshoots at higher flame temperature [98] (p. 734). According to Westenberg [488] (p. 756), the equilibrium $\mathrm{O}$-atom concentration can be obtained from the expression

$$[\mathrm{O}] = k_p [\mathrm{O}_2]^{1/2} \tag{14.10}$$

With $k_p$ included, this expression becomes

$$[\mathrm{O}] = 3.97 \times 10^5 T^{-1/2} [\mathrm{O}_2]^{1/2} e^{-31090/T} \qquad \mathrm{mol/m^3} \tag{14.11}$$

where $T$ is in Kelvin.

#### 14.1.3.5.2. Method 2: Partial Equilibrium Approach

An improvement to method 1 can be made by accounting for third-body reactions in the $\mathrm{O}_2$ dissociation-recombination process:

$$\mathrm{O}_2 + \mathrm{M} \rightleftharpoons \mathrm{O} + \mathrm{O} + \mathrm{M} \tag{14.12}$$

Equation 14.11 (p. 317) is then replaced by the following expression [478] (p. 755):

$$[\mathrm{O}] = 36.64 T^{1/2} [\mathrm{O}_2]^{1/2} e^{-27123/T} \qquad \mathrm{mol/m^3} \tag{14.13}$$

which generally leads to a higher partial $\mathrm{O}$-atom concentration.

#### 14.1.3.5.3. Method 3: Predicted O Approach

When the $\mathrm{O}$-atom concentration is well predicted using an advanced chemistry model (such as the flamelet submodel of the non-premixed model), $[\mathrm{O}]$ can be taken simply from the local $\mathrm{O}$-species mass fraction.

### 14.1.3.6. Approaches for Determining OH Radical Concentration

ANSYS Fluent uses one of three approaches to determine the $\mathrm{OH}$ radical concentration: the exclusion of $\mathrm{OH}$ from the thermal $\mathrm{NO}_x$ calculation approach, the partial equilibrium approach, and the use of the predicted $\mathrm{OH}$ concentration approach.

Release 15.0 - © SAS IP, Inc. All rights reserved. - Contains proprietary and confidential information of ANSYS, Inc. and its subsidiaries and affiliates.

#### 14.1.3.6.1. Method 1: Exclusion of OH Approach

In this approach, the third reaction in the extended Zeldovich mechanism (Equation 14.7 (p. 315)) is assumed to be negligible through the following observation:

$$k_2[O_2]_{eq} \gg k_3[OH]_{eq}$$

This assumption is justified for lean fuel conditions and is a reasonable assumption for most cases.

#### 14.1.3.6.2. Method 2: Partial Equilibrium Approach

In this approach, the concentration of $\mathrm{OH}$ in the third reaction in the extended Zeldovich mechanism (Equation 14.7 (p. 315)) is given by [24] (p. 730), [487] (p. 756)

$$[\mathrm{OH}] = 2.129 \times 10^2 T^{-0.57} e^{-4595/T} [\mathrm{O}]^{1/2} [\mathrm{H_2O}]^{1/2} \qquad \mathrm{mol/m^3} \tag{14.14}$$

#### 14.1.3.6.3. Method 3: Predicted OH Approach

As in the predicted $\mathrm{O}$ approach, when the $\mathrm{OH}$ radical concentration is well predicted using an advanced chemistry model such as the flamelet model, $[\mathrm{OH}]$ can be taken directly from the local $\mathrm{OH}$ species mass fraction.

### 14.1.3.7. Summary

To summarize, the thermal $\mathrm{NO}_x$ formation rate is predicted by Equation 14.9 (p. 316). The $\mathrm{O}$-atom concentration needed in Equation 14.9 (p. 316) is computed using Equation 14.11 (p. 317) for the equilibrium assumption, using Equation 14.13 (p. 317) for a partial equilibrium assumption, or using the local $\mathrm{O}$-species mass fraction. You will make the choice during problem setup. In terms of the transport equation for $\mathrm{NO}$ (Equation 14.1 (p. 314)), the $\mathrm{NO}$ source term due to thermal $\mathrm{NO}_x$ mechanisms is

$$S_{thermal,NO} = M_{w,NO} \frac{d[NO]}{dt} \tag{14.15}$$

where $M_{w,NO}$ is the molecular weight of $\mathrm{NO}$ (kg/mol), and $d[NO]/dt$ is computed from Equation 14.9 (p. 316).

## 14.1.4. Prompt NOx Formation

It is known that during combustion of hydrocarbon fuels, the $\mathrm{NO}_x$ formation rate can exceed that produced from direct oxidation of nitrogen molecules (that is, thermal $\mathrm{NO}_x$).

### 14.1.4.1. Prompt NOx Combustion Environments

The presence of a second mechanism leading to $\mathrm{NO}_x$ formation was first identified by Fenimore [113] (p. 735) and was termed "prompt $\mathrm{NO}_x$". There is good evidence that prompt $\mathrm{NO}_x$ can be formed in a significant quantity in some combustion environments, such as in low-temperature, fuel-rich conditions and where residence times are short. Surface burners, staged combustion systems, and gas turbines can create such conditions [18] (p. 730).


Release 15.0 - © SAS IP, Inc. All rights reserved. - Contains proprietary and confidential information of ANSYS, Inc. and its subsidiaries and affiliates.

At present, the prompt $NO_x$ contribution to total $NO_x$ from stationary combustors is small. However, as $NO_x$ emissions are reduced to very low levels by employing new strategies (burner design or furnace geometry modification), the relative importance of the prompt $NO_x$ can be expected to increase.

### 14.1.4.2. Prompt NOx Mechanism

Prompt $NO_x$ is most prevalent in rich flames. The actual formation involves a complex series of reactions and many possible intermediate species. The route now accepted is as follows:

$$CH + N_2 \rightleftharpoons HCN + N \tag{14.16}$$

$$N + O_2 \rightleftharpoons NO + O \tag{14.17}$$

$$HCN + OH \rightleftharpoons CN + H_2O \tag{14.18}$$

$$CN + O_2 \rightleftharpoons NO + CO \tag{14.19}$$

A number of species resulting from fuel fragmentation have been suggested as the source of prompt $NO_x$ in hydrocarbon flames (for example, $CH$, $CH_2$, $C$, $C_2H$), but the major contribution is from $CH$ (Equation 14.16 (p. 319)) and $CH_2$, via

$$CH_2 + N_2 \rightleftharpoons HCN + NH \tag{14.20}$$

The products of these reactions could lead to formation of amines and cyano compounds that subsequently react to form $NO$ by reactions similar to those occurring in oxidation of fuel nitrogen, for example:

$$HCN + N \rightleftharpoons N_2 + \ldots \tag{14.21}$$

### 14.1.4.3. Prompt NOx Formation Factors

Prompt $NO_x$ formation is proportional to the number of carbon atoms present per unit volume and is independent of the parent hydrocarbon identity. The quantity of $HCN$ formed increases with the concentration of hydrocarbon radicals, which in turn increases with equivalence ratio. As the equivalence ratio increases, prompt $NO_x$ production increases at first, then passes a peak, and finally decreases due to a deficiency in oxygen.

### 14.1.4.4. Primary Reaction

The reaction described by Equation 14.16 (p. 319) is of primary importance. In recent studies [392] (p. 750), comparison of probability density distributions for the location of the peak $NO_x$ with those obtained for the peak $CH$ have shown close correspondence, indicating that the majority of the $NO_x$ at the flame base is prompt $NO_x$ formed by the $CH$ reaction. Assuming that the reaction described by Equation 14.16 (p. 319) controls the prompt $NO_x$ formation rate,

$$\frac{d[NO]}{dt} = k_0 [CH][N_2] \tag{14.22}$$

### 14.1.4.5. Modeling Strategy

There are, however, uncertainties about the rate data for the above reaction. From the reactions described by Equation 14.16 (p. 319) – Equation 14.20 (p. 319), it can be concluded that the prediction of prompt $NO_x$ formation within the flame requires coupling of the $NO_x$ kinetics to an actual hydrocarbon com-

Release 15.0 - © SAS IP, Inc. All rights reserved. - Contains proprietary and confidential information of ANSYS, Inc. and its subsidiaries and affiliates.

bustion mechanism. Hydrocarbon combustion mechanisms involve many steps and, as mentioned previously, are extremely complex and costly to compute. In the present $NO_x$ model, a global kinetic parameter derived by De Soete [90] (p. 733) is used. De Soete compared the experimental values of total $NO_x$ formation rate with the rate of formation calculated by numerical integration of the empirical overall reaction rates of $NO_x$ and $N_2$ formation. He showed that overall prompt formation rate can be predicted from the expression

$$\frac{d[NO]}{dt} = (\text{overall prompt NOx formation rate}) - (\text{overall prompt } N_2 \text{ formation rate}) \tag{14.23}$$

In the early stages of the flame, where prompt $NO_x$ is formed under fuel-rich conditions, the $O$ concentration is high and the $N$ radical almost exclusively forms $NO_x$ rather than nitrogen. Therefore, the prompt $NO_x$ formation rate will be approximately equal to the overall prompt $NO_x$ formation rate:

$$\frac{d[NO]}{dt} = k_{pr}[O_2]^a[N_2][FUEL]e^{-E_a/RT} \tag{14.24}$$

For $C_2H_4$ (ethylene)-air flames,

$$k_{pr} = 1.2\times10^7 (RT/p)^{a+1} \tag{14.25}$$

$E_a$ is 251151 J/mol, $a$ is the oxygen reaction order, $R$ is the universal gas constant, and $p$ is pressure (all in SI units). The rate of prompt $NO_x$ formation is found to be of the first order with respect to nitrogen and fuel concentration, but the oxygen reaction order, $a$, depends on experimental conditions.

### 14.1.4.6. Rate for Most Hydrocarbon Fuels

Equation 14.24 (p. 320) was tested against the experimental data obtained by Backmier et al. [14] (p. 729) for different mixture strengths and fuel types. The predicted results indicated that the model performance declined significantly under fuel-rich conditions and for higher hydrocarbon fuels. To reduce this error and predict the prompt $NO_x$ adequately in all conditions, the De Soete model was modified using the available experimental data. A correction factor, $f$, was developed, which incorporates the effect of fuel type, that is, number of carbon atoms, and the air-to-fuel ratio for gaseous aliphatic hydrocarbons. Equation 14.24 (p. 320) now becomes

$$\frac{d[NO]}{dt} = f\,k'_{pr}[O_2]^a[N_2][FUEL]e^{-E'_a/RT} \tag{14.26}$$

so that the source term due to prompt $NO_x$ mechanism is

$$S_{prompt,NO} = M_{w,NO}\frac{d[NO]}{dt} \tag{14.27}$$

In the above equations,

$$f = 4.75 + 0.0819n - 23.2\phi + 32\phi^2 - 12.2\phi^3 \tag{14.28}$$

$$k'_{pr} = 6.4\times10^6 (RT/p)^{a+1} \tag{14.29}$$

$E'_a$ is 303474.125 J/mol, $n$ is the number of carbon atoms per molecule for the hydrocarbon fuel, and $\phi$ is the equivalence ratio. The correction factor is a curve fit for experimental data, valid for aliphatic alkane hydrocarbon fuels ($C_nH_{2n+2}$) and for equivalence ratios between 0.6 and 1.6. For values outside


Release 15.0 - © SAS IP, Inc. All rights reserved. - Contains proprietary and confidential information of ANSYS, Inc. and its subsidiaries and affiliates.

the range, the appropriate limit should be used. Values of $k'_{pr}$ and $E'_a$ were developed at the Department of Fuel and Energy at The University of Leeds in England.

Here, the concept of equivalence ratio refers to an overall equivalence ratio for the flame, rather than any spatially varying quantity in the flow domain. In complex geometries with multiple burners this may lead to some uncertainty in the specification of $\phi$. However, since the contribution of prompt $\mathrm{NO}_x$ to the total $\mathrm{NO}_x$ emission is often very small, results are not likely to be significantly biased.

#### 14.1.4.7. Oxygen Reaction Order

Oxygen reaction order depends on flame conditions. According to De Soete [90] (p. 733), oxygen reaction order is uniquely related to oxygen mole fraction in the flame:

$$a = \begin{cases} 1.0, & X_{O_2} \le 4.1\times10^{-3} \\ -3.95 - 0.9\ln X_{O_2}, & 4.1\times10^{-3} \le X_{O_2} \le 1.11\times10^{-2} \\ -0.35 - 0.1\ln X_{O_2}, & 1.11\times10^{-2} < X_{O_2} < 0.03 \\ 0, & X_{O_2} \ge 0.03 \end{cases} \tag{14.30}$$

### 14.1.5. Fuel NOx Formation

#### 14.1.5.1. Fuel-Bound Nitrogen

It is well known that nitrogen-containing organic compounds present in liquid or solid fossil fuel can contribute to the total $\mathrm{NO}_x$ formed during the combustion process. This fuel nitrogen is a particularly important source of nitrogen oxide emissions for residual fuel oil and coal, which typically contain 0.3–2% nitrogen by weight. Studies have shown that most of the nitrogen in heavy fuel oils is in the form of heterocycles, and it is thought that the nitrogen components of coal are similar [193] (p. 739). It is believed that pyridine, quinoline, and amine type heterocyclic ring structures are of importance.

#### 14.1.5.2. Reaction Pathways

The extent of the conversion of fuel nitrogen to $\mathrm{NO}_x$ is dependent on the local combustion characteristics and the initial concentration of nitrogen-bound compounds. Fuel-bound compounds that contain nitrogen are released into the gas phase when the fuel droplets or particles are heated during the devolatilization stage. From the thermal decomposition of these compounds (aniline, pyridine, pyrroles, etc.) in the reaction zone, radicals such as $\mathrm{HCN}$, $\mathrm{NH_3}$, $\mathrm{N}$, $\mathrm{CN}$, and $\mathrm{NH}$ can be formed and converted to $\mathrm{NO}_x$. The above free radicals (that is, secondary intermediate nitrogen compounds) are subject to a double competitive reaction path. This chemical mechanism has been subject to several detailed investigations [299] (p. 745). Although the route leading to fuel $\mathrm{NO}_x$ formation and destruction is still not completely understood, different investigators seem to agree on a simplified model:

Release 15.0 - © SAS IP, Inc. All rights reserved. - Contains proprietary and confidential information of ANSYS, Inc. and its subsidiaries and affiliates.

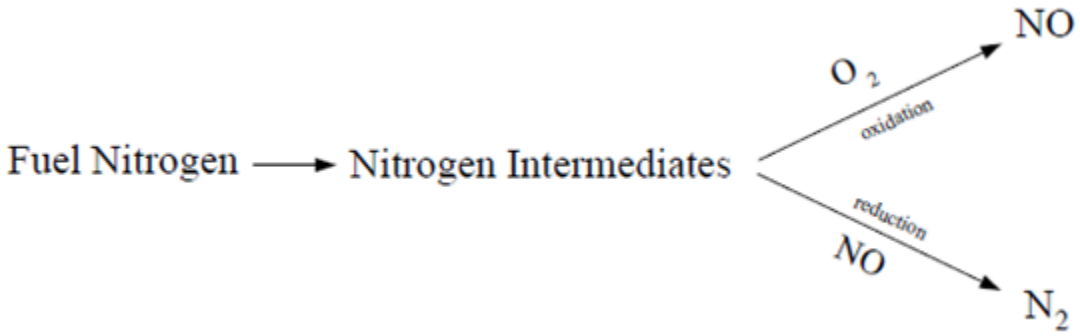


Recent investigations [167] (p. 738) have shown that hydrogen cyanide appears to be the principal product if fuel nitrogen is present in aromatic or cyclic form. However, when fuel nitrogen is present in the form of aliphatic amines, ammonia becomes the principal product of fuel nitrogen conversion.

In the ANSYS Fluent $\mathrm{NO}_x$ model, sources of $\mathrm{NO}_x$ emission for gaseous, liquid, and coal fuels are considered separately. The nitrogen-containing intermediates are grouped as $\mathrm{HCN}$, $\mathrm{NH}_3$, or a combination of both. Transport equations (Equation 14.1 (p. 314) and Equation 14.2 (p. 314) or Equation 14.3 (p. 315)) are solved, after which the source terms $S_{HCN}$, $S_{NH_3}$, and $S_{NO}$ are determined for different fuel types. Discussions to follow refer to fuel $\mathrm{NO}_x$ sources for $S_{NO}$ and intermediate $\mathrm{HCN}$, and $\mathrm{NH}_3$ sources for $S_{HCN}$ and $S_{NH_3}$. Contributions from thermal and prompt mechanisms have been discussed in previous sections.

### 14.1.5.3. Fuel NOx from Gaseous and Liquid Fuels

The fuel $\mathrm{NO}_x$ mechanisms for gaseous and liquid fuels are based on different physics, but the same chemical reaction pathways.

#### 14.1.5.3.1. Fuel NOx from Intermediate Hydrogen Cyanide (HCN)

When $\mathrm{HCN}$ is used as the intermediate species:

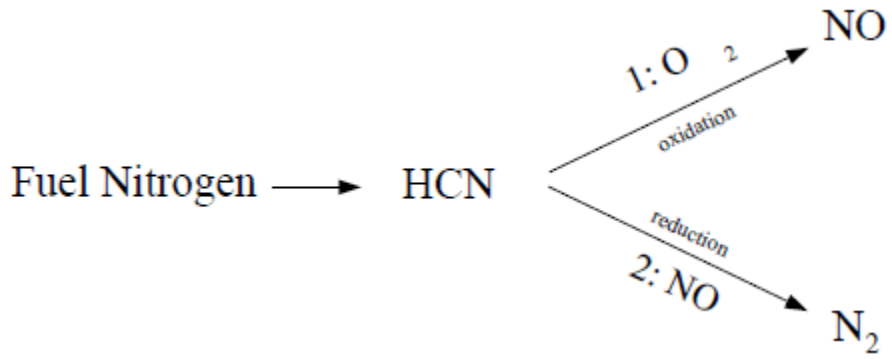


The source terms in the transport equations can be written as follows:

$$S_{HCN} = S_{pl,HCN} + S_{HCN-1} + S_{HCN-2} \tag{14.31}$$

$$S_{NO} = S_{NO-1} + S_{NO-2} \tag{14.32}$$


Release 15.0 - © SAS IP, Inc. All rights reserved. - Contains proprietary and confidential information of ANSYS, Inc. and its subsidiaries and affiliates.

#### 14.1.5.3.1.1. HCN Production in a Gaseous Fuel

The rate of $\mathrm{HCN}$ production is equivalent to the rate of combustion of the fuel:

$$S_{pl,HCN} = \frac{\mathcal{R}_{cf} Y_{N,fuel} M_{w,HCN}}{M_{w,N}} \tag{14.33}$$

where

$S_{pl,HCN}$ = source of $\mathrm{HCN}$ (kg/m$^3$–s)

$\mathcal{R}_{cf}$ = mean limiting reaction rate of fuel (kg/m$^3$–s)

$Y_{N,fuel}$ = mass fraction of nitrogen in the fuel

The mean limiting reaction rate of fuel, $\mathcal{R}_{cf}$, is calculated from the Magnussen combustion model, so the gaseous fuel $\mathrm{NO}_x$ option is available only when the generalized finite-rate model is used.

#### 14.1.5.3.1.2. HCN Production in a Liquid Fuel

The rate of $\mathrm{HCN}$ production is equivalent to the rate of fuel release into the gas phase through droplet evaporation:

$$S_{pl,HCN} = \frac{S_{fuel} Y_{N,fuel} M_{w,HCN}}{M_{w,N} V} \tag{14.34}$$

where

$S_{pl,HCN}$ = source of $\mathrm{HCN}$ (kg/m$^3$–s)

$S_{fuel}$ = rate of fuel release from the liquid droplets to the gas (kg/s)

$Y_{N,fuel}$ = mass fraction of nitrogen in the fuel

$V$ = cell volume (m$^3$)

#### 14.1.5.3.1.3. HCN Consumption

The $\mathrm{HCN}$ depletion rates from reactions (1) and (2) in the above mechanism are the same for both gaseous and liquid fuels, and are given by De Soete [90] (p. 733) as

$$\mathcal{R}_1 = A_1 X_{HCN} X_{O_2}^a e^{-E_1/RT} \tag{14.35}$$

$$\mathcal{R}_2 = A_2 X_{HCN} X_{NO} e^{-E_2/RT} \tag{14.36}$$

where

$\mathcal{R}_1, \mathcal{R}_2$ = conversion rates of $\mathrm{HCN}$ (s$^{-1}$)

$T$ = instantaneous temperature (K)

$X$ = mole fractions

$A_1 = 1.0 \times 10^{10}$ s$^{-1}$

$A_2$ = 3.0 $\times 10^{12}$ $s^{-1}$

$E_1$ = 280451.95 J/mol

$E_2$ = 251151 J/mol

The oxygen reaction order, $a$, is calculated from Equation 14.30 (p. 321).

Since mole fraction is related to mass fraction through molecular weights of the species ($M_{w,i}$) and the mixture ($M_{w,m}$),

$$X_i = Y_i \frac{M_{w,m}}{M_{w,i}} = \frac{Y_i}{M_{w,i}} \left( \frac{\rho RT}{p} \right) \tag{14.37}$$

#### 14.1.5.3.1.4. HCN Sources in the Transport Equation

The mass consumption rates of $\mathrm{HCN}$ that appear in Equation 14.31 (p. 322) are calculated as

$$S_{HCN-1} = -\mathcal{R}_1 \tag{14.38}$$

$$S_{HCN-2} = -\mathcal{R}_2 \frac{M_{w,HCN} p}{R \overline{T}} \tag{14.39}$$

where

$S_{HCN-1}$, $S_{HCN-2}$ = consumption rates of $\mathrm{HCN}$ in reactions 1 and 2, respectively ($kg/m^3$–s)

$p$ = pressure (Pa)

$\overline{T}$ = mean temperature (K)

$R$ = universal gas constant

#### 14.1.5.3.1.5. NOx Sources in the Transport Equation

$\mathrm{NO}_x$ is produced in reaction 1, but destroyed in reaction 2. The sources for Equation 14.32 (p. 322) are the same for a gaseous as for a liquid fuel, and are evaluated as follows:

$$S_{NO-1} = -S_{HCN-1} \frac{M_{w,NO}}{M_{w,HCN}} = \mathcal{R}_1 \frac{M_{w,NO} p}{R \overline{T}} \tag{14.40}$$

$$S_{NO-2} = S_{HCN-2} \frac{M_{w,NO}}{M_{w,HCN}} = -\mathcal{R}_2 \frac{M_{w,NO} p}{R \overline{T}} \tag{14.41}$$

### 14.1.5.3.2. Fuel NOx from Intermediate Ammonia (NH3)

When $\mathrm{NH}_3$ is used as the intermediate species:


Release 15.0 - © SAS IP, Inc. All rights reserved. - Contains proprietary and confidential information of ANSYS, Inc. and its subsidiaries and affiliates.

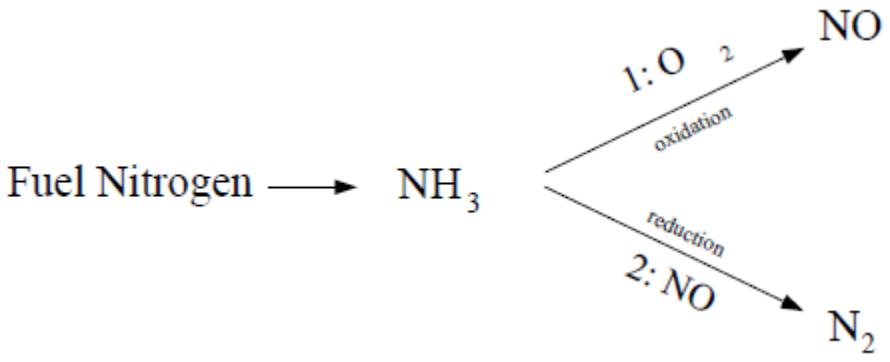


The source terms in the transport equations can be written as follows:

$$S_{NH_3} = S_{pl,NH_3} + S_{NH_3-1} + S_{NH_3-2} \tag{14.42}$$

$$S_{NO} = S_{NO-1} + S_{NO-2} \tag{14.43}$$

#### 14.1.5.3.2.1. NH3 Production in a Gaseous Fuel

The rate of $\mathrm{NH_3}$ production is equivalent to the rate of combustion of the fuel:

$$S_{pl,NH_3} = \frac{\mathcal{R}_{cf} Y_{N,fuel} M_{w,NH_3}}{M_{w,N}} \tag{14.44}$$

where

$S_{pl,NH_3}$ = source of $\mathrm{NH_3}$ ($kg/m^3-s$)

$\mathcal{R}_{cf}$ = mean limiting reaction rate of fuel (kg/m$^3$–s)

$Y_{N,fuel}$ = mass fraction of nitrogen in the fuel

The mean limiting reaction rate of fuel, $\mathcal{R}_{cf}$, is calculated from the Magnussen combustion model, so the gaseous fuel $\mathrm{NO}_x$ option is available only when the generalized finite-rate model is used.

#### 14.1.5.3.2.2. NH3 Production in a Liquid Fuel

The rate of $\mathrm{NH_3}$ production is equivalent to the rate of fuel release into the gas phase through droplet evaporation:

$$S_{pl,NH_3} = \frac{S_{fuel} Y_{N,fuel} M_{w,NH_3}}{M_{w,N} V} \tag{14.45}$$

where

$S_{pl,NH_3}$ = source of $\mathrm{NH_3}$ (kg/m$^3$–s)

$S_{fuel}$ = rate of fuel release from the liquid droplets to the gas (kg/s)

$Y_{N,fuel}$ = mass fraction of nitrogen in the fuel

$V$ = cell volume (m$^3$)

Release 15.0 - © SAS IP, Inc. All rights reserved. - Contains proprietary and confidential information of ANSYS, Inc. and its subsidiaries and affiliates.

#### 14.1.5.3.2.3. NH3 Consumption

The $NH_3$ depletion rates from reactions (1) and (2) in the above mechanism are the same for both gaseous and liquid fuels, and are given by De Soete [90] (p. 733) as

$$\begin{aligned} \mathcal{R}_1 &= A_1 X_{NH_3} X_{O_2}^a e^{-E_1/RT} \\ \mathcal{R}_2 &= A_2 X_{NH_3} X_{NO} e^{-E_2/RT} \end{aligned} \tag{14.46}$$

where

$\mathcal{R}_1, \mathcal{R}_2$ = conversion rates of $NH_3$ ($s^{-1}$)

$T$ = instantaneous temperature (K)

$X$ = mole fractions

$A_1 = 4.0 \times 10^6$ $s^{-1}$

$A_2 = 1.8 \times 10^8$ $s^{-1}$

$E_1$ = 133947.2 J/mol

$E_2$ = 113017.95 J/mol

The oxygen reaction order, $a$, is calculated from Equation 14.30 (p. 321).

Since mole fraction is related to mass fraction through molecular weights of the species ($M_{w,i}$) and the mixture ($M_{w,m}$), $X_i$ can be calculated using Equation 14.37 (p. 324).

#### 14.1.5.3.2.4. NH3 Sources in the Transport Equation

The mass consumption rates of $NH_3$ that appear in Equation 14.42 (p. 325) are calculated as

$$S_{NH_3-1} = -\mathcal{R}_1 \frac{M_{w,NH_3} p}{R\overline{T}} \tag{14.47}$$

$$S_{NH_3-2} = -\mathcal{R}_2 \frac{M_{w,NH_3} p}{R\overline{T}} \tag{14.48}$$

where

$S_{NH_3-1}, S_{NH_3-2}$ = consumption rates of $NH_3$ in reactions 1 and 2, respectively ($kg/m^3$–s)

$p$ = pressure (Pa)

$\overline{T}$ = mean temperature (K)

$R$ = universal gas constant

#### 14.1.5.3.2.5. NOx Sources in the Transport Equation

$NO_x$ is produced in reaction 1, but destroyed in reaction 2. The sources for Equation 14.43 (p. 325) are the same for a gaseous as for a liquid fuel, and are evaluated as follows:


Release 15.0 - © SAS IP, Inc. All rights reserved. - Contains proprietary and confidential information of ANSYS, Inc. and its subsidiaries and affiliates.

$$S_{NO-1} = -S_{NH_3-1}\frac{M_{w,NO}}{M_{w,NH_3}} = \mathcal{R}_1\frac{M_{w,NO}p}{R\overline{T}} \tag{14.49}$$

$$S_{NO-2} = S_{NH_3-2}\frac{M_{w,NO}}{M_{w,NH_3}} = -\mathcal{R}_2\frac{M_{w,NO}p}{R\overline{T}} \tag{14.50}$$

## 14.1.5.3.3. Fuel NOx from Coal

### *14.1.5.3.3.1. Nitrogen in Char and in Volatiles*

For the coal it is assumed that fuel nitrogen is distributed between the volatiles and the char. Since there is no reason to assume that $\mathrm{N}$ is equally distributed between the volatiles and the char, the fraction of $\mathrm{N}$ in the volatiles and the char should be specified separately.

When $\mathrm{HCN}$ is used as the intermediate species, two variations of fuel $\mathrm{NO}_x$ mechanisms for coal are included. When $\mathrm{NH_3}$ is used as the intermediate species, two variations of fuel $\mathrm{NO}_x$ mechanisms for coal are included, much like in the calculation of $\mathrm{NO}_x$ production from the coal via $\mathrm{HCN}$. It is assumed that fuel nitrogen is distributed between the volatiles and the char.

### *14.1.5.3.3.2. Coal Fuel NOx Scheme A*

The first $\mathrm{HCN}$ mechanism assumes that all char $\mathrm{N}$ converts to $\mathrm{HCN}$, which is then converted partially to $\mathrm{NO}$ [420] (p. 752). The reaction pathway is described as follows:

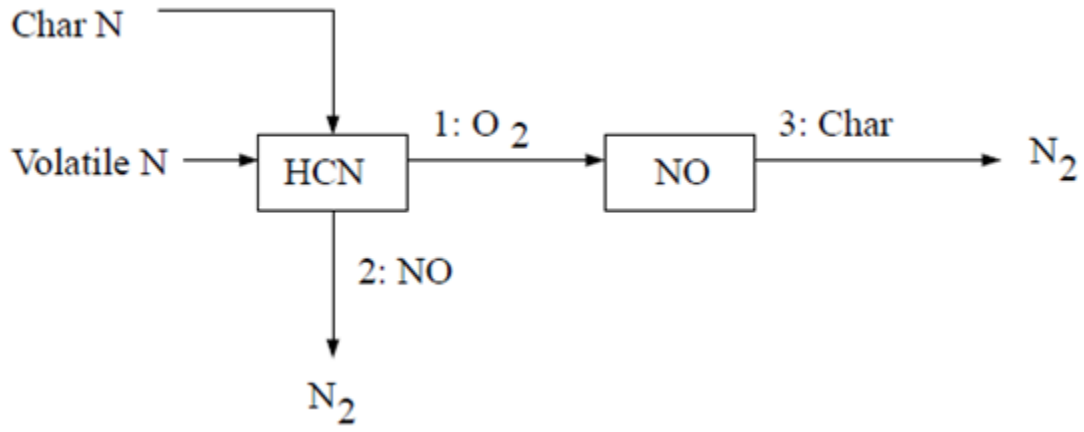


With the first scheme, all char-bound nitrogen converts to $\mathrm{HCN}$. Thus,

$$S_{char,HCN} = \frac{S_c Y_{N,char} M_{w,HCN}}{M_{w,N} V} \tag{14.51}$$

$$S_{char,NO} = 0 \tag{14.52}$$

where

$S_c$ = char burnout rate (kg/s)

$Y_{N,char}$ = mass fraction of nitrogen in char

$V$ = cell volume ($m^3$)

Release 15.0 - © SAS IP, Inc. All rights reserved. - Contains proprietary and confidential information of ANSYS, Inc. and its subsidiaries and affiliates.

#### 14.1.5.3.3.3. Coal Fuel NOx Scheme B

The second $\mathrm{HCN}$ mechanism assumes that all char $\mathrm{N}$ converts to $\mathrm{NO}$ directly [264] (p. 743). The reaction pathway is described as follows:

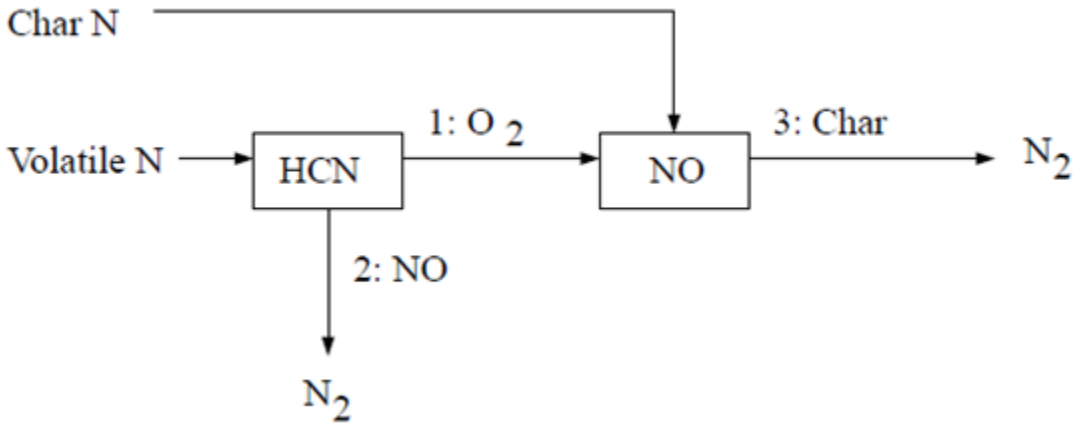


According to Lockwood [264] (p. 743), the char nitrogen is released to the gas phase as $\mathrm{NO}$ directly, mainly as a desorption product from oxidized char nitrogen atoms. If this approach is followed, then

$$S_{char,HCN} = 0 \tag{14.53}$$

$$S_{char,NO} = \frac{S_c Y_{N,char} M_{w,NO}}{M_{w,N} V} \tag{14.54}$$

#### 14.1.5.3.3.4. HCN Scheme Selection

The second $\mathrm{HCN}$ mechanism tends to produce more $\mathrm{NO}_x$ emission than the first. In general, however, it is difficult to say which one outperforms the other.

The source terms for the transport equations are

$$S_{HCN} = S_{pvc,HCN} + S_{HCN-1} + S_{HCN-2} \tag{14.55}$$

$$S_{NO} = S_{char,NO} + S_{NO-1} + S_{NO-2} + S_{NO-3} \tag{14.56}$$

The source contributions $S_{HCN-1}$, $S_{HCN-2}$, $S_{NO-1}$, and $S_{NO-2}$ are described previously. Therefore, only the heterogeneous reaction source, $S_{NO-3}$, the char $\mathrm{NO}_x$ source, $S_{char,NO}$, and the $\mathrm{HCN}$ production source, $S_{pvc,HCN}$, need to be considered.

#### 14.1.5.3.3.5. NOx Reduction on Char Surface

The heterogeneous reaction of $\mathrm{NO}$ reduction on the char surface has been modeled according to the following [245] (p. 742):

$$\mathcal{R}_3 = A_3 e^{-E_3/RT} \overline{p}_{NO} \tag{14.57}$$

where

$\mathcal{R}_3$ = rate of $\mathrm{NO}$ reduction $(\mathrm{mol}/\mathrm{m}^2_{\mathrm{BET}}-\mathrm{s})$


Release 15.0 - © SAS IP, Inc. All rights reserved. - Contains proprietary and confidential information of ANSYS, Inc. and its subsidiaries and affiliates.

$\overline{p}_{NO}$ = mean $\mathrm{NO}$ partial pressure (atm)

$E_3$ = 142737.485 $\mathrm{J/mol}$

$A_3$ = 230 $\mathrm{mol/m^2_{BET}-s-atm}$

$\overline{T}$ = mean temperature (K)

The partial pressure $\overline{p}_{NO}$ is calculated using Dalton's law:

$$\overline{p}_{NO} = \overline{p} X_{NO}$$

The rate of $\mathrm{NO}$ consumption due to reaction 3 will then be

$$S_{NO-3} = c_s A_{BET} M_{w,NO} \mathcal{R}_3$$

where

$A_{BET}$ = BET surface area ($\mathrm{m^2/kg}$)

$c_s$ = concentration of particles ($\mathrm{kg/m^3}$)

$S_{NO-3}$ = $\mathrm{NO}$ consumption ($\mathrm{kg/m^3-s}$)

#### 14.1.5.3.3.5.1. BET Surface Area

The heterogeneous reaction involving char is mainly an adsorption process, whose rate is directly proportional to the pore surface area. The pore surface area is also known as the BET surface area, due to the researchers who pioneered the adsorption theory (Brunauer, Emmett, and Teller [51] (p. 731)). For commercial adsorbents, the pore (BET) surface areas range from 100,000 to 2 million square meters per kilogram, depending on the microscopic structure. For coal, the BET area is typically 25,000 $\mathrm{m^2/kg}$, which is used as the default in ANSYS Fluent. The overall source of $\mathrm{HCN}$ ($S_{pvc,HCN}$) is a combination of volatile contribution ($S_{vol,HCN}$) and char contribution ($S_{char,HCN}$):

$$S_{pvc,HCN} = S_{vol,HCN} + S_{char,HCN}$$

#### 14.1.5.3.3.5.2. HCN from Volatiles

The source of $\mathrm{HCN}$ from the volatiles is related to the rate of volatile release:

$$S_{vol,HCN} = \frac{S_{vol} Y_{N,vol} M_{w,HCN}}{M_{w,N} V}$$

where

$S_{vol}$ = source of volatiles originating from the coal particles into the gas phase (kg/s)

$Y_{N,vol}$ = mass fraction of nitrogen in the volatiles

$V$ = cell volume ($\mathrm{m^3}$)

Calculation of sources related to char-bound nitrogen depends on the fuel $\mathrm{NO}_x$ scheme selection.

Release 15.0 - © SAS IP, Inc. All rights reserved. - Contains proprietary and confidential information of ANSYS, Inc. and its subsidiaries and affiliates.

#### 14.1.5.3.3.6. Coal Fuel NOx Scheme C

The first $NH_3$ mechanism assumes that all char $N$ converts to $NH_3$ which is then converted partially to $NO$ [420] (p. 752). The reaction pathway is described as follows:

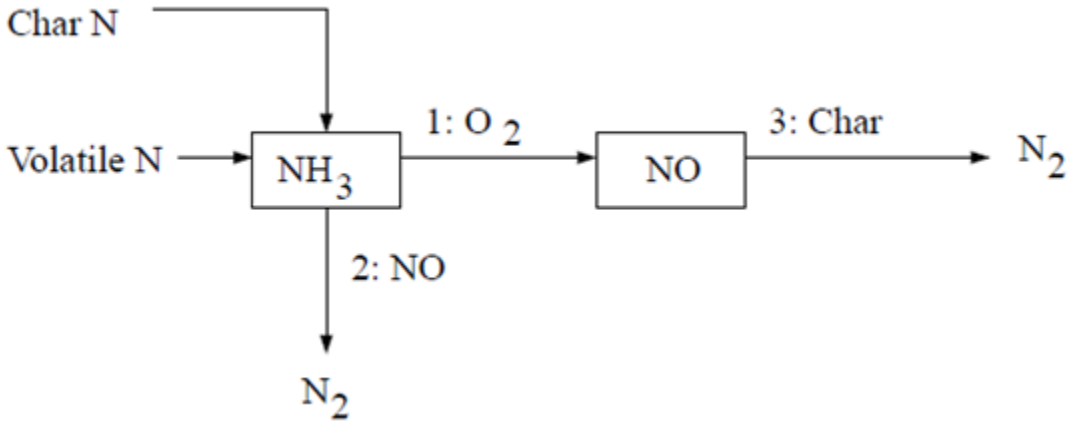


In this scheme, all char-bound nitrogen converts to $NH_3$. Thus,

$$S_{char,NH_3} = \frac{S_c Y_{N,char} M_{w,NH_3}}{M_{w,N} V} \tag{14.58}$$

$$S_{char,NO} = 0 \tag{14.59}$$

where

$S_c$ = char burnout rate (kg/s)

$Y_{N,char}$ = mass fraction of nitrogen in char

$V$ = cell volume ($m^3$)

#### 14.1.5.3.3.7. Coal Fuel NOx Scheme D

The second $NH_3$ mechanism assumes that all char $N$ converts to $NO$ directly [264] (p. 743). The reaction pathway is described as follows:

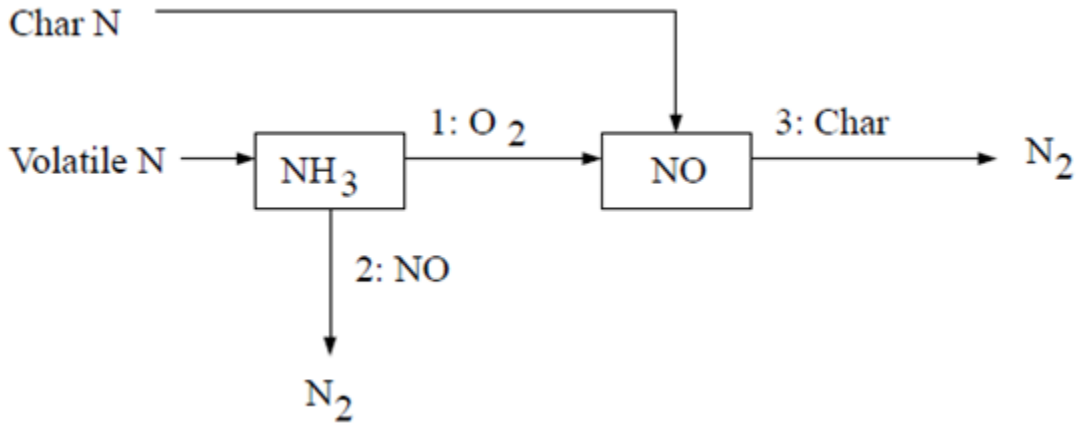



Release 15.0 - © SAS IP, Inc. All rights reserved. - Contains proprietary and confidential information of ANSYS, Inc. and its subsidiaries and affiliates.

According to Lockwood [264] (p. 743), the char nitrogen is released to the gas phase as $NO$ directly, mainly as a desorption product from oxidized char nitrogen atoms. If this approach is followed, then

$$S_{char,NH_3} = 0 \tag{14.60}$$

$$S_{char,NO} = \frac{S_c Y_{N,char} M_{w,NO}}{M_{w,N} V} \tag{14.61}$$

#### *14.1.5.3.3.8. NH3 Scheme Selection*

The second $NH_3$ mechanism tends to produce more $NO_x$ emission than the first. In general, however, it is difficult to say which one outperforms the other.

The source terms for the transport equations are

$$S_{NH_3} = S_{pvc,NH_3} + S_{NH_3-1} + S_{NH_3-2} \tag{14.62}$$

$$S_{NO} = S_{char,NO} + S_{NO-1} + S_{NO-2} + S_{NO-3} \tag{14.63}$$

The source contributions $S_{NH_3-1}$, $S_{NH_3-2}$, $S_{NO-1}$, $S_{NO-2}$, $S_{NO-3}$, and $S_{char,NO}$ are described previously. Therefore, only the $NH_3$ production source, $S_{pvc,NH_3}$, must be considered.

The overall production source of $NH_3$ is a combination of volatile contribution ($S_{vol,NH_3}$), and char contribution ($S_{char,NH_3}$):

$$S_{pvc,NH_3} = S_{vol,NH_3} + S_{char,NH_3} \tag{14.64}$$

##### 14.1.5.3.3.8.1. NH3 from Volatiles

The source of $NH_3$ from the volatiles is related to the rate of volatile release:

$$S_{vol,NH_3} = \frac{S_{vol} Y_{N,vol} M_{w,NH_3}}{M_{w,N} V}$$

where

$S_{vol}$ = source of volatiles originating from the coal particles into the gas phase (kg/s)

$Y_{N,vol}$ = mass fraction of nitrogen in the volatiles

$V$ = cell volume ($m^3$)

Calculation of sources related to char-bound nitrogen depends on the fuel $NO_x$ scheme selection.

### 14.1.5.3.4. Fuel Nitrogen Partitioning for HCN and NH3 Intermediates

In certain cases, especially when the fuel is a solid, both $HCN$ and $NH_3$ can be generated as intermediates at high enough temperatures [318] (p. 746). In particular, low-ranking (lignite) coal has been shown to produce 10 times more $NH_3$ compared to the level of $HCN$, whereas higher-ranking (bituminous) coal has been shown to produce only $HCN$ [317] (p. 746). Studies by Winter et al. [496] (p. 756) have shown that for bituminous coal, using an $HCN/NH_3$ partition ratio of 9:1 gave better $NO_x$ predictions

when compared to measurements than specifying only a single intermediate species. Liu and Gibbs [263] (p. 743) work with woody-biomass (pine wood chips), on the other hand, has suggested an $HCN/NH_3$ ratio of 1:9 due to the younger age of the fuel.

In total, the above work suggests the importance of being able to specify that portions of the fuel nitrogen will be converted to both $HCN$ and $NH_3$ intermediates at the same time. In ANSYS Fluent, fuel nitrogen partitioning can be used whenever $HCN$ or $NH_3$ are intermediates for $NO_x$ production, though it is mainly applicable to solid fuels such as coal and biomass. The reaction pathways and source terms for $HCN$ and $NH_3$ are described in previous sections.

## 14.1.6. NOx Formation from Intermediate N2O

Melte and Pratt [288] (p. 744) proposed the first intermediate mechanism for $NO_x$ formation from molecular nitrogen ($N_2$) via nitrous oxide ($N_2O$). Nitrogen enters combustion systems mainly as a component of the combustion and dilution air. Under favorable conditions, which are elevated pressures and oxygen-rich conditions, this intermediate mechanism can contribute as much as 90% of the $NO_x$ formed during combustion. This makes it particularly important in equipment such as gas turbines and compression-ignition engines. Because these devices are operated at increasingly low temperatures to prevent $NO_x$ formation via the thermal $NO_x$ mechanism, the relative importance of the $N_2O$-intermediate mechanism is increasing. It has been observed that about 30% of the $NO_x$ formed in these systems can be attributed to the $N_2O$-intermediate mechanism.

The $N_2O$-intermediate mechanism may also be of importance in systems operated in flameless mode (for example, diluted combustion, flameless combustion, flameless oxidation, and FLOX systems). In a flameless mode, fuel and oxygen are highly diluted in inert gases so that the combustion reactions and resulting heat release are carried out in the diffuse zone. As a consequence, elevated peaks of temperature are avoided, which prevents thermal $NO_x$. Research suggests that the $N_2O$-intermediate mechanism may contribute about 90% of the $NO_x$ formed in flameless mode, and that the remainder can be attributed to the prompt $NO_x$ mechanism. The relevance of $NO_x$ formation from $N_2O$ has been observed indirectly and theoretically speculated for a number of combustion systems, by a number of researchers [17] (p. 729), [78] (p. 733), [141] (p. 736), [435] (p. 753), [442] (p. 753).

### 14.1.6.1. N2O - Intermediate NOx Mechanism

The simplest form of the mechanism [288] (p. 744) takes into account two reversible elementary reactions:

$$N_2 + O + M \rightleftharpoons N_2O + M \tag{14.65}$$

$$N_2O + O \rightleftharpoons 2NO \tag{14.66}$$

Here, $M$ is a general third body. Because the first reaction involves third bodies, the mechanism is favored at elevated pressures. Both reactions involve the oxygen radical $O$, which makes the mechanism favored for oxygen-rich conditions. While not always justified, it is often assumed that the radical $O$ atoms originate solely from the dissociation of molecular oxygen,

$$\frac{1}{2}O_2 \rightleftharpoons O \tag{14.67}$$

According to the kinetic rate laws, the rate of $NO_x$ formation via the $N_2O$-intermediate mechanism is


Release 15.0 - © SAS IP, Inc. All rights reserved. - Contains proprietary and confidential information of ANSYS, Inc. and its subsidiaries and affiliates.

$$\frac{d[NO]}{dt} = 2\left(k_{f,2}[N_2O][O] - k_{r,2}[NO]^2\right) \qquad \text{mol/m}^3\text{-s} \tag{14.68}$$

To solve Equation 14.68 (p. 333), you will need to have first calculated [O] and [$N_2O$].

It is often assumed that $N_2O$ is at quasi-steady-state (that is, $d[N_2O]/dt = 0$), which implies

$$[N_2O] = \frac{k_{f,1}[N_2][O][M] + k_{r,2}[NO]^2}{k_{r,1}[M] + k_{f,2}[O]} \tag{14.69}$$

The system of Equation 14.68 (p. 333) – Equation 14.69 (p. 333) can be solved for the rate of $NO_x$ formation when the concentration of $N_2$, $O_2$, and M, the kinetic rate constants for Equation 14.65 (p. 332) and Equation 14.66 (p. 332), and the equilibrium constant of Equation 14.67 (p. 332) are known. The appearance of NO in Equation 14.66 (p. 332) entails that coupling of the $N_2O$ mechanism with the thermal $NO_x$ mechanism (and other $NO_x$ mechanisms).

$$k_{f,1} = 4.44\times10^{32}T^{-8.358}e^{-28234/T} \qquad k_{r,1} = 4.00\times10^{8}e^{-28234/T}$$

$$k_{f,2} = 2.90\times10^{7}e^{-11651/T} \qquad k_{r,2} = 1.45\times10^{-29}T^{9.259}e^{-11651/T}$$

In the above expressions, $k_{f,1}$ and $k_{f,2}$ are the forward rate constants of Equation 14.65 (p. 332) and Equation 14.66 (p. 332), and $k_{r,1}$ and $k_{r,2}$ are the corresponding reverse rate constants. The units for $k_{f,2}$, $k_{r,1}$, and $k_{r,2}$ are $\text{m}^3/\text{mol}-\text{s}$, while $k_{f,1}$ has units of $\text{m}^6/\text{mol}^2-\text{s}$.

## 14.1.7. NOx Reduction by Reburning

The design of complex combustion systems for utility boilers, based on air- and fuel-staging technologies, involves many parameters and their mutual interdependence. These parameters include the local stoichiometry, temperature and chemical concentration field, residence time distribution, velocity field, and mixing pattern. A successful application of the in-furnace reduction techniques requires control of these parameters in an optimum manner, so as to avoid impairing the boiler performance. In the mid 1990s, global models describing the kinetics of $NO_x$ destruction in the reburn zone of a staged combustion system became available. Two of these models are described below.

### 14.1.7.1. Instantaneous Approach

The instantaneous $NO_x$ reburning mechanism is a pathway whereby NO reacts with hydrocarbons and is subsequently reduced. In general:

$$CH_i + NO \rightarrow HCN + \text{products} \tag{14.70}$$

Three reburn reactions are modeled by ANSYS Fluent for $1600 \le T \le 2100$:

$$CH + NO \xrightarrow{k_1} HCN + O \tag{14.71}$$

$$CH_2 + NO \xrightarrow{k_2} HCN + OH \tag{14.72}$$

Release 15.0 - © SAS IP, Inc. All rights reserved. - Contains proprietary and confidential information of ANSYS, Inc. and its subsidiaries and affiliates.

$$CH_3 + NO \xrightarrow{k_3} HCN + H_2O \tag{14.73}$$

**Important**

If the temperature is outside of this range, $NO$ reburn will not be computed.

The rate constants for these reactions are taken from Bowman [39] (p. 731) and have units of $m^3/mol-s$:

$$k_1 = 1 \times 10^8;\ k_2 = 1.4 \times 10^6 e^{-550/T};\ k_3 = 2 \times 10^5$$

The $NO$ depletion rate due to reburn is expressed as

$$\frac{d[NO]}{dt} = -k_1[CH][NO] - k_2[CH_2][NO] - k_3[CH_3][NO] \tag{14.74}$$

and the source term for the reburning mechanism in the $NO$ transport equation can be calculated as

$$S_{reburn,NO} = -M_{w,NO}\frac{d[NO]}{dt} \tag{14.75}$$

**Important**

To calculate the $NO$ depletion rate due to reburning, ANSYS Fluent will obtain the concentrations of $CH$, $CH_2$, and $CH_3$ from the species mass fraction results of the combustion calculation. When you use this method, you must be sure to include the species $CH$, $CH_2$, and $CH_3$ in your problem definition.

### 14.1.7.2. Partial Equilibrium Approach

The partial equilibrium approach is based on the model proposed by Kandamby et al. [195] (p. 739), [9] (p. 729). The model adds a reduction path to De Soete's global model [90] (p. 733) that describes the $NO_x$ formation/destruction mechanism in a pulverized coal flame. The additional reduction path accounts for the $NO_x$ destruction in the fuel-rich reburn zone by $CH$ radicals (see Figure 14.1: De Soete's Global NOx Mechanism with Additional Reduction Path (p. 334)).

**Figure 14.1: De Soete's Global NOx Mechanism with Additional Reduction Path**

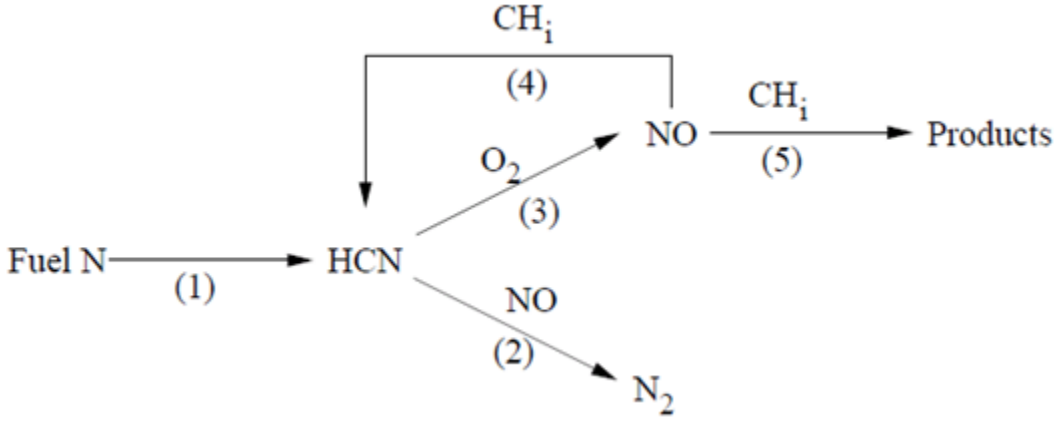



Release 15.0 - © SAS IP, Inc. All rights reserved. - Contains proprietary and confidential information of ANSYS, Inc. and its subsidiaries and affiliates.

This model can be used in conjunction with the eddy-dissipation combustion model and does not require the specification of $CH$ radical concentrations, because they are computed based on the $CH$-radical partial equilibrium. The reburn fuel itself can be an equivalent of $CH_4$, $CH_3$, $CH_2$, or $CH$. How this equivalent fuel is determined is open for debate, and an approximate guide would be to consider the $C/H$ ratio of the fuel itself. A multiplicative constant of $4.0\times10^{-4}$ has been developed for the partial equilibrium of $CH$ radicals to reduce the rates of $HCN$ and $NO$ in the reburn model. This value was obtained by researchers who developed the model, by way of predicting $NO_x$ values for a number of test cases for which experimental data exists.

### 14.1.7.2.1. NOx Reduction Mechanism

In the fuel-rich reburn zone, the $HCN$ oxidation is suppressed and the amount of $NO$ formed in the primary combustion zone is decreased by the reduction reaction from $HCN$ to $N_2$. However, the $NO$ concentration may also decrease due to reactions with $CH$ radicals, which are available in significant amounts in the reburn zone. The following are considered to be the most important reactions of $NO$ reduction by $CH$ radicals:

$$NO+CH_2 \rightarrow HCN+OH \tag{14.76}$$

$$NO+CH \rightarrow HCN+O \tag{14.77}$$

$$NO+C \rightarrow CN+O \tag{14.78}$$

These reactions may be globally described by the addition of pathways (4) and (5) in Figure 14.1: De Soete's Global NOx Mechanism with Additional Reduction Path (p. 334), leading respectively to the formation of $HCN$ and of minor intermediate nitrogen radicals. Assuming that methane is the reburning gas, the global $NO$ reduction rates are then expressed as

$$\mathcal{R}_4 = \left(k_a\chi_1+k_b\chi_1^2\right)[CH_4][NO] \tag{14.79}$$

$$\mathcal{R}_5 = k_c\chi_1^3\chi_2[CH_4][NO] \tag{14.80}$$

where

$$\chi_1=\frac{[H]}{[H_2]};\ \chi_2=\frac{[OH]}{[H_2O]}$$

Therefore, the additional source terms of the $HCN$ and $NO$ transport equations due to reburn reactions are given by

$$\frac{d[HCN]}{dt} = 4\times10^{-4}\mathcal{R}_4 \tag{14.81}$$

$$\frac{d[NO]}{dt} = -4\times10^{-4}(\mathcal{R}_4+\mathcal{R}_5) \tag{14.82}$$

Certain assumptions are required to evaluate the rate constants $k_a$, $k_b$, and $k_c$ and the factors $\chi_1$ and $\chi_2$. For hydrocarbon diffusion flames, the following reaction set can be reasonably considered to be in partial equilibrium:

$$CH_4+H \rightleftharpoons CH_3+H_2 \tag{14.83}$$

Release 15.0 - © SAS IP, Inc. All rights reserved. - Contains proprietary and confidential information of ANSYS, Inc. and its subsidiaries and affiliates.

$$CH_3+OH \rightleftharpoons CH_2+H_2O \tag{14.84}$$

$$CH_2+H \rightleftharpoons CH+H_2 \tag{14.85}$$

$$CH+H \rightleftharpoons C+H_2 \tag{14.86}$$

Thus, the rate constants may be computed as

$$k_a=k_1\frac{k_{f,4}k_{f,5}}{k_{r,4}k_{r,5}};\ k_b=k_2\frac{k_{f,4}k_{f,5}k_{f,6}}{k_{r,4}k_{r,5}k_{r,6}};\ k_c=k_3\frac{k_{f,4}k_{f,5}k_{f,6}k_{f,7}}{k_{r,4}k_{r,5}k_{r,6}k_{r,7}}$$

where $k_1$, $k_2$, and $k_3$ are the rate constants for Equation 14.76 (p. 335) – Equation 14.78 (p. 335). The forward and reverse rate constants for Equation 14.83 (p. 335) – Equation 14.86 (p. 336) are $k_{f,4}$– $k_{f,7}$ and $k_{r,4}$– $k_{r,7}$, respectively. In addition, it is assumed that $\chi_1=1$, because the $H$-radical concentration in the post-flame region of a hydrocarbon diffusion flame has been observed to be of the same order as $[H_2]$. Finally, the $OH$-radical concentration is estimated by considering the reaction

$$OH+H_2 \rightleftharpoons H_2O+H \tag{14.87}$$

to be partially equilibrated, leading to the relationship

$$\chi_2=\frac{k_{r,8}}{k_{f,8}}$$

Values for the rate constants $k_a$, $k_b$, and $k_c$ for different equivalent fuel types are given in Arrhenius form ($AT^be^{-E/RT}$) in Table 14.1: Rate Constants for Different Reburn Fuels (p. 336) [243] (p. 742). All rate constants have units of $m^3/mol-s$, and all values of $E$ have units of $J/mol$.

**Table 14.1: Rate Constants for Different Reburn Fuels**

| Equivalent Fuel Type | $k_a$ | | | $k_b$ | | | $k_c$ | | |
|---|---|---|---|---|---|---|---|---|---|
| | $A$ | $b$ | $E$ | $A$ | $b$ | $E$ | $A$ | $b$ | $E$ |
| $CH_4$ | $5.30\times10^9$ | -1.54 | 27977 | $3.31\times10^{13}$ | -3.33 | 15090 | $3.06\times10^{11}$ | -2.64 | 77077 |
| $CH_3$ | $0.37\times10^9$ | -1.54 | 27977 | $0.23\times10^{13}$ | -3.33 | 15090 | $0.21\times10^{11}$ | -2.64 | 77077 |
| $CH_2$ | $0.23\times10^7$ | -1.54 | 27977 | $0.14\times10^{11}$ | -3.33 | 15090 | $0.13\times10^9$ | -2.64 | 77077 |
| $CH$ | 0.0 | 0.0 | 0.0 | $0.63\times10^8$ | -3.33 | 15090 | $0.58\times10^6$ | -2.64 | 77077 |

For Equation 14.87 (p. 336),

$$k_{f,8}=1.02\times10^5T^{1.60}e^{-13802/RT};\ k_{r,8}=4.52\times10^5T^{1.60}e^{-80815/RT}$$

## 14.1.8. NOx Reduction by SNCR

The selective noncatalytic reduction of $NO_x$ (SNCR), first described by Lyon [275] (p. 744), is a method to reduce the emission of $NO_x$ from combustion by injecting a selective reductant such as ammonia


Release 15.0 - © SAS IP, Inc. All rights reserved. - Contains proprietary and confidential information of ANSYS, Inc. and its subsidiaries and affiliates.

($NH_3$) or urea ($CO(NH_2)_2$) into the furnace, where it can react with $NO$ in the flue gas to form $N_2$. However, the reductant can be oxidized as well to form $NO_x$. The selectivity for the reductive reactions decreases with increasing temperature [297] (p. 745), while the rate of the initiation reaction simultaneously increases. This limits the SNCR process to a narrow temperature interval, or window, where the lower temperature limit for the interval is determined by the residence time.

### 14.1.8.1. Ammonia Injection

Several investigators have modeled the process using a large number of elementary reactions. A simple empirical model has been proposed by Fenimore [114] (p. 735), which is based on experimental measurements. However, the model was found to be unsuitable for practical applications. Ostberg and Dam-Johansen [336] (p. 747) proposed a two-step scheme describing the SNCR process as shown in Figure 14.2: Simplified Reaction Mechanism for the SNCR Process (p. 337), which is a single initiation step followed by two parallel reaction pathways: one leading to $NO$ reduction, and the other to $NO$ formation.

**Figure 14.2: Simplified Reaction Mechanism for the SNCR Process**

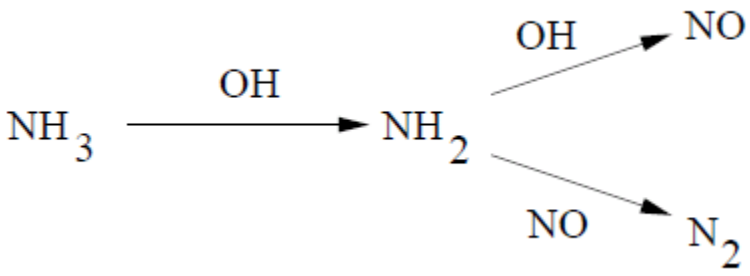


$$NO + NH_3 + \frac{1}{4}O_2 \rightarrow N_2 + \frac{3}{2}H_2O \tag{14.88}$$

$$NH_3 + \frac{5}{4}O_2 \rightarrow NO + \frac{3}{2}H_2O \tag{14.89}$$

The reaction orders of $NO$ and $NH_3$ at 4% volume $O_2$ and the empirical rate constants $k_r$ and $k_{ox}$ for Equation 14.88 (p. 337) Equation 14.89 (p. 337), respectively, have been estimated from work done by Brouwer et al. [48] (p. 731). The reaction order of $NO$ was found to be 1 for Equation 14.88 (p. 337) and the order of $NH_3$ was found to be 1 for both reactions. As such, the following reaction rates for $NO$ and $NH_3$, at 4% volume $O_2$, were proposed:

$$\mathcal{R}_{NO} = -k_r[NO][NH_3] + k_{ox}[NH_3][O_2] \tag{14.90}$$

$$\mathcal{R}_{NH_3} = -k_r[NO][NH_3] - k_{ox}[NH_3][O_2] \tag{14.91}$$

The rate constants $k_r$ and $k_{ox}$ have units of m$^3$/mol-s, and are defined as

$$k_r = 4.24\times10^2 T^{5.30} e^{-E_r/RT};\ k_{ox} = 3.50\times10^{-1} T^{7.65} e^{-E_{ox}/RT}$$

where $E_r = 349937.06$ J/mol and $E_{ox} = 524487.005$ J/mol.

Release 15.0 - © SAS IP, Inc. All rights reserved. - Contains proprietary and confidential information of ANSYS, Inc. and its subsidiaries and affiliates.

This model has been shown to give reasonable predictions of the SNCR process in pulverized coal and fluidized bed combustion applications. The model also captures the influence of the most significant parameters for SNCR, which are the temperature of the flue gas at the injection position, the residence time in the relevant temperature interval, the $NH_3$ to $NO$ molar ratio, and the effect of combustible additives. This model overestimates the $NO$ reduction for temperatures above the optimum temperature by an amount similar to that of the detailed kinetic model of Miller and Bowman [297] (p. 745).

**Important**

The SNCR process naturally occurs when $NH_3$ is present in the flame as a fuel $N$ intermediate. For this reason, even if the SNCR model is not activated and there is no reagent injection, the natural SNCR process may still occur in the flame. The temperature range or "window" at which SNCR may occur is 1073 K < T < 1373 K. If you want to model your case without using the natural SNCR process, contact your support engineer for information on how to deactivate it.

### 14.1.8.2. Urea Injection

Urea as a reagent for the SNCR process is similar to that of injecting ammonia, and has been used in power station combustors to reduce $NO$ emissions successfully. However, both reagents, ammonia and urea, have major limitations as a $NO_x$ reducing agent. The narrow temperature "window" of effectiveness and mixing limitations are difficult factors to handle in a large combustor. The use of urea instead of ammonia as the reducing agent is attractive because of the ease of storage and handling of the reagent.

The SNCR process using urea is a combination of Thermal DeNOx (SNCR with ammonia) and RAPRENOx (SNCR using cyanuric acid that, under heating, sublimes and decomposes into isocyanic acid), because urea most probably decomposes into ammonia and isocyanic acid [297] (p. 745).

One problem of SNCR processes using urea is that slow decay of $HNCO$, as well as the reaction channels leading to $N_2O$ and $CO$, can significantly increase the emission of pollutants other than $NO$. Urea seems to involve a significant emission of carbon-containing pollutants, such as $CO$ and $HNCO$.

Also, some experimental observations [382] (p. 750) show that SNCR using urea is effective in a narrow temperature window that is shifted toward higher temperatures, when compared to Thermal DeNOx processes at the same value of the ratio of nitrogen in the reducing agent and the $NO$ in the feed, $\beta$, where $\beta$ is defined as the ratio of nitrogen in the reducing agent and $NO$ in the feed. The effect of increasing the $\beta$ value is to increase the efficiency of abatement, while the effect of increasing $O_2$ concentration depends on the temperature considered.

The model described here is proposed by Brouwer et al. [48] (p. 731) and is a seven-step reduced kinetic mechanism. Brouwer et al. [48] (p. 731) assumes that the breakdown of urea is instantaneous and 1 mole of urea is assumed to produce 1.1 moles of $NH_3$ and 0.9 moles of $HNCO$. The work of Rota et al. [382] (p. 750) proposed a finite rate two-step mechanism for the breakdown of urea into ammonia and $HNCO$.


Release 15.0 - © SAS IP, Inc. All rights reserved. - Contains proprietary and confidential information of ANSYS, Inc. and its subsidiaries and affiliates.

The seven-step reduced mechanism is given in Table 14.2: Seven-Step Reduced Mechanism for SNCR with Urea (p. 339), and the two-step urea breakdown mechanism is given in Table 14.3: Two-Step Urea Breakdown Process (p. 339).

**Table 14.2: Seven-Step Reduced Mechanism for SNCR with Urea**

| Reaction | A | b | E |
|---|---|---|---|
| $NH_3 + NO \rightarrow N_2 + H_2O + H$ | 4.24E+02 | 5.30 | 349937.06 |
| $NH_3 + O_2 \rightarrow NO + H_2O + H$ | 3.500E-01 | 7.65 | 524487.005 |
| $HNCO + M \rightarrow H + NCO + M$ | 2.400E+08 | 0.85 | 284637.8 |
| $NCO + NO \rightarrow N_2O + CO$ | 1.000E+07 | 0.00 | -1632.4815 |
| $NCO + OH \rightarrow NO + CO + H$ | 1.000E+07 | 0.00 | 0 |
| $N_2O + OH \rightarrow N_2 + O_2 + H$ | 2.000E+06 | 0.00 | 41858.5 |
| $N_2O + M \rightarrow N_2 + O + M$ | 6.900E+17 | -2.5 | 271075.646 |

**Table 14.3: Two-Step Urea Breakdown Process**

| Reaction | A | b | E |
|---|---|---|---|
| $CO(NH_2)_2 \rightarrow NH_3 + HNCO$ | 1.27E+04 | 0 | 65048.109 |
| $CO(NH_2)_2 + H_2O \rightarrow 2NH_3 + CO_2$ | 6.13E+04 | 0 | 87819.133 |

where SI units (m, mol, sec, J) are used in Table 14.2: Seven-Step Reduced Mechanism for SNCR with Urea (p. 339) and Table 14.3: Two-Step Urea Breakdown Process (p. 339).

### 14.1.8.3. Transport Equations for Urea, HNCO, and NCO

When the SNCR model with urea injection is employed in addition to the usual transport equations, ANSYS Fluent solves the following three additional mass transport equations for the urea, $HNCO$, and $NCO$ species.

$$\frac{\partial}{\partial t}\left(\rho Y_{CO(NH_2)_2}\right) + \nabla \cdot \left(\rho \vec{v}\, Y_{CO(NH_2)_2}\right) = \nabla \cdot \left(\rho \mathcal{D} Y_{CO(NH_2)_2}\right) + S_{CO(NH_2)_2} \tag{14.92}$$

$$\frac{\partial}{\partial t}(\rho Y_{HNCO}) + \nabla \cdot (\rho \vec{v}\, Y_{HNCO}) = \nabla \cdot (\rho \mathcal{D} Y_{HNCO}) + S_{HNCO} \tag{14.93}$$

$$\frac{\partial}{\partial t}(\rho Y_{NCO}) + \nabla \cdot (\rho \vec{v}\, Y_{NCO}) = \nabla \cdot (\rho \mathcal{D} Y_{NCO}) + S_{NCO} \tag{14.94}$$

where $Y_{CO(NH_2)_2}$, $Y_{HNCO}$ and $Y_{NCO}$ are mass fractions of urea, $HNCO$, and $NCO$ in the gas phase.

The source terms $S_{CO(NH_2)_2}$, $S_{HNCO}$, and $S_{NCO}$ are determined according to the rate equations given in Table 14.2: Seven-Step Reduced Mechanism for SNCR with Urea (p. 339) and Table 14.3: Two-Step Urea Breakdown Process (p. 339) and the additional source terms due to reagent injection. These additional source terms are determined next. The source terms in the transport equations can be written as follows:

$$S_{CO(NH_2)_2} = S_{pl,CO(NH_2)_2} + S_{CO(NH_2)_2 - reac} \tag{14.95}$$

$$S_{HNCO} = S_{pl,HNCO} + S_{HNCO-reac} \tag{14.96}$$

Release 15.0 - © SAS IP, Inc. All rights reserved. - Contains proprietary and confidential information of ANSYS, Inc. and its subsidiaries and affiliates.

$$S_{NCO}=S_{NCO-reac} \tag{14.97}$$

Apart from the source terms for the above three species, additional source terms for $\mathrm{NO}$, $\mathrm{NH_3}$, and $\mathrm{N_2O}$ are also determined as follows, which should be added to the previously calculated sources due to fuel $\mathrm{NO}_x$:

$$S_{NO}=S_{NO-reac} \tag{14.98}$$

$$S_{NH_3}=S_{pl,NH_3}+S_{NH_3-reac} \tag{14.99}$$

$$S_{N_2O}=S_{N_2O-reac} \tag{14.100}$$

The source terms $S_{i-reac}$ for $i^{th}$ species are determined from the rate equations given in Table 14.2: Seven-Step Reduced Mechanism for SNCR with Urea (p. 339) and Table 14.3: Two-Step Urea Breakdown Process (p. 339).

### 14.1.8.4. Urea Production due to Reagent Injection

The rate of urea production is equivalent to the rate of reagent release into the gas phase through droplet evaporation:

$$S_{pl,CO(NH_2)_2}=\frac{S_{reagent}}{V} \tag{14.101}$$

where $S_{reagent}$ is the rate of reagent release from the liquid droplets to the gas phase (kg/s) and $V$ is the cell volume ($m^3$).

### 14.1.8.5. NH3 Production due to Reagent Injection

If the urea decomposition model is set to the **user-specified** option, then the rate of $\mathrm{NH_3}$ production is proportional to the rate of reagent release into the gas phase through droplet evaporation:

$$S_{pl,NH_3}=MCF_{NH_3}\frac{S_{reagent}}{V} \tag{14.102}$$

where $S_{reagent}$ is the rate of reagent release from the liquid droplets to the gas phase (kg/s), $MCF_{NH_3}$ is the mole fraction of $NH_3$ in the $NH_3/HNCO$ mixture created from urea decomposition, and $V$ is the cell volume ($m^3$).

### 14.1.8.6. HNCO Production due to Reagent Injection

If the urea decomposition model is set to the **user-specified** option, then the rate of $\mathrm{HNCO}$ production is proportional to the rate of reagent release into the gas phase through droplet evaporation:

$$S_{pl,HNCO}=MCF_{HNCO}\frac{S_{reagent}}{V} \tag{14.103}$$


Release 15.0 - © SAS IP, Inc. All rights reserved. - Contains proprietary and confidential information of ANSYS, Inc. and its subsidiaries and affiliates.

where $S_{reagent}$, the injection source term, is the rate of reagent release from the liquid droplets to the gas phase (kg/s), $MCF_{HNCO}$ is the mole fraction of $\mathrm{HNCO}$ in the $\mathrm{NH_3}$/ $HNCO$ mixture created from urea decomposition, and $V$ is the cell volume ($m^3$).

**Important**

The mole conversion fractions (MCF) for species $\mathrm{NH_3}$ and $\mathrm{HNCO}$ are determined through the user species values such that if one mole of urea decomposes into 1.1 moles of $\mathrm{NH_3}$ and 0.9 moles of $\mathrm{HNCO}$, then $MCF_{NH_3}$ = 0.55 and $MCF_{HNCO}$ = 0.45. When the **user-specified** option is used for urea decomposition, then $S_{pl,CO(NH_2)_2}=0$.

However, the default option for urea decomposition is through rate limiting reactions given in Table 14.3: Two-Step Urea Breakdown Process (p. 339), and the source terms are calculated accordingly. In this case, both values of $S_{pl,NH_3}$ and $S_{pl,HNCO}$ are zero.

## 14.1.9. NOx Formation in Turbulent Flows

The kinetic mechanisms of $\mathrm{NO}_x$ formation and destruction described in the preceding sections have all been obtained from laboratory experiments using either a laminar premixed flame or shock-tube studies where molecular diffusion conditions are well defined. In any practical combustion system, however, the flow is highly turbulent. The turbulent mixing process results in temporal fluctuations in temperature and species concentration that will influence the characteristics of the flame.

The relationships among $\mathrm{NO}_x$ formation rate, temperature, and species concentration are highly non-linear. Hence, if time-averaged composition and temperature are employed in any model to predict the mean $\mathrm{NO}_x$ formation rate, significant errors will result. Temperature and composition fluctuations must be taken into account by considering the probability density functions that describe the time variation.

### 14.1.9.1. The Turbulence-Chemistry Interaction Model

In turbulent combustion calculations, ANSYS Fluent solves the density-weighted time-averaged Navier-Stokes equations for temperature, velocity, and species concentrations or mean mixture fraction and variance. To calculate $\mathrm{NO}$ concentration, a time-averaged $\mathrm{NO}$ formation rate must be computed at each point in the domain using the averaged flow-field information.

Methods of modeling the mean turbulent reaction rate can be based on either moment methods [495] (p. 756) or probability density function (PDF) techniques [187] (p. 739). ANSYS Fluent uses the PDF approach.

**Important**

The PDF method described here applies to the $\mathrm{NO}_x$ transport equations only. The preceding combustion simulation can use either the generalized finite-rate chemistry model by Magnussen and Hjertager or the non-premixed combustion model. For details on these models, refer to Species Transport and Finite-Rate Chemistry (p. 187) and Non-Premixed Combustion (p. 215).

Release 15.0 - © SAS IP, Inc. All rights reserved. - Contains proprietary and confidential information of ANSYS, Inc. and its subsidiaries and affiliates.

### 14.1.9.2. The PDF Approach

The PDF method has proven very useful in the theoretical description of turbulent flow [188] (p. 739). In the ANSYS Fluent $NO_x$ model, a single- or joint-variable PDF in terms of a normalized temperature, species mass fraction, or the combination of both is used to predict the $NO_x$ emission. If the non-premixed or partially premixed combustion model is used to model combustion, then a one- or two-variable PDF in terms of mixture fraction(s) is also available. The mean values of the independent variables needed for the PDF construction are obtained from the solution of the transport equations.

### 14.1.9.3. The General Expression for the Mean Reaction Rate

The mean turbulent reaction rate $\overline{w}$ can be described in terms of the instantaneous rate $w$ and a single or joint PDF of various variables. In general,

$$\overline{w} = \int \cdots \int w(V_1, V_2, \ldots) P(V_1, V_2, \ldots) dV_1 dV_2 \ldots \tag{14.104}$$

where $V_1, V_2$,... are temperature and/or the various species concentrations present. $P$ is the probability density function (PDF).

### 14.1.9.4. The Mean Reaction Rate Used in ANSYS Fluent

The PDF is used for weighting against the instantaneous rates of production of $NO$ (for example, Equation 14.15 (p. 318)) and subsequent integration over suitable ranges to obtain the mean turbulent reaction rate. Hence we have

$$\overline{S}_{NO} = \int \rho w_{NO}(V_1) P_1(V_1) dV \tag{14.105}$$

or, for two variables

$$\overline{S}_{NO} = \int \int \rho w_{NO}(V_1, V_2) P(V_1, V_2) dV_1 dV_2 \tag{14.106}$$

where $\overline{S}_{NO}$ is the mean turbulent rate of production of $NO$, $w_{NO}$ is the instantaneous molar rate of $NO$ production, $\rho$ is the instantaneous density, and $P_1(V_1)$ and $P(V_1, V_2)$ are the PDFs of the variables $V_1$ and, if relevant, $V_2$. The same treatment applies for the $HCN$ or $NH_3$ source terms.

Equation 14.105 (p. 342) or Equation 14.106 (p. 342) must be integrated at every node and at every iteration. For a PDF in terms of temperature, the limits of integration are determined from the minimum and maximum values of temperature in the combustion solution (note that you have several options for how the maximum temperature is calculated, as described in Setting Turbulence Parameters in the User's Guide). For a PDF in terms of mixture fraction, the limits of the integrations in Equation 14.105 (p. 342) or Equation 14.106 (p. 342) are determined from the values stored in the look-up tables.

### 14.1.9.5. Statistical Independence

In the case of the two-variable PDF, it is further assumed that the variables $V_1$ and $V_2$ are statistically independent, so that $P(V_1, V_2)$ can be expressed as

$$P(V_1, V_2) = P_1(V_1) P_2(V_2) \tag{14.107}$$


Release 15.0 - © SAS IP, Inc. All rights reserved. - Contains proprietary and confidential information of ANSYS, Inc. and its subsidiaries and affiliates.

### 14.1.9.6. The Beta PDF Option

ANSYS Fluent can assume $P$ to be a two-moment beta function that is appropriate for combustion calculations [155] (p. 737), [301] (p. 745). The equation for the beta function is

$$P(V) = \frac{\Gamma(\alpha+\beta)}{\Gamma(\alpha)\Gamma(\beta)} V^{\alpha-1}(1-V)^{\beta-1} = \frac{V^{\alpha-1}(1-V)^{\beta-1}}{\int_0^1 V^{\alpha-1}(1-V)^{\beta-1} dV} \tag{14.108}$$

where $\Gamma(\,)$ is the Gamma function, and $\alpha$ and $\beta$ depend on the mean value of the quantity in question, $\overline{m}$, and its variance, $\sigma^2$:

$$\alpha = \overline{m}\left(\frac{\overline{m}(1-\overline{m})}{\sigma^2} - 1\right) \tag{14.109}$$

$$\beta = (1-\overline{m})\left(\frac{\overline{m}(1-\overline{m})}{\sigma^2} - 1\right) \tag{14.110}$$

The beta function requires that the independent variable $V$ assumes values between 0 and 1. Thus, field variables such as temperature must be normalized. See Setting Turbulence Parameters in the User's Guide for information on using the beta PDF when using single-mixture fraction models and two-mixture fraction models.

### 14.1.9.7. The Gaussian PDF Option

ANSYS Fluent can also assume $P$ to exhibit a clipped Gaussian form with delta functions at the tails.

The cumulative density function for a Gaussian PDF ($G_{CDF}$) may be expressed in terms of the error function as follows:

$$G_{CDF} = \frac{1}{2}\left(1 + erf\left((m-\overline{m})/\sqrt{2\sigma^2}\right)\right) \tag{14.111}$$

where $erf(\,)$ is the error function, $m$ is the quantity in question, and $\overline{m}$ and $\sigma^2$ are the mean and variance values of $m$, respectively. The error function may be expressed in terms of the incomplete gamma function ($gammp(\,)$):

$$\begin{aligned} \text{for } m<0: erf(m) &= -gammp(0.5,\ m^2) \\ \text{for } m\geq 0: erf(m) &= gammp(0.5,\ m^2) \end{aligned} \tag{14.112}$$

### 14.1.9.8. The Calculation Method for the Variance

The variance, $\sigma^2$, can be computed by solving the following transport equation during the combustion calculation or pollutant postprocessing stage:

$$\frac{\partial}{\partial t}(\rho\sigma^2) + \nabla\cdot(\rho\vec{v}\,\sigma^2) = \nabla\left(\frac{\mu_t}{\sigma_t}\nabla\sigma^2\right) + C_g\mu_t(\nabla\overline{m})^2 - C_d\rho\frac{\varepsilon}{k}\sigma^2 \tag{14.113}$$

where the constants $\sigma_t$, $C_g$, and $C_d$ take the values 0.85, 2.86, and 2.0, respectively.

Release 15.0 - © SAS IP, Inc. All rights reserved. - Contains proprietary and confidential information of ANSYS, Inc. and its subsidiaries and affiliates.

Note that the previous equation may only be solved for temperature. This solution may be computationally intensive, and therefore may not always be applicable for a postprocessing treatment of $NO_x$ prediction. When this is the case or when solving for species, the calculation of $\sigma^2$ is instead based on an approximate form of the variance transport equation (also referred to as the algebraic form). The approximate form assumes equal production and dissipation of variance, and is as follows:

$$\sigma^2 = \frac{\mu_t}{\rho}\frac{k}{\varepsilon}\frac{C_g}{C_d}(\nabla \overline{m})^2 = \frac{\mu_t}{\rho}\frac{k}{\varepsilon}\frac{C_g}{C_d}\left[\left(\frac{\partial \overline{m}}{\partial x}\right)^2 + \left(\frac{\partial \overline{m}}{\partial y}\right)^2 + \left(\frac{\partial \overline{m}}{\partial z}\right)^2\right] \tag{14.114}$$

The term in the brackets is the dissipation rate of the independent variable.

For a PDF in terms of mixture fraction, the mixture fraction variance has already been solved as part of the basic combustion calculation, so no additional calculation for $\sigma^2$ is required.

## 14.2. SOx Formation

The following sections include information on the theory used in the $SO_x$ model. For information about using the $SO_x$ models in ANSYS Fluent, see Using the SOx Model in the User's Guide.

14.2.1. Overview
14.2.2. Governing Equations for SOx Transport
14.2.3. Reaction Mechanisms for Sulfur Oxidation
14.2.4. SO2 and H2S Production in a Gaseous Fuel
14.2.5. SO2 and H2S Production in a Liquid Fuel
14.2.6. SO2 and H2S Production from Coal
14.2.7. SOx Formation in Turbulent Flows

### 14.2.1. Overview

Sulfur exists in coal as organic sulfur, pyretic, and sulfates [1] (p. 729), and exists in liquid fuels mostly in organic form [305] (p. 745), with mass fractions ranging from 0.5% to 3%. All $SO_x$ emissions are produced because of the oxidation of fuel-bound sulfur. During the combustion process, fuel sulfur is oxidized to $SO_2$ and $SO_3$. A portion of the gaseous $SO_x$ will condense on the particles, attaching an amount of water and therefore forming sulfuric acid, or may react further to form sulfates. While $SO_x$ emissions are the main cause of acid rain, $SO_3$ also contributes to particulate emissions, and is responsible for corrosion of combustion equipment. Furthermore, there is a growing interest in the interaction of sulfur species with the nitrogen oxide chemistry [305] (p. 745), as $NO$ levels are affected by the presence of sulfur species. The evidence to date indicates that thermal $NO$ levels (Thermal NOx Formation (p. 315)) are reduced in the presence of $SO_2$. However, the effect of sulfur compounds on the fuel $NO_x$ formation is yet to be clarified.

Sulfur emissions are regulated from stationary sources and from automotive fuels. Sulfur pollutants can be captured during the combustion process or with after treatment methods, such as wet or dry scrubbing. Coal fired boilers are by far the biggest single $SO_x$ emissions source, accounting for over 50% of total $SO_2$ emissions [67] (p. 732).

For higher sulfur concentrations in the fuel, the $SO_x$ concentration field should be resolved together with the main combustion calculation using any of the ANSYS Fluent reaction models. For cases where


Release 15.0 - © SAS IP, Inc. All rights reserved. - Contains proprietary and confidential information of ANSYS, Inc. and its subsidiaries and affiliates.

the sulfur fraction in the fuel is low, the postprocessing option can be used, which solves transport equations for $H_2S$, $SO_2$, $SO$, $SH$, and $SO_3$.

#### 14.2.1.1. The Formation of SOx

The $SO_x$ model incorporates the following stages:

1. Sulfur release from the fuel

   For liquid fuels, one can conveniently assume that sulfur is released as $H_2S$ [305] (p. 745). However, the process is more complicated in the case of coal; here, some of the sulfur is decomposed into the gas phase during devolatilization as $H_2S$, $COS$, $SO_2$, and $CS_2$, while part of the sulfur is retained in the char to be oxidized at a later stage. The percentage of sulfur retained in char is rank dependent [1] (p. 729).

2. Sulfur reaction in the gas phase

   In oxygen rich flames, the predominant sulfur species are $SO$, $SO_2$, and $SO_3$. At lower oxygen concentrations, $H_2S$, $S_2$, and $SH$ are also present in significant proportions, while $SO_3$ becomes negligible [305] (p. 745). In PCGC-3, as well as in the works of Norman et al. [323] (p. 746), the gas phase sulfur species are assumed to be in equilibrium.

3. Sulfur retention in sorbents

   Sulfur pollutants can be absorbed by sorbent particles, injected either in situ, or in the post-flame region.

For low sulfur fuels, we can assume that sulfur is mainly released as $H_2S$. The rate of release can be determined similarly to that of fuel-bound $N$. For the char $S$ it can be assumed that $SO_2$ is produced directly at the same rate as that of char burnout. Transport equations for $H_2S$, $SO_2$, $SO$, $SH$, and $SO_3$ species are incorporated and an appropriate reaction set has been developed, as described in the ensuing sections.

## 14.2.2. Governing Equations for SOx Transport

ANSYS Fluent solves the mass transport equations for the $SO_2$ species, taking into account convection, diffusion, production, and consumption of $SO_2$ and related species. This approach is completely general, being derived from the fundamental principle of mass conservation. The effect of residence time in $SO_x$ mechanisms, a Lagrangian reference frame concept, is included through the convection terms in the governing equations written in the Eulerian reference frame. If all fuel sulfur is assumed to convert directly to $SO_2$ and the other product and intermediate species are assumed negligible, then only the $SO_2$ species transport equation is needed:

$$\frac{\partial}{\partial t}\left(\rho Y_{SO_2}\right)+\nabla\cdot\left(\rho\vec{v}\,Y_{SO_2}\right)=\nabla\cdot\left(\rho\mathcal{D}\nabla Y_{SO_2}\right)+S_{SO_2} \tag{14.115}$$

As described in Reaction Mechanisms for Sulfur Oxidation (p. 346), $SO_x$ formation mechanisms involve multiple reactions among multiple species, and tracking sulfur-containing intermediate species is important. ANSYS Fluent solves transport equations for the $H_2S$, $SO_3$, $SO$, and $SH$ species in addition to the $SO_2$ species:

Release 15.0 - © SAS IP, Inc. All rights reserved. - Contains proprietary and confidential information of ANSYS, Inc. and its subsidiaries and affiliates.

$$\frac{\partial}{\partial t}\left(\rho Y_{H_2S}\right)+\nabla\cdot\left(\rho\vec{v}\,Y_{H_2S}\right)=\nabla\cdot\left(\rho\mathcal{D}Y_{H_2S}\right)+S_{H_2S} \tag{14.116}$$

$$\frac{\partial}{\partial t}\left(\rho Y_{SO_3}\right)+\nabla\cdot\left(\rho\vec{v}\,Y_{SO_3}\right)=\nabla\cdot\left(\rho\mathcal{D}Y_{SO_3}\right)+S_{SO_3} \tag{14.117}$$

$$\frac{\partial}{\partial t}\left(\rho Y_{SO}\right)+\nabla\cdot\left(\rho\vec{v}\,Y_{SO}\right)=\nabla\cdot\left(\rho\mathcal{D}Y_{SO}\right)+S_{SO} \tag{14.118}$$

$$\frac{\partial}{\partial t}\left(\rho Y_{SH}\right)+\nabla\cdot\left(\rho\vec{v}\,Y_{SH}\right)=\nabla\cdot\left(\rho\mathcal{D}Y_{SH}\right)+S_{SH} \tag{14.119}$$

where $Y_{SO_2}$, $Y_{H_2S}$, $Y_{SO_3}$, $Y_{SO}$, and $Y_{SH}$ are mass fractions of $SO_2$, $H_2S$, $SO_3$, SO, and SH in the gas phase. The source terms $S_{SO_2}$, $S_{H_2S}$, $S_{SO_3}$, $S_{SO}$, and $S_{SH}$ are to be determined depending on the form of fuel sulfur release ($SO_2$ and/or $H_2S$) and inclusion of $SO_3$, SO, and SH in the $SO_x$ mechanism.

## 14.2.3. Reaction Mechanisms for Sulfur Oxidation

A detailed reaction mechanism for sulfur oxidation has been proposed by Kramlich [219] (p. 741). The mechanism consists of 20 reversible reactions and includes 12 species (S, $S_2$, SH, SO, $SO_2$, $H_2S$, H, $H_2$, OH, $H_2O$, O, and $O_2$). The mechanism has been reduced to 8 steps and 10 species (with S and $S_2$ removed), and validated in Perfectly Stirred Reactor (PSR) and Plug Flow Reactor (PFR) simulations.

Table 14.4: Eight-Step Reduced Mechanism (p. 347) (for a rate constant $k=AT^b exp(-E/RT)$) lists the reduced mechanism with the modified rate constants. For reduction calculations, O and OH concentrations have been calculated through partial equilibrium assumptions based on $O_2$ and $H_2O$ concentrations, respectively. $N_2$ was used as the dilutant. Since each reaction of the eight-step reduced mechanism is reversible, for each adjacent pair of reactions given in Table 14.4: Eight-Step Reduced Mechanism (p. 347), the second reaction is in fact the reverse reaction of the first.

The reduced mechanism given in Table 14.4: Eight-Step Reduced Mechanism (p. 347) closely follows the $SO_2$ concentration levels, but slightly over-predicts the $H_2S$ concentrations at temperatures below 1500 K. Above 1500 K, both mechanisms are in close agreement for $SO_2$ and $H_2S$ concentration predictions. However, SO and SH are not well correlated by the reduced mechanism when compared against the predictions using the original detailed mechanism.

A major concern in these mechanisms is the presence of H radicals and the method by which to calculate its concentration in the flow field. At present, the concentration of H radicals is assumed to be proportional to the O radical concentration, which can be evaluated from one of the existing methods in ANSYS Fluent; viz. Partial Equilibrium (Method 2: Partial Equilibrium Approach (p. 317)) or Equilibrium (Method 1: Equilibrium Approach (p. 317)). You are then given the option of varying the proportionality constant. Although this assumption is open to debate, the lack of simple relation to calculate the H radical concentration in a flame has prompted the present choice.

The present implementation allows you to either include or remove $SO_3$ from the calculations. Also, depending on the form of fuel sulfur release (for example, $H_2S$ or $SO_2$) the species $H_2S$ may or may not be present for the calculation. You are also given the extended option of partitioning the interme-


Release 15.0 - © SAS IP, Inc. All rights reserved. - Contains proprietary and confidential information of ANSYS, Inc. and its subsidiaries and affiliates.

diate fuel sulfur species to $H_2S$ and $SO_2$. However, there is no literature to guide you on how to select a correct partition fraction.

**Table 14.4: Eight-Step Reduced Mechanism**

| Reaction | A | b | E |
|---|---|---|---|
| $H_2S+H \rightarrow SH+H_2$ | 1.819702E+07 | 0.0E+00 | 7.484300E+03 |
| $SH+H_2 \rightarrow H_2S+H$ | 9.375623E+06 | 0.0E+00 | 6.253660E+04 |
| $OH+H_2S \rightarrow H_2O+SH$ | 1.380385E+02 | 0.0E+00 | 3.742150E+03 |
| $H_2O+SH \rightarrow OH+H_2S$ | 3.104557E+07 | 0.0E+00 | 1.218543E+05 |
| $SO+OH \rightarrow H+SO_2$ | 1.621810E+08 | 0.0E+00 | 2.565926E+03 |
| $H+SO_2 \rightarrow SO+OH$ | 7.691299E+09 | 0.0E+00 | 1.187023E+05 |
| $SH+O \rightarrow SO+H$ | 3.548135E+08 | 0.0E+00 | 2.687316E+03 |
| $SO+H \rightarrow SH+O$ | 2.985385E+09 | 0.0E+00 | 1.694600E+05 |
| $O+H_2S \rightarrow SH+OH$ | 4.365162E+03 | 0.0E+00 | 1.380493E+04 |
| $SH+OH \rightarrow O+H_2S$ | 9.885528E+08 | 0.0E+00 | 6.035996E+04 |
| $SO+O_2 \rightarrow SO_2+O$ | 4.466832E+05 | 0.0E+00 | 2.703222E+04 |
| $SO_2+O \rightarrow SO+O_2$ | 1.663412E+06 | 0.0E+00 | 7.613643E+04 |
| $H+SH+M \rightarrow H_2S+M$ | 1.096478E+03 | 0.0E+00 | 0.000000E+00 |
| $H_2S+M \rightarrow H+SH+M$ | 8.669613E+14 | 0.0E+00 | 3.819463E+05 |
| $SO+O+M \rightarrow SO_2+M$ | 8.709647E+09 k | -1.8E+00 | 0.000000E+00 |
| $SO_2+M \rightarrow SO+O+M$ | 1.905464E+14 | 0.0E+00 | 5.207365E+05 |

A is in $\mathrm{m}^3/\mathrm{mol}-\mathrm{s}$, E is J/mol (assumed 1 cal = 4.18585 J), A units for the thirteenth reaction is $\mathrm{m}^6/\mathrm{mol}^2-\mathrm{s}$, and A units for the fifteenth reaction is $\mathrm{m}^6/\mathrm{mol}^2-\mathrm{s}$.

In addition, the following two reactions were included in ANSYS Fluent to complete the $SO_x$ mechanism, with the rate constants taken from Hunter's work [172] (p. 738).

$$SO_2+O+M \Leftrightarrow SO_3+M \tag{14.120}$$

M = argon, nitrogen, oxygen

$k_{f1} = 3.63 \times 10^2$ exp(+4185.85/RT) $\mathrm{m}^6/\mathrm{mol}^2/\mathrm{sec}$

where R = 8.313 J/mol-K

$k_{r1} = 7.41 \times 10^{14}$ exp(-346123.75/RT) $\mathrm{m}^3/\mathrm{mol}/\mathrm{sec}$.

$$SO_3+O \Leftrightarrow SO_2+O_2 \tag{14.121}$$

Release 15.0 - © SAS IP, Inc. All rights reserved. - Contains proprietary and confidential information of ANSYS, Inc. and its subsidiaries and affiliates.

$k_{f2} = 1.2 \times 10^6 \exp(-39765.575/RT)\ \mathrm{m^3/mol/sec}$

The reverse rate of Equation 14.121 (p. 347) was determined through the equilibrium constant for that equation.

## 14.2.4. SO2 and H2S Production in a Gaseous Fuel

The rate of $SO_2$ or $H_2S$ production is equivalent to the rate of combustion of the fuel:

$$S_{pl,i} = \frac{\mathcal{R}_{cf} Y_{S,fuel} M_{w,i}}{M_{w,S}} \tag{14.122}$$

where

$S_{pl,i}$ = source of $i$ ($kg/m^3-s$), where $i = SO_2$ or $H_2S$

$\mathcal{R}_{cf}$ = mean limiting reaction rate of the fuel (kg/m$^3$–s)

$Y_{S,fuel}$ = mass fraction of sulfur in the fuel

The mean limiting reaction rate of the fuel, $\mathcal{R}_{cf}$, is calculated from the Magnussen combustion model, so the gaseous fuel option for $SO_x$ formation is available only when the generalized finite-rate model is used.

## 14.2.5. SO2 and H2S Production in a Liquid Fuel

The rate of $SO_2$ or $H_2S$ production is equivalent to the rate of fuel release into the gas phase through droplet evaporation:

$$S_{pl,i} = \frac{S_{fuel} Y_{S,fuel} M_{w,i}}{M_{w,S} V} \tag{14.123}$$

where

$S_{pl,i}$ = source of $i$ (kg/m$^3$–s), where $i = SO_2$ or $H_2S$

$S_{fuel}$ = rate of fuel release from the liquid droplets to the gas (kg/s)

$Y_{S,fuel}$ = mass fraction of sulfur in the fuel

$V$ = cell volume (m$^3$)

## 14.2.6. SO2 and H2S Production from Coal

For coal, it is assumed that sulfur is distributed between the volatiles and the char. Since there is no reason to assume that S is equally distributed between the volatiles and the char, the fraction of S in the volatiles and the char should be specified separately.

### 14.2.6.1. SO2 and H2S from Char

The source of $SO_2$ and $H_2S$ from the char is related to the rate of char combustion:


Release 15.0 - © SAS IP, Inc. All rights reserved. - Contains proprietary and confidential information of ANSYS, Inc. and its subsidiaries and affiliates.

$$S_{char,i} = \frac{S_c Y_{S,char} M_{w,i}}{M_{w,S} V} \tag{14.124}$$

where

$S_c$ = char burnout rate (kg/s)

$S_{char,i}$ = source of $i$ (kg/m$^3$–s) in char, where $i = SO_2$ or $H_2S$

$Y_{S,char}$ = mass fraction of sulfur in char

$V$ = cell volume (m$^3$)

#### 14.2.6.2. SO2 and H2S from Volatiles

The source of $\mathrm{SO_2}$ and $\mathrm{H_2S}$ from the volatiles is related to the rate of volatile release:

$$S_{vol,i} = \frac{S_{vol} Y_{S,vol} M_{w,i}}{M_{w,S} V} \tag{14.125}$$

where

$S_{vol,i}$ = source of volatiles originating from the coal particles into the gas phase (kg/s), where $i = SO_2$ or $H_2S$

$Y_{S,vol}$ = mass fraction of sulfur in the volatiles

$V$ = cell volume (m$^3$)

### 14.2.7. SOx Formation in Turbulent Flows

The kinetic mechanisms of $\mathrm{SO}_x$ formation and destruction are obtained from laboratory experiments in a similar fashion to the $\mathrm{NO}_x$ model. In any practical combustion system, however, the flow is highly turbulent. The turbulent mixing process results in temporal fluctuations in temperature and species concentration that will influence the characteristics of the flame.

The relationships among $\mathrm{SO}_x$ formation rate, temperature, and species concentration are highly nonlinear. Hence, if time-averaged composition and temperature are employed in any model to predict the mean $\mathrm{SO}_x$ formation rate, significant errors will result. Temperature and composition fluctuations must be taken into account by considering the probability density functions that describe the time variation.

#### 14.2.7.1. The Turbulence-Chemistry Interaction Model

In turbulent combustion calculations, ANSYS Fluent solves the density-weighted time-averaged Navier-Stokes equations for temperature, velocity, and species concentrations or mean mixture fraction and variance. To calculate $\mathrm{SO_2}$ concentration, a time-averaged $\mathrm{SO_2}$ formation rate must be computed at each point in the domain using the averaged flow-field information.

#### 14.2.7.2. The PDF Approach

The PDF method has proven very useful in the theoretical description of turbulent flow [188] (p. 739). In the ANSYS Fluent $\mathrm{SO}_x$ model, a single- or joint-variable PDF in terms of a normalized temperature,

species mass fraction, or the combination of both is used to predict the $SO_x$ emission. If the non-premixed combustion model is used to model combustion, then a one- or two-variable PDF in terms of mixture fraction(s) is also available. The mean values of the independent variables needed for the PDF construction are obtained from the solution of the transport equations.

#### 14.2.7.3. The Mean Reaction Rate

The mean turbulent reaction rate described in The General Expression for the Mean Reaction Rate (p. 342) for the $NO_x$ model also applies to the $SO_x$ model. The PDF is used for weighting against the instantaneous rates of production of $SO_2$ and subsequent integration over suitable ranges to obtain the mean turbulent reaction rate, as described in Equation 14.105 (p. 342) and Equation 14.106 (p. 342) for $NO_x$.

#### 14.2.7.4. The PDF Options

As is the case with the $NO_x$ model, $P$ can be calculated as either a two-moment beta function or as a clipped Gaussian function, as appropriate for combustion calculations [155] (p. 737), [301] (p. 745).

Equation 14.108 (p. 343) – Equation 14.112 (p. 343) apply to the $SO_x$ model as well, with the variance $\sigma^2$ computed by solving a transport equation during the combustion calculation stage, using Equation 14.113 (p. 343) or Equation 14.114 (p. 344).

## 14.3. Soot Formation

Information about the theory behind soot formation is presented in the following sections. For information about using soot formation models in ANSYS Fluent, see Using the Soot Models in the User's Guide.

14.3.1. Overview and Limitations
14.3.2. Soot Model Theory

### 14.3.1. Overview and Limitations

ANSYS Fluent provides four models for the prediction of soot formation in combustion systems. In addition, the predicted soot concentration can be coupled with radiation absorption when you use the P-1, discrete ordinates, or discrete transfer radiation model with a variable absorption coefficient.

#### 14.3.1.1. Predicting Soot Formation

ANSYS Fluent predicts soot concentrations in a combustion system using one of four available models:

- the one-step Khan and Greeves model [204] (p. 740), in which ANSYS Fluent predicts the rate of soot formation based on a simple empirical rate
- the two-step Tesner model [280] (p. 744), [450] (p. 753), in which ANSYS Fluent predicts the formation of nuclei particles, with soot formation on the nuclei
- the Moss-Brookes model [47] (p. 731), in which ANSYS Fluent predicts soot formation for methane flames (and higher hydrocarbon species, if appropriately modified) by solving transport equations for normalized radical nuclei concentration and the soot mass fraction
- the Moss-Brookes-Hall model [152] (p. 737), which is an extension of the Moss-Brookes model and is applicable for higher hydrocarbon fuels (for example, kerosene)


Release 15.0 - © SAS IP, Inc. All rights reserved. - Contains proprietary and confidential information of ANSYS, Inc. and its subsidiaries and affiliates.

The Khan and Greeves model is the default model used by ANSYS Fluent when you include soot formation.

In the Khan and Greeves model and the Tesner model, combustion of the soot (and particle nuclei) is assumed to be governed by the Magnussen combustion rate [280] (p. 744). Note that this limits the use of these soot formation models to turbulent flows. Both models are empirically-based, approximate models of the soot formation process in combustion systems. The detailed chemistry and physics of soot formation are quite complex and are only approximated in these models. You should view the results of the Khan and Greeves model and the Tesner model as qualitative indicators of your system performance, unless you can undertake experimental validation of the results.

The Moss-Brookes model has less empiricism and should theoretically provide superior accuracy than the Khan and Greeves and Tesner models. The Hall extension provides further options for modeling higher hydrocarbon fuels. Note that the Moss-Brookes-Hall model is only available when the required species are present in the gas phase species list.

#### 14.3.1.2. Restrictions on Soot Modeling

The following restrictions apply to soot formation models:

- You must use the pressure-based solver. The soot models are not available with either of the density-based solvers.
- The Khan and Greeves model and the Tesner model can model soot formation only for turbulent flows (whereas the Moss-Brookes model and the Moss-Brookes-Hall model can be used with both laminar and turbulent flows).
- The soot model cannot be used in conjunction with the premixed combustion model.

## 14.3.2. Soot Model Theory

#### 14.3.2.1. The One-Step Soot Formation Model

In the one-step Khan and Greeves model [204] (p. 740), ANSYS Fluent solves a single transport equation for the soot mass fraction:

$$\frac{\partial}{\partial t}(\rho Y_{soot}) + \nabla \cdot (\rho \vec{v} Y_{soot}) = \nabla \cdot \left( \frac{\mu_t}{\sigma_{soot}} \nabla Y_{soot} \right) + \mathcal{R}_{soot} \tag{14.126}$$

where

$Y_{soot}$ = soot mass fraction

$\sigma_{soot}$ = turbulent Prandtl number for soot transport

$\mathcal{R}_{soot}$ = net rate of soot generation (kg/m$^3$–s)

$\mathcal{R}_{soot}$, the net rate of soot generation, is the balance of soot formation, $\mathcal{R}_{soot,form}$, and soot combustion, $\mathcal{R}_{soot,comb}$:

$$\mathcal{R}_{soot} = \mathcal{R}_{soot,form} - \mathcal{R}_{soot,comb} \tag{14.127}$$

The rate of soot formation is given by a simple empirical rate expression:

$$\mathcal{R}_{soot,form} = C_s p_{fuel} \phi^r e^{-E/RT} \tag{14.128}$$

Release 15.0 - © SAS IP, Inc. All rights reserved. - Contains proprietary and confidential information of ANSYS, Inc. and its subsidiaries and affiliates.

where

$C_s$ = soot formation constant (kg/N-m-s)

$p_{fuel}$ = fuel partial pressure (Pa)

$\phi$ = equivalence ratio

$r$ = equivalence ratio exponent

$E/R$ = activation temperature (K)

The rate of soot combustion is the minimum of two rate expressions [280] (p. 744):

$$\mathcal{R}_{soot,comb} = \min\left[\mathcal{R}_1, \mathcal{R}_2\right] \tag{14.129}$$

The two rates are computed as

$$\mathcal{R}_1 = A\rho Y_{soot}\frac{\varepsilon}{k} \tag{14.130}$$

and

$$\mathcal{R}_2 = A\rho\left(\frac{Y_{ox}}{v_{soot}}\right)\left(\frac{Y_{soot}v_{soot}}{Y_{soot}v_{soot}+Y_{fuel}v_{fuel}}\right)\frac{\varepsilon}{k} \tag{14.131}$$

where

$A$ = constant in the Magnussen model

$Y_{ox}$, $Y_{fuel}$ = mass fractions of oxidizer and fuel

$v_{soot}$, $v_{fuel}$ = mass stoichiometries for soot and fuel combustion

The default constants for the one-step model are valid for a wide range of hydrocarbon fuels.

### 14.3.2.2. The Two-Step Soot Formation Model

The two-step Tesner model [450] (p. 753) predicts the generation of radical nuclei and then computes the formation of soot on these nuclei. ANSYS Fluent therefore solves transport equations for two scalar quantities: the soot mass fraction (Equation 14.126 (p. 351)) and the normalized radical nuclei concentration:

$$\frac{\partial}{\partial t}(\rho b^*_{nuc}) + \nabla\cdot(\rho\vec{v}\, b^*_{nuc}) = \nabla\cdot\left(\frac{\mu_t}{\sigma_{nuc}}\nabla b^*_{nuc}\right) + \mathcal{R}^*_{nuc} \tag{14.132}$$

where

$b^*_{nuc}$ = normalized radical nuclei concentration (particles $\times 10^{-15}$/kg)

$\sigma_{nuc}$ = turbulent Prandtl number for nuclei transport

$\mathcal{R}^*_{nuc}$ = normalized net rate of nuclei generation (particles $\times 10^{-15}$/m$^3$–s)

In these transport equations, the rates of nuclei and soot generation are the net rates, involving a balance between formation and combustion.


Release 15.0 - © SAS IP, Inc. All rights reserved. - Contains proprietary and confidential information of ANSYS, Inc. and its subsidiaries and affiliates.

#### 14.3.2.2.1. Soot Generation Rate

The two-step model computes the net rate of soot generation, $\mathcal{R}_{soot}$, in the same way as the one-step model, as a balance of soot formation and soot combustion:

$$\mathcal{R}_{soot} = \mathcal{R}_{soot,form} - \mathcal{R}_{soot,comb} \tag{14.133}$$

In the two-step model, however, the rate of soot formation, $\mathcal{R}_{soot,form}$, depends on the concentration of radical nuclei, $c_{nuc}$:

$$\mathcal{R}_{soot,form} = m_p(\alpha - \beta N_{soot})\, c_{nuc} \tag{14.134}$$

where

$m_p$ = mean mass of soot particle (kg/particle)

$N_{soot}$ = concentration of soot particles (particles/m$^3$)

$c_{nuc}$ = radical nuclei concentration = $\rho b_{nuc}$ (particles/m$^3$)

$\alpha$ = empirical constant (s$^{-1}$)

$\beta$ = empirical constant (m$^3$/particle-s)

The rate of soot combustion, $\mathcal{R}_{soot,comb}$, is computed in the same way as for the one-step model, using Equation 14.129 (p. 352) – Equation 14.131 (p. 352).

The default constants for the two-step model are applicable for the combustion of acetylene ($C_2H_2$). According to Ahmad et al. [2] (p. 729), these values should be modified for other fuels, as the sooting characteristics of acetylene are known to be different from those of saturated hydrocarbon fuels.

#### 14.3.2.2.2. Nuclei Generation Rate

The net rate of nuclei generation in the two-step model is given by the balance of the nuclei formation rate and the nuclei combustion rate:

$$\mathcal{R}^*_{nuc} = \mathcal{R}^*_{nuc,form} - \mathcal{R}^*_{nuc,comb} \tag{14.135}$$

where

$\mathcal{R}^*_{nuc,form}$ = rate of nuclei formation (particles $\times 10^{-15}$/m$^3$-s)

$\mathcal{R}^*_{nuc,comb}$ = rate of nuclei combustion (particles $\times 10^{-15}$/m$^3$-s)

The rate of nuclei formation, $\mathcal{R}^*_{nuc,form}$, depends on a spontaneous formation and branching process, described by

$$\mathcal{R}^*_{nuc,form} = \eta_0 + (f - g)\, c^*_{nuc} - g_0 c^*_{nuc} N_{soot} \tag{14.136}$$

$$\eta_0 = a_0^* c_{fuel} e^{-E/RT} \tag{14.137}$$

where

$c^*_{nuc}$ = normalized nuclei concentration ($=\rho b^*_{nuc}$)

Release 15.0 - © SAS IP, Inc. All rights reserved. - Contains proprietary and confidential information of ANSYS, Inc. and its subsidiaries and affiliates.

$a_0^* = a_0/10^{15}$

$a_0$ = pre-exponential rate constant (particles/kg-s)

$c_{fuel}$ = fuel concentration (kg/m$^3$)

$f - g$ = linear branching $-$ termination coefficient (s$^{-1}$)

$g_0$ = linear termination on soot particles (m$^3$/particle-s)

Note that the branching term in Equation 14.136 (p. 353), $(f-g)c_{nuc}^*$, is included only when the kinetic rate, $\eta_0$, is greater than the limiting formation rate ($10^5$ particles/m$^3$-s, by default).

The rate of nuclei combustion is assumed to be proportional to the rate of soot combustion:

$$\mathcal{R}_{nuc,comb}^* = \mathcal{R}_{soot,comb}\frac{b_{nuc}^*}{Y_{soot}} \tag{14.138}$$

where the soot combustion rate, $\mathcal{R}_{soot,comb}$, is given by Equation 14.129 (p. 352).

### 14.3.2.3. The Moss-Brookes Model

The Moss-Brookes model solves transport equations for normalized radical nuclei concentration $b_{nuc}^*$ and soot mass fraction $Y_{soot}$:

$$\frac{\partial}{\partial t}(\rho Y_{soot}) + \nabla\cdot(\rho\vec{v}\,Y_{soot}) = \nabla\cdot\left(\frac{\mu_t}{\sigma_{soot}}\nabla Y_{soot}\right) + \frac{dM}{dt} \tag{14.139}$$

$$\frac{\partial}{\partial t}(\rho b_{nuc}^*) + \nabla\cdot(\rho\vec{v}\,b_{nuc}^*) = \nabla\cdot\left(\frac{\mu_t}{\sigma_{nuc}}\nabla b_{nuc}^*\right) + \frac{1}{N_{norm}}\frac{dN}{dt} \tag{14.140}$$

where

$Y_{soot}$ = soot mass fraction

$M$ = soot mass concentration (kg/m$^3$)

$b_{nuc}^*$ = normalized radical nuclei concentration (particles $\times 10^{-15}$/kg) = $\frac{N}{\rho N_{norm}}$

$N$ = soot particle number density (particles/m$^3$)

$N_{norm} = 10^{15}$ particles

The instantaneous production rate of soot particles, subject to nucleation from the gas phase and coagulation in the free molecular regime, is given by

$$\frac{dN}{dt} = \underbrace{C_\alpha N_A\left(\frac{X_{prec}P}{RT}\right)^l \exp\left\{-\frac{T_\alpha}{T}\right\}}_{\text{Nucleation}} - \underbrace{C_\beta\left(\frac{24RT}{\rho_{soot}N_A}\right)^{1/2} d_p^{1/2}N^2}_{\text{Coagulation}} \tag{14.141}$$


Release 15.0 - © SAS IP, Inc. All rights reserved. - Contains proprietary and confidential information of ANSYS, Inc. and its subsidiaries and affiliates.

where $C_\alpha$, $C_\beta$ and $l$ are model constants. Here, $N_A$ (= 6.022045 x $10^{26}$kmol$^{-1}$) is the Avogadro number and $X_{prec}$ is the mole fraction of soot precursor (for methane, the precursor is assumed to be acetylene, whereas for kerosene it is a combination of acetylene and benzene). The mass density of soot, $\rho_{soot}$, is assumed to be 1800 kg/m$^3$ and $d_p$ is the mean diameter of a soot particle. The nucleation rate for soot particles is taken to be proportional to the local acetylene concentration for methane. The activation temperature $T_\alpha$ for the nucleation reaction is that proposed by Lindstedt [256] (p. 743).

The source term for soot mass concentration is modeled by the expression

$$\frac{dM}{dt} = \underbrace{M_P C_\alpha \left(\frac{X_{prec}P}{RT}\right)^l \exp\left\{-\frac{T_\alpha}{T}\right\}}_{\text{Nucleation}} + \underbrace{C_\gamma \left(\frac{X_{sgs}P}{RT}\right)^m \exp\left\{-\frac{T_\gamma}{T}\right\}\left[(\pi N)^{1/3}\left(\frac{6M}{\rho_{soot}}\right)^{2/3}\right]^n}_{\text{Surface Growth}} - \underbrace{C_{oxid}C_\omega\eta_{coll}\left(\frac{X_{OH}P}{RT}\right)\sqrt{T}\,(\pi N)^{1/3}\left(\frac{6M}{\rho_{soot}}\right)^{2/3}}_{\text{Oxidation}} \tag{14.142}$$

where $C_\gamma$, $C_{oxid}$, $C_\omega$, $m$, and $n$ are additional model constants. The constant $M_P$ (= 144 kg/kmol) is the mass of an incipient soot particle, here taken to consist of 12 carbon atoms. Even though the model is not found to be sensitive to this assumption, a nonzero initial mass is needed to begin the process of surface growth. Here, $X_{sgs}$ is the mole fraction of the participating surface growth species. For paraffinic fuels, soot particles have been found to grow primarily by the addition of gaseous species at their surfaces, particularly acetylene that has been found in abundance in the sooting regions of laminar methane diffusion flames.

The model assumes that the hydroxyl radical is the dominant oxidizing agent in methane/air diffusion flames and that the surface-specific oxidation rate of soot by the $\mathrm{OH}$ radical may be formulated according to the model proposed by Fenimore and Jones [115] (p. 735). Assuming a collision efficiency ($\eta_{coll}$) of 0.04, the oxidation rate may be written as Equation 14.142 (p. 355).

The process of determination of the exponents $l$, $m$, and $n$ are explained in detail by Brookes and Moss [47] (p. 731). The constants $C_\alpha$ and $C_\beta$ are determined through numerical modeling of a laminar flame for which experimental data exists.

The set of constants proposed by Brookes and Moss for methane flames are given below:

$C_\alpha$ = 54 s$^{-1}$ (model constant for soot inception rate)

$T_\alpha$ = 21000 K (activation temperature of soot inception)

$C_\beta$ = 1.0 (model constant for coagulation rate)

Release 15.0 - © SAS IP, Inc. All rights reserved. - Contains proprietary and confidential information of ANSYS, Inc. and its subsidiaries and affiliates.

$C_\gamma$ = 11700 $\mathrm{kg \cdot m \cdot kmol^{-1} \cdot s^{-1}}$. (surface growth rate scaling factor)

$T_\gamma$ = 12100 K (activation temperature of surface growth rate)

$C_\omega$ = 105.8125 $\mathrm{kg \cdot m \cdot kmol^{-1} \cdot K^{-1/2} \cdot s^{-1}}$ (oxidation model constant)

$\eta_{coll}$ = 0.04 (collisional efficiency parameter)

$C_{oxid}$ = 0.015 (oxidation rate scaling parameter)

Note that the implementation of the Moss-Brookes model in ANSYS Fluent uses the values listed above, except for $C_{oxid}$, which is set to unity by default.

The closure for the mean soot source terms in the above equations was also described in detail by Brookes and Moss [47] (p. 731). The uncorrelated closure is the preferred option for a tractable solution of the above transport equations.

Moss et al. [310] (p. 746) have shown the above model applied to kerosene flames by modifying only the soot precursor species (in the original model the precursor was acetylene, whereas for kerosene flames the precursor was assumed to be a combination of both acetylene and benzene) and by setting the value of oxidation scaling parameter $C_{oxid}$ to unity. A good comparison against the experimental measurements for the lower pressure (7 bar) conditions was observed. The predictions of soot formation within methane flames have shown the Brooks and Moss [47] (p. 731) model to be superior compared with the standard Tesner et al. [450] (p. 753) formulation.

### 14.3.2.3.1. The Moss-Brookes-Hall Model

Since the Moss-Brookes model was mainly developed and validated for methane flames, a further extension for higher hydrocarbon fuels called the Moss-Brookes-Hall model is available in ANSYS Fluent. Here, the extended version is a model reported by Wen et al. [485] (p. 755), based on model extensions proposed by Hall et al. [152] (p. 737) and an oxidation model proposed by Lee et al. [236] (p. 742). The work of Hall [152] (p. 737) is based on a soot inception rate due to two-ringed and three-ringed aromatics, as opposed to the Moss-Brookes assumption of a soot inception due to acetylene or benzene (for higher hydrocarbons).

Hall et al. [152] (p. 737) proposed a soot inception rate based on the formation rates of two-ringed and three-ringed aromatics ($C_{10}H_7$ and $C_{14}H_{10}$), from acetylene ($C_2H_2$), benzene ($C_6H_6$), and the phenyl radical ($C_6H_5$) based on the following mechanisms:

$$\begin{aligned} 2\,C_2H_2 + C_6H_5 &\rightleftharpoons C_{10}H_7 + H_2 \\ C_2H_2 + C_6H_6 + C_6H_5 &\rightleftharpoons C_{14}H_{10} + H + H_2 \end{aligned} \tag{14.143}$$

Based on their laminar methane flame data, the inception rate of soot particles was given to be eight times the formation rate of species $C_{10}H_7$ and $C_{14}H_{10}$, as shown by

$$\begin{aligned} \left(\frac{dN}{dt}\right)_{inception} &= 8C_{\alpha,1}\frac{N_A}{M_P}\left[\rho^2\left(\frac{Y_{C_2H_2}}{W_{C_2H_2}}\right)^2 \frac{Y_{C_6H_5}W_{H_2}}{W_{C_6H_5}Y_{H_2}}\right]\exp\left\{-\frac{T_{\alpha,1}}{T}\right\} \\ &\quad + 8C_{\alpha,2}\frac{N_A}{M_P}\left[\rho^2\frac{Y_{C_2H_2}}{W_{C_2H_2}}\frac{Y_{C_6H_6}Y_{C_6H_5}W_{H_2}}{W_{C_6H_6}W_{C_6H_5}Y_{H_2}}\right]\exp\left\{-\frac{T_{\alpha,2}}{T}\right\} \end{aligned} \tag{14.144}$$


Release 15.0 - © SAS IP, Inc. All rights reserved. - Contains proprietary and confidential information of ANSYS, Inc. and its subsidiaries and affiliates.

where $C_{\alpha,1}$ = 127 x $10^{8.88}$ $s^{-1}$, $C_{\alpha,2}$ = 178 x $10^{9.50}$ $s^{-1}$, $T_{\alpha,1}$ = 4378 K, and $T_{\alpha,2}$ = 6390 K as determined by Hall et al. [152] (p. 737). In their model, the mass of an incipient soot particle was assumed to be 1200 kg/kmol (corresponding to 100 carbon atoms, as opposed to 12 carbon atoms used by Brookes and Moss [47] (p. 731)). The mass density of soot was assumed to be 2000 kg/$m^3$, which is also slightly different from the value used by Brookes and Moss [47] (p. 731).

Both the coagulation term and the surface growth term were formulated similar to those used by Brookes and Moss [47] (p. 731), with a slight modification to the constant $C_\gamma$ so that the value is 9000.6 $\mathrm{kg \cdot m \cdot kmol^{-1} \cdot s^{-1}}$ (based on the model developed by Lindstedt [257] (p. 743)).

For the soot oxidation term, oxidation due to $O_2$ (based on measurements and a model based on Lee et al. [236] (p. 742)) was added, in addition to the soot oxidation due to the hydroxyl radical. By assuming that the kinetics of surface reactions are the limiting mechanism and that the particles are small enough to neglect the diffusion effect on the soot oxidation, they derived the specific rate of soot oxidation by molecular oxygen. Therefore, the full soot oxidation term, including that due to hydroxyl radical, is of the form

$$\left(\frac{dM}{dt}\right)_{oxid} = -C_{oxid}C_{\omega,1}\eta_{coll}\left(\frac{X_{OH}P}{RT}\right)\sqrt{T}\,(\pi N)^{1/3}\left(\frac{6M}{\rho_{soot}}\right)^{2/3} - C_{oxid}C_{\omega,2}\left(\frac{X_{O_2}P}{RT}\right)\exp\left\{-\frac{T_{\omega,2}}{T}\right\}\sqrt{T}\,(\pi N)^{1/3}\left(\frac{6M}{\rho_{soot}}\right)^{2/3} \quad (14.145)$$

Here, the collision efficiency is assumed to be 0.13 (compared to the value of 0.04 used by Brookes and Moss) and the oxidation rate scaling parameter is assumed to be unity. The model constants used are as follows:

$C_{\omega,1}$ = 105.81 $\mathrm{kg \cdot m \cdot kmol^{-1} \cdot K^{-1/2} \cdot s^{-1}}$ (same as that used by Brookes and Moss)

$C_{\omega,2}$ =8903.51 $\mathrm{kg \cdot m \cdot kmol^{-1} \cdot K^{-1/2} \cdot s^{-1}}$

$T_{\omega,2}$ =19778 K

### 14.3.2.3.2. Soot Formation in Turbulent Flows

The kinetic mechanisms of soot formation and destruction for the Moss-Brookes model and the Hall extension are obtained from laboratory experiments, in a similar fashion to the $NO_x$ model. In any practical combustion system, however, the flow is highly turbulent. The turbulent mixing process results in temporal fluctuations in temperature and species concentration that will influence the characteristics of the flame.

The relationships among soot formation rate, temperature, and species concentration are highly nonlinear. Hence, if time-averaged composition and temperature are employed in any model to predict the mean soot formation rate, significant errors will result. Temperature and composition fluctuations must be taken into account by considering the probability density functions that describe the time variation.

Release 15.0 - © SAS IP, Inc. All rights reserved. - Contains proprietary and confidential information of ANSYS, Inc. and its subsidiaries and affiliates.

#### 14.3.2.3.2.1. The Turbulence-Chemistry Interaction Model

In turbulent combustion calculations, ANSYS Fluent solves the density-weighted time-averaged Navier-Stokes equations for temperature, velocity, and species concentrations or mean mixture fraction and variance. To calculate soot concentration for the Moss-Brookes model and the Hall extension, a time-averaged soot formation rate must be computed at each point in the domain using the averaged flow-field information.

#### 14.3.2.3.2.2. The PDF Approach

The PDF method has proven very useful in the theoretical description of turbulent flow [188] (p. 739). In the ANSYS Fluent Moss-Brookes model and the Hall extension, a single- or joint-variable PDF in terms of a normalized temperature, species mass fraction, or the combination of both is used to predict the soot formation. If the non-premixed combustion model is used to model combustion, then a one- or two-variable PDF in terms of mixture fraction(s) is also available. The mean values of the independent variables needed for the PDF construction are obtained from the solution of the transport equations.

#### 14.3.2.3.2.3. The Mean Reaction Rate

The mean turbulent reaction rate described in The General Expression for the Mean Reaction Rate (p. 342) for the $\mathrm{NO}_x$ model also applies to the Moss-Brookes model and the Hall extension. The PDF is used for weighting against the instantaneous rates of production of soot and subsequent integration over suitable ranges to obtain the mean turbulent reaction rate as described in Equation 14.105 (p. 342) and Equation 14.106 (p. 342) for $\mathrm{NO}_x$.

#### 14.3.2.3.2.4. The PDF Options

As is the case with the $\mathrm{NO}_x$ model, $P$ can be calculated as either a two-moment beta function or as a clipped Gaussian function, as appropriate for combustion calculations [155] (p. 737), [301] (p. 745). Equation 14.108 (p. 343) – Equation 14.112 (p. 343) apply to the Moss-Brookes model and Hall extension as well, with the variance $\sigma^2$ computed by solving a transport equation during the combustion calculation stage, using Equation 14.113 (p. 343) or Equation 14.114 (p. 344).

### 14.3.2.3.3. The Effect of Soot on the Radiation Absorption Coefficient

A description of the modeling of soot-radiation interaction is provided in The Effect of Soot on the Absorption Coefficient (p. 172).

## 14.4. Decoupled Detailed Chemistry Model

The following sections present background information about the detailed chemistry pollutant model. To learn how to use this model, see Using the Decoupled Detailed Chemistry Model in the User's Guide.

14.4.1. Overview
14.4.2. Decoupled Detailed Chemistry Model Theory

## 14.4.1. Overview

Many pollutant species, such as $\mathrm{NO}_x$ and $\mathrm{SO}_x$, are slowly forming relative to the major combustion products, and require a finite-rate chemistry calculation. Further, the mass fractions of these pollutant species are usually very small and they have negligible influence on all other flow fields. Hence, for steady-state simulations, the solution of the pollutant transport equations can be decoupled from the other equations and solved in a postprocessing step. ANSYS Fluent offers several specific pollutant


Release 15.0 - © SAS IP, Inc. All rights reserved. - Contains proprietary and confidential information of ANSYS, Inc. and its subsidiaries and affiliates.

models ($NO_x$, $SO_x$, soot) with fixed chemical mechanisms. The detailed chemistry pollutant model allows pollutant postprocessing using any chemical kinetic mechanism.

#### 14.4.1.1. Limitations

The following limitations exist when using the detailed chemistry pollutant model:

- The detailed chemistry pollutant model is only available with the steady-state solver.
- Since pollutant chemistry is postprocessed on a steady-state solution, pollutant species cannot couple with the flow, energy, or any other field (for example, radiating soot).
- It can be difficult to revert to the original settings of your case file after you have set up the decoupled detailed chemistry pollutant model. This limitation can be addressed by saving case and data files prior to setting up the decoupled detailed chemistry pollutant model.

### 14.4.2. Decoupled Detailed Chemistry Model Theory

A decoupled detailed chemistry pollutant calculation starts from a converged steady-state combustion solution. This original solution can be obtained with the Species Transport, Non-Premixed, Partially-Premixed, or PDF Transport combustion models. After you have imported a detailed chemical mechanism through the CHEMKIN import facility, you will identify the pollutant species. The non-pollutant species in the detailed chemical mechanism that are not already in the original combustion solution are determined by a chemical equilibrium calculation at the fixed temperature of the original solution. Note that species that are not identified as pollutants and do not participate in the reactions amongst the pollutant species are eliminated. Similarly, reactions in the imported CHEMKIN mechanism that do not include any pollutant species are also eliminated.

The sequence of steps that occurs after the pollutant mechanism has been imported and the pollutant species selected is as follows:

1. A mixture material called **pollutant-mixture** is created and set as the default.
2. Non-pollutant, non-original species in the imported mechanism are set to their chemical equilibrium values at the cell temperature.
3. The Species Transport combustion model is enabled with the Laminar sub-model and the stiff chemistry solver.
4. The solution to all transport equations, except the selected pollutant species, is disabled.

Release 15.0 - © SAS IP, Inc. All rights reserved. - Contains proprietary and confidential information of ANSYS, Inc. and its subsidiaries and affiliates.

Release 15.0 - © SAS IP, Inc. All rights reserved. - Contains proprietary and confidential information
of ANSYS, Inc. and its subsidiaries and affiliates.

# Chapter 15: Aerodynamically Generated Noise

The discipline of acoustics is intimately related to fluid dynamics. Many sounds that are technologically important in industrial applications are generated by and propagated in fluid flows. The phenomena associated with sounds can therefore be understood and analyzed in the general framework of fluid dynamics. (The governing equations for acoustics are indeed the same as the ones governing fluid flows.)

The main challenge in numerically predicting sound waves stems from the well-recognized fact that sounds have much lower energy than fluid flows, typically by several orders of magnitude. This poses a great challenge to the computation of sounds in terms of difficulty of numerically resolving sound waves, especially when one is interested in predicting sound propagation to the far field. Another challenge comes from the difficulty of predicting the very flow phenomena (for example, turbulence) in the near field that are responsible for generating sounds.

This chapter provides an overview and theoretical background of ANSYS Fluent's approaches to computing aerodynamically generated sound. For more information about using the acoustics model, see Predicting Aerodynamically Generated Noise in the User's Guide.

15.1. Overview
15.2. Acoustics Model Theory

## 15.1. Overview

Considering the breadth of the discipline and the challenges encountered in aerodynamically generated noise, it is not surprising that a number of computational approaches have been proposed over the years whose sophistication, applicability, and cost widely vary.

ANSYS Fluent offers three approaches to computing aerodynamically generated noise; a direct method, an integral method based on acoustic analogy and a method that utilizes broadband noise source models.

This section is divided into the following sections:

15.1.1. Direct Method
15.1.2. Integral Method Based on Acoustic Analogy
15.1.3. Broadband Noise Source Models

### 15.1.1. Direct Method

In this method, both generation and propagation of sound waves are directly computed by solving the appropriate fluid dynamics equations. Prediction of sound waves always requires time-accurate solutions to the governing equations. Furthermore, in most practical applications of the direct method, one has to employ governing equations that are capable of modeling viscous and turbulence effects, such as unsteady Navier-Stokes equations (that is, DNS), RANS equations, and filtered equations used in DES and LES.

The direct method is therefore computationally difficult and expensive inasmuch as it requires highly accurate numerics, very fine computational meshes all the way to receivers, and acoustically non-reflecting

Release 15.0 - © SAS IP, Inc. All rights reserved. - Contains proprietary and confidential information of ANSYS, Inc. and its subsidiaries and affiliates.

boundary conditions. The computational cost becomes prohibitive when sound is to be predicted in the far field (for example, hundreds of chord-lengths in the case of an airfoil). The direct method becomes feasible when receivers are in the near field (for example, cabin noise). In many such situations involving near-field sound, sounds (or pseudo-sounds for that matter) are predominantly due to local hydrodynamic pressure which can be predicted with a reasonable cost and accuracy.

Since sound propagation is directly resolved in this method, one normally needs to solve the compressible form of the governing equations (for example, compressible RANS equations, compressible form of filtered equations for LES). Only in situations where the flow is low and subsonic, and the receivers in the near field consist primarily of local hydrodynamic pressure fluctuations (that is, pseudo sound), can incompressible flow formulations be used. However, this incompressible treatment will not permit you to simulate resonance and feedback phenomena.

## 15.1.2. Integral Method Based on Acoustic Analogy

For predictions of mid- to far-field noise, the methods based on Lighthill's acoustic analogy [251] (p. 742) offer viable alternatives to the direct method. In this approach, the near-field flow obtained from appropriate governing equations such as unsteady RANS equations, DES, or LES are used to predict the sound with the aid of analytically derived integral solutions to wave equations. The acoustic analogy essentially decouples the propagation of sound from its generation, allowing one to separate the flow solution process from the acoustics analysis.

ANSYS Fluent offers a method based on the Ffowcs-Williams and Hawkings (FW-H) formulation [118] (p. 735). The FW-H formulation adopts the most general form of Lighthill's acoustic analogy, and is capable of predicting sound generated by equivalent acoustic sources. ANSYS Fluent adopts a time-domain integral formulation wherein time histories of sound pressure, or acoustic signals, at prescribed receiver locations are directly computed by evaluating corresponding surface integrals.

Time-accurate solutions of the flow-field variables, such as pressure, velocity components, and density on source (emission) surfaces, are required to evaluate the surface integrals. Time-accurate solutions can be obtained from unsteady Reynolds-averaged Navier-Stokes (URANS) equations, large eddy simulation (LES), or detached eddy simulation (DES) as appropriate for the flow at hand and the features that you want to capture (for example, vortex shedding). The source surfaces can be placed not only on impermeable walls, but also on interior (permeable) surfaces, which enables you to account for the contributions from the quadrupoles enclosed by the source surfaces. Both broadband and tonal noise can be predicted depending on the nature of the flow (noise source) being considered, turbulence model employed, and the time scale of the flow resolved in the flow calculation.

The FW-H acoustics model in ANSYS Fluent allows you to select multiple source surfaces and receivers. Receivers can either be steady in the CFD reference frame or move with a user-specified constant velocity. The latter option enables modeling a "fly over" situation. The model also permits you either to save the source data for a future use, or to carry out an "on the fly" acoustic calculation simultaneously as the transient flow calculation proceeds, or both. Sound pressure signals thus obtained can be processed using the fast Fourier transform (FFT) and associated postprocessing capabilities to compute and plot such acoustic quantities as the overall sound pressure level (SPL) and power spectra.

One important limitation of the integral FW-H formulation is that it is applicable only to predicting the propagation of sound toward *free space*. Thus, while the model can be legitimately used to predict far-field noise due to external aerodynamic flows, such as the flows around ground vehicles and aircraft, it cannot be used for predicting the noise propagation inside ducts or wall-enclosed space.


Release 15.0 - © SAS IP, Inc. All rights reserved. - Contains proprietary and confidential information of ANSYS, Inc. and its subsidiaries and affiliates.

### 15.1.3. Broadband Noise Source Models

In many practical applications involving turbulent flows, noise does not have any distinct tones, and the sound energy is continuously distributed over a broad range of frequencies. In those situations involving *broadband noise*, statistical turbulence quantities readily computable from RANS equations can be utilized, in conjunction with semi-empirical correlations and Lighthill's acoustic analogy, to shed some light on the source of broadband noise.

ANSYS Fluent offers several such *source models* that enable you to quantify the local contribution (per unit surface area or volume) to the total acoustic power generated by the flow. They include the following:

- Proudman's formula
- jet noise source model
- boundary layer noise source model
- source terms in the linearized Euler equations
- source terms in Lilley's equation

Considering that one would ultimately want to come up with some measures to mitigate the noise generated by the flow in question, the source models can be employed to extract useful diagnostics on the noise source to determine which portion of the flow is primarily responsible for the noise generation. Note, however, that these source models do not predict the sound at receivers.

Unlike the direct method and the FW-H integral method, the broadband noise source models do not require transient solutions to any governing fluid dynamics equations. All source models require what typical RANS models would provide, such as the mean velocity field, turbulent kinetic energy ($k$) and the dissipation rate ($\varepsilon$). Therefore, the use of broadband noise source models requires the least computational resources.

## 15.2. Acoustics Model Theory

This section describes the theoretical background for the Ffowcs-Williams and Hawkings model and the broadband noise source models.

This section is divided into the following sections:

15.2.1. The Ffowcs-Williams and Hawkings Model
15.2.2. Broadband Noise Source Models

### 15.2.1. The Ffowcs-Williams and Hawkings Model

The Ffowcs-Williams and Hawkings (FW-H) equation is essentially an inhomogeneous wave equation that can be derived by manipulating the continuity equation and the Navier-Stokes equations. The FW-H [46] (p. 731), [118] (p. 735) equation can be written as:

Release 15.0 - © SAS IP, Inc. All rights reserved. - Contains proprietary and confidential information of ANSYS, Inc. and its subsidiaries and affiliates.

$$\begin{aligned}\frac{1}{a_0^2}\frac{\partial^2 p'}{\partial t^2}-\nabla^2 p' &= \frac{\partial^2}{\partial x_i \partial x_j}\left\{T_{ij}H(f)\right\} \\ &- \frac{\partial}{\partial x_i}\left\{\left[P_{ij}n_j+\rho u_i(u_n-v_n)\right]\delta(f)\right\} \\ &+ \frac{\partial}{\partial t}\left\{\left[\rho_0 v_n+\rho(u_n-v_n)\right]\delta(f)\right\}\end{aligned} \tag{15.1}$$

where

$u_i$ = fluid velocity component in the $x_i$ direction

$u_n$ = fluid velocity component normal to the surface $f=0$

$v_i$ = surface velocity components in the $x_i$ direction

$v_n$ = surface velocity component normal to the surface

$\delta(f)$ = Dirac delta function

$H(f)$ = Heaviside function

$p'$ is the sound pressure at the far field ($p'=p-p_0$). $f=0$ denotes a mathematical surface introduced to "embed" the exterior flow problem ($f>0$) in an unbounded space, which facilitates the use of generalized function theory and the free-space Green function to obtain the solution. The surface ($f=0$) corresponds to the source (emission) surface, and can be made coincident with a body (impermeable) surface or a permeable surface off the body surface. $n_i$ is the unit normal vector pointing toward the exterior region ($f>0$), $a_0$ is the far-field sound speed, and $T_{ij}$ is the Lighthill stress tensor, defined as

$$T_{ij}=\rho u_i u_j+P_{ij}-a_0^2\left(\rho-\rho_0\right)\delta_{ij} \tag{15.2}$$

$P_{ij}$ is the compressive stress tensor. For a Stokesian fluid, this is given by

$$P_{ij}=p\delta_{ij}-\mu\left[\frac{\partial u_i}{\partial x_j}+\frac{\partial u_j}{\partial x_i}-\frac{2}{3}\frac{\partial u_k}{\partial x_k}\delta_{ij}\right] \tag{15.3}$$

The free-stream quantities are denoted by the subscript $0$.

The wave equation Equation 15.1 (p. 364) can be integrated analytically under the assumptions of the free-space flow and the absence of obstacles between the sound sources and the receivers. The complete solution consists of surface integrals and volume integrals. The surface integrals represent the contributions from monopole and dipole acoustic sources and partially from quadrupole sources, whereas the volume integrals represent quadrupole (volume) sources in the region outside the source surface. The contribution of the volume integrals becomes small when the flow is low subsonic and the source surface encloses the source region. In ANSYS Fluent, the volume integrals are dropped. Thus, we have

$$p'(\vec{x},t)=p'_T(\vec{x},t)+p'_L(\vec{x},t) \tag{15.4}$$

where


Release 15.0 - © SAS IP, Inc. All rights reserved. - Contains proprietary and confidential information of ANSYS, Inc. and its subsidiaries and affiliates.

$$
\begin{aligned}
4\pi p'_T(\vec{x},t) &= \int_{f=0}\left[\frac{\rho_0(\dot{U}_n+U_{\dot{n}})}{r(1-M_r)^2}\right]dS \\
&+ \int_{f=0}\left[\frac{\rho_0 U_n\left\{r\dot{M}_r+a_0\left(M_r-M^2\right)\right\}}{r^2(1-M_r)^3}\right]d
\end{aligned}
\tag{15.5}
$$

$$
\begin{aligned}
4\pi p'_L(\vec{x},t) &= \frac{1}{a_0}\int_{f=0}\left[\frac{\dot{L}_r}{r(1-M_r)^2}\right]dS \\
&+ \int_{f=0}\left[\frac{L_r-L_M}{r^2(1-M_r)^2}\right]dS \\
&+ \frac{1}{a_0}\int_{f=0}\left[\frac{L_r\left\{r\dot{M}_r+a_0\left(M_r-M^2\right)\right\}}{r^2(1-M_r)^3}\right]dS
\end{aligned}
\tag{15.6}
$$

where

$$U_i = v_i+\frac{\rho}{\rho_0}(u_i-v_i) \tag{15.7}$$

$$L_i = P_{ij}\hat{n}_j+\rho u_i(u_n-v_n) \tag{15.8}$$

When the integration surface coincides with an impenetrable wall, the two terms on the right in Equation 15.4 (p. 364), $p'_T(\vec{x},t)$ and $p'_L(\vec{x},t)$, are often referred to as thickness and loading terms, respectively, in light of their physical meanings. The square brackets in Equation 15.5 (p. 365) and Equation 15.6 (p. 365) denote that the kernels of the integrals are computed at the corresponding retarded times, $\tau$, defined as follows, given the receiver time, $t$, and the distance to the receiver, $r$,

$$\tau = t-\frac{r}{a_0} \tag{15.9}$$

The various subscripted quantities appearing in Equation 15.5 (p. 365) and Equation 15.6 (p. 365) are the inner products of a vector and a unit vector implied by the subscript. For instance, $L_r=\vec{L}\cdot\hat{\vec{r}}=L_i r_i$ and $U_n=\vec{U}\cdot\vec{n}=U_i n_i$, where $\vec{r}$ and $\vec{n}$ denote the unit vectors in the radiation and wall-normal directions, respectively. The Mach number vector $M_i$ in Equation 15.5 (p. 365) and Equation 15.6 (p. 365) relates to the motion of the integration surface: $M_i=v_i/a_o$. The $L_i$ quantity is a scalar product $L_i M_i$. The dot over a variable denotes source-time differentiation of that variable.

For the calculation of the aerodynamic sound caused by external flow around a body, the **Convective Effects** option must be enabled (see Setting Model Constants in the User's Guide) with the far-field fluid velocity vector $\vec{V}_{conv}$ to be additionally specified. This option is relevant to practical situations such as the flight tests (microphones mounted on an airplane) or wind tunnel measurements (microphones mounted within the wind tunnel core flow region).

With the convective effects taken into account, the retarded time calculation becomes more complicated than the simple form of Equation 15.9 (p. 365). As illustrated in Figure 15.1: Schematic of the Convective

Release 15.0 - © SAS IP, Inc. All rights reserved. - Contains proprietary and confidential information of ANSYS, Inc. and its subsidiaries and affiliates.

Effect on the Retarded Time Calculation (p. 366), the effective sound propagation velocity $a_\theta$ is lower than $a_0$ in the upstream hemisphere and higher than $a_0$ in the downstream hemisphere, where $\theta$ is the direction angle towards the receiver counted from the upstream direction. According to Figure 15.1: Schematic of the Convective Effect on the Retarded Time Calculation (p. 366) the retarded time with the convective effect must be computed as

$$\tau = t - r/a_\theta, \quad a_\theta = \sqrt{a_0^2 - V_{conv}^2 \sin^2\theta} - V_{conv}\cos\theta \tag{15.10}$$

An obvious limitation for the **Convective Effects** option is that the far-field convection must be subsonic $(V_{conv} < a_0)$

**Figure 15.1: Schematic of the Convective Effect on the Retarded Time Calculation**

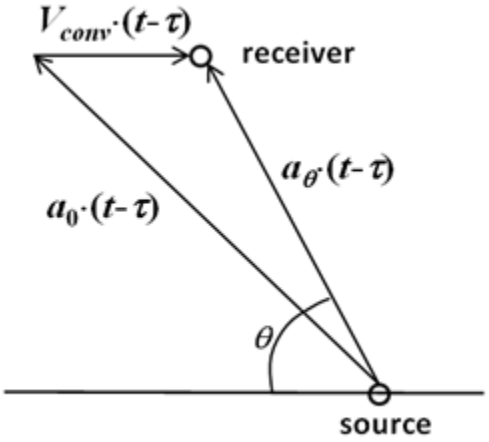


Note the following remarks regarding the applicability of the FW-H integral solution:

- The FW-H formulation in ANSYS Fluent can handle rotating surfaces as well as stationary surfaces.
- It is not required that the surface $f = 0$ coincide with body surfaces or walls. The formulation permits source surfaces to be permeable, and therefore can be placed in the interior of the flow.
- When a permeable source surface (either interior or nonconformal sliding interface) is placed at a certain distance off the body surface, the integral solutions given by Equation 15.5 (p. 365) and Equation 15.6 (p. 365) include the contributions from the quadrupole sources within the region enclosed by the source surface. When using a permeable source surface, the mesh resolution must be fine enough to resolve the transient flow structures inside the volume enclosed by the permeable surface.

## 15.2.2. Broadband Noise Source Models

### *15.2.2.1. Proudman's Formula*

Proudman [363] (p. 749), using Lighthill's acoustic analogy, derived a formula for acoustic power generated by isotropic turbulence without mean flow. More recently, Lilley [252] (p. 743) re-derived the formula by accounting for the retarded time difference that was neglected in Proudman's original derivation.

Both derivations yield acoustic power due to the unit volume of isotropic turbulence (in $\mathrm{W/m^3}$) as

$$P_A = \alpha \rho_0 \left(\frac{u^3}{\ell}\right)\frac{u^5}{a_0^5} \tag{15.11}$$


Release 15.0 - © SAS IP, Inc. All rights reserved. - Contains proprietary and confidential information of ANSYS, Inc. and its subsidiaries and affiliates.

where $u$ and $\ell$ are the turbulence velocity and length scales, respectively, and $a_0$ is the speed of sound. $\alpha$ in Equation 15.11 (p. 366) is a model constant. In terms of $k$ and $\varepsilon$, Equation 15.11 (p. 366) can be re-written as

$$P_A = \alpha_\varepsilon \rho_0 \varepsilon M_t^5 \tag{15.12}$$

where

$$M_t = \frac{\sqrt{2k}}{a_0} \tag{15.13}$$

The rescaled constant, $\alpha_\varepsilon$, is set to 0.1 in ANSYS Fluent based on the calibration of Sarkar and Hussaini [387] (p. 750) in using direct numerical simulation of isotropic turbulence.

ANSYS Fluent can also report the acoustic power in dB, which is computed from

$$L_P = 10 \log\left(\frac{P_A}{P_{ref}}\right) \tag{15.14}$$

where $P_{ref}$ is the reference acoustic power ($P_{ref}$=$10^{-12}$ W/m$^3$ by default).

The Proudman's formula gives an approximate measure of the local contribution to total acoustic power per unit volume in a given turbulence field. Proper caution, however, should be taken when interpreting the results in view of the assumptions made in the derivation, such as high Reynolds number, small Mach number, isotropy of turbulence, and zero mean motion.

### 15.2.2.2. The Jet Noise Source Model

This source model for axisymmetric jets is based on the works of Goldstein [142] (p. 736) who modified the model originally proposed by Ribner [377] (p. 749) to better account for anisotropy of turbulence in axisymmetric turbulent jets.

In Goldstein's model, the total acoustic power emitted by the unit volume of a turbulent jet is computed from

$$\begin{aligned} P_A(\vec{y}) &= \int_0^{2\pi}\int_0^{\pi} I(r,\theta;\ \vec{y})\, r^2 \sin\theta d\theta d\psi \\ &= 2\pi r^2 \int_0^{\pi} I(r,\theta;\ \vec{y})\, \sin\theta d\theta \end{aligned} \tag{15.15}$$

where $r$ and $\theta$ are the radial and angular coordinates of the receiver location, and $I(r,\theta;\ \vec{y})$ is the directional acoustic intensity per unit volume of a jet defined by

$$I(r,\theta;\ \vec{y}) = \frac{12\rho_0 \omega_f^4 L_1 L_2^2 \overline{u_{t1}^2}^2}{5\pi a_0^5 r^2} \frac{D_{self}}{C^5} + \frac{24\rho_0 \omega_f^4 L_1 L_2^4 \overline{u_{t1}^2}}{\pi a_0^5 r^2} \left(\frac{\partial U}{\partial r}\right)^2 \frac{D_{shear}}{C^5} \tag{15.16}$$

$C$ in Equation 15.16 (p. 367) is the modified convection factor defined by

$$C = 1 - M_c \cos\theta \tag{15.17}$$

and

$$D_{self} = 1+2\left(\frac{M}{9}-N\right)\cos^2\theta\sin^2\theta + \frac{1}{3}\left[\frac{M^2}{7}+M-1.5N\left(3-3N+\frac{1.5}{\Delta^2}-\frac{\Delta^2}{2}\right)\right]\sin^4\theta \quad (15.18)$$

$$D_{shear} = \cos^2\theta\left[\cos^2\theta+\frac{1}{2}\left(\frac{1}{\Delta^2}-2N\right)\sin^2\theta\right] \quad (15.19)$$

The remaining parameters are defined as

$$\Delta = \frac{L_2}{L_1} \quad (15.20)$$

$$M = \left[\frac{3}{2}\left(\Delta-\frac{1}{\Delta}\right)\right]^2 \quad (15.21)$$

$$N = 1-\frac{\left(\overline{u_{t2}^2}\right)}{\left(\overline{u_{t1}^2}\right)} \quad (15.22)$$

$$L_1 = \frac{\left(\overline{u_{t1}^2}\right)^{3/2}}{\varepsilon} \quad (15.23)$$

$$L_2 = \frac{\left(\overline{u_{t2}^2}\right)^{3/2}}{\varepsilon} \quad (15.24)$$

$$\omega_f = 2\pi\frac{\varepsilon}{k} \quad (15.25)$$

where $\overline{u_{t1}^2}$ and $\overline{u_{t2}^2}$ are computed differently depending on the turbulence model chosen for the computation. When the RSM is selected, they are computed from the corresponding normal stresses. For all other two-equation turbulence models, they are obtained from

$$\overline{u_{t1}^2} = \frac{8}{9}k \quad (15.26)$$

$$\overline{u_{t2}^2} = \frac{4}{9}k \quad (15.27)$$

ANSYS Fluent reports the acoustic power both in the dimensional units ($W/m^3$) and in dB computed from

$$L_P = 10\log\left(\frac{P_A}{P_{ref}}\right) \quad (15.28)$$


Release 15.0 - © SAS IP, Inc. All rights reserved. - Contains proprietary and confidential information of ANSYS, Inc. and its subsidiaries and affiliates.

where $P_{ref}$ is the reference acoustic power ($P_{ref}$=$10^{-12}$ W/m$^3$ by default).

### 15.2.2.3. The Boundary Layer Noise Source Model

Far-field sound generated by turbulent boundary layer flow over a solid body at low Mach numbers is often of practical interest. The Curle's integral [82] (p. 733) based on acoustic analogy can be used to approximate the local contribution from the body surface to the total acoustic power. To that end, one can start with the Curle's integral

$$p'(\vec{x},t)=\frac{1}{4\pi a_0}\int_S \frac{(x_i-y_i)n_i}{r^2}\frac{\partial p}{\partial t}(\vec{y},\tau)\,dS(\vec{y}) \tag{15.29}$$

where $\tau$ denotes the emission time ($\tau=t-r/a_0$), and $S$ the integration surface.

Using this, the sound intensity in the far field can then be approximated by

$$\overline{p'^2}\approx\frac{1}{16\pi^2 a_0^2}\int_S \frac{\cos^2\theta}{r^2}\overline{\left[\frac{\partial p}{\partial t}(\vec{y},\tau)\right]^2}\,\mathcal{A}_c(\vec{y})\,dS(\vec{y}) \tag{15.30}$$

where $\mathcal{A}_c$ is the correlation area, $r \equiv |\vec{x}-\vec{y}|$, and $\theta$ is the angle between $|\vec{x}-\vec{y}|$ and the wall-normal direction $\vec{n}$.

The total acoustic power emitted from the entire body surface can be computed from

$$\begin{aligned} P_A &= \frac{1}{\rho_0 a_0}\int_0^{2\pi}\int_0^{\pi}\overline{p'^2}\,r^2\sin\theta\,d\theta\,d\psi \\ &= \int_S I(\vec{y})\,dS(\vec{y}) \end{aligned} \tag{15.31}$$

where

$$I(\vec{y})\equiv\frac{\mathcal{A}_c(\vec{y})}{12\rho_0\pi a_0^3}\overline{\left[\frac{\partial p}{\partial t}\right]^2} \tag{15.32}$$

which can be interpreted as the local contribution per unit surface area of the body surface to the total acoustic power. The mean-square time derivative of the surface pressure and the correlation area are further approximated in terms of turbulent quantities like turbulent kinetic energy, dissipation rate, and wall shear.

ANSYS Fluent reports the acoustic surface power defined by Equation 15.32 (p. 369) both in physical (W/m$^2$) and dB units.

### 15.2.2.4. Source Terms in the Linearized Euler Equations

The linearized Euler equations (LEE) can be derived from the Navier-Stokes equations starting from decompositions of the flow variables into mean, turbulent, and acoustic components, and by assuming that the acoustic components are much smaller than the mean and turbulent components. The resulting linearized Euler equations for the acoustic velocity components can be written as

Release 15.0 - © SAS IP, Inc. All rights reserved. - Contains proprietary and confidential information of ANSYS, Inc. and its subsidiaries and affiliates.

$$\frac{\partial u_{ai}}{\partial t}+U_j\frac{\partial u_{ai}}{\partial x_j}+u_{aj}\frac{\partial U_i}{\partial x_j}+\frac{1}{\overline{\rho}}\frac{\partial p_a}{\partial x_i}-\frac{\rho_a}{\overline{\rho}^2}\frac{\partial P}{\partial x_i}= \underbrace{-U_j\frac{\partial u'_i}{\partial x_j}-u'_j\frac{\partial U_i}{\partial x_j}}_{L_{sh}}\underbrace{-u'_j\frac{\partial u'_i}{\partial x_j}}_{L_{se}} -\frac{1}{\overline{\rho}}\frac{\partial p'}{\partial x_i}-\frac{\partial u'_i}{\partial t}+\frac{\partial}{\partial x_j}\overline{u'_j u'_i} \tag{15.33}$$

where the subscript "$a$" refers to the corresponding acoustic components, and the prime superscript refers to the turbulent components.

The right side of Equation 15.33 (p. 370) can be considered as effective source terms responsible for sound generation. Among them, the first three terms involving turbulence are the main contributors. The first two terms denoted by $L_{sh}$ are often referred to as "shear-noise" source terms, since they involve the mean shear. The third term denoted by $L_{se}$ is often called the "self-noise" source term, as it involves turbulent velocity components only.

The turbulent velocity field needed to compute the LEE source terms is obtained using the method of stochastic noise generation and radiation (SNGR) [29] (p. 730). In this method, the turbulent velocity field and its derivatives are computed from a sum of $N$ Fourier modes.

$$\vec{u}\,(\vec{x},t)=2\sum_{n=1}^{N}\tilde{u}_n\cos\left(\vec{k}_n\cdot\vec{x}+\psi_n\right)\vec{\sigma}_n \tag{15.34}$$

where $\tilde{u}_n, \psi_n, \vec{\sigma}_n$ are the amplitude, phase, and directional (unit) vector of the $n^{th}$ Fourier mode associated with the wave-number vector $\vec{k}_n$.

Note that the source terms in the LEE are vector quantities, having two or three components depending on the dimension of the problem at hand.

### 15.2.2.5. Source Terms in Lilley's Equation

Lilley's equation is a third-order wave equation that can be derived by combining the conservation of mass and momentum of compressible fluids. When the viscous terms are omitted, it can be written in the following form:

$$\frac{D}{Dt}\left[\frac{D^2\Pi}{Dt^2}-\frac{\partial}{\partial x_j}\left(a^2\frac{\partial\Pi}{\partial x_j}\right)\right]+2\frac{\partial u_k}{\partial x_j}\frac{\partial}{\partial x_k}\left(a^2\frac{\partial\Pi}{\partial x_j}\right)=-2\frac{\partial u_k}{\partial x_i}\frac{\partial u_j}{\partial x_k}\frac{\partial u_i}{\partial x_j} \tag{15.35}$$

where $\Pi=(1/\gamma)\ln\frac{p}{p_o}$.

Lilley's equation can be linearized about the underlying steady flow as

$$u_i(\vec{x},t)=U_i(\vec{x})+u'_i(\vec{x},t) \tag{15.36}$$

where $u'(\vec{x},t)$ is the turbulent velocity component.

Substituting Equation 15.36 (p. 370) into the source term of Equation 15.35 (p. 370), we have


Release 15.0 - © SAS IP, Inc. All rights reserved. - Contains proprietary and confidential information of ANSYS, Inc. and its subsidiaries and affiliates.

$$
\begin{aligned}
S &\equiv -2\frac{\partial u_k}{\partial x_i}\frac{\partial u_j}{\partial x_k}\frac{\partial u_i}{\partial x_j} \\
&= -2\frac{\partial U_k}{\partial x_i}\frac{\partial U_j}{\partial x_k}\frac{\partial U_i}{\partial x_j} \underbrace{-2\frac{\partial u'_k}{\partial x_i}\frac{\partial u'_j}{\partial x_k}\frac{\partial u'_i}{\partial x_j}}_{\text{Self-Noise Terms}} \underbrace{-6\frac{\partial U_k}{\partial x_i}\frac{\partial U_j}{\partial x_k}\frac{\partial u'_i}{\partial x_j} - 6\frac{\partial u'_k}{\partial x_i}\frac{\partial u'_j}{\partial x_k}\frac{\partial U_i}{\partial x_j}}_{\text{Shear-Noise Terms}}
\end{aligned}
\tag{15.37}
$$

The resulting source terms in Equation 15.37 (p. 371) are evaluated using the mean velocity field and the turbulent (fluctuating) velocity components synthesized by the SNGR method. As with the LEE source terms, the source terms in Equation 15.37 (p. 371) are grouped depending on whether the mean velocity gradients are involved (*shear noise* or *self noise*), and reported separately in ANSYS Fluent.

Release 15.0 - © SAS IP, Inc. All rights reserved. - Contains proprietary and confidential information of ANSYS, Inc. and its subsidiaries and affiliates.

Release 15.0 - © SAS IP, Inc. All rights reserved. - Contains proprietary and confidential information
of ANSYS, Inc. and its subsidiaries and affiliates.

# Chapter 16: Discrete Phase

This chapter describes the theory behind the Lagrangian discrete phase capabilities available in ANSYS Fluent. For information about how to use discrete phase models, see Modeling Discrete Phase in the User's Guide. Information in this chapter is organized into the following sections:


16.1. Introduction
16.2. Particle Motion Theory
16.3. Laws for Drag Coefficients
16.4. Laws for Heat and Mass Exchange
16.5. Vapor Liquid Equilibrium Theory
16.6. Wall-Jet Model Theory
16.7. Wall-Film Model Theory
16.8. Particle Erosion and Accretion Theory
16.9. Atomizer Model Theory
16.10. Secondary Breakup Model Theory
16.11. Collision and Droplet Coalescence Model Theory
16.12. Discrete Element Method Collision Model
16.13. One-Way and Two-Way Coupling
16.14. Node Based Averaging


## 16.1. Introduction

Advances in computational fluid mechanics have provided the basis for further insight into the dynamics of multiphase flows. Currently there are two approaches for the numerical calculation of multiphase flows: the Euler-Lagrange approach (discussed below) and the Euler-Euler approach (discussed in Approaches to Multiphase Modeling (p. 468)).

For more information, see the following section:


16.1.1. The Euler-Lagrange Approach


### 16.1.1. The Euler-Lagrange Approach

The Lagrangian discrete phase model in ANSYS Fluent (described in this chapter) follows the Euler-Lagrange approach. The fluid phase is treated as a continuum by solving the Navier-Stokes equations, while the dispersed phase is solved by tracking a large number of particles, bubbles, or droplets through the calculated flow field. The dispersed phase can exchange momentum, mass, and energy with the fluid phase.

This approach is made considerably simpler when particle-particle interactions can be neglected, and this requires that the dispersed second phase occupies a low volume fraction, even though high mass loading ($\dot{m}_{particles} \geq \dot{m}_{fluid}$) is acceptable. The particle or droplet trajectories are computed individually at specified intervals during the fluid phase calculation. This makes the model appropriate for the modeling of spray dryers, coal and liquid fuel combustion, and some particle-laden flows, but inappropriate for the modeling of liquid-liquid mixtures, fluidized beds, or any application where the volume fraction of the second phase cannot be neglected. For applications such as these, particle-particle interactions can be included using the Discrete Element Model, which is discussed in Discrete Element Method Collision Model (p. 453).


Release 15.0 - © SAS IP, Inc. All rights reserved. - Contains proprietary and confidential information of ANSYS, Inc. and its subsidiaries and affiliates.

Limitations of the discrete phase model are listed in Limitations in the User's Guide.

# 16.2. Particle Motion Theory

This section is composed of the following:

16.2.1. Equations of Motion for Particles
16.2.2. Turbulent Dispersion of Particles
16.2.3. Integration of Particle Equation of Motion

## 16.2.1. Equations of Motion for Particles

### 16.2.1.1. Particle Force Balance

ANSYS Fluent predicts the trajectory of a discrete phase particle (or droplet or bubble) by integrating the force balance on the particle, which is written in a Lagrangian reference frame. This force balance equates the particle inertia with the forces acting on the particle, and can be written as

$$\frac{d\vec{u}_p}{dt} = F_D(\vec{u} - \vec{u}_p) + \frac{\vec{g}(\rho_p - \rho)}{\rho_p} + \vec{F} \tag{16.1}$$

where $\vec{F}$ is an additional acceleration (force/unit particle mass) term, $F_D(\vec{u} - \vec{u}_p)$ is the drag force per unit particle mass and

$$F_D = \frac{18\mu}{\rho_p d_p^2}\frac{C_D Re}{24} \tag{16.2}$$

Here, $\vec{u}$ is the fluid phase velocity, $\vec{u}_p$ is the particle velocity, $\mu$ is the molecular viscosity of the fluid, $\rho$ is the fluid density, $\rho_p$ is the density of the particle, and $d_p$ is the particle diameter. Re is the relative Reynolds number, which is defined as

$$Re \equiv \frac{\rho d_p \left| \vec{u}_p - \vec{u} \right|}{\mu} \tag{16.3}$$

### 16.2.1.2. Inclusion of the Gravity Term

While Equation 16.1 (p. 374) includes a force of gravity on the particle, it is important to note that in ANSYS Fluent the default gravitational acceleration is zero. If you want to include the gravitational force, you must remember to define the magnitude and direction of the gravity vector in the Operating Conditions Dialog Box.

### 16.2.1.3. Other Forces

Equation 16.1 (p. 374) incorporates additional forces ($\vec{F}$) in the particle force balance that can be important under special circumstances. The first of these is the "virtual mass" force, the force required to accelerate the fluid surrounding the particle. This force can be written as

$$\vec{F} = C_{vm}\frac{\rho}{\rho_p}\left(\vec{u}_p \nabla \vec{u} - \frac{d\vec{u}_p}{dt}\right) \tag{16.4}$$

where $C_{vm}$ is the virtual mass factor with a default value of `0.5`.


Release 15.0 - © SAS IP, Inc. All rights reserved. - Contains proprietary and confidential information of ANSYS, Inc. and its subsidiaries and affiliates.

An additional force arises due to the pressure gradient in the fluid:

$$\vec{F} = \frac{\rho}{\rho_p} \vec{u}_p \nabla \vec{u} \tag{16.5}$$

The virtual mass and pressure gradient forces are not important when the density of the fluid is much lower than the density of the particles as is the case for liquid/solid particles in gaseous flows ($\rho/\rho_p \ll 1$). For values of $\rho/\rho_p$ approaching unity, the Virtual Mass and Pressure Gradient forces become significant and it is recommended that they be included when the density ratio is greater than 0.1. See Including the Virtual Mass Force and Pressure Gradient Effects on Particles in Fluent User's Guide for details on how to include these forces in your model.

### 16.2.1.4. Forces in Moving Reference Frames

The additional force term, $\vec{F}$, in Equation 16.1 (p. 374) also includes forces on particles that arise due to rotation of the reference frame. These forces arise when you are modeling flows in moving frames of reference (see Flow in a Moving Reference Frame (p. 18)). For rotation defined about the $z$ axis, for example, the forces on the particles in the Cartesian $x$ and $y$ directions can be written as

$$\left(1 - \frac{\rho}{\rho_p}\right)\Omega^2 x + 2\Omega\left(u_{p,y} - \frac{\rho}{\rho_p}u_y\right) \tag{16.6}$$

where $u_{p,y}$ and $u_y$ are the particle and fluid velocities in the Cartesian $y$ direction, $\Omega$ is the RPM, and

$$\left(1 - \frac{\rho}{\rho_p}\right)\Omega^2 y - 2\Omega\left(u_{p,x} - \frac{\rho}{\rho_p}u_x\right) \tag{16.7}$$

where $u_{p,x}$ and $u_x$ are the particle and fluid velocities in the Cartesian $x$ direction.

### 16.2.1.5. Thermophoretic Force

Small particles suspended in a gas that has a temperature gradient experience a force in the direction opposite to that of the gradient. This phenomenon is known as thermophoresis. ANSYS Fluent can optionally include a thermophoretic effect on particles in the additional acceleration (force/unit mass) term, $F_x$, in Equation 16.1 (p. 374):

$$\vec{F} = -D_{T,p}\frac{1}{m_p T}\nabla T \tag{16.8}$$

where $D_{T,p}$ is the thermophoretic coefficient. You can define the coefficient to be constant, polynomial, or a user-defined function, or you can use the form suggested by Talbot [444] (p. 753):

$$\vec{F} = -\frac{6\pi d_p \mu^2 C_s (K + C_t Kn)}{\rho(1 + 3C_m Kn)(1 + 2K + 2C_t Kn)}\frac{1}{m_p T}\nabla T \tag{16.9}$$

where:

$Kn$ = Knudsen number = $2\lambda/d_p$

Release 15.0 - © SAS IP, Inc. All rights reserved. - Contains proprietary and confidential information of ANSYS, Inc. and its subsidiaries and affiliates.

$\lambda$ = mean free path of the fluid

$K = k/k_p$

$k$ = fluid thermal conductivity based on translational energy only = (15/4) $\mu R$

$k_p$ = particle thermal conductivity

$C_S$ = 1.17

$C_t$ = 2.18

$C_m$ = 1.14

$m_p$ = particle mass

$T$ = local fluid temperature

$\mu$ = fluid viscosity

This expression assumes that the particle is a sphere and that the fluid is an ideal gas.

### 16.2.1.6. Brownian Force

For sub-micron particles, the effects of Brownian motion can be optionally included in the additional force term. The components of the Brownian force are modeled as a Gaussian white noise process with spectral intensity $S_{n,ij}$ given by [246] (p. 742)

$$S_{n,ij} = S_0 \delta_{ij} \tag{16.10}$$

where $\delta_{ij}$ is the Kronecker delta function, and

$$S_0 = \frac{216 \nu k_B T}{\pi^2 \rho d_p^5 \left(\frac{\rho_p}{\rho}\right)^2 C_c} \tag{16.11}$$

$T$ is the absolute temperature of the fluid, $\nu$ is the kinematic viscosity, $C_c$ is the Cunningham correction (defined in Equation 16.69 (p. 386)), and $k_B$ is the Boltzmann constant. Amplitudes of the Brownian force components are of the form

$$F_{b_i} = \zeta_i \sqrt{\frac{\pi S_o}{\Delta t}} \tag{16.12}$$

where $\zeta_i$ are zero-mean, unit-variance-independent Gaussian random numbers. The amplitudes of the Brownian force components are evaluated at each time step. The energy equation must be enabled in order for the Brownian force to take effect. Brownian force is intended only for laminar simulations.

### 16.2.1.7. Saffman's Lift Force

The Saffman's lift force, or lift due to shear, can also be included in the additional force term as an option. The lift force used is from Li and Ahmadi [246] (p. 742) and is a generalization of the expression provided by Saffman [383] (p. 750):

$$\vec{F} = \frac{2K\nu^{1/2}\rho d_{ij}}{\rho_p d_p (d_{lk} d_{kl})^{1/4}} \left(\vec{u} - \vec{u}_p\right) \tag{16.13}$$


Release 15.0 - © SAS IP, Inc. All rights reserved. - Contains proprietary and confidential information of ANSYS, Inc. and its subsidiaries and affiliates.

where $K = 2.594$ and $d_{ij}$ is the deformation tensor. This form of the lift force is intended for small particle Reynolds numbers and is recommended only for sub-micron particles.

## 16.2.2. Turbulent Dispersion of Particles

The dispersion of particles due to turbulence in the fluid phase can be predicted using the stochastic tracking model or the particle cloud model (see Turbulent Dispersion of Particles (p. 377)). The stochastic tracking (random walk) model includes the effect of instantaneous turbulent velocity fluctuations on the particle trajectories through the use of stochastic methods (see Stochastic Tracking (p. 377)). The particle cloud model tracks the statistical evolution of a cloud of particles about a mean trajectory (see Particle Cloud Tracking (p. 379)). The concentration of particles within the cloud is represented by a Gaussian probability density function (PDF) about the mean trajectory. For stochastic tracking a model is available to account for the generation or dissipation of turbulence in the continuous phase (see Coupling Between the Discrete and Continuous Phases (p. 459)).

**Important**

Turbulent dispersion of particles cannot be included if the Spalart-Allmaras turbulence model is used.

### *16.2.2.1. Stochastic Tracking*

When the flow is turbulent, ANSYS Fluent will predict the trajectories of particles using the mean fluid phase velocity, $\overline{u}$, in the trajectory equations (Equation 16.1 (p. 374)). Optionally, you can include the instantaneous value of the fluctuating gas flow velocity,

$$u = \overline{u} + u' \tag{16.14}$$

to predict the dispersion of the particles due to turbulence.

In the stochastic tracking approach, ANSYS Fluent predicts the turbulent dispersion of particles by integrating the trajectory equations for individual particles, using the instantaneous fluid velocity, $\overline{u} + u'(t)$, along the particle path during the integration. By computing the trajectory in this manner for a sufficient number of representative particles (termed the "number of tries"), the random effects of turbulence on the particle dispersion can be included.

ANSYS Fluent uses a stochastic method (random walk model) to determine the instantaneous gas velocity. In the discrete random walk (DRW) model, the fluctuating velocity components are discrete piecewise constant functions of time. Their random value is kept constant over an interval of time given by the characteristic lifetime of the eddies.

The DRW model may give nonphysical results in strongly nonhomogeneous diffusion-dominated flows, where small particles should become uniformly distributed. Instead, the DRW will show a tendency for such particles to concentrate in low-turbulence regions of the flow. In addition, this model is known to give poor prediction of the wall impaction rate of particles with a diameter less than a few microns due to turbulence.

#### 16.2.2.1.1. The Integral Time

Prediction of particle dispersion makes use of the concept of the integral time scale, $T$:

Release 15.0 - © SAS IP, Inc. All rights reserved. - Contains proprietary and confidential information of ANSYS, Inc. and its subsidiaries and affiliates.

$$T = \int_0^\infty \frac{u_p'(t)\,u_p'(t-\tau)}{\overline{u_p'^2}}\,d\tau \tag{16.15}$$

The integral time is proportional to the particle dispersion rate, as larger values indicate more turbulent motion in the flow. It can be shown that the particle diffusivity is given by $\overline{u_i' u_j'} T$.

For small "tracer" particles that move with the fluid (zero drift velocity), the integral time becomes the fluid Lagrangian integral time, $T_L$. This time scale can be approximated as

$$T_L = C_L \frac{k}{\varepsilon} \tag{16.16}$$

where $C_L$ is to be determined as it is not well known. By matching the diffusivity of tracer particles, $\overline{u_i' u_j'} T_L$, to the scalar diffusion rate predicted by the turbulence model, $\nu_t/\sigma$, one can obtain

$$T_L \approx 0.15 \frac{k}{\varepsilon} \tag{16.17}$$

for the $k$- $\varepsilon$ model and its variants, and

$$T_L \approx 0.30 \frac{k}{\varepsilon} \tag{16.18}$$

when the Reynolds stress model (RSM) is used [86] (p. 733). For the $k$- $\omega$ models, substitute $\omega = \varepsilon/k$ into Equation 16.16 (p. 378). The LES model uses the equivalent LES time scales.

### 16.2.2.1.2. The Discrete Random Walk Model

In the discrete random walk (DRW) model, or "eddy lifetime" model, the interaction of a particle with a succession of discrete stylized fluid phase turbulent eddies is simulated [143] (p. 736). Each eddy is characterized by

- a Gaussian distributed random velocity fluctuation, $u'$, $v'$, and $w'$
- a time scale, $\tau_e$

The values of $u'$, $v'$, and $w'$ that prevail during the lifetime of the turbulent eddy are sampled by assuming that they obey a Gaussian probability distribution, so that

$$u' = \zeta \sqrt{\overline{u'^2}} \tag{16.19}$$

where $\zeta$ is a normally distributed random number, and the remainder of the right-hand side is the local RMS value of the velocity fluctuations. Since the kinetic energy of turbulence is known at each point in the flow, these values of the RMS fluctuating components can be defined (assuming isotropy) as

$$\sqrt{\overline{u'^2}} = \sqrt{\overline{v'^2}} = \sqrt{\overline{w'^2}} = \sqrt{2k/3} \tag{16.20}$$

for the $k$- $\varepsilon$ model, the $k$- $\omega$ model, and their variants. When the RSM is used, nonisotropy of the stresses is included in the derivation of the velocity fluctuations:

$$u' = \zeta \sqrt{\overline{u'^2}} \tag{16.21}$$


Release 15.0 - © SAS IP, Inc. All rights reserved. - Contains proprietary and confidential information of ANSYS, Inc. and its subsidiaries and affiliates.

$$v' = \zeta \sqrt{\overline{v'^2}} \tag{16.22}$$

$$w' = \zeta \sqrt{\overline{w'^2}} \tag{16.23}$$

when viewed in a reference frame in which the second moment of the turbulence is diagonal [505] (p. 757). For the LES model, the velocity fluctuations are equivalent in all directions. See Inlet Boundary Conditions for the LES Model (p. 106) for details.

The characteristic lifetime of the eddy is defined either as a constant:

$$\tau_e = 2T_L \tag{16.24}$$

where $T_L$ is given by Equation 16.16 (p. 378) in general (Equation 16.17 (p. 378) by default), or as a random variation about $T_L$:

$$\tau_e = -T_L \ln(r) \tag{16.25}$$

where $r$ is a uniform random number greater than zero and less than 1 and $T_L$ is given by Equation 16.17 (p. 378). The option of random calculation of $\tau_e$ yields a more realistic description of the correlation function.

The particle eddy crossing time is defined as

$$t_{cross} = -\tau \ln\left[1 - \left(\frac{L_e}{\tau \mid u - u_p \mid}\right)\right] \tag{16.26}$$

where $\tau$ is the particle relaxation time, $L_e$ is the eddy length scale, and $|u - u_p|$ is the magnitude of the relative velocity.

The particle is assumed to interact with the fluid phase eddy over the smaller of the eddy lifetime and the eddy crossing time. When this time is reached, a new value of the instantaneous velocity is obtained by applying a new value of $\zeta$ in Equation 16.19 (p. 378).

#### 16.2.2.1.3. Using the DRW Model

The only inputs required for the DRW model are the value for the integral time-scale constant, $C_L$ (see Equation 16.16 (p. 378) and Equation 16.24 (p. 379)) and the choice of the method used for the prediction of the eddy lifetime. You can choose to use either a constant value or a random value by selecting the appropriate option in the Set Injection Properties Dialog Box for each injection, as described in Stochastic Tracking in the User's Guide.

**Important**

Turbulent dispersion of particles cannot be included if the Spalart-Allmaras turbulence model is used.

### 16.2.2.2. Particle Cloud Tracking

Particle dispersion due to turbulent fluctuations can also be modeled with the particle cloud model [26] (p. 730), [27] (p. 730), [183] (p. 739), [261] (p. 743). The turbulent dispersion of particles about a mean trajectory is calculated using statistical methods. The concentration of particles about the mean trajectory

is represented by a Gaussian probability density function (PDF) whose variance is based on the degree of particle dispersion due to turbulent fluctuations. The mean trajectory is obtained by solving the ensemble-averaged equations of motion for all particles represented by the cloud (see Particle Cloud Tracking (p. 379)).

The cloud enters the domain either as a point source or with an initial diameter. The cloud expands due to turbulent dispersion as it is transported through the domain until it exits. As mentioned before, the distribution of particles in the cloud is defined by a probability density function (PDF) based on the position in the cloud relative to the cloud center. The value of the PDF represents the probability of finding particles represented by that cloud with residence time $t$ at location $x_i$ in the flow field. The average particle number density can be obtained by weighting the total flow rate of particles represented by that cloud, $\dot{m}$, as

$$\langle n(x_i) \rangle = \dot{m} P(x_i, t) \tag{16.27}$$

The PDFs for particle position are assumed to be multivariate Gaussian. These are completely described by their mean, $\mu_i$, and variance, $\sigma_i^2$, and are of the form

$$P(x_i, t) = \frac{1}{(2\pi)^{3/2} \prod_{i=1}^{3} \sigma_i} e^{-s/2} \tag{16.28}$$

where

$$s = \sum_{i=1}^{3} \left( \frac{x_i - \mu_i}{\sigma_i} \right)^2 \tag{16.29}$$

The mean of the PDF, or the center of the cloud, at a given time represents the most likely location of the particles in the cloud. The mean location is obtained by integrating a particle velocity as defined by an equation of motion for the cloud of particles:

$$\mu_i(t) \equiv \langle x_i(t) \rangle = \int_0^t \langle V_i(t_1) \rangle dt_1 + \langle x_i(0) \rangle \tag{16.30}$$

The equations of motion are constructed using an ensemble average.

The radius of the particle cloud is based on the variance of the PDF. The variance, $\sigma_i^2(t)$, of the PDF can be expressed in terms of two particle turbulence statistical quantities:

$$\sigma_i^2(t) = 2 \int_0^t \langle u'^2_{p,i}(t_2) \rangle \int_0^{t_2} R_{p,ii}(t_2, t_1) dt_1 dt_2 \tag{16.31}$$

where $\langle u'^2_{p,i} \rangle$ are the mean square velocity fluctuations, and $R_{p,ij}(t_2, t_1)$ is the particle velocity correlation function:

$$R_{p,ij}(t_2, t_1) = \frac{\langle u'_{p,i}(t_2) u'_{p,j}(t_1) \rangle}{\left[ \langle u'^2_{p,i}(t_2) u'^2_{p,j}(t_2) \rangle \right]^{1/2}} \tag{16.32}$$

By using the substitution $\tau = | t_2 - t_1 |$, and the fact that


Release 15.0 - © SAS IP, Inc. All rights reserved. - Contains proprietary and confidential information of ANSYS, Inc. and its subsidiaries and affiliates.

$$R_{p,ij}(t_2,t_1)=R_{p,ij}(t_4,t_3) \tag{16.33}$$

whenever $|t_2-t_1|=|t_4-t_3|$, we can write

$$\sigma_i^2(t)=2\int_0^t \langle u'^2_{p,i}(t_2)\rangle \int_0^{t_2} R_{p,ii}(\tau)\,d\tau dt_2 \tag{16.34}$$

Note that cross correlations in the definition of the variance ($R_{p,ij}, i\neq j$) have been neglected.

The form of the particle velocity correlation function used determines the particle dispersion in the cloud model. ANSYS Fluent uses a correlation function first proposed by Wang [476] (p. 755), and used by Jain [183] (p. 739). When the gravity vector is aligned with the $z$-coordinate direction, $R_{ij}$ takes the form:

$$\begin{aligned} R_{p,11} &= \frac{u'^2}{\theta} e^{-(\tau/\tau_a)}\ \mathrm{St}_T\left(B-0.5m_T\gamma\frac{\mathrm{St}_T^2B^2+1}{\theta}\right) \\ &\quad + \frac{u'^2}{\theta} e^{-(\tau B/T)}\left(-1+\frac{m_T\mathrm{St}_T^2\gamma B}{\theta}+0.5m_T\gamma\frac{\tau}{T}\right) \end{aligned} \tag{16.35}$$

$$R_{p,22}=R_{p,11} \tag{16.36}$$

$$R_{p,33}=\frac{u'^2\mathrm{St}_T B}{\theta}e^{-(\tau/\tau_a)}-\frac{u'^2}{\theta}e^{-(\tau B/T)} \tag{16.37}$$

where $B=\sqrt{1+m_T^2\gamma^2}$ and $\tau_a$ is the aerodynamic response time of the particle:

$$\tau_a=\frac{\rho_p d_p^2}{18\mu} \tag{16.38}$$

and

$$T=\frac{m_T T_{mE}}{m} \tag{16.39}$$

$$T_{fE}=\frac{C_\mu^{3/4}k^{3/2}}{\varepsilon\left(\frac{2}{3}k\right)^{1/2}} \tag{16.40}$$

$$\gamma=\frac{\tau_a g}{u'} \tag{16.41}$$

$$St=\frac{\tau_a}{T_{mE}} \tag{16.42}$$

$$St_T=\frac{\tau_a}{T} \tag{16.43}$$

$$\theta=St_T^2\left(1+m_T^2\gamma^2\right)-1 \tag{16.44}$$

$$m_T=m\left[1-\frac{G(m)}{(1+St)^{0.4(1+0.01St)}}\right] \tag{16.45}$$

Release 15.0 - © SAS IP, Inc. All rights reserved. - Contains proprietary and confidential information of ANSYS, Inc. and its subsidiaries and affiliates.

$$T_{mE}=T_{fE}\frac{\bar{u}}{u'} \tag{16.46}$$

$$m_T=m\left[1-\frac{G(m)}{(1+St)^{0.4(1+0.01St)}}\right] \tag{16.47}$$

$$G(m)=\frac{2}{\sqrt{\pi}}\int_0^{\infty}\frac{e^{-y^2}dy}{\left(1+\frac{m^2}{\pi}\left(\sqrt{\pi}erf(y)y-1+e^{-y^2}\right)\right)^{5/2}} \tag{16.48}$$

Using this correlation function, the variance is integrated over the life of the cloud. At any given time, the cloud radius is set to three standard deviations in the coordinate directions. The cloud radius is limited to three standard deviations since at least $99.2\%$ of the area under a Gaussian PDF is accounted for at this distance. Once the cells within the cloud are established, the fluid properties are ensemble-averaged for the mean trajectory, and the mean path is integrated in time. This is done with a weighting factor defined as

$$W(x_i,t)\equiv\frac{\int_{V_{cell}}P(x_i,t)dV}{\int_{V_{cloud}}P(x_i,t)dV} \tag{16.49}$$

If coupled calculations are performed, sources are distributed to the cells in the cloud based on the same weighting factors.

#### 16.2.2.2.1. Using the Cloud Model

The only inputs required for the cloud model are the values of the minimum and maximum cloud diameters. The cloud model is enabled in the Set Injection Properties Dialog Box for each injection, as described in Cloud Tracking in the User's Guide.

**Important**

The cloud model is not available for unsteady particle tracking, or in parallel, when using the message passing option for the particles.

## 16.2.3. Integration of Particle Equation of Motion

The trajectory equations, and any auxiliary equations describing heat or mass transfer to/from the particle, are solved by stepwise integration over discrete time steps. Integration of time in Equation 16.1 (p. 374) yields the velocity of the particle at each point along the trajectory, with the trajectory itself predicted by

$$\frac{dx}{dt}=u_p \tag{16.50}$$

Note that Equation 16.1 (p. 374) and Equation 16.50 (p. 382) are a set of coupled ordinary differential equations, and Equation 16.1 (p. 374) can be cast into the following general form

$$\frac{du_p}{dt}=\frac{1}{\tau_p}\left(u-u_p\right)+a \tag{16.51}$$


Release 15.0 - © SAS IP, Inc. All rights reserved. - Contains proprietary and confidential information of ANSYS, Inc. and its subsidiaries and affiliates.

where the term $a$ includes accelerations due to all other forces except drag force.

This set can be solved for constant $u$, $a$ and $\tau_p$ by analytical integration. For the particle velocity at the new location $u_p^{n+1}$ we get

$$u_p^{n+1} = u^n + e^{-\frac{\Delta t}{\tau_p}}\left(u_p^n - u^n\right) - a\tau_p\left(e^{-\frac{\Delta t}{\tau_p}} - 1\right) \tag{16.52}$$

The new location $x_p^{n+1}$ can be computed from a similar relationship.

$$x_p^{n+1} = x_p^n + \Delta t\left(u^n + a\tau_p\right) + \tau_p\left(1 - e^{-\frac{\Delta t}{\tau_p}}\right)\left(u_p^n - u^n - a\tau_p\right) \tag{16.53}$$

In these equations $u_p^n$ and $u^n$ represent particle velocities and fluid velocities at the old location. Equation 16.52 (p. 383) and Equation 16.53 (p. 383) are applied when using the **analytic** discretization scheme.

The set of Equation 16.1 (p. 374) and Equation 16.50 (p. 382) can also be solved using numerical discretization schemes. When applying the Euler implicit discretization to Equation 16.51 (p. 382) we get

$$u_p^{n+1} = \frac{u_p^n + \Delta t\left(a + \frac{u^n}{\tau_p}\right)}{1 + \frac{\Delta t}{\tau_p}} \tag{16.54}$$

When applying a trapezoidal discretization to Equation 16.51 (p. 382) the variables $u_p$ and $u_n$ on the right hand side are taken as averages, while accelerations, $a$, due to other forces are held constant. We get

$$\frac{u_p^{n+1} - u_p^n}{\Delta t} = \frac{1}{\tau_p}\left(u^* - u_p^*\right) + a^n \tag{16.55}$$

The averages $u_p^*$ and $u^*$ are computed from

$$u_p^* = \frac{1}{2}\left(u_p^n + u_p^{n+1}\right) \tag{16.56}$$

$$u^* = \frac{1}{2}\left(u^n + u^{n+1}\right) \tag{16.57}$$

$$u^{n+1} = u^n + \Delta t u_p^n \cdot \nabla u^n \tag{16.58}$$

The particle velocity at the new location $n+1$ is computed by

$$u_p^{n+1} = \frac{u_p^n\left(1 - \frac{1}{2}\frac{\Delta t}{\tau_p}\right) + \frac{\Delta t}{\tau_p}\left(u^n + \frac{1}{2}\Delta t u_p^n \cdot \nabla u^n\right) + \Delta t a^n}{1 + \frac{1}{2}\frac{\Delta t}{\tau_p}} \tag{16.59}$$

Release 15.0 - © SAS IP, Inc. All rights reserved. - Contains proprietary and confidential information of ANSYS, Inc. and its subsidiaries and affiliates.

For the **implicit** and the **trapezoidal** schemes the new particle location is always computed by a trapezoidal discretization of Equation 16.50 (p. 382).

$$x_p^{n+1} = x_p^n + \frac{1}{2}\Delta t\left(u_p^n + u_p^{n+1}\right) \tag{16.60}$$

Equation 16.51 (p. 382) and Equation 16.50 (p. 382) can also be computed using a Runge-Kutta scheme which was published by Cash and Karp [58] (p. 732). The ordinary differential equations can be considered as vectors, where the left hand side is the derivative $\vec{y}'$ and the right hand side is an arbitrary function $\vec{f}(t, \vec{y})$.

$$\vec{y}' = \vec{f}(t, \vec{y}) \tag{16.61}$$

We get

$$\vec{y}^{n+1} = \vec{y}^n + c_1\vec{k}_1 + c_2\vec{k}_2 + c_3\vec{k}_3 + c_4\vec{k}_4 + c_5\vec{k}_5 + c_6\vec{k}_6 \tag{16.62}$$

with

$$\begin{aligned}
\vec{k}_1 &= \Delta t\,\vec{f}(t, \vec{y}^n)\\
\vec{k}_2 &= \Delta t\,\vec{f}(t + a_2\Delta t, \vec{y}^n + b_{21}\vec{k}_1)\\
\vec{k}_3 &= \Delta t\,\vec{f}(t + a_3\Delta t, \vec{y}^n + b_{31}\vec{k}_1 + b_{32}\vec{k}_2)\\
\vec{k}_4 &= \Delta t\,\vec{f}(t + a_4\Delta t, \vec{y}^n + b_{41}\vec{k}_1 + b_{42}\vec{k}_2 + b_{43}\vec{k}_3)\\
\vec{k}_5 &= \Delta t\,\vec{f}(t + a_5\Delta t, \vec{y}^n + b_{51}\vec{k}_1 + b_{52}\vec{k}_2 + b_{53}\vec{k}_3 + b_{54}\vec{k}_4)\\
\vec{k}_6 &= \Delta t\,\vec{f}(t + a_6\Delta t, \vec{y}^n + b_{61}\vec{k}_1 + b_{62}\vec{k}_2 + b_{63}\vec{k}_3 + b_{64}\vec{k}_4 + b_{65}\vec{k}_5)
\end{aligned} \tag{16.63}$$

The coefficients $a_2 \ldots a_6$, $b_{21} \ldots b_{65}$, and $c_1 \ldots c_6$ are taken from Cash and Karp [58] (p. 732)

This scheme provides an embedded error control, which is switched off, when no **Accuracy Control** is enabled.

For moving reference frames, the integration is carried out in the moving frame with the extra terms described in Equation 16.6 (p. 375) and Equation 16.7 (p. 375), therefore accounting for system rotation. Using the mechanisms available for accuracy control, the trajectory integration will be done accurately in time.

The **analytic** scheme is very efficient. It can become inaccurate for large steps and in situations where the particles are not in hydrodynamic equilibrium with the continuous flow. The numerical schemes **implicit** and **trapezoidal**, in combination with **Automated Tracking Scheme Selection**, consider most of the changes in the forces acting on the particles and are chosen as default schemes. The **runge-kutta** scheme is recommended if the non-drag force changes along a particle integration step.

The integration step size of the higher-order schemes, **trapezoidal** and **runge-kutta**, is limited to a stable range. Therefore it is recommended that you use them in combination with **Automated Tracking Scheme Selection**.

For the massless particle type, the particle velocity is equal to the velocity of the continuous phase, hence the solution of only the trajectory Equation 16.50 (p. 382) is required where the particle velocity $u_p = u$. The new particle location along the trajectory is always computed by Equation 16.56 (p. 383) and Equation 16.60 (p. 384), with $u_p = u$.


Release 15.0 - © SAS IP, Inc. All rights reserved. - Contains proprietary and confidential information of ANSYS, Inc. and its subsidiaries and affiliates.

## 16.3. Laws for Drag Coefficients

Several laws for drag coefficients, $C_D$, are available for the Euler-Lagrange Model.

16.3.1. Spherical Drag Law
16.3.2. Non-spherical Drag Law
16.3.3. Stokes-Cunningham Drag Law
16.3.4. High-Mach-Number Drag Law
16.3.5. Dynamic Drag Model Theory
16.3.6. Dense Discrete Phase Model Drag Laws

Instructions for selecting the drag law are provided in Drag Laws in the User's Guide.

### 16.3.1. Spherical Drag Law

The drag coefficient, $C_D$, for smooth particles can be taken from

$$C_D = a_1 + \frac{a_2}{Re} + \frac{a_3}{Re^2} \tag{16.64}$$

where $a_1$, $a_2$, and $a_3$ are constants that apply over several ranges of Re given by Morsi and Alexander [309] (p. 746).

### 16.3.2. Non-spherical Drag Law

For non-spherical particles Haider and Levenspiel [150] (p. 737) developed the correlation

$$C_D = \frac{24}{Re_{sph}}\left(1 + b_1 {Re_{sph}}^{b_2}\right) + \frac{b_3 Re_{sph}}{b_4 + Re_{sph}} \tag{16.65}$$

where

$$\begin{aligned} b_1 &= \exp\left(2.3288 - 6.4581\phi + 2.4486\phi^2\right) \\ b_2 &= 0.0964 + 0.5565\phi \\ b_3 &= \exp\left(4.905 - 13.8944\phi + 18.4222\phi^2 - 10.2599\phi^3\right) \\ b_4 &= \exp\left(1.4681 + 12.2584\phi - 20.7322\phi^2 + 15.8855\phi^3\right) \end{aligned} \tag{16.66}$$

The shape factor, $\phi$, is defined as

$$\phi = \frac{s}{S} \tag{16.67}$$

where $s$ is the surface area of a sphere having the same volume as the particle, and $S$ is the actual surface area of the particle. For the purposes of calculating particle mass, drag force, and $Re_{sph}$, the particle size $d_p$ should be the diameter of a sphere having the same volume.

**Important**

The shape factor cannot exceed a value of 1.

Release 15.0 - © SAS IP, Inc. All rights reserved. - Contains proprietary and confidential information of ANSYS, Inc. and its subsidiaries and affiliates.

### 16.3.3. Stokes-Cunningham Drag Law

For sub-micron particles, a form of Stokes' drag law is available [337] (p. 747). In this case, $F_D$ is defined as

$$F_D = \frac{18\mu}{d_p^2 \rho_p C_c} \tag{16.68}$$

The factor $C_c$ is the Cunningham correction to Stokes' drag law, which you can compute from

$$C_c = 1 + \frac{2\lambda}{d_p}\left(1.257 + 0.4e^{-\left(1.1 d_p/2\lambda\right)}\right) \tag{16.69}$$

where $\lambda$ is the molecular mean free path.

### 16.3.4. High-Mach-Number Drag Law

A high-Mach-number drag law is also available. This drag law is similar to the spherical law (Equation 16.64 (p. 385)) with corrections [69] (p. 732) to account for a particle Mach number greater than 0.4 at a particle Reynolds number greater than 20.

### 16.3.5. Dynamic Drag Model Theory

Accurate determination of droplet drag coefficients is crucial for accurate spray modeling. ANSYS Fluent provides a method that determines the droplet drag coefficient dynamically, accounting for variations in the droplet shape.

The dynamic drag model is applicable in almost any circumstance. It is compatible with both the TAB and wave models for droplet breakup. When the collision model is turned on, collisions reset the distortion and distortion velocities of the colliding droplets.

Many droplet drag models assume the droplet remains spherical throughout the domain. With this assumption, the drag of a spherical object is determined by the following [262] (p. 743):

$$C_{d,sphere} = \begin{cases} 0.424 & Re > 1000 \\ \frac{24}{Re}\left(1 + \frac{1}{6}Re^{2/3}\right) & Re \le 1000 \end{cases} \tag{16.70}$$

However, as an initially spherical droplet moves through a gas, its shape is distorted significantly when the Weber number is large. In the extreme case, the droplet shape will approach that of a disk. The drag of a disk, however, is significantly higher than that of a sphere. Since the droplet drag coefficient is highly dependent upon the droplet shape, a drag model that assumes the droplet is spherical is unsatisfactory. The dynamic drag model accounts for the effects of droplet distortion, linearly varying the drag between that of a sphere (Equation 16.70 (p. 386)) and a value of 1.54 corresponding to a disk [262] (p. 743). The drag coefficient is given by

$$C_d = C_{d,sphere}(1 + 2.632y) \tag{16.71}$$

where $y$ is the droplet distortion, as determined by the solution of

$$\frac{d^2y}{dt^2} = \frac{C_F}{C_b}\frac{\rho_g}{\rho_l}\frac{u^2}{r^2} - \frac{C_k\sigma}{\rho_l r^3}y - \frac{C_d\mu_l}{\rho_l r^2}\frac{dy}{dt} \tag{16.72}$$


Release 15.0 - © SAS IP, Inc. All rights reserved. - Contains proprietary and confidential information of ANSYS, Inc. and its subsidiaries and affiliates.

In the limit of no distortion ($y=0$), the drag coefficient of a sphere will be obtained, while at maximum distortion ($y=1$) the drag coefficient corresponding to a disk will be obtained.

Note that Equation 16.72 (p. 386) is obtained from the TAB model for spray breakup, described in Taylor Analogy Breakup (TAB) Model (p. 440), but the dynamic drag model can be used with either of the breakup models.

### 16.3.6. Dense Discrete Phase Model Drag Laws

The drag laws that are suitable for dense gas-solid flow are the Wen and Yu, the Gidaspow, and the Syamlal-O'Brien drag model. A detailed theoretical background to the correlations, along with a recommendation of when to use each model, can be found in Fluid-Solid Exchange Coefficient (p. 524) (see also Specifying the Drag Function in the User's Guide). All three correlations incorporate group effects and therefore are dependent on the particle phase volume fraction. Thus, the new drag models are only available when the DPM volume fraction is computed, that is, in conjunction with the Dense Discrete Phase Model.

## 16.4. Laws for Heat and Mass Exchange

Using ANSYS Fluent's discrete phase modeling capability, reacting particles or droplets can be modeled and their impact on the continuous phase can be examined. Several heat and mass transfer relationships, termed "laws", are available in ANSYS Fluent and the physical models employed in these laws are described in this section.

16.4.1. Inert Heating or Cooling (Law 1/Law 6)
16.4.2. Droplet Vaporization (Law 2)
16.4.3. Droplet Boiling (Law 3)
16.4.4. Devolatilization (Law 4)
16.4.5. Surface Combustion (Law 5)
16.4.6. Multicomponent Particle Definition (Law 7)

The laws that you activate depend upon the particle type that you select. In the Set Injection Properties Dialog Box you will specify the **Particle Type**, and ANSYS Fluent will use a given set of heat and mass transfer laws for the chosen type. All particle types have predefined sequences of physical laws as shown in the table below:

| Particle Type | Description | Laws Activated |
|---|---|---|
| Massless | – | – |
| Inert | inert/heating or cooling | 1, 6 |
| Droplet | heating/evaporation/boiling | 1, 2, 3, 6 |
| Combusting | heating; evolution of volatiles/swelling; heterogeneous surface reaction | 1, 4, 5, 6 |
| Multicomponent | multicomponent droplets/particles | 7 |

In addition to the above laws, you can define your own laws using a user-defined function. More information about user-defined functions can be found in the UDF Manual.

You can also extend combusting particles to include an evaporating/boiling material by selecting **Wet Combustion** in the Set Injection Properties Dialog Box.

Release 15.0 - © SAS IP, Inc. All rights reserved. - Contains proprietary and confidential information of ANSYS, Inc. and its subsidiaries and affiliates.

ANSYS Fluent's physical laws (Laws 1 through 6), which describe the heat and mass transfer conditions listed in this table, are explained in detail in the sections that follow.

## 16.4.1. Inert Heating or Cooling (Law 1/Law 6)

The inert heating or cooling laws (Laws 1 and 6) are applied when the particle temperature is less than the vaporization temperature that you define, $T_{vap}$, and after the volatile fraction, $f_{v,0}$, of a particle has been consumed. These conditions may be written as

**Law 1:**

$$T_p < T_{vap} \tag{16.73}$$

**Law 6:**

$$m_p \le \left(1 - f_{v,0}\right) m_{p,0} \tag{16.74}$$

where $T_p$ is the particle temperature, $m_{p,0}$ is the initial mass of the particle, and $m_p$ is its current mass.

Law 1 is applied until the temperature of the particle/droplet reaches the vaporization temperature. At this point a non-inert particle/droplet may proceed to obey one of the mass-transfer laws (2, 3, 4, and/or 5), returning to Law 6 when the volatile portion of the particle/droplet has been consumed. (Note that the vaporization temperature, $T_{vap}$, is an arbitrary modeling constant used to define the onset of the vaporization/boiling/volatilization laws.)

When using Law 1 or Law 6, ANSYS Fluent uses a simple heat balance to relate the particle temperature, $T_p(t)$, to the convective heat transfer and the absorption/emission of radiation at the particle surface:

$$m_p c_p \frac{dT_p}{dt} = h A_p \left(T_\infty - T_p\right) + \varepsilon_p A_p \sigma \left(\theta_R^4 - T_p^4\right) \tag{16.75}$$

where

$m_p$ = mass of the particle (kg)

$c_p$ = heat capacity of the particle (J/kg-K)

$A_p$ = surface area of the particle ($\mathrm{m}^2$)

$T_\infty$ = local temperature of the continuous phase (K)

$h$ = convective heat transfer coefficient ($\mathrm{W/m^2-K}$)

$\varepsilon_p$ = particle emissivity (dimensionless)

$\sigma$ = Stefan-Boltzmann constant (5.67 x $10^{-8}$ $\mathrm{W/m^2\text{-}K^4}$)

$\theta_R$ = radiation temperature, $\left(\frac{G}{4\sigma}\right)^{1/4}$ (K)

Equation 16.75 (p. 388) assumes that there is negligible internal resistance to heat transfer, that is, the particle is at uniform temperature throughout.

$G$ is the incident radiation in $\mathrm{W/m^2}$:


Release 15.0 - © SAS IP, Inc. All rights reserved. - Contains proprietary and confidential information of ANSYS, Inc. and its subsidiaries and affiliates.

$$G = \int_{\Omega=4\pi} I d\Omega \tag{16.76}$$

where $I$ is the radiation intensity and $\Omega$ is the solid angle.

Radiation heat transfer to the particle is included only if you have enabled the P-1 or discrete ordinates radiation heat transfer to particles using the **Particle Radiation Interaction** option in the Discrete Phase Model Dialog Box.

Equation 16.75 (p. 388) is integrated in time using an approximate, linearized form that assumes that the particle temperature changes slowly from one time value to the next:

$$m_p c_p \frac{dT_p}{dt} = A_p \left\{ -\left[ h + \varepsilon_p \sigma T_p^3 \right] T_p + \left[ h T_\infty + \varepsilon_p \sigma \theta_R^4 \right] \right\} \tag{16.77}$$

As the particle trajectory is computed, ANSYS Fluent integrates Equation 16.77 (p. 389) to obtain the particle temperature at the next time value, yielding

$$T_p(t+\Delta t) = \alpha_p + \left[ T_p(t) - \alpha_p \right] e^{-\beta_p \Delta t} \tag{16.78}$$

where $\Delta t$ is the integration time step and

$$\alpha_p = \frac{h T_\infty + \varepsilon_p \sigma \theta_R^4}{h + \varepsilon_p \sigma T_p^3(t)} \tag{16.79}$$

and

$$\beta_p = \frac{A_p \left( h + \varepsilon_p \sigma T_p^3(t) \right)}{m_p c_p} \tag{16.80}$$

ANSYS Fluent can also solve Equation 16.77 (p. 389) in conjunction with the equivalent mass transfer equation using a stiff coupled solver. See Including Coupled Heat-Mass Solution Effects on the Particles in the User's Guide for details.

The heat transfer coefficient, $h$, is evaluated using the correlation of Ranz and Marshall [366] (p. 749), [367] (p. 749):

$$Nu = \frac{h d_p}{k_\infty} = 2.0 + 0.6 Re_d^{1/2} Pr^{1/3} \tag{16.81}$$

where

$d_p$ = particle diameter (m)

$k_\infty$ = thermal conductivity of the continuous phase (W/m-K)

$\mathrm{Re}_d$ = Reynolds number based on the particle diameter and the relative velocity (Equation 16.3 (p. 374))

Pr = Prandtl number of the continuous phase ($c_p \mu / k_\infty$)

Finally, the heat lost or gained by the particle as it traverses each computational cell appears as a source or sink of heat in subsequent calculations of the continuous phase energy equation. During Laws 1 and

Release 15.0 - © SAS IP, Inc. All rights reserved. - Contains proprietary and confidential information of ANSYS, Inc. and its subsidiaries and affiliates.

6, particles/droplets do not exchange mass with the continuous phase and do not participate in any chemical reaction.

## 16.4.2. Droplet Vaporization (Law 2)

Law 2 is applied to predict the vaporization from a discrete phase droplet. Law 2 is initiated when the temperature of the droplet reaches the vaporization temperature, $T_{vap}$, and continues until the droplet reaches the boiling point, $T_{bp}$, or until the droplet's volatile fraction is completely consumed:

$$T_{vap} \leq T_p < T_{bp} \tag{16.82}$$

$$m_p > \left(1 - f_{v,0}\right) m_{p,0} \tag{16.83}$$

The onset of the vaporization law is determined by the setting of $T_{vap}$, a modeling parameter that has no physical significance. Note that once vaporization is initiated (by the droplet reaching this threshold temperature), it will continue to vaporize even if the droplet temperature falls below $T_{vap}$. Vaporization will be halted only if the droplet temperature falls below the dew point. In such cases, the droplet will remain in Law 2 but no evaporation will be predicted. When the boiling point is reached, the droplet vaporization is predicted by a boiling rate, Law 3, as described in a section that follows.

### 16.4.2.1. Mass Transfer During Law 2—Diffusion Controlled Model

During Law 2, when the rate of vaporization is slow, it can be assumed to be governed by gradient diffusion, with the flux of droplet vapor into the gas phase related to the difference in vapor concentration at the droplet surface and the bulk gas:

$$N_i = k_c \left(C_{i,s} - C_{i,\infty}\right) \tag{16.84}$$

where

$N_i$ = molar flux of vapor $\left(\text{kmol/m}^2\text{-s}\right)$

$k_c$ = mass transfer coefficient $\left(\text{m/s}\right)$

$C_{i,s}$ = vapor concentration at the droplet surface $\left(\text{kmol/m}^3\right)$

$C_{i,\infty}$ = vapor concentration in the bulk gas $\left(\text{kmol/m}^3\right)$

Note that ANSYS Fluent's vaporization law assumes that $N_i$ is positive (evaporation). If conditions exist in which $N_i$ is negative (that is, the droplet temperature falls below the dew point and condensation conditions exist), ANSYS Fluent treats the droplet as inert ($N_i = 0.0$).

The concentration of vapor at the droplet surface is evaluated by assuming that the partial pressure of vapor at the interface is equal to the saturated vapor pressure, $p_{sat}$, at the droplet temperature, $T_p$:

$$C_{i,s} = \frac{p_{sat}\left(T_p\right)}{RT_p} \tag{16.85}$$

where $R$ is the universal gas constant.

The concentration of vapor in the bulk gas is known from solution of the transport equation for species $i$ as:


Release 15.0 - © SAS IP, Inc. All rights reserved. - Contains proprietary and confidential information of ANSYS, Inc. and its subsidiaries and affiliates.

$$C_{i,\infty}=X_i\frac{p}{RT_\infty} \tag{16.86}$$

where $X_i$ is the local bulk mole fraction of species $i$, $p$ is the local absolute pressure, and $T_\infty$ is the local bulk temperature in the gas. The mass transfer coefficient in Equation 16.84 (p. 390) is calculated from the Sherwood number correlation [366] (p. 749), [367] (p. 749):

$$Sh_{AB}=\frac{k_c d_p}{D_{i,m}}=2.0+0.6Re_d^{1/2}Sc^{1/3} \tag{16.87}$$

where

$D_{i,m}$ = diffusion coefficient of vapor in the bulk $(\mathrm{m}^2/\mathrm{s})$

$Sc$ = the Schmidt number, $\mu/\rho D_{i,m}$

$d_p$ = particle (droplet) diameter $(\mathrm{m})$

The vapor flux given by Equation 16.84 (p. 390) becomes a source of species $i$ in the gas phase species transport equation, (see Setting Material Properties for the Discrete Phase in the User's Guide) or in the mixture fraction equation for nonpremixed combustion calculations.

The mass of the droplet is reduced according to

$$m_p(t+\Delta t)=m_p(t)-N_i A_p M_{w,i}\Delta t \tag{16.88}$$

where

$M_{w,i}$ = molecular weight of species $i$ $(\mathrm{kg/kmol})$

$m_p$ = mass of the droplet $(\mathrm{kg})$

$A_p$ = surface area of the droplet $(\mathrm{m}^2)$

ANSYS Fluent can also solve Equation 16.88 (p. 391) in conjunction with the equivalent heat transfer equation using a stiff coupled solver. See Including Coupled Heat-Mass Solution Effects on the Particles in the User's Guide for details.

### 16.4.2.2. Mass Transfer During Law 2—Convection/Diffusion Controlled Model

For high vaporization rates, the effect of the convective flow of the evaporating material from the droplet surface to the bulk gas phase (Stefan Flow) becomes important.

In ANSYS Fluent, the following expression has been adopted following the work of Miller [300] (p. 745) and Sazhin [390] (p. 750):

$$\frac{dm_p}{dt}=k_c A_p \rho_\infty \ln(1+B_m) \tag{16.89}$$

where

$m_p$ = droplet mass $(\mathrm{kg})$

$k_c$ = mass transfer coefficient $(\mathrm{m/s})$

Release 15.0 - © SAS IP, Inc. All rights reserved. - Contains proprietary and confidential information of ANSYS, Inc. and its subsidiaries and affiliates.

$A_p$ = droplet surface area $(\mathrm{m}^2)$

$\rho_\infty$ = density of bulk gas $(\mathrm{kg/m}^3)$

$B_m$ is the Spalding mass number given by:

$$B_m = \frac{Y_{i,s} - Y_{i,\infty}}{1 - Y_{i,s}} \tag{16.90}$$

where

$Y_{i,s}$ = vapor mass fraction at the surface

$Y_{i,\infty}$ = vapor mass fraction in the bulk gas

The mass transfer coefficient $k_c$ is given by Equation 16.87 (p. 391).

### 16.4.2.3. Defining the Saturation Vapor Pressure and Diffusion Coefficient (or Binary Diffusivity)

You must define the saturation vapor pressure as a polynomial or piecewise linear function of temperature ($p_{sat}(T)$) during the problem definition. Note that the saturation vapor pressure definition is critical, as $p_{sat}$ is used to obtain the driving force for the evaporation process (Equation 16.84 (p. 390) and Equation 16.85 (p. 390)). You should provide accurate vapor pressure values for temperatures over the entire range of possible droplet temperatures in your problem. Saturation vapor pressure data can be obtained from a physics or engineering handbook (for example, [344] (p. 748)).

You must also input the diffusion coefficient, $D_{i,m}$, during the setup of the discrete phase material properties. Note that the diffusion coefficient inputs that you supply for the continuous phase are not used in the discrete phase model.

You can define the binary diffusion coefficient (or binary diffusivity) to be either constant, or a function of the continuous phase temperature. Alternatively, you can define the binary diffusion coefficient as function of a film-averaged temperature $T_f$, which is computed by

$$T_f = T_p + a\left(T_\infty - T_p\right) \tag{16.91}$$

where

$T_p$ = droplet temperature (K)

$T_\infty$ = temperature in the bulk gas (K)

$a$ = averaging coefficient

You can also choose to have Fluent compute the diffusion coefficient based on the assumption of unity Lewis number:

$$Le_i = \frac{k}{\rho c_p D_{i,m}} = 1 \tag{16.92}$$

where


Release 15.0 - © SAS IP, Inc. All rights reserved. - Contains proprietary and confidential information of ANSYS, Inc. and its subsidiaries and affiliates.

$D_{i,m}$ = mass diffusivity of species $i$ is the gas-phase mixture

$k$ = mixture thermal conductivity

$\rho$ = mixture density

$c_p$ = mixture specific heat

### 16.4.2.4. Defining the Boiling Point and Latent Heat

The boiling point $T_{bp}$ and the latent heat $h_{fg}$ are defined as constant property inputs for the droplet-particle materials. The default boiling point data in the ANSYS Fluent property database correspond to a pressure of 1 atm (normal boiling point) and the latent heat data correspond to the normal boiling point of the droplets.

During the evaporation process, as the particle changes its temperature, the latent heat will vary according to Equation 16.93 (p. 393)

$$h_{fg} = -\int_{T_p}^{T_{bp}} c_{p,g}\,dT + h_{fg,bp} + \int_{T_p}^{T_{bp}} c_{p,p}\,dT \tag{16.93}$$

where

$T_{\mathrm{bp}}$ = boiling point (K)

$h_{\mathrm{fg,bp}}$ = latent heat at the boiling point (J/kg)

$c_{\mathrm{p,g}}$ and $c_{\mathrm{p,p}}$ = specific heat of gaseous and liquid phase, respectively (J/kg/K)

For simulations at or near atmospheric pressure, the latent heat variation with droplet temperature is generally small and can be ignored, so $h_{fg} \approx h_{fg,bp}$. You may include the droplet temperature effects on the latent heat by selecting the **Temperature Dependent Latent Heat** option in the **Discrete Phase Model** dialog box (see Including the Effect of Droplet Temperature on Latent Heat in the User's Guide).

If the pressure in your simulation differs from atmospheric, you should either modify the boiling point to be consistent with the average pressure in the region where the droplets evaporate, or enable the **Pressure Dependent Boiling** option (see Enabling Pressure Dependent Boiling in the User's Guide). If you modify the boiling point for the droplet material, you should also modify the latent heat value accordingly.

### 16.4.2.5. Heat Transfer to the Droplet

Finally, the droplet temperature is updated according to a heat balance that relates the sensible heat change in the droplet to the convective and latent heat transfer between the droplet and the continuous phase:

$$m_p c_p \frac{dT_p}{dt} = h A_p \left(T_\infty - T_p\right) - \frac{dm_p}{dt} h_{fg} + A_p \varepsilon_p \sigma \left(\theta_R{}^4 - T_p{}^4\right) \tag{16.94}$$

where

$c_p$ = droplet heat capacity (J/kg-K)

$T_p$ = droplet temperature (K)

Release 15.0 - © SAS IP, Inc. All rights reserved. - Contains proprietary and confidential information of ANSYS, Inc. and its subsidiaries and affiliates.

$h$ = convective heat transfer coefficient $(\mathrm{W/m^2\text{-}K})$

$T_\infty$ = temperature of continuous phase (K)

$dm_p/dt$ = rate of evaporation (kg/s)

$h_{fg}$ = latent heat (J/kg)

$\varepsilon_p$ = particle emissivity (dimensionless)

$\sigma$ = Stefan-Boltzmann constant $\left(5.67\times10^{-8}\mathrm{W/m^2\text{-}K^4}\right)$

$\theta_R$ = radiation temperature, $\left(\frac{G}{4\sigma}\right)^{1/4}$, where $G$ is the incident radiation defined by Equation 16.76 (p. 389)

Radiation heat transfer to the particle is included only if you have enabled the P-1 or discrete ordinates radiation heat transfer to particles using the **Particle Radiation Interaction** option in the Discrete Phase Model Dialog Box.

The heat transferred to or from the gas phase becomes a source/sink of energy during subsequent calculations of the continuous phase energy equation.

When the vaporization rate is computed by the Convection/Diffusion Controlled model (Equation 16.89 (p. 391)), the convective heat transfer coefficient $h$ in Equation 16.94 (p. 393) is calculated with a modified $Nu$ number as follows [390] (p. 750):

$$Nu=\frac{hd_p}{k_\infty}=\frac{\ln(1+B_T)}{B_T}(2+0.6\mathrm{Re}_d^{1/2}\mathrm{Pr}^{1/3}) \tag{16.95}$$

where

$d_p$ = particle diameter (m)

$k_\infty$ = thermal conductivity of the continuous phase (W/m-K)

$\mathrm{Re}_d$ = Reynolds number (Equation 16.3 (p. 374))

$\mathrm{Pr}$ = Prandtl number of the continuous phase ($c_p\mu/k_\infty$)

$B_T$ is the Spalding heat transfer number and in the present implementation is assumed to be equal to the Spalding mass transfer number $B_m$ calculated from Equation 16.89 (p. 391):

$$B_T=B_m \tag{16.96}$$

## 16.4.3. Droplet Boiling (Law 3)

Law 3 is applied to predict the convective boiling of a discrete phase droplet when the temperature of the droplet has reached the boiling temperature, $T_{bp}$, and while the mass of the droplet exceeds the nonvolatile fraction, $(1-f_{v,0})$:

$$T_p\geq T_{bp} \tag{16.97}$$

and


Release 15.0 - © SAS IP, Inc. All rights reserved. - Contains proprietary and confidential information of ANSYS, Inc. and its subsidiaries and affiliates.

$$m_p > \left(1 - f_{v,0}\right) m_{p,0} \tag{16.98}$$

When the droplet temperature reaches the boiling point, a boiling rate equation is applied [220] (p. 741):

$$\frac{d\left(d_p\right)}{dt} = \frac{4k_\infty}{\rho_p c_{p,\infty} d_p}\left(1 + 0.23\sqrt{Re_d}\right)\ln\left[1 + \frac{c_{p,\infty}\left(T_\infty - T_p\right)}{h_{fg}}\right] \tag{16.99}$$

where

$c_{p,\infty}$ = heat capacity of the gas (J/kg-K)

$\rho_p$ = droplet density (kg/m$^3$)

$k_\infty$ = thermal conductivity of the gas (W/m-K)

Equation 16.99 (p. 395) was derived assuming steady flow at constant pressure. Note that the model requires $T_\infty > T_{bp}$ in order for boiling to occur and that the droplet remains at fixed temperature ($T_{bp}$) throughout the boiling law.

When radiation heat transfer is active, ANSYS Fluent uses a slight modification of Equation 16.99 (p. 395), derived by starting from Equation 16.94 (p. 393) and assuming that the droplet temperature is constant. This yields

$$\frac{dm_p}{dt} h_{fg} = h A_p\left(T_\infty - T_p\right) + A_p \varepsilon_p \sigma\left(\theta_R{}^4 - T_p{}^4\right) \tag{16.100}$$

or

$$\frac{d\left(d_p\right)}{dt} = \frac{2}{\rho_p h_{fg}}\left[\frac{k_\infty Nu}{d_p}\left(T_\infty - T_p\right) + \varepsilon_p \sigma\left(\theta_R^4 - T_p^4\right)\right] \tag{16.101}$$

Using Equation 16.81 (p. 389) for the Nusselt number correlation and replacing the Prandtl number term with an empirical constant, Equation 16.101 (p. 395) becomes

$$\frac{d\left(d_p\right)}{dt} = \frac{2}{\rho_p h_{fg}}\left[\frac{2k_\infty\left[1 + 0.23\sqrt{Re_d}\right]}{d_p}\left(T_\infty - T_p\right) + \varepsilon_p \sigma\left(\theta_R^4 - T_p^4\right)\right] \tag{16.102}$$

In the absence of radiation, this result matches that of Equation 16.99 (p. 395) in the limit that the argument of the logarithm is close to unity. ANSYS Fluent uses Equation 16.102 (p. 395) when radiation is active in your model and Equation 16.99 (p. 395) when radiation is not active. Radiation heat transfer to the particle is included only if you have enabled the P-1 or discrete ordinates radiation model and you have activated radiation heat transfer to particles using the **Particle Radiation Interaction** option in the Discrete Phase Model Dialog Box.

The droplet is assumed to stay at constant temperature while the boiling rate is applied. Once the boiling law is entered it is applied for the duration of the particle trajectory. The energy required for vaporization appears as a (negative) source term in the energy equation for the gas phase. The evaporated liquid enters the gas phase as species $i$, as defined by your input for the destination species (see Setting Material Properties for the Discrete Phase in the User's Guide).

Release 15.0 - © SAS IP, Inc. All rights reserved. - Contains proprietary and confidential information of ANSYS, Inc. and its subsidiaries and affiliates.

## 16.4.4. Devolatilization (Law 4)

The devolatilization law is applied to a combusting particle when the temperature of the particle reaches the vaporization temperature, $T_{vap}$, and remains in effect while the mass of the particle, $m_p$, exceeds the mass of the nonvolatiles in the particle:

$$T_p \geq T_{vap} \text{ and } T_p \geq T_{bp} \tag{16.103}$$

and

$$m_p > \left(1 - f_{v,0}\right)\left(1 - f_{w,0}\right) m_{p,0} \tag{16.104}$$

where $f_{w,0}$ is the mass fraction of the evaporating/boiling material if **Wet Combustion** is selected (otherwise, $f_{w,0} = 0$). As implied by Equation 16.103 (p. 396), the boiling point, $T_{bp}$, and the vaporization temperature, $T_{vap}$, should be set equal to each other when Law 4 is to be used. When wet combustion is active, $T_{bp}$ and $T_{vap}$ refer to the boiling and evaporation temperatures for the droplet material only.

ANSYS Fluent provides a choice of four devolatilization models:

- the constant rate model (the default model)
- the single kinetic rate model
- the two competing rates model (the Kobayashi model)
- the chemical percolation devolatilization (CPD) model

Each of these models is described, in turn, in the following sections.

### 16.4.4.1. Choosing the Devolatilization Model

You will choose the devolatilization model when you are setting physical properties for the combusting-particle material in the Create/Edit Materials Dialog Box, as described in Description of the Properties in the User's Guide. By default, the constant rate model (Equation 16.105 (p. 396)) will be used.

### 16.4.4.2. The Constant Rate Devolatilization Model

The constant rate devolatilization law dictates that volatiles are released at a constant rate [25] (p. 730):

$$-\frac{1}{f_{v,0}\left(1 - f_{w,0}\right) m_{p,0}} \frac{dm_p}{dt} = A_0 \tag{16.105}$$

where

$m_p$ = particle mass (kg)

$f_{v,0}$ = fraction of volatiles initially present in the particle

$m_{p,0}$ = initial particle mass (kg)

$A_0$ = rate constant ($s^{-1}$)


Release 15.0 - © SAS IP, Inc. All rights reserved. - Contains proprietary and confidential information of ANSYS, Inc. and its subsidiaries and affiliates.

The rate constant $A_0$ is defined in the material properties of the combusting particle(s). The Fluent materials database includes default values for each of the available combusting particle materials. A representative value is 12 $s^{-1}$ derived from the work of Pillai [350] (p. 748) on coal combustion. Proper use of the constant devolatilization rate requires that the vaporization temperature, which controls the onset of devolatilization, be set appropriately. Values in the literature show this temperature to be about 600 K [25] (p. 730).

The volatile fraction of the particle enters the gas phase as the devolatilizing species $i$, defined by you (see Setting Material Properties for the Discrete Phase in the User's Guide). Once in the gas phase, the volatiles may react according to the inputs governing the gas phase chemistry.

### 16.4.4.3. The Single Kinetic Rate Model

The single kinetic rate devolatilization model assumes that the rate of devolatilization is first-order dependent on the amount of volatiles remaining in the particle [15] (p. 729):

$$-\frac{dm_p}{dt}=k\left[m_p-\left(1-f_{v,0}\right)\left(1-f_{w,0}\right)m_{p,0}\right] \tag{16.106}$$

where

$m_p$ = particle mass (kg)

$f_{v,0}$ = mass fraction of volatiles initially present in the particle

$f_{w,0}$ = mass fraction of evaporating/boiling material (if wet combustion is modeled)

$m_{p,0}$ = initial particle mass (kg)

$k$ = kinetic rate ($s^{-1}$)

Note that $f_{v,0}$, the fraction of volatiles in the particle, should be defined using a value slightly in excess of that determined by proximate analysis. The kinetic rate, $k$, is defined by input of an Arrhenius type pre-exponential factor and an activation energy:

$$k=A_1 e^{-(E/RT)} \tag{16.107}$$

The Fluent materials database includes default values for the rate constants, $A_1$ and $E$, for each of the available combusting particle materials.

Equation 16.106 (p. 397) has the approximate analytical solution:

$$\begin{aligned} m_p(t+\Delta t) &= \left(1-f_{v,0}\right)\left(1-f_{w,0}\right)m_{p,0} \\ &+\left[m_p(t)-\left(1-f_{v,0}\right)\left(1-f_{w,0}\right)m_{p,0}\right]e^{-k\,\Delta t} \end{aligned} \tag{16.108}$$

which is obtained by assuming that the particle temperature varies only slightly between discrete time integration steps.

ANSYS Fluent can also solve Equation 16.106 (p. 397) in conjunction with the equivalent heat transfer equation using a stiff coupled solver. See Including Coupled Heat-Mass Solution Effects on the Particles in the User's Guide for details.

Release 15.0 - © SAS IP, Inc. All rights reserved. - Contains proprietary and confidential information of ANSYS, Inc. and its subsidiaries and affiliates.

### 16.4.4.4. The Two Competing Rates (Kobayashi) Model

ANSYS Fluent also provides the kinetic devolatilization rate expressions of the form proposed by Kobayashi [213] (p. 740):

$$\mathcal{R}_1 = A_1 e^{-\left(E_1/RT_p\right)} \tag{16.109}$$

$$\mathcal{R}_2 = A_2 e^{-\left(E_2/RT_p\right)} \tag{16.110}$$

where $\mathcal{R}_1$ and $\mathcal{R}_2$ are competing rates that may control the devolatilization over different temperature ranges. The two kinetic rates are weighted to yield an expression for the devolatilization as

$$\frac{m_v(t)}{\left(1-f_{w,0}\right)m_{p,0}-m_a} = \int_0^t \left(\alpha_1\mathcal{R}_1+\alpha_2\mathcal{R}_2\right)\exp\left(-\int_0^t \left(\mathcal{R}_1+\mathcal{R}_2\right)dt\right)dt \tag{16.111}$$

where

$m_v(t)$ = volatile yield up to time $t$

$m_{p,0}$ = initial particle mass at injection

$\alpha_1, \alpha_2$ = yield factors

$m_a$ = ash content in the particle

The Kobayashi model requires input of the kinetic rate parameters, $A_1$, $E_1$, $A_2$, and $E_2$, and the yields of the two competing reactions, $\alpha_1$ and $\alpha_2$. ANSYS Fluent uses default values for the yield factors of 0.3 for the first (slow) reaction and 1.0 for the second (fast) reaction. It is recommended in the literature [213] (p. 740) that $\alpha_1$ be set to the fraction of volatiles determined by proximate analysis, since this rate represents devolatilization at low temperature. The second yield parameter, $\alpha_2$, should be set close to unity, which is the yield of volatiles at very high temperature.

By default, Equation 16.111 (p. 398) is integrated in time analytically, assuming the particle temperature to be constant over the discrete time integration step. ANSYS Fluent can also solve Equation 16.111 (p. 398) in conjunction with the equivalent heat transfer equation using a stiff coupled solver. See Including Coupled Heat-Mass Solution Effects on the Particles in the User's Guide for details.

### 16.4.4.5. The CPD Model

In contrast to the coal devolatilization models presented above, which are based on empirical rate relationships, the chemical percolation devolatilization (CPD) model characterizes the devolatilization behavior of rapidly heated coal based on the physical and chemical transformations of the coal structure [123] (p. 735), [124] (p. 735), [146] (p. 737).

#### 16.4.4.5.1. General Description

During coal pyrolysis, the labile bonds between the aromatic clusters in the coal structure lattice are cleaved, resulting in two general classes of fragments. One set of fragments has a low molecular weight (and correspondingly high vapor pressure) and escapes from the coal particle as a light gas. The other set of fragments consists of tar gas precursors that have a relatively high molecular weight (and correspondingly low vapor pressure) and tend to remain in the coal for a long period of time during typical devolatilization conditions. During this time, reattachment with the coal lattice (which is referred to as cross-linking) can occur. The high molecular weight compounds plus the residual lattice are referred to


Release 15.0 - © SAS IP, Inc. All rights reserved. - Contains proprietary and confidential information of ANSYS, Inc. and its subsidiaries and affiliates.

as metaplast. The softening behavior of a coal particle is determined by the quantity and nature of the metaplast generated during devolatilization. The portion of the lattice structure that remains after devolatilization is comprised of char and mineral-compound-based ash.

The CPD model characterizes the chemical and physical processes by considering the coal structure as a simplified lattice or network of chemical bridges that link the aromatic clusters. Modeling the cleavage of the bridges and the generation of light gas, char, and tar precursors is then considered to be analogous to the chemical reaction scheme shown in Figure 16.1: Coal Bridge (p. 399).

**Figure 16.1: Coal Bridge**

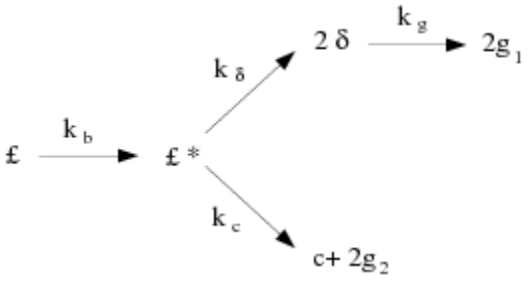


The variable $£$ represents the original population of labile bridges in the coal lattice. Upon heating, these bridges become the set of reactive bridges, $£^*$. For the reactive bridges, two competing paths are available. In one path, the bridges react to form side chains, $\delta$. The side chains may detach from the aromatic clusters to form light gas, $g_1$. As bridges between neighboring aromatic clusters are cleaved, a certain fraction of the coal becomes detached from the coal lattice. These detached aromatic clusters are the heavy-molecular-weight tar precursors that form the metaplast. The metaplast vaporizes to form coal tar. While waiting for vaporization, the metaplast can also reattach to the coal lattice matrix (crosslinking). In the other path, the bridges react and become a char bridge, $c$, with the release of an associated light gas product, $g_2$. The total population of bridges in the coal lattice matrix can be represented by the variable $p$, where $p = £ + c$.

## 16.4.4.5.2. Reaction Rates

Given this set of variables that characterizes the coal lattice structure during devolatilization, the following set of reaction rate expressions can be defined for each, starting with the assumption that the reactive bridges are destroyed at the same rate at which they are created ($\frac{\partial £^*}{\partial t} = 0$):

$$\frac{d£}{dt} = -k_b £ \tag{16.112}$$

$$\frac{dc}{dt} = k_b \frac{£}{\rho + 1} \tag{16.113}$$

$$\frac{d\delta}{dt} = \left[ 2\rho k_b \frac{£}{\rho + 1} \right] - k_g \delta \tag{16.114}$$

$$\frac{dg_1}{dt} = k_g \delta \tag{16.115}$$

Release 15.0 - © SAS IP, Inc. All rights reserved. - Contains proprietary and confidential information of ANSYS, Inc. and its subsidiaries and affiliates.

$$\frac{dg_2}{dt} = 2\frac{dc}{dt} \tag{16.116}$$

where the rate constants for bridge breaking and gas release steps, $k_b$ and $k_g$, are expressed in Arrhenius form with a distributed activation energy:

$$k = Ae^{-(E \pm E_\sigma)/RT} \tag{16.117}$$

where $A$, $E$, and $E_\sigma$ are, respectively, the pre-exponential factor, the activation energy, and the distributed variation in the activation energy, $R$ is the universal gas constant, and $T$ is the temperature. The ratio of rate constants, $\rho = k_\delta / k_c$, is set to 0.9 in this model based on experimental data.

### 16.4.4.5.3. Mass Conservation

The following mass conservation relationships are imposed:

$$g = g_1 + g_2 \tag{16.118}$$

$$g_1 = 2f - \sigma \tag{16.119}$$

$$g_2 = 2(c - c_0) \tag{16.120}$$

where $f$ is the fraction of broken bridges ($f = 1 - p$). The initial conditions for this system are given by the following:

$$c(0) = c_0 \tag{16.121}$$

$$£(0) = £_0 = p_0 - c_0 \tag{16.122}$$

$$\delta(0) = 2f_0 = 2(1 - c_0 - £_0) \tag{16.123}$$

$$g(0) = g_1(0) = g_2(0) = 0 \tag{16.124}$$

where $c_0$ is the initial fraction of char bridges, $p_0$ is the initial fraction of bridges in the coal lattice, and $£_0$ is the initial fraction of labile bridges in the coal lattice.

### 16.4.4.5.4. Fractional Change in the Coal Mass

Given the set of reaction equations for the coal structure parameters, it is necessary to relate these quantities to changes in coal mass and the related release of volatile products. To accomplish this, the fractional change in the coal mass as a function of time is divided into three parts: light gas ($f_{gas}$), tar precursor fragments ($f_{frag}$), and char ($f_{char}$). This is accomplished by using the following relationships, which are obtained using percolation lattice statistics:

$$f_{gas}(t) = \frac{r\left(g_1 + g_2\right)(\sigma + 1)}{4 + 2r(1 - c_0)(\sigma + 1)} \tag{16.125}$$

$$f_{frag}(t) = \frac{2}{2 + r(1 - c_0)(\sigma + 1)}\left[\Phi F(p) + r\Omega K(p)\right] \tag{16.126}$$


Release 15.0 - © SAS IP, Inc. All rights reserved. - Contains proprietary and confidential information of ANSYS, Inc. and its subsidiaries and affiliates.

$$f_{char}(t) = 1 - f_{gas}(t) - f_{frag}(t) \tag{16.127}$$

The variables $\Phi, \Omega, F(p)$, and $K(p)$ are the statistical relationships related to the cleaving of bridges based on the percolation lattice statistics, and are given by the following equations:

$$\Phi = 1 + r\left[\frac{£}{p} + \frac{(\sigma - 1)\delta}{4(1-p)}\right] \tag{16.128}$$

$$\Omega = \frac{\delta}{2(1-p)} - \frac{£}{p} \tag{16.129}$$

$$F(p) = \left(\frac{p'}{p}\right)^{\frac{\sigma+1}{\sigma-1}} \tag{16.130}$$

$$K(p) = \left[1 - \left(\frac{\sigma+1}{2}\right)p'\right]\left(\frac{p'}{p}\right)^{\frac{\sigma+1}{\sigma-1}} \tag{16.131}$$

$r$ is the ratio of bridge mass to site mass, $m_b/m_a$, where

$$m_b = 2M_{w,\delta} \tag{16.132}$$

$$m_a = M_{w,1} - (\sigma+1)M_{w,\delta} \tag{16.133}$$

where $M_{w,\delta}$ and $M_{w,1}$ are the side chain and cluster molecular weights respectively. $\sigma + 1$ is the lattice coordination number, which is determined from solid-state nuclear magnetic Resonance (NMR) measurements related to coal structure parameters, and $p'$ is the root of the following equation in $p$ (the total number of bridges in the coal lattice matrix):

$$p'(1-p')^{\sigma-1} = p(1-p)^{\sigma-1} \tag{16.134}$$

In accounting for mass in the metaplast (tar precursor fragments), the part that vaporizes is treated in a manner similar to flash vaporization, where it is assumed that the finite fragments undergo vapor/liquid phase equilibration on a time scale that is rapid with respect to the bridge reactions. As an estimate of the vapor/liquid that is present at any time, a vapor pressure correlation based on a simple form of Raoult's Law is used. The vapor pressure treatment is largely responsible for predicting pressure-dependent devolatilization yields. For the part of the metaplast that reattaches to the coal lattice, a cross-linking rate expression given by the following equation is used:

$$\frac{dm_{cross}}{dt} = m_{frag}A_{cross}e^{-(E_{cross}/RT)} \tag{16.135}$$

where $m_{cross}$ is the amount of mass reattaching to the matrix, $m_{frag}$ is the amount of mass in the tar precursor fragments (metaplast), and $A_{cross}$ and $E_{cross}$ are rate expression constants.

### 16.4.4.5.5. CPD Inputs

Given the set of equations and corresponding rate constants introduced for the CPD model, the number of constants that must be defined to use the model is a primary concern. For the relationships defined previously, it can be shown that the following parameters are coal independent [123] (p. 735):

Release 15.0 - © SAS IP, Inc. All rights reserved. - Contains proprietary and confidential information of ANSYS, Inc. and its subsidiaries and affiliates.

- $A_b$, $E_b$, $E_{\sigma b}$, $A_g$, $E_g$, and $E_{\sigma g}$ for the rate constants $k_b$ and $k_g$
- $A_{cross}$, $E_{cross}$, and $\rho$

These constants are included in the submodel formulation and are not input or modified during problem setup.

There are an additional five parameters that are coal-specific and must be specified during the problem setup:

- initial fraction of bridges in the coal lattice, $p_0$
- initial fraction of char bridges, $c_0$
- lattice coordination number, $\sigma+1$
- cluster molecular weight, $M_{w,1}$
- side chain molecular weight, $M_{w,\delta}$

The first four of these are coal structure quantities that are obtained from NMR experimental data. The last quantity, representing the char bridges that either exist in the parent coal or are formed very early in the devolatilization process, is estimated based on the coal rank. These quantities are entered in the **Create/Edit Materials** dialog box, as described in Description of the Properties in the User's Guide. Values for the coal-dependent parameters for a variety of coals are listed in Table 16.1: Chemical Structure Parameters for C NMR for 13 Coals (p. 402).

**Table 16.1: Chemical Structure Parameters for C NMR for 13 Coals**

| Coal Type | $\sigma+1$ | $p_0$ | $M_{w,1}$ | $M_{w,\delta}$ | $c_0$ |
|---|---|---|---|---|---|
| Zap (AR) | 3.9 | .63 | 277 | 40 | .20 |
| Wyodak (AR) | 5.6 | .55 | 410 | 42 | .14 |
| Utah (AR) | 5.1 | .49 | 359 | 36 | 0 |
| Ill6 (AR) | 5.0 | .63 | 316 | 27 | 0 |
| Pitt8 (AR) | 4.5 | .62 | 294 | 24 | 0 |
| Stockton (AR) | 4.8 | .69 | 275 | 20 | 0 |
| Freeport (AR) | 5.3 | .67 | 302 | 17 | 0 |
| Pocahontas (AR) | 4.4 | .74 | 299 | 14 | .20 |
| Blue (Sandia) | 5.0 | .42 | 410 | 47 | .15 |
| Rose (AFR) | 5.8 | .57 | 459 | 48 | .10 |
| 1443 (lignite, ACERC) | 4.8 | .59 | 297 | 36 | .20 |
| 1488 (subbituminous, ACERC) | 4.7 | .54 | 310 | 37 | .15 |
| 1468 (anthracite, ACERC) | 4.7 | .89 | 656 | 12 | .25 |

AR refers to eight types of coal from the Argonne premium sample bank [423] (p. 752), [473] (p. 755). Sandia refers to the coal examined at Sandia National Laboratories [122] (p. 735). AFR refers to coal ex-


Release 15.0 - © SAS IP, Inc. All rights reserved. - Contains proprietary and confidential information of ANSYS, Inc. and its subsidiaries and affiliates.

amined at Advanced Fuel Research. ACERC refers to three types of coal examined at the Advanced Combustion Engineering Research Center.

### 16.4.4.5.6. Particle Swelling During Devolatilization

The particle diameter changes during devolatilization according to the swelling coefficient, $C_{sw}$, which is defined by you and applied in the following relationship:

$$\frac{d_p}{d_{p,0}} = 1 + (C_{sw} - 1)\frac{\left(1 - f_{w,0}\right)m_{p,0} - m_p}{f_{v,0}\left(1 - f_{w,0}\right)m_{p,0}} \tag{16.136}$$

where

$d_{p,0}$ = particle diameter at the start of devolatilization

$d_p$ = current particle diameter

The term $(1-f_{w,0})m_{p,0} - m_p \Big/ f_{v,0}(1-f_{w,0})m_{p,0}$ is the ratio of the mass that has been devolatilized to the total volatile mass of the particle. This quantity approaches a value of 1.0 as the devolatilization law is applied. When the swelling coefficient is equal to 1.0, the particle diameter stays constant. When the swelling coefficient is equal to 2.0, the final particle diameter doubles when all of the volatile component has vaporized, and when the swelling coefficient is equal to 0.5 the final particle diameter is half of its initial diameter.

### 16.4.4.5.7. Heat Transfer to the Particle During Devolatilization

Heat transfer to the particle during the devolatilization process includes contributions from convection and radiation (if active):

$$m_p c_p \frac{dT_p}{dt} = hA_p\left(T_\infty - T_p\right) - \frac{dm_p}{dt}h_{fg} + A_p\varepsilon_p\sigma\left(\theta_R{}^4 - T_p{}^4\right) \tag{16.137}$$

where the variables have already been defined for Equation 16.94 (p. 393).

Radiation heat transfer to the particle is included only if you have enabled the P-1 or discrete ordinates radiation heat transfer to particles using the **Particle Radiation Interaction** option in the Discrete Phase Model Dialog Box.

By default, Equation 16.137 (p. 403) is solved analytically, by assuming that the temperature and mass of the particle do not change significantly between time steps:

$$T_p(t + \Delta t) = \alpha_p + \left[T_p(t) - \alpha_p\right]e^{-\beta_p \Delta t} \tag{16.138}$$

where

$$\alpha_p = \frac{hA_pT_\infty + \frac{dm_p}{dt}h_{fg} + A_p\varepsilon_p\sigma\theta_R{}^4}{hA_p + \varepsilon_pA_p\sigma T_p{}^3} \tag{16.139}$$

and

$$\beta_p = \frac{A_p\left(h + \varepsilon_p\sigma T_p{}^3\right)}{m_pc_p} \tag{16.140}$$

ANSYS Fluent can also solve Equation 16.137 (p. 403) in conjunction with the equivalent mass transfer equation using a stiff coupled solver. See Including Coupled Heat-Mass Solution Effects on the Particles in the User's Guide for details.

## 16.4.5. Surface Combustion (Law 5)

After the volatile component of the particle is completely evolved, a surface reaction begins that consumes the combustible fraction, $f_{comb}$, of the particle. Law 5 is therefore active (for a combusting particle) after the volatiles are evolved:

$$m_p < \left(1 - f_{v,0}\right)\left(1 - f_{w,0}\right)m_{p,0} \tag{16.141}$$

and until the combustible fraction is consumed:

$$m_p > \left(1 - f_{v,0} - f_{comb}\right)\left(1 - f_{w,0}\right)m_{p,0} \tag{16.142}$$

When the combustible fraction, $f_{comb}$, has been consumed in Law 5, the combusting particle may contain residual "ash" that reverts to the inert heating law, Law 6 (described previously).

With the exception of the multiple surface reactions model, the surface combustion law consumes the reactive content of the particle as governed by the stoichiometric requirement, $S_b$, of the surface "burnout" reaction:

$$char\,(s) + S_b ox\,(g) \rightarrow products\,(g) \tag{16.143}$$

where $S_b$ is defined in terms of mass of oxidant per mass of char, and the oxidant and product species are defined in the Set Injection Properties Dialog Box.

ANSYS Fluent provides a choice of four heterogeneous surface reaction rate models for combusting particles:

- the diffusion-limited rate model (the default model)
- the kinetics/diffusion-limited rate model
- the intrinsic model
- the multiple surface reactions model

Each of these models is described in detail below. You will choose the surface combustion model when you are setting physical properties for the combusting-particle material, as described in Description of the Properties in the User's Guide. By default, the diffusion-limited rate model will be used.

### 16.4.5.1. The Diffusion-Limited Surface Reaction Rate Model

The diffusion-limited surface reaction rate model, which is the default model in ANSYS Fluent, assumes that the surface reaction proceeds at a rate determined by the diffusion of the gaseous oxidant to the surface of the particle:

$$\frac{dm_p}{dt} = -4\pi d_p D_{i,m} \frac{Y_{ox} T_\infty \rho}{S_b\left(T_p + T_\infty\right)} \tag{16.144}$$

where


Release 15.0 - © SAS IP, Inc. All rights reserved. - Contains proprietary and confidential information of ANSYS, Inc. and its subsidiaries and affiliates.

$D_{i,m}$ = diffusion coefficient for oxidant in the bulk ($m^2/s$)

$Y_{ox}$ = local mass fraction of oxidant in the gas

$\rho$ = gas density ($kg/m^3$)

$S_b$ = stoichiometry of Equation 16.143 (p. 404)

Equation 16.144 (p. 404) is derived from the model of Baum and Street [25] (p. 730) with the kinetic contribution to the surface reaction rate ignored. The diffusion-limited rate model assumes that the diameter of the particles does not change. Since the mass of the particles is decreasing, the effective density decreases, and the char particles become more porous.

### 16.4.5.2. The Kinetic/Diffusion Surface Reaction Rate Model

The kinetic/diffusion-limited rate model assumes that the surface reaction rate is determined either by kinetics or by a diffusion rate. ANSYS Fluent uses the model of Baum and Street [25] (p. 730) and Field [119] (p. 735), in which a diffusion rate coefficient

$$D_0 = C_1 \frac{\left[\left(T_p + T_\infty\right)/2\right]^{0.75}}{d_p} \tag{16.145}$$

and a kinetic rate

$$\mathcal{R} = C_2 e^{-\left(E/RT_p\right)} \tag{16.146}$$

are weighted to yield a char combustion rate of

$$\frac{dm_p}{dt} = -A_p p_{ox} \frac{D_0 \mathcal{R}}{D_0 + \mathcal{R}} \tag{16.147}$$

where $A_p$ is the surface area of the droplet ($\pi d_p^2$), $p_{ox}$ is the partial pressure of oxidant species in the gas surrounding the combusting particle, and the kinetic rate, $\mathcal{R}$, incorporates the effects of chemical reaction on the internal surface of the char particle (intrinsic reaction) and pore diffusion. In ANSYS Fluent, Equation 16.147 (p. 405) is recast in terms of the oxidant mass fraction, $Y_{ox}$, as

$$\frac{dm_p}{dt} = -A_p \frac{\rho R T_\infty Y_{ox}}{M_{w,ox}} \frac{D_0 \mathcal{R}}{D_0 + \mathcal{R}} \tag{16.148}$$

The particle size is assumed to remain constant in this model while the density is allowed to decrease.

When this model is enabled, the rate constants used in Equation 16.145 (p. 405) and Equation 16.146 (p. 405) are entered in the Create/Edit Materials Dialog Box, as described in Setting Material Properties for the Discrete Phase in the User's Guide.

### 16.4.5.3. The Intrinsic Model

The intrinsic model in ANSYS Fluent is based on Smith's model [417] (p. 752), assuming the order of reaction is equal to unity. Like the kinetic/diffusion model, the intrinsic model assumes that the surface reaction rate includes the effects of both bulk diffusion and chemical reaction (see Equation 16.148 (p. 405)). The intrinsic model uses Equation 16.145 (p. 405) to compute the diffusion rate

Release 15.0 - © SAS IP, Inc. All rights reserved. - Contains proprietary and confidential information of ANSYS, Inc. and its subsidiaries and affiliates.

coefficient, $D_0$, but the chemical rate, $\mathcal{R}$, is explicitly expressed in terms of the intrinsic chemical and pore diffusion rates:

$$\mathcal{R}=\eta\frac{d_p}{6}\rho_p A_g k_i \tag{16.149}$$

$\eta$ is the effectiveness factor, or the ratio of the actual combustion rate to the rate attainable if no pore diffusion resistance existed [233] (p. 741):

$$\eta=\frac{3}{\phi^2}(\phi\coth\phi-1) \tag{16.150}$$

where $\phi$ is the Thiele modulus:

$$\phi=\frac{d_p}{2}\left[\frac{S_b\rho_p A_g k_i p_{ox}}{D_e\rho_{ox}}\right]^{1/2} \tag{16.151}$$

$\rho_{ox}$ is the density of oxidant in the bulk gas (kg/$\mathrm{m}^3$) and $D_e$ is the effective diffusion coefficient in the particle pores. Assuming that the pore size distribution is unimodal and the bulk and Knudsen diffusion proceed in parallel, $D_e$ is given by

$$D_e=\frac{\theta}{\tau^2}\left[\frac{1}{D_{Kn}}+\frac{1}{D_0}\right]^{-1} \tag{16.152}$$

where $D_0$ is the bulk molecular diffusion coefficient and $\theta$ is the porosity of the char particle:

$$\theta=1-\frac{\rho_p}{\rho_t} \tag{16.153}$$

$\rho_p$ and $\rho_t$ are, respectively, the apparent and true densities of the pyrolysis char.

$\tau$ (in Equation 16.152 (p. 406)) is the tortuosity of the pores. The default value for $\tau$ in ANSYS Fluent is $\sqrt{2}$, which corresponds to an average intersecting angle between the pores and the external surface of 45 $^\circ$ [233] (p. 741).

$D_{Kn}$ is the Knudsen diffusion coefficient:

$$D_{Kn}=97.0\bar{r}_p\sqrt{\frac{T_p}{M_{w,ox}}} \tag{16.154}$$

where $T_p$ is the particle temperature and $\bar{r}_p$ is the mean pore radius of the char particle, which can be measured by mercury porosimetry. Note that macropores ($\bar{r}_p>150$ Å) dominate in low-rank chars while micropores ($\bar{r}_p<10$ Å) dominate in high-rank chars [233] (p. 741).

$A_g$ (in Equation 16.149 (p. 406) and Equation 16.151 (p. 406)) is the specific internal surface area of the char particle, which is assumed in this model to remain constant during char combustion. Internal surface area data for various pyrolysis chars can be found in [416] (p. 751). The mean value of the internal surface area during char combustion is higher than that of the pyrolysis char [233] (p. 741). For example, an estimated mean value for bituminous chars is 300 $\mathrm{m}^2$/g [62] (p. 732).


Release 15.0 - © SAS IP, Inc. All rights reserved. - Contains proprietary and confidential information of ANSYS, Inc. and its subsidiaries and affiliates.

$k_i$ (in Equation 16.149 (p. 406) and Equation 16.151 (p. 406)) is the intrinsic reactivity, which is of Arrhenius form:

$$k_i = A_i e^{-\left(E_i / R T_p\right)} \tag{16.155}$$

where the pre-exponential factor $A_i$ and the activation energy $E_i$ can be measured for each char. In the absence of such measurements, the default values provided by ANSYS Fluent (which are taken from a least squares fit of data of a wide range of porous carbons, including chars [416] (p. 751)) can be used.

To allow a more adequate description of the char particle size (and hence density) variation during combustion, you can specify the burning mode $\alpha$, relating the char particle diameter to the fractional degree of burnout $U$ (where $U = 1 - m_p / m_{p,0}$) by [415] (p. 751)

$$\frac{d_p}{d_{p,0}} = (1 - U)^{\alpha} \tag{16.156}$$

where $m_p$ is the char particle mass and the subscript zero refers to initial conditions (that is, at the start of char combustion). Note that $0 \le \alpha \le 1/3$ where the limiting values 0 and $1/3$ correspond, respectively, to a constant size with decreasing density (zone 1) and a decreasing size with constant density (zone 3) during burnout. In zone 2, an intermediate value of $\alpha = 0.25$, corresponding to a decrease of both size and density, has been found to work well for a variety of chars [415] (p. 751).

When this model is enabled, the rate constants used in Equation 16.145 (p. 405), Equation 16.149 (p. 406), Equation 16.151 (p. 406), Equation 16.152 (p. 406), Equation 16.154 (p. 406), Equation 16.155 (p. 407), and Equation 16.156 (p. 407) are entered in the Create/Edit Materials Dialog Box, as described in Setting Material Properties for the Discrete Phase in the User's Guide.

### 16.4.5.4. The Multiple Surface Reactions Model

Modeling multiple particle surface reactions follows a pattern similar to the wall surface reaction models, where the surface species is now a "particle surface species". For the mixture material defined in the **Species Model** dialog box, the particle surface species can be depleted or produced by the stoichiometry of the particle surface reaction (defined in the **Reactions** dialog box). The particle surface species constitutes the reactive char mass of the particle, hence, if a particle surface species is depleted, the reactive "char" content of the particle is consumed, and in turn, when a surface species is produced, it is added to the particle "char" mass. Any number of particle surface species and any number of particle surface reactions can be defined for any given combusting particle.

Multiple injections can be accommodated, and combusting particles reacting according to the multiple surface reactions model can coexist in the calculation, with combusting particles following other char combustion laws. The model is based on oxidation studies of char particles, but it is also applicable to gas-solid reactions in general, not only to char oxidation reactions.

See Particle Surface Reactions (p. 204) for information about particle surface reactions.

#### 16.4.5.4.1. Limitations

Note the following limitations of the multiple surface reactions model:

- The model is available only with the species transport model for volumetric reactions, and not with the nonpremixed, premixed, or partially premixed combustion models.

Release 15.0 - © SAS IP, Inc. All rights reserved. - Contains proprietary and confidential information of ANSYS, Inc. and its subsidiaries and affiliates.

### 16.4.5.5. Heat and Mass Transfer During Char Combustion

The surface reaction consumes the oxidant species in the gas phase; that is, it supplies a (negative) source term during the computation of the transport equation for this species. Similarly, the surface reaction is a source of species in the gas phase: the product of the heterogeneous surface reaction appears in the gas phase as a user-selected chemical species. The surface reaction also consumes or produces energy, in an amount determined by the heat of reaction defined by you.

The particle heat balance during surface reaction is

$$m_p c_p \frac{dT_p}{dt} = h A_p \left( T_\infty - T_p \right) - f_h \frac{dm_p}{dt} H_{reac} + A_p \varepsilon_p \sigma \left( {\theta_R}^4 - {T_p}^4 \right) \tag{16.157}$$

where $H_{reac}$ is the heat released by the surface reaction. Note that only a portion $(1 - f_h)$ of the energy produced by the surface reaction appears as a heat source in the gas-phase energy equation: the particle absorbs a fraction $f_h$ of this heat directly. For coal combustion, it is recommended that $f_h$ be set to 1.0 if the char burnout product is $CO$ and 0.3 if the char burnout product is $CO_2$ [40] (p. 731).

Radiation heat transfer to the particle is included only if you have enabled the P-1 or discrete ordinates radiation heat transfer to particles using the **Particle Radiation Interaction** option in the Discrete Phase Model Dialog Box.

By default, Equation 16.157 (p. 408) is solved analytically, by assuming that the temperature and mass of the particle do not change significantly between time steps. ANSYS Fluent can also solve Equation 16.157 (p. 408) in conjunction with the equivalent mass transfer equation using a stiff coupled solver. See Including Coupled Heat-Mass Solution Effects on the Particles in the User's Guide for details.

## 16.4.6. Multicomponent Particle Definition (Law 7)

Multicomponent particles are described in ANSYS Fluent as droplet particles containing a mixture of several components or species. The particle mass $m$ is the sum of the masses of the components

$$m = \sum_i m_i \tag{16.158}$$

The density of the particle $\rho_p$ can be either constant, or volume-averaged:

$$\rho_p = \left( \sum_i \frac{m_i}{m \rho_i} \right)^{-1} \tag{16.159}$$

The multicomponent droplet vaporization rate is calculated as the sum of the vaporization rates of the individual components.

For the **diffusion-controlled** Vaporization model, the vaporization rate of component $i$ is given by Equation 16.160 (p. 408)

$$\frac{dm_i}{dt} = A_p M_{w,i} k_{c,i} \left( C_{i,s} - C_{i,\infty} \right) \tag{16.160}$$

while for the **convection/diffusion controlled** model, it is given by Equation 16.161 (p. 408)

$$\frac{dm_i}{dt} = A_p k_{c,i} \rho_\infty \ln\left( 1 + B_{m,i} \right) \tag{16.161}$$


Release 15.0 - © SAS IP, Inc. All rights reserved. - Contains proprietary and confidential information of ANSYS, Inc. and its subsidiaries and affiliates.

where

$m_i$ = mass of component $i$ in droplet (kg)

$k_{c,i}$ = mass transfer coefficient of component $i$ (m/s) given by Equation 16.87 (p. 391)

$A_p$ = droplet surface area ($m^2$)

$\rho_\infty$ = density of bulk gas ($kg/m^3$)

$M_{w,i}$ = molecular weight of species $i$

$C_{i,s}$ and $C_{i,\infty}$ = concentration of species $i$ at the droplet surface and the bulk, respectively ($kmol/m^3$).

$B_{m,i}$ = Spalding mass number for species $i$ and is given by Equation 16.90 (p. 392)

When the total vapor pressure at the droplet surface exceeds the cell pressure, the multicomponent droplet is in the boiling regime and ANSYS Fluent applies the boiling rate equation (Equation 16.162 (p. 409)). The total vapor pressure is computed as $P_t = \sum P_i$ where $P_i$ is the partial pressure of component $i$.

The boiling rate equation is

$$\frac{dm_i}{dt} = x_i \frac{\pi d_p k_\infty}{c_{p\infty}} (2 + 0.6 \mathrm{Re}_d^{1/2} \mathrm{Pr}^{1/3}) \ln(1 + B_{T,i}) \tag{16.162}$$

where

$x_i$ = volume fraction of component $i$ in the droplet

$d_p$ = droplet diameter (m)

$k_\infty$ = thermal conductivity of the continuous phase (W/m–K)

$c_{p\infty}$ = specific heat of the continuous phase (J/kg–K)

$B_{T,i}$ = Spalding heat transfer number for component $i$ computed by Equation 16.163 (p. 409)

$$B_{T,i} = \frac{c_{p\infty}(T_\infty - T_p)}{h_{vap,i}} \tag{16.163}$$

The equation for the multicomponent particle temperature $T$ consists of terms for radiation, convective heating and vaporization, and is cast similarly to the single component particle energy equation (Equation 16.75 (p. 388)). Radiation heat transfer to the particle is included only if you have enabled **P-1** or **Discrete-Ordinates (DO)** radiation heat transfer to the particles using the **Particle Radiation Interaction** option in the **Discrete Phase Model** dialog box.

The energy equation is written for the multicomponent particle as follows:

$$m_p c_p \frac{dT}{dt} = A_p \varepsilon_p \sigma \left( \Theta_R^4 - T_p^4 \right) + h A_p \left( T_\infty - T_p \right) + \sum_i \frac{dm_i}{dt} \left( h_{vap,i} \right) \tag{16.164}$$

Release 15.0 - © SAS IP, Inc. All rights reserved. - Contains proprietary and confidential information of ANSYS, Inc. and its subsidiaries and affiliates.

where $^{dm_i}/_{dt}$ is computed from Equation 16.160 (p. 408), Equation 16.161 (p. 408), or Equation 16.162 (p. 409). The heat transfer coefficient $h$ is computed from Equation 16.81 (p. 389) for the **diffusion-controlled** Vaporization model and Equation 16.95 (p. 394) for the **convection/diffusion-controlled** Vaporization model and the boiling regime.

In Equation 16.163 (p. 409) and Equation 16.164 (p. 409) $h_{vap,i}$ is the latent heat of vaporization for component $i$.

When radiation heat transfer is active, the boiling rate $^{dm_i}/_{dt}$ calculated by Equation 16.162 (p. 409), is augmented by the radiation term,

$$\frac{x_i}{h_{vap,i}} A_p \varepsilon_p \sigma \left( \Theta_R^4 - T_p^4 \right) \tag{16.165}$$

### 16.4.6.1. Raoult's Law

The correlation between the vapor concentration of a species $C_{i,s}$ over the surface and its mole fraction in the condensed phase $x_i^L$ is described by Raoult's law:

$$C_{i,s} = \frac{p_i}{RT} = \frac{x_i^L p_{sat,i}}{RT} \tag{16.166}$$

### 16.4.6.2. Peng-Robinson Real Gas Model

In the Peng-Robinson Real Gas Model, the vapor concentration of each species at the surface is deduced from the calculations of vapor mole fraction and compressibility:

$$C_{i,S} = x_i^V \frac{p}{Z^V RT} \tag{16.167}$$

These calculations are described in Vapor Liquid Equilibrium Theory (p. 410). The vapor-liquid equilibrium is deduced from the inputs for the Peng-Robinson model in the evaporating vapor species, so it is not necessary to specify vapor pressure separately.

Instead of using Raoult's Law or the Peng-Robinson equation of state, you can define your own user-defined function for delivering the vapor concentration at the particle surface. For more information, see `DEFINE_DPM_VP_EQUILIB` in the UDF Manual.

## 16.5. Vapor Liquid Equilibrium Theory

A number of industrially important processes, such as distillation, absorption, and extraction, bring into contact two phases that are not at equilibrium. The rate at which a species is transferred from one phase to the other depends on the departure of the system from equilibrium. The quantitative treatment of these rate processes requires knowledge of the equilibrium states of the system. Apart from these cases, vapor-liquid equilibrium (VLE) relationships in multicomponent systems are needed for the solution of many other classes of engineering problems, such as the computation of evaporation rates in spray combustion applications.

For the multicomponent particle, the vaporization rate of component $i$ is computed from Equation 16.160 (p. 408) or Equation 16.161 (p. 408) and requires knowledge of the component concentration or the mass fraction at the droplet surface.


Release 15.0 - © SAS IP, Inc. All rights reserved. - Contains proprietary and confidential information of ANSYS, Inc. and its subsidiaries and affiliates.

The concentration or mass fraction of species $i$ at the particle surface is computed from the mole fraction $x_i$, which can be obtained from the general expression for two phase equilibrium, equating the fugacity of the liquid and vapor mixture components [356] (p. 748):

$$f_i^V = x_i^V \phi_i^V p = x_i^L \phi_i^L p = f_i^L \tag{16.168}$$

where $x_i$ is the mole fraction, $\phi_i$ is the fugacity coefficient for the species $i$ in the mixture, and $p$ is the absolute pressure. The superscripts $V$ and $L$ are the vapor and the liquid phase variables, respectively. The fugacity coefficients account for the nonideality in the gas and liquid mixture. The fugacity of the liquid phase can be calculated from the pure component's saturation pressure $p_{sat,i}$ [418] (p. 752):

$$f_i^L = x_i^L \phi_i^L p = \gamma_i x_i^L \phi_{sat,i}^L p_{sat,i} exp\left[\frac{V_i^L\left(p - p_{sat,i}\right)}{RT}\right] \tag{16.169}$$

Here, $\phi_{sat,i}^L$ is the fugacity coefficient for pure $i$ at the saturation pressure; $\gamma_i$ is the activity coefficient for species $i$ in the mixture, and accounts for the nonideality in the liquid phase; $T$ is the particle surface temperature. We assume perfect thermal conductivity inside the particle, so the particle temperature is used instead; $R$ is the universal gas constant; $V_i^L$ is the molar volume of the liquid. The exponential term is the Poynting correction factor and accounts for the compressibility effects within the liquid. Except at high pressures, the Poynting factor is usually negligible. Under low pressure conditions where the gas phase may be assumed to be ideal, $\phi_i^V \approx 1$ and $\phi_{sat,i} \approx 1$. Furthermore, if the liquid is also assumed to be ideal, $\gamma \approx 1$, then Equation 16.168 (p. 411) reduces to Raoult's law,

$$x_i^V p = x_i^L p_{sat,i} \tag{16.170}$$

Raoult's law is the default vapor-liquid equilibrium expression used in the ANSYS Fluent multicomponent droplet model. However, there is a UDF hook available for user-defined vapor-liquid equilibrium models.

While Raoult's law represents the simplest form of the VLE equation, keep in mind that it is of limited use, as the assumptions made for its derivation are usually unrealistic. The most critical assumption is that the liquid phase is an ideal solution. This is not likely to be valid, unless the system is made up of species of similar molecular sizes and chemical nature, such as in the case of benzene and toluene, or n-heptane and n-hexane.

For higher pressures, especially near or above the critical point of the components, real gas effects must be considered. Most models describing the fugacity coefficients use a cubic equation of state with the general form:

$$p = \frac{RT}{V-b} - \frac{a(V-\eta)}{(V-b)\left(V^2+\delta V+\varepsilon\right)} \tag{16.171}$$

where $V$ is the molar volume. For in-cylinder applications, the Peng-Robinson equation of state is often used [343] (p. 748), where $\delta = 2b$, $\varepsilon = -b^2$, and $\eta = b$:

$$p = \frac{RT}{V-b} - \frac{a}{V^2+2bV-b^2} \tag{16.172}$$

This equation defines the compressibility

$$Z=\frac{pV}{RT}=\frac{V}{V-b}-\frac{aV/RT}{V^2+2bV-b^2} \tag{16.173}$$

The implementation of the Peng-Robinson equation of state in ANSYS Fluent uses this expression for both phases, the particle liquid and the vapor phase. The parameters $a$ and $b$ are determined by the composition using a simple mixing law:

$$\begin{aligned} a&=\sum_{i=1}^{N}\sum_{j=1}^{N}x_i x_j\sqrt{a_i a_j} \\ b&=\sum_{i=1}^{N}x_i b_i \end{aligned} \tag{16.174}$$

where $N$ is the number of components in the mixture. The pure component parameters can be obtained using the relationship with the Peng-Robinson constants:

$$a_i=\left(0.457247\frac{R^2T_{c,i}^2}{p_{c,i}}\right)\left[1+\left(0.37464+1.54226\omega_i-0.26992\omega_i^2\right)\left(1-\left(\frac{T}{T_{c,i}}\right)^{1/2}\right)\right]^2 \tag{16.175}$$

$$b_i=0.07780\frac{RT_{c,i}}{P_{c,i}}$$

where $T_{c,i}$ is the critical temperature, $p_{c,i}$ is the critical pressure and $\omega_i$ is the acentric factor of the component $i$.

The fugacities of the components depend on the compressibility of the liquid and vapor phase:

$$ln\phi_i=\left(\frac{\partial\left(A^{\gamma}/RT\right)}{\partial N_i}\right)_{T,V,N_{j\neq i}}-lnZ \tag{16.176}$$

where $A^{\gamma}$ is the residual Helmholtz energy, which is a function of the compressibility:

$$\frac{A^{\gamma}}{RT}=\int_V^{\infty}\left[1-Z\right]\frac{dV}{V}+lnZ \tag{16.177}$$

In summary, the vapor mole fraction $x_i^V$, the pressure $p$, and the compressibilities of the vapor ($Z^V$) and the liquid ($Z^L$) phase at the surface of the particle are determined from the liquid particle mole fraction of the components $x_i^L$ and the particle temperature $T_p$. The surface vapor concentrations are calculated using the following equation:

$$C_{i,S}=x_i^V\frac{p}{Z^VRT} \tag{16.178}$$

## 16.6. Wall-Jet Model Theory

The **wall-jet** boundary condition provides a range of rebound directions and velocities when a liquid droplet collides with a wall. It is suitable for situations where droplets impact a hot wall, where no liquid


Release 15.0 - © SAS IP, Inc. All rights reserved. - Contains proprietary and confidential information of ANSYS, Inc. and its subsidiaries and affiliates.

film is formed, but the droplets reflect or stick on the wall depending on their impact properties. The direction and velocity of the droplet particles are given by the resulting momentum flux, which is a function of the impingement angle, $\phi$, and Weber number. See Figure 16.2: "Wall Jet" Boundary Condition for the Discrete Phase (p. 413).

**Figure 16.2: "Wall Jet" Boundary Condition for the Discrete Phase**

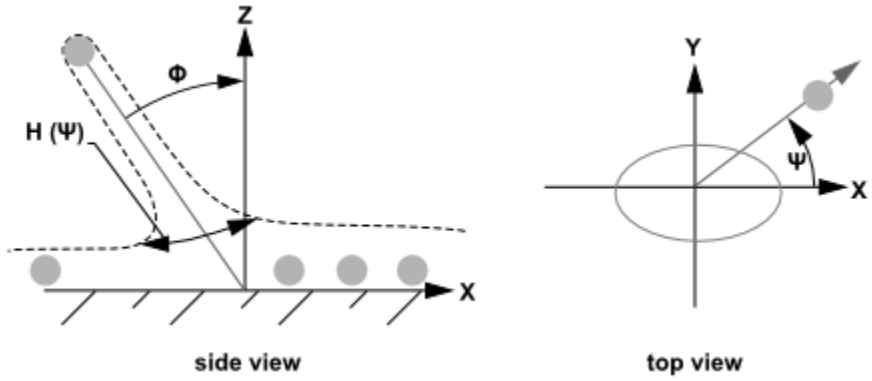


The **wall-jet** type boundary condition assumes an analogy with an inviscid jet impacting a solid wall. Equation 16.179 (p. 413) shows the analytical solution for an axisymmetric impingement assuming an empirical function for the sheet height ($H$) as a function of the angle that the drop leaves the impingement ($\Psi$).

$$H(\Psi) = H_{\pi} e^{\beta\left(1-\frac{\Psi}{\pi}\right)} \tag{16.179}$$

where $H_{\pi}$ is the sheet height at $\Psi = \pi$ and $\beta$ is a constant determined from conservation of mass and momentum. The probability that a drop leaves the impingement point at an angle between $\Psi$ and $\Psi + \delta\Psi$ is given by integrating the expression for $H(\Psi)$

$$\Psi = -\frac{\pi}{\beta} \ln\left[1 - P\left(1 - e^{-\beta}\right)\right] \tag{16.180}$$

where $P$ is a random number between 0 and 1. The expression for $\beta$ is given in Naber and Reitz [315] (p. 746) as

$$\sin(\phi) = \frac{e^{\beta}+1}{\left(e^{\beta}-1\right)\left(1+\left(\frac{\pi}{\beta}\right)^2\right)} \tag{16.181}$$

Fluent uses a simplified expression for computing $\beta$ from Equation 16.181 (p. 413).

## 16.7. Wall-Film Model Theory

This section is composed of the following:

16.7.1. Introduction
16.7.2. Interaction During Impact with a Boundary
16.7.3. Splashing
16.7.4. Separation Criteria
16.7.5. Conservation Equations for Wall-Film Particles

Release 15.0 - © SAS IP, Inc. All rights reserved. - Contains proprietary and confidential information of ANSYS, Inc. and its subsidiaries and affiliates.

## 16.7.1. Introduction

ANSYS Fluent has a specific boundary condition for simulation of liquid droplets colliding with walls and forming thin films. This model is particularly aimed at simulation of internal combustion engines. The wall film model uses transient Lagrangian particles to discretize physical effects and is therefore well suited for fast transient effects. Besides this, an Eulerian wall film model exists that is able to deal with steady wall films (Eulerian Wall Films (p. 611)).

Spray-wall interaction is an important part of the mixture formation process in port fuel injected (PFI) engines. A fuel spray impinges on a surface, usually at the intake port near the intake valve, as well as at the intake valve itself, where it splashes and subsequently evaporates. The evaporated mixture is entrained into the cylinder of the engine, where it is mixed with the fresh charge and any residual gas in the cylinder. The mixture that is compressed and burned, finally exits through the exhaust port. The process repeats itself between 200 and 8000 times per minute, depending on the engine.

Several cycles worth of fuel remain in the intake tract due to film formation on the walls. This in turn makes the film important in hydrocarbon emissions for PFI engines. Additionally, film can form inside combustion chambers of direct injection (DI) types of engines. In a direct injection engine, fuel is injected directly into the combustion chamber, where the spray can impinge upon the piston if the injection event is early or late in the cycle. The modeling of the wall-film inside a DI engine, especially in diesel engines, is compounded by the presence of carbon deposits on the surfaces of the engine. This carbon deposit absorbs the liquid film as it impinges upon it. It is believed that the carbon deposits adsorb the fuel later in the cycle, however this phenomenon is very complex and is not well understood.

DPM particles are used to model the wall-film. The wall-film model in ANSYS Fluent allows a single component liquid drop to impinge upon a boundary surface and form a thin film. The model can be broken down into four major subtopics: interaction during the initial impact with a wall boundary, subsequent tracking on surfaces, calculation of film variables, and coupling to the gas phase. Figure 16.3: Mechanisms of Splashing, Momentum, Heat and Mass Transfer for the Wall-Film (p. 414) schematically shows the basic mechanisms considered for the wall-film model.

**Figure 16.3: Mechanisms of Splashing, Momentum, Heat and Mass Transfer for the Wall-Film**

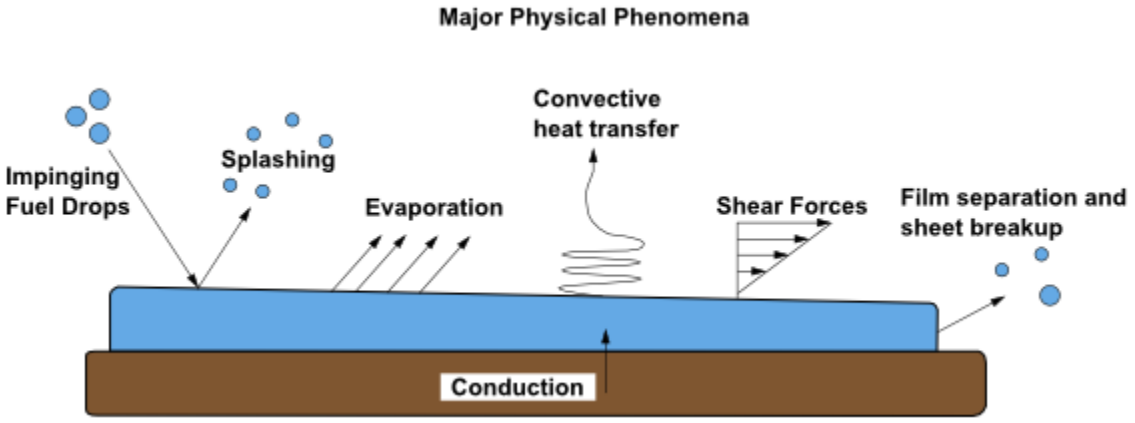


The main assumptions and restrictions for the wall-film model are as follows:

- The layer is thin, less than 500 microns in thickness. This limitation is due to the assumption of a linear velocity profile in the film.
- The temperature in the film particles change relatively slowly so that an analytical integration scheme can be utilized.


Release 15.0 - © SAS IP, Inc. All rights reserved. - Contains proprietary and confidential information of ANSYS, Inc. and its subsidiaries and affiliates.

- Film particles are assumed to be in direct contact with the wall surface and the heat transfer from the wall to the film takes place by conduction.
- The film temperature never exceeds the boiling temperature for the liquid.
- The simulation is transient.
- The wall-film model is not available with the **Workpile Algorithm** shared memory option in parallel processing.

If you want to model a spray impacting a very hot wall, the wall-jet model may be more appropriate as the assumption in the wall-jet impingement model is that there is a vapor layer underneath the drops that keeps them from making direct contact with the boundary surface. This may be a more accurate assumption for in-cylinder diesel computations at typical operating conditions.

## 16.7.2. Interaction During Impact with a Boundary

The wall interaction is based on the work of Stanton [433] (p. 752) and O'Rourke [332] (p. 747), where the regimes are calculated for a drop-wall interaction based on local information. The four regimes, stick, rebound, spread, and splash are based on the impact energy and wall temperature. The following chart is helpful in showing the cutoffs.

**Figure 16.4: Simplified Decision Chart for Wall Interaction Criterion**

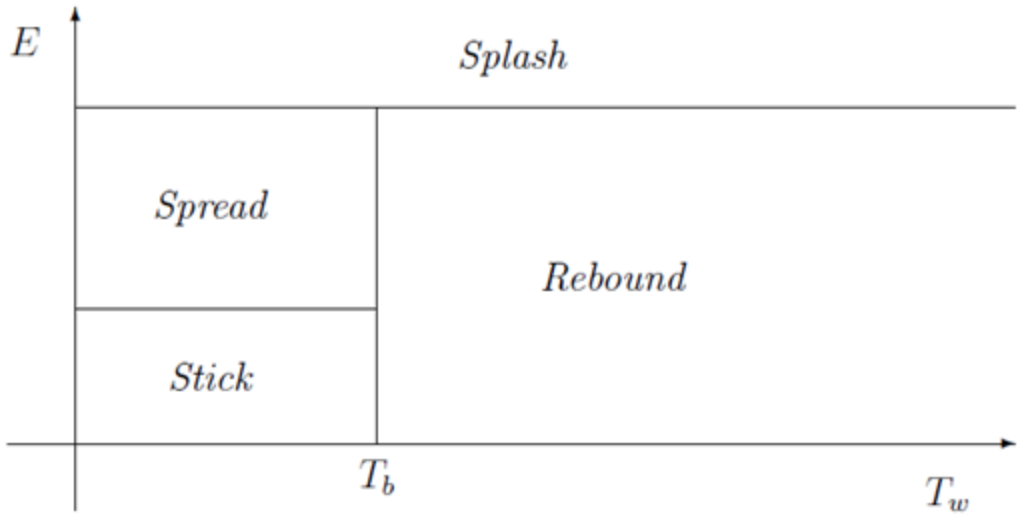


Below the boiling temperature of the liquid, the impinging droplet can either stick, spread or splash, while above the boiling temperature, the particle can either rebound or splash.

The criteria by which the regimes are partitioned are based on the impact energy and the boiling temperature of the liquid. The impact energy is defined by

$$E^2 = \frac{\rho V_r^2 d_p}{\sigma}\left(\frac{1}{\min\left(h_0/d_p, 1\right)+\delta_{bl}/d_p}\right) \tag{16.182}$$

where $\rho$ is the liquid density, $V_r$ is the relative velocity of the particle in the frame of the wall (that is $V_r^2 = \left(V_p - V_w\right)^2$), where $\rho$ is the liquid density, $d_p$ is the diameter of the droplet, $\sigma$ is the surface tension of the liquid, and $h_0$ is the film height. Here, $\delta_{bl}$ is a boundary layer thickness, defined by

$$\delta_{bl} = \frac{d_p}{\sqrt{Re}} \tag{16.183}$$

where the Reynolds number is defined as $Re = \rho V_r d_p / \mu$. By defining the energy as in Equation 16.182 (p. 415), the presence of the film on the wall suppresses the splash, but does not give unphysical results when the film height approaches zero.

The sticking regime is applied when the dimensionless energy $E$ is less than 16, and the particle velocity is set equal to the wall velocity. In the spreading regime, the initial direction and velocity of the particle are set using the wall-jet model, where the probability of the drop having a particular direction along the surface is given by an analogy of an inviscid liquid jet with an empirically defined radial dependence for the momentum flux.

If the wall temperature is above the boiling temperature of the liquid, impingement events below a critical impact energy ($E_{cr}$) results in the particles rebounding from the wall. For the rebound regime, the particle rebounds with the following coefficient of restitution:

$$e = 0.993 - 1.76\Theta_I + 1.56\Theta_I^2 - 0.49\Theta_I^3 \tag{16.184}$$

where $\Theta_I$ is the impingement angle in radians as measured from the wall surface.

Splashing occurs when the impingement energy is above a critical energy threshold, defined as $E_{cr} = 57.7$. The number of splashed droplet parcels is set in the **Wall** boundary condition dialog box with a default number of 4, however, you can select numbers between zero and ten. The splashing algorithm follows that described by Stanton [433] (p. 752) and is detailed in Splashing (p. 416).

## 16.7.3. Splashing

If the particle impinging on the surface has a sufficiently high energy, the particle splashes and several new particles are created. You can explicitly set the number of particles created by each impact in the **DPM** tab of the **Wall** boundary condition dialog box. The minimum number of splashed parcels is three. The properties (diameter, magnitude, and direction) of the splashed parcels are randomly sampled from the experimentally obtained distribution functions described in the following sections. Setting the number of splashed parcels to zero in the Lagrangian wall film model turns off the splashing calculation for the Lagrangian model. Bear in mind that each splashed parcel can be considered a discrete sample of the distribution curves and that selecting the number of splashed drops in the **Wall** boundary condition dialog box does not limit the number of splashed drops, only the number of *parcels* representing those drops.

Therefore, for each splashed parcel, a different diameter is obtained by sampling a cumulative probability distribution function (CPDF), also referred to as F, which is obtained from a Weibull distribution function and fitted to the data from Mundo, et al. [312] (p. 746). The equation is

$$f(d) = 2\frac{d}{D^2}\exp\left[-\left(\frac{d}{D}\right)^2\right] \tag{16.185}$$


Release 15.0 - © SAS IP, Inc. All rights reserved. - Contains proprietary and confidential information of ANSYS, Inc. and its subsidiaries and affiliates.

and it represents the probability of finding drops of diameter $d_i$ in a sample of splashed drops. This distribution is similar to the Nakamura-Tanasawa distribution function used by O'Rourke [332] (p. 747), but with the peak of the distribution function being $D = d_{max}/\sqrt{2}$. To ensure that the distribution functions produce physical results with an increasing Weber number, the following expression for $d_{max}$ from O'Rourke [332] (p. 747) is used. The peak of the splashed diameter distribution is

$$d_{max}/d_0 = \max\left(\frac{E_{crit}^2}{E^2}, \frac{6.4}{We}, 0.06\right) \tag{16.186}$$

where the expression for energy is given by Equation 16.182 (p. 415). Low Weber number impacts are described by the second term in Equation 16.186 (p. 417) and the peak of the minimum splashed diameter distribution is never less than 0.06 for very high energy impacts in any of the experiments analyzed by O'Rourke [332] (p. 747). The Weber number in Equation 16.186 (p. 417) is defined using the relative velocity and drop diameter:

$$We = \frac{\rho V_r^2 D}{\sigma} \tag{16.187}$$

The cumulative probability distribution function (CPDF) is needed so that a diameter can be sampled from the experimental data. The CPDF is obtained from integrating Equation 16.185 (p. 416) to obtain

$$F(d) = 1 - \exp\left[-\left(\frac{d}{D}\right)^2\right] \tag{16.188}$$

which is bounded by zero and one. An expression for the diameter (which is a function of $D$, the impingement Weber number $We$, and the impingement energy) is obtained by inverting Equation 16.188 (p. 417) and sampling the CPDF between zero and one. The expression for the diameter of the $i^{th}$ splashed parcel is therefore given by, $d_i = D\sqrt{-\ln(1-c_i)}$ where $c_i$ is the $i^{th}$ random sample. Once the diameter of the splashed drop has been determined, the probability of finding that drop in a given sample is determined by evaluating Equation 16.185 (p. 416) at the given diameter. The number of droplets in each parcel is proportional to the value of the PDF for that droplet size. The total number of particles is then determined by the total mass that is splashed.

The amount of mass splashed from the surface is a quadratic function of the splashing energy, obtained from the experimental data from Mundo [312] (p. 746). The splashed mass fraction $y_s$ is given by

$$y_s = \begin{cases} 1.8\text{x}10^{-4}\left(E^2 - E_{crit}^2\right) & , E_{crit}^2 < E^2 < 7500 \\ 0.70 & , E^2 > 7500 \end{cases} \tag{16.189}$$

The authors (O'Rourke et al. [332] (p. 747)) noted that nearly all of the impacts for typical diesel sprays are well above the upper bound and so the splashing event nearly always ejects 70% of the mass of the impinging drop. To obtain an expression for the total number of drops, we note that overall conservation of mass requires that the sum of the total mass of the splashed parcel(s) must equal the splashed mass fraction, or

$$\frac{\rho\pi}{6} N_{tot} \sum_{n=1}^{N_{parcels}} \left(f_n d_n^3\right) = y_s m_0 \tag{16.190}$$

Release 15.0 - © SAS IP, Inc. All rights reserved. - Contains proprietary and confidential information of ANSYS, Inc. and its subsidiaries and affiliates.

where $m_0$ is the total mass of the impinging parcel. The expression for the total number of splashed drops is

$$N_{tot}=\frac{y_s m_0}{\frac{\rho\pi}{6}\sum_{n=1}^{N_{parcels}}\left(f_n d_n^3\right)}$$

The number of splashed drops per parcel is then determined by $N_{tot}$ multiplied by the value of the PDF for that droplet size.

To calculate the velocity with which the splashed drops leave the surface, additional correlations are sampled for the normal component of the velocity. A Weibull function, fit to the data from Mundo [312] (p. 746), is used as the PDF for the normal component. The probability density is given by

$$f\left(\frac{V_{ni}}{V_{nd}}\right)=\left[\frac{b_v}{\Theta_v}\left(\frac{V_{ni}/V_{nd}}{\Theta_v}\right)^{b_v-1}\right]\exp\left[-\left(\frac{V_{ni}/V_{nd}}{\Theta_v}\right)^{b_v}\right] \tag{16.191}$$

where indices $i$ and $d$ refer to the $i^{\text{th}}$ splashed droplet and the impinging droplet, respectively. The terms $b_v$ and $\Theta_v$ are functions of $\Theta_I$, the impingement angle measured from the surface normal:

$$b_v=\begin{cases}2.1, & \Theta_I\le 50^\circ\\ 1.10+0.02\Theta_I, & \Theta_I>50^\circ\end{cases}$$

$$\Theta_v=0.158e^{0.017\Theta_I}$$

The tangential component of the velocity is obtained from the expression for the reflection angle $\Theta_s$:

$$\Theta_s=65.4+0.226\Theta_l \tag{16.192}$$

combined with

$$V_{ti}=\frac{V_{ni}}{\tan(\Theta_s)} \tag{16.193}$$

Note that units of angles $\Theta_V$, $\Theta_I$, and $\Theta_s$ are in degrees.

Finally, an energy balance is performed for the new parcels so that the sum of the kinetic and surface energies of the new drops does not exceed that of the old drops. The energy balance is given by

$$\frac{1}{2}\sum_{i=1}^{N_{parcel}}\left(m_i V_i^2\right)+\pi\sigma\sum_{i=1}^{N_{parcel}}\left(N_i d_i^2\right)=\frac{1}{2}m_d V_d^2 m_i V_i^2+\pi\sigma\left(N_d d^2\right)-E_{crit} \tag{16.194}$$

where $E_{crit}$ is the threshold energy for splashing to occur. To ensure conservation of energy, the following correction factor is computed:


Release 15.0 - © SAS IP, Inc. All rights reserved. - Contains proprietary and confidential information of ANSYS, Inc. and its subsidiaries and affiliates.

$$K = \frac{\frac{1}{2} m_d V_d^2 m_i V_i^2 + \pi\sigma\left(N_d d^2\right) - E_{crit} - \pi\sigma \sum_{i=1}^{N_{parcel}} \left(N_i d_i^2\right)}{\frac{1}{2} \sum_{i=1}^{N_{parcel}} \left(m_i V_i^2\right)} \tag{16.195}$$

This correction factor is needed due to the relatively small number of sampled points for the velocity of the splashed drops (see Stanton [434] (p. 752) for more detail). The components of the splashed parcel are multiplied by the square root of $K$ in Equation 16.195 (p. 419) so that energy will be conserved. The normal and tangential velocity components of the splashed parcels are therefore given by

$$V_{ni}' = \sqrt{K} V_{ni} \quad \text{and} \quad V_{ti}' = \sqrt{K} V_{ti}$$

ANSYS Fluent will limit the velocity of the splashed parcels so that they do not exceed the impact velocity of the original parcel. It is important to note that splashing events are inherently transient, so the splashing submodel is only available with unsteady tracking in ANSYS Fluent. Splashing can also cause large increases in source terms in the cells in which it occurs, which can cause difficulty in convergence between time steps. Thus, it may be necessary to use a smaller time step during the simulation when splashing is enabled.

## 16.7.4. Separation Criteria

The film can separate from the wall when the stress at an edge of the film exceeds the adhesion forces holding the film to the wall. These forces are complex and highly dependent on local surface conditions. An order of magnitude analysis of a film rounding a sharp corner shows that the stresses at the edge of a film are proportional to the angle that the film negotiates. In ANSYS Fluent, you can specify the maximum angle that the film can negotiate using a special text command. For more information, contact your ANSYS Fluent support engineer.

## 16.7.5. Conservation Equations for Wall-Film Particles

Conservation equations for momentum, mass, and energy for individual parcels in the wall-film are described below. The particle-based approach for thin films was first formulated by O'Rourke [331] (p. 747) and most of the following derivation is based closely on that work.

### 16.7.5.1. Momentum

The equation for the momentum of a parcel on the film is

$$\begin{aligned} \rho h \frac{d\vec{u}_p}{dt} + h\left(\nabla_s p_f\right)_\alpha &= \tau_g \vec{t}_g + \tau_w \vec{t}_w + \dot{\vec{P}}_{imp,\alpha} \\ &\quad - \dot{M}_{imp,\alpha} \vec{u}_p + \dot{\vec{F}}_{n,\alpha} + \rho h\left(\vec{g} - \vec{a}_w\right) \end{aligned} \tag{16.196}$$

where $\alpha$ denotes the current face on which the particle resides, $h$ denotes the current film height at the particle location, $\nabla_s$ is the gradient operator restricted to the surface, and $p_f$ is the pressure on the surface of the film. On the right-hand side of Equation 16.196 (p. 419), $\tau_g$ denotes the magnitude of the shear stress of the gas flow on the surface of the film, $\vec{t}_g$ is the unit vector in the direction of the relative motion of the gas and the film surface, $\mu_l$ is the liquid viscosity, and $\tau_w$ is the magnitude of

the stress that the wall exerts on the film. Similarly to the expression for $\vec{t_g}$, $\vec{t_w}$ is the unit vector in the direction of the relative motion of the film and the wall. The remaining expressions on the right-hand side of Equation 16.196 (p. 419) are $\dot{\vec{P}}_{imp,\alpha}$ which denotes the impingement pressure on the film surface, $\dot{M}_{imp,\alpha}$ is the impingement mass source, and $\dot{\vec{F}}_{n,\alpha}$ is the force necessary to keep the film on the surface, as determined by

$$\vec{u}_p \cdot \hat{n}_\alpha = 0 . \tag{16.197}$$

Here, $\rho h ( \vec{g} - \vec{a}_w )$ is the body force term. Note that the body force term can be very significant, despite the small values of film thickness due to the very high acceleration rates seen in simulations with moving boundaries. The requirement represented by Equation 16.197 (p. 420) is explicitly enforced at each time step in ANSYS Fluent for all particles representing the wall-film.

The term $h\left( \nabla_s p_f \right)_\alpha$ is the surface gradient of the pressure on the face, $p_f$. This pressure, $p_f$, is the sum of the fluid pressure and the impingement pressure from the drops on the face, given by

$$p_f = P_{cell} - \dot{\vec{P}}_{imp,\alpha} \cdot \hat{n} + \dot{M}_{imp,\alpha} \vec{u}_p \cdot \hat{n}$$

where the impingement mass $\dot{M}_{imp,\alpha}$ is given by

$$\dot{M}_{imp,\alpha} = \int \int \int \rho V_p \vec{v} \cdot \hat{n} f ( \vec{x}_s, \vec{v}, r, T_d, t ) \, dr d\vec{v} \, dT_d \tag{16.198}$$

and the impingement pressure is given by

$$\dot{\vec{P}}_{imp,\alpha} = \int \int \int \rho V_p \vec{v} \, \vec{v} \cdot \hat{n} f ( \vec{x}_s, \vec{v}, r, T_d, t ) \, dr d\vec{v} \, dT_d \tag{16.199}$$

where $V_p$ is the volume of the parcel, and f() is the distribution function of impinging droplets with respect to size, velocity, and droplet temperature $T_{\mathrm{dp}}$. An approximation of the impingement mass in Equation 16.198 (p. 420) is given by

$$\dot{M}_{imp,\alpha} = \left( \sum_{n=0}^{N_s} \rho V_p \right) \Big/ \, A_\alpha \Delta t , \tag{16.200}$$

and the corresponding expression of the impingement pressure in Equation 16.199 (p. 420) is given by

$$\dot{\vec{P}}_{imp,\alpha} = \left( \sum_{n=0}^{N_i} \rho V_p \left( \vec{u}_p^{\,n+1} - \vec{u}_p^{\,n} \right) \right) \Big/ \, A_\alpha \Delta t . \tag{16.201}$$

The summation in Equation 16.201 (p. 420) is over *all* the particles that impinge upon the face during the same interval ($N_i$).

The expression for the stress that the gas exerts on the surface of the wall-film, $\vec{\tau}_g$, in Equation 16.196 (p. 419) is given by


Release 15.0 - © SAS IP, Inc. All rights reserved. - Contains proprietary and confidential information of ANSYS, Inc. and its subsidiaries and affiliates.

$$\vec{\tau}_g = C_f \left| \vec{u}_g - 2\vec{u}_p \right| \left( \vec{u}_g - 2\vec{u}_p \right) = C_f \left| \vec{V}_{rel_g} \right| \vec{V}_{rel_g}$$

where $C_f$ is the skin friction coefficient and $\vec{u}_g$ is the gas velocity evaluated at the film height above the wall. The assumption made in evaluating the skin friction coefficient is that the wall shear stress from the gas is constant over the thickness of the film and the boundary layer above the film (in the normal direction from the face).

where $\hat{n}$ is the normal face. The expression for the stress that the wall exerts on the film, $\vec{\tau}_w$, in Equation 16.196 (p. 419) is given by

$$\vec{\tau}_w = -\frac{\mu_l}{h}\left(2\vec{u}_p - \vec{u}_w\right) = -\frac{\mu_l}{h}\left(\vec{V}_{rel_w}\right)$$

where $\mu_l$ is the liquid viscosity and $\vec{u}_w$ is the velocity of the wall.

Since ANSYS Fluent solves a particle position equation of the form

$$\frac{d\vec{u}_p}{dt} = \alpha - \beta \vec{u}_p,$$

Equation 16.196 (p. 419) must be rearranged. The film particle acceleration is then given by

$$\begin{aligned} \frac{d\vec{u}_p}{dt} = & \left( \frac{C_f \left| V_{rel_g} \right|}{\rho h} \vec{u}_g - \frac{\left(\nabla_s p_f\right)_\alpha}{\rho} + \frac{\mu_l \left| \vec{u_w} \right|}{\rho h^2} \vec{u}_w + \frac{\dot{\vec{P}}_{imp}}{\rho h} + \vec{g} \right) \\ & - \left( \frac{2C_f \left| V_{rel_g} \right|}{\rho h} + \frac{2\mu_l}{\rho h^2} + \frac{\dot{M}_{imp}}{\rho h} \right) \vec{u}_p \end{aligned} \tag{16.202}$$

The terms for $\dot{M}_{imp}$ and $\dot{\vec{P}}_{imp}$ are used from the previous time step and the differential equations for the particle motion are solved with the existing integration routines.

### 16.7.5.2. Mass Transfer from the Film

The film vaporization law is applied when the film particle is above the vaporization temperature $T_{vap}$. A wall particle has the temperature limited by the boiling temperature $T_{bp}$ and does not have a specific boiling law associated with the physics of film boiling.

The vaporization rate of the film is governed by gradient diffusion from the surface exposed to the gas phase. The gradient of vapor concentration between the film surface and the gas phase is

$$\dot{N}_i = B_f \left( C_{i,s} - C_{i,\infty} \right) \tag{16.203}$$

where $\dot{N}_i$ is the molar flux of vapor (with units of kmol/$\mathrm{m}^2$-s), $B_f$ is the mass transfer coefficient (in m/s), and $C_{i,s}$ and $C_{i,\infty}$ are the vapor concentrations on the film surface and in the bulk gas, respectively. The units of vapor concentration are kmol/$\mathrm{m}^3$.

The vapor concentration at the surface is evaluated using the saturated vapor pressure at the film surface temperature and the bulk gas concentration is obtained from the flow field solution. The vaporization rate is sensitive to the saturated vapor pressure, similar to droplet vaporization.

The mass transfer coefficient is obtained using a Nusselt correlation for the heat transfer coefficient and replacing the Prandtl number with the Schmidt number. The equation is

$$Nu_x = \frac{B_f x}{k_f} = \begin{cases} 0.332 Re_x^{1/2} Sc^{1/3} & Re_x < 2500, 0.6 < Sc < 50 \\ 0.0296 Re_x^{4/5} Sc^{1/3} & Re_x > 2500, 0.6 < Sc < 60 \end{cases} \tag{16.204}$$

where the Reynolds number is based on a representative length derived from the face area. The temperature for the film surface is equal to the gas temperature, but is limited by the boiling temperature of the liquid. The particle properties are evaluated at the surface temperature when used in the correlation defined by Equation 16.204 (p. 422).

For multicomponent vaporization, the Schmidt number based on the diffusivity of each species is used to calculate the correlation in Equation 16.204 (p. 422) for each component.

The mass of the particle is decreased by

$$m_p(t+\Delta t) = m_p(t) - N_i A_p M_{w,i} \Delta t \tag{16.205}$$

where $M_{w,i}$ is the molecular weight of the gas phase species to which the vapor from the liquid is added. The diameter of the film particle is decreased to account for the mass loss in the individual parcel. This keeps the number of drops in the parcel constant and acts only as a place holder. When the parcel detaches from the boundary, the diameter is set to the height of the film and the number in the parcel is adjusted so that the overall mass of the parcel is conserved.

### 16.7.5.3. Energy Transfer from the Film

To obtain an equation for the temperature in the film, energy flux from the gas side as well as energy flux from the wall side must be considered. The assumed temperature profile in the liquid is bilinear, with the surface temperature $T_s$ being the maximum temperature of the gas at the film height. Furthermore, the boiling point of the liquid and the wall temperature will be the maximum of the wall face temperature $T_w$, and will be the same boiling temperature as the liquid. An energy balance on a film particle yields

$$\frac{d}{dt}\left\{m_p C_p T_p\right\} = Q_{cond} + Q_{conv} \tag{16.206}$$

where $Q_{cond}$ is the conduction from the wall, given by

$$Q_{cond} = \frac{\kappa A_p}{h}\left(T_w - T_p\right)$$

where $\kappa$ is the thermal conductivity of the liquid and $h$ is the film height at the location of the particle, as seen in Figure 16.5: Assumption of a Bilinear Temperature Profile in the Film (p. 423). The convection from the top surface, $Q_{conv}$ is given by

$$Q_{conv} = h_f A_p\left(T_g - T_p\right)$$


Release 15.0 - © SAS IP, Inc. All rights reserved. - Contains proprietary and confidential information of ANSYS, Inc. and its subsidiaries and affiliates.

where $h_f$ is the film heat transfer coefficient given by Equation 16.204 (p. 422) and $A_p$ is the area represented by a film particle, taken to be a mass weighted percentage of the face area, $A_f$. Contributions from the impingement terms are neglected in this formulation, as well as contributions from the gradients of the mean temperature on the edges of the film.

**Figure 16.5: Assumption of a Bilinear Temperature Profile in the Film**

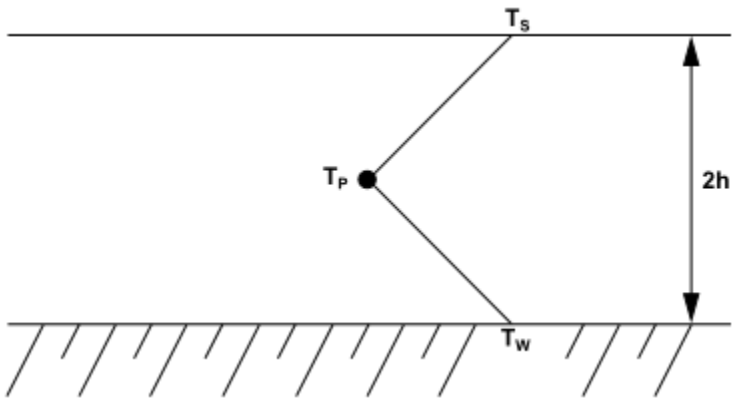


Assuming that the temperature changes slowly for each particle in the film, the equation for the change in temperature of a non vaporizing particle can be written as

$$m_p C_p \frac{dT_p}{dt} = A_p \left( -\left[ h_f + \frac{\kappa}{h} \right] T_p + h T_g + \frac{\kappa}{h} T_w \right) \tag{16.207}$$

As the particle trajectory is computed, ANSYS Fluent integrates Equation 16.207 (p. 423) to obtain the particle temperature at the next time value, yielding

$$T_p(t+\Delta t) = \alpha_p + \left[ T_p(t) - \alpha_p \right] e^{-\beta_p \Delta t} \tag{16.208}$$

where $\Delta t$ is the integration time step and $\alpha_p$ and $\beta_p$ are given by

$$\alpha_p = \frac{h_f T_g + \frac{\kappa}{h} T_w}{h_f + \frac{\kappa}{h}} \tag{16.209}$$

and

$$\beta_p = \frac{A_p \left( h_f + \frac{\kappa}{h} \right)}{m_p C_p} \tag{16.210}$$

When the particle changes its mass during vaporization, an additional term is added to Equation 16.207 (p. 423) to account for the enthalpy of vaporization, which is given by

$$m_p C_p \frac{dT_p}{dt} = A_p \left( -\left[ h_f + \frac{\kappa}{h} \right] T_p + h T_g + \frac{\kappa}{h} T_w \right) + \dot{m}_p h_{fg} \tag{16.211}$$

where $h_{fg}$ is the latent heat of vaporization (with units of J/kg) and the expression $\dot{m}_p$ is the rate of evaporation in kg/s. This alters the expression for $\alpha_p$ in Equation 16.209 (p. 423) so that

Release 15.0 - © SAS IP, Inc. All rights reserved. - Contains proprietary and confidential information of ANSYS, Inc. and its subsidiaries and affiliates.

$$\alpha_p = \frac{h_f T_g + \frac{\kappa}{h} T_w + \dot{m}_p h_{fg} / A_p}{h_f + \frac{\kappa}{h}} \tag{16.212}$$

When the wall-film model is active, the heat flux from the wall to the liquid film is subtracted from the heat flux from the wall to the gas phase. Additionally, enthalpy from vaporization of the liquid from the wall is subtracted from the cell to which the vapor mass goes. Since film boiling is modeled by limiting the liquid phase temperature to the boiling point of the material, energy in excess of that absorbed by the liquid will be put into the gas phase. When the thermal boundary conditions on the wall are set to a constant heat flux, the local temperature of the wall face is used as the thermal boundary condition for the wall-film particles.

**Important**

The wall-film model has been specifically implemented for in-cylinder flows and should be used with caution for other applications.

## 16.8. Particle Erosion and Accretion Theory

Particle erosion and accretion rates can be monitored at wall boundaries. The erosion rate is defined as

$$R_{erosion} = \sum_{p=1}^{N_{particles}} \frac{\dot{m}_p C\left(d_p\right) f\left(\alpha\right) v^{b(v)}}{A_{face}} \tag{16.213}$$

where $C\left(d_p\right)$ is a function of particle diameter, $\alpha$ is the impact angle of the particle path with the wall face, $f\left(\alpha\right)$ is a function of impact angle, $v$ is the relative particle velocity, $b\left(v\right)$ is a function of relative particle velocity, and $A_{face}$ is the area of the cell face at the wall. Default values are $C = 1.8 \times 10^{-9}$, $f = 1$, and $b = 0$. Note that $C$, $f$, and $b$ are defined as boundary conditions at a wall, rather than properties of a material, so the default values are not updated to reflect the actual materials being used. Therefore, you should specify values appropriate to your problem at all walls as described in Setting Particle Erosion and Accretion Parameters in the *Fluent User's Guide*. Values of these functions for sand eroding both carbon steel and aluminum are given by Edwards et al. [106] (p. 734).

Functions for $C$, $f$, and $b$ must be expressed as piecewise-linear, piecewise-polynomial or polynomial functions in order to define them as part of the wall boundary conditions. Therefore, it may be necessary to approximate functions found in the literature by one of these methods.

The erosion rate as calculated above is displayed in units of removed material/(area-time), that is, mass flux, and can therefore be changed accordingly to the defined units in ANSYS Fluent. The functions $C$ and $f$ have to be specified in consistent units to build a dimensionless group with the relative particle velocity and its exponent. To compute an erosion rate in terms of length/time (mm/year, for example) you can either define a custom field function to divide the erosion rate by the density of the wall material or include this division in the units for $C$ and/or $f$. Note that the units given by ANSYS Fluent when displaying the erosion rate are no longer valid in the latter case.

A variety of erosion models [120] (p. 735), [286] (p. 744), [105] (p. 734), [321] (p. 746), [158] (p. 737), [385] (p. 750) containing model constants [158] (p. 737), [105] (p. 734) and angle functions can be easily


Release 15.0 - © SAS IP, Inc. All rights reserved. - Contains proprietary and confidential information of ANSYS, Inc. and its subsidiaries and affiliates.

implemented into ANSYS Fluent. The equations describing some of the erosion models can be modified to appear in the form of the general equation describing the erosion rate, Equation 16.213 (p. 424).

For example, the Tulsa Angle Dependent Model [105] (p. 734) described by Equation 16.214 (p. 425)

$$ER = 1.559e^{-6}B^{-0.59}F_s v^{1.73} f(\alpha) \tag{16.214}$$

can be rewritten in the form of Equation 16.213 (p. 424) with the following substitutions:

$$v^{1.73} = v^{b(v)}$$

$$1.559e^{-6}B^{-0.59}F_s = C(d_p)$$

where $ER$ is the erosion ratio (mass of surface eroded per mass of particles impinging), $B$ is the Brinell hardness, and $F_s$ is a particle shape coefficient. The Tulsa model [105] (p. 734) suggests values for $F_s$ of 1.0 for sharp/angular sand, 0.53 for semi-rounded sand, and 0.2 for fully rounded sand. As noted above, the impact angle function can be approximated by a piecewise-polynomial fit. The following is an approximation of the impact angle function for steel being eroded by sand.

$$f(\alpha) = \begin{cases} 0 + 22.7\alpha - 38.4\alpha^2 & \alpha \le 0.267\text{rad} \\ 2.00 + 6.80\alpha - 7.50\alpha^2 + 2.25\alpha^3 & \alpha > 0.267\text{rad} \end{cases}$$

User-defined functions can be used to describe erosion models of any form. For more complex models, such as those in which $f$ cannot be approximated by linear or polynomial functions of $\alpha$ only, the default **Erosion Model** in the **Wall** boundary condition dialog box cannot be used. Hence, a user-defined function should be used instead. For information on how to apply user-defined functions for DPM erosion models, see `DEFINE_DPM_EROSION` in the UDF Manual, or contact your support engineer for further assistance.

Note that the particle erosion and accretion rates can be displayed only when coupled calculations are enabled.

The accretion rate is defined as

$$R_{accretion} = \sum_{p=1}^{N_{particles}} \frac{\dot{m}_p}{A_{face}} \tag{16.215}$$

## 16.9. Atomizer Model Theory

In addition to the simple injection types described in Injection Types in the User's Guide, ANSYS Fluent also provides more complex injection types for sprays describing primary breakup phenomena. For most types of injections, you will need to provide the initial diameter, position, and velocity of the particles. For sprays, however, there are models available to predict the droplet size and velocity distributions.

All of the atomization models use physical atomizer parameters, such as orifice diameter and mass flow rate, to calculate initial droplet size, velocity, and position.

For realistic atomizer simulations, the droplets must be randomly distributed, both spatially through a dispersion angle and in their time of release. For other types of injections in ANSYS Fluent (nonatomizer), all of the droplets are released along fixed trajectories at the beginning of the time step. The atomizer

Release 15.0 - © SAS IP, Inc. All rights reserved. - Contains proprietary and confidential information of ANSYS, Inc. and its subsidiaries and affiliates.

models use stochastic trajectory selection and staggering to attain a random distribution. Further information on staggering can be found in section Staggering of Particles in Space and Time in the User's Guide.

Stochastic trajectory selection is the random dispersion of initial droplet directions. All of the atomizer models provide an initial dispersion angle, and the stochastic trajectory selection picks an initial direction within this angle. This approach improves the accuracy of the results for spray-dominated flows. The droplets will be more evenly spread among the computational cells near the atomizer, which improves the coupling to the gas phase by spreading drag more smoothly over the cells near the injection. Source terms in the energy and species conservation equations are also more evenly distributed among neighboring cells, improving solution convergence.

Five atomizer models are available in ANSYS Fluent to predict the spray characteristics from knowledge of global parameters such as nozzle type and liquid flow rate. You can choose them as injection types and define the associated parameters in the **Set Injection Properties** dialog box, as described in Injection Types in the User's Guide. Details about the atomizer models are provided below.

Information is organized into the following subsections:

16.9.1. The Plain-Orifice Atomizer Model
16.9.2. The Pressure-Swirl Atomizer Model
16.9.3. The Air-Blast/Air-Assist Atomizer Model
16.9.4. The Flat-Fan Atomizer Model
16.9.5. The Effervescent Atomizer Model

## 16.9.1. The Plain-Orifice Atomizer Model

The plain-orifice is the most common type of atomizer and the most simply made. However there is nothing simple about the physics of the internal nozzle flow and the external atomization. In the plain-orifice atomizer model in ANSYS Fluent, the liquid is accelerated through a nozzle, forms a liquid jet and then breaks up to form droplets. This apparently simple process is dauntingly complex. The plain orifice may operate in three different regimes: single-phase, cavitating and flipped [424] (p. 752). The transition between regimes is abrupt, producing dramatically different sprays. The internal regime determines the velocity at the orifice exit, as well as the initial droplet size and the angle of droplet dispersion. Diagrams of each case are shown in Figure 16.6: Single-Phase Nozzle Flow (Liquid Completely Fills the Orifice) (p. 427), Figure 16.7: Cavitating Nozzle Flow (Vapor Pockets Form Just After the Inlet Corners) (p. 427), and Figure 16.8: Flipped Nozzle Flow (Downstream Gas Surrounds the Liquid Jet Inside the Nozzle) (p. 427).


Release 15.0 - © SAS IP, Inc. All rights reserved. - Contains proprietary and confidential information of ANSYS, Inc. and its subsidiaries and affiliates.

**Figure 16.6: Single-Phase Nozzle Flow (Liquid Completely Fills the Orifice)**

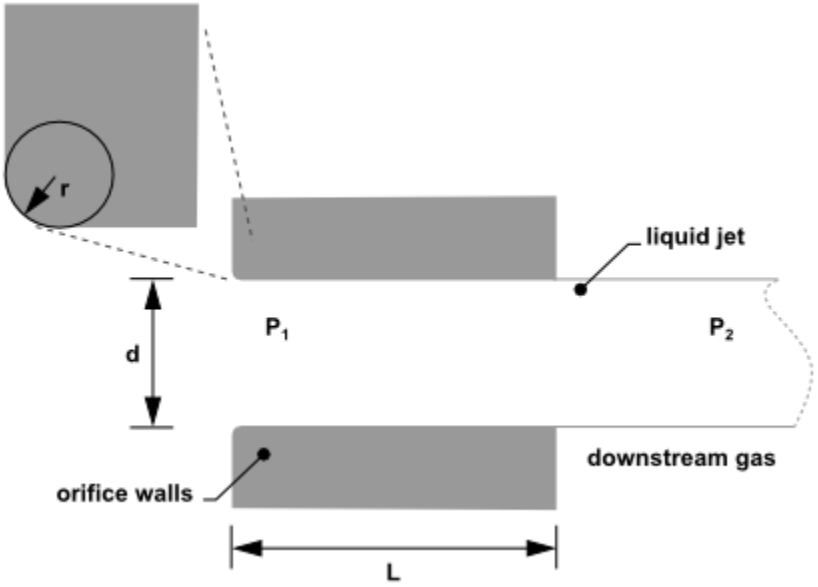


**Figure 16.7: Cavitating Nozzle Flow (Vapor Pockets Form Just After the Inlet Corners)**

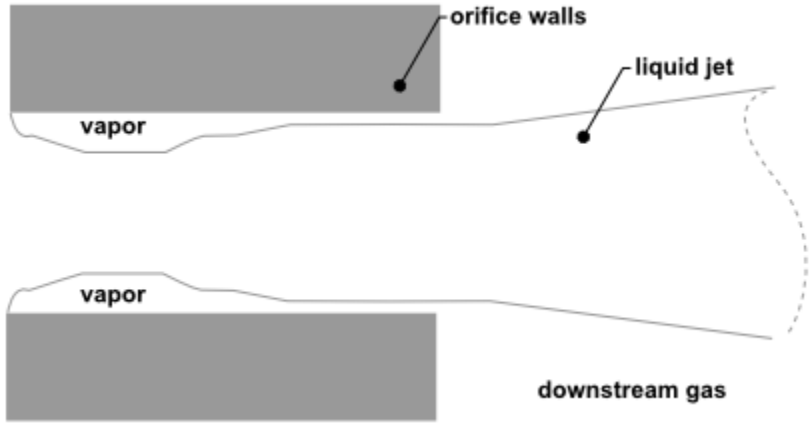


**Figure 16.8: Flipped Nozzle Flow (Downstream Gas Surrounds the Liquid Jet Inside the Nozzle)**

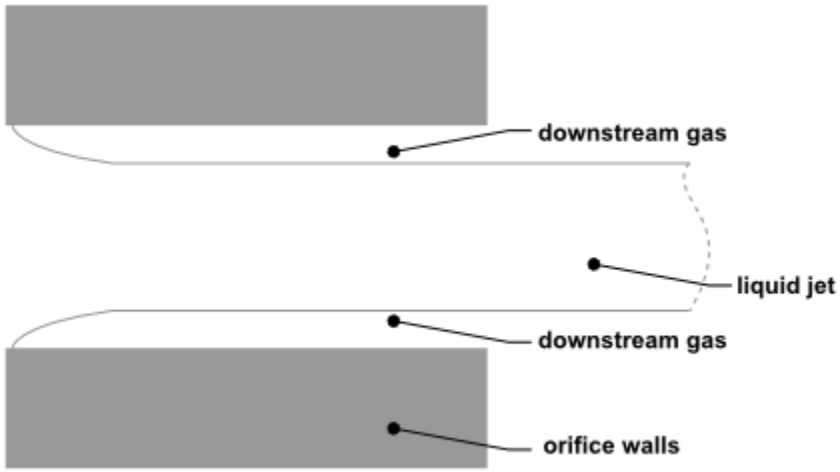


Release 15.0 - © SAS IP, Inc. All rights reserved. - Contains proprietary and confidential information
of ANSYS, Inc. and its subsidiaries and affiliates.

### 16.9.1.1. Internal Nozzle State

To accurately predict the spray characteristics, the plain-orifice model in ANSYS Fluent must identify the correct state of the internal nozzle flow because the nozzle state has a tremendous effect on the external spray. Unfortunately, there is no established theory for determining the nozzle state. One must rely on empirical models obtained from experimental data. ANSYS Fluent uses several dimensionless parameters to determine the internal flow regime for the plain-orifice atomizer model. These parameters and the decision-making process are summarized below.

A list of the parameters that control internal nozzle flow is given in Table 16.2: List of Governing Parameters for Internal Nozzle Flow (p. 428). These parameters may be combined to form nondimensional characteristic lengths such as *r/d* and *L/d*, as well as nondimensional groups like the Reynolds number based on hydraulic "head" ($\mathrm{Re}_h$) and the cavitation parameter (K).

**Table 16.2: List of Governing Parameters for Internal Nozzle Flow**

| | |
|---|---|
| nozzle diameter | $d$ |
| nozzle length | $L$ |
| radius of curvature of the inlet corner | $r$ |
| upstream pressure | $p_1$ |
| downstream pressure | $p_2$ |
| viscosity | $\mu$ |
| liquid density | $\rho_l$ |
| vapor pressure | $p_v$ |

$$Re_h = \frac{d\rho_l}{\mu}\sqrt{\frac{2\left(p_1 - p_2\right)}{\rho_l}} \tag{16.216}$$

$$K = \frac{p_1 - p_v}{p_1 - p_2} \tag{16.217}$$

The liquid flow often contracts in the nozzle, as can be seen in Figure 16.7: Cavitating Nozzle Flow (Vapor Pockets Form Just After the Inlet Corners) (p. 427) and Figure 16.8: Flipped Nozzle Flow (Downstream Gas Surrounds the Liquid Jet Inside the Nozzle) (p. 427). Nurick [324] (p. 747) found it helpful to use a coefficient of contraction ($C_c$) to represent the reduction in the cross-sectional area of the liquid jet. The coefficient of contraction is defined as the area of the stream of contracting liquid over the total cross-sectional area of the nozzle. ANSYS Fluent uses Nurick's fit for the coefficient of contraction:

$$C_c = \frac{1}{\sqrt{\frac{1}{C_{ct}^2} - \frac{11.4r}{d}}} \tag{16.218}$$

Here, $C_{ct}$ is a theoretical constant equal to 0.611, which comes from potential flow analysis of flipped nozzles.


Release 15.0 - © SAS IP, Inc. All rights reserved. - Contains proprietary and confidential information of ANSYS, Inc. and its subsidiaries and affiliates.

### 16.9.1.2. Coefficient of Discharge

Another important parameter for describing the performance of nozzles is the coefficient of discharge ($C_d$). The coefficient of discharge is the ratio of the mass flow rate through the nozzle to the theoretical maximum mass flow rate:

$$C_d = \frac{\dot{m}_{eff}}{A\sqrt{2\rho_l\left(p_1 - p_2\right)}} \tag{16.219}$$

where $\dot{m}_{eff}$ is the *effective* mass flow rate of the nozzle, defined by

$$\dot{m}_{eff} = \frac{2\pi\dot{m}}{\Delta\phi} \tag{16.220}$$

Here, $\dot{m}$ is the mass flow rate specified in the user interface, and $\Delta\phi$ is the difference between the azimuthal stop angle and the azimuthal start angle

$$\Delta\phi = \phi_{stop} - \phi_{start} \tag{16.221}$$

as input by you (see Point Properties for Plain-Orifice Atomizer Injections in the User's Guide). Note that the mass flow rate that you input should be for the appropriate start and stop angles, in other words the correct mass flow rate for the sector being modeled. Note also that for $\Delta\phi$ of $2\pi$, the effective mass flow rate is identical to the mass flow rate in the interface.

The cavitation number ($K$ in Equation 16.217 (p. 428)) is an essential parameter for predicting the inception of cavitation. The inception of cavitation is known to occur at a value of $K_{incep} \approx$ 1.9 for short, sharp-edged nozzles. However, to include the effects of inlet rounding and viscosity, an empirical relationship is used:

$$K_{incep} = 1.9\left(1 - \frac{r}{d}\right)^2 - \frac{1000}{Re_h} \tag{16.222}$$

Similarly, a critical value of $K$ where flip occurs is given by

$$K_{crit} = 1 + \frac{1}{\left(1 + \frac{L}{4d}\right)\left(1 + \frac{2000}{Re_h}\right)e^{70r/d}} \tag{16.223}$$

If $r/d$ is greater than 0.05, then flip is deemed impossible and $K_{crit}$ is set to 1.0.

The cavitation number, $K$, is compared to the values of $K_{incep}$ and $K_{crit}$ to identify the nozzle state. The decision tree is shown in Figure 16.9: Decision Tree for the State of the Cavitating Nozzle (p. 430). Depending on the state of the nozzle, a unique closure is chosen for the above equations.

For a single-phase nozzle ($K > K_{incep}, K \geq K_{crit}$) [249] (p. 742), the coefficient of discharge is given by

$$C_d = \frac{1}{\frac{1}{C_{du}} + 20\frac{(1 + 2.25L/d)}{Re_h}} \tag{16.224}$$

where $C_{du}$ is the ultimate discharge coefficient, and is defined as

Release 15.0 - © SAS IP, Inc. All rights reserved. - Contains proprietary and confidential information of ANSYS, Inc. and its subsidiaries and affiliates.

$$C_{du} = 0.827 - 0.0085\frac{L}{d} \tag{16.225}$$

For a cavitating nozzle ($K_{crit} \le K \le K_{incep}$) [324] (p. 747) the coefficient of discharge is determined from

$$C_d = C_c\sqrt{K} \tag{16.226}$$

For a flipped nozzle ($K < K_{crit}$) [324] (p. 747),

$$C_d = C_{ct} = 0.611 \tag{16.227}$$

**Figure 16.9: Decision Tree for the State of the Cavitating Nozzle**

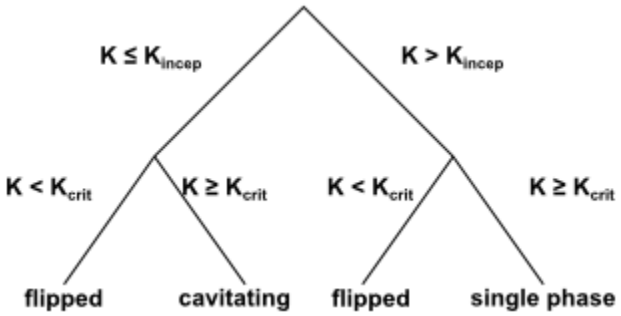


All of the nozzle flow equations are solved iteratively, along with the appropriate relationship for coefficient of discharge as given by the nozzle state. The nozzle state may change as the upstream or downstream pressures change. Once the nozzle state is determined, the exit velocity is calculated, and appropriate correlations for spray angle and initial droplet size distribution are determined.

### 16.9.1.3. Exit Velocity

For a single-phase nozzle, the estimate of exit velocity ($u$) comes from the conservation of mass and the assumption of a uniform exit velocity:

$$u = \frac{\dot{m}_{eff}}{\rho_l A} \tag{16.228}$$

For the cavitating nozzle, Schmidt and Corradini [395] (p. 750) have shown that the uniform exit velocity is not accurate. Instead, they derived an expression for a higher velocity over a reduced area:

$$u = \frac{2C_c p_1 - p_2 + (1 - 2C_c)p_v}{C_c\sqrt{2\rho_l\left(p_1 - p_v\right)}} \tag{16.229}$$

This analytical relation is used for cavitating nozzles in ANSYS Fluent. For the case of flipped nozzles, the exit velocity is found from the conservation of mass and the value of the reduced flow area:

$$u = \frac{\dot{m}_{eff}}{\rho_l C_{ct} A} \tag{16.230}$$

### 16.9.1.4. Spray Angle

The correlation for the spray angle ($\theta$) comes from the work of Ranz [365] (p. 749):


Release 15.0 - © SAS IP, Inc. All rights reserved. - Contains proprietary and confidential information of ANSYS, Inc. and its subsidiaries and affiliates.

$$\frac{\theta}{2}=\begin{cases}\tan^{-1}\left[\frac{4\pi}{C_A}\sqrt{\frac{\rho_g}{\rho_l}}\frac{\sqrt{3}}{6}\right] & single phase, cavitating \\ 0.01 & flipped\end{cases} \tag{16.231}$$

The spray angle for both single-phase and cavitating nozzles depends on the ratio of the gas and liquid densities and also the parameter $C_A$. For flipped nozzles, the spray angle has a constant value.

The parameter $C_A$, which you must specify, is thought to be a constant for a given nozzle geometry. The larger the value, the narrower the spray. Reitz [372] (p. 749) suggests the following correlation for $C_A$:

$$C_A = 3 + \frac{L}{3.6d} \tag{16.232}$$

The spray angle is sensitive to the internal flow regime of the nozzle. Hence, you may want to choose smaller values of $C_A$ for cavitating nozzles than for single-phase nozzles. Typical values range from 4.0 to 6.0. The spray angle for flipped nozzles is a small, arbitrary value that represents the lack of any turbulence or initial disturbance from the nozzle.

### 16.9.1.5. Droplet Diameter Distribution

One of the basic characteristics of an injection is the distribution of drop size. For an atomizer, the droplet diameter distribution is closely related to the nozzle state. ANSYS Fluent's spray models use a two-parameter Rosin-Rammler distribution, characterized by the most probable droplet size and a spread parameter. The most probable droplet size, $d_0$ is obtained in ANSYS Fluent from the Sauter mean diameter, $d_{32}$ [238] (p. 742). For more information about the Rosin-Rammler size distribution, see Using the Rosin-Rammler Diameter Distribution Method in the User's Guide.

For single-phase nozzle flows, the correlation of Wu et al. [498] (p. 756) is used to calculate $d_{32}$ and relate the initial drop size to the estimated turbulence quantities of the liquid jet:

$$d_{32} = 133.0\lambda We^{-0.74}, \tag{16.233}$$

where $\lambda = d/8$, $\lambda$ is the radial integral length scale at the jet exit based upon fully-developed turbulent pipe flow, and We is the Weber number, defined as

$$We \equiv \frac{\rho_l u^2 \lambda}{\sigma}. \tag{16.234}$$

Here, $\sigma$ is the droplet surface tension. For a more detailed discussion of droplet surface tension and the Weber number, see Secondary Breakup Model Theory (p. 439). For more information about mean particle diameters, see Summary Reporting of Current Particles in the User's Guide.

For cavitating nozzles, ANSYS Fluent uses a slight modification of Equation 16.233 (p. 431). The initial jet diameter used in Wu's correlation, $d$, is calculated from the effective area of the cavitating orifice exit, and therefore represents the effective diameter of the exiting liquid jet, $d_{eff}$. For an explanation of effective area of cavitating nozzles, see Schmidt and Corradini [395] (p. 750).

The length scale for a cavitating nozzle is $\lambda = d_{eff}/8$, where

$$d_{eff}=\sqrt{\frac{4\dot{m}_{eff}}{\pi\rho_l u}}\,. \tag{16.235}$$

For the case of the flipped nozzle, the initial droplet diameter is set to the diameter of the liquid jet:

$$d_0=d\sqrt{C_{ct}} \tag{16.236}$$

where $d_0$ is defined as the most probable diameter.

The second parameter required to specify the droplet size distribution is the spread parameter, $s$. The values for the spread parameter are chosen from past modeling experience and from a review of experimental observations. Table 16.3: Values of Spread Parameter for Different Nozzle States (p. 432) lists the values of s for the three nozzle states. The larger the value of the spread parameter, the narrower the droplet size distribution.

**Table 16.3: Values of Spread Parameter for Different Nozzle States**

| State | Spread Parameter |
|---|---|
| single phase | 3.5 |
| cavitating | 1.5 |
| flipped | ∞ |

Since the correlations of Wu et al. provide the Sauter mean diameter, $d_{32}$, these are converted to the most probable diameter, $d_0$. Lefebvre [238] (p. 742) gives the most general relationship between the Sauter mean diameter and most probable diameter for a Rosin-Rammler distribution. The simplified version for $s$=3.5 is as follows:

$$d_0=1.2726d_{32}\left(1-\frac{1}{s}\right)^{1/s} \tag{16.237}$$

At this point, the droplet size, velocity, and spray angle have been determined and the initialization of the injections is complete.

## 16.9.2. The Pressure-Swirl Atomizer Model

Another important type of atomizer is the pressure-swirl atomizer, sometimes referred to by the gas-turbine community as a simplex atomizer. This type of atomizer accelerates the liquid through nozzles known as swirl ports into a central swirl chamber. The swirling liquid pushes against the walls of the swirl chamber and develops a hollow air core. It then emerges from the orifice as a thinning sheet, which is unstable, breaking up into ligaments and droplets. The pressure-swirl atomizer is very widely used for liquid-fuel combustion in gas turbines, oil furnaces, and direct-injection spark-ignited automobile engines. The transition from internal injector flow to fully-developed spray can be divided into three steps: film formation, sheet breakup, and atomization. A sketch of how this process is thought to occur is shown in Figure 16.10: Theoretical Progression from the Internal Atomizer Flow to the External Spray (p. 433).


Release 15.0 - © SAS IP, Inc. All rights reserved. - Contains proprietary and confidential information of ANSYS, Inc. and its subsidiaries and affiliates.

**Figure 16.10: Theoretical Progression from the Internal Atomizer Flow to the External Spray**

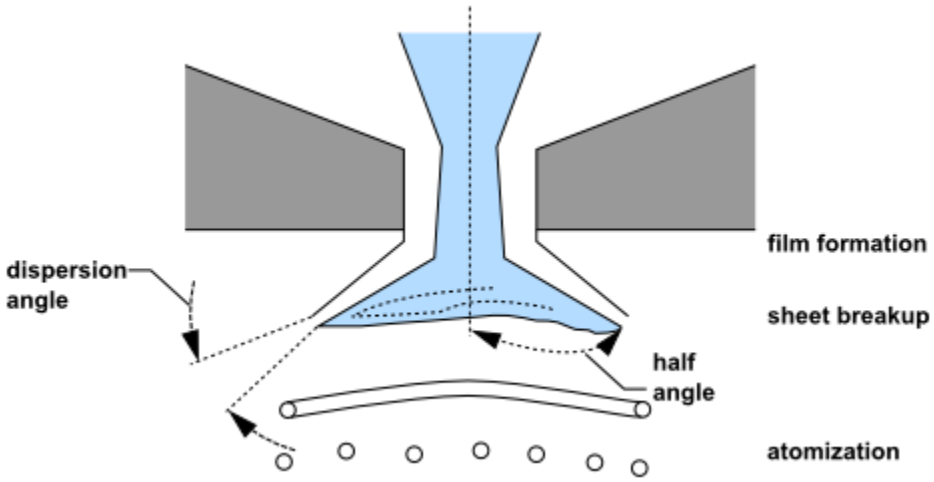


The interaction between the air and the sheet is not well understood. It is generally accepted that an aerodynamic instability causes the sheet to break up. The mathematical analysis below assumes that Kelvin-Helmholtz waves grow on the sheet and eventually break the liquid into ligaments. It is then assumed that the ligaments break up into droplets due to varicose instability. Once the liquid droplets are formed, the spray evolution is determined by drag, collision, coalescence, and secondary breakup.

The pressure-swirl atomizer model used in ANSYS Fluent is called the Linearized Instability Sheet Atomization (LISA) model of Schmidt et al. [397] (p. 750). The LISA model is divided into two stages:

1. film formation

2. sheet breakup and atomization

Both parts of the model are described below.

### 16.9.2.1. Film Formation

The centrifugal motion of the liquid within the injector creates an air core surrounded by a liquid film. The thickness of this film, $t$, is related to the mass flow rate by

$$\dot{m}_{eff} = \pi \rho u t \left( d_{inj} - t \right) \tag{16.238}$$

where $d_{inj}$ is the injector exit diameter, and $\dot{m}_{eff}$ is the effective mass flow rate, which is defined by Equation 16.220 (p. 429). The other unknown in Equation 16.238 (p. 433) is $u$, the axial component of velocity at the injector exit. This quantity depends on internal details of the injector and is difficult to calculate from first principles. Instead, the approach of Han et al. [154] (p. 737) is used. The total velocity is assumed to be related to the injector pressure by

$$U = k_v \sqrt{\frac{2 \Delta p}{\rho_l}} \tag{16.239}$$

where $k_v$ is the velocity coefficient. Lefebvre [238] (p. 742) has noted that $k_v$ is a function of the injector design and injection pressure. If the swirl ports are treated as nozzles and if it is assumed that the dominant portion of the pressure drop occurs at those ports, $k_v$ is the expression for the discharge coefficient ($C_d$). For single-phase nozzles with sharp inlet corners and $L/d$ ratios of 4, a typical $C_d$ value

Release 15.0 - © SAS IP, Inc. All rights reserved. - Contains proprietary and confidential information of ANSYS, Inc. and its subsidiaries and affiliates.

is 0.78 or less [249] (p. 742). If the nozzles are cavitating, the value of $C_d$ may be as low as 0.61. Hence, 0.78 should be a practical upper bound for $k_v$. Reducing $k_v$ by 10% to 0.7 approximates the effect of other momentum losses on the discharge coefficient.

Physical limits on $k_v$ require that it be less than unity from conservation of energy, yet be large enough to permit sufficient mass flow. To guarantee that the size of the air core is non-negative, the following expression is used for $k_v$:

$$k_v = \max\left[0.7, \frac{4\dot{m}_{eff}}{d_0^2 \rho_l \cos\theta \sqrt{\frac{\rho_l}{2\Delta p}}}\right] \tag{16.240}$$

Assuming that $\Delta p$ is known, Equation 16.239 (p. 433) can be used to find $U$. Once $U$ is determined, $u$ is found from

$$u = U\cos\theta \tag{16.241}$$

where $\theta$ is the spray angle, which is assumed to be known. At this point, the thickness and axial component of the liquid film are known at the injector exit. The tangential component of velocity ($w = U\sin\theta$) is assumed to be equal to the radial velocity component of the liquid sheet downstream of the nozzle exit. The axial component of velocity is assumed to remain constant.

### 16.9.2.2. Sheet Breakup and Atomization

The pressure-swirl atomizer model includes the effects of the surrounding gas, liquid viscosity, and surface tension on the breakup of the liquid sheet. Details of the theoretical development of the model are given in Senecal et al. [399] (p. 751) and are only briefly presented here. For a more robust implementation, the gas-phase velocity is neglected in calculating the relative liquid-gas velocity and is instead set by you. This avoids having the injector parameters depend too heavily on the usually under-resolved gas-phase velocity field very near the injection location.

The model assumes that a two-dimensional, viscous, incompressible liquid sheet of thickness $2h$ moves with velocity $U$ through a quiescent, inviscid, incompressible gas medium. The liquid and gas have densities of $\rho_l$ and $\rho_g$, respectively, and the viscosity of the liquid is $\mu_l$. A coordinate system is used that moves with the sheet, and a spectrum of infinitesimal wavy disturbances of the form

$$\eta = \eta_0 e^{ikx+\omega t} \tag{16.242}$$

is imposed on the initially steady motion. The spectrum of disturbances results in fluctuating velocities and pressures for both the liquid and the gas. In Equation 16.242 (p. 434), $\eta_0$ is the initial wave amplitude, $k = 2\pi/\lambda$ is the wave number, and $\omega = \omega_r + i\omega_i$ is the complex growth rate. The most unstable disturbance has the largest value of $\omega_r$, denoted here by $\Omega$, and is assumed to be responsible for sheet breakup. Thus, it is desired to obtain a dispersion relation $\omega = \omega(k)$ from which the most unstable disturbance can be calculated as a function of wave number.

Squire [432] (p. 752), Li and Tankin [248] (p. 742), and Hagerty and Shea [149] (p. 737) have shown that two solutions, or modes, exist that satisfy the governing equations subject to the boundary conditions at the upper and lower interfaces. The first solution, called the sinuous mode, has waves at the upper and lower interfaces in phase. The second solution is called the varicose mode, which has the waves at the upper and lower interfaces $\pi$ radians out of phase. It has been shown by numerous authors (for example, Senecal et al. [399] (p. 751)) that the sinuous mode dominates the growth of varicose waves for low velocities and low gas-to-liquid density ratios. In addition, it can be shown that the sinuous and


Release 15.0 - © SAS IP, Inc. All rights reserved. - Contains proprietary and confidential information of ANSYS, Inc. and its subsidiaries and affiliates.

varicose modes become indistinguishable for high-velocity flows. As a result, the atomization model in ANSYS Fluent is based upon the growth of sinuous waves on the liquid sheet.

As derived in Senecal et al. [399] (p. 751), the dispersion relation for the sinuous mode is given by

$$\omega^2[\tanh(kh)+Q]+\left[4\nu_l k^2\tanh(kh)+2iQkU\right]+ \tag{16.243}$$

$$4\nu_l k^4\tanh(kh)-4\nu_l^2 k^3\ell\tanh(\ell h)-QU^2k^2+\frac{\sigma k^3}{\rho_l}=0 \tag{16.244}$$

where $Q=\rho_g/\rho_l$ and $\ell^2=k^2+\omega/\nu_l$.

Above a critical Weber number of $We_g$ = 27/16 (based on the liquid velocity, gas density, and sheet half-thickness), the fastest-growing waves are short. For $We_g<27/16$, the wavelengths are long compared to the sheet thickness. The speed of modern high pressure fuel injection systems is high enough to ensure that the film Weber number is well above this critical limit.

An order-of-magnitude analysis using typical values shows that the terms of second order in viscosity can be neglected in comparison to the other terms in Equation 16.244 (p. 435). Using this assumption, Equation 16.244 (p. 435) reduces to

$$\omega_r=\frac{1}{\tanh(kh)+Q}\left\{-2\nu_l k^2\tanh(kh)+\right. \tag{16.245}$$

$$\left.\sqrt{4\nu_l^2k^4\tanh^2(kh)-Q^2U^2k^2-[\tanh(kh)+Q]\left[-QU^2k^2+\frac{\sigma k^3}{\rho_l}\right]}\right\} \tag{16.246}$$

For waves that are long compared with the sheet thickness, a mechanism of sheet disintegration proposed by Dombrowski and Johns [94] (p. 734) is adopted. For long waves, ligaments are assumed to form from the sheet breakup process once the unstable waves reach a critical amplitude. If the surface disturbance has reached a value of $\eta_b$ at breakup, a breakup time, $\tau$, can be evaluated:

$$\eta_b=\eta_0 e^{\Omega\tau}\Rightarrow\frac{1}{\Omega}\ln\left(\frac{\eta_b}{\eta_0}\right) \tag{16.247}$$

where $\Omega$, the maximum growth rate, is found by numerically maximizing Equation 16.246 (p. 435) as a function of $k$. The maximum is found using a binary search that checks the sign of the derivative. The sheet breaks up and ligaments will be formed at a length given by

$$L_b=U\tau=\frac{U}{\Omega}\ln\left(\frac{\eta_b}{\eta_0}\right) \tag{16.248}$$

where the quantity $\ln\left(\eta_b/\eta_0\right)$ is an empirical *sheet* constant that you must specify. The default value of 12 was obtained theoretically by Weber [480] (p. 755) for liquid jets. Dombrowski and Hooper [93] (p. 734) showed that a value of 12 for the sheet constant agreed favorably with experimental sheet breakup lengths over a range of Weber numbers from 2 to 200.

Release 15.0 - © SAS IP, Inc. All rights reserved. - Contains proprietary and confidential information of ANSYS, Inc. and its subsidiaries and affiliates.

The diameter of the ligaments formed at the point of breakup can be obtained from a mass balance. If it is assumed that the ligaments are formed from tears in the sheet twice per wavelength, the resulting diameter is given by

$$d_L = \sqrt{\frac{8h}{K_s}} \tag{16.249}$$

where $K_s$ is the wave number corresponding to the maximum growth rate, $\Omega$. The ligament diameter depends on the sheet thickness, which is a function of the breakup length. The film thickness is calculated from the breakup length and the radial distance from the center line to the mid-line of the sheet at the atomizer exit, $r_0$:

$$h_{end} = \frac{r_0 h_0}{r_0 + L_b \sin\left(\frac{\theta}{2}\right)} \tag{16.250}$$

This mechanism is not used for waves that are short compared to the sheet thickness. For short waves, the ligament diameter is assumed to be linearly proportional to the wavelength that breaks up the sheet,

$$d_L = \frac{2\pi C_L}{K_s} \tag{16.251}$$

where $C_L$, or the ligament constant, is equal to 0.5 by default.

In either the long-wave or the short-wave case, the breakup from ligaments to droplets is assumed to behave according to Weber's [480] (p. 755) analysis for capillary instability.

$$d_0 = 1.88 d_L (1 + 3Oh)^{1/6} \tag{16.252}$$

Here, $Oh$ is the Ohnesorge number, which is a combination of the Reynolds number and the Weber number (see Jet Stability Analysis (p. 444) for more details about Oh). Once $d_0$ has been determined from Equation 16.252 (p. 436), it is assumed that this droplet diameter is the most probable droplet size of a Rosin-Rammler distribution with a spread parameter of 3.5 and a default dispersion angle of 6 $^\circ$ (which can be modified in the GUI). The choice of spread parameter and dispersion angle is based on past modeling experience [396] (p. 750). It is important to note that the spray cone angle must be specified by you when using this model.

## 16.9.3. The Air-Blast/Air-Assist Atomizer Model

In order to accelerate the breakup of liquid sheets from an atomizer, an additional air stream is often directed through the atomizer. The liquid is formed into a sheet by a nozzle, and air is then directed against the sheet to promote atomization. This technique is called air-assisted atomization or air-blast atomization, depending on the quantity of air and its velocity. The addition of the external air stream past the sheet produces smaller droplets than without the air. Though the exact mechanism for this enhanced performance is not completely understood, it is thought that the assisting air may accelerate the sheet instability. The air may also help disperse the droplets, preventing collisions between them. Air-assisted atomization is used in many of the same applications as pressure-swirl atomization, where especially fine atomization is required.

ANSYS Fluent's air-blast atomization model is a variation of the pressure-swirl model. One important difference between them is that the sheet thickness is set directly in the air-blast atomizer model. This input is necessary because of the variety of sheet formation mechanisms used in air-blast atomizers. Hence the air-blast atomizer model does not contain the sheet formation equations that were included


Release 15.0 - © SAS IP, Inc. All rights reserved. - Contains proprietary and confidential information of ANSYS, Inc. and its subsidiaries and affiliates.

in the pressure-swirl atomizer model (Equation 16.238 (p. 433) – Equation 16.241 (p. 434)). You will also specify the maximum relative velocity that is produced by the sheet and air. Though this quantity could be calculated, specifying a value relieves you from the necessity of finely resolving the atomizer internal flow. This feature is convenient for simulations in large domains, where the atomizer is very small by comparison.

An additional difference is that the air-blast atomizer model assumes that the sheet breakup is always due to short waves. This assumption is a consequence of the greater sheet thickness commonly found in air-blast atomizers. Hence the ligament diameter is assumed to be linearly proportional to the wavelength of the fastest-growing wave on the sheet, and is calculated from Equation 16.251 (p. 436).

Other inputs are similar to the pressure-swirl model – you must provide the mass flow rate and spray angle. The angle in the case of the air-blast atomizer is the initial trajectory of the film as it leaves the end of the orifice. The value of the angle is negative if the initial film trajectory is inward, towards the centerline. Specification of the inner and outer diameters of the film at the atomizer exit are also required, in addition to the dispersion angle whose default value is 6 $^{\circ}$ (which can be modified in the GUI).

Since the air-blast atomizer model does not include internal gas flows, you must create the air streams surrounding the injector as boundary conditions within the ANSYS Fluent simulation. These streams are ordinary continuous-phase flows and require no special treatment.

## 16.9.4. The Flat-Fan Atomizer Model

The flat-fan atomizer is very similar to the pressure-swirl atomizer, but it makes a flat sheet and does not use swirl. The liquid emerges from a wide, thin orifice as a flat liquid sheet that breaks up into droplets. The primary atomization process is thought to be similar to the pressure-swirl atomizer. Some researchers believe that flat-fan atomization, because of jet impingement, is very similar to the atomization of a flat sheet. The flat-fan model could serve doubly for this application.

The flat-fan atomizer is available only for 3D models. An image of the three-dimensional flat fan is shown in Figure 16.11: Flat Fan Viewed from Above and from the Side (p. 438). The model assumes that the fan originates from a virtual origin. You need to provide the location of this origin, which is the intersection of the lines that mark the sides of the fan as well as the location of the center point of the arc from which the fan originates. ANSYS Fluent will find the vector that points from the origin to the center point in order to determine the direction of the injection. You also need to provide the half-angle of the fan arc, the width of the orifice (in the normal direction) and the mass flow rate of the liquid to use the flat-fan atomizer model.

Release 15.0 - © SAS IP, Inc. All rights reserved. - Contains proprietary and confidential information of ANSYS, Inc. and its subsidiaries and affiliates.

**Figure 16.11: Flat Fan Viewed from Above and from the Side**

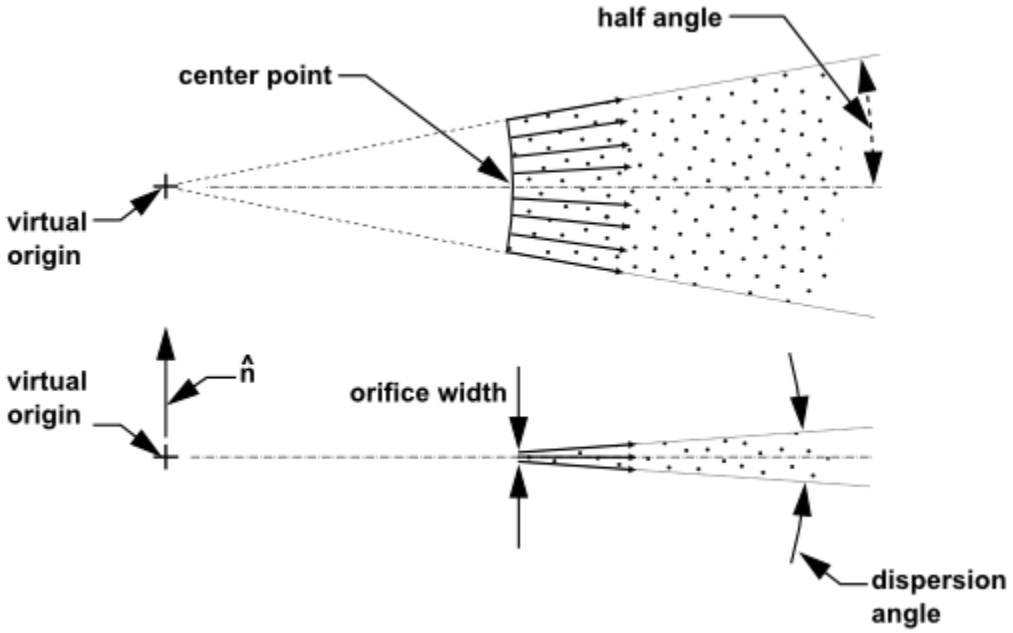


The breakup of the flat fan is calculated very much like the breakup of the sheet in the pressure-swirl atomizer. The sheet breaks up into ligaments that then form individual droplets. The only difference is that for short waves, the flat fan sheet is assumed to form ligaments at half-wavelength intervals. Hence the ligament diameter for short waves is given by

$$d_L = \sqrt{\frac{16h}{K_s}} \tag{16.253}$$

In this case, $d_L$ in Equation 16.253 (p. 438) is taken to be the most probable diameter, with a Rosin-Rammler spread parameter of 3.5 and a default dispersion angle of $6^\circ$. This angle can be set in the **Set Injection Properties** dialog box. In all other respects, the flat-fan atomizer model is like the sheet breakup portion of the pressure-swirl atomizer.

## 16.9.5. The Effervescent Atomizer Model

Effervescent atomization is the injection of liquid infused with a super-heated (with respect to down-stream conditions) liquid or propellant. As the volatile liquid exits the nozzle, it rapidly changes phase. This phase change quickly breaks up the stream into small droplets with a wide dispersion angle. The model also applies to cases where a very hot liquid is discharged.

Since the physics of effervescence is not well understood, the model must rely on rough empirical fits. The photographs of Reitz and Bracco [372] (p. 749) provide some insights. These photographs show a dense liquid core to the spray, surrounded by a wide shroud of smaller droplets.

The initial velocity of the droplets is computed from conservation of mass, assuming the exiting jet has a cross-sectional area that is $C_{ct}$ times the nozzle area, where $C_{ct}$ is a fixed constant, equal to `0.611` as specified in Equation 16.218 (p. 428) and Equation 16.227 (p. 430).

$$u = \frac{\dot{m}_{eff}}{\rho_l C_{ct} A} \tag{16.254}$$

The maximum droplet diameter is set to the effective diameter of the exiting jet:


Release 15.0 - © SAS IP, Inc. All rights reserved. - Contains proprietary and confidential information of ANSYS, Inc. and its subsidiaries and affiliates.

$$d_{max} = d\sqrt{C_{ct}} \tag{16.255}$$

The droplet size is then sampled from a Rosin-Rammler distribution with a spread parameter of 4.0. (See Using the Rosin-Rammler Diameter Distribution Method in the User's Guide for details on the Rosin-Rammler distribution.) The most probable droplet size depends on the angle, $\theta$, between the droplet's stochastic trajectory and the injection direction:

$$d_0 = d_{max} e^{-(\theta/\Theta_s)^2} \tag{16.256}$$

The dispersion angle multiplier, $\Theta_s$, is computed from the quality, $x$, and the specified value for the dispersion constant, $C_{eff}$:

$$x = \frac{\dot{m}_{\text{vapor}}}{(\dot{m}_{\text{vapor}} + \dot{m}_{\text{liquid}})} \tag{16.257}$$

$$\Theta s = \frac{x}{C_{eff}} \tag{16.258}$$

This technique creates a spray with large droplets in the central core and a shroud of smaller surrounding droplets. The droplet temperature is initialized to 0.99 times the saturation temperature, such that the temperature of the droplet is close to boiling. To complete the model, the flashing vapor must also be included in the calculation. This vapor is part of the continuous phase and not part of the discrete phase model. You must create an inlet at the point of injection when you specify boundary conditions for the continuous phase. When the effervescent atomizer model is selected, you will need to specify the nozzle diameter, mass flow rate, mixture quality, saturation temperature of the volatile substance, spray half-angle and dispersion constant in addition to specifying the position and direction of the injector.

## 16.10. Secondary Breakup Model Theory

ANSYS Fluent offers four droplet breakup models: the Taylor Analogy Breakup (TAB) model, the Wave model, the KHRT model, and the Stochastic Secondary Droplet (SSD) Model. The TAB model is recommended for low-Weber-number injections and is well suited for low-speed sprays into a standard atmosphere. For Weber numbers greater than 100, the Wave model is more applicable. The KHRT offers a transition between both application areas, because it considers the competing effects of aerodynamic breakup and instabilities due to droplet acceleration. It is combined with the Levich model for the liquid core length. The Wave and KHRT models are popular for use in high-speed fuel-injection applications. The SSD model treats breakup at high Weber numbers as a discrete random event resulting in a distribution of diameter scales over a range. The choice of model depends on the relative importance of momentum and surface tension in the droplet breakup; this is described by the Weber number, which is defined in Equation 16.266 (p. 441).

Details for each model are provided in the following sections:

16.10.1. Taylor Analogy Breakup (TAB) Model
16.10.2. Wave Breakup Model
16.10.3. KHRT Breakup Model
16.10.4. Stochastic Secondary Droplet (SSD) Model

Release 15.0 - © SAS IP, Inc. All rights reserved. - Contains proprietary and confidential information of ANSYS, Inc. and its subsidiaries and affiliates.

## 16.10.1. Taylor Analogy Breakup (TAB) Model

### 16.10.1.1. Introduction

The Taylor analogy breakup (TAB) model is a classic method for calculating droplet breakup, which is applicable to many engineering sprays. This method is based upon Taylor's analogy [446] (p. 753) between an oscillating and distorting droplet and a spring mass system. Table 16.4: Comparison of a Spring-Mass System to a Distorting Droplet (p. 440) illustrates the analogous components.

**Table 16.4: Comparison of a Spring-Mass System to a Distorting Droplet**

| Spring-Mass System | Distorting and Oscillating Droplet |
|---|---|
| restoring force of spring | surface tension forces |
| external force | droplet drag force |
| damping force | droplet viscosity forces |

The resulting TAB model equation set, which governs the oscillating and distorting droplet, can be solved to determine the droplet oscillation and distortion at any given time. As described in detail below, when the droplet oscillations grow to a critical value the "parent" droplet will break up into a number of smaller "child" droplets. As a droplet is distorted from a spherical shape, the drag coefficient changes. A drag model that incorporates the distorting droplet effects is available in ANSYS Fluent. See Dynamic Drag Model Theory (p. 386) for details.

### 16.10.1.2. Use and Limitations

The TAB model is best for low-Weber-number sprays. Extremely high-Weber-number sprays result in shattering of droplets, which is not described well by the spring-mass analogy.

### 16.10.1.3. Droplet Distortion

The equation governing a damped, forced oscillator is [330] (p. 747)

$$F - kx - d\frac{dx}{dt} = m\frac{d^2x}{dt^2} \tag{16.259}$$

where $x$ is the displacement of the droplet equator from its spherical (undisturbed) position. The coefficients of this equation are taken from Taylor's analogy:

$$\frac{F}{m} = C_F\frac{\rho_g u^2}{\rho_l r} \tag{16.260}$$

$$\frac{k}{m} = C_k\frac{\sigma}{\rho_l r^3} \tag{16.261}$$

$$\frac{d}{m} = C_d\frac{\mu_l}{\rho_l r^2} \tag{16.262}$$


Release 15.0 - © SAS IP, Inc. All rights reserved. - Contains proprietary and confidential information of ANSYS, Inc. and its subsidiaries and affiliates.

where $\rho_l$ and $\rho_g$ are the discrete phase and continuous phase densities, $u$ is the relative velocity of the droplet, $r$ is the undisturbed droplet radius, $\sigma$ is the droplet surface tension, and $\mu_l$ is the droplet viscosity. The dimensionless constants $C_F$, $C_k$, and $C_d$ will be defined later.

The droplet is assumed to break up if the distortion grows to a critical ratio of the droplet radius. This breakup requirement is given as

$$x > C_b r \tag{16.263}$$

Where $C_b$ is a constant equal to 0.5, if breakup is assumed to occur when the distortion is equal to half the droplet radius, that is, oscillations at the north and south pole with this amplitude will meet at the droplet center. This implicitly assumes that the droplet is undergoing only one (fundamental) oscillation mode. Equation 16.259 (p. 440) is nondimensionalized by setting $y = x/(C_b r)$ and substituting the relationships in Equation 16.260 (p. 440) – Equation 16.262 (p. 440):

$$\frac{d^2y}{dt^2} = \frac{C_F}{C_b}\frac{\rho_g}{\rho_l}\frac{u^2}{r^2} - \frac{C_k\sigma}{\rho_l r^3}y - \frac{C_d\mu_l}{\rho_l r^2}\frac{dy}{dt} \tag{16.264}$$

where breakup now occurs for $y > 1$. For under-damped droplets, the equation governing $y$ can easily be determined from Equation 16.264 (p. 441) if the relative velocity is assumed to be constant:

$$y(t) = We_c + e^{-(t/t_d)}\left[\left(y_0 - We_c\right)\cos(\omega t) + \frac{1}{\omega}\left(\frac{dy_0}{dt} + \frac{y_0 - We_c}{t_d}\right)\sin(\omega t)\right] \tag{16.265}$$

where

$$We = \frac{\rho_g u^2 r}{\sigma} \tag{16.266}$$

$$We_c = \frac{C_F}{C_k C_b}We \tag{16.267}$$

$$y_0 = y(0) \tag{16.268}$$

$$\frac{dy_0}{dt} = \frac{dy}{dt}(0) \tag{16.269}$$

$$\frac{1}{t_d} = \frac{C_d}{2}\frac{\mu_l}{\rho_l r^2} \tag{16.270}$$

$$\omega^2 = C_k\frac{\sigma}{\rho_l r^3} - \frac{1}{t_d^2} \tag{16.271}$$

In Equation 16.265 (p. 441), $u$ is the relative velocity between the droplet and the gas phase and We is the droplet Weber number, a dimensionless parameter defined as the ratio of aerodynamic forces to surface tension forces. The droplet oscillation frequency is represented by $\omega$. The default value of $y_0$ is 0, based upon the work of Liu et al. [262] (p. 743). The constants have been chosen to match experiments and theory [222] (p. 741):

Release 15.0 - © SAS IP, Inc. All rights reserved. - Contains proprietary and confidential information of ANSYS, Inc. and its subsidiaries and affiliates.

$$\begin{aligned} C_k &= 8 \\ C_d &= 5 \\ C_F &= \frac{1}{3} \end{aligned} \tag{16.272}$$

If Equation 16.265 (p. 441) is solved for all droplets, those with $y > 1$ are assumed to break up. The size and velocity of the new child droplets must be determined.

### 16.10.1.4. Size of Child Droplets

The size of the child droplets is determined by equating the energy of the parent droplet to the combined energy of the child droplets. The energy of the parent droplet is [330] (p. 747)

$$E_{parent} = 4\pi r^2\sigma + K\frac{\pi}{5}\rho_l r^5\left[\left(\frac{dy}{dt}\right)^2 + \omega^2 y^2\right] \tag{16.273}$$

where $K$ is the ratio of the total energy in distortion and oscillation to the energy in the fundamental mode, of the order ($\frac{10}{3}$). The child droplets are assumed to be non-distorted and non-oscillating. Thus, the energy of the child droplets can be shown to be

$$E_{child} = 4\pi r^2\sigma\frac{r}{r_{32}} + \frac{\pi}{6}\rho_l r^5\left(\frac{dy}{dt}\right)^2 \tag{16.274}$$

where $r_{32}$ is the Sauter mean radius of the droplet size distribution. $r_{32}$ can be found by equating the energy of the parent and child droplets (that is, Equation 16.273 (p. 442) and Equation 16.274 (p. 442)), setting $y = 1$, and $\omega^2 = 8\sigma/\rho_l r^3$:

$$r_{32} = \frac{r}{1 + \frac{8K y^2}{20} + \frac{\rho_l r^3 (dy/dt)^2}{\sigma}\left(\frac{6K-5}{120}\right)} \tag{16.275}$$

Once the size of the child droplets is determined, the number of child droplets can easily be determined by mass conservation.

### 16.10.1.5. Velocity of Child Droplets

The TAB model allows for a velocity component normal to the parent droplet velocity to be imposed upon the child droplets. When breakup occurs, the equator of the parent droplet is traveling at a velocity of $dx/dt = C_b r\,(dy/dt)$. Therefore, the child droplets will have a velocity normal to the parent droplet velocity given by

$$v_{normal} = C_v C_b r\frac{dy}{dt} \tag{16.276}$$

where $C_v$ is a constant of order (1).

### 16.10.1.6. Droplet Breakup

To model droplet breakup, the TAB model first determines the amplitude for an undamped oscillation ($t_d \approx \infty$) for each droplet at time step $n$ using the following:


Release 15.0 - © SAS IP, Inc. All rights reserved. - Contains proprietary and confidential information of ANSYS, Inc. and its subsidiaries and affiliates.

$$A=\sqrt{(y^n-We_c)^2+\left(\frac{(dy/dt)^n}{\omega}\right)^2} \tag{16.277}$$

According to Equation 16.277 (p. 443), breakup is possible only if the following condition is satisfied:

$$We_c+A>1 \tag{16.278}$$

This is the limiting case, as damping will only reduce the chance of breakup. If a droplet fails the above criterion, breakup does not occur. The only additional calculations required then, are to update $y$ using a discretized form of Equation 16.265 (p. 441) and its derivative, which are both based on work done by O'Rourke and Amsden [330] (p. 747):

$$\begin{aligned} y^{n+1} &= We_c+e^{-(\Delta t/t_d)}\{(y^n-We_c)\cos(\omega t) \\ &\quad +\frac{1}{\omega}\left[\left(\frac{dy}{dt}\right)^n+\frac{y^n-We_c}{t_d}\right]\sin(\omega t)\Bigg\} \end{aligned} \tag{16.279}$$

$$\begin{aligned} \left(\frac{dy}{dt}\right)^{n+1} &= \frac{We_c-y^{n+1}}{t_d} \\ &\quad +\omega e^{-(\Delta t/t_d)}\left\{\frac{1}{\omega}\left[\left(\frac{dy}{dt}\right)^n+\frac{y^n-We_c}{t_d}\right]\cos(\omega\Delta t)-(y^n-We_c)\sin(\omega\Delta t)\right\} \end{aligned} \tag{16.280}$$

All of the constants in these expressions are assumed to be constant throughout the time step.

If the criterion of Equation 16.278 (p. 443) is met, then breakup is possible. The breakup time, $t_{bu}$, must be determined to see if breakup occurs within the time step $\Delta t$. The value of $t_{bu}$ is set to the time required for oscillations to grow sufficiently large that the magnitude of the droplet distortion, $y$, is equal to unity. The breakup time is determined under the assumption that the droplet oscillation is undamped for its first period. The breakup time is therefore the smallest root greater than $t^n$ of an undamped version of Equation 16.265 (p. 441):

$$We_c+A\cos[\omega(t-t^n)+\phi]=1 \tag{16.281}$$

where

$$\cos\phi=\frac{y^n-We_c}{A} \tag{16.282}$$

and

$$\sin\phi=-\frac{(dy/dt)^n}{A\omega} \tag{16.283}$$

If $t_{bu}>t^{n+1}$, then breakup will not occur during the current time step, and $y$ and $(dy/dt)$ are updated by Equation 16.279 (p. 443) and Equation 16.280 (p. 443). The breakup calculation then continues with the next droplet. Conversely, if $t^n<t_{bu}<t^{n+1}$,then breakup will occur and the child droplet radii are determined by Equation 16.275 (p. 442). The number of child droplets, $N$, is determined by mass conservation:

Release 15.0 - © SAS IP, Inc. All rights reserved. - Contains proprietary and confidential information of ANSYS, Inc. and its subsidiaries and affiliates.

$$N^{n+1} = N^n \left( \frac{r^n}{r^{n+1}} \right)^3 \tag{16.284}$$

It is assumed that the child droplets are neither distorted nor oscillating; that is, $y = (dy/dt) = 0$. The child droplets are represented by a number of child parcels which are created from the original parcel. These child parcels are distributed equally along the equator of the parent droplet in a plane normal to the parent relative velocity vector. The diameter of each of the child parcels is sampled from a Rosin Rammler distribution based on the Sauter mean radius (Equation 16.275 (p. 442)) and a spread parameter of 3.5.

A velocity component normal to the relative velocity vector, with magnitude computed by Equation 16.276 (p. 442), is imposed upon the child droplets. It is decomposed at the equator into components pointing radially outward.

**Important**

A large number of child parcels ensures a smooth distribution of particle diameters and source terms which is needed when simulating, for example, evaporating sprays.

## 16.10.2. Wave Breakup Model

### 16.10.2.1. Introduction

An alternative to the TAB model that is appropriate for high-Weber-number flows is the wave breakup model of Reitz [371] (p. 749), which considers the breakup of the droplets to be induced by the relative velocity between the gas and liquid phases. The model assumes that the time of breakup and the resulting droplet size are related to the fastest-growing Kelvin-Helmholtz instability, derived from the jet stability analysis described below. The wavelength and growth rate of this instability are used to predict details of the newly-formed droplets.

### 16.10.2.2. Use and Limitations

The wave model is appropriate for high-speed injections, where the Kelvin-Helmholtz instability is believed to dominate droplet breakup ($We > 100$). Because this breakup model can increase the number of computational parcels, you may want to inject a modest number of droplets initially.

### 16.10.2.3. Jet Stability Analysis

The jet stability analysis described in detail by Reitz and Bracco [373] (p. 749) is presented briefly here. The analysis considers the stability of a cylindrical, viscous, liquid jet of radius $a$ issuing from a circular orifice at a velocity $v$ into a stagnant, incompressible, inviscid gas of density $\rho_2$. The liquid has a density, $\rho_1$, and viscosity, $\mu_1$, and a cylindrical polar coordinate system is used, which moves with the jet. An arbitrary infinitesimal axisymmetric surface displacement of the form

$$\eta = \eta_0 e^{ikz + \omega t} \tag{16.285}$$

is imposed on the initially steady motion and it is therefore desired to find the dispersion relation $\omega = \omega(k)$ which relates the real part of the growth rate, $\omega$, to its wave number, $k = 2\pi/\lambda$.


Release 15.0 - © SAS IP, Inc. All rights reserved. - Contains proprietary and confidential information of ANSYS, Inc. and its subsidiaries and affiliates.

In order to determine the dispersion relation, the linearized equations for the hydrodynamics of the liquid are solved assuming wave solutions of the form

$$\phi_1 = C_1 I_0(kr)\, e^{ikz+\omega t} \tag{16.286}$$

$$\psi_1 = C_2 I_1(Lr)\, e^{ikz+\omega t} \tag{16.287}$$

where $\phi_1$ and $\psi_1$ are the velocity potential and stream function, respectively, $C_1$ and $C_2$ are integration constants, $I_0$ and $I_1$ are modified Bessel functions of the first kind, $L^2=k^2+\omega/v_1$, and $v_1$ is the liquid kinematic viscosity [371] (p. 749). The liquid pressure is obtained from the inviscid part of the liquid equations. In addition, the inviscid gas equations can be solved to obtain the fluctuating gas pressure at $r=a$:

$$-p_{21}=-\rho_2(U-i\omega k)^2 k\eta\frac{K_0(ka)}{K_1(ka)} \tag{16.288}$$

where $K_0$ and $K_1$ are modified Bessel functions of the second kind and $u$ is the relative velocity between the liquid and the gas. The linearized boundary conditions are

$$v_1 = \frac{\partial \eta}{\partial t} \tag{16.289}$$

$$\frac{\partial u_1}{\partial r}=-\frac{\partial v_1}{\partial z} \tag{16.290}$$

and

$$-p_1+2\mu_1-\frac{\sigma}{a^2}\left(\eta+a^2\frac{\partial^2\eta}{\partial z^2}\right)+p_2=0 \tag{16.291}$$

which are mathematical statements of the liquid kinematic free surface condition, continuity of shear stress, and continuity of normal stress, respectively. Note that $u_1$ is the axial perturbation liquid velocity, $v_1$ is the radial perturbation liquid velocity, and $\sigma$ is the surface tension. Also note that Equation 16.290 (p. 445) was obtained under the assumption that $v_2=0$.

As described by Reitz [371] (p. 749), Equation 16.289 (p. 445) and Equation 16.290 (p. 445) can be used to eliminate the integration constants $C_1$ and $C_2$ in Equation 16.286 (p. 445) and Equation 16.287 (p. 445). Thus, when the pressure and velocity solutions are substituted into Equation 16.291 (p. 445), the desired dispersion relation is obtained:

$$\begin{aligned}\omega^2+2v_1k^2\omega\left[\frac{I_1'(ka)}{I_0(ka)}-\frac{2kL}{k^2+L^2}\frac{I_1(ka)}{I_0(ka)}\frac{I_1'(La)}{I_1(La)}\right] &= \frac{\sigma k}{\rho_1 a^2}\left(1-k^2a^2\right)\left(\frac{L^2-a^2}{L^2+a^2}\right)\frac{I_1(ka)}{I_0(ka)} \\ &+\frac{\rho_2}{\rho_1}\left(U-i\frac{\omega}{k}\right)^2\left(\frac{L^2-a^2}{L^2+a^2}\right)\frac{I_1(ka)}{I_0(ka)}\frac{K_0(ka)}{K_1(ka)}\end{aligned} \tag{16.292}$$

As shown by Reitz [371] (p. 749), Equation 16.292 (p. 445) predicts that a maximum growth rate (or most unstable wave) exists for a given set of flow conditions. Curve fits of numerical solutions to Equation 16.292 (p. 445) were generated for the maximum growth rate, $\Omega$, and the corresponding wavelength, $\Lambda$, and are given by Reitz [371] (p. 749):

Release 15.0 - © SAS IP, Inc. All rights reserved. - Contains proprietary and confidential information of ANSYS, Inc. and its subsidiaries and affiliates.

$$\frac{\Lambda}{a} = 9.02\frac{\left(1+0.45Oh^{0.5}\right)\left(1+0.4Ta^{0.7}\right)}{\left(1+0.87We_2^{1.67}\right)^{0.6}} \tag{16.293}$$

$$\Omega\sqrt{\frac{\rho_1 a^3}{\sigma}} = \frac{(0.34+0.38We_2^{1.5})}{(1+Oh)\ (1+1.4Ta^{0.6})} \tag{16.294}$$

where $Oh=\sqrt{We_1}/Re_1$ is the Ohnesorge number and $Ta=Oh\sqrt{We_2}$ is the Taylor number. Furthermore, $We_1=\rho_1 U^2 a/\sigma$ and $We_2=\rho_2 U^2 a/\sigma$ are the liquid and gas Weber numbers, respectively, and $Re_1=Ua/v_1$ is the Reynolds number.

### 16.10.2.4. Droplet Breakup

In the wave model, breakup of droplet parcels is calculated by assuming that the radius of the newly-formed droplets is proportional to the wavelength of the fastest-growing unstable surface wave on the parent droplet. In other words,

$$r=B_0\Lambda \tag{16.295}$$

where $B_0$ is a model constant set equal to 0.61 based on the work of Reitz [371] (p. 749). Furthermore, the rate of change of droplet radius in the parent parcel is given by

$$\frac{da}{dt}=-\frac{(a-r)}{\tau}, r\le a \tag{16.296}$$

where the breakup time, $\tau$, is given by

$$\tau=\frac{3.726B_1 a}{\Lambda\Omega} \tag{16.297}$$

and $\Lambda$ and $\Omega$ are obtained from Equation 16.293 (p. 446) and Equation 16.294 (p. 446), respectively. The breakup time constant, $B_1$, is set to a value of 1.73 as recommended by Liu et al. [262] (p. 743). Values of $B_1$ can range between 1 and 60, depending on the injector characterization.

In the wave model, mass is accumulated from the parent drop at a rate given by Equation 16.297 (p. 446) until the shed mass is equal to 5% of the initial parcel mass. At this time, a new parcel is created with a radius given by Equation 16.295 (p. 446). The new parcel is given the same properties as the parent parcel (that is, temperature, material, position, etc.) with the exception of radius and velocity. The new parcel is given a component of velocity randomly selected in the plane orthogonal to the direction vector of the parent parcel, and the momentum of the parent parcel is adjusted so that momentum is conserved. The velocity magnitude of the new parcel is the same as the parent parcel.

You must also specify the model constants that determine how the gas phase interacts with the liquid droplets. For example, the breakup time constant B1 is the constant multiplying the time scale that determines how quickly the parcel will lose mass. Therefore, a larger number means that it takes longer for the particle to lose a given amount. A larger number for B1 in the context of interaction with the gas phase would mean that the interaction with the subgrid is less intense. B0 is the constant for the drop size and is generally taken to be 0.61.

In the initial breakup of a cylindrical liquid jet at low gas Weber numbers (Rayleigh regime), Equation 16.295 (p. 446) can predict droplet diameters that are larger than the initial (jet) diameter. In that


Release 15.0 - © SAS IP, Inc. All rights reserved. - Contains proprietary and confidential information of ANSYS, Inc. and its subsidiaries and affiliates.

case, the size of the droplets is calculated from the fastest growing wavelength, which determines the spacing of the initial droplets, and mass conservation considerations. You can suppress this accounting for the Rayleight regime as described in Breakup in the *Fluent User's Guide*.

## 16.10.3. KHRT Breakup Model

### 16.10.3.1. Introduction

ANSYS Fluent provides an alternative model for droplet breakup called KHRT ([28] (p. 730), [342] (p. 748)), which combines the effects of Kelvin-Helmholtz waves driven by aerodynamic forces with Rayleigh-Taylor instabilities due to acceleration of shed drops ejected into freestream conditions. Both mechanisms model droplet breakup by tracking wave growth on the surface of the droplet, with breakup occurring due to the fastest growing instability based on local conditions. To model the liquid core in the near nozzle region, a Levich core length is applied that only allows breakup due to Kelvin-Helmholtz wave growth.

### 16.10.3.2. Use and Limitations

The KHRT model was developed to simulate high Weber number sprays and should not be applied to low pressure sprays.

### 16.10.3.3. Liquid Core Length

The KHRT model assumes that a liquid core exists in the near nozzle region. Child droplets are shed from this liquid core and are subjected to sudden acceleration when they are ejected into the freestream and a Rayleigh-Taylor instability becomes the dominant effect. The length of the liquid core is obtained from Levich theory [244] (p. 742):

$$L = C_L d_0 \sqrt{\frac{\rho_l}{\rho_g}} \tag{16.298}$$

Where $C_L$ is the Levich constant and $d_0$ is a reference nozzle diameter. The reference diameter must be specified for atomizer injections in ANSYS Fluent, however the cone and solid cone injections assume that the reference diameter is the minimum of the droplet diameter and the inner diameter of the cone. Surface injections use the surface area specified to calculate an equivalent hydraulic diameter for use as $d_0$. When a Rosin-Rammler distribution is specified for non-atomizer injections, the maximum diameter of the Rosin-Rammler becomes the reference diameter.

A liquid core is approximated by 'blobs' [28] (p. 730) as shown in Figure 16.12: Liquid Core Approximation (p. 448).

Release 15.0 - © SAS IP, Inc. All rights reserved. - Contains proprietary and confidential information of ANSYS, Inc. and its subsidiaries and affiliates.

**Figure 16.12: Liquid Core Approximation**

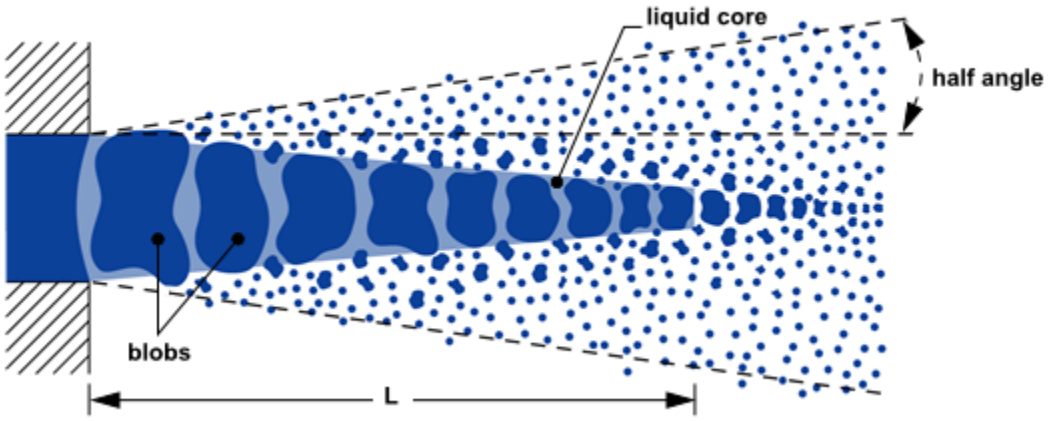


The 'blobs' are introduced into the domain with the diameter specified in the injection. It is often best to use an effective droplet diameter by considering a contraction coefficient, which can be computed with

$$D_e = \sqrt{C_a} \cdot d_0 \tag{16.299}$$

Where $C_a$ denotes the contraction coefficient.

You can disable the Liquid Core Approximation entirely by setting the Levich constant, $C_L$, to zero as described in Breakup in the *Fluent User's Guide*.

### 16.10.3.4. Rayleigh-Taylor Breakup

As with the Kelvin-Helmholtz model, the Rayleigh-Taylor (RT) model is based on wave instabilities on the droplet surface. The frequency of the fastest growing wave is computed by

$$\Omega_{RT} = \sqrt{\frac{2\left(-g_t(\rho_p - \rho_g)\right)^{3/2}}{3\sqrt{3\sigma}(\rho_p + \rho_g)}} \tag{16.300}$$

Where $g_t$ is the droplet acceleration in the direction of the droplet travel. The corresponding wave number is given by

$$K_{RT} = \sqrt{\frac{-g_t(\rho_p - \rho_g)}{3\sigma}} \tag{16.301}$$

Breakup occurs after RT waves have been growing for a time larger than the breakup time $\tau_{RT}$, defined as

$$\tau_{RT} = \frac{C_\tau}{\Omega_{RT}} \tag{16.302}$$

Here $C_\tau$ is the Rayleigh-Taylor breakup time constant which has a default value of $0.5$.

The wave growth is tracked when the predicted wave length $2\pi C_{RT}/K_{RT}$, corresponding to the fastest wave growth rate, is smaller than the local droplet diameter. The radius of the smaller child droplets is calculated with


Release 15.0 - © SAS IP, Inc. All rights reserved. - Contains proprietary and confidential information of ANSYS, Inc. and its subsidiaries and affiliates.

$$r_c = \frac{\pi C_{RT}}{K_{RT}} \tag{16.303}$$

where $C_{RT}$ is the breakup radius constant which has a default value of $0.1$.

### 16.10.3.5. Droplet Breakup Within the Liquid Core

Within the liquid core only aerodynamic breakup is considered. It is computed based on the Wave breakup model, described in the previous section.

### 16.10.3.6. Droplet Breakup Outside the Liquid Core

Outside the liquid core, both KH and RT effects are calculated and both are considered for breakup. Typically, the RT instability grows faster when droplet acceleration is high and this effect dominates for high Weber number sprays. In both cases, a new parcel is generated only when the accumulated shed parcel mass exceeds 5% of the initial parcel mass.

## 16.10.4. Stochastic Secondary Droplet (SSD) Model

In the **Wave** and **TAB** spray models, droplet breakup is determined using a single diameter scale. The **SSD** model [10] (p. 729) treats breakup as a discrete random event resulting in a distribution of diameter scales over a range. With the **SSD** model, the probability of breakup is independent of the parent droplet size and the secondary droplet size is sampled from an analytical solution of the Fokker-Planck equation for the probability distribution. In addition, parameters for the size distribution are based on local conditions.

### 16.10.4.1. Theory

The initial diameter of the parcels injected into the domain is set in the DPM injection dialog box. The breakup model predicts the time at which breakup occurs and the number and properties of the new drops. Drops larger than a critical radius are subject to breakup:

$$r_c = \frac{We_{cr}\sigma_l}{\rho_g u_{rel}^2} \tag{16.304}$$

where $We_{cr}$ is the critical Weber number, which you will need to specify. The default value of the critical Weber number is 6.

The breakup time is defined as

$$t_{bu} = B\sqrt{\frac{\rho_l}{\rho_g}}\frac{r}{|u_{rel}|} \tag{16.305}$$

where $B$ is the user-specified breakup constant, with a default value of 1.73.

Drops with a radius larger than the critical radius (derived from the critical Weber number) have their breakup times incremented. When the breakup time on the parcel is larger than the critical breakup time (locally calculated from conditions in the cell and on the parcel), breakup occurs.

When a parcel reaches breakup, it is destroyed and new parcels are created. The diameters of these child parcels are obtained by sampling a distribution function in the log of the diameter, $\mathrm{x} = \ln(\mathrm{r})$:

Release 15.0 - © SAS IP, Inc. All rights reserved. - Contains proprietary and confidential information of ANSYS, Inc. and its subsidiaries and affiliates.

$$T(x) = \frac{1}{\sqrt{2\pi\langle\xi^2\rangle}} \exp\left[\frac{-(x - x_0 - \langle\xi\rangle)^2}{2\langle\xi^2\rangle}\right] \tag{16.306}$$

where $\langle\xi\rangle$ and $\langle\xi^2\rangle$ are parameters of the model.

The parameter $\langle\xi\rangle$ has a negative dimensionless value and must be set by you: $\exp(\langle\xi\rangle)$ is a typical factor by which child particles are smaller than the original parcel.

The parameter $\langle\xi^2\rangle$ defines the variance, in logarithmic terms, of the distribution of child particles. It has a positive, dimensionless value, which should be significantly less than $\langle\xi\rangle^2$ (to avoid child particles that are larger than the original). It is computed from $\langle\xi^2\rangle = -0.1\ln\left(\frac{We_{cr}}{We}\right)$.

When breakup occurs, enough parcels are created so that the number of drops represented by each parcel is approximately equal to a target number in the parcel (NP), which you set. Parcels are created, with diameters sampled randomly from the distribution, and provisionally given the target NP. This continues until the mass of the parent parcel is used up. A scaling factor is then applied to the number of drops in all the new parcels to conserve the mass of the parent parcel.

This methodology results in improved statistics and gives you control over error during a simulation. A smaller NP will mean more parcels but lower statistical error. However, there is a limit to the number of parcels that can be created during a single breakup event; the default value for this limit is 50. Therefore, the number of drops in each parcel will sometimes deviate significantly from the target NP.

For information on how to apply this model, refer to Breakup in the User's Guide.

## 16.11. Collision and Droplet Coalescence Model Theory

For information about this model, see the following sections:

16.11.1. Introduction
16.11.2. Use and Limitations
16.11.3. Theory

### 16.11.1. Introduction

When your simulation includes tracking of droplets, ANSYS Fluent provides an option for estimating the number of droplet collisions and their outcomes in a computationally efficient manner. The difficulty in any collision calculation is that for $N$ droplets, each droplet has $N-1$ possible collision partners. Thus, the number of possible collision pairs is approximately $\frac{1}{2}N^2$. (The factor of $\frac{1}{2}$ appears because droplet A colliding with droplet B is identical to droplet B colliding with droplet A. This symmetry reduces the number of possible collision events by half.)

An important consideration is that the collision algorithm must calculate $\frac{1}{2}N^2$ possible collision events at every time step. Since a spray can consist of several million droplets, the computational cost of a collision calculation from first principles is prohibitive. This motivates the concept of parcels. Parcels are statistical representations of a number of individual droplets. For example, if ANSYS Fluent tracks a set of parcels, each of which represents 1000 droplets, the cost of the collision calculation is reduced by a factor of $10^6$. Because the cost of the collision calculation still scales with the square of $N$, the re-


Release 15.0 - © SAS IP, Inc. All rights reserved. - Contains proprietary and confidential information of ANSYS, Inc. and its subsidiaries and affiliates.

duction of cost is significant; however, the effort to calculate the possible intersection of so many parcel trajectories would still be prohibitively expensive.

The algorithm of O'Rourke [329] (p. 747) efficiently reduces the computational cost of the spray calculation. Rather than using geometry to see if parcel paths intersect, O'Rourke's method is a stochastic estimate of collisions. O'Rourke also makes the assumption that two parcels may collide only if they are located in the same continuous-phase cell. These two assumptions are valid only when the continuous-phase cell size is small compared to the size of the spray. For these conditions, the method of O'Rourke is second-order accurate at estimating the chance of collisions. The concept of parcels together with the algorithm of O'Rourke makes the calculation of collision possible for practical spray problems.

Once it is decided that two parcels of droplets collide, the algorithm further determines the type of collision. Only coalescence and bouncing outcomes are considered. The probability of each outcome is calculated from the collisional Weber number ($We_c$) and a fit to experimental observations. Here,

$$We_c = \frac{\rho U_{rel}^2 \overline{D}}{\sigma} \tag{16.307}$$

where $U_{rel}$ is the relative velocity between two parcels and $\overline{D}$ is the arithmetic mean diameter of the two parcels. The state of the two colliding parcels is modified based on the outcome of the collision.

## 16.11.2. Use and Limitations

The collision model assumes that the frequency of collisions is much less than the particle time step. If the particle time step is too large, then the results may be time-step-dependent. You should adjust the particle length scale accordingly. Additionally, the model is most applicable for low-Weber-number collisions where collisions result in bouncing and coalescence. Above a Weber number of about 100, the outcome of collision could be shattering.

Sometimes the collision model can cause mesh-dependent artifacts to appear in the spray. This is a result of the assumption that droplets can collide only within the same cell. These tend to be visible when the source of injection is at a mesh vertex. The coalescence of droplets tends to cause the spray to pull away from cell boundaries. In two dimensions, a finer mesh and more computational droplets can be used to reduce these effects. In three dimensions, best results are achieved when the spray is modeled using a polar mesh with the spray at the center.

If the collision model is used in a transient simulation, multiple DPM iterations per time step cannot be specified in the **Number of Continuous Phase Iterations per DPM Iteration** field in the Discrete Phase Model Dialog Box. In such cases, only one DPM iteration per time step will be calculated.

## 16.11.3. Theory

As noted above, O'Rourke's algorithm assumes that two droplets may collide only if they are in the same continuous-phase cell. This assumption can prevent droplets that are quite close to each other, but not in the same cell, from colliding, although the effect of this error is lessened by allowing some droplets that are farther apart to collide. The overall accuracy of the scheme is second-order in space.

### *16.11.3.1. Probability of Collision*

The probability of collision of two droplets is derived from the point of view of the larger droplet, called the collector droplet and identified below with the number 1. The smaller droplet is identified in the following derivation with the number 2. The calculation is in the frame of reference of the larger droplet so that the velocity of the collector droplet is zero. Only the relative distance between the collector and

Release 15.0 - © SAS IP, Inc. All rights reserved. - Contains proprietary and confidential information of ANSYS, Inc. and its subsidiaries and affiliates.

the smaller droplet is important in this derivation. If the smaller droplet is on a collision course with the collector, the centers will pass within a distance of $r_1+r_2$. More precisely, if the smaller droplet center passes within a flat circle centered around the collector of area $\pi(r_1+r_2)^2$ perpendicular to the trajectory of the smaller droplet, a collision will take place. This disk can be used to define the collision volume, which is the area of the aforementioned disk multiplied by the distance traveled by the smaller droplet in one time step, namely $\pi(r_1+r_2)^2 v_{rel}\Delta t$.

The algorithm of O'Rourke uses the concept of a collision volume to calculate the probability of collision. Rather than calculating whether or not the position of the smaller droplet center is within the collision volume, the algorithm calculates the probability of the smaller droplet being within the collision volume. It is known that the smaller droplet is somewhere within the continuous-phase cell of volume $V$. If there is a uniform probability of the droplet being anywhere within the cell, then the chance of the droplet being within the collision volume is the ratio of the two volumes. Thus, the probability of the collector colliding with the smaller droplet is

$$P_1=\frac{\pi(r_1+r_2)^2 v_{rel}\Delta t}{V} \tag{16.308}$$

Equation 16.308 (p. 452) can be generalized for parcels, where there are $n_1$ and $n_2$ droplets in the collector and smaller droplet parcels, respectively. The collector undergoes a mean expected number of collisions given by

$$\overline{n}=\frac{n_2\pi(r_1+r_2)^2 v_{\mathrm{rel}}\Delta t}{V} \tag{16.309}$$

The actual number of collisions that the collector experiences is not generally the mean expected number of collisions. The probability distribution of the number of collisions follows a Poisson distribution, according to O'Rourke, which is given by

$$P(n)=e^{-\overline{n}}\frac{\overline{n}^{\,n}}{n!} \tag{16.310}$$

where $n$ is the number of collisions between a collector and other droplets.

For each DPM timestep, the mean expected number of collisions is calculated for each pair of tracked parcels in each cell. A random sample from the Poisson distribution is generated, to detect whether this pair collides.

### 16.11.3.2. Collision Outcomes

Once it is determined that two parcels collide, the outcome of the collision must be determined. In general, the outcome tends to be coalescence if the droplets collide head-on, and bouncing if the collision is more oblique. In the reference frame being used here, the probability of coalescence can be related to the offset of the collector droplet center and the trajectory of the smaller droplet. The critical offset is a function of the collisional Weber number and the relative radii of the collector and the smaller droplet.

The critical offset is calculated by O'Rourke using the expression

$$b_{crit}=(r_1+r_2)\sqrt{\min\left(1.0,\frac{2.4f}{We}\right)} \tag{16.311}$$

where $f$ is a function of $r_1/r_2$, defined as


Release 15.0 - © SAS IP, Inc. All rights reserved. - Contains proprietary and confidential information of ANSYS, Inc. and its subsidiaries and affiliates.

$$f\left(\frac{r_1}{r_2}\right)=\left(\frac{r_1}{r_2}\right)^3-2.4\left(\frac{r_1}{r_2}\right)^2+2.7\left(\frac{r_1}{r_2}\right) \tag{16.312}$$

The value of the actual collision parameter, $b$, is $(r_1+r_2)\sqrt{Y}$, where $Y$ is a random number between 0 and 1. The calculated value of $b$ is compared to $b_{crit}$, and if $b<b_{crit}$, the result of the collision is coalescence. Equation 16.310 (p. 452) gives the number of smaller droplets that coalesce with the collector. The properties of the coalesced droplets are found from the basic conservation laws.

In the case of a grazing collision, the new velocities are calculated based on conservation of momentum and kinetic energy. It is assumed that some fraction of the kinetic energy of the droplets is lost to viscous dissipation and angular momentum generation. This fraction is related to $b$, the collision offset parameter. Using assumed forms for the energy loss, O'Rourke derived the following expression for the new velocity:

$$v_1'=\frac{m_1v_1+m_2v_2}{m_1+m_2}+\frac{m_2(v_1-v_2)}{m_1+m_2}\left(\frac{b-b_{crit}}{r_1+r_2-b_{crit}}\right) \tag{16.313}$$

This relation is used for each of the components of velocity. No other droplet properties are altered in grazing collisions.

## 16.12. Discrete Element Method Collision Model

ANSYS Fluent allows you to use the discrete element method (DEM) as part of the DPM capability. To use the DEM model, refer to Modeling Collision Using the DEM Model in the User's Guide.

The discrete element method is suitable for simulating granular matter (such as gravel, coal, beads of any material). Such simulations are characterized by a high volume fraction of particles, where particle-particle interaction is important. Note that interaction with the fluid flow may or may not be important. Typical applications include:

- hoppers
- risers
- packed beds
- fluidized beds
- pneumatic transport

### 16.12.1. Theory

The DPM capabilities allow you to simulate moving particles as moving mass points, where abstractions are used for the shape and volume of the particles. Note that the details of the flow around the particles (for example, vortex shedding, flow separation, boundary layers) are neglected. Using Newton's second law, the ordinary differential equations that govern the particle motion are represented as follows:

$$m\frac{d\vec{v}}{dt}=\vec{F}_{\text{drag}}+\vec{F}_{\text{pressure}}+\vec{F}_{\text{virtual_mass}}+\vec{F}_{\text{gravitation}}+\vec{F}_{\text{other}} \tag{16.314}$$

$$\frac{dx}{dt}=\vec{v} \tag{16.315}$$

Release 15.0 - © SAS IP, Inc. All rights reserved. - Contains proprietary and confidential information of ANSYS, Inc. and its subsidiaries and affiliates.

The DEM implementation is based on the work of Cundall and Strack [81] (p. 733), and accounts for the forces that result from the collision of particles (the so-called "soft sphere" approach). These forces then enter through the $\vec{F}_{\text{other}}$ term in Equation 16.314 (p. 453). The forces from the particle collisions are determined by the deformation, which is measured as the overlap between pairs of spheres (see Figure 16.13: Particles Represented by Spheres (p. 454)) or between a sphere and a boundary. Equation 16.314 (p. 453) is integrated over time to capture the interaction of the particles, using a time scale for the integration that is determined by the rigidity of the materials.

**Figure 16.13: Particles Represented by Spheres**

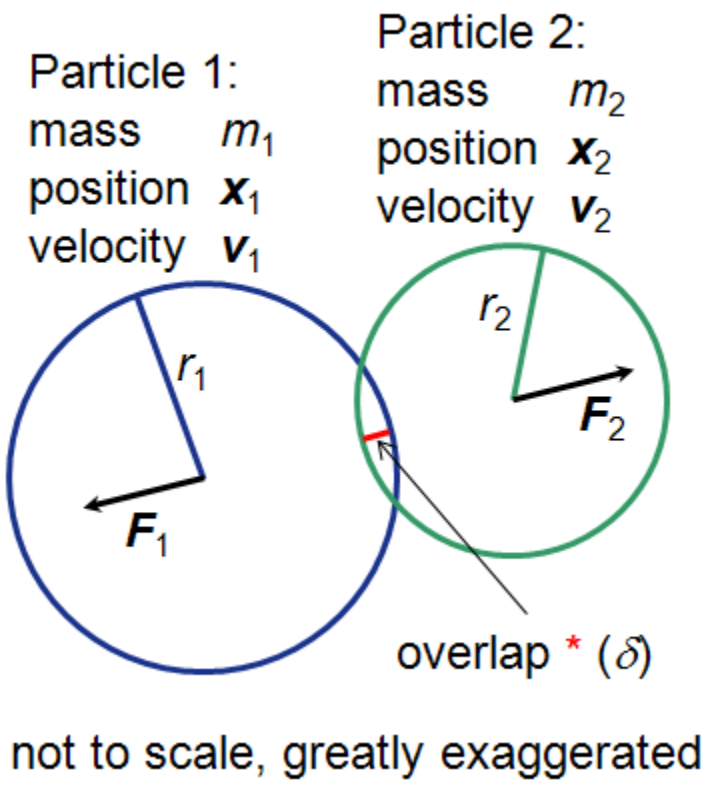


The following collision force laws are available:

- spring
- spring-dashpot
- friction

The size of the spring constant of the normal contact force for a given collision pair should at least satisfy the condition that for the biggest parcels in that collision pair and the highest relative velocity, the spring constant should be high enough to make two parcels in a collision recoil with a maximum overlap that is not too large compared to the parcel diameter. You can estimate the value of the spring constant $k$ using the following equation:

$$k = \frac{\pi v^2}{3\varepsilon_D^2} D\rho \tag{16.316}$$


Release 15.0 - © SAS IP, Inc. All rights reserved. - Contains proprietary and confidential information of ANSYS, Inc. and its subsidiaries and affiliates.

where $D$ is the parcel diameter, $\rho$ is the particle mass density, $v$ is the relative velocity between two colliding particles, and $\varepsilon_D$ is the fraction of the diameter for allowable overlap. The collision time scale is evaluated as $\pi\sqrt{\frac{m}{k}}$, where $m$ is the parcel mass (defined by $\frac{\rho D^3 \pi}{6}$)

### 16.12.1.1. The Spring Collision Law

For the linear spring collision law, a unit vector ($\vec{e}_{12}$) is defined from particle 1 to particle 2:

$$\vec{e}_{12} = (x_2 - x_1) \; / \| x_2 - x_1 \| \tag{16.317}$$

where $x_1$ and $x_2$ represent the position of particle 1 and 2, respectively.

The overlap $\delta$ (which is less than zero during contact) is defined as follows:

$$\delta = \| x_2 - x_1 \| - (r_1 + r_2) \tag{16.318}$$

where $r_1$ and $r_2$ represent the radii of particle 1 and 2, respectively.

The force on particle 1 ($\vec{F}_1$) is then calculated using a spring constant $K$ that you define (and that must be greater than zero):

$$\vec{F}_1 = K\delta\vec{e}_{12} \tag{16.319}$$

and then by Newton's third law, the force on particle 2 ($\vec{F}_2$) is:

$$\vec{F}_2 = -\vec{F}_1 \tag{16.320}$$

Note that $\vec{F}_1$ is directed away from particle 2, because $\delta$ is less than zero for contact.

### 16.12.1.2. The Spring-Dashpot Collision Law

The spring-dashpot collision law is a linear spring force law as described previously, augmented with a dashpot term described below.

For the spring-dashpot collision law, you define a spring constant $K$ as in the spring collision law, along with a coefficient of restitution for the dashpot term ($\eta$). Note that $0 < \eta \leq 1$.

In preparation for the force calculations, the following expressions are evaluated:

$$f_{\text{loss}} = \sqrt{\pi^2 + \ln^2 \eta} \tag{16.321}$$

$$m_{12} = \frac{m_1 m_2}{m_1 + m_2} \tag{16.322}$$

$$t_{\text{coll}} = f_{\text{loss}} \sqrt{\frac{m_{12}}{K}} \tag{16.323}$$

$$\gamma = -2\frac{m_{12}\ln\eta}{t_{\text{coll}}} \tag{16.324}$$

$$\vec{v}_{12} = \vec{v}_2 - \vec{v}_1 \tag{16.325}$$

where $f_{\text{loss}}$ is a loss factor, $m_1$ and $m_2$ are the masses of particle 1 and 2, respectively, $m_{12}$ is the so-called "reduced mass", $t_{\text{coll}}$ is the collision time scale, $\vec{v}_1$ and $\vec{v}_2$ are the velocities of particle 1 and

Release 15.0 - © SAS IP, Inc. All rights reserved. - Contains proprietary and confidential information of ANSYS, Inc. and its subsidiaries and affiliates.

2, respectively, $\vec{v}_{12}$ is the relative velocity, and $\gamma$ is the damping coefficient. Note that $\gamma \geq 0$, because $\ln\eta \leq 0$.

With the previous expressions, the force on particle 1 can be calculated as:

$$\vec{F}_1 = (K\delta + \gamma(\vec{v}_{12} \cdot \vec{e}_{12}))\,\vec{e}_{12} \tag{16.326}$$

$\vec{F}_2$ is calculated using Equation 16.320 (p. 455).

### 16.12.1.3. The Friction Collision Law

The friction collision law is based on the equation for Coulomb friction ($\vec{F}_{\text{friction}}$):

$$\vec{F}_{\text{friction}} = \mu \vec{F}_{\text{normal}} \tag{16.327}$$

where $\mu$ is the friction coefficient and $\vec{F}_{\text{normal}}$ is the force that is normal to the surface. The direction of the friction force is opposite to the relative tangential motion, and may or may not inhibit the relative tangential motion depending on the following:

- the size of the tangential momentum
- the size of other tangential forces (for example, tangential components from gravity and drag)

The friction coefficient is a function of the relative tangential velocity magnitude ($v_{\text{rt}}$):

- $v_r \leq v_{\text{glide}}$:
  - $\mu(v_r) = \mu_{\text{stick}} + \left(\mu_{\text{stick}} - \mu_{\text{glide}}\right)\left(v_r / v_{\text{glide}} - 2.0\right)\left(v_r / v_{\text{glide}}\right)$
- $v_{\text{glide}} < v_r \leq v_{\text{limit}}$:
  - $\mu(v_r) = \mu_{\text{glide}}$
- $v_r > v_{\text{limit}}$:
  - $v_{\text{ratio}} = (v_r - v_{\text{limit}}) / slope_{\text{limit}}$
  - $\mu_{\text{ratio}} = \mu_{\text{glide}} / \mu_{\text{limit}}$
  - $\mu(v_r) = \mu_{\text{glide}} \dfrac{1 + v_{\text{ratio}}}{1 + \mu_{\text{ratio}} v_{\text{ratio}}}$

where

$\mu_{\text{stick}}$ is the sticking friction coefficient

$\mu_{\text{glide}}$ is the gliding friction coefficient

$\mu_{\text{limit}}$ is the high velocity limit friction coefficient


Release 15.0 - © SAS IP, Inc. All rights reserved. - Contains proprietary and confidential information of ANSYS, Inc. and its subsidiaries and affiliates.

$v_{\text{glide}}$ is the gliding velocity — for lower velocities, $\mu$ is interpolated quadratically between $\mu_{\text{stick}}$ and $\mu_{\text{glide}}$

$v_{\text{limit}}$ is the limit velocity — for higher velocities, $\mu(v_r)$ approaches $\mu_{\text{limit}}$

$slope_{\text{limit}}$ is a parameter determining the how fast $\mu(v_r)$ approaches $\mu_{\text{limit}}$

For an example of a plot of $\mu(v_{\text{rt}})$, see Figure 16.14: An Example of a Friction Coefficient Plot (p. 457).

**Figure 16.14: An Example of a Friction Coefficient Plot**

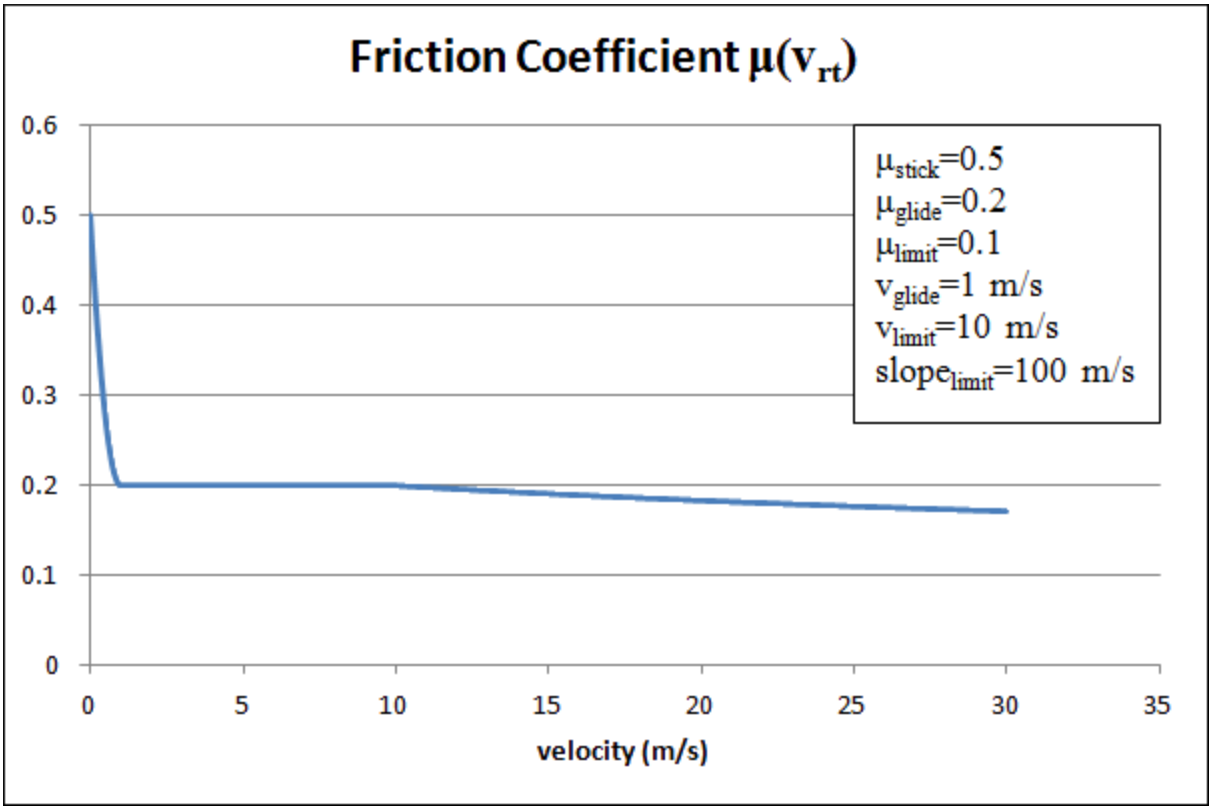


## 16.12.1.4. DEM Parcels

For typical applications, the computational cost of tracking all of the particles individually is prohibitive. Instead, the approach for the discrete element method is similar to that of the DPM, in that like particles are divided into parcels, and then the position of each parcel is determined by tracking a single representative particle. The DEM approach differs from the DPM in the following ways:

- The mass used in the DEM calculations of the collisions is that of the entire parcel, not just that of the single representative particle.
- The radius of the DEM parcel is that of a sphere whose volume is the mass of the entire parcel divided by the particle density.

## 16.12.1.5. Cartesian Collision Mesh

When evaluating the collisions between parcels, it is too costly to conduct a direct force evaluation that involves all of the parcels. Consider that for $N$ parcels, the number of pairs that would need to be in-

Release 15.0 - © SAS IP, Inc. All rights reserved. - Contains proprietary and confidential information of ANSYS, Inc. and its subsidiaries and affiliates.

spected for every time step would be on the order of $N^2$. To address this issue, a geometric approach is used: the domain is divided by a suitable Cartesian mesh (where the edge length of the mesh cells is a multiple of the largest parcel diameter), and then the force evaluation is only conducted for parcels that are in neighboring mesh cells, because particles in more remote cells of the collision mesh are *a priori* known to be out of reach. See Figure 16.15: Force Evaluation for Parcels (p. 458) for an illustration.

**Figure 16.15: Force Evaluation for Parcels**

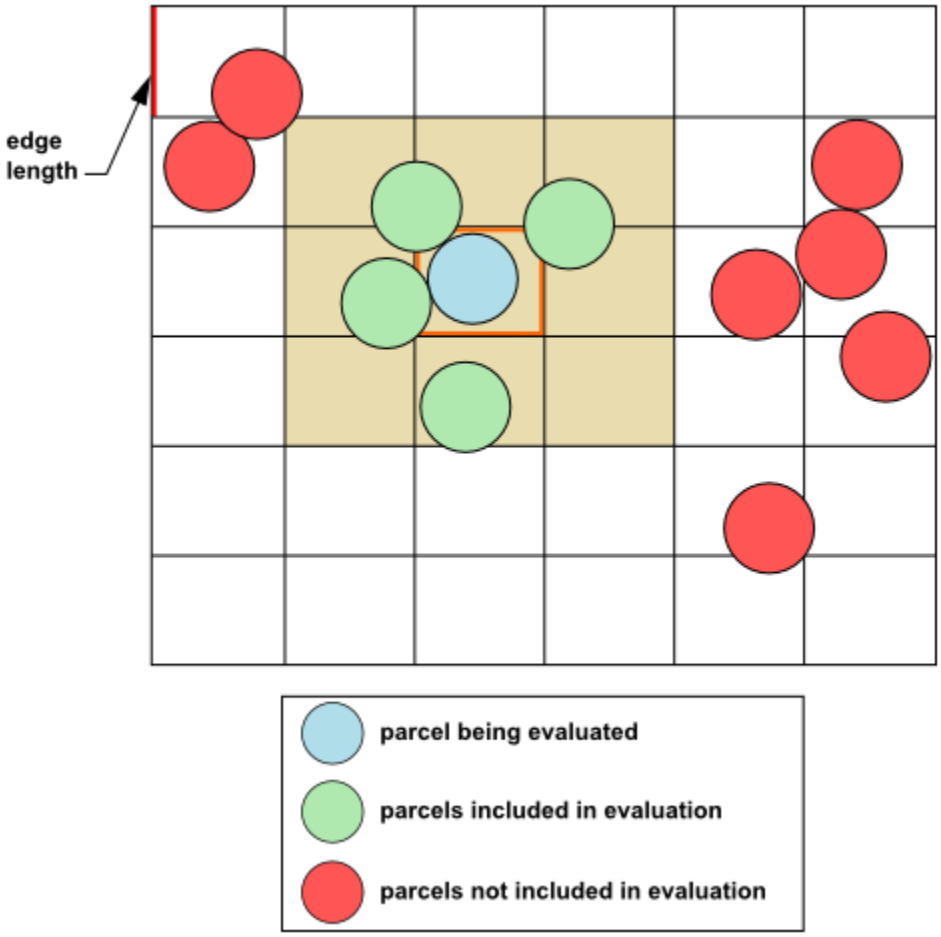


## 16.13. One-Way and Two-Way Coupling

You can use ANSYS Fluent to predict the discrete phase patterns based on a fixed continuous phase flow field (an *uncoupled* approach or "one-way coupling"), or you can include the effect of the discrete phase on the continuum (a *coupled* approach or "two-way coupling"). In the coupled approach, the continuous phase flow pattern is impacted by the discrete phase (and vice versa), and you can alternate calculations of the continuous phase and discrete phase equations until a converged coupled solution is achieved.

For more information, see the following sections:

16.13.1. Coupling Between the Discrete and Continuous Phases
16.13.2. Momentum Exchange
16.13.3. Heat Exchange
16.13.4. Mass Exchange
16.13.5. Under-Relaxation of the Interphase Exchange Terms
16.13.6. Interphase Exchange During Stochastic Tracking


Release 15.0 - © SAS IP, Inc. All rights reserved. - Contains proprietary and confidential information of ANSYS, Inc. and its subsidiaries and affiliates.

16.13.7. Interphase Exchange During Cloud Tracking

## 16.13.1. Coupling Between the Discrete and Continuous Phases

As the trajectory of a particle is computed, ANSYS Fluent keeps track of the heat, mass, and momentum gained or lost by the particle stream that follows that trajectory and these quantities can be incorporated in the subsequent continuous phase calculations. Thus, while the continuous phase always impacts the discrete phase, you can also incorporate the effect of the discrete phase trajectories on the continuum. This two-way coupling is accomplished by alternately solving the discrete and continuous phase equations until the solutions in both phases have stopped changing. This interphase exchange of heat, mass, and momentum from the particle to the continuous phase is depicted qualitatively in Figure 16.16: Heat, Mass, and Momentum Transfer Between the Discrete and Continuous Phases (p. 459). Note that no interchange terms are computed for particles defined as massless, where the discrete phase trajectories have no impact on the continuum.

**Figure 16.16: Heat, Mass, and Momentum Transfer Between the Discrete and Continuous Phases**

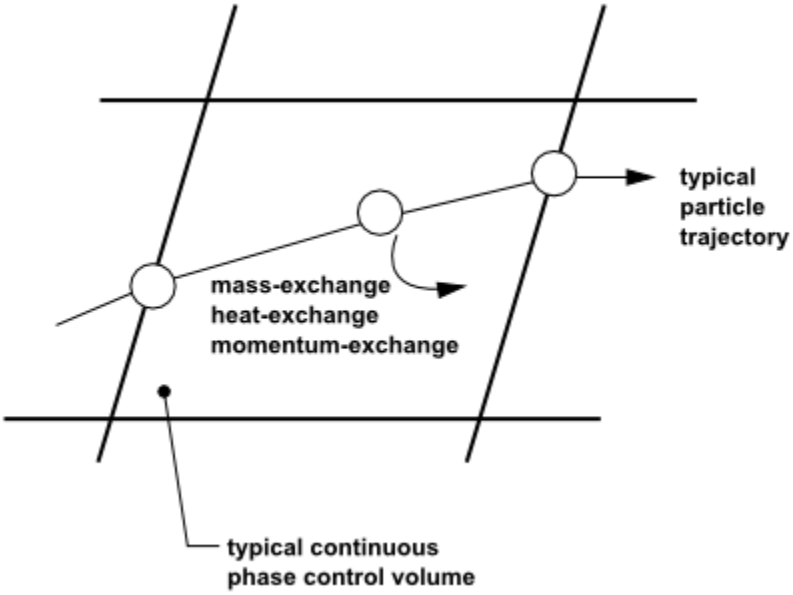


## 16.13.2. Momentum Exchange

The momentum transfer from the continuous phase to the discrete phase is computed in ANSYS Fluent by examining the change in momentum of a particle as it passes through each control volume in the ANSYS Fluent model. This momentum change is computed as

$$F = \sum \left( \frac{18\mu C_D Re}{\rho_p d_p^2 24} \left( u_p - u \right) + F_{other} \right) \dot{m}_p \Delta t \tag{16.328}$$

where

$\mu$ = viscosity of the fluid

$\rho_p$ = density of the particle

$d_p$ = diameter of the particle

$\mathrm{Re}$ = relative Reynolds number

Release 15.0 - © SAS IP, Inc. All rights reserved. - Contains proprietary and confidential information of ANSYS, Inc. and its subsidiaries and affiliates.

$u_p$ = velocity of the particle

$u$ = velocity of the fluid

$C_D$ = drag coefficient

$\dot{m}_p$ = mass flow rate of the particles

$\Delta t$ = time step

$F_{other}$ = other interaction forces

This momentum exchange appears as a momentum source in the continuous phase momentum balance in any subsequent calculations of the continuous phase flow field and can be reported by ANSYS Fluent as described in Postprocessing for the Discrete Phase in the User's Guide.

## 16.13.3. Heat Exchange

The heat transfer from the continuous phase to the discrete phase is computed in ANSYS Fluent by examining the change in thermal energy of a particle as it passes through each control volume in the ANSYS Fluent model. In the absence of a chemical reaction (that is, for all particle laws except Law 5) the heat exchange is computed as

$$Q = \frac{\dot{m}_{p,0}}{m_{p,0}} \left[ \left( m_{p_{in}} - m_{p_{out}} \right) \left[ -H_{lat_{ref}} + H_{pyrol} \right] - m_{p_{out}} \int_{T_{ref}}^{T_{p_{out}}} c_{p_p} dT + m_{p_{in}} \int_{T_{ref}}^{T_{p_{in}}} c_{p_p} dT \right] \tag{16.329}$$

where

$\dot{m}_{p,0}$ = initial mass flow rate of the particle injection (kg/s)

$m_{p,0}$ = initial mass of the particle (kg)

$m_{p_{in}}$ = mass of the particle on cell entry (kg)

$m_{p_{out}}$ = mass of the particle on cell exit (kg)

$c_{p_p}$ = heat capacity of the particle (J/kg-K)

$H_{pyrol}$ = heat of pyrolysis as volatiles are evolved (J/kg)

$T_{p_{in}}$ = temperature of the particle on cell entry (K)

$T_{p_{out}}$ = temperature of the particle on cell exit (K)

$T_{ref}$ = reference temperature for enthalpy (K)

$H_{lat_{ref}}$ = latent heat at reference conditions (J/kg)

The latent heat at the reference conditions $H_{lat_{ref}}$ for droplet particles is computed as the difference of the liquid and gas standard formation enthalpies, and can be related to the latent heat at the boiling point as follows:


Release 15.0 - © SAS IP, Inc. All rights reserved. - Contains proprietary and confidential information of ANSYS, Inc. and its subsidiaries and affiliates.

$$H_{lat_{ref}} = H_{lat} - \int_{T_{ref}}^{T_{bp}} c_{p_g} dT + \int_{T_{ref}}^{T_{bp}} c_{p_p} dT \tag{16.330}$$

where

$c_{p_g}$ = heat capacity of gas product species (J/kg-K)

$T_{bp}$ = boiling point temperature (K)

$H_{lat}$ = latent heat at the boiling point temperature (J/kg)

For the volatile part of the combusting particles, some constraints are applied to ensure that the enthalpy source terms do not depend on the particle history. The formulation should be consistent with the mixing of two gas streams, one consisting of the fluid and the other consisting of the volatiles. Hence $H_{pyrol_{ref}}$ is derived by applying a correction to $H_{pyrol}$, which accounts for different heat capacities in the particle and gaseous phase:

$$H_{pyrol_{ref}} = H_{pyrol} - \int_{T_{ref}}^{T_{p,init}} c_{p_g} dT + \int_{T_{ref}}^{T_{p,init}} c_{p_p} dT \tag{16.331}$$

where

$T_{p,init}$ = particle initial temperature (K)

## 16.13.4. Mass Exchange

The mass transfer from the discrete phase to the continuous phase is computed in ANSYS Fluent by examining the change in mass of a particle as it passes through each control volume in the ANSYS Fluent model. The mass change is computed simply as

$$M = \frac{\Delta m_p}{m_{p,0}} \dot{m}_{p,0} \tag{16.332}$$

This mass exchange appears as a source of mass in the continuous phase continuity equation and as a source of a chemical species defined by you. The mass rates per cell (in kg/s) are included in any subsequent calculations of the continuous phase flow field and are reported by ANSYS Fluent as described in Postprocessing for the Discrete Phase in the User's Guide.

## 16.13.5. Under-Relaxation of the Interphase Exchange Terms

Note that the interphase exchange of momentum, heat, and mass is under-relaxed during the calculation, so that

$$F_{new} = F_{old} + \alpha \left( F_{calculated} - F_{old} \right) \tag{16.333}$$

$$Q_{new} = Q_{old} + \alpha \left( Q_{calculated} - Q_{old} \right) \tag{16.334}$$

$$M_{new} = M_{old} + \alpha \left( M_{calculated} - M_{old} \right) \tag{16.335}$$

where $\alpha$ is the under-relaxation factor for particles/droplets. The default value for $\alpha$ is 0.5. This value may be reduced to improve the stability of coupled calculations. Note that the value of $\alpha$ does not influence the predictions obtained in the final converged solution.

Release 15.0 - © SAS IP, Inc. All rights reserved. - Contains proprietary and confidential information of ANSYS, Inc. and its subsidiaries and affiliates.

Two options exist when updating the new particle source terms $F_{new}$, $Q_{new}$ and $M_{new}$. The first option is to compute the new source terms and the particle source terms, $F_{calculated}$, $Q_{calculated}$ and $M_{calculated}$, at the same time. The second option is to update the new source terms, $F_{new}$, $Q_{new}$ and $M_{new}$, every flow iteration, while the particle source terms, $F_{calculated}$, $Q_{calculated}$ and $M_{calculated}$, are calculated every Discrete Phase Model iteration. The latter option is recommended for transient flows, where the particles are updated once per flow time step.

Figure 16.17: Effect of Number of Source Term Updates on Source Term Applied to Flow Equations (p. 462) shows how the source term, $S$, when applied to the flow equations, changes with the number of updates for varying under-relaxation factors. In Figure 16.17: Effect of Number of Source Term Updates on Source Term Applied to Flow Equations (p. 462), $S_\infty$ is the final source term for which a value is reached after a certain number of updates and $S_0$ is the initial source term at the start of the computation. The value of $S_0$ is typically zero at the beginning of the calculation.

**Figure 16.17: Effect of Number of Source Term Updates on Source Term Applied to Flow Equations**

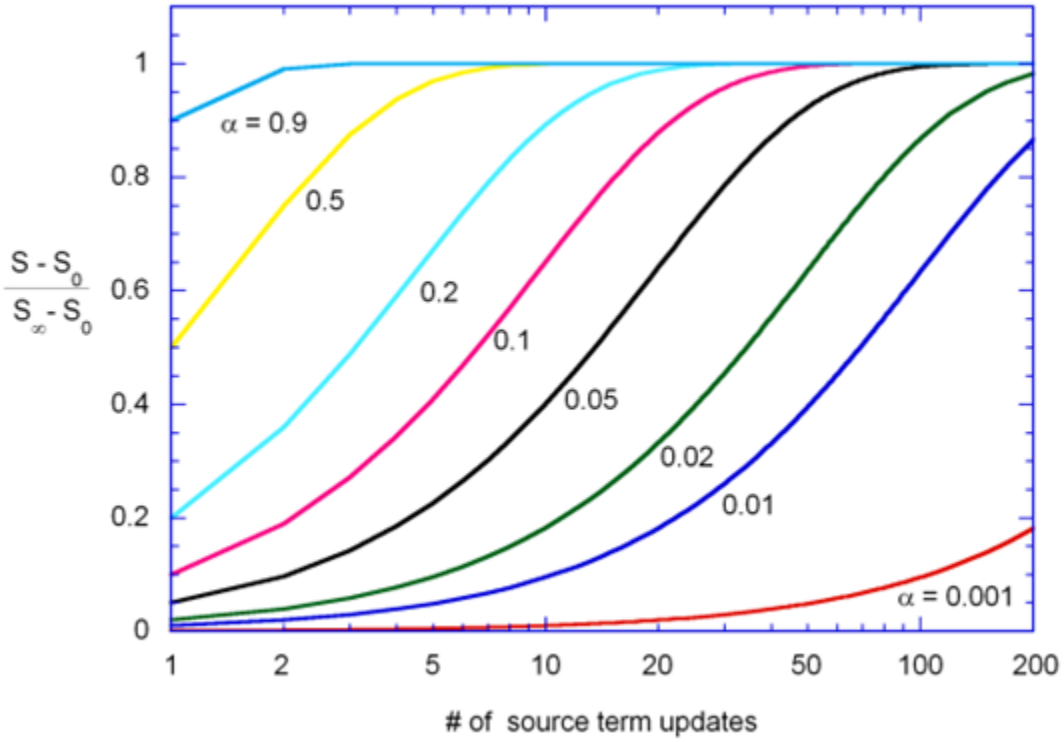


Figure 16.17: Effect of Number of Source Term Updates on Source Term Applied to Flow Equations (p. 462) can be applied to this option as well. Keep in mind that the DPM source terms are updated every continuous flow iteration.

## 16.13.6. Interphase Exchange During Stochastic Tracking

When stochastic tracking is performed, the interphase exchange terms, computed via Equation 16.328 (p. 459) to Equation 16.335 (p. 461), are computed for each stochastic trajectory with the particle mass flow rate, $\dot{m}_{p0}$, divided by the number of stochastic tracks computed. This implies that an equal mass flow of particles follows each stochastic trajectory.


Release 15.0 - © SAS IP, Inc. All rights reserved. - Contains proprietary and confidential information of ANSYS, Inc. and its subsidiaries and affiliates.

## 16.13.7. Interphase Exchange During Cloud Tracking

When the particle cloud model is used, the interphase exchange terms are computed via Equation 16.328 (p. 459) to Equation 16.335 (p. 461) based on ensemble-averaged flow properties in the particle cloud. The exchange terms are then distributed to all the cells in the cloud based on the weighting factor defined in Equation 16.49 (p. 382).

# 16.14. Node Based Averaging

Various DPM parcel quantities can affect the continuous fluid flow by being integrated into the flow solver equations. By default, ANSYS Fluent applies the effects of a DPM parcel only to the fluid cell that contains the parcel. As an alternative, mesh node averaging can be used to distribute the parcel's effects to neighboring mesh nodes. This reduces the grid dependency of DPM simulations, since the parcel's effects on the flow solver are distributed more smoothly across neighboring cells.

A variable $\varphi$ is averaged on a mesh node using the following equation:

$$\bar{\varphi}_{node} = \sum_k N_{in\,parcel} w\left(\vec{x}^{\,k}_p - \vec{x}_{node}\right)\varphi_p \tag{16.336}$$

Here $\varphi_p$ is the particle variable, $N_{in\,parcel}$ is the number in the parcel, and $\bar{\varphi}_{node}$ is the accumulation of the particle variable on the node for all parcels $k$. The function $w$ is a weighting function, or "kernel."

The following kernels are available in ANSYS Fluent:

- **nodes-per-cell**

$$w_k\left(\vec{x}^{\,k}_p - \vec{x}_{node}\right) = \frac{1}{n_{nodes}} \tag{16.337}$$

- **shortest-distance**

$$w_k\left(\vec{x}^{\,k}_p - \vec{x}_{node}\right) = \frac{1 - \dfrac{\left|\vec{x}^{\,k}_p - \vec{x}_{node}\right|}{\sum_i \left|\vec{x}^{\,i}_p - \vec{x}_{node}\right|}}{\sum_j \left(1 - \dfrac{\left|\vec{x}^{\,j}_p - \vec{x}_{node}\right|}{\sum_i \left|\vec{x}^{\,i}_p - \vec{x}_{node}\right|}\right)} \tag{16.338}$$

- **inverse-distance**

$$w_k\left(\vec{x}^{\,k}_p - \vec{x}_{node}\right) = \frac{\dfrac{1}{\left|\vec{x}^{\,k}_p - \vec{x}_{node}\right|}}{\sum_i \left(\dfrac{1}{\left|\vec{x}^{\,i}_p - \vec{x}_{node}\right|}\right)} \tag{16.339}$$

- **gaussian**

Release 15.0 - © SAS IP, Inc. All rights reserved. - Contains proprietary and confidential information of ANSYS, Inc. and its subsidiaries and affiliates.

$$w\left(\vec{x}_p^{\,k}-\vec{x}_{node}\right)=\left(\frac{a}{\pi}\right)^{3/2}\exp\left(-a\frac{\left|\vec{x}_p^{\,k}-\vec{x}_{node}\right|^2}{\Delta x^2}\right) \tag{16.340}$$

where $\Delta x$ is a characteristic length scale of the cell containing the parcel.

For the Gaussian kernel, an additional parameter $a$ is necessary to control the width of the Gaussian distribution. Kaufmann et al. [199] (p. 740) had good success with a small width and using $a=6$, while Apte et al. [11] (p. 729) used a broad distribution and a value of $a=0.5$. The default value is $a=1$.

For information on using node based averaging, refer to Node Based Averaging of Particle Data in the User's Guide.


Release 15.0 - © SAS IP, Inc. All rights reserved. - Contains proprietary and confidential information of ANSYS, Inc. and its subsidiaries and affiliates.

# Chapter 17: Multiphase Flows

This chapter discusses the general multiphase models that are available in ANSYS Fluent. Introduction (p. 465) provides a brief introduction to multiphase modeling, Discrete Phase (p. 373) discusses the Lagrangian dispersed phase model, and Solidification and Melting (p. 601) describes ANSYS Fluent's model for solidification and melting. For information about using the general multiphase models in ANSYS Fluent, see Modeling Multiphase Flows in the User's Guide. Information about the various theories behind the multiphase models is presented in the following sections:


17.1. Introduction
17.2. Choosing a General Multiphase Model
17.3. Volume of Fluid (VOF) Model Theory
17.4. Mixture Model Theory
17.5. Eulerian Model Theory
17.6. Wet Steam Model Theory
17.7. Modeling Mass Transfer in Multiphase Flows
17.8. Modeling Species Transport in Multiphase Flows


## 17.1. Introduction

A large number of flows encountered in nature and technology are a mixture of phases. Physical phases of matter are gas, liquid, and solid, but the concept of phase in a multiphase flow system is applied in a broader sense. In multiphase flow, a phase can be defined as an identifiable class of material that has a particular inertial response to and interaction with the flow and the potential field in which it is immersed. For example, different-sized solid particles of the same material can be treated as different phases because each collection of particles with the same size will have a similar dynamical response to the flow field.

Information is organized into the following subsections:


17.1.1. Multiphase Flow Regimes
17.1.2. Examples of Multiphase Systems


### 17.1.1. Multiphase Flow Regimes

Multiphase flow regimes can be grouped into four categories: gas-liquid or liquid-liquid flows; gas-solid flows; liquid-solid flows; and three-phase flows.

#### *17.1.1.1. Gas-Liquid or Liquid-Liquid Flows*

The following regimes are gas-liquid or liquid-liquid flows:

- Bubbly flow: This is the flow of discrete gaseous or fluid bubbles in a continuous fluid.
- Droplet flow: This is the flow of discrete fluid droplets in a continuous gas.
- Slug flow: This is the flow of large bubbles in a continuous fluid.
- Stratified/free-surface flow: This is the flow of immiscible fluids separated by a clearly-defined interface.


Release 15.0 - © SAS IP, Inc. All rights reserved. - Contains proprietary and confidential information of ANSYS, Inc. and its subsidiaries and affiliates.

See Figure 17.1: Multiphase Flow Regimes (p. 467) for illustrations of these regimes.

#### 17.1.1.2. Gas-Solid Flows

The following regimes are gas-solid flows:

- Particle-laden flow: This is flow of discrete particles in a continuous gas.
- Pneumatic transport: This is a flow pattern that depends on factors such as solid loading, Reynolds numbers, and particle properties. Typical patterns are dune flow, slug flow, and homogeneous flow.
- Fluidized bed: This consists of a vessel containing particles, into which a gas is introduced through a distributor. The gas rising through the bed suspends the particles. Depending on the gas flow rate, bubbles appear and rise through the bed, intensifying the mixing within the bed.

See Figure 17.1: Multiphase Flow Regimes (p. 467) for illustrations of these regimes.

#### 17.1.1.3. Liquid-Solid Flows

The following regimes are liquid-solid flows:

- Slurry flow: This flow is the transport of particles in liquids. The fundamental behavior of liquid-solid flows varies with the properties of the solid particles relative to those of the liquid. In slurry flows, the Stokes number (see Equation 17.4 (p. 471)) is normally less than 1. When the Stokes number is larger than 1, the characteristic of the flow is liquid-solid fluidization.
- Hydrotransport: This describes densely-distributed solid particles in a continuous liquid.
- Sedimentation: This describes a tall column initially containing a uniform dispersed mixture of particles. At the bottom, the particles will slow down and form a sludge layer. At the top, a clear interface will appear, and in the middle a constant settling zone will exist.

See Figure 17.1: Multiphase Flow Regimes (p. 467) for illustrations of these regimes.

#### 17.1.1.4. Three-Phase Flows

Three-phase flows are combinations of the other flow regimes listed in the previous sections.


Release 15.0 - © SAS IP, Inc. All rights reserved. - Contains proprietary and confidential information of ANSYS, Inc. and its subsidiaries and affiliates.

**Figure 17.1: Multiphase Flow Regimes**

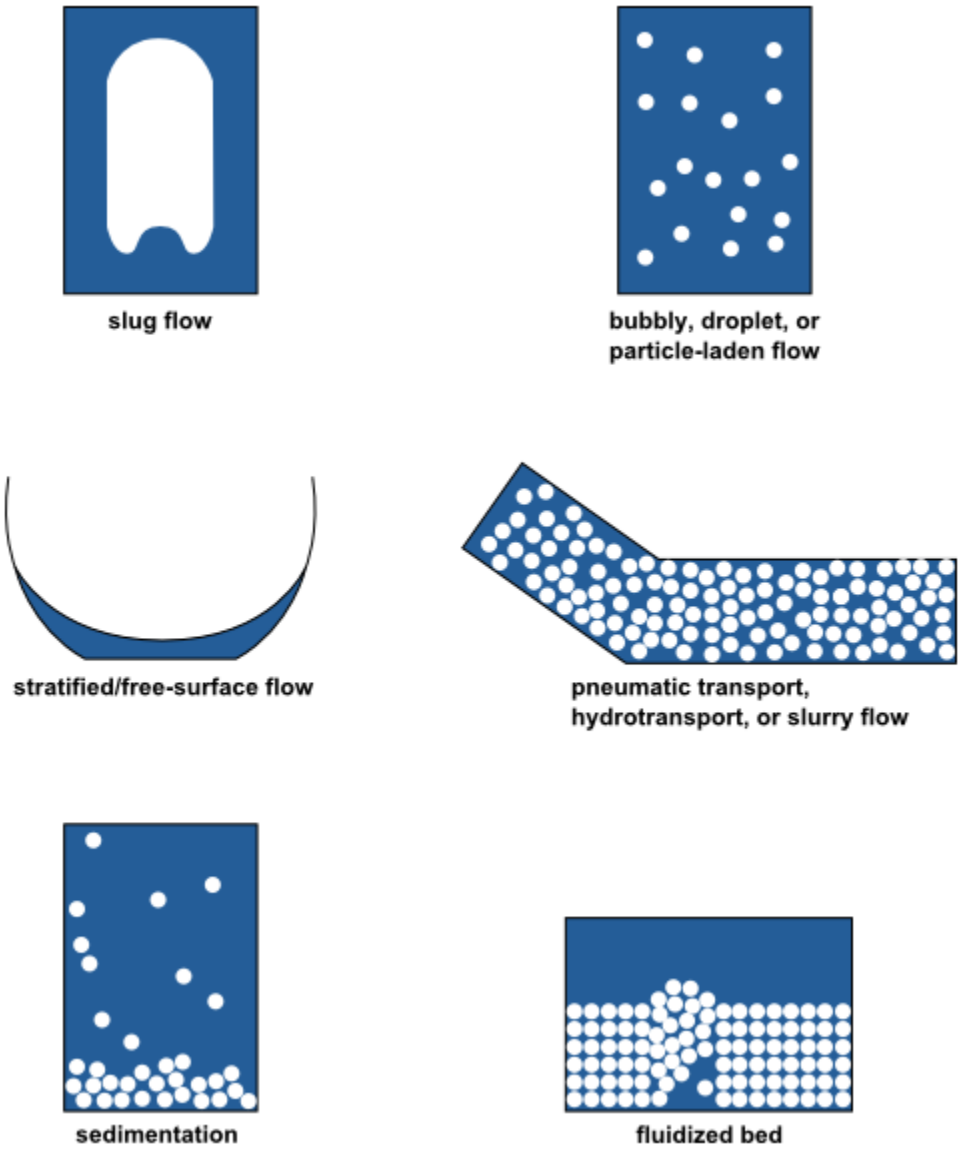


## 17.1.2. Examples of Multiphase Systems

Specific examples of each regime described in Multiphase Flow Regimes (p. 465) are listed below:

- Bubbly flow examples include absorbers, aeration, air lift pumps, cavitation, evaporators, flotation, and scrubbers.
- Droplet flow examples include absorbers, atomizers, combustors, cryogenic pumping, dryers, evaporation, gas cooling, and scrubbers.
- Slug flow examples include large bubble motion in pipes or tanks.
- Stratified/free-surface flow examples include sloshing in offshore separator devices and boiling and condensation in nuclear reactors.
- Particle-laden flow examples include cyclone separators, air classifiers, dust collectors, and dust-laden environmental flows.

Release 15.0 - © SAS IP, Inc. All rights reserved. - Contains proprietary and confidential information
of ANSYS, Inc. and its subsidiaries and affiliates.

- Pneumatic transport examples include transport of cement, grains, and metal powders.
- Fluidized bed examples include fluidized bed reactors and circulating fluidized beds.
- Slurry flow examples include slurry transport and mineral processing
- Hydrotransport examples include mineral processing and biomedical and physiochemical fluid systems
- Sedimentation examples include mineral processing.

# 17.2. Choosing a General Multiphase Model

The first step in solving any multiphase problem is to determine which of the regimes described in Multiphase Flow Regimes (p. 465) best represents your flow. Model Comparisons (p. 469) provides some broad guidelines for determining appropriate models for each regime, and Detailed Guidelines (p. 470) provides details about how to determine the degree of interphase coupling for flows involving bubbles, droplets, or particles, and the appropriate model for different amounts of coupling.

Information is organized into the following subsections:

17.2.1. Approaches to Multiphase Modeling
17.2.2. Model Comparisons
17.2.3. Time Schemes in Multiphase Flow
17.2.4. Stability and Convergence

## 17.2.1. Approaches to Multiphase Modeling

Advances in computational fluid mechanics have provided the basis for further insight into the dynamics of multiphase flows. Currently there are two approaches for the numerical calculation of multiphase flows: the Euler-Lagrange approach (discussed in Introduction (p. 373)) and the Euler-Euler approach (discussed in the following section).

### *17.2.1.1. The Euler-Euler Approach*

In the Euler-Euler approach, the different phases are treated mathematically as interpenetrating continua. Since the volume of a phase cannot be occupied by the other phases, the concept of phasic volume fraction is introduced. These volume fractions are assumed to be continuous functions of space and time and their sum is equal to one. Conservation equations for each phase are derived to obtain a set of equations, which have similar structure for all phases. These equations are closed by providing constitutive relations that are obtained from empirical information, or, in the case of granular flows , by application of kinetic theory.

In ANSYS Fluent, three different Euler-Euler multiphase models are available: the volume of fluid (VOF) model, the mixture model, and the Eulerian model.

#### 17.2.1.1.1. The VOF Model

The VOF model (described in Volume of Fluid (VOF) Model Theory (p. 474)) is a surface-tracking technique applied to a fixed Eulerian mesh. It is designed for two or more immiscible fluids where the position of the interface between the fluids is of interest. In the VOF model, a single set of momentum equations is shared by the fluids, and the volume fraction of each of the fluids in each computational cell is tracked throughout the domain. Applications of the VOF model include stratified flows, free-surface flows, filling, sloshing, the motion of large bubbles in a liquid, the motion of liquid after a dam break, the prediction of jet breakup (surface tension), and the steady or transient tracking of any liquid-gas interface.


Release 15.0 - © SAS IP, Inc. All rights reserved. - Contains proprietary and confidential information of ANSYS, Inc. and its subsidiaries and affiliates.

#### 17.2.1.1.2. The Mixture Model

The mixture model (described in Mixture Model Theory (p. 500)) is designed for two or more phases (fluid or particulate). As in the Eulerian model, the phases are treated as interpenetrating continua. The mixture model solves for the mixture momentum equation and prescribes relative velocities to describe the dispersed phases. Applications of the mixture model include particle-laden flows with low loading, bubbly flows, sedimentation , and cyclone separators. The mixture model can also be used without relative velocities for the dispersed phases to model homogeneous multiphase flow.

#### 17.2.1.1.3. The Eulerian Model

The Eulerian model (described in Eulerian Model Theory (p. 511)) is the most complex of the multiphase models in ANSYS Fluent. It solves a set of $n$ momentum and continuity equations for each phase. Coupling is achieved through the pressure and interphase exchange coefficients. The manner in which this coupling is handled depends upon the type of phases involved; granular (fluid-solid) flows are handled differently than nongranular (fluid-fluid) flows. For granular flows, the properties are obtained from application of kinetic theory. Momentum exchange between the phases is also dependent upon the type of mixture being modeled. ANSYS Fluent's user-defined functions allow you to customize the calculation of the momentum exchange. Applications of the Eulerian multiphase model include bubble columns, risers, particle suspension, and fluidized beds.

### 17.2.2. Model Comparisons

In general, once you have determined the flow regime that best represents your multiphase system, you can select the appropriate model based on the following guidelines:

- For bubbly, droplet, and particle-laden flows in which the phases mix and/or dispersed-phase volume fractions exceed 10%, use either the mixture model (described in Mixture Model Theory (p. 500)) or the Eulerian model (described in Eulerian Model Theory (p. 511)).
- For slug flows, use the VOF model. See Volume of Fluid (VOF) Model Theory (p. 474) for more information about the VOF model.
- For stratified/free-surface flows, use the VOF model. See Volume of Fluid (VOF) Model Theory (p. 474) for more information about the VOF model.
- For pneumatic transport, use the mixture model for homogeneous flow (described in Mixture Model Theory (p. 500)) or the Eulerian model for granular flow (described in Eulerian Model Theory (p. 511)).
- For fluidized beds, use the Eulerian model for granular flow. See Eulerian Model Theory (p. 511) for more information about the Eulerian model.
- For slurry flows and hydrotransport, use the mixture or Eulerian model (described, respectively, in Mixture Model Theory (p. 500), Eulerian Model Theory (p. 511)).
- For sedimentation, use the Eulerian model. See Eulerian Model Theory (p. 511) for more information about the Eulerian model.
- For general, complex multiphase flows that involve multiple flow regimes, select the aspect of the flow that is of most interest, and choose the model that is most appropriate for that aspect of the flow. Note that the accuracy of results will not be as good as for flows that involve just one flow regime, since the model you use will be valid for only part of the flow you are modeling.

Release 15.0 - © SAS IP, Inc. All rights reserved. - Contains proprietary and confidential information of ANSYS, Inc. and its subsidiaries and affiliates.

As discussed in this section, the VOF model is appropriate for stratified or free-surface flows, and the mixture and Eulerian models are appropriate for flows in which the phases mix or separate and/or dispersed-phase volume fractions exceed 10%. (Flows in which the dispersed-phase volume fractions are less than or equal to 10% can be modeled using the discrete phase model described in Discrete Phase (p. 373).)

To choose between the mixture model and the Eulerian model, you should consider the following guidelines:

- If there is a wide distribution of the dispersed phases (that is, if the particles vary in size and the largest particles do not separate from the primary flow field), the mixture model may be preferable (that is, less computationally expensive). If the dispersed phases are concentrated just in portions of the domain, you should use the Eulerian model instead.
- If interphase drag laws that are applicable to your system are available (either within ANSYS Fluent or through a user-defined function), the Eulerian model can usually provide more accurate results than the mixture model. Even though you can apply the same drag laws to the mixture model, as you can for a non-granular Eulerian simulation, if the interphase drag laws are unknown or their applicability to your system is questionable, the mixture model may be a better choice. For most cases with spherical particles, the Schiller-Naumann law is more than adequate. For cases with non-spherical particles, a user-defined function can be used.
- If you want to solve a simpler problem, which requires less computational effort, the mixture model may be a better option, since it solves a smaller number of equations than the Eulerian model. If accuracy is more important than computational effort, the Eulerian model is a better choice. Keep in mind, however, that the complexity of the Eulerian model can make it less computationally stable than the mixture model.

ANSYS Fluent's multiphase models are compatible with ANSYS Fluent's dynamic mesh modeling feature. For more information on the dynamic mesh feature, see Flows Using Sliding and Dynamic Meshes (p. 33). For more information about how other ANSYS Fluent models are compatible with ANSYS Fluent's multiphase models, see Appendix A in the User's Guide.

### 17.2.2.1. Detailed Guidelines

For stratified and slug flows, the choice of the VOF model, as indicated in Model Comparisons (p. 469), is straightforward. Choosing a model for the other types of flows is less straightforward. As a general guide, there are some parameters that help to identify the appropriate multiphase model for these other flows: the particulate loading, $\beta$, and the Stokes number, St. (Note that the word "particle" is used in this discussion to refer to a particle, droplet, or bubble.)

#### 17.2.2.1.1. The Effect of Particulate Loading

Particulate loading has a major impact on phase interactions. The particulate loading is defined as the mass density ratio of the dispersed phase ($d$) to that of the carrier phase ($c$):

$$\beta = \frac{\alpha_d \rho_d}{\alpha_c \rho_c} \tag{17.1}$$

The material density ratio

$$\gamma = \frac{\rho_d}{\rho_c} \tag{17.2}$$


Release 15.0 - © SAS IP, Inc. All rights reserved. - Contains proprietary and confidential information of ANSYS, Inc. and its subsidiaries and affiliates.

is greater than 1000 for gas-solid flows, about 1 for liquid-solid flows, and less than 0.001 for gas-liquid flows.

Using these parameters it is possible to estimate the average distance between the individual particles of the particulate phase. An estimate of this distance has been given by Crowe et al. [79] (p. 733):

$$\frac{L}{d_d} = \left( \frac{\pi}{6} \frac{1+\kappa}{\kappa} \right)^{1/3} \tag{17.3}$$

where $\kappa = \frac{\beta}{\gamma}$. Information about these parameters is important for determining how the dispersed phase should be treated. For example, for a gas-particle flow with a particulate loading of 1, the interparticle space $\frac{L}{d_d}$ is about 8; the particle can therefore be treated as isolated (that is, very low particulate loading).

Depending on the particulate loading, the degree of interaction between the phases can be divided into the following three categories:

- For very low loading, the coupling between the phases is one-way (that is, the fluid carrier influences the particles via drag and turbulence, but the particles have no influence on the fluid carrier). The discrete phase (Discrete Phase (p. 373)), mixture, and Eulerian models can all handle this type of problem correctly. Since the Eulerian model is the most expensive, the discrete phase or mixture model is recommended.
- For intermediate loading, the coupling is two-way (that is, the fluid carrier influences the particulate phase via drag and turbulence, but the particles in turn influence the carrier fluid via reduction in mean momentum and turbulence). The discrete phase (Discrete Phase (p. 373)), mixture, and Eulerian models are all applicable in this case, but you need to take into account other factors in order to decide which model is more appropriate. See below for information about using the Stokes number as a guide.
- For high loading, there is two-way coupling plus particle pressure and viscous stresses due to particles (four-way coupling). Only the Eulerian model will handle this type of problem correctly.

#### 17.2.2.1.2. The Significance of the Stokes Number

For systems with intermediate particulate loading, estimating the value of the Stokes number can help you select the most appropriate model. The Stokes number can be defined as the relation between the particle response time and the system response time:

$$St = \frac{\tau_d}{t_s} \tag{17.4}$$

where $\tau_d = \frac{\rho_d d_d^2}{18\mu_c}$ and $t_s$ is based on the characteristic length ($L_s$) and the characteristic velocity ($V_s$) of the system under investigation: $t_s = \frac{L_s}{V_s}$.

For $St \ll 1.0$, the particle will follow the flow closely and any of the three models (discrete phase(Discrete Phase (p. 373)), mixture, or Eulerian) is applicable; you can therefore choose the least expensive (the mixture model, in most cases), or the most appropriate considering other factors. For $St > 1.0$, the particles will move independently of the flow and either the discrete phase model (Discrete Phase (p. 373)) or the Eulerian model is applicable. For $St \approx 1.0$, again any of the three models is applicable; you can choose the least expensive or the most appropriate considering other factors.

Release 15.0 - © SAS IP, Inc. All rights reserved. - Contains proprietary and confidential information of ANSYS, Inc. and its subsidiaries and affiliates.

#### *17.2.2.1.2.1. Examples*

For a coal classifier with a characteristic length of 1 m and a characteristic velocity of 10 m/s, the Stokes number is 0.04 for particles with a diameter of 30 microns, but 4.0 for particles with a diameter of 300 microns. Clearly the mixture model will not be applicable to the latter case.

For the case of mineral processing, in a system with a characteristic length of 0.2 m and a characteristic velocity of 2 m/s, the Stokes number is 0.005 for particles with a diameter of 300 microns. In this case, you can choose between the mixture and Eulerian models. The volume fractions are too high for the discrete phase model (Discrete Phase (p. 373)), as noted below.

### 17.2.2.1.3. Other Considerations

Keep in mind that the use of the discrete phase model (Discrete Phase (p. 373)) is limited to low volume fractions, unless you are using the dense discrete phase model formulation. In addition, for the discrete phase model simulation, you can choose many more advanced combustion models compared to the Eulerian models. To account for particle distributions, you will need to use the population balance models (see the Population Balance Module Manual) or the discrete phase model and the dense discrete phase model.

## 17.2.3. Time Schemes in Multiphase Flow

In many multiphase applications, the process can vary spatially as well as temporally. In order to accurately model multiphase flow, both higher-order spatial and time discretization schemes are necessary. In addition to the first-order time scheme in ANSYS Fluent, the second-order time scheme is available in the Mixture and Eulerian multiphase models, and with the VOF Implicit Scheme.

---

**Important**

The second-order time scheme cannot be used with the VOF Explicit Schemes.

---

The second-order time scheme has been adapted to all the transport equations, including mixture phase momentum equations, energy equations, species transport equations, turbulence models, phase volume fraction equations, the pressure correction equation, and the granular flow model. In multiphase flow, a general transport equation (similar to that of Equation 20.19 (p. 639)) may be written as

$$\frac{\partial(\alpha\rho\phi)}{\partial t} + \nabla\cdot(\alpha\rho\vec{V}\phi) = \nabla\cdot\overline{\overline{\tau}} + S_{\phi} \tag{17.5}$$

Where $\phi$ is either a mixture (for the mixture model) or a phase variable, $\alpha$ is the phase volume fraction (unity for the mixture equation), $\rho$ is the mixture phase density, $\vec{V}$ is the mixture or phase velocity (depending on the equations), $\overline{\overline{\tau}}$ is the diffusion term, and $S_{\phi}$ is the source term.

As a fully implicit scheme, this second-order time-accurate scheme achieves its accuracy by using an Euler backward approximation in time (see Equation 20.21 (p. 639)). The general transport equation, Equation 17.5 (p. 472) is discretized as


Release 15.0 - © SAS IP, Inc. All rights reserved. - Contains proprietary and confidential information of ANSYS, Inc. and its subsidiaries and affiliates.

$$\frac{3\left(\alpha_p\rho_p\phi_p Vol\right)^{n+1}-4\left(\alpha_p\rho_p\phi_p Vol\right)^{n}+\left(\alpha_p\rho_p\phi_p\right)^{n-1}}{2\Delta t}= \sum\left[A_{nb}\left(\phi_{nb}-\phi_p\right)\right]^{n+1}+S_U{}^{n+1}-S_p{}^{n+1}\phi_p{}^{n+1} \tag{17.6}$$

Equation 17.6 (p. 473) can be written in simpler form:

$$A_p\phi_p=\sum A_n b\phi_n b+S_\phi \tag{17.7}$$

where

$$A_p=\sum A_{nb}{}^{n+1}+S_p{}^{n+1}+\frac{1.5\left(\alpha_p\rho_p Vol\right)^{n+1}}{\Delta t}$$

$$S_\phi=S_U{}^{n+1}+\frac{2\left(\alpha_p\rho_p\phi_p Vol\right)^{n}-0.5\left(\alpha_p\rho_p\phi_p Vol\right)^{n-1}}{\Delta t}$$

This scheme is easily implemented based on ANSYS Fluent's existing first-order Euler scheme. It is unconditionally stable, however, the negative coefficient at the time level $t_{n-1}$, of the three-time level method, may produce oscillatory solutions if the time steps are large.

This problem can be eliminated if a bounded second-order scheme is introduced. However, oscillating solutions are most likely seen in compressible liquid flows. Therefore, in this version of ANSYS Fluent, a bounded second-order time scheme has been implemented for compressible liquid flows only. For single phase and multiphase compressible liquid flows, the second-order time scheme is, by default, the bounded scheme.

## 17.2.4. Stability and Convergence

The process of solving a multiphase system is inherently difficult and you may encounter some stability or convergence problems.

When solving a time-dependent problem, a proper initial field is required to avoid instabilities, which usually arise from poor initial fields. If the CPU time is a concern for transient problems, then the best option is to use PC SIMPLE. When body forces are significant, or if the solution requires higher order numerical schemes, it is recommended that you start with a small time step, which can be increased after performing a few time steps to get a better approximation of the pressure field.

For a steady solution, it is recommended that you use the Multiphase Coupled solver, described in detail in Coupled Solution for Eulerian Multiphase Flows in the User's Guide. The iterative nature of this solver requires a good starting patched field. If difficulties are encountered due to higher order schemes, or due to the complexities of the problem, you may need to reduce the Courant number. The default Courant number is 200 but it can be reduced to as low as 4. This can later be increased if the iteration process runs smoothly. In addition, there are explicit under-relaxation factors for velocities and pressure. All other under-relaxation factors are implicit. Lower under-relaxation factors for the volume fraction equation may delay the solution dramatically with the Coupled solver (any value 0.5 or above is adequate); on the contrary, PC SIMPLE would normally need a low under-relaxation for the volume fraction equation.

Release 15.0 - © SAS IP, Inc. All rights reserved. - Contains proprietary and confidential information of ANSYS, Inc. and its subsidiaries and affiliates.

In addition, ANSYS Fluent offers a Full Multiphase Coupled solver where all velocities, pressure correction and volume fraction correction are solved simultaneously, which currently is not as robust as the others.

Furthermore, ANSYS Fluent has an option to solve stratified immiscible fluids within the Eulerian multiphase formulation. This feature is similar to the single fluid VOF solution, but in the context of multiple velocities.

# 17.3. Volume of Fluid (VOF) Model Theory

Information is organized into the following subsections:

17.3.1. Overview of the VOF Model
17.3.2. Limitations of the VOF Model
17.3.3. Steady-State and Transient VOF Calculations
17.3.4. Volume Fraction Equation
17.3.5. Material Properties
17.3.6. Momentum Equation
17.3.7. Energy Equation
17.3.8. Additional Scalar Equations
17.3.9. Time Dependence
17.3.10. Surface Tension and Adhesion
17.3.11. Open Channel Flow
17.3.12. Open Channel Wave Boundary Conditions
17.3.13. Coupled Level-Set and VOF Model

## 17.3.1. Overview of the VOF Model

The VOF model can model two or more immiscible fluids by solving a single set of momentum equations and tracking the volume fraction of each of the fluids throughout the domain. Typical applications include the prediction of jet breakup, the motion of large bubbles in a liquid, the motion of liquid after a dam break, and the steady or transient tracking of any liquid-gas interface.

## 17.3.2. Limitations of the VOF Model

The following restrictions apply to the VOF model in ANSYS Fluent:

- You must use the pressure-based solver. The VOF model is not available with the density-based solver.
- All control volumes must be filled with either a single fluid phase or a combination of phases. The VOF model does not allow for void regions where no fluid of any type is present.
- Only one of the phases can be defined as a compressible ideal gas. There is no limitation on using compressible liquids using user-defined functions.
- Streamwise periodic flow (either specified mass flow rate or specified pressure drop) cannot be modeled when the VOF model is used.
- The second-order implicit time-stepping formulation cannot be used with the VOF explicit scheme.
- When tracking particles in parallel, the DPM model cannot be used with the VOF model if the shared memory option is enabled (Parallel Processing for the Discrete Phase Model in the User's Guide). (Note that using the message passing option, when running in parallel, enables the compatibility of all multiphase flow models with the DPM model.)


Release 15.0 - © SAS IP, Inc. All rights reserved. - Contains proprietary and confidential information of ANSYS, Inc. and its subsidiaries and affiliates.

## 17.3.3. Steady-State and Transient VOF Calculations

The VOF formulation in ANSYS Fluent is generally used to compute a time-dependent solution, but for problems in which you are concerned only with a steady-state solution, it is possible to perform a steady-state calculation. A steady-state VOF calculation is sensible only when your solution is independent of the initial conditions and there are distinct inflow boundaries for the individual phases. For example, since the shape of the free surface inside a rotating cup depends on the initial level of the fluid, such a problem must be solved using the time-dependent formulation. On the other hand, the flow of water in a channel with a region of air on top and a separate air inlet can be solved with the steady-state formulation.

The VOF formulation relies on the fact that two or more fluids (or phases) are not interpenetrating. For each additional phase that you add to your model, a variable is introduced: the volume fraction of the phase in the computational cell. In each control volume, the volume fractions of all phases sum to unity. The fields for all variables and properties are shared by the phases and represent volume-averaged values, as long as the volume fraction of each of the phases is known at each location. Thus the variables and properties in any given cell are either purely representative of one of the phases, or representative of a mixture of the phases, depending upon the volume fraction values. In other words, if the $q^{th}$ fluid's volume fraction in the cell is denoted as $\alpha_q$, then the following three conditions are possible:

- $\alpha_q = 0$: The cell is empty (of the $q^{th}$ fluid).
- $\alpha_q = 1$: The cell is full (of the $q^{th}$ fluid).
- $0 < \alpha_q < 1$: The cell contains the interface between the $q^{th}$ fluid and one or more other fluids.

Based on the local value of $\alpha_q$, the appropriate properties and variables will be assigned to each control volume within the domain.

## 17.3.4. Volume Fraction Equation

The tracking of the interface(s) between the phases is accomplished by the solution of a continuity equation for the volume fraction of one (or more) of the phases. For the $q^{th}$ phase, this equation has the following form:

$$\frac{1}{\rho_q}\left[\frac{\partial}{\partial t}\left(\alpha_q \rho_q\right) + \nabla \cdot \left(\alpha_q \rho_q \vec{v}_q\right) = S_{\alpha_q} + \sum_{p=1}^{n}\left(\dot{m}_{pq} - \dot{m}_{qp}\right)\right] \tag{17.8}$$

where $\dot{m}_{qp}$ is the mass transfer from phase $q$ to phase $p$ and $\dot{m}_{pq}$ is the mass transfer from phase $p$ to phase $q$. By default, the source term on the right-hand side of Equation 17.8 (p. 475), $S_{\alpha_q}$, is zero, but you can specify a constant or user-defined mass source for each phase. See Modeling Mass Transfer in Multiphase Flows (p. 579) for more information on the modeling of mass transfer in ANSYS Fluent's general multiphase models.

The volume fraction equation will not be solved for the primary phase; the primary-phase volume fraction will be computed based on the following constraint:

Release 15.0 - © SAS IP, Inc. All rights reserved. - Contains proprietary and confidential information of ANSYS, Inc. and its subsidiaries and affiliates.

$$\sum_{q=1}^{n} \alpha_q = 1 \tag{17.9}$$

The volume fraction equation may be solved either through implicit or explicit time discretization.

### 17.3.4.1. The Implicit Scheme

When the implicit scheme is used for time discretization, ANSYS Fluent's standard finite-difference interpolation schemes, **QUICK**, **Second Order Upwind** and **First Order Upwind**, and the **Modified HRIC** schemes, are used to obtain the face fluxes for all cells, including those near the interface.

$$\frac{\alpha_q^{n+1}\rho_q^{n+1} - \alpha_q^n \rho_q^n}{\Delta t} V + \sum_f \left( \rho_q^{n+1} U_f^{n+1} \alpha_{q,f}^{n+1} \right) = \left[ S_{\alpha_q} + \sum_{p=1}^{n} \left( \dot{m}_{pq} - \dot{m}_{qp} \right) \right] V \tag{17.10}$$

Since this equation requires the volume fraction values at the current time step (rather than at the previous step, as for the explicit scheme), a standard scalar transport equation is solved iteratively for each of the secondary-phase volume fractions at each time step.

The implicit scheme can be used for both time-dependent and steady-state calculations. See Choosing a Volume Fraction Formulation in the User's Guide for details.

### 17.3.4.2. The Explicit Scheme

In the explicit approach, ANSYS Fluent's standard finite-difference interpolation schemes are applied to the volume fraction values that were computed at the previous time step.

$$\frac{\alpha_q^{n+1}\rho_q^{n+1} - \alpha_q^n \rho_q^n}{\Delta t} V + \sum_f \left( \rho_q U_f^n \alpha_{q,f}^n \right) = \left[ \sum_{p=1}^{n} \left( \dot{m}_{pq} - \dot{m}_{qp} \right) + S_{\alpha_q} \right] V \tag{17.11}$$

where

$n+1$ = index for new (current) time step

$n$ = index for previous time step

$\alpha_{q,f}$ = face value of the $q^{th}$ volume fraction, computed from the first- or second-order upwind, QUICK, modified HRIC, compressive, or CICSAM scheme

$V$ = volume of cell

$U_f$ = volume flux through the face, based on normal velocity

This formulation does not require iterative solution of the transport equation during each time step, as is needed for the implicit scheme.

**Important**

When the explicit scheme is used, a time-dependent solution must be computed.

When the explicit scheme is used for time discretization, the face fluxes can be interpolated either using interface reconstruction or using a finite volume discretization scheme (Interpolation Near the Interface (p. 477)). The schemes available in ANSYS Fluent for the explicit formulation are discussed in Explicit Schemes in the User's Guide.


Release 15.0 - © SAS IP, Inc. All rights reserved. - Contains proprietary and confidential information of ANSYS, Inc. and its subsidiaries and affiliates.

### 17.3.4.3. Interpolation Near the Interface

ANSYS Fluent's control-volume formulation requires that convection and diffusion fluxes through the control volume faces be computed and balanced with source terms within the control volume itself.

In the geometric reconstruction and donor-acceptor schemes, ANSYS Fluent applies a special interpolation treatment to the cells that lie near the interface between two phases. Figure 17.2: Interface Calculations (p. 477) shows an actual interface shape along with the interfaces assumed during computation by these two methods.

**Figure 17.2: Interface Calculations**

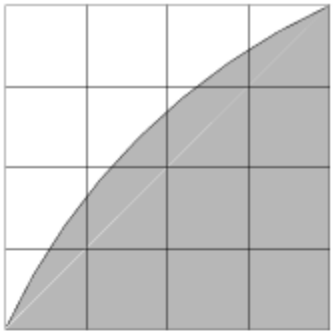

actual interface shape

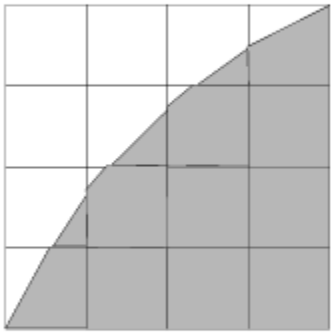

interface shape represented by the geometric reconstruction (piecewise-linear) scheme

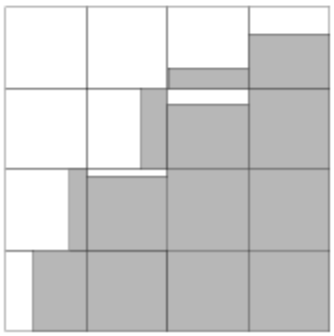

interface shape represented by the donor-acceptor scheme

The explicit scheme and the implicit scheme treat these cells with the same interpolation as the cells that are completely filled with one phase or the other (that is, using the standard upwind (First-Order Upwind Scheme (p. 633)), second-order (Second-Order Upwind Scheme (p. 634)), QUICK (QUICK Scheme (p. 636)), modified HRIC (Modified HRIC Scheme (p. 638)), compressive (The Compressive and Zonal Discretization Schemes (p. 479)), or CICSAM scheme (The Compressive Interface Capturing Scheme for Arbitrary Meshes (CICSAM) (p. 479)), rather than applying a special treatment.

Release 15.0 - © SAS IP, Inc. All rights reserved. - Contains proprietary and confidential information of ANSYS, Inc. and its subsidiaries and affiliates.

#### 17.3.4.3.1. The Geometric Reconstruction Scheme

In the geometric reconstruction approach, the standard interpolation schemes that are used in ANSYS Fluent are used to obtain the face fluxes whenever a cell is completely filled with one phase or another. When the cell is near the interface between two phases, the geometric reconstruction scheme is used.

The geometric reconstruction scheme represents the interface between fluids using a piecewise-linear approach. In ANSYS Fluent this scheme is the most accurate and is applicable for general unstructured meshes. The geometric reconstruction scheme is generalized for unstructured meshes from the work of Youngs [504] (p. 756). It assumes that the interface between two fluids has a linear slope within each cell, and uses this linear shape for calculation of the advection of fluid through the cell faces. (See Figure 17.2: Interface Calculations (p. 477).)

The first step in this reconstruction scheme is calculating the position of the linear interface relative to the center of each partially-filled cell, based on information about the volume fraction and its derivatives in the cell. The second step is calculating the advecting amount of fluid through each face using the computed linear interface representation and information about the normal and tangential velocity distribution on the face. The third step is calculating the volume fraction in each cell using the balance of fluxes calculated during the previous step.

---

**Important**

When the geometric reconstruction scheme is used, a time-dependent solution must be computed. Also, if you are using a conformal mesh (that is, if the mesh node locations are identical at the boundaries where two subdomains meet), you must ensure that there are no two-sided (zero-thickness) walls within the domain. If there are, you will need to slit them, as described in Slitting Face Zones in the User's Guide.

---

#### 17.3.4.3.2. The Donor-Acceptor Scheme

In the donor-acceptor approach, the standard interpolation schemes that are used in ANSYS Fluent are used to obtain the face fluxes whenever a cell is completely filled with one phase or another. When the cell is near the interface between two phases, a "donor-acceptor" scheme is used to determine the amount of fluid advected through the face [165] (p. 738). This scheme identifies one cell as a donor of an amount of fluid from one phase and another (neighbor) cell as the acceptor of that same amount of fluid, and is used to prevent numerical diffusion at the interface. The amount of fluid from one phase that can be convected across a cell boundary is limited by the minimum of two values: the filled volume in the donor cell or the free volume in the acceptor cell.

The orientation of the interface is also used in determining the face fluxes. The interface orientation is either horizontal or vertical, depending on the direction of the volume fraction gradient of the $q^{th}$ phase within the cell, and that of the neighbor cell that shares the face in question. Depending on the interface's orientation as well as its motion, flux values are obtained by pure upwinding, pure downwinding, or some combination of the two.

---

**Important**

When the donor-acceptor scheme is used, a time-dependent solution must be computed. Also, the donor-acceptor scheme can be used only with quadrilateral or hexahedral meshes. In addition, if you are using a conformal mesh (that is, if the mesh node locations are identical at the boundaries where two subdomains meet), you must ensure that there are


Release 15.0 - © SAS IP, Inc. All rights reserved. - Contains proprietary and confidential information of ANSYS, Inc. and its subsidiaries and affiliates.

no two-sided (zero-thickness) walls within the domain. If there are, you will need to slit them, as described in Slitting Face Zones in the User's Guide.

### 17.3.4.3.3. The Compressive Interface Capturing Scheme for Arbitrary Meshes (CICSAM)

The compressive interface capturing scheme for arbitrary meshes (CICSAM), based on Ubbink's work [457] (p. 754), is a high resolution differencing scheme. The CICSAM scheme is particularly suitable for flows with high ratios of viscosities between the phases. CICSAM is implemented in ANSYS Fluent as an explicit scheme and offers the advantage of producing an interface that is almost as sharp as the geometric reconstruction scheme.

### 17.3.4.3.4. The Compressive and Zonal Discretization Schemes

The compressive scheme is a second order reconstruction scheme based on the slope limiter. The theory below is applicable to zonal discretization and the phase localized compressive scheme, which use the framework of the compressive scheme.

$$\phi_f = \phi_d + \beta \nabla \phi_d \tag{17.12}$$

where

$\varphi_f$ is the face VOF value

$\varphi_d$ is the donor cell VOF value

$\beta$ is the slope limiter value

$\nabla \varphi_d$ is the donor cell VOF gradient value

- The slope limiter for the compressive scheme $\beta$ is bound between 0 and 2. This scheme is available for the VOF model, for both the implicit and explicit volume fraction schemes. It is also available for the Eulerian multiphase model when the explicit scheme for the volume fraction is selected. Note that the compressive scheme can be made available for the Eulerian multiphase model when the implicit volume fraction scheme is selected as described in Implicit Schemes in the User's Guide.
- The slope limiter for the zonal discretization and phase localized compressive schemes can be summarized in the table below:

**Table 17.1: Slope Limiter Discretization Scheme**

| **Slope Limiter Value** $\beta$ | **Scheme** |
|---|---|
| 0 | first order upwind |
| 1 | second order reconstruction bounded by the global minimum/maximum of the volume fraction |
| 2 | compressive |

Release 15.0 - © SAS IP, Inc. All rights reserved. - Contains proprietary and confidential information of ANSYS, Inc. and its subsidiaries and affiliates.

| Slope Limiter Value $\beta$ | Scheme |
|---|---|
| $0<\beta<1$ and $1<\beta<2$ | blended: where a value between 0 and 1 means blending of the first order and second order and a value between 1 and 2 means blending of the second order and compressive scheme |

**Note**

1. $\beta=0$ represents the first order upwind scheme described in First-Order Upwind Scheme (p. 633).
2. $\beta=1$ is analogous to the second order upwind scheme (Second-Order Upwind Scheme (p. 634)), where the slope limiter is bounded between 0 and 1.
3. $\beta=2$ represents the compressive scheme described above, where the slope limiter is bounded between 0 and 2.

- The slope limiter for the phase localized compressive scheme is calculated based on the specified values of the interfacial slope limiters.

#### 17.3.4.3.5. Bounded Gradient Maximization (BGM)

The BGM scheme is introduced to obtain sharp interfaces with the VOF model, comparable to that obtained by the Geometric Reconstruction scheme. Currently this scheme is available only with the steady state solver and cannot be used for transient problems. In the BGM scheme, discretization occurs in such a way so as to maximize the local value of the gradient, by maximizing the degree to which the face value is weighted towards the extrapolated downwind value [475] (p. 755).

## 17.3.5. Material Properties

The properties appearing in the transport equations are determined by the presence of the component phases in each control volume. In a two-phase system, for example, if the phases are represented by the subscripts 1 and 2, and if the volume fraction of the second of these is being tracked, the density in each cell is given by

$$\rho=\alpha_2\rho_2+(1-\alpha_2)\rho_1 \tag{17.13}$$

In general, for an $n$-phase system, the volume-fraction-averaged density takes on the following form:

$$\rho=\sum\alpha_q\rho_q \tag{17.14}$$

All other properties (for example, viscosity) are computed in this manner.

## 17.3.6. Momentum Equation

A single momentum equation is solved throughout the domain, and the resulting velocity field is shared among the phases. The momentum equation, shown below, is dependent on the volume fractions of all phases through the properties $\rho$ and $\mu$.

$$\frac{\partial}{\partial t}(\rho\vec{v})+\nabla\cdot(\rho\vec{v}\,\vec{v})=-\nabla p+\nabla\cdot\left[\mu\left(\nabla\vec{v}+\nabla\vec{v}^{\,T}\right)\right]+\rho\vec{g}+\vec{F} \tag{17.15}$$


Release 15.0 - © SAS IP, Inc. All rights reserved. - Contains proprietary and confidential information of ANSYS, Inc. and its subsidiaries and affiliates.

One limitation of the shared-fields approximation is that in cases where large velocity differences exist between the phases, the accuracy of the velocities computed near the interface can be adversely affected.

Note that if the viscosity ratio is more than $1x10^3$, this may lead to convergence difficulties. The compressive interface capturing scheme for arbitrary meshes (CICSAM) (The Compressive Interface Capturing Scheme for Arbitrary Meshes (CICSAM) (p. 479)) is suitable for flows with high ratios of viscosities between the phases, therefore solving the problem of poor convergence.

## 17.3.7. Energy Equation

The energy equation, also shared among the phases, is shown below.

$$\frac{\partial}{\partial t}(\rho E) + \nabla \cdot (\vec{v}(\rho E + p)) = \nabla \cdot \left(k_{eff} \nabla T\right) + S_h \tag{17.16}$$

The VOF model treats energy, $E$, and temperature, $T$, as mass-averaged variables:

$$E = \frac{\sum_{q=1}^{n} \alpha_q \rho_q E_q}{\sum_{q=1}^{n} \alpha_q \rho_q} \tag{17.17}$$

where $E_q$ for each phase is based on the specific heat of that phase and the shared temperature.

The properties $\rho$ and $k_{eff}$ (effective thermal conductivity) are shared by the phases. The source term, $S_h$, contains contributions from radiation, as well as any other volumetric heat sources.

As with the velocity field, the accuracy of the temperature near the interface is limited in cases where large temperature differences exist between the phases. Such problems also arise in cases where the properties vary by several orders of magnitude. For example, if a model includes liquid metal in combination with air, the conductivities of the materials can differ by as much as four orders of magnitude. Such large discrepancies in properties lead to equation sets with anisotropic coefficients, which in turn can lead to convergence and precision limitations.

## 17.3.8. Additional Scalar Equations

Depending upon your problem definition, additional scalar equations may be involved in your solution. In the case of turbulence quantities, a single set of transport equations is solved, and the turbulence variables (for example, $k$ and $\varepsilon$ or the Reynolds stresses) are shared by the phases throughout the field.

## 17.3.9. Time Dependence

For time-dependent VOF calculations, Equation 17.8 (p. 475) is solved using an explicit time-marching scheme. ANSYS Fluent automatically refines the time step for the integration of the volume fraction equation, but you can influence this time step calculation by modifying the Courant number. You can choose to update the volume fraction once for each time step, or once for each iteration within each time step. These options are discussed in more detail in Setting Time-Dependent Parameters for the VOF Model in the User's Guide.

## 17.3.10. Surface Tension and Adhesion

The VOF model can also include the effects of surface tension along the interface between each pair of phases. The model can be augmented by the additional specification of the contact angles between

Release 15.0 - © SAS IP, Inc. All rights reserved. - Contains proprietary and confidential information of ANSYS, Inc. and its subsidiaries and affiliates.

the phases and the walls, as well as the at porous jumps. You can specify a surface tension coefficient as a constant, as a function of temperature through a polynomial, or as a function of any variable through a UDF. The solver will include the additional tangential stress terms (causing what is termed as Marangoni convection) that arise due to the variation in surface tension coefficient. Variable surface tension coefficient effects are usually important only in zero/near-zero gravity conditions.

## 17.3.10.1. Surface Tension

Surface tension arises as a result of attractive forces between molecules in a fluid. Consider an air bubble in water, for example. Within the bubble, the net force on a molecule due to its neighbors is zero. At the surface, however, the net force is radially inward, and the combined effect of the radial components of force across the entire spherical surface is to make the surface contract, thereby increasing the pressure on the concave side of the surface. The surface tension is a force, acting only at the surface, that is required to maintain equilibrium in such instances. It acts to balance the radially inward intermolecular attractive force with the radially outward pressure gradient force across the surface. In regions where two fluids are separated, but one of them is not in the form of spherical bubbles, the surface tension acts to minimize free energy by decreasing the area of the interface.

In ANSYS Fluent, two surface tension models exist: the continuum surface force (CSF) and the continuum surface stress (CSS). The two models are described in detail in the sections that follow.

**Note**

The calculation of surface tension effects on triangular and tetrahedral meshes is not as accurate as on quadrilateral and hexahedral meshes. The region where surface tension effects are most important should therefore be meshed with quadrilaterals or hexahedra.

### 17.3.10.1.1. The Continuum Surface Force Model

The continuum surface force (CSF) model proposed by Brackbill et al. [41] (p. 731) has been implemented such that the addition of surface tension to the VOF calculation results in a source term in the momentum equation. To understand the origin of the source term, consider the special case where the surface tension is constant along the surface, and where only the forces normal to the interface are considered. It can be shown that the pressure drop across the surface depends upon the surface tension coefficient, $\sigma$, and the surface curvature as measured by two radii in orthogonal directions, $R_1$ and $R_2$:

$$p_2 - p_1 = \sigma \left( \frac{1}{R_1} + \frac{1}{R_2} \right) \tag{17.18}$$

where $p_1$ and $p_2$ are the pressures in the two fluids on either side of the interface.

In ANSYS Fluent, a formulation of the CSF model is used, where the surface curvature is computed from local gradients in the surface normal at the interface. Let $n$ be the surface normal, defined as the gradient of $\alpha_q$, the volume fraction of the $q^{th}$ phase.

$$n = \nabla \alpha_q \tag{17.19}$$

The curvature, $\kappa$, is defined in terms of the divergence of the unit normal, $\hat{n}$ [41] (p. 731):

$$\kappa = \nabla \cdot \hat{n} \tag{17.20}$$

where


Release 15.0 - © SAS IP, Inc. All rights reserved. - Contains proprietary and confidential information of ANSYS, Inc. and its subsidiaries and affiliates.

$$\hat{n} = \frac{n}{|n|} \tag{17.21}$$

The surface tension can be written in terms of the pressure jump across the surface. The force at the surface can be expressed as a volume force using the divergence theorem. It is this volume force that is the source term that is added to the momentum equation. It has the following form:

$$F_{vol} = \sum_{pairsij, i<j} \sigma_{ij} \frac{\alpha_i \rho_i \kappa_j \nabla \alpha_j + \alpha_j \rho_j \kappa_i \nabla \alpha_i}{\frac{1}{2}\left(\rho_i + \rho_j\right)} \tag{17.22}$$

This expression allows for a smooth superposition of forces near cells where more than two phases are present. If only two phases are present in a cell, then $\kappa_i = -\kappa_j$ and $\nabla \alpha_i = -\nabla \alpha_j$, and Equation 17.22 (p. 483) simplifies to

$$F_{vol} = \sigma_{ij} \frac{\rho \kappa_i \nabla \alpha_i}{\frac{1}{2}\left(\rho_i + \rho_j\right)} \tag{17.23}$$

where $\rho$ is the volume-averaged density computed using Equation 17.14 (p. 480). Equation 17.23 (p. 483) shows that the surface tension source term for a cell is proportional to the average density in the cell.

### 17.3.10.1.2. The Continuum Surface Stress Model

The Continuum Surface Stress (CSS) method is an alternative way to modeling surface tension in a conservative manner, unlike the non-conservative formulation of the Continuum Surface Force (CSF) method. CSS avoids the explicit calculation of curvature, and could be represented as an anisotropic variant of modeling capillary forces based on surface stresses.

In the CSS method, the surface stress tensor due to surface tension is represented as

$$T = \sigma\left(I - \hat{\hat{n}} \otimes \hat{\hat{n}}\right) \ |\vec{n}| \tag{17.24}$$

$$\vec{n} = \nabla \alpha \tag{17.25}$$

$$\hat{\hat{n}} = \frac{\vec{n}}{|\vec{n}|} \tag{17.26}$$

where,

$I$ = unit tensor

$\sigma$ = surface tension coefficient

$\otimes$ = tensor product of the two vectors: the original normal and the transformed normal

$\alpha$ = volume fraction

$\vec{n}$ = volume fraction gradient

$$T = \sigma\left(|\nabla \alpha| I - \frac{\nabla \alpha \otimes \nabla \alpha}{|\nabla \alpha|}\right) \tag{17.27}$$

The surface tension force is represented as

$$F_{CSS} = \nabla \cdot T \tag{17.28}$$

Release 15.0 - © SAS IP, Inc. All rights reserved. - Contains proprietary and confidential information of ANSYS, Inc. and its subsidiaries and affiliates.

#### 17.3.10.1.3. Comparing the CSS and CSF Methods

The CSS method provides few added advantages over the CSF method, especially for cases involving variable surface tension. Both CSS and CSF methods introduce parasitic currents at the interface due to the imbalance of the pressure gradient and surface tension force.

In the CSF method, the surface tension force is represented in a nonconservative manner as follows:

$$F_{CSF} = \sigma\, k\, \nabla \alpha \tag{17.29}$$

where k is the curvature. This expression is valid only for constant surface tension.

For variable surface tension, the CSF formulation requires you to model an additional term in the tangential direction to the interface based on the surface tension gradient.

In the CSS method, surface tension force is represented in a conservative manner as follows:

$$F_{CSS} = \nabla \cdot \left[ \sigma \left( |\nabla \alpha| I - \frac{\nabla \alpha \otimes \nabla \alpha}{|\nabla \alpha|} \right) \right] \tag{17.30}$$

The CSS method does not require any explicit calculation for the curvature. Therefore, It performs more physically in under-resolved regions, such as sharp corners.

The CSS method does not require any additional terms for modeling variable surface tension due to its conservative formulation.

#### 17.3.10.1.4. When Surface Tension Effects Are Important

The importance of surface tension effects is determined based on the value of two dimensionless quantities: the Reynolds number, Re, and the capillary number, $Ca$; or the Reynolds number, Re, and the Weber number, $We$. For Re $\ll 1$, the quantity of interest is the capillary number:

$$Ca = \frac{\mu U}{\sigma} \tag{17.31}$$

and for Re $\gg 1$, the quantity of interest is the Weber number:

$$We = \frac{\rho L U^2}{\sigma} \tag{17.32}$$

where $U$ is the free-stream velocity. Surface tension effects can be neglected if $Ca \gg 1$ or $We \gg 1$.

To include the effects of surface tension in your model, refer to Including Surface Tension and Adhesion Effects in the User's Guide.

### 17.3.10.2. Wall Adhesion

An option to specify a wall adhesion angle in conjunction with the surface tension model is also available in the VOF model. The model is taken from work done by Brackbill et al. [41] (p. 731). Rather than impose this boundary condition at the wall itself, the contact angle that the fluid is assumed to make with the wall is used to adjust the surface normal in cells near the wall. This so-called dynamic boundary condition results in the adjustment of the curvature of the surface near the wall.

If $\theta_w$ is the contact angle at the wall, then the surface normal at the live cell next to the wall is

$$\hat{n} = \hat{n}_w \cos\theta_w + \hat{t}_w \sin\theta_w \tag{17.33}$$


Release 15.0 - © SAS IP, Inc. All rights reserved. - Contains proprietary and confidential information of ANSYS, Inc. and its subsidiaries and affiliates.

where $\hat{n}_w$ and $\hat{t}_w$ are the unit vectors normal and tangential to the wall, respectively. The combination of this contact angle with the normally calculated surface normal one cell away from the wall determine the local curvature of the surface, and this curvature is used to adjust the body force term in the surface tension calculation.

To include wall adhesion in your model, refer to Including Surface Tension and Adhesion Effects in the User's Guide.

### 17.3.10.3. Jump Adhesion

Similar to wall adhesion, there is also an option to provide jump adhesion when using the VOF model. Here, the contact angle treatment is applicable to each side of the porous jump boundary by assuming the same contact angle at both the sides.

Therefore, if $\theta_w$ is the contact angle at the porous jump, then the surface normal at the neighboring cell to the porous jump is

$$\hat{n} = \hat{n}_w \cos\theta_w + \hat{t}_w \sin\theta_w \tag{17.34}$$

where $\hat{n}_w$ and $\hat{t}_w$ are the unit vectors normal and tangential to the porous jump, respectively.

To include jump adhesion in your model, refer to Steps for Setting Boundary Conditions in the User's Guide.

ANSYS Fluent provides two methods of jump adhesion treatment at the porous jump boundary:

- **Constrained Two-Sided Adhesion Treatment:**

  The constrained two-sided adhesion treatment option imposes constraints on the adhesion treatment. Here, the contact angle treatment will be applied to only the side(s) of the porous jump that is(are) adjacent to the non-porous fluid zones. Hence, the contact angle treatment will not be applied to the side(s) of the porous jump that is(are) adjacent to porous media zones. If the constrained two-sided adhesion treatment is disabled, the contact angle treatment will be applied to all sides of the porous jump.

  **Note**

  This is the default treatment in ANSYS Fluent.

- **Forced Two-Sided Adhesion:**

  ANSYS Fluent allows you to use forced two-sided contact angle treatment for fluid zones without any imposed constraints. Refer to Steps for Setting Boundary Conditions in the User's Guide to learn how to apply this option.

## 17.3.11. Open Channel Flow

ANSYS Fluent can model the effects of open channel flow (for example, rivers, dams, and surface-piercing structures in unbounded stream) using the VOF formulation and the open channel boundary condition. These flows involve the existence of a free surface between the flowing fluid and fluid above it (generally the atmosphere). In such cases, the wave propagation and free surface behavior becomes important.

Release 15.0 - © SAS IP, Inc. All rights reserved. - Contains proprietary and confidential information of ANSYS, Inc. and its subsidiaries and affiliates.

Flow is generally governed by the forces of gravity and inertia. This feature is mostly applicable to marine applications and the analysis of flows through drainage systems.

Open channel flows are characterized by the dimensionless Froude Number, which is defined as the ratio of inertia force and hydrostatic force.

$$Fr = \frac{V}{\sqrt{gy}} \tag{17.35}$$

where $V$ is the velocity magnitude, $g$ is gravity, and $y$ is a length scale, in this case, the distance from the bottom of the channel to the free surface. The denominator in Equation 17.35 (p. 486) is the propagation speed of the wave. The wave speed as seen by the fixed observer is defined as

$$V_w = V \pm \sqrt{gy} \tag{17.36}$$

Based on the Froude number, open channel flows can be classified in the following three categories:

- When $Fr < 1$, that is, $V < \sqrt{gy}$ (therefore $V_w < 0$ or $V_w > 0$), the flow is known to be *subcritical* where disturbances can travel upstream as well as downstream. In this case, downstream conditions might affect the flow upstream.
- When $Fr = 1$ (therefore $V_w = 0$), the flow is known to be critical, where upstream propagating waves remain stationary. In this case, the character of the flow changes.
- When $Fr > 1$, that is, $V > \sqrt{gy}$ (therefore $V_w > 0$), the flow is known to be *supercritical* where disturbances cannot travel upstream. In this case, downstream conditions do not affect the flow upstream.

### 17.3.11.1. Upstream Boundary Conditions

There are two options available for the upstream boundary condition for open channel flows:

- pressure inlet
- mass flow rate

#### 17.3.11.1.1. Pressure Inlet

The total pressure $p_0$ at the inlet can be given as

$$p_0 = \frac{1}{2}\rho V^2 + \left(\rho - \rho_0\right) \mid \vec{g} \mid (\hat{g} \cdot (\vec{b} - \vec{a})) \tag{17.37}$$

where $\vec{b}$ and $\vec{a}$ are the position vectors of the face centroid and any point on the free surface, respectively, Here, free surface is assumed to be horizontal and normal to the direction of gravity. $\vec{g}$ is the gravity vector, $|\vec{g}|$ is the gravity magnitude, $\hat{g}$ is the unit vector of gravity, $V$ is the velocity magnitude, $\rho$ is the density of the mixture in the cell, and $\rho_0$ is the reference density.

From this, the dynamic pressure $q$ is

$$q = \frac{\rho}{2} V^2 \tag{17.38}$$

and the static pressure $p_s$ is


Release 15.0 - © SAS IP, Inc. All rights reserved. - Contains proprietary and confidential information of ANSYS, Inc. and its subsidiaries and affiliates.

$$p_s = \left(\rho - \rho_0\right) \mid \vec{g} \mid (\hat{g} \cdot (\vec{b} - \vec{a})) \tag{17.39}$$

which can be further expanded to

$$p_s = \left(\rho - \rho_0\right) \mid \vec{g} \mid \left((\hat{g} \cdot \vec{b}) + y_{local}\right) \tag{17.40}$$

where the distance from the free surface to the reference position, $y_{local}$, is

$$y_{local} = -(\vec{a} \cdot \hat{g}) \tag{17.41}$$

#### 17.3.11.1.2. Mass Flow Rate

The mass flow rate for each phase associated with the open channel flow is defined by

$$\dot{m}_{phase} = \rho_{phase}\left(Area_{phase}\right)(Velocity) \tag{17.42}$$

#### 17.3.11.1.3. Volume Fraction Specification

In open channel flows, ANSYS Fluent internally calculates the volume fraction based on the input parameters specified in the boundary conditions dialog box, therefore this option has been disabled.

For subcritical inlet flows (Fr < 1), ANSYS Fluent reconstructs the volume fraction values on the boundary by using the values from the neighboring cells. This can be accomplished using the following procedure:

- Calculate the node values of volume fraction at the boundary using the cell values.
- Calculate the volume fraction at the each face of boundary using the interpolated node values.

For supercritical inlet flows (Fr > 1), the volume fraction value on the boundary can be calculated using the fixed height of the free surface from the bottom.

### *17.3.11.2. Downstream Boundary Conditions*

#### 17.3.11.2.1. Pressure Outlet

Determining the static pressure is dependent on the **Pressure Specification Method**. Using the **Free Surface Level**, the static pressure is dictated by Equation 17.39 (p. 487) and Equation 17.41 (p. 487), otherwise you must specify the static pressure as the **Gauge Pressure**.

For subcritical outlet flows (Fr <1), if there are only two phases, then the pressure is taken from the pressure profile specified over the boundary, otherwise the pressure is taken from the neighboring cell. For supercritical flows (Fr > 1), the pressure is always taken from the neighboring cell.

#### 17.3.11.2.2. Outflow Boundary

Outflow boundary conditions can be used at the outlet of open channel flows to model flow exits where the details of the flow velocity and pressure are not known prior to solving the flow problem. If the conditions are unknown at the outflow boundaries, then ANSYS Fluent will extrapolate the required information from the interior.

It is important, however, to understand the limitations of this boundary type:

Release 15.0 - © SAS IP, Inc. All rights reserved. - Contains proprietary and confidential information of ANSYS, Inc. and its subsidiaries and affiliates.

- You can only use single outflow boundaries at the outlet, which is achieved by setting the flow rate weighting to 1. In other words, outflow splitting is not permitted in open channel flows with outflow boundaries.
- There should be an initial flow field in the simulation to avoid convergence issues due to flow reversal at the outflow, which will result in an unreliable solution.
- An outflow boundary condition can only be used with mass flow inlets. It is not compatible with pressure inlets and pressure outlets. For example, if you choose the inlet as **pressure-inlet**, then you can only use **pressure-outlet** at the outlet. If you choose the inlet as **mass-flow-inlet**, then you can use either **outflow** or **pressure-outlet** boundary conditions at the outlet. Note that this only holds true for open channel flow.
- Note that the outflow boundary condition assumes that flow is fully developed in the direction perpendicular to the outflow boundary surface. Therefore, such surfaces should be placed accordingly.

#### 17.3.11.2.3. Backflow Volume Fraction Specification

ANSYS Fluent internally calculates the volume fraction values on the outlet boundary by using the neighboring cell values, therefore, this option is disabled.

### *17.3.11.3. Numerical Beach Treatment*

In certain applications, it is desirable to suppress the numerical reflection caused by an outlet boundary for passing waves. To avoid wave reflection, a damping sink term is added in the momentum equation for the cell zone in the vicinity of the pressure outlet boundary [341] (p. 748), [512] (p. 757).

$$S = -\left[C_1 \rho V + \frac{1}{2} C_2 \rho \left| V \right| V \right] f(z) f(x) \tag{17.43}$$

where

$\hat{z}$ = vertical direction along gravity

$\hat{x}$ = flow direction

$S$ = momentum sink term in the $\hat{z}$ direction

$C_1$ = linear damping resistance (1/s) (default value is 10)

$C_2$ = quadratic damping resistance (1/m) (default value is 10)

$V$ = velocity along the $\hat{z}$ direction

$z$ = distance from the free surface level

$x$ = distance along the flow direction $\hat{x}$

$f(x)$ = damping function in the $\hat{x}$ direction

$f(z)$ = damping function in the $\hat{z}$ direction

The scaling factors in the $\hat{x}$ and $\hat{z}$ directions are defined by Equation 17.44 (p. 488) and Equation 17.45 (p. 489), respectively:

$$r_x = \frac{x - x_s}{x_e - x_s} \tag{17.44}$$


Release 15.0 - © SAS IP, Inc. All rights reserved. - Contains proprietary and confidential information of ANSYS, Inc. and its subsidiaries and affiliates.

$$r_z = \frac{z - z_{fs}}{z_b - z_{fs}} \tag{17.45}$$

where the damping functions in the $\hat{x}$ and $\hat{z}$ directions, respectively, are

$$f(x) = (r_x)^2 \tag{17.46}$$

$$f(z) = 1 - r_z \tag{17.47}$$

In Equation 17.44 (p. 488), $x_s$ and $x_e$ are the start and end points of the damping zone in the $\hat{x}$ direction. In Equation 17.45 (p. 489), $z_{\text{fs}}$ and $z_b$ are the free surface and bottom level along the $\hat{z}$ direction.

**Note**

Numerical beach treatment in ANSYS Fluent uses linear damping in the $\hat{z}$ direction and quadratic damping in the $\hat{x}$ direction.

**Note**

This option is available with Open Channel Flow (p. 485) and Open Channel Wave Boundary Conditions (p. 489).

To include numerical beach in your simulation, see Numerical Beach Treatment for Open Channels

## 17.3.12. Open Channel Wave Boundary Conditions

Open channel wave boundary conditions allow you to simulate the propagation of waves, which is useful in the marine industry. Small amplitude wave theories are generally applicable to lower wave steepness and lower relative depth, while finite amplitude wave theories are more appropriate for either increasing wave steepness or increasing relative depth. Wave steepness is generally defined as the ratio of wave height to wave length, and relative depth is defined as the ratio of wave height to the liquid depth.

ANSYS Fluent provides the following wave theories for incoming surface gravity waves through velocity inlet boundary conditions:

- First order Airy wave theory is applied to small amplitude waves in shallow to deep liquid depth ranges, and is linear in nature.
- Higher order Stokes wave theories are applied to finite amplitude waves in intermediate to deep liquid depth ranges, and are nonlinear in nature.
- Higher order Cnoidal/Solitary wave theories are applied to finite amplitude waves in shallow depth ranges, and are nonlinear in nature.

Short gravity wave expressions for each wave theory are based on infinite liquid height, whereas shallow or intermediate wave expressions are based on finite liquid height.

The wave height $H$ is defined as follows:

$$H = 2A = A_t + A_c \tag{17.48}$$

where $A$ is the wave amplitude, $A_t$ is the wave amplitude at the trough, and $A_c$ is the wave amplitude at the crest. For linear wave theory, $A_t = A_c$ and for nonlinear wave theory, $A_t \neq A_c$.

The wave number ($k$) is:

$$k = \frac{2\pi}{\lambda} \tag{17.49}$$

where $\lambda$ is the wave length.

The vector form for the wave number $K$ is

$$\vec{K} = k_x \hat{x} + k_y \hat{y} \tag{17.50}$$

where $\hat{x}$ is the reference wave propagation direction, $\hat{z}$ is the direction opposite to gravity and $\hat{y}$ is the direction normal to $\hat{x}$ and $\hat{z}$. The wave numbers in the $\hat{x}$ and $\hat{y}$ directions are defined by Equation 17.51 (p. 490) and Equation 17.52 (p. 490), respectively:

$$k_x = k\cos\theta \tag{17.51}$$

$$k_y = k\sin\theta \tag{17.52}$$

$\theta$ is the wave heading angle, which is defined as the angle between the wave front and reference wave propagation direction, in the plane of $\hat{x}$ and $\hat{y}$.

The effective wave frequency $\omega_e$ is defined as

$$\omega_e = \omega + \vec{K} \cdot \vec{U} \tag{17.53}$$

where $\omega$ is the wave frequency and $\vec{U}$ is the averaged velocity of the flow current. The effects of a moving object could also be incorporated with the flow current when the flow is specified relative to the motion of the moving object.

The wave speed or celerity $c$ is defined as

$$c = \frac{\omega}{k} \tag{17.54}$$

The final velocity vector for incoming waves obtained by superposing all the velocity components is represented as:

$$\vec{V} = \vec{U} + u\,\hat{x} + v\,\hat{y} + w\,\hat{z} \tag{17.55}$$

where $u, v$, and $w$ are the velocity components of the surface gravity wave in the $\hat{x}$, $\hat{y}$, and $\hat{z}$ directions, respectively.

### 17.3.12.1. Airy Wave Theory

The wave profile for a linear wave is given as

$$\zeta(X,t) = A\cos\alpha \tag{17.56}$$

where $\alpha$ is defined as follows:

$$\alpha = k_x x + k_y y - \omega_e t + \varepsilon \tag{17.57}$$


Release 15.0 - © SAS IP, Inc. All rights reserved. - Contains proprietary and confidential information of ANSYS, Inc. and its subsidiaries and affiliates.

$x$ and $y$ are the space coordinates in the $\hat{x}$ and $\hat{y}$ directions, respectively, $\varepsilon$ is the phase difference, and $t$ is the time.

The wave frequency $\omega$ is defined as follows for shallow/intermediate waves:

$$\omega = \sqrt{gk \tanh(kh)} \tag{17.58}$$

and as follows for short gravity waves:

$$\omega = \sqrt{gk} \tag{17.59}$$

where $h$ is the liquid height, $k$ is the wave number, and $g$ is the gravity magnitude.

The velocity components for the incident wave boundary condition can be described in terms of shallow/intermediate waves and short gravity waves.

**Velocity Components for Shallow/Intermediate Waves**

$$\begin{pmatrix} u \\ v \end{pmatrix} = \frac{gkA}{\omega} \frac{\cosh[k(z+h)]}{\cosh(kh)} \begin{pmatrix} \cos\theta \\ \sin\theta \end{pmatrix} \cos\alpha \tag{17.60}$$

$$w = \frac{gkA}{\omega} \frac{\sinh[k(z+h)]}{\cosh(kh)} \sin\alpha \tag{17.61}$$

**Velocity Components for Short Gravity Waves**

$$\begin{pmatrix} u \\ v \end{pmatrix} = \frac{gkA}{\omega} e^{kz} \begin{pmatrix} \cos\theta \\ \sin\theta \end{pmatrix} \cos\alpha \tag{17.62}$$

$$w = \frac{gkA}{\omega} e^{kz} \sin\alpha \tag{17.63}$$

where $z$ is the height from the free surface level in the direction $\hat{z}$, which is opposite to that of gravity. For more information on how to use and set up this model, refer to Modeling Open Channel Wave Boundary Conditions in the User's Guide.

## 17.3.12.2. Stokes Wave Theories

The generalized expression for wave profiles for higher order theories (second to fifth order) is

$$\begin{aligned} \zeta(X,t) \quad &= A\cos\alpha + A^2 k \left(b_{22} + A^2 k^2 b_{24}\right) \cos 2\alpha \\ &+ A^3 k^2 \left(b_{33} + A^2 k^2 b_{35}\right) \cos 3\alpha + A^4 k^3 b_{44} \cos 4\alpha + A^5 k^4 b_{55} \cos 5\alpha \end{aligned} \tag{17.64}$$

The generalized expression for the associated velocity potential for shallow/intermediate waves is

Release 15.0 - © SAS IP, Inc. All rights reserved. - Contains proprietary and confidential information of ANSYS, Inc. and its subsidiaries and affiliates.

$$\Phi(X,t)=c\left[\begin{array}{l} A\left(a_{11}+A^2k^2a_{13}+A^4k^4a_{15}\right)\cosh kh\sin\alpha+ \\ A^2k\left(a_{22}+A^2k^2a_{24}\right)\cosh 2kh\sin 2\alpha+ \\ A^3k^2\left(a_{33}+A^2k^2a_{35}\right)\cosh 3kh\sin 3\alpha+ \\ A^4k^3\left(a_{44}\right)\cosh 4kh\sin 4\alpha+ \\ A^5k^4\left(a_{55}\right)\cosh 5kh\sin 5\alpha \end{array}\right] \tag{17.65}$$

and for short gravity waves, the velocity potential is

$$\Phi(X,t)=cA\,e^{kz}\sin\alpha \tag{17.66}$$

The wave frequency $\omega$ is defined as

$$\omega=\left[gk\left(1+A^2k^2c_3+A^4k^4c_5\right)\tanh kh\right]^{1/2} \tag{17.67}$$

where $c$ is the wave speed, $g$ is the gravity magnitude, $a_{mn}$, $b_{mn}$, and $c_{mn}$ are functions of wave length and liquid height for shallow/intermediate waves and constant values for short gravity waves. Velocity components for surface gravity waves are derived from the velocity potential function.

$$u=\frac{\partial\Phi}{\partial x}\cos\theta \tag{17.68}$$

$$v=\frac{\partial\Phi}{\partial x}\sin\theta \tag{17.69}$$

$$w=\frac{\partial\Phi}{\partial z} \tag{17.70}$$

Refer to Lin's book for details on the numerical expressions [254] (p. 743).

### 17.3.12.3. Cnoidal/Solitary Wave Theory

Fluent formulates the Cnoidal/Solitary wave theories that are expressed using complex Jacobian and elliptic functions based on the work by John D. Fenton (1998) [116] (p. 735). The cnoidal solution displays long flat troughs and narrow crests of real waves in shallow waters. In the limit of infinite wavelength, the cnoidal solution describes a solitary wave as a wave with a single hump, having no troughs. Due to the complexity of the cnoidal wave theories, solitary wave theories are more widely used for shallow depth regimes.

**Note**

For simplicity, the higher order terms, which are functions of relative depth, have been omitted from the numerical details below. Refer to the work of John D. Fenton [116] (p. 735) for detailed numerical expressions.

The elliptic function parameter, $m$, is calculated by solving the following nonlinear equation:

$$\frac{\lambda}{h}=4K(m)\sqrt{\frac{3H}{h}}\left[1+Higher\cdot order\cdot terms\right] \tag{17.71}$$


Release 15.0 - © SAS IP, Inc. All rights reserved. - Contains proprietary and confidential information of ANSYS, Inc. and its subsidiaries and affiliates.

Tough height from the bottom, $h_{tr}$, is derived from the following relationship:

$$\frac{h_{tr}}{h} = 1 - \frac{H}{h}\frac{E(m)}{K(m)} + Higher \cdot order \cdot terms \tag{17.72}$$

Wave number, $k$, is defined as:

$$k = \frac{1}{h_{tr}}\sqrt{\frac{3H}{4h_{tr}}}\left[1 + Higher \cdot order \cdot terms\right] \tag{17.73}$$

Wave celerity, $c$, is defined as:

$$c = \sqrt{gh_{tr}}\left(1 + \frac{H}{h}\left[\frac{1}{2} - \frac{E(m)}{K(m)}\right] + Higher \cdot order \cdot terms\right) \tag{17.74}$$

Wave frequency, $\omega$, is defined as:

$$\omega = kc \tag{17.75}$$

The wave profile for a shallow wave is defined as:

$$\zeta(X,t) = -h + h_{tr}\left[1 + \frac{H}{h_{tr}}cn^2(\alpha,m) + Higher \cdot order \cdot terms\right] \tag{17.76}$$

Where $\alpha$ is defined as:

$$\alpha = k_x(x - x_0) + k_y y - \omega_e t \tag{17.77}$$

where $x_0$ is the translational distance from reference frame origin in the $\hat{x}$ direction.

Velocity components for the fifth order wave theories are expressed as:

$$u = \left[c - \sqrt{gh_{tr}}\left\{1 - \sum_{i=1}^{5}\left(\frac{4(kh_{tr})^2}{3}\right)^i \sum_{j=0}^{i-1}\left(\frac{z+h}{h_{tr}}\right)^{2j}\sum_{l=0}^{i} cn^{2l}(\alpha,m)\,C_{ijl}\right\}\right]\cos(\theta) \tag{17.78}$$

$$v = \left[c - \sqrt{gh_{tr}}\left\{1 - \sum_{i=1}^{5}\left(\frac{4(kh_{tr})^2}{3}\right)^i \sum_{j=0}^{i-1}\left(\frac{z+h}{h_{tr}}\right)^{2j}\sum_{l=0}^{i} cn^{2l}(\alpha,m)\,C_{ijl}\right\}\right]\sin(\theta) \tag{17.79}$$

$$w = \sqrt{gh_{tr}}2kh_{tr}cn(\alpha,m)\,sn(\alpha,m)\,dn(\alpha,m) \left[\sum_{i=1}^{5}\left(\frac{4(kh_{tr})^2}{3}\right)^i \sum_{j=0}^{i-1}\left(\frac{z+h}{h_{tr}}\right)^{2j+1}\sum_{l=1}^{i} cn^{2(l-1)}(\alpha,m)\,\frac{1}{2j+1}C_{ijl}\right] \tag{17.80}$$

where $C_{ijl}$ are the numerical coefficients mentioned in the reference [116] (p. 735).

**Note**

Solitary wave theory expressions are derived by assuming that the waves have infinite wave length. Based on this assumption we get:

Release 15.0 - © SAS IP, Inc. All rights reserved. - Contains proprietary and confidential information of ANSYS, Inc. and its subsidiaries and affiliates.

$m = 1$

$h_{tr} = h$

## 17.3.12.4. Nomenclature for Open Channel Waves

| Symbol | Description |
|---|---|
| $\hat{x}$ | Reference wave propagation direction |
| $\hat{y}$ | direction normal to $\hat{x}$ and $\hat{z}$ |
| $\hat{z}$ | Direction opposite to gravity |
| $H$ | Wave Height |
| $A$ | Wave Amplitude |
| $h$ | Liquid Height |
| $h_{tr}$ | Trough Height |
| $\lambda$ | Wave Length |
| $\theta$ | Wave Heading Angle |
| $k$ | Wave Number |
| $k_x$ | Wave Number in the $\hat{x}$ direction |
| $k_y$ | Wave Number in the $\hat{y}$ direction |
| $c$ | Wave Celerity |
| $\omega$ | Wave Frequency |
| $\omega_e$ | Effective Wave Frequency |
| $m$ | Elliptical Function Parameter |
| $K\ (m)$ | Complete Elliptical Integral of the First Kind |
| $E\ (m)$ | Complete Elliptical Integral of the Second Kind |
| $cn\ (\alpha, m)$, $sn\ (\alpha, m)$, $dn\ (\alpha, m)$ | Jacobian Elliptic Functions |
| $x$ | Spatial coordinate in the $\hat{x}$ direction |
| $y$ | Spatial coordinate in the $\hat{y}$ direction |
| $z$ | Spatial coordinate in the $\hat{z}$ direction |


Release 15.0 - © SAS IP, Inc. All rights reserved. - Contains proprietary and confidential information of ANSYS, Inc. and its subsidiaries and affiliates.

| Symbol | Description |
|---|---|
| $x_0$ | Translational distance from reference frame origin in the $\hat{x}$ direction |
| $\Phi$ | Velocity Potential |
| $\vec{U}$ | Averaged velocity of flow current |
| $u, v, w$ | Velocity components for surface gravity waves in the $\hat{x}$, $\hat{y}$, and $\hat{z}$ directions, respectively. |

### 17.3.12.5. Choosing a Wave Theory

Applying linear versus nonlinear wave theories to shallow waves is limited by the Ursell number. For nonlinear waves, the Ursell number criterion is based on waves being single-crested, without producing any secondary crests at the trough. Wave theories should be chosen in accordance with wave steepness and relative depth, as waves try to acquire a nonlinear pattern with increasing wave steepness or relative depth. Second and fourth order wave theories are more prone to produce secondary crests. Choosing the correct wave theory for a particular application depends on the input parameters within the wave breaking limit, as described below:

- **Mandatory Check for Complete Wave Regime within Wave Breaking Limit**

  The wave height to liquid depth ratio $H/h$ (relative depth) within the wave breaking limit is defined as:

$$\left[\frac{H}{h}\right]_{\max,theoretical} = 0.78 \tag{17.81}$$

$$\left[\frac{H}{h}\right]_{\max,practical} = 0.55 \tag{17.82}$$

  The wave height to wave length depth ratio $H/\lambda$ (wave steepness) within the breaking limit is defined as:

$$\left[\frac{H}{\lambda}\right]_{\max,theoretical} = 0.142 \tag{17.83}$$

$$\left[\frac{H}{\lambda}\right]_{\max,practical} = 0.1 \tag{17.84}$$

- **Check for Wave Theories within Wave Breaking Limit**

  For this check, the wave type is represented with the appropriate wave theory in the following manner:

  – **Linear Wave**: Airy Wave Theory

  – **Stoke Wave**: Fifth Order Stoke Wave Theory

Release 15.0 - © SAS IP, Inc. All rights reserved. - Contains proprietary and confidential information of ANSYS, Inc. and its subsidiaries and affiliates.

– **Shallow Wave**: Fifth Order Cnoidal/Solitary Wave Theory

Checks for wave theories between second to fourth order are performed between linear and fifth order Stokes wave.

– **Wave Regime Check**

The liquid height to wave length ratio $h/\lambda$ for short gravity waves is defined as:

$$\left[\frac{h}{\lambda}\right]_{\min} = 0.5 \tag{17.85}$$

For Stokes wave in shallow regime the ratio is defined as:

$$\left[\frac{h}{\lambda}\right]_{\min} = 0.06 \tag{17.86}$$

For shallow waves, the ratio is defined as:

$$\left[\frac{h}{\lambda}\right]_{\max} = 0.085 \tag{17.87}$$

– **Wave Steepness Check**

The wave height to wave length ratio $H/\lambda$ for linear waves is defined as:

$$\left[\frac{H}{\lambda}\right]_{\max} = 0.02\tanh\left(2\pi\frac{h}{\lambda}\right) \tag{17.88}$$

For Stokes wave in shallow regime, the ratio is defined as:

$$\left[\frac{H}{\lambda}\right]_{\max} = 0.142\tanh\left(2\pi\frac{h}{\lambda}\right) \tag{17.89}$$

For shallow waves, the ratio is defined as:

$$\left[\frac{H}{\lambda}\right]_{\max} = 0.142\left(2\pi\frac{h}{\lambda}\right) \tag{17.90}$$

- **Relative Depth Check**

The wave height to liquid depth ratio $H/h$ for a linear wave is defined as:

$$\left[\frac{H}{h}\right]_{\max} = 0.1 \tag{17.91}$$

For Stokes wave in shallow regime the ratio is defined as:

$$\left[\frac{H}{h}\right]_{\max} = 0.5 \tag{17.92}$$

For shallow waves, the ratio is defined as:

$$\left[\frac{H}{h}\right]_{\max} = 0.55 \tag{17.93}$$


Release 15.0 - © SAS IP, Inc. All rights reserved. - Contains proprietary and confidential information of ANSYS, Inc. and its subsidiaries and affiliates.

- **Ursell Number Stability Criterion**

  The Ursell number is defined as:

$$Ur = \frac{H\lambda^2}{h^3} \tag{17.94}$$

  The Ursell number stability criterion for a linear wave is defined as:

$$(Ur)_{\max} = \frac{32\pi^2}{3} \tag{17.95}$$

  The criterion for Stokes wave in shallow regime is defined as:

$$(Ur)_{\max} = \frac{8\pi^2}{3} \tag{17.96}$$

  The criterion for shallow waves is defined as:

$$(Ur)_{\min} = \frac{8\pi^2}{3} \tag{17.97}$$

### 17.3.12.6. Superposition of Waves

The principle of superposition of waves can be applied to two or more waves simultaneously passing through the same medium. The resultant wave pattern is produced by the summation of wave profiles and velocity potentials of the individual waves. Depending on the nature of the superposition, the following phenomena are possible:

- Interference: Superposition of waves of the same frequency and wave heights, travelling in the same direction. Constructive interference occurs in cases of waves travelling in the same phase, while destructive interference occurs in cases of waves travelling in opposite phases.
- Beats/Wave Group: Superposition of waves of same wave heights travelling in the same direction with nearly equal frequencies. The beats are generated by increase/decrease in the resultant frequency of the waves over time.

  For marine applications, this concept of wave superposition is known as a Wave Group. In a wave group, packets (group) of waves move with a group velocity that is slower than the phase speed of each individual wave within the packet.
- Stationary/Standing Waves: Superposition of identical waves travelling in opposite directions. This superposition forms a stationary wave where each particle executes simple harmonic motion with the same frequency but different amplitudes.
- Irregular Waves: Superposition of waves with different wave heights, frequencies, phase differences, and direction of propagation. Irregular sea waves are quite common in marine applications, and can be modeled by superimposing multiple waves.

**Note**

The superposition principle is only valid for linear and small-amplitude waves. Superposition of finite amplitude waves may be approximate or invalid because of their nonlinear behavior and dependency of the wave dispersion on wave height.

Release 15.0 - © SAS IP, Inc. All rights reserved. - Contains proprietary and confidential information of ANSYS, Inc. and its subsidiaries and affiliates.

## 17.3.13. Coupled Level-Set and VOF Model

The level-set method is a popular interface-tracking method for computing two-phase flows with topologically complex interfaces. This is similar to the interface tracking method of the VOF model. In the level-set method [335] (p. 747), the interface is captured and tracked by the level-set function, defined as a signed distance from the interface. Because the level-set function is smooth and continuous, its spatial gradients can be accurately calculated. This in turn will produce accurate estimates of interface curvature and surface tension force caused by the curvature. However, the level-set method is found to have a deficiency in preserving volume conservation [327] (p. 747). On the other hand, the VOF method is naturally volume-conserved, as it computes and tracks the volume fraction of a particular phase in each cell rather than the interface itself. The weakness of the VOF method lies in the calculation of its spatial derivatives, since the VOF function (the volume fraction of a particular phase) is discontinuous across the interface. To overcome the deficiencies of the level-set method and the VOF method, a coupled level-set and VOF approach is provided in ANSYS Fluent.

**Important**

The coupled level-set and VOF model is specifically designed for two-phase flows, where no mass transfer is involved and is applied to transient flow problems only. The mesh should be restricted to quadrilateral, triangular or a combination of both for 2D cases and restricted to hexahedral, tetrahedral or a combination of both for 3D cases.

To learn how to use this model, refer to Including Coupled Level Set with the VOF Model

### 17.3.13.1. Theory

The level-set function $\varphi$ is defined as a signed distance to the interface. Accordingly, the interface is the zero level-set, $\varphi(x,t)$ and can be expressed as $\Gamma = \{x \mid \varphi(x,t) = 0\}$ in a two-phase flow system:

$$\varphi(x,t) = \begin{cases} +|d| & \text{if } x \in \text{the primary phase} \\ 0 & \text{if } x \in \Gamma \\ -|d| & \text{if } x \in \text{the secondary phase} \end{cases} \tag{17.98}$$

where $d$ is the distance from the interface.

The normal and curvature of the interface, which is needed in the computation of the surface tension force, can be estimated as

$$\vec{n} = \frac{\nabla \varphi}{|\nabla \varphi|} \Big|_{\varphi=0} \tag{17.99}$$

$$\kappa = \nabla \cdot \frac{\nabla \varphi}{|\nabla \varphi|} \Big|_{\varphi=0} \tag{17.100}$$

The evolution of the level-set function can be given in a similar fashion as to the VOF model:

$$\frac{\partial \varphi}{\partial t} + \nabla \cdot (\vec{u} \varphi) = 0 \tag{17.101}$$

Where $\vec{u}$ is the underlying velocity field.

And the momentum equation can be written as


Release 15.0 - © SAS IP, Inc. All rights reserved. - Contains proprietary and confidential information of ANSYS, Inc. and its subsidiaries and affiliates.

$$\frac{\partial(\rho\vec{u})}{\partial t}+\nabla\cdot(\rho\vec{u}\,\vec{u})=-\nabla p+\nabla\cdot\mu[\nabla\vec{u}+(\nabla\vec{u})^T]-\sigma\kappa\delta(\varphi)\nabla\varphi+\rho\vec{g} \tag{17.102}$$

$\delta(\varphi)=\frac{1+\cos(\pi\varphi/a)}{2a}$ if $|\varphi|<a$ and $a=1.5h$ (where $h$ is the grid spacing), otherwise $\delta(\varphi)=0.\sigma$ is the surface tension coefficient.

### 17.3.13.1.1. Re-initialization of the Level-set Function via the Geometrical Method

By nature of the transport equation of the level-set function Equation 17.101 (p. 498), it is unlikely that the distance constraint of $|\nabla\varphi|=1$ is maintained after its solution. The reasons for the lack of maintenance is due to the deformation of the interface, uneven profile, and thickness across the interface. Those errors will accumulate during the iteration process and cause large errors in mass and momentum solutions. A re-initialization process is therefore required for each time step. The geometrical interface-front construction method is used here. The geometrical method involves a simple concept and is reliable in producing accurate geometrical data for the interface front. The values of the VOF and the level-set function are both used to reconstruct the interface-front. Namely, the VOF model provides the size of the cut in the cell where the likely interface passes through, and the gradient of the level-set function determines the direction of the interface.

The concept of piecewise linear interface construction (PLIC) is also employed to construct the interface-front. The procedure for the interface–front reconstruction can be briefly described as follows and as shown in Figure 17.3: Schematic View of the Interface Cut Through the Front Cell (p. 499):

1. Locate the interface front cells, where the sign($\varphi$) is alternating or the value of the volume fraction is between 0 and 1, that is, a partially filled cell.
2. Calculate the normal of the interface segment in each front cell from the level-set function gradients.
3. Position the cut-through, making sure at least one corner of the cell is occupied by the designated phase in relation to the neighboring cells.
4. Find the intersection between the cell centerline normal to the interface and the interface so that the VOF is satisfied.
5. Find the intersection points between the interface line and the cell boundaries; these intersection points are designated as front points.

**Figure 17.3: Schematic View of the Interface Cut Through the Front Cell**

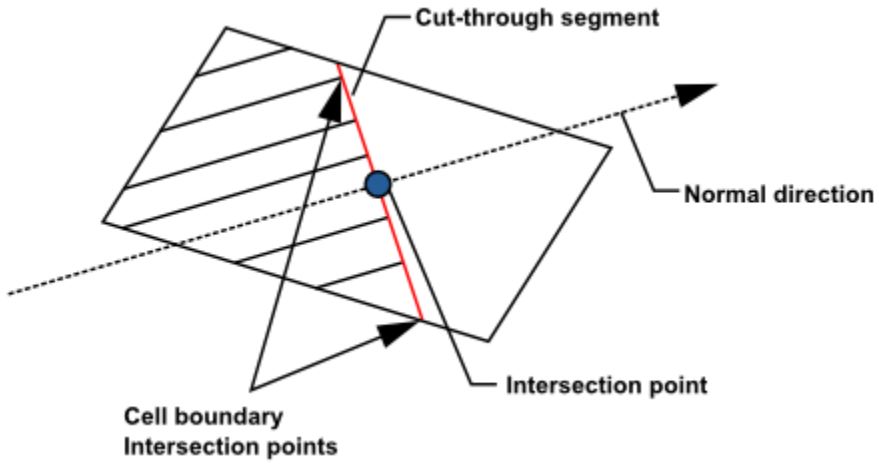

Once the interface front is reconstructed, the procedure for the minimization of the distance from a given point to the interface can begin as follows:

1. Calculate the distance of the given point in the domain to each cut-segment of the front cell. The method for the distance calculation is as follows:

   a. If the normal line starting from the given point to the interface intersects within the cut-segment, then the calculated distance will be taken as the distance to the interface.

   b. If the intersection point is beyond the end points of the cut-segment, the shortest distance from the given point to the end points of the cut-segment will be taken as the distance to the interface cut-segment, as shown in Figure 17.4: Distance to the Interface Segment (p. 500).

2. Minimize all possible distances from the given point to all front cut-segments, so as to represent the distance from the given point to the interface. Thus, the values of these distances will be used to re-initialize the level-set function.

**Figure 17.4: Distance to the Interface Segment**

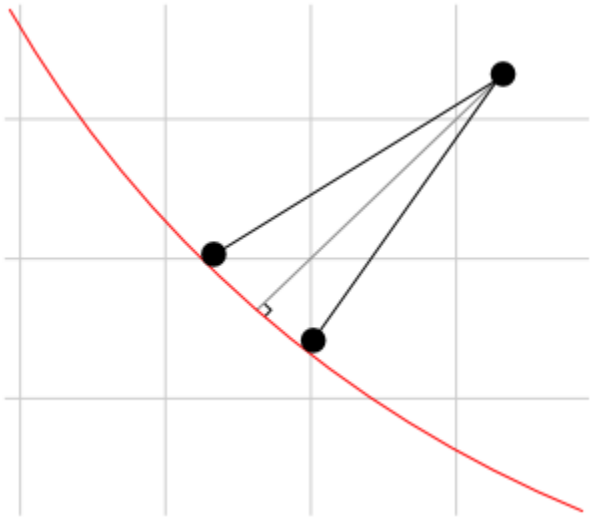

### *17.3.13.2. Limitations*

The current implementation of the model is only suitable for two-phase flow regime, where two fluids are not interpenetrating. The level-set model can only be used when the VOF model is activated. Note that no mass transfer is permitted.

## 17.4. Mixture Model Theory

Information is organized into the following subsections:

17.4.1. Overview
17.4.2. Limitations
17.4.3. Continuity Equation
17.4.4. Momentum Equation
17.4.5. Energy Equation
17.4.6. Relative (Slip) Velocity and the Drift Velocity
17.4.7. Volume Fraction Equation for the Secondary Phases
17.4.8. Granular Properties
17.4.9. Granular Temperature


Release 15.0 - © SAS IP, Inc. All rights reserved. - Contains proprietary and confidential information of ANSYS, Inc. and its subsidiaries and affiliates.

17.4.10. Solids Pressure
17.4.11. Interfacial Area Concentration

## 17.4.1. Overview

The mixture model is a simplified multiphase model that can be used in different ways. It can be used to model multiphase flows where the phases move at different velocities, but assume local equilibrium over short spatial length scales. It can be used to model homogeneous multiphase flows with very strong coupling and phases moving at the same velocity and lastly, the mixture models are used to calculate non-Newtonian viscosity.

The mixture model can model $n$ phases (fluid or particulate) by solving the momentum, continuity, and energy equations for the mixture, the volume fraction equations for the secondary phases, and algebraic expressions for the relative velocities. Typical applications include sedimentation, cyclone separators, particle-laden flows with low loading, and bubbly flows where the gas volume fraction remains low.

The mixture model is a good substitute for the full Eulerian multiphase model in several cases. A full multiphase model may not be feasible when there is a wide distribution of the particulate phase or when the interphase laws are unknown or their reliability can be questioned. A simpler model like the mixture model can perform as well as a full multiphase model while solving a smaller number of variables than the full multiphase model.

The mixture model allows you to select granular phases and calculates all properties of the granular phases. This is applicable for liquid-solid flows.

## 17.4.2. Limitations

The following limitations apply to the mixture model in ANSYS Fluent:

- You must use the pressure-based solver. The mixture model is not available with the density-based solver.
- Only one of the phases can be defined as a compressible ideal gas. There is no limitation on using compressible liquids using user-defined functions.
- When the mixture model is used, do not model streamwise periodic flow with specified mass flow rate.
- Do not model solidification and melting in conjunction with the mixture model.
- The Singhal et al. cavitation model (available with the mixture model) is not compatible with the LES turbulence model.
- Do not use the relative formulation in combination with the MRF and mixture model (see Limitations in the User's Guide).
- The mixture model does not allow for inviscid flows.
- When tracking particles in parallel, do not use the DPM model with the mixture model if the shared memory option is enabled (Parallel Processing for the Discrete Phase Model in the User's Guide). (Note that using the message passing option, when running in parallel, enables the compatibility of all multiphase flow models with the DPM model.)

The mixture model, like the VOF model, uses a *single-fluid* approach. It differs from the VOF model in two respects:

Release 15.0 - © SAS IP, Inc. All rights reserved. - Contains proprietary and confidential information of ANSYS, Inc. and its subsidiaries and affiliates.

- The mixture model allows the phases to be interpenetrating. The volume fractions $\alpha_q$ and $\alpha_p$ for a control volume can therefore be equal to any value between 0 and 1, depending on the space occupied by phase $q$ and phase $p$.
- The mixture model allows the phases to move at different velocities, using the concept of slip velocities. (Note that the phases can also be assumed to move at the same velocity, and the mixture model is then reduced to a homogeneous multiphase model.)

The mixture model solves the continuity equation for the mixture, the momentum equation for the mixture, the energy equation for the mixture, and the volume fraction equation for the secondary phases, as well as algebraic expressions for the relative velocities (if the phases are moving at different velocities).

## 17.4.3. Continuity Equation

The continuity equation for the mixture is

$$\frac{\partial}{\partial t}\left(\rho_m\right)+\nabla\cdot\left(\rho_m\vec{v}_m\right)=0 \tag{17.103}$$

where $\vec{v}_m$ is the mass-averaged velocity:

$$\vec{v}_m=\frac{\sum_{k=1}^{n}\alpha_k\rho_k\vec{v}_k}{\rho_m} \tag{17.104}$$

and $\rho_m$ is the mixture density:

$$\rho_m=\sum_{k=1}^{n}\alpha_k\rho_k \tag{17.105}$$

$\alpha_k$ is the volume fraction of phase $k$.

## 17.4.4. Momentum Equation

The momentum equation for the mixture can be obtained by summing the individual momentum equations for all phases. It can be expressed as

$$\begin{aligned}\frac{\partial}{\partial t}\left(\rho_m\vec{v}_m\right)+\nabla\cdot\left(\rho_m\vec{v}_m\vec{v}_m\right) &= -\nabla p+\nabla\cdot\left[\mu_m\left(\nabla\vec{v}_m+\nabla\vec{v}_m^{\,T}\right)\right]\\ &\quad+\rho_m\vec{g}+\vec{F}+\nabla\cdot\left(\sum_{k=1}^{n}\alpha_k\rho_k\vec{v}_{dr,k}\vec{v}_{dr,k}\right)\end{aligned} \tag{17.106}$$

where $n$ is the number of phases, $\vec{F}$ is a body force, and $\mu_m$ is the viscosity of the mixture:

$$\mu_m=\sum_{k=1}^{n}\alpha_k\mu_k \tag{17.107}$$

$\vec{v}_{dr,k}$ is the drift velocity for secondary phase $k$:

$$\vec{v}_{dr,k}=\vec{v}_k-\vec{v}_m \tag{17.108}$$


Release 15.0 - © SAS IP, Inc. All rights reserved. - Contains proprietary and confidential information of ANSYS, Inc. and its subsidiaries and affiliates.

## 17.4.5. Energy Equation

The energy equation for the mixture takes the following form:

$$\frac{\partial}{\partial t}\sum_{k=1}^{n}\left(\alpha_k\rho_k E_k\right)+\nabla\cdot\sum_{k=1}^{n}\left(\alpha_k\vec{v}_k\left(\rho_k E_k+p\right)\right)=\nabla\cdot\left(k_{eff}\nabla T\right)+S_E \tag{17.109}$$

where $k_{eff}$ is the effective conductivity ($\sum\alpha_k(k_k+k_t)$), where $k_t$ is the turbulent thermal conductivity, defined according to the turbulence model being used. The first term on the right-hand side of Equation 17.109 (p. 503) represents energy transfer due to conduction. $S_E$ includes any other volumetric heat sources.

In Equation 17.109 (p. 503),

$$E_k=h_k-\frac{p}{\rho_k}+\frac{v_k^2}{2} \tag{17.110}$$

for a compressible phase, and $E_k=h_k$ for an incompressible phase, where $h_k$ is the sensible enthalpy for phase $k$.

## 17.4.6. Relative (Slip) Velocity and the Drift Velocity

The relative velocity (also referred to as the slip velocity) is defined as the velocity of a secondary phase ($p$) relative to the velocity of the primary phase ($q$):

$$\vec{v}_{pq}=\vec{v}_p-\vec{v}_q \tag{17.111}$$

The mass fraction for any phase ($k$) is defined as

$$c_k=\frac{\alpha_k\rho_k}{\rho_m} \tag{17.112}$$

The drift velocity and the relative velocity ($\vec{v}_{qp}$) are connected by the following expression:

$$\vec{v}_{dr,p}=\vec{v}_{pq}-\sum_{k=1}^{n}c_k\vec{v}_{qk} \tag{17.113}$$

ANSYS Fluent's mixture model makes use of an algebraic slip formulation. The basic assumption of the algebraic slip mixture model is that to prescribe an algebraic relation for the relative velocity, a local equilibrium between the phases should be reached over a short spatial length scale. Following Manninen et al. [281] (p. 744), the form of the relative velocity is given by:

$$\vec{v}_{pq}=\frac{\tau_p}{f_{drag}}\frac{\left(\rho_p-\rho_m\right)}{\rho_p}\vec{a} \tag{17.114}$$

where $\tau_p$ is the particle relaxation time

$$\tau_p=\frac{\rho_p d_p^2}{18\mu_q} \tag{17.115}$$

Release 15.0 - © SAS IP, Inc. All rights reserved. - Contains proprietary and confidential information of ANSYS, Inc. and its subsidiaries and affiliates.

$d$ is the diameter of the particles (or droplets or bubbles) of secondary phase $p$, $\vec{a}$ is the secondary-phase particle's acceleration. The default drag function $f_{drag}$ is taken from Schiller and Naumann [393] (p. 750):

$$f_{drag} = \begin{cases} 1 + 0.15Re^{0.687} & Re \le 1000 \\ 0.0183Re & Re > 1000 \end{cases} \tag{17.116}$$

and the acceleration $\vec{a}$ is of the form

$$\vec{a} = \vec{g} - (\vec{v}_m \cdot \nabla)\vec{v}_m - \frac{\partial \vec{v}_m}{\partial t} \tag{17.117}$$

The simplest algebraic slip formulation is the so-called drift flux model, in which the acceleration of the particle is given by gravity and/or a centrifugal force and the particulate relaxation time is modified to take into account the presence of other particles.

In turbulent flows the relative velocity should contain a diffusion term due to the dispersion appearing in the momentum equation for the dispersed phase. ANSYS Fluent adds this dispersion to the relative velocity:

$$\vec{v}_{pq} = \frac{\left(\rho_p - \rho_m\right) d_p^2}{18\mu_q f_{drag}} \vec{a} - \frac{\eta_t}{\sigma_t}\left(\frac{\nabla \alpha_p}{\alpha_p} - \frac{\nabla \alpha_q}{\alpha_q}\right) \tag{17.118}$$

where $\sigma_t$ is a Prandtl/Schmidt number set to 0.75 and $\eta_t$ is the turbulent diffusivity. This diffusivity is calculated from the continuous-dispersed fluctuating velocity correlation, such that

$$\eta_t = C_\mu \frac{k^2}{\varepsilon}\left[\frac{\gamma_\gamma}{1+\gamma_\gamma}\right]\left(1 + C_\beta \zeta_\gamma^2\right)^{-1/2} \tag{17.119}$$

$$\zeta_\gamma = \frac{|\vec{v}_{pq}|}{\sqrt{2/3k}} \tag{17.120}$$

where $C_\beta = 1.8 - 1.35\cos^2\theta$

and

$$\cos\theta = \frac{\vec{v}_{pq} \cdot \vec{v}_p}{|\vec{v}_{pq}||\vec{v}_p|}$$

$\gamma_\gamma$ is the time ratio between the time scale of the energetic turbulent eddies affected by the crossing-trajectories effect and the particle relaxation time.

When you are solving a mixture multiphase calculation with slip velocity, you can directly prescribe formulations for the drag function. The following choices are available:

- Schiller-Naumann (the default formulation)
- Morsi-Alexander
- symmetric


Release 15.0 - © SAS IP, Inc. All rights reserved. - Contains proprietary and confidential information of ANSYS, Inc. and its subsidiaries and affiliates.

- Grace et al.
- Tomiyama et al.
- universal drag laws
- constant
- user-defined

See Interphase Exchange Coefficients (p. 518) for more information on these drag functions and their formulations, and Defining the Phases for the Mixture Model in the User's Guide for instructions on how to enable them.

Note that, if the slip velocity is not solved, the mixture model is reduced to a homogeneous multiphase model. In addition, the mixture model can be customized (using user-defined functions) to use a formulation other than the algebraic slip method for the slip velocity. See the UDF Manual for details.

## 17.4.7. Volume Fraction Equation for the Secondary Phases

From the continuity equation for secondary phase $p$, the volume fraction equation for secondary phase $p$ can be obtained:

$$\frac{\partial}{\partial t}\left(\alpha_p \rho_p\right) + \nabla \cdot \left(\alpha_p \rho_p \vec{v}_m\right) = -\nabla \cdot \left(\alpha_p \rho_p \vec{v}_{dr,p}\right) + \sum_{q=1}^{n}\left(\dot{m}_{qp} - \dot{m}_{pq}\right) \tag{17.121}$$

## 17.4.8. Granular Properties

Since the concentration of particles is an important factor in the calculation of the effective viscosity for the mixture, we may use the granular viscosity to get a value for the viscosity of the suspension. The volume weighted averaged for the viscosity would now contain shear viscosity arising from particle momentum exchange due to translation and collision.

The collisional and kinetic parts, and the optional frictional part, are added to give the solids shear viscosity:

$$\mu_s = \mu_{s,col} + \mu_{s,kin} + \mu_{s,fr} \tag{17.122}$$

Refer to Solids Pressure (p. 538) for definitions of the constants used in granular flow.

### 17.4.8.1. Collisional Viscosity

The collisional part of the shear viscosity is modeled as [139] (p. 736), [441] (p. 753)

$$\mu_{s,col} = \frac{4}{5}\alpha_s \rho_s d_s g_{0,ss}\left(1 + e_{ss}\right)\left(\frac{\Theta_s}{\pi}\right)^{1/2}\alpha_s \tag{17.123}$$

### 17.4.8.2. Kinetic Viscosity

ANSYS Fluent provides two expressions for the kinetic viscosity.

The default expression is from Syamlal et al. [441] (p. 753):

Release 15.0 - © SAS IP, Inc. All rights reserved. - Contains proprietary and confidential information of ANSYS, Inc. and its subsidiaries and affiliates.

$$\mu_{s,kin}=\frac{\alpha_s d_s \rho_s \sqrt{\Theta_s \pi}}{6\,(3-e_{ss})}\left[1+\frac{2}{5}\,(1+e_{ss})\,(3e_{ss}-1)\,\alpha_s g_{0,ss}\right] \tag{17.124}$$

The following optional expression from Gidaspow et al. [139] (p. 736) is also available:

$$\mu_{s,kin}=\frac{10\rho_s d_s \sqrt{\Theta_s \pi}}{96\alpha_s\,(1+e_{ss})\,g_{0,ss}}\left[1+\frac{4}{5}g_{0,ss}\alpha_s\,(1+e_{ss})\right]^2\alpha_s \tag{17.125}$$

## 17.4.9. Granular Temperature

The viscosities need the specification of the granular temperature for the $s^{th}$ solids phase. Here we use an algebraic equation from the **granular temperature** transport equation. This is only applicable for dense fluidized beds where the convection and the diffusion term can be neglected under the premise that production and dissipation of granular energy are in equilibrium.

$$0=\left(-p_s\overline{\overline{I}}+\overline{\overline{\tau}}_s\right):\nabla\vec{v}_s-\gamma_{\Theta_s}+\phi_{ls} \tag{17.126}$$

where

$\left(-p_s\overline{\overline{I}}+\overline{\overline{\tau}}_s\right):\nabla\vec{v}_s$ = the generation of energy by the solid stress tensor

$\gamma_{\Theta_s}$ = the collisional dissipation of energy

$\phi_{ls}$ = the energy exchange between the $l^{th}$ fluid or solid phase and the $s^{th}$ solid phase

The collisional dissipation of energy, $\gamma_{\Theta_s}$, represents the rate of energy dissipation within the $s^{th}$ solids phase due to collisions between particles. This term is represented by the expression derived by Lun et al. [271] (p. 744)

$$\gamma_{\Theta m}=\frac{12\left(1-e_{ss}^2\right)g_{0,ss}}{d_s\sqrt{\pi}}\rho_s\alpha_s^2\Theta_s^{3/2} \tag{17.127}$$

The transfer of the kinetic energy of random fluctuations in particle velocity from the $s^{th}$ solids phase to the $l^{th}$ fluid or solid phase is represented by $\phi_{ls}$ [139] (p. 736):

$$\phi_{ls}=-3K_{ls}\Theta_s \tag{17.128}$$

ANSYS Fluent allows you to solve for the granular temperature with the following options:

- algebraic formulation (the default)

  This is obtained by neglecting convection and diffusion in the transport equation (Equation 17.126 (p. 506)) [441] (p. 753).

- constant granular temperature

  This is useful in very dense situations where the random fluctuations are small.

- UDF for granular temperature


Release 15.0 - © SAS IP, Inc. All rights reserved. - Contains proprietary and confidential information of ANSYS, Inc. and its subsidiaries and affiliates.

## 17.4.10. Solids Pressure

The total solid pressure is calculated and included in the mixture momentum equations:

$$P_{s,total} = \sum_{q=1}^{N} p_q \tag{17.129}$$

where $p_q$ is presented in the section for granular flows by Equation 17.279 (p. 539)

## 17.4.11. Interfacial Area Concentration

Interfacial area concentration is defined as the interfacial area between two phases per unit mixture volume. This is an important parameter for predicting mass, momentum and energy transfers through the interface between the phases. In two-fluid flow systems, one discrete (particles) and one continuous, the size and its distribution of the discrete phase or particles can change rapidly due to growth (mass transfer between phases), expansion due to pressure changes, coalescence, breakage and/or nucleation mechanisms. The Population Balance model (see the Population Balance Module Manual) ideally captures this phenomenon, but is computationally expensive since several transport equations need to be solved using moment methods, or more if the discrete method is used. The interfacial area concentration model uses a single transport equation per secondary phase and is specific to bubbly flows in liquid at this stage.

The transport equation for the interfacial area concentration can be written as

$$\frac{\partial \left(\rho_g \chi_p\right)}{\partial t} + \nabla \cdot \left(\rho_g \vec{u}_g \chi_p\right) = \frac{1}{3}\frac{D\rho_g}{Dt}\chi_p + \frac{2}{3}\frac{\dot{m}_g}{\alpha_g}\chi_p + \rho_g\left(S_{RC} + S_{WE} + S_{TI}\right) \tag{17.130}$$

where $\chi_p$ is the interfacial area concentration ($m^2/m^3$), and $\alpha_g$ is the gas volume fraction. The first two terms on the right hand side of Equation 17.130 (p. 507) are of gas bubble expansion due to compressibility and mass transfer (phase change). $\dot{m}_g$ is the mass transfer rate into the gas phase per unit mixture volume ($kg/m^3/s$). $S_{RC}$ and $S_{WE}$ are the coalescence sink terms due to random collision and wake entrainment, respectively. $S_{TI}$ is the breakage source term due to turbulent impact.

Two sets of models, the Hibiki-Ishii model [163] (p. 738) and the Ishii-Kim model [207] (p. 740), [178] (p. 738), exist for those source and sink terms for the interfacial area concentration, which are based on the works of Ishii et al. [163] (p. 738), [207] (p. 740). According to their study, the mechanisms of interactions can be summarized in five categories:

- Coalescence due to random collision driven by turbulence.
- Breakage due to the impact of turbulent eddies.
- Coalescence due to wake entrainment.
- Shearing-off of small bubbles from large cap bubbles.
- Breakage of large cap bubbles due to flow instability on the bubble surface.

In ANSYS Fluent, only the first three effects will be considered.

Release 15.0 - © SAS IP, Inc. All rights reserved. - Contains proprietary and confidential information of ANSYS, Inc. and its subsidiaries and affiliates.

### 17.4.11.1. Hibiki-Ishii Model

$$\begin{aligned} S_{RC} &= -\frac{1}{3\phi}\left(\frac{\alpha_g}{\chi_p}\right)^2 f_c n_b \lambda_c \\ &= -\left(\frac{\alpha_g}{\chi_p}\right)^2 \frac{\Gamma_c \alpha_g^2 \epsilon^{1/3}}{d_b^{11/3}\left(\alpha_{gmax}-\alpha_g\right)} exp\left(-K_c \frac{d_b^{5/6}\rho_f^{1/2}\epsilon^{1/3}}{\sigma^{1/2}}\right) \\ &= -\frac{\Gamma_c}{\psi^{11/3}} \frac{\epsilon^{1/3}}{\left(\alpha_{gmax}-\alpha_g\right)} \alpha_g^{1/3}\chi_p^{5/3} exp\left[-K_c \psi^{5/6} \frac{\rho_f^{1/2}\epsilon^{1/3}}{\sigma^{1/2}}\left(\frac{\alpha_g}{\chi_p}\right)^{5/6}\right] \end{aligned} \tag{17.131}$$

where $f_c$, $\lambda_c$ and $n_b$ are the frequency of particle/bubble collision, the efficiency of coalescence from the collision, and the number of particles per unit mixture volume, respectively. The averaged size of the particle/bubble $d_b$ is assumed to be calculated as

$$d_b = \psi \frac{\alpha_g}{\chi_p} \tag{17.132}$$

and

$$\lambda_c = exp\left(-K_c \frac{d_b^{5/6}\rho_f^{1/2}\varepsilon^{1/3}}{\sigma^{1/2}}\right) \tag{17.133}$$

$$\begin{aligned} S_{TI} &= \frac{1}{3\phi}\left(\frac{\alpha_g}{\chi_p}\right)^2 f_B n_e \lambda_B \\ &= \left(\frac{\alpha_g}{\chi_p}\right)^2 \frac{\Gamma_B \alpha_g\left(1-\alpha_g\right)\epsilon^{1/3}}{d_b^{11/3}\left(\alpha_{gmax}-\alpha_g\right)} exp\left(-K_B \frac{\sigma}{\rho_f d_b^{5/3}\epsilon^{2/3}}\right) \\ &= \frac{\Gamma_B}{\psi^{11/3}} \frac{\left(1-\alpha_g\right)\epsilon^{1/3}\chi_p^{5/3}}{\alpha_g^{2/3}\left(\alpha_{gmax}-\alpha_g\right)} exp\left[-\frac{K_B}{\psi^{5/3}} \frac{\sigma}{\rho_f \epsilon^{2/3}}\left(\frac{\chi_p}{\alpha_g}\right)^{5/3}\right] \end{aligned} \tag{17.134}$$

where $f_B$, $\lambda_B$ and $n_e$ are the frequency of collision between particles/bubbles and turbulent eddies of the primary phase, the efficiency of breakage from the impact, and the number of turbulent eddies per unit mixture volume, respectively. In Equation 17.134 (p. 508)

$$\lambda_B = exp\left(-K_B \frac{\sigma}{\rho_f d_b^{5/3}\varepsilon^{2/3}}\right) \tag{17.135}$$

The experimental adjustable coefficients are given as follows:


Release 15.0 - © SAS IP, Inc. All rights reserved. - Contains proprietary and confidential information of ANSYS, Inc. and its subsidiaries and affiliates.

$\Gamma_C = 0.188; K_C = 0.129; \Gamma_B = 0.264; K_B = 1.37.$

The shape factor $\psi$ is given as 6 and $\phi$ as $\frac{1}{36\pi}$ for spherical particles/bubbles. There is no model for $S_{WE}$ in the Hibiki-Ishii formulation.

### 17.4.11.2. Ishii-Kim Model

$$\begin{aligned} S_{RC} &= -\frac{1}{3\phi}\left(\frac{\alpha_g}{\chi_p}\right)^2 C_{RC}\left[\frac{n_b^2 u_t d_b^2}{\alpha_{g\max}^{1/3}\left(\alpha_{g\max}^{1/3}-\alpha_g^{1/3}\right)}\right]\left[1-exp\left(-C\frac{\alpha_{g\max}^{1/3}\alpha_g^{1/3}}{\alpha_{g\max}^{1/3}-\alpha_g^{1/3}}\right)\right] \\ &= -\frac{1}{3\pi}C_{RC}u_t\chi_p^2\left[\frac{1}{\alpha_{g\max}^{1/3}\left(\alpha_{g\max}^{1/3}-\alpha_g^{1/3}\right)}\right]\left[1-exp\left(-C\frac{\alpha_{g\max}^{1/3}\alpha_g^{1/3}}{\alpha_{g\max}^{1/3}-\alpha_g^{1/3}}\right)\right] \end{aligned} \tag{17.136}$$

$$S_{WE} = -\frac{1}{3\phi}\left(\frac{\alpha_g}{\chi_p}\right)^2 n_b^2 d_b^2 u_r C_D^{1/3} = -\frac{1}{3\pi}C_{WE}u_r\chi_p^2 C_D^{1/3} \tag{17.137}$$

$$\begin{aligned} S_{TI} &= \frac{1}{3\phi}\left(\frac{\alpha_g}{\chi_p}\right)^2 C_{TI}\left(\frac{n_b u_t}{d_b}\right)\left(1-\frac{We_{cr}}{We}\right)^{1/2} exp\left(-\frac{We_{cr}}{We}\right) \\ &= \frac{1}{18}C_{TI}u_t\frac{\chi_p^2}{\alpha_g}\left(1-\frac{We_{cr}}{We}\right)^{1/2} exp\left(-\frac{We_{cr}}{We}\right) \end{aligned} \tag{17.138}$$

where the mean bubble fluctuating velocity, $u_t$, is given by $\varepsilon^{1/3}d_b^{1/3}$. The bubble terminal velocity, $u_r$, is a function of the bubble diameter and local time-averaged void fraction.

$$u_r = \left(\frac{d_b g \Delta\rho}{3C_D\rho_f}\right)^{1/2} \tag{17.139}$$

$$C_D = 24\frac{\left(1+0.1Re_D^{0.75}\right)}{Re_D} \quad and \quad Re_D \equiv \frac{\rho_f u_r d_b}{\mu_f}\left(1-\alpha_g\right) \tag{17.140}$$

$$We = \frac{\rho_f u_t^2 d_b}{\sigma} \tag{17.141}$$

where $\mu_f$ is the molecular viscosity of the fluid phase, $g$ is the gravitational acceleration and $\sigma$ is the interfacial tension. In this model, when the Weber number, $We$, is less than the critical Weber number, $We_{cr}$, the breakage rate equals zero, that is, $S_{TI} = 0$. The coefficients used are given as follows [178] (p. 738):

$C_{RC}$ = 0.004

$C_{WE}$ = 0.002

$C_{TI}$ = 0.085

$C$ = 3.0

$We_{cr}$ = 6.0

$\alpha_{g\max}$ = 0.75

**Important**

Currently, this model is only suitable for two-phase flow regimes, one phase being gas and another liquid, that is, bubbly column applications. However, you can always use UDFs to include your own interfacial area concentration models, which can apply to other flow regimes.

See the UDF Manual for details.

### 17.4.11.3. Yao-Morel Model

The volumetric interfacial area is an important quantity that appears in the calculation of the interphase exchange forces like momentum, mass, and heat transfer. In ANSYS Fluent, the Hibiki and Ishii model ([163] (p. 738)) and the Ishii and Kim model (Hibiki-Ishii Model (p. 508)) have been implemented In the context of bubbly flows with bulk mass transfer. An extension to these two models exists. This will include heterogeneous mass transfer effects on wall based on the work done by Yao and Morel [500] (p. 756) for nucleate boiling applications. The volumetric interfacial area transport Equation 17.130 (p. 507) contains a nucleation term and models for coalescence and breakup. Yao and Morel [500] (p. 756) modeled the coalescence term as follows:

$$\Phi^{CO} = \frac{1}{2}\frac{\eta_c n}{T_{cf}+T_{ci}} \tag{17.142}$$

where $T_{cf}$ and $T_{cI}$ are the free traveling time and the interaction time for coalescence, $n$ is the bubble number density, $\eta_c$ is the coalescence efficiency and the factor one-half has been included to avoid double counting on the same events between bubble pairs. The final expression for the above equation is

$$\Phi^{CO} = -K_{c1}\frac{\varepsilon^{1/3}\alpha^2}{d_b^{11/3}}\frac{1}{g(\alpha)+K_{c2}\alpha\sqrt{\frac{We}{We_c}}}\cdot\exp\left(K_{c3}\sqrt{\frac{We}{We_c}}\right) \tag{17.143}$$

where $We_c = 1.24$ is the critical Weber number and the coefficients have the values $K_{c1} = 2.86$, $K_{c2} = 1.922, K_{c3} = 1.017, We$ is the Weber number, $\varepsilon$ is the dissipation obtained from the k-epsilon turbulence model, $g(\alpha)$ is a modification factor defined as $1 - \left({}^{\alpha}/_{\alpha_{\max}}\right)^{1/3}$ and $\alpha_{\max} = 0.52$ is the packing limit. Regarding Equation 17.130 (p. 507), the coalescence sink terms due to random collision and wake entrainment are as follows:

$$S_{RC}+S_{WE} = \frac{1}{3\phi}\left(\frac{\alpha}{\chi_p}\right)^2\Phi^{CO} \tag{17.144}$$

The breakage term, as modeled by Yao and Morel [500] (p. 756), is


Release 15.0 - © SAS IP, Inc. All rights reserved. - Contains proprietary and confidential information of ANSYS, Inc. and its subsidiaries and affiliates.

$$\Phi^{BK}=\frac{\eta_b n}{T_{bf}+T_{bi}} \tag{17.145}$$

where $T_{bf}$ and $T_{bi}$ are the free traveling time and the interaction time for breakage and , $\eta_b$ is the breakage efficiency. The final expression for the above equation is of the form

$$\Phi^{BK}=K_{b1}\frac{\varepsilon^{1/3}\alpha(1-\alpha)}{d_b^{11/3}}\frac{1}{1+K_{b2}(1-\alpha)\sqrt{\frac{We}{We_c}}}\cdot\exp\left(-\frac{We}{We_c}\right) \tag{17.146}$$

Here, the coefficients have the values $K_{b1}=1.6$ and $K_{b2}=0.42$

Regarding Equation 17.130 (p. 507), the $S_{TI}$ breakage source term due to turbulent impact is of the form

$$S_{TI}=\frac{1}{3\phi}\left(\frac{\alpha}{\chi_p}\right)^2\Phi^{BK} \tag{17.147}$$

When including source terms due to bubble nucleation at the heated wall a new term should be added to Equation 17.130 (p. 507). This is of the form

$$\Phi^{NUC}=\pi d_{bw}^2 N_w f\frac{A_{heated}}{Volume} \tag{17.148}$$

where $d_{bw}$ is the diameter of the nucleation bubble, $N_w$ is the nucleation site density, and $f$ is the frequency of the bubble. These parameters can be connected to the boiling models described in Wall Boiling Models (p. 565). The bubble departure frequency is given by Equation 17.400 (p. 566), the nucleate site density by Equation 17.401 (p. 567), the bubble departure diameter by Equation 17.404 (p. 567), Equation 17.405 (p. 567), or Equation 17.406 (p. 567), while the interface to liquid mass transfer ($\dot{m}_v$ here) is defined by Equation 17.421 (p. 573) and Equation 17.424 (p. 573).

To learn how to apply this model, refer to Defining the Interfacial Area Concentration in the User's Guide.

## 17.5. Eulerian Model Theory

Details about the Eulerian multiphase model are presented in the following subsections:

17.5.1. Overview of the Eulerian Model
17.5.2. Limitations of the Eulerian Model
17.5.3. Volume Fraction Equation
17.5.4. Conservation Equations
17.5.5. Interfacial Area Concentration
17.5.6. Interphase Exchange Coefficients
17.5.7. Lift Force
17.5.8. Wall Lubrication Force
17.5.9. Turbulent Dispersion Force
17.5.10. Virtual Mass Force
17.5.11. Solids Pressure
17.5.12. Maximum Packing Limit in Binary Mixtures
17.5.13. Solids Shear Stresses
17.5.14. Granular Temperature
17.5.15. Description of Heat Transfer

Release 15.0 - © SAS IP, Inc. All rights reserved. - Contains proprietary and confidential information of ANSYS, Inc. and its subsidiaries and affiliates.

17.5.16. Turbulence Models
17.5.17. Solution Method in ANSYS Fluent
17.5.18. Dense Discrete Phase Model
17.5.19. Multi-Fluid VOF Model
17.5.20. Wall Boiling Models

## 17.5.1. Overview of the Eulerian Model

The Eulerian multiphase model in ANSYS Fluent allows for the modeling of multiple separate, yet interacting phases. The phases can be liquids, gases, or solids in nearly any combination. An Eulerian treatment is used for each phase, in contrast to the Eulerian-Lagrangian treatment that is used for the discrete phase model.

With the Eulerian multiphase model, the number of secondary phases is limited only by memory requirements and convergence behavior. Any number of secondary phases can be modeled, provided that sufficient memory is available. For complex multiphase flows, however, you may find that your solution is limited by convergence behavior. See Eulerian Model in the User's Guide for multiphase modeling strategies.

ANSYS Fluent's Eulerian multiphase model does not distinguish between fluid-fluid and fluid-solid (granular) multiphase flows. A granular flow is simply one that involves at least one phase that has been designated as a granular phase.

The ANSYS Fluent solution is based on the following:

- A single pressure is shared by all phases.
- Momentum and continuity equations are solved for each phase.
- The following parameters are available for granular phases:
  - Granular temperature (solids fluctuating energy) can be calculated for each solid phase. You can select either an algebraic formulation, a constant, a user-defined function, or a partial differential equation.
  - Solid-phase shear and bulk viscosities are obtained by applying kinetic theory to granular flows. Frictional viscosity for modeling granular flow is also available. You can select appropriate models and user-defined functions for all properties.
- Several interphase drag coefficient functions are available, which are appropriate for various types of multiphase regimes. (You can also modify the interphase drag coefficient through user-defined functions, as described in the UDF Manual.)
- All of the $k$- $\varepsilon$ and $k$- $\omega$ turbulence models are available, and may apply to all phases or to the mixture.

## 17.5.2. Limitations of the Eulerian Model

All other features available in ANSYS Fluent can be used in conjunction with the Eulerian multiphase model, except for the following limitations:

- The Reynolds Stress turbulence model is not available on a per phase basis.
- Particle tracking (using the Lagrangian dispersed phase model) interacts only with the primary phase.


Release 15.0 - © SAS IP, Inc. All rights reserved. - Contains proprietary and confidential information of ANSYS, Inc. and its subsidiaries and affiliates.

- Streamwise periodic flow with specified mass flow rate cannot be modeled when the Eulerian model is used (you are allowed to specify a pressure drop).
- Inviscid flow is not allowed.
- Melting and solidification are not allowed.
- When tracking particles in parallel, the DPM model cannot be used with the Eulerian multiphase model if the shared memory option is enabled (Parallel Processing for the Discrete Phase Model in the User's Guide). (Note that using the message passing option, when running in parallel, enables the compatibility of all multiphase flow models with the DPM model.)

To change from a single-phase model to a multiphase model, you will have to do this in a series of steps. You will have to set up a mixture solution and then a multiphase solution. However, since multiphase problems are strongly linked, it is better to start directly solving a multiphase problem with an initial conservative set of parameters (first order in time and space). This is of course problem dependent. The modifications involve, among other things, the introduction of the volume fractions $\alpha_1, \alpha_2, \ldots \alpha_n$ for the multiple phases, as well as mechanisms for the exchange of momentum, heat, and mass between the phases.

## 17.5.3. Volume Fraction Equation

The description of multiphase flow as interpenetrating continua incorporates the concept of phasic volume fractions, denoted here by $\alpha_q$. Volume fractions represent the space occupied by each phase, and the laws of conservation of mass and momentum are satisfied by each phase individually. The derivation of the conservation equations can be done by ensemble averaging the local instantaneous balance for each of the phases [6] (p. 729) or by using the mixture theory approach [38] (p. 731).

The volume of phase $q$, $V_q$, is defined by

$$V_q = \int_V \alpha_q dV \tag{17.149}$$

where

$$\sum_{q=1}^{n} \alpha_q = 1 \tag{17.150}$$

The effective density of phase $q$ is

$$\hat{\rho}_q = \alpha_q \rho_q \tag{17.151}$$

where $\rho_q$ is the physical density of phase $q$.

The volume fraction equation may be solved either through implicit or explicit time discretization. For detailed information about both VOF schemes, refer to The Implicit Scheme (p. 476) and The Explicit Scheme (p. 476).

## 17.5.4. Conservation Equations

The general conservation equations from which the equations solved by ANSYS Fluent are derived are presented in this section, followed by the solved equations themselves.

Release 15.0 - © SAS IP, Inc. All rights reserved. - Contains proprietary and confidential information of ANSYS, Inc. and its subsidiaries and affiliates.

## 17.5.4.1. Equations in General Form

### 17.5.4.1.1. Conservation of Mass

The continuity equation for phase $q$ is

$$\frac{\partial}{\partial t}\left(\alpha_q \rho_q\right) + \nabla \cdot \left(\alpha_q \rho_q \vec{v}_q\right) = \sum_{p=1}^{n}\left(\dot{m}_{pq} - \dot{m}_{qp}\right) + S_q \tag{17.152}$$

where $\vec{v}_q$ is the velocity of phase $q$ and $\dot{m}_{pq}$ characterizes the mass transfer from the $p^{th}$ to $q^{th}$ phase, and $\dot{m}_{qp}$ characterizes the mass transfer from phase $q$ to phase $p$, and you are able to specify these mechanisms separately.

By default, the source term $S_q$ on the right-hand side of Equation 17.152 (p. 514) is zero, but you can specify a constant or user-defined mass source for each phase. A similar term appears in the momentum and enthalpy equations. See Modeling Mass Transfer in Multiphase Flows (p. 579) for more information on the modeling of mass transfer in ANSYS Fluent's general multiphase models.

### 17.5.4.1.2. Conservation of Momentum

The momentum balance for phase $q$ yields

$$\begin{aligned}\frac{\partial}{\partial t}\left(\alpha_q \rho_q \vec{v}_q\right) + \nabla \cdot \left(\alpha_q \rho_q \vec{v}_q \vec{v}_q\right) &= -\alpha_q \nabla p + \nabla \cdot \overline{\overline{\tau}}_q + \alpha_q \rho_q \vec{g} \\ &+ \sum_{p=1}^{n}\left(\vec{R}_{pq} + \dot{m}_{pq}\vec{v}_{pq} - \dot{m}_{qp}\vec{v}_{qp}\right) \\ &+ \left(\vec{F}_q + \vec{F}_{lift,q} + \vec{F}_{wl,q} + \vec{F}_{vm,q} + \vec{F}_{td,q}\right)\end{aligned} \tag{17.153}$$

where $\overline{\overline{\tau}}_q$ is the $q^{th}$ phase stress-strain tensor

$$\overline{\overline{\tau}}_q = \alpha_q \mu_q \left(\nabla \vec{v}_q + \nabla \vec{v}_q^{\,T}\right) + \alpha_q\left(\lambda_q - \frac{2}{3}\mu_q\right)\nabla \cdot \vec{v}_q \overline{\overline{I}} \tag{17.154}$$

Here $\mu_q$ and $\lambda_q$ are the shear and bulk viscosity of phase $q$, $\vec{F}_q$ is an external body force, $\vec{F}_{lift,q}$ is a lift force (described in Lift Force (p. 528)), $\vec{F}_{wl,q}$ is a wall lubrication force (described in Wall Lubrication Force (p. 532)), $\vec{F}_{vm,q}$ is a virtual mass force, and $\vec{F}_{td,q}$ is a turbulent dispersion force (in the case of turbulent flows only). $\vec{R}_{pq}$ is an interaction force between phases, and $p$ is the pressure shared by all phases.

$\vec{v}_{pq}$ is the interphase velocity, defined as follows. If $\dot{m}_{pq} > 0$ (that is, phase $p$ mass is being transferred to phase $q$), $\vec{v}_{pq} = \vec{v}_p$; if $\dot{m}_{pq} < 0$ (that is, phase $q$ mass is being transferred to phase $p$), $\vec{v}_{pq} = \vec{v}_q$. Likewise, if $\dot{m}_{qp} > 0$ then $v_{qp} = v_q$, if $\dot{m}_{qp} < 0$ then $v_{qp} = v_p$.


Release 15.0 - © SAS IP, Inc. All rights reserved. - Contains proprietary and confidential information of ANSYS, Inc. and its subsidiaries and affiliates.

Equation 17.153 (p. 514) must be closed with appropriate expressions for the interphase force $\vec{R}_{pq}$. This force depends on the friction, pressure, cohesion, and other effects, and is subject to the conditions that $\vec{R}_{pq} = -\vec{R}_{qp}$ and $\vec{R}_{qq} = 0$.

ANSYS Fluent uses a simple interaction term of the following form:

$$\sum_{p=1}^{n} \vec{R}_{pq} = \sum_{p=1}^{n} K_{pq} \left( \vec{v}_p - \vec{v}_q \right) \tag{17.155}$$

where $K_{pq}$ ($=K_{qp}$) is the interphase momentum exchange coefficient (described in Interphase Exchange Coefficients (p. 518)), and $\vec{v}_p$ and $\vec{v}_q$ are the phase velocities. Note that Equation 17.155 (p. 515) represents the mean interphase momentum exchange and does not include any contribution due to turbulence. The turbulent interphase momentum exchange is modeled with the turbulent dispersion force term, $\vec{F}_{td,q}$ in Equation 17.153 (p. 514), as described in Turbulent Dispersion Force (p. 534).

#### 17.5.4.1.3. Conservation of Energy

To describe the conservation of energy in Eulerian multiphase applications, a separate enthalpy equation can be written for each phase:

$$\begin{aligned} \frac{\partial}{\partial t}\left(\alpha_q \rho_q h_q\right) + \nabla \cdot \left(\alpha_q \rho_q \vec{u}_q h_q\right) &= \alpha_q \frac{\partial p_q}{\partial t} + \overline{\overline{\tau}}_q : \nabla \vec{u}_q - \nabla \cdot \vec{q}_q \\ &\quad + S_q + \sum_{p=1}^{n} \left( Q_{pq} + \dot{m}_{pq} h_{pq} - \dot{m}_{qp} h_{qp} \right) \end{aligned} \tag{17.156}$$

where $h_q$ is the specific enthalpy of the $q^{th}$ phase, $\vec{q}_q$ is the heat flux, $S_q$ is a source term that includes sources of enthalpy (for example, due to chemical reaction or radiation), $Q_{pq}$ is the intensity of heat exchange between the $p^{th}$ and $q^{th}$ phases, and $h_{pq}$ is the interphase enthalpy (for example, the enthalpy of the vapor at the temperature of the droplets, in the case of evaporation). The heat exchange between phases must comply with the local balance conditions $Q_{pq} = -Q_{qp}$ and $Q_{qq} = 0$.

### 17.5.4.2. Equations Solved by ANSYS Fluent

The equations for fluid-fluid and granular multiphase flows, as solved by ANSYS Fluent, are presented here for the general case of an $n$-phase flow.

#### 17.5.4.2.1. Continuity Equation

The volume fraction of each phase is calculated from a continuity equation:

$$\frac{1}{\rho_{rq}} \left( \frac{\partial}{\partial t}\left(\alpha_q \rho_q\right) + \nabla \cdot \left(\alpha_q \rho_q \vec{v}_q\right) = \sum_{p=1}^{n} \left( \dot{m}_{pq} - \dot{m}_{qp} \right) \right) \tag{17.157}$$

where $\rho_{rq}$ is the phase reference density, or the volume averaged density of the $q^{th}$ phase in the solution domain.

Release 15.0 - © SAS IP, Inc. All rights reserved. - Contains proprietary and confidential information of ANSYS, Inc. and its subsidiaries and affiliates.

The solution of this equation for each secondary phase, along with the condition that the volume fractions sum to one (given by Equation 17.150 (p. 513)), allows for the calculation of the primary-phase volume fraction. This treatment is common to fluid-fluid and granular flows.

### 17.5.4.2.2. Fluid-Fluid Momentum Equations

The conservation of momentum for a fluid phase $q$ is

$$\frac{\partial}{\partial t}\left(\alpha_q \rho_q \vec{v}_q\right) + \nabla \cdot \left(\alpha_q \rho_q \vec{v}_q \vec{v}_q\right) = -\alpha_q \nabla p + \nabla \cdot \bar{\bar{\tau}}_q + \alpha_q \rho_q \vec{g} + \sum_{p=1}^{n}\left(K_{pq}\left(\vec{v}_p - \vec{v}_q\right) + \dot{m}_{pq}\vec{v}_{pq} - \dot{m}_{qp}\vec{v}_{qp}\right) + \left(\vec{F}_q + \vec{F}_{lift,q} + \vec{F}_{wl,q} + \vec{F}_{vm,q} + \vec{F}_{td,q}\right) \tag{17.158}$$

Here $\vec{g}$ is the acceleration due to gravity and $\bar{\bar{\tau}}_q$, $\vec{F}_q$, $\vec{F}_{lift,q}$, $\vec{F}_{wl,q}$, $\vec{F}_{vm,q}$, and $\vec{F}_{td,q}$ are as defined for Equation 17.153 (p. 514).

### 17.5.4.2.3. Fluid-Solid Momentum Equations

Following the work of [3] (p. 729), [60] (p. 732), [91] (p. 734), [139] (p. 736), [235] (p. 742), [271] (p. 744), [326] (p. 747), [441] (p. 753), ANSYS Fluent uses a multi-fluid granular model to describe the flow behavior of a fluid-solid mixture. The solid-phase stresses are derived by making an analogy between the random particle motion arising from particle-particle collisions and the thermal motion of molecules in a gas, taking into account the inelasticity of the granular phase. As is the case for a gas, the intensity of the particle velocity fluctuations determines the stresses, viscosity, and pressure of the solid phase. The kinetic energy associated with the particle velocity fluctuations is represented by a "pseudothermal" or granular temperature which is proportional to the mean square of the random motion of particles.

The conservation of momentum for the fluid phases is similar to Equation 17.158 (p. 516), and that for the $s^{th}$ solid phase is

$$\frac{\partial}{\partial t}\left(\alpha_s \rho_s \vec{v}_s\right) + \nabla \cdot \left(\alpha_s \rho_s \vec{v}_s \vec{v}_s\right) = -\alpha_s \nabla p - \nabla p_s + \nabla \cdot \bar{\bar{\tau}}_s + \alpha_s \rho_s \vec{g} + \sum_{l=1}^{N}\left(K_{ls}\left(\vec{v}_l - \vec{v}_s\right) + \dot{m}_{ls}\vec{v}_{ls} - \dot{m}_{sl}\vec{v}_{sl}\right) + \left(\vec{F}_s + \vec{F}_{lift,s} + \vec{F}_{vm,s} + \vec{F}_{td,s}\right) \tag{17.159}$$

where $p_s$ is the $s^{th}$ solids pressure, $K_{ls}=K_{sl}$ is the momentum exchange coefficient between fluid or solid phase $l$ and solid phase $s$, $N$ is the total number of phases, and $\vec{F}_s$, $\vec{F}_{lift,s}$, $\vec{F}_{vm,s}$, and $\vec{F}_{td,s}$ are defined in the same manner as the analogous terms in Equation 17.153 (p. 514).

### 17.5.4.2.4. Conservation of Energy

The equation solved by ANSYS Fluent for the conservation of energy is Equation 17.156 (p. 515).


Release 15.0 - © SAS IP, Inc. All rights reserved. - Contains proprietary and confidential information of ANSYS, Inc. and its subsidiaries and affiliates.

## 17.5.5. Interfacial Area Concentration

Interfacial area concentration is defined as the interfacial area between two phases per unit mixture volume. This is an important parameter for predicting mass, momentum and energy transfers through the interface between the phases. When using the Eulerian multiphase model with non-granular secondary phases, you can have ANSYS Fluent compute the interfacial area in one of two ways:

- use a transport equation for interfacial area concentration as described in Interfacial Area Concentration (p. 507). This allows for a distribution of bubble diameters and coalescence/breakage effects.
- use an algebraic relationship between a specified bubble diameter and the interfacial area concentration.

The algebraic interfacial area models are derived from the surface area to volume ratio, $A_p$, for a spherical bubble or droplet:

$$A_p = \frac{\pi d_p^2}{\frac{1}{6}\pi d_p^3} = \frac{6}{d_p} \tag{17.160}$$

where $d_p$ is the bubble or droplet diameter. The algebraic models available when using the Eulerian multiphase model are:

**Particle Model**

For a dispersed phase, $p$, with volume fraction, $\alpha_p$, the particle model estimates the interfacial area concentration, $A_i$ as

$$A_i = \alpha_p A_p = \frac{6\alpha_p}{d_p} \tag{17.161}$$

**Symmetric Model (default)**

The symmetric model differs from the particle model in that it introduces the complimentary volume fraction (corresponding to the primary phase volume fraction for a two-phase flow) which ensures that the interfacial area concentration approaches 0 as $\alpha_p$ approaches 1.

$$A_i = \frac{6\alpha_p(1-\alpha_p)}{d_p} \tag{17.162}$$

**Ishii Model (boiling flows only)**

The Ishii model, which is only available when the boiling model is activated, also modifies the particle model and results in a piecewise linear function of $\alpha_p$ that approaches 0 as $\alpha_p$ approaches 1.

$$A_i = \frac{6(1-\alpha_p)\min(\alpha_p, \alpha_{p,crit})}{d_p(1-\min(\alpha_p, \alpha_{p,crit}))} \tag{17.163}$$

In Fluent, $\alpha_{p,crit}$ is chosen as 0.25.

**User-Defined (boiling flows only)**

See `DEFINE_EXCHANGE_PROPERTY` in the Fluent UDF Manual.

Release 15.0 - © SAS IP, Inc. All rights reserved. - Contains proprietary and confidential information of ANSYS, Inc. and its subsidiaries and affiliates.

## 17.5.6. Interphase Exchange Coefficients

It can be seen in Equation 17.158 (p. 516) and Equation 17.159 (p. 516) that momentum exchange between the phases is based on the value of the fluid-fluid exchange coefficient $K_{pq}$ and, for granular flows, the fluid-solid and solid-solid exchange coefficients $K_{ls}$.

### 17.5.6.1. Fluid-Fluid Exchange Coefficient

For fluid-fluid flows, each secondary phase is assumed to form droplets or bubbles. This has an impact on how each of the fluids is assigned to a particular phase. For example, in flows where there are unequal amounts of two fluids, the predominant fluid should be modeled as the primary fluid, since the sparser fluid is more likely to form droplets or bubbles. The exchange coefficient for these types of bubbly, liquid-liquid or gas-liquid mixtures can be written in the following general form:

$$K_{pq} = \frac{\rho_p f}{6\tau_p} d_p A_i \tag{17.164}$$

where $A_i$ is the interfacial area (see Interfacial Area Concentration (p. 517)), $f$, the drag function, is defined differently for the different exchange-coefficient models (as described below) and $\tau_p$, the "particulate relaxation time", is defined as

$$\tau_p = \frac{\rho_p d_p^2}{18\mu_q} \tag{17.165}$$

where $d_p$ is the diameter of the bubbles or droplets of phase $p$.

Nearly all definitions of $f$ include a drag coefficient ($C_D$) that is based on the relative Reynolds number ($Re$). It is this drag function that differs among the exchange-coefficient models. For all these situations, $K_{pq}$ should tend to zero whenever the primary phase is not present within the domain. To enforce this, the drag function $f$ is always multiplied by the volume fraction of the primary phase $q$, as is reflected in Equation 17.164 (p. 518).

For each pair of phases in fluid-fluid flows you may use one of the available drag function models in ANSYS Fluent or a user-defined function to specify the interphase exchange coefficient. If the exchange coefficient is equal to zero (that is, if no exchange coefficient is specified), the flow fields for the fluids will be computed independently, with the only "interaction" being their complementary volume fractions within each computational cell. You can specify different exchange coefficients for each pair of phases.

The following drag models are available in ANSYS Fluent.

17.5.6.1.1. Schiller and Naumann Model
17.5.6.1.2. Morsi and Alexander Model
17.5.6.1.3. Symmetric Model
17.5.6.1.4. Grace et al. Model
17.5.6.1.5. Tomiyama et al. Model
17.5.6.1.6. Ishii Model
17.5.6.1.7. Universal Drag Laws for Bubble-Liquid and Droplet-Gas Flows

#### 17.5.6.1.1. Schiller and Naumann Model

For the model of Schiller and Naumann [393] (p. 750)


Release 15.0 - © SAS IP, Inc. All rights reserved. - Contains proprietary and confidential information of ANSYS, Inc. and its subsidiaries and affiliates.

$$f = \frac{C_D Re}{24} \tag{17.166}$$

where

$$C_D = \begin{cases} 24\left(1 + 0.15 Re^{0.687}\right)/Re & Re \le 1000 \\ 0.44 & Re > 1000 \end{cases} \tag{17.167}$$

and Re is the relative Reynolds number. The relative Reynolds number for the primary phase $q$ and secondary phase $p$ is obtained from

$$Re = \frac{\rho_q \mid \vec{v}_p - \vec{v}_q \mid d_p}{\mu_q} \tag{17.168}$$

The relative Reynolds number for secondary phases $p$ and $r$ is obtained from

$$Re = \frac{\rho_{rp} \mid \vec{v}_r - \vec{v}_p \mid d_{rp}}{\mu_{rp}} \tag{17.169}$$

where $\mu_{rp} = \alpha_p \mu_p + \alpha_r \mu_r$ is the mixture viscosity of the phases $p$ and $r$.

The Schiller and Naumann model is the default method, and it is acceptable for general use for all fluid-fluid pairs of phases.

### 17.5.6.1.2. Morsi and Alexander Model

For the Morsi and Alexander model [309] (p. 746)

$$f = \frac{C_D Re}{24} \tag{17.170}$$

where

$$C_D = a_1 + \frac{a_2}{Re} + \frac{a_3}{Re^2} \tag{17.171}$$

and Re is defined by Equation 17.168 (p. 519) or Equation 17.169 (p. 519). The constants, $a_i$, are defined as follows:

$$a_1, a_2, a_3 = \begin{cases} 0, 24, 0 & 0 < Re < 0.1 \\ 3.690, 22.73, 0.0903 & 0.1 < Re < 1 \\ 1.222, 29.1667, -3.8889 & 1 < Re < 10 \\ 0.6167, 46.50, -116.67 & 10 < Re < 100 \\ 0.3644, 98.33, -2778 & 100 < Re < 1000 \\ 0.357, 148.62, -47500 & 1000 < Re < 5000 \\ 0.46, -490.546, 578700 & 5000 < Re < 10000 \\ 0.5191, -1662.5, 5416700 & Re \ge 10000 \end{cases} \tag{17.172}$$

The Morsi and Alexander model is the most complete, adjusting the function definition frequently over a large range of Reynolds numbers, but calculations with this model may be less stable than with the other models.

Release 15.0 - © SAS IP, Inc. All rights reserved. - Contains proprietary and confidential information of ANSYS, Inc. and its subsidiaries and affiliates.

### 17.5.6.1.3. Symmetric Model

For the symmetric model, the density and the viscosity are calculated from volume averaged properties:

$$\rho_{pq}=\alpha_p\rho_p+\alpha_q\rho_q \tag{17.173}$$

$$\mu_{pq}=\alpha_p\mu_p+\alpha_q\mu_q \tag{17.174}$$

and the diameter is defined as

$$d_{pq}=\frac{1}{2}\left(d_p+d_q\right) \tag{17.175}$$

in turn

$$K_{pq}=\frac{\rho_{pq}f}{6\tau_{pq}}d_pA_i \tag{17.176}$$

$$\tau_{pq}=\frac{\rho_{pq}\left(d_{pq}\right)^2}{18\mu_{pq}} \tag{17.177}$$

$$Re=\frac{\varrho_{pq}\mid v_p-v_q\mid d_{pq}}{\mu_{pq}} \tag{17.178}$$

$$f=\frac{C_DRe}{24} \tag{17.179}$$

and $C_D$ is defined by Equation 17.167 (p. 519).

Note that if there is only one dispersed phase, then $d_p=d_q$ in Equation 17.177 (p. 520).

The symmetric model is recommended for flows in which the secondary (dispersed) phase in one region of the domain becomes the primary (continuous) phase in another. For example, if air is injected into the bottom of a container filled halfway with water, the air is the dispersed phase in the bottom half of the container; in the top half of the container, the air is the continuous phase. This model can also be used for the interaction between secondary phases.

### 17.5.6.1.4. Grace et al. Model

For the model of Grace, et al. [69] (p. 732)

$$f=\frac{C_DRe}{24} \tag{17.180}$$

where

$$Re=\frac{\rho_q\mid\vec{v}_p-\vec{v}_q\mid d_p}{\mu_q} \tag{17.181}$$

$$C_D=\max\left(\min\left(C_{D_{ellipse}},C_{D_{cap}}\right),C_{D_{sphere}}\right) \tag{17.182}$$

In Equation 17.182 (p. 520) $C_{D_{ellipse}}$, $C_{D_{cap}}$, and $C_{D_{sphere}}$ are defined as follows:


Release 15.0 - © SAS IP, Inc. All rights reserved. - Contains proprietary and confidential information of ANSYS, Inc. and its subsidiaries and affiliates.

$$C_{D_{sphere}} = \begin{cases} 24/Re & Re < 0.01 \\ 24\left(1 + 0.15Re^{0.687}\right)/Re & Re \geq 0.01 \end{cases} \tag{17.183}$$

$$C_{D_{cap}} = \frac{8}{3} \tag{17.184}$$

$$C_{D_{ellipse}} = \frac{4}{3}\frac{gd_p}{U_t^2}\frac{\left(\rho_q - \rho_p\right)}{\rho_q} \tag{17.185}$$

where

$$U_t = \frac{\mu_q}{\rho_q d_p} Mo^{-0.149}(J - 0.857)$$

where $Mo$ is the Morton number given by:

$$Mo = \frac{\mu_q^4 g(\rho_q - \rho_p)}{\rho_q^2 \sigma^3}$$

$J$ is given by the piecewise function:

$$J = \begin{cases} 0.94H^{0.757} & 2 < H \leq 59.3 \\ 3.42H^{0.441} & H > 59.3 \end{cases}$$

$$H = \frac{4}{3} EoMo^{-0.149}\left(\frac{\mu_q}{\mu_{ref}}\right)^{-0.14}$$

where $Eo$ is the Eötvös number:

$$Eo = \frac{g(\rho_q - \rho_p)d_p^2}{\sigma}$$

and $\mu_{ref} = 0.0009 \, {kg}/{(m-s)}$.

The Grace et al. model is well suited to gas-liquid flows in which the bubbles can have a range of shapes.

### 17.5.6.1.5. Tomiyama et al. Model

For the model of Tomiyama, et al. [443] (p. 753)

$$f = \frac{C_D Re}{24} \tag{17.186}$$

where

$$Re = \frac{\rho_q \mid \vec{v}_p - \vec{v}_q \mid d_p}{\mu_q} \tag{17.187}$$

$$C_D = \max\left( \min\left( \frac{24}{Re}(1+0.15Re^{0.687}), \frac{72}{Re} \right), \frac{8}{3}\frac{Eo}{Eo+4} \right) \tag{17.188}$$

In Equation 17.188 (p. 522),

$$Eo = \frac{g(\rho_q - \rho_p) d_p^2}{\sigma}$$

Like the Grace et al. model, the Tomiyama et al. model is well suited to gas-liquid flows in which the bubbles can have a range of shapes.

### 17.5.6.1.6. Ishii Model

For boiling flows only, you can use the model of Ishii [177] (p. 738). For the Ishii model, the drag coefficient $C_D$ is determined by choosing the minimum of the viscous regime $\left(C_D^{\text{vis}}\right)$ and the distorted regime $\left(C_D^{\text{dis}}\right)$, defined as follows:

$$C_D = \min\left(C_D^{\text{vis}}, C_D^{\text{dis}}\right) \tag{17.189}$$

where $C_D^{\text{vis}}$ and $C_D^{\text{dis}}$ are given by the following formulas:

$$C_D^{\text{vis}} = \frac{24}{\text{Re}}\left(1 + 0.15\text{Re}^{0.75}\right) \tag{17.190}$$

$$C_D^{\text{dis}} = \frac{2}{3}\frac{d_p}{\sqrt{\frac{\sigma}{g|\rho_q - \rho_p|}}} \tag{17.191}$$

where $\text{Re}$ is the relative Reynolds number, $\sigma$ is the surface tension, and $g$ is gravity.

The bubble diameter $d_p$ is determined as in Bubble and Droplet Diameters (p. 571).

### 17.5.6.1.7. Universal Drag Laws for Bubble-Liquid and Droplet-Gas Flows

The universal drag laws [216] (p. 741) are suitable for the calculation of the drag coefficients in a variety of gas-liquid flow regimes. The drag laws can apply to non-spherical droplets/bubbles with the constraint of a pool flow regime, that is, the hydraulic diameter of the flow domain which is far larger than the averaged size of the particles.

The exchange coefficient for bubbly and droplet flows can be written in the general form

$$K_{pq} = \frac{\rho_p f}{6\tau_p} d_p A_i \tag{17.192}$$

Where $q$ represents the primary phase and $p$ the dispersed phase and $A_i$ is the interfacial area (see Interfacial Area Concentration (p. 517)). The dispersed phase relaxation time $\tau_p$ is defined as


Release 15.0 - © SAS IP, Inc. All rights reserved. - Contains proprietary and confidential information of ANSYS, Inc. and its subsidiaries and affiliates.

$$\tau_p = \frac{\rho_p d_p^2}{18\mu_e} \tag{17.193}$$

The drag function $f$ is defined as

$$f = \frac{C_D Re}{24} \tag{17.194}$$

The relative Reynolds number for the primary phase $q$ and the secondary phase $p$ is obtained based on the relative velocity of the two phases.

$$Re = \frac{\rho_q \mid \vec{v_q} - \vec{v_p} \mid d_p}{\mu_e} \tag{17.195}$$

Where $\mu_e$ is the effective viscosity of the primary phase accounting for the effects of family of particles in the continuum.

The Rayleigh-Taylor instability wavelength is

$$\lambda_{RT} = \left( \frac{\sigma}{g \Delta \rho_{pq}} \right)^{0.5} \tag{17.196}$$

Where $\sigma$ is the surface tension, $g$ the gravity, and $\Delta \rho_{pq}$ the absolute value of the density difference between phases $p$ and $q$.

The drag coefficient is defined differently for bubbly and droplet flows.

#### *17.5.6.1.7.1. Bubble-Liquid Flow*

$$C_{D_{vis}} = \frac{24}{Re}\left(1 + 0.1 Re^{0.75}\right) \tag{17.197}$$

$$C_{D_{dis}} = 2/3 \left( \frac{d_p}{\lambda_{RT}} \right) \left\{ \frac{1 + 17.67 f^{*6/7}}{18.67 f^*} \right\}^2 ; \; f^* = \left(1 - \alpha_p\right)^{1.5} \tag{17.198}$$

$$C_{D_{cap}} = \frac{8}{3}\left(1 - \alpha_p\right)^2 \tag{17.199}$$

- In the viscous regime, the following condition is satisfied:

  $$C_{D_{dis}} < C_{D_{vis}} \tag{17.200}$$

  The drag coefficient, $C_D$, is defined as

  $$C_D = C_{D_{vis}} \tag{17.201}$$

- In the distorted bubble regime, the following condition is satisfied:

  $$C_{D_{vis}} < C_{D_{dis}} < C_{D_{cap}} \tag{17.202}$$

  The drag coefficient is calculated as

  $$C_D = C_{D_{dis}} \tag{17.203}$$

Release 15.0 - © SAS IP, Inc. All rights reserved. - Contains proprietary and confidential information of ANSYS, Inc. and its subsidiaries and affiliates.

- In the strongly deformed, capped bubble regime, the following condition is satisfied:

$$C_{D_{dis}} > C_{D_{cap}} \tag{17.204}$$

The drag coefficient can be written as

$$C_D = C_{D_{cap}} \tag{17.205}$$

The effective viscosity for the bubble-liquid mixture is

$$\mu_e = \frac{\mu_q}{1-\alpha_p} \tag{17.206}$$

#### *17.5.6.1.7.2. Droplet-Gas Flow*

- When $\mathrm{Re} < 1$, the drag coefficient for the stokes regime is

$$C_D = \frac{24}{Re} \tag{17.207}$$

- When $1 \leq \mathrm{Re} \leq 1000$, the drag coefficient for the viscous regime is

$$C_D = \frac{24}{Re}\left(1 + 0.1Re^{0.75}\right) \tag{17.208}$$

- For the Newton's regime ($\mathrm{Re} \geq 1000$), the drag coefficient is

$$C_D = 2/3\left(\frac{d_p}{\lambda_{RT}}\right)\left\{\frac{1+17.67f^{*6/7}}{18.67f^*}\right\}^2 ; f^* = \left(1-\alpha_p\right)^3 \tag{17.209}$$

The effective viscosity for a bubble-liquid mixture is

$$\mu_e = \frac{\mu_q}{\left(1-\alpha_p\right)^{2.5}} \tag{17.210}$$

**Important**

The universal drag models are currently suitable for bubble-liquid and/or droplet-gas flow where the characteristic length of the flow domain is much larger than the averaged size of the particles.

### *17.5.6.2. Fluid-Solid Exchange Coefficient*

The fluid-solid exchange coefficient $K_{sl}$ can be written in the following general form:

$$K_{sl} = \frac{\alpha_s \rho_s f}{\tau_s} \tag{17.211}$$

where $f$ is defined differently for the different exchange-coefficient models (as described below), and $\tau_s$, the "particulate relaxation time", is defined as

$$\tau_s = \frac{\rho_s d_s^2}{18\mu_l} \tag{17.212}$$


Release 15.0 - © SAS IP, Inc. All rights reserved. - Contains proprietary and confidential information of ANSYS, Inc. and its subsidiaries and affiliates.

where $d_s$ is the diameter of particles of phase $s$.

All definitions of $f$ include a drag function ($C_D$) that is based on the relative Reynolds number ($\mathrm{Re}_s$). It is this drag function that differs among the exchange-coefficient models.

- For the Syamlal-O'Brien model [440] (p. 753)

$$f = \frac{C_D Re_s \alpha_l}{24 v_{r,s}^2} \tag{17.213}$$

where the drag function has a form derived by Dalla Valle [85] (p. 733)

$$C_D = \left( 0.63 + \frac{4.8}{\sqrt{Re_s / v_{r,s}}} \right)^2 \tag{17.214}$$

This model is based on measurements of the terminal velocities of particles in fluidized or settling beds, with correlations that are a function of the volume fraction and relative Reynolds number [379] (p. 750):

$$Re_s = \frac{\rho_l d_s \mid \vec{v}_s - \vec{v}_l \mid}{\mu_l} \tag{17.215}$$

where the subscript $l$ is for the $l^{th}$ fluid phase, $s$ is for the $s^{th}$ solid phase, and $d_s$ is the diameter of the $s^{th}$ solid phase particles.

The fluid-solid exchange coefficient has the form

$$K_{sl} = \frac{3 \alpha_s \alpha_l \rho_l}{4 v_{r,s}^2 d_s} C_D \left( \frac{Re_s}{v_{r,s}} \right) \mid \vec{v}_s - \vec{v}_l \mid \tag{17.216}$$

where $v_{r,s}$ is the terminal velocity correlation for the solid phase [132] (p. 736):

$$v_{r,s} = 0.5 \left( A - 0.06 Re_s + \sqrt{(0.06 Re_s)^2 + 0.12 Re_s (2B - A) + A^2} \right) \tag{17.217}$$

with

$$A = \alpha_l^{4.14} \tag{17.218}$$

and

$$B = 0.8 \alpha_l^{1.28} \tag{17.219}$$

for $\alpha_l \leq 0.85$, and

$$B = \alpha_l^{2.65} \tag{17.220}$$

for $\alpha_l > 0.85$.

This model is appropriate when the solids shear stresses are defined according to Syamlal et al. [441] (p. 753) (Equation 17.294 (p. 542)).

- The parameterized Syamlal-O'Brien model is an enhancement of the Syamlal-O'Brien model in which the values of 0.8 and 2.65 in Equation 17.219 (p. 525) and Equation 17.220 (p. 525) are replaced by parameters that are adjusted based on the fluid flow properties and the expected minimum fluidization velocity [439] (p. 753). This overcomes the tendency of the original Syamlal-O'Brien model to under/over-predict bed expansion in fluid bed reactors, for example.

  The parameters are derived from the velocity correlation between single and multiple particle systems at terminal settling or minimum fluidization conditions. For a multiple particle system, the relative Reynolds number at the minimum fluidization condition is expressed as:

$$\mathrm{Re}_s = \mathrm{Re}_{single}\left[\frac{A + 0.06B\mathrm{Re}_{single}}{1 + 0.06\mathrm{Re}_{single}}\right] \tag{17.221}$$

  where $\mathrm{Re}_{single}$ is the Reynolds number at the terminal settling condition for a single particle and can be expressed as:

$$\mathrm{Re}_{single} = \left[\frac{\left(4.8^2 + 2.52\sqrt{{}^{4\mathrm{Ar}}/_{s}}\right)^{0.5} - 4.8}{1.26}\right]^2 \tag{17.222}$$

  The Archimedes number, $\mathrm{Ar}$, can be written as a function of the drag coefficient, $C_D$, and the Reynolds number, $\mathrm{Re}_s$:

$$\mathrm{Ar} = \frac{3}{4}C_D\mathrm{Re}_s^2 \tag{17.223}$$

  where $C_D$ can be obtained from the terminal velocity correlation, $v_{r,s}$, and the Reynolds number:

$$C_D = \left(\frac{0.63}{v_{r,s}} + \frac{4.8}{\sqrt{v_{r,s}\mathrm{Re}_s}}\right)^2 \tag{17.224}$$

  $v_{r,s}$ is found from Equation 17.217 (p. 525) with $A$ from Equation 17.218 (p. 525) and B rewritten as follows:

$$B = \begin{cases} c1\alpha_l^{1.28} & \alpha_l \le 0.85 \\ \alpha_l^{d1} & \alpha_l > 0.85 \end{cases} \tag{17.225}$$

  where $d1 = 1.28 + {}^{\log_{10}c1}\!/_{\log_{10}0.85}$

  Once the particle diameter and the expected minimum fluidization velocity are given, the coefficients $c1$ and $d1$ can be found by iteratively solving Equation 17.221 (p. 526) – Equation 17.225 (p. 526).

  This model implementation is restricted to use in gas-solid flows in which the gas phase is the primary phase and is incompressible. Furthermore, the model is appropriate only for Geldart Group B particles.

- For the model of Wen and Yu [484] (p. 755), the fluid-solid exchange coefficient is of the following form:

$$K_{sl} = \frac{3}{4}C_D\frac{\alpha_s\alpha_l\rho_l\,|\,\vec{v}_s - \vec{v}_l\,|}{d_s}\alpha_l^{-2.65} \tag{17.226}$$

  where


Release 15.0 - © SAS IP, Inc. All rights reserved. - Contains proprietary and confidential information of ANSYS, Inc. and its subsidiaries and affiliates.

$$C_D = \frac{24}{\alpha_l Re_s}\left[1 + 0.15(\alpha_l Re_s)^{0.687}\right] \tag{17.227}$$

and $\mathrm{Re}_s$ is defined by Equation 17.215 (p. 525).

This model is appropriate for dilute systems.

- The Gidaspow model [139] (p. 736) is a combination of the Wen and Yu model [484] (p. 755) and the Ergun equation [109] (p. 734).

  When $\alpha_l > 0.8$, the fluid-solid exchange coefficient $K_{sl}$ is of the following form:

  $$K_{sl} = \frac{3}{4} C_D \frac{\alpha_s \alpha_l \rho_l |\vec{v}_s - \vec{v}_l|}{d_s} \alpha_l^{-2.65} \tag{17.228}$$

  where

  $$C_D = \frac{24}{\alpha_l Re_s}\left[1 + 0.15(\alpha_l Re_s)^{0.687}\right] \tag{17.229}$$

  When $\alpha_l \leq 0.8$,

  $$K_{sl} = 150 \frac{\alpha_s (1-\alpha_l)\mu_l}{\alpha_l d_s^2} + 1.75 \frac{\rho_l \alpha_s |\vec{v}_s - \vec{v}_l|}{d_s} \tag{17.230}$$

  This model is recommended for dense fluidized beds.

- The Huilin-Gidaspow model [171] (p. 738) is also a combination of the Wen and Yu model [484] (p. 755) and the Ergun equation [109] (p. 734). The smooth switch is provided by the function when the solid volume fraction is less than 0.2:

  $$K_{sl} = \psi K_{sl-Ergun} + (1-\psi) K_{sl-Wen\&Yu} \tag{17.231}$$

  where the stitching function is of the form

  $$\psi = \frac{1}{2} + \frac{\arctan(262.5(\alpha_s - 0.2))}{\pi} \tag{17.232}$$

- The Gibilaro model [136] (p. 736) is of the form

  $$K_{sl} = \left(\frac{18}{\mathrm{Re}} + 0.33\right)\frac{\rho_f |v_s - v_l|}{d_p} \alpha_s \alpha_l^{-1.8} \tag{17.233}$$

  with the Reynolds number as

  $$\mathrm{Re} = \frac{\alpha_l \rho_l d_p |v_s - v_l|}{\mu_l} \tag{17.234}$$

### 17.5.6.3. Solid-Solid Exchange Coefficient

The solid-solid exchange coefficient $K_{ls}$ has the following form [438] (p. 753):

$$K_{ls} = \frac{3(1+e_{ls})\left(\frac{\pi}{2} + C_{fr,ls}\frac{\pi^2}{8}\right)\alpha_s \rho_s \alpha_l \rho_l (d_l + d_s)^2 g_{0,ls}}{2\pi\left(\rho_l d_l^3 + \rho_s d_s^3\right)} |\vec{v}_l - \vec{v}_s| \tag{17.235}$$

where

$e_{ls}$ = the coefficient of restitution

$C_{fr,ls}$ = the coefficient of friction between the $l^{th}$ and $s^{th}$ solid-phase particles $\left(C_{fr,ls}=0\right)$

$d_l$ = the diameter of the particles of solid $l$

$g_{0,ls}$ = the radial distribution coefficient

Note that the coefficient of restitution is described in Solids Pressure (p. 538) and the radial distribution coefficient is described in Radial Distribution Function (p. 539).

### 17.5.6.4. Drag Modification

When using the Eulerian or Mixture multiphase models, ANSYS Fluent can include a user-specified drag modification term in the calculation of interphase momentum exchange. This is introduced by replacing $K_{pq}$ in Equation 17.158 (p. 516) with $K_{pq}^{'}$ where

$$K_{pq}^{'}=\eta K_{pq} \tag{17.236}$$

and $K_{pq}$ is defined as in Equation 17.164 (p. 518). You can specify the modification factor, $\eta$, as a constant, a user-defined function, or defined by the Brucato correlation.

#### 17.5.6.4.1. Brucato Correlation

The Brucato correlation, [50] (p. 731) [223] (p. 741), is appropriate for gas-liquid flows where the drag coefficient is increased by the liquid phase turbulence. For the Brucato correlation, the drag modification factor is expressed as

$$\eta=(1+\gamma) \tag{17.237}$$

where

$$\gamma=K\left(\frac{d}{\lambda}\right)^3 \tag{17.238}$$

Here, $K=6.5\times10^{-6}$, $d$ is the bubble diameter and $\lambda$ is the Kolmogrov length scale given by:

$$\lambda=\left(\frac{v_l^3}{\varepsilon}\right)^{1/4} \tag{17.239}$$

where $v_l$ is the specific molecular viscosity of the liquid phase and $\varepsilon$ is the average liquid phase turbulent eddy dissipation.

## 17.5.7. Lift Force

For multiphase flows, ANSYS Fluent can include the effect of lift forces on the secondary phase particles, droplets, or bubbles. These lift forces act on a particle mainly due to velocity gradients in the primary-phase flow field. The lift force will be more significant for larger particles, but the ANSYS Fluent model


Release 15.0 - © SAS IP, Inc. All rights reserved. - Contains proprietary and confidential information of ANSYS, Inc. and its subsidiaries and affiliates.

assumes that the particle diameter is much smaller than the interparticle spacing. Thus, the inclusion of lift forces is not appropriate for closely packed particles or for very small particles.

From Drew (1993) [100] (p. 734), the lift force acting on a secondary phase $p$ in a primary phase $q$ can be calculated as:

$$\vec{F}_{lift} = -C_l \rho_q \alpha_p \left( \vec{v}_q - \vec{v}_p \right) \times \left( \nabla \times \vec{v}_q \right) \tag{17.240}$$

where

$C_l$ = the lift coefficient (Lift Coefficient Models (p. 529))

$\rho_q$ = the primary phase density

$\alpha_p$ = the secondary phase volume fraction

$\vec{v}_q$ = the primary phase velocity

$\vec{v}_p$ = the secondary phase velocity

The lift force $\vec{F}_{lift}$ will be added to the right-hand side of the momentum equation for both phases ($\vec{F}_{lift,q} = -\vec{F}_{lift,p}$).

In most cases, the lift force is insignificant compared to the drag force, so there is no reason to include this extra term. If the lift force is significant (for example, if the phases separate quickly), it may be appropriate to include this term. By default, $\vec{F}_{lift}$ is not included. The lift force and lift coefficient can be specified for each pair of phases, if desired.

**Important**

It is important that if you include the lift force in your calculation, you need not include it everywhere in the computational domain since it is computationally expensive to converge. For example, in the wall boundary layer for turbulent bubbly flows in channels the lift force is significant when the slip velocity is large in the vicinity of high strain rates for the primary phase.

### 17.5.7.1. Lift Coefficient Models

Fluent offers a variety of models for the lift coefficient, $C_l$, in Equation 17.240 (p. 529). These models are described in the following sections.

17.5.7.1.1. Moraga Lift Force Model
17.5.7.1.2. Saffman-Mei Lift Force Model
17.5.7.1.3. Legendre-Magnaudet Lift Force Model
17.5.7.1.4. Tomiyama Lift Force Model

Alternatively, you can specify a constant, or a User-Defined Function for the Lift Coefficient (`DEFINE_EXCHANGE_PROPERTY`). Refer to Including the Lift Force in the Fluent User's Guide for details about how to include lift force in your simulation.

Release 15.0 - © SAS IP, Inc. All rights reserved. - Contains proprietary and confidential information of ANSYS, Inc. and its subsidiaries and affiliates.

### 17.5.7.1.1. Moraga Lift Force Model

The model developed by Moraga et al (1999) [308] (p. 746) is applicable mainly to the lift force on spherical solid particles, though it can be applied to liquid drops and bubbles. In this model the lift coefficient combines opposing actions of two phenomena:

- classical aerodynamic lift resulting from the interaction between the dispersed phase particles and the primary phase shear
- the vorticity-induced lift resulting from interaction between particles and vortices shed by particle wakes

As a result, the lift coefficient is defined in terms of both particle Reynolds number and vorticity Reynolds number:

$$\mathrm{Re}_p = \frac{\rho_q \left| \vec{V}_q - \vec{V}_p \right| d_p}{\mu_q} \tag{17.241}$$

$$\mathrm{Re}_\omega = \frac{\rho_q \left| \nabla \times \vec{V}_q \right| d_p^2}{\mu_q} \tag{17.242}$$

Defining $\varphi = \mathrm{Re}_p \mathrm{Re}_\omega$, the Moraga lift coefficient is formulated as:

$$C_l = \begin{cases} 0.0767 & \varphi \le 6000 \\ -\left(0.12 - 0.2e^{-\frac{\varphi}{3.6}\times 10^{-5}}\right) e^{\frac{\varphi}{3}\times 10^{-7}} & 6000 < \varphi < 5\times 10^7 \\ -0.6353 & \varphi \ge 5\times 10^7 \end{cases} \tag{17.243}$$

### 17.5.7.1.2. Saffman-Mei Lift Force Model

The Saffman-Mei model is applicable mainly to spherical solid particles, though it can be applied to liquid drops that are not significantly distorted. As in the Moraga model (Moraga Lift Force Model (p. 530)), the lift coefficient is correlated in terms of particle Reynolds number and vorticity Reynolds number. According to Saffman (1965, 1968) [383] (p. 750), [384] (p. 750), for low Reynolds number flow past a spherical particle, the lift coefficient can be defined as:

$$C_l = \frac{3}{2\pi\sqrt{\mathrm{Re}_\omega}} C_l' \tag{17.244}$$

where $C_l' = 6.46$ and $0 \le \mathrm{Re}_p \le \mathrm{Re}_\omega \le 1$.

Mei and Klausner (1994) [287] (p. 744) extended the model to a higher range of particle Reynolds numbers. The Saffman-Mei model is empirically represented as:

$$C_l' = \begin{cases} 6.46 \times f\left(\mathrm{Re}_p, \mathrm{Re}_\omega\right) & \mathrm{Re}_p \le 40 \\ 6.46 \times 0.0524 \left(\beta \mathrm{Re}_p\right)^{1/2} & 40 < \mathrm{Re}_p < 100 \end{cases} \tag{17.245}$$

where


Release 15.0 - © SAS IP, Inc. All rights reserved. - Contains proprietary and confidential information of ANSYS, Inc. and its subsidiaries and affiliates.

$$\beta = 0.5\left(\mathrm{Re}_\omega / \mathrm{Re}_p\right)$$
$$f\left(\mathrm{Re}_p, \mathrm{Re}_\omega\right) = \left(1 - 0.3314\beta^{0.5}\right)e^{-0.1\mathrm{Re}_p} + 0.3314\beta^{0.5}$$

#### 17.5.7.1.3. Legendre-Magnaudet Lift Force Model

The Legendre-Magnaudet model (1998) [239] (p. 742) is applicable primarily to small diameter spherical fluid particles, though it can be applied to non-distorted liquid drops and bubbles. In contrast to the Saffman-Mei model for rigid solid particles, the Legendre-Magnaudet model accounts for the momentum transfer between the flow around the particle and the inner recirculation flow inside the fluid particle caused by the fluid friction/stresses at the fluid interface. Therefore, the predicted lift force coefficients are approximately 2–5 times smaller than for rigid solid particles.

The range of validity given by Legendre and Magnaudet is as follows:

$$0.1 < \mathrm{Re}_p < 500 \quad , \quad Sr = 2\beta \le 1$$

where $\beta$ is defined as in the Saffman-Mei model (Saffman-Mei Lift Force Model (p. 530)). The lift force coefficient is then estimated as:

$$C_l = \sqrt{\left(C_{l,low\mathrm{Re}}\right)^2 + \left(C_{l,high\mathrm{Re}}\right)^2} \tag{17.246}$$

where:

$$C_{l,low\mathrm{Re}} = \frac{6}{\pi^2}\left(\mathrm{Re}_p Sr\right)^{-0.5}\frac{2.55}{\left(1 + 0.2\frac{\mathrm{Re}_p}{Sr}\right)^{1.5}}$$
$$Cl,high\mathrm{Re} = \frac{1}{2}\frac{1 + 16\mathrm{Re}_p^{-1}}{1 + 29\mathrm{Re}_p^{-1}} \tag{17.247}$$

#### 17.5.7.1.4. Tomiyama Lift Force Model

The Tomiyama model is applicable to the lift force on larger-scale deformable bubbles in the ellipsoidal and spherical cap regimes. As with the Tomiyama drag and wall lubrication models, this model depends on the Eötvös number. Its main feature is prediction of the cross-over point in bubble size at which particle distortion causes a reversal in the sign of the lift force. The model implemented in Fluent is a lightly modified version of the original Tomiyama lift model (1998) [452] (p. 753) by Frank et al. (2004) [128] (p. 735):

$$\mathrm{C}_l = \begin{cases} \min\left[0.288\tanh\left(0.121\mathrm{Re}_p\right), f\left(Eo'\right)\right] & Eo' \le 4 \\ f\left(Eo'\right) & 4 < Eo' \le 10 \\ -0.27 & 10 < Eo' \end{cases} \tag{17.248}$$

where

$$f\left(Eo'\right)=0.00105Eo'^{3}-0.0159Eo'^{2}-0.0204Eo'+0.474 \tag{17.249}$$

$Eo'$ is a modified Eötvös number based on the long axis of the deformable bubble, $d_h$:

$$Eo'=\frac{g\left(\rho_q-\rho_p\right)d_h^2}{\sigma} \tag{17.250}$$

$$d_h=d_b\left(1+0.163Eo^{0.757}\right)^{1/3} \tag{17.251}$$

$$Eo=\frac{g\left(\rho_q-\rho_p\right)d_b^2}{\sigma} \tag{17.252}$$

where $\sigma$ is the surface tension, $g$ is gravity, and $d_b$ is the bubble diameter.

## 17.5.8. Wall Lubrication Force

For liquid-gas bubbly flows using the Eulerian model ANSYS Fluent can include the effect of wall lubrication forces on the secondary phases (bubbles). The wall lubrication force tends to push the secondary phases away from walls. For example, in a bubbly upward flow in a vertical pipe this force results in the dispersed phase concentrating in a region near, but not immediately adjacent to, the wall.

The wall lubrication force acting on a secondary phase, $p$, in a primary phase, $q$, has the general form:

$$\vec{F}_{wl}=C_{wl}\rho_q\alpha_p\left|\left(\vec{v}_q-\vec{v}_p\right)_{||}\right|^2\vec{n}_w \tag{17.253}$$

where

$C_{wl}$ = the wall lubrication coefficient (Wall Lubrication Models (p. 532))

$\rho_q$ = the primary phase density

$\alpha_p$ = the secondary phase volume fraction

$\left|\left(\vec{v}_q-\vec{v}_p\right)_{||}\right|$ = the phase relative velocity component tangential to the wall surface

$\vec{n}_w$ = the unit normal pointing away from the wall

### 17.5.8.1. Wall Lubrication Models

The wall lubrication models in ANSYS Fluent differ in how they compute the wall lubrication coefficient, $C_{wl}$ in Equation 17.253 (p. 532).

ANSYS Fluent offers the following models:

17.5.8.1.1. Antal et al. Model
17.5.8.1.2. Tomiyama Model
17.5.8.1.3. Frank Model
17.5.8.1.4. Hosokawa Model


Release 15.0 - © SAS IP, Inc. All rights reserved. - Contains proprietary and confidential information of ANSYS, Inc. and its subsidiaries and affiliates.

You can also specify a user-defined wall lubrication coefficient with a User Defined Function using the DEFINE_EXCHANGE_PROPERTY macro. For details on using a UDF to define the wall lubrication coefficient, see DEFINE_EXCHANGE_PROPERTY in the Fluent UDF Manual.

#### 17.5.8.1.1. Antal et al. Model

The model proposed by Antal et al. [8] (p. 729) computes the coefficient, $C_{wl}$, as:

$$C_{wl}=\max\left(0,\frac{C_{w1}}{d_b}+\frac{C_{w2}}{y_w}\right) \tag{17.254}$$

where $C_{w1}=-0.01$ and $C_{w2}=0.05$ are non-dimensional coefficients, $d_b$ is the bubble/particle diameter, and $y_w$ is the distance to the nearest wall.

Note that $C_{wl}$ is non-zero only within a thin layer adjacent to the wall that satisfies:

$$y_w \le -\left(C_{w2}/C_{w1}\right)d_b \tag{17.255}$$

corresponding to $y_w \le 5d_b$ with the default values of $C_{w1}$ and $C_{w2}$. As a result, the Antal model will only be active on a sufficiently fine mesh and grid independence can only be achieved with very fine meshes.

#### 17.5.8.1.2. Tomiyama Model

The Tomiyama model [452] (p. 753) modifies the wall lubrication force formulation of Antal [8] (p. 729) based on the results of experiments with flow of air bubbles in glycerin in a pipe. The expression for $C_{wl}$ for the Tomiyama model is:

$$C_{wl}=C_w\frac{d_b}{2}\left(\frac{1}{y_w^2}-\frac{1}{\left(D-y_w\right)^2}\right) \tag{17.256}$$

In Equation 17.256 (p. 533), $D$ is the pipe diameter and $C_w$ depends on the Eotvos number, $Eo$. $C_w$ is defined as

$$C_w=\begin{cases}0.47 & Eo<1\\ e^{-0.933Eo+0.179} & 1\le Eo\le 5\\ 0.00599Eo-0.0187 & 5<Eo\le 33\\ 0.179 & 33\le Eo\end{cases} \tag{17.257}$$

where the Eotvos number, $Eo$ is defined as

$$Eo=\frac{g(\rho_q-\rho_p)d_b^2}{\sigma}$$

and $\sigma$ is the surface tensions coefficient. It has been noted by Frank et al. [128] (p. 735) that, though the Tomiyama model has been found to be superior to the Antal model, it is restricted to flows in pipe geometries due to the dependence on pipe diameter in Equation 17.256 (p. 533).

Release 15.0 - © SAS IP, Inc. All rights reserved. - Contains proprietary and confidential information of ANSYS, Inc. and its subsidiaries and affiliates.

#### 17.5.8.1.3. Frank Model

The model of Frank et al. [128] (p. 735), [129] (p. 736) removes the dependence on pipe diameters in the Tomiyama model [452] (p. 753). The Frank model defines the coefficient $C_{wl}$ as

$$C_{wl} = C_w \max\left(0, \frac{1}{C_{wd}} \cdot \frac{1 - \frac{y_w}{C_{wc} d_b}}{y_w \left(\frac{y_w}{C_{wc} d_b}\right)^{m-1}}\right) \tag{17.258}$$

where

$C_w$ is determined as a function of $\mathrm{Eo}$ as in Equation 17.257 (p. 533).

$C_{wd}$ is the damping coefficient and determines the relative magnitude of the force.

$C_{wc}$ is the cut-off coefficient and determines the distance to the wall within which the force is active.

$m$ is the power law constant and is recommended to be between 1.5 and 2.

By default, $C_{wd} = 6.8$, $C_{wc} = 10$, and $m = 1.7$.

#### 17.5.8.1.4. Hosokawa Model

The model from Hosokawa et al. [168] (p. 738) is based on experimental measurements that indicate that, for bubbles, the coefficient, $C_w$ (Equation 17.257 (p. 533)) used in the Tomiyama and Frank models depends not only on the Eotvos number, but on the phase relative Reynolds number. The model proposes the following expression for $C_w$.

$$C_w = \max\left(\frac{7}{\mathrm{Re}_d^{1.9}}, 0.0217 Eo\right) \tag{17.259}$$

where the phase relative Reynolds number, $\mathrm{Re}_d$, is defined

$$\mathrm{Re}_d = \frac{\rho_q \left|\vec{v_q} - \vec{v_p}\right| d_b}{\mu_q} \tag{17.260}$$

By default, the Hosokawa model computes $C_{wl}$ as in Equation 17.258 (p. 534). Note that Equation 17.259 (p. 534) is only valid for liquid-gas bubble flows.

### 17.5.9. Turbulent Dispersion Force

For multiphase turbulent flows using the Eulerian model, ANSYS Fluent can include the effects of turbulent dispersion forces which account for the interphase turbulent momentum transfer. The turbulent dispersion force acts as a turbulent diffusion in dispersed flows. For example for a boiling flow in a heated vertical pipe, vapor is generated on heated wall surfaces. The turbulent dispersion force plays a crucial role in driving the vapor away from the vicinity of the wall towards the center of the pipe.

The turbulent dispersion force arises from averaging the interphase drag term. For a dispersed phase, $p$, and a continuous phase, $q$, the turbulent drag is modeled as:


Release 15.0 - © SAS IP, Inc. All rights reserved. - Contains proprietary and confidential information of ANSYS, Inc. and its subsidiaries and affiliates.

$$K_{pq}(\tilde{\vec{v}}_p - \tilde{\vec{v}}_q) = K_{pq}(\vec{v}_p - \vec{v}_q) - K_{pq}\vec{v}_{dr} \tag{17.261}$$

The term on the left side is the instantaneous drag. The first term on the right hand side, $K_{pq}(\vec{v}_p - \vec{v}_q)$, appears in Equation 17.155 (p. 515) and represents the mean momentum exchange between the two phases. $K_{pq}$ is the interphase exchange coefficient, described in Interphase Exchange Coefficients (p. 518), and $\vec{v}_p$ and $\vec{v}_q$ are the mean phase velocity vectors. The second term, $K_{pq}\vec{v}_{dr}$, is commonly referred to as the turbulent dispersion force:

$$\vec{F}_{td,q} = -\vec{F}_{td,p} = -f_{td,limiting}K_{pq}\vec{v}_{dr} \tag{17.262}$$

where $\vec{v}_{dr}$ is the drift velocity and accounts for the dispersion of the secondary phases due to transport by turbulent fluid motion. $f_{td,limiting}$ is a factor that can be used to impose a limiting function on the turbulent dispersion force. For clarity, the limiting factor is omitted from the descriptions of the turbulent dispersion models that follow. See Limiting Functions for the Turbulent Dispersion Force (p. 537) for details about the implementation of the limiting factor.

## 17.5.9.1. Models for Turbulent Dispersion Force

The following sections describe the models for turbulent dispersion force that are available in ANSYS Fluent:

17.5.9.1.1. Lopez de Bertodano Model
17.5.9.1.2. Simonin Model
17.5.9.1.3. Burns et al. Model
17.5.9.1.4. Diffusion in VOF Model

You can also specify the turbulent dispersion force with a User Defined Function. For information on enabling turbulent dispersion force in your model, see Including the Turbulent Dispersion Force in the User's Guide.

### 17.5.9.1.1. Lopez de Bertodano Model

Instead of following Equation 17.262 (p. 535) and modeling the drift velocity, Lopez de Bertodano proposed the following formulation [266] (p. 743):

$$\vec{F}_{td,q} = -\vec{F}_{td,p} = C_{TD}\rho_q k_q \nabla \alpha_p \tag{17.263}$$

where $\rho_q$ is the continuous phase density, $k_q$ is the turbulent kinetic energy in the continuous phase, and $\nabla \alpha_p$ is the gradient of dispersed phase volume fraction, and $C_{TD}$ is a user-modifiable constant. By default, $C_{TD} = 1$.

### 17.5.9.1.2. Simonin Model

Simonin and Viollet [408] (p. 751) proposed that the drift velocity, $\vec{v}_{dr}$, is calculated from:

$$\vec{v}_{dr} = -\mathbf{D}_{pq} \cdot \left( \frac{\nabla \alpha_p}{\alpha_p} - \frac{\nabla \alpha_q}{\alpha_q} \right) \tag{17.264}$$

In Equation 17.264 (p. 535), $\mathbf{D}_{pq}$ is the fluid-particulate dispersion tensor.

For the dispersed two-equation turbulence model (k- ε Dispersed Turbulence Model (p. 550)), ANSYS Fluent uses Tchen theory [164] (p. 738) and assumes that $\mathbf{D}_{pq}$ is a scalar, expressed as given by $D_{t,pq}$ in Equation 17.364 (p. 558) with a dispersion Prandtl number, $\sigma_{pq}$ ($\sigma_{pq}=0.75$ by default). The turbulent dispersion force is then given by:

$$\vec{F}_{td,q}=-\vec{F}_{td,p}=C_{TD}K_{pq}\frac{D_{t,pq}}{\sigma_{pq}}\left(\frac{\nabla\alpha_p}{\alpha_p}-\frac{\nabla\alpha_q}{\alpha_q}\right) \tag{17.265}$$

Here, $C_{TD}$ is a user-modifiable constant that is set to 1 by default.

For the mixture turbulence model (k- ε Mixture Turbulence Model (p. 549)), the dispersion scalar is equal to the mixture turbulent kinematic viscosity.

### 17.5.9.1.3. Burns et al. Model

Burns et al. [53] (p. 731) derived a formulation based on Favre averaging of the drag term. The final expression is similar to Simonin's model. For the Burns model, the dispersion scalar is estimated by the turbulent viscosity of the continuous phase:

$$D_q=D_p=D_{tq}=\frac{\mu_{tq}}{\rho_q} \tag{17.266}$$

and

$$\vec{F}_{td,q}=-\vec{F}_{td,p}=C_{TD}K_{pq}\frac{D_q}{\sigma_{pq}}\left(\frac{\nabla\alpha_p}{\alpha_p}-\frac{\nabla\alpha_q}{\alpha_q}\right) \tag{17.267}$$

By default, $C_{TD}=1$ and $\sigma_{pq}=0.9$. As in the Simonin model, when using the mixture turbulence model the dispersion scalar is equal to the mixture turbulent kinetic viscosity.

### 17.5.9.1.4. Diffusion in VOF Model

Instead of treating the turbulent dispersion as an interfacial momentum force in the phase momentum equations, you can model it as a turbulent diffusion term in the governing equations of phase volume fractions [422] (p. 752). With the turbulent dispersion term, the governing equation for the volume fraction in phase $q$, Equation 17.152 (p. 514), becomes:

$$\frac{\partial}{\partial t}(\alpha_q\rho_q)+\nabla\cdot(\alpha_q\rho_q\vec{v}_q)=\nabla\left(\gamma_q\nabla\alpha_q\right)+\sum_{p=1}^{n}\left(\dot{m}_{pq}-\dot{m}_{qp}\right)+S_q \tag{17.268}$$

where $\gamma_q$ is the diffusion coefficient in the $q^{\text{th}}$ phase, and the term $\nabla\left(\gamma_q\nabla\alpha_q\right)$ is the turbulent dispersion term that must satisfy the constraint:

$$\sum_{q=1}^{n}\nabla\left(\gamma_q\nabla\alpha_q\right)=0 \tag{17.269}$$

In order to satisfy Equation 17.269 (p. 536) the diffusion coefficients for the secondary phases are estimated from the phase turbulent viscosities, $\mu_{t,q}$ as


Release 15.0 - © SAS IP, Inc. All rights reserved. - Contains proprietary and confidential information of ANSYS, Inc. and its subsidiaries and affiliates.

$$\gamma_q = \frac{\mu_{t,q}}{\sigma_q} \quad q = 2 \cdots n \tag{17.270}$$

where $\sigma_q = 0.75$ by default.

For the primary phase, $q = 1$, the diffusion term is

$$D_q = -\sum_{p=2}^{n} D_p \tag{17.271}$$

### 17.5.9.2. Limiting Functions for the Turbulent Dispersion Force

In some applications it is desirable to apply the turbulent dispersion force only in particular flow regimes or conditions. For example, a user may want to include the turbulent dispersion force only in a bubbly flow regime. To accommodate this, a limiting function can be applied through the factor, $f_{td,limiting}$, in Equation 17.262 (p. 535).

ANSYS Fluent provides three options for determining $f_{td,limiting}$:

**None**

By default, no limiting is performed on the turbulent dispersion force ($f_{td,limiting} = 1$).

**Standard**

ANSYS Fluent includes a standard limiting function that varies linearly from `0` to `1` based on the volume fraction of the dispersed phase(s), $\alpha_p$:

$$f_{td,limiting}\left(\alpha_p\right) = \max\left(0, \min\left(1, \frac{\alpha_{p,2} - \alpha_p}{\alpha_{p,2} - \alpha_{p,1}}\right)\right) \tag{17.272}$$

By default,

$$\alpha_{p,1} = 0.3$$
$$\alpha_{p,2} = 0.7$$

If necessary, the values of $\alpha_{p,1}$ and $\alpha_{p,2}$ can be changed using the following `domainsetvar` scheme commands:

(domainsetvar <phase-id> 'mp/td/vof-lower-limit <$\alpha_{p,1}$—value>)

(domainsetvar <phase-id> 'mp/td/vof-upper-limit <$\alpha_{p,2}$—value>)

with appropriate values substituted for <phase-id> and <$\alpha_{p,i}$—value>. Note that the value for <phase-id> for a given phase can be found from the **Phases** Task Page in the GUI.

**User-Defined**

You can specify your own limiting function by creating a User-Defined Function (UDF) using the `DEFINE_EXCHANGE_PROPERTY` macro (`DEFINE_EXCHANGE_PROPERTY`). Note that $f_{td,limiting}$ must

Release 15.0 - © SAS IP, Inc. All rights reserved. - Contains proprietary and confidential information of ANSYS, Inc. and its subsidiaries and affiliates.

have a value between 0 and 1, and should vary continuously to ensure numerical stability and physical solutions.

## 17.5.10. Virtual Mass Force

For multiphase flows, ANSYS Fluent includes the "virtual mass effect" that occurs when a secondary phase $p$ accelerates relative to the primary phase $q$. The inertia of the primary-phase mass encountered by the accelerating particles (or droplets or bubbles) exerts a "virtual mass force" on the particles [100] (p. 734). The virtual mass force is defined as:

$$\vec{F}_{vm} = 0.5\alpha_p\rho_q\left(\frac{d_q\vec{v}_q}{dt} - \frac{d_p\vec{v}_p}{dt}\right) \tag{17.273}$$

The term $\frac{d_q}{dt}$ denotes the phase material time derivative of the form

$$\frac{d_q(\phi)}{dt} = \frac{\partial(\phi)}{\partial t} + \left(\vec{v}_q \cdot \nabla\right)\phi \tag{17.274}$$

The virtual mass force $\vec{F}_{vm}$ will be added to the right-hand side of the momentum equation for both phases ($\vec{F}_{vm,q} = -\vec{F}_{vm,p}$).

The virtual mass effect is significant when the secondary phase density is much smaller than the primary phase density (for example, for a transient bubble column). By default, $\vec{F}_{vm}$ is not included.

## 17.5.11. Solids Pressure

For granular flows in the compressible regime (that is, where the solids volume fraction is less than its maximum allowed value), a solids pressure is calculated independently and used for the pressure gradient term, $\nabla p_s$, in the granular-phase momentum equation. Because a Maxwellian velocity distribution is used for the particles, a granular temperature is introduced into the model, and appears in the expression for the solids pressure and viscosities. The solids pressure is composed of a kinetic term and a second term due to particle collisions:

$$p_s = \alpha_s\rho_s\Theta_s + 2\rho_s(1+e_{ss})\alpha_s^2 g_{0,ss}\Theta_s \tag{17.275}$$

where $e_{ss}$ is the coefficient of restitution for particle collisions, $g_{0,ss}$ is the radial distribution function, and $\Theta_s$ is the granular temperature. ANSYS Fluent uses a default value of 0.9 for $e_{ss}$, but the value can be adjusted to suit the particle type. The granular temperature $\Theta_s$ is proportional to the kinetic energy of the fluctuating particle motion, and will be described later in this section. The function $g_{0,ss}$ (described below in more detail) is a distribution function that governs the transition from the "compressible" condition with $\alpha < \alpha_{s,max}$, where the spacing between the solid particles can continue to decrease, to the "incompressible" condition with $\alpha = \alpha_{s,max}$, where no further decrease in the spacing can occur. A value of 0.63 is the default for $\alpha_{s,max}$, but you can modify it during the problem setup.

Other formulations that are also available in ANSYS Fluent are [441] (p. 753)

$$p_s = 2\rho_s(1+e_{ss})\alpha_s^2 g_{0,ss}\Theta_s \tag{17.276}$$

and [276] (p. 744)


Release 15.0 - © SAS IP, Inc. All rights reserved. - Contains proprietary and confidential information of ANSYS, Inc. and its subsidiaries and affiliates.

$$p_s=\alpha_s\rho_s\Theta_s\left[\left(1+4\alpha_s g_{0,ss}\right)+\frac{1}{2}\left[\left(1+e_{ss}\right)\left(1-e_{ss}+2\mu_{fric}\right)\right]\right] \tag{17.277}$$

where $\mu_{fric}$ is defined in [276] (p. 744).

When more than one solids phase are calculated, the above expression does not take into account the effect of other phases. A derivation of the expressions from the Boltzman equations for a granular mixture are beyond the scope of this manual, however there is a need to provide a better formulation so that some properties may feel the presence of other phases. A known problem is that N solid phases with identical properties should be consistent when the same phases are described by a single solids phase. Equations derived empirically may not satisfy this property and need to be changed accordingly without deviating significantly from the original form. From [138] (p. 736), a general solids pressure formulation in the presence of other phases could be of the form

$$p_q=\alpha_q\rho_q\Theta_q+\sum_{p=1}^{N}\frac{\pi}{3}g_{0,pq}d_{qp}^3 n_q n_p\left(1+e_{qp}\right)f\left(m_p,m_q,\Theta_p,\Theta_q\right) \tag{17.278}$$

where $d_{pq}=\frac{d_p+d_q}{2}$ is the average diameter, $n_p$, $n_q$ are the number of particles, $m_p$ and $m_q$ are the masses of the particles in phases $p$ and $q$, and $f$ is a function of the masses of the particles and their granular temperatures. For now, we have to simplify this expression so that it depends only on the granular temperature of phase $q$

$$p_q=\alpha_q\rho_q\Theta_q+\sum_{p=1}^{N}2\frac{d_{pq}^3}{d_q^3}\left(1+e_{pq}\right)g_{0,pq}\alpha_q\alpha_p\rho_q\Theta_q \tag{17.279}$$

Since all models need to be cast in the general form, it follows that

$$p_q=\alpha_q\rho_q\Theta_q+\left(\sum_{p=1}^{N}\frac{d_{pq}^3}{d_q^3}p_{c,qp}\right)\rho_q\Theta_q \tag{17.280}$$

where $p_{c,qp}$ is the collisional part of the pressure between phases $q$ and $p$. In Equation 17.279 (p. 539), $p_{c,qp}=2\left(1+e_{pq}\right)g_{0,pq}\alpha_q\alpha_p$.

The above expression reverts to the one solids phase expression when $N=1$ and $q=p$ but also has the property of feeling the presence of other phases.

### 17.5.11.1. Radial Distribution Function

The radial distribution function, $g_0$, is a correction factor that modifies the probability of collisions between grains when the solid granular phase becomes dense. This function may also be interpreted as the nondimensional distance between spheres:

$$g_0=\frac{s+d_p}{s} \tag{17.281}$$

where $s$ is the distance between grains. From Equation 17.281 (p. 539) it can be observed that for a dilute solid phase $s\to\infty$, and therefore $g_0\to 1$. In the limit when the solid phase compacts, $s\to 0$ and $g_0\to\infty$. The radial distribution function is closely connected to the factor $\chi$ of Chapman and Cowling's [60] (p. 732)

Release 15.0 - © SAS IP, Inc. All rights reserved. - Contains proprietary and confidential information of ANSYS, Inc. and its subsidiaries and affiliates.

theory of nonuniform gases. $\chi$ is equal to 1 for a rare gas, and increases and tends to infinity when the molecules are so close together that motion is not possible.

In the literature there is no unique formulation for the radial distribution function. ANSYS Fluent has a number of options:

- For one solids phase, use [326] (p. 747):

$$g_0 = \left[ 1 - \left( \frac{\alpha_s}{\alpha_{s,max}} \right)^{\frac{1}{3}} \right]^{-1} \tag{17.282}$$

  This is an empirical function and does not extend easily to $n$ phases. For two identical phases with the property that $\alpha_s = \alpha_1 + \alpha_2$, the above function is not consistent for the calculation of the partial pressures $p_1$ and $p_2$, $p_s = p_1 + p_2$. In order to correct this problem, ANSYS Fluent uses the following consistent formulation:

$$g_{0,ll} = \left[ 1 - \left( \frac{\alpha_s}{\alpha_{s,max}} \right)^{\frac{1}{3}} \right]^{-1} + \frac{1}{2} d_l \sum_{k=1}^{N} \frac{\alpha_k}{d_k} \tag{17.283}$$

  where $\alpha_{s,\max}$ is the packing limit, $N$ is the total number of solid phases, $d$ is the diameter of the phases, and

$$\alpha_s = \sum_{k=1}^{N} \alpha_k \tag{17.284}$$

  and $k$ are solid phases only.

- The following expression is also available [174] (p. 738):

$$g_{0,ll} = \frac{1}{\left( 1 - \frac{\alpha_s}{\alpha_{s,max}} \right)} + \frac{3}{2} d_l \sum_{k=1}^{N} \frac{\alpha_k}{d_k} \tag{17.285}$$

- Also available [276] (p. 744), slightly modified for $n$ solids phases, is the following:

$$g_{0,ll} = \frac{1 + 2.5\alpha_s + 4.59\alpha_s^2 + 4.52\alpha_s^3}{\left( 1 - \left( \frac{\alpha_s}{\alpha_{s,max}} \right)^3 \right)^{0.678}} + \frac{1}{2} d_l \sum_{k=1}^{N} \frac{\alpha_k}{d_k} \tag{17.286}$$

- The following equation [441] (p. 753) is available:

$$g_{0,kl} = \frac{1}{(1 - \alpha_s)} + \frac{3 \left( \sum_{k=1}^{N} \frac{\alpha_k}{d_k} \right)}{(1 - \alpha_s)^2 \left( d_j + d_k \right)} d_k d_l \tag{17.287}$$


Release 15.0 - © SAS IP, Inc. All rights reserved. - Contains proprietary and confidential information of ANSYS, Inc. and its subsidiaries and affiliates.

When the number of solid phases is greater than 1, Equation 17.283 (p. 540), Equation 17.285 (p. 540) and Equation 17.286 (p. 540) are extended to

$$g_{0,lm}=\frac{d_m g_{0,ll}+d_l g_{0,mm}}{d_m+d_l} \tag{17.288}$$

It is interesting to note that Equation 17.285 (p. 540) and Equation 17.286 (p. 540) compare well with [3] (p. 729) experimental data, while Equation 17.287 (p. 540) reverts to the [56] (p. 732) derivation.

## 17.5.12. Maximum Packing Limit in Binary Mixtures

The packing limit is not a fixed quantity and may change according to the number of particles present within a given volume and the diameter of the particles. Small particles accumulate in between larger particles increasing the packing limit. For a binary mixture ANSYS Fluent uses the correlations proposed by [112] (p. 735).

For a binary mixture with diameters $d1>d2$, the mixture composition is defined as $X_1=\frac{\alpha_1}{\alpha_1+\alpha_2}$

where

$$X_1<=\frac{\alpha_{1,max}}{\left(\alpha_{1,max}+\left(1-\alpha_{1,max}\right)\alpha_{2,max}\right)} \tag{17.289}$$

as this is a condition for application of the maximum packing limit for binary mixtures.

The maximum packing limit for the mixture $\alpha_{s,max}$ is the minimum of the two expressions (Equation 17.290 (p. 541) and Equation 17.291 (p. 541)):

$$\begin{aligned}&(\alpha_{1,max}-\alpha_{2,max}+[1-\sqrt{\frac{d2}{d1}}](1-\alpha_{1,max})\alpha_{2,max})\\&*(\alpha_{1,max}+(1-\alpha_{1,max})\alpha_{2,max})\frac{X_1}{\alpha_{1,max}}\\&+\alpha_{2,max}\end{aligned} \tag{17.290}$$

$$\left[1-\sqrt{\frac{d2}{d1}}\right]\left(\alpha_{1,max}+\left(1-\alpha_{1,max}\right)\alpha_{2,max}\right)(1-X_1)+\alpha_{1,max} \tag{17.291}$$

The packing limit is used for the calculation of the radial distribution function.

## 17.5.13. Solids Shear Stresses

The solids stress tensor contains shear and bulk viscosities arising from particle momentum exchange due to translation and collision. A frictional component of viscosity can also be included to account for the viscous-plastic transition that occurs when particles of a solid phase reach the maximum solid volume fraction.

The collisional and kinetic parts, and the optional frictional part, are added to give the solids shear viscosity:

$$\mu_s=\mu_{s,col}+\mu_{s,kin}+\mu_{s,fr} \tag{17.292}$$

Release 15.0 - © SAS IP, Inc. All rights reserved. - Contains proprietary and confidential information of ANSYS, Inc. and its subsidiaries and affiliates.

### 17.5.13.1. Collisional Viscosity

The collisional part of the shear viscosity is modeled as [139] (p. 736), [441] (p. 753)

$$\mu_{s,col} = \frac{4}{5}\alpha_s \rho_s d_s g_{0,ss}(1+e_{ss})\left(\frac{\Theta_s}{\pi}\right)^{1/2}\alpha_s \tag{17.293}$$

### 17.5.13.2. Kinetic Viscosity

ANSYS Fluent provides two expressions for the kinetic part.

The default expression is from Syamlal et al. [441] (p. 753):

$$\mu_{s,kin} = \frac{\alpha_s d_s \rho_s \sqrt{\Theta_s \pi}}{6(3-e_{ss})}\left[1+\frac{2}{5}(1+e_{ss})(3e_{ss}-1)\alpha_s g_{0,ss}\right] \tag{17.294}$$

The following optional expression from Gidaspow et al. [139] (p. 736) is also available:

$$\mu_{s,kin} = \frac{10\rho_s d_s \sqrt{\Theta_s \pi}}{96\alpha_s (1+e_{ss}) g_{0,ss}}\left[1+\frac{4}{5}g_{0,ss}\alpha_s (1+e_{ss})\right]^2 \alpha_s \tag{17.295}$$

### 17.5.13.3. Bulk Viscosity

The solids bulk viscosity accounts for the resistance of the granular particles to compression and expansion. It has the following form from Lun et al. [271] (p. 744):

$$\lambda_s = \frac{4}{3}\alpha_s^2 \rho_s d_s g_{0,ss}(1+e_{ss})\left(\frac{\Theta_s}{\pi}\right)^{1/2} \tag{17.296}$$

Note that the bulk viscosity is set to a constant value of zero, by default. It is also possible to select the Lun et al. expression or use a user-defined function.

### 17.5.13.4. Frictional Viscosity

In dense flow at low shear, where the secondary volume fraction for a solid phase nears the packing limit, the generation of stress is mainly due to friction between particles. The solids shear viscosity computed by ANSYS Fluent does not, by default, account for the friction between particles.

If the frictional viscosity is included in the calculation, ANSYS Fluent uses Schaeffer's [391] (p. 750) expression:

$$\mu_{s,fr} = \frac{p_s \sin\phi}{2\sqrt{I_{2D}}} \tag{17.297}$$

where $p_s$ is the solids pressure, $\phi$ is the angle of internal friction, and $I_{2D}$ is the second invariant of the deviatoric stress tensor. It is also possible to specify a constant or user-defined frictional viscosity.

In granular flows with high solids volume fraction, instantaneous collisions are less important. The application of kinetic theory to granular flows is no longer relevant since particles are in contact and the resulting frictional stresses need to be taken into account. ANSYS Fluent extends the formulation of the frictional viscosity and employs other models, as well as providing new hooks for UDFs. See the UDF Manual for details.


Release 15.0 - © SAS IP, Inc. All rights reserved. - Contains proprietary and confidential information of ANSYS, Inc. and its subsidiaries and affiliates.

The frictional stresses are usually written in Newtonian form:

$$\tau_{friction} = -P_{friction}\,\overrightarrow{\overrightarrow{I}} + \mu_{friction}\left(\nabla \vec{u}_s + (\nabla \vec{u}_s)^T\right) \tag{17.298}$$

The frictional stress is added to the stress predicted by the kinetic theory when the solids volume fraction exceeds a critical value. This value is normally set to 0.5 when the flow is three-dimensional and the maximum packing limit is about 0.63. Then

$$P_S = P_{kinetic} + P_{friction} \tag{17.299}$$

$$\mu_S = \mu_{kinetic} + \mu_{friction} \tag{17.300}$$

The derivation of the frictional pressure is mainly semi-empirical, while the frictional viscosity can be derived from the first principles. The application of the modified Coulomb law leads to an expression of the form

$$\mu_{friction} = \frac{P_{friction}\sin\phi}{2\sqrt{I_{2D}}} \tag{17.301}$$

Where $\phi$ is the angle of internal friction and $I_{2D}$ is the second invariant of the deviatoric stress tensor.

Two additional models are available in ANSYS Fluent: the Johnson and Jackson [190] (p. 739) model for frictional pressure and Syamlal et al [441] (p. 753).

The Johnson and Jackson [190] (p. 739) model for frictional pressure is defined as

$$P_{friction} = Fr\frac{\left(\alpha_s - \alpha_{s,min}\right)^n}{\left(\alpha_{s,max} - \alpha_s\right)^p} \tag{17.302}$$

With coefficient $Fr$ = 0.05, $n$ = 2 and $p$ = 5 [325] (p. 747). The critical value for the solids volume fraction is 0.5. The coefficient $Fr$ was modified to make it a function of the volume fraction:

$$Fr = 0.1\alpha_s \tag{17.303}$$

The frictional viscosity for this model is of the form

$$\mu_{friction} = P_{friction}\sin\phi \tag{17.304}$$

The second model that is employed is Syamlal et al. [441] (p. 753). Comparing the two models results in the frictional normal stress differing by orders of magnitude.

The radial distribution function is an important parameter in the description of the solids pressure resulting from granular kinetic theory. If we use the models of Lun et al. [271] (p. 744) or Gidaspow [138] (p. 736) the radial function tends to infinity as the volume fraction tends to the packing limit. It would then be possible to use this pressure directly in the calculation of the frictional viscosity, as it has the desired effect. This approach is also available in ANSYS Fluent by default.

**Important**

The introduction of the frictional viscosity helps in the description of frictional flows, however a complete description would require the introduction of more physics to capture the elastic regime with the calculation of the yield stress and the use of the flow-rule. These effects can be added by you via UDFs to model static regime. Small time steps are required to get good convergence behavior.

Release 15.0 - © SAS IP, Inc. All rights reserved. - Contains proprietary and confidential information of ANSYS, Inc. and its subsidiaries and affiliates.

## 17.5.14. Granular Temperature

The granular temperature for the $s^{th}$ solids phase is proportional to the kinetic energy of the particles' random motion. The formal expression is:

$$\Theta_s = \frac{1}{3} u_{s,i} u_{s,i} \tag{17.305}$$

In Equation 17.305 (p. 544) $u_{s,i}$ represents the $i^{th}$ component of the fluctuating solids velocity in the Cartesian coordinate system. This is defined as an ensemble average of the particles' random velocity within a finite volume and time period. The averaging basis is particle number per unit volume following [60] (p. 732) and [91] (p. 734).

The transport equation derived from kinetic theory takes the form [91] (p. 734)

$$\begin{aligned} \frac{3}{2}\left[\frac{\partial}{\partial t}\left(\rho_s \alpha_s \Theta_s\right) + \nabla \cdot \left(\rho_s \alpha_s \vec{v}_s \Theta_s\right)\right] &= \left(-p_s \overline{\overline{I}} + \overline{\overline{\tau}}_s\right) : \nabla \vec{v}_s \\ &+ \nabla \cdot \left(k_{\Theta_s} \nabla \Theta_s\right) - \gamma_{\Theta_s} + \phi_{ls} \end{aligned} \tag{17.306}$$

where

$\left(-p_s \overline{\overline{I}} + \overline{\overline{\tau}}_s\right) : \nabla \vec{v}_s$ = the generation of energy by the solid stress tensor

$k_{\Theta_s} \nabla \Theta_s$ = the diffusion of energy ($k_{\Theta s}$ is the diffusion coefficient)

$\gamma_{\Theta_s}$ = the collisional dissipation of energy

$\phi_{ls}$ = the energy exchange between the $l^{th}$ fluid or solid phase and the $s^{th}$ solid phase

Equation 17.306 (p. 544) contains the term $k_{\Theta_s} \nabla \Theta_s$ describing the diffusive flux of granular energy. When the default Syamlal et al. model [441] (p. 753) is used, the diffusion coefficient for granular energy, $k_{\Theta_s}$ is given by

$$k_{\Theta_s} = \frac{15 d_s \rho_s \alpha_s \sqrt{\Theta_s \pi}}{4(41-33\eta)} \left[1 + \frac{12}{5}\eta^2 (4\eta - 3)\alpha_s g_{0,ss} + \frac{16}{15\pi}(41-33\eta)\eta \alpha_s g_{0,ss}\right] \tag{17.307}$$

where

$$\eta = \frac{1}{2}(1 + e_{ss})$$

ANSYS Fluent uses the following expression if the optional model of Gidaspow et al. [139] (p. 736) is enabled:

$$k_{\Theta_s} = \frac{150 \rho_s d_s \sqrt{(\Theta \pi)}}{384 (1 + e_{ss}) g_{0,ss}} \left[1 + \frac{6}{5}\alpha_s g_{0,ss}(1 + e_s)\right]^2 + 2\rho_s {\alpha_s}^2 d_s (1 + e_{ss}) g_{0,ss} \sqrt{\frac{\Theta_s}{\pi}} \tag{17.308}$$


Release 15.0 - © SAS IP, Inc. All rights reserved. - Contains proprietary and confidential information of ANSYS, Inc. and its subsidiaries and affiliates.

The collisional dissipation of energy, $\gamma_{\Theta_s}$, represents the rate of energy dissipation within the $s^{th}$ solids phase due to collisions between particles. This term is represented by the expression derived by Lun et al. [271] (p. 744)

$$\gamma_{\Theta m} = \frac{12\left(1-e_{ss}^2\right)g_{0,ss}}{d_s\sqrt{\pi}}\rho_s\alpha_s^2\Theta_s^{3/2} \tag{17.309}$$

The transfer of the kinetic energy of random fluctuations in particle velocity from the $s^{th}$ solids phase to the $l^{th}$ fluid or solid phase is represented by $\phi_{ls}$ [139] (p. 736):

$$\phi_{ls} = -3K_{ls}\Theta_s \tag{17.310}$$

ANSYS Fluent allows you to solve for the granular temperature with the following options:

- algebraic formulation (the default)

  It is obtained by neglecting convection and diffusion in the transport equation, Equation 17.306 (p. 544) [441] (p. 753).

- partial differential equation

  This is given by Equation 17.306 (p. 544) and it is allowed to choose different options for it properties.

- dpm-averaged granular temperature

  An alternative formulation available only with the Dense Discrete Phase Model (DDPM).

- constant granular temperature

  This is useful in very dense situations where the random fluctuations are small.

- UDF for granular temperature

For a granular phase $s$, we may write the shear force at the wall in the following form:

$$\overrightarrow{\tau_s} = -\frac{\pi}{6}\sqrt{3}\,\phi\frac{\alpha_s}{\alpha_{s,max}}\rho_s g_0\sqrt{\Theta_s}\,\overrightarrow{U_{s,||}} \tag{17.311}$$

Here $\overrightarrow{U_{s,||}}$ is the particle slip velocity parallel to the wall, $\phi$ is the specularity coefficient between the particle and the wall, $\alpha_{s,max}$ is the volume fraction for the particles at maximum packing, and $g_0$ is the radial distribution function that is model dependent.

The general boundary condition for granular temperature at the wall takes the form [190] (p. 739)

$$q_s = \frac{\pi}{6}\sqrt{3}\,\phi\frac{\alpha_s}{\alpha_{s,max}}\rho_s g_0\sqrt{\Theta_s}\,\overrightarrow{U_{s,||}}\cdot\overrightarrow{U_{s,||}} - \frac{\pi}{4}\sqrt{3}\frac{\alpha_s}{\alpha_{s,max}}\left(1-e_{sw}^2\right)\rho_s g_0\Theta_s^{\frac{3}{2}} \tag{17.312}$$

## 17.5.15. Description of Heat Transfer

The internal energy balance for phase $q$ is written in terms of the phase enthalpy, Equation 17.156 (p. 515), defined by

$$H_q = \int c_{p,q} dT_q \tag{17.313}$$

where $c_{p,q}$ is the specific heat at constant pressure of phase $q$. The thermal boundary conditions used with multiphase flows are the same as those for a single-phase flow. See Cell Zone and Boundary Conditions in the User's Guide for details.

### 17.5.15.1. The Heat Exchange Coefficient

The volumetric rate of energy transfer between phases, $Q_{pq}$, is assumed to be a function of the temperature difference and the interfacial area, $A_i$:

$$Q_{pq} = h_{pq} A_i \left( T_p - T_q \right) \tag{17.314}$$

where $h_{pq} \left( = h_{qp} \right)$ is the volumetric heat transfer coefficient between the $p^{th}$ phase and the $q^{th}$ phase. The heat transfer coefficient is related to the $p^{th}$ phase Nusselt number, $Nu_p$, by

$$h_{pq} = \frac{\kappa_q N u_p}{d_p} \tag{17.315}$$

Here $\kappa_q$ is the thermal conductivity of the $q^{th}$ phase, $d_p$ is the bubble diameter.

When using the Eulerian multiphase, ANSYS Fluent provides several methods for determining the volumetric heat transfer coefficient, $h_{pq}$, detailed in the following sections.

17.5.15.1.1. Constant
17.5.15.1.2. Nusselt Number
17.5.15.1.3. Ranz-Marshall Model
17.5.15.1.4. Tomiyama Model
17.5.15.1.5. Hughmark Model
17.5.15.1.6. Gunn Model
17.5.15.1.7. Two-Resistance Model
17.5.15.1.8. User Defined

#### 17.5.15.1.1. Constant

You can specify a constant value for the volumetric heat transfer coefficient, $h_{pq}$, by selecting the **constant-htc** method for heat transfer coefficient. If the Two-Resistance model is selected, the constant can be specified for each phase.

#### 17.5.15.1.2. Nusselt Number

You can specify the Nusselt number, $Nu_p$, used in Equation 17.315 (p. 546) by selecting the **nusselt-number** method for heat transfer coefficient. For the Two-Resistance model, the Nusselt number can be specified for each phase. In such cases, the Nusselt number is always defined relative to the physical properties to which it pertains.

#### 17.5.15.1.3. Ranz-Marshall Model

The correlation of Ranz and Marshall [366] (p. 749), [367] (p. 749) computes the Nusselt number as follows:


Release 15.0 - © SAS IP, Inc. All rights reserved. - Contains proprietary and confidential information of ANSYS, Inc. and its subsidiaries and affiliates.

$$Nu_p = 2.0 + 0.6\mathrm{Re}_p^{1/2}\mathrm{Pr}^{1/3} \tag{17.316}$$

where $\mathrm{Re}_p$ is the relative Reynolds number based on the diameter of the $p^{th}$ phase and the relative velocity $|\vec{u_p} - \vec{u_q}|$, and Pr is the Prandtl number of the $q^{th}$ phase:

$$Pr = \frac{c_{p_q}\mu_q}{\kappa_q} \tag{17.317}$$

### 17.5.15.1.4. Tomiyama Model

Tomiyama [452] (p. 753) proposed a slightly different correlation for the interfacial heat transfer, applicable to turbulent bubbly flows with relatively low Reynolds number. For the Tomiyama model, the Nusselt number, $Nu_p$, is expressed:

$$Nu_p = 2.0 + 0.15\mathrm{Re}_p^{0.8}\mathrm{Pr}^{0.5} \tag{17.318}$$

### 17.5.15.1.5. Hughmark Model

In order to extend the Ranz-Marshall model to a wider range of Reynolds numbers, Hughmark [170] (p. 738) proposed the following correction:

$$\mathrm{Nu_p} = \begin{cases} 2 + 0.6\mathrm{Re_p}^{1/2}\mathrm{Pr}^{1/3} & 0 \le \mathrm{Re_p} < 776.06 \quad 0 \le \mathrm{Pr} < 250 \\ 2 + 0.27\mathrm{Re_p}^{0.62}\mathrm{Pr}^{1/3} & 776.06 \le \mathrm{Re_p} \quad 0 \le \mathrm{Pr} < 250 \end{cases} \tag{17.319}$$

The Reynolds number crossover point is chosen to achieve continuity. The Hughmark model should not be used outside the recommended Prandtl number range

### 17.5.15.1.6. Gunn Model

In the case of granular flows (where $p = s$), you can also choose a Nusselt number correlation by Gunn [147] (p. 737), applicable to a porosity range of 0.35–1.0 and a Reynolds number of up to $10^5$:

$$Nu_s = \left(7 - 10\alpha_f + 5\alpha_f^2\right)\left(1 + 0.7Re_s^{0.2}Pr^{1/3}\right) + \left(1.33 - 2.4\alpha_f + 1.2\alpha_f^2\right)Re_s^{0.7}Pr^{1/3} \tag{17.320}$$

The Prandtl number is defined as above with $q = f$.

### 17.5.15.1.7. Two-Resistance Model

In some special situations, the use of an overall volumetric heat transfer coefficient is not sufficient to model the interphase heat transfer process accurately. A more general approach is to consider separate heat transfer processes with different heat transfer coefficients on either side of the phase interface. This generalization is referred to in Fluent as the two-resistance model.

At the interface between the $q^{\text{th}}$ phase and the $p^{\text{th}}$ phase, the temperature is assumed to be the same on both sides of the interface and is represented by $T_s$. Then the volumetric rates of phase heat exchange can be expressed as follows:

From the interface to the $q^{\text{th}}$ phase:

Release 15.0 - © SAS IP, Inc. All rights reserved. - Contains proprietary and confidential information of ANSYS, Inc. and its subsidiaries and affiliates.

$$Q_q = h_q A_i \left( T_s - T_q \right) + \dot{m}_{pq} H_{qs} \tag{17.321}$$

From the interface to the $p^{\text{th}}$ phase:

$$Q_p = h_p A_i \left( T_s - T_p \right) - \dot{m}_{pq} H_{ps} \tag{17.322}$$

where $h_q$ and $h_p$ are the $q^{\text{th}}$ and $p^{\text{th}}$ phase heat transfer coefficients, and $H_{qs}$ and $H_{ps}$ are the $q^{\text{th}}$ and $p^{\text{th}}$ phase enthalpies, respectively.

Since neither heat nor mass can be stored on the phase interface, the overall heat balance must be satisfied:

$$Q_q + Q_p = 0 \tag{17.323}$$

Therefore, in the absence of interphase mass transfer ($\dot{m}_{pq} = 0$) the interfacial temperature is determined as follows:

$$T_s = \frac{h_q T_q + h_p T_p}{h_q + h_p} \tag{17.324}$$

and the interphase heat transfer is given by

$$Q_q = -Q_p = h_{pq} A_i \left( T_p - T_q \right), \quad \frac{1}{h_{pq}} = \frac{1}{h_q} + \frac{1}{h_p} \tag{17.325}$$

Hence, in the absence of interphase mass transfer the two-resistance model works somewhat similar to coupled wall thermal boundaries, wherein the interface temperature and the overall heat transfer coefficient are determined by the heat transfer rates on the two sides.

The phase heat transfer coefficients, $h_q$ and $h_p$, can be computed using the same correlations that are available for computing the overall heat transfer coefficient, $h_{pq}$. In addition you can specify a zero-resistance condition on one side of the phase interface. This is equivalent to an infinite phase specific heat transfer coefficient. For example, if $h_q \to \infty$ its effect is to force the interface temperature to be the same as the phase temperature, $T_s = T_q$. You can also choose to use the *constant time scale return to saturation* method proposed by Lavieville et al. [234] (p. 742) which is used by default for the interface to vapor heat transfer coefficient in the wall boiling models. Refer to Interface to Vapor Heat Transfer (p. 573) for details of the formulation of the Lavieville et al method.

#### 17.5.15.1.8. User Defined

You can also specify the volumetric heat transfer coefficient, $h_{pq}$, as a user defined function using the DEFINE_PROPERTY UDF macro. See DEFINE_PROPERTY UDFs in the Fluent UDF Manual for details.

## 17.5.16. Turbulence Models

To describe the effects of turbulent fluctuations of velocities and scalar quantities in a single phase, ANSYS Fluent uses various types of closure models, as described in Turbulence (p. 39). In comparison to single-phase flows, the number of terms to be modeled in the momentum equations in multiphase flows is large, and this makes the modeling of turbulence in multiphase simulations extremely complex.


Release 15.0 - © SAS IP, Inc. All rights reserved. - Contains proprietary and confidential information of ANSYS, Inc. and its subsidiaries and affiliates.

ANSYS Fluent provides three methods for modeling turbulence in multiphase flows within the context of the $k$- $\varepsilon$ and $k$- $\omega$ models. In addition, ANSYS Fluent provides two turbulence options within the context of the Reynolds stress models (RSM).

The $k$- $\varepsilon$ and $k$- $\omega$ turbulence model options are:

- mixture turbulence model (the default)
- dispersed turbulence model
- turbulence model for each phase

**Important**

Note that the descriptions of each method below are presented based on the standard $k$-$\varepsilon$ model. The multiphase modifications to the $k$- $\omega$, RNG and realizable $k$- $\varepsilon$ models are similar, and are therefore not presented explicitly.

The RSM turbulence model options are:

- mixture turbulence model (the default)
- dispersed turbulence model

For either category, the choice of model depends on the importance of the secondary-phase turbulence in your application.

## 17.5.16.1. k- $\varepsilon$ Turbulence Models

ANSYS Fluent provides three turbulence model options in the context of the $k$- $\varepsilon$ models: the mixture turbulence model (the default), the dispersed turbulence model, or a per-phase turbulence model.

### 17.5.16.1.1. k- ε Mixture Turbulence Model

The mixture turbulence model is the default multiphase turbulence model. It represents the first extension of the single-phase $k$- $\varepsilon$ model, and it is applicable when phases separate, for stratified (or nearly stratified) multiphase flows, and when the density ratio between phases is close to 1. In these cases, using mixture properties and mixture velocities is sufficient to capture important features of the turbulent flow.

The $k$ and $\varepsilon$ equations describing this model (and without including buoyancy, dilation, and source terms) are as follows:

$$\frac{\partial}{\partial t}(\rho_m k) + \nabla \cdot (\rho_m \vec{v}_m k) = \nabla \cdot \left( \left( \mu_m + \frac{\mu_{t,m}}{\sigma_k} \right) \nabla k \right) + G_{k,m} - \rho_m \epsilon + \Pi_{k_m} \tag{17.326}$$

and

$$\frac{\partial}{\partial t}(\rho_m \varepsilon) + \nabla \cdot (\rho_m \vec{v}_m \varepsilon) = \nabla \cdot \left( \left( \mu_m + \frac{\mu_{t,m}}{\sigma_\varepsilon} \right) \nabla \varepsilon \right) + \frac{\varepsilon}{k} \left( C_{1\varepsilon} G_{k,m} - C_{2\varepsilon} \rho_m \varepsilon \right) + \Pi_{\varepsilon_m} \tag{17.327}$$

where the mixture density, $\rho_m$, molecular viscosity, $\mu_m$, and velocity, $\vec{v}_m$, are computed from

$$\rho_m = \sum_{i=1}^{N} \alpha_i \rho_i \tag{17.328}$$

$$\mu_m = \sum_{i=1}^{n} \alpha_i \mu_i \tag{17.329}$$

and

$$\vec{v}_m = \frac{\sum_{i=1}^{N} \alpha_i \rho_i \vec{v}_i}{\sum_{i=1}^{N} \alpha_i \rho_i} \tag{17.330}$$

where $\alpha_i$, $\rho_i$, $\mu_i$, and $\vec{v}_i$ are, respectively, the volume fraction, density, viscosity, and velocity of the i$^{th}$ phase.

The turbulent viscosity for the mixture, $\mu_{t,m}$, is computed from

$$\mu_{t,m} = \rho_m C_\mu \frac{k^2}{\varepsilon} \tag{17.331}$$

and the production of turbulence kinetic energy, $G_{k,m}$, is computed from

$$G_{k,m} = \mu_{t,m} \left( \nabla \vec{v}_m + (\nabla \vec{v}_m)^T \right) : \nabla \vec{v}_m \tag{17.332}$$

The terms, $\Pi_{k_m}$ and $\Pi_{\varepsilon_m}$ are source terms that can be included to model the turbulent interaction between the dispersed phases and the continuous phase (Turbulence Interaction Models (p. 556)).

The turbulent viscosity for phase $i$ is computed from

$$\mu_{t,i} = \frac{\rho_i}{\rho_m} \mu_{t,m} \tag{17.333}$$

The constants in these equations are the same as those described in Standard k-ε Model (p. 47) for the single-phase $k$- $\varepsilon$ model.

### 17.5.16.1.2. k- ε Dispersed Turbulence Model

The dispersed turbulence model is the appropriate model when the concentrations of the secondary phases are dilute, or when using the granular model. Fluctuating quantities of the secondary phases can be given in terms of the mean characteristics of the primary phase and the ratio of the particle relaxation time and eddy-particle interaction time.

The model is applicable when there is clearly one primary continuous phase and the rest are dispersed dilute secondary phases.

#### *17.5.16.1.2.1. Assumptions*

The dispersed method for modeling turbulence in ANSYS Fluent assumes the following:

- a modified $k$- $\varepsilon$ model for the continuous phase


Release 15.0 - © SAS IP, Inc. All rights reserved. - Contains proprietary and confidential information of ANSYS, Inc. and its subsidiaries and affiliates.

Turbulent predictions for the continuous phase are obtained using the standard $k$- $\varepsilon$ model supplemented with extra terms that include the interphase turbulent momentum transfer.

- Tchen-theory correlations for the dispersed phases

  Predictions for turbulence quantities for the dispersed phases are obtained using the Tchen theory of dispersion of discrete particles by homogeneous turbulence [164] (p. 738).

- interphase turbulent momentum transfer

  In turbulent multiphase flows, the momentum exchange terms contain the correlation between the instantaneous distribution of the dispersed phases and the turbulent fluid motion. It is possible to take into account the dispersion of the dispersed phases transported by the turbulent fluid motion.

- a phase-weighted averaging process

  The choice of averaging process has an impact on the modeling of dispersion in turbulent multiphase flows. A two-step averaging process leads to the appearance of fluctuations in the phase volume fractions. When the two-step averaging process is used with a phase-weighted average for the turbulence, however, turbulent fluctuations in the volume fractions do not appear. ANSYS Fluent uses phase-weighted averaging, so no volume fraction fluctuations are introduced into the continuity equations.

#### *17.5.16.1.2.2. Turbulence in the Continuous Phase*

The eddy viscosity model is used to calculate averaged fluctuating quantities. The Reynolds stress tensor for continuous phase $q$ takes the following form:

$$\overline{\overline{\tau}}''_q = -\frac{2}{3}\left(\rho_q k_q + \rho_q v_{t,q} \nabla \cdot \vec{U}_q\right)\overline{\overline{I}} + \rho_q v_{t,q}\left(\nabla \vec{U}_q + \nabla \vec{U}_q{}^T\right) \tag{17.334}$$

where $\vec{U}_q$ is the phase-weighted velocity.

The turbulent viscosity $\mu_{t,q}$ is written in terms of the turbulent kinetic energy of phase $q$:

$$\mu_{t,q} = \rho_q C_\mu \frac{k_q^2}{\varepsilon_q} \tag{17.335}$$

and a characteristic time of the energetic turbulent eddies is defined as

$$\tau_{t,q} = \frac{3}{2} C_\mu \frac{k_q}{\varepsilon_q} \tag{17.336}$$

where $\varepsilon_q$ is the dissipation rate and $C_\mu = 0.09$.

The length scale of the turbulent eddies is

$$L_{t,q} = \sqrt{\frac{3}{2}} C_\mu \frac{k_q^{3/2}}{\varepsilon_q} \tag{17.337}$$

Turbulent predictions are obtained from the modified $k$- $\varepsilon$ model. The transport equations (excluding buoyancy, dilation, and user-defined source terms) are:

Release 15.0 - © SAS IP, Inc. All rights reserved. - Contains proprietary and confidential information of ANSYS, Inc. and its subsidiaries and affiliates.

$$\frac{\partial}{\partial t}(\alpha_q \rho_q k_q) + \nabla \cdot (\alpha_q \rho_q \vec{U}_q k_q) = \nabla \cdot \left( \alpha_q \left( \mu_q + \frac{\mu_{t,q}}{\sigma_k} \right) \nabla k_q \right) + \alpha_q G_{k,q} - \alpha_q \rho_q \epsilon_q + \alpha_q \rho_q \Pi_{k_q} \tag{17.338}$$

and

$$\frac{\partial}{\partial t}\left(\alpha_q \rho_q \varepsilon_q\right) + \nabla \cdot \left(\alpha_q \rho_q \vec{U}_q \varepsilon_q\right) = \nabla \cdot \left( \alpha_q \left( \mu_q + \frac{\mu_{t,q}}{\sigma_\varepsilon} \right) \nabla \varepsilon_q \right) + \alpha_q \frac{\varepsilon_q}{k_q} \left( C_{1\varepsilon} G_{k,q} - C_{2\varepsilon} \rho_q \varepsilon_q \right) + \alpha_q \rho_q \Pi_{\varepsilon_q} \tag{17.339}$$

Here, the terms containing $\Pi_{k_q}$ and $\Pi_{\varepsilon_q}$ are source terms that can be included to model the influence of the dispersed phases on the continuous phase $q$ (Turbulence Interaction Models (p. 556)). $G_{k,q}$ is the production of turbulent kinetic energy, as defined in Modeling Turbulent Production in the k-ε Models (p. 54). All other terms have the same meaning as in the single-phase $k$- $\varepsilon$ model.

#### *17.5.16.1.2.3. Turbulence in the Dispersed Phase*

The turbulence quantities for the dispersed phase are not obtained from transport equations. Time and length scales that characterize the motion are used to evaluate dispersion coefficients, correlation functions, and the turbulent kinetic energy of each dispersed phase.

### 17.5.16.1.3. k- ε Turbulence Model for Each Phase

The most general multiphase turbulence model solves a set of $k$ and $\varepsilon$ transport equations for each phase. This turbulence model is the appropriate choice when the turbulence transfer among the phases plays a dominant role.

Note that, since ANSYS Fluent is solving two additional transport equations for each secondary phase, the per-phase turbulence model is more computationally intensive than the dispersed turbulence model.

#### *17.5.16.1.3.1. Transport Equations*

The Reynolds stress tensor and turbulent viscosity are computed using Equation 17.334 (p. 551) and Equation 17.335 (p. 551). Turbulence predictions are obtained from


Release 15.0 - © SAS IP, Inc. All rights reserved. - Contains proprietary and confidential information of ANSYS, Inc. and its subsidiaries and affiliates.

$$\begin{aligned}\frac{\partial}{\partial t}\left(\alpha_q\rho_q k_q\right)+\nabla\cdot\left(\alpha_q\rho_q\vec{U}_q k_q\right) &= \nabla\cdot\left(\alpha_q\left(\mu_q+\frac{\mu_{t,q}}{\sigma_k}\right)\nabla k_q\right)\\ &+\left(\alpha_q G_{k,q}-\alpha_q\rho_q\varepsilon_q\right)\\ &+\sum_{l=1}^{N}K_{lq}\left(C_{lq}k_l-C_{ql}k_q\right)\\ &-\sum_{l=1}^{N}K_{lq}\left(\vec{U}_l-\vec{U}_q\right)\cdot\frac{\mu_{t,l}}{\alpha_l\sigma_l}\nabla\alpha_l\\ &+\sum_{l=1}^{N}K_{lq}\left(\vec{U}_l-\vec{U}_q\right)\cdot\frac{\mu_{t,q}}{\alpha_q\sigma_q}\nabla\alpha_q\\ &+\Pi_{k_q}\end{aligned} \tag{17.340}$$

and

$$\begin{aligned}\frac{\partial}{\partial t}\left(\alpha_q\rho_q\varepsilon_q\right)+\nabla\cdot\left(\alpha_q\rho_q\vec{U}_q\varepsilon_q\right) &= \nabla\cdot\left(\alpha_q\left(\mu_q+\frac{\mu_{t,q}}{\sigma_\varepsilon}\right)\nabla\varepsilon_q\right)\\ &+\frac{\varepsilon_q}{k_q}\Bigg[C_{1\varepsilon}\alpha_q G_{k,q}-C_{2\varepsilon}\alpha_q\rho_q\varepsilon_q\\ &+C_{3\varepsilon}\Bigg(\sum_{l=1}^{N}K_{lq}\left(C_{lq}k_l-C_{ql}k_q\right)\\ &-\sum_{l=1}^{N}K_{lq}\left(\vec{U}_l-\vec{U}_q\right)\cdot\frac{\mu_{t,l}}{\alpha_l\sigma_l}\nabla\alpha_l\\ &+\sum_{l=1}^{N}K_{lq}\left(\vec{U}_l-\vec{U}_q\right)\cdot\frac{\mu_{t,q}}{\alpha_q\sigma_q}\nabla\alpha_q\Bigg)\Bigg]\\ &+\Pi_{\varepsilon_q}\end{aligned} \tag{17.341}$$

The terms $C_{lq}$ and $C_{ql}$ can be approximated as

$$C_{lq}=2\,,C_{ql}=2\left(\frac{\eta_{lq}}{1+\eta_{lq}}\right) \tag{17.342}$$

where $\eta_{lq}$ is defined by Equation 17.363 (p. 558). The terms $\Pi_{k_q}$ and $\Pi_{\varepsilon_q}$ are source terms which can be included to model the influence of the inter-phase turbulence interaction (Turbulence Interaction Models (p. 556)).

### 17.5.16.2. RSM Turbulence Models

Multiphase turbulence modeling typically involves two equation models that are based on single-phase models and often cannot accurately capture the underlying flow physics. Additional turbulence modeling

Release 15.0 - © SAS IP, Inc. All rights reserved. - Contains proprietary and confidential information of ANSYS, Inc. and its subsidiaries and affiliates.

for multiphase flows is diminished even more when the basic underlying single-phase model cannot capture the complex physics of the flow. In such situations, the logical next step is to combine the Reynolds stress model with the multiphase algorithm in order to handle challenging situations in which both factors, RSM for turbulence and the Eulerian multiphase formulation, are a precondition for accurate predictions [73] (p. 733).

The phase-averaged continuity and momentum equations for a continuous phase are:

$$\frac{\partial}{\partial t}\left(\overline{\alpha_c}\rho_c\right)+\nabla\cdot\left(\overline{\alpha_c}\rho_c\tilde{U}_c\right)=0 \tag{17.343}$$

$$\frac{\partial}{\partial t}\left(\overline{\alpha_c}\rho_{rmc}\tilde{U}_c\right)+\nabla\cdot\left(\overline{\alpha_c}\rho_{rmc}\tilde{U}_c\otimes\tilde{U}_c\right)=-\overline{\alpha_c}\nabla\tilde{p}+\nabla\cdot\tilde{\tau}_c^t+F_{Dc} \tag{17.344}$$

For simplicity, the laminar stress-strain tensor and other body forces such as gravity have been omitted from Equation 17.343 (p. 554) - Equation 17.344 (p. 554). The tilde denotes phase-averaged variables while an overbar (for example, $\overline{\alpha_c}$) reflects time-averaged values. In general, any variable $\Phi$ can have a phase-average value defined as

$$\tilde{\Phi}_c=\frac{\overline{\alpha_c\Phi_c}}{\overline{\alpha_c}} \tag{17.345}$$

Considering only two phases for simplicity, the drag force between the continuous and the dispersed phases can be defined as:

$$F_{Dc}=K_{dc}\left[\left(\tilde{U}_d-\tilde{U}_c\right)-\left(\frac{\overline{\alpha_d u'_d}}{\overline{\alpha_d}}-\frac{\overline{\alpha_c u'_c}}{\overline{\alpha_c}}\right)\right] \tag{17.346}$$

where $K_{dc}$ is the drag coefficient. Several terms in the Equation 17.346 (p. 554) need to be modeled in order to close the phase-averaged momentum equations. Full descriptions of all modeling assumptions can be found in [72] (p. 732). This section only describes the different modeling definition of the turbulent stresses $\tilde{\tau}^t$ that appears in Equation 17.344 (p. 554).

The turbulent stress that appears in the momentum equations need to be defined on a per-phase basis and can be calculated as:

$$\tilde{\tau^t}_k=-\overline{\alpha_k}\rho_k\tilde{R}_{k,ij} \tag{17.347}$$

where the subscript $k$ is replaced by $c$ for the primary (that is, continuous) phase or by $d$ for any secondary (that is, dispersed) phases. As is the case for single-phase flows, the current multiphase Reynolds stress model (RSM) also solves the transport equations for Reynolds stresses $R_{ij}$. ANSYS Fluent includes two methods for modeling turbulence in multiphase flows within the context of the RSM model: the dispersed turbulence model, and the mixture turbulence model.

### 17.5.16.2.1. RSM Dispersed Turbulence Model

The dispersed turbulence model is used when the concentrations of the secondary phase are dilute and the primary phase turbulence is regarded as the dominant process. Consequently, the transport equations for turbulence quantities are only solved for the primary (continuous) phase, while the predictions of turbulence quantities for dispersed phases are obtained using the Tchen theory. The transport equation for the primary phase Reynolds stresses in the case of the dispersed model are:


Release 15.0 - © SAS IP, Inc. All rights reserved. - Contains proprietary and confidential information of ANSYS, Inc. and its subsidiaries and affiliates.

$$\frac{\partial}{\partial t}(\overline{\alpha}\rho\widetilde{R}_{ij}) + \frac{\partial}{\partial x_k}(\overline{\alpha}\rho\widetilde{U}_k\widetilde{R}_{ij}) = -\overline{\alpha}\rho\left(\widetilde{R}_{ik}\frac{\partial\widetilde{U}_j}{\partial x_k} + \widetilde{R}_{jk}\frac{\partial\widetilde{U}_i}{\partial x_k}\right) + \frac{\partial}{\partial x_k}\left[\overline{\alpha}\mu\frac{\partial}{\partial x_k}(\widetilde{R}_{ij})\right] - \frac{\partial}{\partial x_k}\left[\overline{\alpha}\rho\overline{u'_i u'_j u'_k} + \overline{\alpha}p'\left(\delta_{jk}u'_i + \delta_{ik}u'_j\right)\right] + \overline{\alpha p'\left(\frac{\partial u'_i}{\partial x_j} + \frac{\partial u'_j}{\partial x_i}\right)} - \overline{\alpha}\rho\widetilde{\epsilon}_{ij} - 2\overline{\alpha}\rho\Omega_k\left(\widetilde{R}_{jm}\epsilon_{ikm} + \widetilde{R}_{im}\epsilon_{jkm}\right) + \Pi_{R,ij} \quad (17.348)$$

The variables in Equation 17.348 (p. 555) are per continuous phase $c$ and the subscript is omitted for clarity. In general, the terms in Equation 17.348 (p. 555) are modeled in the same way as for the single phase case described in Reynolds Stress Model (RSM) (p. 83). The last term, $\Pi_{R,ij}$, takes into account the interaction between the continuous and the dispersed phase turbulence. A general model for this term can be of the form:

$$\Pi_{R,ij} = K_{dc}C_{1,dc}\left(R_{dc,ij} - R_{c,ij}\right) + K_{dc}C_{2,dc}a_{dc,i}b_{dc,j} \quad (17.349)$$

where $C_1$ and $C_2$ are unknown coefficients, $a_{dc,i}$ is the relative velocity, $b_{dc,j}$ represents the drift or the relative velocity, and $R_{dc,ij}$ is the unknown particulate-fluid velocity correlation. To simplify this unknown term, the following assumption has been made:

$$\Pi_{R,ij} = \frac{2}{3}\delta_{ij}\Pi_k \quad (17.350)$$

where $\delta_{ij}$ is the Kronecker delta, and $\Pi_k$ represents the modified version of the original Simonin model [409] (p. 751).

$$\Pi_{kc} = K_{dc}\left(\tilde{k}_{dc} - 2\tilde{k}_c + \tilde{V}_{rel}\cdot\tilde{V}_{drift}\right) \quad (17.351)$$

where $\tilde{K}_c$ represents the turbulent kinetic energy of the continuous phase, $\tilde{k}_{dc}$ is the continuous-dispersed phase velocity covariance and finally, $\tilde{V}_{rel}$ and $\tilde{V}_{drift}$ stand for the relative and the drift velocities, respectively. In order to achieve full closure, the transport equation for the turbulent kinetic energy dissipation rate ($\tilde{\varepsilon}$) is required. The modeling of $\tilde{\varepsilon}$ together with all other unknown terms in Equation 17.351 (p. 555) are modeled in the same way as in [72] (p. 732).

### 17.5.16.2.2. RSM Mixture Turbulence Model

The main assumption for the mixture model is that all phases share the same turbulence field which consequently means that the term $\Pi_R$ in the Reynolds stress transport equations (Equation 17.348 (p. 555)) is neglected. Apart from that, the equations maintain the same form but with phase properties and phase velocities being replaced with mixture properties and mixture velocities. The mixture density, for example, can be expressed as

$$\rho_m = \sum_{i=1}^{N}\overline{\alpha}_i\rho_i \quad (17.352)$$

while mixture velocities can be expressed as

$$\tilde{U}_m = \frac{\sum_{i=1}^{N} \overline{\alpha}_i \rho_i \tilde{U}_i}{\sum_{i=1}^{N} \overline{\alpha}_i \rho_i} \tag{17.353}$$

where $N$ is the number of species.

## 17.5.16.3. Turbulence Interaction Models

When using a turbulence model in an Eulerian multiphase simulation, Fluent can optionally include the influence of the dispersed phase on the multiphase turbulence equations. The influence of the dispersed phases is represented by source terms ($\Pi_{k_q}$ and $\Pi_{\varepsilon_q}$ in Equation 17.338 (p. 552) and Equation 17.339 (p. 552)) whose form will depend on the model chosen.

You can choose from the following models for turbulence interaction.

17.5.16.3.1. Simonin et al.
17.5.16.3.2. Troshko-Hassan
17.5.16.3.3. Sato
17.5.16.3.4. None

Turbulence interaction can be included with any of the multiphase turbulence models and formulations in Fluent.

See Including Turbulence Interaction Source Terms in the *Fluent User's Guide* for details about how to include turbulence interaction in your simulation.

### 17.5.16.3.1. Simonin et al.

In the Simonin et al. model [409] (p. 751), the turbulence interaction is modeled by additional source terms in the turbulence transport equation(s). The Simonin model is only available with Dispersed and Per Phase turbulence models.

#### *17.5.16.3.1.1. Formulation in Dispersed Turbulence Models*

##### 17.5.16.3.1.1.1. Continuous Phase

The term $\Pi_{k_q}$ is derived from the instantaneous equation of the continuous phase and takes the following form, where $M$ represents the number of secondary phases:

$$\Pi_{k_q} = C_s \sum_{p=1}^{M} \frac{K_{pq}}{\alpha_q \rho_q} X_{pq} \left( < \vec{v}''_q \cdot \vec{v}''_p > + \left( \vec{U}_p - \vec{U}_q \right) \cdot \vec{v}_{dr} \right) \tag{17.354}$$

which can be simplified to

$$\Pi_{k_q} = C_s \sum_{p=1}^{M} \frac{K_{pq}}{\alpha_q \rho_q} X_{pq} \left( k_{pq} - 2k_q + \vec{v}_{pq} \cdot \vec{v}_{dr} \right) \tag{17.355}$$

where:


Release 15.0 - © SAS IP, Inc. All rights reserved. - Contains proprietary and confidential information of ANSYS, Inc. and its subsidiaries and affiliates.

$C_s$ is a user-modifiable model constant. By default, $C_s = 1$.

$k_{pq}$ is the covariance of the velocities of the continuous phase $q$ and the dispersed phase $p$, calculated from Equation 17.364 (p. 558).

$\vec{v}_{pq}$ is the relative velocity.

$\vec{v}_{dr}$ is the drift velocity, calculated from Equation 17.264 (p. 535).

$X_{pq} = \frac{\rho_p}{\rho_p + C_{VM}\rho_q}$ For granular flows, $X_{pq} \sim 1$.

Equation 17.355 (p. 556) can be split into two terms as follows:

$$\Pi_{k_q} = C_s \sum_{p=1}^{M} \frac{K_{pq}}{\alpha_q \rho_q} X_{pq} \left( k_{pq} - 2k_q \right) + C_s \sum_{p=1}^{M} \frac{K_{pq}}{\alpha_q \rho_q} X_{pq} \vec{v}_{pq} \cdot \vec{v}_{dr} \tag{17.356}$$

The second term in Equation 17.356 (p. 557) is related to drift velocity and is referred to as the drift turbulent source. It is an option term in the turbulent kinetic energy source and can be included as described in Including Turbulence Interaction Source Terms in the *Fluent User's Guide*

$\Pi_{\varepsilon_q}$ is modeled according to Elgobashi et al. [108] (p. 734):

$$\Pi_{\varepsilon_q} = C_{3\varepsilon} \frac{\varepsilon_q}{k_q} \Pi_{k_q} \tag{17.357}$$

where $C_{3\varepsilon} = 1.2$.

#### 17.5.16.3.1.1.2. Dispersed Phases

For the dispersed phases, the characteristic particle relaxation time connected with inertial effects acting on a dispersed phase $p$ is defined as

$$\tau_{pq}^{F} = \frac{\rho_q d_p^2}{18 \mu_c f\left(\mathrm{Re}, \alpha_q\right)} \left( 1 + C_{VM} \frac{\rho_q}{\rho_p} \right) \tag{17.358}$$

The time scale of the energetic turbulent eddies is defined as:

$$\tau_q^t = \frac{3}{2} C_\mu \frac{k_q}{\varepsilon_q} \tag{17.359}$$

The eddy particle interaction time is mainly affected by the crossing-trajectory effect [80] (p. 733), and is defined as

$$\tau_{pq}^t = \frac{\tau_q^t}{\sigma_1 \sqrt{\left(1 + C_\beta \xi_\tau^2\right)}} \tag{17.360}$$

where $\sigma_1 = 1$, the parameter, $\xi_\tau$, is given by

$$\xi_\tau = \frac{\left|\vec{U}_p - \vec{U}_q\right|}{\sqrt{\frac{2}{3}k_q}} \tag{17.361}$$

and

$$C_\beta = 1.8 - 1.35\cos^2\theta \tag{17.362}$$

where $\theta$ is the angle between the mean particle velocity and the mean relative velocity. The ratio between these two characteristic times is written as

$$\eta_{pq} = \frac{\tau^t_{pq}}{\tau^F_{pq}} \tag{17.363}$$

Following Simonin [409] (p. 751), ANSYS Fluent writes the turbulence quantities for dispersed phase $p$ as follows:

$$\begin{aligned} k_p &= k_q\left(\frac{b^2+\eta_{pq}}{1+\eta_{pq}}\right) \\ k_{pq} &= 2k_q\left(\frac{b+\eta_{pq}}{1+\eta_{pq}}\right) \\ D_{t,pq} &= \frac{1}{3}k_{pq}\tau_{t,pq} \\ D_p &= D_{t,pq} + \left(\frac{2}{3}k_p - b\frac{1}{3}k_{pq}\right)\tau_{F,pq} \\ b &= (1+C_{\mathrm{VM}})\left(\frac{\rho_p}{\rho_q}+1\right)^{-1} \end{aligned} \tag{17.364}$$

and $C_{\mathrm{VM}} = 0.5$ is the added-mass coefficient. For granular flows, $b$ is negligible. The viscosity for the secondary phase, $p$ for granular flows is approximated as:

$$\nu_p = \frac{1}{3}k_{pq}\tau^t_{pq} + \frac{2}{3}k_p\tau^F_{pq} \tag{17.365}$$

while for bubbly flows it can be left as $D_{t,pq}$.

#### *17.5.16.3.1.2. Formulation in Per Phase Turbulence Models*

For Per Phase turbulence models, only the second term from Equation 17.356 (p. 557) (the drift turbulence source) is added in the phase turbulence modeling equations.

For the turbulent kinetic energy equations:


Release 15.0 - © SAS IP, Inc. All rights reserved. - Contains proprietary and confidential information of ANSYS, Inc. and its subsidiaries and affiliates.

**Continuous Phase**

$$\Pi_{k_q} = C_s \alpha_q \sum_{p=1}^{M} K_{pq} \vec{v}_{pq} \cdot \vec{v}_{dr} \tag{17.366}$$

**Dispersed Phases**

$$\Pi_{k_p} = C_s \alpha_p K_{pq} \vec{v}_{pq} \cdot \vec{v}_{dr} \quad p = 1 \ldots m \tag{17.367}$$

Turbulence dissipation sources for all phases are computed as:

$$\Pi_{\varepsilon_r} = C_{3\varepsilon} \frac{\varepsilon_k}{k_r} \Pi_{k_r} \quad r = 0 \ldots m \tag{17.368}$$

## 17.5.16.3.2. Troshko-Hassan

Troshko and Hassan [455] (p. 754) proposed an alternative model to account for the turbulence of the dispersed phase in the $k$- $\varepsilon$ equations.

### *17.5.16.3.2.1. Troshko-Hassan Formulation in Mixture Turbulence Models*

In the Mixture turbulence models, the Troshko-Hassan turbulence interaction terms are:

$$\Pi_{k_m} = C_{ke} \sum_{p=1}^{M} K_{pq} |\vec{U}_p - \vec{U}_q|^2 \tag{17.369}$$

$$\Pi_{\varepsilon_m} = C_{td} \frac{1}{\tau_p} \Pi_{k_m} \tag{17.370}$$

By default, $C_{ke} = 0.75$ and $C_{td} = 0.45$. These values are user-modifiable as described in Including Turbulence Interaction Source Terms in the *Fluent User's Guide*. $\tau_p$ is the characteristic time of the induced turbulence defined as

$$\tau_p = \frac{2 C_{VM} d_p}{3 C_D \left| \vec{U}_p - \vec{U}_q \right|} \tag{17.371}$$

$C_{VM}$ is the virtual mass coefficient and $C_D$ is the drag coefficient.

### *17.5.16.3.2.2. Troshko-Hassan Formulation in Dispersed Turbulence Models*

#### 17.5.16.3.2.2.1. Continuous Phase

In the Dispersed turbulence models, the term $\Pi_{k_q}$ is calculated as follows:

$$\Pi_{k_q} = C_{ke} \sum_{p=1}^{M} \frac{K_{pq}}{\alpha_q \rho_q} | \vec{U}_p - \vec{U}_q |^2 \tag{17.372}$$

and $\Pi_{\varepsilon_q}$ is calculated as

$$\Pi_{\varepsilon_q} = C_{td} \frac{1}{\tau_p} \Pi_{k_q} \tag{17.373}$$

Release 15.0 - © SAS IP, Inc. All rights reserved. - Contains proprietary and confidential information of ANSYS, Inc. and its subsidiaries and affiliates.

By default, $C_{ke} = 0.75$ and $C_{td} = 0.45$. These values are user-modifiable as described in Including Turbulence Interaction Source Terms in the *Fluent User's Guide*.$\tau_p$ is the characteristic time of the induced turbulence defined as in Equation 17.371 (p. 559)

#### 17.5.16.3.2.2.2. Dispersed Phases

For the Troshko-Hassan model, the kinematic turbulent viscosity of the dispersed phase is calculated as

$$v_p = v_q \tag{17.374}$$

### *17.5.16.3.2.3. Troshko-Hassan Formulation in Per-Phase Turbulence Models*

#### 17.5.16.3.2.3.1. Continuous Phase

In the Per-Phase turbulence models, the continuous phase equations are modified with the following terms:

$$\Pi_{k_q} = C_{ke}\alpha_q \sum_{p=1}^{M} K_{pq} \left| \vec{U}_p - \vec{U}_q \right|^2 \tag{17.375}$$

$$\Pi_{\varepsilon_q} = C_{td}\frac{1}{\tau_p}\Pi_{k_q} \tag{17.376}$$

By default, $C_{ke} = 0.75$ and $C_{td} = 0.45$. These values are user-modifiable as described in Including Turbulence Interaction Source Terms in the *Fluent User's Guide*.$\tau_p$ is the characteristic time of the induced turbulence defined as in Equation 17.371 (p. 559)

#### 17.5.16.3.2.3.2. Dispersed Phases

The dispersed phase equations are also modified with source terms defined as follows:

$$\Pi_{k_p} = C_{ke}\alpha_p K_{pq} \left| \vec{U}_p - \vec{U}_q \right|^2 \quad p = 1 \ldots M \tag{17.377}$$

$$\Pi_{\varepsilon_p} = C_{td}\frac{1}{\tau_p}\Pi_{k_p} \quad p = 1 \ldots M \tag{17.378}$$

## 17.5.16.3.3. Sato

Unlike the Simonin and Troshko-Hassan models, the Sato model [388] (p. 750) does not add explicit source terms to the turbulence equations. Instead, in an attempt to incorporate the effect of the random primary phase motion induced by the dispersed phase in bubbly flow, Sato et al. proposed the following relation:

$$v_q = C_\mu \frac{k_q^2}{\varepsilon_q} + C_{\mu,p}\alpha_p d_p \left| \vec{U}_p - \vec{U}_q \right| \tag{17.379}$$

where the relative velocity and the diameter of the dispersed phase represent velocity and time scales and $C_{\mu,p} = 0.6$. The kinematic viscosity for the dispersed secondary phase is defined as in Equation 17.374 (p. 560).


Release 15.0 - © SAS IP, Inc. All rights reserved. - Contains proprietary and confidential information of ANSYS, Inc. and its subsidiaries and affiliates.

#### 17.5.16.3.4. None

If None is selected, then no source terms are added to account for turbulent interaction. This is appropriate if you prefer to add your own source terms using the DEFINE_SOURCE UDF macro ( DEFINE_SOURCE in the *Fluent UDF Manual*).

## 17.5.17. Solution Method in ANSYS Fluent

For Eulerian multiphase calculations, ANSYS Fluent can solve the phase momentum equations, the shared pressure, and phasic volume fraction equations in a coupled and segregated fashion. The coupled solution for multiphase flows is discussed in detail in Coupled Solution for Eulerian Multiphase Flows in the User's Guide. When solving the equations in a segregated manner, ANSYS Fluent uses the phase coupled SIMPLE (PC-SIMPLE) algorithm [462] (p. 754) for the pressure-velocity coupling. PC-SIMPLE is an extension of the SIMPLE algorithm [340] (p. 747) to multiphase flows. The velocities are solved coupled by phases, but in a segregated fashion. The block algebraic multigrid scheme used by the density-based solver described in [482] (p. 755) is used to solve a vector equation formed by the velocity components of all phases simultaneously. Then, a pressure correction equation is built based on total volume continuity rather than mass continuity. Pressure and velocities are then corrected so as to satisfy the continuity constraint.

### 17.5.17.1. The Pressure-Correction Equation

For incompressible multiphase flow, the pressure-correction equation takes the form

$$\sum_{k=1}^{n}\frac{1}{\rho_{rk}}\left\{\frac{\partial}{\partial t}\alpha_k\rho_k+\nabla\cdot\alpha_k\rho_k\vec{v}'_k+\nabla\cdot\alpha_k\rho_k\vec{v}^{\,*}_k-\left(\sum_{l=1}^{n}(\dot{m}_{lk}-\dot{m}_{kl})\right)\right\}=0 \tag{17.380}$$

where $\rho_{rk}$ is the phase reference density for the $k^{th}$ phase (defined as the total volume average density of phase $k$), $\vec{v}'_k$ is the velocity correction for the $k^{th}$ phase, and $\vec{v}^{\,*}_k$ is the value of $\vec{v}_k$ at the current iteration. The velocity corrections are themselves expressed as functions of the pressure corrections.

### 17.5.17.2. Volume Fractions

The volume fractions are obtained from the phase continuity equations. In discretized form, the equation of the $k^{th}$ volume fraction is

$$a_{p,k}\alpha_k=\sum_{nb}\left(a_{nb,k}\alpha_{nb,k}\right)+b_k=R_k \tag{17.381}$$

In order to satisfy the condition that all the volume fractions sum to one,

$$\sum_{k=1}^{n}\alpha_k=1 \tag{17.382}$$

## 17.5.18. Dense Discrete Phase Model

In the standard formulation of the Lagrangian multiphase model, described in Discrete Phase (p. 373), the assumption is that the volume fraction of the discrete phase is sufficiently low: it is not taken into account when assembling the continuous phase equations. The general form of the mass and momentum conservation equations in ANSYS Fluent is given in Equation 17.383 (p. 562) and Equation 17.384 (p. 562) (and also defined in Continuity and Momentum Equations (p. 2)).

Release 15.0 - © SAS IP, Inc. All rights reserved. - Contains proprietary and confidential information of ANSYS, Inc. and its subsidiaries and affiliates.

$$\frac{\partial \rho}{\partial t} + \nabla \cdot (\rho \vec{v}) = S_{DPM} + S_{other} \tag{17.383}$$

$$\frac{\partial \rho \vec{v}}{\partial t} + \nabla \cdot (\rho \vec{v} \vec{v}) = -\nabla p + \nabla \cdot \tau + \rho \vec{g} + \vec{F}_{DPM} + \vec{F}_{other} \tag{17.384}$$

To overcome this limitation of the Lagrangian multiphase model, the volume fraction of the particulate phase is accounted for by extending Equation 17.383 (p. 562) and Equation 17.384 (p. 562) to the following set of equations (see also Conservation Equations (p. 513), written for phase $p$):

$$\frac{\partial}{\partial t}\left(\alpha_p \rho_p\right) + \nabla \cdot \left(\alpha_p \rho_p \vec{v}_p\right) = \sum_{q=1}^{nphases} \left(\dot{m}_{qp} - \dot{m}_{pq}\right) \tag{17.385}$$

$$\begin{aligned} \frac{\partial}{\partial t}\left(\alpha_p \rho_p \vec{v}_p\right) + \nabla \cdot \left(\alpha_p \rho_p \vec{v}_p \vec{v}_p\right) &= -\alpha_p \nabla p + \nabla \cdot \left[\alpha_p \mu_p \left(\nabla \vec{v}_p + \nabla \vec{v}_p^{\,T}\right)\right] \\ &\quad + \alpha_p \rho_p \vec{g} + F_{vm,lift,user} \\ &\quad + \sum_{q=1}^{nphases} \left(\vec{K}_{qp}\left(\vec{v}_q - \vec{v}_p\right) + \dot{m}_{qp}\vec{v}_{qp} - \dot{m}_{qp}\vec{v}_{qp}\right) \\ &\quad + K_{DPM}\left(\vec{v}_{DPM} - \vec{v}_p\right) + S_{DPM,explicit} \end{aligned} \tag{17.386}$$

Here, Equation 17.385 (p. 562) is the mass conservation equation for an individual phase $p$ and Equation 17.386 (p. 562) is the corresponding momentum conservation equation. Currently, the momentum exchange terms (denoted by $DPM$) are considered only in the primary phase equations.

In the resulting set of equations (one continuity and one momentum conservation equation per phase), those corresponding to a discrete phase are not solved. The solution, such as volume fraction or velocity field, is taken from the Lagrangian tracking solution.

In versions prior to ANSYS Fluent 13, one drawback of the dense discrete phase model was that it did not prevent the actual concentration of particles from becoming unphysically high. Hence, the model had only a limited applicability to flows close to the packing regime, such as fluidized bed reactors. To overcome this, ANSYS Fluent now applies a special treatment to the particle momentum equation as soon as the particle volume fraction exceeds a certain user specified limit. Thus, the unlimited accumulation of particles is prevented. In turn, this will allow you to simulate suspensions and flows like bubbling fluidized bed reactors, operating at the packing limit conditions, allowing for polydispersed particle systems. However, no Discrete Element Method (DEM) type collision treatment is applied, which would otherwise allow the efficient simulation of systems with a large number of particles.

In the context of the phase coupled SIMPLE algorithm (Solution Method in ANSYS Fluent (p. 561)) and the coupled algorithm for pressure-velocity coupling (Selecting the Pressure-Velocity Coupling Method in the User's Guide), a higher degree of implicitness is achieved in the treatment of the drag coupling terms. All drag related terms appear as coefficients on the left hand side of the linear equation system.

### 17.5.18.1. Limitations

Since the given approach makes use of the Eulerian multiphase model framework, all its limitations are adopted:

- The turbulence models: LES and DES turbulence models are not available.


Release 15.0 - © SAS IP, Inc. All rights reserved. - Contains proprietary and confidential information of ANSYS, Inc. and its subsidiaries and affiliates.

- The combustion models: PDF Transport model, Premixed, Non-premixed and partially premixed combustion models are not available.
- The solidification and melting models are not available.
- The Wet Steam model is not available.
- The real gas model (pressure-based and density-based) is not available.
- The density-based solver and models dependent on it are not available.
- Parallel DPM with the shared memory option is disabled.

### 17.5.18.2. Granular Temperature

The solids stress acting on particles in a dense flow situation is modeled via an additional acceleration in the particle force balance Equation 16.1 (p. 374).

$$\frac{du_p}{dt} = F_D\left(u - u_p\right) + \frac{g_x\left(\rho_p - \rho\right)}{\rho_p} + F_x + F_{interaction} \tag{17.387}$$

The term $F_{interaction}$ models the additional acceleration acting on a particle, resulting from interparticle interaction. It is computed from the stress tensor given by the Kinetic Theory of Granular Flows as

$$F_{interaction} = -\frac{1}{\rho_p}\nabla \cdot \overline{\overline{\tau}}_s \tag{17.388}$$

Following the same theory, the granular temperature is used in the model for the granular stress. For a more detailed description on the Kinetic Theory of Granular Flows refer to Solids Pressure (p. 538), Maximum Packing Limit in Binary Mixtures (p. 541), and Solids Shear Stresses (p. 541).

The granular temperature can be estimated using any of the available options described in Granular Temperature (p. 544). By default, the algebraic formulation is used. The conservation equation for the granular temperature (kinetic energy of the fluctuating particle motion) is solved with the averaged particle velocity field. Therefore, a sufficient statistical representation of the particle phase is needed to ensure the stable behavior of the granular temperature equation. For details, refer to Conservation Equations (p. 513) – Granular Temperature (p. 544).

The main advantage over the Eulerian model is that, there is no need to define classes to handle particle size distributions. This is done in a natural way in the Lagrangian formulation [361] (p. 749).

## 17.5.19. Multi-Fluid VOF Model

The multi-fluid VOF model for Eulerian multiphase allows you to use the Geo-Reconstruct, compressive, and CICSAM sharpening schemes with the explicit VOF option. This model should be enabled only for cases requiring sharp interface treatment between phases. This model might help in overcoming some limitations of the VOF model because of the shared velocity and temperature formulation.

The multi-fluid VOF model for the Eulerian multiphase model provides the anisotropic drag law, which can be used when modeling free surface flow. This drag law is also used when there is higher drag in the normal direction to the interface and lower drag in the tangential direction to the interface.

Release 15.0 - © SAS IP, Inc. All rights reserved. - Contains proprietary and confidential information of ANSYS, Inc. and its subsidiaries and affiliates.

In some cases, where the flow for a particular phase is important in both the directions (tangential and normal to the interface), using a higher anisotropy ratio will result in numerical instability. Therefore, in those cases, an anisotropy ratio of up to 1000 is recommended, where the anisotropy ratio is defined as

$$anisotropy\ ratio = \frac{friction\ factor_{normal\ to\ interface}}{friction\ factor_{tangential\ to\ interface}}$$

In cases, where flow for a particular phase is important only in one direction (tangential or normal to the interface), a higher anisotropy ratio could be used. The principal directions for this drag are based on the normal and tangential direction to the interface.

Two types of drag formulations exist within the anisotropic drag law: one that is based on the symmetric drag law and the other is based on different viscosity options.

**Formulation 1**

This is based on the symmetric drag law, where the effective drag coefficient in the principal direction $p$ is described as follows:

$$K_p = K_{symmetric} \lambda_p \tag{17.389}$$

where $\lambda_p$ is the friction factor vector in the principal direction. $K_{symmetric}$ is the isotropic drag coefficient obtained from the symmetric drag law.

**Formulation 2**

The effective drag coefficient in the principal direction $p$ is described as follows:

$$K_p = (K_{visc})_p vof_i\ vof_j \tag{17.390}$$

where $vof_i$ is the volume fraction for phase $i$ and $vof_j$ is the volume fraction for phase $j$.

The viscous drag component in the principal direction $K_{visc}, p$ is

$$(K_{visc})_p = \frac{\mu}{l_c^2} \lambda_p \tag{17.391}$$

where the viscosity options can be any one of the following:

$$\mu = 0.5\left(\mu_i + \mu_j\right)$$

$$\mu = \frac{2\mu_i\mu_j}{\left(\mu_i + \mu_j\right)}$$

$$\mu = \frac{\mu_i\mu_j}{\left(\mu_i vof_j + \mu_j vof_i\right)}$$

$$\mu = \mu_i vof_i + \mu_j vof_j$$

$$\mu = \mu_i$$

$$\mu = \mu_j$$


Release 15.0 - © SAS IP, Inc. All rights reserved. - Contains proprietary and confidential information of ANSYS, Inc. and its subsidiaries and affiliates.

and $l_c$ is the length scale.

To learn how to use the multi-fluid VOF model and the two drag formulations, refer to Including the Multi-Fluid VOF Model in the User's Guide.

## 17.5.20. Wall Boiling Models

### 17.5.20.1. Overview

The term "subcooled boiling" is used to describe the physical situation where the wall temperature is high enough to cause boiling to occur at the wall even though the bulk volume averaged liquid temperature is less than the saturation value. In such cases, the energy is transferred directly from the wall to the liquid. Part of this energy will cause the temperature of the liquid to increase and part will generate vapor. Interphase heat transfer will also cause the average liquid temperature to increase, however, the saturated vapor will condense. Additionally, some of the energy may be transferred directly from the wall to the vapor. These basic mechanisms are the foundations of the so called Rensselaer Polytechnic Institute (RPI) models.

In ANSYS Fluent, the wall boiling models are developed in the context of the Eulerian multiphase model. The multiphase flows are governed by the conservation equations for phase continuity (Equation 17.152 (p. 514)), momentum (Equation 17.153 (p. 514)), and energy (Equation 17.156 (p. 515)). The wall boiling phenomenon is modeled by the RPI nucleate boiling model of Kurual and Podowski [221] (p. 741) and an extended formulation for the departed nucleate boiling regime (DNB) by Lavieville et al [234] (p. 742).

The wall boiling models are compatible with three different wall boundaries: isothermal wall, specified heat flux, and specified heat transfer coefficient (coupled wall boundary).

Specific submodels have been considered to account for the interfacial transfers of momentum, mass, and heat, as well as turbulence models in boiling flows, as described below.

To learn how to set up the boiling model, refer to Including the Boiling Model.

### 17.5.20.2. RPI Model

According to the basic RPI model, the total heat flux from the wall to the liquid is partitioned into three components, namely the convective heat flux, the quenching heat flux, and the evaporative heat flux:

$$\dot{q}_W = \dot{q}_C + \dot{q}_Q + \dot{q}_E \tag{17.392}$$

The heated wall surface is subdivided into area $A_b$, which is covered by nucleating bubbles and a portion $(1 - A_b)$, which is covered by the fluid.

- The convective heat flux $\dot{q}_C$ is expressed as

$$\dot{q}_C = h_C (T_w - T_l)(1 - A_b) \tag{17.393}$$

where $h_C$ is the single phase heat transfer coefficient, and $T_w$ and $T_l$ are the wall and liquid temperatures, respectively.

- The quenching heat flux $\dot{q}_Q$ models the cyclic averaged transient energy transfer related to liquid filling the wall vicinity after bubble detachment, and is expressed as

$$\dot{q}_Q = \frac{2k_l}{\sqrt{\pi \lambda_l T}} (T_w - T_l) \tag{17.394}$$

Where $k_l$ is the conductivity, $T$ is the periodic time, and $\lambda_l = \frac{k_l}{\rho_l C_{pl}}$ is the diffusivity.

- The evaporative flux $\dot{q}_E$ is given by

$$\dot{q}_E = V_d N_w \rho_v h_{fv} \tag{17.395}$$

Where $V_d$ is the volume of the bubble based on the bubble departure diameter, $N_w$ is the active nucleate site density, $\rho_v$ is the vapor density, and $h_{fv}$ is the latent heat of evaporation, and $f$ is the bubble departure frequency. These equations need closure for the following parameters:

- **Area of Influence**

Its definition is based on the departure diameter and the nucleate site density:

$$A_b = K \frac{N_w \pi D_w^2}{4} \tag{17.396}$$

Note that in order to avoid numerical instabilities due to unbound empirical correlations for the nucleate site density, the area of influence has to be restricted. The area of influence is limited as follows:

$$A_b = \min(1, K \frac{N_w \pi D_w^2}{4}) \tag{17.397}$$

The value of the empirical constant $K$ is usually set to 4, however it has been found that this value is not universal and may vary between 1.8 and 5. The following relation for this constant has also been implemented based on Del Valle and Kenning's findings [88] (p. 733):

$$K = 4.8 e^{(-\frac{Ja_{sub}}{80})} \tag{17.398}$$

and $Ja_{sub}$ is the subcooled Jacob number defined as

$$Ja_{sub} = \frac{\rho_l C_{pl} \Delta T_{sub}}{\rho_v h_{fv}} \tag{17.399}$$

where $\Delta T = T_{sat} - T_l$

- **Frequency of Bubble Departure**

Implementation of the RPI model normally uses the frequency of bubble departure as the one based on inertia controlled growth (not really applicable to subcooled boiling) [74] (p. 733)

$$f = \frac{1}{T} = \sqrt{\frac{4g(\rho_l - \rho_v)}{3\rho_l D_w}} \tag{17.400}$$

- **Nucleate Site Density**

The nucleate site density is usually represented by a correlation based on the wall superheat. The general expression is of the form


Release 15.0 - © SAS IP, Inc. All rights reserved. - Contains proprietary and confidential information of ANSYS, Inc. and its subsidiaries and affiliates.

$$N_w = C^n (T_w - T_{sat})^n \tag{17.401}$$

Here the empirical parameters from Lemmert and Chawla [240] (p. 742) are used, where $n = 1.805$ and $C = 210$. Other formulations are also available, such as Kocamustafaogullari and Ishii [215] (p. 741) where

$$N_w^* = f(\rho^*) r_c^{*-4.4} \tag{17.402}$$

Here

$$N_w^* = N_w D_w^2$$
$$r_c^* = 2 r_c / D_w$$
$$r_c = \frac{2\sigma T_{sat}}{\rho_v h_{fv} \Delta T_w}$$
$$\rho^* = (\rho_l - \rho_v) / \rho_v$$

Where $D_w$ is the bubble departure diameter and the density function is defined as

$$f(\rho^*) = 2.157 \times 10^{-7} \rho^{*-3.2} (1 + 0.0049 \rho^*)^{4.13} \tag{17.403}$$

- **Bubble Departure Diameter**

The default bubble departure diameter for the RPI model is based on empirical correlations [451] (p. 753) and is calculated in meters as

$$D_w = \min(0.0014, 0.0006 e^{-\frac{\Delta T_w}{45.0}}) \tag{17.404}$$

while Kocamustafaogullari and Ishii [214] (p. 740) use

$$D_w = 0.0012 \left(\rho^*\right)^{0.9} 0.0208 \varnothing \sqrt{\frac{\sigma}{g(\rho_l - \rho_v)}} \tag{17.405}$$

with $\varnothing$ being the contact angle in degrees.

The bubble departure diameter in millimeters based on the Unal relationship [458] (p. 754) is calculated as

$$D_w = 2.4210^{-5} P^{0.709} \left( \frac{a}{b\sqrt{\varphi}} \right) \tag{17.406}$$

$$a = \frac{\Delta T_{sup}}{2\rho_g H_{lv}} \sqrt{\frac{\rho_s C_{ps} k_s}{\pi}} \tag{17.407}$$

$$b = \begin{cases} \dfrac{\Delta T_{sub}}{2\left(1 - \frac{\rho_g}{\rho_l}\right)} e^{\left(\frac{\Delta T_{sub}}{3} - 1\right)} & \Delta T_{sub} \le 3 \\ \dfrac{\Delta T_{sub}}{2\left(1 - \frac{\rho_g}{\rho_l}\right)} & \Delta T_{sub} > 3 \end{cases} \tag{17.408}$$

Release 15.0 - © SAS IP, Inc. All rights reserved. - Contains proprietary and confidential information of ANSYS, Inc. and its subsidiaries and affiliates.

$$\varphi = \max\left( \left( \frac{U_b}{U_0} \right)^{0.47}, 1.0 \right) \tag{17.409}$$

where $P$ is the flow pressure, $\Delta T_{sup} = T_w - T_{sat}$ is the wall superheat, $H_{lv}$ is latent heat, $U_b$ is the near wall bulk velocity, and $U_b = 0.61$ m/s. The subscripts $s$, $l$, and $g$ denote the solid material, liquid, and vapor phase, respectively.

### 17.5.20.3. Non-equilibrium Subcooled Boiling

When using the basic RPI model (RPI Model (p. 565)), the temperature of the vapor is not calculated, but instead is fixed at the saturation temperature. To model boiling departing from the nucleate boiling regime (DNB), or to model it up to the critical heat flux and post dry-out condition, it is necessary to include the vapor temperature in the solution process. The wall heat partition is now modified as follows:

$$\dot{q}_W = (\dot{q}_C + \dot{q}_Q + \dot{q}_E) f(\alpha_l) + (1 - f(\alpha_l))\dot{q}_V + \dot{q}_G \tag{17.410}$$

Here $\dot{q}_C$, $\dot{q}_Q$, and $\dot{q}_E$ are the liquid-phase convective heat flux, quenching heat flux, and evaporation heat flux, respectively (described in detail in RPI Model (p. 565)). The extra heat fluxes are $\dot{q}_V$ representing the convective heat flux of the vapor phase, and $\dot{q}_G$ representing heat flux to any other possible gas phases in a system. These can be expressed as

$$\dot{q}_V = h_V (T_W - T_V) \tag{17.411}$$

$$\dot{q}_G = h_G (T_W - T_G) \tag{17.412}$$

Similar to the liquid phase $\dot{q}_C$, the convective heat transfer coefficients $h_V$ and $h_G$ are computed from the wall function formulations.

The function $f(\alpha_l)$ depends on the local liquid volume fraction with similar limiting values as the liquid volume fraction. Lavieville et al [234] (p. 742) proposed the following expression:

$$f(\alpha_l) = \begin{cases} 1 - \frac{1}{2} e^{-20(\alpha_l - \alpha_{l,crit})} \\ \frac{1}{2} \left( \frac{\alpha_l}{\alpha_{l,crit}} \right)^{20\alpha_{l,crit}} \end{cases} \tag{17.413}$$

Here, the critical value for the vapor fraction is $\alpha_{l,crit} = 0.2$

### 17.5.20.4. Critical Heat Flux

In wall boiling, the critical heat flux (CHF) condition is characterized by a sharp reduction of local heat transfer coefficients and the excursion of wall surface temperatures. It occurs when heated surfaces are no longer wetted by boiling liquid with the increase of vapor content. At critical heat flux conditions, vapor replaces the liquid and occupies the space adjacent to heated walls. The energy is therefore directly transferred from the wall to the vapor. In turn, it results in rapid reduction of the heat removal ability and sharp rise of the vapor temperature, and most importantly, the wall temperatures. In addition, wall boiling departs from the nucleating boiling regime, and the multiphase flow regime changes from a bubbly flow to a mist flow.


Release 15.0 - © SAS IP, Inc. All rights reserved. - Contains proprietary and confidential information of ANSYS, Inc. and its subsidiaries and affiliates.

To model the critical heat flux conditions, the basic approach adopted in ANSYS Fluent is to extend the RPI model from the nucleate boiling regime to critical heat flux and post dry-out conditions, while considering the following:

- The generalized and non-equilibrium wall heat flux partition
- The flow regime transition from bubbly to mist flows

### 17.5.20.4.1. Wall Heat Flux Partition

The wall heat partition is defined in the same way as Equation 17.410 (p. 568), with the exception of the function definition. Here, the function $f(\alpha_l)$ depends on the local liquid/vapor volume fraction with the same limiting values as the liquid volume fraction, that is, between zero and one. Lavieville et al. [234] (p. 742) proposed the following expression:

$$f(\alpha_l) = \begin{cases} 1 - \frac{1}{2}\exp\left[-20\left(\alpha_l - \alpha_{l,crit}\right)\right] & \alpha_l \geq \alpha_{l,crit} \\ \frac{1}{2}\left(\frac{\alpha_l}{\alpha_{l,crit}}\right)^{20\alpha_{l,crit}} & \alpha_l < \alpha_{l,crit} \end{cases} \tag{17.414}$$

The critical value for the liquid volume fraction is $0.2$, and for the vapor phase, it is $\alpha_{v,crit} = 1 - \alpha_{l,crit} = 0.8$.

There are also some other functions available to define the wall heat flux partition. When defining wall boiling regimes, Tentner et al. [448] (p. 753) suggested the following expression based on the vapor volume fraction:

$$f(\alpha_v) = 1 - f(\alpha_l) = \begin{cases} 0 & \alpha_v < \alpha_{v,1} \\ \frac{1}{2}\left(1 - \cos\left(\pi \frac{\alpha_v - \alpha_{v,1}}{\alpha_{v,2} - \alpha_{v,1}}\right)\right) & \alpha_{v,1} \leq \alpha_v \leq \alpha_{v,2} \\ 1 & \alpha_v > \alpha_{v,2} \end{cases} \tag{17.415}$$

Taking the thin film boiling into consideration in the wall heat flux partition, Ioilev et al. [175] (p. 738) used a linear function to extend Equation 17.415 (p. 569) to the critical heat flux condition:

$$f(\alpha_v) = \max\left(0, \min\left\{\frac{\alpha_v - \alpha_{v,1}}{\alpha_{v,2} - \alpha_{v,1}}\right\}\right) \tag{17.416}$$

Where the breakpoints have been set to $\alpha_{v,1} = 0.9$ and $\alpha_{v,2} = 0.95$.

In ANSYS Fluent, Equation 17.415 (p. 569) is chosen as the default formulation for the wall heat flux partition.

### 17.5.20.4.2. Flow Regime Transition

When wall boiling departs from the nucleate boiling regime and reaches the critical heat flux and post dry-out conditions, the multiphase flow regime changes from a bubbly flow to a mist flow. Consequently, the liquid phase switches from the continuous phase to the dispersed phase, while the vapor phase becomes the continuous phase from the originally dispersed phase in the bubbly flow regime. With

Release 15.0 - © SAS IP, Inc. All rights reserved. - Contains proprietary and confidential information of ANSYS, Inc. and its subsidiaries and affiliates.

the flow regime transition, the interfacial area, momentum transfer terms (drag, lift, turbulent dispersion, interfacial area, and so on), heat transfer and turbulence quantities will change accordingly.

To mimic the change of the flow regime and compute the interfacial transfers, the so-called flow regime maps, based on cross-section averaged flow parameters, are traditionally used in sub-channel one-dimensional thermal-hydraulic codes. In CFD solvers, the concept of flow regime maps has been expanded into a local, cell-based interfacial surface topology to evaluate the flow regime transitions from local flow parameters. The ensemble of all the computational cells with their usually simple local interfacial surface topologies can provide complex global topologies to represent the different flow regimes as the traditional sub-channel flow regime maps.

As a first step, this implementation adopts a simple local interfacial surface topology to control the transition smoothly from a continuous liquid bubbly flow to a continuous vapor droplet flow configuration [448] (p. 753), [175] (p. 738). It assumes that inside a computational cell, the local interfacial surface topology contains multi-connected interfaces, and the flow regimes are determined by a single local flow quantity — the vapor volume fraction $\alpha_v$:

- Bubbly flow topology: the vapor phase is dispersed in the continuous liquid in the form of bubbles. Typically $\alpha_v \leq 0.3$
- Mist flow topology: the liquid phase is dispersed in the continuous vapor in the form of droplets. Typically $\alpha_v \geq 0.7$
- Churn flow: this is an intermediate topology between the bubbly and mist flow topology, where $0.3 < \alpha_v < 0.7$

The interfacial surface topologies are used to compute the interfacial area and interfacial transfers of momentum and heat. Introducing $\phi$ to represent interfacial quantities (interfacial area, drag, lift, turbulent drift force and heat transfer), then they are calculated using the following general form:

$$\phi = (1 - f(\alpha_v))\phi_{bubbly} + f(\alpha_v)\phi_{droplet} \tag{17.417}$$

Here $f(\alpha_v)$ is computed using equation Equation 17.415 (p. 569) or Equation 17.416 (p. 569), but with different lower and upper limits of the breakpoints. Typically, the values of 0.3 and 0.7 are used and $\phi_{bubbly}$ and $\phi_{droplet}$ are the interfacial quantities from bubbly flow and mist flow, respectively. They are calculated using the interfacial sub-models presented in Interfacial Momentum Transfer (p. 570) and Interfacial Heat Transfer (p. 572).

It may be noted that in the boiling models, the liquid is usually defined as the first phase, and the vapor as the second phase. Once this is defined, it remains unchanged with the flow regime transition. When $\phi_{bubbly}$ and $\phi_{droplet}$ are calculated, however, the primary or secondary phases are switched. For $\phi_{bubbly}$, the liquid is treated as the primary phase, while the vapor is the secondary phase. Contrary to this, for $\phi_{droplet}$, the vapor becomes the primary phase and the liquid is the secondary phase.

### 17.5.20.5. Interfacial Momentum Transfer

The interfacial momentum transfer may include five parts: drag, lift, wall lubrication, turbulent drift forces, and virtual mass (described in Interphase Exchange Coefficients (p. 518)). Various models are available for each of these effects, some of which are specifically formulated for boiling flows. Also, user-defined options are available.


Release 15.0 - © SAS IP, Inc. All rights reserved. - Contains proprietary and confidential information of ANSYS, Inc. and its subsidiaries and affiliates.

### 17.5.20.5.1. Interfacial Area

The interfacial area can be calculated using either a transport equation or algebraic models as described in Interfacial Area Concentration (p. 517). For boiling flows, the algebraic formulations are typically chosen. See Interfacial Area Concentration (p. 517) for model details.

### 17.5.20.5.2. Bubble and Droplet Diameters

#### *17.5.20.5.2.1. Bubble Diameter*

By default, Fluent uses the following model for bubble diameter as a function of the local subcooling, $\Delta T_{sub} = T_{sat} - T_l$:

$$D_b = \begin{cases} \max\left[1.0\times10^{-5}, d_{\min}\exp\left(\frac{-K\,(\Delta T_{sub} - \Delta T_{\max})}{d_{\min}}\right)\right] & \Delta T_{sub} > 13.5\ K \\ d_{\max} - K\,(\Delta T_{sub} - \Delta T_{\min}) & \Delta T_{sub} \le 13.5\ K \end{cases} \tag{17.418}$$

where:

$$d_{\min} = 0.00015\ m$$
$$d_{\max} = 0.001\ m$$
$$\Delta T_{\min} = 0\ K$$
$$\Delta T_{\max} = 13.5\ K$$
$$K = \frac{d_{\max} - d_{\min}}{\Delta T_{\max} - \Delta T_{\min}}$$

As an alternative, the bubble diameter, $D_b$, can be given by the Unal correlation [458] (p. 754) :

$$D_b = \begin{cases} 0.0015 & \Delta T_{sub} < 0 \\ 0.0015 - 0.0001\,\Delta T_{sub} & 0 \le \Delta T_{sub} \le 13.5K \\ 0.00015 & \Delta T_{sub} > 13.5K \end{cases} \tag{17.419}$$

To use the Unal correlation, Equation 17.419 (p. 571), you can use the following scheme command:

```
(rpsetvar 'mp/boiling/bubble-diameter-model 2)
```

To return to the default formulation, Equation 17.418 (p. 571), you can use the scheme command:

```
(rpsetvar 'mp/boiling/bubble-diameter-model 1)
```

#### *17.5.20.5.2.2. Droplet Diameter*

When the flow regime transitions to mist flow, the droplet diameter can be assumed to be constant or estimated by the Kataoka-Ishii correlation [197] (p. 739):

$$D_d = C_{ds}\frac{\sigma}{\rho_v j_v^2}\mathrm{Re}_l^{-1/6}\mathrm{Re}_v^{2/3}\left(\frac{\rho_v}{\rho_l}\right)^{-1/3}\left(\frac{\mu_v}{\mu_l}\right)^{2/3} \tag{17.420}$$

where:

$C_{ds}=0.28$

$j_v$ is the vapor volumetric flux (superficial velocity)

$\mathrm{Re}_l$ is the local liquid Reynolds number

$\mathrm{Re}_v$ is the local vapor Reynolds number

$\mu_l$ is the liquid viscosity

$\mu_v$ is the vapor viscosity

#### 17.5.20.5.3. Interfacial Drag Force

The interfacial drag force is calculated using the standard model described in Interphase Exchange Coefficients (p. 518) (and defined in the context of the interfacial area from Interfacial Area Concentration (p. 517)). As described in Fluid-Fluid Exchange Coefficient (p. 518), ANSYS Fluent offers several options to calculate the drag force on dispersed phases. For boiling flows, the Ishii model (Ishii Model (p. 522)) is typically chosen, though any of the models listed in Fluid-Fluid Exchange Coefficient (p. 518) are available.

#### 17.5.20.5.4. Interfacial Lift Force

As described in Lift Force (p. 528), ANSYS Fluent offers several options to calculate the lift forces on the dispersed phases. For boiling flows, this force is important in the nucleating boiling regime. In the RPI model, the Tomiyama model (Tomiyama Lift Force Model (p. 531)) is usually chosen to account for the effects of the turbulent dispersion force.

#### 17.5.20.5.5. Turbulent Dispersion Force

As described in Turbulent Dispersion Force (p. 534), ANSYS Fluent offers several options to calculate the turbulent dispersion force. For boiling flows, this force is important in transporting the vapor from walls to the core fluid flow regions. In the RPI model, the Lopez de Bertodano model (Lopez de Bertodano Model (p. 535)) is usually chosen to account for the effects of the turbulent dispersion force.

#### 17.5.20.5.6. Wall Lubrication Force

As described in Wall Lubrication Force (p. 532), ANSYS Fluent offers several options to calculate the wall lubrication force on the dispersed phases. For boiling flows, this force can be important in the nucleating boiling regime. In the RPI model, the Antal et al. model (Antal et al. Model (p. 533)) is usually chosen to account for the effects of the wall lubrication force.

#### 17.5.20.5.7. Virtual Mass Force

In the wall boiling models, the virtual mass force can be modeled using the standard correlation implemented for the Eulerian multiphase model as described in Virtual Mass Force (p. 538).

### *17.5.20.6. Interfacial Heat Transfer*

#### 17.5.20.6.1. Interface to Liquid Heat Transfer

As the bubbles depart from the wall and move towards the subcooled region, there is heat transfer from the bubble to the liquid, that is defined as


Release 15.0 - © SAS IP, Inc. All rights reserved. - Contains proprietary and confidential information of ANSYS, Inc. and its subsidiaries and affiliates.

$$\dot{q}_{lt} = h_{sl}(T_{sat} - T_l) \tag{17.421}$$

where $h_{sl}$ is the volumetric heat transfer coefficient. The heat transfer coefficient can be computed using either the Ranz-Marshall or Tomiyama models described in The Heat Exchange Coefficient (p. 546).

#### 17.5.20.6.2. Interface to Vapor Heat Transfer

The interface to vapor heat transfer is calculated using the *constant time scale return to saturation* method [234] (p. 742). It is assumed that the vapor retains the saturation temperature by rapid evaporation/condensation. The formulation is as follows:

$$\dot{q}_{vt} = \frac{\alpha_v \rho_v C_{p,v}}{\delta t}(T_{sat} - T_v) \tag{17.422}$$

Where $\delta t$ is the time scale set to a default value of 0.05 and $C_{p,v}$ is the isobaric heat capacity.

### 17.5.20.7. Mass Transfer

#### 17.5.20.7.1. Mass Transfer From the Wall to Vapor

The evaporation mass flow is applied at the cell near the wall and it is derived from the evaporation heat flux, Equation 17.422 (p. 573)

$$\dot{m}_E = \frac{\dot{q}_E}{h_{fv} + C_{p,l}\Delta T_{sub}} \tag{17.423}$$

#### 17.5.20.7.2. Interfacial Mass Transfer

The interfacial mass transfer depends directly on the interfacial heat transfer. Assuming that all the heat transferred to the interface is used in mass transfer (that is, evaporation or condensation), the interfacial mass transfer rate can be written as:

$$\dot{m} = \dot{m}_{lt} + \dot{m}_{vt} = \frac{\dot{q}_{lt} + \dot{q}_{vt}}{h_{fv}} \tag{17.424}$$

### 17.5.20.8. Turbulence Interactions

To model boiling flows, turbulence interaction models are usually included in the multiphase turbulence models to describe additional bubble stirring and dissipation. As described in Turbulence Models (p. 548), three options are available for boiling flows: Troshko-Hassan (default), Simonin et al, and Sato.

## 17.6. Wet Steam Model Theory

Information is organized into the following subsections:

17.6.1. Overview of the Wet Steam Model
17.6.2. Limitations of the Wet Steam Model
17.6.3. Wet Steam Flow Equations
17.6.4. Phase Change Model
17.6.5. Built-in Thermodynamic Wet Steam Properties

Release 15.0 - © SAS IP, Inc. All rights reserved. - Contains proprietary and confidential information of ANSYS, Inc. and its subsidiaries and affiliates.

## 17.6.1. Overview of the Wet Steam Model

During the rapid expansion of steam, a condensation process will take place shortly after the state path crosses the vapor-saturation line. The expansion process causes the super-heated dry steam to first subcool and then nucleate to form a two-phase mixture of saturated vapor and fine liquid droplets known as wet steam.

Modeling wet steam is very important in the analysis and design of steam turbines. The increase in steam turbine exit wetness can cause severe erosion to the turbine blades at the low-pressure stages, and a reduction in aerodynamic efficiency of the turbine stages operating in the wet steam region [307] (p. 746).

ANSYS Fluent has adopted the Eulerian-Eulerian approach for modeling wet steam flow. The flow mixture is modeled using the compressible Navier-Stokes equations, in addition to two transport equations for the liquid-phase mass-fraction ($\beta$), and the number of liquid-droplets per unit volume ($\eta$). The phase change model, which involves the formation of liquid-droplets in a homogeneous nonequilibrium condensation process, is based on the classical non-isothermal nucleation theory.

This section describes the theoretical aspects of the wet steam model. Information about enabling the model and using your own property functions and data with the wet steam model is provided in Setting Up the Wet Steam Model in the User's Guide. Solution settings and strategies for the wet steam model can be found in Wet Steam Model in the User's Guide. Postprocessing variables are described in Model-Specific Variables in the User's Guide.

## 17.6.2. Limitations of the Wet Steam Model

The following restrictions and limitations currently apply to the wet steam model in ANSYS Fluent:

- The wet steam model is available for the density-based solver only.
- Pressure inlet, mass-flow inlet, and pressure outlet are the only inflow and outflow boundary conditions available.
- When the wet steam model is active, the access to the **Create/Edit Materials** dialog box is restricted because the fluid mixture properties are determined from the built-in steam property functions or from the user-defined wet steam property functions. Therefore, if solid properties need to be set and adjusted, then it must be done in the **Create/Edit Materials** dialog box before activating the wet steam model.

## 17.6.3. Wet Steam Flow Equations

The wet steam is a mixture of two-phases. The primary phase is the gaseous-phase consisting of water-vapor (denoted by the subscript *v*) while the secondary phase is the liquid-phase consisting of condensed-water droplets (denoted by the subscript *l*).

The following assumptions are made in this model:

- The velocity slip between the droplets and gaseous-phase is negligible.
- The interactions between droplets are neglected.
- The mass fraction of the condensed phase, $\beta$ (also known as wetness factor), is small ($\beta < 0.2$).


Release 15.0 - © SAS IP, Inc. All rights reserved. - Contains proprietary and confidential information of ANSYS, Inc. and its subsidiaries and affiliates.

- Since droplet sizes are typically very small (from approximately 0.1 microns to approximately 100 microns), it is assumed that the volume of the condensed liquid phase is negligible.

From the preceding assumptions, it follows that the mixture density ($\rho$) can be related to the vapor density ($\rho_v$) by the following equation:

$$\rho = \frac{\rho_v}{(1-\beta)} \tag{17.425}$$

In addition, the temperature and the pressure of the mixture will be equivalent to the temperature and pressure of the vapor-phase.

The mixture flow is governed by the compressible Navier-Stokes equations given in vector form by Equation 20.70 (p. 659):

$$\frac{\partial W}{\partial Q}\frac{\partial}{\partial t}\int_V Q dV + \oint [F-G]\cdot dA = \int_V H dV \tag{17.426}$$

where $Q$=(P,u,v,w,T) are mixture quantities. The flow equations are solved using the same density-based solver algorithms employed for general compressible flows.

To model wet steam, two additional transport equations are needed [176] (p. 738). The first transport equation governs the mass fraction of the condensed liquid phase ($\beta$):

$$\frac{\partial \rho\beta}{\partial t} + \nabla\cdot(\rho\vec{v}\beta) = \Gamma \tag{17.427}$$

where $\Gamma$ is the mass generation rate due to condensation and evaporation (kg per unit volume per second). The second transport equation models the evolution of the number density of the droplets per unit volume:

$$\frac{\partial \rho\eta}{\partial t} + \nabla\cdot(\rho\vec{v}\eta) = \rho I \tag{17.428}$$

where $I$ is the nucleation rate (number of new droplets per unit volume per second).

To determine the number of droplets per unit volume, Equation 17.425 (p. 575) and the average droplet volume $V_d$ are combined in the following expression:

$$\eta = \frac{\beta}{(1-\beta)V_d\left(\rho_l/\rho_v\right)} \tag{17.429}$$

where $\rho_l$ is the liquid density and the average droplet volume is defined as

$$V_d = \frac{4}{3}\pi\bar{r}_d^3 \tag{17.430}$$

where $r_d$ is the droplet radius.

Together, Equation 17.426 (p. 575), Equation 17.427 (p. 575), and Equation 17.428 (p. 575) form a closed system of equations that, along with Equation 17.425 (p. 575), permit the calculation of the wet steam flow field.

Release 15.0 - © SAS IP, Inc. All rights reserved. - Contains proprietary and confidential information of ANSYS, Inc. and its subsidiaries and affiliates.

## 17.6.4. Phase Change Model

The following is assumed in the phase change model:

- The condensation is homogeneous (that is, no impurities present to form nuclei).
- The droplet growth is based on average representative mean radii.
- The droplet is assumed to be spherical.
- The droplet is surrounded by infinite vapor space.
- The heat capacity of the fine droplet is negligible compared with the latent heat released in condensation.

The mass generation rate $\Gamma$ in the classical nucleation theory during the nonequilibrium condensation process is given by the sum of mass increase due to nucleation (the formation of critically sized droplets) and also due to growth/demise of these droplets [176] (p. 738).

Therefore, $\Gamma$ is written as:

$$\Gamma = \frac{4}{3}\pi\rho_l I r_*^{\,3} + 4\pi\rho_l \eta \bar{r}^{\,2}\frac{\partial \bar{r}}{\partial t} \tag{17.431}$$

where $\bar{r}$ is the average radius of the droplet, and $r_*$ is the Kelvin-Helmholtz critical droplet radius, above which the droplet will grow and below which the droplet will evaporate. An expression for $r_*$ is given by [503] (p. 756).

$$r_* = \frac{2\sigma}{\rho_l RT \ln S} \tag{17.432}$$

where $\sigma$ is the liquid surface tension evaluated at temperature $T$, $\rho_l$ is the condensed liquid density (also evaluated at temperature $T$), and $S$ is the super saturation ratio defined as the ratio of vapor pressure to the equilibrium saturation pressure:

$$s = \frac{P}{P_{sat}(T)} \tag{17.433}$$

The expansion process is usually very rapid. Therefore, when the state path crosses the saturated-vapor line, the process will depart from equilibrium, and the supersaturation ratio $S$ can take on values greater than one.

The condensation process involves two mechanisms, the transfer of mass from the vapor to the droplets and the transfer of heat from the droplets to the vapor in the form of latent heat. This energy transfer relation was presented in [501] (p. 756) and used in [176] (p. 738) and can be written as:

$$\frac{\partial \bar{r}}{\partial t} = \frac{P}{h_{lv}\rho_l\sqrt{2\pi RT}}\frac{\gamma+1}{2\gamma}C_p(T_0 - T) \tag{17.434}$$

where $T_0$ is the droplet temperature.

The classical homogeneous nucleation theory describes the formation of a liquid-phase in the form of droplets from a supersaturated phase in the absence of impurities or foreign particles. The nucleation rate described by the steady-state classical homogeneous nucleation theory [503] (p. 756) and corrected for non-isothermal effects, is given by:


Release 15.0 - © SAS IP, Inc. All rights reserved. - Contains proprietary and confidential information of ANSYS, Inc. and its subsidiaries and affiliates.

$$I=\frac{q_c}{(1+\theta)}\left(\frac{\rho_v^2}{\rho_l}\right)\sqrt{\frac{2\sigma}{{M_m}^3\pi}}e^{-\left(\frac{4\pi {r_*}^2\sigma}{3k_BT}\right)} \tag{17.435}$$

where $q_c$ is evaporation coefficient, $k_B$ is the Boltzmann constant, $M_m$ is mass of one molecule, $\sigma$ is the liquid surface tension, and $\rho_l$ is the liquid density at temperature $T$.

A non-isothermal correction factor, $\theta$, is given by:

$$\theta=\frac{2(\gamma-1)}{(\gamma+1)}\left(\frac{h_{lv}}{RT}\right)\left(\frac{h_{lv}}{RT}-0.5\right) \tag{17.436}$$

where $h_{lv}$ is the specific enthalpy of evaporation at pressure $p$ and $\gamma$ is the ratio of specific heat capacities.

## 17.6.5. Built-in Thermodynamic Wet Steam Properties

There are many equations that describe the thermodynamic state and properties of steam. While some of these equations are accurate in generating property tables, they are not suitable for fast CFD computations. Therefore, ANSYS Fluent uses a simpler form of the thermodynamic state equations [502] (p. 756) for efficient CFD calculations that are accurate over a wide range of temperatures and pressures. These equations are described below.

### 17.6.5.1. Equation of State

The steam equation of state used in the solver, which relates the pressure to the vapor density and the temperature, is given by [502] (p. 756):

$$P=\rho_v RT\left(1+B\rho_v+C{\rho_v}^2\right) \tag{17.437}$$

where $B$, and $C$ are the second and the third virial coefficients given by the following empirical functions:

$$B=a_1\left(1+\frac{\tau}{\alpha}\right)^{-1}+a_2e^{\tau}(1-e^{-\tau})^{\frac{5}{2}}+a_3\tau \tag{17.438}$$

where $B$ is given in m$^3$/kg, $\tau = \frac{1500}{T}$ with $T$ given in Kelvin, $\alpha$ = 10000.0, $a_1$= 0.0015, $a_2$= -0.000942, and $a_3$= -0.0004882.

$$C=a(\tau-\tau_0)e^{-\alpha\tau}+b \tag{17.439}$$

where $C$ is given in m$^6$/kg$^2$, $\tau = \frac{T}{647.286}$ with $T$ given in Kelvin, $\tau_o$= 0.8978, $\alpha$=11.16, $a$= 1.772, and $b$= 1.5E-06.

The two empirical functions that define the virial coefficients $B$ and $C$ cover the temperature range from 273 K to 1073 K.

The vapor isobaric specific heat capacity $Cp_v$ is given by:

Release 15.0 - © SAS IP, Inc. All rights reserved. - Contains proprietary and confidential information of ANSYS, Inc. and its subsidiaries and affiliates.

$$\begin{aligned} Cp_v &= Cp_0(T) \\ &+ R\left[ [(1-\alpha_v T)(B-B_1) - B_2]\rho_v \right. \\ &+ \left. \left[ (1-2\alpha_v T)C + \alpha_v T C_1 - \frac{C_2}{2} \right] \rho_v{}^2 \right] \end{aligned} \tag{17.440}$$

The vapor specific enthalpy, $h_v$ is given by:

$$h_v = h_0(T) + RT\left[ (B-B_1)\rho_v + \left( C - \frac{C_1}{2} \right) \rho_v{}^2 \right] \tag{17.441}$$

The vapor specific entropy, $s_v$ is given by:

$$s_v = s_0(T) - R\left[ \ln\rho_v + (B+B_1)\rho_v + \frac{(C+C_1)}{2}\rho_v{}^2 \right] \tag{17.442}$$

The isobaric specific heat at zero pressure is defined by the following empirical equation:

$$Cp_0(T) = \sum_{i=1}^{6} a_i T^{i-2} \tag{17.443}$$

where $Cp_0$ is in KJ/kg K, $a_1$ = 46.0, $a_2$ = 1.47276, $a_3$ = 8.38930E-04, $a_4$ = -2.19989E-07, $a_5$ = 2.46619E-10, and $a_6$ = -9.70466E-14.

and

$B_1 = T\frac{dB}{dT}$, $C_1 = T\frac{dC}{dT}$, $B_2 = T^2\frac{dB^2}{dT^2}$, and $C_2 = T^2\frac{dC^2}{dT^2}$.

Both $h_0(T)$ and $s_0(T)$ are functions of temperature and they are defined by:

$$h_0(T) = \int Cp_0 dT + h_c \tag{17.444}$$

$$s_0(T) = \int \frac{Cp_0}{T} dT + s_c \tag{17.445}$$

where $h_c$ and $s_c$ are arbitrary constants.

The vapor dynamic viscosity $\mu_v$ and thermal conductivity $k_v$ are also functions of temperature and were obtained from [501] (p. 756).

### 17.6.5.2. Saturated Vapor Line

The saturation pressure equation as a function of temperature was obtained from [374] (p. 749). The example provided in UDWSPF Example in the User's Guide contains a function called `wetst_satP()` that represents the formulation for the saturation pressure.

### 17.6.5.3. Saturated Liquid Line

At the saturated liquid-line, the liquid density, surface tension, specific heat $Cp$, dynamic viscosity, and thermal conductivity must be defined. The equation for liquid density, $\rho_l$, was obtained from [374] (p. 749).


Release 15.0 - © SAS IP, Inc. All rights reserved. - Contains proprietary and confidential information of ANSYS, Inc. and its subsidiaries and affiliates.

The liquid surface tension equation was obtained from [501] (p. 756). While the values of $Cp_l$, $\mu_l$ and $Kt_l$ were curve fit using published data from [103] (p. 734) and then written in polynomial forms. The example provided in UDWSPF Example in the User's Guide contains functions called `wetst_cpl()`, `wetst_mul()`, and `wetst_ktl()` that represent formulations for $Cp_l$, $\mu_l$ and $Kt_l$.

#### 17.6.5.4. Mixture Properties

The mixture properties are related to vapor and liquid properties via the wetness factor using the following mixing law:

$$\phi_m = \phi_l \beta + (1-\beta)\phi_v \tag{17.446}$$

where $\phi$ represents any of the following thermodynamic properties: $h$, $s$, $Cp$, $Cv$, $\mu$ or $Kt$.

## 17.7. Modeling Mass Transfer in Multiphase Flows

This section describes the modeling of mass transfer in the framework of ANSYS Fluent's general multiphase models (that is, Eulerian multiphase, mixture multiphase, VOF multiphase). There are numerous kinds of mass transfer processes that can be modeled in ANSYS Fluent. You can use models available in ANSYS Fluent (for example ANSYS Fluent's cavitation model), or define your own mass transfer model via user-defined functions. See UDF-Prescribed Mass Transfer (p. 581) and the UDF Manual for more information about the modeling of mass transfer via user-defined functions.

Information about mass transfer is presented in the following subsections:

17.7.1. Source Terms due to Mass Transfer
17.7.2. Unidirectional Constant Rate Mass Transfer
17.7.3. UDF-Prescribed Mass Transfer
17.7.4. Cavitation Models
17.7.5. Evaporation-Condensation Model

### 17.7.1. Source Terms due to Mass Transfer

ANSYS Fluent adds contributions due to mass transfer only to the momentum, species, and energy equations. No source term is added for other scalars such as turbulence or user-defined scalars.

Let $m_{p^i q^j}$ be the mass transfer rate per unit volume from the $i^{th}$ species of phase $p$ to the $j^{th}$ species of phase $q$. In case a particular phase does not have a mixture material associated with it, the mass transfer will be with the bulk phase.

#### 17.7.1.1. Mass Equation

The contribution to the mass source for phase $p$ in a cell is

$$m_p = -m_{p^i q^j} \tag{17.447}$$

and for phase $q$ is

$$m_q = m_{p^i q^j} \tag{17.448}$$

#### 17.7.1.2. Momentum Equation

For VOF or mixture models, there is no momentum source.

Release 15.0 - © SAS IP, Inc. All rights reserved. - Contains proprietary and confidential information of ANSYS, Inc. and its subsidiaries and affiliates.

For the Eulerian model, the momentum source in a cell for phase $p$ is

$$m_p \vec{u}_p = -m_{p^i q^j} \vec{u}_p \tag{17.449}$$

and for phase $q$ is

$$m_q \vec{u}_q = m_{p^i q^j} \vec{u}_p \tag{17.450}$$

### 17.7.1.3. Energy Equation

For all multiphase models, the following energy sources are added.

The energy source in a cell for phase $p$ is

$$H_p = -m_{p^i q^j} \left( h_q^{f^j} - h_p^{f^i} \right) \tag{17.451}$$

and for phase $q$ is

$$H_q = m_{p^i q^j} \left( h_q^{f^j} - h_p^{f^i} \right) \tag{17.452}$$

where $h_p^{f^i}$ and $h_q^{f^j}$ are the formation enthalpies of species $i$ of phase $p$ and species $j$ of phase $q$, respectively. The difference between $h_p^{f^i}$ and $h_q^{f^j}$ is the latent heat.

### 17.7.1.4. Species Equation

The species source in a cell for species $i$ of phase $p$ is

$$m_p^i = -m_{p^i q^j} \tag{17.453}$$

and for species $j$ of phase $q$ is

$$m_q^j = m_{p^i q^j} \tag{17.454}$$

### 17.7.1.5. Other Scalar Equations

No source/sink terms are added for turbulence quantities and other scalars. The transfer of these scalar quantities due to mass transfer could be modeled using user-defined source terms.

## 17.7.2. Unidirectional Constant Rate Mass Transfer

The unidirectional mass transfer model defines a positive mass flow rate per unit volume from phase $p$ to phase $q$:

$$\dot{m}_{pq} = \max\left[0, \lambda_{pq}\right] - \max\left[0, -\lambda_{pq}\right] \tag{17.455}$$

where

$$\lambda_{pq} = \dot{r} \alpha_p \rho_q \tag{17.456}$$

and $\dot{r}$ is a constant rate of particle shrinking or swelling, such as the rate of burning of a liquid droplet. This is not available for the VOF model.


Release 15.0 - © SAS IP, Inc. All rights reserved. - Contains proprietary and confidential information of ANSYS, Inc. and its subsidiaries and affiliates.

If phase $p$ is a mixture material and a mass transfer mechanism is defined for species $i$ of phase $p$, then

$$\lambda_{pq} = \dot{r}\alpha_p y_{p,i}\rho_q \tag{17.457}$$

where $y_{p,i}$ is the mass fraction of species $i$ in phase $p$.

## 17.7.3. UDF-Prescribed Mass Transfer

Because there is no universal model for mass transfer, ANSYS Fluent provides a UDF that you can use to input models for different types of mass transfer, for example, evaporation, condensation, boiling, and so on. Note that when using this UDF, ANSYS Fluent will automatically add the source contribution to all relevant momentum and scalar equations. This contribution is based on the assumption that the mass "created" or "destroyed" will have the same momentum and energy of the phase from which it was created or destroyed. If you would like to input your source terms directly into momentum, energy, or scalar equations, then the appropriate path is to use UDFs for user-defined sources for all equations, rather than the UDF for mass transfer. See the UDF Manual for more information about UDF-based mass transfer in multiphase.

## 17.7.4. Cavitation Models

A liquid at constant temperature can be subjected to a decreasing pressure, which may fall below the saturated vapor pressure. The process of rupturing the liquid by a decrease of pressure at constant temperature is called cavitation. The liquid also contains the micro-bubbles of noncondensable (dissolved or ingested) gases, or nuclei, which under decreasing pressure may grow and form cavities. In such processes, very large and steep density variations happen in the low-pressure/cavitating regions.

This section provides information about the following three cavitation models used in ANSYS Fluent.

- Singhal et al. model [410] (p. 751): You can use this model to include cavitation effects in two-phase flows when the mixture model is used. This is also known as the Full Cavitation Model, which has been implemented in ANSYS Fluent since Version 6.1.
- Zwart-Gerber-Belamri model [511] (p. 757): You can use this model in both the mixture and Eulerian multiphase models.
- Schnerr and Sauer model [398] (p. 750): This is the default model. You can use this model in both the mixture and Eulerian multiphase models.

The following assumptions are made in the standard two-phase cavitation models:

- The system under investigation must consist of a liquid and a vapor phase.
- Mass transfer between the liquid and vapor phase is assumed to take place. Both bubble formation (evaporation) and collapse (condensation) are taken into account in the cavitation models.
- For the cavitation model, ANSYS Fluent defines positive mass transfer as being from the liquid to the vapor.
- The cavitation models are based on the Rayleigh-Plesset equation, describing the growth of a single vapor bubble in a liquid.
- In the Singhal et al. model, noncondensable gases have been introduced into the system. The mass fraction of the noncondensable gases is assumed to be a known constant.

Release 15.0 - © SAS IP, Inc. All rights reserved. - Contains proprietary and confidential information of ANSYS, Inc. and its subsidiaries and affiliates.

- The input material properties used in the cavitation models can be constants, functions of temperature or user-defined.

The cavitation models offer the following capabilities:

- The Singhal et al. model can be used to account for the effect of noncondensable gases. The Zwart-Gerber-Belamri and Schnerr and Sauer models do not include the noncondensable gases in the basic model terms.
- The Zwart-Gerber-Belamri and Schnerr and Sauer models are compatible with all the turbulence models available in ANSYS Fluent.
- Both the pressure-based segregated and coupled solvers are available with the cavitation models.
- They are all fully compatible with dynamic mesh and non-conformal interfaces.
- Both liquid and vapor phases can be incompressible or compressible. For compressible liquids, the density is described using a user-defined function. See the UDF Manual for more information on user-defined density functions.

### 17.7.4.1. Limitations of the Cavitation Models

The following limitations apply to the cavitation models in ANSYS Fluent:

- None of the cavitation models can be used with the explicit VOF option because the surface tracking schemes are incompatible with the interpenetrating continua assumption of the cavitation models. However, all the cavitation models are compatible with the implicit VOF option.
- They can only be used for a single cavitation process. In other words, only a single liquid fluid is subjected to cavitation. Note that this liquid can be a phase or a species in a mixture phase. ANSYS Fluent cannot simulate multiple cavitation processes.
- The Singhal et al. model requires the primary phase to be a liquid and the secondary phase to be a vapor. This model is only compatible with the multiphase mixture model.
- The Singhal et al. model cannot be used with the Eulerian multiphase model.
- The Singhal et al. model is not compatible with the LES turbulence model.
- The Zwart-Gerber-Belamri and Schnerr and Sauer models do not take the effect of noncondensable gases into account by default.

### 17.7.4.2. Vapor Transport Equation

With the multiphase cavitation modeling approach, a basic two-phase cavitation model consists of using the standard viscous flow equations governing the transport of mixture (Mixture model) or phases (Eulerian multiphase), and a conventional turbulence model (k- $\varepsilon$ model). In cavitation, the liquid-vapor mass transfer (evaporation and condensation) is governed by the vapor transport equation:

$$\frac{\partial}{\partial t}\left(\alpha\rho_v\right)+\nabla\cdot\left(\alpha\rho_v\vec{V}_v\right)=R_e-R_c \tag{17.458}$$

where

$v$ = vapor phase

$\alpha$ = vapor volume fraction


Release 15.0 - © SAS IP, Inc. All rights reserved. - Contains proprietary and confidential information of ANSYS, Inc. and its subsidiaries and affiliates.

$\rho_v$ = vapor density

$\vec{V}_v$ = vapor phase velocity

$R_e$, $R_c$ = mass transfer source terms connected to the growth and collapse of the vapor bubbles respectively

In Equation 17.458 (p. 582), the terms $R_e$ and $R_c$ account for the mass transfer between the liquid and vapor phases in cavitation. In ANSYS Fluent, they are modeled based on the Rayleigh-Plesset equation describing the growth of a single vapor bubble in a liquid.

### 17.7.4.3. Bubble Dynamics Consideration

In most engineering situations we assume that there are plenty of nuclei for the inception of cavitation. Thus, our primary focus is on proper accounting of bubble growth and collapse. In a flowing liquid with zero velocity slip between the fluid and bubbles, the bubble dynamics equation can be derived from the generalized Rayleigh-Plesset equation as [45] (p. 731)

$$\Re_b \frac{D^2\Re_b}{Dt^2} + \frac{3}{2}\left(\frac{D\Re_b}{Dt}\right)^2 = \left(\frac{P_b - P}{\rho_l}\right) - \frac{4\nu_\ell}{\Re_b}\dot{\Re}_b - \frac{2\sigma}{\rho_l \Re_b} \tag{17.459}$$

where,

$\Re_b$ = bubble radius

$\sigma$ = liquid surface tension coefficient

$\rho_l$ = liquid density

$P_b$ = bubble surface pressure

$P$ = local far-field pressure

Neglecting the second-order terms and the surface tension force, Equation 17.459 (p. 583) is simplified to

$$\frac{D\Re_B}{Dt} = \sqrt{\frac{2}{3}\frac{P_b - P}{\rho_l}} \tag{17.460}$$

This equation provides a physical approach to introduce the effects of bubble dynamics into the cavitation model. It can also be considered to be an equation for void propagation and, hence, mixture density.

### 17.7.4.4. Singhal et al. Model

This cavitation model is based on the "full cavitation model", developed by Singhal et al. [410] (p. 751). It accounts for all first-order effects (that is, phase change, bubble dynamics, turbulent pressure fluctuations, and noncondensable gases). It has the capability to account for multiphase (N-phase) flows or flows with multiphase species transport, the effects of slip velocities between the liquid and gaseous phases, and the thermal effects and compressibility of both liquid and gas phases. The cavitation model can be used with the mixture multiphase model, with or without slip velocities. However, it is always preferable to solve for cavitation using the mixture model without slip velocity; slip velocities can be turned on if the problem suggests that there is significant slip between phases.

Release 15.0 - © SAS IP, Inc. All rights reserved. - Contains proprietary and confidential information of ANSYS, Inc. and its subsidiaries and affiliates.

To derive an expression of the net phase change rate, Singhal et al. [410] (p. 751) uses the following two-phase continuity equations:

Liquid phase:

$$\frac{\partial}{\partial t}\left[ (1-\alpha)\rho_l \right] + \nabla \cdot \left[ (1-\alpha)\rho_l \vec{V} \right] = -R \tag{17.461}$$

Vapor phase:

$$\frac{\partial}{\partial t}\left(\alpha\rho_v\right) + \nabla \cdot \left(\alpha\rho_v \vec{V}\right) = R \tag{17.462}$$

Mixture:

$$\frac{\partial}{\partial t}(\rho) + \nabla \cdot (\rho \vec{V}) = 0 \tag{17.463}$$

where,

$l$ = liquid phase

$\rho$ = mixture density (function of phase volume fraction and density)

Mixture density $\rho$ is defined as

$$\rho = \alpha\rho_v + (1-\alpha)\rho_l \tag{17.464}$$

Combining Equation 17.461 (p. 584), Equation 17.462 (p. 584), and Equation 17.463 (p. 584) yields a relationship between the mixture density and vapor volume fraction ($\alpha$):

$$\frac{D\rho}{Dt} = -\left(\rho_l - \rho_v\right)\frac{D\alpha}{Dt} \tag{17.465}$$

The vapor volume fraction ($\alpha$) can be related to the bubble number density ($n$) and the radius of bubble ($\Re_B$) as

$$\alpha = n \times \left( \frac{4}{3}\pi \Re_B{}^3 \right) \tag{17.466}$$

Substituting Equation 17.466 (p. 584) into Equation 17.465 (p. 584) gives the following:

$$\frac{D\rho}{Dt} = -\left(\rho_l - \rho_v\right)(n4\pi)^{\frac{1}{3}}(3\alpha)^{\frac{2}{3}}\frac{D\Re_B}{Dt} \tag{17.467}$$

Using the Equation 17.460 (p. 583), and combining Equation 17.461 (p. 584), Equation 17.462 (p. 584), Equation 17.465 (p. 584), and Equation 17.467 (p. 584), the expression for the net phase change rate ($R$) is finally obtained as

$$R = (n4\pi)^{\frac{1}{3}}(3\alpha)^{\frac{2}{3}}\frac{\rho_v\rho_l}{\rho}\left[\frac{2}{3}\left(\frac{P_B - P}{\rho_\ell}\right)\right]^{\frac{1}{2}} \tag{17.468}$$

Here $R$ represents the vapor generation or evaporation rate, that is, the source term $R_e$ in Equation 17.458 (p. 582). All terms, except $n$, are either known constants or dependent variables. In the absence of a general model for estimation of the bubble number density, the phase change rate expression is rewritten in terms of bubble radius ($\Re_B$), as follows:


Release 15.0 - © SAS IP, Inc. All rights reserved. - Contains proprietary and confidential information of ANSYS, Inc. and its subsidiaries and affiliates.

$$R=\frac{3\alpha}{\Re_B}\frac{\rho_v\rho_l}{\rho}\sqrt{\frac{2}{3}\frac{(P_B-P)}{\rho_\ell}} \tag{17.469}$$

Equation 17.469 (p. 585) indicates that the unit volume mass transfer rate is not only related to the vapor density ($\rho_v$), but the function of the liquid density ($\rho_\ell$), and the mixture density ($\rho$) as well. Since Equation 17.469 (p. 585) is derived directly from phase volume fraction equations, it is exact and should accurately represent the mass transfer from liquid to vapor phase in cavitation (bubble growth or evaporation). Though the calculation of mass transfer for bubble collapse or condensation is expected to be different from that of bubble growth, Equation 17.469 (p. 585) is often used as a first approximation to model the bubble collapse. In this case, the right side of the equation is modified by using the absolute value of the pressure difference and is treated as a sink term.

It may be noted that in practical cavitation models, the local far-field pressure $P$ is usually taken to be the same as the cell center pressure. The bubble pressure $P_B$ is equal to the saturation vapor pressure in the absence of dissolved gases, mass transport and viscous damping, that is, $P_B=P_v$.

where,

$P_B$ = bubble pressure

$P_v$ = saturation vapor pressure

Based on Equation 17.469 (p. 585), Singhal et al. [510] (p. 757) proposed a model where the vapor mass fraction is the dependent variable in the transport equation. This model accommodates also a single phase formulation where the governing equations is given by:

$$\frac{\partial}{\partial t}\left(f_v\rho\right)+\nabla\cdot\left(f_v\rho\vec{V}_v\right)=\nabla\cdot\left(\Gamma\nabla f_v\right)+R_e-R_c \tag{17.470}$$

where,

$f_v$ = vapor mass fraction

$f_g$ = noncondensable gases

$\Gamma$ = diffusion coefficient

The rates of mass exchange are given by the following equations:

If $P\le P_v$

$$R_e=F_{vap}\frac{max\left(1.0,\sqrt{k}\right)\left(1-f_v-f_g\right)}{\sigma}\rho_l\rho_v\sqrt{\frac{2}{3}\frac{(P_v-P)}{\rho_l}} \tag{17.471}$$

If $P>P_v$

$$R_c=F_{cond}\frac{max\left(1.0,\sqrt{k}\right)f_v}{\sigma}\rho_l\rho_l\sqrt{\frac{2}{3}\frac{(P-P_v)}{\rho_l}} \tag{17.472}$$

The saturation pressure is corrected by an estimation of the local values of the turbulent pressure fluctuations:

Release 15.0 - © SAS IP, Inc. All rights reserved. - Contains proprietary and confidential information of ANSYS, Inc. and its subsidiaries and affiliates.

$$P_v = P_{sat} + \frac{1}{2}(0.39\rho k) \tag{17.473}$$

The constants have the values $F_{vap} = 0.02$ and $F_{cond} = 0.01$. In this model, the liquid-vapor mixture is assumed to be compressible. Also, the effects of turbulence and the noncondensable gases have been taken into account.

### 17.7.4.5. Zwart-Gerber-Belamri Model

Assuming that all the bubbles in a system have the same size, Zwart-Gerber-Belamri [511] (p. 757) proposed that the total interphase mass transfer rate per unit volume ($R$) is calculated using the bubble density numbers ($n$), and the mass change rate of a single bubble:

$$R = n \times \left( 4\pi \Re_B^{\,2} \rho_v \frac{D\Re_B}{Dt} \right) \tag{17.474}$$

Substituting the value of $n$ in Equation 17.474 (p. 586) into Equation 17.466 (p. 584), we have the expression of the net mass transfer:

$$R = \frac{3\alpha\rho_v}{\Re_B} \sqrt{\frac{2}{3}\frac{P_B - P}{\rho_l}} \tag{17.475}$$

Comparing Equation 17.475 (p. 586) and Equation 17.469 (p. 585), you will notice that the difference is only in the density terms in the mass transfer rate. In Equation 17.475 (p. 586), the unit volume mass transfer rate is only related to the vapor phase density ($\rho_v$). Unlike Equation 17.469 (p. 585), $R$ has no relation with the liquid phase and mixture densities in this model.

As in Equation 17.469 (p. 585), Equation 17.475 (p. 586) is derived assuming bubble growth (evaporation). To apply it to the bubble collapse process (condensation), the following generalized formulation is used:

$$R_e = F\frac{3\alpha\rho_v}{\Re_B} \sqrt{\frac{2}{3}\frac{|P_B - P|}{\rho_l}} sign(P_B - P) \tag{17.476}$$

where $F$ is an empirical calibration coefficient. Though it is originally derived from evaporation, Equation 17.476 (p. 586) only works well for condensation. It is physically incorrect and numerically unstable if applied to evaporation. The fundamental reason is that one of the key assumptions is that the cavitation bubble does not interact with each other. This is plausible only during the earliest stage of cavitation when the cavitation bubble grows from the nucleation site. As the vapor volume fraction increases, the nucleation site density must decrease accordingly. To model this process, Zwart-Gerber-Belamri proposed to replace $\alpha_v$ with $\alpha_{nuc}(1 - \alpha_v)$ in Equation 17.476 (p. 586). Then the final form of this cavitation model is as follows:

If $P \le P_v$

$$R_e = F_{vap}\frac{3\alpha_{nuc}(1 - \alpha_v)\rho_v}{\Re_B} \sqrt{\frac{2}{3}\frac{P_v - P}{\rho_l}} \tag{17.477}$$

If $P \ge P_v$

$$R_c = F_{cond}\frac{3\alpha_v\rho_v}{\Re_B} \sqrt{\frac{2}{3}\frac{P - P_v}{\rho_l}} \tag{17.478}$$


Release 15.0 - © SAS IP, Inc. All rights reserved. - Contains proprietary and confidential information of ANSYS, Inc. and its subsidiaries and affiliates.

where,

$\Re_B$ = bubble radius = $10^{-6}$m

$\alpha_{nuc}$ = nucleation site volume fraction = $5\times10^{-4}$

$F_{vap}$ = evaporation coefficient = $50$

$F_{cond}$ = condensation coefficient = $0.01$

### 17.7.4.6. Schnerr and Sauer Model

As in the Singhal et al. model, Schnerr and Sauer [398] (p. 750) follow a similar approach to derive the exact expression for the net mass transfer from liquid to vapor. The equation for the vapor volume fraction has the general form:

$$\frac{\partial}{\partial t}\left(\alpha\rho_v\right)+\nabla\cdot\left(\alpha\rho_v\vec{V}\right)=\frac{\rho_v\rho_l}{\rho}\frac{D\alpha}{Dt} \tag{17.479}$$

Here, the net mass source term is as follows:

$$R=\frac{\rho_v\rho_l}{\rho}\frac{d\alpha}{dt} \tag{17.480}$$

Unlike Zwart-Gerber-Belamri and Singhal et al., Schnerr and Sauer use the following expression to connect the vapor volume fraction to the number of bubbles per volume of liquid:

$$\alpha=\frac{n_b\frac{4}{3}\pi\Re_B{}^3}{1+n_b\frac{4}{3}\pi\Re_B{}^3} \tag{17.481}$$

Following a similar approach to Singhal et al., they derived the following equation:

$$R=\frac{\rho_v\rho_l}{\rho}\alpha(1-\alpha)\frac{3}{\Re_B}\sqrt{\frac{2}{3}\frac{(P_v-P)}{\rho_l}} \tag{17.482}$$

$$\Re_B=\left(\frac{\alpha}{1-\alpha}\frac{3}{4\pi}\frac{1}{n}\right)^{\frac{1}{3}} \tag{17.483}$$

where,

$R$ = mass transfer rate

$\Re_B$ = bubble radius

Comparing Equation 17.482 (p. 587) with Equation 17.469 (p. 585) and Equation 17.475 (p. 586), it is obvious that unlike the two previous models, the mass transfer rate in the Schnerr and Sauer model is proportional to $\alpha_v(1-\alpha_v)$. Moreover, the function $f\left(\alpha_v,\rho_v,\rho_l\right)=\frac{\rho_v\rho_l}{\rho}\alpha(1-\alpha)$ has the interesting property that it approaches zero when $\alpha=0$ and $\alpha=1$, and reaches the maximum in between. Also in this model, the only parameter that must be determined is the number of spherical bubbles per volume of liquid. If you assume that no bubbles are created or destroyed, the bubble number density would be constant. The initial conditions for the nucleation site volume fraction and the equilibrium bubble radius would therefore be sufficient to specify the bubble number density ($n$) from Equation 17.481 (p. 587) and then the phase transition by Equation 17.482 (p. 587).

Release 15.0 - © SAS IP, Inc. All rights reserved. - Contains proprietary and confidential information of ANSYS, Inc. and its subsidiaries and affiliates.

As in the two other models, Equation 17.482 (p. 587) is also used to model the condensation process. The final form of the model is as follows:

When $P_v \geq P$,

$$R_e = \frac{\rho_v \rho_l}{\rho} \alpha (1-\alpha) \frac{3}{\Re_B} \sqrt{\frac{2}{3} \frac{(P_v - P)}{\rho_l}} \tag{17.484}$$

When $P_v \leq P$,

$$R_c = \frac{\rho_v \rho_l}{\rho} \alpha (1-\alpha) \frac{3}{\Re_B} \sqrt{\frac{2}{3} \frac{(P - P_v)}{\rho_l}} \tag{17.485}$$

### 17.7.4.7. Additional Guidelines for the Cavitation Models

In practical applications of a cavitation model, several factors greatly influence numerical stability. For instance, the high pressure difference between the inlet and exit, large ratio of liquid to vapor density, and large phase change rates between the liquid and vapor all have unfavorable effects on solution convergence. In addition, poor initial conditions very often lead to an unrealistic pressure field and unexpected cavitating zones, which, once present, are usually difficult to correct. You may consider the following factors/tips when choosing a cavitation model and addressing potential numerical problems:

- Choice of the cavitation models

  In ANSYS Fluent, there are three available cavitation models. The Zwart-Gerber-Belamri and the Schnerr and Sauer models have been implemented following an entirely different numerical procedure from the Singhal et al. model developed in ANSYS Fluent 6.1. Numerically, these two models are robust and converge quickly. It is therefore highly recommended that you should use the Schnerr and Sauer or the Zwart-Gerber-Bleamri model. The Singhal et al. model, though physically similar to the other two, is numerically less stable and more difficult to use.

- Choice of the solvers

  In ANSYS Fluent, both the segregated (SIMPLE, SIMPLEC, and PISO) and coupled pressure-based solvers can be used in cavitation. As usual, the coupled solver is generally more robust and converges faster, particularly for cavitating flows in rotating machinery (liquid pumps, inducers, impellers, etc). For fuel injector applications, however, the segregated solver also performs very well with the Schnerr and Sauer and the Zwart-Gerber-Belamri models.

  As for the Singhal et al. model, since the coupled solver does not show any significant advantages, it is suggested that the segregated solver is used.

- Initial conditions

  Though no special initial condition settings are required, we suggest that the vapor fraction is always set to inlet values. The pressure is set close to the highest pressure among the inlets and outlets to avoid unexpected low pressure and cavitating spots. In general, the Schnerr and Sauer and Zwart-Gerber-Belamri models are robust enough so that there is no need for specific initial conditions. But in some very complicated cases, it may be beneficial to obtain a realistic pressure field before substantial cavities are formed. This can be achieved by obtaining a converged/near-converged solution for a single phase liquid flow, and then enabling the cavitation model. Again, the Singhal et al.model is much more sensitive to initial conditions. The above mentioned treatments are generally required.


Release 15.0 - © SAS IP, Inc. All rights reserved. - Contains proprietary and confidential information of ANSYS, Inc. and its subsidiaries and affiliates.

- Pressure discretization schemes

  As for general multiphase flows, it is more desirable to use the following pressure discretization schemes in cavitation applications in this order:

  – PRESTO!

  – body force weighted

  – second order

  The standard and linear schemes generally are not very effective in complex cavitating flows and you should avoid using them.

- Relaxation factors

  – Schnerr and Sauer and Zwart-Gerber-Belamri models

    The default settings generally work well. To achieve numerical efficiency, however, the following values may be recommended:

    → The relaxation factor for vapor is 0.5 or higher unless the solution diverges or all the residuals oscillate excessively.

    → The density and the vaporization mass can be relaxed, but in general set them to 1.

    → For the segregated solver, the relaxation factor for pressure should be no less than the value for the momentum equations.

    → For the coupled solver, the default value for the Courant number (200) may need to be reduced to 20-50 in some complex 3D cases.

  – Singhal et al. model

    In general, small relaxation factors are recommended for momentum equations, usually between 0.05 – 0.4. The relaxation factor for the pressure-correction equation should generally be larger than those for momentum equations, say in the range of 0.2 – 0.7. The density and the vaporization mass (source term in the vapor equation) can also be relaxed to improve convergence. Typically, the relaxation factor for density is set between the values of 0.3 and 1.0, while for the vaporization mass, values between 0.1 and 1.0 may be appropriate. For some extreme cases, even smaller relaxation factors may be required for all the equations.

- Special tips for the Singal et al. model

  – Noncondensable gases

    Noncondensable gases are usually present in liquids. Even a small amount (for example, 15 ppm) of noncondensable gases can have significant effects on both the physical results and the convergence characteristics of the solution. A value of zero for the mass fraction of noncondensable gases should generally be avoided. In some cases, if the liquid is purified of noncondensable gases, a much smaller value (for example, $10^{-8}$) may be used to replace the default value of $1.5 \times 10^{-5}$. In fact, higher mass fractions of the noncondensable gases may in many cases enhance numerical stability and lead to more realistic results. In particular, when the saturation pressure of a liquid at

Release 15.0 - © SAS IP, Inc. All rights reserved. - Contains proprietary and confidential information of ANSYS, Inc. and its subsidiaries and affiliates.

a certain temperature is zero or very small, noncondensable gases will play a crucial role both numerically and physically.

– Limits for dependent variables

In many cases, setting the pressure upper limit to a reasonable value can help convergence greatly at the early stage of the solution. It is advisable to always limit the maximum pressure when possible.

By default, ANSYS Fluent sets the maximum pressure limit to 5.0 $\times 10^{10}$ Pascal.

– Relaxation factor for the pressure correction equation

For cavitating flows, a special relaxation factor is introduced for the pressure correction equation. By default, this factor is set to 0.7, which should work well for most of the cases. For some very complicated cases, however, you may experience the divergence of the AMG solver. Under those circumstances, this value may be reduced to no less than 0.4. You can set the value of this relaxation factor by typing a text command. For more information, contact your ANSYS Fluent support engineer.

### 17.7.4.8. Extended Cavitation Model Capabilities

When cavitation occurs, in many practical applications other gaseous species exist in the systems. For instance, in a ventilated supercavitating vehicle, air is injected into a liquid to stabilize or increase the cavitation along the vehicle surfaces. In some cases, the incoming flow is a mixture of a liquid and some gaseous species. To predict those types of cavitating flows, the basic two-phase cavitation model must be extended to a multiphase (N-phase) flow, or a multiphase species transport cavitation model.

### 17.7.4.9. Multiphase Cavitation Models

The multiphase cavitation models are the extensions of the three basic two-phase cavitation models to multiphase flows. In addition to the primary liquid and secondary vapor phase, more secondary gaseous phases can be included into the computational system under the following assumptions:

- Mass transfer (cavitation) only occurs between the liquid and vapor phase.
- The basic two-phase cavitation models are still used to model the phase changes between the liquid and vapor.
- Only one secondary phase can be defined as compressible gas phase, while a user-defined density may be applied to all the phases.
- In the Singhal et al. model, the predescribed noncondensable gases can be included in the system. To exclude noncondensable gases from the system, the mass fraction must be set to 0, and the noncondensable gas must be modeled by a separate compressible gas phase.
- For non-cavitating phase ($i$), the general transport equation governing the vapor phase is the volume fraction equation in the Zwart-Gerber-Belamri and Schnerr and Sauer models, while in the Singhal et al. model, a mass transfer equation is solved and the vapor must be the second phase.

### 17.7.4.10. Multiphase Species Transport Cavitation Model

In some cases, there are several gas phase components in a system that can be considered compressible. Since only one compressible gas phase is allowed in the general multiphase approach, the multiphase species transport approach offers an option to handle these types of applications by assuming that there is one compressible gas phase with multiple species.


Release 15.0 - © SAS IP, Inc. All rights reserved. - Contains proprietary and confidential information of ANSYS, Inc. and its subsidiaries and affiliates.

The detailed description of the multiphase species transport approach can be found in Modeling Species Transport in Multiphase Flows (p. 595). The multiphase species transport cavitation model can be summarized as follows:

- All the assumptions/limitations for the multiphase cavitation model apply here.
- The primary phase can only be a single-species liquid.
- All the secondary phases allow more than one species.
- The mass transfer between a liquid and a vapor phase/species is modeled by the basic cavitation models.
- The mass transfer between other phases or species are modeled with the standard mass transfer approach. In the standard model, zero constant rates should be chosen.
- For the phases with multiple species, the phase shares the same pressure as the other phases, but each species has its own pressure (that is, partial pressure). As a result, the vapor density and the pressure used in Equation 17.472 (p. 585) are the partial density and pressure of the vapor.

## 17.7.5. Evaporation-Condensation Model

ANSYS Fluent uses one of two models for interphase mass transfer through evaporation-condensation depending on the multiphase and interfacial heat transfer models being used. In most cases the Lee model is used. The single exception is in the case that the Eulerian multiphase model is used in conjunction with the two-resistance model for interfacial heat transfer, in which case the Thermal Phase Change model is used.

### *17.7.5.1. Lee Model*

The Lee model [237] (p. 742) is a mechanistic model with a physical basis. It is used with the mixture and VOF multiphase models as well as with the Eulerian multiphase model if one of the overall interfacial heat transfer coefficient models is used (as opposed to the two-resistance model). In the Lee model, the liquid-vapor mass transfer (evaporation and condensation) is governed by the vapor transport equation:

$$\frac{\partial}{\partial t}(\alpha_v \rho_v) + \nabla \cdot (\alpha_v \rho_v \vec{V}_v) = \dot{m}_{lv} - \dot{m}_{vl} \tag{17.486}$$

where

$v$ = vapor phase

$\alpha_v$ = vapor volume fraction

$\rho_v$ = vapor density

$\vec{V}_v$ = vapor phase velocity

$\dot{m}_{lv}$, $\dot{m}_{vl}$ = the rates of mass transfer due to evaporation and condensation, respectively. These rates use units of kg/s/m$^3$

As shown in the right side of Equation 17.486 (p. 591), ANSYS Fluent defines positive mass transfer as being from the liquid to the vapor for evaporation-condensation problems.

Based on the following temperature regimes, the mass transfer can be described as follows:

Release 15.0 - © SAS IP, Inc. All rights reserved. - Contains proprietary and confidential information of ANSYS, Inc. and its subsidiaries and affiliates.

If $T_l > T_{sat}$ (evaporation):

$$\dot{m}_{lv} = coeff * \alpha_l \rho_l \frac{(T_l - T_{sat})}{T_{sat}} \tag{17.487}$$

If $T_v < T_{sat}$ (condensation):

$$\dot{m}_{vl} = coeff * \alpha_v \rho_v \frac{(T_{sat} - T_v)}{T_{sat}} \tag{17.488}$$

$coeff$ is a coefficient that must be fine tuned and can be interpreted as a relaxation time. $\alpha$ and $\rho$ are the phase volume fraction and density, respectively. The source term for the energy equation can be obtained by multiplying the rate of mass transfer by the latent heat.

Consider the Hertz Knudsen formula [160] (p. 737) [212] (p. 740), which gives the evaporation-condensation flux based on the kinetic theory for a flat interface:

$$F = \beta \sqrt{\frac{M}{2\pi R T_{sat}}} (P^* - P_{sat}) \tag{17.489}$$

The flux has units of kg/s/m$^2$, $P$ is the pressure, $T$ is the temperature, and $R$ is the universal gas constant. The coefficient $\beta$ is the so-called accommodation coefficient that shows the portion of vapor molecules going into the liquid surface and adsorbed by this surface. $P^*$ represents the vapor partial pressure at the interface on the vapor side. The Clapeyron-Clausius equation relates the pressure to the temperature for the saturation condition. (It is obtained by equating the vapor and liquid chemical potentials):

$$\frac{dP}{dT} = \frac{L}{T(v_v - v_l)} \tag{17.490}$$

$v_v$ and $v_l$ are the inverse of the density for the vapor and liquid (volume per mass unit), respectively. $L$ is the latent heat (J/kg).

Based on this differential expression, we can obtain variation of temperature from variation of pressure close to the saturation condition.

**Figure 17.5: The Stability Phase Diagram**

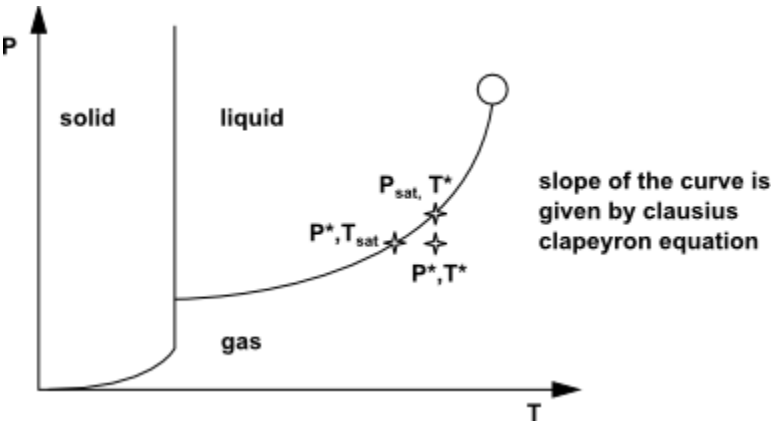


The Clausius Clapeyron equation yields the following formula as long as $P^*$ and $T^*$ are close to the saturation condition:


Release 15.0 - © SAS IP, Inc. All rights reserved. - Contains proprietary and confidential information of ANSYS, Inc. and its subsidiaries and affiliates.

$$(P^* - P_{sat}) = -\frac{L}{T(v_v - v_l)}(T^* - T_{sat}) \tag{17.491}$$

Using this relation in the above Hertz Knudsen equation yields [445] (p. 753)

$$F = \beta\sqrt{\frac{M}{2\pi RT_{sat}}}L\left(\frac{\rho_v\rho_l}{\rho_l - \rho_v}\right)\frac{(T^* - T_{sat})}{T_{sat}} \tag{17.492}$$

The factor $\beta$ is defined by means of the accommodation coefficient and the physical characteristics of the vapor. $\beta$ approaches 1.0 at near equilibrium conditions.

In the Eulerian and mixture multiphase models, the flow regime is assumed to be dispersed. If we assume that all vapor bubbles, for example, have the same diameter, then the interfacial area density is given by the following formula:

$$A_i = \frac{6\alpha_v\alpha_l}{d_b} \tag{17.493}$$

where $d_b$ is the bubble diameter ($m$) and the phase source term (kg/s/m$^3$) should be of the form:

$$FA_i = \frac{6}{d_b}\beta\sqrt{\frac{M}{2\pi RT_{sat}}}L\left(\frac{\alpha_v\rho_v}{\rho_l - \rho_v}\right)\left[\alpha_l\rho_l\frac{(T^* - T_{sat})}{T_{sat}}\right] \tag{17.494}$$

From the above equation, $coeff$, which is the inverse of the relaxation time (1/s) is defined as

$$coeff = \frac{6}{d_b}\beta\sqrt{\frac{M}{2\pi RT_{sat}}}L\left(\frac{\alpha_v\rho_v}{\rho_l - \rho_v}\right) \tag{17.495}$$

This leads to the final expression for the evaporation process defined in Equation 17.487 (p. 592). It can be treated implicitly as a source term in the phase conservation equation.

A similar expression can be obtained for condensation. In this case, we consider small droplets in a continuous vapor phase even if your primary phase is a liquid.

Note that the coefficient $coeff$ should theoretically be different for the condensation and evaporation expression. Furthermore, the theoretical expression is based on a few strong assumptions:

- flat interface
- dispersed regime with constant diameter
- known $\beta$

The bubble diameter and accommodation coefficient are usually not very well known, which is why the coefficient $coeff$ must be fine tuned to match experimental data. By default, the coefficient for both evaporation and condensation is 0.1. However, in practical cases, the order of magnitude of $coeff$ can be as high $10^3$.

Release 15.0 - © SAS IP, Inc. All rights reserved. - Contains proprietary and confidential information of ANSYS, Inc. and its subsidiaries and affiliates.

### 17.7.5.2. Thermal Phase Change Model

The thermal phase change model is used for evaporation-condensation when the Eulerian multiphase model is used with the two-resistance approach for computing phase heat transfer coefficients (Two-Resistance Model (p. 547)).

Applying Equation 17.321 (p. 548) and Equation 17.322 (p. 548) to a liquid-vapor pair gives:

From the interface to the liquid phase:

$$Q_l = h_l A_i (T_s - T_l) - \dot{m}_{lv} H_{ls} \tag{17.496}$$

From the interface to the vapor phase:

$$Q_v = h_v A_i (T_s - T_v) + \dot{m}_{lv} H_{vs} \tag{17.497}$$

where $h_l$ and $h_v$ are the liquid and vapor phase heat transfer coefficients and $H_{ls}$ and $H_{vs}$ are the liquid and vapor phase enthalpies. The interfacial temperature, $T_s$, is determined from consideration of thermodynamic equilibrium. Ignoring effects of surface tension on pressure, we can assume that $T_s = T_{sat}$, the saturation temperature.

Because neither heat nor mass can be stored on the phase interface, the overall heat balance must be satisfied:

$$Q_l + Q_v = 0 \tag{17.498}$$

From the preceding equations, the mass transfer through evaporation from the liquid to the vapor phase can be expressed as:

$$\dot{m}_{lv} = -\frac{h_l A_i (T_{sat} - T_l) + h_v A_i (T_{sat} - T_v)}{H_{vs} - H_{ls}} \tag{17.499}$$

The phase enthalpies, $H_{vs}$ and $H_{ls}$, need to be computed correctly to take account of the discontinuity in static enthalpy due to latent heat between the two phases as well as the heat transfer from either phase to the phase interface. Using the Prakash formulation [362] (p. 749) with the bulk fluid enthalpy carried out of the outgoing phase and the saturation enthalpy carried into the incoming phase we have:

If $\dot{m}_{lv} \geq 0$ (evaporation, the liquid phase is the outgoing phase):

$$\begin{aligned} H_{ls} &= H_l (T_l) \\ H_{vs} &= H_v (T_{sat}) \end{aligned} \tag{17.500}$$

If $\dot{m}_{lv} < 0$ (condensation, the liquid phase is the incoming phase):

$$\begin{aligned} H_{ls} &= H_l (T_{sat}) \\ H_{vs} &= H_v (T_v) \end{aligned} \tag{17.501}$$

This leads to a formulation that is stable both physically and numerically. It implies that the denominator in Equation 17.499 (p. 594) is non-zero, being greater than or equal to the latent heat:

$$L = H_v (T_{sat}) - H_l (T_{sat}) \tag{17.502}$$


Release 15.0 - © SAS IP, Inc. All rights reserved. - Contains proprietary and confidential information of ANSYS, Inc. and its subsidiaries and affiliates.

It may be noted that with the presence of mass transfer $H_l$ and $H_v$ are total phase enthalpies, which can be expressed in a general form:

$$H(T) = H\left(T_{ref}\right) + \int_{T_{ref}}^{T} C_p(T)\, dT \tag{17.503}$$

where $T_{ref}$ is the reference temperature and $H\left(T_{ref}\right)$ is the standard state enthalpy at $T_{ref}$. Equation 17.503 (p. 595) applies for phases as well as species on each phase.

Note that in the thermal phase change model the evaporation-condensation mass transfer process is governed entirely by the interphase heat transfer processes and the overall heat balance. There is no calibration required for the mass transfer coefficients as there is in the Lee model. Therefore, it is generally recommended that you use the Eulerian multiphase formulation with the two-resistance heat transfer method when simulating evaporation-condensation processes.

## 17.8. Modeling Species Transport in Multiphase Flows

Species transport, as described in Species Transport and Finite-Rate Chemistry (p. 187), can also be applied to multiphase flows. You can choose to solve the conservation equations for chemical species in multiphase flows by having ANSYS Fluent, for each phase $k$, predict the local mass fraction of each species, $Y_i^k$, through the solution of a convection-diffusion equation for the $i^{th}$ species. The generalized chemical species conservation equation (Equation 7.1 (p. 187)), when applied to a multiphase mixture can be represented in the following form:

$$\begin{aligned}\frac{\partial}{\partial t}\left(\rho^q \alpha^q Y_i^q\right) + \nabla \cdot \left(\rho^q \alpha^q \vec{v}^{\,q} Y_i^q\right) = \quad & -\nabla \cdot \alpha^q \vec{J}_i^{\,q} + \alpha^q R_i^q + \alpha^q S_i^q \\ & + \sum_{p=1}^{n}\left(\dot{m}_{p^i q^j} - \dot{m}_{q^j p^i}\right) + \mathcal{R}\end{aligned} \tag{17.504}$$

where $R_i^q$ is the net rate of production of homogeneous species $i$ by chemical reaction for phase $q$, $\dot{m}_{q^j p^i}$ is the mass transfer source between species $i$ and $j$ from phase $q$ to $p$, and $\mathcal{R}$ is the heterogeneous reaction rate. In addition, $\alpha^q$ is the volume fraction for phase $q$ and $S_i^q$ is the rate of creation by addition from the dispersed phase plus any user-defined sources.

ANSYS Fluent treats homogeneous gas phase chemical reactions the same as a single-phase chemical reaction. The reactants and the products belong to the same mixture material (set in the **Species Model** dialog box), and hence the same phase. The reaction rate is scaled by the volume fraction of the particular phase in the cell.

The set-up of a homogeneous gas phase chemical reaction in ANSYS Fluent is the same as it is for a single phase. For more information, see Species Transport and Finite-Rate Chemistry (p. 187). For most multiphase species transport problems, boundary conditions for a particular species are set in the associated phase boundary condition dialog box (see Defining Multiphase Cell Zone and Boundary Conditions in the User's Guide), and postprocessing and reporting of results is performed on a per-phase basis (see Postprocessing for Multiphase Modeling in the User's Guide).

For multiphase species transport simulations, the **Species Model** dialog box allows you to include **Volumetric**, **Wall Surface**, and **Particle Surface** reactions. ANSYS Fluent treats multiphase surface reac-

Release 15.0 - © SAS IP, Inc. All rights reserved. - Contains proprietary and confidential information of ANSYS, Inc. and its subsidiaries and affiliates.

tions as it would a single-phase reaction. The reaction rate is scaled with the volume fraction of the particular phase in the cell. For more information, see Species Transport and Finite-Rate Chemistry (p. 187).

**Important**

To turn off reactions for a particular phase, while keeping the reactions active for other phases, turn on **Volumetric** under **Reactions** in the **Species Model** dialog box. Then, in the **Create/Edit Materials** dialog box, select **none** from the **Reactions** drop-down list.

The species of different phases is entirely independent. There is no implicit relationship between them even if they share the same name. Explicit relationships between species of different phases can be specified through mass transfer and heterogeneous reactions. For more information on mass transfer and heterogeneous reactions, see Including Mass Transfer Effects and Specifying Heterogeneous Reactions in the User's Guide, respectively.

Some phases may have a fluid material associated with them instead of a mixture material. The species equations are solved in those phases that are assigned a mixture material. The species equation above is solved for the mass fraction of the species in a particular phase. The mass transfer and heterogeneous reactions will be associated with the bulk fluid for phases with a single fluid material.

Additional information about modeling species transport is presented in the following subsections:

17.8.1. Limitations
17.8.2. Mass and Momentum Transfer with Multiphase Species Transport
17.8.3. The Stiff Chemistry Solver
17.8.4. Heterogeneous Phase Interaction

## 17.8.1. Limitations

The following limitations exist for the modeling of species transport for multiphase flows:

- The nonpremixed, premixed, partially-premixed combustion, or the composition PDF transport species transport models are not available for multiphase species reactions.
- Only the laminar finite-rate, finite-rate/eddy-dissipation, and eddy-dissipation turbulence-chemistry models of homogeneous reactions are available for multiphase species transport.
- The discrete phase model (DPM) is not compatible with multiphase species transport.

## 17.8.2. Mass and Momentum Transfer with Multiphase Species Transport

The ANSYS Fluent multiphase mass transfer model accommodates mass transfer between species belonging to different phases. Instead of a matrix-type input, multiple mass transfer mechanisms need to be input. Each mass transfer mechanism defines the mass transfer phenomenon from one entity to another entity. An entity is either a particular species in a phase, or the bulk phase itself if the phase does not have a mixture material associated with it. The mass transfer phenomenon could be specified either through the built-in unidirectional "constant-rate" mass transfer (Unidirectional Constant Rate Mass Transfer (p. 580)) or through user-defined functions.

ANSYS Fluent loops through all the mass transfer mechanisms to compute the net mass source/sink of each species in each phase. The net mass source/sink of a species is used to compute species and mass source terms. ANSYS Fluent will also automatically add the source contribution to all relevant momentum and energy equations based on that assumption that the momentum and energy carried along with


Release 15.0 - © SAS IP, Inc. All rights reserved. - Contains proprietary and confidential information of ANSYS, Inc. and its subsidiaries and affiliates.

the transferred mass. For other equations, the transport due to mass transfer must be explicitly modeled by you.

### 17.8.2.1. Source Terms Due to Heterogeneous Reactions

Consider the following reaction:

$$aA + bB \rightarrow cC + dD \tag{17.505}$$

Let as assume that $A$ and $C$ belong to phase $1$ and $B$ and $D$ to phase $2$.

#### 17.8.2.1.1. Mass Transfer

Mass source for the phases are given by:

$$S_1 = \mathcal{R}(cM_c - aM_a) \tag{17.506}$$

$$S_2 = \mathcal{R}(dM_d - bM_b) \tag{17.507}$$

where $S$ is the mass source, $M$ is the molecular weight, and $\mathcal{R}$ is the reaction rate.

The general expression for the mass source for the $i^{th}$ phase is

$$S_{r_i} = -\mathcal{R}\sum_{r_i}\gamma_j^r M_j^r \tag{17.508}$$

$$S_{p_i} = \mathcal{R}\sum_{p_i}\gamma_j^p M_j^p \tag{17.509}$$

$$S_i = S_{p_i} + S_{r_i} \tag{17.510}$$

where $\gamma$ is the stoichiometric coefficient, $p$ represents the product, and $r$ represents the reactant.

#### 17.8.2.1.2. Momentum Transfer

Momentum transfer is more complicated, but we can assume that the reactants mix (conserving momentum) and the products take momentum in the ratio of the rate of their formation.

The net velocity, $\vec{u}_{net}$, of the reactants is given by:

$$\vec{u}_{net} = \frac{aM_a\vec{u}_1 + bM_b\vec{u}_2}{aM_a + bM_b} \tag{17.511}$$

The general expression for the net velocity of the reactants is given by:

$$\vec{u}_{net} = \frac{\sum_r \gamma_j^r M_j^r \vec{u}_{r_j}}{\sum_r \gamma_j^r M_j^r} \tag{17.512}$$

where $j$ represents the $j^{th}$ item (either a reactant or a product).

Momentum transfer for the phases is then given by:

$$S_1^{\vec{u}} = \mathcal{R}(cM_c\vec{u}_{net} - aM_a\vec{u}_1) \tag{17.513}$$

Release 15.0 - © SAS IP, Inc. All rights reserved. - Contains proprietary and confidential information of ANSYS, Inc. and its subsidiaries and affiliates.

$$S_2^{\vec{u}} = \mathcal{R}(dM_d\vec{u}_{net} - bM_b\vec{u}_2) \tag{17.514}$$

The general expression is

$$S_i^{\vec{u}} = S_{p_i}\vec{u}_{net} - \mathcal{R}\sum_{r_i}\gamma_j^r M_j^r \vec{u}_i \tag{17.515}$$

If we assume that there is no momentum transfer, then the above term will be zero.

### 17.8.2.1.3. Species Transfer

The general expression for source for $k^{th}$ species in the $j^{th}$ phase is

$$S_{r_i^k} = -\mathcal{R}\sum_{r_i^k}\gamma_j^{r^k} M_j^{r^k} \tag{17.516}$$

$$S_{p_i^k} = \mathcal{R}\sum_{p_i^k}\gamma_j^{p^k} M_j^{p^k} \tag{17.517}$$

$$S_i^k = S_{p_i^k} + S_{r_i^k} \tag{17.518}$$

### 17.8.2.1.4. Heat Transfer

For heat transfer, we need to consider the formation enthalpies of the reactants and products as well:

The net enthalpy of the reactants is given by:

$$H_{net} = \frac{aM_a\left(H_a + h_a^f\right) + bM_b\left(H_b + h_b^f\right)}{aM_a + bM_b} \tag{17.519}$$

where $h^f$ represents the formation enthalpy, and $H$ represents the enthalpy.

The general expression for $H_{net}$ is:

$$H_{net} = \frac{\sum_r \gamma_j^r M_j^r\left(H_j^r + h^{f^r}{}_j\right)}{\sum_r \gamma_j^r M_j^r} \tag{17.520}$$

If we assume that this enthalpy gets distributed to the products in the ratio of their mass production rates, heat transfer for the phases are given by:

$$S_1^H = \mathcal{R}\left(cM_cH_{net} - aM_aH^a - cM_ch_f^c\right) \tag{17.521}$$

$$S_2^H = \mathcal{R}\left(dM_dH_{net} - bM_bH^b - dM_dh_f^d\right) \tag{17.522}$$

The last term in the above equations appears because our enthalpy is with reference to the formation enthalpy.

The general expression for the heat source is:


Release 15.0 - © SAS IP, Inc. All rights reserved. - Contains proprietary and confidential information of ANSYS, Inc. and its subsidiaries and affiliates.

$$S_i^H = S_{p_i} H_{net} - \mathcal{R}\left( \sum_{r_i} \gamma_j^r M_j^r H_j^r + \sum_{p_i} \gamma_j^p M_j^p h^{f\,p}_{\;j} \right) \tag{17.523}$$

If we assume that there is no heat transfer, we can assume that the different species only carry their formation enthalpies with them. Thus the expression for $H_{net}$ will be:

$$H_{net} = \frac{\sum_r \gamma_j^r M_j^r h^{f\,r}_{\;j}}{\sum_r \gamma_j^r M_j^r} \tag{17.524}$$

The expression $S_i^H$ will be

$$S_i^H = S_{p_i} H_{net} - \mathcal{R} \sum_{p_i} \gamma_j^p M_j^p h^{f\,p}_{\;j} \tag{17.525}$$

## 17.8.3. The Stiff Chemistry Solver

ANSYS Fluent has the option of solving intraphase and interphase chemical reactions with a stiff chemistry solver. This option is only available for unsteady cases, where a fractional step scheme is applied. In the first fractional step, the multiphase species Equation 17.504 (p. 595) is solved spatially with the reaction term $R_i^q$ set to zero. In the second fractional step, the reaction term is integrated in every cell using a stiff ODE solver. To use this option, refer to Specifying Heterogeneous Reactions in the User's Guide.

## 17.8.4. Heterogeneous Phase Interaction

To compute the heterogeneous phase interaction rates, a modified Arrhenius type rate expression is provided, which you can define using the graphical user interface (see Specifying Heterogeneous Reactions in the User's Guide), or a user-defined function (see `DEFINE_HET_RXN_RATE` in the UDF Manual).

The rate expression is in the general form:

$$Rate = k \Pi_{i=1}^{NR} \left( \frac{Y_i \rho_{ip} VOF_{ip}}{MW_i} \right)^{st} kmol/m^3 - sec \tag{17.526}$$

where

$$k = A \left( \frac{T_{ip}}{T_{ref}} \right)^b exp\left( \frac{-E}{RT_{ip}} \right) \tag{17.527}$$

Here, $Y_i$ is the $i^{th}$ species mass fraction, $NR$ is the total number of reactants in a given inter-phase reaction, $\rho_{ip}$ is the bulk density of the phase $ip$, $VOF_{ip}$ is the volume fraction of the phase $ip$, $MW_i$ the molecular weight (kg/kmol) of the reactant species, $st$ is the stoichiometric coefficient of the reactant in the given reaction, and $k$ is the rate constant.

The rate constant in the modified Arrhenius form is given by Equation 17.527 (p. 599). $T_{ip}$ is the phase temperature (phase-1, phase-2, and so on) as required by the expression. Make sure you provide the

Release 15.0 - © SAS IP, Inc. All rights reserved. - Contains proprietary and confidential information of ANSYS, Inc. and its subsidiaries and affiliates.

correct phase for the temperature to be extracted. Usually, $T_{ref}$ is set to unity for most reactions, but certain reaction rate constants may have a given $T_{ref}$ value, which is normally 298.15 K.

The reaction rate given in Equation 17.527 (p. 599) will be valid above the kick-off temperature specified by you, where the temperature for the rate calculation is taken from the selected phase.


Release 15.0 - © SAS IP, Inc. All rights reserved. - Contains proprietary and confidential information of ANSYS, Inc. and its subsidiaries and affiliates.

# Chapter 18: Solidification and Melting

This chapter describes how you can model solidification and melting in ANSYS Fluent. For information about using the model, see Modeling Solidification and Melting of the User's Guide. Information about the theory behind the model is organized into the following sections:


18.1. Overview
18.2. Limitations
18.3. Introduction
18.4. Energy Equation
18.5. Momentum Equations
18.6. Turbulence Equations
18.7. Species Equations
18.8. Back Diffusion
18.9. Pull Velocity for Continuous Casting
18.10. Contact Resistance at Walls
18.11. Thermal and Solutal Buoyancy


## 18.1. Overview

ANSYS Fluent can be used to solve fluid flow problems involving solidification and/or melting taking place at one temperature (for example, in pure metals) or over a range of temperatures (for example, in binary alloys). Instead of tracking the liquid-solid front explicitly, ANSYS Fluent uses an enthalpy-porosity formulation. The liquid-solid mushy zone is treated as a porous zone with porosity equal to the liquid fraction, and appropriate momentum sink terms are added to the momentum equations to account for the pressure drop caused by the presence of solid material. Sinks are also added to the turbulence equations to account for reduced porosity in the solid regions.

ANSYS Fluent provides the following capabilities for modeling solidification and melting:

- calculation of liquid-solid solidification/melting in pure metals as well as in binary alloys
- modeling of continuous casting processes (that is, "pulling" of solid material out of the domain)
- modeling of the thermal contact resistance between solidified material and walls (for example, due to the presence of an air gap)
- modeling of species transport with solidification/melting
- postprocessing of quantities related to solidification/melting (that is, liquid fraction and pull velocities)

These modeling capabilities allow ANSYS Fluent to simulate a wide range of solidification/melting problems, including melting, freezing, crystal growth, and continuous casting. The physical equations used for these calculations are described in Introduction (p. 602), and instructions for setting up and solving a solidification/melting problem are provided in Modeling Solidification and Melting of the User's Guide.


Release 15.0 - © SAS IP, Inc. All rights reserved. - Contains proprietary and confidential information of ANSYS, Inc. and its subsidiaries and affiliates.

## 18.2. Limitations

As mentioned in Overview (p. 601), the formulation in ANSYS Fluent can be used to model the solidification/melting of pure materials, as well as alloys. In the case of alloys, ANSYS Fluent offers two rules to determine the liquid fraction versus temperature relationship, namely the linear Lever rule and the non-linear Scheil rule.

The following limitations apply to the solidification/melting model in ANSYS Fluent:

- The solidification/melting model can be used only with the pressure-based solver; it is not available with the density-based solvers.
- The solidification/melting model cannot be used for compressible flows.
- Of the general multiphase models (VOF, mixture, and Eulerian), only the VOF model can be used with the solidification/melting model.
- With the exception of species diffusivities, you cannot specify separate material properties for the solid and liquid materials through the GUI. However, if needed, separate solid and liquid properties can be specified with user-defined functions using the DEFINE_PROPERTY macro. For details on using the DEFINE_PROPERTY macro, refer to DEFINE_PROPERTY UDFs in the UDF Manual.
- When using the solidification/melting model in conjunction with modeling species transport with reactions, there is no mechanism to restrict the reactions to only the liquid region; that is, the reactions are solved everywhere.

## 18.3. Introduction

An enthalpy-porosity technique [468] (p. 754), [470] (p. 755), [471] (p. 755) is used in ANSYS Fluent for modeling the solidification/melting process. In this technique, the melt interface is not tracked explicitly. Instead, a quantity called the liquid fraction, which indicates the fraction of the cell volume that is in liquid form, is associated with each cell in the domain. The liquid fraction is computed at each iteration, based on an enthalpy balance.

The mushy zone is a region in which the liquid fraction lies between 0 and 1. The mushy zone is modeled as a "pseudo" porous medium in which the porosity decreases from 1 to 0 as the material solidifies. When the material has fully solidified in a cell, the porosity becomes zero and hence the velocities also drop to zero.

In this section, an overview of the solidification/melting theory is given. Refer to Voller and Prakash [471] (p. 755) for details on the enthalpy-porosity method.

## 18.4. Energy Equation

The enthalpy of the material is computed as the sum of the sensible enthalpy, $h$, and the latent heat, $\Delta H$:

$$H = h + \Delta H \tag{18.1}$$

where

$$h = h_{ref} + \int_{T_{ref}}^{T} c_p dT \tag{18.2}$$


Release 15.0 - © SAS IP, Inc. All rights reserved. - Contains proprietary and confidential information of ANSYS, Inc. and its subsidiaries and affiliates.

and

$h_{ref}$ = reference enthalpy

$T_{ref}$ = reference temperature

$c_p$ = specific heat at constant pressure

The liquid fraction, $\beta$, can be defined as

$$\begin{aligned} &\beta = 0 && \text{if} \quad T < T_{solidus} \\ &\beta = 1 && \text{if} \quad T > T_{liquidus} \\ &\beta = \frac{T - T_{solidus}}{T_{liquidus} - T_{solidus}} && \text{if} \quad T_{solidus} < T < T_{liquidus} \end{aligned} \tag{18.3}$$

The latent heat content can now be written in terms of the latent heat of the material, $L$:

$$\Delta H = \beta L \tag{18.4}$$

The latent heat content can vary between zero (for a solid) and $L$ (for a liquid).

For solidification/melting problems, the energy equation is written as

$$\frac{\partial}{\partial t}(\rho H) + \nabla \cdot (\rho \vec{v} H) = \nabla \cdot (k \nabla T) + S \tag{18.5}$$

where

$H$ = enthalpy (see Equation 18.1 (p. 602))

$\rho$ = density

$\vec{v}$ = fluid velocity

$S$ = source term

The solution for temperature is essentially an iteration between the energy equation (Equation 18.5 (p. 603)) and the liquid fraction equation (Equation 18.3 (p. 603)). Directly using Equation 18.3 (p. 603) [472] (p. 755) to update the liquid fraction usually results in poor convergence of the energy equation. In ANSYS Fluent, the method suggested by Voller and Swaminathan is used to update the liquid fraction. For pure metals, where $T_{solidus}$ and $T_{liquidus}$ are equal, a method based on specific heat, given by Voller and Prakash [471] (p. 755), is used instead.

## 18.5. Momentum Equations

The enthalpy-porosity technique treats the mushy region (partially solidified region) as a porous medium. The porosity in each cell is set equal to the liquid fraction in that cell. In fully solidified regions, the porosity is equal to zero, which extinguishes the velocities in these regions. The momentum sink due to the reduced porosity in the mushy zone takes the following form:

$$S = \frac{(1-\beta)^2}{\left(\beta^3 + \varepsilon\right)} A_{mush} \left(\vec{v} - \vec{v}_p\right) \tag{18.6}$$

Release 15.0 - © SAS IP, Inc. All rights reserved. - Contains proprietary and confidential information of ANSYS, Inc. and its subsidiaries and affiliates.

where $\beta$ is the liquid volume fraction, $\varepsilon$ is a small number (0.001) to prevent division by zero, $A_{mush}$ is the mushy zone constant, and $\vec{v}_p$ is the solid velocity due to the pulling of solidified material out of the domain (also referred to as the pull velocity).

The mushy zone constant measures the amplitude of the damping; the higher this value, the steeper the transition of the velocity of the material to zero as it solidifies. Very large values may cause the solution to oscillate.

The pull velocity is included to account for the movement of the solidified material as it is continuously withdrawn from the domain in continuous casting processes. The presence of this term in Equation 18.6 (p. 603) allows newly solidified material to move at the pull velocity. If solidified material is not being pulled from the domain, $\vec{v}_p = 0$. More details about the pull velocity are provided in Pull Velocity for Continuous Casting (p. 607).

## 18.6. Turbulence Equations

Sinks are added to all of the turbulence equations in the mushy and solidified zones to account for the presence of solid matter. The sink term is very similar to the momentum sink term (Equation 18.6 (p. 603)):

$$S = \frac{(1-\beta)^2}{\left(\beta^3+\varepsilon\right)} A_{mush}\phi \tag{18.7}$$

where $\phi$ represents the turbulence quantity being solved ($k$, $\varepsilon$, $\omega$, and so on), and the mushy zone constant, $A_{mush}$, is the same as the one used in Equation 18.6 (p. 603).

## 18.7. Species Equations

For solidification and melting of a pure substance, phase change occurs at a distinct melting temperature, $T_{melt}$. For a multicomponent mixture, however, a mushy freeze/melt zone exists between a lower solidus and an upper liquidus temperature. When a multicomponent liquid solidifies, solutes diffuse from the solid phase into the liquid phase. This effect is quantified by the partition coefficient of solute $i$, denoted $K_i$, which is the ratio of the mass fraction in the solid to that in the liquid at the interface.

ANSYS Fluent computes the solidus and liquidus temperatures in a species mixture as,

$$T_{solidus} = T_{melt} + \sum_{solutes} m_i Y_i / K_i \tag{18.8}$$

$$T_{liquidus} = T_{melt} + \sum_{solutes} m_i Y_i \tag{18.9}$$

where $K_i$ is the partition coefficient of solute $i$, $Y_i$ is the mass fraction of solute $i$, and $m_i$ is the slope of the liquidus surface with respect to $Y_i$. If the value of the mass fraction $Y_i$ exceeds the value of the eutectic mass fraction $Y_{i,\mathrm{Eut}}$, then $Y_i$ is clipped to $Y_{i,\mathrm{Eut}}$ when calculating the liquidus and solidus temperatures. It is assumed that the last species material of the mixture is the solvent and that the other species are the solutes.


Release 15.0 - © SAS IP, Inc. All rights reserved. - Contains proprietary and confidential information of ANSYS, Inc. and its subsidiaries and affiliates.

ANSYS Fluent expects that you will input a negative value for the liquidus slope of species $i$ ($m_i$). If you input a positive slope for $m_i$, ANSYS Fluent will disregard your input and instead calculate it using the Eutectic temperature $T_{\text{Eut}}$ and the Eutectic mass fraction $Y_{i,\text{Eut}}$:

$$m_i = \frac{T_{Eut} - T_{melt}}{Y_{i,Eut}} \tag{18.10}$$

Updating the liquid fraction via Equation 18.3 (p. 603) can cause numerical errors and convergence difficulties in multicomponent mixtures. Instead, the liquid fraction is updated as,

$$\beta^{n+1} = \beta^n - \lambda \frac{a_p (T - T^*)\, \Delta t}{\rho V L - a_p \Delta t L \frac{\partial T^*}{\partial \beta}} \tag{18.11}$$

where the superscript $n$ indicates the iteration number, $\lambda$ is a relaxation factor with a default value of 0.9, $a_p$ is the cell matrix coefficient, $\Delta t$ is the time-step, $\rho$ is the current density, $V$ is the cell volume, $T$ is the current cell temperature and $T^*$ is the interface temperature.

ANSYS Fluent offers two models for species segregation at the micro-scale, namely the Lever rule and the Scheil rule. The former assumes infinite diffusion of the solute species in the solid, and the latter assumes zero diffusion. For the Lever rule, the interface temperature $T^*$, is calculated as:

$$T^* = T_{\text{melt}} + \sum_{i=0}^{N_s - 1} m_i \left( \frac{Y_i}{K_i + \beta (1 - K_i)} \right) \tag{18.12}$$

where $N_s$ is the number of species.

The Scheil rule evaluates $T^*$ as:

$$T^* = T_{\text{melt}} + \sum_{i=0}^{N_s - 1} m_i Y_i \beta^{K_i - 1} \tag{18.13}$$

For information about how back diffusion (that is, a finite amount of diffusion of the solute species) can be incorporated into the formulation, see the section that follows.

For the Lever rule, species transport equations are solved for the total mass fraction of species $i$, $Y_i$:

$$\frac{\partial}{\partial t}(\rho Y_i) + \nabla \cdot \left( \rho \left[ \beta \vec{v}_{liq} Y_{i,liq} + (1 - \beta) \vec{v}_p Y_{i,sol} \right] \right) = -\nabla \cdot \vec{J}_i + R_i \tag{18.14}$$

where $R_i$ is the reaction rate and $\vec{J}_i$ is given by

$$\vec{J}_i = -\rho \left[ \beta D_{i,m,liq} \nabla Y_{i,liq} + (1 - \beta) D_{i,m,sol} \nabla Y_{i,sol} \right] \tag{18.15}$$

$\vec{v}_{liq}$ is the velocity of the liquid and $\vec{v}_p$ is the solid (pull) velocity. $\vec{v}_p$ is set to zero if pull velocities are not included in the solution. The liquid velocity can be found from the average velocity (as determined by the flow equation) as

$$\vec{v}_{liq} = \frac{\left( \vec{v} - \vec{v}_p (1 - \beta) \right)}{\beta} \tag{18.16}$$

Release 15.0 - © SAS IP, Inc. All rights reserved. - Contains proprietary and confidential information of ANSYS, Inc. and its subsidiaries and affiliates.

The liquid ($Y_{i,liq}$) and solid ($Y_{i,sol}$) mass fractions are related to each other by the partition coefficient $K_i$:

$$Y_{i,sol}=K_i Y_{i,liq} \tag{18.17}$$

When the Scheil model is selected, ANSYS Fluent solves for $Y_{i,liq}$ as the dependent variable [469] (p. 755):

$$\begin{aligned}\frac{\partial}{\partial t}\left(\rho Y_{i,liq}\right)+\nabla\cdot\left(\rho\left[\beta\vec{v}_{liq}Y_{i,liq}+(1-\beta)\vec{v}_{p}Y_{i,sol}\right]\right) &= R_i \\ &+\nabla\cdot\left(\rho\beta D_{i,m,liq}\nabla Y_{i,liq}\right) \\ &-K_i Y_{i,liq}\frac{\partial}{\partial t}(\rho(1-\beta)) \\ &+\frac{\partial}{\partial t}\left(\rho(1-\beta)Y_{i,liq}\right)\end{aligned} \tag{18.18}$$

## 18.8. Back Diffusion

The Scheil rule assumes zero solute diffusion in the solid zone, while the Lever rule assumes infinite solute diffusion in the solid. Back diffusion models a finite solid diffusion at the micro level using a non-dimensional parameter (denoted by $\gamma$) between 0 (no diffusion, as in the Scheil rule) and 1 (infinite diffusion, as in the Lever Rule). $\gamma$ typically depends on the solidification conditions such as the solid diffusivity, the local solidification time, and the secondary dendritic arm spacing. The interface temperature is calculated as follows:

$$T^{*}=T_{\text{melt}}+\sum_{i=0}^{N_s-1}m_i Y_i\left(1-(1-\gamma K_i)(1-\beta)\right)^{\frac{K_i-1}{1-\gamma K_i}} \tag{18.19}$$

When back diffusion is included with the Scheil rule formulation, the species transport equation is solved with the liquid species mass fraction as the dependent variable:

$$\begin{aligned}\frac{\partial(\rho Y_{i,\text{liq}})}{\partial t}+\nabla\cdot\left(\rho\left[\beta\vec{v}\,Y_{i,\text{liq}}+(1-\beta)\vec{v}_p Y_{i,\text{sol}}\right]\right) &= R_i \\ &+\nabla\cdot(\rho\beta D_{i,m,\text{liq}}\nabla Y_{i,\text{liq}}) \\ &-K_i Y_{i,\text{liq}}\frac{\partial(\rho(1-\beta))}{\partial t} \\ &+\frac{\partial(\rho(1-\beta)Y_{i,\text{liq}})}{\partial t} \\ &-\gamma(1-\beta)\frac{\partial(\rho Y_{i,\text{liq}})}{\partial t}\end{aligned} \tag{18.20}$$

The total species mass fraction and liquid species mass fraction are related as

$$Y_{i,\text{sol}}=K_i Y_i\left[1-(1-\gamma K_i)(1-\beta)\right]^{\frac{K_i-1}{1-\gamma K_i}}=K_i Y_{i,\text{liq}} \tag{18.21}$$


Release 15.0 - © SAS IP, Inc. All rights reserved. - Contains proprietary and confidential information of ANSYS, Inc. and its subsidiaries and affiliates.

## 18.9. Pull Velocity for Continuous Casting

In continuous casting processes, the solidified matter is usually continuously pulled out from the computational domain, as shown in Figure 18.1: "Pulling" a Solid in Continuous Casting (p. 607). Consequently, the solid material will have a finite velocity that must be accounted for in the enthalpy-porosity technique.

**Figure 18.1: "Pulling" a Solid in Continuous Casting**

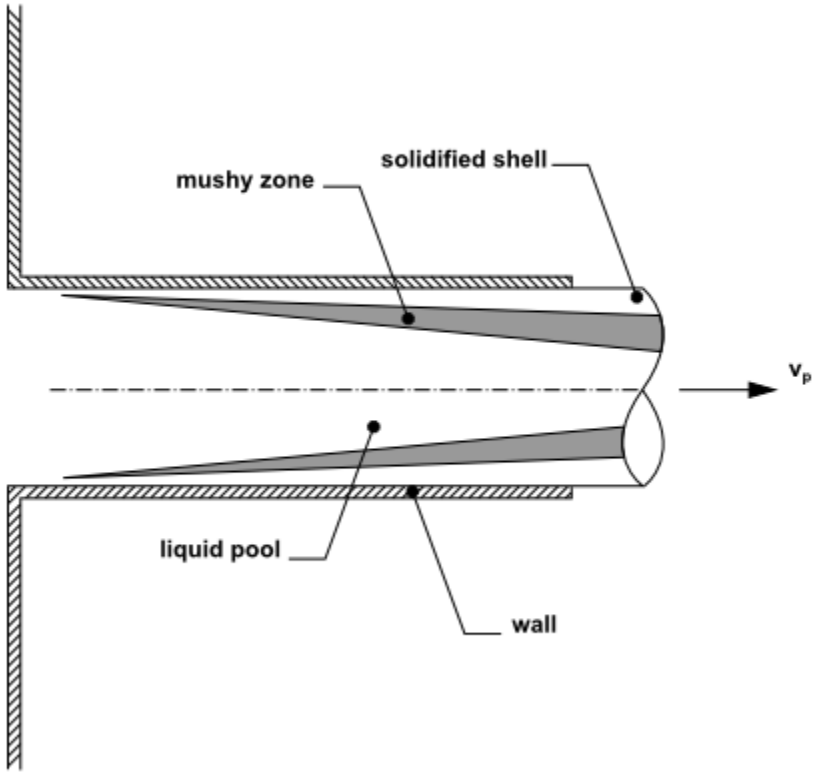


As mentioned in Momentum Equations (p. 603), the enthalpy-porosity approach treats the solid-liquid mushy zone as a porous medium with porosity equal to the liquid fraction. A suitable sink term is added in the momentum equation to account for the pressure drop due to the porous structure of the mushy zone. For continuous casting applications, the relative velocity between the molten liquid and the solid is used in the momentum sink term (Equation 18.6 (p. 603)) rather than the absolute velocity of the liquid.

The exact computation of the pull velocity for the solid material is dependent on Young's modulus and Poisson's ratio of the solid and the forces acting on it. ANSYS Fluent uses a Laplacian equation to approximate the pull velocities in the solid region based on the velocities at the boundaries of the solidified region:

$$\nabla^2 \vec{v}_p = 0 \tag{18.22}$$

ANSYS Fluent uses the following boundary conditions when computing the pull velocities:

- At a velocity inlet, a stationary wall, or a moving wall, the specified velocity is used.
- At all other boundaries (including the liquid-solid interface between the liquid and solidified material), a zero-gradient velocity is used.

The pull velocities are computed only in the solid region.

Release 15.0 - © SAS IP, Inc. All rights reserved. - Contains proprietary and confidential information of ANSYS, Inc. and its subsidiaries and affiliates.

Note that ANSYS Fluent can also use a specified constant value or custom field function for the pull velocity, instead of computing it. See Procedures for Modeling Continuous Casting of the User's Guide for details.

## 18.10. Contact Resistance at Walls

ANSYS Fluent's solidification/melting model can account for the presence of an air gap between the walls and the solidified material, using an additional heat transfer resistance between walls and cells with liquid fractions less than 1. This contact resistance is accounted for by modifying the conductivity of the fluid near the wall. Thus, the wall heat flux, as shown in Figure 18.2: Circuit for Contact Resistance (p. 608), is written as

$$q = \frac{(T - T_w)}{(l/k + R_c(1-\beta))} \tag{18.23}$$

where $T$, $T_w$, and $l$ are defined in Figure 18.2: Circuit for Contact Resistance (p. 608), $k$ is the thermal conductivity of the fluid, $\beta$ is the liquid volume fraction, and $R_c$ is the contact resistance, which has the same units as the inverse of the heat transfer coefficient.

**Figure 18.2: Circuit for Contact Resistance**

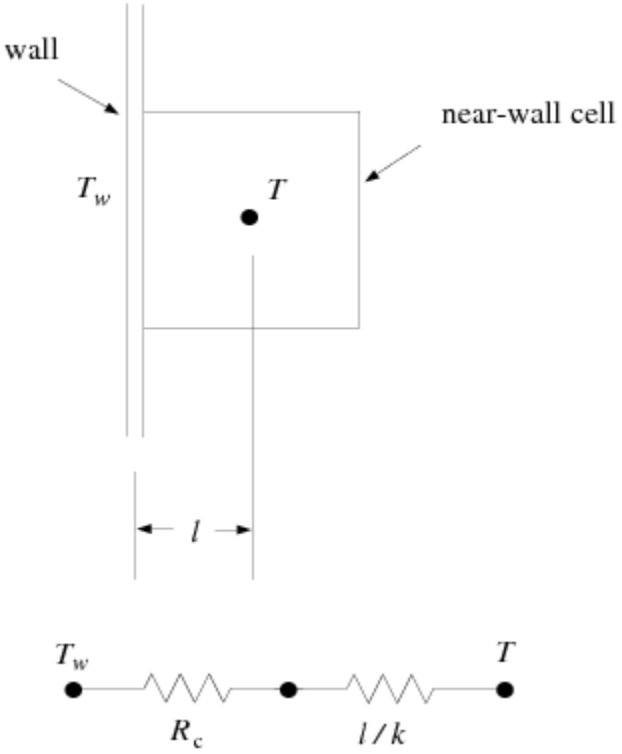


## 18.11. Thermal and Solutal Buoyancy

When multiple species are involved in the solidification/melting process, the density of the liquid pool varies with temperature as well as species composition. In the presence of a gravitational field, buoyancy will be induced by two mechanisms:

- **Thermal buoyancy**: is the gravitational force due to the variation of density with temperature.


Release 15.0 - © SAS IP, Inc. All rights reserved. - Contains proprietary and confidential information of ANSYS, Inc. and its subsidiaries and affiliates.

- **Solutal buoyancy**: is the gravitational force due to the variation of density with the change in the species composition of the melt. In multi-component solidification problems, the solutes are continuously rejected near the liquid solid interface, leading to the enrichment of the liquid pool with the solutes. This enrichment of the solutes causes a concentration gradient in the immediate vicinity of the solid-liquid interface, and consequently a density gradient.

Modeling of thermal and solutal buoyancy is often important for the accurate prediction of the overall solidification behavior. The flow due to thermal buoyancy tends to promote mixing and smooths out temperature gradients. Therefore, excluding this term can lead to inaccurate predictions of solidification time. Solutal buoyancy moves the enriched liquid away from the liquid-solid interface and replaces it with the far field nominal composition liquid. Excluding solutal buoyancy can lead to an over prediction of segregation patterns for multi-component materials.

For multi-component solidification problems, the buoyancy induced flows are modeled in ANSYS Fluent using the Boussinesq approach. The thermal buoyancy is calculated as described in Natural Convection and Buoyancy-Driven Flows Theory (p. 137). The body forces due to solutal buoyancy are calculated using a similar approach:

$$\vec{F}_s = \rho_{ref}\vec{g}\sum_{i=0}^{N_s}\beta_{s,i}\left(y_{l,i}-y_{ref,i}\right) \tag{18.24}$$

where $y_{l,i}$ is the mass fraction of the $i$th solute in the liquid phase and $y_{ref,i}$ is the reference mass fraction of the $i^{\text{th}}$ species. $\beta_{s,i}$ is the solutal expansion coefficient of the $i^{\text{th}}$ species and $N_s$ is the total number of solute species, $g$ is the gravity vector, and $\rho_{ref}$ is the reference density.

The total body force is the sum of the solutal and thermal buoyancy, which can have similar or opposite signs, and their relative importance can change significantly during the course of the simulation.

Refer to Modeling Thermal and Solutal Buoyancy in the User's Guide to learn how to include thermal and solutal buoyancy.

Release 15.0 - © SAS IP, Inc. All rights reserved. - Contains proprietary and confidential information of ANSYS, Inc. and its subsidiaries and affiliates.

Release 15.0 - © SAS IP, Inc. All rights reserved. - Contains proprietary and confidential information
of ANSYS, Inc. and its subsidiaries and affiliates.

# Chapter 19: Eulerian Wall Films

The Eulerian Wall Film (EWF) model can be used to predict the creation and flow of thin liquid films on the surface of walls. This chapter presents an overview of the theory and the governing equations for the methods used in the Eulerian Wall Film (EWF) model.

19.1. Introduction
19.2. Mass, Momentum, and Energy Conservation Equations for Wall Film
19.3. Numerical Schemes and Solution Algorithm

For more information about using the Eulerian Wall Film model, see Modeling Eulerian Wall Films in the User's Guide.

## 19.1. Introduction

The fundamental picture of a film model consists of a two dimensional thin film of liquid on a wall surface, as shown in Figure 19.1: Subgrid Processes That Require a Wall Film Model (p. 611). A thin liquid film forms as liquid drops impinge on a solid surface in the domain. There are several possible outcomes from this impingement: *stick*, where the droplet impacts the wall with little energy and remains nearly spherical; *rebound*, where the drop leaves the surface relatively intact but with changed velocity; *spread*, where the drop hits the wall with moderate energy and spreads out into the film; and *splash*, where part of the impinging drop joins the film and another part of the drop leaves the wall in several other smaller drops.

The thin film assumption is one usually made in both Eulerian and Lagrangian film modeling approaches, specifically that the thickness of the film is small compared to the radius of curvature of the surface so that the properties do not vary across the thickness of the film and that films formed are thin enough so that the liquid flow in the film can be considered parallel to the wall, with an assumed quadratic shape. Further modeling assumptions are needed to close the problem.

**Figure 19.1: Subgrid Processes That Require a Wall Film Model**

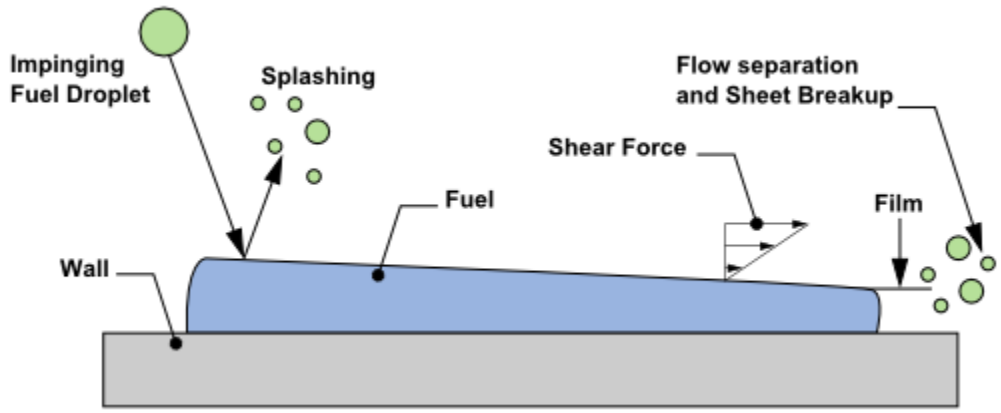


Release 15.0 - © SAS IP, Inc. All rights reserved. - Contains proprietary and confidential information of ANSYS, Inc. and its subsidiaries and affiliates.

## 19.2. Mass, Momentum, and Energy Conservation Equations for Wall Film

Conservation of mass for a two dimensional film in a three dimensional domain is:

$$\frac{\partial h}{\partial t}+\nabla_s\cdot[h\vec{V}_l]=\frac{\dot{m}_s}{\rho_l} \tag{19.1}$$

where $\rho_l$ is the liquid density, $h$ the film height, $\nabla_s$ the surface gradient operator, $\vec{V}_l$ the mean film velocity and $\dot{m}_s$ the mass source per unit wall area due to droplet collection, film separation, film stripping, and phase change.

Conservation of film momentum is given,

$$\frac{\partial h\vec{V}_l}{\partial t}+\nabla_s\cdot(h\vec{V}_l\vec{V}_l)=-\frac{h\nabla_s P_L}{\rho_l}+(\vec{g}_\tau)h+\frac{3}{2\rho_l}\vec{\tau}_{fs}-\frac{3\nu_l}{h}\vec{V}_l+\frac{\dot{q}}{\rho_l} \tag{19.2}$$

where

$$P_L=P_{gas}+P_h+P_\sigma$$
$$P_h=-\rho h(\vec{n}\cdot\vec{g})$$
$$P_\sigma=-\sigma\nabla_s\cdot(\nabla_s h)$$

The terms on the left hand side of Equation 19.2 (p. 612) represent transient and convection effects, respectively. On the right hand side, the first term includes the effects of gas-flow pressure, the gravity component normal to the wall surface (known as *spreading*), and surface tension; the second term represents the effect of gravity in the direction parallel to the film; the third term is the viscous shear force at the gas-film interface; the fourth term represents the viscous force in the film, and the last term is associated with droplet collection or separation. Note that in arriving at the shear and viscous terms on the RHS, a parabolic film velocity profile has been assumed.

Conservation of film energy is given as:

$$\begin{aligned}\frac{\partial(hT_f)}{\partial t}+\nabla_s\cdot(\vec{V}_f hT_f) &=\frac{1}{\rho C_P}\left\{k_f\left[\frac{T_s-T_f}{h/2}-\frac{T_f-T_w}{h/2}\right]+\dot{q}_{imp}+\dot{m}_{vap}L(T_s)\right\}\\ &=\frac{1}{\rho C_P}\left\{2k_f\left[\frac{T_s+T_w}{h}-\frac{2T_f}{h}\right]+\dot{q}_{imp}+\dot{m}_{vap}L(T_s)\right\}\end{aligned} \tag{19.3}$$

In the above equation, $T_s$ is the temperature at the film-gas interface; $T_f$ is the average film temperature and it is the dependent variable of the above equation; $T_w$ the wall temperature; It is clear that a piecewise linear profile has been assumed: the film temperature varies from $T_w$ to $T_f$ in the lower half of the film and from $T_f$ to $T_s$ in the upper half. $\dot{q}_{imp}$ is the source term due to liquid impingement from the bulk flow to the wall. $\dot{m}_{vap}$ is the mass vaporization or condensation rate and $L$ is the latent heat associated with the phase change.

Equation 19.1 (p. 612) and Equation 19.2 (p. 612) form the foundation of EWF modeling, with the solution of Equation 19.3 (p. 612) being optional only when thermal modeling is desired. These equations are solved on the surface of a wall boundary. Since the film considered here is thin, the lubrication approx-


Release 15.0 - © SAS IP, Inc. All rights reserved. - Contains proprietary and confidential information of ANSYS, Inc. and its subsidiaries and affiliates.

imation (parallel flow) is valid and therefore these equations are solved in local coordinates that are parallel to the surface.

Subsequent sections present the EWF sub-models and numerical solution procedures adopted in ANSYS Fluent.

## 19.2.1. Film Sub-Models

The Eulerian wall film model can interact with the discrete phase model (DPM) and Eulerian multiphase model through source terms to the film equations. During the interaction with the DPM model, the discrete particles are collected to form a wall film. The discrete particles can splash when interacting with a film boundary, creating additional particles in the same way as described in the Lagrangian film model. Additional particles can be created when the film separates from the wall, or when the shear stress is sufficient that large particles can be stripped from the film. Mass leaving the film surface by separation or stripping is accounted for through source terms to the film equations. In the Eulerian multiphase interaction, a secondary phase in the multiphase flow is captured on solid surfaces, forming liquid films. Collection efficiency can be computed for the solid surfaces. Mass and momentum leaving the liquid film due to separation and stripping is added to the secondary phase in the multiphase flow.

### 19.2.1.1. DPM Collection

Discrete particle streams or discrete particles hitting a face on a wall boundary are absorbed into the film. When particles are absorbed, their mass and momentum are added to the source terms in Equation 19.1 (p. 612) and Equation 19.2 (p. 612), continuity and momentum equations, respectively. The mass source term is given by

$$\dot{m}_s = \dot{m}_p \tag{19.4}$$

where $\dot{m}_p$ is the flow rate of the particle stream impinging on the face. The momentum source term is

$$\dot{\vec{q}}_s = \dot{m}_p \cdot (\vec{V}_p - \vec{V}_l) \tag{19.5}$$

where $\vec{V}_p$ denotes the velocity of the particle stream and $\vec{V}_l$ denotes the film velocity.

### 19.2.1.2. Splashing

During the interaction with the DPM model, the discrete particles are collected to form a wall film. The discrete particles can splash when interacting with a film boundary, creating additional particles in the same way as described in the Lagrangian film model (Splashing (p. 416)).

### 19.2.1.3. Film Separation

The film can separate from an edge if two criteria are met – first that the angle between faces is sufficiently large and second if the film inertia is above a critical value (defined by you). If separation occurs, a source term in the film equation is used to remove mass and momentum from the face corresponding to the edge upstream of where the separation occurs. This source term is accumulated at each film time step, and particle streams are created at DPM iterations using this source. New particle streams are created only during the DPM iteration, however the source terms due to film separating from an edge are updated each film step.

Release 15.0 - © SAS IP, Inc. All rights reserved. - Contains proprietary and confidential information of ANSYS, Inc. and its subsidiaries and affiliates.

#### 19.2.1.3.1. Separation Criteria

Based on the work by Foucart, separation can occur at an edge if a critical angle, $\theta$, is exceeded and a Weber number based on the film, $We_f$, is above a minimum value.

The Weber number is defined as,

$$We_f = \frac{\rho_l h |\vec{V}_l|^2}{\sigma} \tag{19.6}$$

and $\sigma$ is surface tension of the film. The separation criteria become,

$$\begin{cases} \theta > \theta_{critical} \\ We_f > We_{critical} \end{cases} \tag{19.7}$$

**Figure 19.2: Separation Criteria**

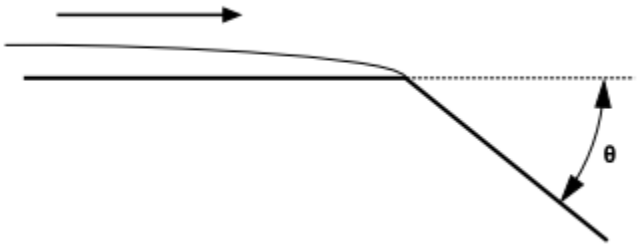


Once separation occurs, you can specify three different models to calculate the number and diameter of the shed particle stream at an edge, based on work by Foucart ([127] (p. 735)), O'Rourke ([331] (p. 747)) and Friedrich ([130] (p. 736)).

##### *19.2.1.3.1.1. Foucart Separation*

The Foucart model for edge separation assumes that the drop diameter is given by

$$d = \left( \frac{3h^2 l}{4\pi} \right)^{\frac{1}{3}} \tag{19.8}$$

where $l$ is the length of the edge and $h$ the height of the film. The flow rate $q$ of the particles from the film is equal to the mass flux of the film across the edge

$$q = V_l \bullet \hat{n}_e h l \rho_l \tag{19.9}$$

where $\hat{n}_e$ is the inward pointing normal from the edge centroid to the face center. The particles separated from an edge using Foucart's criterion are given the velocity of the film at the edge where the separation occurs.

##### *19.2.1.3.1.2. O'Rourke Separation*

The O'Rourke model for edge separation assumes that the drop diameter is equal to the height of the film at the edge, and the flow rate of the particles from the film is equal to the mass flux of the film across the edge.


Release 15.0 - © SAS IP, Inc. All rights reserved. - Contains proprietary and confidential information of ANSYS, Inc. and its subsidiaries and affiliates.

#### 19.2.1.3.1.3. Friedrich Separation

Friedrich's separation model assumes that the drop diameter is equal to the height of the film at the edge, but the flow rate of the particles from the film is calculated from an experimentally derived force ratio between the inertia of the film and the surface tension forces.

The force ratio is given by

$$F_{ratio} = \frac{We_f}{1 + {}^{1}/_{\sin(\theta)} + Fr_f We_f \left({}^{L_b}/_{h}\right)\left({}^{1}/_{\tan(\theta)}\right)} \tag{19.10}$$

where $Fr_f = \frac{gh}{V_l^2}$ and the characteristic breakup length $L_b$ is given by:

$$L_b = 0.0388 h^{0.5} \mathrm{Re}_h^{0.6} We_{rel}^{-0.5} \tag{19.11}$$

and the relative Weber number $We_{rel}$ and the film flow Reynolds number are defined as follows,

$$We_{rel} = \frac{\rho_{gas} h \left(V_{gas} - V_l\right)^2}{2\sigma} \tag{19.12}$$

$$\mathrm{Re}_h = \frac{\rho_f V_l h}{\mu_l} \tag{19.13}$$

Unlike the O'Rourke or Foucart separation methods, the mass flux into the particle stream is an experimentally derived percentage of the flux across the edge as given in Equation 19.9 (p. 614). The flux across the edge is assumed to be a function of the force ratio given by:

$$\gamma = 1 - \exp\left(0.411544\left(\frac{1 - F_{ratio}^2}{F_{ratio}}\right)\right) \tag{19.14}$$

which is a curve fit to the data in Friedrich, et.al. ([130] (p. 736)) and is valid for force ratios greater than one (that is, separated flows). If the force ratio in the Friedrich correlation is less than one, the curve fit is clipped to 0.05, implying that 5% of the film mass flux crossing the edge is shed into the particle phase if separation does take place.

### 19.2.1.4. Film Stripping

Film stripping occurs when high relative velocities exist between the gas phase and the liquid film on a wall surface. At sufficiently high shear rates, Kelvin-Helmholtz waves form on the surface of the film and grow, eventually stripping off droplets from the surface. The model for this behavior in the current implementation of the wall film model in ANSYS Fluent is based on work by Lopez de Bertodano, et al. ([267] (p. 743)) and Mayer ([285] (p. 744)).

As described in Mayer, in a thin liquid sheet in a shear flow, waves of length $\lambda$ are formed due a Kelvin-Helmholtz type of instability, but the waves are damped out by viscous forces in the film. The balance of wave growth and damping provides a term for the frequency $\omega$

$$\omega = \frac{f}{\lambda^{1/2}} - \frac{\nu}{\lambda^2} \tag{19.15}$$

where

$$f = \sqrt{\frac{\pi}{2}} \frac{\beta \rho_g V_g^2}{\sqrt{\sigma \rho_l}} \tag{19.16}$$

with $\beta$ as a sheltering parameter with a value of 0.3, and

$$v = \frac{8\pi^2 \mu_l}{\rho_l} \tag{19.17}$$

For waves to grow and eventually break off from the film, ω must be greater than zero which implies that the minimum wave length for growing waves should be:

$$0 = \frac{f}{\lambda^{1/2}} - \frac{v}{\lambda^2} \Rightarrow \lambda_{\min} = \left( \frac{v}{f} \right)^{2/3} = 2\pi \sqrt[3]{16} \left( \frac{\mu_l \sqrt{\sigma / \rho_l}}{\beta \rho_g V_g^2} \right)^{2/3} \tag{19.18}$$

An expression for frequency from Taylor's theory can be derived using linear stability analysis, and is given by Lopez de Bertodano et al [267] (p. 743)

$$\omega = 0.384 \frac{\rho_g U_g^3}{\sigma} \sqrt{\frac{\rho_g}{\rho_l}} \tag{19.19}$$

Following Mayer, the average droplet size of the stripped droplets is

$$\overline{d} = F \overline{\lambda} = F \cdot \frac{9}{2} \lambda_{\min} \tag{19.20}$$

where $F$ (with a default value of 0.14) is a numerical factor that is equivalent to the **Diameter Coefficient** in the graphical user interface.

To obtain a mass flow rate at the surface of the liquid, it is assumed that $\dot{m} \cong \frac{1}{2} \rho_l \overline{\lambda} \omega$ where $\overline{\lambda}$ is the average wavelength of the disturbance. Mayer uses the expression $\overline{\lambda} = 4.5 \lambda_{\min}$ which results in the following expression for the flow rate of drops stripped from the surface:

$$\dot{m} = C \frac{9}{2} \rho_l \omega \lambda_{\min} \tag{19.21}$$

where $C$ (with a default value of 0.5) is a numerical factor that is equivalent to the **Mass Coefficient** in the graphical user interface. Mass sources are accumulated during the course of the film calculation according to the above expression, and are injected into the free stream with the velocity of the film and the calculated mass flow rate from the face during the DPM iteration.

No mass will be taken from the film unless a minimum (critical) shear rate (defined in the graphical user interface) is exceeded on the face where liquid film exists.

### 19.2.1.5. Secondary Phase Accretion

In an Eulerian multiphase flow, the secondary phase to be collected on a solid surface must have the same material as defined in the Eulerian wall film model. When the secondary phase is captured by the wall surface, its mass and momentum are removed from the multiphase flow, and added as source terms to the continuity and momentum equations, Equation 19.1 (p. 612) and Equation 19.2 (p. 612) respectively, of the wall film.


Release 15.0 - © SAS IP, Inc. All rights reserved. - Contains proprietary and confidential information of ANSYS, Inc. and its subsidiaries and affiliates.

The mass source term is given by

$$\dot{m}_s = \alpha_d \rho_d V_{dn} A \tag{19.22}$$

where $\alpha_d$ is the secondary phase volume fraction, $\rho_d$ is the secondary phase density, $V_{dn}$ is the phase velocity normal to the wall surface, and $A$ is the wall surface area.

The momentum source is give by

$$\dot{\vec{q}}_s = \dot{m}_s \vec{V}_d \tag{19.23}$$

where $\vec{V}_d$ is the secondary phase velocity vector.

The collection efficiency of the secondary phase is computed as

$$\beta = \frac{\rho_d V_{dn}}{C_d V_d} \tag{19.24}$$

where $C_d$ and $V_d$ are the reference (far field) secondary phase concentration and velocity, respectively.

### 19.2.1.6. Coupling of Wall Film with Mixture Species Transport

The Eulerian wall film model can also be coupled with the mixture species transport model to consider phase changes between film material (liquid) and the gas species (vapor). The rate of phase change is governed by

$$\dot{m}_{phase} = \frac{(\rho D/\delta)}{\rho D/\delta + C_{phase}} C_{phase}(y_{sat} - y_i) \qquad \left[ kg/m^2 - s \right] \tag{19.25}$$

where $\rho$ is the density of the gas mixture, $D$ is the mass diffusivity of the vapor species, $\delta$ is the cell-center-to-wall distance, $C_{phase}$ is the phase change constant, and $y_i$ represents the cell-center mass fraction of the vapor species. The saturation species mass fraction is computed as

$$y_{sat} = \frac{P_{sat}(T)}{P} \frac{M_i}{\overline{M}} \tag{19.26}$$

where $P$ is the absolute pressure of the gas mixture and, $M_i$ and $\overline{M}$ is the molecular weight of the vapor species and the mixture, respectively. The saturation pressure $P_{sat}$ is a function of temperature only. By default, water vapor is assumed to be the vapor species and its saturation pressure is computed, following Springer et al ([431] (p. 752)), as

$$\begin{aligned} \log_{10} P_{sat} &= -2.1794 + 0.02953(T - 273.17) - 9.1837e^{-5}(T - 273.17)^2 \\ &\quad + 1.4454e^{-7}(T - 273.17)^3 \end{aligned} \tag{19.27}$$

However, you can replace the above default formulation by using a user-defined property when defining the vapor material in the **Materials** task page.

It is clear from Equation 19.25 (p. 617) that when the vapor mass fraction exceeds the saturation mass fraction, condensation takes place (that is, negative $\dot{m}_{phase}$) instead, when the vapor mass fraction is less than the saturation mass fraction, the liquid film vaporizes. The phase change constant in Equation 19.25 (p. 617) takes different values for condensation and vaporization, respectively.

Release 15.0 - © SAS IP, Inc. All rights reserved. - Contains proprietary and confidential information of ANSYS, Inc. and its subsidiaries and affiliates.

$$C_{phase}=\begin{cases} C_{con} \\ C_{vap}h\cdot 10^{-4} \end{cases} \tag{19.28}$$

where the film height $h$ is used to prevent generating vapor without the presence of liquid.

## 19.2.2. Boundary Conditions

Boundary conditions for Equation 19.1 (p. 612) and Equation 19.2 (p. 612), film mass and momentum equations, are specified only at the wall on which film modeling is enabled. There are two types of conditions: one is the fixed mass and momentum fluxes and the other specified initial film height and velocity. When the fluxes are specified, they are added to the equations as source terms. When the initial film height and velocity are specified, these values are enforced only at the first film time step.

## 19.2.3. Obtaining Film Velocity Without Solving the Momentum Equations

Equation 19.2 (p. 612) is used to obtain film average velocity through momentum conservation. However, one can estimate the film velocity without solving Equation 19.2 (p. 612). In this case, the film velocity is assumed to have a component that is driven by the shear due to the external flow and a component that is driven by gravity.

### 19.2.3.1. Shear-Driven Film Velocity

As shown in Figure 19.3: Shear-Driven Film Velocity (p. 618), it is assumed that the film velocity varies linearly from the wall to the air-film interface.

**Figure 19.3: Shear-Driven Film Velocity**

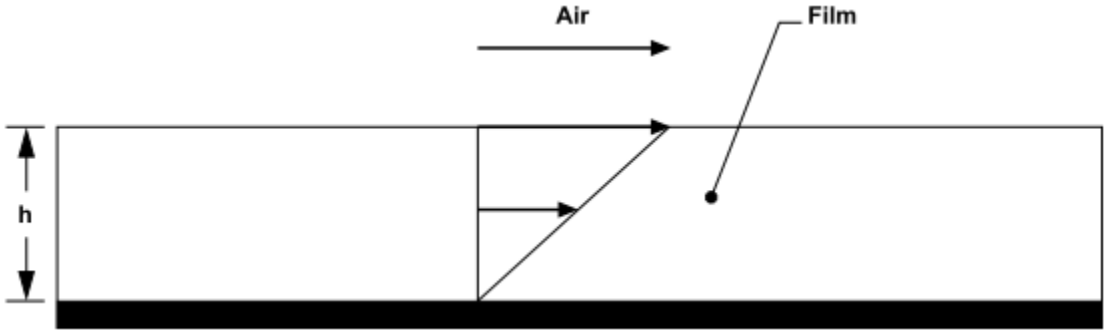


By equating the two shear forces at the film-air interface, one from the air side and one from the film side, we have,

$$\vec{\tau}_{air}=\mu_l\frac{\partial \vec{V}}{\partial n}=\mu_l\frac{\vec{V}_s}{h} \tag{19.29}$$

where $\vec{V}_s$ is the surface velocity. The film average velocity is therefore,

$$\vec{V}_l=\frac{\vec{\tau}_{air}h}{2\mu_l} \tag{19.30}$$


Release 15.0 - © SAS IP, Inc. All rights reserved. - Contains proprietary and confidential information of ANSYS, Inc. and its subsidiaries and affiliates.

### 19.2.3.2. Gravity-Driven Film Velocity

It is assumed that the film movement is entirely controlled by the balance of gravity force and the wall shear force, and that the film velocity has a parabolic profile with a zero-gradient at the air-film interface, as shown in Figure 19.4: Gravity-Driven Film Velocity (p. 619).

**Figure 19.4: Gravity-Driven Film Velocity**

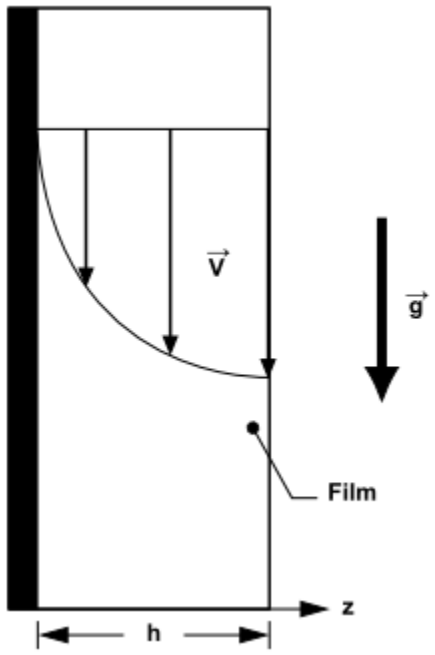


Assuming no-slip at the wall, the parabolic film velocity becomes $\vec{V}(z) = \vec{a}\,z^2 + \vec{b}\,z$.

Balancing the weight of the film and the wall shear force, we have,

$$\rho_l A h \vec{g} = A \mu_l \frac{\partial \vec{V}}{\partial z}\Big|_{z=0} = \mu_l (2\vec{a}\,z + \vec{b})_{z=0} \tag{19.31}$$

therefore,

$$\vec{b} = \frac{\rho_l h}{\mu_l}\vec{g} \tag{19.32}$$

Applying the zero-gradient assumption at the air-film interface, we have,

$$\vec{a} = -\frac{\vec{b}}{2h} = -\frac{\rho_l}{2\mu_l}\vec{g} \tag{19.33}$$

Thus the gravity-induced film velocity is,

$$\vec{V}(z) = \frac{\rho_l h}{\mu_l} z \left(1 - \frac{z}{2h}\right)\vec{g} \tag{19.34}$$

The film average velocity is,

Release 15.0 - © SAS IP, Inc. All rights reserved. - Contains proprietary and confidential information of ANSYS, Inc. and its subsidiaries and affiliates.

$$\vec{V}_l = \frac{\rho_l h^2}{3\mu_l}\vec{g} \tag{19.35}$$

## 19.3. Numerical Schemes and Solution Algorithm

This section describes the temporal and spatial differencing schemes, as well as the solution algorithms used with the Eulerian Wall Film (EWF) model.

19.3.1. Temporal Differencing Schemes
19.3.2. Spatial Differencing Schemes
19.3.3. Solution Algorithm

### 19.3.1. Temporal Differencing Schemes

The following temporal differencing schemes are available for the Eulerian Wall Film (EWF) model.

19.3.1.1. First-Order Explicit Method
19.3.1.2. First-Order Implicit Method
19.3.1.3. Second-Order Implicit Method

#### *19.3.1.1. First-Order Explicit Method*

Defining *F* and *G* as follows, with the subscript $i$ indicates the previous time-step values:

$$\begin{aligned} F_i &\equiv \left\{ -\nabla_s \cdot [h\vec{V}_l] + \frac{\dot{m}_s}{\rho_l} \right\}_i \\ G_i &\equiv \left( -\frac{h\nabla_s P_L}{\rho_l} + (\vec{g}_\tau)h + \frac{3}{2\rho_l}\vec{\tau}_{fs} + \frac{\dot{q}}{\rho_l} - \nabla_s \cdot (h\vec{V}_l\vec{V}_l) \right)_i \end{aligned} \tag{19.36}$$

We have the following discretized film mass and momentum equations, with subscript $i$+1 represents the current time-step values, and $\Delta t$ the time step used for film computations.

$$\begin{aligned} \frac{h_{i+1} - h_i}{\Delta t} &= F_i \\ \frac{(h\vec{V}_l)_{i+1} - (h\vec{V}_l)_i}{\Delta t} &= -\left( \frac{3\nu_l}{h}\vec{V}_l \right)_{i+1} + G_i \end{aligned} \tag{19.37}$$

Film height and velocity are then computed as follows,

$$\begin{aligned} h_{i+1} &= h_i + \Delta t F_i \\ (\vec{V}_l)_{i+1} &= \frac{(h\vec{V}_l)_i + \Delta t G_i}{h_{i+1} + \Delta t \frac{3\nu_l}{h_{i+1}}} \end{aligned} \tag{19.38}$$

The above set of equations complete the *explicit* differencing scheme in which film height is computed first, based upon values of $F_i$ evaluated at the previous film time-step; then film velocity is calculated using the latest film height and values of $G_i$ evaluated at the previous film time-step.


Release 15.0 - © SAS IP, Inc. All rights reserved. - Contains proprietary and confidential information of ANSYS, Inc. and its subsidiaries and affiliates.

### 19.3.1.2. First-Order Implicit Method

With the explicit method, evaluations of $F$ and $G$ are done based upon the previous time-step film height and velocity vector. In order to improve accuracy of this explicit method, a first-order implicit method is introduced in which $F$ and $G$ values are updated during an iterative loop within a film time step. This new method can be described as a predictor-corrector procedure. At the beginning, that is, the predictor step, the explicit scheme is used to compute film height and velocity vector,

**Predictor:**

$$h_{i+1}^{0} = h_i + \Delta t F_i$$
$$(\vec{V}_l)_{i+1}^{0} = \frac{(h\vec{V}_l)_i + \Delta t G_i}{h_{i+1}^{0} + \Delta t \frac{3\nu_l}{h_{i+1}^{0}}} \tag{19.39}$$

The superscript $0$ indicates the first step in the iteration loop.

**Corrector:**

The latest film height and velocity vector are used to update $F$ and $G$; then film height and velocity are recomputed,

$$h_{i+1}^{n+1} = h_i + \Delta t F[h_{i+1}^{n}, (\vec{V}_l)_{i+1}^{n}]$$
$$(\vec{V}_l)_{i+1}^{n+1} = \frac{(h\vec{V}_l)_i + \Delta t G[h_{i+1}^{n}, (\vec{V}_l)_{i+1}^{n}]}{h_{i+1}^{n+1} + \Delta t \frac{3\nu_l}{h_{i+1}^{n+1}}} \tag{19.40}$$

The superscript $n$+1 and $n$ represent the current and the previous iterations, respectively. The iteration procedure ends with the following convergence criteria:

$$|h_{i+1}^{n+1} - h_{i+1}^{n}| \le \varepsilon$$
$$|(u_\alpha)_{i+1}^{n+1} - (u_\alpha)_{i+1}^{n}| \le \varepsilon \tag{19.41}$$

where $u_\alpha$ represent each component of the velocity vector.

### 19.3.1.3. Second-Order Implicit Method

With the above discussed explicit and first-order implicit methods, time differencing is only first-order accurate. A second-order implicit method is introduced below. The iterative procedure is very similar to that used in the first-order implicit method, but two time-steps ($i$ and $i$–1) are used for time differencing in the predictor step.

**Predictor:**

Release 15.0 - © SAS IP, Inc. All rights reserved. - Contains proprietary and confidential information of ANSYS, Inc. and its subsidiaries and affiliates.

$$h_{i+1}^{0}=h_i+\frac{\Delta t}{2}\{3F_i-F_{i-1}\}$$
$$(\vec{V}_l)_{i+1}^{0}=\frac{(h\vec{V}_l)_i+\frac{\Delta t}{2}\{3G_i-G_{i-1}\}}{h_{i+1}^{0}+\Delta t\frac{3v_l}{h_{i+1}^{0}}} \tag{19.42}$$

**Corrector:**

$$h_{i+1}^{n+1}=h_i+\frac{\Delta t}{2}\left\{F[h_{i+1}^{n},\ (\vec{V}_l)_{i+1}^{n}]+F[h_{i+1}^{n-1},\ (\vec{V}_l)_{i+1}^{n-1}]\right\}$$
$$(\vec{V}_l)_{i+1}^{n+1}=\frac{(h\vec{V}_l)_i+\frac{\Delta t}{2}\left\{G[h_{i+1}^{n},\ (\vec{V}_l)_{i+1}^{n}]-G[h_{i+1}^{n-1},\ (\vec{V}_l)_{i+1}^{n-1}]\right\}}{h_{i+1}^{n+1}+\Delta t\frac{3v_l}{h_{i+1}^{n+1}}} \tag{19.43}$$

The iteration procedure ends with the following convergence criteria:

$$|h_{i+1}^{n+1}-h_{i+1}^{n}|\le\varepsilon$$
$$|(u_\alpha)_{i+1}^{n+1}-(u_\alpha)_{i+1}^{n}|\le\varepsilon \tag{19.44}$$

where $u_\alpha$ represent each component of the velocity vector.

## 19.3.2. Spatial Differencing Schemes

Computing $F$ and $G$, defined in Equation 19.36 (p. 620), involves evaluations of spatial gradients for various quantities at face centers. Applying Green-Gauss theorem the gradient of a scalar $\varphi$ at face center $0$ is computed as,

$$\nabla\varphi=\frac{1}{A}\sum_e\varphi_e\vec{l}_e \tag{19.45}$$

where the subscript $e$ represents the center of each edge of a film face, $A$ the area of the face and $\vec{l}$ the length vector (whose magnitude is the length of the edge and whose direction is normal to the edge), as in the sketch below,

**Figure 19.5: Spatial Gradient**

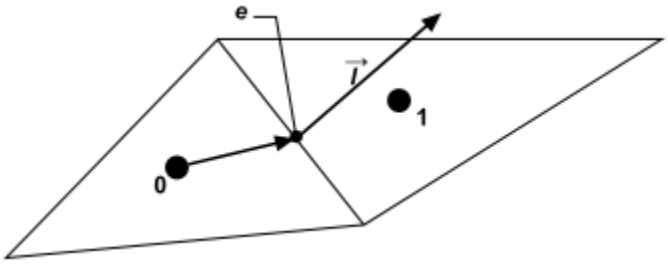


Clearly, at the center of the gradient calculation is how to obtain $\varphi_e$. The following describes the steps taken in the current implementation.


Release 15.0 - © SAS IP, Inc. All rights reserved. - Contains proprietary and confidential information of ANSYS, Inc. and its subsidiaries and affiliates.

**(1) Primary gradient computation**

A primary gradient is calculated using Green-Gauss theorem by simply estimating edge center value as,

$$\varphi_e = \frac{1}{2}(\varphi_P + \varphi_E) \tag{19.46}$$

$$\nabla \varphi_P = \frac{1}{A}\sum_e \varphi_e \vec{l}_e \tag{19.47}$$

**(2) Reconstruction of edge-center values**

The edge-center values are then computed using either the first-order upwind or the second-order upwind schemes,

1st-order upwind: $\varphi_e^* = \varphi_{UP}$

2nd-order upwind: $\varphi_e^* = \varphi_{UP} + \vec{d} r_{UP} \cdot \nabla \varphi_P$

$\varphi_{UP}$ is the value of $\varphi$ at the UPWIND face center; $\vec{d} r_{UP}$ is the distance vector from the UPWIND face center to the edge center.

**(3) Final gradient calculation**

Finally the gradient at face center is computed as,

$$\nabla \varphi = \frac{1}{A}\sum_e \varphi_e^* \vec{l}_e \tag{19.48}$$

## 19.3.3. Solution Algorithm

While film movement is always tracked with time, the EWF model can be run with both steady and transient flow simulations.

### *19.3.3.1. Steady Flow*

It is assumed that while flow affects its movement, the thin film does not, however, affect the flow field. In this case the flow field has converged and is kept unchanged (frozen flow field). The elapsed time for film development is increased by the film time step, $\Delta t$. This time step can either be a user-specified constant or can be computed automatically using an adaptive time-stepping method depending upon the maximum Courant number, described as follows:

1. When the computed maximum Courant number exceeds the user-specified value, the film time step is reduced by a factor of 2.

2. When the computed maximum Courant number is less than half the user-specified value, the film time step is increased by a factor of 1.5.

### *19.3.3.2. Transient Flow*

Within each flow time step, $\Delta t_{flow}$, a number of film sub-time steps are used to advance the film time to the same physical time of flow. The film sub-time step is determined as follows,

Release 15.0 - © SAS IP, Inc. All rights reserved. - Contains proprietary and confidential information of ANSYS, Inc. and its subsidiaries and affiliates.

$$\Delta t = \frac{\Delta t_{flow}}{N_{film}} \tag{19.49}$$

$N_{film}$ is the number of film time steps; $\Delta t_{flow}$ is the flow time step.

Since film computation starts at the end of each flow time step, the effect of the film on flow is lagged by one flow time step.


Release 15.0 - © SAS IP, Inc. All rights reserved. - Contains proprietary and confidential information of ANSYS, Inc. and its subsidiaries and affiliates.

# Chapter 20: Solver Theory

This chapter describes the ANSYS Fluent solver theory. Details about the solver algorithms used by ANSYS Fluent are provided in Overview of Flow Solvers (p. 625) – Multigrid Method (p. 670). For more information about using the solver, see Using the Solver in the User's Guide.


20.1. Overview of Flow Solvers
20.2. General Scalar Transport Equation: Discretization and Solution
20.3. Discretization
20.4. Pressure-Based Solver
20.5. Density-Based Solver
20.6. Pseudo Transient Under-Relaxation
20.7. Multigrid Method
20.8. Hybrid Initialization
20.9. Full Multigrid (FMG) Initialization


## 20.1. Overview of Flow Solvers

ANSYS Fluent allows you to choose one of the two numerical methods:

- pressure-based solver (see Pressure-Based Solver (p. 626))
- density-based solver (see Density-Based Solver (p. 628))

Historically speaking, the pressure-based approach was developed for low-speed incompressible flows, while the density-based approach was mainly used for high-speed compressible flows. However, recently both methods have been extended and reformulated to solve and operate for a wide range of flow conditions beyond their traditional or original intent.

In both methods the velocity field is obtained from the momentum equations. In the density-based approach, the continuity equation is used to obtain the density field while the pressure field is determined from the equation of state.

On the other hand, in the pressure-based approach, the pressure field is extracted by solving a pressure or pressure correction equation which is obtained by manipulating continuity and momentum equations.

Using either method, ANSYS Fluent will solve the governing integral equations for the conservation of mass and momentum, and (when appropriate) for energy and other scalars such as turbulence and chemical species. In both cases a control-volume-based technique is used that consists of:

- Division of the domain into discrete control volumes using a computational grid.
- Integration of the governing equations on the individual control volumes to construct algebraic equations for the discrete dependent variables ("unknowns") such as velocities, pressure, temperature, and conserved scalars.
- Linearization of the discretized equations and solution of the resultant linear equation system to yield updated values of the dependent variables.


Release 15.0 - © SAS IP, Inc. All rights reserved. - Contains proprietary and confidential information of ANSYS, Inc. and its subsidiaries and affiliates.

The two numerical methods employ a similar discretization process (finite-volume), but the approach used to linearize and solve the discretized equations is different.

The general solution methods are described in Pressure-Based Solver (p. 626) and Density-Based Solver (p. 628). To learn how to apply the solvers, see Choosing the Solver in the User's Guide.

## 20.1.1. Pressure-Based Solver

The pressure-based solver employs an algorithm which belongs to a general class of methods called the projection method [66] (p. 732). In the projection method, wherein the constraint of mass conservation (continuity) of the velocity field is achieved by solving a pressure (or pressure correction) equation. The pressure equation is derived from the continuity and the momentum equations in such away that the velocity field, corrected by the pressure, satisfies the continuity. Since the governing equations are nonlinear and coupled to one another, the solution process involves iterations wherein the entire set of governing equations is solved repeatedly until the solution converges.

Two pressure-based solver algorithms are available in ANSYS Fluent. A segregated algorithm, and a coupled algorithm. These two approaches are discussed in the sections below.

### *20.1.1.1. The Pressure-Based Segregated Algorithm*

The pressure-based solver uses a solution algorithm where the governing equations are solved sequentially (that is, segregated from one another). Because the governing equations are non-linear and coupled, the solution loop must be carried out iteratively in order to obtain a converged numerical solution.

In the segregated algorithm, the individual governing equations for the solution variables (for example, $u, v, w, p, T, k, \varepsilon$, and so on) are solved one after another. Each governing equation, while being solved, is "decoupled" or "segregated" from other equations, hence its name. The segregated algorithm is memory-efficient, since the discretized equations need only be stored in the memory one at a time. However, the solution convergence is relatively slow, inasmuch as the equations are solved in a decoupled manner.

With the segregated algorithm, each iteration consists of the steps illustrated in Figure 20.1: Overview of the Pressure-Based Solution Methods (p. 627) and outlined below:

1. Update fluid properties (for example, density, viscosity, specific heat) including turbulent viscosity (diffusivity) based on the current solution.

2. Solve the momentum equations, one after another, using the recently updated values of pressure and face mass fluxes.

3. Solve the pressure correction equation using the recently obtained velocity field and the mass-flux.

4. Correct face mass fluxes, pressure, and the velocity field using the pressure correction obtained from Step 3.

5. Solve the equations for additional scalars, if any, such as turbulent quantities, energy, species, and radiation intensity using the current values of the solution variables.

6. Update the source terms arising from the interactions among different phases (for example, source term for the carrier phase due to discrete particles).

7. Check for the convergence of the equations.


Release 15.0 - © SAS IP, Inc. All rights reserved. - Contains proprietary and confidential information of ANSYS, Inc. and its subsidiaries and affiliates.

These steps are continued until the convergence criteria are met.

**Figure 20.1: Overview of the Pressure-Based Solution Methods**

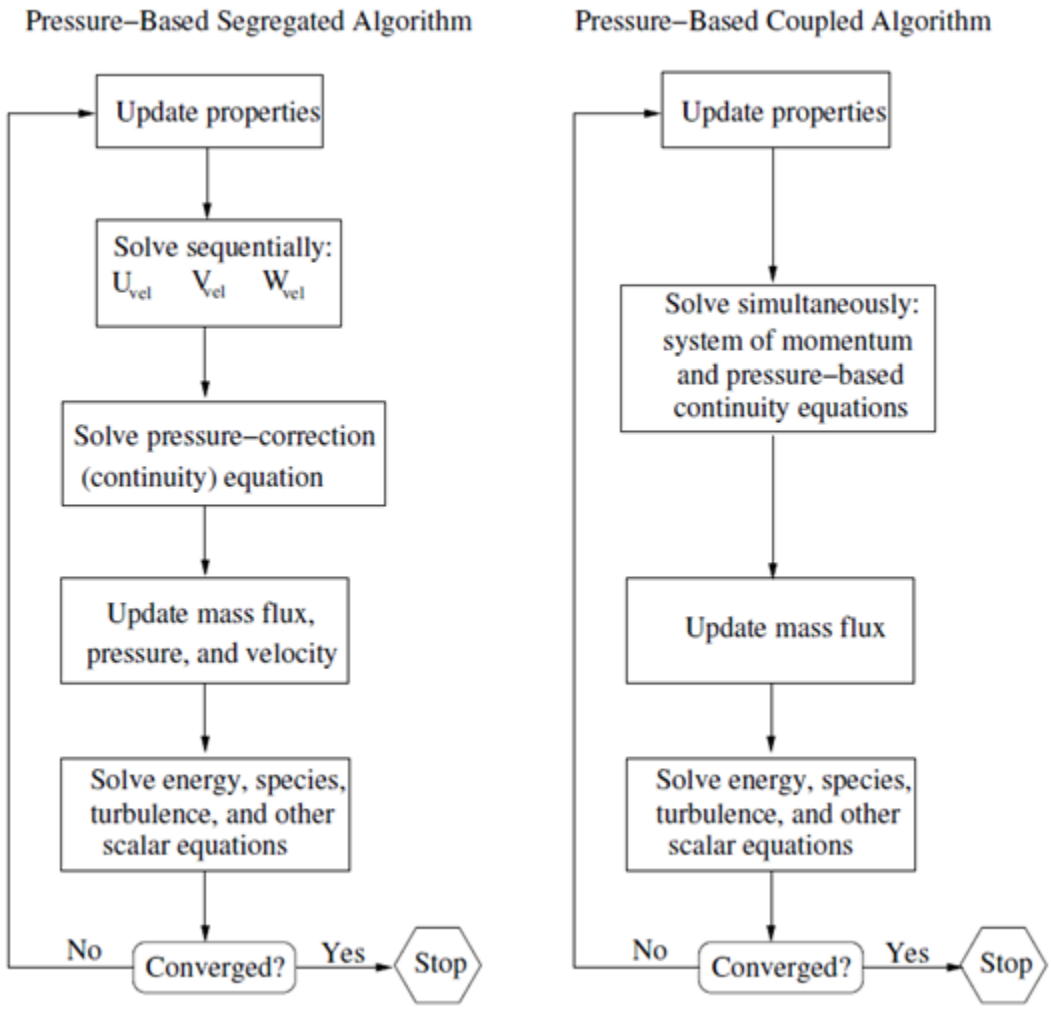


## 20.1.1.2. The Pressure-Based Coupled Algorithm

Unlike the segregated algorithm described above, the pressure-based coupled algorithm solves a coupled system of equations comprising the momentum equations and the pressure-based continuity equation. Thus, in the coupled algorithm, Steps 2 and 3 in the segregated solution algorithm are replaced by a single step in which the coupled system of equations are solved. The remaining equations are solved in a decoupled fashion as in the segregated algorithm.

Since the momentum and continuity equations are solved in a closely coupled manner, the rate of solution convergence significantly improves when compared to the segregated algorithm. However, the memory requirement increases by 1.5 – 2 times that of the segregated algorithm since the discrete system of all momentum and pressure-based continuity equations must be stored in the memory when solving for the velocity and pressure fields (rather than just a single equation, as is the case with the segregated algorithm).

Release 15.0 - © SAS IP, Inc. All rights reserved. - Contains proprietary and confidential information of ANSYS, Inc. and its subsidiaries and affiliates.

## 20.1.2. Density-Based Solver

The density-based solver solves the governing equations of continuity, momentum, and (where appropriate) energy and species transport simultaneously (that is, coupled together). Governing equations for additional scalars will be solved afterward and sequentially (that is, segregated from one another and from the coupled set) using the procedure described in General Scalar Transport Equation: Discretization and Solution (p. 630). Because the governing equations are non-linear (and coupled), several iterations of the solution loop must be performed before a converged solution is obtained. Each iteration consists of the steps illustrated in Figure 20.2: Overview of the Density-Based Solution Method (p. 629) and outlined below:

1. Update the fluid properties based on the current solution. (If the calculation has just begun, the fluid properties will be updated based on the initialized solution.)

2. Solve the continuity, momentum, and (where appropriate) energy and species equations simultaneously.

3. Where appropriate, solve equations for scalars such as turbulence and radiation using the previously updated values of the other variables.

4. When interphase coupling is to be included, update the source terms in the appropriate continuous phase equations with a discrete phase trajectory calculation.

5. Check for convergence of the equation set.

These steps are continued until the convergence criteria are met.


Release 15.0 - © SAS IP, Inc. All rights reserved. - Contains proprietary and confidential information of ANSYS, Inc. and its subsidiaries and affiliates.

**Figure 20.2: Overview of the Density-Based Solution Method**

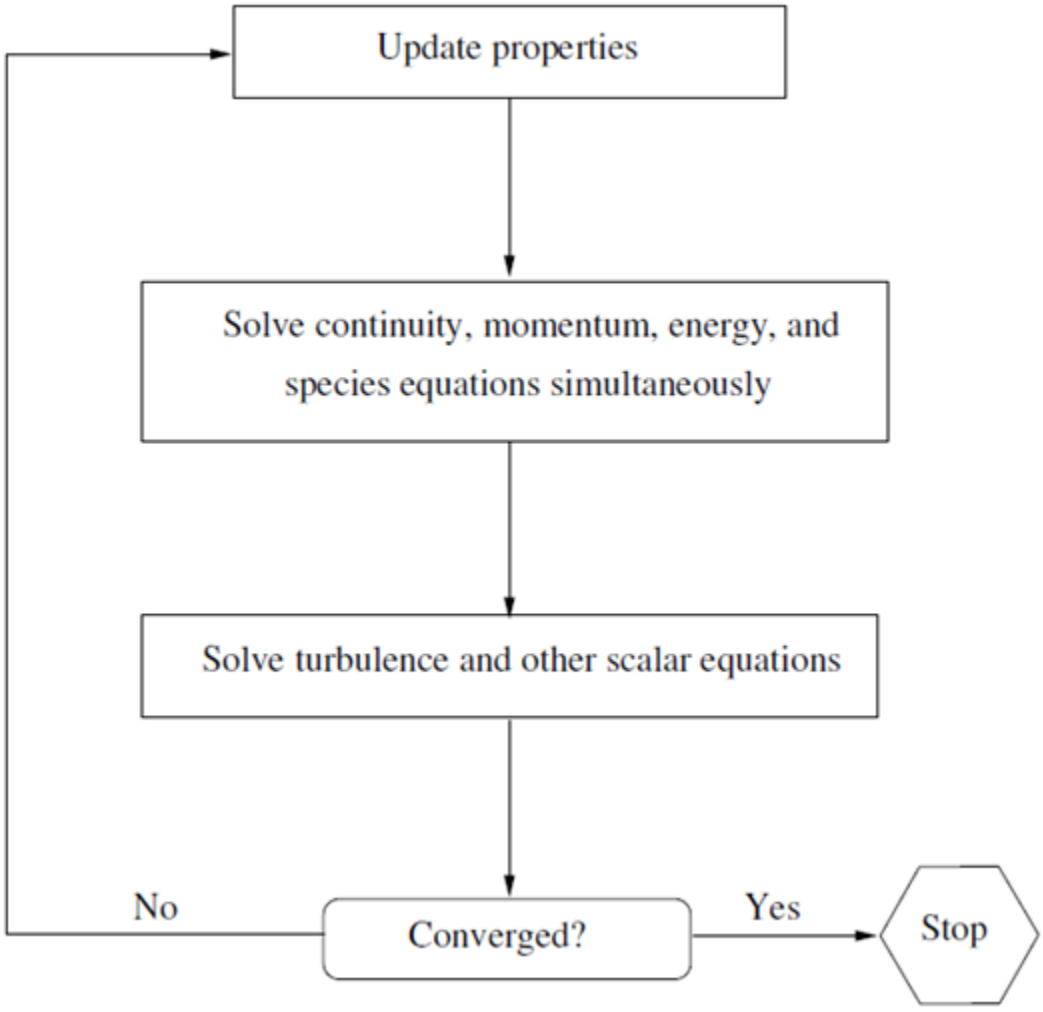


In the density-based solution method, you can solve the coupled system of equations (continuity, momentum, energy and species equations if available) using, either the coupled-explicit formulation or the coupled-implicit formulation. The main distinction between the density-based explicit and implicit formulations is described next.

In the density-based solution methods, the discrete, non-linear governing equations are linearized to produce a system of equations for the dependent variables in every computational cell. The resultant linear system is then solved to yield an updated flow-field solution.

The manner in which the governing equations are linearized may take an "implicit" or "explicit" form with respect to the dependent variable (or set of variables) of interest. By implicit or explicit we mean the following:

- implicit: For a given variable, the unknown value in each cell is computed using a relation that includes both existing and unknown values from neighboring cells. Therefore each unknown will appear in more than one equation in the system, and these equations must be solved simultaneously to give the unknown quantities.

Release 15.0 - © SAS IP, Inc. All rights reserved. - Contains proprietary and confidential information of ANSYS, Inc. and its subsidiaries and affiliates.

- explicit: For a given variable, the unknown value in each cell is computed using a relation that includes only existing values. Therefore each unknown will appear in only one equation in the system and the equations for the unknown value in each cell can be solved one at a time to give the unknown quantities.

In the density-based solution method you have a choice of using either an implicit or explicit linearization of the governing equations. This choice applies only to the coupled set of governing equations. Transport equations for additional scalars are solved segregated from the coupled set (such as turbulence, radiation, and so on). The transport equations are linearized and solved implicitly using the method described in General Scalar Transport Equation: Discretization and Solution (p. 630). Regardless of whether you choose the implicit or explicit methods, the solution procedure shown in Figure 20.2: Overview of the Density-Based Solution Method (p. 629) is followed.

If you choose the implicit option of the density-based solver, each equation in the coupled set of governing equations is linearized implicitly with respect to all dependent variables in the set. This will result in a system of linear equations with $N$ equations for each cell in the domain, where $N$ is the number of coupled equations in the set. Because there are $N$ equations per cell, this is sometimes called a "block" system of equations.

A point implicit linear equation solver (Incomplete Lower Upper (ILU) factorization scheme or a symmetric block Gauss-Seidel) is used in conjunction with an algebraic multigrid (AMG) method to solve the resultant block system of equations for all $N$ dependent variables in each cell. For example, linearization of the coupled continuity, $x$-, $y$-, $z$-momentum, and energy equation set will produce a system of equations in which $p$, $u$, $v$, $w$, and $T$ are the unknowns. Simultaneous solution of this equation system (using the block AMG solver) yields at once updated pressure, $u$-, $v$-, $w$-velocity, and temperature fields.

In summary, the coupled implicit approach solves for all variables ($p$, $u$, $v$, $w$, $T$) in all cells at the same time.

If you choose the explicit option of the density-based solver, each equation in the coupled set of governing equations is linearized explicitly. As in the implicit option, this too will result in a system of equations with $N$ equations for each cell in the domain and likewise, all dependent variables in the set will be updated at once. However, this system of equations is explicit in the unknown dependent variables. For example, the $x$-momentum equation is written such that the updated $x$ velocity is a function of existing values of the field variables. Because of this, a linear equation solver is not needed. Instead, the solution is updated using a multi-stage (Runge-Kutta) solver. Here you have the additional option of employing a full approximation storage (FAS) multigrid scheme to accelerate the multi-stage solver.

In summary, the density-based explicit approach solves for all variables ($p$, $u$, $v$, $w$, $T$) one cell at a time.

Note that the FAS multigrid is an optional component of the explicit approach, while the AMG is a required element in both the pressure-based and density-based implicit approaches.

## 20.2. General Scalar Transport Equation: Discretization and Solution

ANSYS Fluent uses a control-volume-based technique to convert a general scalar transport equation to an algebraic equation that can be solved numerically. This control volume technique consists of integrating the transport equation about each control volume, yielding a discrete equation that expresses the conservation law on a control-volume basis.

Discretization of the governing equations can be illustrated most easily by considering the unsteady conservation equation for transport of a scalar quantity $\phi$. This is demonstrated by the following equation written in integral form for an arbitrary control volume $V$ as follows:


Release 15.0 - © SAS IP, Inc. All rights reserved. - Contains proprietary and confidential information of ANSYS, Inc. and its subsidiaries and affiliates.

$$\int_V \frac{\partial \rho \phi}{\partial t} dV + \oint \rho \phi \vec{v} \cdot d\vec{A} = \oint \Gamma_\phi \nabla \phi \cdot d\vec{A} + \int_V S_\phi dV \tag{20.1}$$

where

$\rho$ = density

$\vec{v}$ = velocity vector (= $u\hat{i} + v\hat{j}$ in 2D)

$\vec{A}$ = surface area vector

$\Gamma_\phi$ = diffusion coefficient for $\phi$

$\nabla \phi$ = gradient of $\phi = (\partial \phi / \partial x)\hat{i} + (\partial \phi / \partial y)\hat{j}$ in 2D)

$S_\phi$ = source of $\phi$ per unit volume

Equation 20.1 (p. 631) is applied to each control volume, or cell, in the computational domain. The two-dimensional, triangular cell shown in Figure 20.3: Control Volume Used to Illustrate Discretization of a Scalar Transport Equation (p. 632) is an example of such a control volume. Discretization of Equation 20.1 (p. 631) on a given cell yields

$$\frac{\partial \rho \phi}{\partial t} V + \sum_f^{N_{faces}} \rho_f \vec{v}_f \phi_f \cdot \vec{A}_f = \sum_f^{N_{faces}} \Gamma_\phi \nabla \phi_f \cdot \vec{A}_f + S_\phi V \tag{20.2}$$

where

$N_{faces}$ = number of faces enclosing cell

$\phi_f$ = value of $\phi$ convected through face $f$

$\rho_f \vec{v}_f \cdot \vec{A}_f$ = mass flux through the face

$\vec{A}_f$ = area of face $f$, $|A|$ (= $|A_x\hat{i} + A_y\hat{j}|$ in 2D)

$\nabla \phi_f$ = gradient of $\phi$ at face $f$

$V$ = cell volume

Where $\frac{\partial \rho \phi}{\partial t} V$ is defined in Temporal Discretization (p. 639). The equations solved by ANSYS Fluent take the same general form as the one given above and apply readily to multi-dimensional, unstructured meshes composed of arbitrary polyhedra.

Release 15.0 - © SAS IP, Inc. All rights reserved. - Contains proprietary and confidential information of ANSYS, Inc. and its subsidiaries and affiliates.

**Figure 20.3: Control Volume Used to Illustrate Discretization of a Scalar Transport Equation**

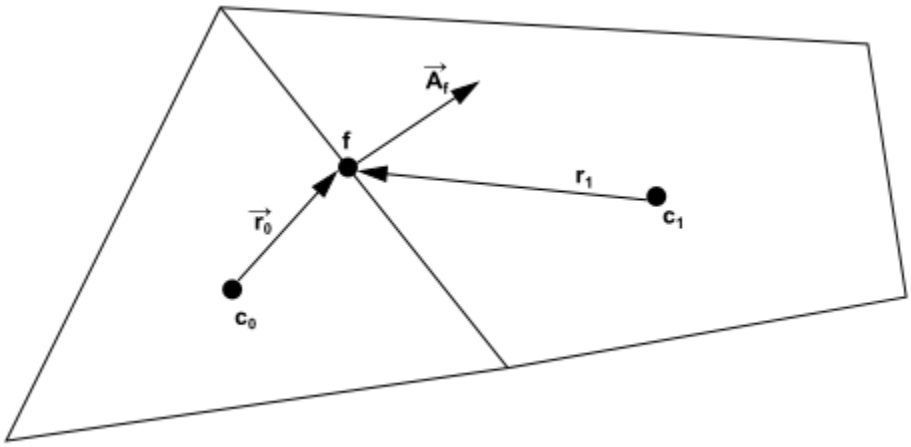


For more information, see the following section:
20.2.1. Solving the Linear System

## 20.2.1. Solving the Linear System

The discretized scalar transport equation (Equation 20.2 (p. 631)) contains the unknown scalar variable $\phi$ at the cell center as well as the unknown values in surrounding neighbor cells. This equation will, in general, be non-linear with respect to these variables. A linearized form of Equation 20.2 (p. 631) can be written as

$$a_P \phi = \sum_{nb} a_{nb} \phi_{nb} + b \tag{20.3}$$

where the subscript $nb$ refers to neighbor cells, and $a_P$ and $a_{nb}$ are the linearized coefficients for $\phi$ and $\phi_{nb}$.

The number of neighbors for each cell depends on the mesh topology, but will typically equal the number of faces enclosing the cell (boundary cells being the exception).

Similar equations can be written for each cell in the mesh. This results in a set of algebraic equations with a sparse coefficient matrix. For scalar equations, ANSYS Fluent solves this linear system using a point implicit (Gauss-Seidel) linear equation solver in conjunction with an algebraic multigrid (AMG) method that is described in Algebraic Multigrid (AMG) (p. 676).

# 20.3. Discretization

Information is organized into the following subsections:
20.3.1. Spatial Discretization
20.3.2. Temporal Discretization
20.3.3. Evaluation of Gradients and Derivatives
20.3.4. Gradient Limiters

## 20.3.1. Spatial Discretization

By default, ANSYS Fluent stores discrete values of the scalar $\phi$ at the cell centers ($c_0$ and $c_1$ in Figure 20.3: Control Volume Used to Illustrate Discretization of a Scalar Transport Equation (p. 632)). However,


Release 15.0 - © SAS IP, Inc. All rights reserved. - Contains proprietary and confidential information of ANSYS, Inc. and its subsidiaries and affiliates.

face values $\phi_f$ are required for the convection terms in Equation 20.2 (p. 631) and must be interpolated from the cell center values. This is accomplished using an upwind scheme.

Upwinding means that the face value $\phi_f$ is derived from quantities in the cell upstream, or "upwind," relative to the direction of the normal velocity $v_n$ in Equation 20.2 (p. 631). ANSYS Fluent allows you to choose from several upwind schemes: first-order upwind, second-order upwind, power law, and QUICK. These schemes are described in First-Order Upwind Scheme (p. 633) – QUICK Scheme (p. 636).

The diffusion terms in Equation 20.2 (p. 631) are central-differenced and are always second-order accurate.

For information on how to use the various spatial discretization schemes, see Choosing the Spatial Discretization Scheme in the User's Guide.

### 20.3.1.1. First-Order Upwind Scheme

When first-order accuracy is desired, quantities at cell faces are determined by assuming that the cell-center values of any field variable represent a cell-average value and hold throughout the entire cell; the face quantities are identical to the cell quantities. Thus when first-order upwinding is selected, the face value $\phi_f$ is set equal to the cell-center value of $\phi$ in the upstream cell.

**Important**

First-order upwind is available in the pressure-based and density-based solvers.

### 20.3.1.2. Power-Law Scheme

The power-law discretization scheme interpolates the face value of a variable, $\phi$, using the exact solution to a one-dimensional convection-diffusion equation

$$\frac{\partial}{\partial x}(\rho u \phi) = \frac{\partial}{\partial x}\Gamma\frac{\partial \phi}{\partial x} \tag{20.4}$$

where $\Gamma$ and $\rho u$ are constant across the interval $\partial x$. Equation 20.4 (p. 633) can be integrated to yield the following solution describing how $\phi$ varies with $x$:

$$\frac{\phi(x)-\phi_0}{\phi_L-\phi_0} = \frac{\exp\left(Pe\frac{x}{L}\right)-1}{\exp(Pe)-1} \tag{20.5}$$

where

$$\phi_0 = \phi\,|_{x=0}$$
$$\phi_L = \phi\,|_{x=L}$$

and $Pe$ is the Peclet number:

$$Pe = \frac{\rho u L}{\Gamma} \tag{20.6}$$

The variation of $\phi(x)$ between $x=0$ and $x=L$ is depicted in Figure 20.4: Variation of a Variable Phi Between x=0 and x=L (p. 634) (Equation 20.4 (p. 633)) for a range of values of the Peclet number. Fig-

ure 20.4: Variation of a Variable Phi Between x=0 and x=L (p. 634) shows that for large $Pe$, the value of $\phi$ at $x = L/2$ is approximately equal to the upstream value. This implies that when the flow is dominated by convection, interpolation can be accomplished by simply letting the face value of a variable be set equal to its "upwind" or upstream value. This is the standard first-order scheme for ANSYS Fluent.

**Figure 20.4: Variation of a Variable Phi Between x=0 and x=L**

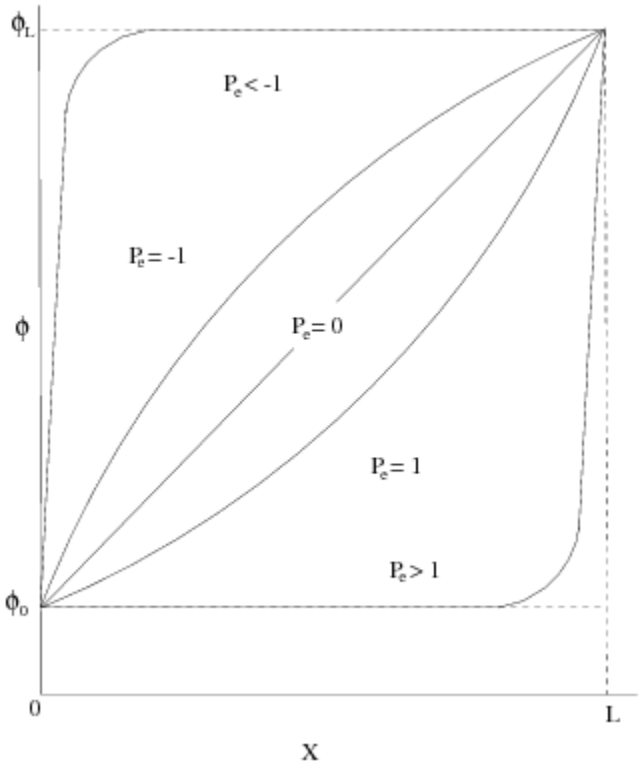


If the power-law scheme is selected, ANSYS Fluent uses Equation 20.5 (p. 633) in an equivalent "power law" format [340] (p. 747), as its interpolation scheme.

As discussed in First-Order Upwind Scheme (p. 633), Figure 20.4: Variation of a Variable Phi Between x=0 and x=L (p. 634) shows that for large Pe, the value of $\phi$ at $x = L/2$ is approximately equal to the upstream value. When $Pe$ = 0 (no flow, or pure diffusion), Figure 20.4: Variation of a Variable Phi Between x=0 and x=L (p. 634) shows that $\phi$ may be interpolated using a simple linear average between the values at $x = 0$ and $x = L$. When the Peclet number has an intermediate value, the interpolated value for $\phi$ at $x = L/2$ must be derived by applying the "power law" equivalent of Equation 20.5 (p. 633).

**Important**

The power-law scheme is available in the pressure-based solver and when solving additional scalar equations in the density-based solver.

### 20.3.1.3. Second-Order Upwind Scheme

When second-order accuracy is desired, quantities at cell faces are computed using a multidimensional linear reconstruction approach [19] (p. 730). In this approach, higher-order accuracy is achieved at cell faces through a Taylor series expansion of the cell-centered solution about the cell centroid. Thus when second-order upwinding is selected, the face value $\phi_f$ is computed using the following expression:


Release 15.0 - © SAS IP, Inc. All rights reserved. - Contains proprietary and confidential information of ANSYS, Inc. and its subsidiaries and affiliates.

$$\phi_{f,SOU} = \phi + \nabla\phi \cdot \vec{r} \tag{20.7}$$

where $\phi$ and $\nabla\phi$ are the cell-centered value and its gradient in the upstream cell, and $\vec{r}$ is the displacement vector from the upstream cell centroid to the face centroid. This formulation requires the determination of the gradient $\nabla\phi$ in each cell, as discussed in Evaluation of Gradients and Derivatives (p. 641). Finally, the gradient $\nabla\phi$ is limited so that no new maxima or minima are introduced.

**Important**

Second-order upwind is available in the pressure-based and density-based solvers.

### 20.3.1.4. First-to-Higher Order Blending

In some instances, and at certain flow conditions, a converged solution to steady-state may not be possible with the use of higher-order discretization schemes due to local flow fluctuations (physical or numerical). On the other hand, a converged solution for the same flow conditions maybe possible with a first-order discretization scheme. For this type of flow and situation, if a better than first-order accurate solution is desired, then first-to-higher-order blending can be used to obtain a converged steady-state solution.

The first-order to higher-order blending is applicable only when higher-order discretization is used. It is applicable with the following discretization schemes: second-order upwinding, central-differencing schemes, QUICK, and third-order MUSCL. The blending is not applicable to first-order, power-law, modified HRIC schemes, or the Geo-reconstruct and CICSAM schemes.

In the density-based solver, the blending is applied as a scaling factor to the reconstruction gradients. While in the pressure-based solver, the blending is applied to the higher-order terms for the convective transport variable.

To learn how to apply this option, refer to First-to-Higher Order Blending in the User's Guide.

### 20.3.1.5. Central-Differencing Scheme

A second-order-accurate central-differencing discretization scheme is available for the momentum equations when you are using the LES turbulence model. This scheme provides improved accuracy for LES calculations.

The central-differencing scheme calculates the face value for a variable ($\phi_f$) as follows:

$$\phi_{f,CD} = \frac{1}{2}\left(\phi_0 + \phi_1\right) + \frac{1}{2}\left(\nabla\phi_0 \cdot \vec{r}_0 + \nabla\phi_1 \cdot \vec{r}_1\right) \tag{20.8}$$

where the indices 0 and 1 refer to the cells that share face $f$, $\nabla\phi_{r,0}$ and $\nabla\phi_{r,1}$ are the reconstructed gradients at cells 0 and 1, respectively, and $\vec{r}$ is the vector directed from the cell centroid toward the face centroid.

It is well known that central-differencing schemes can produce unbounded solutions and non-physical wiggles, which can lead to stability problems for the numerical procedure. These stability problems can often be avoided if a deferred correction is used for the central-differencing scheme. In this approach, the face value is calculated as follows:

Release 15.0 - © SAS IP, Inc. All rights reserved. - Contains proprietary and confidential information of ANSYS, Inc. and its subsidiaries and affiliates.

$$\phi_f = \underbrace{\phi_{f,UP}}_{\text{implicit part}} + \underbrace{\left(\phi_{f,CD} - \phi_{f,UP}\right)}_{\text{explicit part}} \tag{20.9}$$

where UP stands for upwind. As indicated, the upwind part is treated implicitly while the difference between the central-difference and upwind values is treated explicitly. Provided that the numerical solution converges, this approach leads to pure second-order differencing.

**Important**

The central differencing scheme is available only in the pressure-based solver.

### 20.3.1.6. Bounded Central Differencing Scheme

The central differencing scheme described in Central-Differencing Scheme (p. 635) is an ideal choice for LES in view of its meritoriously low numerical diffusion. However, it often leads to unphysical oscillations in the solution fields. In LES, the situation is exacerbated by usually very low subgrid-scale turbulent diffusivity. The bounded central differencing scheme is essentially based on the normalized variable diagram (NVD) approach [241] (p. 742) together with the convection boundedness criterion (CBC). The bounded central differencing scheme is a composite NVD-scheme that consists of a pure central differencing, a blended scheme of the central differencing and the second-order upwind scheme, and the first-order upwind scheme. It should be noted that the first-order scheme is used only when the CBC is violated.

**Important**

The bounded central differencing scheme is the default convection scheme for LES. When you select LES, the convection discretization schemes for all transport equations are automatically switched to the bounded central differencing scheme.

**Important**

The bounded central differencing scheme is available only in the pressure-based solver.

### 20.3.1.7. QUICK Scheme

For quadrilateral and hexahedral meshes, where unique upstream and downstream faces and cells can be identified, ANSYS Fluent also provides the QUICK scheme for computing a higher-order value of the convected variable $\phi$ at a face. QUICK-type schemes [242] (p. 742) are based on a weighted average of second-order-upwind and central interpolations of the variable. For the face $e$ in Figure 20.5: One-Dimensional Control Volume (p. 637), if the flow is from left to right, such a value can be written as

$$\phi_e = \theta\left[\frac{S_d}{S_c+S_d}\phi_P + \frac{S_c}{S_c+S_d}\phi_E\right] + (1-\theta)\left[\frac{S_u+2S_c}{S_u+S_c}\phi_P - \frac{S_c}{S_u+S_c}\phi_W\right] \tag{20.10}$$


Release 15.0 - © SAS IP, Inc. All rights reserved. - Contains proprietary and confidential information of ANSYS, Inc. and its subsidiaries and affiliates.

**Figure 20.5: One-Dimensional Control Volume**

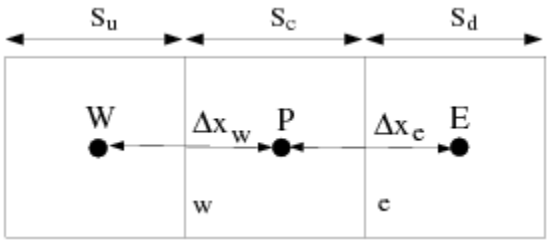


$\theta = 1$ in the above equation results in a central second-order interpolation while $\theta = 0$ yields a second-order upwind value. The traditional QUICK scheme is obtained by setting $\theta = 1/8$. The implementation in ANSYS Fluent uses a variable, solution-dependent value of $\theta$, chosen so as to avoid introducing new solution extrema.

The QUICK scheme will typically be more accurate on structured meshes aligned with the flow direction. Note that ANSYS Fluent allows the use of the QUICK scheme for unstructured or hybrid meshes as well; in such cases the usual second-order upwind discretization scheme (described in Second-Order Upwind Scheme (p. 634)) will be used at the faces of non-hexahedral (or non-quadrilateral, in 2D) cells. The second-order upwind scheme will also be used at partition boundaries when the parallel solver is used.

**Important**

The QUICK scheme is available in the pressure-based solver and when solving additional scalar equations in the density-based solver.

### 20.3.1.8. Third-Order MUSCL Scheme

This third-order convection scheme was conceived from the original MUSCL (Monotone Upstream-Centered Schemes for Conservation Laws) [459] (p. 754) by blending a central differencing scheme and second-order upwind scheme as

$$\phi_f = \theta \phi_{f,CD} + (1-\theta)\phi_{f,SOU} \tag{20.11}$$

where $\phi_{f,CD}$ is defined in Equation 20.8 (p. 635), and $\phi_{f,SOU}$ is computed using the second-order upwind scheme as described in Second-Order Upwind Scheme (p. 634).

Unlike the QUICK scheme, which is applicable to structured hex meshes only, the MUSCL scheme is applicable to arbitrary meshes. Compared to the second-order upwind scheme, the third-order MUSCL has a potential to improve spatial accuracy for all types of meshes by reducing numerical diffusion, most significantly for complex three-dimensional flows, and it is available for all transport equations.

**Important**

The third-order MUSCL currently implemented in ANSYS Fluent does not contain any Gradient limiter. As a result, it can produce undershoots and overshoots when the flow-field under consideration has discontinuities such as shock waves.

**Important**

The MUSCL scheme is available in the pressure-based and density-based solvers.

Release 15.0 - © SAS IP, Inc. All rights reserved. - Contains proprietary and confidential information of ANSYS, Inc. and its subsidiaries and affiliates.

### 20.3.1.9. Modified HRIC Scheme

For simulations using the VOF multiphase model, upwind schemes are generally unsuitable for interface tracking because of their overly diffusive nature. Central differencing schemes, while generally able to retain the sharpness of the interface, are unbounded and often give unphysical results. In order to overcome these deficiencies, ANSYS Fluent uses a modified version of the High Resolution Interface Capturing (HRIC) scheme. The modified HRIC scheme is a composite NVD scheme that consists of a non-linear blend of upwind and downwind differencing [314] (p. 746).

First, the normalized cell value of volume fraction, $\tilde{\phi}_c$, is computed and is used to find the normalized face value, $\tilde{\phi}_f$, as follows:

$$\tilde{\phi}_c = \frac{\phi_D - \phi_U}{\phi_A - \phi_U} \tag{20.12}$$

**Figure 20.6: Cell Representation for Modified HRIC Scheme**

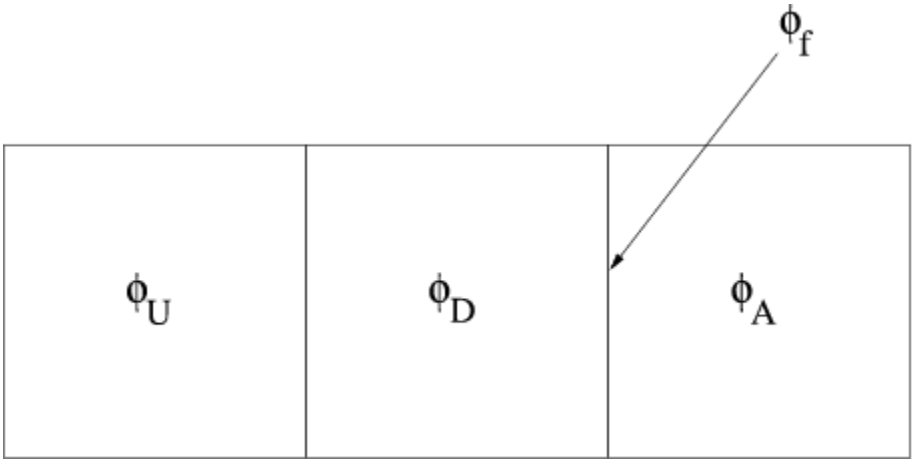


where $A$ is the acceptor cell, $D$ is the donor cell, and $U$ is the upwind cell, and

$$\tilde{\phi}_f = \begin{cases} \tilde{\phi}_c & \tilde{\phi}_c < 0 \text{ or } \tilde{\phi}_c > 1 \\ 2\tilde{\phi}_c & 0 \le \tilde{\phi}_c \le 0.5 \\ 1 & 0.5 \le \tilde{\phi}_c \le 1 \end{cases} \tag{20.13}$$

Here, if the upwind cell is not available (for example, unstructured mesh), an extrapolated value is used for $\phi_U$. Directly using this value of $\tilde{\phi}_f$ causes wrinkles in the interface, if the flow is parallel to the interface. So, ANSYS Fluent switches to the ULTIMATE QUICKEST scheme (the one-dimensional bounded version of the QUICK scheme [241] (p. 742)) based on the angle between the face normal and interface normal:

$$\phi_f^{\tilde{U}Q} = \begin{cases} \tilde{\phi}_c & \tilde{\phi}_c < 0 \text{ or } \tilde{\phi}_c > 1 \\ MIN\left(\tilde{\phi}_f, \frac{6\tilde{\phi}_c + 3}{8}\right) & 0 \le \tilde{\phi}_c \le 1 \end{cases} \tag{20.14}$$


Release 15.0 - © SAS IP, Inc. All rights reserved. - Contains proprietary and confidential information of ANSYS, Inc. and its subsidiaries and affiliates.

This leads to a corrected version of the face volume fraction, $\tilde{\phi}_f^*$:

$$\tilde{\phi}_f^* = \tilde{\phi}_f \sqrt{\cos\theta} + (1 - \sqrt{\cos\theta})\,\phi_f^{\tilde{U}Q} \tag{20.15}$$

where

$$\cos\theta = \frac{\nabla\phi \cdot \vec{d}}{|\nabla\phi \parallel \vec{d}|} \tag{20.16}$$

and $\vec{d}$ is a vector connecting cell centers adjacent to the face $f$.

The face volume fraction is now obtained from the normalized value computed above as follows:

$$\phi_f = \tilde{\phi}_f^* \left(\phi_A - \phi_U\right) + \phi_U \tag{20.17}$$

The modified HRIC scheme provides improved accuracy for VOF calculations when compared to QUICK and second-order schemes, and is less computationally expensive than the **Geo-Reconstruct** scheme.

### 20.3.1.10. High Order Term Relaxation

Higher order schemes can be written as a first-order scheme plus additional terms for the higher-order scheme. The higher-order relaxation can be applied to these additional terms.

The under-relaxation of high order terms follows the standard formulation for any generic property $\varphi$

$$\varphi_{new} = \varphi_{old} + f\left(\varphi_{intermediate} - \varphi_{old}\right) \tag{20.18}$$

Where $f$ is the under-relaxation factor. note that the default value of $f$ for steady state cases is 0.25 and for transient cases is 0.75. The same factor is applied to all equations solved.

For information about this solver option, see High Order Term Relaxation (HOTR) in the User's Guide.

## 20.3.2. Temporal Discretization

For transient simulations, the governing equations must be discretized in both space and time. The spatial discretization for the time-dependent equations is identical to the steady-state case. Temporal discretization involves the integration of every term in the differential equations over a time step $\Delta t$. The integration of the transient terms is straightforward, as shown below.

A generic expression for the time evolution of a variable $\phi$ is given by

$$\frac{\partial\phi}{\partial t} = F(\phi) \tag{20.19}$$

where the function $F$ incorporates any spatial discretization. If the time derivative is discretized using backward differences, the first-order accurate temporal discretization is given by

$$\frac{\phi^{n+1} - \phi^n}{\Delta t} = F(\phi) \tag{20.20}$$

and the second-order discretization is given by

$$\frac{3\phi^{n+1} - 4\phi^n + \phi^{n-1}}{2\Delta t} = F(\phi) \tag{20.21}$$

Release 15.0 - © SAS IP, Inc. All rights reserved. - Contains proprietary and confidential information of ANSYS, Inc. and its subsidiaries and affiliates.

where

$\phi$ = a scalar quantity

$n+1$ = value at the next time level, $t+\Delta t$

$n$ = value at the current time level, $t$

$n-1$ = value at the previous time level, $t-\Delta t$

Once the time derivative has been discretized, a choice remains for evaluating $F(\phi)$: in particular, which time level values of $\phi$ should be used in evaluating $F$.

### 20.3.2.1. Implicit Time Integration

One method is to evaluate $F(\phi)$ at the future time level:

$$\frac{\phi^{n+1}-\phi^{n}}{\Delta t}=F\left(\phi^{n+1}\right) \tag{20.22}$$

This is referred to as "implicit" integration since $\phi^{n+1}$ in a given cell is related to $\phi^{n+1}$ in neighboring cells through $F\left(\phi^{n+1}\right)$:

$$\phi^{n+1}=\phi^{n}+\Delta tF\left(\phi^{n+1}\right) \tag{20.23}$$

This implicit equation can be solved iteratively at each time level before moving to the next time step.

The advantage of the fully implicit scheme is that it is unconditionally stable with respect to time step size.

### 20.3.2.2. Bounded Second Order Implicit Time Integration

Any independent variable could be discretized in time as

$$\frac{\partial\phi}{\partial t}=\frac{\phi_{n+1/2}-\phi_{n-1/2}}{dt} \tag{20.24}$$

$$\phi_{n+1/2}=\phi_{n}+\frac{1}{2}\beta_{n+1/2}\left(\phi_{n}-\phi_{n-1}\right) \tag{20.25}$$

$$\phi_{n-1/2}=\phi_{n-1}+\frac{1}{2}\beta_{n-1/2}\left(\phi_{n-1}-\phi_{n-2}\right) \tag{20.26}$$

Where $n, n-1, n-2, n+1/2, n-1/2$ are different time levels.

$\beta_{n+1/2}$ and $\beta_{n-1/2}$ are bounding factors for each variable at the $n+1/2$ and $n-1/2$ level.

Bounded variables include the following:

- Multiphase flows: Volume fraction
- Turbulent flows: Turbulence kinetic energy, dissipation rate, specific dissipation rate
- Reacting flows: Species mass fraction, premixed/non-premixed variables


Release 15.0 - © SAS IP, Inc. All rights reserved. - Contains proprietary and confidential information of ANSYS, Inc. and its subsidiaries and affiliates.

#### 20.3.2.2.1. Limitations

The following limitations exist when using the bounded second order implicit formulation:

- It is not available with the density-based solver, only the pressure-based solver.
- It is not available with moving deforming meshes.
- It is only applicable to the implicit volume fraction discretization schemes for multiphase, and not to the explicit volume fraction schemes.
- It does not support the Singhal et al. cavitation model.

### *20.3.2.3. Explicit Time Integration*

The explicit time integration is only available when using the explicit density-based solver, in which $F(\phi)$ is evaluated explicitly (based on the existing solution of the dependent variable $\phi$:

$$\frac{\phi^{n+1}-\phi^{n}}{\Delta t}=F(\phi^{n}) \tag{20.27}$$

and is referred to as "explicit" integration since $\phi^{n+1}$ can be expressed explicitly in terms of the existing solution values, $\phi^{n}$:

$$\phi^{n+1}=\phi^{n}+\Delta tF(\phi^{n}) \tag{20.28}$$

Here, the time step $\Delta t$ is restricted to the stability limit of the underlying solver (that is, a time step is limited by the Courant-Friedrichs-Lewy condition). In order to be time-accurate, all cells in the domain must use the same time step. For stability, this time step must be the minimum of all the local time steps in the domain. This method is also referred to as "global time stepping".

The use of explicit time stepping is fairly restrictive. It is used primarily to capture the transient behavior of moving waves, such as shocks, because it is more accurate and less expensive than the implicit time stepping methods in such cases. You *cannot* use explicit time stepping in the following cases:

- Calculations with the pressure-based solver or density-based implicit formulation: The explicit time stepping formulation is available only with the density-based explicit formulation. ANSYS Fluent also uses multi-stage Runge-Kutta explicit time integration for the density-based solver, as detailed in Steady-State Flow Solution Methods (p. 663) and Unsteady Flows Solution Methods (p. 666)
- Incompressible flow: Explicit time stepping cannot be used to compute time-accurate incompressible flows.
- FAS multigrid and residual smoothing cannot be used with explicit time stepping because they destroy the time accuracy of the underlying solver.

## 20.3.3. Evaluation of Gradients and Derivatives

Gradients are needed not only for constructing values of a scalar at the cell faces, but also for computing secondary diffusion terms and velocity derivatives. The gradient $\nabla\phi$ of a given variable $\phi$ is used to discretize the convection and diffusion terms in the flow conservation equations. The gradients are computed in ANSYS Fluent according to the following methods:

Release 15.0 - © SAS IP, Inc. All rights reserved. - Contains proprietary and confidential information of ANSYS, Inc. and its subsidiaries and affiliates.

- Green-Gauss Cell-Based
- Green-Gauss Node-Based
- Least Squares Cell-Based

To learn how to apply the various gradients, see Choosing the Spatial Discretization Scheme in the User's Guide.

### 20.3.3.1. Green-Gauss Theorem

When the Green-Gauss theorem is used to compute the gradient of the scalar $\phi$ at the cell center $c0$, the following discrete form is written as

$$(\nabla\phi)_{c0} = \frac{1}{\nu}\sum_{f}\bar{\phi}_{f}\vec{A}_{f} \tag{20.29}$$

where $\phi_f$ is the value of $\phi$ at the cell face centroid, computed as shown in the sections below. The summation is over all the faces enclosing the cell.

### 20.3.3.2. Green-Gauss Cell-Based Gradient Evaluation

By default, the face value, $\bar{\phi}_f$, in Equation 20.29 (p. 642) is taken from the arithmetic average of the values at the neighboring cell centers, that is,

$$\bar{\phi}_{f}=\frac{\phi_{c0}+\phi_{c1}}{2} \tag{20.30}$$

### 20.3.3.3. Green-Gauss Node-Based Gradient Evaluation

Alternatively, $\bar{\phi}_f$ can be computed by the arithmetic average of the nodal values on the face.

$$\bar{\phi}_{f}=\frac{1}{N_f}\sum_{n}^{N_f}\bar{\phi}_{n} \tag{20.31}$$

where $N_f$ is the number of nodes on the face.

The nodal values, $\bar{\phi}_n$ in Equation 20.31 (p. 642), are constructed from the weighted average of the cell values surrounding the nodes, following the approach originally proposed by Holmes and Connel [166] (p. 738) and Rauch et al. [369] (p. 749). This scheme reconstructs exact values of a linear function at a node from surrounding cell-centered values on arbitrary unstructured meshes by solving a constrained minimization problem, preserving a second-order spatial accuracy.

The node-based gradient is known to be more accurate than the cell-based gradient particularly on irregular (skewed and distorted) unstructured meshes, however, it is relatively more expensive to compute than the cell-based gradient scheme.


Release 15.0 - © SAS IP, Inc. All rights reserved. - Contains proprietary and confidential information of ANSYS, Inc. and its subsidiaries and affiliates.

### 20.3.3.4. Least Squares Cell-Based Gradient Evaluation

In this method the solution is assumed to vary linearly. In Figure 20.7: Cell Centroid Evaluation (p. 643), the change in cell values between cell $c0$ and $ci$ along the vector $\delta r_i$ from the centroid of cell $c0$ to cell $ci$, can be expressed as

$$(\nabla\phi)_{c0} \cdot \Delta r_i = \left(\phi_{ci} - \phi_{c0}\right) \tag{20.32}$$

**Figure 20.7: Cell Centroid Evaluation**

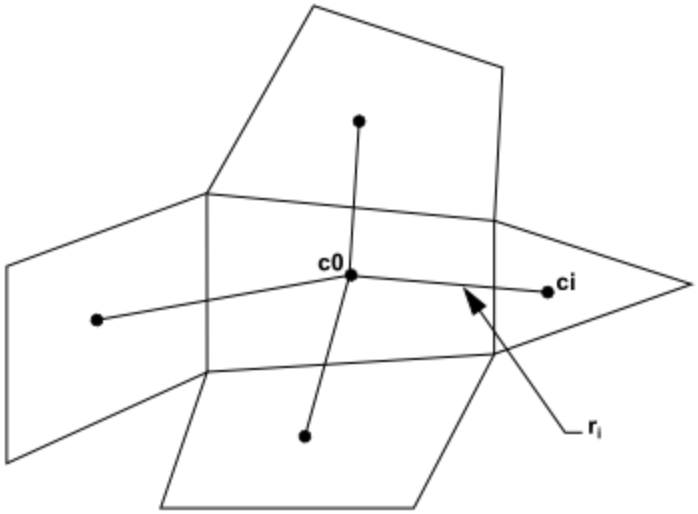


If we write similar equations for each cell surrounding the cell c0, we obtain the following system written in compact form:

$$[J](\nabla\phi)_{c0} = \Delta\phi \tag{20.33}$$

Where [J] is the coefficient matrix that is purely a function of geometry.

The objective here is to determine the cell gradient ($\nabla\phi_0 = \phi_x \hat{i} + \phi_y \hat{j} + \phi_z \hat{k}$) by solving the minimization problem for the system of the non-square coefficient matrix in a least-squares sense.

The above linear-system of equation is over-determined and can be solved by decomposing the coefficient matrix using the Gram-Schmidt process [7] (p. 729). This decomposition yields a matrix of weights for each cell. Thus for our cell-centered scheme this means that the three components of the weights ($W^x{}_{i0}$, $W^y{}_{i0}$, $W^z{}_{i0}$) are produced for each of the faces of cell c0.

Therefore, the gradient at the cell center can then be computed by multiplying the weight factors by the difference vector $\Delta\phi = \left(\phi_{c1} - \phi_{c0}\right)$,

$$\left(\phi_x\right)_{c0} = \sum_{i=1}^{n} W^x{}_{i0} \cdot \left(\phi_{ci} - \phi_{c0}\right) \tag{20.34}$$

$$\left(\phi_y\right)_{c0} = \sum_{i=1}^{n} W^y{}_{i0} \cdot \left(\phi_{ci} - \phi_{c0}\right) \tag{20.35}$$

Release 15.0 - © SAS IP, Inc. All rights reserved. - Contains proprietary and confidential information of ANSYS, Inc. and its subsidiaries and affiliates.

$$\left(\phi_z\right)_{c0} = \sum_{i=1}^{n} W^z{}_{i0} \cdot \left(\phi_{ci} - \phi_{c0}\right) \tag{20.36}$$

On irregular (skewed and distorted) unstructured meshes, the accuracy of the least-squares gradient method is comparable to that of the node-based gradient (and both are much more superior compared to the cell-based gradient). However, it is less expensive to compute the least-squares gradient than the node-based gradient. Therefore, it has been selected as the default gradient method in the ANSYS Fluent solver.

## 20.3.4. Gradient Limiters

Gradient limiters, also known as slope limiters, are used on the second-order upwind (SOU) scheme to prevent spurious oscillations, which would otherwise appear in the solution flow field near shocks, discontinuities, or near rapid local changes in the flow field. The gradient limiter attempts to invoke and enforce the monotonicity principle by prohibiting the linearly reconstructed field variable on the cell faces to exceed the maximum or minimum values of the neighboring cells.

There are three gradient limiters in the ANSYS Fluent solvers:

- Standard limiter
- Multidimensional limiter
- Differentiable limiter

Gradient limiters can be categorized into two general groups: non-differentiable limiters and differentiable limiters. Both, the standard limiter and multidimensional limiter are of the non-differentiable form, since they use minimum and maximum types of functions for limiting the solution variables. The third limiter in ANSYS Fluent, as the name indicates, is a differentiable type of limiter, which uses a smooth function to impose the monotonicity principle.

For each of the above mentioned limiter methods, ANSYS Fluent provides two limiting directions:

- cell to face limiting, where the limited value of the reconstruction gradient is determined at cell face centers. This is the default method.
- cell to cell limiting, where the limited value of the reconstruction gradient is determined along a scaled line between two adjacent cell centroids. On an orthogonal mesh (or when cell-to-cell direction is parallel to face area direction) this method becomes equivalent to the default cell to face method. For smooth field variation, cell to cell limiting may provide less numerical dissipation on meshes with skewed cells.

For more information about how to access the limiter functions in ANSYS Fluent through the GUI or TUI, see Selecting Gradient Limiters in the User's Guide.

**Important**

On unstructured meshes, ANSYS Fluent uses the scalar form of the gradient limiter given by the following equation:

$$\Phi_{f_{SOU}} = \Phi + \psi \nabla \phi \cdot r \tag{20.37}$$

Where $\psi$ is a scalar value that limits the gradient $\nabla \Phi$.


Release 15.0 - © SAS IP, Inc. All rights reserved. - Contains proprietary and confidential information of ANSYS, Inc. and its subsidiaries and affiliates.

### 20.3.4.1. Standard Limiter

The standard limiter is the default limiter function in ANSYS Fluent and is derived from the work of Barth and Jespersen [19] (p. 730). This limiter is of a non-differentiable type and uses the Minmod function (Minimum Modulus) to limit and clip the reconstructed solution overshoots and undershoots on the cell faces.

### 20.3.4.2. Multidimensional Limiter

The multidimensional limiter in ANSYS Fluent [206] (p. 740) has a similar form to the standard limiter. Since the multidimensional limiter uses a Minmod function for limiting the gradient, it is also classified as a non-differentiable type of limiter. However, in the standard limiter formulation, if limiting took place on any face of the cell, then this will cause the cell gradient to be clipped in an equal manner, in all directions, regardless of whether or not limiting is needed on the other cell faces. This limiting method is rather severe and adds unnecessary dissipation to the numerical scheme. The multidimensional limiter, on the other hand, attempts to lessen the severity of the gradient limiting by carefully examining the gradient on each cell and clipping only the normal components of the gradient to the cell faces. For this procedure to work on a scalar form limiter, the normal components of gradients on cell faces are first sorted out in ascending order of their magnitude so that only the necessary clipping can be applied. The multidimensional limiter is therefore less dissipative than the standard limiter.

### 20.3.4.3. Differentiable Limiter

One disadvantage with non-differentiable limiters is that they tend to stall the apparent residual's convergence after a few orders of reduction in residual magnitude. Note that this does not mean that the solution is not converging, but rather the solution continues to converge while the residuals are stalling. This annoying behavior can be directly traced to the non-differentiable nature of the limiting functions. Therefore, the differentiable limiter uses a smooth function to impose the monotonicity condition while allowing the residuals to converge. The differentiable limiter used in ANSYS Fluent is a modified form [477] (p. 755) of a limiter which was originally proposed by Venkatakrishnan [463] (p. 754).

**Important**

ANSYS Fluent uses gradient or slope limiters and not flux limiters. Gradient limiters are applied to the gradients of the variable field being linearly reconstructed at the cell faces, while flux limiters are used on the system fluxes.

## 20.4. Pressure-Based Solver

In this section, special practices related to the discretization of the momentum and continuity equations and their solution by means of the pressure-based solver are addressed. Information is organized into the following subsections:

20.4.1. Discretization of the Momentum Equation
20.4.2. Discretization of the Continuity Equation
20.4.3. Pressure-Velocity Coupling
20.4.4. Steady-State Iterative Algorithm
20.4.5. Time-Advancement Algorithm

These special practices are most easily described by considering the steady-state continuity and momentum equations in integral form:

$$\oint \rho \vec{v} \cdot d\vec{A} = 0 \tag{20.38}$$

Release 15.0 - © SAS IP, Inc. All rights reserved. - Contains proprietary and confidential information of ANSYS, Inc. and its subsidiaries and affiliates.

$$\oint \rho \vec{v}\,\vec{v}\cdot d\vec{A} = -\oint pI\cdot d\vec{A} + \oint \bar{\bar{\tau}}\cdot d\vec{A} + \int_V \vec{F}\,dV \tag{20.39}$$

where $I$ is the identity matrix, $\bar{\bar{\tau}}$ is the stress tensor, and $\vec{F}$ is the force vector.

## 20.4.1. Discretization of the Momentum Equation

The discretization scheme described in Discretization (p. 632) for a scalar transport equation is also used to discretize the momentum equations. For example, the $x$-momentum equation can be obtained by setting $\phi = u$:

$$a_P u = \sum_{nb} a_{nb} u_{nb} + \sum p_f A\cdot\hat{i} + S \tag{20.40}$$

If the pressure field and face mass fluxes are known, Equation 20.40 (p. 646) can be solved in the manner outlined in Discretization (p. 632), and a velocity field obtained. However, the pressure field and face mass fluxes are not known a priori and must be obtained as a part of the solution. There are important issues with respect to the storage of pressure and the discretization of the pressure gradient term; these are addressed next.

ANSYS Fluent uses a co-located scheme, whereby pressure and velocity are both stored at cell centers. However, Equation 20.40 (p. 646) requires the value of the pressure at the face between cells $c0$ and $c1$, shown in Figure 20.3: Control Volume Used to Illustrate Discretization of a Scalar Transport Equation (p. 632). Therefore, an interpolation scheme is required to compute the face values of pressure from the cell values.

### 20.4.1.1. Pressure Interpolation Schemes

ANSYS Fluent offers the following options for interpolating the pressure values at the faces. By default the **Second Order** scheme is used except in the case of mixture or VOF multiphase simulations in which case **PRESTO!** is the default.

- The **Linear** scheme computes the face pressure as the average of the pressure values in the adjacent cells.
- The **Standard** scheme interpolates the pressure values at the faces using momentum equation coefficients [376] (p. 749):

$$P_f = \frac{\frac{P_{c_0}}{a_{p,c_0}} + \frac{P_{c_1}}{a_{p,c_1}}}{\frac{1}{a_{p,c_0}} + \frac{1}{a_{p,c_1}}} \tag{20.41}$$

  This procedure works well as long as the pressure variation between cell centers is smooth. When there are jumps or large gradients in the momentum source terms between control volumes, the pressure profile has a high gradient at the cell face, and cannot be interpolated using this scheme. If this scheme is used, the discrepancy shows up in overshoots/undershoots of cell velocity.

  Flows for which the standard pressure interpolation scheme will have trouble include flows with large body forces, such as in strongly swirling flows, in high-Rayleigh-number natural convection and the like. In such cases, it is necessary to pack the mesh in regions of high gradient to resolve the pressure variation adequately.


Release 15.0 - © SAS IP, Inc. All rights reserved. - Contains proprietary and confidential information of ANSYS, Inc. and its subsidiaries and affiliates.

Another source of error is that ANSYS Fluent assumes that the normal pressure gradient at the wall is zero. This is valid for boundary layers, but not in the presence of body forces or curvature. Again, the failure to correctly account for the wall pressure gradient is manifested in velocity vectors pointing in/out of walls.

- The **Second Order** scheme reconstructs the face pressure using a central differencing scheme. The pressure values at the faces are given by:

$$P_f = \frac{1}{2}\left(P_{c_0} + P_{c_1}\right) + \frac{1}{2}\left(\nabla P_{c_0} \cdot \vec{r}_{c_0} + \nabla P_{c_1} \cdot \vec{r}_{c_1}\right) \tag{20.42}$$

  This scheme may provide improved accuracy over the **Standard** and **Linear** schemes. The **Second Order** scheme is not applicable for the VOF or mixture model for multiphase flow.

- The **Body Force Weighted** scheme computes the face pressure by assuming that the normal gradient of the difference between pressure and body forces is constant. This works well if the body forces are known a priori in the momentum equations (for example, buoyancy and axisymmetric swirl calculations).

  **Important**

  When a case contains porous media, the body-force-weighted scheme is applied only for non-porous faces, where the scheme takes into account the discontinuity of explicit body forces (for example, gravity, swirl, Coriolis) and the discontinuity of pressure gradients for flows with rapidly changing densities (for example, natural convection, VOF). All interior and exterior porous faces are treated with a special scheme that preserves the continuity of the normal velocity across cell faces in spite of the discontinuity of the resistance.

- The **PRESTO!** (PREssure STaggering Option) scheme uses the discrete continuity balance for a "staggered" control volume about the face to compute the "staggered" (that is, face) pressure. This procedure is similar in spirit to the staggered-grid schemes used with structured meshes [340] (p. 747). Note that for triangular, tetrahedral, hybrid, and polyhedral meshes, comparable accuracy is obtained using a similar algorithm. The PRESTO! scheme is available for all meshes.

For recommendations on when to use these alternate schemes, see Choosing the Pressure Interpolation Scheme in the User's Guide.

## 20.4.2. Discretization of the Continuity Equation

Equation 20.38 (p. 645) may be integrated over the control volume in Figure 20.3: Control Volume Used to Illustrate Discretization of a Scalar Transport Equation (p. 632) to yield the following discrete equation

$$\sum_{f}^{N_{faces}} J_f A_f = 0 \tag{20.43}$$

where $J_f$ is the mass flux through face $f$, $\rho v_n$.

In order to proceed further, it is necessary to relate the face values of velocity, $\vec{v}_n$, to the stored values of velocity at the cell centers. Linear interpolation of cell-centered velocities to the face results in unphysical checkerboarding of pressure. ANSYS Fluent uses a procedure similar to that outlined by Rhie and Chow [376] (p. 749) to prevent checkerboarding. The face value of velocity is not averaged linearly;

Release 15.0 - © SAS IP, Inc. All rights reserved. - Contains proprietary and confidential information of ANSYS, Inc. and its subsidiaries and affiliates.

instead, momentum-weighted averaging, using weighting factors based on the $a_P$ coefficient from Equation 20.40 (p. 646), is performed. Using this procedure, the face flux,

$J_f$, may be written as

$$\begin{aligned} Jf &= \rho_f \frac{a_{p,c_0} v_{n,c_0} + a_{p,c_1} v_{n,c_1}}{a_{p,c_0} + a_{p,c_1}} + d_f \left( \left( p_{c_0} + (\nabla p)_{c_0} \cdot \vec{r_0} \right) - \left( p_{c_1} + (\nabla p)_{c_1} \cdot \vec{r_1} \right) \right) \\ &= \hat{J}_f + d_f \left( p_{c_0} - p_{c_1} \right) \end{aligned} \tag{20.44}$$

where $p_{c_0}$, $p_{c_1}$ and $v_{n,c_0}$, $v_{n,c_1}$ are the pressures and normal velocities, respectively, within the two cells on either side of the face, and $\hat{J}_f$ contains the influence of velocities in these cells (see Figure 20.3: Control Volume Used to Illustrate Discretization of a Scalar Transport Equation (p. 632)). The term $d_f$ is a function of $\bar{a}_P$, the average of the momentum equation $a_P$ coefficients for the cells on either side of face $f$.

### 20.4.2.1. Density Interpolation Schemes

For incompressible flows, ANSYS Fluent uses arithmetic averaging for density. For compressible flow calculations (that is, calculations that use the ideal gas law for density), ANSYS Fluent applies upwind interpolation of density at cell faces. Several interpolation schemes are available for the density upwinding at cell faces: first-order upwind, second-order upwind (default), QUICK, MUSCL, and when applicable, central differencing and bounded central differencing.

The first-order upwind scheme (based on [196] (p. 739)) sets the density at the cell face to be the upstream cell-center value. This scheme provides stability for the discretization of the pressure-correction equation, and gives good results for most classes of flows. Although this scheme provides the best stability for compressible flow calculations, it gives very diffusive representations of shocks.

The second-order upwind scheme provides stability for supersonic flows and captures shocks better than the first-order upwind scheme. The QUICK scheme for density is similar to the QUICK scheme used for other variables. See QUICK Scheme (p. 636) for details.

**Important**

In the case of multiphase flows, the selected density scheme is applied to the compressible phase and arithmetic averaging is used for incompressible phases.

**Important**

If solution instability is encountered for compressible flow, it is recommended that you achieve a solution with a first order scheme and then switch to a higher order schemes.

For recommendations on choosing an appropriate density interpolation scheme for your compressible flow, see Choosing the Density Interpolation Scheme in the User's Guide.


Release 15.0 - © SAS IP, Inc. All rights reserved. - Contains proprietary and confidential information of ANSYS, Inc. and its subsidiaries and affiliates.

## 20.4.3. Pressure-Velocity Coupling

Pressure-velocity coupling is achieved by using Equation 20.44 (p. 648) to derive an additional condition for pressure by reformatting the continuity equation (Equation 20.43 (p. 647)). The pressure-based solver allows you to solve your flow problem in either a segregated or coupled manner. ANSYS Fluent provides the option to choose among five pressure-velocity coupling algorithms: SIMPLE, SIMPLEC, PISO, Coupled, and (for unsteady flows using the non-iterative time advancement scheme (NITA)) Fractional Step (FSM). All the aforementioned schemes, except the "coupled" scheme, are based on the predictor-corrector approach. For instructions on how to select these algorithms, see Choosing the Pressure-Velocity Coupling Method in the User's Guide.

Note that **SIMPLE**, **SIMPLEC**, **PISO**, and **Fractional Step** use the pressure-based segregated algorithm, while **Coupled** uses the pressure-based coupled solver.

**Important**

The pressure-velocity coupling schemes that are applicable when using the Eulerian multiphase model are **Phase Coupled SIMPLE**, **Multiphase Coupled**, and **Full Multiphase Coupled**. These are discussed in detail in Selecting the Pressure-Velocity Coupling Method in the User's Guide.

### *20.4.3.1. Segregated Algorithms*

#### 20.4.3.1.1. SIMPLE

The SIMPLE algorithm uses a relationship between velocity and pressure corrections to enforce mass conservation and to obtain the pressure field.

If the momentum equation is solved with a guessed pressure field $p^*$, the resulting face flux, $J_f^*$, computed from Equation 20.44 (p. 648)

$$J_f^* = \hat{J}_f^* + d_f\left(p_{c0}^* - p_{c1}^*\right) \tag{20.45}$$

does not satisfy the continuity equation. Consequently, a correction $J_f'$ is added to the face flux $J_f^*$ so that the corrected face flux, $J_f$

$$J_f = J_f^* + J_f' \tag{20.46}$$

satisfies the continuity equation. The SIMPLE algorithm postulates that $J_f'$ be written as

$$J_f' = d_f\left(p_{c0}' - p_{c1}'\right) \tag{20.47}$$

where $p'$ is the cell pressure correction.

The SIMPLE algorithm substitutes the flux correction equations (Equation 20.46 (p. 649) and Equation 20.47 (p. 649)) into the discrete continuity equation (Equation 20.43 (p. 647)) to obtain a discrete equation for the pressure correction $p'$ in the cell:

$$a_P p' = \sum_{nb} a_{nb} p_{nb}' + b \tag{20.48}$$

Release 15.0 - © SAS IP, Inc. All rights reserved. - Contains proprietary and confidential information of ANSYS, Inc. and its subsidiaries and affiliates.

where the source term $b$ is the net flow rate into the cell:

$$b = \sum_{f}^{N_{faces}} J_f^* A_f \tag{20.49}$$

The pressure-correction equation (Equation 20.48 (p. 649)) may be solved using the algebraic multigrid (AMG) method described in Algebraic Multigrid (AMG) (p. 676). Once a solution is obtained, the cell pressure and the face flux are corrected using

$$p = p^* + \alpha_p p' \tag{20.50}$$

$$J_f = J_f^* + d_f\left(p'_{c0} - p'_{c1}\right) \tag{20.51}$$

Here $\alpha_p$ is the under-relaxation factor for pressure (see Under-Relaxation of Variables (p. 653) for information about under-relaxation). The corrected face flux, $J_f$, satisfies the discrete continuity equation identically during each iteration.

### 20.4.3.1.2. SIMPLEC

A number of variants of the basic SIMPLE algorithm are available in the literature. In addition to SIMPLE, ANSYS Fluent offers the SIMPLEC (SIMPLE-Consistent) algorithm [461] (p. 754). SIMPLE is the default, but many problems will benefit from the use of SIMPLEC, as described in SIMPLE vs. SIMPLEC in the User's Guide.

The SIMPLEC procedure is similar to the SIMPLE procedure outlined above. The only difference lies in the expression used for the face flux correction, $J'_f$. As in SIMPLE, the correction equation may be written as

$$J_f = J_f^* + d_f\left(p'_{c0} - p'_{c1}\right) \tag{20.52}$$

However, the coefficient $d_f$ is redefined as a function of $\left(\overline{a_P - \sum_{nb} a_{nb}}\right)$. The use of this modified correction equation has been shown to accelerate convergence in problems where pressure-velocity coupling is the main deterrent to obtaining a solution.

#### *20.4.3.1.2.1. Skewness Correction*

For meshes with some degree of skewness, the approximate relationship between the correction of mass flux at the cell face and the difference of the pressure corrections at the adjacent cells is very rough. Since the components of the pressure-correction gradient along the cell faces are not known in advance, an iterative process similar to the PISO neighbor correction described below is desirable. After the initial solution of the pressure-correction equation, the pressure-correction gradient is recalculated and used to update the mass flux corrections. This process, which is referred to as "skewness correction", significantly reduces convergence difficulties associated with highly distorted meshes. The SIMPLEC skewness correction allows ANSYS Fluent to obtain a solution on a highly skewed mesh in approximately the same number of iterations as required for a more orthogonal mesh.

### 20.4.3.1.3. PISO

The Pressure-Implicit with Splitting of Operators (PISO) pressure-velocity coupling scheme, part of the SIMPLE family of algorithms, is based on the higher degree of the approximate relation between the corrections for pressure and velocity. One of the limitations of the SIMPLE and SIMPLEC algorithms is


Release 15.0 - © SAS IP, Inc. All rights reserved. - Contains proprietary and confidential information of ANSYS, Inc. and its subsidiaries and affiliates.

that new velocities and corresponding fluxes do not satisfy the momentum balance after the pressure-correction equation is solved. As a result, the calculation must be repeated until the balance is satisfied. To improve the efficiency of this calculation, the PISO algorithm performs two additional corrections: neighbor correction and skewness correction.

#### *20.4.3.1.3.1. Neighbor Correction*

The main idea of the PISO algorithm is to move the repeated calculations required by SIMPLE and SIMPLEC inside the solution stage of the pressure-correction equation [180] (p. 738). After one or more additional PISO loops, the corrected velocities satisfy the continuity and momentum equations more closely. This iterative process is called a momentum correction or "neighbor correction". The PISO algorithm takes a little more CPU time per solver iteration, but it can dramatically decrease the number of iterations required for convergence, especially for transient problems.

#### *20.4.3.1.3.2. Skewness Correction*

For meshes with some degree of skewness, the approximate relationship between the correction of mass flux at the cell face and the difference of the pressure corrections at the adjacent cells is very rough. Since the components of the pressure-correction gradient along the cell faces are not known in advance, an iterative process similar to the PISO neighbor correction described above is desirable [117] (p. 735). After the initial solution of the pressure-correction equation, the pressure-correction gradient is recalculated and used to update the mass flux corrections. This process, which is referred to as "skewness correction", significantly reduces convergence difficulties associated with highly distorted meshes. The PISO skewness correction allows ANSYS Fluent to obtain a solution on a highly skewed mesh in approximately the same number of iterations as required for a more orthogonal mesh.

#### *20.4.3.1.3.3. Skewness - Neighbor Coupling*

For meshes with a high degree of skewness, the simultaneous coupling of the neighbor and skewness corrections at the same pressure correction equation source may cause divergence or a lack of robustness. An alternate, although more expensive, method for handling the neighbor and skewness corrections inside the PISO algorithm is to apply one or more iterations of skewness correction for each separate iteration of neighbor correction. For each individual iteration of the classical PISO algorithm from [180] (p. 738), this technique allows a more accurate adjustment of the face mass flux correction according to the normal pressure correction gradient.

### *20.4.3.2. Fractional-Step Method (FSM)*

In the FSM, the momentum equations are decoupled from the continuity equation using a mathematical technique called operator-splitting or approximate factorization. The resulting solution algorithm is similar to the segregated solution algorithms described earlier. The formalism used in the approximate factorization allows you to control the order of splitting error. Because of this, the FSM is adopted in ANSYS Fluent as a velocity-coupling scheme in a non-iterative time-advancement (NITA) algorithm (Non-Iterative Time-Advancement Scheme (p. 656)).

### *20.4.3.3. Coupled Algorithm*

As previously mentioned, the pressure-based solver allows you to solve your flow problem in either a segregated or coupled manner. Using the coupled approach offers some advantages over the non-coupled or segregated approach. The coupled scheme obtains a robust and efficient single phase implementation for steady-state flows, with superior performance compared to the segregated solution schemes. This pressure-based coupled algorithm offers an alternative to the density-based and pressure-

Release 15.0 - © SAS IP, Inc. All rights reserved. - Contains proprietary and confidential information of ANSYS, Inc. and its subsidiaries and affiliates.

based segregated algorithm with SIMPLE-type pressure-velocity coupling. For transient flows, using the coupled algorithm is necessary when the quality of the mesh is poor, or if large time steps are used.

The pressure-based segregated algorithm solves the momentum equation and pressure correction equations separately. This semi-implicit solution method results in slow convergence.

The coupled algorithm solves the momentum and pressure-based continuity equations together. The full implicit coupling is achieved through an implicit discretization of pressure gradient terms in the momentum equations, and an implicit discretization of the face mass flux, including the Rhie-Chow pressure dissipation terms.

In the momentum equations (Equation 20.40 (p. 646)), the pressure gradient for component $k$ is of the form

$$\sum_f p_f A_k = -\sum_j a^{u_k p} p_j \tag{20.53}$$

Where $a^{u_k p}$ is the coefficient derived from the Gauss divergence theorem and coefficients of the pressure interpolation schemes (Equation 20.41 (p. 646)). Finally, for any $i$th cell, the discretized form of the momentum equation for component $u_k$ is defined as

$$\sum_j a_{ij}{}^{u_k u_k} u_{kj} + \sum_j a_{ij}{}^{u_k p} p_j = b_i{}^{u_k} \tag{20.54}$$

In the continuity equation, Equation 20.43 (p. 647), the balance of fluxes is replaced using the flux expression in Equation 20.44 (p. 648), resulting in the discretized form

$$\sum_k \sum_j a_{ij}{}^{p u_k} u_{kj} + \sum_j a_{ij}{}^{pp} p_j = b_i{}^{p} \tag{20.55}$$

As a result, the overall system of equations (Equation 20.54 (p. 652) and Equation 20.55 (p. 652)), after being transformed to the $\delta$-form, is presented as

$$\sum_j [A]_{ij} \vec{X}_j = \vec{B}_i \tag{20.56}$$

where the influence of a cell $i$ on a cell $j$ has the form

$$A_{ij} = \begin{bmatrix} a_{ij}^{pp} & a_{ij}^{pu} & a_{ij}^{pv} & a_{ij}^{pw} \\ a_{ij}^{up} & a_{ij}^{uu} & a_{ij}^{uv} & a_{ij}^{uw} \\ a_{ij}^{vp} & a_{ij}^{vu} & a_{ij}^{vv} & a_{ij}^{vw} \\ a_{ij}^{wp} & a_{ij}^{wu} & a_{ij}^{wv} & a_{ij}^{ww} \end{bmatrix} \tag{20.57}$$

and the unknown and residual vectors have the form

$$\vec{X}_j = \begin{bmatrix} p_i' \\ u_i' \\ v_i' \\ w_i' \end{bmatrix} \tag{20.58}$$


Release 15.0 - © SAS IP, Inc. All rights reserved. - Contains proprietary and confidential information of ANSYS, Inc. and its subsidiaries and affiliates.

$$\vec{B}_i = \begin{bmatrix} -r_i^p \\ -r_i^u \\ -r_i^v \\ -r_i^w \end{bmatrix} \tag{20.59}$$

Note that Equation 20.56 (p. 652) is solved using the coupled AMG, which is detailed in The Coupled and Scalar AMG Solvers (p. 679).

#### 20.4.3.3.1. Limitations

The pressure-based coupled algorithm is not compatible with

- The non-iterative time advancement solver (NITA)
- The fixed velocity option

## 20.4.4. Steady-State Iterative Algorithm

If you are performing a steady-state calculation, the governing equations for the pressure-based solver do not contain time-dependent terms. For steady-state flows, Discretization (p. 632) describes control-volume-based discretization of the steady-state transport equation (see Equation 20.1 (p. 631)).

### 20.4.4.1. Under-Relaxation of Variables

The under-relaxation of variables is used in all cases for some material properties, in the NITA solver for solution variables, and in the pressure-based coupled algorithm where this explicit under-relaxation is used for momentum and pressure.

Because of the nonlinearity of the equation set being solved by ANSYS Fluent, it is necessary to control the change of $\phi$. This is typically achieved by under-relaxation of variables (also referred to as explicit relaxation), which reduces the change of $\phi$ produced during each iteration. In a simple form, the new value of the variable $\phi$ within a cell depends upon the old value, $\phi_{old}$, the computed change in $\phi$, $\Delta\phi$, and the under-relaxation factor, $\alpha$, as follows:

$$\phi = \phi_{old} + \alpha \Delta\phi \tag{20.60}$$

### 20.4.4.2. Under-Relaxation of Equations

The under-relaxation of equations, also known as implicit relaxation, is used in the pressure-based solver to stabilize the convergence behavior of the outer nonlinear iterations by introducing selective amounts of $\phi$ in the system of discretized equations. This is equivalent to the location-specific time step.

$$\frac{a_p \phi}{\alpha} = \sum_{nb} a_{nb} \phi_{nb} + b + \frac{1-\alpha}{\alpha} a_p \phi_{old} \tag{20.61}$$

The CFL number is a solution parameter in the pressure-based coupled algorithm and can be written in terms of $\alpha$:

$$\frac{1-\alpha}{\alpha} = \frac{1}{CFL} \tag{20.62}$$

Release 15.0 - © SAS IP, Inc. All rights reserved. - Contains proprietary and confidential information of ANSYS, Inc. and its subsidiaries and affiliates.

## 20.4.5. Time-Advancement Algorithm

For time-dependent flows, the discretized form of the generic transport equations is of the following form:

$$\int_V \frac{\partial \rho \phi}{\partial t} dV + \oint \rho \phi \vec{v} \cdot d\vec{A} = \oint \Gamma_\phi \nabla \phi \cdot d\vec{A} + \int_V S_\phi dV \tag{20.63}$$

where

$\frac{\partial \rho \phi}{\partial t}$ = conservative form of transient derivative of transported variable $\phi$

$\rho$ = density

$\vec{v}$ = velocity vector (= $u\hat{i} + v\hat{j}$ in 2D)

$\vec{A}$ = surface area vector

$\Gamma_\phi$ = diffusion coefficient for $\phi$

$\nabla \phi$ = gradient of $\phi$ (= $(\partial \phi / \partial x)\hat{i} + (\partial \phi / \partial y)\hat{j}$ in 2D)

$S_\phi$ = source of $\phi$ per unit volume

The temporal discretization of the transient derivative in the Equation 20.63 (p. 654) is described in Temporal Discretization (p. 639), including first-order and second-order schemes in time. The pressure-based solver in ANSYS Fluent uses an implicit discretization of the transport equation (Equation 20.63 (p. 654)). As a standard default approach, all convective, diffusive, and source terms are evaluated from the fields for time level n+1.

$$\int_V \frac{\partial \rho \phi}{\partial t} dV + \oint \rho^{n+1} \phi^{n+1} \vec{v}^{\,n+1} \cdot d\vec{A} = \oint \Gamma_\phi^{n+1} \nabla \phi^{n+1} \cdot d\vec{A} + \int_V S_\phi^{n+1} dV \tag{20.64}$$

In the pressure-based solver, the overall time-discretization error is determined by both the choice of temporal discretization (for example, first-order, second-order) and the manner in which the solutions are advanced to the next time step (time-advancement scheme). Temporal discretization introduces the corresponding truncation error; $O(\Delta t)$, $O\left[(\Delta t)^2\right]$, for first-order and second-order, respectively.

The segregated solution process by which the equations are solved one by one introduces splitting error. There are two approaches to the time-advancement scheme depending on how you want to control the splitting error.

### 20.4.5.1. Iterative Time-Advancement Scheme

In the iterative scheme, all the equations are solved iteratively, for a given time-step, until the convergence criteria are met. Thus, advancing the solutions by one time-step normally requires a number of outer iterations as shown in Figure 20.1: Overview of the Pressure-Based Solution Methods (p. 627) and Figure 20.8: Overview of the Iterative Time Advancement Solution Method For the Segregate Solver (p. 655). With this iterative scheme, non-linearity of the individual equations and inter-equation couplings are fully accounted for, eliminating the splitting error. The iterative scheme is the default in ANSYS Fluent.


Release 15.0 - © SAS IP, Inc. All rights reserved. - Contains proprietary and confidential information of ANSYS, Inc. and its subsidiaries and affiliates.

**Figure 20.8: Overview of the Iterative Time Advancement Solution Method For the Segregate Solver**

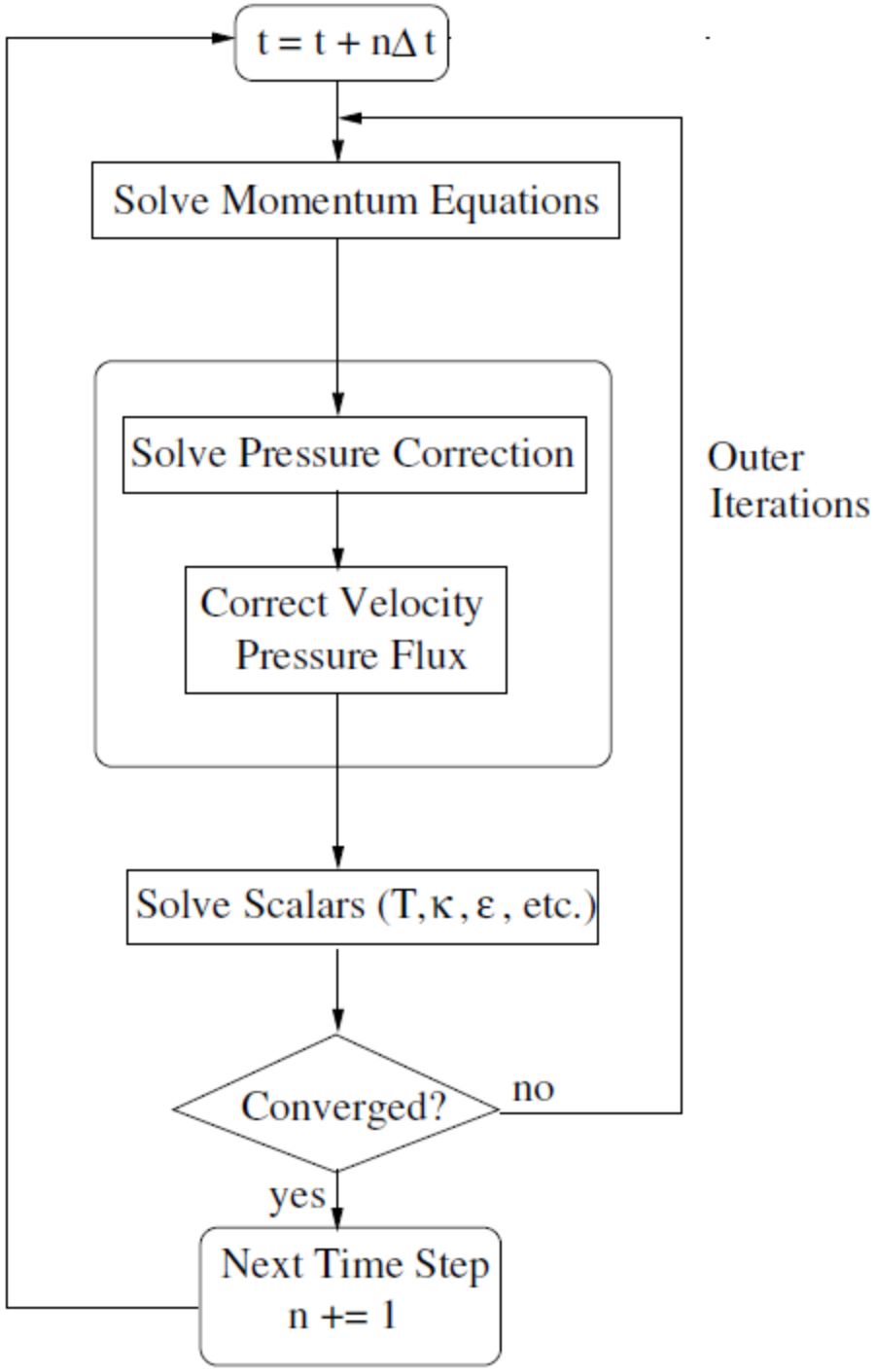


### 20.4.5.1.1. The Frozen Flux Formulation

The standard fully-implicit discretization of the convective part of Equation 20.64 (p. 654) produces non-linear terms in the resulting equations. In addition, solving these equations generally requires numerous iterations per time step. As an alternative, ANSYS Fluent provides an optional way to discretize the convective part of Equation 20.63 (p. 654) using the mass flux at the cell faces from the previous time level $n$.

Release 15.0 - © SAS IP, Inc. All rights reserved. - Contains proprietary and confidential information of ANSYS, Inc. and its subsidiaries and affiliates.

$$\oint \rho\phi\vec{v}\cdot d\vec{A} = \oint \rho^{n}\phi^{n+1}\vec{v}^{\,n}\cdot d\vec{A} \tag{20.65}$$

The solution still has the same order of accuracy but the non-linear character of the discretized transport equation is essentially reduced and the convergence within each time step is improved.

The **Frozen Flux Formulation** option is accessible from the **Solution Methods** dialog box.

**Important**

This option is only available for single-phase transient problems that use the segregated iterative solver and do not use a moving/deforming mesh model.

### 20.4.5.2. Non-Iterative Time-Advancement Scheme

The iterative time-advancement scheme requires a considerable amount of computational effort due to a large number of outer iterations performed for each time-step. The idea underlying the non-iterative time-advancement (NITA) scheme is that, in order to preserve overall time accuracy, you do not really need to reduce the splitting error to zero, but only have to make it the same order as the truncation error. The NITA scheme, as seen in Figure 20.9: Overview of the Non-Iterative Time Advancement Solution Method (p. 657), does not need the outer iterations, performing only a single outer iteration per time-step, which significantly speeds up transient simulations. However, the NITA scheme still allows for an inner iteration to solve the individual set of equations.


Release 15.0 - © SAS IP, Inc. All rights reserved. - Contains proprietary and confidential information of ANSYS, Inc. and its subsidiaries and affiliates.

**Figure 20.9: Overview of the Non-Iterative Time Advancement Solution Method**

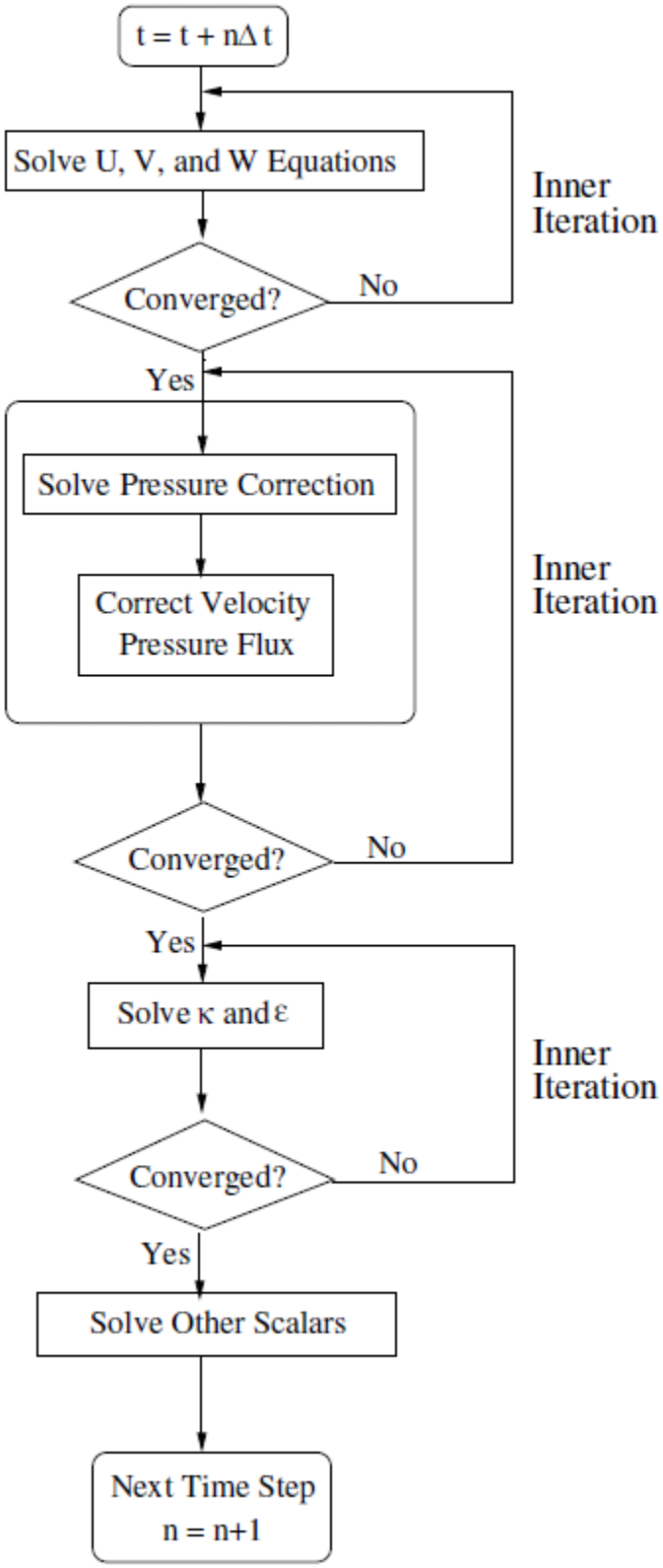


Release 15.0 - © SAS IP, Inc. All rights reserved. - Contains proprietary and confidential information of ANSYS, Inc. and its subsidiaries and affiliates.

ANSYS Fluent offers two versions of NITA schemes; the non-iterative fractional step method (FSM) ([12] (p. 729), [101] (p. 734), [181] (p. 739), and [182] (p. 739)) and the non-iterative PISO method [179] (p. 738). Both NITA schemes are available for first-order and second-order time integration.

**Important**

In general, the NITA solver is not recommended for highly viscous fluid flow.

## 20.5. Density-Based Solver

The density-based solver in ANSYS Fluent solves the governing equations of continuity, momentum, and (where appropriate) energy and species transport simultaneously as a set, or vector, of equations. Governing equations for additional scalars will be solved sequentially (that is, segregated from one another and from the coupled set), in a manner described in General Scalar Transport Equation: Discretization and Solution (p. 630). Two algorithms are available for solving the coupled set of equations, the coupled-explicit formulation and the coupled-implicit formulation.

Information is organized into the following subsections:

20.5.1. Governing Equations in Vector Form
20.5.2. Preconditioning
20.5.3. Convective Fluxes
20.5.4. Steady-State Flow Solution Methods
20.5.5. Unsteady Flows Solution Methods

### 20.5.1. Governing Equations in Vector Form

The system of governing equations for a single-component fluid, written to describe the mean flow properties, is cast in integral Cartesian form for an arbitrary control volume $V$ with differential surface area $dA$ as follows:

$$\frac{\partial}{\partial t}\int_V W\,dV + \oint [F-G]\cdot dA = \int_V H\,dV \tag{20.66}$$

where the vectors $W$, $F$, and $G$ are defined as

$$W=\begin{Bmatrix}\rho\\ \rho u\\ \rho v\\ \rho w\\ \rho E\end{Bmatrix}, F=\begin{Bmatrix}\rho v\\ \rho v u+p\hat{i}\\ \rho v v+p\hat{j}\\ \rho v w+p\hat{k}\\ \rho v E+pv\end{Bmatrix}, G=\begin{Bmatrix}0\\ \tau_{xi}\\ \tau_{yi}\\ \tau_{zi}\\ \tau_{ij}v_j+q\end{Bmatrix} \tag{20.67}$$

and the vector $H$ contains source terms such as body forces and energy sources.

Here $\rho$, $v$, $E$, and $p$ are the density, velocity, total energy per unit mass, and pressure of the fluid, respectively. $\tau$ is the viscous stress tensor, and $q$ is the heat flux.

Total energy $E$ is related to the total enthalpy $H$ by

$$E=H-p/\rho \tag{20.68}$$

where


Release 15.0 - © SAS IP, Inc. All rights reserved. - Contains proprietary and confidential information of ANSYS, Inc. and its subsidiaries and affiliates.

$$H = h + |v|^2/2 \tag{20.69}$$

The Navier-Stokes equations as expressed in Equation 20.66 (p. 658) become (numerically) very stiff at low Mach number due to the disparity between the fluid velocity $v$ and the acoustic speed $c$ (speed of sound). This is also true for incompressible flows, regardless of the fluid velocity, because acoustic waves travel infinitely fast in an incompressible fluid (speed of sound is infinite). The numerical stiffness of the equations under these conditions results in poor convergence rates. This difficulty is overcome in ANSYS Fluent's density-based solver by employing a technique called (time-derivative) preconditioning [483] (p. 755).

## 20.5.2. Preconditioning

Time-derivative preconditioning modifies the time-derivative term in Equation 20.66 (p. 658) by pre-multiplying it with a preconditioning matrix. This has the effect of re-scaling the acoustic speed (eigenvalue) of the system of equations being solved in order to alleviate the numerical stiffness encountered in low Mach numbers and incompressible flow.

Derivation of the preconditioning matrix begins by transforming the dependent variable in Equation 20.66 (p. 658) from conserved quantities $W$ to primitive variables $Q$ using the chain-rule as follows:

$$\frac{\partial W}{\partial Q}\frac{\partial}{\partial t}\int_V Q dV + \oint [F - G]\cdot dA = \int_V H dV \tag{20.70}$$

where $Q$ is the vector $\{p, u, v, w, T\}^T$ and the Jacobian $\partial W/\partial Q$ is given by

$$\frac{\partial W}{\partial Q} = \begin{bmatrix} \rho_p & 0 & 0 & 0 & \rho_T \\ \rho_p u & \rho & 0 & 0 & \rho_T u \\ \rho_p v & 0 & \rho & 0 & \rho_T v \\ \rho_p w & 0 & 0 & \rho & \rho_T w \\ \rho_p H - \delta & \rho u & \rho v & \rho w & \rho_T H + \rho C_p \end{bmatrix} \tag{20.71}$$

where

$$\rho_p = \left.\frac{\partial \rho}{\partial p}\right|_T, \rho_T = \left.\frac{\partial \rho}{\partial T}\right|_p \tag{20.72}$$

and $\delta = 1$ for an ideal gas and $\delta = 0$ for an incompressible fluid.

The choice of primitive variables $Q$ as dependent variables is desirable for several reasons. First, it is a natural choice when solving incompressible flows. Second, when we use second-order accuracy we need to reconstruct $Q$ rather than $W$ in order to obtain more accurate velocity and temperature gradients in viscous fluxes, and pressure gradients in inviscid fluxes. And finally, the choice of pressure as a dependent variable allows the propagation of acoustic waves in the system to be singled out [464] (p. 754).

We precondition the system by replacing the Jacobian matrix $\partial W/\partial Q$ (Equation 20.71 (p. 659)) with the preconditioning matrix $\Gamma$ so that the preconditioned system in conservation form becomes

Release 15.0 - © SAS IP, Inc. All rights reserved. - Contains proprietary and confidential information of ANSYS, Inc. and its subsidiaries and affiliates.

$$\Gamma \frac{\partial}{\partial t} \int_V Q dV + \oint [F - G] \cdot d A = \int_V H dV \tag{20.73}$$

where

$$\Gamma = \begin{bmatrix} \Theta & 0 & 0 & 0 & \rho_T \\ \Theta u & \rho & 0 & 0 & \rho_T u \\ \Theta v & 0 & \rho & 0 & \rho_T v \\ \Theta w & 0 & 0 & \rho & \rho_T w \\ \Theta H - \delta & \rho u & \rho v & \rho w & \rho_T H + \rho C_p \end{bmatrix} \tag{20.74}$$

The parameter $\Theta$ is given by

$$\Theta = \left( \frac{1}{U_r^2} - \frac{\rho_T}{\rho C_p} \right) \tag{20.75}$$

The reference velocity $U_r$ appearing in Equation 20.75 (p. 660) is chosen locally such that the eigenvalues of the system remain well conditioned with respect to the convective and diffusive time scales [483] (p. 755).

The resultant eigenvalues of the preconditioned system (Equation 20.73 (p. 660)) are given by

$$u, u, u, u' + c', u' - c' \tag{20.76}$$

where

$$u = v \cdot \hat{n}$$
$$u' = u (1 - \alpha)$$
$$c' = \sqrt{\alpha^2 u^2 + U_r^2}$$
$$\alpha = \left( 1 - \beta U_r^2 \right) / 2$$
$$\beta = \left( \rho_p + \frac{\rho_T}{\rho C_p} \right)$$

For an ideal gas, $\beta = (\gamma RT)^{-1} = 1/c^2$. Thus, when $U_r = c$ (at sonic speeds and above), $\alpha = 0$ and the eigenvalues of the preconditioned system take their traditional form, $u \pm c$. At low speed, however, as $U_r \to 0, \alpha \to 1/2$ and all eigenvalues become of the same order as $u$. For constant-density flows, $\beta = 0$ and $\alpha = 1/2$ regardless of the values of $U_r$. As long as the reference velocity is of the same order as the local velocity, all eigenvalues remain of the order $u$. Thus, the eigenvalues of the preconditioned system remain well conditioned at all speeds.

Note that the non-preconditioned Navier-Stokes equations are recovered exactly from Equation 20.73 (p. 660) by setting $1/U_r^2$ to $\rho_p$, the derivative of density with respect to pressure. In this case $\Gamma$ reduces exactly to the Jacobian $\partial W / \partial Q$.


Release 15.0 - © SAS IP, Inc. All rights reserved. - Contains proprietary and confidential information of ANSYS, Inc. and its subsidiaries and affiliates.

Although Equation 20.73 (p. 660) is conservative in the steady state, it is not, in a strict sense, conservative for time-dependent flows. This is not a problem, however, since the preconditioning has already destroyed the time accuracy of the equations and we will not employ them in this form for unsteady calculations.

For unsteady calculations, an unsteady preconditioning is available when the dual-time stepping method is used (Implicit Time Stepping (Dual-Time Formulation) (p. 666)). The unsteady preconditioning enhances the solution accuracy by improving the scaling of the artificial dissipation and maximizes the efficiency by optimizing the number of sub-iterations required at each physical time step [339] (p. 747). For low Mach number flows in particular, for both low frequency problems (large time steps) and high frequency problems (small time step), significant savings in computational time are possible when compared with the non-preconditioned case.

The unsteady preconditioning adapts the level of preconditioning based on the user-specified time-step and on the local advective and acoustic time scales of the flow. For acoustic problems, the physical time-step size is small as it is based on the acoustic CFL number. In this case the preconditioning parameter $U_r^2$ will approach $c^2$, which in effect will turn off the low-Mach preconditioning almost completely. For advection dominated problems, like the transport of turbulent vortical structures, and so on, the physical time-step is large as it is based on the particle CFL number. The corresponding unsteady preconditioning parameter $U_r^2$ will then approach $u^2$, which corresponds to the steady preconditioning choice. For intermediate physical time-step sizes, the unsteady preconditioning parameter will be adapted to provide optimum convergence efficiency of the pseudo-time iterations and accurate scaling of the artificial dissipation terms, regardless of the choice of the physical time step.

## 20.5.3. Convective Fluxes

### *20.5.3.1. Roe Flux-Difference Splitting Scheme*

The inviscid flux vector $F$ appearing in Equation 20.73 (p. 660) is evaluated by a standard upwind, flux-difference splitting [381] (p. 750). This approach acknowledges that the flux vector $F$ contains characteristic information propagating through the domain with speed and direction according to the eigenvalues of the system. By splitting $F$ into parts, where each part contains information traveling in a particular direction (that is, characteristic information), and upwind differencing the split fluxes in a manner consistent with their corresponding eigenvalues, we obtain the following expression for the discrete flux at each face:

$$F=\frac{1}{2}(F_R+F_L)-\frac{1}{2}\Gamma\,|\,\hat{\mathrm{A}}\,|\,\delta Q \tag{20.77}$$

Here $\delta Q$ is the spatial difference $Q_R-Q_L$. The fluxes $F_R=F\left(Q_R\right)$ and $F_L=F\left(Q_L\right)$ are computed using the (reconstructed) solution vectors $Q_R$ and $Q_L$ on the "right" and "left" side of the face. The matrix $|\hat{\mathrm{A}}|$ is defined by

$$|\,\hat{\mathrm{A}}\,|=M\,|\,\Lambda\,|\,M^{-1} \tag{20.78}$$

where $\Lambda$ is the diagonal matrix of eigenvalues and M is the modal matrix that diagonalizes $\Gamma^{-1}$A, where A is the inviscid flux Jacobian $\partial F/\partial Q$.

For the non-preconditioned system (and an ideal gas) Equation 20.77 (p. 661) reduces to Roe's flux-difference splitting [381] (p. 750) when Roe-averaged values are used to evaluate $\Gamma\,|\,\hat{\mathrm{A}}\,|$. At present, arithmetic averaging of states $Q_R$ and $Q_L$ is used.

In its current form, Equation 20.77 (p. 661) can be viewed as a second-order central difference plus an added matrix dissipation. The added matrix dissipation term is not only responsible for producing an upwinding of the convected variables, and of pressure and flux velocity in supersonic flow, but it also provides the pressure-velocity coupling required for stability and efficient convergence of low-speed and incompressible flows.

### 20.5.3.2. AUSM+ Scheme

An alternative way to compute the flux vector $F$ appearing in Equation 20.73 (p. 660) is by using a flux-vector splitting scheme [65] (p. 732). The scheme, called Advection Upstream Splitting Method (AUSM), was first introduced by Liou and Steffen in 1993 [259] (p. 743). The AUSM scheme first computes a cell interface Mach number based on the characteristic speeds from the neighboring cells. The interface Mach number is then used to determine the upwind extrapolation for the convection part of the inviscid fluxes. A separate Mach number splitting is used for the pressure terms. Generalized Mach number based convection and pressure splitting functions were proposed by Liou [258] (p. 743) and the new scheme was termed AUSM+. The AUSM+ scheme has several desirable properties:

1. Provides exact resolution of contact and shock discontinuities
2. Preserves positivity of scalar quantities
3. Free of oscillations at stationary and moving shocks

The AUSM+ scheme avoids using an explicit artificial dissipation, by proposing a numerical flux of the form:

$$F = m_f \phi + p_i \tag{20.79}$$

Here $m_f$ is the mass flux through the interface, which is computed using the fourth order polynomial functions of the left and right side (of the interface) Mach numbers.

ANSYS Fluent utilizes an all-speed version of the AUSM+ scheme based on the low-Mach preconditioning.

### 20.5.3.3. Low Diffusion Roe Flux Difference Splitting Scheme

In order to reduce dissipation in LES calculations, ANSYS Fluent uses a modified version of the Roe Flux Difference Splitting scheme, called the Low Diffusion Roe Flux Difference Splitting scheme. The scheme includes low Mach number preconditioning, in which the artificial dissipation term has been reduced [52] (p. 731) through the use of a hybrid scheme that combines a central scheme and a second-order upwind scheme (Roe's Flux Difference scheme).


Release 15.0 - © SAS IP, Inc. All rights reserved. - Contains proprietary and confidential information of ANSYS, Inc. and its subsidiaries and affiliates.

The Low Diffusion Roe-FDS is available in special circumstances when the LES viscous model is selected and when using the implicit-time formulation (dual-time-stepping). It is recommended that you use the second-order upwind scheme for maximum accuracy when selecting this flux scheme.

**Important**

The low diffusion discretization must be used only for subsonic flows. For high Mach number flows, it is recommended that you switch to standard Roe-FDS or AUSM+ flux schemes and second-order upwind discretization.

**Important**

When running LES with the explicit-time formulation, Low Diffusion Roe-FDS is not available and you will need to either use the standard Roe-FDS or the AUSM+ flux scheme and second-order upwind discretization.

To learn how to apply the different convective fluxes, see Convective Flux Types in the User's Guide.

## 20.5.4. Steady-State Flow Solution Methods

The coupled set of governing equations (Equation 20.73 (p. 660)) in ANSYS Fluent is discretized in time for both steady and unsteady calculations. In the steady case, it is assumed that time marching proceeds until a steady-state solution is reached. Temporal discretization of the coupled equations is accomplished by either an implicit or an explicit time-marching algorithm. These two algorithms are described below. To learn how to apply the two formulations, see Density-Based Solver Settings in the User's Guide.

### 20.5.4.1. Explicit Formulation

In the explicit scheme a multi-stage, time-stepping algorithm [185] (p. 739) is used to discretize the time derivative in Equation 20.73 (p. 660). The solution is advanced from iteration $n$ to iteration $n+1$ with an $m$-stage Runge-Kutta scheme, given by

$$Q^0 = Q^n$$
$$\Delta Q^i = -\alpha_i \Delta t \Gamma^{-1} R^{i-1}$$
$$Q^{n+1} = Q^m$$

where $\Delta Q^i \equiv Q^i - Q^n$ and $i = 1, 2, \ldots, m$ is the stage counter for the $m$-stage scheme. $\alpha_i$ is the multi-stage coefficient for the $i^{th}$ stage. The residual $R^i$ is computed from the intermediate solution $Q^i$ and, for Equation 20.73 (p. 660), is given by

$$R^i = \sum^{N_{faces}} \left( F\left(Q^i\right) - G\left(Q^i\right) \right) \cdot A - VH \tag{20.80}$$

The time step $\Delta t$ is computed from the CFL (Courant-Friedrichs-Lewy) condition

$$\Delta t = \frac{2 \quad CFL \quad V}{\sum_f \lambda_f^{\max} A_f} \tag{20.81}$$

where $V$ is the cell volume, $A_f$ is the face area, and ${\lambda_f}^{max}$ is the maximum of the local eigenvalues defined by Equation 20.76 (p. 660).

For steady-state solutions, convergence acceleration of the explicit formulation can be achieved with the use of local time stepping, residual smoothing, and full-approximation storage multigrid.

Local time stepping is a method by which the solution at each control volume is advanced in time with respect to the cell time step, defined by the local stability limit of the time-stepping scheme.

Residual smoothing, on the other hand, increases the bound of stability limits of the time-stepping scheme and hence allows for the use of a larger CFL value to achieve fast convergence (Implicit Residual Smoothing (p. 664)).

The convergence rate of the explicit scheme can be accelerated through use of the full-approximation storage (FAS) multigrid method described in Full-Approximation Storage (FAS) Multigrid (p. 681).

By default, ANSYS Fluent uses a 3-stage Runge-Kutta scheme based on the work by Lynn [274] (p. 744) for steady-state flows that use the density-based explicit solver.

#### 20.5.4.1.1. Implicit Residual Smoothing

The maximum time step can be further increased by increasing the support of the scheme through implicit averaging of the residuals with their neighbors. The residuals are filtered through a Laplacian smoothing operator:

$$\overline{R}_i = R_i + \varepsilon \sum \left( \overline{R}_j - \overline{R}_i \right) \tag{20.82}$$

This equation can be solved with the following Jacobi iteration:

$$\overline{R}_i^{\,m} = \frac{R_i + \epsilon \sum_1^N \overline{R}_j^{\,m-1}}{1 + \epsilon N} \tag{20.83}$$

where $N$ is the number of neighbors. Two Jacobi iterations are usually sufficient to allow doubling the time step with a value of $\varepsilon = 0.5$.

### 20.5.4.2. Implicit Formulation

In the implicit scheme, an Euler implicit discretization in time of the governing equations (Equation 20.73 (p. 660)) is combined with a Newton-type linearization of the fluxes to produce the following linearized system in delta form [481] (p. 755):

$$\left[ D + \sum_j^{N_{faces}} S_{j,k} \right] \Delta Q^{n+1} = -R^n \tag{20.84}$$

The center and off-diagonal coefficient matrices, $D$ and $S_{j,k}$ are given by

$$D = \frac{V}{\Delta t} \Gamma + \sum_j^{N_{faces}} S_{j,i} \tag{20.85}$$


Release 15.0 - © SAS IP, Inc. All rights reserved. - Contains proprietary and confidential information of ANSYS, Inc. and its subsidiaries and affiliates.

$$S_{j,k} = \left( \frac{\partial F_j}{\partial Q_k} - \frac{\partial G_j}{\partial Q_k} \right) A_j \tag{20.86}$$

and the residual vector $R^n$ and time step $\Delta t$ are defined as in Equation 20.80 (p. 663) and Equation 20.81 (p. 663), respectively.

Equation 20.84 (p. 664) is solved using either Incomplete Lower Upper factorization (ILU) by default or symmetric point Gauss-Seidel algorithm, in conjunction with an algebraic multigrid (AMG) method (see Algebraic Multigrid (AMG) (p. 676)) adapted for coupled sets of equations.

Explicit relaxation can improve the convergence to steady state of the implicit formulation. By default, explicit relaxation is enabled for the implicit solver and uses a factor of `0.75`. You can specify a factor $\alpha$ to control the amount that the solution vector $Q$ changes between iterations after the end of the algebraic multigrid (AMG) cycle:

$$Q_{new} = Q_{old} + \alpha \Delta Q \tag{20.87}$$

By specifying a value less than the default value of `1` for $\alpha$, the variables in the solution vector will be under-relaxed and the convergence history can be improved. For information on how to set this value, see Specifying the Explicit Relaxation in the User's Guide.

**Important**

Note that explicit relaxation is available for the density-based implicit solver in steady state mode only.

### 20.5.4.2.1. Convergence Acceleration for Stretched Meshes

When the flow is solved on meshes containing highly stretched cells (cells with large aspect ratio typically found near wall boundaries), the traditional implicit solution method will suffer from convergence slow down due to the small local time step values defined by equation Equation 20.81 (p. 663). The larger the cell aspect ratio, the smaller the local time step and the slower the local rate change of the solution. The time step definition in equation Equation 20.81 (p. 663) is based effectively on the minimum cell characteristic distance. A more optimum time step definition for the implicit solution method can be based on the maximum characteristic length of the cell [247] (p. 742) to give a new time step definition:

$$\Delta t = \frac{2 \quad CFL \quad V \quad AR}{\sum_f \lambda_f^{\max} A_f} \tag{20.88}$$

where AR is the cell aspect ratio defined as the ratio of maximum length to minimum length in the cell

$$AR = \frac{l_{\max}}{l_{\min}}$$

Effectively, the new definition will vary the local CFL value from one cell to another proportional to the value of the cell aspect ratio. When the cell aspect ratio is near unity, the local CFL value will be similar to the one entered by you. On the other hand, on stretched high aspect ratio cells, the local CFL value is a multiple of the cell aspect ratio. The new time step definition will accelerate the solution convergence particularly on meshes with Y+ near 1.

Release 15.0 - © SAS IP, Inc. All rights reserved. - Contains proprietary and confidential information of ANSYS, Inc. and its subsidiaries and affiliates.

## 20.5.5. Unsteady Flows Solution Methods

For time-accurate calculations, explicit and implicit time-stepping schemes are available. (The time-implicit approach is also referred to as "dual time stepping".)

### 20.5.5.1. Explicit Time Stepping

The explicit time stepping approach, is available only for the explicit scheme described above. The time step is determined by the CFL condition. To maintain time accuracy of the solution the explicit time stepping employs the same time step in each cell of the domain (this is also known as global-time step), and with preconditioning disabled. By default, ANSYS Fluent uses a 4-stage Runge-Kutta scheme for unsteady flows.

### 20.5.5.2. Implicit Time Stepping (Dual-Time Formulation)

The implicit-time stepping method (also known as dual-time formulation) is available in the density-based explicit and implicit formulation.

When performing unsteady simulations with implicit-time stepping (dual-time stepping), ANSYS Fluent uses a low Mach number time-derivative unsteady preconditioner to provide accurate results both for pure convective processes (for example, simulating unsteady turbulence) and for acoustic processes (for example, simulating wave propagation) [456] (p. 754), [339] (p. 747).

Here we introduce a preconditioned pseudo-time-derivative term into Equation 20.66 (p. 658) as follows:

$$\frac{\partial}{\partial t}\int_V W\,dV + \Gamma\frac{\partial}{\partial \tau}\int_V Q\,dV + \oint [F-G]\cdot dA = \int_V H\,dV \tag{20.89}$$

where $t$ denotes physical-time and $\tau$ is a pseudo-time used in the time-marching procedure. Note that as $\tau \rightarrow \infty$, the second term on the left side of Equation 20.89 (p. 666) vanishes and Equation 20.66 (p. 658) is recovered.

The time-dependent term in Equation 20.89 (p. 666) is discretized in an implicit fashion by means of either a first- or second-order accurate, backward difference in time.

The dual-time formulation is written in semi-discrete form as follows:

$$\left[\frac{\Gamma}{\Delta\tau} + \frac{\varepsilon_0}{\Delta t}\frac{\partial W}{\partial Q}\right]\Delta Q^{k+1} + \frac{1}{V}\oint [F-G]\cdot dA = H - \frac{1}{\Delta t}\left(\varepsilon_0 W^k - \varepsilon_1 W^n + \varepsilon_2 W^{n-1}\right)$$

where $\{\varepsilon_0 = \varepsilon_1 = 1/2\,, \varepsilon_2 = 0\}$ gives first-order time accuracy, and $\{\varepsilon_0 = 3/2\,, \varepsilon_1 = 2\,, \varepsilon_2 = 1/2\}$ gives second-order. $k$ is the inner iteration counter and $n$ represents any given physical-time level.

The pseudo-time-derivative is driven to zero at each physical time level by a series of inner iterations using either the implicit or explicit time-marching algorithm.

Throughout the (inner) iterations in pseudo-time, $W^n$ and $W^{n-1}$ are held constant and $W^k$ is computed from $Q^k$. As $\tau \rightarrow \infty$, the solution at the next physical time level $W^{n+1}$ is given by $W\left(Q^k\right)$.


Release 15.0 - © SAS IP, Inc. All rights reserved. - Contains proprietary and confidential information of ANSYS, Inc. and its subsidiaries and affiliates.

Note that the physical time step $\Delta t$ is limited only by the level of desired temporal accuracy. The pseudo-time-step $\Delta \tau$ is determined by the CFL condition of the (implicit or explicit) time-marching scheme.

Table 20.1: Summary of the Density-Based Solver (p. 667) summarizes all operation modes for the density-based solver from the iterative scheme in steady-state calculations to time-marching schemes for transient calculations.

**Table 20.1: Summary of the Density-Based Solver**

| Solution Method | Density-Based Solver - Explicit Formulation | Density-Based Solver - Implicit Formulation |
|---|---|---|
| Steady-State | – 3-stages Runge-Kutta | – local time step |
| | – local time step | – time-derivative preconditioning |
| | – time-derivative preconditioning | |
| | — FAS | |
| Unsteady - Explicit Time Stepping | – 4-stages Runge-Kutta | N/A |
| | – global time step | |
| | – no time-derivative preconditioning | |
| | – No FAS | |
| Unsteady - Implicit Time Stepping (dual-time formulation) First Order | – dual-time formulation | – dual-time formulation |
| | – Physical time: first order Euler backward | – Physical time: first order Euler backward |
| | – preconditioned pseudo-time derivative | – preconditioned pseudo-time derivative |
| | – inner iteration: explicit pseudo-time marching, 3-stage Runge-Kutta | – inner iteration: implicit pseudo-time marching |
| Unsteady - Implicit Time Stepping (dual-time formulation) Second Order | – dual-time formulation | – dual-time formulation |
| | – Physical time: second order Euler backward | – Physical time: second order Euler backward |
| | – preconditioned pseudo-time derivative | – preconditioned pseudo-time derivative |
| | – inner iteration: explicit pseudo-time marching, 3-stage Runge-Kutta | – inner iteration: implicit pseudo-time marching |

## 20.6. Pseudo Transient Under-Relaxation

The pseudo transient under-relaxation method is a form of implicit under-relaxation. Here, the under-relaxation is controlled through the pseudo time step size. The pseudo time step size can be the same or different for different equations solved.

$$\rho_p \Delta V \frac{\phi_p - \phi_p^{old}}{\Delta t} + a_p \phi_p = \sum_{nb} a_{nb} \phi_{nb} + b \tag{20.90}$$

where $\Delta t$ is the pseudo time step.

To learn how to apply pseudo transient under-relaxation, refer to Performing Pseudo Transient Calculations.

For more information, see the following section:
20.6.1. Automatic Pseudo Transient Time Step

## 20.6.1. Automatic Pseudo Transient Time Step

During a pseudo transient calculation, you have the option of specifying the pseudo time step or you can have ANSYS Fluent calculate it automatically. In general, ANSYS Fluent computes a fluid time scale for fluid zones. A solid time scale is used in the energy equation for the following zones or models:

- Solid zones
- Porous zones
- Solidification and melting model

The automatic time step is treated as follows:

- *Fluid Time Scale*

  The automatic fluid time scale for fluid zones is calculated using the minimum of the different time-scales:

  $$\Delta t_{fluid} = Min\left(\Delta t_u, \Delta t_p, \Delta t_g, \Delta t_{rot}, \Delta t_{compress}, \Delta t_{viscous}\right) \tag{20.91}$$

  Each time scale is obtained by dividing a representative length scale $L_{scale}$ over an appropriate representative velocity scale that depends on the physics present in the flow domain. Therefore, the convective time scale $\Delta t_u$, the dynamic time scale $\Delta t_p$, and the gravitational time scale $\Delta t_g$ are given by the following equations:

  $$\Delta t_u = \frac{0.3 L_{scale}}{Max\left(U_{bc}, U_{domain}\right)} \tag{20.92}$$

  $$\Delta t_p = \frac{0.3 L_{scale}}{U_{\Delta P}} \tag{20.93}$$

  $$\Delta t_g = \sqrt{\frac{L_{scale}}{g}} \tag{20.94}$$

  where $g = |\vec{g}|$ is the magnitude of the gravitational vector.

  For natural convection cases (the Boussinesq approximation is used) $g$ is modified as follows:

  $$g = |\vec{g}|\beta\left(T_{\max} - T_{\min}\right) \tag{20.95}$$

  The velocity $U_{bc}$ is the maximum of the arithmetic average of the velocity at the domain boundary faces, and $U_{domain}$ is the arithmetic average of the velocity over the cells in the domain. For the VOF and mixture models, the average velocity is calculated using the velocity in interfacial cells only.

  For cases with rotational velocities, the rotational time scale is calculated as

  $$\Delta t_{rot} = \frac{0.1}{\omega} \tag{20.96}$$

  where $\omega = |\vec{\omega}|$ is the magnitude of the angular velocity vector.

  The diffusion time scale is expressed in terms of the kinematic viscosity $v$, and is given by


Release 15.0 - © SAS IP, Inc. All rights reserved. - Contains proprietary and confidential information of ANSYS, Inc. and its subsidiaries and affiliates.

$$\Delta t_{viscous} = \frac{L_{scale}^2}{v} \tag{20.97}$$

If the simulation Mach number is greater than 0.3, then the compressible time scale is obtained from the following formula:

$$\Delta t_{compress} = \frac{0.3 L_{scale}}{Max\left(U_{bc}, U_{domain}, U_{\Delta P}, \overline{c}\right)} \tag{20.98}$$

Where the simulation Mach number $M$ is computed as

$$M = \frac{\mathrm{MAX}\left(U_{bc}, U_{domain}, U_{\Delta P}\right)}{\overline{c}} \tag{20.99}$$

where $\overline{c}$ is the average speed of sound over all cells, and the velocity scale $U_{\Delta P}$ is based on the pressure difference at open boundaries, such as pressure inlet, pressure outlet or velocity inlet, and is defined by the following:

$$U_{\Delta \mathrm{P}} = \sqrt{\left(\frac{P_{bc,max} - P_{bc,min}}{\overline{\rho}_{cells}}\right)} \tag{20.100}$$

where $P_{bc,max}$ is the maximum pressure value at the open boundary, $P_{bc,mIn}$ is the minimum pressure value at the open boundary, and $\overline{\rho}_{cells}$ is the average density over the domain.

Two length scale calculation methods are available: *aggressive* and *conservative*. If the aggressive length scale method is applied, then the length scale in all of the equations shown above are defined as

$$L_{scale} = MAX\left(L_{vol}, L_{ext}\right) \tag{20.101}$$

On the other hand, if the *conservative* length scale method is applied, then the length scale is defined as

$$L_{scale} = MIN\left(L_{vol}, L_{ext}\right) \tag{20.102}$$

where the length scale is defined as

$$L_{vol} = \sqrt[3]{V} \tag{20.103}$$

and the domain length scale is defined as

$$L_{ext} = MAX\left(L_x, L_y, L_z\right) \tag{20.104}$$

where $V$ is the volume of the domain and ($L_x, L_y, L_z$) are the domain extents in the x, y, and z direction, respectively.

- *Solid Time Scale*

The automatic solid time scale for solid zones, porous zones, and solidification/melting model, with the energy equation enabled, is computed using the following formula:

$$\Delta t_{solid} = \frac{L_{scale_solid}^2}{a} \tag{20.105}$$

where $L_{scale_solid}$ is the representative length scale and $\alpha = \frac{k}{\rho C_p}$ is the representative velocity scale, where $k$ is the conductivity of the solid material, $\rho$ is the density of the solid material, and $C_p$ is the specific heat of the solid material. The length scale for the solid zone is calculated as

Release 15.0 - © SAS IP, Inc. All rights reserved. - Contains proprietary and confidential information of ANSYS, Inc. and its subsidiaries and affiliates.

the cube root of the solid volume. All solid properties are volume averaged over solid zones. Since the time scale in the solid zone is governed by the diffusion phenomenon, it is usually very high compared to the time step predicted in fluid zones.

To learn how to apply the automatic time step for pseudo transient cases, refer to Performing Pseudo Transient Calculations in the User's Guide.

# 20.7. Multigrid Method

The ANSYS Fluent solver contains two forms of multigrid: algebraic (AMG) and full-approximation storage (FAS). AMG is an essential component of both the pressure-based and density-based implicit solvers, while FAS is an important, but optional, component of the density-based explicit solver. (Note that when the density-based explicit solver is used, AMG will also be used, since the scalar equations (for example, turbulence) are solved using the approach described in General Scalar Transport Equation: Discretization and Solution (p. 630).)

This section describes the mathematical basis of the multigrid approach. Common aspects of AMG and FAS are presented first, followed by separate sections that provide details unique to each method.

Information is organized into the following subsections:

20.7.1. Approach
20.7.2. Multigrid Cycles
20.7.3. Algebraic Multigrid (AMG)
20.7.4. Full-Approximation Storage (FAS) Multigrid

For information about user inputs and controls for the multigrid solver, see Modifying Algebraic Multigrid Parameters and Setting FAS Multigrid Parameters in the User's Guide.

## 20.7.1. Approach

ANSYS Fluent uses a multigrid scheme to accelerate the convergence of the solver by computing corrections on a series of coarse grid levels. The use of this multigrid scheme can greatly reduce the number of iterations and the CPU time required to obtain a converged solution, particularly when your model contains a large number of control volumes.

### *20.7.1.1. The Need for Multigrid*

Implicit solution of the linearized equations on unstructured meshes is complicated by the fact that there is no equivalent of the line-iterative methods that are commonly used on structured meshes. Since direct matrix inversion is out of the question for realistic problems and "whole-field" solvers that rely on conjugate-gradient (CG) methods have robustness problems associated with them, the methods of choice are point implicit solvers like Gauss-Seidel and ILU. Although the Gauss-Seidel and ILU schemes rapidly remove local (high-frequency) errors in the solution, global (low-frequency) errors are reduced at a rate inversely related to the mesh size. Thus, for a large number of nodes, the solver "stalls" and the residual reduction rate becomes prohibitively low.

The multi-stage scheme used in the density-based explicit solver can efficiently remove local (high-frequency) errors as well. That is, the effect of the solution in one cell is communicated to adjacent cells relatively quickly. However, the scheme is less effective at reducing global (low-frequency) errors–errors that exist over a large number of control volumes. Thus, global corrections to the solution across a large number of control volumes occur slowly, over many iterations. This implies that performance of the multi-stage scheme will deteriorate as the number of control volumes increases.


Release 15.0 - © SAS IP, Inc. All rights reserved. - Contains proprietary and confidential information of ANSYS, Inc. and its subsidiaries and affiliates.

Multigrid techniques allow global error to be addressed by using a sequence of successively coarser meshes. This method is based upon the principle that global (low-frequency) error existing on a fine mesh can be represented on a coarse mesh where it again becomes accessible as local (high-frequency) error: because there are fewer coarse cells overall, the global corrections can be communicated more quickly between adjacent cells. Since computations can be performed at an exponentially decaying expense in both CPU time and memory storage on coarser meshes, there is the potential for very efficient elimination of global error. The fine-grid relaxation scheme or "smoother", in this case either the point-implicit linear solvers (The Coupled and Scalar AMG Solvers (p. 679)) or the explicit multi-stage scheme, is not required to be particularly effective at reducing global error and can be tuned for efficient reduction of local error.

### 20.7.1.2. The Basic Concept in Multigrid

Consider the set of discretized linear (or linearized) equations given by

$$A\phi_e + b = 0 \tag{20.106}$$

where $\phi_e$ is the exact solution. Before the solution has converged there will be a defect $d$ associated with the approximate solution $\phi$:

$$A\phi + b = d \tag{20.107}$$

We seek a correction $\psi$ to $\phi$ such that the exact solution is given by

$$\phi_e = \phi + \psi \tag{20.108}$$

Substituting Equation 20.108 (p. 671) into Equation 20.106 (p. 671) gives

$$A\,(\phi + \psi)\, + b = 0 \tag{20.109}$$

$$A\psi + \,(A\phi + b)\, = 0 \tag{20.110}$$

Now using Equation 20.107 (p. 671) and Equation 20.109 (p. 671) we obtain

$$A\psi + d = 0 \tag{20.111}$$

which is an equation for the correction in terms of the original fine level operator $A$ and the defect $d$. Assuming the local (high-frequency) errors have been sufficiently damped by the relaxation scheme on the fine level, the correction $\psi$ will be smooth and therefore more effectively solved on the next coarser level.

### 20.7.1.3. Restriction and Prolongation

Solving for corrections on the coarse level requires transferring the defect down from the fine level (restriction), computing corrections, and then transferring the corrections back up from the coarse level (prolongation). We can write the equations for coarse level corrections $\psi^H$ as

$$A^H\psi^H + Rd = 0 \tag{20.112}$$

where $A^H$ is the coarse level operator and $R$ the restriction operator responsible for transferring the fine level defect down to the coarse level. Solution of Equation 20.112 (p. 671) is followed by an update of the fine level solution given by

$$\phi^{new} = \phi + P\psi^H \tag{20.113}$$

where $P$ is the prolongation operator used to transfer the coarse level corrections up to the fine level.

Release 15.0 - © SAS IP, Inc. All rights reserved. - Contains proprietary and confidential information of ANSYS, Inc. and its subsidiaries and affiliates.

#### 20.7.1.4. Unstructured Multigrid

The primary difficulty with using multigrid on unstructured meshes is the creation and use of the coarse grid hierarchy. On a structured mesh, the coarse meshes can be formed simply by removing every other mesh line from the fine meshes and the prolongation and restriction operators are simple to formulate (for example, injection and bilinear interpolation).

The difficulties of applying multigrid on unstructured meshes are overcome in a separate fashion by each of the two multigrid methods used in ANSYS Fluent. While the basic principles discussed so far and the cycling strategy described in Multigrid Cycles (p. 672) are the same, the techniques for construction of restriction, prolongation, and coarse mesh operators are different, as discussed in Algebraic Multigrid (AMG) (p. 676) and Full-Approximation Storage (FAS) Multigrid (p. 681) for the AMG and FAS methods, respectively.

### 20.7.2. Multigrid Cycles

A multigrid cycle can be defined as a recursive procedure that is applied at each grid level as it moves through the grid hierarchy. Four types of multigrid cycles are available in ANSYS Fluent: the V, W, F, and flexible ("flex") cycles. The V and W cycles are available in both AMG and FAS, while the F and flexible cycles are restricted to the AMG method only. (The W and flexible AMG cycles are not available for solving the coupled equation set due to the amount of computation required.)

#### 20.7.2.1. The V and W Cycles

Figure 20.10: V-Cycle Multigrid (p. 673) and Figure 20.11: W-Cycle Multigrid (p. 674) show the V and W multigrid cycles (defined below). In each figure, the multigrid cycle is represented by a square, and then expanded recursively to show the individual steps that are performed within the cycle. The individual steps are represented by a circle, one or more squares, and a triangle, connected by lines: circle-square-triangle for a V cycle, or circle-square-square-triangle for a W cycle. The squares in this group expand again, into circle-square-triangle or circle-square-square-triangle, and so on. You may want to follow along in the figures as you read the steps below.


Release 15.0 - © SAS IP, Inc. All rights reserved. - Contains proprietary and confidential information of ANSYS, Inc. and its subsidiaries and affiliates.

**Figure 20.10: V-Cycle Multigrid**

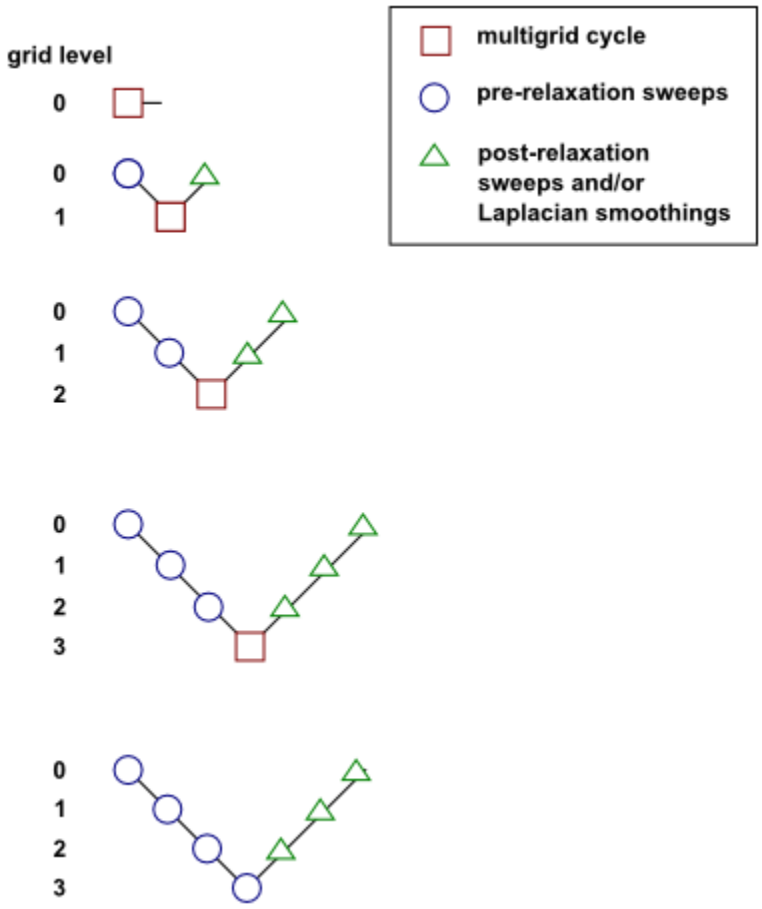

**Figure 20.11: W-Cycle Multigrid**

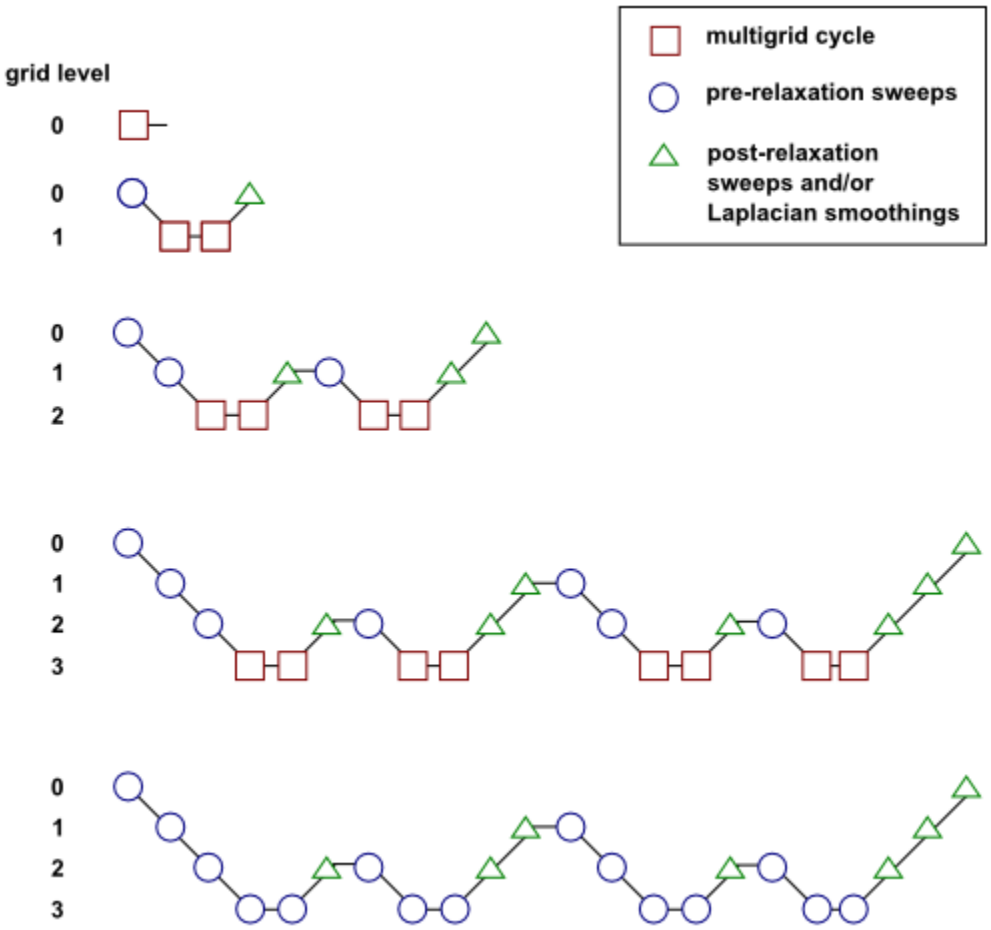


For the V and W cycles, the traversal of the hierarchy is governed by three parameters, $\beta_1$, $\beta_2$, and $\beta_3$, as follows:

1. First, iterations are performed on the current grid level to reduce the high-frequency components of the error (local error). For AMG, one iteration consists of one forward and one backward Gauss-Seidel sweep. For FAS, one iteration consists of one pass of the multi-stage scheme (described in Explicit Formulation (p. 663)).

   These iterations are referred to as pre-relaxation sweeps because they are performed before moving to the next coarser grid level. The number of pre-relaxation sweeps is specified by $\beta_1$.

   In Figure 20.10: V-Cycle Multigrid (p. 673) and Figure 20.11: W-Cycle Multigrid (p. 674) this step is represented by a circle and marks the start of a multigrid cycle. The high-wave-number components of error should be reduced until the remaining error is expressible on the next coarser mesh without significant aliasing.


Release 15.0 - © SAS IP, Inc. All rights reserved. - Contains proprietary and confidential information of ANSYS, Inc. and its subsidiaries and affiliates.

If this is the coarsest grid level, then the multigrid cycle on this level is complete. (In so the square representing the multigrid cycle on level 3 is equivalent to a circle, as shown in the final diagram in each figure.)

**Important**

In the AMG method, the default value of $\beta_1$ is zero (that is, no pre-relaxation sweeps are performed).

2. Next, the problem is "restricted" to the next coarser grid level using Equation 20.112 (p. 671).

   In Figure 20.10: V-Cycle Multigrid (p. 673) and Figure 20.11: W-Cycle Multigrid (p. 674), the restriction from a finer grid level to a coarser grid level is designated by a downward-sloping line.

3. The error on the coarse grid is reduced by performing a specified number ($\beta_2$) of multigrid cycles (represented in Figure 20.10: V-Cycle Multigrid (p. 673) and Figure 20.11: W-Cycle Multigrid (p. 674) as squares). Commonly, for fixed multigrid strategies $\beta_2$ is either 1 or 2, corresponding to V-cycle and W-cycle multigrid, respectively.

4. Next, the cumulative correction computed on the coarse grid is "interpolated" back to the fine grid using Equation 20.113 (p. 671) and added to the fine grid solution. In the FAS method, the corrections are additionally smoothed during this step using the Laplacian smoothing operator discussed in Implicit Residual Smoothing (p. 664).

   In Figure 20.10: V-Cycle Multigrid (p. 673) and Figure 20.11: W-Cycle Multigrid (p. 674) the prolongation is represented by an upward-sloping line.

   The high-frequency error now present at the fine grid level is due to the prolongation procedure used to transfer the correction.

5. In the final step, iterations are performed on the fine grid to remove the high-frequency error introduced on the coarse grid by the multigrid cycles. These iterations are referred to as post-relaxation sweeps because they are performed after returning from the next coarser grid level. The number of post-relaxation sweeps is specified by $\beta_3$.

   In Figure 20.10: V-Cycle Multigrid (p. 673) and Figure 20.11: W-Cycle Multigrid (p. 674), this relaxation procedure is represented by a single triangle.

   For AMG, the default value of $\beta_3$ is 1.

**Important**

Note, however, that if you are using AMG with V-cycle to solve an energy equation with a solid conduction model presented with anisotropic or very high conductivity coefficient, there is a possibility of divergence with a default post-relaxation sweep of 1. In such cases you should increase the post-relaxation sweep (for example, to 2) in the AMG section for better convergence, or change the cycle type to F-cycle or W-cycle, with an under-relaxation factor set to 1. This is especially effective when calculating pure heat conduction or conjugate heat transfer. Any instability observed when using the F-cycle or W-cycle

Release 15.0 - © SAS IP, Inc. All rights reserved. - Contains proprietary and confidential information of ANSYS, Inc. and its subsidiaries and affiliates.

can be remedied by increasing the pre-relaxation sweep count to 1. Although the default value of 0 is optimal for most cases, increasing the pre-relaxation sweep value to 1 or 2 can improve convergence.

Since the default value for $\beta_1$ is 0 (that is, pre-relaxation sweeps are not performed), this procedure is roughly equivalent to using the solution from the coarse level as the initial guess for the solution at the fine level.

For FAS, the default value of $\beta_3$ is zero (that is, post-relaxation sweeps are not performed); post-relaxation sweeps are never performed at the end of the cycle for the finest grid level, regardless of the value of $\beta_3$. This is because for FAS, post-relaxation sweeps at the fine level are equivalent to pre-relaxation sweeps during the next cycle.

## 20.7.3. Algebraic Multigrid (AMG)

This algorithm is referred to as an "algebraic" multigrid scheme because, as we shall see, the coarse level equations are generated without the use of any geometry or re-discretization on the coarse levels; a feature that makes AMG particularly attractive for use on unstructured meshes. The advantage being that no coarse meshes have to be constructed or stored, and no fluxes or source terms need to be evaluated on the coarse levels. This approach is in contrast with FAS (sometimes called "geometric") multigrid in which a hierarchy of meshes is required and the discretized equations are evaluated on every level. In theory, the advantage of FAS over AMG is that the former should perform better for non-linear problems since non-linearities in the system are carried down to the coarse levels through the re-discretization; when using AMG, once the system is linearized, non-linearities are not "felt" by the solver until the fine level operator is next updated.

### *20.7.3.1. AMG Restriction and Prolongation Operators*

The restriction and prolongation operators used here are based on the additive correction (AC) strategy described for structured meshes by Hutchinson and Raithby [173] (p. 738). Inter-level transfer is accomplished by piecewise constant interpolation and prolongation. The defect in any coarse level cell is given by the sum of those from the fine level cells it contains, while fine level corrections are obtained by injection of coarse level values. In this manner the prolongation operator is given by the transpose of the restriction operator

$$P = R^T \tag{20.114}$$

The restriction operator is defined by a coarsening or "grouping" of fine level cells into coarse level ones. In this process each fine level cell is grouped with one or more of its "strongest" neighbors, with a preference given to currently ungrouped neighbors. The algorithm attempts to collect cells into groups of fixed size, typically two or four, but any number can be specified.

By default, the "strongest" neighbor is evaluated as the neighbor $j$ of the current cell $i$ for which the coefficient $A_{ij}$ is largest. For sets of coupled equations $A_{ij}$ is a block matrix and the measure of its magnitude is simply taken to be the magnitude of its first element. In addition, the set of coupled equations for a given cell are treated together and not divided amongst different coarse cells. This results in the same coarsening for each equation in the system.

Alternatively, you can choose to have ANSYS Fluent use Laplace coefficients as the strength factors in determining the coarsening. Refer to Coarsening Parameters in the *Fluent User's Guide* for details about using the Laplace coarsening option.


Release 15.0 - © SAS IP, Inc. All rights reserved. - Contains proprietary and confidential information of ANSYS, Inc. and its subsidiaries and affiliates.

### 20.7.3.2. AMG Coarse Level Operator

The coarse level operator $A^H$ is constructed using a Galerkin approach. Here we require that the defect associated with the corrected fine level solution must vanish when transferred back to the coarse level. Therefore we may write

$$Rd^{new}=0 \tag{20.115}$$

Upon substituting Equation 20.107 (p. 671) and Equation 20.113 (p. 671) for $d^{new}$ and $\phi^{new}$ we have

$$\begin{aligned} &R\left[A\phi^{new}+b\right]=0 \\ &R\left[A\left(\phi+P\psi^H\right)+b\right]=0 \end{aligned} \tag{20.116}$$

Now rearranging and using Equation 20.107 (p. 671) once again gives

$$\begin{aligned} &RAP\psi^H+R\left(A\phi+b\right)=0 \\ &RAP\psi^H+Rd=0 \end{aligned} \tag{20.117}$$

Comparison of Equation 20.117 (p. 677) with Equation 20.112 (p. 671) leads to the following expression for the coarse level operator:

$$A^H=RAP \tag{20.118}$$

The construction of coarse level operators therefore reduces to a summation of diagonal and corresponding off-diagonal blocks for all fine level cells within a group to form the diagonal block of that group's coarse cell.

### 20.7.3.3. The F Cycle

The multigrid F cycle is essentially a combination of the V and W cycles described in The V and W Cycles (p. 672).

Recall that the multigrid cycle is a recursive procedure. The procedure is expanded to the next coarsest grid level by performing a single multigrid cycle on the current level. Referring to Figure 20.10: V-Cycle Multigrid (p. 673) and Figure 20.11: W-Cycle Multigrid (p. 674), this means replacing the square on the current level (representing a single cycle) with the procedure shown for the 0-1 level cycle (the second diagram in each figure). We see that a V cycle consists of:

$$\text{pre sweep}\rightarrow\text{restrict}\rightarrow\text{V cycle}\rightarrow\text{prolongate}\rightarrow\text{post sweep} \tag{20.119}$$

and a W cycle:

$$\text{pre sweep}\rightarrow\text{restrict}\rightarrow\text{W cycle}\rightarrow\text{W cycle}\rightarrow\text{prolongate}\rightarrow\text{post sweep} \tag{20.120}$$

An F cycle is formed by a W cycle followed by a V cycle:

$$\text{pre sweep}\rightarrow\text{restrict}\rightarrow\text{W cycle}\rightarrow\text{V cycle}\rightarrow\text{prolongate}\rightarrow\text{post sweep} \tag{20.121}$$

As expected, the F cycle requires more computation than the V cycle, but less than the W cycle. However, its convergence properties turn out to be better than the V cycle and roughly equivalent to the W cycle. The F cycle is the default AMG cycle type for the coupled equation set and for the scalar energy equation.

Release 15.0 - © SAS IP, Inc. All rights reserved. - Contains proprietary and confidential information of ANSYS, Inc. and its subsidiaries and affiliates.

### 20.7.3.4. The Flexible Cycle

For the flexible cycle, the calculation and use of coarse grid corrections is controlled in the multigrid procedure by the logic illustrated in Figure 20.12: Logic Controlling the Flex Multigrid Cycle (p. 678). This logic ensures that coarser grid calculations are invoked when the rate of residual reduction on the current grid level is too slow. In addition, the multigrid controls dictate when the iterative solution of the correction on the current coarse grid level is sufficiently converged and should therefore be applied to the solution on the next finer grid. These two decisions are controlled by the parameters $\alpha$ and $\beta$ shown in Figure 20.12: Logic Controlling the Flex Multigrid Cycle (p. 678), as described in detail below. Note that the logic of the multigrid procedure is such that grid levels may be visited repeatedly during a single global iteration on an equation. For a set of 4 multigrid levels, referred to as 0, 1, 2, and 3, the flex-cycle multigrid procedure for solving a given transport equation might consist of visiting grid levels as 0-1-2-3-2-3-2-1-0-1-2-1-0, for example.

**Figure 20.12: Logic Controlling the Flex Multigrid Cycle**

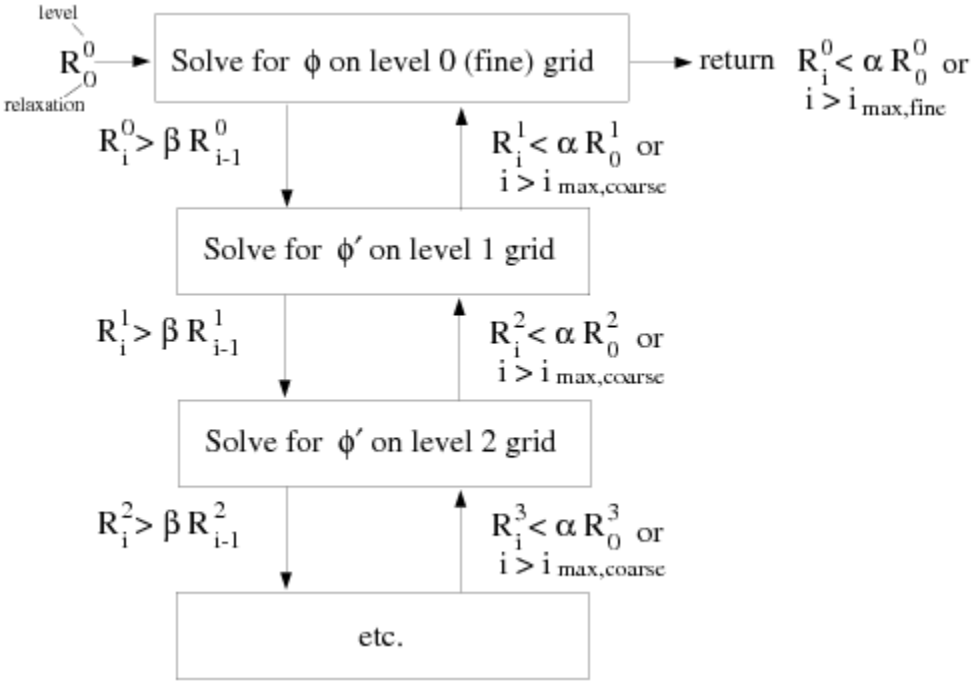


The main difference between the flexible cycle and the V and W cycles is that the satisfaction of the residual reduction tolerance and termination criterion determine when and how often each level is visited in the flexible cycle, whereas in the V and W cycles the traversal pattern is explicitly defined.

#### 20.7.3.4.1. The Residual Reduction Rate Criteria

The multigrid procedure invokes calculations on the next coarser grid level when the error reduction rate on the current level is insufficient, as defined by

$$R_i > \beta R_{i-1} \tag{20.122}$$

Here $R_i$ is the absolute sum of residuals (defect) computed on the current grid level after the $i$th relaxation on this level. The above equation states that if the residual present in the iterative solution after $i$ relaxations is greater than some fraction, $\beta$ (between 0 and 1), of the residual present after the $(i-1)$th relaxation, the next coarser grid level should be visited. Thus $\beta$ is referred to as the residual reduction tolerance, and determines when to "give up" on the iterative solution at the current grid level and move


Release 15.0 - © SAS IP, Inc. All rights reserved. - Contains proprietary and confidential information of ANSYS, Inc. and its subsidiaries and affiliates.

to solving the correction equations on the next coarser grid. The value of $\beta$ controls the frequency with which coarser grid levels are visited. The default value is 0.7. A larger value will result in less frequent visits, and a smaller value will result in more frequent visits.

#### 20.7.3.4.2. The Termination Criteria

Provided that the residual reduction rate is sufficiently rapid, the correction equations will be converged on the current grid level and the result applied to the solution field on the next finer grid level.

The correction equations on the current grid level are considered sufficiently converged when the error in the correction solution is reduced to some fraction, $\alpha$ (between 0 and 1), of the original error on this grid level:

$$R_i < \alpha R_0 \tag{20.123}$$

Here, $R_i$ is the residual on the current grid level after the $i$th iteration on this level, and $R_0$ is the residual that was initially obtained on this grid level at the current global iteration. The parameter $\alpha$, referred to as the termination criterion, has a default value of 0.1. Note that the above equation is also used to terminate calculations on the lowest (finest) grid level during the multigrid procedure. Thus, relaxations are continued on each grid level (including the finest grid level) until the criterion of this equation is obeyed (or until a maximum number of relaxations has been completed, in the case that the specified criterion is never achieved).

### *20.7.3.5. The Coupled and Scalar AMG Solvers*

The scalar AMG solver is used for the solution of linear systems obtained from the discretization of the individual transport equations.

$$a_{ij} x_j = b_i \tag{20.124}$$

where the above equation contains scalar variables.

The coupled AMG solver is used to solve linear transport equations using implicit discretization from coupled systems such as flow variables for the density-based solver, pressure-velocity variables for the coupled pressure-based schemes and inter-phase coupled individual equations for Eulerian multiphase flows.

$$[A]_{ij} \vec{X}_j = \vec{B}_i \tag{20.125}$$

where the influence of a cell $i$ on a cell $j$ has the form

$$A_{ij} = \begin{bmatrix} a_{ij}^{11} & a_{ij}^{12} & \dots & a_{ij}^{1N} \\ a_{ij}^{21} & \cdot & & \cdot \\ \vdots & & \cdot & \cdot \\ a_{ij}^{N1} & & & a_{ij}^{NN} \end{bmatrix} \tag{20.126}$$

and the unknown and source vectors have the form

$$\vec{X}_j = \begin{bmatrix} x_j^1 \\ \vdots \\ x_j^N \end{bmatrix} \tag{20.127}$$

Release 15.0 - © SAS IP, Inc. All rights reserved. - Contains proprietary and confidential information of ANSYS, Inc. and its subsidiaries and affiliates.

$$\vec{B}_i = \begin{bmatrix} b_i^1 \\ \vdots \\ b_i^N \end{bmatrix} \tag{20.128}$$

The above resultant system of equations is solved in ANSYS Fluent using either the Gauss-Seidel smoother or the Incomplete Lower Upper decomposition (ILU) smoother. If a scalar system of equations is to be solved then the point-method (Gauss-Seidel or ILU) smoother is used, while for a coupled system of equations the block-method (Gauss-Seidel or ILU) smoother is used.

### 20.7.3.5.1. Gauss-Seidel

The Gauss-Seidel method is a technique for solving a linear system of equations one at a time and in sequence. It uses the previously computed results as soon as they become available. It performs two sweeps on the unknowns in forward and backward directions. Both point or block method Gauss-Seidel smoothers are available in ANSYS Fluent to solve for either the scalar AMG system of equations or the coupled AMG system of equations.

The Gauss-Seidel procedure can be illustrated using the scalar system, Equation 20.124 (p. 679). The forward sweep can be written as:

$$x_i^{k+1/2} = \left( b_i - \sum_{j<i} a_{ij} x_j^{k+1/2} - \sum_{j>i} a_{ij} x_j^k \right) / a_{ii} \quad (i = 1, \ldots, N) \tag{20.129}$$

where N is the number of unknowns. The forward sweep is followed by a backward sweep that can be written as:

$$x_i^{k+1} = \left( b_i - \sum_{j<i} a_{ij} x_j^{k+1/2} - \sum_{j>i} a_{ij} x_j^{k+1} \right) / a_{ii} \tag{20.130}$$

Following from Equation 20.129 (p. 680) and Equation 20.130 (p. 680), symmetric Gauss-Seidel can be expressed in matrix form as a two-step recursive solution of the system

$$(D_A + L_A) D_A^{-1} (D_A + U_A) (x^{k+1} - x^k) = b - A x^k \tag{20.131}$$

where $D_A$, $L_A$, and $U_A$ represent diagonal, lower tridiagonal, and upper tridiagonal parts of matrix $A$, respectively.

Symmetric Gauss-Seidel has a somewhat limited rate of smoothing of residuals between levels of AMG, unless the coarsening factor is set to 2.

### 20.7.3.5.2. Incomplete Lower Upper (ILU)

A more effective AMG smoother is based on the ILU decomposition technique. In general, any iterational method can be represented as

$$M \left( x^{k+1} - x^k \right) = b - A x^k \tag{20.132}$$

where matrix M is some approximation of the original matrix A from

$$Ax = b \tag{20.133}$$


Release 15.0 - © SAS IP, Inc. All rights reserved. - Contains proprietary and confidential information of ANSYS, Inc. and its subsidiaries and affiliates.

$M$ should be close to A and the calculation of $M^{-1}$ should have a low operation count. We consider $M$ as an incomplete lower upper factorization of the matrix A such that

$$M = LU = (D + L_A) D^{-1} (D + U_A) \tag{20.134}$$

where $L_A$ and $U_A$ are the lower tridiagonal and upper tridiagonal parts of matrix A. The diagonal matrix D is calculated in a special way to satisfy the following condition for diagonal $D_M$ of matrix M:

$$D_M = D_A \tag{20.135}$$

In this case, the $i$th element of the diagonal of D will be calculated using

$$d_{ii} = a_{ii} - \sum_{j<1} \left( \frac{a_{ij} a_{ji}}{d_{jj}} \right) \tag{20.136}$$

The calculation of the new solution $x^{k+1}$ is then performed in two symmetric recursive sweeps, similar to Gauss-Seidel sweeps. Diagonal elements $d_{ii}$ of the ILU decomposition are calculated during the construction of levels and stored in the memory. ILU smoother is slightly more expensive compared to Gauss-Seidel, but has better smoothing properties, especially for block-coupled systems solved by coupled AMG. In this case, coarsening of levels can be more aggressive using coarsening factors between 8 and 12 for 3D problems compared to 2 for Gauss-Seidel.

**Important**

When solving the coupled systems, shorter solution times and more robust performance can be obtained by using the default ILU smoother, rather than the Gauss-Seidel smoother, which is the default for scalar systems. ILU is recommended whenever the coupled AMG solver is used. It is used by default for the coupled equations and, when pseudo-transient is used, for the scalar equations.

### 20.7.4. Full-Approximation Storage (FAS) Multigrid

ANSYS Fluent's approach to forming the multigrid grid hierarchy for FAS is simply to coalesce groups of cells on the finer grid to form coarse grid cells. Coarse grid cells are created by agglomerating the cells surrounding a node, as shown in Figure 20.13: Node Agglomeration to Form Coarse Grid Cells (p. 682). Depending on the grid topology, this can result in cells with irregular shapes and variable numbers of faces. The grid levels are, however, simple to construct and are embedded, resulting in simple prolongation and relaxation operators.

Release 15.0 - © SAS IP, Inc. All rights reserved. - Contains proprietary and confidential information of ANSYS, Inc. and its subsidiaries and affiliates.

**Figure 20.13: Node Agglomeration to Form Coarse Grid Cells**

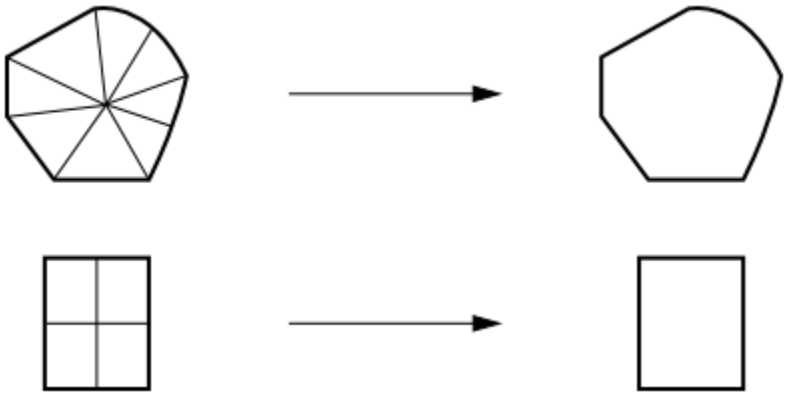

It is interesting to note that although the coarse grid cells look very irregular, the discretization cannot "see" the jaggedness in the cell faces. The discretization uses only the area projections of the cell faces and therefore each group of "jagged" cell faces separating two irregularly-shaped cells is equivalent to a single straight line (in 2D) connecting the endpoints of the jagged segment. (In 3D, the area projections form an irregular, but continuous, geometrical shape.) This optimization decreases the memory requirement and the computation time.

### 20.7.4.1. FAS Restriction and Prolongation Operators

FAS requires restriction of both the fine grid solution $\phi$ and its residual (defect) $d$. The restriction operator $R$ used to transfer the solution to the next coarser grid level is formed using a full-approximation scheme [42] (p. 731). That is, the solution for a coarse cell is obtained by taking the volume average of the solution values in the embedded fine grid cells. Residuals for the coarse grid cell are obtained by summing the residuals in the embedded fine grid cells.

The prolongation operator $P$ used to transfer corrections up to the fine level is constructed to simply set the fine grid correction to the associated coarse grid value.

The coarse grid corrections $\psi^H$, which are brought up from the coarse level and applied to the fine level solution, are computed from the difference between the solution calculated on the coarse level $\phi^H$ and the initial solution restricted down to the coarse level $R\phi$. Thus correction of the fine level solution becomes

$$\phi^{new} = \phi + P\left(\phi^H - R\phi\right) \tag{20.137}$$

### 20.7.4.2. FAS Coarse Level Operator

The FAS coarse grid operator $A^H$ is simply that which results from a re-discretization of the governing equations on the coarse level mesh. Since the discretized equations presented in Discretization (p. 632) and Density-Based Solver (p. 658) place no restrictions on the number of faces that make up a cell, there is no problem in performing this re-discretization on the coarse grids composed of irregularly shaped cells.

There is some loss of accuracy when the finite-volume scheme is used on the irregular coarse grid cells, but the accuracy of the multigrid solution is determined solely by the finest grid and is therefore not affected by the coarse grid discretization.


Release 15.0 - © SAS IP, Inc. All rights reserved. - Contains proprietary and confidential information of ANSYS, Inc. and its subsidiaries and affiliates.

In order to preserve accuracy of the fine grid solution, the coarse level equations are modified to include source terms [184] (p. 739) which insure that corrections computed on the coarse grid $\phi^H$ will be zero if the residuals on the fine grid $d^h$ are zero as well. Thus, the coarse grid equations are formulated as

$$A^H\phi^H + d^H = d^H(R\phi) - Rd^h \tag{20.138}$$

Here $d^H$ is the coarse grid residual computed from the current coarse grid solution $\phi^H$, and $d^H(R\phi)$ is the coarse grid residual computed from the restricted fine level solution $R\phi$. Initially, these two terms will be the same (because initially we have $\phi^H = R\phi$) and cancel from the equation, leaving

$$A^H\phi^H = -Rd^h \tag{20.139}$$

So there will be no coarse level correction when the fine grid residual $d^h$ is zero.

## 20.8. Hybrid Initialization

Hybrid Initialization is a collection of recipes and boundary interpolation methods. It solves the Laplace equation to produce a velocity field that conforms to complex domain geometries, and a pressure field which smoothly connects high and low pressure values in the computational domain. All other variables (that is temperature, turbulence, VOF, species, and so on) will be patched based on domain averaged values or a predetermined recipe. These recipes are detailed below.

- **Velocity Field:** Laplace's equation is solved with appropriate boundary conditions to produce the velocity field in the domain.

  $$\nabla^2\varphi = 0 \tag{20.140}$$

  where $\varphi$ is the velocity potential. The velocity components are given by the gradient potential:

  $$\vec{V} = \nabla\varphi \tag{20.141}$$

  Velocity potential is expressed as follows for the various boundary conditions:

  - **Wall Boundaries:** The velocity normal to the wall is zero.

    $$\frac{\partial\varphi}{\partial n}\Big|_{wall} = 0 \tag{20.142}$$

  - **Inlet Boundaries:** The velocity normal to the inlet boundaries are computed from the user-specified boundary values.

    $$\frac{\partial\varphi}{\partial n}\Big|_{inlet} = V_\perp \tag{20.143}$$

  - **Far Field Boundaries:** At the far-field boundaries the velocity normal to the boundaries is computed from the user-specified free stream conditions.

    $$\frac{\partial\varphi}{\partial n}\Big|_{inlet} = V_\perp \tag{20.144}$$

    Far away from the body the flow approaches the free stream conditions:

    $$\frac{\partial\varphi}{\partial x}\Big|_{\infty} = u_\infty \tag{20.145}$$

Release 15.0 - © SAS IP, Inc. All rights reserved. - Contains proprietary and confidential information of ANSYS, Inc. and its subsidiaries and affiliates.

$$\frac{\partial \varphi}{\partial y}\Big|_{\infty} = v_{\infty} \tag{20.146}$$

$$\frac{\partial \varphi}{\partial z}\Big|_{\infty} = w_{\infty} \tag{20.147}$$

  - **Outlet Boundaries:** They are specified as zero potential.

$$\varphi = 0 \tag{20.148}$$

A uniform initial velocity magnitude with the direction taken from the solution of the velocity potential solution can be specified by selecting the **Maintain Constant Velocity Magnitude** option under the **General Setting** tab.

- **Pressure Field:** An additional Laplace equation is solved with the appropriate boundary condition to produce the smooth pressure field in the domain, only if the pressure information is available in at least one inlet and one outlet in the domain. Otherwise, the pressure field will be initialized with the averaged constant value from all the boundaries.

$$\nabla^2 P = 0 \tag{20.149}$$

where $P$ is expressed as follows for the various boundary conditions:

  - Pressure inlet boundaries: by default, $P$ is computed as 1% less than the specified **Total Pressure** or, if you selected the **Use Specified Pressure on the Inlet** option under the **General Settings** tab, then it takes the $P$ from the specified **Supersonic/Initial Gauge Pressure**.

  - Pressure outlet boundaries: $P$ is computed as 1% more than the specified **Gauge Pressure** at this boundary.

  - Velocity/Mass flow inlet boundaries: $P$ uses the value of the specified **Supersonic/Initial Gauge Pressure** only if you have selected the **Use specified pressure on the inlet** option under the **General Settings** tab.

  - Wall Boundaries: the normal gradient of $P$ is set to zero.

$$\frac{\partial p}{\partial n}\Big|_{wall} = 0 \tag{20.150}$$

- **Temperature Field:** Temperature will be initialized with a constant value (domain averaged).

- **Turbulent Parameters:** By default, turbulent parameters are initialized with constant values (domain averaged). However, if you want to initialize the flow with variable turbulence parameters, then you will need to select the appropriate option in the **Hybrid Initialization** dialog box, described in Steps in Using Hybrid Initialization.

- **Species Fractions:** By default, secondary species mass/mole fractions are initialized with a 0.0 value. However, if you want to specify the initialization values, then you will need to select the appropriate option in the **Hybrid Initialization** dialog box, described in Steps in Using Hybrid Initialization.

- **Volume Fractions:** For a two-phase case, the secondary VOF phase will be initialized with the minimum VOF from all inlets. If the case has more than two phases, then the secondary phases will be initialized with a zero VOF.

For information about using hybrid initialization in ANSYS Fluent, see Hybrid Initialization in the User's Guide.


Release 15.0 - © SAS IP, Inc. All rights reserved. - Contains proprietary and confidential information of ANSYS, Inc. and its subsidiaries and affiliates.

# 20.9. Full Multigrid (FMG) Initialization

For many complex flow problems such as those found in rotating machinery, or flows in expanding or spiral ducts, flow convergence can be accelerated if a better initial solution is used at the start of the calculation. The Full Multigrid initialization (FMG initialization) can provide this initial and approximate solution at a minimum cost to the overall computational expense.

For more information about using FMG initialization in ANSYS Fluent, see Full Multigrid (FMG) Initialization in the User's Guide.

For more information about FMG initialization, see the following sections:

20.9.1. Overview of FMG Initialization
20.9.2. Limitations of FMG Initialization

## 20.9.1. Overview of FMG Initialization

FMG initialization utilizes the ANSYS Fluent FAS Multigrid technology (see Full-Approximation Storage (FAS) Multigrid (p. 681)) to obtain the initial solution. Starting from a uniform solution (after performing standard initialization), the FMG initialization procedure constructs the desirable number of geometric grid levels using the procedure outlined in Full-Approximation Storage (FAS) Multigrid (p. 681). To begin the process, the initial solution is restricted all the way down to the coarsest level. The FAS multigrid cycle is then applied until a given order of residual reduction is obtained or the maximum number of cycles is reached. The solution is then interpolated one grid level up and the FAS multigrid cycle is applied again between the current level all the way down to the coarsest level. This process will repeat until the finest level is reached. The FMG initialization iteration is illustrated in Figure 20.14: The FMG Initialization (p. 685).

**Figure 20.14: The FMG Initialization**

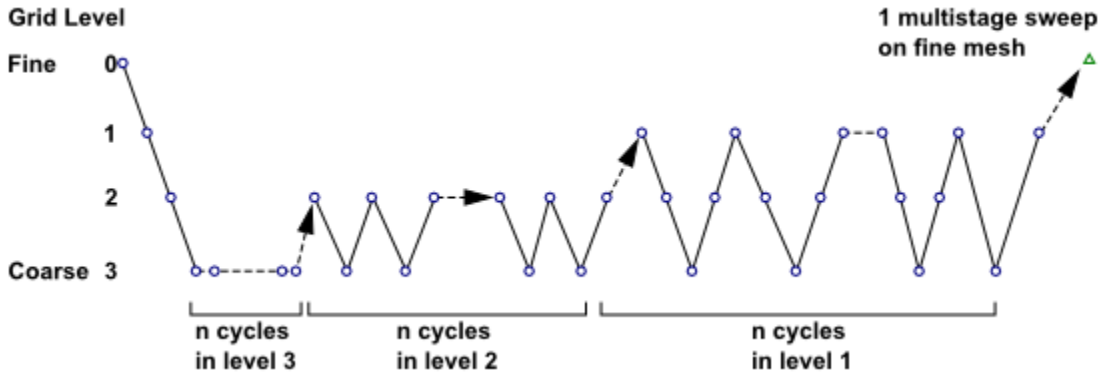


Since FMG initialization does most of the work on coarse levels, this initialization procedure is computationally inexpensive and, for large problems, a good initial solution can be obtained in a fraction of the time spent to converge on a final solution. Note that FMG initialization can be used with the pressure-based and density-based solvers.

When FMG initialization is started, the algorithm will perform the following steps:

1. Records the current solver selection and all current solver parameters.

2. Switches from the selected solver to the density-based explicit formulation.

3. Performs one FMG iteration using the FMG parameters given in the text command interface (see below).

Release 15.0 - © SAS IP, Inc. All rights reserved. - Contains proprietary and confidential information of ANSYS, Inc. and its subsidiaries and affiliates.

4. Switches back to the initially selected solver and resets all solver parameters back to the original solver settings.

In the FMG iteration, the Euler equations for inviscid flow are solved using first order-discretization to obtain the approximate solution. If species are present, then the FMG initialization will solve the species equations. However, turbulence equations or any other transport scalars are not solved in the FMG initialization.

## 20.9.2. Limitations of FMG Initialization

- FMG initialization is not available for unsteady flows.

  **Important**

  If an initial solution is needed for an unsteady calculation, then you must first switch to the steady state solver, perform FMG initialization and other necessary iterations to get an initial solution, and then perform unsteady calculations.

- FMG will not initialize turbulence or other transport equations field variables.

  **Important**

  If you are solving for turbulent flow, then you can still use FMG initialization, however the FMG will not initialize the turbulence field variables. For this reason, a good initial guess of the turbulence field quantities are important for achieving fast convergence after the FMG initialization has been performed.

- FMG should not be used with multiphase flow.


Release 15.0 - © SAS IP, Inc. All rights reserved. - Contains proprietary and confidential information of ANSYS, Inc. and its subsidiaries and affiliates.

# Chapter 21: Adapting the Mesh

The solution-adaptive mesh refinement feature of ANSYS Fluent allows you to refine and/or coarsen your mesh based on geometric and numerical solution data. In addition, ANSYS Fluent provides tools for creating and viewing adaption fields customized to particular applications. For information about using mesh adaption in ANSYS Fluent, see Adapting the Mesh in the User's Guide. Theoretical information about the adaption process is described in detail in the following sections.


21.1. Static Adaption Process
21.2. Boundary Adaption
21.3. Gradient Adaption
21.4. Dynamic Gradient Adaption
21.5. Isovalue Adaption
21.6. Region Adaption
21.7. Volume Adaption
21.8. Yplus/Ystar Adaption
21.9. Anisotropic Adaption
21.10. Geometry-Based Adaption
21.11. Registers


## 21.1. Static Adaption Process

The adaption process is separated into two distinct tasks.

1. The individual cells are marked for refinement or coarsening based on the adaption function, which is created from geometric and/or solution data.

2. The cell is refined or considered for coarsening based on these adaption marks.

   The primary advantages of this modularized approach are the abilities to create sophisticated adaption functions and to experiment with various adaption functions without modifying the existing mesh.

---

**Important**

Write a case and data file before starting the adaption process. If you generate an undesirable mesh, you can restart the process with the saved files.

---

For more information, see the following section:


21.1.1. Hanging Node Adaption


### 21.1.1. Hanging Node Adaption

Hanging node adaption is the procedure used in ANSYS Fluent. Meshes produced by this method are characterized by nodes on edges and faces that are not vertices of all the cells sharing those edges or faces, as shown in Figure 21.1: Example of a Hanging Node (p. 688).


Release 15.0 - © SAS IP, Inc. All rights reserved. - Contains proprietary and confidential information of ANSYS, Inc. and its subsidiaries and affiliates.

**Figure 21.1: Example of a Hanging Node**

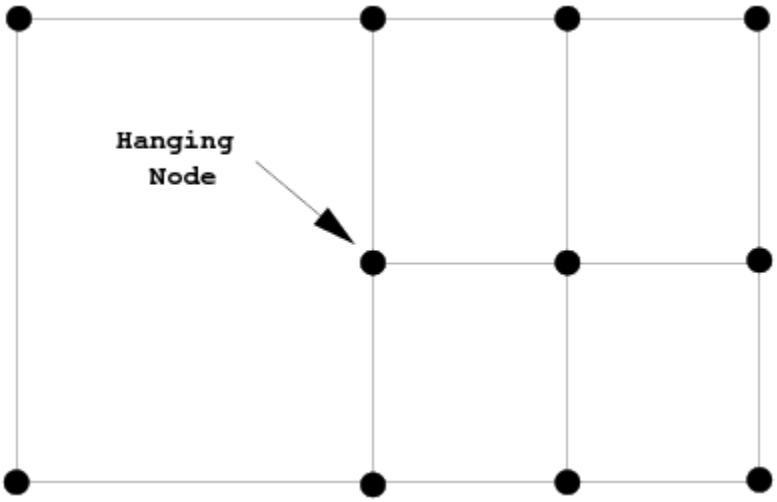


Hanging node mesh adaption provides the ability to operate on meshes with a variety of cell shapes, including hybrid meshes. Although the hanging node scheme provides significant mesh flexibility, it requires additional memory to maintain the mesh hierarchy which is used by the rendering and mesh adaption operations.

### *21.1.1.1. Hanging Node Refinement*

The cells marked for refinement are divided as described here:

- A triangle is split into 4 triangles.
- A quadrilateral is split into 4 quadrilaterals.
- A tetrahedron is split into eight tetrahedra. The subdivision consists of trimming each corner of the tetrahedron, and subdividing the enclosed octahedron by introducing the shortest diagonal.
- A hexahedron is split into 8 hexahedra.
- A wedge is split into 8 wedges.
- A pyramid is split into 6 pyramids and 4 tetrahedra.

Figure 21.2: Hanging Node Adaption of 2D Cell Types (p. 689) and Figure 21.3: Hanging Node Adaption of 3D Cell Types (p. 689) illustrate the division of the supported cell shapes.

To maintain accuracy, neighboring cells are not allowed to differ by more than one level of refinement. This prevents the adaption from producing excessive cell volume variations (reducing truncation error) and ensures that the positions of the parent (original) and child (refined) cell centroids are similar (reducing errors in the flux evaluations).


Release 15.0 - © SAS IP, Inc. All rights reserved. - Contains proprietary and confidential information of ANSYS, Inc. and its subsidiaries and affiliates.

**Figure 21.2: Hanging Node Adaption of 2D Cell Types**

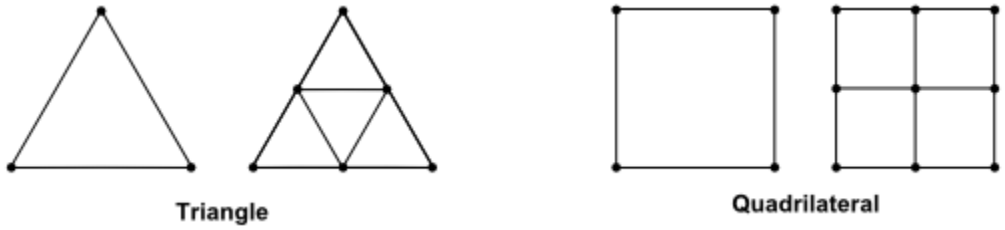


**Figure 21.3: Hanging Node Adaption of 3D Cell Types**

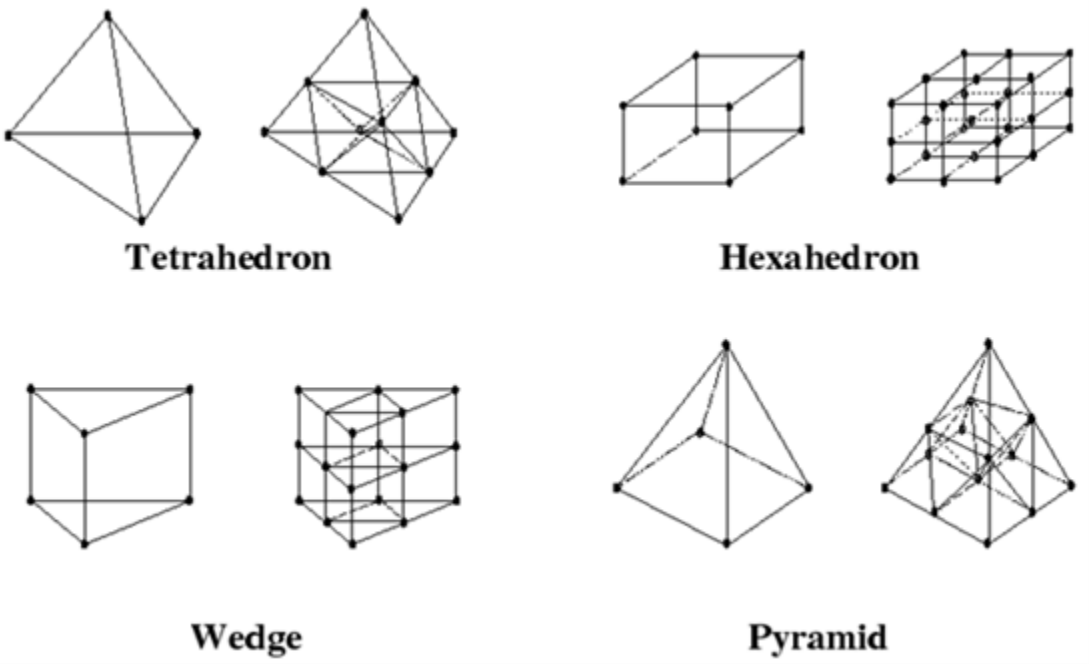


### *21.1.1.2. Hanging Node Coarsening*

The mesh is coarsened by reintroducing inactive parent cells (uniting the child cells to reclaim the previously subdivided parent cell). An inactive parent cell is reactivated if all its children are marked for coarsening. You will eventually reclaim the original mesh with repeated application of the hanging node coarsening. Using the hanging node adaption process, you cannot coarsen the mesh further than the original mesh.

## 21.2. Boundary Adaption

If more cells are required on a boundary, they can be added using boundary adaption, which allows you to mark or refine cells in the proximity of the selected boundary zones. The ability to refine the mesh near one or more boundary zones is provided because important fluid interactions often occur in these regions (for example, the development of strong velocity gradients in the boundary layer near a wall).

An example of a mesh that can be improved with boundary adaption is shown in Figure 21.4: Mesh Before Adaption (p. 690). This mesh has only four cells on the vertical face of a step. Boundary adaption on the zone corresponding to the face of the step can be used to increase the number of cells, as shown in Figure 21.5: Mesh after Boundary Adaption (p. 691). This procedure cannot increase the resolution of

Release 15.0 - © SAS IP, Inc. All rights reserved. - Contains proprietary and confidential information of ANSYS, Inc. and its subsidiaries and affiliates.

a curved surface. Therefore, if more cells are required on a curved surface where the shape of the surface is important, create the mesh with sufficient surface nodes before reading it into the solver.

**Figure 21.4: Mesh Before Adaption**

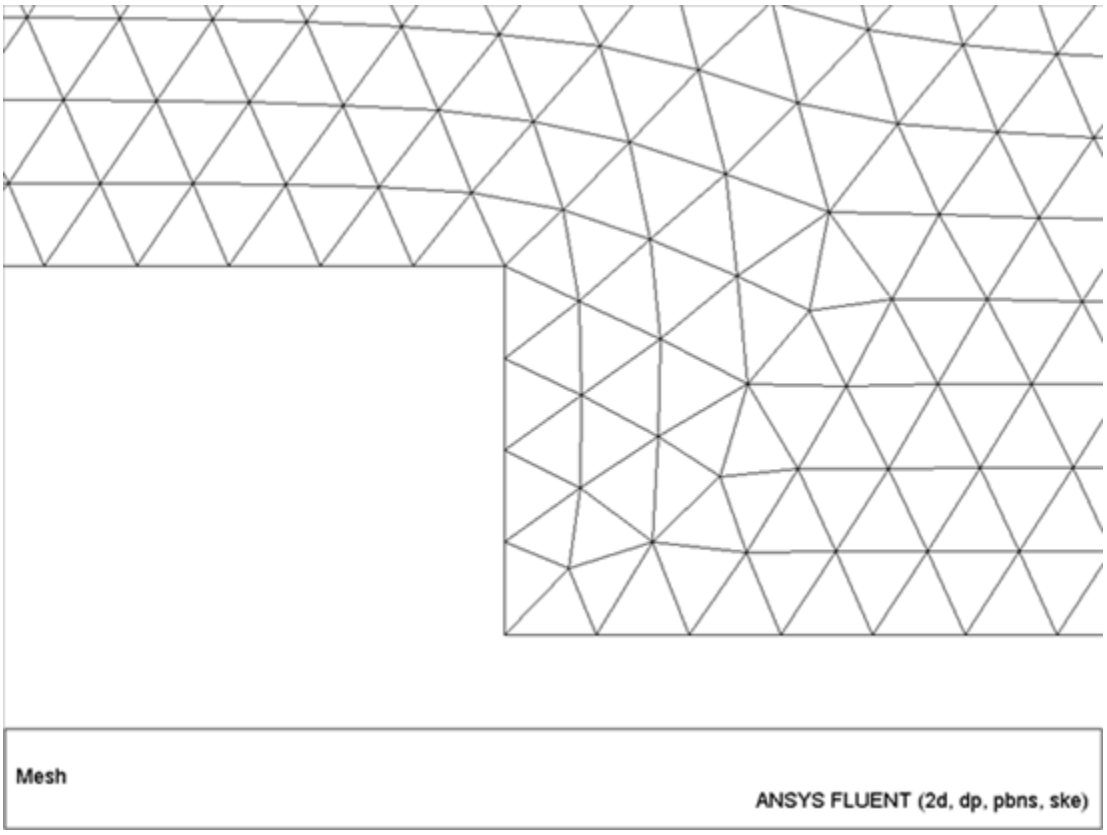



Release 15.0 - © SAS IP, Inc. All rights reserved. - Contains proprietary and confidential information of ANSYS, Inc. and its subsidiaries and affiliates.

**Figure 21.5: Mesh after Boundary Adaption**

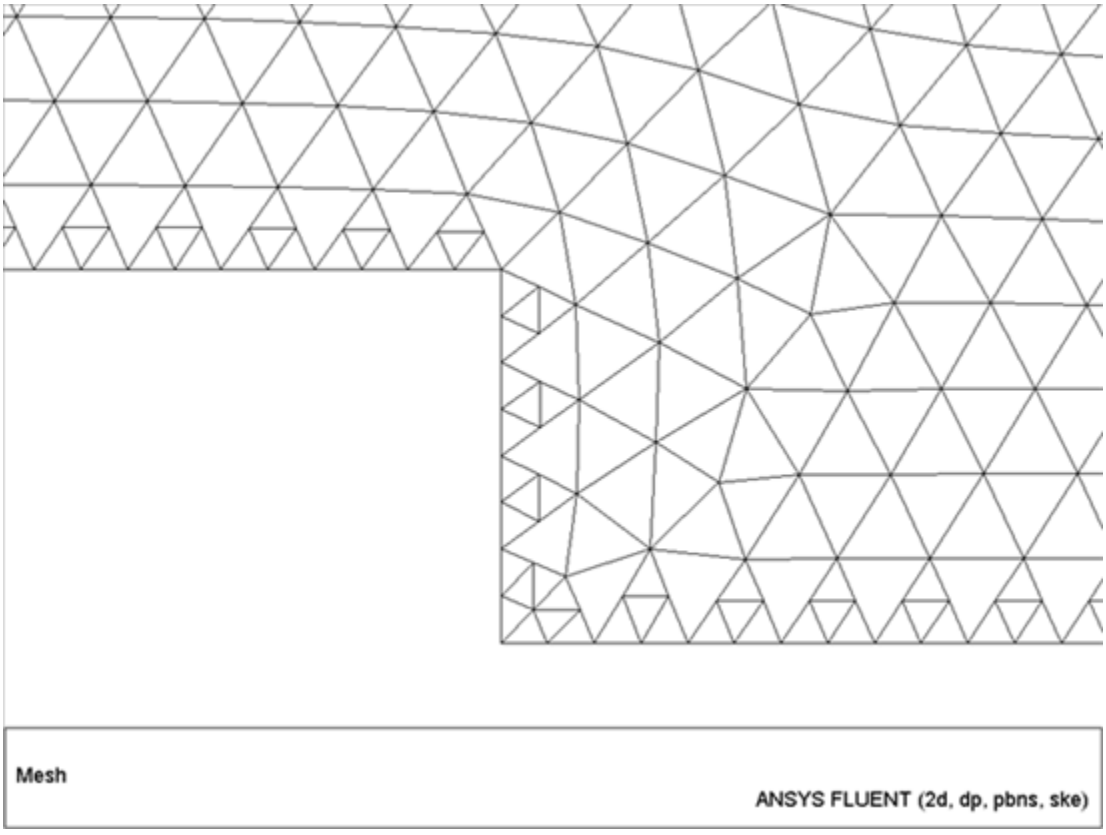


## 21.3. Gradient Adaption

The gradient adaption function allows you to mark cells or adapt the mesh based on the gradient, curvature, or isovalue of the selected field variables.

Information can be found in the following subsections:

21.3.1. Gradient Adaption Approach
21.3.2. Example of Steady Gradient Adaption

### 21.3.1. Gradient Adaption Approach

Solution-adaptive mesh refinement is performed to efficiently reduce the numerical error in the digital solution, with minimal numerical cost. Unfortunately, direct error estimation for point-insertion adaption schemes is difficult because of the complexity of accurately estimating and modeling the error in the adapted meshes. A comprehensive mathematically rigorous theory for error estimation and convergence is not yet available for CFD simulations. Assuming that maximum error occurs in high-gradient regions, the readily available physical features of the evolving flow field may be used to drive the mesh adaption process.

Three approaches for using this information for mesh adaption are available in ANSYS Fluent:

- **Gradient approach**: In this approach, ANSYS Fluent multiplies the Euclidean norm of the gradient of the selected solution variable by a characteristic length scale [87] (p. 733). For example, the gradient function in two dimensions has the following form:

$$|e_{i1}| = (A_{cell})^{\frac{r}{2}} |\nabla f| \tag{21.1}$$

where $e_{i1}$ is the error indicator, $A_{cell}$ is the cell area, $r$ is the gradient volume weight, and $\nabla f$ is the Euclidean norm of the gradient of the desired field variable, $f$.

The default value of the gradient volume weight is unity, which corresponds to full volume weighting. A value of zero will eliminate the volume weighting, and values between 0 and 1 will use proportional weighting of the volume.

If you specify adaption based on the gradient of a scalar, then the value of $|e_{i1}|$ is displayed when you plot contours of the adaption function.

This approach is recommended for problems with strong shocks, for example, supersonic inviscid flows.

- **Curvature approach**: This is an equidistribution adaption technique that multiplies the undivided Laplacian of the selected solution variable by a characteristic length scale [479] (p. 755).

  For example, the gradient function in two dimensions has the following form:

  $$|e_{i2}| = (A_{cell})^{\frac{r}{2}} |\nabla^2 f| \tag{21.2}$$

  where $e_{i2}$ is the error indicator, $A_{cell}$ is the cell area, $r$ is the gradient volume weight, and $\nabla^2 f$ is the undivided Laplacian of the desired field variable ($f$).

  The default value of the gradient volume weight is unity, which corresponds to full volume weighting. A value of zero will eliminate the volume weighting, and values between 0 and 1 will use proportional weighting of the volume.

  This approach is recommended for problems with smooth solutions.

- **Isovalue approach**: This approach is not based on derivatives. Instead, the isovalues of the required field variable $f$, are used to control the adaption. Therefore, the function is of the form:

  $$e_{i3} = f \tag{21.3}$$

  where $e_{i3}$ is the error indicator. This approach is recommended for problems where derivatives are not helpful. For example, if you want to refine the mesh where the reaction is taking place, you can use the isovalues of the reaction rate and mark for refinement at high reaction rates. This approach also allows you to customize the criteria for controlling the adaption using custom field functions, user-defined scalars, and so on

The length scale is the square (2D) or cube (3D) root of the cell volume. Introducing the length scale allows resolution of both strong and weak disturbances, increasing the potential for more accurate solutions. However, you can reduce or eliminate the volume weighting by changing the gradient **Volume Weight** in the Mesh Adaption Controls Dialog Box (see Mesh Adaption Controls in the User's Guide for details).

Any of the field variables available for contouring can be used in the gradient adaption function. These scalar functions include both geometric and physical features of the numerical solution. Therefore, in addition to traditional adaption to physical features, such as the velocity, you may choose to adapt to the cell volume field to reduce rapid variations in cell volume.

In addition to the **Standard** (no normalization) approach formerly used by ANSYS Fluent, two options are available for **Normalization** [135] (p. 736):


Release 15.0 - © SAS IP, Inc. All rights reserved. - Contains proprietary and confidential information of ANSYS, Inc. and its subsidiaries and affiliates.

- **Scale**, which scales the values of $e_{i1}$, $e_{i2}$, or $e_{i3}$ by their average value in the domain, that is:

$$\frac{|e_i|}{\overline{|e_i|}} \tag{21.4}$$

  When using the **Scale** option, suitable first-cut values for the **Coarsen Threshold** and the **Refine Threshold** are 0.3 to 0.5, and 0.7 to 0.9, respectively. Smaller values will result in larger adapted regions.

- **Normalize**, which scales the values of $e_{i1}$, $e_{i2}$, or $e_{i3}$ by their maximum value in the domain, therefore always returning a problem-independent range of [0, 1] for any variable used for adaption, that is:

$$\frac{|e_i|}{\max|e_i|} \tag{21.5}$$

  When using the **Normalize** option, suitable first-cut values for the **Coarsen Threshold** and the **Refine Threshold** are 0.2 to 0.4, and 0.5 to 0.9, respectively. Smaller values will result in larger adapted regions.

## 21.3.2. Example of Steady Gradient Adaption

An example of the use of steady gradient adaption is the solution of the supersonic flow over a bluff body. The initial mesh, shown in Figure 21.6: Bluff-Body Mesh Before Adaption (p. 694), is very coarse, even though it contains sufficient cells to adequately describe the shape of the bluff body. The mesh ahead of the bluff body is too coarse to resolve the shock wave that forms in front of the bluff body. In this instance, pressure is a suitable variable to be used in gradient adaption. This is because there will be a jump in pressure across the shock. However, several adaptions are necessary before the shock can be properly resolved. After several adaptions the mesh will be as shown in Figure 21.7: Bluff-Body Mesh after Gradient Adaption (p. 694).

A typical application of gradient adaption for an incompressible flow might be a mixing layer, which involves a discontinuity.

Release 15.0 - © SAS IP, Inc. All rights reserved. - Contains proprietary and confidential information of ANSYS, Inc. and its subsidiaries and affiliates.

**Figure 21.6: Bluff-Body Mesh Before Adaption**

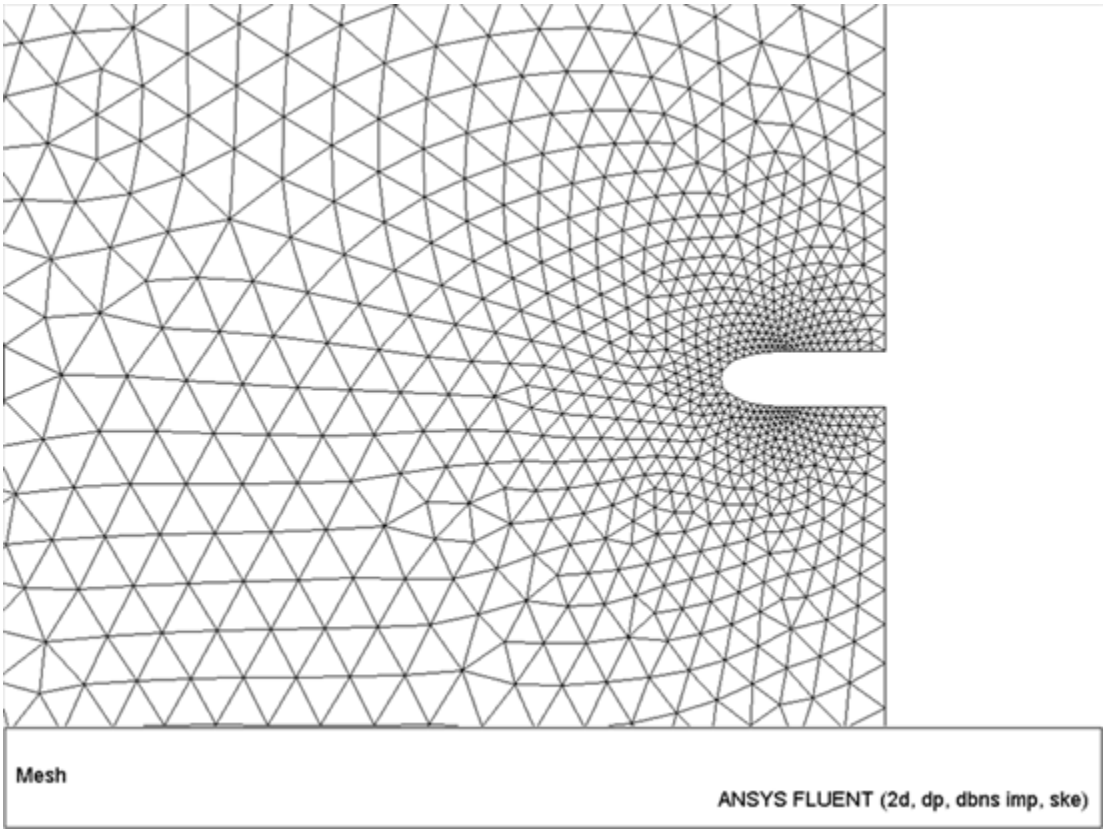


**Figure 21.7: Bluff-Body Mesh after Gradient Adaption**

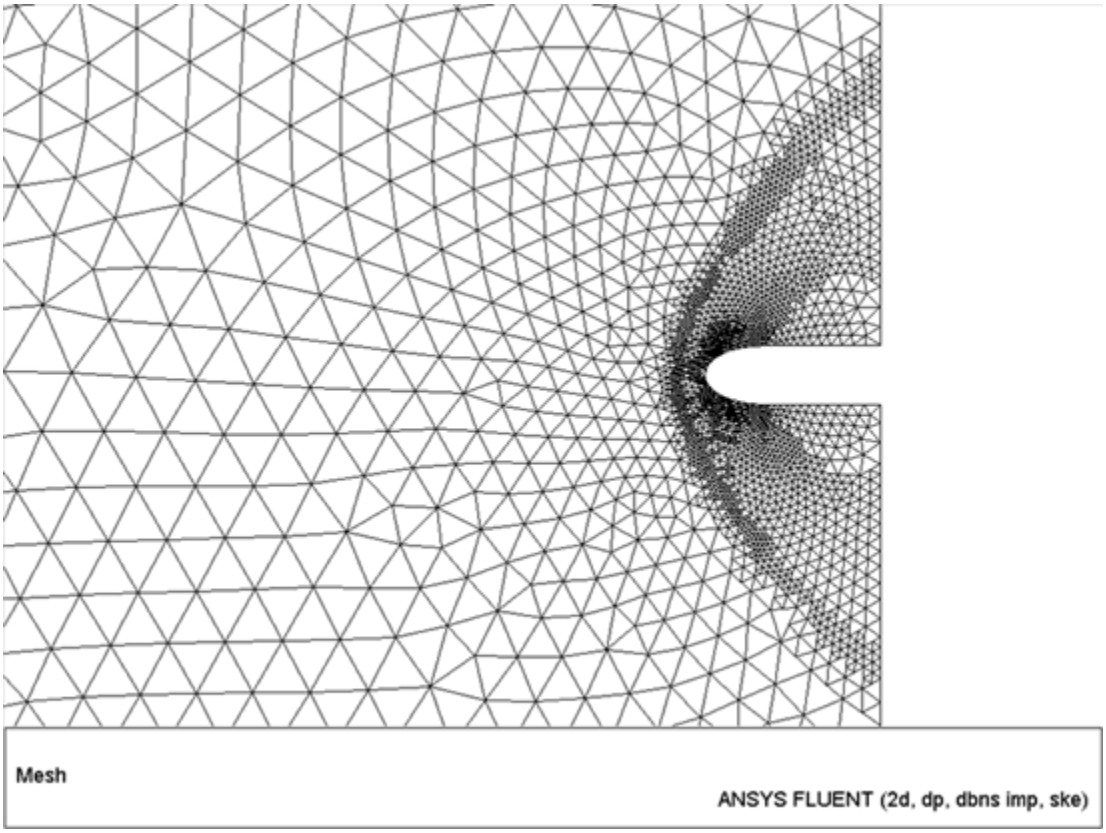



Release 15.0 - © SAS IP, Inc. All rights reserved. - Contains proprietary and confidential information of ANSYS, Inc. and its subsidiaries and affiliates.

## 21.4. Dynamic Gradient Adaption

In contrast with the static gradient adaption (Gradient Adaption (p. 691)), dynamic gradient adaption is a fully automated process. For time dependent and for steady state problems, you can perform the entire solution without changing the initial settings. That is, you can let the solver periodically perform adaptions without changing/entering any parameter.

## 21.5. Isovalue Adaption

Some flows may contain flow features that are easy to identify based on values of a certain quantity. For instance, wakes represent a total pressure deficit, and jets are identifiable by a region of relatively high-velocity fluid. Since it is known that these regions also contain large gradients of important flow quantities (such as $k$ and $\varepsilon$ in turbulent flows), it is more convenient to perform an isovalue adaption on the relevant flow quantity than to refine on gradients of the individual flow variables.

The isovalue adaption function allows you to mark or refine cells inside or outside a specified range of a selected field variable function. The mesh can be refined or marked for refinement based on geometric and/or solution vector data. Specifically, any quantity in the display list of field variables can be used for the isovalue adaption. Some examples of how you might use the isovalue marking/adaption feature include the following:

- Create masks using coordinate values or the quadric function.
- Refine cells that have a velocity magnitude within a specified range.
- Mark and display cells with a pressure or continuity residual outside of a desired range to determine where the numerical solution is changing rapidly.

The approach used in isovalue adaption is to compute the specified value for each cell (velocity, quadric function, centroid $x$ coordinate, and so on), and then visit each cell, marking for refinement the cells that have values inside (or outside) the specified ranges.

An example of a problem in which isovalue adaption is useful is an impinging jet with axial velocity contours as shown in Figure 21.8: Impinging Jet Axial Velocity Contours Before Adaption (p. 696). The axisymmetric mesh for the problem is displayed in Figure 21.9: Impinging Jet Mesh Before Adaption (p. 696). An isovalue adaption based on axial velocity allows refinement of the mesh only in the jet (Figure 21.10: Impinging Jet Mesh after Isovalue Adaption (p. 697)).

Release 15.0 - © SAS IP, Inc. All rights reserved. - Contains proprietary and confidential information of ANSYS, Inc. and its subsidiaries and affiliates.

**Figure 21.8: Impinging Jet Axial Velocity Contours Before Adaption**

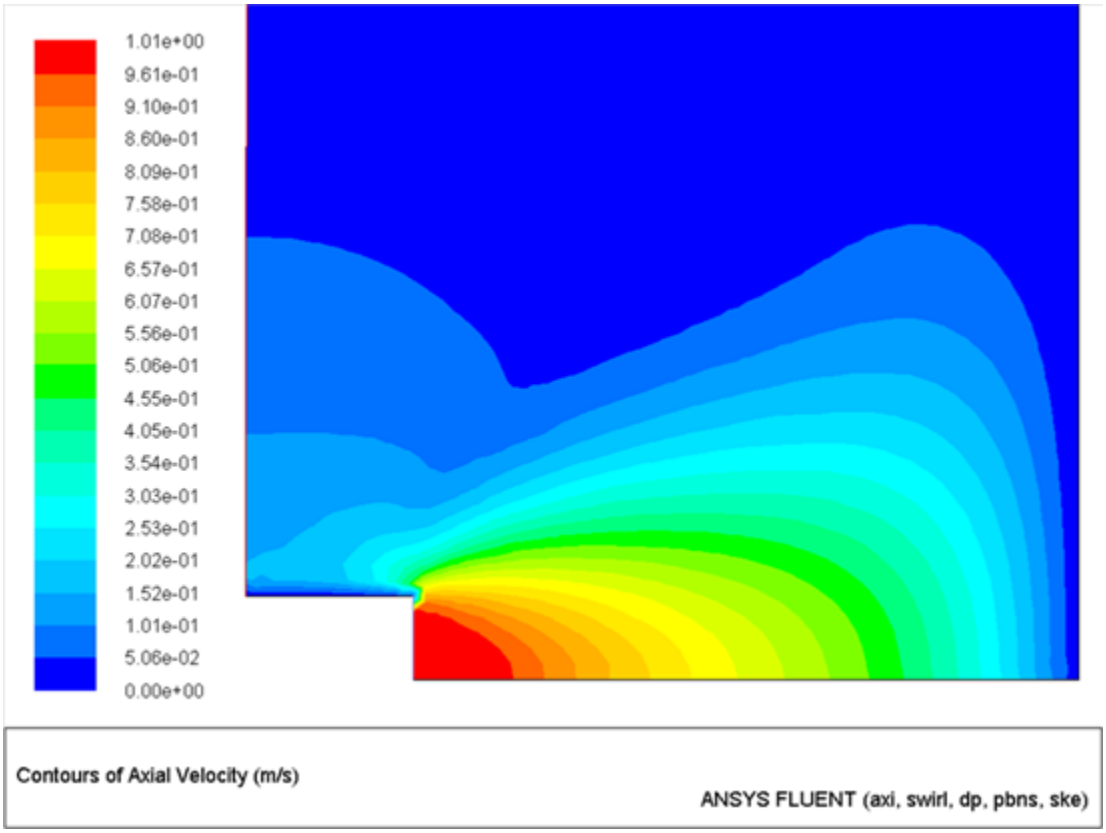


**Figure 21.9: Impinging Jet Mesh Before Adaption**

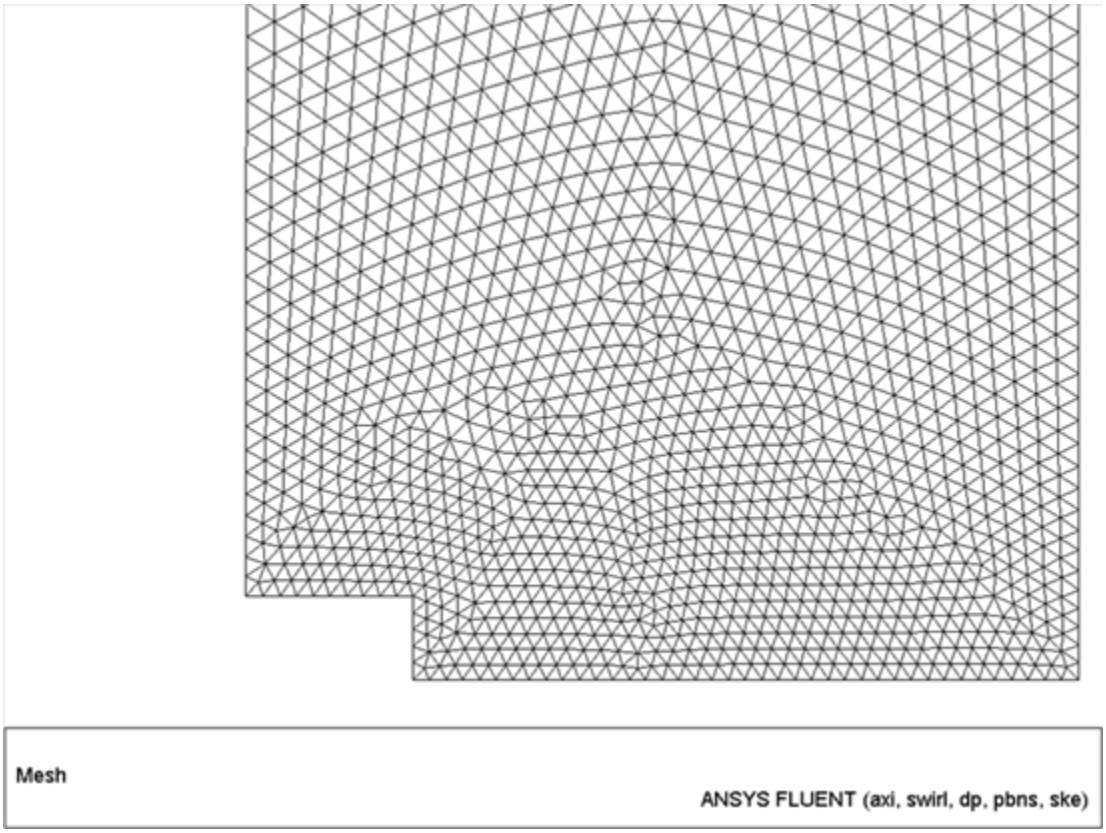



Release 15.0 - © SAS IP, Inc. All rights reserved. - Contains proprietary and confidential information of ANSYS, Inc. and its subsidiaries and affiliates.

**Figure 21.10: Impinging Jet Mesh after Isovalue Adaption**

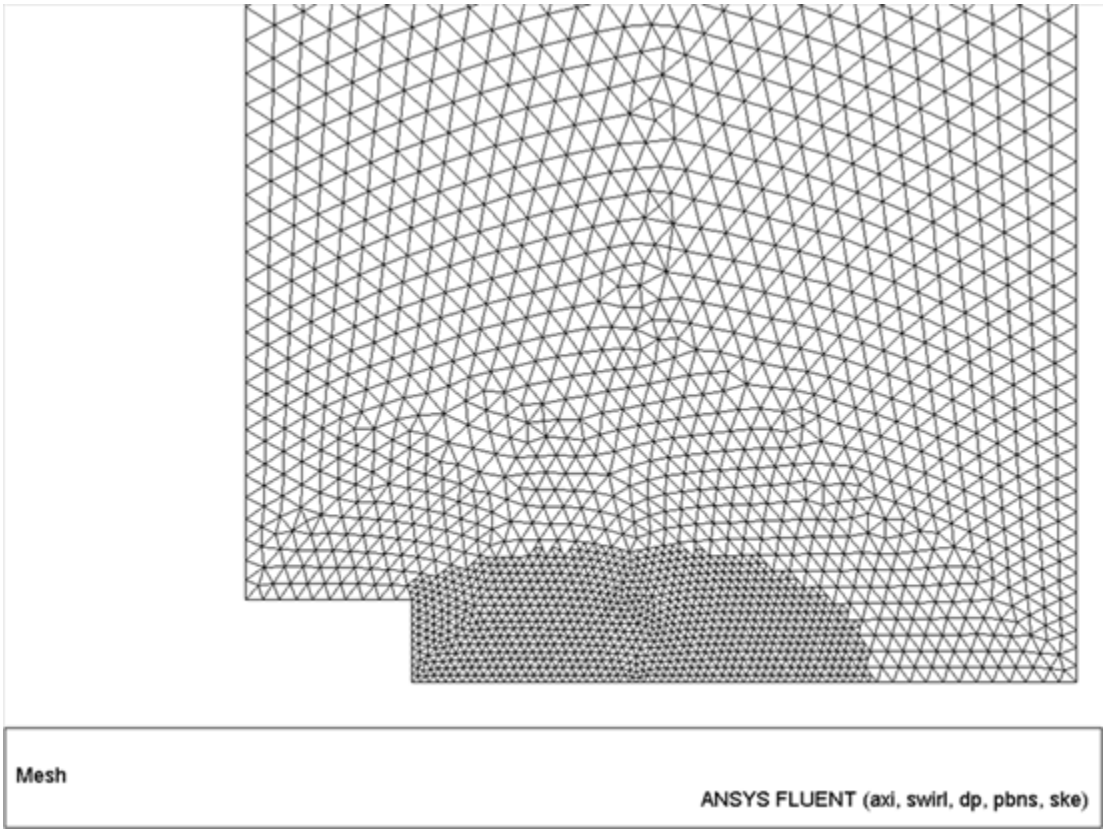


## 21.6. Region Adaption

Many mesh generators create meshes with cell volumes that grow very rapidly with distance from boundaries. While this avoids an overly dense mesh as a matter of course, it might also create problems if the mesh is not fine enough to resolve the flow. But if it is known a priori that a finer mesh is required in a certain region of the solution domain, the mesh can be refined using region adaption.

The region adaption function marks or refines cells inside or outside a region defined by text or mouse input. Presently, the mesh can be refined or marked inside or outside a hexahedron (quadrilateral in 2D), a sphere (circle in 2D), or a cylinder. The region-based marking/adaption feature is particularly useful for refining regions that intuitively require good resolution: for example, the wake region of a blunt-body flow field. In addition, you can use the region marking to create mask adaption registers that can be used to limit the extent of the refinement and coarsening.

Information can be found in the following subsections:

21.6.1. Defining a Region
21.6.2. Region Adaption Example

### 21.6.1. Defining a Region

The basic approach to the region adaption function is to first define a region:

- The hexahedron (quadrilateral) is defined by entering the coordinates of two points defining the diagonal.
- The sphere (circle) is defined by entering the coordinates of the center of the sphere and its radius.

Release 15.0 - © SAS IP, Inc. All rights reserved. - Contains proprietary and confidential information of ANSYS, Inc. and its subsidiaries and affiliates.

- To define a cylinder, specify the coordinates of the points defining the cylinder axis, and the radius. In 3D this will define a cylinder. In 2D, you will have an arbitrarily oriented rectangle with length equal to the cylinder axis length and width equal to the radius.

  A rectangle defined using the cylinder option differs from one defined with the quadrilateral option in that the former can be arbitrarily oriented in the domain, while the latter must be aligned with the coordinate axes.

  You can either enter the exact coordinates into the appropriate real entry fields or select the locations with the mouse on displays of the mesh or solution field. After the region is defined, each cell that has a centroid inside/outside the specified region is marked for refinement.

## 21.6.2. Region Adaption Example

Figure 21.11: Flap-Airfoil Mesh Before Adaption (p. 698) shows a mesh that was created for solving the flow around a flap airfoil. The mesh is very fine near the surface of the airfoil, particularly at the trailing edge of the main airfoil. In order to ensure that the flow separation known to occur on the suction surface of the flap is properly predicted, the mesh is adapted within a circular region (selected by mouse probe) surrounding the flap. The result is shown in Figure 21.12: Flap-Airfoil Mesh after Region Adaption (p. 699).

**Figure 21.11: Flap-Airfoil Mesh Before Adaption**

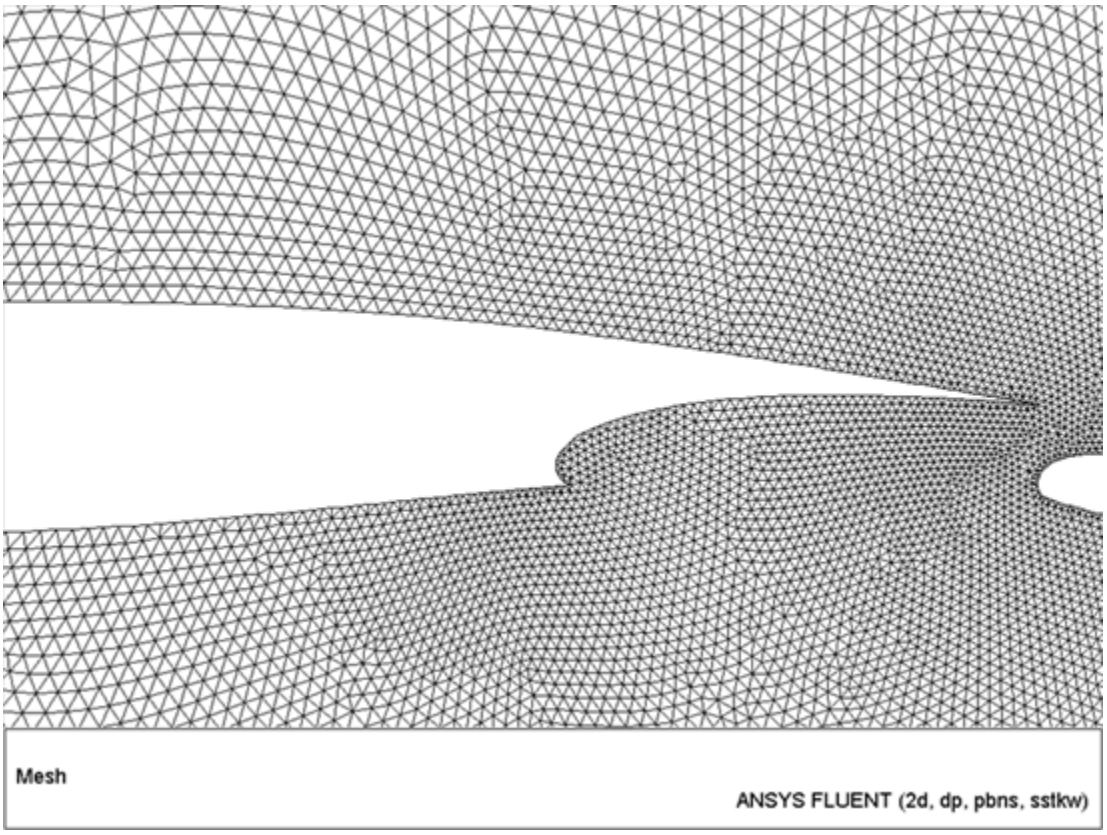



Release 15.0 - © SAS IP, Inc. All rights reserved. - Contains proprietary and confidential information of ANSYS, Inc. and its subsidiaries and affiliates.

**Figure 21.12: Flap-Airfoil Mesh after Region Adaption**

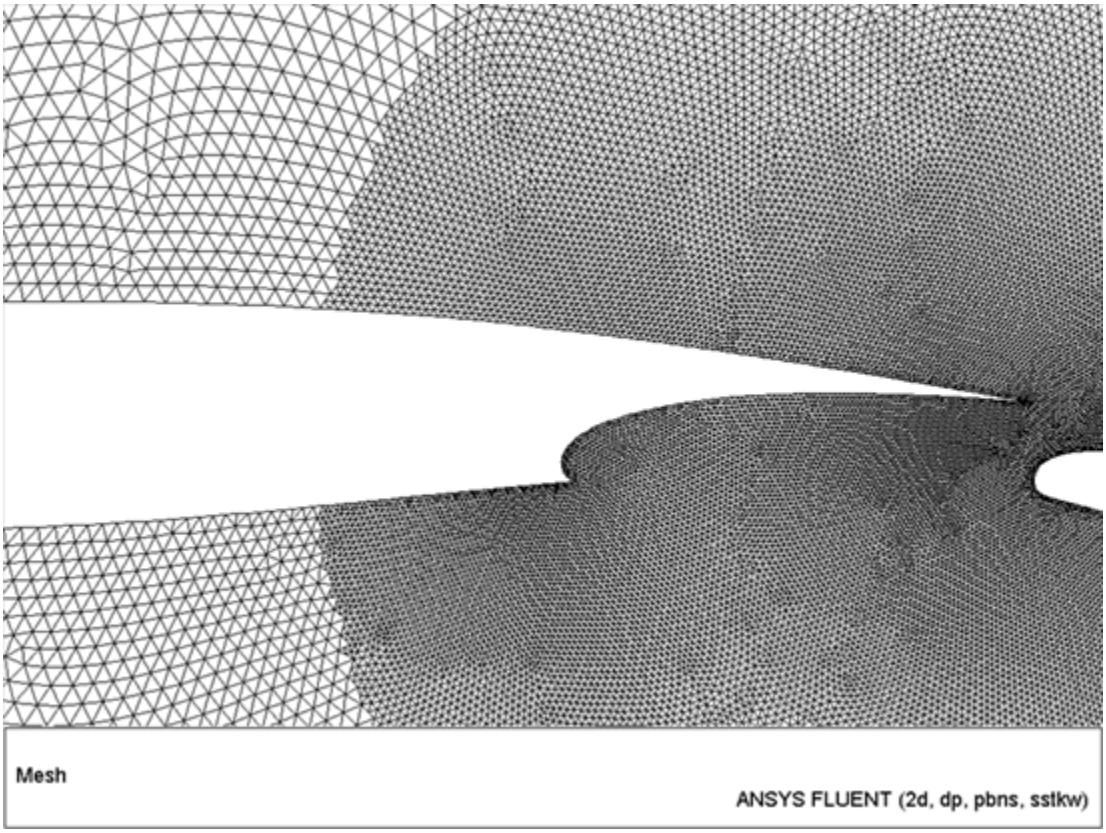


## 21.7. Volume Adaption

As mentioned in Using Adaption in the User's Guide, it is best for both accuracy and convergence to have a mesh in which the changes in cell volume are gradual. If the mesh creation or adaption process results in a mesh that does not have this property, the mesh can be improved by using volume adaption with the option of refining, based on either the cell volume or the change in volume between the cell and its neighbors.

Information can be found in the following subsections:

21.7.1. Volume Adaption Approach
21.7.2. Volume Adaption Example

### 21.7.1. Volume Adaption Approach

Marking or refining the mesh based on volume magnitude is often used to remove large cells or to globally refine the mesh. The procedure is to mark for refinement any cell with a volume greater than the specified threshold value.

Marking or refining the mesh based on the change in cell volume is used to improve the smoothness of the mesh. The procedure is to mark for refinement any cell that has a volume change greater than the specified threshold value. The volume change is computed by looping over the faces and comparing the ratio of the cell neighbors to the face.

For example, in Figure 21.13: Volume Change—Ratio of the Volumes of the Cells (p. 700) the ratio of V1/V2 and the ratio of V2/V1 is compared to the threshold value. If V2/V1 is greater than the threshold, then C2 is marked for refinement.

Release 15.0 - © SAS IP, Inc. All rights reserved. - Contains proprietary and confidential information of ANSYS, Inc. and its subsidiaries and affiliates.

**Figure 21.13: Volume Change—Ratio of the Volumes of the Cells**

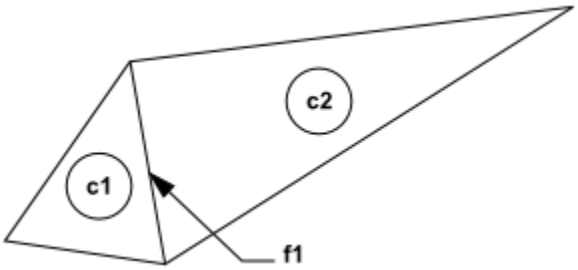


## 21.7.2. Volume Adaption Example

The mesh in Figure 21.14: Duct Mesh Before Adaption (p. 700) was created for a duct with a slot on the bottom boundary that acts as an inlet. Local refinement was used to create a mesh that is fine in the region above the slot, but coarse elsewhere. This created a very sharp change in cell volume.

To improve the mesh, it was refined using volume adaption with the criterion that the maximum cell volume change should be less than 2.5. The resulting mesh is shown in Figure 21.15: Duct Mesh after Volume Adaption Based on Change in Cell Volume (p. 701). It can be seen that the interface between the refined region and the surrounding mesh is no longer as sharp.

**Figure 21.14: Duct Mesh Before Adaption**

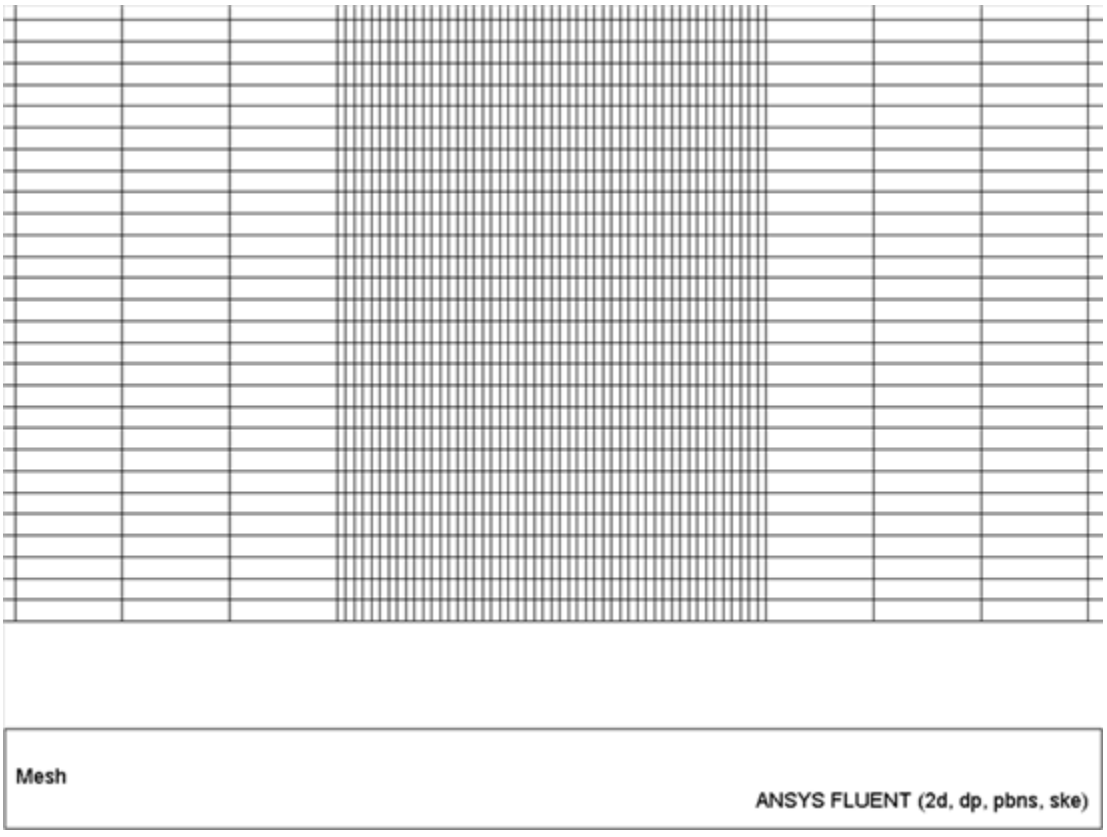



Release 15.0 - © SAS IP, Inc. All rights reserved. - Contains proprietary and confidential information of ANSYS, Inc. and its subsidiaries and affiliates.

**Figure 21.15: Duct Mesh after Volume Adaption Based on Change in Cell Volume**

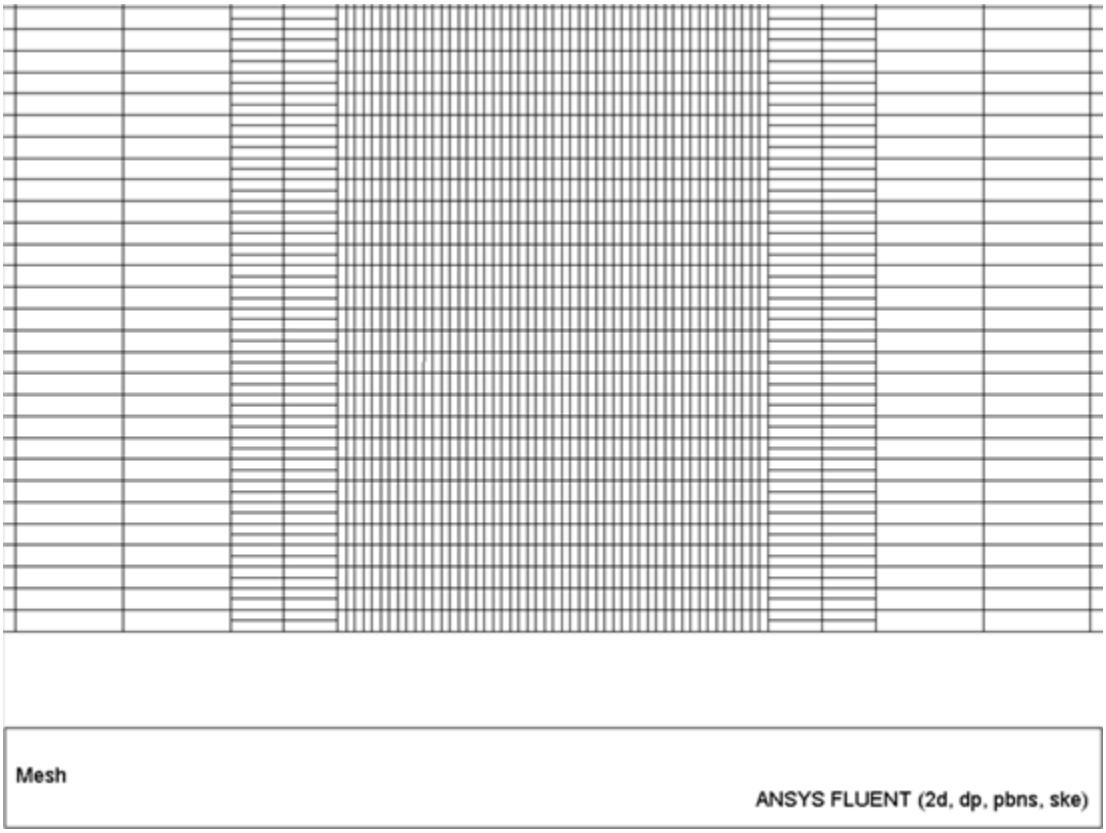


## 21.8. Yplus/Ystar Adaption

It is often difficult to gauge the near-wall resolution requirements when creating the mesh for a turbulent flow. Hence, Yplus and Ystar adaption have been provided to appropriately refine or coarsen the mesh along the wall during the solution process.

For more information, see the following section:
21.8.1. Yplus/Ystar Adaption Approach

### 21.8.1. Yplus/Ystar Adaption Approach

The approach is to compute $y^+$ or $y^*$ for boundary cells on the specified viscous wall zones, define the minimum and maximum allowable $y^+$ or $y^*$, and mark and/or adapt the appropriate cells. Cells with $y^+$ or $y^*$ values below the minimum allowable threshold will be marked for coarsening and cells with $y^+$ or $y^*$ values above the maximum allowable threshold will be marked for refinement (unless coarsening or refinement has been disabled).

Figure 21.16: Duct Flow Mesh Before Adaption (p. 702) shows a mesh created to solve the flow over an airfoil, where the bottom boundary of the mesh that is shown is the top surface of the airfoil. After an initial solution, it was determined that $y^+$ values of some of the cells on the top surface were too large, and $y^+$ adaption was used to refine them. The resulting mesh is shown in Figure 21.17: Duct Flow Mesh After y+ Adaption (p. 703). Note that the cell-size distribution on the wall after refinement is much less uniform than in the original mesh, which is an adverse effect of $y^+$ adaption. Modifying the adaption

Release 15.0 - © SAS IP, Inc. All rights reserved. - Contains proprietary and confidential information of ANSYS, Inc. and its subsidiaries and affiliates.

thresholds (in this case, the upper threshold) can often improve the uniformity by marking cells that were not marked when the original adaption threshold values were used.

**Figure 21.16: Duct Flow Mesh Before Adaption**

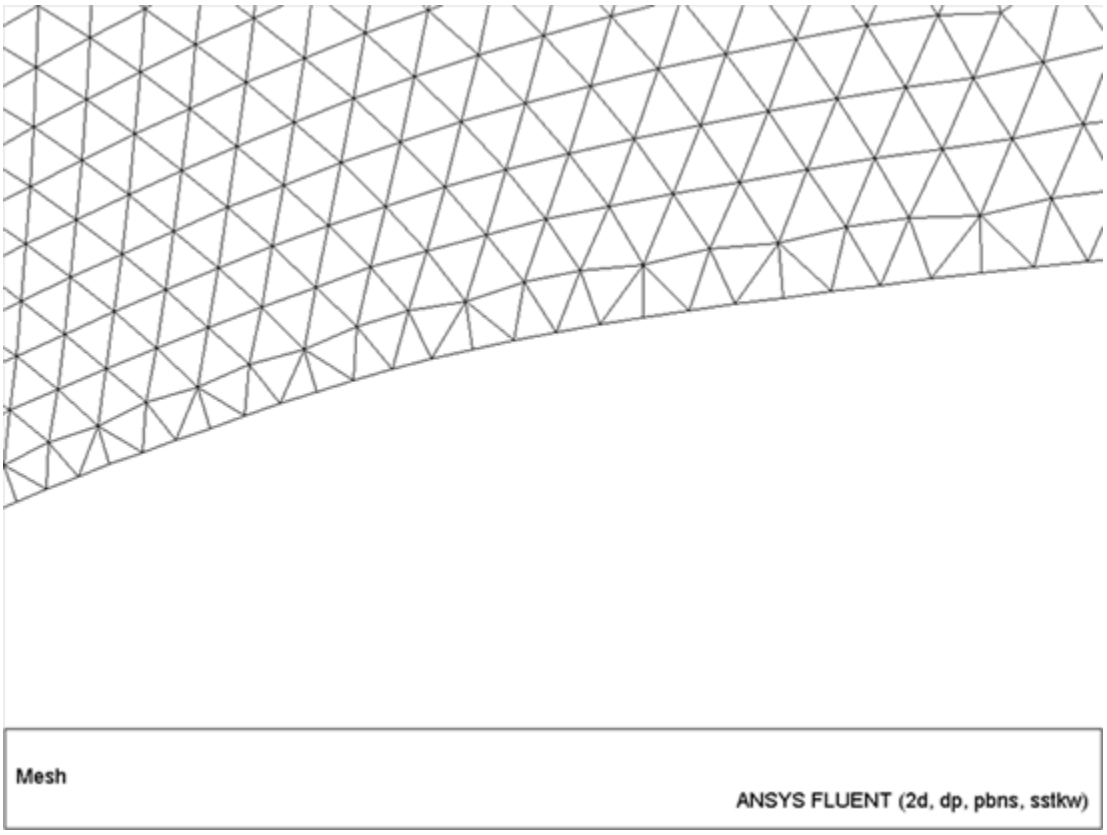



Release 15.0 - © SAS IP, Inc. All rights reserved. - Contains proprietary and confidential information of ANSYS, Inc. and its subsidiaries and affiliates.

**Figure 21.17: Duct Flow Mesh After y+ Adaption**

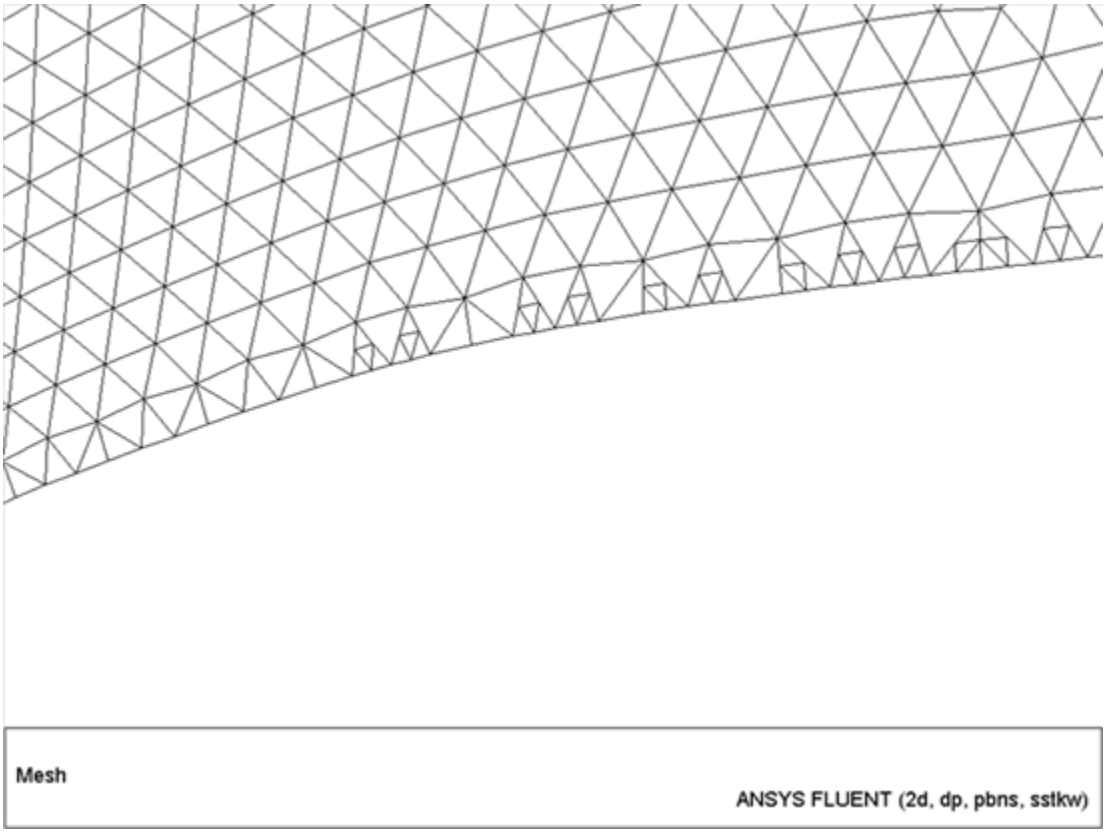


## 21.9. Anisotropic Adaption

The purpose of anisotropic adaption is to refine hexahedral or prism layer cells in 3D meshes. Anisotropic adaption is considered to be more of a mesh manipulation tool rather than an adaption feature, allowing you to refine some hexahedral or prism cells that are adjacent to one or a few boundary face zones using the GUI. The hexahedral or prism cells are split in one direction each time, giving you control of the different splitting ratios, therefore achieving anisotropic refinement.

---

**Important**

Note that anisotropic adaption is different from other mesh adaption features, because it only refines the mesh and does not allow coarsening after refinement.

---

For information on how to use anisotropic adaption, see Anisotropic Adaption in the User's Guide.

## 21.10. Geometry-Based Adaption

The purpose of adaption is to produce a mesh that is fine enough and adequately represents all important features of the geometry. However, when you have a coarse mesh of a geometry that has curved profiles and sharp corners, the adapted mesh may not recover the curved profiles and corners at the perimeter of the geometry. In such cases, you can use geometry-based adaption to reconstruct the geometry (or to recover the finer details of the geometry), while you are also performing the adaption process.

For more information, see the following section:

21.10.1. Geometry-Based Adaption Approach

Release 15.0 - © SAS IP, Inc. All rights reserved. - Contains proprietary and confidential information of ANSYS, Inc. and its subsidiaries and affiliates.

## 21.10.1. Geometry-Based Adaption Approach

Geometry-based adaption works on the principle of geometry reconstruction. In this approach, the cell count of the mesh is increased by creating the new nodes in the domain in between the existing nodes of the mesh. The newly created nodes are projected in such a way that the resulting mesh is finer and has a shape that is closer to the original geometry.

The following sections explain how nodes are projected and the parameters that control the node propagation.

### *21.10.1.1. Node Projection*

Consider a coarse mesh created for a circular geometry. A section of the mesh close to the circular edge is shown in Figure 21.18: Mesh Before Adaption (p. 704). The edge is not smooth and has sharp corners, such that its shape does not closely resemble that of the original geometry. Using boundary adaption along with the geometry reconstruction option will result in a mesh with smoother edges, as shown in Figure 21.19: Projection of Nodes (p. 705).

In Figure 21.19: Projection of Nodes (p. 705), the dotted lines represent the original edge of the mesh. The boundary adaption process creates new nodes in between the original nodes. These nodes are projected towards the edge of the geometry, and as a result the resulting mesh has smooth edges and its shape is closer to the original geometry.

**Important**

Only the nodes created in the adaption process (newly created nodes) are projected; the original nodes retain their positions.

**Figure 21.18: Mesh Before Adaption**

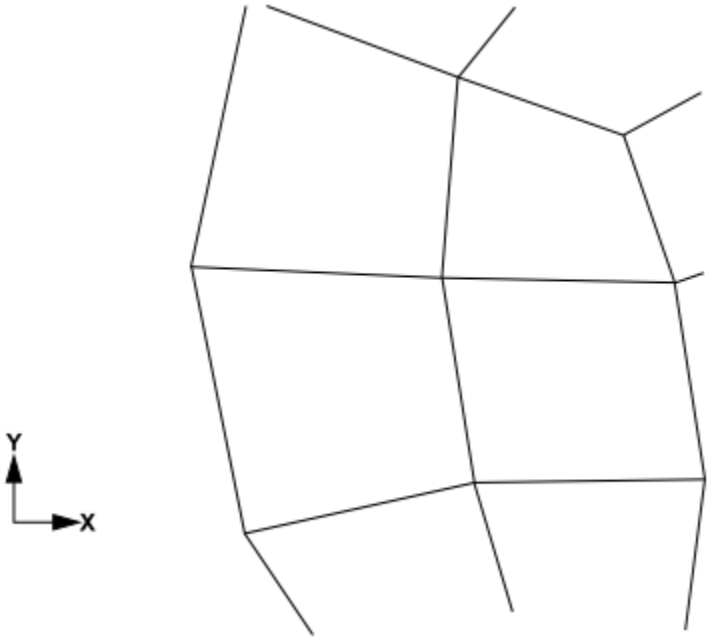



Release 15.0 - © SAS IP, Inc. All rights reserved. - Contains proprietary and confidential information of ANSYS, Inc. and its subsidiaries and affiliates.

**Figure 21.19: Projection of Nodes**

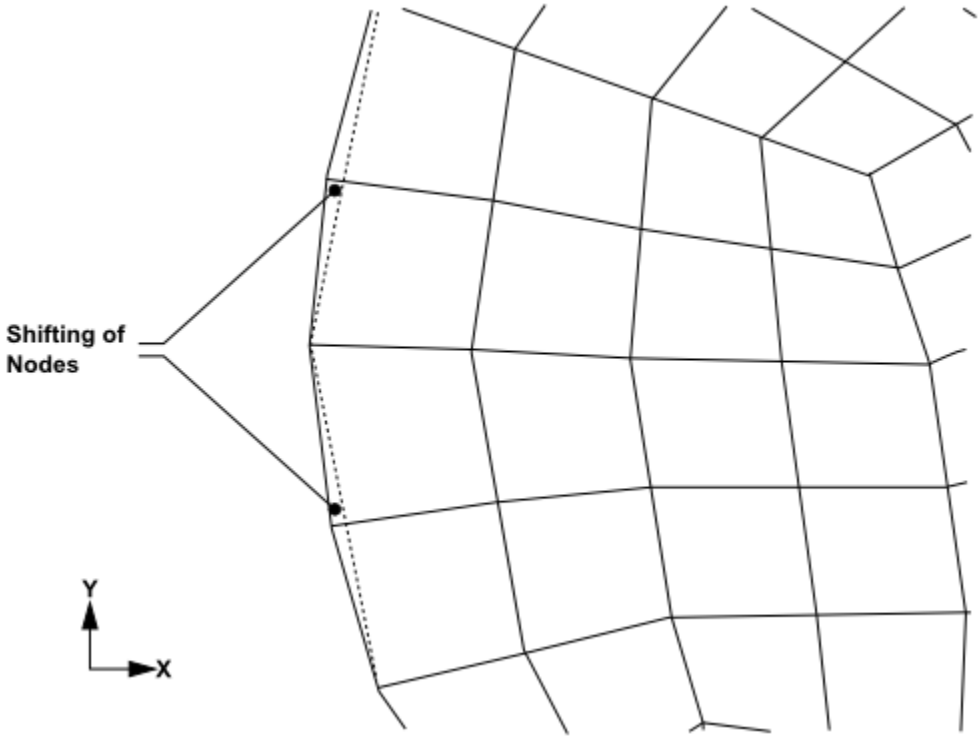


The following parameters control node projection and are specified in the Geometry Based Adaption Dialog Box.

- **Levels of Projection Propagation**: This parameter allows you to specify the number of node layers across which node propagation should take place for geometry reconstruction. A value of 1 means only the nodes at the boundary will be projected, a value of 2 means the nodes at the boundary and the nodes in the next layer will be projected, and so on.

---

**Note**

The nodes in the first level are projected by a maximum magnitude and the node in the last level are projected by a minimum magnitude. The magnitude of projection decreases gradually from the first level to the last level.

For example, a value of 3 for **Levels of Projection Propagation** means, the level 1 node is projected by maximum magnitude and level 3 node is projected by minimum magnitude. Figure 21.20: Levels Projection Propagation and Magnitude (p. 706) illustrates the level of propagation and magnitude of projection of newly created nodes.

---

Release 15.0 - © SAS IP, Inc. All rights reserved. - Contains proprietary and confidential information of ANSYS, Inc. and its subsidiaries and affiliates.

**Figure 21.20: Levels Projection Propagation and Magnitude**

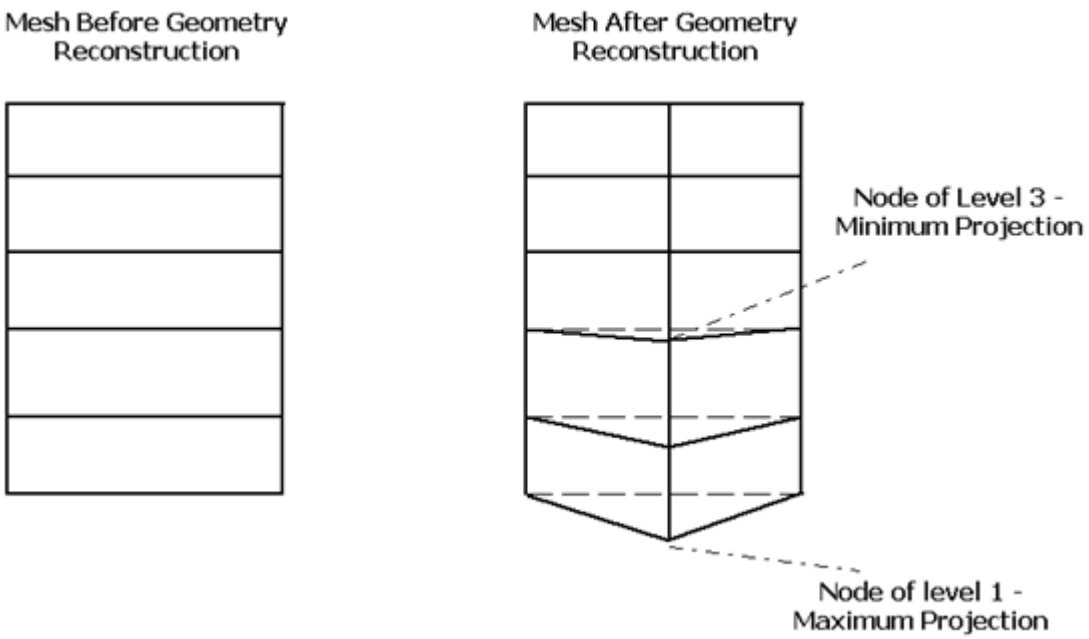


- **Direction of Projection**: This parameter allows you to specify the direction, X, Y, or Z (for 3D), for node projection. If you do not specify any direction, the node projection takes place at the nearest point of the newly created node.
- **Background Mesh**: This option allows you to use a fine surface mesh as a background mesh, which is then used to reconstruct the geometry. When you read the surface mesh, the node projection will take place based on the node positions of the background mesh.

  *This option is useful when the mesh you want to adapt is very coarse and geometry is highly curved. In such cases, node projection, only by specifying the parameters may not result in a good quality mesh. However, you can also modify the propagation criteria by specifying the parameters.*

  **Important**

  You can read only one surface mesh at a time. The various zones of the surface mesh will be listed in the **Background Mesh** drop-down list.

## *21.10.1.2. Example of Geometry-Based Adaption*

Consider a mesh created for a spherical geometry. The initial mesh is very coarse, resulting in sharp corners (as in Figure 21.21: Coarse Mesh of a Sphere (p. 707)). It does not represent the spherical geometry accurately. You can recover the original spherical geometry from this coarse mesh by using geometry-based adaption.


Release 15.0 - © SAS IP, Inc. All rights reserved. - Contains proprietary and confidential information of ANSYS, Inc. and its subsidiaries and affiliates.

**Figure 21.21: Coarse Mesh of a Sphere**

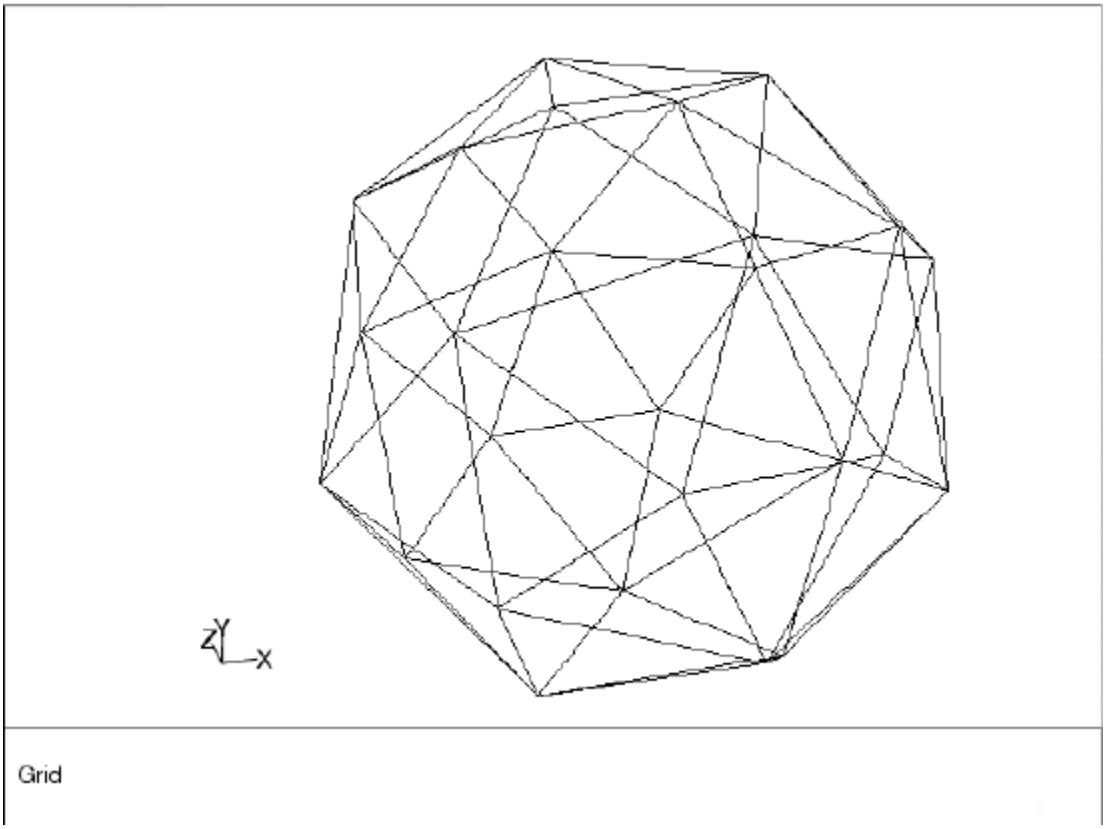


If you adapt boundaries of the domain without activating the **Reconstruct Geometry** option, the resulting mesh (see Figure 21.22: Adapted Mesh Without Geometry Reconstruction (p. 708)) has a sufficient number of cells, but the boundary of the domain still contains sharp corners.

Boundary adaption only creates new nodes in between the existing nodes to increase the cell count of the mesh. Since it does not project the nodes, the shape of the mesh remains as it is.

If you adapt the boundary with the **Reconstruct Geometry** option, the resulting mesh (Figure 21.23: Mesh after Geometry-Based Adaption (p. 708)) has more cells and less sharp corners at the boundary. In addition, the newly created nodes are projected in a direction such that its shape is closer to the original geometry (that is, a sphere with smooth boundary).

Release 15.0 - © SAS IP, Inc. All rights reserved. - Contains proprietary and confidential information of ANSYS, Inc. and its subsidiaries and affiliates.

**Figure 21.22: Adapted Mesh Without Geometry Reconstruction**

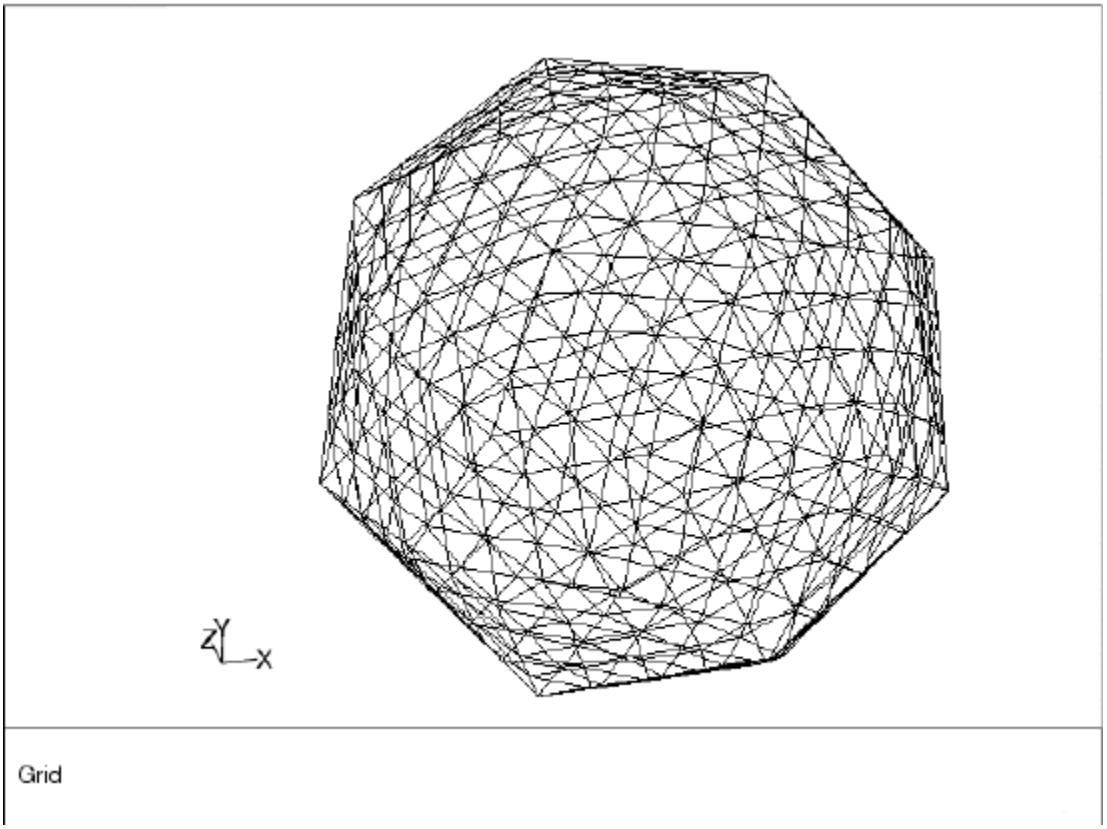


**Figure 21.23: Mesh after Geometry-Based Adaption**

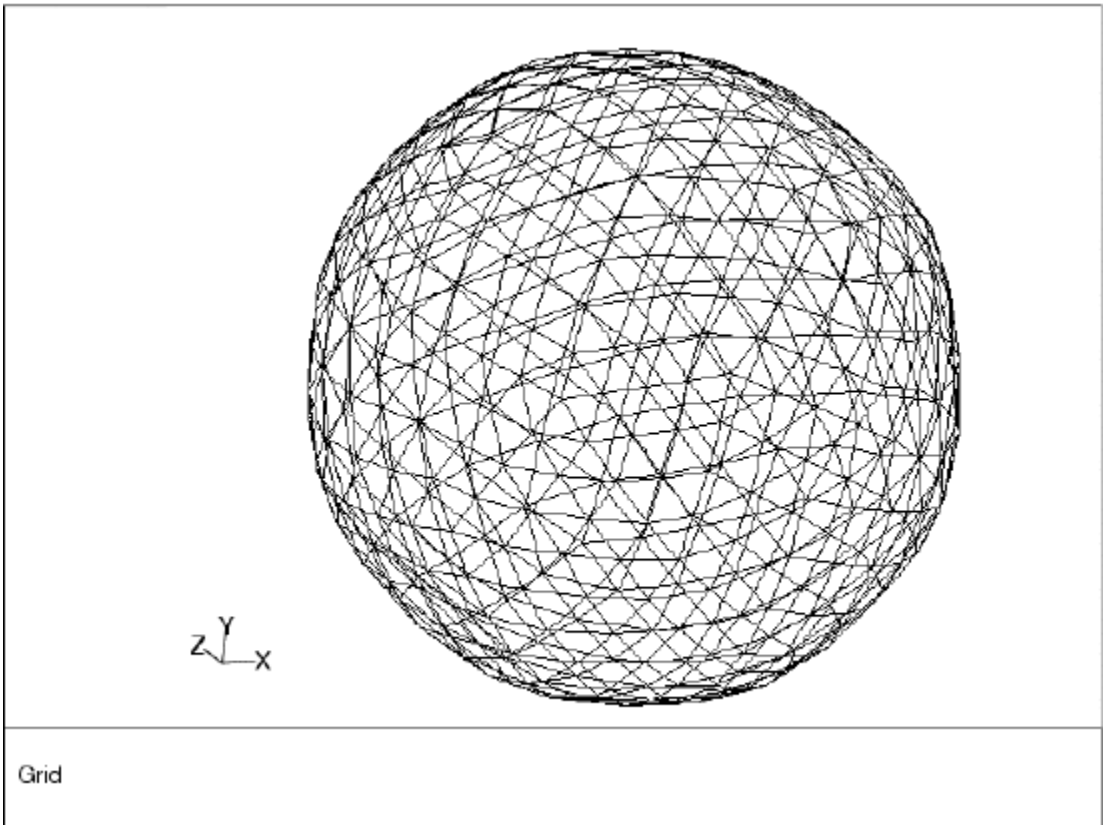



Release 15.0 - © SAS IP, Inc. All rights reserved. - Contains proprietary and confidential information
of ANSYS, Inc. and its subsidiaries and affiliates.

# 21.11. Registers

A register is the group of cells that are marked for refinement/coarsening but not adapted.

There are two types of registers:

- adaption registers
- mask registers

For more information, see the following sections:
21.11.1. Adaption Registers
21.11.2. Mask Registers

## 21.11.1. Adaption Registers

An adaption register is basically a list of identifiers for each cell in the domain. The identifiers designate whether a cell is neutral (not marked), marked for refinement, or marked for coarsening. Invoking the **Mark** command creates an adaption register. It is called a register because it is used in a manner similar to the way memory registers are used in calculators. For example, one adaption register holds the result of an operation, another register holds the results of a second operation, and these registers can be used to produce a third register.

The adaption function is used to set the appropriate identifier. For example, to refine the cells based on pressure gradient, the solver computes the gradient adaption function for each cell. The cell value is compared with the refining and coarsening threshold values and assigned the appropriate identifier.

- If the cell value < coarsen threshold value, the cell is marked for coarsening.
- If the coarsen threshold value < cell value < refine threshold value, the cell is neutral (not marked).
- If the cell value > refine threshold value, the cell is marked for refinement.

Adaption registers can be created using geometric data, physical features of the flow field, and combinations of these information. After they are created, the adaption registers can be listed, displayed, deleted, combined, exchanged, inverted, and changed to mask registers.

**Hybrid Adaption Functions**

The hybrid adaption functions are created to confine the adaption to a specific region (using masks) and/or create a more accurate error indicator. ANSYS Fluent provides a few basic tools to aid in creating hybrid adaption functions.

1. Create the initial adaption registers using geometric and/or solution vector information.
2. Manipulate these registers and their associated refinement and coarsening marks.
   - Manipulate the registers by changing the type and/or combining them to create the desired hybrid function.
   - Manipulate the marks by using **Exchange**, **Invert**, **Limit**, and **Fill** operations.
3. Delete, display, and/or adapt based on the hybrid adaption functions.

*Release 15.0 - © SAS IP, Inc. All rights reserved. - Contains proprietary and confidential information of ANSYS, Inc. and its subsidiaries and affiliates.*

For example, you can capture the shock wave generated on a wedge in a supersonic flow field by adapting the mesh based on the gradients of pressure. The pressure gradient near the surface of the wedge, however, is relatively small. You can therefore use the velocity field to resolve the equally important boundary layer near the surface of the wedge.

- If you adapt based on pressure, regions near the surface might be coarsened.
- If you subsequently adapted based on velocity, these regions may be refined, but the net result will not gain in resolution.
- If you combine the velocity and pressure gradient adaption functions, the new adaption function will allow increased resolution in both regions.

The relative weight of the two functions in the hybrid function is determined by the values of the refinement and coarsening thresholds you specify for each of the flow field variables.

To refine the shock and boundary layer only near the leading edge of the wedge, create a circle at the leading edge of the wedge using the region adaption function, change this new register to a mask, and combine it with the hybrid gradient function.

*The GUI and text interface commands generate adaption registers that designate the cells marked for refinement or coarsening. These registers can be converted to mask registers.*

## 21.11.2. Mask Registers

Mark registers maintain only two states: ACTIVE and INACTIVE. If the adaption register is converted to a mask, cells marked for refinement become ACTIVE cells, while those that are unmarked or marked for coarsening become INACTIVE.

*You can use a mask register to limit adaption to cells within a certain region.*

This process is illustrated in Figure 21.24: Adaption Register with Marked Cells (p. 710), Figure 21.25: Mask Register with Active Cells (p. 711), and Figure 21.26: New Adaption Register Created from Application of Mask (p. 711).

Figure 21.24: Adaption Register with Marked Cells (p. 710) shows a cloud of cells representing an adaption register (shaded cells are marked cells). Figure 21.25: Mask Register with Active Cells (p. 711) illustrates the active cells associated with a mask register. If the mask is applied to (combined with) the adaption register, the new adaption register formed from the combination has the marked cells shown in Figure 21.26: New Adaption Register Created from Application of Mask (p. 711).

**Figure 21.24: Adaption Register with Marked Cells**

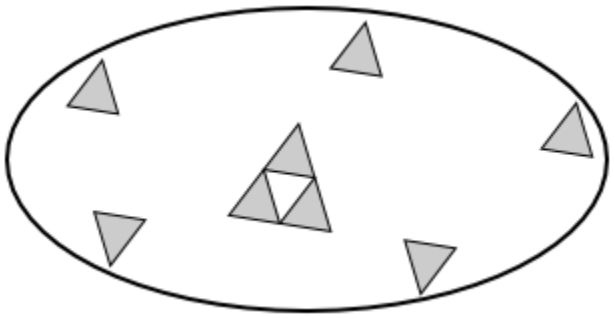


Release 15.0 - © SAS IP, Inc. All rights reserved. - Contains proprietary and confidential information of ANSYS, Inc. and its subsidiaries and affiliates.

**Figure 21.25: Mask Register with Active Cells**

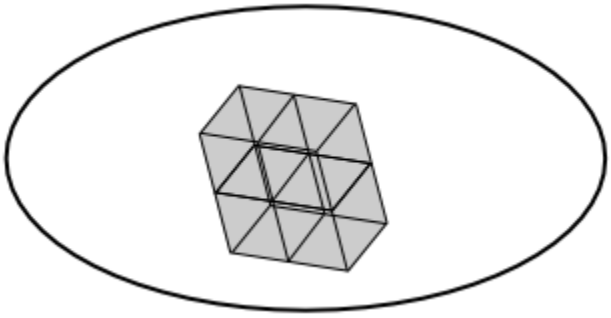

**Figure 21.26: New Adaption Register Created from Application of Mask**

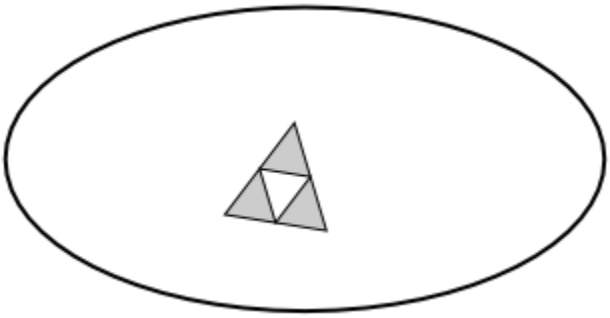

This example does not differentiate between refinement or coarsening marks because the mask is applied to both types of marks. For more information on combining registers, see Manipulating Adaption Registers in the User's Guide.

Release 15.0 - © SAS IP, Inc. All rights reserved. - Contains proprietary and confidential information of ANSYS, Inc. and its subsidiaries and affiliates.

Release 15.0 - © SAS IP, Inc. All rights reserved. - Contains proprietary and confidential information
of ANSYS, Inc. and its subsidiaries and affiliates.

# Chapter 22: Reporting Alphanumeric Data

ANSYS Fluent provides tools for computing and reporting integral quantities at surfaces and boundaries. These tools enable you to find the mass flow rate and heat transfer rate through boundaries, the forces and moments on boundaries, and the area, integral, flow rate, average, and mass average (among other quantities) on a surface or in a volume. In addition, you can print histograms of geometric and solution data, set reference values for the calculation of non-dimensional coefficients, and compute projected surface areas. You can also print or save a summary report of the models, boundary conditions, and solver settings in the current case.

This chapter describes some of the background behind ANSYS Fluent's reporting features. These features are described in the following sections.

22.1. Fluxes Through Boundaries
22.2. Forces on Boundaries
22.3. Surface Integration
22.4. Volume Integration

Additional information about using these reporting tools can be found in Reporting Alphanumeric Data in the User's Guide. Reporting tools for the discrete phase are described in Postprocessing for the Discrete Phase in the User's Guide.

## 22.1. Fluxes Through Boundaries

This section describes the quantities that you can compute for boundaries. For more information about generating flux reports, see Generating a Flux Report in the User's Guide.

For selected boundary zones, you can compute the following quantities:

- The mass flow rate through a boundary is computed by summing the dot product of the density times the velocity vector and the area projections over the faces of the zone.
- The total heat transfer rate through a boundary is computed by summing the total heat transfer rate, $q = q_c + q_r$, over the faces, where $q_c$ is the convective heat transfer rate and $q_r$ is the radiation heat transfer rate. The computation of the heat transfer through the face depends on the specified boundary condition. For example, the conduction heat transfer on a constant-temperature wall face would be the product of the thermal conductivity with the dot product of the area projection and the temperature gradient. For flow boundaries, the total heat transfer rate is the flow rate of the conserved quantity. Depending on the models that are being used, the total heat transfer rate may include the convective flow of sensible or total enthalpy, diffusive flux of energy, etc. Note that the reference temperature in all enthalpy calculations is always 298.15 K.

  **Important**

  Note that in the case of moving walls with compressible flow, the pressure work is also added while reporting heat flux.

Release 15.0 - © SAS IP, Inc. All rights reserved. - Contains proprietary and confidential information of ANSYS, Inc. and its subsidiaries and affiliates.

- The radiation heat transfer rate through a boundary is computed by summing the radiation heat transfer rate $q_r$ over the faces. The computation of the radiation model used.

For example, you might use flux reporting to compute the mass flow through a duct with pressure boundaries specified at the inlet and exit after running a simulation with these settings.

## 22.2. Forces on Boundaries

For selected wall zones, you can compute and report the forces along a specified vector, the moments about a specified center and along a specified axis, and the coordinates of the center of pressure. This feature is useful for reporting, for instance, aerodynamic quantities such as lift, drag, and moment coefficients, as well as the center of pressure for an airfoil.

For information about how ANSYS Fluent computes forces, moments, and centers of pressure, see Computing Forces, Moments, and the Center of Pressure (p. 714). Otherwise, for more information about generating a report on forces, moments, or centers of pressure, see Generating a Force, Moment, or Center of Pressure Report in the User's Guide.

### 22.2.1. Computing Forces, Moments, and the Center of Pressure

The total force component along the specified force vector $\vec{a}$ on a wall zone is computed by summing the dot product of the pressure and viscous forces on each face with the specified force vector. The terms in this summation represent the pressure and viscous force components in the direction of the vector $\vec{a}$:

$$\underbrace{F_a}_{total\ force\ component} = \underbrace{\vec{a}\cdot\vec{F_p}}_{pressure\ force\ component} + \underbrace{\vec{a}\cdot\vec{F_v}}_{viscous\ force\ component} \tag{22.1}$$

where

$\vec{a}$ = specified force vector

$\vec{F_p}$ = pressure force vector

$\vec{F_v}$ = viscous force vector

In addition to the actual pressure, viscous, and total forces, the associated force coefficients are also computed for each of the selected wall zones, using the reference values (as described in Reference Values in the User's Guide). The force coefficient is defined as force divided by $\frac{1}{2}\rho v^2 A$, where $\rho, v$, and $A$ are the density, velocity, and area. Finally, the net values of the pressure, viscous, and total forces and coefficients for all of the selected wall zones are also computed.

The total moment vector about a specified center $A$ is computed by summing the cross products of the pressure and viscous force vectors for each face with the moment vector $\vec{r}_{AB}$, which is the vector from the specified moment center $A$ to the force origin $B$ (see Figure 22.1: Moment About a Specified Moment Center (p. 715)). The terms in this summation represent the pressure and viscous moment vectors:

$$\underbrace{\vec{M}_A}_{total\ moment} = \underbrace{\vec{r}_{AB}\times\vec{F_p}}_{pressure\ moment} + \underbrace{\vec{r}_{AB}\times\vec{F_v}}_{viscous\ moment} \tag{22.2}$$

where


Release 15.0 - © SAS IP, Inc. All rights reserved. - Contains proprietary and confidential information of ANSYS, Inc. and its subsidiaries and affiliates.

$A$ = specified moment center

$B$ = force origin

$\vec{r}_{AB}$ = moment vector

$\vec{F_p}$ = pressure force vector

$\vec{F_v}$ = viscous force vector

**Figure 22.1: Moment About a Specified Moment Center**

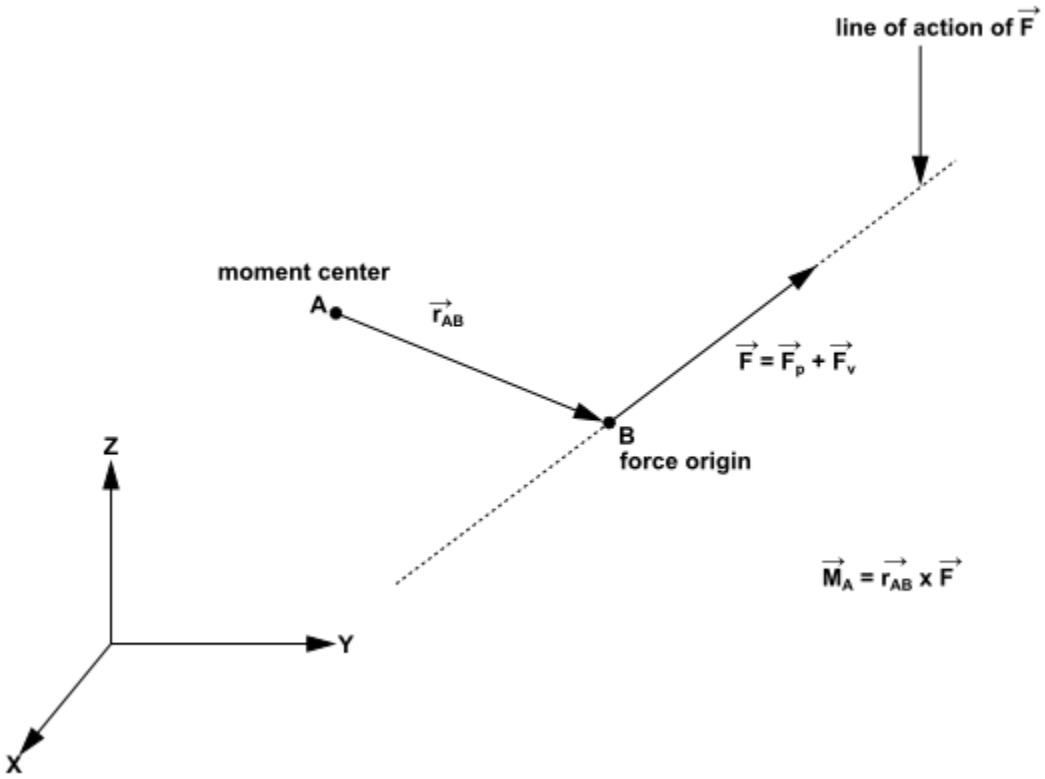


Direction of the total moment vector follows the right hand rule for cross products.

Along with the actual components of the pressure, viscous, and total moments, the moment coefficients are computed for each of the selected wall zones, using the reference values (as described in Reference Values in the User's Guide). The moment coefficient is defined as the moment divided by $\frac{1}{2}\rho v^2 AL$, where $\rho, v$, $A$, and $L$ are the density, velocity, area, and length. The coefficient values for the individual wall zones are also summed to yield the net values of the pressure, viscous, and total moments and coefficients for all of the selected wall zones.

Furthermore, the moments along a specified axis are computed. These moments, also known as torques, are defined as the dot product of a unit vector in the direction of the specified axis and the individual and net values of the pressure, viscous, and total moments and coefficients.

To reduce round-off error, a reference pressure is used to normalize the cell pressure for computation of the pressure force. For example, the net pressure force vector, acting on a wall zone, is computed as the vector sum of the individual force vectors for each cell face:

Release 15.0 - © SAS IP, Inc. All rights reserved. - Contains proprietary and confidential information of ANSYS, Inc. and its subsidiaries and affiliates.

$$\overrightarrow{F_p} = \sum_{i=1}^{n} \left(p - p_{ref}\right) A\hat{n} \tag{22.3}$$

$$\overrightarrow{F_p} = \sum_{i=1}^{n} pA\hat{n} - p_{ref} \sum_{i=1}^{n} A\hat{n} \tag{22.4}$$

where $n$ is the number of faces, $A$ is the area of the face, and $\hat{n}$ is the unit normal to the face.

For a 2D shape, the resulting force due to pressure and viscous stresses is applied along a line (parallel to the resulting force). The center of pressure is the intersecting point of this line with a user-specified reference line (for example, the chord line is generally selected for a 2D airfoil). The resultant moment about this point is then zero.

For a general body in 3D, the pressure and viscous wall stress distribution can be represented by a force (and its application axis) and a moment about a moment center. In general, the problem of finding the translation of the application axis that zeroes the moment does not have a solution. For certain symmetric geometries (for example a non spinning missile), however, this solution exists. In such cases, the center of pressure is usually defined as the intersection of the application axis of the resulting force with a user-specified reference plane.

ANSYS Fluent calculates the center of pressure as follows. For a generic moment center and axes, the resultant moment is expressed as

$$\begin{aligned} \mathrm{M}_x &= \mathrm{F}_z\mathrm{Y} - \mathrm{F}_y\mathrm{Z} \\ \mathrm{M}_y &= \mathrm{F}_x\mathrm{Z} - \mathrm{F}_z\mathrm{X} \\ \mathrm{M}_z &= \mathrm{F}_y\mathrm{X} - \mathrm{F}_x\mathrm{Y} \end{aligned} \tag{22.5}$$

In 3D, zeroing two of these equations and using the equation of the user-specified (constraining) reference plane, the intersection point between the application axis and the specified reference plane can be obtained. In 2D, only the last equation in Equation 22.5 (p. 716) is used in combination with the user-specified reference line to calculate the center of pressure.

## 22.3. Surface Integration

You can compute the area or mass flow rate, or the integral, standard deviation, flow rate, volume flow rate, area-weighted average, mass-weighted average, sum, facet average, facet maximum, facet minimum, uniformity index (weighted by area or mass), vertex average, vertex minimum, and vertex maximum for a selected field variable on selected surfaces in the domain. These surfaces are sets of data points created by ANSYS Fluent for each of the zones in your model, or defined by you using the methods described in Creating Surfaces for Displaying and Reporting Data in the User's Guide, or by using the Text User Interface, described in Text User Interface (TUI) in the User's Guide.

The following list provides information on the data reported for the various surface integrals:

- For the vertex average, vertex maximum, and the vertex minimum, ANSYS Fluent reports the node values of the selected variable on the selected surface.
- For mass flow rate, volume flow rate, and flow rate, ANSYS Fluent reports the rate. Of these, flow rate is the only one associated with a selected variable. The values used in the computation depend on the kind of surface selected:


Release 15.0 - © SAS IP, Inc. All rights reserved. - Contains proprietary and confidential information of ANSYS, Inc. and its subsidiaries and affiliates.

  - The face flux values are used for face zone surfaces.
  - The cell values are used for postprocessing surfaces. See Cell Values in the User's Guide for further details.

- For all other surface integrals, ANSYS Fluent reports the integral, using values that are appropriate for the particular surface:
  - For face zone surfaces, the face values are used when they are available, that is, when they are calculated by the solver or specified as a boundary condition. Otherwise, the cell values are used. The cell value for non-internal faces (that is, faces that only have `c0` and no `c1`) is the `c0` value. The cell value for internal faces (that is, faces that have `c0` and `c1`) is the average of the `c0` and `c1` values.
  - For postprocessing surfaces, the cell values are used. See Cell Values in the User's Guide for further details.

Example uses of several types of surface integral reports are given below:

- Area: You can compute the area of a velocity inlet zone, and then estimate the velocity from the mass flow rate:

$$v = \frac{\dot{m}}{\rho A} \tag{22.6}$$

- Area-weighted average: You can find the average value on a solid surface, such as the average heat flux on a heated wall with a specified temperature.
- Mass average: You can find the average value on a surface in the flow, such as average enthalpy at a velocity inlet.
- Mass flow rate: You can compute the mass flow rate through a velocity inlet zone, and then estimate the velocity from the area, as described above.
- Flow rate: To calculate the heat transfer rate through a surface, you can calculate the flow rate of enthalpy.
- Integral: You can use integrals for more complex calculations, which may involve the use of the Custom Field Function Calculator Dialog Box, described in Custom Field Functions in the User's Guide, to calculate a function that requires integral computations (for example, swirl number).
- Standard deviation: You can find the standard deviation of a specified field variable on a surface, such as enthalpy, viscosity, and velocity.
- Volume flow rate: This will report the volume flow rate through the specified surface.

For information about how ANSYS Fluent computes surface integrals, see Computing Surface Integrals (p. 717). Otherwise, for more information about generating a surface integral report, see Generating a Surface Integral Report in the User's Guide.

## 22.3.1. Computing Surface Integrals

### *22.3.1.1. Area*

The area of a surface is computed by summing the areas of the facets that define the surface. Facets on a surface are either triangular or quadrilateral in shape.

$$\int dA = \sum_{i=1}^{n} |A_i| \tag{22.7}$$

Release 15.0 - © SAS IP, Inc. All rights reserved. - Contains proprietary and confidential information of ANSYS, Inc. and its subsidiaries and affiliates.

### 22.3.1.2. Integral

An integral on a surface is computed by summing the product of the facet area and the selected field variable facet value, such as density or pressure. For details on the computation of the facet values, see Surface Integration (p. 716).

### 22.3.1.3. Area-Weighted Average

The area-weighted average of a quantity is computed by dividing the summation of the product of the selected field variable and facet area by the total area of the surface:

$$\frac{1}{A}\int \phi dA = \frac{1}{A}\sum_{i=1}^{n} \phi_i |A_i| \tag{22.8}$$

### 22.3.1.4. Flow Rate

The flow rate of a quantity through a surface is computed by summing the value of the selected field variable multiplied by the density and the dot product of the facet area vector and the facet velocity vector.

$$\int \phi \rho \vec{v} \cdot d\vec{A} = \sum_{i=1}^{n} \phi_i \rho_i \vec{v_i} \cdot \vec{A_i} \tag{22.9}$$

### 22.3.1.5. Mass Flow Rate

The mass flow rate through a surface is computed by summing the value of the selected field variable multiplied by the density and the dot product of the facet area vector and the facet velocity vector.

$$\int \rho \vec{v} \cdot d\vec{A} = \sum_{i=1}^{n} \rho_i \vec{v_i} \cdot \vec{A_i} \tag{22.10}$$

### 22.3.1.6. Mass-Weighted Average

The mass-weighted average of a quantity is computed by dividing the summation of the value of the selected field variable multiplied by the absolute value of the dot product of the facet area and momentum vectors by the summation of the absolute value of the dot product of the facet area and momentum vectors (surface mass flux):

$$\frac{\int \phi \rho \, |\vec{v} \cdot d\vec{A}|}{\int \rho \, |\vec{v} \cdot d\vec{A}|} = \frac{\sum_{i=1}^{n} \phi_i \rho_i \, |\vec{v_i} \cdot \vec{A_i}|}{\sum_{i=1}^{n} \rho_i \, |\vec{v_i} \cdot \vec{A_i}|} \tag{22.11}$$

### 22.3.1.7. Sum of Field Variable

The sum of a specified field variable on a surface is computed by summing the value of the selected variable at each facet:

$$\sum_{i=1}^{n} \phi_i \tag{22.12}$$


Release 15.0 - © SAS IP, Inc. All rights reserved. - Contains proprietary and confidential information of ANSYS, Inc. and its subsidiaries and affiliates.

### 22.3.1.8. Facet Average

The facet average of a specified field variable on a surface is computed by dividing the summation of the facet values of the selected variable by the total number of facets. See Node, Cell, and Facet Values in the User's Guide for definitions of facet values.

$$\frac{\sum_{i=1}^{n} \phi_i}{n} \tag{22.13}$$

### 22.3.1.9. Facet Minimum

The facet minimum of a specified field variable on a surface is the minimum facet value of the selected variable on the surface. See Node, Cell, and Facet Values in the User's Guide for definitions of facet values.

### 22.3.1.10. Facet Maximum

The facet maximum of a specified field variable on a surface is the maximum facet value of the selected variable on the surface. See Node, Cell, and Facet Values in the User's Guide for definitions of facet values.

### 22.3.1.11. Vertex Average

The vertex average of a specified field variable on a surface is computed by dividing the summation of the vertex values of the selected variable by the total number of vertices. See Node, Cell, and Facet Values in the User's Guide for definitions of vertex values.

$$\frac{\sum_{i=1}^{n} \phi_i}{n} \tag{22.14}$$

### 22.3.1.12. Vertex Minimum

The vertex minimum of a specified field variable on a surface is the minimum vertex value of the selected variable on the surface. See Node, Cell, and Facet Values in the User's Guide for definitions of vertex values.

### 22.3.1.13. Vertex Maximum

The vertex maximum of a specified field variable on a surface is the maximum vertex value of the selected variable on the surface. See Node, Cell, and Facet Values in the User's Guide for definitions of vertex values.

### 22.3.1.14. Standard-Deviation

The standard deviation of a specified field variable on a surface is computed using the mathematical expression below:

$$\sqrt{\frac{\sum_{i=1}^{n} (x - x_0)^2}{n}} \tag{22.15}$$

Release 15.0 - © SAS IP, Inc. All rights reserved. - Contains proprietary and confidential information of ANSYS, Inc. and its subsidiaries and affiliates.

where $x$ is the cell value of the selected variables at each facet, $x_0$ is the mean of $x$

$$x_0 = \frac{\sum_{i=1}^{n} x}{n}$$

and $n$ is the total number of facets. See Node, Cell, and Facet Values in the User's Guide for definitions of facet values.

### 22.3.1.15. Uniformity Index

The uniformity index represents how a specified field variable varies over a surface, where a value of 1 indicates the highest uniformity. The uniformity index can be weighted by area or mass: the area-weighted uniformity index captures the variation of the quantity (for example, the species concentration), whereas the mass-weighted uniformity index captures the variation of the flux (for example, the species flux).

The area-weighted uniformity index ($\gamma_a$) of a specified field variable $\phi$ is calculated using the following equation:

$$\gamma_a = 1 - \frac{\sum_{i=1}^{n} \left[ \left( \left| \phi_i - \overline{\phi}_a \right| \right) A_i \right]}{2 \left| \overline{\phi}_a \right| \sum_{i=1}^{n} A_i} \tag{22.16}$$

where $i$ is the facet index of a surface with $n$ facets, and $\overline{\phi}_a$ is the average value of the field variable over the surface:

$$\overline{\phi}_a = \frac{\sum_{i=1}^{n} \phi_i A_i}{\sum_{i=1}^{n} A_i} \tag{22.17}$$

The equation for the mass-weighted uniformity index ($\gamma_m$) is different than Equation 22.16 (p. 720) in that it incorporates flux terms:

$$\gamma_m = 1 - \frac{\sum_{i=1}^{n} \left[ \left( \left| \phi_i - \overline{\phi}_m \right| \right) \left( \left| \rho_i \vec{v}_i A_i \right| \right) \right]}{2 \left| \overline{\phi}_m \right| \sum_{i=1}^{n} \left[ \left| \rho_i \vec{v}_i A_i \right| \right]} \tag{22.18}$$

where $\overline{\phi}_m$ is the average flux of the field variable through the surface:

$$\overline{\phi}_m = \frac{\sum_{i=1}^{n} \left[ \phi_i \left( \left| \rho_i \vec{v}_i A_i \right| \right) \right]}{\sum_{i=1}^{n} \left[ \left| \rho_i \vec{v}_i A_i \right| \right]} \tag{22.19}$$

### 22.3.1.16. Volume Flow Rate

The volume flow rate through a surface is computed by summing the value of the facet area vector multiplied by the facet velocity vector:


Release 15.0 - © SAS IP, Inc. All rights reserved. - Contains proprietary and confidential information of ANSYS, Inc. and its subsidiaries and affiliates.

$$\int \vec{v} \cdot d\vec{A} = \sum_{i=1}^{n} \vec{v}_i \cdot \vec{A}_i \tag{22.20}$$

## 22.4. Volume Integration

The volume, sum, maximum, minimum, volume integral, volume-weighted average, mass integral, and mass-weighted average can be obtained for a selected field variable in selected cell zones in the domain.

Example uses of the different types of volume integral reports are given below:

- **Volume**: You can compute the total volume of a fluid region, or the volume of a phase within the fluid region.
- **Sum**: You can add up the discrete-phase mass or energy sources to determine the net transfer from the discrete phase. You can also sum user-defined sources of mass or energy.
- **Sum*2Pi**: In a 2D axisymmetric model, you can add up the discrete-phase mass or energy sources to determine the net transfer from the discrete phase in the entire revolved domain. You can also sum user-defined sources of mass or energy. This report type is only available in 2D axisymmetric cases.
- **Maximum**: The maximum value of the selected variable among all cells in the selected zone.
- **Minimum**: The minimum value of the selected variable among all cells in the selected zone.
- **Volume Integral**: For quantities that are stored per unit volume, you can use volume integrals to determine the net value (for example, integrate density to determine mass).
- **Volume-Average**: You can obtain volume averages of mass sources, energy sources, or discrete-phase exchange quantities.
- **Mass Integral**: You can determine the total mass of a particular species by integrating its mass fraction.
- **Mass**: You can determine the total mass of the mixture phase or an individual phase in the selected fluid zone.
- **Mass-Average**: You can find the average value (such as average temperature) in a fluid zone.

For information about how ANSYS Fluent computes volume integrals, see Computing Volume Integrals (p. 721). Otherwise, for more information about generating a volume integral report, see Generating a Volume Integral Report in the User's Guide.

### 22.4.1. Computing Volume Integrals

#### *22.4.1.1. Volume*

The volume of a fluid phase in a cell zone is computed by summing the product of the phase volume fraction and cell volume for the cells that comprise the zone:

Release 15.0 - © SAS IP, Inc. All rights reserved. - Contains proprietary and confidential information of ANSYS, Inc. and its subsidiaries and affiliates.

$$\int \alpha_p dV = \sum_{i=1}^{n} \alpha_{p_i} |V_i| \tag{22.21}$$

**Note**

For single-phase flow, or for the mixture phase in a multiphase flow, $\alpha_{p_i} = 1$ and the volume of the cell zone is recovered.

### 22.4.1.2. Sum

The sum of a specified field variable in a cell zone is computed by summing the value of the selected variable at each cell in the selected zone:

$$\sum_{i=1}^{n} \phi_i \tag{22.22}$$

### 22.4.1.3. Sum*2Pi

The sum*2pi of a specified field variable in a cell zone of a 2D axisymmetric model is computed by summing the value of the selected variable at each cell in the selected zone and multiplying it by $2\pi$:

$$2\pi \sum_{i=1}^{n} \phi_i \tag{22.23}$$

### 22.4.1.4. Volume Integral

A volume integral is computed by summing the product of the cell volume and the selected field variable:

$$\int \phi dV = \sum_{i=1}^{n} \phi_i |V_i| \tag{22.24}$$

### 22.4.1.5. Volume-Weighted Average

The volume-weighted average of a quantity is computed by dividing the summation of the product of the selected field variable and cell volume by the total volume of the cell zone:

$$\frac{1}{V} \int \phi dV = \frac{1}{V} \sum_{i=1}^{n} \phi_i |V_i| \tag{22.25}$$

### 22.4.1.6. Mass-Weighted Integral

The mass-weighted integral is computed by summing the product of density, cell volume, and the selected field variable:

$$\int \phi \rho dV = \sum_{i=1}^{n} \phi_i \rho_i |V_i| \tag{22.26}$$

**Note**

For multiphase cases, the density, $\rho_i$, used in Equation 22.26 (p. 722) is the mixture density.


Release 15.0 - © SAS IP, Inc. All rights reserved. - Contains proprietary and confidential information of ANSYS, Inc. and its subsidiaries and affiliates.

### 22.4.1.7. Mass

The mass of a particular phase is computed by summing the product of phase density, cell volume, and phase volume fraction:

$$\int \alpha_p \rho_p dV = \sum_{i=1}^{n} \alpha_{p_i} \rho_{p_i} |V_i| \tag{22.27}$$

### 22.4.1.8. Mass-Weighted Average

The mass-weighted average of a quantity is computed by dividing the summation of the product of density, cell volume, and the selected field variable by the summation of the product of density and cell volume:

$$\frac{\int \phi \rho dV}{\int \rho dV} = \frac{\sum_{i=1}^{n} \phi_i \rho_i |V_i|}{\sum_{i=1}^{n} \rho_i |V_i|} \tag{22.28}$$

**Note**

For multiphase cases, the density, $\rho_i$, used in Equation 22.28 (p. 723) is the mixture density.

Release 15.0 - © SAS IP, Inc. All rights reserved. - Contains proprietary and confidential information
of ANSYS, Inc. and its subsidiaries and affiliates.

# Appendix A. Nomenclature

| | |
|---|---|
| $A$ | Area ($m^2$, $ft^2$) |
| $\vec{a}$ | Acceleration ($m/s^2$, $ft/s^2$) |
| $a$ | Local speed of sound (m/s, ft/s) |
| $c$ | Concentration (mass/volume, moles/volume) |
| $C_D$ | Drag coefficient, defined different ways (dimensionless) |
| $c_{p'}$ $c_v$ | Heat capacity at constant pressure, volume (J/kg-K, Btu/$lb_m$- $^\circ$F) |
| $d$ | Diameter; $d_p, D_p$, particle diameter (m, ft) |
| $D_H$ | Hydraulic diameter (m, ft) |
| $_{ij}, D$ | Mass diffusion coefficient ($m^2/s$, $ft^2/s$) |
| $E$ | Total energy, activation energy (J, kJ, cal, Btu) |
| $f$ | Mixture fraction (dimensionless) |
| $\vec{F}$ | Force vector (N, $lb_f$) |
| $F_D$ | Drag force (N, $lb_f$) |
| $\vec{g}$ | Gravitational acceleration ($m/s^2$, $ft/s^2$); standard values = 9.80665 $m/s^2$, 32.1740 $ft/s^2$ |
| Gr | Grashof number ≡ ratio of buoyancy forces to viscous forces (dimensionless) |
| $H$ | Total enthalpy (energy/mass, energy/mole) |
| $h$ | Heat transfer coefficient (W/$m^2$-K, Btu/$ft^2$-h- $^\circ$F) |
| $h$ | Species enthalpy; $h^0$, standard state enthalpy of formation (energy/mass, energy/mole) |
| $I$ | Radiation intensity (energy per area of emitting surface per unit solid angle) |
| $J$ | Mass flux; diffusion flux (kg/$m^2$-s, $lb_m/ft^2$-s) |
| $K$ | Equilibrium constant = forward rate constant/backward rate constant (units vary) |
| $k$ | Kinetic energy per unit mass (J/kg, Btu/$lb_m$) |
| $k$ | Reaction rate constant, for example, $k_1, k_{-1}, k_{f,r}, k_{b,r}$ (units vary) |
| $k$ | Thermal conductivity (W/m-K, Btu/ft-h- $^\circ$F) |
| $k_B$ | Boltzmann constant ($1.38\times10^{-23}$ J/molecule-K) |
| $k,$ $k_c$ | Mass transfer coefficient (units vary); also $K, K_c$ |
| $\ell, l, L$ | Length scale (m, cm, ft, in) |

Release 15.0 - © SAS IP, Inc. All rights reserved. - Contains proprietary and confidential information of ANSYS, Inc. and its subsidiaries and affiliates.

| | |
|---|---|
| Le | Lewis number ≡ ratio of thermal diffusivity to mass diffusivity (dimensionless) |
| $m$ | Mass (g, kg, $\mathrm{lb}_m$) |
| $\dot{m}$ | Mass flow rate (kg/s, $\mathrm{lb}_m$/s) |
| $M_w$ | Molecular weight (kg/kmol, $\mathrm{lb}_m/\mathrm{lb}_m$mol) |
| M | Mach number ≡ ratio of fluid velocity magnitude to local speed of sound (dimensionless) |
| Nu | Nusselt number ≡ dimensionless heat transfer or mass transfer coefficient (dimensionless); usually a function of other dimensionless groups |
| $p$ | Pressure (Pa, atm, mm Hg, $\mathrm{lb}_f/\mathrm{ft}^2$) |
| Pe | Peclet number $\equiv Re \times Pr$ for heat transfer, and $\equiv Re \times Sc$ for mass transfer (dimensionless) |
| Pr | Prandtl number ≡ ratio of momentum diffusivity to thermal diffusivity (dimensionless) |
| $Q$ | Flow rate of enthalpy (W, Btu/h) |
| $q$ | Heat flux (W/m$^2$, Btu/$\mathrm{ft}^2$-h) |
| $R$ | Gas-law constant (8.31447 $\times 10^3$ J/kmol-K, 1.98588 Btu/$\mathrm{lb}_m$mol- $^\circ$F) |
| $r$ | Radius (m, ft) |
| $\mathcal{R}$ | Reaction rate (units vary) |
| Ra | Rayleigh number $\equiv Gr \times Pr$; measure of the strength of buoyancy-induced flow in natural (free) convection (dimensionless) |
| Re | Reynolds number ≡ ratio of inertial forces to viscous forces (dimensionless) |
| $S$ | Total entropy (J/K, J/kmol-K, Btu/$\mathrm{lb}_m$mol- $^\circ$F) |
| $s$ | Species entropy; $s^0$, standard state entropy (J/kmol-K, Btu/$\mathrm{lb}_m$mol- $^\circ$F) |
| Sc | Schmidt number ≡ ratio of momentum diffusivity to mass diffusivity (dimensionless) |
| $S_{ij}$ | Mean rate-of-strain tensor (s$^{-1}$) |
| $T$ | Temperature (K, $^\circ$C, $^\circ$R, $^\circ$F) |
| $t$ | Time (s) |
| $U$ | Free-stream velocity (m/s, ft/s) |
| $u, v, w$ | Velocity magnitude (m/s, ft/s); also written with directional subscripts (for example, $v_x$, $v_y$, $v_z$, $v_r$) |
| $V$ | Volume (m$^3$, $\mathrm{ft}^3$) |
| $\vec{v}$ | Overall velocity vector (m/s, ft/s) |
| We | Weber number ≡ ratio of aerodynamic forces to surface tension forces (dimensionless) |
| $X$ | Mole fraction (dimensionless) |
| $Y$ | Mass fraction (dimensionless) |
| $\alpha$ | Permeability, or flux per unit pressure difference (L/m$^2$-h-atm, $\mathrm{ft}^3/\mathrm{ft}^2$-h-($\mathrm{lb}_f/\mathrm{ft}^2$)) |
| $\alpha$ | Thermal diffusivity (m$^2$/s, $\mathrm{ft}^2$/s) |
| $\alpha$ | Volume fraction (dimensionless) |


Release 15.0 - © SAS IP, Inc. All rights reserved. - Contains proprietary and confidential information of ANSYS, Inc. and its subsidiaries and affiliates.

| | |
|---|---|
| $\beta$ | Coefficient of thermal expansion ($K^{-1}$) |
| $\gamma$ | Porosity (dimensionless) |
| $\gamma$ | Ratio of specific heats, $c_p/c_v$ (dimensionless) |
| $\Delta$ | Change in variable, final − initial (for example, $\Delta p$, $\Delta t$, $\Delta H$, $\Delta S$, $\Delta T$) |
| $\delta$ | Delta function (units vary) |
| $\varepsilon$ | Emissivity (dimensionless) |
| $\varepsilon$ | Lennard-Jones energy parameter (J/molecule) |
| $\varepsilon$ | Turbulent dissipation rate ($m^2/s^3$, $ft^2/s^3$) |
| $\varepsilon$ | Void fraction (dimensionless) |
| $\eta$ | Effectiveness factor (dimensionless) |
| $\eta', \eta''$ | Rate exponents for reactants, products (dimensionless) |
| $\theta_r$ | Radiation temperature (K) |
| $\lambda$ | Molecular mean free path (m, nm, ft) |
| $\lambda$ | Wavelength (m, nm, Å, ft) |
| $\mu$ | Dynamic viscosity (cP, Pa-s, $lb_m$/ft-s) |
| $\nu$ | Kinematic viscosity ($m^2/s$, $ft^2/s$) |
| $\nu', \nu''$ | Stoichiometric coefficients for reactants, products (dimensionless) |
| $\rho$ | Density ($kg/m^3$, $lb_m/ft^3$) |
| $\sigma$ | Stefan-Boltzmann constant ($5.67 \times 10^{-8}$ $W/m^2$-$K^4$) |
| $\sigma$ | Surface tension (kg/m, dyn/cm, $lb_f$/ft) |
| $\sigma_s$ | Scattering coefficient ($m^{-1}$) |
| $\overline{\overline{\tau}}$ | Stress tensor (Pa, $lb_f/ft^2$) |
| $\tau$ | Shear stress (Pa, $lb_f/ft^2$) |
| $\tau$ | Time scale, for example, $\tau_c$, $\tau_p$, $\tau_c$ (s) |
| $\tau$ | Tortuosity, characteristic of pore structure (dimensionless) |
| $\phi$ | Equivalence ratio (dimensionless) |
| $\phi$ | Thiele modulus (dimensionless) |
| $\Omega$ | Angular velocity; $\Omega_{ij}$, Mean rate of rotation tensor ($s^{-1}$) |
| $\omega$ | Specific dissipation rate ($s^{-1}$) |
| $\Omega, \Omega'$ | Solid angle (degrees, radians, gradians) |
| $\Omega_D$ | Diffusion collision integral (dimensionless) |

Release 15.0 - © SAS IP, Inc. All rights reserved. - Contains proprietary and confidential information of ANSYS, Inc. and its subsidiaries and affiliates.

Release 15.0 - © SAS IP, Inc. All rights reserved. - Contains proprietary and confidential information
of ANSYS, Inc. and its subsidiaries and affiliates.

# Bibliography


[1] *User Manual for 1993 Version Pulverized Coal Gasification and Combustion 3-Dimensional (pcgc-3)*. Advanced Combustion Engineering Research Center, Brigham Young University. 1993.

[2] T. Ahmad, S. L. Plee, and J. P. Myers. *"Computation of Nitric Oxide and Soot Emissions from Turbulent Diffusion Flames"*. *J. of Engineering for Gas Turbines and Power*. 107. 48–53. 1985.

[3] B. J. Alder and T. E. Wainwright. *"Studies in Molecular Dynamics II: Behaviour of a Small Number of Elastic Spheres*. *J. Chem. Phys*. 33. 1439. 1960.

[4] M. J. Augenstein, A. M. Tenenbaum, Y. Langsam. *Data Structures Using C*. Prentice Hall. 1990.

[5] A. A. Amsden. *"KIVA-3: A KIVA Program with Block-Structured Mesh for Complex Geometries"*. *Technical Report LA-12503-MS, UC-361*. Los Alamos National Laboratory, Los Alamos, New Mexico. March 1993.

[6] T. B. Anderson and R. Jackson. *"A Fluid Mechanical Description of Fluidized Beds"*. *I & EC Fundam*. 6. 527–534. 1967.

[7] W. Anderson and D. L. Bonhus. *"An Implicit Upwind Algorithm for Computing Turbulent Flows on Unstructured Grids"*. *Computers Fluids*. 23(1). 1–21. 1994.

[8] S. P. Antal, R. T. Lahey, and J.E. Flaherty. *"Analysis of phase distribution in fully developed laminar bubbly two-phase flow"*. *International Journal of Multiphase Flow*. 17. 5. 635–652. 1991.

[9] A. Antifora, M. Sala, A. Perera, and L. Vigevano. *"NOx Emissions in Combustion Systems of Coal Fired Furnaces with a Reducing Environment: Predictions and Measurements"*. *Fourth International Conference on Technologies and Combustion for a Clean Environment*. Lisbon, Portugal. 1997.

[10] S. V. Apte, M. Gorokhovski and P. Moin. *"LES of Atomizing Spray with Stochastic Modeling of Secondary Breakup"*. *International Journal of Multiphase Flow*. 29. 1503 –1522. 2003.

[11] S. V. Apte, K. Mahesh, and T. Lundgren. *"Accounting for finite-size effects in simulations of dispersed particle-laden flows"*. *International Journal of Multiphase Flow*. 34(3). 260–271. 2008.

[12] S. Armsfield and R. Street. *"The Fractional-Step Method for the Navier-Stokes Equations on Staggered Grids: Accuracy of Three Variations"*. *Journal of Computational Physics*. 153. 660–665. 1999.

[13] D. Arnal, M. Habiballah, and E. Coustols. *"Théorie de l'instabilité laminaire et critères de transition en écoulement bi et tridimensionnel"*. *La Recherche aérospatiale*. 2. 125–143. 1984.

[14] F. Backmier, K. H. Eberius, and T. Just. *Comb. Sci. Tech*. 7. 77. 1973.

[15] S. Badzioch and P. G. W. Hawksley. *"Kinetics of Thermal Decomposition of Pulverized Coal Particles"*. *Ind. Eng. Chem. Process Design and Development*. 9. 521–530. 1970.

[16] J. Baldyga. *"Turbulent mixer model with application to homogeneous instantaneous chemical reactions"*. *Chem. Eng. Sci*. 44. 1175–1182. 1989.

[17] R. S. Barlow, G. J. Fiechtner, C. D. Carter, and J. Y. Chen. *"Experiments on the Scalar Structure of Turbulent CO/$H_2$/$N_2$ Jet Flames"*. *Combustion and Flame*. 120. 549–569. 2000.


*Release 15.0 - © SAS IP, Inc. All rights reserved. - Contains proprietary and confidential information of ANSYS, Inc. and its subsidiaries and affiliates.*

[18] F. J. Barnes, J. H. Bromly, T. J. Edwards, and R. Madngezewsky. *"NOx Emissions from Radiant Gas Burners"*. *Journal of the Institute of Energy*. 155. 184–188. 1988.

[19] T. J. Barth and D. Jespersen. *"The design and application of upwind schemes on unstructured meshes"*. *Technical Report AIAA-89-0366*. AIAA 27th Aerospace Sciences Meeting, Reno, Nevada. 1989.

[20] H. Barths, C. Antoni, and N. Peters. *"Three-Dimensional Simulation of Pollutant Formation in a DI-Diesel Engine Using Multiple Interactive Flamelets"*. *SAE Paper*. SAE. 1998.

[21] H. Barths, N. Peters, N. Brehm, A. Mack M. Pfitzner, and V. Smiljanowski. *"Simulation of pollutant formation in a gas turbine combustor using unsteady flamelets"*. *27th Symp. (Int'l.) on Combustion*. The Combustion Institute. 1841–1847. 1998.

[22] G. K. Batchelor. *An Introduction to Fluid Dynamics*. Cambridge Univ.Press. Cambridge, England. 1967.

[23] D. L. Baulch, D. D. Drysdall, D. G. Horne, and A. C. Lloyd. *Evaluated Kinetic Data for High Temperature Reactions*. 1,2,3. Butterworth. 1973.

[24] D. L. Baulch et al.. *"Evaluated Kinetic Data for Combustion Modelling"*. *J. Physical and Chemical Reference Data*. 21(3). 1992.

[25] M. M. Baum and P. J. Street. *"Predicting the Combustion Behavior of Coal Particles"*. *Combust. Sci. Tech.*. 3(5). 231–243. 1971.

[26] L. L. Baxter. *"Turbulent Transport of Particles"*. *PhD Thesis*. Brigham Young University, Provo, Utah. 1989.

[27] L. L. Baxter and P. J. Smith. *"Turbulent Dispersion of Particles: The STP Model"*. *Energy & Fuels*. 7. 852–859. 1993.

[28] J. C. Beale and R. D. Reitz. *"Modeling Spray Atomization with the Kelvin-Helmholtz/Rayleigh-Taylor Hybrid Model"*. *Atomization and Sprays*. 9. 623–650. 1999.

[29] W. Bechara, C. Bailly, P. Lafon, and S. Candel. *"Stochastic Approach to Noise Modeling for Free Turbulent Flows"*. *AIAA Journal*. 32. 3. 1994.

[30] M. Behnia, S. Parneix, Y. Shabany, and P. A. Durbin. *"Numerical Study of Turbulent Heat Transfer in Confined and Unconfined Impinging Jets"*. *International Journal of Heat and Fluid Flow*. 20. 1–9. 1999.

[31] R. W. Bilger and R. E. Beck. *15th Symp. (Int'l.) on Combustion*. The Combustion Institute. 541. 1975.

[32] R. W. Bilger, M. B. Esler, and S. H. Starner. *"On Reduced Mechanisms for Methane-Air Combustion"*. *Lecture Notes in Physics*. Springer-Verlag. 384. page 86. 1991.

[33] B. Binniger, M. Chan, G. Paczkko, and M. Herrmann. *"Numerical Simulation of Turbulent Partially Pre-mixed Hydrogen Flames with the Flamelet Model"*. Technical reportAdvanced Combustion Gmbh. Internal Report. 1998.

[34] G. A. Bird. *Molecular Gas Dynamics and the direct Simulation of Gas Flows*. Oxford University Press, New York. 1994.

[35] J. Blauvens, B. Smets, and J. Peters. *In 16th Symp.(Int'l.) on Combustion*. The Combustion Institute. 1977.

*Release 15.0 - © SAS IP, Inc. All rights reserved. - Contains proprietary and confidential information of ANSYS, Inc. and its subsidiaries and affiliates.*

[36] Blint. *Principles of Combustion*. Wiley-Interscience. New York1988.

[37] P. Boudier and et al. *"A model for Turbulent Flame Ignition and Propagation in Spark Ignition Engines"*. *In Twenty Fourth Symposium (international) on Combustion, Sydney, Australia*. 1992.

[38] R. M. Bowen. *"Theory of Mixtures"*. In A. C. Eringen, editor*Continuum Physics*. Academic Press, New York. 1–127. 1976.

[39] C. T. Bowman. *"Chemistry of Gaseous Pollutant Formation and Destruction"*. In W. Bartok and A. F. Sarofim, editors*Fossil Fuel Combustion*. J. Wiley and Sons, Canada. 1991.

[40] R. K. Boyd and J. H. Kent. *"Three-dimensional furnace computer modeling"*. *In 21st Symp. (Int'l.) on Combustion*. The Combustion Institute. 265–274. 1986.

[41] J. U. Brackbill, D. B. Kothe, and C. Zemach. *"A Continuum Method for Modeling Surface Tension"*. *J. Comput. Phys*. 100. 335–354. 1992.

[42] A. Brandt. *"Multi-level Adaptive Computations in Fluid Dynamics"*. *Technical Report AIAA-79-1455*. AIAA, Williamsburg, VA. 1979.

[43] K. Bray, P. Domingo and L. Vervisch. *"Role of the Progress Variable in Models for Partially Premixed Turbulent Combustion"*. *Combustion and Flame*. 141. 431–437. 2005.

[44] K. N. Bray and N. Peters. *"Laminar Flamelets in Turbulent Flames"*. In P. A. Libby and F. A. Williams, editors*Turbulent Reacting Flows*. Academic Press. 63–114. 1994.

[45] C. E. Brennen. *Cavitation and Bubble Dynamics*. Oxford University Press. 1995.

[46] K. S. Brentner and F. Farassat. *"An Analytical Comparison of the Acoustic Analogy and Kirchhoff Formulations for Moving Surfaces"*. *AIAA Journal*. 36(8). 1998.

[47] S. J. Brookes and J. B. Moss. *"Prediction of Soot and Thermal Radiation in Confined Turbulent Jet Diffusion Flames"*. *Combustion and Flame*. 116. 486–503. 1999.

[48] J. Brouwer, M. P. Heap, D. W. Pershing, and P. J. Smith. *"A Model for Prediction of Selective Non-Catalytic Reduction of Nitrogen Oxides by Ammonia, Urea, and Cyanuric Acid with Mixing Limitations in the Presence of CO"*. *In 26th Symposium (Int'l) on Combustion*. The Combustion Institute. 1996.

[49] A. L. Brown. *"Modeling Soot in Pulverized Coal Flames"*. *MSc thesis*. Brigham Young University, Utah, USA. 1997.

[50] A. Brucato, F. Grisafi, and G. Montante. *"Particle drag coefficients in turbulent fluids"*. *Chemical Engineering Science*. 53(18). 3295–3314. 1998.

[51] S. Brunauer. *The Absorption of Gases and Vapors*. Princeton University Press, Princeton, NJ. 1943.

[52] Trong T. Bui. *"A Parallel Finite-Volume Algorithm for Large-Eddy Simulation of Turbulent Flows"*. *Technical Memorandum NASA/TM-1999-206570*. 1999.

[53] A. D. B. Burns, Th. Frank, I. Hamill, and J.-M. Shi. *The Favre Averaged Drag Model for Turbulent Dispersion in Eulerian Multi-Phase Flows*. *Fifth International Conference on Multiphase Flow, ICMF-2004, Yokohama, Japan*. 2004.

[54] S. Candel and T. Poinsot. *"Flame stretch and the balance equation for the flame area"*. *Combustion Science and Technology*. 70. 1–15. 1990.

*Release 15.0 - © SAS IP, Inc. All rights reserved. - Contains proprietary and confidential information of ANSYS, Inc. and its subsidiaries and affiliates.*

[55] R. Cao and S. B. Pope. *"Numerical Integration of Stochastic Differential Equations: Weak Second-Order Mid-Point Scheme for Application in the Composition PDF Method"*. *Journal of Computational Physics*. 185(1). 194–212. 2003.

[56] N. F.Carnahan and K. E. Starling. *"Equations of State for Non-Attracting Rigid Spheres"*. *J. Chem. Phys*. 51. 635–636. 1969.

[57] M. G. Carvalho, T. Farias, and P. Fontes. *"Predicting Radiative Heat Transfer in Absorbing, Emitting, and Scattering Media Using the Discrete Transfer Method"*. In W. A. Fiveland et al., editor*Fundamentals of Radiation Heat Transfer*. 160. ASME HTD. pages 17–26. 1991.

[58] J. R. Cash and A. H. Karp. *"A variable order Runge-Kutta method for initial value problems with rapidly varying right-hand sides"*. *ACM Transactions on Mathematical Software*. 16. 201–222. 1990.

[59] Cantera. *http://sourceforge.net/projects/cantera/*. 2012.

[60] S. Chapman and T. G. Cowling. *The Mathematical Theory of Non-Uniform Gases*. 3rd edition. Cambridge University Press, Cambridge, England. 1990.

[61] F. Charlette, C. Meneveau, and D. Veynante. *"A Power-Law Flame Wrinkling Model for LES of Premixed Turbulent Combustion, Part I: Non-Dynamic Formulation and Initial Tests"*. *Combustion and Flame*. 131. 1–2. 159–180. 2002.

[62] S. Charpenay, M. A. Serio, and P. R. Solomon. *In 24th Symp. (Int'l.) on Combustion*. 1189–1197. The Combustion Institute. 1992.

[63] H. C. Chen and V. C. Patel. *"Near-Wall Turbulence Models for Complex Flows Including Separation"*. *AIAA Journal*. 26(6). 641–648. 1988.

[64] P. Cheng. *"Two-Dimensional Radiating Gas Flow by a Moment Method"*. *AIAA Journal*. 2. 1662–1664. 1964.

[65] R. V. Chima and M. S. Liou. *"Comparison of the AUSM+ and H-CUSP Schemes for Turbomachinery Applications"*. *NASA TM-2003-212457*. 2003.

[66] A. J. Chorin. *"Numerical solution of navier-stokes equations"*. *Mathematics of Computation*. 22. 745–762. 1968.

[67] B. H. Chowdhury. *"Emission Control Alternatives for Electric Utility Power Plants"*. *Energy Sources*. 18(4). 393–406. October 1996.

[68] E. H. Chui and G. D. Raithby. *"Computation of Radiant Heat Transfer on a Non-Orthogonal Mesh Using the Finite-Volume Method"*. *Numerical Heat Transfer, Part B*. 23. 269–288. 1993.

[69] Clift, Grace, and Weber. *"Bubbles, Drops, and Particles"*. *Technical Report*. Academic Press. 1978.

[70] P.J. Coelho and N. Peters. *"Unsteady Modelling of a Piloted Methane/Air Jet Flame Based on the Eulerian Particle Flamelet Model"*. *Combustion and Flame*. 122. 444–465. 2001.

[71] M.F. Cohen and D.P. Greenberg. *"The hemi-cube: a radiosity solution for complex environments"*. *ACM SIGGRAPH Computer Graphics*. 19(3). 31–40. 1985.

[72] D. Cokljat, V. A. Ivanov, F. J. Sarasola, and S. A. Vasquez. *"Multiphase k-epsilon Models for Unstructured Meshes"*. *In ASME 2000 Fluids Engineering Division Summer Meeting*. Boston, MA, USA. 2000.

*Release 15.0 - © SAS IP, Inc. All rights reserved. - Contains proprietary and confidential information of ANSYS, Inc. and its subsidiaries and affiliates.*

[73] D. Cokljat, M. Slack, and S. A. Vasquez. *"Reynolds-Stress Model for Eulerian Multiphase"*. In Y. Nagano K. Hanjalic and M. J. Tummers, editors. *Proceedings of the 4th International Symposium on Turbulence Heat and Mass Transfer*. Begell House, Inc. 1047–1054. 2003.

[74] R. Cole. *"A Photographic Study of Pool Boiling in the Region of the Critical Heat Flux"*. *AIChE J.*. 6. 533–542. 1960.

[75] H. W. Coleman and B. K. Hodge and R. P. Taylor. *"A Re-Evaluation of Schlichting's Surface Roughness Experiment"*. *Journal of Fluids Engineering*. 106. 1984.

[76] O. Colin, C. Angelberger, and A. Benkenida. *"3D Modeling of Mixing, Ignition and Combustion Phenomena in Highly Stratified Gasoline Engines"*. *Oil & Gas Science and Technology*. Rev IFP. 58. 1. 47–62. 2003.

[77] A. Coppalle and P. Vervisch. *"The Total Emissivities of High-Temperature Flames"*. *Combustion and Flame*. 49. 101–108. 1983.

[78] S. M. Correa. *"A Review of NOx Formation Under Gas-Turbine Combustion Conditions"*. *Combustion Science and Technology*. 87. 329–362. 1992.

[79] C. Crowe, M. Sommerfield, and Yutaka Tsuji. *Multiphase Flows with Droplets and Particles*. CRC Press. 1998.

[80] G. T. Csanady. *"Turbulent Diffusion of Heavy Particles in the Atmosphere"*. *J. Atmos. Science*. 20. 201–208. 1963.

[81] P. A. Cundall and O. D. L. Strack. *"A Discrete Numerical Model for Granular Assemblies"*. *Geotechnique*. 29. 47–65. 1979.

[82] N. Curle. *"The Influence of Solid Boundaries upon Aerodynamic Sound"*. *Proceedings of the Royal Society of London*. Series A, Mathematical and Physical Sciences, 231. 505–514. 1955.

[83] J. Dacles-Mariani, G. G. Zilliac, J. S. Chow, and P. Bradshaw.. *"Numerical/Experimental Study of a Wingtip Vortex in the Near Field"*. *AIAA Journal*. 33(9). 1561–1568. 1995.

[84] D. Dajnak and F. C. Lockwood. *"Modelling of Toxic Heavy Metal Mercury Partitioning from Pulverized Fuel Combustion"*. *IFRF Combustion Journal*.

[85] J. M. Dalla Valle. *Micromeritics*. Pitman, London. 1948.

[86] B. J. Daly and F. H. Harlow. *"Transport Equations in Turbulence"*. *Phys. Fluids*. 13. 2634–2649. 1970.

[87] J. F. Daunenhofer and J. R. Baron. *"Grid Adaption for the 2D Euler Equations"*. *Technical Report AIAA-85-0484*. American Institute of Aeronautics and Astronautics. 1985.

[88] V. H. Del Valle and D. B. R. Kenning. *"Subcooled flow boiling at high heat flux"*. *International Journal of Heat and Mass Transfer*. 28(10). 1907–1920. 1985.

[89] M. K. Denison and B. W. Webb. *"A Spectral Line-Based Weighted-Sum-of-Gray-Gases Model for Arbitrary RTE Solvers"*. *J. Heat Transfer*. 115. 1002–1012. 1993.

[90] G. G. DeSoete. *"Overall Reaction Rates of NO and $N_2$ Formation from Fuel Nitrogen"*. *In 15th Symp. (Int'l.) on Combustion*. The Combustion Institute. 1093–1102. 1975.

*Release 15.0 - © SAS IP, Inc. All rights reserved. - Contains proprietary and confidential information of ANSYS, Inc. and its subsidiaries and affiliates.*

[91] J. Ding and D. Gidaspow. *"A Bubbling Fluidization Model Using Kinetic Theory of Granular Flow"*. *AIChE J*. 36(4). 523–538. 1990.

[92] G. Dixon-Lewis. *"Structure of Laminar Flames"*. *In 23rd Symp. (Int'l.) on Combustion*. The Combustion Institute. 305–324. 1990.

[93] N. Dombrowski and P. C. Hooper. *"The effect of ambient density or drop formation in sprays"*. *Chemical Engineering Science*. 17. 291–305. 1962.

[94] N. Dombrowski and W. R. Johns. *"The Aerodynamic Instability and Disintegration of Viscous Liquid Sheets"*. *Chemical Engineering Science*. 18. 203. 1963.

[95] C. Dopazo and E. E. O'Brien. *"Functional Formulation of Nonisothermal Turbulent Reactive Flows"*. *Phys. Fluids*. 17. 1968. 1975.

[96] A. M. Douaud and P. Eyzat. *"Four-Octane-Number Method for Predicting the Anti-Knock Behavior of Fuels in Engines"*. *SAE Technical Paper*. v87 780080. SAE. 1978.

[97] M. C. Drake and R. J. Blint. *"Relative Importance of Nitrogen Oxide Formation Mechanisms in Laminar Opposed-Flow Diffusion Flames"*. *Combustion and Flame*. 83. 185–203. 1991.

[98] M. C. Drake, S. M. Correa, R. W. Pitz, W. Shyy, and C. P. Fenimore. *"Superequilibrium and Thermal Nitric Oxide Formation in Turbulent Diffusion Flames"*. *Combustion and Flame*. 69. 347–365. 1987.

[99] M. C. Drake, R. W. Pitz, M. Lapp, C. P. Fenimore, R. P. Lucht, D. W. Sweeney, and N. M. Laurendeau. *In 20th Symp. (Int'l.) on Combustion*. The Combustion Institute. 327. 1984.

[100] D. A. Drew and R. T. Lahey. *In Particulate Two-Phase Flow*. Butterworth-Heinemann. Boston, MA509–566. 1993.

[101] J. K. Dukowwicz and A. S. Dvinsky. *"Approximate Factorization as a High-Order Splitting for the Implicit Incompressible Flow Equations"*. *Journal of Computational Physics*. 102. 336–347. 1992.

[102] P. A. Durbin. *"Separated Flow Computations with the* $k$*-* $\varepsilon$*-* $v^2$ *Model"*. *AIAA Journal*. 33(4). 659–664. 1995.

[103] E. R. G. Eckert and R. M. Drake. *Analysis of Heat and Mass Transfer*. McGraw-Hill Co.. 1972.

[104] D. K. Edwards and R. Matavosian. *"Scaling Rules for Total Absorptivity and Emissivity of Gases"*. *J. Heat Transfer*. 106. 684–689. 1984.

[105] J. K. Edwards, B. S. McLaury, and S. A. Shirazi. *"Supplementing a CFD Code with Erosion Prediction Capabilities"*. *In Proceedings of ASME FEDSM'98: ASME 1998 Fluids Engineering Division Summer Meeting, Washington DC*. June 1998.

[106] J. K. Edwards, B. S. McLaury, and S. A.Shirazi. *"Evaluation of Alternative Pipe Bend Fittings in Erosive Service"*. *In Proceedings of ASME FEDSM'00: ASME 2000 Fluids Engineering Division Summer Meeting, Boston, MA*. June 2000.

[107] Y. Egorov. *"Contact Condensation in Stratified Steam-Water Flow"*. *EVOL-ECORDA-D 07*. 2004.

[108] S. E. Elgobashi and T. W. Abou-Arab. *"A Two-Equation Turbulence Model for Two-Phase Flows"*. *Phys. Fluids*. 26(4). 931–938. 1983.

[109] S. Ergun. *"Fluid Flow through Packed Columns"*. *Chem. Eng. Prog*. 48(2). 89–94. 1952.


*Release 15.0 - © SAS IP, Inc. All rights reserved. - Contains proprietary and confidential information of ANSYS, Inc. and its subsidiaries and affiliates.*

[110] G. Erlebacher, M. Y. Hussaini, C. G. Speziale, and T. A. Zang.. *"Toward the Large-Eddy Simulation of Compressible Turbulent Flows"*. *J. Fluid Mech*. 238. 155–185. 1992.

[111] J. Ewald. *"A Level Set Based Flamelet Model for the Prediction of Combustion in Homogeneous Charge and Direct Injection Spark Ignition Engines"*. *PhD Thesis*. Aachen University. 2006.

[112] R. F. Fedors and R. F. Landell. *"An Empirical Method of Estimating the Void Fraction in Mixtures of Uniform Particles of Different Size"*. *Powder Technology*. 23. 225–231.

[113] C. P. Fenimore. *"Formation of Nitric Oxide in Premixed Hydrocarbon Flames"*. *In 13th Symp.(Int'l.)on Combustion*. The Combustion Institute. 373. 1971.

[114] C. P. Fenimore. *"Destruction of NO by $NH_3$ in Lean Burnt Gas"*. *Combustion and Flame*. 37. 245. 1980.

[115] C. P. Fenimore and G. W. Jones. *"Oxidation of soot by hydroxyl radicals"*. *J. Phys. Chem*. 71. 593–597. 1967.

[116] John D. Fenton. *"The Cnoidal Theory of Water Waves"*. *Developments in Offshore Engineering*. J.B. Herbich, Houston. 1998.

[117] J. L. Ferzieger and M. Peric. *Computational Methods for Fluid Dynamics*. Springer-Verlag, Heidelberg. 1996.

[118] J. E. Ffowcs-Williams and D. L. Hawkings. *"Sound Generation by Turbulence and Surfaces in Arbitrary Motion"*. *Proc. Roy. Soc. London*. A264. 321–342. 1969.

[119] M. A. Field. *"Rate of Combustion of Size-Graded Fractions of Char from a Low Rank Coal between 1200 K–2000 K"*. *Combustion and Flame*. 13. 237–252. 1969.

[120] I. Finnie. *"Erosion of Surfaces by Solid Particles"*. *Wear*. 3. 87–103. 1960.

[121] W. A. Fiveland and A. S. Jamaluddin. *"Three-Dimensional Spectral Radiative Heat Transfer Solutions by the Discrete Ordinates Method"*. *Heat Transfer Phenomena in Radiation, Combustion and Fires*. HTD Vol. 10643–48. 1989.

[122] T. H. Fletcher and D. R. Hardesty. *"Compilation of Sandia coal devolatilization data: Milestone report"*. *Sandia Report SAND92-8209*. 1992.

[123] T. H. Fletcher and A. R. Kerstein. *"Chemical percolation model for devolatilization: 3. Direct use of $^{13}C$ NMR data to predict effects of coal type"*. *Energy and Fuels*. 6. 414. 1992.

[124] T. H. Fletcher, A. R. Kerstein, R. J. Pugmire, and D. M. Grant.. *"Chemical percolation model for devolatilization: 2. Temperature and heating rate effects on product yields"*. *Energy and Fuels*. 4. 54. 1990.

[125] W. L. Flower, R. K. Hanson, and C. H. Kruger. *In 15th Symp. (Int'l.) on Combustion*. The Combustion Institute. 823. 1975.

[126] R. O. Fox. *Computational Models for Turbulent Reacting Flows*. Cambridge University Press, Cambridge, England. 2003.

[127] J. A. Foucart, *Private Communication*.

[128] Th. Frank, J. M. Shi, and A. D. Burns. *"Validation of Eulerian Multiphase Flow Models for Nuclear Safety Applications"*. *Third International Symposium on Two-Phase Flow Modeling and Experimentation, Pisa, Italy*. Sept. 22–24, 2004.

*Release 15.0 - © SAS IP, Inc. All rights reserved. - Contains proprietary and confidential information of ANSYS, Inc. and its subsidiaries and affiliates.*

[129] Th. Frank, P. J. Zwart, E. Krepper, H.-M. Prasser, and D. Lucas. *"Validation of CFD models for mono- and polydisperse air-water two-phase flows in pipes"*. *J. Nuclear Engineering & Design*. 238. 647–659. March 2008.

[130] M. A. Friedrich, H. Lan, J. L. Wegner, J. A. Drallmeier, and B. F. Armaly . *"A Separation Criterion with Experimental Validation for Shear-Driven Films in Separated Flows"*. *Journal of Fluids Engineering*. 130,. May 2008.

[131] S. Fu, B. E. Launder, and M. A. Leschziner. *"Modeling Strongly Swirling Recirculating Jet Flow with Reynolds-Stress Transport Closures"*. *In Sixth Symposium on Turbulent Shear Flows*. Toulouse, France. 1987.

[132] J. Garside and M. R. Al-Dibouni. *"Velocity-Voidage Relationships for Fluidization and Sedimentation"*. *I & EC Process Des. Dev*. 16. 206–214. 1977.

[133] J. A. Gasper, N. C. Widmer, J. A. Cole, and W. R. Seeker. *"Study of Mercury Speciation in a Simulated Municipal Waste Incinerator Flue"*. *In Proceedings of 1997 International Conference on Incineration and Thermal Treatment Technologies*. Oakland, California. 1997.

[134] M. Germano, U. Piomelli, P. Moin, and W. H. Cabot. *"Dynamic Subgrid-Scale Eddy Viscosity Model"*. *In Summer Workshop*. Center for Turbulence Research, Stanford, CA. 1996.

[135] T. Gessner. *"Dynamic Mesh Adaption for Supersonic Combustion Waves Modeled with Detailed Reaction Mechanisms"*. *PhD thesis*. University of Freiburg, Freiburg, Germany. 2001.

[136] L. G. Gibilaro, R. Di Felice and S. P. Waldram. *"Generalized Friction Factor and Drag Coefficient Correlations for Fluid-particle Interactions"*. *Chem. Eng. Sci*. 40(10). 1817-1823. 1985.

[137] M. M. Gibson and B. E. Launder. *"Ground Effects on Pressure Fluctuations in the Atmospheric Boundary Layer"*. *J. Fluid Mech*. 86. 491–511. 1978.

[138] D. Gidaspow. *Multiphase Flow and Fluidization*. Academic Press, Boston, MA. 1994.

[139] D. Gidaspow, R. Bezburuah, and J. Ding. *"Hydrodynamics of Circulating Fluidized Beds, Kinetic Theory Approach"*. *In Fluidization VII, Proceedings of the 7th Engineering Foundation Conference on Fluidization*. 75–82. 1992.

[140] R. G. Gilbert, K. Luther, and J. Troe. *Ber. Bunsenges. Phys. Chem*. 87. 1983.

[141] P. Glarborg, J. E. Johnsson, and K. Dam-Johansen. *"Kinetics of Homogeneous Nitrous Oxide Decomposition"*. *Combustion and Flame*. ,99. 523–532. 1994.

[142] M. E. Goldstein and B. Rosenbaum. *"Effect of Anisotropic Turbulence on Aerodynamic Noise*. *Journal of the Acoustical Society of America*. 54. 630–645. 1973.

[143] A. D. Gosman and E. Ioannides. *"Aspects of computer simulation of liquid-fuelled combustors"*. *J. Energy*. 7(6). 482–490. 1983.

[144] J. Gottgens, F. Mauss, and N. Peters. *"Analytic Approximations of Burning Velocities and Flame Thicknesses of Lean Hydrogen, Methane, Ethylene, Ethane, Acetylene and Propane Flames"*. *In Twenty-Fourth Symposium (Int.) on Combustion, Pittsburgh*. 29–135. 1992.

[145] I. R. Gran and B. F. Magnussen. *"A numerical study of a bluff-body stabilized diffusion flame. part 2. influence of combustion modeling and finite-rate chemistry"*. *Combustion Science and Technology*. 119. 191. 1996.

*Release 15.0 - © SAS IP, Inc. All rights reserved. - Contains proprietary and confidential information of ANSYS, Inc. and its subsidiaries and affiliates.*

[146] D. M. Grant, R. J. Pugmire, T. H. Fletcher, and A. R. Kerstein.. *"Chemical percolation model of coal devolatilization using percolation lattice statistics"*. *Energy and Fuels*. 3. 175. 1989.

[147] D. J. Gunn. *"Transfer of Heat or Mass to Particles in Fixed and Fluidized Beds"*. *Int. J. Heat Mass Transfer*. 21. 467–476. 1978.

[148] F. Menter and Y. Egorov. *The Scale-Adaptive Simulation Method for Unsteady Turbulent Flow Predictions. Part 1: Theory and Model Description*. *Journal Flow Turbulence and Combustion*. 85. 113–138. 2010.

[149] W. W. Hagerty and J. F. Shea. *"A Study of the Stability of Plane Fluid Sheets"*. *Journal of Applied Mechanics*. 22. 509. 1955.

[150] A. Haider and O. Levenspiel. *"Drag Coefficient and Terminal Velocity of Spherical and Nonspherical Particles"*. *Powder Technology*. 58. 63–70. 1989.

[151] B. Hall. *"An Experimental Study of Mercury Reactions in Combustion Flue Gases"*. *PhD thesis*. Chalmers University of Technology, Sweden. 1991.

[152] R. J. Hall, M. D. Smooke, and M. B. Colket. *Physical and Chemical Aspects of Combustion*. Gordon and Breach. 1997.

[153] M. P. Halstead, L. J. Kirsch, and C. P. Quinn. *"Autoignition of Hydrocarbon Fuels at High Temperatures and Pressures – Fitting of a Mathematical Model"*. *Combustion and Flame*. 30. 45–60. 1977.

[154] Z. Han, S. Perrish, P. V. Farrell, and R. D. Reitz. *"Modeling Atomization Processes of Pressure-Swirl Hollow-Cone Fuel Sprays"*. *Atomization and Sprays*. 7(6). 663–684. Nov.-Dec. 1997.

[155] G. Hand, M. Missaghi, M. Pourkashanian, and A. Williams. *"Experimental Studies and Computer Modeling of Nitrogen Oxides in a Cylindrical Furnace"*. *In Proceedings of the Ninth Members Conference*. volume 2. IFRF Doc No K21/g/301989.

[156] R. K. Hanson and S. Salimian. *"Survey of Rate Constants in H/N/O Systems"*. In W. C. Gardiner, editor*Combustion Chemistry*. 361. 1984.

[157] H. O. Hardenburg and F. W. Hase. *"An Empirical Formula for Computing the Pressure Rise Delay of a Fuel from its Cetane Number and from the Relevant Parameters of Direct Injection Diesel Engines"*. *SAE Technical Paper 790493*. SAE. 1979.

[158] K. Haugen, O. Kvernvold, A. Ronald, and R. Sandberg. *"Sand Erosion of Wear-resistant Materials: Erosion in Choke Valves.Wear"*. 186-187. 179–188. 1995.

[159] R. A. W. M. Henkes, F. F. van der Flugt, and C. J. Hoogendoorn. *"Natural Convection Flow in a Square Cavity Calculated with Low-Reynolds-Number Turbulence Models"*. *Int. J. Heat Mass Transfer*. 34. 1543–1557. 1991.

[160] H. Hertz. *"On the Evaporation of Liquids, Especially Mercury, in Vacuo"*. *Annalen der Physik (Leipzig)*. 17. 177. 1882.

[161] J. B.Heywood. *Internal Combustion Engine Fundamentals*. McGraw-Hill, New York, rev. edition. 1988.

[162] R. Herweg and R.R. Maly. *A Fundamental Model for Flame Kernel Formation in S.I. Engines*. SAE 922243. 1947-1976. 1992.

*Release 15.0 - © SAS IP, Inc. All rights reserved. - Contains proprietary and confidential information of ANSYS, Inc. and its subsidiaries and affiliates.*

[163] T. Hibiki and M. Ishii. *"One-group Interfacial Area Transport of Bubbly Flows in Vertical Round Tubes"*. *International Journal of Heat and Mass Transfer*. 43. 2711–2726. 2000.

[164] J. O. Hinze. *Turbulence*. McGraw-Hill Publishing Co., New York. 1975.

[165] C. W. Hirt and B. D. Nichols. *"Volume of Fluid (VOF) Method for the Dynamics of Free Boundaries"*. *J. Comput. Phys*. 39. 201–225. 1981.

[166] D. G. Holmes and S. D. Connell. *"Solution of the 2D Navier-Stokes Equations on Unstructured Adaptive Grids"*. *Presented at the AIAA 9th Computational Fluid Dynamics Conference*. June 1989.

[167] T. J. Houser, M. Hull, R. Alway, and T. Biftu. *Int. Journal of Chem. Kinet*. 12. 579. 1980.

[168] S. Hosokawa, A. Tomiyama, S. Misaki, and T. Hamada. *"Lateral Migration of Single Bubbles Due to the Presence of Wall"*. *ASME 2002 Joint U.S.-European Fluids Engineering Division Conference, Montreal, QC, Canada*. July 14–18, 2002.

[169] P. Huang, P. Bradshaw, and T. Coakley. *"Skin Friction and Velocity Profile Family for Compressible Turbulent Boundary Layers"*. *AIAA Journal*. 31(9). 1600–1604. September 1993.

[170] G. A. Hughmark. *"Mass and heat transfer from rigid spheres"*. *AICHE Journal*. 13. 1219–1221. November 1967.

[171] L. Huilin and D. Gidaspow. *"Hydrodynamics of binary fluidization in a riser: CFD simulation using two granular temperatures"*. *Chemical Engineering Science*. 58. 3777–3792. 2003.

[172] S. C. Hunter. *"Formation of so3 in gas turbines"*. *Transactions of the ASME*. 104. 44–51. 1982.

[173] B. R. Hutchinson and G. D. Raithby. *"A Multigrid Method Based on the Additive Correction Strategy"*. *Numerical Heat Transfer*. 9. 511–537. 1986.

[174] H. Ibdir and H. Arastoopour. *"Modeling of multi-type particle flow using kinetic approach"*. *AICHE Journal*. May 2005.

[175] A. Ioilev, M. Samigulin and V. Ustinenko. *"Advances in the Modeling of Cladding Heat Transfer and Critical Heat Flux in Boiling Water Reactor Fuel Assemblies"*. *The 12th International Topical Meeting on Nuclear Reactor Thermal Hydraulics (NURETH-12)*. Pittsburgh, Pennsylvania. 2007.

[176] K. Ishazaki, T. Ikohagi, and H. Daiguji. *"A High-Resolution Numerical Method for Transonic Non-equilibrium Condensation Flows Through a Steam Turbine Cascade"*. *In Proceedings of the 6th International Symposium on Computational Fluid Dynamics*. 1. 479–484. 1995.

[177] M. Ishii. *"Two-fluid model for two-phase flow"*. *2nd International Workshop on Two-phase Flow Fundamentals*. RPI, Troy, NY. 1979.

[178] M. Ishii and S. Kim. *"Micro Four-Sensor Probe Measurement of Interfacial Area Transport for Bubbly Flow in Round Pipes"*. *Nuclear Engineering and Design*. 205. 123–131. 2001.

[179] R. I. Issa. *"Solution of the Implicitly Discretized Fluid Flow Equations by Operator-Splitting"*. *Journal of Computational Physics*. 62. 40–65. 1985.

[180] R. I. Issa. *"Solution of Implicitly Discretized Fluid Flow Equations by Operator Splitting"*. *Journal of Computational Physics*. 62. 40–65. 1986.

*Release 15.0 - © SAS IP, Inc. All rights reserved. - Contains proprietary and confidential information of ANSYS, Inc. and its subsidiaries and affiliates.*

[181] H. M. Glaz J. B. Bell, P. Colella. *"Second-Order Projection Method for the Incompressible Navier-Stokes Equations"*. *Journal of Computational Physics*. 85. 257. 1989.

[182] H. M. Glaz J. B. Bell, P. Colella. *"An Analysis of the Fractional-Step Method"*. *Journal of Computational Physics*. 108. 51–58. 1993.

[183] S. Jain. *"Three-Dimensional Simulation of Turbulent Particle Dispersion"*. *PhD thesis*. University of Utah, Utah. 1995.

[184] A. Jameson. *"Solution of the Euler Equations for Two Dimensional Transonic Flow by a Multigrid Method"*. *MAE Report 1613*. Princeton University. June 1983.

[185] A. Jameson, W. Schmidt, and E. Turkel. *"Numerical Solution of the Euler Equations by Finite Volume Methods Using Runge-Kutta Time-Stepping Schemes"*. *Technical Report AIAA-81-1259*. AIAA 14th Fluid and Plasma Dynamics Conference, Palo Alto, California. June 1981.

[186] J. Janicka, W. Kolbe, and W. Kollmann. *"Closure of the transport equation for the pdf of turbulent scalar fields"*. *Journal Non-Equilibrium Thermodynamics*. 4. 47. 1978.

[187] J. Janicka and W. Kollmann. *"A Two-Variable Formulation for the Treatment of Chemical Reactions in Turbulent* $H_2$*-Air Diffusion Flames"*. *In 17th Symp. (Int'l.) on Combustion*. The Combustion Institute. 1978.

[188] J. Janicka and W. Kollmann. *"A Numerical Study of Oscillating Flow Around a Circular Cylinder"*. *Combustion and Flame*. 44. 319–336. 1982.

[189] C. Jayatillaka. *"The Influence of Prandtl Number and Surface Roughness on the Resistance of the Laminar Sublayer to Momentum and Heat Transfer"*. *Prog. Heat Mass Transfer*. 1. 193–321. 1969.

[190] P. C. Johnson and R. Jackson. *"Frictional-Collisional Constitutive Relations for Granular Materials, with Application to Plane Shearing"*. *J. Fluid Mech*. 176. 67–93. 1987.

[191] W. P. Jones and J. H. Whitelaw. *"Calculation Methods for Reacting Turbulent Flows: A Review"*. *Combustion and Flame*. 48. 1–26. 1982.

[192] T. Jongen. *"Simulation and Modeling of Turbulent Incompressible Flows"*. *PhD thesis*. EPF Lausanne, Lausanne, Switzerland. 1992.

[193] T. Just and S. Kelm. *"Die Industry*. 38. 76. 1986.

[194] B. Kader. *"Temperature and Concentration Profiles in Fully Turbulent Boundary Layers"*. *Int. J. Heat Mass Transfer*. 24(9). 1541–1544. 1981.

[195] N. Kandamby, G. Lazopoulos, F. C. Lockwood, A. Perera, and L. Vigevano. *"Mathematical Modeling of NOx Emission Reduction by the Use of Reburn Technology in Utility Boilers"*. *In ASME Int. Joint Power Generation Conference and Exhibition, Houston, Texas*. 1996.

[196] K. C. Karki and S. V. Patankar. *"Pressure-Based Calculation Procedure for Viscous Flows at All Speeds in Arbitrary Configurations"*. *AIAA Journal*. 27. 1167–1174. 1989.

[197] I. Kataoka, M. Ishii, and K. Mishima. *"Generation and size distribution of droplet in annular two-phase flow"*. *J. of Fluids Engineering*. 105. 230–238. 1983.

[198] Kato, M., Launder B.E.. *"The modelling of turbulent flow around stationary and vibrating square cylinders"*. *Ninth Symposium on "Turbulent Shear Flows"*. Kyoto, Japan. August 16-18, 1993.

*Release 15.0 - © SAS IP, Inc. All rights reserved. - Contains proprietary and confidential information of ANSYS, Inc. and its subsidiaries and affiliates.*

[199] A. Kaufmann, M. Moreau, O. Simonin, J. Helie. *"Comparison between Lagrangian and mesoscopic Eulerian modelling approaches for inertial particles suspended in decaying isotropic turbulence"*. *Journal of Computational Physics*. 277. 13. 6448–6472. Academic Press Professional, Inc., San Diego, CA, USA. June, 2008.

[200] W. M. Kays. *"Loss coefficients for abrupt changes in flow cross section with low reynolds number flow in single and multiple tube systems"*. *Transactions of the ASME*. 72. 1067–1074. January 1950.

[201] W. M. Kays. *"Turbulent Prandtl Number - Where Are We?"*. *J. Heat Transfer*. 116. 284–295. 1994.

[202] W. M. Kays and A. L. London. *Compact Heat Exchangers*. McGraw-Hill, New York. 1964.

[203] R. J. Kee, F. M. Rupley, J. A. Miller, M. E. Coltrin, J. F. Grcar, E. Meeks, H. K. Moffat, A. E. Lutz, G. Dixon-Lewis, M. D. Smooke, J. Warnatz, G. H. Evans, R. S. Larson, R. E. Mitchell, L. R. Petzold, W. C. Reynolds, M. Caracotsios, W. E. Stewart, P. Glarborg, C. Wang, O. Adigun, W. G. Houf, C. P. Chou, S. F. Miller, P. Ho, and D. J. Young. CHEMKIN v. 4.0*Technical Report*. Reaction Design, Inc., San Diego, CA. 2004.

[204] I. M. Khan and G. Greeves. *"A Method for Calculating the Formation and Combustion of Soot in Diesel Engines"*. In N. H.Afgan and J. M.Beer, editors*Heat Transfer in Flames*. Chapter 25Scripta, Washington DC. 1974.

[205] J. S. Kim and F. A. Williams. *"Extinction of Diffusion Flames with Non-Unity Lewis Number"*. *Eng. Math*. 31. 101–118. 1997.

[206] S. Kim, D. Caraeni, and B. Makarov. *"A Multidimensional Linear Reconstruction Scheme for Arbitrary Unstructured Grids"*. *Technical report*. AIAA 16th Computational Fluid Dynamics Conference, Orlando,FloridaAmerican Institute of Aeronautics and Astronautics. June 2003.

[207] S. Kim, Q. Wu, and M. Ishii. *"One-group Interfacial Area Transport in Vertical Bubbly Flow"*. *International Journal of Heat and Mass Transfer*. 41. 1103–1112. 1997.

[208] S.-E. Kim. *"Large eddy simulation using unstructured meshes and dynamic subgrid-scale turbulence models"*. *Technical Report AIAA-2004-2548*. 34th Fluid Dynamics Conference and ExhibitAmerican Institute of Aeronautics and Astronautics,. June 2004.

[209] S.-E. Kim and D. Choudhury. *"A Near-Wall Treatment Using Wall Functions Sensitized to Pressure Gradient"*. In ASME FED Vol. 217, *Separated and Complex Flows*. ASME. 1995.

[210] S.-E. Kim, D. Choudhury, and B. Patel. *"Computations of Complex Turbulent Flows Using the Commercial Code ANSYS Fluent"*. *In Proceedings of the ICASE/LaRC/AFOSR Symposium on Modeling Complex Turbulent Flows*. Hampton, Virginia1997.

[211] W.-W. Kim and S. Menon. *"Application of the localized dynamic subgrid-scale model to turbulent wall-bounded flows"*. *Technical Report AIAA-97-0210*. 35th Aerospace Sciences Meeting, Reno, NVAmerican Institute of Aeronautics and Astronautics. January 1997.

[212] M. Knudsen. *"Maximum Rate of Vaporization of Mercury"*. *Annalen der Physik (Leipzig)*. 47. 697. 1915.

[213] H. Kobayashi, J. B. Howard, and A. F. Sarofim. *"Coal Devolatilization at High Temperatures"*. *In 16th Symp. (Int'l.) on Combustion*. The Combustion Institute. 1976.

[214] G. Kocamustafaogullari and M. Ishii. *"Interfacial area and nucleation site density in boiling systems"*. *International Journal of Heat and Mass Transfer*. 26. 9. 1377–1387. 1983.

*Release 15.0 - © SAS IP, Inc. All rights reserved. - Contains proprietary and confidential information of ANSYS, Inc. and its subsidiaries and affiliates.*

[215] G. Kocamustafaogullari and M. Ishii. *"Foundation of the Interfacial Area Transport Equation and its Closure Relations"*. *International Journal of Heat and Mass Transfer*. 38. 481–493. 1995.

[216] N. I. Kolev. *Multiphase Flow Dynamics 2: Thermal and Mechanical Interactions*. Springer, Berlin, Germany, 2nd edition. 2005.

[217] S. C. Kong, Z. W. Han, and R. D. Reitz. *"The Development and Application of a Diesel Ignition and Combustion Model for Multidimensional Engine Simulations"*. *SAE Paper 950278*. SAE. 1995.

[218] R. Kraichnan. *"Diffusion by a Random Velocity Field"*. *Physics of Fluids*. 11. 21–31. 1970.

[219] J. C. Kramlich. *"The Fate and Behavior of Fuel-Sulfur in Combustion Systems"*. *PhD thesis*. Washington State University, Washington, USA. 1980.

[220] K. K. Y. Kuo. *Principles of Combustion*. John Wiley and Sons, New York. 1986.

[221] N. Kurul and M. Z. Podowski. *"On the modeling of multidimensional effects in boiling channels"*. *In Proceedings of the 27th National Heat Transfer Conference, Minneapolis, Minnesota, USA*. 1991.

[222] H. Lamb. *Hydrodynamics, Sixth Edition*. Dover Publications, New York. 1945.

[223] G. L. Lane, M. P. Schwarz, and G. M. Evans. *Modelling of the Interaction between Gas and Liquid in Stirred Vessels*. *10th European Conference on Mixing*. 197–204. 2000.

[224] R. B. Langtry, F. R. Menter, S. R. Likki, Y. B. Suzen, P. G. Huang, and S. Volker. *"A Correlation-Based Transition Model Using Local Variables: Part II — Test Cases and Industrial Applications"*. (ASME-GT2004-53454) 2004.

[225] R. B. Langtry and F. R. Menter. *"Correlation-Based Transition Modeling for Unstructured Parallelized Computational Fluid Dynamics Codes"*. *AIAA Journal*. 47(12). 2894–2906. December 2009.

[226] M. E. Larsen and J. R. Howell. *"Least Squares Smoothing of Direct Exchange Areas in Zonal Analysis"*. *J. Heat Transfer*. 108. 239–242. 1986.

[227] B. E. Launder. *"Second-Moment Closure and Its Use in Modeling Turbulent Industrial Flows"*. *International Journal for Numerical Methods in Fluids*. 9. 963–985. 1989.

[228] B. E. Launder. *"Second-Moment Closure: Present... and Future?"*. *Inter. J. Heat Fluid Flow*. 10(4). 282–300. 1989.

[229] B. E. Launder, G. J. Reece, and W. Rodi. *"Progress in the Development of a Reynolds-Stress Turbulence Closure"*. *J. Fluid Mech*. 68(3). 537–566. April 1975.

[230] B. E. Launder and N. Shima. *"Second-Moment Closure for the Near-Wall Sublayer: Development and Application"*. *AIAA Journal*. 27(10). 1319–1325. 1989.

[231] B. E. Launder and D. B. Spalding. *Lectures in Mathematical Models of Turbulence*. Academic Press, London, England. 1972.

[232] B. E. Launder and D. B.Spalding. *"The Numerical Computation of Turbulent Flows"*. *Computer Methods in Applied Mechanics and Engineering*. 3. 269–289. 1974.

[233] N. M. Laurendeau. *"Heterogeneous Kinetics of Coal Char Gasification and Combustion"*. *Prog. Energy Comb. Sci*. 4. 221–270. 1978.

*Release 15.0 - © SAS IP, Inc. All rights reserved. - Contains proprietary and confidential information of ANSYS, Inc. and its subsidiaries and affiliates.*

[234] J. Lavieville, E. Quemerais, S. Mimouni, M. Boucker and N. Mechitoua. *"NEPTUNE CFD V1.0 Theory Manual"*. *EDF*. 2005.

[235] J. L. Lebowitz. *"Exact Solution of Generalized Percus-Yevick Equation for a Mixture of Hard Spheres"*. *The Phy. Rev*. 133(4A). A895–A899. 1964.

[236] K. B. Lee, M. W. Thring, and J. M. Beer. *Combustion and Flame*. 6. 137–145. 1962.

[237] W. H. Lee. *"A Pressure Iteration Scheme for Two-Phase Modeling"*. *Technical Report LA-UR 79-975*. Los Alamos Scientific Laboratory, Los Alamos, New Mexico. 1979.

[238] A. H. Lefebvre. *Atomization and Sprays*. Hemisphere Publishing Corporation. 1989.

[239] D. Legendre and J. Magnaudet. *"The Lift Force on a Spherical Bubble in a Viscous Linear Shear Flow"*. *J. Fluid Mech*. 368. 81–126. 1998.

[240] M. Lemmert and L. M. Chawla. *Influence of flow velocity on surface boiling heat transfer coefficient in Heat Transfer in Boiling*. E. Hahne and U. Grigull, Eds., Academic Press and Hemisphere, New York, NY, USA. 1977.

[241] B. P. Leonard. *"The ULTIMATE conservative difference scheme applied to unsteady one-dimensional advection"*. *Comp. Methods Appl. Mech. Eng*. 88. 17–74. 1991.

[242] B. P. Leonard and S. Mokhtari. *"ULTRA-SHARP Nonoscillatory Convection Schemes for High-Speed Steady Multidimensional Flow"*. *NASATM1-2568 (ICOMP-90-12)*. NASA Lewis Research Center. 1990.

[243] K. M. Leung and R. P. Lindsted. *"Detailed Kinetic Modeling of C1-C3 Alkane Diffusion Flames"*. *Combustion and Flame*. 102. 129–160. 1995.

[244] V. G. Levich. *Physicochemical Hydrodynamics*. Prentice Hall. 1962.

[245] J. M. Levy, L. K. Chen, A. F. Sarofim, and J. M. Beer. *"NO/Char Reactions at Pulverized Coal Flame Conditions"*. *In 18th Symp. (Int'l.) on Combustion*. The Combustion Institute. 1981.

[246] A. Li and G. Ahmadi. *"Dispersion and Deposition of Spherical Particles from Point Sources in a Turbulent Channel Flow"*. *Aerosol Science and Technology*. 16. 209–226. 1992.

[247] D. Li , S. Venkateswaran, K. Fakhari and C. Merkle. *"Convergence Assessment of General Fluid Equations on Unstructured Hybrid Grids"*. *Technical Report AIAA-2001-2557*. AIAA 15th Computational Fluid Dynamics Conference, Anaheim, CaliforniaAmerican Institute of Aeronautics and Astronautics. June 2001.

[248] X. Li and R. S. Tankin. *"On the Temporal Instability of a Two-Dimensional Viscous Liquid Sheet"*. *Journal of Fluid Mechanics*. 226. 425. 1991.

[249] A. K. Lichtarowicz, R. K. Duggins, and E. Markland. *"Discharge Coefficients for Incompressible Non-Cavitating Flow Through Long Orifices"*. *Journal of Mechanical Engineering Science*. 7. 2. 1965.

[250] F. S. Lien and M. A. Leschziner. *"Assessment of Turbulent Transport Models Including Non-Linear RNG Eddy-Viscosity Formulation and Second-Moment Closure"*. *Computers and Fluids*. 23(8). 983–1004. 1994.

[251] M. J. Lighthill. *"On Sound Generated Aerodynamically"*. *Proc. Roy. Soc. London*. A211564–587. 1952.

*Release 15.0 - © SAS IP, Inc. All rights reserved. - Contains proprietary and confidential information of ANSYS, Inc. and its subsidiaries and affiliates.*

[252] G. M. Lilley. *"The radiated noise from isotropic turbulence revisited"*. *NASA Contract Report 93-75*. NASA Langley Research Center, Hampton, VA. 1993.

[253] D. K. Lilly. *"A Proposed Modification of the Germano Subgrid-Scale Closure Model"*. *Physics of Fluids*. 4. 633–635. 1992.

[254] P. Lin. *Numerical Modeling of Water Waves*. Taylor & Francis. 2008.

[255] F. Lindemann. *Trans. Faraday Soc*. 7. 1922.

[256] R. P. Lindstedt. *In Proc. IUTAM Conf. on Aerothermo-Chemistry in Combustion*. Taipei, Taiwan1991.

[257] R. P. Lindstedt. *"Soot Formation in Combustion*. Springer-Verlag, Berlin. 1994.

[258] M. S. Liou. *"A sequel to AUSM: AUSM+"*. *Journal of Computational Physics*. 129. 364–382. 1996.

[259] M. S. Liou and C. J. Steffen, Jr.. *"A new flux splitting scheme"*. *Journal of Computational Physics*. 107(1). 23–39. 1993.

[260] A. N. Lipatnikov and J. Chomiak. *"Turbulent Flame Speed and Thickness: Phenomenology, Evaluation and Application in Multi-dimensional Simulations"*. *Progress in Energy& Combustion Science*. 28. 1–74. January 2002.

[261] R. J. Litchford and S. M. Jeng. *"Efficient Statistical Transport Model for Turbulent Particle Dispersion in Sprays"*. *AIAA Journal*. 29. 1443. 1991.

[262] A. B. Liu, D. Mather, and R. D. Reitz. *"Modeling the Effects of Drop Drag and Breakup on Fuel Sprays"*. *SAE Technical Paper 930072*. SAE. 1993.

[263] H. Liu and B. M. Gibbs. *"Modeling of NO and* $N_2O$ *Emissions from Biomass-Fired Circulating Fluidized Bed Combustors"*. *Fuel*. 81. 271–280. 2002.

[264] F. C. Lockwood and C. A Romo-Millanes. *"Mathematical Modelling of Fuel - NO Emissions From PF Burners"*. *J. Int. Energy*. 65. 144–152. September 1992.

[265] G. Lodier, L. Vervisch, V. Moureau and P. Domingo. *"Composition-Space Premixed Flamelet Solution with Differential Diffusion for In Situ Flamelet-Generated Manifolds"*. *Combustion and Flame*. 158. 10. 2009-2016. 2011.

[266] M. Lopez de Bertodano. *"Turbulent Bubbly Flow in a Triangular Duct"*. *Ph.D. Thesis*. Rensselaer Polytechnic Institute, Troy, New York. 1991.

[267] M. A. Lopez de Bertodano, C. S. Jan, S.G. Beus. *"Annular Flow Entrainment Rate Experiment in a Small Vertical Pipe"*. *Nuclear Engineering and Design*. 178. 61-70. 1997.

[268] T. F. Lu and C.K. Law. *"A Directed Relation Graph Method for Mechanism Reduction"*. Proc. Combust. Inst. 30(1). 1333-1341. 2005.

[269] T. F. Lu and C.K. Law. *"On the Applicability of Directed Relation Graph to the Reduction of Reaction Mechanisms"*. *Combust. Flame*. 146(3). 472-483. 2006.

[270] T. F. Lu and C.K. Law. *"Toward Accommodating Realistic Fuel Chemistry in Large-Scale Computation"*. *Prog. Energy Combust. Sci*. 35(1). 192-215. 2009.

*Release 15.0 - © SAS IP, Inc. All rights reserved. - Contains proprietary and confidential information of ANSYS, Inc. and its subsidiaries and affiliates.*

[271] C. K. K. Lun, S. B. Savage, D. J. Jeffrey, and N. Chepurniy. *"Kinetic Theories for Granular Flow: Inelastic Particles in Couette Flow and Slightly Inelastic Particles in a General Flow Field"*. *J. Fluid Mech*. 140. 223–256. 1984.

[272] J. Y. Luo, R. I. Issa, and A. D. Gosman. *"Prediction of Impeller-Induced Flows in Mixing Vessels Using Multiple Frames of Reference"*. *In IChemE Symposium Series*. 136. 549–556. 1994.

[273] A. E. Lutz, R. J. Kee, J. F. Grcar, and F. M. Rupley. *"OPPDIF: A FORTRAN Program for Computing Opposed-Flow Diffusion Flames"*. *Sandia National Laboratories Report SAND96-8243*. 1997.

[274] J. F. Lynn. *"Multigrid Solution of the Euler Equations with Local Preconditioning"*. *PhD thesis*. University of Michigan. 1995.

[275] R. K. Lyon. *"The $NH_3$-NO-O $O_2$ Reaction"*. *Int. Journal of Chem. Kinetics*. 8. 315–318. 1976.

[276] D. Ma and G. Ahmadi. *"A Thermodynamical Formulation for Dispersed Multiphase Turbulent Flows"*. *Int.J.Multiphase Flow*. 16. 323–351. 1990.

[277] J. Ma. *"Soot Formation and Soot Secondary Reactions During Coal Pyrolysis"*. *PhD thesis*. Brigham Young University, Utah, USA. 1996.

[278] J. I. Madsen, W. A. Rogers, and T. J. OBrien. *"Unstructured Multigrid Through Agglomeration In Computational Modelling of Mercury Control by Sorbent Injection"*. Baltimore, Maryland 2004.

[279] B. F. Magnussen. *"On the Structure of Turbulence and a Generalized Eddy Dissipation Concept for Chemical Reaction in Turbulent Flow"*. Nineteenth AIAA Meeting, St. Louis 1981.

[280] B. F. Magnussen and B. H. Hjertager. *"On mathematical models of turbulent combustion with special emphasis on soot formation and combustion"*. *In 16th Symp. (Int'l.) on Combustion*. The Combustion Institute. 1976.

[281] M. Manninen, V. Taivassalo, and S. Kallio. *"On the mixture model for multiphase flow"*. VTT Publications 288, Technical Research Centre of Finland. 1996.

[282] D. L. Marchisio and R. O. Fox. *"Solution of Population Balance Equations Using the Direct Quadrature Method of Moments"*. *Aerosol Science and Technology*. 36. 43–73. 2005.

[283] F. Mathey, D. Cokljat, J. P. Bertoglio, and E. Sergent. *"Specification of LES Inlet Boundary Condition Using Vortex Method"*. In K. Hanjali , Y. Nagano, and M. Tummers, editors*4th International Symposium on Turbulence, Heat and Mass Transfer, Antalya, Turkey*. Begell House, Inc. 2003.

[284] S. R. Mathur and J. Y. Murthy. *"Coupled ordinates method for multigrid acceleration of radiation calculations"*. *J. of Thermophysics and Heat Transfer*. 13(4). 1783-1785. 1999.

[285] S. Mayer, . *"Theory of Liquid Atomization in High Velocity Gas Streams"*. *ARS Journal*. 31. 467–473. 1961.

[286] B. S. McLaury, J. Wang, S. A. Shirazi, J. R. Shadley, and E. F. Rybicki. *"Solid Particle Erosion in Long Radius Elbows and Straight Pipes"*. *SPE Annual Technical Conference and Exhibition, II Production Operations and Engineering/General, San Antonio, Texas*. SPE Paper 38842 October 1997.

[287] R. Mei and J. F. Klausner. *"Shear Lift Force on Spherical Bubbles"*. *J.Fluid Mech*. 15. 62–65. 1994.

[288] P. C. Melte and D. T. Pratt. *"Measurement of Atomic Oxygen and Nitrogen Oxides in Jet Stirred Combustion"*. *In 15th Symposium (Int'l) on Combustion*. The Combustion Institute. 1061–1070. 1974.


*Release 15.0 - © SAS IP, Inc. All rights reserved. - Contains proprietary and confidential information of ANSYS, Inc. and its subsidiaries and affiliates.*

[289] C. Meneveau and T. Poinsot. *"Stretching and Quenching of Flamelets in Premixed Turbulent Combustion"*. *Combustion and Flame*. 86. 311–332. 1991.

[290] F. R. Menter. *"Two-Equation Eddy-Viscosity Turbulence Models for Engineering Applications"*. *AIAA Journal*. 32(8). 1598–1605. August 1994.

[291] F. R. Menter. *"Review of the SST Turbulence Model Experience from an Industrial Perspective"*. *International Journal of Computational Fluid Dynamics*. Volume 23, Issue 4. 2009.

[292] F. R. Menter and Y. Egorov. *"Re-visiting the Turbulent Scale Equation"*. *Proc. IUTAM Symp. One Hundred Years of Boundary Layer Research, Göttingen*. Springer. 2004.

[293] F. R. Menter, M. Kuntz, and R. Langtry. *"Ten Years of Experience with the SST Turbulence Model"*. In K. Hanjalic, Y. Nagano, and M. Tummers, editors*Turbulence, Heat and Mass Transfer*. 4. Begell House Inc. 625–632. 2003.

[294] F. R. Menter, R. B. Langtry, S. R. Likki, Y. B. Suzen, P. G. Huang, and S. Volker. *"A Correlation-Based Transition Model Using Local Variables: Part I — Model Formulation"*. (ASME-GT2004-53452) 2004.

[295] F. R. Menter, . M. Kuntz and R. Bender. *"A scale-adaptive simulation model for turbulent flow predictions"*. *AIAA Journal*. January 2003.

[296] M. Metghalchi and J. C. Keck. *"Burning velocities of mixtures of air with methanol, isooctane and indolene at high pressures and temperatures"*. *Combustion and Flame*. 48. 191–210. 1982.

[297] J. A. Miller and C. T. Bowman. *"Mechanism and Modeling of Nitrogen Chemistry in Combustion"*. *Prog. in Energy and Comb. Sci*. 15. 287–338. 1989.

[298] J. A. Miller, M. C. Branch, W. J. McLean, D. W. Chandler, M. D. Smooke, and R. J. Kee. *In 20th Symp. (Int'l.) on Combustion*. The Combustion Institute. 673. 1985.

[299] J. A. Miller and G. A. Fisk. *Chemical and Engineering News*. 31. 1987.

[300] R. S. Miller, K. Harstad and J. Bellan. *"Evaluation of Equilibrium and Non-Equilibrium Evaporation Models for Many Droplet Gas-Liquid Flow Simulations"*. *International Journal of Multiphase Flow*. 24. 6. 1025 –1055. 1998.

[301] M. Missaghi. *"Mathematical Modelling of Chemical Sources in Turbulent Combustion"*. *PhD thesis*. The University of Leeds, England. 1987.

[302] M. Missaghi, M. Pourkashanian, A. Williams, and L. Yap. *In Proceedings of American Flame Days Conference, USA*. 1990.

[303] M. F. Modest. *"The Weighted-Sum-of-Gray-Gases Model for Arbitrary Solution Methods in Radiative Transfer"*. *J. Heat Transfer*. 113. 650–656. 1991.

[304] M. F. Modest. *Radiative Heat Transfer*. Series in Mechanical EngineeringMcGraw-Hill. 1993.

[305] L. J. Molero de Blas. *"Pollutant Formation and Interaction in the Combustion of Heavy Liquid Fuels"*. *PhD thesis*. University of London, England. 1998.

[306] J. P. Monat, R. K. Hanson, and C. H. Kruger. *In 17th Symp. (Int'l.) on Combustion*. The Combustion Institute. 543. 1979.

*Release 15.0 - © SAS IP, Inc. All rights reserved. - Contains proprietary and confidential information of ANSYS, Inc. and its subsidiaries and affiliates.*

[307] M. J. Moore and C. H. Sieverding. *"Two-Phase Steam Flow in Turbines and Separator*. McGraw-Hill. 1976.

[308] F. J. Moraga, R. T. Bonetto and R. T. Lahey. *"Lateral forces on spheres in turbulent uniform shear flow"*. *International Journal of Multiphase Flow*. 25. 1321–1372. 1999.

[309] S. A. Morsi and A. J. Alexander. *"An Investigation of Particle Trajectories in Two-Phase Flow Systems"*. *J. Fluid Mech*. 55(2). 193–208. September 26 1972.

[310] J. B. Moss, S. A. L. Perera,C. D. Stewart, and M. Makida. *"Radiation Heat Transfer in Gas Turbine Combustors"*. *In Proc. 16th (Int'l.) Symp. on Airbreathing Engines, Cleveland, OH*. 2003.

[311] C. M. Muller, H. Breitbach, and N. Peters. *"Partially Premixed Turbulent Flame Propagation in Jet Flames"*. *In 25th Symposium (Int) on Combustion*. The Combustion Institute. 1994.

[312] C. Mundo, M. Sommerfeld, and C. Tropea. *"Droplet-Wall Collisions: Experimental Studies of the Deformation and Breakup Process"*. *International Journal of Multiphase Flow*. 21(2). 151–173. 1995.

[313] J. Y. Murthy and S. R. Mathur. *"A Finite Volume Method For Radiative Heat Transfer Using Unstructured Meshes"*. *AIAA-98-0860*. January 1998.

[314] S. Muzaferija, M. Peric, P. Sames, and T. Schellin. *"A Two-Fluid Navier-Stokes Solver to Simulate Water Entry"*. *In Proc 22nd Symposium on Naval Hydrodynamics, Washington, DC*. 277–289. 1998.

[315] J. D. Naber and R. D. Reitz. *"Modeling Engine Spray/Wall Impingement"*. *Technical Report 880107, Society of Automotive Engineers*. General Motors Research Laboratories, Warren, MI. 1988.

[316] M. Namazian and J. B. Heywood. *"Flow in the Piston Cylinder Ring Crevices of a Spark Ignition Engine: Effect on Hydrocarbon Emissions, Efficiency, and Power"*. *SAE Technical Paper 820088*. SAE. 1982.

[317] I. Naruse, Y. Yamamoto, Y. Itoh, and K. Ohtake. *"Fundamental Study on $N_2O$ Formation/Decomposition Characteristics by Means of Low-Temperature Pulverized Coal Combustion"*. *In 26th Symposium (Int'l) on Combustion*. The Combustion Institute. 3213–3221. 1996.

[318] P. F. Nelson, A. N. Buckley, and M. D. Kelly. *"Functional Forms of Nitrogen in Coals and the Release of Coal Nitrogen as NOx Precursors (HCN and $NH_3$)"*. *In 24th Symposium (Int'l) on Combustion*. The Combustion Institute. 1259. 1992.

[319] P. Nguyen, L. Vervisch, V. Subramanian and P. Domingo. *"Multi-Dimensional Flamelet-Generated Manifolds for Partially Premixed Combustion"*. *Combustion and Flame*. 157. 43–61. 2010.

[320] F. Nicoud and F. Ducros. *"Subgrid-Scale Stress Modelling Based on the Square of the Velocity Gradient Tensor.Flow"*. *Turbulence, and Combustion*. 62(3). 183–200. 1999.

[321] L. Nokleberg and T. Sontvedt. *"Erosion of Oil and Gas Industry Choke Valves Using Computational Fluid Dynamics and Experiment"*. *International Journal of Heat and Fluid Flow*. 636–643. 1998.

[322] P. A. Nooren, H. A. Wouters, T. W. J. Peeters, D. Roekaerts, U. Maas, and D. Schmidt. *"Monte carlo pdf modeling of a turbulent natural-gas diffusion flame"*. *Combustion Theory and Modeling*. 1. 79–96. 1997.

[323] J. Norman, M. Porkashanian, and A. Williams. *"Modelling the Formation and Emission of Environmentally Unfriendly Coal Species in Some Gasification Processes"*. *Fuel*. 76(13). 1201–1216. October 1997.


*Release 15.0 - © SAS IP, Inc. All rights reserved. - Contains proprietary and confidential information of ANSYS, Inc. and its subsidiaries and affiliates.*

[324] W. H. Nurick. *"Orifice Cavitation and Its Effects on Spray Mixing"*. *Journal of Fluids Engineering*. 98. 1976.

[325] R. Ocone, S. Sundaresan, and R. Jackson. *"Gas-particle flow in a duct of arbitrary inclination with particle-particle interaction"*. *AIChE J*. 39. 1261–1271. 1993.

[326] S. Ogawa, A. Umemura, and N. Oshima. *"On the Equation of Fully Fluidized Granular Materials"*. *J. Appl. Math. Phys*. 31. 483. 1980.

[327] E. Olsson, G. Kreiss and S. Zahedi. *"A Conservative Level Set Method for Two Phase Flow II"*. *J. Comput. Phys*. 225. 785–807. 2007.

[328] O. O. Oluwole, H.-W. Wong, R. C. Miake-Lye, and W. H. Green Jr. *"Dynamic Spatial and Temporal Allocation of Reduced Chemical Kinetics Models in Combustion Computational Fluid Dynamics Simulations"*. *46th AIAA/ASME/SAE/ASEE Joint Propulsion Conference*. AIAA 2010-6827, 2010.

[329] P. J. O'Rourke. *"Collective Drop Effects on Vaporizing Liquid Sprays"*. *PhD thesis*. Princeton University, Princeton, New Jersey. 1981.

[330] P. J. O'Rourke and A. A. Amsden. *"The TAB Method for Numerical Calculation of Spray Droplet Breakup"*. *SAE Technical Paper 872089*. SAE. 1987.

[331] P. J. O'Rourke and A. A. Amsden. *"A Particle Numerical Model for Wall Film Dynamics in Port-Fuel Injected Engines"*. *SAE Paper 961961*. 1996.

[332] P. J. O'Rourke and A. A. Amsden. *"A Spray/Wall Interaction Submodel for the KIVA-3 Wall Film Model"*. *SAE Paper 2000-01-0271*. 2000.

[333] P.J. O'Rourke and F. V. Bracco. *"Two Scaling Transformations for the Numerical Computation of Multidimensional Unsteady Laminar Flames"*. *Journal of Computational Physics*. 33 (2). 185 –203. 1979.

[334] S. A. Orszag, V. Yakhot, W. S. Flannery, F. Boysan, D. Choudhury, J. Maruzewski, and B. Patel. *"Renormalization Group Modeling and Turbulence Simulations"*. *In International Conference on Near-Wall Turbulent Flows, Tempe, Arizona*. 1993.

[335] S. Osher and J. A. Sethian,. *"Fronts Propagating with Curvature-dependent Speed: Algorithms Based on Hamilton-Jacobi Formulations"*. *J. Comput. Phys*. 79. 12–49. 1988.

[336] M. Ostberg and K. Dam-Johansen. *"Empirical Modeling of the Selective Non-Catalytic Reduction of NO Comparison with Large-Scale Experiments and Detailed Kinetic Modeling"*. *Chem. Engineering Science*. 49(12). 1897–1904. 1994.

[337] H. Ounis, G. Ahmadi, and J. B. McLaughlin. *"Brownian Diffusion of Submicrometer Particles in the Viscous Sublayer"*. *Journal of Colloid and Interface Science*. 143(1). 66–277. 1991.

[338] M. N. Ozisik. *Radiative Transfer and Interactions with Conduction and Convection"*. Wiley, New York. 1973.

[339] S. A. Pandya, S. Venkateswaran, and T. H. Pulliam. *"Implementation of dual-time procedures in overflow"*. *Technical Report AIAA-2003-0072*. American Institute of Aeronautics and Astronautics. 2003.

[340] S. V. Patankar. *Numerical Heat Transfer and Fluid Flow*. Hemisphere, Washington, DC. 1980.

*Release 15.0 - © SAS IP, Inc. All rights reserved. - Contains proprietary and confidential information of ANSYS, Inc. and its subsidiaries and affiliates.*

[341] J. C. Park, M. H. Kim and H. Miyata. *"Fully Non-linear Free-surface Simulations By a 3D Viscous Numerical Wave Tank"*. *International Journal for Numerical Methods in Fluids*. 29. 685–703. 1999.

[342] M. A. Patterson and R. D. Reitz. *"Modeling the Effects of Fuel Spray Characteristics on Diesel Engine Combustion and Emission"*. *SAE Paper*. SAE. 1998.

[343] D. Y. Peng and D. B. Robinson. *"A New Two-Constant Equation of State"*. *Industrial and Engineering Chemistry: Fundamentals*. 15. 59–64. 1976.

[344] R. H. Perry, D. W. Gree, and J. O. Maloney. *Perry's Chemical Engineers' Handbook*. McGraw-Hill, New York. 6th edition. 1984.

[345] N. Peters. *"Laminar Diffusion Flamelet Models in Non Premixed Combustion"*. *Prog. Energy Combust. Sci*. 10. 319–339. 1984.

[346] N. Peters. *"Laminar Flamelet Concepts in Turbulent Combustion"*. *In 21st Symp. (Int'l.) on Combustion*. The Combustion Institute. 1231–1250. 1986.

[347] N. Peters. *Turbulent Combustion*. Cambridge University Press, Cambridge, England. 2000.

[348] N. Peters and S. Donnerhack. *In 18th Symp. (Int'l.) on Combustion*. The Combustion Institute. 33. 1981.

[349] N. Peters and B. Rogg. *"Reduced Kinetic Mechanisms for Applications in Combustion Systems"*. *In Lecture Notes in Physics*. m15. Springer-Verlag. 1992.

[350] K. K. Pillai. *"The Influence of Coal Type on Devolatilization and Combustion in Fluidized Beds"*. *J. Inst. Energy*. 142. 1981.

[351] U. Piomelli, P. Moin and J. H. Ferziger. *"Model Consistency in Large-Eddy Simulation of Turbulent Channel Flow"*. *Physics of Fluids*. 31. 1884–1894. 1988.

[352] H. Pitsch. *"A Consistent Level Set Formulation For Large-Eddy Simulation of Premixed Turbulent Combustion"*. *Combustion and Flame*. 143. 587–598. 2005.

[353] H. Pitsch, H. Barths, and N. Peters. *"Three-Dimensional Modeling of NOx and Soot Formation in DI-Diesel Engines Using Detailed Chemistry Based on the Interactive Flamelet Approach"*. *SAE Paper 962057*. SAE. 1996.

[354] H. Pitsch and N. Peters. *"A Consistent Flamelet Formulation for Non-Premixed Combustion Considering Differential Diffusion Effects"*. *Combustion and Flame*. 114. 26–40. 1998.

[355] T. Poinsot and D. Veynante. *Theoretical and Numerical Combustion*. McGraw-Hill, New York. 2001.

[356] B. E. Poling, J. M. Prausnitz, and J.P. OConnell. *The Properties of Gases and Liquids*. McGraw-Hill, New York, 5th edition. 2001.

[357] S. B. Pope. *"Pdf methods for turbulent reactive flows"*. *Progress Energy Combustion Science*. 11. 119. 1985.

[358] S. B. Pope. *"Computationally efficient implementation of combustion chemistry using in-situ adaptive tabulation"*. *Combustion Theory and Modeling*. 1. 41–63. 1997.

[359] S. B. Pope. *Turbulent Flows*. Cambridge University Press, Cambridge, England. 2000.

*Release 15.0 - © SAS IP, Inc. All rights reserved. - Contains proprietary and confidential information of ANSYS, Inc. and its subsidiaries and affiliates.*

[360] S. B. Pope. *"Gibbs Function Continuation for the Stable Computation of Chemical Equilibrium"*. *Combustion and Flame*. 139. 222–226. 2004.

[361] B. Popoff and M. Braun. *"A Lagrangian Approach to Dense Particulate Flows"*. *In International Conference on Multiphase Flow*. Leipzig, Germany. 2007.

[362] C. Prakash. *"Two phase model for binary liquid-solid phase change: Parts I and II"*. *Numerical Heat Transfer*. 18. 2. 131–167. 1990.

[363] I. Proudman. *"The Generation of Noise by Isotropic Turbulence"*. *Proc. Roy. Soc*. A214. 119. 1952.

[364] G. D. Raithby and E. H. Chui. *"A Finite-Volume Method for Predicting a Radiant Heat Transfer in Enclosures with Participating Media"*. *J. Heat Transfer*. 112. 415–423. 1990.

[365] W. E. Ranz. *"Some Experiments on Orifice Sprays"*. *Canadian Journal of Chemical Engineering*. 175. 1958.

[366] W. E. Ranz and W. R. Marshall, Jr.. *"Vaporation from Drops, Part I"*. *Chem. Eng. Prog*. 48(3). 141–146. March 1952.

[367] W. E. Ranz and W. R. Marshall, Jr.. *"Evaporation from Drops, Part I and Part II"*. *Chem. Eng. Prog*. 48(4). 173–180. April 1952.

[368] A. V. Rao. *Dynamics of Particles and Rigid Bodies. A Systematic Approach*. Cambridge University Press. Cambridge, England 2006.

[369] R. D. Rauch, J. T. Batira, and N. T. Y. Yang. *"Spatial Adaption Procedures on Unstructured Meshes for Accurate Unsteady Aerodynamic Flow Computations"*. *Technical Report AIAA-91-1106*. AIAA. 1991.

[370] Reaction Design. *http://www.reactiondesign.com*. 2012.

[371] R. D. Reitz. *"Mechanisms of Atomization Processes in High-Pressure Vaporizing Sprays"*. *Atomization and Spray Technology*. 3. 309–337. 1987.

[372] R. D. Reitz and F. V. Bracco. *"Mechanism of Atomization of a Liquid Jet"*. *Phys. Fluids*. 26(10). 1982.

[373] R. D. Reitz and F. V. Bracco. *"Mechanisms of Breakup of Round Liquid Jets"*. *The Encyclopedia of Fluid Mechanics, ed. N. Cheremisnoff*. 3. 223–249. 1986.

[374] W. C. Reynolds. *"Thermodynamic Properties in SI: Graphs, Tables, and Computational Equations for 40 Substances"*. Department of Mechanical Engineering, Stanford University. 1979.

[375] W. C. Reynolds. *"Fundamentals of turbulence for turbulence modeling and simulation"*. *Lecture Notes for Von Karman Institute Agard Report No. 755*. 1987.

[376] C. M. Rhie and W. L. Chow. *"Numerical Study of the Turbulent Flow Past an Airfoil with Trailing Edge Separation"*. *AIAA Journal*. 21(11). 1525–1532. November 1983.

[377] H. S. Ribner. *"The Generation of Sound by turbulent jets"*. *In Advances in Applied Mathematics*. Academic, New York. 1964.

[378] S. Richard, O. Colin, O. Vermorel, A. Benkenida, C. Angelberger, and D. Veynante. *"Towards Large Eddy Simulation of Combustion in Spark Ignition Engines"*. *Proceedings of the Combustion Institute*. 31. 2. 3059–3066. 2007.

*Release 15.0 - © SAS IP, Inc. All rights reserved. - Contains proprietary and confidential information of ANSYS, Inc. and its subsidiaries and affiliates.*

[379] J. R. Richardson and W. N. Zaki. *"Sedimentation and Fluidization: Part I"*. *Trans. Inst. Chem. Eng*. 32. 35–53. 1954.

[380] C. E. Roberts and R. D. Matthews. *"Development and Application of an Improved Ring Pack Model for Hydrocarbon Emissions Studies"*. *SAE Technical Paper 961966*. SAE. 1996.

[381] P. L. Roe. *"Characteristic based schemes for the Euler equations"*. *Annual Review of Fluid Mechanics*. 18. 337–365. 1986.

[382] R. Rota, D. Antos, E. F. Zanoelo, and M. Morbidelli. *"Experimental and Modeling Analysis of the NOxOUT Process"*. *Chemical Engineering Science*. 57. 27–38. 2002.

[383] P. G. Saffman. *"The Lift on a Small Sphere in a Slow Shear Flow"*. *J.Fluid Mech*. 22. 385–400. 1965.

[384] P. G. Saffman. *Corrigendum to: "The Lift on a Small Sphere in a Slow Shear Flow"*. *J.Fluid Mech*. 31. 624. 1968.

[385] M. M. Salama and E. S. Venkatesh. *"Evaluation of api rp14e erosional velocity limitations for offshore gas wells"*. *In OTC Conference, Houston, TX*. 371–376. May 1983.

[386] S. Sarkar and L. Balakrishnan. *"Application of a Reynolds-Stress Turbulence Model to the Compressible Shear Layer"*. ICASE Report 90-18*NASA CR 182002*. 1990.

[387] S. Sarkar and M. Y. Hussaini. *"Computation of the sound generated by isotropic turbulence"*. *NASA Contract Report 93-74*. NASA Langley Research Center, Hampton, VA. 1993.

[388] Y. Sato and K. Sekoguchi. *"Liquid Velocity Distribution in Two-Phase Bubbly Flow"*. *Int. J. Multiphase Flow*. 2. 79. 1979.

[389] S. S. Sazhin. *"An Approximation for the Absorption Coefficient of Soot in a Radiating Gas"*. *Manuscript*. Fluent Europe, Ltd. 1994.

[390] S. S. Sazhin. *"Advanced Models of Fuel Droplet Heating and Evaporation"*. *Progress in Energy and Combustion Science*. Elsevier Science. 32. 162–214. 2006.

[391] D. G. Schaeffer. *"Instability in the Evolution Equations Describing Incompressible Granular Flow"*. *J. Diff. Eq*. 66. 19–50. 1987.

[392] R. W. Schefer, M. Namazian, and J. Kelly. *"In Combustion Research Facility News*. 3:4. Sandia. 1991.

[393] L. Schiller and Z. Naumann. *"Z. Ver. Deutsch. Ing*. 77. 318. 1935.

[394] H. Schlichting and K. Gersten. *Grenzschicht-Theorie*. Springer-Verlag, Berlin, Heidelberg, New York. 1997.

[395] D. P. Schmidt and M. L. Corradini. *"Analytical Prediction of the Exit Flow of Cavitating Orifices"*. *Atomization and Sprays*. 7. 6. 1997.

[396] D. P. Schmidt, M. L. Corradini, and C. J. Rutland. *"A Two-Dimensional, Non-Equilibrium Model of Flashing Nozzle Flow"*. *In 3rd ASME/JSME Joint Fluids Engineering Conference*. 1999.

[397] D. P. Schmidt, I. Nouar, P. K. Senecal, C. J. Rutland, J. K. Martin, and R. D. Reitz. *"Pressure-Swirl Atomization in the Near Field"*. *SAE Paper 01-0496*. SAE. 1999.

[398] G. H. Schnerr and J. Sauer. *"Physical and Numerical Modeling of Unsteady Cavitation Dynamics"*. *In Fourth International Conference on Multiphase Flow, New Orleans, USA*. 2001.


*Release 15.0 - © SAS IP, Inc. All rights reserved. - Contains proprietary and confidential information of ANSYS, Inc. and its subsidiaries and affiliates.*

[399] P. K. Senecal, D. P. Schmidt, I. Nouar, C. J. Rutland, and R. D.Reitz. *"Modeling High Speed Viscous Liquid Sheet Atomization"*. *International Journal of Multiphase Flow*. 25(6–7). 1073–1097. 1999.

[400] E. Sergent. *"Vers une methodologie de couplage entre la Simulation des Grandes Echelles et les modeles statistiques"*. *PhD thesis*. L'Ecole Centrale de Lyon, Lyon, France. 2002.

[401] N. G. Shah. *"A New Method of Computation of Radiant Heat Transfer in Combustion Chambers"*. *PhD thesis*. Imperial College of Science and Technology, London, England. 1979.

[402] T.-H. Shih, W. W. Liou, A. Shabbir, Z. Yang, and J. Zhu. *"A New $k$- $\varepsilon$ Eddy-Viscosity Model for High Reynolds Number Turbulent Flows - Model Development and Validation"*. *Computers Fluids*. 24(3). 227–238. 1995.

[403] M. L. Shur, P. R. Spalart, M. K. Strelets, and A. K. Travin. *"A Hybrid RANS-LES Approach With Delayed-DES and Wall-Modelled LES Capabilities"*. *International Journal of Heat and Fluid Flow*. 29:6. December 2008. 1638-1649.

[404] M. Shur, P. R. Spalart, M. Strelets, and A. Travin. *"Detached-Eddy Simulation of an Airfoil at High Angle of Attack"*. *In 4th Int. Symposium on Eng. Turb. Modeling and Experiments, Corsica, France*. May 1999.

[405] M. L. Shur, M. K. Strelets, A. K. Travin and P. R. Spalart. *"Turbulence Modeling in Rotating and Curved Channels: Assessing the Spalart-Shur Correction"*. *AIAA Journal*. 38(5). 2000. 2000.

[406] R. Siegel and J. R. Howell. *"Thermal Radiation Heat Transfer*. Hemisphere Publishing Corporation, Washington DC. 1992.

[407] R. Siegel and C. M. Spuckler. *"Effect of Refractive Index and Diffuse or Specular Boundaries on a Radiating Isothermal Layer"*. *J. Heat Transfer*. 116. 787–790. 1994.

[408] O. Simonin and P. L. Viollet. *"Modeling of Turbulent Two-Phase Jets Loaded with Discrete Particles"*. *Phenomena in Multiphase Flows*. 259–269. 1990.

[409] O. Simonin and P. L. Viollet. *"Predictions of an Oxygen Droplet Pulverization in a Compressible Subsonic Coflowing Hydrogen Flow"*. *Numerical Methods for Multiphase Flows*. FED91. 65–82. 1990.

[410] A. K. Singhal, H. Y. Li, M. M. Athavale, and Y. Jiang. *"Mathematical Basis and Validation of the Full Cavitation Model"*. *ASME FEDSM'01*. New Orleans, Louisiana 2001.

[411] Y. R. Sivathanu and G. M. Faeth. *"Generalized State Relationships for Scalar Properties in Non-Premixed Hydrocarbon/AirFlames"*. *Combustion and Flame*. 82. 211–230. 1990.

[412] J. Smagorinsky. *"General Circulation Experiments with the Primitive Equations. I. The Basic Experiment"*. *Month. Wea. Rev*. 91. 99–164. 1963.

[413] P. E. Smirnov and F. R. Menter. *"Sensitization of the SST Turbulence Model to Rotation and Curvature by Applying the Spalart-Shur Correction Term"*. *ASME Paper GT 2008-50480*. Berlin, Germany. 2008.

[414] R. Smirnov, S. Shi, and I. Celik. *"Random Flow Generation Technique for Large Eddy Simulations and Particle-Dynamics Modeling"*. *Journal of Fluids Engineering*. 123. 359–371. 2001.

[415] I. W. Smith. *"Combustion and Flame*. 17. 421. 1971.

[416] I. W. Smith. *"The Intrinsic Reactivity of Carbons to Oxygen"*. *Fuel*. 57. 409–414. 1978.

*Release 15.0 - © SAS IP, Inc. All rights reserved. - Contains proprietary and confidential information of ANSYS, Inc. and its subsidiaries and affiliates.*

[417] I. W. Smith. *"The Combustion Rates of Coal Chars: A Review"*. *In 19th Symp. (Int'l.) on Combustion*. The Combustion Institute. 1045–1065. 1982.

[418] J. M. Smith and H. C. Van Ness. *Introduction to Chemical Engineering Thermodynamics"*. McGraw Hill, New Jersey. 1986.

[419] T. F. Smith, Z. F. Shen, and J. N. Friedman. *"Evaluation of Coefficients for the Weighted Sum of Gray Gases Model"*. *J. Heat Transfer*. 104. 602–608. 1982.

[420] L. D. Smoot and P. J. Smith. *"NOx Pollutant Formation in a Turbulent Coal System"*. *In Coal Combustion and Gasification*. Plenum, Plenum, NY373. 1985.

[421] D. O. Snyder, E. K. Koutsavdis, and J. S. R. Anttonen. *"Transonic store separation using unstructured CFD with dynamic meshing"*. *Technical Report AIAA-2003-3913*. 33rd AIAA Fluid Dynamics Conference and Exhibit American Institute of Aeronautics and Astronautics. 2003.

[422] A. Sokolichen, G. Eigenberger, and A. Lapin. *"Simulation of Buoyancy Driver Bubbly Flow: Established Simplifications and Open Questions"*. *Journal Review, AIChE Journal*. 50:1. 24–45. January 2004.

[423] M. S. Solum, R. J. Pugmire, and D. M. Grant. *"Energy and Fuels*. 3. 187. 1989.

[424] C. Soteriou, R. Andrews, and M. Smith. *"Direct Injection Diesel Sprays and the Effect of Cavitation and Hydraulic Flip on Atomization"*. *SAE Paper 950080*. SAE. 1995.

[425] P. R. Spalart. *"Young-person's guide to detached-eddy simulation grids"*. *NASA NASA/CR-2001-211032*. NASA Langley Research Center. 2001.

[426] P. Spalart and S. Allmaras. *"A one-equation turbulence model for aerodynamic flows"*. *Technical Report AIAA-92-0439*. American Institute of Aeronautics and Astronautics. 1992.

[427] P. R. Spalart, S. Deck, M. L. Shur, K. D. Squires, M. K. Strelets, and A. Travin. *"A new version of detached-eddy simulation, resistant to ambiguous grid densities"*. *Theoretical and Computational Fluid Dynamics*. 20. 181–195. 2006.

[428] P. R. Spalart and M. L. Shur. *"On the Sensitization of Turbulence Models to Rotation and Curvature"*. *Aerospace Sci. Tech*. 1(5). 297–302. 1997.

[429] D. B. Spalding. *"Mixing and chemical reaction in steady confined turbulent flames"*. *In 13th Symp. (Int'l.) on Combustion*. The Combustion Institute. 1970.

[430] C. G. Speziale, S. Sarkar, and T. B.Gatski. *"Modelling the Pressure-Strain Correlation of Turbulence: An Invariant Dynamical Systems Approach"*. *J. Fluid Mech*. 227. 245–272. 1991.

[431] T. E. Springer, T. A. Zawodzinski, and S. Gottesfeld. *"Polymer Electrolyte Fuel Cell Model"*. *J. Electrochemical Soc*. 138:8. August 1991.

[432] H. B. Squire. *"Investigation of the Instability of a Moving Liquid Film"*. *British Journal of Applied Physics*. 4. 167. 1953.

[433] D. W. Stanton and C. J. Rutland. *"Modeling Fuel Film Formation and Wall Interaction in Diesel Engines"*. *SAE Paper 960628*. 1996.

[434] D. W. Stanton and C. J. Rutland. *"Multi-Dimensional Modeling of Thin Liquid Films and Spray-Wall Interactions Resulting from Impinging Sprays"*. *International Journal of Heat and Mass Transfer*. 41. 3037–3054. 1998.


*Release 15.0 - © SAS IP, Inc. All rights reserved. - Contains proprietary and confidential information of ANSYS, Inc. and its subsidiaries and affiliates.*

[435] R. C. Steele, P. C. Malte, D. G. Nichol, and J. C. Kramlich. *"NOx and $N_2O$ in Lean-Premixed Jet-Stirred Flames"*. *Combustion and Flame*. 100. 440–449. 1995.

[436] P. H. Steward, C. W. Larson, and D. Golden. *"Combustion and Flame*. 75. 1989.

[437] S. Subramaniam and S. B. Pope. *"A Mixing Model for Turbulent Reactive Flows Based on Euclidean Minimum Spanning Trees"*. *Combustion and Flame*. 115. 487–514. 1998.

[438] M. Syamlal. *"The Particle-Particle Drag Term in a Multiparticle Model of Fluidization"*. *National Technical Information Service, Springfield, VA*. DOE/MC/21353-2373, NTIS/DE87006500, 1987.

[439] M. Syamlal and T. O'Brien. *"The Derivation of a Drag Coefficient Formula from Velocity-Voidage Correlations"*. 1987.

[440] M. Syamlal and T. J. O'Brien. *"Computer Simulation of Bubbles in a Fluidized Bed"*. *AIChE Symp. Series*. 85. 22–31. 1989.

[441] M. Syamlal, W. Rogers, and O'Brien T. J.. *MFIX Documentation: Volume1, Theory Guide*>. National Technical Information Service, Springfield, VA. DOE/METC-9411004, NTIS/DE9400087, 1993.

[442] D. Tabacco, C. Innarella, and C. Bruno. *"Theoretical and Numerical Investigation on Flameless Combustion"*. *Combustion Science and Technology*. 2002.

[443] T. Takamasa and A. Tomiyama. . *"Three-Dimensional Gas-Liquid Two-Phase Bubbly Flow in a C-Shaped Tube"*. *Ninth International Topical Meeting on Nuclear Reactor Thermal Hydraulics (NURETH-9)*. San Francisco, CA. 1999.

[444] L. Talbot et al. *"Thermophoresis of Particles in a Heated Boundary Layer"*. *J. Fluid Mech*. 101(4). 737–758. 1980.

[445] I. Tanasawa. *"Advances in Condensation Heat Transfer"*. *Advances in Heat Transfer*. 21. 55–139. 1991.

[446] G. I. Taylor. *"The Shape and Acceleration of a Drop in a High Speed Air Stream, Technical Report"*. *In the Scientific Papers of G. I. Taylor*. ed., G. K. Batchelor. 1963.

[447] P. B. Taylor and P. J. Foster. *"Some Gray Weighting Coefficients for $CO_2$-$H_2O$-Soot Mixtures"*. *Int. J. Heat Transfer*. 18. 1331–1332. 1974.

[448] A. Tentner, S. Lo and V. Kozlov. *"Advances in Computational Fluid Dynamics Modeling of Two-Phase Flow in a Boiling Water Reactor Fuel Assembly"*. *In International Conference on Nuclear Engineering*. Miami, Florida. 2006.

[449] A. Teraji, T. Tsuda, T. Noda, M. Kubo, and T. Itoh. *"Development of a Novel Flame Propagation Model (UCFM: Universal Coherent Flamelet Model) for SI Engines and Its Application to Knocking Prediction"*. *SAE 2005 World Congress & Exhibition*. 2005.

[450] P. A. Tesner, T. D. Snegiriova, and V. G. Knorre. *"Kinetics of Dispersed Carbon Formation"*. *Combustion and Flame*. 17. 253–260. 1971.

[451] V. I. Tolubinski and D. M. Kostanchuk. *Vapor bubbles growth rate and heat transfer intensity at subcooled water boiling*. *4th International Heat Transfer Conference, Paris, France*. 1970.

[452] A. Tomiyama. *"Struggle with computational bubble dynamics"*. *Third International Conference on Multiphase Flow, Lyon, France*. June 8–12, 1998.

*Release 15.0 - © SAS IP, Inc. All rights reserved. - Contains proprietary and confidential information of ANSYS, Inc. and its subsidiaries and affiliates.*

[453] A. Tomiyama, H. Tarnai, I. Zun and S. Hosokama. *"Transverse Migration of Single Bubbles in Simple Shear Flow"*. *Chem. Eng. Sci.*. 57. 1849–1858. 2002.

[454] B. Toole-ONeil, S. J. Tewalt, R. B. Finkleman, and D. J. Akers. *"Mercury Concentration in Coal Unravelling the Puzzle"*. *Fuel*. 78(1). 47–74,. January 1999.

[455] A. A. Troshko and Y. A. Hassan. *"A Two-Equation Turbulence Model of Turbulent Bubbly Flow"*. *International Journal of Multiphase Flow*. 22(11). 1965–2000. 2001.

[456] E. Turkel and V. N. Vatsa. *"Choice of variables and preconditioning for time dependent problems"*. *Technical Report AIAA-2003-3692*. 16th AIAA Computational Fluid Dynamics Conference, Orlando, FloridaAmerican Institute of Aeronautics and Astronautics. June 2003.

[457] O. Ubbink. *"Numerical Prediction of Two Fluid Systems With Sharp Interfaces"*. *PhD thesis*. Imperial College of Science, Technology and Medicine, London, England. 1997.

[458] H. C. Unal. *"Maximum Bubble Diameter, Maximum Bubble Growth Time and Bubble Growth Rate During Subcooled Nucleate Flow Boiling of Water Up To* $17.7MN/m^2$*"*. *Int. J. Heat Mass Transfer*. 19. 643–649. 1976.

[459] B. Van Leer. *"Toward the Ultimate Conservative Difference Scheme. IV. A Second Order Sequel to Godunov's Method"*. *Journal of Computational Physics*. 32. 101–136. 1979.

[460] A. van Oijen and L.P.H. de Goey. *"Modelling of Premixed Laminar Flames Using Flamelet-Generated Manifolds"*. *Combust. Sci. Tech*. 161. 113–137. 2000.

[461] J. P. Vandoormaal and G. D. Raithby. *"Enhancements of the SIMPLE Method for Predicting Incompressible Fluid Flows"*. *Numer.Heat Transfer*. 7. 147–163. 1984.

[462] S. A. Vasquez and V. A. Ivanov. *"A Phase Coupled Method for Solving Multiphase Problems on Unstructured Meshes"*. *In Proceedings of ASME FEDSM'00*. ASME 2000 Fluids Engineering Division Summer Meeting, Boston. June 2000.

[463] V. Venkatakrishnan. *"On The Accuracy of Limiters and Convergence to Steady State Solutions"*. *Technical Report AIAA-93-0880*. American Institute of Aeronautics and Astronautics. January 1993.

[464] S. Venkateswaran, J. M. Weiss, and C. L. Merkle. *"Propulsion Related Flowfields Using the Preconditioned Navier-Stokes Equations"*. *Technical Report AIAA-92-3437*. AIAA/ASME/SAE/ASEE 28th Joint Propulsion Conference, Nashville, TN. July 1992.

[465] O. Vermorel, S. Richard, O. Colin, C. Angelberger, A. Benkenida, and D. Veynante. *"Towards the Understanding of Cyclic Variability in a Spark Ignited Engine Using Multi-Cycle LES"*. *Combustion and Flame*. 156. 8. 1525–1541. 2009.

[466] D. Veynante and L. Vervisch. *"Turbulent Combustion Modeling"*. *Progress in Energy and Combustion Science*. Elsevier Science. 28. 3. 193–266. 2002.

[467] J. R. Viegas, M. W. Rubesin, and C. C. Horstman. *"On the Use of Wall Functions as Boundary Conditions for Two-Dimensional Separated Compressible Flows"*. *Technical Report AIAA-85-0180*. AIAA 23rd Aerospace Sciences Meeting, Reno, Nevada1985.

[468] V. R. Voller. *"Modeling Solidification Processes"*. *Technical report*. Mathematical Modeling of Metals Processing Operations Conference, Palm Desert, CAAmerican Metallurgical Society. 1987.

*Release 15.0 - © SAS IP, Inc. All rights reserved. - Contains proprietary and confidential information of ANSYS, Inc. and its subsidiaries and affiliates.*

[469] V. R. Voller, A. D. Brent, and C. Prakash. *"The Modeling of Heat, Mass and Solute Transport in Solidification Systems"*. *Int. J. Heat Mass Transfer*. 32(9). 1719–1731. 1989.

[470] V. R. Voller, A. D. Brent, and K. J. Reid. *"A Computational Modeling Framework for the Analysis of Metallurgical Solidification Process and Phenomena"*. *Technical report*. Conference for Solidification ProcessingRanmoor House, Sheffield, England. September 1987.

[471] V. R. Voller and C. Prakash. *"A Fixed-Grid Numerical Modeling Methodology for Convection-Diffusion Mushy Region Phase-Change Problems"*. *Int. J. Heat Mass Transfer*. 30. 1709–1720. 1987.

[472] V. R. Voller and C. R. Swaminathan. *"Generalized Source-Based Method for Solidification Phase Change"*. *Numer. Heat Transfer B,*. 19(2). 175–189. 1991.

[473] K. S. Vorres. *"User's handbook for the Argonne premium coal sample bank"*. Argonne National Laboratory, supported by DOE contract W-31-109-ENG-38, September 1989. Also K. S. Vorres, ACS Div. Fuel Chem. preprint 32. 4. 1987.

[474] D. Keith Walters and Davor Cokljat. *"A three-equation eddy-viscosity model for reynolds-averaged navier-stokes simulations of transitional flows"*. *Journal of Fluids Engineering*. 130. December 2008.

[475] D. Keith Walters and Nicole M. Wolgemuth. *"A new interface-capturing discretization for numerical solution of the volume fraction equation in two-phase flows"*. *International Journal for Numerical Methods in Fluids*. 60. 893-918. 2009.

[476] L. P. Wang. *"On the Dispersion of Heavy Particles by Turbulent Motion"*. *PhD thesis*. Washington State University. 1990.

[477] Z. J. Wang. *"A Fast Nested Multi-grid Viscous Flow Solver for Adaptive Cartesian/Quad Grids"*. *International Journal for Numerical Methods in Fluids*. 33. 657–680. 2000.

[478] J. Warnatz. *"NOx Formation in High Temperature Processes"*. University of Stuttgart, Germany.

[479] G. P. Warren, W. K. Anderson, J. L. Thomas, and S. L. Krist. *"Grid convergence for adaptive methods"*. *Technical Report AIAA-91-1592*. AIAA10th Computational Fluid Dynamics Conference, Honolulu, HawaiiAmerican Institute of Aeronautics and Astronautics. June 1991.

[480] C. Weber. *"Zum Zerfall eines Flüssigkeitsstrahles"*. *ZAMM*. 11. 136–154. 1931.

[481] J. M. Weiss, J. P. Maruszewski, and W. A. Smith. *"Implicit Solution of the Navier-Stokes Equations on Unstructured Meshes"*. *Technical Report AIAA-97-2103*. 13th AIAA CFD Conference, Snowmass, COJuly 1997.

[482] J. M. Weiss, J. P. Maruszewski, and W. A. Smith. *"Implicit Solution of Preconditioned Navier-Stokes Equations Using Algebraic Multigrid"*. *AIAA Journal*. 37(1). 29–36. 1999.

[483] J. M. Weiss and W. A. Smith. *"Preconditioning Applied to Variable and Constant Density Flows"*. *AIAA Journal*. 33(11). 2050–2057. November 1995.

[484] C.-Y. Wen and Y. H. Yu. *"Mechanics of Fluidization"*. *Chem. Eng. Prog. Symp. Series*. 62. 100–111. 1966.

[485] Z. Wen, S. Yun, M. J. Thomson, and M. F. Lightstone. *"Modeling Soot Formation in Turbulent Kerosene/Air Jet Diffusion Flames"*. *Combustion and Flame*. 135. 323–340. 2003.

[486] H. Werner and H. Wengle. *"Large-Eddy Simulation of Turbulent Flow Over and Around a Cube in a Plate Channel"*. *In Eighth Symposium on Turbulent Shear Flows, Munich, Germany*. 1991.

*Release 15.0 - © SAS IP, Inc. All rights reserved. - Contains proprietary and confidential information of ANSYS, Inc. and its subsidiaries and affiliates.*

[487] C. Westbrook and F. Dryer. *"Chemical Kinetic Modelling of Hydrocarbon Combustion"*. *Prog. Energy Comb. Sci*. 1. 1984.

[488] A. A. Westenberg. *"Comb. Sci. Tech*. 4. 59. 1971.

[489] F. White and G. Christoph. *"A Simple New Analysis of Compressible Turbulent Skin Friction Under Arbitrary Conditions"*. *Technical Report AFFDL-TR-70-133*. February 1971.

[490] D. C. Wilcox. *Turbulence Modeling for CFD*. DCW Industries, Inc. La Canada, California. 1998.

[491] J. Wilcox. *"On the Path to Elucidating the Speciation of Mercury in the Flue Gases of Coal Combustion"*. *PhD thesis*. Dept. of Chemical and Environmental Engineering. The University of Arizona, Arizona, U.S.A. January 2004.

[492] J. Wilcox. *"A Kinetic Investigation of High-Temperature Mercury Oxidation by Chlorine"*. *Journal of Physical Chemistry A,*. 113(24). 6633–6639. 2009.

[493] J. Wilcox, D. C. J. Marsden, and P. Blowers. *"Evaluation of Basis Sets and Theoretical Methods for Estimating Rate Constants of Mercury Oxidation Reactions Involving Chlorine"*. *Fuel Processing Technology*. 85(5). 391–400. 2004.

[494] J. Wilcox, J. Robles, D. C. J. Marsden, and P. Blowers. *"Theoretically Predicted Rate Constants for Mercury Oxidation by Hydrogen Chloride in Coal Combustion Flue Gases"*. *Environmental Science and Technology*. 37(18). 4199–4204. September 2003.

[495] F. A. Williams. *Turbulent Mixing in Nonreactive and Reactive Flows*. Plenum Press, New York. 1975.

[496] F. Winter, C. Wartha, G. Loffler, and H. Hofbauer. *"The NO and* $N_2O$ *Formation Mechanism During Devolatilization and Char Combustion Under Fluidized Bed Conditions"*. *In 26th Symposium (Int'l) on Combustion*. The Combustion Institute. 3325–3334. 1996.

[497] M. Wolfshtein. *"The Velocity and Temperature Distribution of One-Dimensional Flow with Turbulence Augmentation and Pressure Gradient"*. *Int. J. Heat Mass Transfer*. 12. 301–318. 1969.

[498] P.-K. Wu, L.-K.Tseng, and G. M. Faeth. *"Primary Breakup in Gas/Liquid Mixing Layers for Turbulent Liquids"*. *Atomization and Sprays*. 2. 295–317. 1995.

[499] V. Yakhot and S. A. Orszag. *"Renormalization Group Analysis of Turbulence I Basic Theory"*. *Journal of Scientific Computing*. 1(1). 1–51. 1986.

[500] W. Yao and C. Morel. *"Volumetric Interfacial Area Prediction in Upward Bubbly Two-Phase Flow"*. *International Journal of Heat and Mass Transfer*. 47. 307-328. 2004.

[501] J. B. Young. *"The Spontaneous Condensation od Steam in Supersonic Nozzles"*. *Physico Chemical Hydrodynamics*. 3(2). 57–82. July 1982.

[502] J. B. Young. *"An Equation of State for Steam for Turbomachinery and Other Flow Calculations"*. *Journal of Engineering for Gas Turbines and Power*. 110. 1–7. January 1988.

[503] J. B. Young.. *"Two-Dimensional Nonequilibrium, Wet-Steam Calculations for Nozzles and Turbine Cascades"*. *Journal of Turbomachinery*. 114. 569–579. July 1992.

[504] D. L. Youngs. *"Time-Dependent Multi-Material Flow with Large Fluid Distortion"*. *Numerical Methods for Fluid Dynamics*. K. W. Morton and M. J. Baines, editors. Academic Press. 1982.

*Release 15.0 - © SAS IP, Inc. All rights reserved. - Contains proprietary and confidential information of ANSYS, Inc. and its subsidiaries and affiliates.*

[505] Q. Zhou and M. A. Leschziner. *"Technical report"*. *8th Turbulent Shear Flows Symp, Munich*. 1991.

[506] V. Zimont. *"Gas Premixed Combustion at High Turbulence. Turbulent Flame Closure Model Combustion Model"*. *Experimental Thermal and Fluid Science*. 21. 179–186. 2000.

[507] V. Zimont, W. Polifke, M. Bettelini, and W. Weisenstein. *"An Efficient Computational Model for Premixed Turbulent Combustion at High Reynolds Numbers Based on a Turbulent Flame Speed Closure"*. *J. of Gas Turbines Power*. 120. 526–532. 1998.

[508] V. L. Zimont, F. Biagioli, and K. J. Syed. *"Modelling Turbulent Premixed Combustion in the Intermediate Steady Propagation Regime"*. *Progress in Computational Fluid Dynamics*. 1(1). 14–28. 2001.

[509] V. L. Zimont and A. N. Lipatnikov. *"A Numerical Model of Premixed Turbulent Combustion of Gases"*. *Chem. Phys. Report*. 14(7). 993–1025. 1995.

[510] P. J. Zwart. *"Numerical Modelling of Free Surface and Cavitating Flows"*. *VKI Lecture Series*. 2005.

[511] P. J. Zwart, A. G. Gerber, and T. Belamri. *"A Two-Phase Flow Model for Predicting Cavitation Dynamics"*. *In Fifth International Conference on Multiphase Flow, Yokohama, Japan*. 2004.

[512] P. J. Zwart, P. G. Godin, J. Penrose, S. H. Rhee. *"Ship Hull Simulations with a Coupled Solution Algorithm"*. In Y. Nagano K. Hanjalic and M. J. Tummers, editors*Proceedings of the 10th International Symposium on Practical Designs of Ships and Other Floating Structures*. Houston, TX. 2007.

*Release 15.0 - © SAS IP, Inc. All rights reserved. - Contains proprietary and confidential information of ANSYS, Inc. and its subsidiaries and affiliates.*

Release 15.0 - © SAS IP, Inc. All rights reserved. - Contains proprietary and confidential information
of ANSYS, Inc. and its subsidiaries and affiliates.

# Index


## A

absolute velocity formulation, 21, 25
absorption coefficient, 141
  composition-dependent, 141, 170
  effect of particles on, 172
  effect of soot on, 172
  WSGGM, 170
accuracy
  diffusion terms, 632
  first-order, 633
  first-to-higher order, 635
  second-order, 634
acoustic signals, 362
acoustics model, 361
  acoustic analogy, 362
  boundary layer noise, 369
  broadband noise, 363, 366
  direct method, 361
  FW-H
    formulation, 363
  integral method, 362
  jet noise, 367
  Lilley's equation, 370
  linearized Euler equation, 369
  Proudman's formula, 366
  quadrupoles, 362
adaption, 687
  adaption registers, 709
  anisotropic, 703
  boundary, 689
  coarsening, 689
  dynamic gradient, 695
  geometry-based, 703
  gradient, 691
  hanging node, 687
  hybrid adaption, 709
  isovalue, 695
  marking, 687
  mask registers, 710
  process, 687
  refinement, 688
  region, 697
  volume, 699
  y+ and y*, 701
added mass effect, 538
aerodynamic noise, 361
algebraic multigrid (AMG), 632, 670, 676
  Laplace coarsening, 676
alloys
  solidification of, 601
alphanumeric reporting, 713
ammonia
  injection, 337
  production, 340
angular discretization, 153
angular momentum, 11
anisotropic
  adaption, 703
  diffusivity, 4
  thermal conductivity, 137
anisotropic scattering
  discrete ordinates radiation model, 156
  DO radiation model, 156
  P-1 model, 144
  Rosseland model, 147
area averaging, 28
area-weighted average, 716
Arrhenius
  reaction rate, 189
Arrhenius rate
  multiphase, 599
atomizer models, 425
  air-blast atomizer, 436
  effervescent atomizer, 438
  plain-orifice atomizer, 426
  pressure-swirl atomizer, 432
autoignition
  flamelet model for, 249-250
  model, 303
    ignition delay modeling, 306
    knock modeling, 305
    limitations, 304
automated grid refinement
  lookup tables, 230
automatic time step
  pseudo transient, 668
axisymmetric swirl flows, 9

## B

back diffusion
  Scheil, 606
beam width, 164
binning algorithm, 295
blending
  first-to-higher order, 635
body forces, 646
boiling, 390
  point, 393
  rate equation, 394
boiling model, 565
  critical heat flux, 568


*Release 15.0 - © SAS IP, Inc. All rights reserved. - Contains proprietary and confidential information of ANSYS, Inc. and its subsidiaries and affiliates.*

non-equilibrium subcooled, 568
RPI, 565
boundary adaption, 689
boundary conditions
discrete ordinates (DO) radiation model
opaque walls, 157
periodic boundaries, 167
specular walls, 167
symmetry boundaries, 167
low-pressure gas slip, 202
radiation
discrete ordinates (DO) model, 159-160, 167
P-1 model, 145-146
Rosseland model, 147
radiation model (DTRM), 150
species, 201
surface reaction, 201
turbulence, 90, 106
boundary layers, 689
Bounded Central Differencing Scheme, 636
bounded second order implicit
time stepping, 640
Boussinesq hypothesis, 42
breakup model
SSD model, 449
Brinkman number, 135
broadband noise, 366
Brownian force, 376
Brucato correlation, 528
bubble columns, 469
bubbly flow, 465, 467, 469
buoyancy
forces, 137
solutal, 608
thermal, 608
buoyancy-driven flows, 137
theory, 137
burnt mixture, 254


## C


capabilities, 1
capillary number, 484
Cartesian mesh
to bin cells, 295
cavitation model, 581, 583
additional guidelines, 588
Schnerr and Sauer, 587
Singhal et al., 583
Zwart-Gerber-Belamri, 586
cell
values, 632
volume
change, 695
center of pressure, 714
computing, 714
CFL condition, 663
CFX-RIF, 242
char, 328, 348
burnout, 404
characteristic strain rate, 240
chemical
database, 215
equilibrium, 274
chemical mechanism
dimension reduction, 296
chemical reaction, 136
equilibrium chemistry, 215, 220
non-equilibrium chemistry, 220, 244
laminar flamelet model, 238
steady diffusion flamelet model, 244
unsteady diffusion flamelet model, 246
non-premixed combustion model, 215
reversible, 191
chemical vapor
deposition, 199
chemistry
acceleration
cell agglomeration method, 293
dimension reduction method, 296
ISAT method, 289
agglomeration, 293
chemistry model
detailed, 358
CHEMKIN mechanism, 359
CICSAM, 479
circumferential average, 27
cloud tracking, 379
clustering, 149, 169
co-located scheme, 646
coal combustion, 405
char burnout, 404
devolatilization, 396
models for, 404
particle heating, 403
swelling, 403
coalescence
discrete phase, 452
coarsening, 689
coefficient of restitution, 527
collision model
discrete element method (DEM), 453
friction collision law, 456
spring collision law, 455
spring-dashpot collision law, 455



*Release 15.0 - © SAS IP, Inc. All rights reserved. - Contains proprietary and confidential information of ANSYS, Inc. and its subsidiaries and affiliates.*

combusting flow radiation models, 170
combustion
  applications, 4
  coal, 235, 396
  ECFM, 262
    with LES, 267
  equilibrium chemistry, 215
  finite-rate model, 189
  flamelet model
    theory, 239
  inert model, 237
  laminar flamelet model, 238
  liquid fuel, 235, 390
  non-equilibrium chemistry, 220
    laminar flamelet model, 238
    steady diffusion flamelet model, 244
    unsteady diffusion flamelet model, 246
  non-premixed, 215
  partially premixed, 273
  pollutant formation, 313
  premixed, 253
  steady diffusion flamelet model, 244
  unsteady diffusion flamelet model, 246
combustors
  gaseous, 247
COMET, 150
composition PDF transport
  Eulerian, 286
composition PDF transport model, 281
  IEM model, 284
  Modified Curl model, 284
  Monte Carlo method, 282
    Lagrangian method, 282
compressible flows, 12
  equations for, 14
  gas law equation, 14
  higher-order density interpolation, 648
  model usage of, 13
  physics of, 13
  turbulence modeling, 56, 61
compression-ignition engines, 249-250
compressive, 479
compressive scheme
  phase localized, 479
computing
  centers of pressure, 714
  forces and force coefficients, 714
  moments and moment coefficients, 714
conduction, 133, 136
conductive heat transfer
  energy equation, 133
  modeling, 133
  theory, 133
conjugate-gradient methods, 670
conservation equations, 2
  discretization of, 632
  in integral form, 645, 658
contact resistance in solidification and melting, 608
continuity equation, 2
continuous casting, 601, 607
continuum surface force, 482
continuum surface stress, 483
control volume technique, 625
convection in moving solids, 136
convective flux, 4
convective heat transfer
  energy equation, 133
  modeling, 133
  theory, 133
conventions used in this guide, xxix
convergence, 695, 699
  criteria, 626, 628
convergence acceleration
  stretched meshes, 665
coupled level-set
  theory, 498
coupled ordinates method, 150
Courant number, 663
CPD model, 398
crevice model, 308
  parameters, 309
  theory, 310
critical heat flux, 568
crossflow transition, 79
crystal growth, 601
curvature correction, 128
CVD, 199
  low-pressure gas slip, 202
cyclones, 83

## D

damping
  turbulence, 66
decoupled detailed chemistry model, 358
define/models/energy?, 135, 137
define/models/viscous/turbulence-expert/rke-cmu-rotation-term?, 53
Delta-Eddington scattering phase function, 156
dense discrete phase model
  granular temperature, 563
density
  for premixed turbulent combustion, 270
  interpolation schemes, 648
density-based solver, 628, 658

discretization, 663
explicit, 629
flux difference splitting, 661
flux vector splitting, 662
implicit, 629
implicit formulation
convergence acceleration, 665
preconditioning, 659
temporal discretization, 663
derivative evaluation, 641
detached eddy simulation (DES) model, 95
curvature correction, 128
with realizable k-epsilon, 96
with Spalart-Allmaras, 95
with SST k-omega, 97
with transition SST, 97
detailed chemistry pollutant model, 358
devolatilization models, 396
diesel
engines, 308
unsteady laminar flamelet model, 249-250
differentiable limiter, 645
diffuse semi-transparent walls, 163
diffusion
coefficient, 4, 188
flames, 215
species, 188
diffusion flame
stretching, 221
diffusion flamelet model
steady
non-adiabatic, 246
dimension reduction, 296
direct numerical simulation, 99
discrete element method (DEM)
collision model, 453
friction collision law, 456
spring collision law, 455
spring-dashpot collision law, 455
discrete ordinates (DO) radiation model, 138
advantages, 140
angular discretization, 153
anisotropic scattering, 156
boundary conditions
diffuse semi-transparent walls, 163
exterior semi-transparent walls, 164
flow inlets and exits, 167
gray-diffuse walls, 159
periodic boundaries, 167
semi-transparent walls, 160
solid semi-transparent media, 167
specular semi-transparent walls, 161
specular walls, 167
symmetry boundaries, 167
COMET, 150
coupled ordinates method, 150
energy coupling
limitations, 153
theory, 152
finite-volume scheme, 150
irradiation, 164
limitations, 140
non-gray, 151
angular discretization, 153
diffuse walls, 159
limitations, 140
particulate effects, 157
opaque walls, 157
particulate effects, 157
pixelation, 153
semi-transparent wall limitations, 166
theory, 150
discrete phase, 373
air-blast atomizer, 436
atomizer models, 425
boiling, 390
boiling point, 393
Brownian force, 376
cloud tracking, 379
coalescence, 452
collision model
discrete element method (DEM), 453
coupled calculations, 458-459, 462, 626, 628
devolatilization, 396
discrete element method (DEM)
collision model, 453
drag coefficient, 385
drag force, 374
droplet
collision model, 450
droplet breakup models, 439
dynamic drag model, 386
effervescent atomizer, 438
flat-fan atomizer, 437
heat transfer, 388, 459-460
high mach number, 386
injections, 425
latent heat, 393
lift force, 376
limitations of, 512
mass transfer, 392, 459, 461
moving reference frames, 375
multicomponent particles, 410
numerics, 382



*Release 15.0 - © SAS IP, Inc. All rights reserved. - Contains proprietary and confidential information of ANSYS, Inc. and its subsidiaries and affiliates.*

one-way, 458
particle cloud tracking, 379
Peng-Robinson real gas model, 410
plain-orifice atomizer, 426
pressure gradient force, 374
pressure-swirl atomizer, 432
primary breakup, 425
radiation heat transfer to, 389, 394, 408
Raoult's law, 410
secondary breakup models, 439
sources
node based averaging, 463
spray modeling
atomizers, 425
breakup, 439
droplet collision, 450
dynamic drag, 386
wall-film, 413
wall-jet, 412
stochastic tracking, 377
thermophoretic force, 375
time step, 460
trajectory calculations, 374
turbulent dispersion, 377, 379
two-way, 458
vapor pressure, 392
vaporization, 390
variables
node based averaging, 463
virtual mass force, 374
wall-film model, 413
wall-jet model, 412
discrete phase model
secondary breakup model
stochastic secondary droplet (SSD) model, 449
discrete random walk (DRW) model, 377-378
discrete transfer radiation model (DTRM), 138
advantages, 139
boundary conditions
inlets/outlets, 150
walls, 150
clustering, 149
limitations, 139
ray tracing, 148
theory, 148
discrete values
storage points for, 632
discretization, 632, 646
bounded central differencing scheme, 636
first-order scheme, 633
first-to-higher order blending, 635
frozen flux formulation, 655
iterative time advancement, 654
low diffusion second-order scheme, 662
modified HRIC scheme, 638
node vs. cell, 641
non-iterative time advancement, 654
power-law scheme, 633
QUICK scheme, 636
second-order scheme, 634
temporal, 639, 653, 663, 666
third-order MUSCL scheme, 637
discretization scheme
compressive, 479
zonal, 479
dispersion angle
atomizers, 425
effervescent atomizer, 438
flat-fan atomizer, 437
DNS, 99
donor-acceptor scheme, 478
DPM sources
node based averaging, 463
DPM variables
node based averaging, 463
drag coefficient, 714
discrete phase, 385
in Eulerian multiphase model, 469
drag modification, 528
Brucato correlation, 528
drift flux model, 503
drift velocity, 503
droplet
boiling, 394
devolatilization, 396
inert heating or cooling, 388
multicomponent, 408
surface combustion, 404
vaporization, 390
droplet breakup models, 439
KHRT breakup, 447
Rayleigh-Taylor breakup, 448
stochastic secondary droplet (SSD), 449
Taylor analogy breakup (TAB), 440
wave breakup, 444
droplet flow, 465, 467, 469
DRW model, 377-378
dual cell
heat rejection, 184
ntu relations, 184
restrictions, 183
dual time stepping, 640, 666
dynamic kinetic energy subgrid-scale model, 106
dynamic mesh model, 34

conservation equation, 35
six DOF solver, 36
theory, 34
dynamic meshes
crevice model, 308
dynamic Smagorinsky-Lilly subgrid-scale model, 101


## E


EDC model, 195
eddy-dissipation model, 193
effective density, 513
effective diffusivity modeling, 59, 63
effectiveness
heat exchangers, 179
effectiveness factor, 206
eight-step reduced mechanism, 346
ELES, 109
embedded large eddy simulation (ELES), 109
emissivity, 172
weighted-sum-of-gray-gases model (WSGGM), 170
energy
equation, 133
in solid regions, 136
sources, 136
due to radiation, 136
due to reaction, 136
interphase, 136
energy coupling, 152
energy equation
convection and conduction, 133
in solids, 136
engine ignition
auto, 303
spark, 299
engines
diesel, 249-250
enhanced wall treatment, 122, 124, 127
enthalpy
equation, 134
enthalpy-porosity method, 602
equilibrium chemistry, 215, 220
partial equilibrium, 220
equivalence ratio, 219
error reduction
rate, 678
using multigrid, 670
Euler
equations, 15
scheme, 382
Euler-Euler multiphase modeling, 468
Euler-Lagrange multiphase modeling, 373
Eulerian composition PDF transport, 286
Eulerian multiphase model, 469, 512
added mass effect, 538
boiling model, 565
critical heat flux, 568
non-equilibrium subcooled, 568
RPI, 565
bulk viscosity, 542
conservation equations, 513
exchange coefficients, 518
frictional viscosity, 542
granular temperature, 544
heat exchange coefficient, 546
constant-htc, 546
Gunn model, 547
Hughmark model, 547
Nusselt number, 546
Ranz-Marshall model, 546
Tomiyama model, 547
two-resistance model, 547
heat transfer, 545
interfacial area concentration, 517
Hibiki-Ishii model, 508
Ishii-Kim model, 509
Yao-Morel model, 510
interphase exchange coefficients
drag modification, 528
k-epsilon, 549
k-epsilon dispersed turbulence model, 550
k-epsilon per-phase turbulence model, 552
kinetic viscosity, 542
lift forces, 528
Legendre-Magnaudet model, 531
Moraga model, 530
Saffman-Mei model, 530
Tomiyama model, 531
limitations of, 512
mass transfer, 579
multi-fluid VOF model, 563
overview, 512
RSM turbulence models, 553
dispersed turbulence model, 554
mixture turbulence model, 555
solids pressure, 538
solids shear stresses, 541
theory, 511
turbulence in, 512, 548
turbulent dispersion, 534
turbulent dispersion force
Burns et al. model, 536
diffusion-in-vof model, 536
Lopez de Bertodano model, 535
Simonin model, 535



Release 15.0 - © SAS IP, Inc. All rights reserved. - Contains proprietary and confidential information of ANSYS, Inc. and its subsidiaries and affiliates.

virtual mass force, 538
volume fraction, 513
wall lubrication force, 532
Eulerian unsteady laminar flamelet model, 247
Eulerian wall film
boundary conditions, 618
conservation equations, 612
coupling with mixture species transport, 617
DPM collection, 613
film velocity, 618
model theory, 611
secondary phase accretion, 616
separation, 613
solution schemes, 620
algorithm, 623
spatial differencing, 622
temporal differencing, 620
splashing, 613
stripping, 615
sub-models, 613
evaporation, 390
evaporation-condensation model, 591
Lee model, 591
thermal phase change model, 594
explicit interpolation scheme, 476
explicit time stepping, 641, 666
exponential scheme, 382
extended coherent flamelet model (ECFM), 262
with LES, 267
exterior semi-transparent walls, 164
external radiation, 173

## F

F-cycle multigrid, 677
face flux, 647
FAS multigrid, 681
FGM
see also flamelet generated manifold, 278
see also flamelet model, 275
finite-rate reactions, 189
particle surface, 204
reacting channel model, 208
volumetric, 187
wall surface, 199
finite-volume scheme, 150, 632
first-order accuracy, 633
first-to-higher order blending, 635
flame
speed, 257
speed, Peters model, 260
stretching, 221, 259
flame front, 254
thickening, 257
flamelet generated manifold (FGM)
turbulent closure, 278
flamelet model, 220, 238
approaches
generation, 242
import, 242
assumptions, 238
CFX-RIF format files, 243
flamelet generated manifold (FGM), 275
diffusion, 277
premixed, 275
flamelet generation approach, 242
flamelet import approach, 242
multiple flamelet libraries, 245
multiple-flamelet import approach
CFX-RIF files, 243
OPPDIF files, 243
standard format files, 243
OPPDIF files, 243
predicting slow-forming product species, 246
restrictions, 238
scalar dissipation, 240
single-flamelet import approach
CFX-RIF files, 242
OPPDIF files, 242
standard format files, 242
standard format files, 242-243
steady diffusion, 244
assumptions and limitations, 244
automated grid refinement, 245
introduction, 244
strain rate, 240
theory, 239
unsteady diffusion, 246
unsteady laminar
diesel, 249-250
Eulerian, 247
flames
slow-chemistry, 244
flexible-cycle multigrid, 678
flow rate, 716
flue gas recycle
non-premixed model with, 236
fluid flow
compressible, 12
equations
continuity and momentum, 2
mass conservation, 2
momentum conservation, 3
UDS transport, 4
inviscid, 15

*Release 15.0 - © SAS IP, Inc. All rights reserved. - Contains proprietary and confidential information of ANSYS, Inc. and its subsidiaries and affiliates.*

overview, 1
periodic, 6
physical models of, 1
swirling and rotating, 8
fluid-fluid multiphase flows, 516
fluidized beds, 466-467, 469
flux
reports, 713
through boundaries, 713
flux-difference splitting, 661
flux-vector splitting, 662
FMG multigrid, 685
limitations, 686
forces
coefficients of, 714
computing, 714
on boundaries, 714
Fractional Step algorithm
non-iterative scheme (NITA), 656
free vortex, 11
free-surface flow, 465, 467, 469
freezing, 601
friction collision law
discrete element method (DEM), 456
frictional viscosity, 542
frozen flux formulation, 655
fuel rich flames, 220
full multigrid (FMG), 685
limitations, 686
full-approximation storage (FAS) multigrid, 670, 681
fully-developed flow, 6
FW-H acoustics model, 363

## G

gaseous combustors, 247
gaseous solid catalyzed reactions, 208
Gauss-Seidel method, 670
Gauss-Seidel smoother, 680
gaussian, 463
geometric reconstruction scheme, 478
geometry-based adaption, 703
Gidaspow model, 524
global time stepping, 641
glossary, 725
governing equations, 2
discretization of, 632
in integral form, 645, 658
Grace et al. model, 518
gradient adaption, 691
dynamic, 695
gradient limiters, 644
differentiable limiter, 645
multidimensional limiter, 645
standard limiter, 645
gradient option, 641
granular flows, 468-469, 516
stresses in, 516
granular temperature, 506, 544
Grashof number, 137
gravitational acceleration, 374
gray-band model
discrete ordinates (DO) radiation model, 151
P-1 radiation model, 143
boundary conditions, 145
gray-diffuse
model, 167
walls, 159
Green-Gauss cell-based, 642
Green-Gauss node-based, 642

## H

hanging node adaption, 687
hanging nodes, 687
heat exchanger groups, 175, 182
heat exchanger models, 175
dual cell
heat rejection, 184
ntu relations, 184
restrictions, 183
effectiveness, 179
group connectivity, 182
heat rejection, 180
ntu-model, 175
features, 177
restrictions, 176
restrictions, 176, 183
simple-effectiveness-model, 175
features, 177
restrictions, 176
heat flux, 713
critical, 568
heat rejection, 180, 184
dual cell, 184
heat exchangers, 180
heat sources, 136
heat transfer, 133
buoyancy-driven flows, 137
convective and conductive, 133
theory, 133
modeling, 133
natural convection flows, 137
overview of models, 133
radiation, 138
radiative theory, 141


Release 15.0 - © SAS IP, Inc. All rights reserved. - Contains proprietary and confidential information of ANSYS, Inc. and its subsidiaries and affiliates.

heterogeneous reactions
multiphase, 599
source terms, 597
Hibiki-Ishii model
interfacial area concentration, 508
high mach number
discrete phase, 386
high order term relaxation, 639
HNCO production, 340
hybrid
initialization, 683
hydrotransport, 466-467, 469

## I

IDDES, 98
ignition
delay modeling, 306
spark model, 299
species transport equation, 304
ILU
method, 670
smoother, 680
impeller-baffle interaction, 22
impellers
multiple, 23
implicit Euler scheme, 382
implicit formulation
convergence acceleration
stretched meshes, 665
implicit interpolation scheme, 476
implicit time stepping, 640, 666
improved delayed detached eddy simulation (IDDES), 98
in-cylinder model
crevice model
theory, 310
inert model
combustion, 237
initialization
hybrid, 683
integral reporting, 716, 721
integral time scale, 377
interfacial area concentration, 507, 517
Hibiki-Ishii model, 508
Ishii-Kim model, 509
Yao-Morel model, 510
intermittency transition model, 79
rough walls, 82
interphase exchange coefficients, 518
drag modification, 528
interpolation, 632, 646
inverse-distance, 463
inviscid flows, 15
continuity equation, 15
energy equation, 16
equations, 15
momentum equation, 16
irradiation, 164
ISAT, 289
algorithm, 193
chemistry agglomeration, 293
dimension reduction, 296
Ishii model, 518
Ishii-Kim model
interfacial area concentration, 509
isotropic diffusivity, 4
isovalue
adaption, 695
iterative procedure, 628
iterative time advancement, 654

## J

jet breakup, 468, 474
jump
adhesion, 485

## K

k-epsilon model, 46
curvature correction, 128
realizable, 51
with DES, 96
RNG, 48
standard, 47
k-kl-omega model, 67
k-omega model
curvature correction, 128
SST, 62
with DES, 97
standard, 58
KHRT breakup model, 447
liquid core length, 447
kinetic theory
in granular flows, 468
knock modeling, 305
Knudsen number, 202, 375
Kobayashi model, 398

## L

Lagrangian method, 282
laminar finite-rate model, 189
Laplace coarsening, 676
large eddy simulation (LES), 99
boundary conditions, 106
no perturbations, 106

Release 15.0 - © SAS IP, Inc. All rights reserved. - Contains proprietary and confidential information of ANSYS, Inc. and its subsidiaries and affiliates.

spectral synthesizer, 108
subgrid-scale models, 100
dynamic kinetic energy model, 106
dynamic Smagorinsky-Lilly model, 101
Smagorinsky-Lilly model, 101
WALE model, 102
wall-modeled LES model, 103
wall-modeled LES S-omega model, 105
vortex method, 106
latent heat, 393
Lavieville et al model, 547
least squares cell-based, 643
Lee model, 591
Legendre-Magnaudet lift model, 531
LES, 99
Lewis number, 188
lift coefficient, 714
lift force, 376
in multiphase flow, 528
Legendre-Magnaudet model, 531
Moraga model, 530
Saffman-Mei model, 530
Tomiyama model, 531
limiter, 644
line solvers, 670
linear pressure-strain model, 85
linear-anisotropic scattering phase function, 144, 147, 156
liquid fraction, 602
liquid fuel combustion, 390
liquid reactions, 285
liquid reactors, 247, 249
lookup tables
generating
automated grid refinement, 230
Low Diffusion Second-Order scheme, 662
low-pressure gas system
slip boundary formulation, 202
low-Re stress-omega, 87
low-Reynolds number flows, 49

## M

Mach number, 13
macro heat exchanger models, 175
mass
average, 716
averaging, 28
diffusion, 188
flux, 713
transfer, 579
mass and momentum transfer, 596
mass flow rate, 4, 716
through a surface, 718
mass-averaged quantities, 718, 723
Maxwell-Stefan equation, 188
Maxwell's models, 202
mean
beam length, 170
free path, 202, 375
mean reaction rate
NOx, 342
soot, 358
SOx, 350
mesh
adaption, 687
coarsening, 689
near walls, 701
interfaces, 37
motion of, 17, 34
moving reference frame, 17
refinement, 688
at boundaries, 689
based on cell volume, 699
based on gradient, 691
based on isovalue, 695
dynamic, 695
in a region, 697
near walls, 701
spacing at walls
in turbulent flows, 701
storage points, 632
metallurgy, 601
mixed convection, 137
mixed-out averaging, 29
mixing plane, 17
mixing plane model, 24-25
area averaging, 28
mass averaging, 28
mass conservation, 30
mixed-out averaging, 29
swirl conservation, 30
theory, 26
total enthalpy conservation, 31
mixing tanks, 23
mixture diffusivity, 5
mixture fraction, 216
conservation of, 218
limitations on, 232
variance, 218
mixture multiphase model, 469
cavitation model, 581
collisional viscosity, 505
drift flux model, 503
drift velocity, 503


Release 15.0 - © SAS IP, Inc. All rights reserved. - Contains proprietary and confidential information of ANSYS, Inc. and its subsidiaries and affiliates.

evaporation-condensation model, 591
granular temperature, 506
interfacial area concentration, 507
Hibiki-Ishii model, 508
Ishii-Kim model, 509
Yao-Morel model, 510
kinetic viscosity, 505
limitations, 501
mass transfer, 579
momentum equation, 502
overview, 501
relative velocity, 503
slip velocity, 503
solids shear stresses, 505
theory, 500
volume fraction, 505
modified HRIC scheme, 638
moments
coefficients of, 714
computing, 714
reporting, 714
momentum equation, 3
Monte Carlo method, 282
Moraga lift model, 530
Morsi and Alexander model, 518
Moss-Brookes soot formation model
theory, 354
turbulence-chemistry interaction, 357
Moss-Brookes-Hall soot formation model
theory, 356
turbulence-chemistry interaction, 357
moving mesh, 17
moving reference frame, 17, 22
discrete phase, 375
mathematical equations, 19
multi-fluid VOF model, 563
multi-stage scheme, 663
multicomponent droplet, 408
Raoult's Law, 410
multicomponent particle
Raoult's Law, 410
multicomponent particles, 408, 410
multidimensional limiter, 645
multigrid solver, 670
algebraic (AMG), 676
cycles, 672
F cycle, 677
flexible cycle, 678
full (FMG), 685
limitations, 686
full-approximation storage (FAS), 681
prolongation, 671
residual reduction rate, 678
restriction, 671
termination criteria, 679
V cycle, 672, 674
W cycle, 672, 674
multiphase flows, 565
boiling model
critical heat flux, 568
non-equilibrium subcooled, 568
RPI, 565
cavitation model, 581, 583, 586-587
choosing a model for, 468
Euler-Euler approach, 468
Euler-Lagrange approach, 373
Eulerian model, 469, 511-512
evaporation-condensation model, 591
Lee model, 591
thermal phase change model, 594
examples, 467
fluid-fluid, 516
fluid-solid, 516
gas-liquid, 465
gas-solid, 466
granular, 516
homogeneous, 503
interphase exchange coefficients, 518
liquid-liquid, 465
liquid-solid, 466
mixture model, 469, 500-501
multi-fluid VOF model, 563
particulate loading, 470
regimes, 465
second-order time scheme, 472
Stokes number, 471
volume of fluid (VOF) model, 468, 474
wet steam model, 573
properties, 577
restrictions, 574
multiphase species transport, 595
Arrhenius rate, 599
heterogeneous reaction, 599
heterogeneous reactions, 597
limitations, 596
momentum transfer, 596
stiff chemistry, 599
multiple reference frame, 22
restrictions of, 22
steady flow approximation, 22
theory of, 24
multiple surface reactions model, 407
mushy zone, 602-603

*Release 15.0 - © SAS IP, Inc. All rights reserved. - Contains proprietary and confidential information of ANSYS, Inc. and its subsidiaries and affiliates.*

## N

natural convection, 137, 646
Navier-Stokes equations, 2
  filtered, 40
near-wall flows, 49
near-wall treatments, 112
neighbor correction, 651
node based averaging, 463
  kernels, 463
    gaussian, 463
    inverse-distance, 463
    nodes-per-cell, 463
    shortest-distance, 463
node values, 632
nodes-per-cell, 463
noise, 362
nomenclature, 725
non-equilibrium chemistry, 220
  laminar flamelet model, 238
  steady diffusion flamelet model, 244
  unsteady diffusion flamelet model, 246
non-equilibrium subcooled boiling, 568
non-equilibrium wall functions, 120
non-gray discrete ordinates (DO) radiation model, 151
  angular discretization, 153
  diffuse walls, 159
  limitations, 140
  particulate effects, 157
  pixelation, 153
non-gray P-1 radiation model, 143
  boundary conditions, 145
  limitations, 139
non-gray radiation, 172
  discrete ordinates (DO) radiation model, 151
    boundary conditions, 159
    limitations, 140
    particulate effects, 157
  P-1 radiation model, 143
    boundary conditions, 145
    limitations, 139
non-iterative time advancement (NITA), 654
non-premixed combustion model, 215
  enthalpy equation, 134
  equilibrium chemistry, 215, 220
  flamelet model
    theory, 239
  flue gas recycle, 236
  laminar flamelet model, 238
  limitations of, 232
  look-up tables, 224-225, 227
  multiple fuel inlets, 225, 232
  non-adiabatic form, 224
  non-equilibrium chemistry, 220
    laminar flamelet model, 238
    steady diffusion flamelet model, 244
    unsteady diffusion flamelet model, 246
  PDF functions in, 222
  rich flammability limit, 221
  steady diffusion flamelet model, 244
  unsteady diffusion flamelet model, 246
NOx, 244
  reduction, 336
    ammonia, 337
    urea, 338
NOx model, 313
  coal, 327
  formation, 314
  fuel, 321
  liquid fuel, 322
  PDF functions in, 341
  prompt, 318
  reburn, 333
  selective noncatalytic reduction (SNCR), 336
  thermal, 315
  turbulence-chemistry interaction, 341
ntu relations, 184
ntu-model, 175
  features, 177
  restrictions, 176
nuclei formation, 353
numerical beach
  open channel, 488
  open channel wave boundary condition, 488
numerical scheme, 625

## O

O radical concentration, 316
OH radical concentration, 317
one-step soot formation model
  theory, 351
opaque walls, 157
open channel boundary condition, 485
open channel flow, 485
  downstream boundary condition, 487
  mass flow rate, 487
  upstream boundary condition, 486
  wave boundary condition, 489
Operating Conditions dialog box, 374
OPPDIF, 242
opposed-flow diffusion flamelet, 239
optical thickness, 172

## P

P-1 radiation model, 138


Release 15.0 - © SAS IP, Inc. All rights reserved. - Contains proprietary and confidential information of ANSYS, Inc. and its subsidiaries and affiliates.

advantages, 139
anisotropic scattering, 144
boundary conditions
inlets/outlets, 146
walls, 145
limitations, 139
non-gray, 143
boundary conditions, 145
limitations, 139
particulate effects in, 144
theory, 142
parameterized Syamlal-O'Brien model, 524
partially premixed combustion model, 273
chemical equilibrium, 274
FGM turbulent closure, 278
flamelet generated manifold (FGM), 275
diffusion, 277
premixed, 275
limitations of, 273
overview, 273
steady diffusion flamelet model, 274
theory, 274
unburnt properties
calculation of, 279
partially premixed flames, 253-254, 273
partially specular boundaries, 172
particle
boiling, 394
cloud tracking, 379
coupling, 458
devolatilization, 396
dispersion prediction, 377
erosion, 424
inert heating or cooling, 388
laws, 387
motion, 374
multicomponent particles, 408, 410
radiation, 389, 394
splashing, 416
sub-micron, 376, 386
surface combustion, 404
trajectory calculations, 374
turbulent dispersion, 377
vaporization, 390
particle surface reactions, 204
gaseous solid catalyzed reactions, 208
solid decomposition reactions, 207
solid deposition reactions, 207
solid-solid reactions, 207
theory, 204
particle-laden flow, 466-467, 469
particulate
loading, 470
particulate effects
absorption coefficient, 172
DO model, 157
P-1 radiation model, 144
radiation, 172
PDF reaction, 285
Peclet number, 633
Peng-Robinson real gas model, 410
periodic flows, 6
limitations, 7
overview, 6
pressure, 8
theory, 7
Peters flame speed model, 260
phase, 465
phase localized compressive scheme, 479
PISO algorithm, 650
neighbor correction, 651
non-iterative scheme (NITA), 656
skewness correction, 651
skewness-neighbor coupling, 651
pixelation, 153
plasma-enhanced surface reaction modeling, 4
pneumatic transport, 466-467, 469
pollutant formation, 313
decoupled detailed chemistry model, 358
NOx, 313
soot, 350
SOx, 344-345
postprocessing
pollutants, 358
reports, 713
power-law scheme, 633
Prandtl numbers
calculating inverse effective, 50
preconditioning, 659
matrix, 659
premixed combustion model
G-equation, 255
premixed flames, 253
premixed model
G-equation
Peters, 260
premixed turbulent combustion, 253
adiabatic, 270
C-Equation
theory, 254
density, 270
flame front, 254
wrinkling, 257
flame speed, 257

*Release 15.0 - © SAS IP, Inc. All rights reserved. - Contains proprietary and confidential information of ANSYS, Inc. and its subsidiaries and affiliates.*

flame stretching, 259
non-adiabatic, 270
product formation, 254
progress variable, 254
restrictions, 254
stretch factor, 259
wall damping, 260
pressure
drop
heat exchanger, 178
gradient force, 374
interpolation schemes, 646
work, 135
pressure-based coupled algorithm, 651
pressure-based solver, 626, 645
density interpolation schemes, 648
discretization, 646
frozen flux formulation, 655
iterative time advancement, 654
non-iterative time advancement (NITA), 654
pressure interpolation schemes, 646
pressure-velocity coupling, 649
steady-state flows, 653
time-dependent flows, 653
pressure-correction equation, 649
pressure-velocity coupling, 649
coupled algorithm, 651
PRESTO!, 646
primary breakup, 425
probability density function (PDF), 221
product formation, 254
slowly forming, 221, 246
production of
ammonia, 340
HNCO, 340
urea, 340
progress variable, 254
prolongation, 671
properties
database, 215
Proudman's formula, 366
pseudo transient
time step
automatic, 668
under-relaxation, 667
pull velocity, 603, 607


## Q


quadratic pressure-strain model, 86
quadrupoles, 362
QUICK scheme, 636


## R


radiation
DO/energy coupling
limitations, 153
theory, 152
radiation heat flux, 713
radiation models, 138
combusting flows, 170
discrete ordinates (DO), 140
discrete transfer radiation model (DTRM), 139, 148
P-1, 139
Rosseland, 140
S2S, 140
solar load, 138
surface-to-surface (S2S), 140
theory, 141
radiative heat transfer, 138
applications, 138
choosing a model, 172
discrete ordinates (DO) model, 150
discrete transfer radiation model (DTRM), 148
emissivity, 172
external radiation, 173
modeling, 138
non-gray, 172
discrete ordinates (DO) model, 140, 151
P-1 model, 139, 143, 145
optical thickness, 172
P-1 model, 142
particulate effects, 172
radiative transfer equation (RTE), 141
Rosseland model, 146
scattering, 172
semi-transparent media, 160
semi-transparent walls, 172
soot effects on, 172
surface-to-surface (S2S) radiation model, 167
theory, 141
radiative transfer equation, 141
radiosity, 169
RANS-LES
hybrid formulations, 41
Raoult's law, 410
ray tracing, 148
Rayleigh number, 137
reacting channel model, 208
flow inside, 209
outer flow in the shell, 211
surface reactions, 210-211
reacting flows, 187
equilibrium chemistry, 215
heterogeneous reactions, 404



*Release 15.0 - © SAS IP, Inc. All rights reserved. - Contains proprietary and confidential information of ANSYS, Inc. and its subsidiaries and affiliates.*

non-premixed combustion model, 215
partially premixed combustion, 273
pollutant formation in, 313
premixed combustion, 253
reaction progress variable, 254
reaction rate
surface reactions, 199
reactions
liquid, 285
pressure-dependent, 192
reversible, 191
reactor network model, 212
reactors
liquid, 247, 249
realizable k-epsilon model, 51
limitation, 51
with DES, 96
reburning, 333
reference frame
multiple, 22-23
reference pressure, 715
reference values
for force and moment coefficient reports, 714
refinement, 688
refractive index, 141
region adaption, 697
registers, 709
adaption, 709
mask, 710
types, 709
relative velocity, 25
for mixture model, 503
relative velocity formulation, 20, 24
relax to chemical equilibrium model, 198
relaxation scheme, 670, 674
relaxation sweeps, 674
renormalization group (RNG) theory, 48
reporting
center of pressure, 714
data, 713
drag coefficients, 714
fluxes through boundaries, 713
forces, 714
heat flux, 713
lift coefficients, 714
mass flux, 713
moments and moment coefficients, 714
radiation heat flux, 713
surface integrals, 716
volume integrals, 721
residual
reduction rate criteria, 678-679
smoothing, 664
restriction, 671
reversible reactions, 191
Reynolds
averaging, 39
number, 137, 713
stresses, 42
Reynolds stress model (RSM), 83
boundary conditions, 90
linear pressure-strain model, 85
low-Re stress-omega, 87
pressure-strain term in, 85
quadratic pressure-strain model, 86
Reynolds-averaged Navier-Stokes (RANS) equations, 39
rich flammability limit option, 221
rich limit, 220
risers, 469
RNG k-epsilon model, 48
swirl modification, 50
Rosseland radiation model, 138
advantages, 140
anisotropic scattering, 147
boundary conditions
inlets/outlets, 147
walls, 147
limitations, 140
theory, 146
rotating flows, 8-9
moving reference frame, 11
multiple reference frame, 23
overview, 9
physics of, 11
three-dimensional, 10
turbulence modeling in, 51, 83
RPI boiling model, 565
RSM, 83
RTE, 141
RUN-1DL, 242
Runge Kutta, 382

## S

S2S radiation model
advantages, 140
clustering, 169
equations, 168
gray-diffuse model, 167
limitations, 140
theory, 167
Saffman-Mei lift model, 530
Saffman's lift force, 376
Sato model
turbulence interaction, 556

*Release 15.0 - © SAS IP, Inc. All rights reserved. - Contains proprietary and confidential information of ANSYS, Inc. and its subsidiaries and affiliates.*

scalable wall functions, 119
scalar
  dissipation, 240
  transport equations, 4
scale-adaptive simulation (SAS) model, 92
  curvature correction, 128
scattering, 172
  phase function
    Delta-Eddington, 156
    linear-anisotropic, 144, 147, 156
    user-defined, 156
Schiller and Naumann model, 518
Schmidt number, 188
Schnerr and Sauer
  cavitation model, 587
second-order accuracy, 634
secondary breakup
  discrete phase, 439
secondary mixture fraction, 216
sedimentation, 466-467, 469
segregated algorithm, 626
segregated solver
  density interpolation schemes, 648
  frozen flux formulation, 655
  pressure interpolation schemes, 646
selective noncatalytic reduction (SNCR), 336
  ammonia injection, 337
  urea injection, 338
semi-transparent
  interior walls, 160
  media, 160
  walls, 172
sensible enthalpy, 133
sequential solution, 626
seven-step reduced mechanism, 338
shell conduction
  DO/energy coupling, 153
shock waves, 693
shortest-distance, 463
Simonin et al. model
  turbulence interaction, 556
SIMPLE algorithm, 649
simple-effectiveness-model, 175
  features, 177
  restrictions, 176
SIMPLEC algorithm, 650
  skewness correction, 650
Singhal et al.
  cavitation model, 583
single reference frame, 17
site species, 201
six DOF solver, 34
skewness
  correction, 650-651
skewness-neighbor coupling, 651
sliding mesh model, 33
  initial conditions for, 22
sliding meshes
  theory, 37
slip boundary
  condition at walls, 147
  formulation, 202
slip regime, 202
slip velocity, 503
slope limiter, 644
sloshing, 468
slow-chemistry flames, 244
slug flow, 465, 467, 469
slurry flow, 466-467, 469
Smagorinsky-Lilly subgrid-scale model, 101
smoother
  Gauss-Seidel, 680
  ILU, 680
smoothing
  residuals, 664
solid
  deposition reactions, 207
  species, 201
solid decomposition
  reactions, 207
solid zone
  convection in a moving, 136
solid-solid reactions, 207
solidification and melting, 601
  back diffusion, 606
  limitations, 602
  overview, 601
  theory, 602
solids pressure, 538
  radial distribution function, 539
solutal buoyancy, 608
solution, 625
  accuracy, 632
  numerical scheme, 625
  process, 625
  under-relaxation, 653
solver, 625
  density-based, 628, 658
    explicit, 629
    implicit, 629
  differentiable limiter, 645
  discretization, 632
  gradient limiters, 644
    differentiable limiter, 645


Release 15.0 - © SAS IP, Inc. All rights reserved. - Contains proprietary and confidential information of ANSYS, Inc. and its subsidiaries and affiliates.

multidimensional limiter, 645
standard limiter, 645
Green-Gauss cell-based, 642
Green-Gauss node-based, 642
least squares cell-based, 643
linearization
explicit, 629
implicit, 629
multi-stage scheme, 663
multidimensional limiter, 645
multigrid, 632, 670
algebraic (AMG), 670, 676
full (FMG), 685
full (FMG) limitations on, 686
full-approximation storage (FAS), 670, 681
node vs. cell discretization, 641
numerical scheme, 625
overview of, 625
pressure-based, 626, 645
standard limiter, 645
soot model, 350
Moss-Brookes, 354
turbulence-chemistry interaction, 357
Moss-Brookes-Hall, 356
turbulence-chemistry interaction, 357
one-step, 351
radiation effects, 172
restrictions, 351
theory, 351
two-step, 352
source terms
heterogeneous reactions, 597
SOx model, 344
coal, 348
formation, 344-345
gaseous fuel, 348
liquid fuel, 348
PDF functions in, 349
turbulence-chemistry interaction, 349
Spalart-Allmaras model, 42
curvature correction, 128
with DES, 95
spark model, 299
limitations, 299
overview, 299
species
diffusion, 135, 188
slow-forming product, 221
sources, 199
transport equation, 187
species diffusion terms, 135
species transport
multiphase, 595
heterogeneous reactions, 597
limitations, 596
momentum transfer, 596
specular
boundaries, 172
specular semi-transparent walls, 161
specular walls, 172
splashing, 416
spray modeling
atomizers, 425
breakup, 439
droplet collision, 450
dynamic drag, 386
wall-film, 413
wall-jet, 412
spring collision law
discrete element method (DEM), 455
spring-dashpot collision law
discrete element method (DEM), 455
SSD model, 449
SST k-omega model, 62
with DES, 97
SST transition model
with DES, 97
stability, 653
stagnation pressure, 13
stagnation temperature, 13
standard deviation, 716
on a surface, 719
standard k-epsilon model, 47
weaknesses, 51
standard k-omega model, 58
standard limiter, 645
standard wall functions vs. non-equilibrium wall functions, 121
steady diffusion flamelet model, 244, 274
assumptions and limitations, 244
introduction, 244
non-adiabatic, 246
stiff chemistry
multiphase, 599
stochastic
particle tracking, 377
secondary droplet model, 449
stoichiometric ratio, 219
Stokes number, 471
Stokes-Cunningham law, 386
strain rate, 240
stratified flow, 465, 467-469
streamwise-periodic flow, 6
stretch factor, 259

*Release 15.0 - © SAS IP, Inc. All rights reserved. - Contains proprietary and confidential information of ANSYS, Inc. and its subsidiaries and affiliates.*

stretched meshes
convergence acceleration, 665
sub-micron particles, 376, 386
subgrid-scale models, 100
dynamic kinetic energy model, 106
dynamic Smagorinsky-Lilly model, 101
Smagorinsky-Lilly model, 101
WALE model, 102
wall-modeled LES model, 103
S-omega, 105
subsonic, 13
supersonic, 13
surface coverage reaction
rate modification, 201
surface deposition, 201
surface integrals, 716
area, 717
area-weighted average, 718
computing, 717
facet field variables, 719
facet maximum, 719
facet minimum, 719
field variable sum, 718
flow rate, 718
integral, 718
mass flow rate, 718
mass-weighted average, 718
standard deviation, 719
uniformity index, 720
vertex field variables, 719
vertex maximum, 719
vertex minimum, 719
volume flow rate, 720
surface integration, 716
surface tension, 481
continuum surface force, 482
continuum surface stress, 483
surface-to-surface (S2S) radiation model, 138
advantages, 140
clustering, 169
equations, 168
gray-diffuse model, 167
limitations, 140
theory, 167
surfaces
computing integrals, 717
swelling
coefficient, 403
swirl
axisymmetric flow modeling, 9
swirl velocity, 10
swirling flows, 8-9, 646
moving reference frame, 11
overview, 9
physics of, 11
swirl velocity, 10
three-dimensional, 10
turbulence modeling in, 48, 50-51, 83
Syamlal-O'Brien model, 524
symmetric model, 518

## T

TAB model, 440
Taylor analogy breakup (TAB) model, 440
Taylor-Foster approximation, 172
temporal discretization, 653, 663, 666
solver, 639
termination criteria, 679
TFM, 196
thermal buoyancy, 608
thermal conductivity
anisotropic, 137
thermal mixing, 133
thermal phase change model, 594
thermophoretic force, 375
thickened flame model (TFM), 196
third-body efficiencies, 190
third-order MUSCL scheme, 637
time advancement schemes, 654
time step, 666
discrete phase, 460
time stepping
bounded second order implicit, 640
dual, 640, 666
explicit, 641, 666
global, 641
implicit, 640, 666
Tomiyama lift model, 518, 531
torque, 715
total pressure, 13
total temperature, 13
trajectory calculations, 374
transition SST model, 71
with DES, 97
translating
reference frame, 22
transonic, 13
transport equation
coupling SST transport and intermittency transition model, 82
coupling SST transport and transition model, 74
ignition species, 304
intermittency transition model, 80
k-kl-omega model, 67


Release 15.0 - © SAS IP, Inc. All rights reserved. - Contains proprietary and confidential information of ANSYS, Inc. and its subsidiaries and affiliates.

realizable k-epsilon model, 52
Reynolds stress model, 83
RNG k-epsilon model, 48
SAS model
with omega-based turbulence models, 94
with SST k-omega, 93
species, 187
SST k-omega model, 63
standard k-epsilon model, 47
standard k-omega model, 58
transition SST model, 71
transport equations
user-defined scalar, 4
trapezoidal Euler scheme, 382
Troshko-Hassan model
turbulence interaction, 556
turbulence, 39
buoyancy effects, 55, 89
compressibility effects, 56, 61
crossflow transition, 79
damping, 66
DES model, 95
with realizable k-epsilon, 96
with Spalart-Allmaras, 95
with SST k-omega, 97
with transition SST, 97
discrete phase interaction, 377
dissipation modeling, 60, 65
dissipation rate modeling, 90
embedded large eddy simulation (ELES), 109
enhanced wall treatment, 122, 124, 127
improved delayed detached eddy simulation (IDDES), 98
intermittency transition model, 79
rough walls, 82
k-epsilon model, 46
realizable, 51, 96
RNG, 48
standard, 47
k-kl-omega model
transition, 67
k-kl-omega transition model, 67
k-omega model
SST, 62, 97
standard, 58
kinetic energy modeling, 84
large eddy simulation (LES), 99
mesh considerations for, 701
modeling, 39, 42
in multiphase flows, 512
near-wall treatments, 112
no perturbations, 106
principles, 39
production, 44, 54, 60
realizable k-epsilon model, 51
with DES, 96
Reynolds stress model (RSM), 83
RNG k-epsilon model, 48
SAS model, 92
Spalart-Allmaras model, 42
with DES, 95
spectral synthesizer, 108
SST k-omega model, 62
with DES, 97
SST transition model, 71
with DES, 97
standard k-epsilon model, 47
standard k-omega model, 58
two-layer model, 113, 122
V2F model, 82
vortex method, 106
wall functions, 113, 115
limitations of, 121
non-equilibrium, 120
scalable, 119
standard, 115
turbulence interaction
Eulerian multiphase
Sato model, 556
Simonin et al. model, 556
Troshko-Hassan model, 556
turbulence production
modeling, 64
turbulence-chemistry interaction, 193, 215, 221, 341
NOx, 341
soot, 357
SOx, 349
turbulent destruction
modeling, 45
turbulent dispersion, 534
turbulent dispersion force
Burns et al. model, 536
diffusion-in-vof model, 536
Lopez de Bertodano model, 535
Simonin model, 535
turbulent flow
mass diffusion, 188
turbulent production
modeling, 44
turbulent viscosity
in RSM, 90
in the k-epsilon model, 47
modeling in realizable k-epsilon model, 43
modeling in the realizable k-epsilon model, 53

*Release 15.0 - © SAS IP, Inc. All rights reserved. - Contains proprietary and confidential information of ANSYS, Inc. and its subsidiaries and affiliates.*

modeling in the RNG k-epsilon model, 49
two-layer model, 113, 122
two-step soot formation model
theory, 352

## U

UDS
isotropic diffusivity, 4
UDS transport equations, 4
about, 4
anisotropic diffusivity, 4
diffusion coefficient, 4
multiphase flows, 5
multiphase mass flux, 5
single phase flow, 4
unburnt mixture, 254
unburnt properties, 279
under-relaxation, 653
discrete phase, 461
pseudo transient, 667
uniformity index, 716, 720
universal drag laws for bubble-liquid and droplet-gas flows , 518
unsteady diffusion flamelet model, 246
unsteady laminar flamelet model
diesel approach, 249-250
Eulerian approach, 247
upwind schemes, 632
first-order, 633
second-order, 634
urea
injection, 338
production, 340
seven-step reduced mechanism, 338
user-defined functions (UDFs)
in multiphase models, 469
user-defined mass flux, 4
user-defined scalar (UDS) equations, 4
user-defined scalars
theory
multiphase flow, 5
single phase flow, 4

## V

V-cycle multigrid, 672, 674
V2F model, 82
vaporization, 388, 390, 396
temperature, 388
velocity
swirl, 10
view factors, 168
clustering, 169
virtual mass force, 374, 538
viscous dissipation terms, 135
VOF
coupled level-set, 498
volatile fraction, 388
volatiles, 329, 331, 349
volume adaption, 699
volume flow rate, 716
through a surface, 720
volume fraction, 468, 513
in Eulerian multiphase model, 513
in mixture model, 505
in VOF model, 475
volume integrals
computing, 721
mass-weighted average, 723
mass-weighted integral, 722
sum, 722
volume-weighted average, 722
volume integration, 721
volume of fluid (VOF) model, 468
CICSAM, 479
compressive, 479
discretization scheme
compressive, 479
donor-acceptor scheme, 478
explicit scheme, 476
geometric reconstruction scheme, 478
implicit scheme, 476
interpolation, 477
CICSAM, 479
donor-acceptor scheme, 478
explicit scheme, 476
geometric reconstruction scheme, 478
implicit scheme, 476
jump adhesion, 485
limitations, 474
mass transfer, 579
momentum equation, 480
numerical beach, 488
open channel
numerical beach, 488
open channel flow, 485
overview, 474
phase localized
compressive scheme, 479
properties, 480
steady-state calculations, 475
surface tension, 481
continuum surface force, 482
continuum surface stress, 483
theory, 474


Release 15.0 - © SAS IP, Inc. All rights reserved. - Contains proprietary and confidential information of ANSYS, Inc. and its subsidiaries and affiliates.

time-dependent calculations, 475
volume fraction, 475
wall adhesion, 484
volumetric heat sources, 136

## W

W-cycle multigrid, 672, 674
WALE subgrid-scale model, 102
wall
adhesion, 484
functions, 113, 115
limitations of, 118, 121
non-equilibrium, 120
scalable, 119
standard, 115
rotation, 11
wall damping, 260
wall lubrication
models
Antal et al., 533
Frank et al., 534
Hosokawa, 534
Tomiyama, 533
wall lubrication force, 532
models, 532
wall surface reactions, 199
boundary conditions, 201
reaction rate, 199
site species, 201
solid species, 201
wall-film model, 413
separation criteria, 419
splashing, 416
wall-jet model, 412
wall-modeled LES model (WMLES), 103
wall-modeled LES S-omega model (WMLES S-omega), 105
wave boundary condition
Airy wave theory, 490
Stokes wave theory, 491
wave breakup model, 444
wavelength bands, 151
Weber number, 431, 484
weighted-sum-of-gray-gases model (WSGGM), 141
combusting flows, 170
mean beam length, 170
Wen and Yu model, 524
wet steam multiphase model
limitations, 574
properties, 577
theory, 573

## Y

y*, 115
adaption, 701
y+, 115
adaption, 701
Yao-Morel model
interfacial area concentration, 510

## Z

zones
deforming, 34
moving, 17
Zwart-Gerber-Belamri
cavitation model, 586

*Release 15.0 - © SAS IP, Inc. All rights reserved. - Contains proprietary and confidential information of ANSYS, Inc. and its subsidiaries and affiliates.*

Release 15.0 - © SAS IP, Inc. All rights reserved. - Contains proprietary and confidential information
of ANSYS, Inc. and its subsidiaries and affiliates.